NASA SP 33 PART 2

SPACE FLIGHT HANDBOOKS

Volume 1

Orbital Flight Handbook

NATIONAL AERONAUTICS AND SPACE ADMINISTRATION

SPACE FLIGHT HANDBOOKS

Volume 1

Orbital Flight Handbook

PART 2 - MISSION SEQUENCING PROBLEMS

Prepared for the
GEORGE C.
MARSHALL SPACE FLIGHT CENTER
Huntsville, Alabama
Under Contract NAS 8-5031

Office of Scientific and Technical Information
NATIONAL AERONAUTICS AND SPACE ADMINISTRATION
Washington, D. C. **1963**

FOREWORD

This handbook has been produced by the Space Systems Division of the Martin Company under Contract NAS8-5031 with the George C. Marshall Space Flight Center of the National Aeronautics and Space Administration. The handbook expands and updates work previously done by the Martin Company and also incorporates, as indicated in the text, some of the work done by Space Technology Laboratories, Inc. and Norair Division of Northrop Corporation under previous contracts with the George C. Marshall Space Flight Center. The Orbital Flight Handbook is considered the first in a series of volumes by various contractors, sponsored by MSFC, treating the dynamics of space flight in a variety of aspects of interest to the mission designer and evaluator. The primary purpose of these books is to serve as a basic tool in preliminary mission planning. In condensed form, they provide background data and material collected through several years of intensive studies in each space mission area, such as earth orbital flight, lunar flight, and interplanetary flight.

Volume I, the present volume, is concerned with earth orbital missions. The volume consists of three parts presented in three separate books. The parts are:

Part 1 - Basic Techniques and Data
Part 2 - Mission Sequencing Problems
Part 3 - Requirements

The Martin Company Program Manager for this project has been Jorgen Jensen, George Townsend has been Technical Director. George Townsend has also had the direct responsibility for the coordination and preparation of this volume. Donald Kraft is one of the principal contributors to this volume; information has also been supplied by Jyri Kork and Sidney Russak. Barclay E. Tucker and John Magnus have assisted in preparing the handbook for publication.

The assistance given by the Future Projects Office at MSFC and by the MSFC Contract Management Panel, directed by Conrad D. Swanson, is gratefully acknowledged.

CONTENTS

Volume I, Part 2 - Mission Sequencing Problems

VI Maneuvers VI-1

VII Rendezvous VII-1

VIII Orbital Departure VIII-1

IX Satellite Re-Entry IX-1

The preceding contents are Part 2 of Volume I. The remaining two parts of Volume I contain the following:

Volume I, Part 1 - Basic Techniques and Data

I Introduction I-1

II Physical Data II-1

III Orbital Mechanics III-1

IV Perturbations IV-1

V Satellite Lifetimes V-1

Volume I, Part 3 - Requirements

X Waiting Orbit Criteria X-1

XI Orbit Computations XI-1

XII Guidance and Control Requirements XII-1

XIII Mission Requirements XIII-1

Appendix A A-1

Appendix B B-1

Index i

CHAPTER VI

MANEUVERS

Prepared by:

G. E. Townsend, Jr.
Martin Company (Baltimore)
Aerospace Mechanics Department
March 1963

		Page
	Symbols	VI-1
A.	Introduction	VI-2
B.	Impulsive Corrections	VI-2
C.	Independent Adjustment of Orbital Elements	VI-3
D.	Small Maneuvers in Nearly Circular Orbits	VI-15
E.	General Two-Impulse Maneuvers	VI-23
F.	Propulsion Requirements for Canceling the Effects of Drag and Oblateness	VI-26
G.	Differential Corrections in Orbit Transfer	VI-33
H.	The Statistical Distribution of the Elements of the Final Orbit	VI-39
I.	Transfer Trajectory Optimization	VI-43
J.	The Effects of Finite Burning Time	VI-50
K.	In-Orbit Propulsion System	VI-53
L.	Micro-Thrust Study	VI-56
M.	References	VI-64
N.	Bibliography	VI-65
	Illustrations	VI-75

LIST OF ILLUSTRATIONS

Figure		Page
1	Solution to the Law of Cosines	VI-77
2	Solution to the Law of Sines	VI-78
3	Total Velocity Increment Required for Two-Pulse Correction to a Circular Orbit	VI-79
4	Effects of Variations in Characteristic Velocity on the Velocity After the Manuever	VI-80
5	Effects of Variations in the Pulse Attitude Angle on Vehicle Velocity After the Maneuver	VI-81
6	Effects of Variations in Characteristic Velocity on the Turn Angle.	VI-82
7	Effects of Variations in Thrust Pulse Angle on the Turn Angle	VI-83
8	Maneuvers in Circular Orbits to Change Orbital Inclination and/or the Node	VI-84
9	Nondimensionalized Impulsive Velocity Required to Transfer to a New Altitude, Rotate the Orbital Plane (at that altitude), and Recircularize Upon Arrival at the Initial Orbit	VI-85
10	Ratio of the Interceptor's Apogee Radius to the Radius of the Target's Circular Orbit as a Function of the Azimuth Change for Minimum Energy	VI-86
11	Nondimensionalized Orbital Period of the Interceptor in Its Maneuvering Orbit (elliptic orbit with apsidal radii equal to r_a and r_c)	VI-87
12	Fuel Required for Lateral Maneuvers in a Circular Orbit	VI-88
13	Nondimensionalized Impulsive Velocity Required to Rotate a Satellite's Orbital Plane	VI-89
14	Maneuver Angle as a Function of Thrust Attitude . . .	VI-90

LIST OF ILLUSTRATIONS (continued)

Figure		Page
15	Total Velocity Increment Required for Two-Pulse Correction to a Circular Orbit	VI-91
16	Velocity Increment for Maintenance of Circular Orbits by an Impulse at Orbit Intersection	VI-92
17	Error Analysis of Two-Pulse Correction of a Circular Orbit	VI-93
18	Absolute Magnitudes of the Nondimensionalized Components of the Thrust Vector as a Function of the True Anomaly for Orbit Inclinations from 0° to 90°	VI-94
19	Absolute Magnitude of the Nondimensionalized Thrust Vector as a Function of True Anomaly	VI-95
20	Magnitudes of the Nondimensionalized Corrective Force and Its Components, Averaged over the Orbit	VI-96
21	Discrete Velocity Sustaining System (h_0 = 300 naut mi = 555 km; I_{sp} = 300 sec)	VI-97
22	Discrete Velocity Sustaining System (h_0 = 200 naut mi = 370 km; I_{sp} = 300 sec)	VI-97
23	Discrete Velocity Sustaining System (h_0 = 100 naut mi = 185 km; I_{sp} = 300 sec)	VI-98
24	Discrete Velocity Sustaining System (h_0 = 50 naut mi = 93 km; I_{sp} = 300 sec)	VI-98
25	Velocity Required for Optimum 2-D Transfers Between Circular Orbits	VI-99
26	Independent Impulses for Optimum 2-D Transfers Between Circular Orbits	VI-100
27	Flight Path Angles for Optimum 2-D Transfer Between Circular Orbits	VI-101

LIST OF ILLUSTRATIONS (continued)

Figure		Page
28	Velocity Required for Optimum 3-D Transfers Between Circular Orbits	VI-102
29	Central Angles for Optimum 3-D Transfers Between Circular Orbits	VI-103
30	Flight Path Angles for Optimum 3-D Transfer Between Circular Orbits	VI-104
31	Total Energy Requirement for the Three-Pulse Transfer Between Circular Orbits as a Function of r_1, r_2 and r_3	VI-105
32	Energy Requirements for Transfer Between Coplanar Circular Orbits via the Hohmann Ellipse	VI-106
33	Lead Time Versus Acceleration Time	VI-107
34	Lead Time Versus Acceleration Time	VI-107
35	Velocity Difference Between Finite and Zero Time Acceleration Assumptions	VI-108
36	Difference in Velocity Increments Due to Zero and Finite Thrust Time Assumptions	VI-108
37	The Maximum Uncertainty in the Velocity Increment for Present Control Parameters as a Function of the Initial Thrust-to-Weight Ratio (specific impulse = 300 sec)	VI-109
38a	The Maximum Error in the Velocity Increment for a Velocity Monitored Propulsion System	VI-110
38b	The Maximum Error in the Velocity Increment for a Velocity Monitored Propulsion System (error in the integrated velocity increment = $10^{-4} \Delta V$)	VI-111
39	Characteristic Chamber Length for a UDMH-IRFNA Motor	VI-112

LIST OF ILLUSTRATIONS (continued)

Figure		Page
40	Relative Total Pressure Loss (measured at the throat) as a Function of Chamber Cross Section for a UDMH-IRFNA Rocket Motor	VI-113
41	Sea Level Specific Impulse for a UDMH-IRFNA Motor as a Function of Chamber Pressure (mixture ratio = 2.60:1)	VI-113

VI. MANEUVERS

SYMBOLS

A	Right ascension
A_T	Throat area
a	Semimajor axis
C_F	Coefficient of Thrust
D	Drag force
ΔV	Velocity increment due to impulsive thrusts
E	Eccentric anomaly
e	Eccentricity
$\mathfrak{F}(\ )$	Hypergeometric series
F	Force; Function
g_0	Gravity acceleration
h	Altitude
$I_0(z)$	Modified Bessel function of the first kind
I_{sp}	Specific impulse
i	Inclination
J, J_2	First coefficients of the potential function
L	Latitude
m	Mean anomaly relative to the injection point
M	Mean anomaly relative to perigee; Mach number
m, $\dot{m}$	Mass and mass rate
$P_n^m(z)$	Generalized Legendre polynomial
p	Semiparameter of ellipse
R	Range, equatorial radius
r	radius
r_a, r_p	Apogee and perigee radii
T_s	Period of sustained lifetime
t	Time
t_b	Burning time
U	Potential function
V	Velocity
V_c	Circular speed $\sqrt{\mu/r}$
W_o	Initial weight
W_p	Propellant weight
X_K	Acceleration
x, y, z	Coordinate components
β	Azimuth relative to north point on horizon; Log-log slope of atmospheric density approximation
γ	Flight path angle relative to local horizontal; ratio of specific heats for a gas
ϵ	Base of natural logarithms utilized to prevent confusion with eccentricity
ζ	Mass ratio W_p/W_o
θ	Central angle measured from perigee, i.e., true anomaly
μ	Gravitational constant = GM ; statistical mean
ν	Angle in the equatorial plane measured from the ascending node to the intersection of the equatorial plane and the instantaneous meridian
ρ	Atmospheric mass density
σ	Variance of a statistical density function
τ	Orbital period
ϕ	Central angle measured from the ascending node = $\theta + \omega$
ϕ_T	Thrust orientation angle relative to velocity vector
Ω	Right ascension of the ascending node
Ω_e	Rotational rate of the earth
$\dot{\Omega}$	Secular regression rate of the line of nodes due to the earth's oblateness
ω	Argument of perigee
ω'	Secular precession rate of the argument of perigee due to the earth's oblateness

A. INTRODUCTION

Because of many reasons, including guidance inaccuracies in launch and ascent, change of mission for the satellite, and evasion or rendezvous maneuvers, a requirement exists to transfer from one position and velocity in space to another at some subsequent time. This chapter treats some of the problems associated with such maneuvers and presents computation routines and data useful in analyses of these maneuvers.

Due to the fact that two general trajectories do not intersect, it is necessary to perform at least two maneuvers in order to produce the desired trajectory. Thus, the first order of business is the analyses of impulses (the mechanism of investigation) and of the independent adjustment of the six constants of integration or elements. These discussions will be followed by the analysis of small maneuvers in nearly circular orbits, a general two-impulse transfer discussion, propulsion requirements for correcting the effect of atmospheric drag and the earth's oblateness. At this point, the emphasis changes slightly to the presentation of material pertinent to differential corrections, the errors in the final orbit and trajectory optimization. These discussions are followed in turn by the analysis of the effects of finite burning time and the in-orbit propulsion system. The chapter concludes with a discussion of the adaptability of microthrusts for orbital corrections.

B. IMPULSIVE CORRECTIONS

Because the impulse is the medium of analysis in these discussions, the accompanying assumptions and methods will first be reviewed. Because the burning time is infinitesimal, the effects of gravity, variations in position due to thrust, etc., can be neglected and the governing law considered to be the law of cosines.

By this law, the characteristic velocity of the maneuver (ΔV) may be expressed as a function of the velocity vector prior to maneuver (V_1), the velocity vector after the maneuver (V_2), the turning angle of the maneuver (ψ) and the angle of thrust application relative to the initial flight direction (ϕ_T).

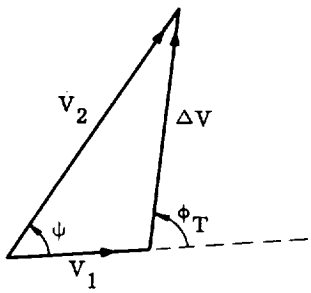

$$\Delta V^2 = V_1^2 + V_2^2 - 2 V_1 V_2 \cos \psi \qquad (1)$$

where

$$\Delta V = g_0 I_{sp} \ell n \left(\frac{1}{1 - \frac{\dot{m} t_b}{m_0}} \right) \qquad (2)$$

= the ideal velocity increment obtainable.

A convenient graphical representation of this law can be found if it is first nondimensionalized.

$$\left(\frac{\Delta V}{V_1} \right)^2 = 1 + \left(\frac{V_2}{V_1} \right)^2 - 2 \left(\frac{V_2}{V_1} \right) \cos \psi \qquad (3)$$

Similarly the law of sines is:

$$\frac{\Delta V}{V_1} \sin \phi_T = \frac{V_2}{V_1} \sin \psi \qquad (4)$$

These equations are presented in Figs. 1 and 2. The velocity increment itself is related to the mass fraction $\left(\frac{\dot{m} t_b}{m_0} \right)$ in Fig. 3. The form of these figures is the nomogram; the philosophy of construction along with a general description of the utilization of such a figure is presented in Chapter III. The effects of errors in ΔV and ϕ_T on the final velocity V_2 can be seen immediately from the law of cosines to be

$$\left(\frac{\partial x}{\partial y} \right)_{\phi_T} = \frac{y + \cos \phi_T}{x} \qquad (5)$$

$$\left(\frac{\partial x}{\partial \phi_T} \right)_y = - \frac{y}{x} \sin \phi_T \qquad (6)$$

$$\left(\frac{\partial \psi}{\partial y} \right)_{\phi_T} = \frac{\sin \phi_T}{x^2} \qquad (7)$$

$$\left(\frac{\partial \psi}{\partial \phi_T} \right)_y = \frac{y}{x} \left(\frac{\partial x}{\partial y} \right)_{\phi_T} \qquad (8)$$

where

$$x = \frac{V_2}{V_1}$$

$$y = \frac{\Delta V}{V_1}$$

and the subscript on the partial derivative indicates the parameter held constant. Figures 4 through 7 show these error coefficients.

C. INDEPENDENT ADJUSTMENT OF ORBITAL ELEMENTS

The impulse having been considered, attention can be turned to the correction of the orbital elements. This series of corrections will be treated first for the case when the target orbit is circular then for the case of elliptic orbits. (The distinction is made because of minor differences in the maneuver formulation.)

1. Circular Orbits

In general, the ascent guidance system will not be capable of placing the vehicle in a specified precisely circular orbit (even for a spherical earth). Therefore, maneuvers to change each element must be defined.

a. Correction of eccentricity and semimajor axis

The first of these maneuvers is the placement of the satellite in the proper orbit. This problem is considered in three cases, in which the planar orbit will be described by apogee and perigee radii and the time of perigee crossing. The three cases are:

(1) $r_a > r_n > r_p$

(2) $r_a > r_p > r_n$

(3) $r_n > r_a > r_p$.

The r_n is that radius which is specified for the satellite.

Case 1--$r_a > r_n > r_p$. Consider first the pulse necessary to change an initially elliptical orbit to a circular orbit.

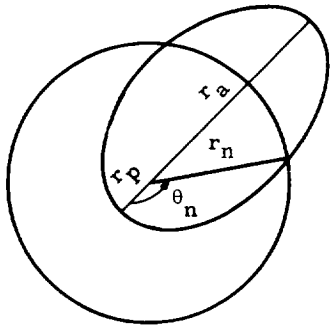

From the law of cosines

$$\Delta V_\epsilon^2 = V_c^2 + V_n^2 - 2 V_c V_n \cos \Delta\gamma$$

where

$V_c = \sqrt{\frac{\mu}{r_n}}$

V_n = velocity in the incorrect orbit at r_n

$\Delta\gamma$ = change in flight path angle

This expression may be written in terms of the knowns by considering

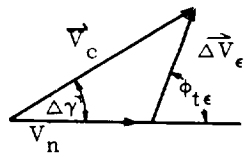

$$\Delta\gamma = \cos^{-1} \sqrt{\frac{r_a r_p}{r_n (r_a + r_p - r_n)}}$$

$$V_n^2 = \frac{\mu p}{r_n^2 \cos^2 \Delta\gamma} = 2 V_c^2 \left(1 - \frac{r_n}{r_a + r_p}\right)$$

$$2 V_c V_n \cos \Delta\gamma = 2 \sqrt{\frac{\mu}{r_n}} \frac{\sqrt{\mu p}}{r_n \cos \Delta\gamma} \cos \Delta\gamma$$

$$= 2 V_c^2 \sqrt{\frac{2 r_a r_p}{r_n (r_a + r_p)}}$$

Then, the nondimension solution for the corrective pulse may be written so as to involve only two ratios.

$$\left(\frac{\Delta V_\epsilon}{2 V_c}\right)^2 = \frac{3}{2} - \frac{\frac{r_n}{r_p}}{\frac{r_a}{r_p} + 1} - \sqrt{\frac{2 \frac{r_a}{r_p}}{\frac{r_n}{r_p}\left(\frac{r_a}{r_p} + 1\right)}} \qquad (9)$$

The direction of thrust application is determined by noting that

$$\Delta V_\epsilon \sin \phi_{t\epsilon} = V_c \sin \Delta\gamma$$

or

$$\phi_{t\epsilon} = \sin^{-1} \left(\frac{V_c}{\Delta V_\epsilon} \sin \Delta\gamma\right) \qquad (10)$$

If a timer signal is used to trigger the pulse, the time to make the correction must also be computed.

$$t = \frac{1}{\sqrt{\mu}} \left(\frac{r_a + r_p}{2}\right)^{3/2} \left[E - \frac{r_a - r_p}{r_a + r_p} \sin E\right] + t_p \qquad (11)$$

where

$$\sin E = \frac{r_n}{r_a - r_p} \left[\frac{r_a}{r_p}\left(1 + 2 \frac{r_p}{r_n}\right) + \frac{r_p}{r_a}\left(1 + 2 \frac{r_a}{r_n}\right) + \right.$$

(continued)

$$- 2 \left(1 + 2 \frac{r_a}{r_n} \frac{r_p}{r_n}\right)\Bigg]^{1/2}$$

and t is the time to initiate the correction.

The orbit resulting from the correction(s), the magnitude, direction and time of which are given by Eqs (9), (10) and (11) is a circular orbit of the desired period. However, this orbit may be slightly in error due to inherent inaccuracies. For this reason, the following error analysis for changing the size and shape of the orbit to a circular orbit was conducted.

$$\sin \Delta\gamma = \frac{\Delta V}{V_c} \sin \phi_t$$

$$\cos \Delta\gamma \, \partial(\Delta\gamma) = \frac{\partial(\Delta V)}{V_c} \sin \phi_t + \frac{\Delta V}{V_c} \cos \phi_t \, \partial \phi_t - \frac{\Delta V}{V_c^2} \sin \phi_t \, \Delta V_c$$

where

$$V_c = \sqrt{\frac{\mu}{r}} \quad \text{and}$$

$$\frac{\partial V_c}{\partial r} = - \frac{V_c}{2r} .$$

Thus,

$$\cos \Delta\gamma \, \delta(\Delta\gamma) = \frac{\delta(\Delta V)}{V_c} \sin \phi_t + \frac{\Delta V}{V_c} \cos \phi_t \, \Delta\phi_t + \frac{\Delta V \, \Delta r}{2 V_c r} \sin \phi_t$$

or

$$\frac{\cos \Delta\gamma \, \delta(\Delta\gamma)}{\sin \phi_t} = \frac{\delta(\Delta V)}{V_c} + \frac{\Delta V}{V_c} \left[\frac{\Delta r}{2r} + \cot \phi_t \, \Delta\phi_t\right] .$$

It is noted that both sides of the last equation become infinite as ϕ_t goes to zero. This problem may be resolved by going back one step to the preceding equation and noting that for $\phi_t = 0$, $\Delta\gamma = 0$.

$$\delta(\Delta\gamma) = \frac{\Delta V \, \Delta\phi_t}{V_c}$$

b. Correction of the plane

The second maneuver to be considered is that necessary to change the orbital plane. Consider the case of maneuvers in circular orbits to change orbital inclination or the node (Fig. 8). A vehicle in a circular orbit with inclination angle (i) and nodal longitude (Ω) is given a horizontal thrust pulse (ΔV, the characteristic velocity of the maneuver) at latitude (L) so that the orbital velocity remains constant in magnitude, but changes in azimuth by an angle $\Delta\beta$. (Azimuth is determined by the intersection of the meridian at the point of the maneuver and the great circle projection of the orbital path.) Using primes to indicate quantities after the maneuver,

$$\beta' = \beta + \Delta\beta.$$

A new node (Ω') and new inclination (i') result from such a maneuver. If d is the longitude of the maneuver, measured from the reference axis, then

$$\nu = \Omega \pm d.$$

(Note: Use a plus sign if Ω and d are on opposite sides of the reference axis, and a minus sign if they are on the same side.)

Since d is fixed, the longitude of the new node is

$$\Omega' = \nu' - d.$$

From spherical trigonometry,

$$\cos i = \cos L \sin \beta$$

$$\sin \nu = \tan L \cot i$$

$$\cot \beta = \sin L \cot \nu$$

These expressions can be manipulated by maintaining L constant to yield

$$\nu' = \tan^{-1} (\sin L \tan \beta'), \tag{12}$$

and

$$i' = \cos^{-1} (\cos L \sin \beta'). \tag{13}$$

The energy requirement to accomplish this constant speed turn is then simply

$$\frac{\Delta V}{V_c} = 2 \sin \Delta\beta / 2 \tag{14}$$

and the impulse must be directed according to

$$\phi_t = \pm \left(\frac{\Delta\beta}{2} + 90°\right)$$

in the plane normal to the radius vector.

The error derivatives $\left(\frac{\partial i}{\partial \beta}\right)_{L = \text{constant}}$ and $\left(\frac{\partial \nu}{\partial \beta}\right)_{L = \text{constant}}$ may be readily determined as

$$\left(\frac{\partial i}{\partial \beta}\right)_L = - \frac{\cos L \cos \beta}{\sin i} = - \sin L \cot i \cot \nu \tag{15}$$

and

$$\left(\frac{\partial \nu}{\partial \beta}\right)_L = \frac{\sin L \sec^2 \beta}{\sec^2 \nu} = \cos^2 \nu \sin L + \frac{\sin^2 \nu}{\sin L} . \tag{16}$$

At this point, it is of interest to note that if it is desired that the nodal position be maintained constant, the maneuver must occur at one of the equatorial crossings. If, however, the inclination is to be maintained constant, all maneuvers must be made at $\pm \frac{\Delta\Omega}{2}$ (sign depends on the direction of the $\Delta\Omega$) from the longitude corresponding to the maximum latitude.

Equation (14) shows the very large energy requirements for significant changes in azimuth at low altitudes where V_c is of the order of 8000 mps and suggests that a more efficient procedure might result if the maneuver could be made at a point where the velocity is low. Pursuing this thought further, consider the following sketch.

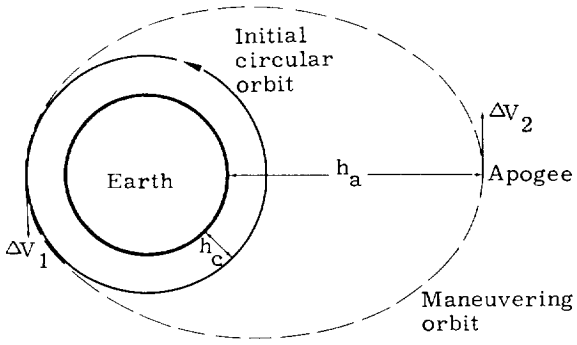

The philosophy is first to inject into an elliptic orbit the parameters of which will be investigated, secondly to change azimuth at the maximum radius (minimum velocity) and thirdly, reestablish the desired circular orbit but in a new plane. Now

$$V_p = V_c + \Delta V_1$$

$$V_p^2 - V_a^2 = 2\mu \left(\frac{1}{r_p} - \frac{1}{r_a}\right)$$

or

$$V_a = \frac{2V_c^2}{V_p} - V_p$$

Having reached apogee, the second increment of magnitude defined by

$$\frac{\Delta V_2}{V_a} = 2 \sin \frac{\Delta\beta_2}{2}$$

is applied.

Then at perigee, the initial velocity adjustment must be canceled; thus

$$\Delta V_{total} = 2\Delta V_1 + \Delta V_2 .$$

By combining the above equations, the following explicit expression for ΔV_T in terms of the radius of the circular orbit and the ratio of apogee to perigee radii can be obtained.

$$\Delta V_T = 2V_c \left\{ \left(\frac{r_a}{r_c}\right)^{1/2} \left[1 + \left(\frac{r_a}{r_c}\right)^{-1} \cdot \sin \frac{\Delta\beta}{2}\right] \left[\frac{1}{2}\left(1 + \frac{r_a}{r_c}\right)\right]^{-1/2} - 1 \right\}$$

$$(r_a \geq r_c) \tag{15}$$

This function has been plotted in Fig. 9 ($r_a \geq r_c$) in nondimensionalized form (by dividing through by V_c) for various values of $\Delta\beta$. For the smaller values of $\Delta\beta$, the impulsive incremental velocity required to perform the transfer maneuver is seen to be greater when the vehicle is injected into an elliptic orbit, that is, when the nodal point is stretched or lengthened. On the other hand, for the larger values of $\Delta\beta$, the three-impulse maneuver becomes more efficient, and, in fact, there is a definite ratio of r_a/r_c at which the total energy required for the maneuver is a minimum.

This condition is more clearly illustrated by analyzing the variation of ΔV_T with respect to r_a for a given value of r_c. Performing the indicated differentiation yields

$$\frac{\partial(\Delta V_T)}{\partial r_a} = \frac{V_c}{2r_c} \left\{ \left[\frac{1}{2}\frac{r_a}{r_c}\left(1 + \frac{r_a}{r_c}\right)\right]^{-3/2} \cdot \left[\frac{r_a}{r_c} - \left(1 + 2\frac{r_a}{r_c}\right) \sin \frac{\Delta\beta}{2}\right] \right\} \tag{16}$$

This function defines the minimum points when

$$\frac{\partial(\Delta V_T)}{\partial r_a} = 0 \tag{17}$$

that is, when

$$\frac{r_a}{r_c} = \left(1 + 2\frac{r_a}{r_c}\right) \sin \frac{\Delta\beta}{2} \tag{18}$$

or when

$$\frac{r_a}{r_c} = \frac{\sin \frac{\Delta ß}{2}}{1 - 2 \sin \frac{\Delta ß}{2}} \qquad (19)$$

The right-hand side of Eq (19) is plotted in Fig. 10 for the range $0° \leq \Delta i \leq 90°$ and also in Fig. 9 as a dotted line. The values given by the curve are the minima, while values selected within the shaded area represent choices which require more energy than the minimum, but less than that required to make the correction on the initial circular orbit itself. Another factor which in inferred from this curve is that since $r_a \geq r_c$, the value of $\Delta ß$, at which the function is exactly unity (about 39°), defines the minimum azimuth change for which it becomes profitable to effect the transfer to an eccentric orbit.

The vertical boundary at $\Delta ß = 60°$ arises because of the fact that the formulation breaks down at this point because the vehicle is required to transfer to infinity (i.e., escape) maneuver, then return. In this region all maneuvers will require the same energy, since the velocities at these large radii are essentially zero. However, this solution is of academic interest because of the impracticality of such an approach.

Another factor of interest in this study is the period T of the elliptical orbits being considered, since one would normally want to keep the transfer time within reasonable limits. The equation for the period of a vehicle in an elliptic orbit about the spherical earth is

$$\tau = \frac{2\pi}{\mu^{1/2}} a^{3/2} \qquad (20)$$

which may be reduced in terms of the variables used in the previous equations to the form:

$$\tau = \frac{2\pi r_c^{3/2}}{\mu^{1/2}} \left[\frac{1}{2}\left(1 + \frac{r_a}{r_c}\right)\right]^{3/2}$$

$$= \tau_c \left[\frac{1}{2}\left(1 + \frac{r_a}{r_c}\right)\right]^{3/2} \qquad (21)$$

where τ_c is the period of the (target's) circular orbit. Figure 11 is a plot of the nondimensionalized orbital period of the interceptor

$$\frac{\tau}{\tau_c} = \left[\frac{1}{2}\left(1 + \frac{r_a}{r_c}\right)\right]^{3/2} \qquad (22)$$

as a function of the parameter r_a/r_c for the same range as was considered previously, with the same equation applying in this case, for the entire range of r_a/r_c.

The factor of interest here, however, is the additional amount of time required to perform the eccentric maneuver, as compared to the period of the circular orbit. This factor is given by

$$\tau - \tau_c = \left(\frac{\tau}{\tau_c} - 1\right) \tau_c \qquad (23)$$

The new circular orbit may also be described in terms of the lateral separation from the old orbit as a function of the central angle from the point at which the maneuver is made (ϕ_0) if the maneuver is small. Let the spherical separation of the new orbit from the original orbit be $\bar{z}$ expressed in radians.

Then

$$\frac{\sin \bar{z}}{\sin \Delta ß} = \frac{\sin \phi_0}{\sin \phi_T}$$

but $\sin \Delta ß = \Delta V / V_c \sin \phi_T$ from pulse geometry.

Therefore,

$$\sin \bar{z} = \frac{\Delta V}{V_c} \sin \phi_0.$$

For small angles ($\bar{z} < 0.1$ radian) $\sin \bar{z} \tilde{=} \bar{z}$ (radian) $\tilde{=} \frac{z}{r_0} \frac{(km)}{(km)}$, and with a maximum error of about 1% we have:

$$\frac{z}{r_0} \tilde{=} \frac{\Delta V}{V_0} \sin \phi_0 \qquad (24)$$

The separation z (km) versus mass ratio required is plotted in nomograph form in Fig. 12 for circular orbits at altitudes of 0, 200, 400, 600, 800 and 1000 km for various ϕ_0 and I_{sp} = 200, 250, 300, 350 and 400 sec. The maximum separation between the orbits is seen to occur at

$$\phi_0 = (2n - 1)\ 90°, \quad n = 1, 2, \ldots$$

This fact is true because both orbits must contain the original radius vector.

There is no time separation between satellites because the satellite is in a circular orbit at the same altitude with the same period both before and after the maneuver.

c. Correction of position

The equations to correct the position of the satellite in its corrected circular orbit are derived as follows. If it is assumed the satellite is displaced $\Delta\theta$ from some desired position, then the time in which the satellite passes through $\Delta\theta$ is

$$\Delta t = \frac{\tau}{2\pi} \Delta\theta \qquad (25)$$

This Δt must be lost or made up, depending upon whether the satellite is ahead of, or behind its desired zenith. The simplest solution, from the standpoint of computations involved, is to cause the satellite to enter an elliptical orbit possessing a period $\tau \pm \Delta t/n$ (with perigee or apogee, as the case may be, at the altitude of the desired orbit) by a pulse tangent to the original orbit, and to re-enter the original orbit by an equal and opposite pulse after n periods of the transfer orbit. Then, if τ_t and a are parameters of the transfer orbit,

$$\frac{\Delta t}{n} = \pm (\tau_t - \tau) = \pm \tau \left\{ \left(\frac{a}{r_n} \right)^{3/2} - 1 \right\} \quad (26)$$

Combining Eqs (25) and (26) and noting that

$$a = \frac{\mu r_n}{2\mu - r_n V_n^2},$$

V_n is determined as

$$\left(\frac{V_n}{V_c} \right)^2 = 2 - \frac{1}{\left(\frac{\Delta\theta}{2\pi} + 1 \right)^{2/3}}.$$

Then,

$$\frac{\Delta V_{\theta 1}}{n V_c} = \frac{V_n}{V_c} - 1 = \sqrt{2 - \frac{1}{\left(\frac{\Delta\theta}{2\pi} + 1 \right)^{2/3}}} - 1 \quad (27a)$$

and

$$\Delta V_{\theta 2} = - \Delta V_{\theta 1}$$

where:

$\Delta V_{\theta 1}$, $\Delta V_{\theta 2}$ are the first and second corrective pulses applied tangentially at an interval $n\tau \left(1 \pm \frac{\Delta\theta}{2\pi n} \right)$.

n = number of revolutions in transfer orbit

$\Delta\theta$ = + if vehicle is to move backward in orbit (i.e., ΔV along velocity vector)
= - if vehicle is to move ahead in orbit (i.e., ΔV opposes velocity vector)

Equation (27a) is presented in Fig. 13.

For large values of $\Delta\theta$, ΔV approaches

$$\Delta V = \sqrt{\frac{\mu}{r}} \, (\sqrt{2} - 1),$$

which is the difference between escape and circular orbit velocities. For small values of $\Delta\theta$,

$$\Delta V \approx \sqrt{\frac{\mu}{r}} \left(\frac{\Delta\theta}{6\pi} \right).$$

The time required for carrying out the maneuver is

$$t = \frac{2\pi n}{\sqrt{\mu}} \sqrt{\left(\frac{r\mu}{2\mu - r(V + \Delta V)^2} \right)^3}$$

where ΔV is negative if $\Delta\theta$ is + and positive if $\Delta\theta$ is -.

The more general case where thrust is not assumed to be along the velocity vector results in the following expression

$$\Delta\theta = (1 - K_2)\,\pi \left\{ 1 - \frac{1}{\left(2 - K_2^2 \right)^{3/2}} \right\} + 2 K_2 \left\{ \tan^{-1} \left[\frac{\tan\alpha}{K_2^2 - 1} \right] + \alpha - \frac{E - e \sin E}{\left[2 - K_2^2 \right]^{3/2}} \right\} \quad (27b)$$

where

$$\alpha = \tan^{-1} \left\{ \frac{(K_2 - K_1)\,|\sin \phi_T|}{1 + (K_2 - K_1) \cos \phi_T} \right\}$$

$$K = \sqrt{2 - \frac{r}{a}}$$

and

$$E = \tan^{-1} \left\{ (K_2 - K_1) \sqrt{\frac{2 - K_2^2}{K_2^2 - 1}} \, |\sin \phi_T| \right\}$$

This relationship is presented in Fig. 14.

Equation (27) assumes that the maneuver may be initiated at any time and considers only the magnitude of the error in the central angle. If it is desired to produce a specific node (on a rotating earth) at a specified time, the basic approach must be altered. The new problem may be restated as follows: Assume that it is desired to move from a known position B (relative to the ascending node) to a nodal position Ω_2 on a rotating earth in the same time that it takes to move from a position α to the node Ω_1. This problem is illustrated in the following sketch.

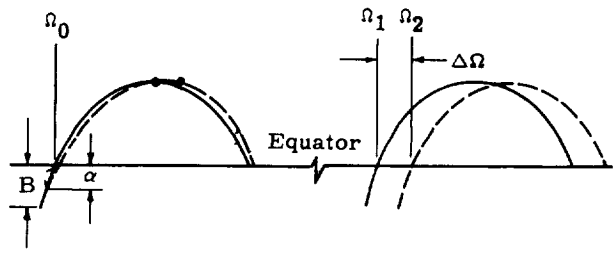

For the case of nearly circular orbits, this implies that ($t_1 = t_2$):

$$\frac{\tau}{2\pi}\left[2\pi n + \alpha - n\dot{\omega}\right] = \frac{\tau'}{2\pi}\left[2\pi n' + B - n'\dot{\omega}'\right] \tag{28}$$

If $n = n'$ and $\dot{\omega}' \approx \dot{\omega}$,

$$\frac{\tau}{\tau'} = \frac{n'(2\pi - \dot{\omega}') + B}{n(2\pi - \dot{\omega}) + \alpha}$$

$$\simeq 1 + \frac{B - \alpha}{n(2\pi - \dot{\omega}) + \alpha} .$$

Another relationship between τ and τ' can be obtained by observing the nodal motion as a function of period change:

$$n\Delta\tau\Omega_e = \Delta\Omega + \dot{\Omega}n$$

and

$$\frac{\tau}{\tau'} = 1 + \frac{\Delta\Omega + n\dot{\Omega}}{n\Omega_e \tau'}$$

Equating

$$\frac{B - \alpha}{n(2\pi - \dot{\omega}) + \alpha} = \frac{\Delta\Omega + n\dot{\Omega}}{n\Omega_e \tau'} \tag{29}$$

The angle α is included in the analysis for the sole purpose of providing a means for including errors in the time of passage through the node Ω_0. Therefore,

$$\alpha = f(t_{error}) = \frac{2\pi\Delta t_0}{\tau} .$$

Substituting this relationship into Eq (29) yields

$$\frac{B}{2\pi} = \left[1 - \frac{\dot{\omega}}{2\pi} + \frac{\Delta t_0}{n\tau}\right]\left[\frac{\Delta\Omega + n\dot{\Omega}}{\Omega_e\tau + \frac{\Delta\Omega}{n} + \dot{\Omega}}\right] + \frac{\Delta t_0}{\tau} \tag{30}$$

Thus, the position of the point at which the first corrective pulse is to be made is defined, but the magnitude of the correction itself has not yet been evaluated. This portion of the analysis can be accomplished when it is noted that the orbits of interest for this study are circular.

Thus,

$$\Delta\tau = 3\tau\left[\frac{\Delta r}{r} + \frac{\Delta V}{V_c}\right] \tag{31}$$

If the period change is to result solely from a velocity pulse (that is, no change in radius during the application of the pulse), the period change is:

$$\Delta\tau = \frac{3\tau\Delta V}{V_c} .$$

Again,

$$\Delta\tau = \frac{\Delta\Omega + n\dot{\Omega}}{n\Omega_e} .$$

Therefore,

$$\Delta V = \frac{\mu}{6\pi r^2}\left[\frac{\Delta\Omega + n\dot{\Omega}}{n\Omega_e}\right] \tag{32}$$

This equation defines the first pulse, which alters the period to produce the desired position change. However, a second pulse approximately equal to, but in the opposite direction from the first, is required at the desired node to produce the correct orbit. Both of these pulses should be directed along the velocity vector. The magnitude of this second pulse is:

$$\Delta V_2 = \Delta V_1 + (V_c - \delta V_1)$$

where the corrective term is included to compensate for the small radius and velocity errors which produced the initial displacement.

Case 2. $r_a > r_p > r_n$. For this case, the determination of ΔV_ϵ must be modified as follows:

$$\frac{\Delta V_\epsilon}{\sqrt{2}V_{ca}} = \frac{1}{\sqrt{\frac{r_a}{r_n} + 1}} - \frac{1}{\sqrt{\frac{r_a}{r_p} + 1}} \tag{33}$$

$$\frac{\Delta V_{\epsilon 2}}{V_c} = 1 - \sqrt{\frac{2}{1 + \frac{r_n}{r_a}}} \tag{34}$$

where $V_{ca} = \sqrt{\frac{\mu}{r_a}}$. Tangential pulses ($\Delta V_{\epsilon 1}$ and $\Delta V_{\epsilon 2}$) are applied at

$$t_p + \frac{\pi}{\sqrt{\mu}}\left(\frac{r_a + r_p}{2}\right)^{3/2}$$

and

$$t_p + \frac{2\pi}{\sqrt{\mu}}\left(\frac{r_a + r_p}{2}\right)^{3/2}, \text{ respectively.}$$

The subsequent corrections for i, Ω proceed exactly as in the first case.

Case 3. $r_n > r_a > r_p$. Proceeding in a manner similar to Case 2,

$$\frac{\Delta V_{\epsilon 1}}{\sqrt{2}V_{cp}} = \frac{1}{\sqrt{1 + \frac{r_p}{r_n}}} - \frac{1}{\sqrt{1 + \frac{r_p}{r_a}}} \tag{35}$$

$$\frac{\Delta V_{\epsilon 2}}{V_c} = 1 - \sqrt{\frac{2}{\frac{r_n}{r_p} + 1}} \tag{36}$$

where $V_{cp} = \sqrt{\frac{\mu}{r_p}}$ and $\Delta V_{\epsilon 1}$ and $\Delta V_{\epsilon 2}$ are applied tangentially at times

$$t_p + \frac{2\pi}{\sqrt{\mu}} \left(\frac{r_a + r_p}{2}\right)^{3/2}$$

and

$$t_p + \frac{3\pi}{\sqrt{\mu}} \left(\frac{r_a + r_p}{2}\right)^{3/2} .$$

The subsequent corrections for i, Ω proceed exactly as in the first case.

2. Elliptical Orbits

The presentation here considers the orbit to be defined in terms of the six usual elements a, e, t_p, i, ω, Ω and discusses the adjustment of each.

a. Transition from incorrect orbit

The first step in the final correction of an elliptical orbit is a transition from the incorrect orbit to an orbit of the desired size and shape in the plane of the incorrect orbit, but rotated in the plane through an angle $\omega - \omega'$, where ω' is the angle from perigee to node for the incorrect orbit and ω the angle from perigee to node in the orbit ultimately desired.

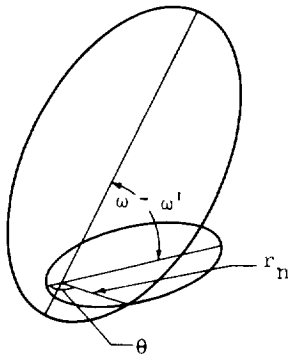

Known or calculable quantities are r'_a, r'_p, r_a, r_p, ω and ω', where primes denote quantities in the incorrect orbit. The angle from perigee to intersection in the original orbit (θ) may be determined as follows.

$$r_n = \frac{p'}{1 + e' \cos\theta} = \frac{p}{1 + e \cos(\theta - \omega + \omega')}$$

Writing this expression in terms of the known radii,

$$\left(\frac{r'_a}{r'_p} - 1\right) \cos\theta + \frac{r'_a}{r'_p} + 1 = \frac{r'_a}{r_a}\left[\frac{r_a}{r_p} + 1 + \left(\frac{r_a}{r_p} - 1\right)\cos(\theta - \psi)\right] \quad (37)$$

where

$$\psi = \omega - \omega' .$$

This expression can be easily solved for θ by an iteration technique. However, a direct solution is also available

$$\cos\theta = \frac{B(1 - A\cos\psi)}{1 + A^2 - 2A\cos\psi} \pm \left[B^2(1 - A\cos\psi)^2 - (1 + A^2 - 2A\cos\psi)(B^2 - A^2\sin^2\psi)\right]^{1/2} \cdot (1 + A^2 - 2A\cos\psi)^{-1}$$

where

$$A = \frac{1/r_p - 1/r_a}{1/r'_p - 1/r'_a} = \frac{e' p}{e p'} ,$$

$$B = \frac{1/r_a + 1/r_p}{1/r'_p - 1/r'_a} - \frac{\frac{r'_a}{r'_p} + 1}{\frac{r'_a}{r'_p} - 1} = \frac{e' p'}{p} - \frac{1}{e'}$$

$$\psi = \omega - \omega' .$$

The change in flight path angle in the maneuver is

$$\Delta\gamma = \cos^{-1}\sqrt{\frac{r'_a/r_n}{r'_a/r'_p - (r_n/r'_p) + 1}} - \cos^{-1}\sqrt{\frac{r_a/r_n}{\frac{r_a}{r_p} - \frac{r_n}{r_p} + 1}} \quad (38)$$

The characteristic velocity necessary to effect the maneuver may be determined from the law of cosines.

$$\frac{\Delta V_\epsilon^2}{2 V_{cr}^2} = 2 - \frac{1}{\frac{r'_a}{r_n} + \frac{r'_p}{r_n}} - \frac{1}{\frac{r_a}{r_n} + \frac{r_p}{r_n}} - 2\sqrt{\left[1 - \frac{1}{\frac{r'_a}{r_n} + \frac{r'_p}{r_n}}\right]\left[1 - \frac{1}{\frac{r_a}{r_n} + \frac{r_p}{r_n}}\right]} \cos\Delta\gamma , \quad (39)$$

where ΔV_ϵ is the characteristic velocity of the correction and V_{cr} is the circular velocity at r.

Thus, if r_p, r_a, r'_a, r'_p, ω and ω' are known, θ (and hence r_n and the time for correction), ΔV and $\Delta\gamma$ are determined.

b. Correction of inclination

After the size and shape correction is completed, it is possible to correct inclination to the desired value by a constant speed turn at the node (ω). The error in inclination (Δi) will be determined as data. The characteristic velocity of the inclination correction is then

$$\Delta V_i = 2V_n \sin \frac{\Delta i}{2} \tag{40}$$

where the velocity at the node (V_n) is determined as

$$V_n = \sqrt{\mu\left(\frac{2}{r_n} - \frac{1}{a}\right)}$$

$$= V_{ca}\left[\frac{r_a}{r_p} + 1 + \left(\frac{r_a}{r_p} - 1\right)\cos\omega - \frac{2\frac{r_a}{r_p}}{\frac{r_a}{r_p} + 1}\right]^{1/2}$$

(V_{ca} is circular velocity at r_a.)

Then, the inclination correction may be expressed in nondimensional form as

$$\frac{\Delta V_i}{V_{ca}} = 2 \sin \frac{\Delta i}{2} \sqrt{\frac{r_a}{r_p} + 1 + \left(\frac{r_a}{r_p} - 1\right)\cos\omega - \frac{2\frac{r_a}{r_p}}{\frac{r_a}{r_p} + 1}} \tag{41}$$

and the direction of thrust application is

$$\phi_{ti} = \frac{\Delta i}{2} + 90° \tag{42}$$

from the initial direction of motion because the thrust possesses no component along the principal normal to the orbit.

The thrust is applied at a time

$$t - t_p = \frac{\tau}{2\pi}(E_n - e \sin E_n)$$

where

$$E_n = 2 \tan^{-1}\left[\sqrt{\frac{r_p}{r_a}} \tan \frac{\omega}{2}\right]. \tag{43}$$

c. Correction of nodal position

The next corrective maneuver is the correction of nodal position.

The inclination (i) is to be maintained and the latitude of the satellite at transition is L. Consider the spherical triangles formed by the projections of the original and corrected orbits on a spherical earth.

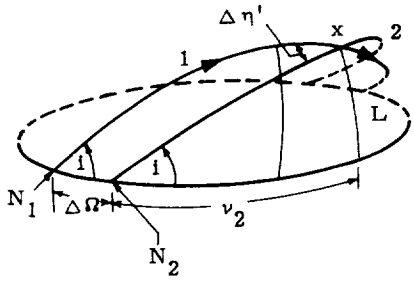

$$\tan i = \frac{\tan L}{\sin(\nu_2 + \Delta\Omega)} = \frac{\tan L}{\sin \nu_2}$$

$$\sin(\nu_2 + \Delta\Omega) = \sin \nu_2$$

Thus

$$\nu_2 = 90° - \frac{\Delta\Omega}{2}$$

Let the angle from node to transition (x) at the incorrect orbit be ϕ_x.

Then,

$$\phi_x = \tan^{-1}\left[\frac{\tan\left(90° + \frac{\Delta\Omega}{2}\right)}{\cos i}\right].$$

The velocity at x should be changed to the velocity possessed in the original orbit at $90° - \frac{\Delta\Omega}{2}$ longitude from N_1. To obtain this condition, a constant speed turn, the change in yaw angle at x in the actual orbits ($\Delta\eta$), and a consequent rotation of the orbit through an angle in its plane is necessary.

Again considering spherical trigonometry, the projected change in yaw angle is

$$\Delta\eta' = 180 - 2 \cos^{-1}\left(\sin \frac{\Delta\Omega}{2} \sin i\right) \tag{44}$$

The actual change in yaw angle is given by

$$\Delta\eta = 2 \sin^{-1}\left(\cos \gamma_x \sin \frac{\Delta\eta'}{2}\right) \tag{45}$$

where γ_x is the flight path angle in both orbits at the transition point.

The first pulse required in the nodal correction is then

$$\Delta V'_n = 2V_x \sin \frac{\Delta\eta}{2} = 2V_x \cos \gamma_x \sin \frac{\Delta\Omega}{2} \sin i.$$

However, $r_x V_x \cos \gamma_x = \sqrt{\mu p}$.

Then,

$$\Delta V'_n = 2\sqrt{\frac{\mu}{p}}\,(1 + e\cos\theta_x)\sin\frac{\Delta\Omega}{2}\sin i \qquad (46)$$

where $\theta_x = \phi_x - \omega_1$ and $\Delta\eta'$ is given by Eq (44). The time for the correction is determined by θ_t.

Since the orbit is elliptic and since this orbit rotates about the line through the point of thrust application and the center of the earth, the line of apsides is rotated in the orbit plane during this maneuver. For some satellite applications, this rotation is very objectionable and must be canceled. Therefore, a second pulse is required ($\Delta V''_n$) to rotate the orbit a specified angle (α) in its plane. If r' is the radius at transition, $\Delta V''_n = 2\,V'\sin\gamma'$.

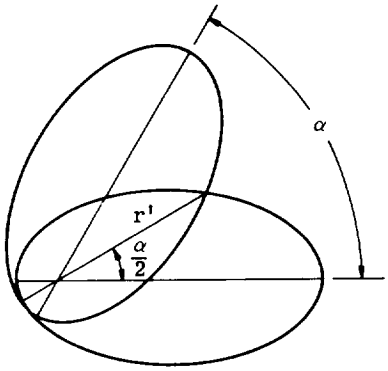

But, $V' = \dfrac{\sqrt{p\mu}}{r'\cos\gamma'} = \sqrt{\dfrac{\mu}{p}}\,\dfrac{1 - e\cos\frac{\alpha}{2}}{\cos\gamma'}$

and, therefore, since $\tan\gamma' = \dfrac{-e\sin\frac{\alpha}{2}}{1 - e\cos\frac{\alpha}{2}}$

$$V' = \sqrt{\frac{\mu}{p}}\left(\frac{-e\sin\frac{\alpha}{2}}{\sin\gamma'}\right)$$

Then

$$\Delta V''_n = 2V'\sin\gamma' = -2\sqrt{\frac{\mu}{p}}\,e\sin\frac{\alpha}{2} \qquad (47)$$

where p, e are parameters of the desired orbit, and α is determined as

$$\alpha = 180° - 2\tan^{-1}\left[\frac{\tan\left(90 - \frac{\Delta\Omega}{2}\right)}{\cos i}\right] \qquad (48)$$

The corrective pulse is applied at

$$t = \frac{\tau}{2\pi}\,(E' - e\sin E')$$

seconds after the time of perigee passage, where

$$E' = 2\tan^{-1}\left(\sqrt{\frac{r_p}{r_a}}\cot\frac{\alpha}{4}\right) \qquad (49)$$

Note is made at this point that the analysis of the second nodal pulse is identically that which is required to change the argument of perigee an amount $\Delta\omega$ for the case where this element alone is to be changed.

d. Correction of position

The elliptical orbit is now correct with the exception of the position correction or analogously the correction to the time of perigee passage. Since the orientation of the orbit is correct, this final adjustment must be made either at apogee or perigee.

If the observed time of perigee passage is t'_p and the time at which the satellite should cross perigee is t_p, the period of the transfer orbit tangent at perigee is $\tau + \Delta t$, where $\Delta t = t'_p - t_p$.

And, the corrective pulse to be applied at perigee is

$$\frac{\Delta V_t}{n} = \sqrt{\frac{\mu}{r_p}}\left[\sqrt{2 - r_p\left(\frac{2\pi}{\sqrt{\mu}\,(\tau + \Delta t)}\right)^{2/3}} - \sqrt{\frac{2}{1 + \frac{r_p}{r_a}}}\right] \qquad (50)$$

An equal and opposite pulse applied at $t_p + n\,(\tau + \Delta t)$ completes the maneuver and prevents further drift.

Equations (10) to (50) comprise a method of correction calculation which is theoretically sufficient to achieve the desired properties in a given orbit.

Repetitions of the various maneuvers may be required to achieve desired accuracies. The number of repetitions will depend on sensor and control accuracies, and on the mission itself.

3. Sequence for Corrections for Maneuvers

Several requirements restrict the selection of a routine to correct the positions of a satellite. Since the mission of most satellites is intrinsically one of long duration, and corrections to an accurate orbit might be required daily, economy is an important factor. Secondly, the transfer orbits involved in the correction should closely approximate the nominal orbit, so that the mission (communication, surveillance, etc.) will not be interrupted. Also, the correction routine should be as simple as possible with the other imposed conditions. The following correction calculation routine has been selected on the basis of these requirements.

At any given reference time t_0, the data for the correction calculation are a_0, e_0, i_0, Ω_0, ω_0, θ_0. These quantities are in error compared to the corresponding parameters of the nominal orbit at the same time, a_n, e_n, i_n, Ω_{0n}, ω_{0n}, θ_{0n}.

Because of their frequent occurrence in the correction equations chosen, it is convenient to define six parameters, η, λ, ξ, σ, $\varkappa$, ψ. These parameters are defined (for the case of the incorrect orbit, denoted by subscript "0") as follows:

$$\begin{aligned}
\eta_0 &= \cos\omega_0 \sin\Omega_0 + \cos i_0 \cos\Omega_0 \sin\omega_0 \\
\lambda_0 &= -\sin\omega_0 \sin\Omega_0 + \cos i_0 \cos\Omega_0 \cos\omega_0 \\
\xi_0 &= \cos\omega_0 \cos\Omega_0 - \cos i_0 \sin\Omega_0 \sin\omega_0 \\
\sigma_0 &= -\sin\omega_0 \cos\Omega_0 - \cos i_0 \sin\Omega_0 \cos\omega_0 \\
\varkappa_0 &= \sin i_0 \sin\omega_0 \\
\psi_0 &= \sin i_0 \cos\omega_0
\end{aligned} \tag{51}$$

Then the incorrect orbit may be expressed in spherical coordinates (r, A, L) by the three equations:

$$\begin{aligned}
r &= \frac{a_0 (1 - e_0^2)}{1 + e_0 \cos\theta} \\
A &= \tan^{-1}\left(\frac{\eta_0 \cos\theta + \lambda_0 \sin\theta}{\xi_0 \cos\theta + \sigma_0 \sin\theta}\right) \\
L &= \sin^{-1}(\varkappa_0 \cos\theta + \psi_0 \sin\theta)
\end{aligned} \tag{52}$$

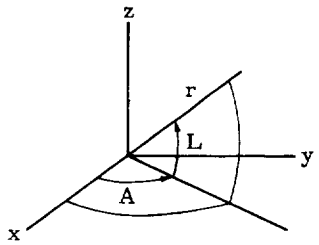

Although all six orbital elements may require correction, economy can be improved by correcting more than one element with a single thrust. The corrections of inclination and the node, which are both nonplanar corrections, can be simply combined, as can the planar corrections (size, shape and position of the satellite within the orbit). Although, for maximum economy, the order in which the planar and nonplanar corrections are made depends on the energies of the incorrect and required orbits, the increased economy derived from employing separate corrective routines for each case is not sufficient to justify the increased complexity of the routine (for small changes in the orbital elements). For example, in the case of circular orbits of radii $r_n = 5.488164 \times 10^7 \pm 6000$ ft ($1.672792 \times 10^7 \pm 1830$ m) the velocity increments required to rotate the orbit planes through 0.10° are 27.961 fps and 27.965 fps (8.5225 and 8.5237 mps), a difference in the fifth significant figure or third decimal place. Even though the error in radius should approach $r_n \pm 25,000$ ft (7620 m), the difference in the increments is in the fourth place. Thus, for orbital maintenance the order of correction for the nodal and inclination changes has very little effect on the resultant energy requirement. Even though the errors to be corrected during initial placement are much larger and the differences in the velocity increments more significant, the order still produces only minor differences. For this reason the position of the planar change in the routine will be considered inmaterial for simplicity.

The first thrust in the corrective sequence is chosen as a thrust to eliminate error in inclination and node by a constant speed turn at the intersection of the incorrect orbit and the nominal orbit plane. If quantities associated with this intersection point are denoted by the subscript 1, this point may be determined by setting $r = r_1$, $\theta = \theta_1$ in Eq (52) and simultaneously solving this equation and Eq (53) of the nominal orbit plane for θ_1 and r_1

$$\cos L \cos A \sin i_n \sin\Omega_{0n} - \cos L \sin A \sin i_n \cos\Omega_{0n} + \sin L \cos i_n = 0$$

which yields (53)

$$\begin{aligned}
&(\xi_0 \cos\theta_1 + \sigma_0 \sin\theta_1) \sin i_n \sin\Omega_n \\
&- (\eta_0 \cos\theta_1 + \lambda_0 \sin\theta_1) \sin i_n \cos\Omega_{0n} \\
&+ (\varkappa_0 \cos\theta_1 + \psi_0 \sin\theta_1) \cos i_n = 0
\end{aligned}$$

Solving this equation for θ_1 gives

$$\cos\theta_1 = \pm \frac{Q}{\sqrt{T^2 + Q^2}} \tag{54}$$

where

$$\begin{aligned}
Q &= \sigma_0 \sin i_n \sin\Omega_{0n} - \lambda_0 \sin i_n \cos\Omega_{0n} \\
&\quad + \psi_0 \cos i_n, \\
T &= \xi_0 \sin i_n \sin\Omega_{0n} - \eta_0 \sin i_n \cos\Omega_{0n} \\
&\quad + \varkappa_0 \cos i_n,
\end{aligned}$$

and the sign chosen in Eq (54) is that which satisfies

$$\cos\theta_1 = -\frac{Q}{T} \sin\theta_1.$$

In computing the velocity increment required at the intersection point, latitude, flight path angle, orbit velocity and change of flight path azimuth during the maneuver are necessary.

$$L_1 = \sin^{-1}\left[\sin i_n \sin(\theta_1 + \omega_1)\right] \tag{55}$$

where

$$\omega_1 = \sin^{-1}\left[\frac{\sin i_0 \sin(\theta_1 + \omega_0)}{\sin i_n}\right]$$

$$\gamma_1 = \tan^{-1}\left[\frac{e_0 \sin\theta_1}{1 + e_0 \cos\theta_1}\right] \quad (56)$$

$$V_1 = \sqrt{\mu\left(\frac{2}{r_1} - \frac{1}{a_0}\right)} \quad (57)$$

$$\Delta\beta_1 = \sin^{-1}\left(\frac{\cos i_n}{\cos L_1}\right) - \sin^{-1}\left(\frac{\cos i_0}{\cos L_1}\right) \quad (58)$$

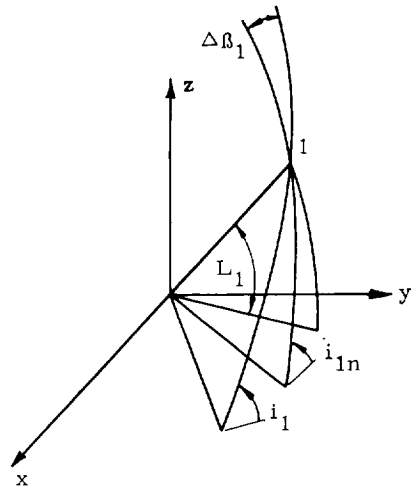

The magnitude of the velocity increment required to correct the orbit inclination and node is

$$\Delta V_1 = 2V_1 \sin\frac{\Delta\beta_1}{2} \cos\gamma_1 \quad (59)$$

The parameters in the corrected orbit corresponding to Eq 51 are:

$$\eta_1 = \cos\omega_1 \sin\Omega_{1n} + \cos i_n \cos\Omega_{1n} \sin\omega_1$$

$$\lambda_1 = -\sin\omega_1 \sin\Omega_{1n} + \cos i_n \cos\Omega_{1n} \cos\omega_1$$

$$\xi_1 = \cos\omega_1 \cos\Omega_{1n} - \cos i_n \sin\Omega_{1n} \sin\omega_1$$

$$\sigma_1 = -\sin\omega_1 \cos\Omega_{1n} - \cos i_n \sin\Omega_{1n} \cos\omega_1$$

$$\chi_1 = \sin i_n \sin\omega_1$$

$$\psi_1 = \sin i_n \cos\omega_1 \quad (60)$$

The orientation of the corrective thrust can then be obtained. Since the general elliptical orbit in three dimensions may be expressed as:

$$\vec{r} = \left[\xi p \frac{\cos\theta}{1 + e\cos\theta} + \sigma p \frac{\sin\theta}{1 + e\cos\theta}\right] \vec{i}$$

(continued)

$$+ \left[\eta p \frac{\cos\theta}{1 + e\cos\theta} + \lambda p \frac{\sin\theta}{1 + e\cos\theta}\right] \vec{j}$$

$$+ \left[\chi p \frac{\cos\theta}{1 + e\cos\theta} + \psi p \frac{\sin\theta}{1 + e\cos\theta}\right] \vec{k}, \quad (61)$$

the orbital velocity may be determined as $\frac{\vec{dr}}{dt}$.

$$\vec{V} = \sqrt{\frac{\mu}{p}}\left[\sigma(\cos\theta + e) - \xi\sin\theta\right]\vec{i} + \sqrt{\frac{\mu}{p}}\left[\lambda(\cos\theta + e) - \eta\sin\theta\right]\vec{j} + \sqrt{\frac{\mu}{p}}\left[\psi(\cos\theta + e) - \chi\sin\theta\right]\vec{k} \quad (62)$$

Orbital velocity in spherical coordinates may then be expressed as:

$$V = \sqrt{\mu\left(\frac{2}{r} - \frac{1}{a}\right)}$$

$$\nu^* = \tan^{-1}\left[\frac{\lambda(\cos\theta + e) - \eta\sin\theta}{\sigma(\cos\theta + e) - \xi\sin\theta}\right]$$

$$\phi^* = \sin^{-1}\left[\frac{1}{V}\sqrt{\frac{\mu}{p}}\left\{\psi(\cos\theta + e) - \chi\sin\theta\right\}\right]. \quad (63)$$

where

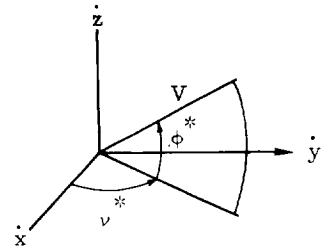

Corresponding to Eq (63), the orientation of the velocity increment ΔV_1 is given by:

$$\Delta\nu_1^* = \tan^{-1}\left\{\left[(\lambda_1 - \lambda_0)(\cos\theta_1 + e_0) - (\eta_1 - \eta_0)\sin\theta_1\right]\left[(\sigma_1 - \sigma_0)(\cos\theta_1 + e_0) - (\xi_1 - \xi_0)\sin\theta_1\right]^{-1}\right\}$$

$$\Delta\phi_1^* = \sin^{-1}\left[\frac{1}{\Delta V_1}\sqrt{\frac{\mu}{p_0}}\left\{(\psi_1 - \psi_0)(\cos\theta_1 + e_0) - (\chi_1 - \chi_0)\sin\theta_1\right\}\right] \quad (64)$$

After addition of the velocity increment defined by Eqs (59) and (64), the vehicle occupies an orbit which lies in the correct plane, but which has the original incorrect size and shape. The next step in the selected correction routine is a transfer from apogee of the incorrect orbit to a point in the nominal orbit (for this case assumed

circular). This approach is not always the most efficient means of making a transfer, however, for the small period changes required (even for the initial placement problem), the energy differences are extremely small. The equations defining this correction are:

$$\Delta V_2 = \sqrt{\frac{\mu}{r_a}}\left(\sqrt{\frac{2r_n}{r_a + r_n}} - \sqrt{2 - \frac{r_a}{a_0}}\right)$$

$$\Delta\nu_2^* = \tan^{-1}\left(\frac{\lambda_1}{\sigma_1}\right)$$

$$\Delta\phi_2^* = \sin^{-1}(-\psi_1), \qquad (65)$$

where

$$r_a = a_0(1 + e_0)$$

When the vehicle completes the transfer to nominal orbit altitude, a tangential thrust could be applied to cause the vehicle to enter a circular orbit at this altitude. However, the vehicle would still not be synchronized because the orbital central angle would remain uncorrected. Correction of this quantity, which is discussed earlier, involves two thrusts applied tangentially at any point in the circular orbit. Selecting the terminus of the Hohmann transfer orbit, i.e. the point at which the vehicle first reaches nominal altitude, as the point for initiating the change of position improves the economy of the correction routine in certain cases. For example, if the vehicle reaches the nominal radius, r_n, with a velocity greater than circular velocity, and the vehicle is ahead of the nominal position desired in the orbit, part or all of the excess velocity can be used as part or all of the first velocity increment of the angular position correction.

The third corrective thrust, computed as the combination of the tangential thrust to achieve circularity and the first of two tangential thrusts to change the orbital central angle, is

$$\Delta V_3 = \sqrt{\frac{\mu}{r_n}}\left(\sqrt{2 - \left(1 - \frac{\Delta\theta}{2\pi}\right)^{-2/3}} - \sqrt{\frac{2r_a}{r_n + r_a}}\right)$$

$$\Delta\nu_3^* = \tan^{-1}\left(\frac{\lambda_1}{\sigma_1}\right) + 180°$$

$$\Delta\phi_3^* = -\sin^{-1}(-\psi_1) \qquad (66)$$

The direction of $\Delta\vec{V}_3$ is opposite to that of $\Delta\vec{V}_2$. In Eq (66), the angle of required position change, $\Delta\theta$, is positive for the case in which the vehicle lags its nominal position in the pattern orbit. The first equation of (66) holds whether $r_a > r_n$ or $r_n > r_a$. The final corrective thrust is

$$\Delta V_4 = \sqrt{\frac{\mu}{r_n}}\left(\sqrt{2 - \left(1 - \frac{\Delta\theta}{2\pi}\right)^{-2/3}} - 1\right)$$

$$\Delta\nu_4^* = \tan^{-1}\left(\frac{\lambda_1}{\sigma_1}\right)$$

$$\Delta\phi_4^* = \sin^{-1}(-\psi_1). \qquad (67)$$

As noted, economy can be improved by substituting $\frac{\Delta\theta}{n}$ (n = an integer) for $\Delta\theta$ in the first equation of (67) and increasing the transfer time by a factor of n.

If the value of $\Delta\theta$ in Eqs (66) and (67) is to be computed from the initial data (e_0, e_n, a_0, a_n, etc.), the time interval from the time of data sensing to the time of initiating the correction of orbital central angle is

$$\Delta t = a_0\sqrt{\frac{a_0}{\mu}}\left[\pi - \sin^{-1}\left(\frac{\sqrt{1 - e_0^2}\sin\theta}{1 + e_0\cos\theta_0}\right) + \frac{e_0\sqrt{1 - e_0^2}\sin\theta_0}{1 + e_0\cos\theta_0}\right] + \frac{\pi}{2}\left(\frac{p_0}{1 - e_0} + r\right)\sqrt{\frac{1}{2\mu}\left(\frac{p_0}{1 - e_0} + r\right)} \qquad (68)$$

The location of the nominal position at the time of initiation of the angular position correction is:

$$r_{3n} = r_n$$

$$L_{3n} = \sin^{-1}\left[\sin L_{0n}\cos\frac{\Delta t}{\tau_n}\,2\pi + \sqrt{\sin^2 i_n - \sin^2 L_{0n}}\sin\frac{\Delta t}{\tau_n}\,2\pi\right]$$

$$A_{3n} = \tan^{-1}\left[\frac{\cos i_n}{\sqrt{\left(\frac{\sin i_n}{\sin L_{3_n}}\right)^2 - 1}}\right] + A_{0n} - \sin^{-1}\left(\frac{\tan L_{0n}}{\tan i_n}\right) \qquad (69)$$

and the position of the vehicle at this time is given by:

$$r_3 = r_n$$

$$L_3 = \sin^{-1}(x_1)$$

$$A_3 = \tan^{-1}\left(\frac{\eta_1}{\xi_1}\right). \qquad (70)$$

The required change in central angle is then

$$\Delta\theta = \cos^{-1}\left[\cos L_3 \cos L_{3n} \cos (A_3 - A_{3n}) + \sin L_3 \sin L_{3n}\right]$$

The four maneuvers given by Eqs (59), (65), (66) and (67) comprise the complete correction routine.

Although the proximity of the correction transfer orbits to the nominal orbit means that the difference in perturbation of the transfer and nominal (perturbed) orbits is negligible, the perturbations affect the times of correction initiation and must, therefore, be included in the routine. This may be done by considering the orbit parameters ω and Ω involved in the equations as functions of time and adding a perturbation correction to the computed times.

A sample problem has been calculated using this routine in order to provide an appreciation of the magnitude of the propulsion requirement for each correction. The data for the sample problem are:

$a_{0n} = 5.488164 \times 10^7$ ft (1.672792×10^7 m)	$a_0 = 5.4889664 \times 10^7$ ft (1.673037×10^7 m)
$e_{0n} = 0$	$e_0 = 0.0001$
$i_{0n} = 54.736°$	$i_0 = 54.741°$
$\Omega_{0n} = 0$	$\Omega_0 = 0.005°$
$\omega_{0n} = 0$	$\omega_0 = -60°$
$\theta_{0n} = 0$	$\theta_0 = 60.005°$

The radius at this time is $r_0 = 5.488692 \times 10^7$ ft (1.672953×10^7 m) which is r_n plus 1 stat mi or 1.609 km.

Proceeding through the correction routine yields the following correction magnitudes.

ΔV_1 = 1.804 fps (0.5499 m/s)

ΔV_2 = 0.185 fps (0.0564 m/s)

ΔV_3 = 1.899 fps (0.5788 m/s)

ΔV_4 = 0.914 fps (0.2786 m/s)

Total ΔV = 4.802 fps (1.463 m/s).

Thus if the satellite possesses propellants capable of supplying a total of 5000 fps (1524 m/s) and 5 fps (1.524 m/s) is assumed to be the average correction required twice per day, the system can function for about 500 days.

Thus, the routine seems adequate to satisfy the requirements of economy and proximity of the transfer and nominal orbits with a reasonably simple calculation routine.

D. SMALL MANEUVERS IN NEARLY CIRCULAR ORBITS (REF. 1)

1. Linearization of Maneuvers

The discussions of Section B have been general and are not restricted to small eccentricities. Generally, however, for the cases in which the target orbit is circular and no intermediate orbits are utilized, the actual orbit obtainable will deviate slightly from circularity. If this deviation is to be corrected, some of the maneuvers of the previous discussions can be simplified using first order differentials. This approach has two major advantages:

(1) The functional form of the solution can be simplified.

(2) The roundoff error arising from subtracting to nearly equal quantities can be reduced.

As before, the discussions will be divided into three cases for investigation:

(1) Correction by means of two velocity increments tangent to the flight path, the first impulse (ΔV_1) being applied at apogee in the incorrect orbit and the second at the altitude of the nominal circular orbit.

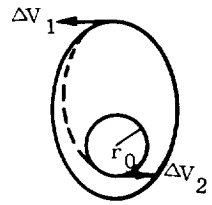

(2) Correction by means of two tangential impulses, the first (ΔV_1) being applied at perigee in the incorrect orbit.

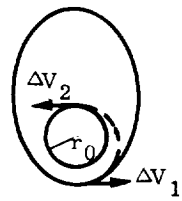

(3) Correction by means of one impulse (ΔV) applied at the intersection of the incorrect and correct orbits, if the orbits intersect.

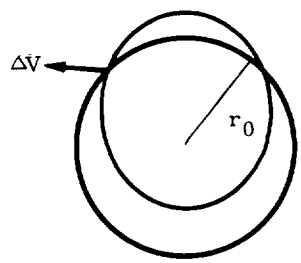

It is noted that while the circular orbit is shown within the ellipse for Cases (1) and (2), the cases for exterior circular orbits will also be discussed.

Consider

$$\Delta a = a - r_0$$

$$\Delta e = e \qquad e^2 << 1$$

for Case 1

$$r_1 = a(1+e) = r_0 + \Delta a + e(r_0 + \Delta a)$$

$$\approx r_0 + \Delta a + e r_0$$

$$\Delta V_1 \approx \sqrt{\frac{\mu}{r_0}} \left[\left(1 - \frac{\Delta a}{2 r_0} - \frac{e}{2}\right) \left(1 - \frac{\Delta a}{4 r_0} - \frac{e}{4}\right) - \left(1 - \frac{\Delta a}{2 r_0}\right)(1 - e) \right], \quad e^2 << 1, \quad \left(\frac{\Delta a}{r_0}\right)^2 << 1$$

The latter approximation utilizes the following expansions.

$$(1 \pm \epsilon)^{-1} = 1 \mp \epsilon + \epsilon^2 \mp \epsilon^3 + \ldots$$

$$(1 \pm \epsilon)^{1/2} = 1 \pm \frac{\epsilon}{2} - \frac{\epsilon^2}{8} \pm \frac{\epsilon^3}{16} - \ldots$$

Then

$$\Delta V_1 \approx \frac{1}{4} \left[\frac{\mu}{r_0}\right]^{1/2} \left[e - \frac{\Delta a}{r_0}\right]$$

$$\Delta V_2 = \left[\frac{\mu}{r_0}\right]^{1/2} - \left[\frac{2\mu \left(1 + \frac{\Delta a}{r_0}\right)(1+e)}{r_0 \left[\left(1 + \frac{\Delta a}{r_0}\right)(1+e) + 1\right]} \right]^{1/2}$$

$$\approx \left[\frac{\mu}{r_0}\right]^{1/2} \left\{ 1 - \left[\left(1 + \frac{\Delta a}{2 r_0} + \frac{e}{2}\right) \cdot \left(1 - \frac{\Delta a}{4 r_0} - \frac{e}{4}\right) \right] \right\}$$

The procedure is similar in Case (2), the results being summarized below. For Case (3),

$$\Delta V^2 = \frac{\mu}{r_0} \left[3 - \frac{1}{1 + \frac{\Delta a}{r_0}} - 2 \sqrt{\left(1 + \frac{\Delta a}{r_0}\right)\left(1 - e^2\right)} \right]$$

$$\Delta V^2 \approx \frac{\mu}{r_0} \left[3 - \left\{ 1 - \frac{\Delta a}{r_0} + \left(\frac{\Delta a}{r_0}\right)^2 \right\} - 2 \left\{ 1 + \frac{\Delta a}{2 r_0} - \frac{1}{8} \left(\frac{\Delta a}{r_0}\right)^2 \right\} \left(1 - \frac{e^2}{2}\right) \right]$$

$$\Delta V^2 \approx \frac{\mu}{r_0} \left[e^2 - \frac{3}{4} \left(\frac{\Delta a}{r_0}\right)^2 \right]$$

The final results are as follows. For Case (1):

$$\Delta V_1 \approx \frac{1}{4} \sqrt{\frac{\mu}{r_0}} \left(e - \frac{\Delta a}{r_0}\right) \tag{71}$$

$$\Delta V_2 \approx \frac{1}{4} \sqrt{\frac{\mu}{r_0}} \left(-e - \frac{\Delta a}{r_0}\right) \tag{72}$$

$$\Delta V_T = \left|\Delta V_1\right| + \left|\Delta V_2\right|$$

$e^2 << 1$,
$\Delta a = a - r_0$

Case (2):

$$\Delta V_1 \approx \frac{1}{4} \sqrt{\frac{\mu}{r_0}} \left(-e - \frac{\Delta a}{r_0}\right) \tag{73}$$

$$\Delta V_2 \approx \frac{1}{4} \sqrt{\frac{\mu}{r_0}} \left(e - \frac{\Delta a}{r_0}\right) \tag{74}$$

$$\Delta V_{total} = \left|\Delta V_1\right| + \left|\Delta V_2\right|$$

$e^2 << 1$

Case (3):

$$\Delta V \approx \left[\frac{\mu}{r_0}\right]^{1/2} \left[e^2 - \frac{3}{4} \left(\frac{\Delta a}{r_0}\right)^2\right]^{1/2}, \quad e^2 << 1; \quad \frac{\Delta a}{r_0} < e \tag{75}$$

The symmetry is obvious in Cases (1) and (2), and the total velocity requirement is the same in these cases:

$$\frac{\Delta V_{total}}{V_0} \approx \frac{1}{2} e, \qquad -e < \frac{\Delta a}{r_0} < e$$

$$\approx \frac{1}{2} \frac{\Delta a}{r_0}, \quad \left|\frac{\Delta a}{r_0}\right| > e$$

Since for intersection of the correct and incorrect orbits

$$a(1-e) = r_p < r_0 < r_a = a(1+e)$$

then

$$r_0 + \Delta a - e r_0 < r_0 < r_0 + \Delta a + e r_0$$

or

$$\left|\frac{\Delta a}{r_0}\right| < e,$$

and, from Eq (75), the impulses required for Case (3) have the range

$$\frac{e}{2}\sqrt{\frac{\mu}{r_0}} < \Delta V < e\sqrt{\frac{\mu}{r_0}}$$

However, if the orbits intersect (i.e., $e > \left|\frac{\Delta a}{r_0}\right|$), the total velocity required for correction by two tangential impulses at extrema, Case (1) or Case (2), is

$$\Delta V_{total} \approx \frac{e}{2}\sqrt{\frac{\mu}{r_0}},$$

which indicates the anticipated superiority of efficiency in Cases (1) and (2). Equations (71) through (74) are plotted in Fig. 15 for the error ranges of interest. Equation (75) is plotted in Fig. 16. As an example, consider the following table.

Errors in Original Orbit		Velocity Increment Required for Correction ΔV_{total} (mps)
Δa (km)	e	
10	0.00167	6.72
9.3	0.001	5.44
0	0.001	3.91 2 pulse 7.77 1 pulse

2. Error Analysis

Orbit correction sensitivities will also be developed for the case of correction of a slightly eccentric orbit to a circular orbit by two impulses tangent to the flight path. The following nomenclature will be involved:

V_1 = orbit speed at r_1 before the first correction

V_1' = orbit speed at r_1 after the first correction

ΔV_1 = characteristic velocity of the first corrective impulse

r_2 = radius at extremum where second impulse is applied (nominally r_0)

V_2 = orbit speed at r_2 before the second correction

V_2' = orbit speed at r_2 after the second correction

ΔV_2 = characteristic velocity of the second corrective impulse

γ = flight path angle with respect to local horizontal

Φ_T = thrust attitude angle

Primes will denote corrected parameters.

The errors in the final orbit parameters, $\Delta a'$ and e', will be functions of errors in the injection parameters (Δr_2, $\Delta V_2'$ and γ_2), which, in turn, will be functions of errors in the magnitude and orientation of the second corrective thrust and errors in the conditions r_2, V_2 and γ_2 before thrust. The errors in r_2, V_2 and γ_2 are functions of errors in magnitude and orientation of the first corrective impulse and errors in the determined values of r_1, V_1 and γ_1. Therefore, the error equations are conveniently developed in several steps.

a. Errors contributed by corrective thrusts

The orbit errors contributed by errors in the corrective thrusts may be induced intuitively, but a rigorous general analysis is not difficult. The equations describing addition of a vector impulse ΔV are

$$f_1 = -\Delta V^2 + V^2 + V'^2 - 2VV'\cos(\gamma' - \gamma) = 0 \quad (76)$$

$$f_2 = -\Delta V \sin\Phi_T + V' \sin(\gamma' - \gamma) = 0 \quad (77)$$

Symbols are consistent with previous notation and are further defined in the sketch.

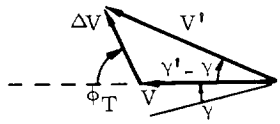

Errors in V' and γ' are to be determined as functions of errors in V, γ, Φ_T and ΔV. From Eqs (76) and (77) the error relationships, to the order of linear differentials, can be expressed as follows.

$$-\Delta V\, d(\Delta V) + V'\, dV' + VV'\left[\sin(\gamma' - \gamma)\cdot(d\gamma' - d\gamma)\right] - \left[\cos(\gamma' - \gamma)\cdot(V\, dV' + V'\, dV)\right] + V\, dV = 0$$

and

$$- \sin \phi_T \, d(\Delta V) - \Delta V \cos \phi_T \, d\phi_T + \sin (\gamma' - \gamma) \, dV' + V' \left[\cos (\gamma' - \gamma) \cdot (d\gamma' - d\gamma) \right] = 0$$

Terms may be collected, and the resulting expressions solved by application of Cramer's rule for the errors dV' and $d\gamma'$: In this solution the Jacobian

$$\frac{\partial (f_1, f_2)}{\partial (V', \gamma')} = 2 \begin{vmatrix} V' - V \cos (\gamma' - \gamma) & VV' \sin (\gamma' - \gamma) \\ \sin (\gamma' - \gamma) & V' \cos (\gamma' - \gamma) \end{vmatrix} = 2V' \left[V' \cos (\gamma' - \gamma) - V \right]$$

is useful. The results are

$$dV' = \left[\frac{\Delta V \cos (\gamma' - \gamma) - \frac{VV'}{\Delta V} \sin^2 (\gamma' - \gamma)}{V' \cos (\gamma' - \gamma) - V} \right] d(\Delta V) + \cos (\gamma' - \gamma) \, dV - V \sin (\gamma' - \gamma) \, d\phi_T$$

$$d\gamma' = \frac{\sin (\gamma' - \gamma) \left[\left\{ V' - V \cos (\gamma' - \gamma) \right\} \frac{V'}{\Delta V} - \Delta V \right]}{V' \left[V' \cos (\gamma' - \gamma) - V \right]} d(\Delta V) - \frac{\sin (\gamma' - \gamma)}{V'} dV + \left[1 - \frac{V}{V'} \cos (\gamma' - \gamma) \right] d\phi_T + d\gamma$$

In terms of $(\gamma' - \gamma)$ or, in terms of ϕ_T,

$$dV' = \left(\frac{\Delta V}{V'} + \frac{V}{V'} \cos \phi_T \right) d(\Delta V) + \left(\frac{\Delta V}{V'} \cos \phi_T + \frac{V}{V'} \right) dV - V \frac{\Delta V}{V'} \sin \phi_T \, d\phi_T \qquad (78)$$

$$d\gamma' = \frac{V}{V'^2} \sin \phi_T \, d(\Delta V) - \frac{\Delta V}{V'^2} \sin \phi_T \, dV + \frac{\Delta V}{V'^2} (\Delta V + V \cos \phi) \, d\phi_T + d\gamma \qquad (79)$$

For the case of interest, tangential corrective impulses applied at orbit extrema, the following nominal values are involved in evaluation of the sensitivities.

$$\phi_T = 0$$

$$V' = V + \Delta V$$

$$\gamma' - \gamma = 0$$

Then Eqs (78) and (79) become

$$dV' = d(\Delta V) + dV \qquad (80)$$

$$d\gamma' = \frac{\Delta V}{V'} d\phi + d\gamma \qquad (81)$$

(tangential impulses at extrema)

which agree with intuition for this simple case.

b. Errors prior to second impulse

Errors in the orbit conditions r_2, V_2, γ_2 prior to the second impulse will be developed from a general analysis giving errors at extrema in terms of errors in any injection condition r, V, γ. Specification of the conditions (r, V, γ) at any time completely determines the planar properties of the orbit. From the energy equation and the geometry of an ellipse, simple expressions can be developed relating r_a, r_p, v_a and v_p to a and e:

$$r_a = a (1 + e) \qquad (82)$$

$$r_p = a (1 - e) \qquad (83)$$

$$v_a = \sqrt{\frac{\mu}{a} \left(\frac{1 - e}{1 + e} \right)} \qquad (84)$$

$$v_p = \sqrt{\frac{\mu}{a} \left(\frac{1 + e}{1 - e} \right)} \qquad (85)$$

Then

$$dr_a = (1 + e) \, da + ade \qquad (86)$$

$$dr_p = (1 - e) \, da - ade \qquad (87)$$

$$dv_a = - \frac{V_a}{2a} da - \frac{V_p}{(1 + e)^2} de \qquad (88)$$

$$dv_p = - \frac{V_p}{2a} da + \frac{V_a}{(1 - e)^2} de \qquad (89)$$

In turn, from the energy equation,

$$a = \left[\frac{2}{r} - \frac{V^2}{\mu} \right]^{-1},$$

and Kepler's second law, which can be restated in the form

$$e = \sqrt{1 - \left(\frac{2}{r} - \frac{V^2}{\mu} \right) \left(\frac{r^2 V^2 \cos^2 \gamma}{\mu} \right)}$$

the differentials of a and e are

$$da = \frac{2a^2}{r^2} dr + \frac{2a^2 V}{\mu} dV$$

$$de = \frac{1}{2e} \left[- \frac{1}{a} \left(-2 \frac{r^2 V^2}{\mu} \cos \gamma \sin \gamma \, d\gamma + \right. \right.$$

(continued)

$$+\frac{\cos^2\gamma}{\mu}\left\{2rV^2\,dr+2Vr^2\,dV\right\}\Big)$$
$$-\frac{r^2V^2\cos^2\gamma}{\mu}\left(-\frac{2}{r^2}\,dr-\frac{2V}{\mu}\,dV\right)\Bigg]$$

which, after simplification and substitution of

$$r=\frac{a(1-e^2)}{1+e\cos\theta}$$

give

$$da=\frac{2(1+e\cos\theta)^2}{(1-e^2)^2}\,dr+2a\left[\sqrt{\frac{a}{\mu}}\sqrt{\frac{1+2e\cos\theta+e^2}{1-e^2}}\right]dV \tag{90}$$

$$de=\frac{(e+\cos\theta)(1+e\cos\theta)}{a(1-e^2)}\,dr+2(e+\cos\theta)\sqrt{\frac{a(1-e^2)}{\mu(1+2e\cos\theta+e^2)}}\,dV+(1-e^2)\frac{\sin\theta}{1+e\cos\theta}\,d\gamma \tag{91}$$

Substitution of Eqs (90) and (91) in Eqs (86) through (89) gives the required error relationships:

$$dr_a=\frac{1+e}{(1-e^2)^2}(1+e\cos\theta)(2+e-e^2+e\cos\theta+\cos\theta)\,dr+2a\sqrt{\frac{a}{\mu}}\frac{(1+e)^2}{\sqrt{1-e^2}}\frac{1+\cos\theta}{\sqrt{1+2e\cos\theta+e^2}}\,dV+a(1-e^2)\frac{\sin\theta}{1+e\cos\theta}\,d\gamma \tag{92}$$

$$dr_p=\frac{1-e}{(1-e^2)^2}(1+e\cos\theta)(2-e-e^2+e\cos\theta-\cos\theta)\,dr+2a\sqrt{\frac{a}{\mu}}\frac{(1-e)^2}{\sqrt{1-e^2}}\frac{1-\cos\theta}{\sqrt{1+2e\cos\theta+e^2}}\,dV-a(1-e^2)\frac{\sin\theta}{1+e\cos\theta}\,d\gamma \tag{93}$$

$$dV_a=-\frac{(1+e\cos\theta)}{1-e^2}\left[\frac{V_a}{a}\frac{(1+e\cos\theta)}{1-e^2}+\frac{V_p}{a}\frac{(e+\cos\theta)}{(1-e)^2}\right]dr+$$

(continued)

$$-\sqrt{\frac{a}{\mu}}\left[V_a\sqrt{\frac{1+2e\cos\theta+e^2}{1-e^2}}+2V_p\frac{\sqrt{1-e^2}}{(1+e)^2}\frac{(e+\cos\theta)}{\sqrt{1+2e\cos\theta+e^2}}\right]dV-V_p\frac{1-e^2}{(1+e)^2}\frac{\sin\theta}{1+e\cos\theta}\,d\gamma \tag{94}$$

$$dV_p=-\frac{(1+e\cos\theta)}{1-e^2}\left[\frac{V_p}{a}\frac{(1+e\cos\theta)}{1-e^2}-\frac{V_a}{a}\frac{(e+\cos\theta)}{(1-e)^2}\right]dr-\sqrt{\frac{a}{\mu}}\left[V_p\sqrt{\frac{1+2e\cos\theta+e^2}{1-e^2}}-2V_a\frac{\sqrt{1-e^2}}{(1-e)^2}\frac{(e+\cos\theta)}{\sqrt{1+2e\cos\theta+e^2}}\right]dV+V_a\frac{1+e}{1-e}\frac{\sin\theta}{1+e\cos\theta}\,d\gamma \tag{95}$$

These equations relate errors in conditions at orbit extrema to errors in injection conditions (r, V, γ).

For $e^2 \ll 1$ Eqs (92) through (95) reduce to

$$dr_a\approx\left[2+\cos\theta+2e(3+\cos\theta)\cos^2\frac{\theta}{2}\right]dr+2a\sqrt{\frac{a}{\mu}}\left[1+\cos\theta+2e(2-\cos\theta)\cos^2\frac{\theta}{2}\right]dV+\left[a\sin\theta-\frac{ea}{2}\sin 2\theta\right]d\gamma \tag{96}$$

$$dr_p\approx\left[2-\cos\theta-2e(3-\cos\theta)\sin^2\frac{\theta}{2}\right]dr+2a\sqrt{\frac{a}{\mu}}\left[1-\cos\theta-2e(2+\cos\theta)\sin^2\frac{\theta}{2}\right]dV+\left[-a\sin\theta+\frac{ea}{2}\sin 2\theta\right]d\gamma \tag{97}$$

$$dV_a\approx-\frac{1}{a}\sqrt{\frac{\mu}{a}}(1+\cos\theta)(1+e\cos\theta)\,dr-\left[(1-e\cos\theta)(1+2\cos\theta)+e\right]dV-\sqrt{\frac{\mu}{a}}\sin\theta(1-e\cos\theta-e)\,d\gamma \tag{98}$$

$$dV_p\approx-\frac{1}{a}\sqrt{\frac{\mu}{a}}(1-\cos\theta)(1+e\cos\theta)\,dr-\left[(1-e\cos\theta)(1-2\cos\theta)-e\right]dV+\sqrt{\frac{\mu}{a}}\sin\theta(1+e-\cos\theta)\,d\gamma \tag{99}$$

For $e^2 \ll 1$ and impulses applied near apogee or perigee ($\theta = 0°$ or $180°$), the case of interest for the two-impulse correction previously described, Eqs (96) through (99) reduce still further to the following results: perigee injection, $e^2 \ll 1$:

$$dr_a \approx (3 + 8\,e)\,dr_p + 4\,a\sqrt{\frac{a}{\mu}}\,(1 + e)\,dV_p \qquad (100)$$

$$dV_a \approx -\frac{2}{a}\sqrt{\frac{\mu}{a}}\,(1 + e)\,dr_p - (3 - 2\,e)\,dV_p \qquad (101)$$

apogee injection, $e^2 \ll 1$:

$$dr_p \approx (3 - 8\,e)\,dr_a + 4\,a\sqrt{\frac{a}{\mu}}\,(1 - e)\,dV_a \qquad (102)$$

$$dV_p \approx -\frac{2}{a}\sqrt{\frac{\mu}{a}}\,(1 - e)\,dr_a - (3 + 2\,e)\,dV_a \qquad (103)$$

For e, $\frac{\Delta a}{r_.} < 0.001$ the errors are given to three significant figures by the following very simple formulas.

$$\frac{dr_2}{r_0} \approx 3\,\frac{dr_1}{r_0} + 4\,\frac{dV_1}{V_0} \qquad (104)$$

$$\frac{dV_2}{V_1} \approx -2\,\frac{dr_1}{r_0} - 3\,\frac{dV_1}{V_0} \qquad (105)$$

The relation of errors in conditions before the second impulse to errors just after the first impulse must also consider errors in orbit central angle, θ, and local flight path angle, γ. Because the orbits of interest are nearly circular, a variational approach is necessary to define errors in these angular quantities. Therefore, a general analysis of errors in r, V, θ and γ anywhere in a near-circular orbit as functions of launch errors will be performed, and the results for r and V will be compared to Eqs (104) and (105).

Series expansions for the variables of interest are available in Chapter III.

$$\frac{r}{a} = 1 - e\cos M - \frac{e^2}{2}(\cos 2M - 1) - \frac{e^3}{2!\,2^2}(3\cos 3M - 3\cos M) - \cdots$$

$$\frac{V}{\sqrt{\frac{\mu}{a}}} = 1 + e\cos\theta + \frac{e^2}{4}(3 - \cos 2\theta) + \frac{e^3}{8}(4\cos\theta - \cos 3\theta - 7) + \cdots$$

$$\theta = M + 2\,e\sin M + \frac{5e^2}{4}\sin 2M + \frac{e^3}{12}(13\sin 3M - 3\sin M) + \cdots$$

$$\gamma = e\sin\theta - \frac{e^2}{2}\sin 2\theta + \frac{e^3}{3}\sin 3\theta - \cdots$$

$$M = \text{mean anomaly} = \sqrt{\frac{\mu}{a^3}}\,(t - t_p) \qquad (106)$$

For $e^2 \ll 1$, approximate relations can be written.

$$r \approx a\,(1 - e\cos M) \qquad (107)$$

$$V \approx \sqrt{\frac{\mu}{a}}\,(1 + e\cos M) \qquad (108)$$

$$\theta \approx M + 2\,e\sin M \qquad (109)$$

$$\gamma \approx e\sin M \qquad (110)$$

Deviations from the nominal circle r_0 and v_0 at launch are $\delta r_1 = r_1 - r_0$, $\delta V_1 = V_1 - V_o$, $\delta\gamma_1 = \gamma_1$ and $\delta\theta_1 = \theta_1 - \theta_0$. From Eq (47)

$$M = M_0 + \Delta M = \sqrt{\frac{\mu}{r_0^3\left(1 + \frac{\Delta a}{r_0}\right)^3}}\,(t - t_{po} - \Delta t_p)$$

or

$$\Delta M = -\frac{3}{2}\,\frac{\Delta a}{r_0}\,M_0 - \sqrt{\frac{\mu}{r_0^3}}\,\Delta t_p. \qquad (111)$$

The errors at any later time δr_2, δV_2, γ and $\delta\theta_2$ will be determined by varying one injection parameter at a time and assuming a linear combination of the individual errors.

Case (1) $[\delta r_1 = 0,\ \delta V_1 = 0,\ \delta\gamma_1 \neq 0]$. If γ_1 is the only launch parameter which is in error, $\delta r_1 = 0$, $\delta V_1 = 0$, $\gamma_1 = \delta\gamma_1$, and from Eq (133), $e \approx |\delta\gamma_1|$, where $\delta\gamma_1$ is an error due to a velocity component normal to the desired circular orbit velocity at launch. For the circular orbit, M and t_p are referenced to the perigee direction in the incorrect orbit. Since the semimajor axis a is a function of r and V but not γ, $\delta a = 0$ for this case. That is, if only the orientation of the injection velocity is varied, there will be generated a family of orbits in which the eccentricity varies, but the semimajor axis remains constant. Then, from Eqs (107) through (111),

$$\delta r_{(1)} \approx -\,e r_0\cos M_0 \approx -\,r_0\,|\delta\gamma_1|\cos M_0$$

$$\frac{\delta V_{(1)}}{V_0} \approx |\delta\gamma_1|\cos M_0$$

$$\delta\theta_{(1)} \approx -\sqrt{\frac{\mu}{r_0^3}}\,\Delta t_p + 2\,|\delta\gamma_1|\sin M_0$$

$$\delta\gamma_{(1)} \approx |\delta\gamma_1|\sin M_0$$

From the δr_1 equation, $\delta r = 0$ when $\cos M_0 = 0$. Therefore, for Case (1), $M_0 = 90°$ (for γ_1 positive) or $M_0 = 270°$ (for γ_1 negative). The absolute magnitudes in these equations may be removed by

defining a mean anomaly m_0, referenced to the launch point. Then $m_0 = M_0 - 90°$ for positive $\delta\gamma_1$, and $m_0 = M_0 + 90°$ for negative $\delta\gamma_1$. Substitution in the previous equations gives, for either positive or negative $\delta\gamma_1$,

$$\frac{\delta r_{(1)}}{r_0} \approx \Delta\gamma_1 \sin m_0 \tag{112}$$

$$\frac{\delta V_{(1)}}{V_0} \approx -\Delta\gamma_1 \sin m_0 \tag{113}$$

$$\delta\theta_{(1)} \approx 2\,\Delta\gamma_1 (\cos m_0 - 1) \tag{114}$$

$$\delta\gamma_{(1)} \approx \Delta\gamma_1 \cos m_0 \tag{115}$$

In derivation of Eq (114) use is made of the fact that $\delta\theta_{(1)} = 0$ at $m_0 = 0$ since the correct and incorrect orbits intersect at launch.

Case (2) $[\delta\gamma_1 = 0,\ \delta V_1 = 0,\ \delta r_1 \neq 0]$. For $\delta\gamma_1 = 0,\ \delta V_1 = 0,\ \delta r_1 \neq 0$, Eqs (90) and (91) give $\frac{\delta a}{r_0}(2) \approx 2\frac{\delta r_1}{r_0}$

$$e_{(2)} \approx \left|\frac{\Delta r_1}{r_0}\right|.$$

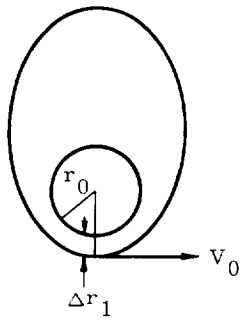

Then, from Eqs (48) through (52)

$$\frac{\delta r_{(3)}}{r_0} \approx 2\frac{\delta r_1}{r_0} - \frac{|\delta r_1|}{r_0}\cos M_0$$

$$\frac{\delta V_{(2)}}{V_0} \approx -\frac{\delta r_1}{r_0} + \frac{|\delta r_1|}{r_0}\cos M_0$$

$$\delta\theta_{(2)} \approx -3\frac{\delta r_1}{r_0} M_0 - \sqrt{\frac{\mu}{r_0^3}}\,\delta t_p + 2\frac{|\delta r_1|}{r_0}\sin M_0$$

$$\delta\gamma_{(2)} \approx \frac{|\delta r_1|}{r_0}\sin M_0$$

But $M_0 = 0°$ for Δr_1 positive, and $M = 180°$ for δr_1 negative. Then, for $m_0 = 0°$ at launch,

$$\frac{\delta r_{(2)}}{r_0} \approx \frac{\delta r_1}{r_0}(2 - \cos m_0) \tag{116}$$

$$\frac{\delta V_{(2)}}{V_0} \approx \frac{\delta r_1}{r_0}(\cos m_0 - 1) \tag{117}$$

$$\delta\theta_{(2)} \approx \frac{\delta r_1}{r_0}(2\sin m_0 - 3 m_0) \tag{118}$$

$$\delta\gamma_{(2)} \approx \frac{\delta r_1}{r_0}\sin m_0 \tag{119}$$

Case (3) $[\delta r_1 = 0,\ \delta\gamma_1 = 0,\ \delta V_1 \neq 0]$. For the remaining case, where $\delta r_1 = 0$, $\delta\gamma_1 = 0$ and $\delta V_1 \neq 0$, Eqs (90) and (91) give

$$\frac{\delta a_{(3)}}{r_0} \approx 2\frac{\delta V_1}{V_0}$$

$$e_{(3)} \approx 2\frac{|\delta V_1|}{V_0}.$$

A procedure similar to that used in Cases (1) and (2) gives

$$\frac{\delta r_{(3)}}{r_0} \approx 2\frac{\delta V_1}{V_0}(1 - \cos m_0) \tag{120}$$

$$\frac{\delta V_{(3)}}{V_0} \approx \frac{\delta V_1}{V_0}(2\cos m_0 - 1) \tag{121}$$

$$\delta\theta_{(3)} \approx -3 m_0\frac{\delta V_1}{V_0} + 4\frac{\delta V_1}{V_0}\sin m_0 \tag{122}$$

$$\delta\gamma_{(3)} \approx 2\frac{\delta V_1}{V_0}\sin m_0. \tag{123}$$

The total error solutions are obtained by adding Eqs (112), (116) and (120); Eqs (113), (117) and (121); etc.

$$\frac{\delta r}{r_0} \approx \sin m_0\,\delta\gamma_1 + (2 - \cos m_0)\frac{\delta r_1}{r_0} + 2(1 - \cos m_0)\frac{\delta V_1}{V_0} \tag{124}$$

$$\frac{\delta V}{V_0} \approx -\sin m_0\,\delta\gamma_1 + (\cos m_0 - 1)\frac{\delta r_1}{r_0} + (2\cos m_0 - 1)\frac{\delta V_1}{V_0} \tag{125}$$

$$\delta\theta \approx \delta\theta_1 + 2(\cos m_0 - 1)\,\delta\gamma_1 + (2\sin m_0 - 3 m_0)\frac{\delta r_1}{r_0} + (4\sin m_0 - 3 m_0)\frac{\delta V_1}{V_0} \tag{126}$$

$$\delta\gamma \approx \cos m_0\,\delta\gamma_1 + \sin m_0\frac{\delta r_1}{r_0} + 2\sin m_0\frac{\delta V_1}{V_0} \tag{127}$$

for $e^2 \ll 1$

For the problem of relating errors at one orbit extremum to those at the previous extremum, $\mathcal{M}_0 = 180°$ in Eqs (124) through (127).

$$\frac{\delta r_2}{r_0} \approx 3\frac{\delta r_1}{r_0} + 4\frac{\delta V_1}{V_0} \tag{128}$$

$$\frac{\delta V_2}{V_0} \approx -2\frac{\delta r_1}{r_0} - 3\frac{\delta V_1}{V_0} \tag{129}$$

$$\delta\theta_2 \approx \delta\theta_1 - 4\delta\gamma_1 - 3\pi\frac{\delta r_1}{r_0} - 3\pi\frac{\delta V_1}{V_0} \tag{130}$$

$$\delta\gamma_2 \approx -\delta\gamma_1 \tag{131}$$

$e^2 << 1$, points 1 and 2 extrema

Eqs (128) and (129) agree exactly with Eqs (104) and (105), in which the errors were derived as differentials.

c. Errors in final orbit elements

Errors in the final orbit elements $\delta a'$ and e' may be determined as functions of errors in the orbit conditions just after the second impulse, r_2, V'_2, γ'_2 by letting $r = r_0 + \delta r$, $V = V_0 + \delta V$ and $\cos^2\gamma = 1 - \gamma^2 + \ldots$ in

$$e^2 = 1 - \left(\frac{2}{r} - \frac{V^2}{\mu}\right)\left(\frac{r^2V^2\cos^2\gamma}{\mu}\right)$$

(neglecting terms of third and higher orders) and in

$$a = \left(\frac{2}{r} - \frac{V^2}{\mu}\right)^{-1}$$

(neglecting terms of second and higher orders). The results are

$$\Delta a \approx 2\delta r + 2\frac{r_0}{V_0}\delta V \tag{132}$$

$$e^2 \approx \left(2\frac{\delta V}{V_0} + \frac{\delta r}{r_0}\right)^2 + \gamma^2 \tag{133}$$

d. Combination of the errors

The errors in the final orbit parameters can now be written completely in terms of errors in tracking and prediction of the original orbit and errors in the corrective thrusts by adding the individual errors derived previously. Let the errors in tracking and prediction of the original orbit at the time of the first corrective impulse be δr_1, δV_1, and $\delta\gamma_1$, and let the errors in the first corrective impulse magnitude and orientation be $\delta(\Delta V_1)$ and $\delta\phi_1$. Then, from Eqs (80) and (81), the errors just after the corrective maneuvers are

$$\delta r_1' \approx \delta r_1$$

$$\delta V_1' \approx \delta(\Delta V_1) + \delta V_1$$

$$\delta\theta_1' \approx \delta\theta$$

$$\delta\gamma' \approx \frac{\Delta V_1}{V_0}\delta\phi_{T_1} + \delta\gamma_1.$$

These errors are transformed to errors at the next orbit extremum, where the second corrective impulse is to be applied by Eqs (104), (105) and (128) through (131).

$$\frac{\delta r_2}{r_0} \approx 3\frac{\delta r_1'}{r_0} + 4\frac{\delta V_1'}{V_0} \approx 3\frac{\delta r_1}{r_0} + 4\left[\frac{\delta(\Delta V_1)}{V_0} + \frac{\delta V_1}{V_0}\right]$$

$$\frac{\delta V_2}{V_0} \approx -2\frac{\delta r_1'}{r_0} - 3\frac{\delta V_1'}{V_0} \approx -2\frac{\delta r_1}{r_0} - 3\left[\frac{\delta(\Delta V_1)}{V_0} + \frac{\delta V_1}{V_0}\right]$$

$$\delta\theta_2 \approx \delta\theta_1' - 4\delta\gamma' - 3\pi\frac{\delta r_1'}{r_0} - 3\pi\frac{\delta V_1'}{V_0}$$

$$\approx \delta\theta_1 - 4\left(\frac{\Delta V_1}{V_0}\delta\phi_{T_1} + \delta\gamma_1\right) - 3\pi\left[\frac{\delta r_1}{r_0} + \frac{\delta(\Delta V_1)}{V_0} + \frac{\delta V_1}{V_0}\right]$$

$$\delta\gamma_2 \approx -\delta\gamma_1' \approx -\frac{\Delta V_1}{V_0}\delta\phi_{T_1} - \delta\gamma_1$$

Equations (80) and (81) are then applied to these equations to include the errors in the second impulse magnitude and orientation, $\delta(\Delta V_2)$ and $\delta\phi_{T_2}$

$$\frac{\delta r_2'}{r_0} = \frac{\delta r_2}{r_0} \approx 3\frac{\delta r_1}{r_0} + 4\left(\frac{\delta(\Delta V_1)}{V_0} + \frac{\delta V_1}{V_0}\right)$$

$$\frac{\delta V_2'}{V_0} \approx \frac{\delta(\Delta V_2)}{V_0} + \frac{\delta V_2}{V_0} \approx \frac{\delta(\Delta V_2)}{V_0} - 2\frac{\delta r_1}{r_0} - 3\left(\frac{\delta(\Delta V_1)}{V_0} + \frac{\delta V_1}{V_0}\right)$$

$$\delta\theta_2' = \delta\theta_2 \approx \delta\theta_1 - 4\left(\frac{\Delta V_1}{V_0}\delta\phi_{T_1} + \delta\gamma_1\right) - 3\pi\left(\frac{\delta r_1}{r_0} + \frac{\delta(\Delta V_1)}{V_0} + \frac{\delta V_1}{V_0}\right)$$

$$\delta\gamma_2' \approx \frac{\Delta V_2}{V_0}\,\Delta\phi_{T_2} + \delta\gamma_2 \approx \frac{\Delta V_2}{V_0}\,\delta\phi_{T_2} - \frac{\Delta V_1}{V_0}\,\delta\phi_{T_1} - \delta\gamma_1$$

Finally, these errors are transformed to the errors in final orbit elements by Eqs (132) and (133).

$$\frac{\delta a'}{r_0} \approx 2\left[\frac{\delta r_1}{r_0} + \frac{\delta V_1}{V_0} + \frac{\delta(\Delta V_1)}{V_0} + \frac{\delta(\Delta V_2)}{V_0}\right] \quad (134)$$

$$e'^2 \approx \left[-\frac{\delta r_1}{r_0} - 2\frac{\delta V_1}{V_0} - 2\frac{\delta(\Delta V_1)}{V_0} + 2\frac{\delta(\Delta V_2)}{V_0}\right]^2 + \left[\frac{\Delta V_2}{V_0}\,\delta\phi_{T_2} - \frac{\Delta V_1}{V_0}\,\delta\phi_{T_1} - \delta\gamma_1\right]^2 \quad (135)$$

Equation (134) is plotted in Fig. 17. For the assumption that $\delta(\Delta V_1) = \delta(\Delta V_2)$.

E. GENERAL TWO-IMPULSE MANEUVERS

For the case where it is desired to transfer between orbits and where the maximum change in the azimuth is not large, it is possible to accomplish the transfer efficiently with two impulses. This may be visualized from the following sketch.

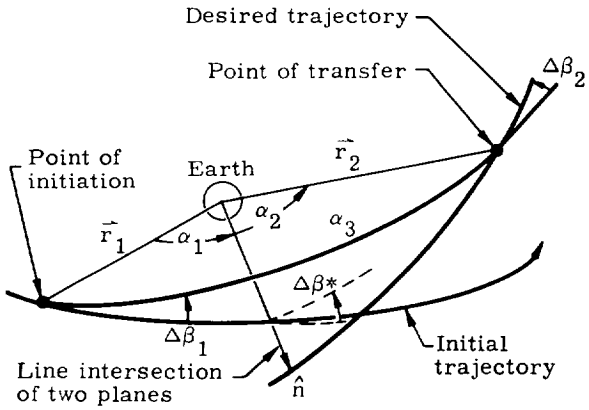

The plane of the transfer is thus defined by $\vec{r} \cdot \vec{r}_1 \times \vec{r}_2 = 0$ where $\vec{r}$ is a general radius vector for points on the transfer trajectory. However, this expression will not serve the purposes we desire. Thus, consider the unit vector $\hat{n}$ along the intersection of the planes.

$$\cos\alpha_1 = \frac{\vec{r}_1 \cdot \hat{n}}{r_1} = \hat{r}_1 \cdot \hat{n}$$

$$\cos\alpha_2 = \hat{r}_2 \cdot \hat{n}$$

$$\cos\alpha_3 = \hat{r}_1 \cdot \hat{r}_2$$

$$\sin\Delta\beta_1 = \sin\Delta\beta^* \frac{\sin\alpha_2}{\sin\alpha_3}$$

where $\Delta\beta^*$ is a known angle for the two orbits as a function of the latitude at which the planes intersect.

Now at this point, the plane of motion is defined. The initial and final radii and the angle between are known; however, the transfer has not been uniquely defined because many elliptical trajectories could be constructed to satisfy these conditions. To completely define the problem, one additional parameter must thus be selected. This parameter could be a geometrical element such as a, p, or e, a time variant parameter at r_1 or r_2 at the time of transfer. Since the latter piece of data is more general than the others, it is assumed to apply for this purpose.

Thus the problem evolves into the solution of a set of simultaneous equations for the planar elements of the orbit.

$$\Delta t = t_{arrival} - t_{injection} = \sqrt{\frac{\mu}{a^3}}\left[E_2 - E_1 - e(\sin E_2 - \sin E_1)\right]$$

$$\alpha_3 = \theta_2 - \theta_1 = \cos^{-1}\left[\frac{a(1-e^2) - r_2}{e r_2}\right] - \cos^{-1}\left[\frac{a(1-e^2) - r_1}{e r_1}\right]$$

where

$$\cos E_2 = \frac{a - r_2}{e a}$$

$$\cos E_1 = \frac{2 - r_1}{e a}$$

This solution is transcendental and thus requires the simultaneous iteration of 4 equations unless Lambert's theorem (discussed in Chapter III) is utilized in place of Kepler's equation. (If Lambert's theorem is utilized, the semimajor axis is evaluated by an iteration which does not involve eccentricity, and the equation for α_3 can then be utilized to define eccentricity.) Two iterative processes are valid for this solution and are sufficiently simple that their use is justified in automatic computation. The first such process is the Newton-Raphson iteration. This procedure is applicable for functions

$$y_1 = f_1(E_1, E_2, a, e) = f_1(x_i) \equiv 0 \qquad i = 1, 2, 3, 4$$

$$y_2 = f_2(E_1, E_2, a, e) = f_2(x_i) \equiv 0$$

$$y_3 = f_3(E_1, E_2, a, e) = f_3(x_i) \equiv 0$$

$$y_4 = f_4(E_1, E_2, a, e) = f_4(x_i) \equiv 0$$

Now assume

$$x_1 = x_{1,0} + h$$

$$x_2 = x_{2,0} + k$$

$$x_3 = x_{3,0} + m$$

$$x_4 = x_{4,0} + n$$

Thus

$$f_i (x_{1,0} + h, x_{2,0} + k, x_{3,0} + m, x_{4,0} + n) = 0$$

etc.

Expanding these f_i in Taylor series and neglecting higher order terms in h, k, m and n now yields

$$f_1(x_{1,0} + h, \cdots x_{4,0} + n) = f_1 (x_{1,0}, x_{2,0}, x_{3,0}, x_{4,0}) + h \left(\frac{\partial f_1}{\partial x_1}\right)_{x_i = x_{i,0}} + k \left(\frac{\partial f_1}{\partial x_2}\right)_{x_i = x_{i,0}} + m \left(\frac{\partial f_1}{\partial x_3}\right)_{x_i = x_{i,0}} + n \left(\frac{\partial f_1}{\partial x_4}\right)_{x_i = x_{i,0}}$$

and similarly for f_2, f_3 and f_4. Now treating the coefficients h, k, m and n as the unknowns, the solution is

$$h = \frac{\begin{vmatrix} f_1 & \partial f_1/\partial x_2 & \partial f_1/\partial x_3 & \partial f_1/\partial x_4 \\ f_2 & . & . & . \\ f_3 & . & . & . \\ f_4 & \partial f_4/\partial x_2 & \partial f_4/\partial x_3 & \partial f_4/\partial x_4 \end{vmatrix}}{\begin{vmatrix} \partial f_1/\partial x_1 & . & . & \partial f_1/\partial x_4 \\ . & . & . & . \\ . & . & . & . \\ \partial f_4/\partial x_1 & . & . & \partial f_4/\partial x_4 \end{vmatrix}}$$

and k, m and n are determined in a similar manner (i.e., by replacing in turn the second, third and fourth columns of the determinant by the column f_1, f_2, f_3, f_4 and dividing the resultant determinant by the same denominator as presented above). Once the process is completed numerically, it is repeated until the values of the increments h, k, m and n are smaller than some value which must be specified.

This solution has been tested and proven to converge; however, it must be noted that the functions which are being iterated are of a very complex nature and have many relative minima and maxima. Thus, unless the first guesses for a and e are reasonably valid, the method will not converge to the proper root. First estimates may be obtained from series expansions or approximate forms discussed in Chapter III.

The second iterative solution which has been checked is a purely numerical evaluation and proceeds as follows. First, the variable E is eliminated by direct substitution into the equations for Δt and $\Delta\theta$. Then functions f_1, f_2 and f_3 are defined as follows

$$f_1 = (\Delta t_{given} - \Delta t_{computed})\, 2\pi/\tau$$

$$f_2 = \Delta\theta_{given} - \Delta\theta_{computed}$$

$$f_3 = |f_1| + |f_2|$$

As before, a value for each of the variables a and e is guessed, but this time one value (say a) is incremented positively and negatively and the function f_3 evaluated for each set of variables (a + Δa, e); (a, e); and (a - Δa, e). The value of a which results in the smallest value of f_3 is then selected and the process is repeated after incrementing e. A fairly coarse grid (i.e., large Δa and Δe) can be utilized initially, and this grid is halved each time the previous root is selected as the minimizing value. Once the grid is sufficiently small or once the value of f_3 (which is the total error of the solution) is less than a specified number the solution can be halted. In all cases f_3 should be checked because unless it is nearly zero, the set of variables selected corresponds to a local minimum, not the true root. In such cases, both a and e can be incremented varying amounts to see if there is any set of roots in the vicinity yielding a smaller f_3. If so, the procedure continues. This solution is illustrated below for the case in which point A represents the first repeated root

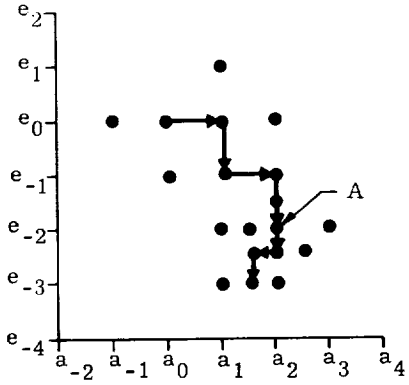

This solution was found ideally suited to automatic computation, since no functions other than those required in the definition of the problem

need be programmed and since the logic involved is very simple. In addition, it is possible to ascertain whether convergence to the proper roots has been obtained by checking the value of f_3. This method also proved to require less accurate initial estimates of a and e and was never subject to the problem of division by zero as is possible in the definition of h, k, m and n of the Newton-Raphson method.

Once the elements a and e are known to the desired accuracy, the development of the maneuvers can continue. The term $\Delta\beta$, was defined previously; therefore, consider the azimuths in the two orbits at the point of the second maneuver

$$\sin \beta_1 = \frac{\cos i_1}{\cos L}$$

$$\sin \beta_2 = \frac{\cos i_2}{\cos L}$$

$$\sin \beta_1 = \frac{\cos i_1}{\cos i_2} \sin \beta_2$$

but

$$\Delta\beta_2 = \beta_2 - \beta_1$$

Thus

$$1 = \frac{\cos i_1}{\cos i_2} \left[\cos \Delta\beta_2 + \sin \Delta\beta_2 \cot \beta_1\right]$$

or

$$\frac{\cos i_2}{\cos i_1} = \cos \Delta\beta_2 + \sin \Delta\beta_2 \cot \beta_1$$

$\Delta\beta_2$ can be evaluated directly from this equation; however, unless $\Delta\beta_2$ is small a simple solution would be to evaluate both β_1 and β_2 then subtract. For the case where $\Delta\beta_2$ is small (as is in general true)

$$\Delta\beta_2 \approx \left(\frac{\cos i_2}{\cos i_1} - 1\right) \left[\left(\frac{\cos L}{\cos i_1}\right)^2 - 1\right]^{-1/2}$$

But the velocity vector must be rotated through another angle ($\Delta\gamma$) in order to change the direction of the velocity in the plane to attain the correct ellipse. This angle is obtained from

$$\Delta\gamma_1 = \cos^{-1} \sqrt{\frac{a^2(1 - e^2)}{r_1(2a - r_1)}} - \cos^{-1} \sqrt{\frac{a_0^2(1 - e_0^2)}{r_1(2a_0 - r_1)}}$$

$$\Delta\gamma_2 = \cos^{-1} \sqrt{\frac{a_f^2(1 - e_f^2)}{r_2(2a_f - r_2)}} + \cos^{-1} \sqrt{\frac{a(1 - e^2)}{r_2(2a - r_2)}}$$

(continued)

where: the absence of a subscript denotes the transfer orbit
subscript 0 denotes the initial orbit
subscript f denotes the final orbit

Now the total turn angle for the velocity vector is obtained from the following sketch to be

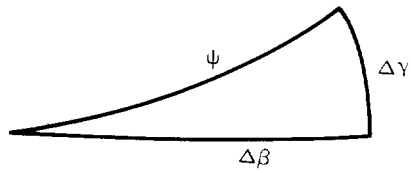

$$\psi_1 = \cos^{-1} (\cos \Delta\gamma_1 \cos \Delta\beta_1)$$

$$\psi_2 = \cos^{-1} (\cos \Delta\gamma_2 \cos \Delta\beta_2)$$

and the changes in the required velocities are:

$$\Delta V_1^2 = V_0^2 + V_1^2 - 2V_0V_1 \cos \psi_1$$

$$= \mu \left[\frac{4}{r_1} - \frac{1}{a_0} - \frac{1}{a} - \sqrt{\left(\frac{2}{r_1} - \frac{1}{a_0}\right)\left(\frac{2}{r_1} - \frac{1}{a}\right)} \cdot \cos \Delta\gamma_1 \cos \Delta\beta_1\right]$$

and

$$\Delta V_2^2 = \mu \left[\frac{4}{r_2} - \frac{1}{a} - \frac{1}{a_f} - \sqrt{\left(\frac{2}{r_2} - \frac{1}{a}\right)\left(\frac{2}{r_2} - \frac{1}{a_f}\right)} \cos \Delta\gamma_2 \cos \Delta\beta_2\right]$$

No provision has been made at any point in this analysis for nonzero burning times. Actually, however, these equations have been utilized in a digital program to simulate powered maneuvers. The process was as follows.

(1) The impulsive analysis was made.

(2) A finite burning simulation was attempted.

(3) The error in the position and velocity at burnout was determined from the computed position and velocity and the values were predicted for the transfer orbit the same number of seconds after the impulse.

(4) The magnitude of the errors was utilized to adjust the time for initiating the thrust and the thrust program.

(5) The process was repeated until the desired transfer orbit was obtained to a specified accuracy. The allowable errors for the initial computations were $(\Delta x, \Delta y, \Delta z)_{B0} \leq 1000$ ft (or 300 m) and $(\Delta \dot{x}, \Delta \dot{y}, \Delta \dot{z})_{B0} \leq 0.1$ fps (or 0.03 mps).

The validity of the impulsive analysis was in this manner proven for moderate to large accelerations. The low acceleration runs, however, required more computations in order to converge to a proper thrust program. This fact should be expected, since the accuracy of the impulsive analysis deteriorates as the time of thrusting increases. The results of these runs indicated generally good agreement for the computation of the actual propellant mass required but indicated that the maneuver should be anticipated in order to find the proper thrust program in a limited number of trials. The physical significance of this statement is seen directly from the following sketch.

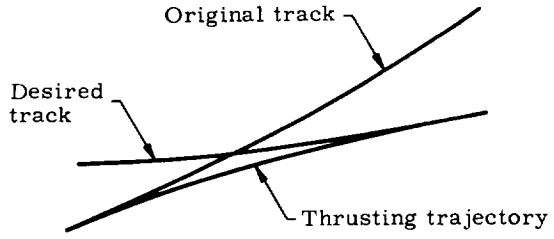

F. PROPULSION REQUIREMENTS FOR CANCELLING THE EFFECTS OF DRAG AND OBLATENESS

For most earth satellites only two relatively large perturbing accelerations act on the vehicle, the first due to earth's oblateness and the second due to atmospheric drag. Generally these effects are sufficiently large that it is necessary to accept them; however, for some orbits and for some specific satellite applications it may be desirable to cancel them. This section treats these two problems.

1. Counteracting the Effects of the Earth's Oblateness (Ref. 2)

The potential function of the earth in Jeffrey's notation is:

$$U(r, L) = -\frac{\mu}{R}\left[\frac{R}{r} + \frac{JR^3}{3r^3}(1 - 3\sin^2 L) + O(J^2)\right]$$

where

$J = 3/2\, J_2$

and where terms of the order J^2 have been neglected

while for a spherical earth it is

$$U_s = -\frac{\mu}{r}$$

The gravitational force acting on the satellite is given by the negative gradient of the potential function. In polar coordinates

$$\text{grad } U = \hat{r}\frac{\partial U}{\partial r} + \hat{L}\frac{1}{r}\frac{\partial U}{\partial L} + \hat{\phi}\frac{1}{r\cos L}\frac{\partial U}{\partial \phi}$$

therefore

$$F_{ob} = -\text{grad } U(r, L) = -\hat{r}\frac{\mu}{R^2\rho^2}\left[1 + \frac{J}{\rho^2}(1 - 3\sin^2 L)\right] + \frac{\hat{L}\mu}{R^2\rho^4} J \sin 2L \qquad (136)$$

and

$$F_s = -\text{grad } U_s = -\hat{r}\frac{\mu}{R^2\rho^2}$$

where

$$\rho = \frac{r}{R} \qquad (137)$$

The corrective force which must be exerted on the satellite to remain in an unperturbed orbit is the difference between these two forces represented by Eqs (136) and (137).

$$\vec{F}_{req} = -m(F_{ob} - F_s)$$

$$\vec{F}_{req} = m(\text{grad } U - \text{grad } U_s)$$

so that the general force equation giving the corrective force per unit mass is

$$\vec{F}_{req} = \hat{r}\frac{\mu}{R^2\rho^4}\left[J(1 - 3\sin^2 L)\right] - \hat{L}\frac{\mu}{R^2\rho^4} J \sin 2L \qquad (138)$$

Consider the following sketch which shows the projection of the actual orbit on a sphere of radius equal to that value of r occurring at the highest latitude of the orbit. The X-axis in this case is 90° out of phase with the ascending node.

By inspection, the relation between the latitude L and the angle from perigee θ is

$$\sin L = \sin i \cos \tau \qquad (139)$$

where

$$\tau = \theta - \alpha$$

$$\alpha = 90 - \omega$$

From the standard form of the conic for the orbit of a satellite about a spherical earth,

$$r = \frac{p}{1 + e\cos\theta} \qquad (140)$$

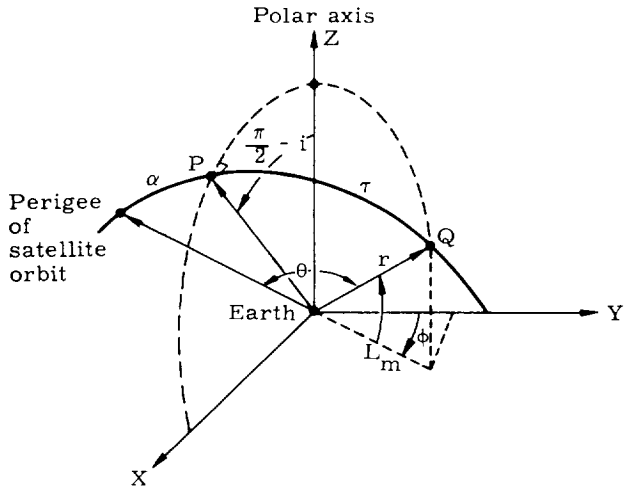

Substituting these expressions into the force equation per unit mass (Eq (138)) yields

$$\vec{F}_{req} = \hat{r}\,\frac{\mu R^2}{p^4}\,(1 + e\cos\theta)^4 \left[J\left(1 - 3\sin^2 i\cos^2(\theta - \alpha)\right)\right] - \frac{\hat{L}\,2J\mu R^2}{p^4}\,(1 + e\cos\theta)^4 \sin i\cos(\theta - \alpha)\sqrt{1 - \sin^2 i\cos^2(\theta - \alpha)} \tag{141}$$

Now to relate the force to time, rather than true anomaly, replace θ by E, using the geometric relationship

$$\cos\theta = \frac{\cos E - e}{1 - e\cos E} \tag{142}$$

and

$$\cos(\theta - \alpha) = \frac{H}{1 - e\cos E} \tag{143}$$

where

$$H = (\cos E - e)\cos\alpha + \sqrt{1 - e^2}\,\sin E\sin\alpha \tag{144}$$

Substitution of Eqs (142) and (143) into Eq (68) to get the corrective thrust requirements in terms of obital elements gives

$$\vec{F}_{req} = m\left(\hat{r}\,F_r + \hat{L}\,F_L\right) \tag{145}$$

where

$$F_r = \frac{J\mu R^2}{p^4}\left(\frac{1 - e^2}{1 - e\cos E}\right)^4 \left[1 - \frac{3H^2\sin^2 i}{(1 - e\cos E)^2}\right]$$

and

$$F_L = \frac{J\,2\mu R^2 H\sin i}{p^4(1 - e\cos E)}\left(\frac{1 - e^2}{1 - e\cos E}\right)^4 \left[1 - \frac{H^2\sin^2 i}{(1 - e\cos E)^2}\right]^{\frac{1}{2}}$$

Now the mass of the satellite must be considered a function of time. If the mass rate is small relative to the mass of the satellite, this time variation can be written as

$$m = m_o\left(1 - \frac{\dot{m}t}{m_0} + O(\dot{m}/m)^2\right)$$

or as a function of the eccentric anomaly

$$m = m_o - \frac{dm}{dE}\frac{dE}{dt}\,t = m_o - \frac{dm}{dE}\left(\frac{dt}{dE}\right)^{-1} t. \tag{146}$$

But for a spherical earth,

$$t = \frac{\tau}{2\pi}\,(E - e\sin E) \tag{147}$$

so that

$$\frac{dt}{dE} = \frac{\tau}{2\pi}\,(1 - e\cos E) \tag{147a}$$

and hence m (and therefore W in units of weight) can be expressed as a function only of the eccentric anomaly:

$$W = W_0 - \frac{E - e\sin E}{1 - e\cos E}\,\frac{dW}{dE}. \tag{148}$$

Substituting Eq (148) into the force equation (145) gives

$$F_{req} = \frac{1}{g_0}\left[W_0 - \frac{E - e\sin E}{1 - e\cos E}\,\frac{dW}{dE}\right]\left[\hat{r}\,F_r + \hat{L}\,F_L\right] \tag{149}$$

Now expressing the thrust as a function of the specific impulse

$$F_{req} = I_{sp}\,\dot{W}$$

or as a function of eccentric anomaly and weight

$$F_{req} = I_{sp} \frac{dW}{dE} \left(\frac{dt}{dE}\right)^{-1} \tag{150}$$

Therefore

$$I_{sp} \frac{dW}{dE} = \frac{\tau}{2\pi g_0} \left[W_0 (1 - e \cos E) - (E - e \sin E) \frac{dW}{dE} \right] \sqrt{F_r^2 + F_L^2} \tag{151}$$

thus,

$$\frac{dW}{dE} = \frac{W_0 (1 - e \cos E) \sqrt{F_r^2 + F_L^2}}{\frac{2\pi I_{sp} g_0}{\tau} + (E - e \sin E) \sqrt{F_r^2 + F_L^2}} \tag{151a}$$

Integration of Eq (151a) over limits of one revolution (0 to 2π) gives the amount of propellant used in that orbital pass

$$W_p = \int_0^{2\pi} \frac{dW}{dE} \, dE \tag{152}$$

Also, by a slight rearrangement of terms, using Eqs (147a) and (151), the integral equation for the corrective thrust is

$$|F_{req}| = W_0 \int_0^E \frac{\sqrt{F_r^2 + F_L^2}}{g_0 + \frac{T}{2\pi I_{sp}} (E - e \sin E) \sqrt{F_r^2 + F_L^2}} \, dE \tag{153}$$

Both of these equations are difficult if not impossible to integrate analytically. However, a simplification will result if the mass of the vehicle is assumed constant for a complete revolution. The magnitude of the error of this assumption is small as will be apparent in subsequent discussions.

Each component of the force can be related to the propellant flow by Eq (151)

$$I_{sp} \frac{dW_r}{dE} = \frac{W\tau}{2\pi g_0} (1 - e \cos E) F_r \tag{154}$$

$$I_{sp} \frac{dW_L}{dE} = \frac{W\tau}{2\pi g_0} (1 - e \cos E) F_L \tag{154a}$$

The actual propellant flow rate is

$$I_{sp} \frac{dW}{dE} = \frac{W\tau}{2\pi g_0} (1 - e \cos E) F_{req} \tag{155}$$

or upon substituting for F_{req} in terms of its components

$$I_{sp} \frac{dW}{dE} = \frac{W\tau}{2\pi g_0} (1 - e \cos E) \sqrt{F_r^2 + F_L^2} \tag{155a}$$

so that

$$\frac{dW}{dE} = \sqrt{\left(\frac{dW_r}{dE}\right)^2 + \left(\frac{dW_L}{dE}\right)^2} \tag{156}$$

and hence, the weight of propellant consumption per revolution is

$$W_P = \frac{W\tau \mu R^2 J}{2\pi g_0 a^4 I_{sp}} \int_0^{2\pi} \left\{ \left[\frac{1}{(1 - e \cos E)^5} \right] \cdot \left[5H^4 \sin^4 i - 2H^2 (1 \quad e \cos E)^2 \sin^2 i + (1 - e \cos E)^4 \right]^{1/2} \right\} dE \tag{157}$$

Probably the most common case for which the oblateness correction will be made will be for satellites in circular orbits. It would therefore be of interest at this time to determine the thrust and propellant equations for circular orbits.

The simplifying conditions for circular orbits are: (1) eccentricity is by definition zero, (2) perigee is undefined and may be selected to make the angle a zero, and (3) the eccentric anomaly E and the true anomaly θ are coincident. Then

$$F_r = \frac{\mu R^2}{a^4} J (1 - 3 \sin^2 L) \tag{158}$$

$$F_L = - \frac{\mu R^2}{a^4} J \sin^2 L \tag{158a}$$

$$F_{req} = m \sqrt{F_r^2 + F_L^2} \tag{158b}$$

$$W_p = \frac{W \tau \mu R^2 J}{2\pi g_0 a^4 I_{sp}} \int_0^{2\pi} \left[5 \cos^4 E \sin^4 i - 2 \cos^2 E \sin^2 i + 1 \right]^{1/2} dE \tag{159}$$

Also, for circular orbits, the true anomaly is related to the time since perigee passage by

$$\theta = \frac{2\pi t}{\tau} .$$

Thus, the corrective thrust F_{req} can be rewritten from Eqs (158) and (159) as

$$F_r = \frac{\mu R^2 J}{a^4} (1 - 3 \sin^2 \cos^2 \theta) \qquad (160)$$

$$F_L = \frac{-2\mu R^2 J}{a^4} \sin i \cos \theta \sqrt{1 - \sin^2 i \cos^2 \theta} \qquad (160a)$$

$$F_{req} = M \sqrt{F_r^2 + F_L^2} \qquad (160b)$$

The variation of the absolute values of these functions as functions of the true anomaly θ, and orbit inclination i are illustrated in Figs. 18 and 19. The parameter for these figures is a non-dimensional acceleration x defined as follows:

$$x_r = \frac{a^4}{\mu R^2 J} |F_r|$$

$$x_\theta = \frac{a^4}{\mu R^2 J} |F_\theta|$$

$$x_{req} = \frac{a^4}{\mu R^2 J} |F_{req}|$$

Estimated average values derived from these curves are illustrated in Fig. 20 as a function of the orbit inclination i. The curve for $\bar{x}_{req}$ represents the averages derived from the curves in Fig. 19, not from $\bar{x}_r$ and $\bar{x}_L$, since

$$\bar{x}_{req} \neq \sqrt{\bar{x}_r^2 + \bar{x}_L^2}$$

but rather

$$\bar{x}_{req} = \overline{\sqrt{x_r^2 + x_L^2}}$$

Evaluation of the propellant requirement is now a simple matter, since

$$I_{sp} \int_0^{W_p} dW_p = \int_0^{\tau} F_{req} \, dt$$

hence,

$$W_p = \frac{\tau}{I_{sp}} F_{req}$$

or

$$W_p = \frac{W \tau \mu R^2 J}{g_0 I_{sp} a^4} \bar{x}_{req}$$

where $\bar{x}_{req}$ is as illustrated in Fig. 20.

Example 1. Consider a 10,000-lb (44,500 newton) satellite on a 300-naut mi or 556-km equatorial circular orbit. The parameters for this case would be as follows:

$m = 311$ slugs $= 4530$ kg

$I_{sp} = 500$ sec (assumed)

$R = 20.9264 \times 10^6$ ft $= 6378.2$ km

$a = 22.72 \times 10^6$ ft $= 6930$ km

$\mu = 1.407645 \times 10^{16}$ ft^3/sec^2 $=$ 398601.5 km^3/sec^2

$i = 0$ deg

$\tau = 5740$ sec

$J = 1.637 \times 10^{-3}$

For this case

$\bar{x}_{req} = 1$

$F_{req} = 11.8$ lb (average value) $= 52.5$ newton

and

$W_p = 136$ lb/orbit $= 605$ newtons/orbit

Example 2. Consider the same 10,000-lb (44,500 newton) vehicle on a 300-naut mi (556-km) polar circular orbit. The parameters are the same as before, except that now,

$i = 90°$.

For this case

$\bar{x}_{req} = 1.31$

Hence,

$F_{req} = 15.5$ lb (average value) $= 69$ newton

$W_p = 178$ lb/orbit $= 794$ newtons/orbit

Example 3. Consider the same 10,000-lb (44,500 newton) vehicle on a 300-naut mi (556-km) circular orbit inclined 28° to the equator (east-launching from the AMR). The parameters are the same as in Example 1, except that now,

$i = 28°$.

For this case

$$\bar{x}_{req} = 0.935$$

Hence,

$$F_{req} = 11.05 \text{ lb (average value)} = 49.2 \text{ newtons}$$

$$W_p = 127 \text{ lb/orbit} = 566 \text{ newtons/orbit}$$

Example 4. Consider the same 10,000-lb (44,500 newton) vehicle on a "24-hr" circular equatorial orbit. The parameters are the same as in Example 1, except that now,

$$a = 1.4 \times 10^8 \text{ ft} = 0.42 \times 10^8 \text{ m}$$

$$\tau = 86,164 \text{ sec}$$

For this case

$$\bar{x}_{req} = 1$$

Hence,

$$F_{req} = 0.00815 \text{ lb (average value)} = 0.0363 \text{ newton}$$

$$W_p = 1.4 \text{ lb/orbit} = 6.24 \text{ newtons/orbit}$$

Conclusions. Some general observations may be made from Figs. 18, 19 and 20.

(1) In an equatorial orbit, the corrective force required to maintain an unperturbed orbit is constant and directed away from the earth (Fig. 18). As the inclination of the orbit is increased to about 30° the radial component of the force decreases somewhat, indicating the diminishing effect of the equatorial bulge as the vehicle gets farther away from it. Beyond an inclination of 30°, the vehicle begins to feel the full effect of the oblate shape of the earth and results in the high values of F_{req} (Fig. 19) for low values of θ.

(2) The correction required on a polar orbit is greater than that required on an equatorial orbit. As an illustrative example, consider a satellite on a polar orbit. Beginning with its position at $\theta = 0$ (over the earth's North Pole), the field is symmetric, and only a negative component of radial force exists (i.e., thrust directed toward center of earth). As the vehicle's latitude decreases (increasing θ) the force decreases and rotates away from the center of the earth until at $\theta = 55°$, it is tangent to the orbit, and directed away from the equator. Finally, as the vehicle passes over the equator on its way toward the South Pole, the only force is the radial component acting away from the earth.

(3) Another result is that an orbit inclination of about 30° requires the least amount of energy expenditure to maintain the orbit (Fig. 20).

2. Propulsion Requirements for Counteracting Drag

Corrective propulsion needed for drag cancellation may be applied either by a continuous thrust device or in discrete impulses. In the first case, either thrust must be varied in such a manner that the drag is balanced at every instant or the time integral of the thrust dotted into the velocity around the orbit must be equal to the work done by the drag force. This drag force is

$$\frac{\vec{D}}{m} = -\frac{1}{2}\frac{C_D A}{m}\rho(\vec{V}+\vec{V}_{aT})\cdot(\vec{V}+\vec{V}_{aT})\frac{\vec{V}+\vec{V}_{aT}}{\left|\vec{V}+\vec{V}_{aT}\right|}$$

where

$\vec{V}_{aT}$ = the velocity of the atmosphere

V = the velocity due to elliptic motion

ρ = mass density as function of position

Thus

$$\frac{\vec{T}}{m} = \frac{\vec{D}}{m}$$

Assuming that the orbit is specified (both planar and orientation elements) and that a model of atmospheric density is available which includes as many of the effects due to solar radiation, atmospheric oblateness, etc., as desirable, and that the product $C_D A$ can be defined with some accuracy, the time history of thrust can be computed. This procedure would best be handled numerically though the possibility exists that series expansions in the various terms might also prove useful. The major drawbacks, however, that the method is cumbersome and requires a variable thrust, are sufficient to eliminate this method from consideration in a parametric study of this nature.

The time integral approach to drag cancellation may be stated as

$$W_{thrust} = -W_{drag}$$

$$\int_0^\tau \vec{F}\cdot(\vec{V}+\vec{V}_{aT})\,dt = \int_0^\tau \vec{D}\cdot(\vec{V}+\vec{V}_{aT})\,dt$$

$$= \int_0^\tau \frac{1}{2} C_D A \rho \frac{\left[(\vec{V}+\vec{V}_{aT})\cdot(\vec{V}+\vec{V}_{aT})\right]^2}{\left|\vec{V}+\vec{V}_{aT}\right|}\,dt$$

where τ is the orbital period

But if

$$F = F \frac{(\vec{V} + \vec{V}_{aT})}{\left|\vec{V} + \vec{V}_{aT}\right|}$$

where

F = scalar constant

The left-hand side of the previous integral reduces to:

$$F \int_0^\tau \frac{(\vec{V} + \vec{V}_{aT}) \cdot (\vec{V} + \vec{V}_{aT})}{\left|\vec{V} + \vec{V}_{aT}\right|} \, dt$$

which is by definition

$$F \int_0^\tau \left|\vec{V} + \vec{V}_{aT}\right| \, dt$$

Similarly the right-hand side of the equation is

$$\frac{1}{2} \int_0^\tau C_D A \rho \left|\vec{V} + \vec{V}_{aT}\right|^3 dt$$

This solution, like the first, is such that a numerical solution is quite attractive for the general case. For special cases when the term $\vec{V}_{aT}$ can be neglected or considered to be colinear with $\vec{V}$ (that is for very high satellites or nearly circular equatorial orbits). The general order of complexity can be reduced and analytic solutions become attractive. Material pertinent to these cases is covered in Chapter V. Because of the restrictive nature of this material it is not presented here. Rather, it is noted that the procedure is simply the matching of the work done by thrust and by drag. The matching procedure is at times very tedious but may nonetheless be accomplished. An approximation to this impulse could be obtained by integrating the drag force over a revolution and observing the change in the orbital elements; then via the methods described in previous sections the impulse required to correct elements could be computed and the average thrust obtained by dividing by the orbital period.

The final approach to this maintenance maneuver is one in which the orbit is allowed to decay until one of the elements has changed an amount equal to or greater than a prescribed tolerance for that element. At this time a two-impulse maneuver is initiated which transfers the vehicle back to the original orbit. Since atmospheric velocity is small compared to the vehicle velocity, the perturbing forces occur approximately in the plane of motion and thus the transfer will be approximately coplanar. Chapter V again presents all of the data pertinent to the decay of satellites and the first section of this chapter ties these changes into the propulsion requirements. Thus, the procedure to be followed for an analysis of this nature is:

(1) The specification of the geometrical elements.

(2) The establishment of tolerances for the elements.

(3) The evaluation of the rates of change of the elements.

(4) The assessment of the times at which corrective action is required, the same maneuver being required each time.

(5) The calculation of the maneuver requirements.

Since each of these discussions is presented in detail in the respective sections of pertinent chapters repetition of this material for the general solution is superfluous. However, because circular orbits pose a unique problem the solution of which can be obtained, the following paragraphs are presented for this restricted problem. The discussions follow those of Ref. (3).

The total required velocity, ΔV, is the sum of the separate velocity additions ΔV_1 and ΔV_2, where ΔV_1 refers to the velocity addition necessary to obtain a Hohmann transfer back to the desired altitude, and where ΔV_2 is the velocity addition necessary to circularize the orbit having once reached the desired altitude. The total required velocity for a single two-impulse correction maneuver is just ΔV. The following sketch describes the geometry of these maneuvers.

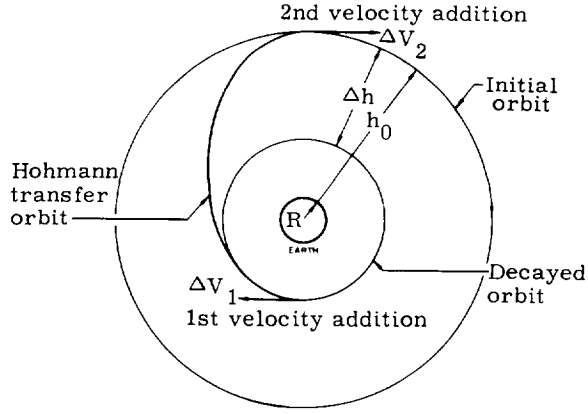

The separate velocity additions, ΔV_1 and ΔV_2, may be determined from the energy equation to be

$$\Delta V_1 = \sqrt{\mu \left(\frac{1}{R + h_0 - \Delta h} - \frac{1}{R + h_0 - \Delta h/2}\right)} - \sqrt{\mu \frac{1}{R + h_0 - \Delta h}} \qquad (161)$$

$$\Delta V_2 = \sqrt{\mu \frac{1}{R + h_0}} - \left[\mu \left(\frac{2}{R + h_0} - \frac{1}{R + h_0 - \Delta h/2}\right)\right]^{\frac{1}{2}} \quad (162)$$

The velocity addition available from a given engine is related to the propellant mass fraction, W_p/W_0, by the familiar rocket equation

$$\Delta V_i = I_{sp} g_0 \ln \frac{1}{1 - W_{pi}/W_{0i}} \quad (163)$$

or

$$\frac{W_{pi}}{W_{0i}} = 1 - e^{-\Delta V_i / I_{sp} g_0} \quad (164)$$

where ΔV_i is the ith total velocity addition and W_{pi} is the amount of propellant required for that particular velocity addition.

Since all the ΔV requirements are the same for each maneuver, it follows that

$$\frac{W_{p1}}{W_0} = \frac{W_{p2}}{W_0 - W_{p1}} = \frac{W_{p3}}{W_0 - W_{p1} - W_{p2}} = 1 - e^{-\Delta V / I_{sp} g_0} \quad (165)$$

where the subscripts 1, 2, 3, etc., denote successive corrective maneuvers. The total amount of propellant used after n maneuvers is then,

$$W_p = \sum_{i=1}^{n} W_{pi} \quad (166)$$

where,

$$W_{p1} = W_0 \left(1 - e^{-\Delta V / I_{sp} g_0}\right) \quad (167)$$

$$W_{p2} = (W_0 - W_{p1}) \left(1 - e^{-\Delta V / I_{sp} g_0}\right) \quad (168)$$

$$W_{pn} = \left\{\left(W_0 - W_{p1} - W_{p2} - \cdots - W_{pn-1}\right) \cdot \left[1 - \exp\left(\Delta V / I_{sp}\, g_0\right)\right]\right\} \quad (169)$$

The total time elapsed after n maneuvers is the summation of the increments of time between successive maneuvers, where it is recalled that the amount Δh has been lost in altitude from one maneuver to the next. This time may be found as follows:

$$dE_T = -\frac{\mu m}{2(R + h)^2}\, dh \quad (170)$$

(where E_T is the total energy of a satellite of mass m in a circular orbit at an altitude h.)

From the drag force D acting on the satellite.

$$dE_T = DV\, dt = \frac{1}{2} \rho V^3 C_D A\, dt \quad (171)$$

(if the atmospheric velocity is neglected).

Now combining Equations (170) and (171) with the expression for circular velocity, and approximating the atmospheric density, to make integration possible, by

$$\rho = \rho_0 e^{-\beta h} \quad (172)$$

yields

$$\frac{(W/C_D A)}{g_0 \rho_0 \sqrt{\mu R}} \int_{h_0}^{h_0 - \Delta h} e^{\beta h}\, dh = -\int_0^{\Delta T} dt \quad (L \ll R) \quad (173)$$

which after integrating and rearranging is the time interval between maneuvers

$$\Delta T = \frac{(W/C_D A)}{\beta g_0 \rho_0 \sqrt{\mu R}} e^{\beta h_0} \left(1 - e^{-\beta \Delta h}\right) + \pi \sqrt{\frac{\left[2(R + h) - \Delta h\right]^3}{\mu}} \quad (174)$$

where the corrective term is 1/2 of the period of the transfer orbit.

An appreciation of the validity of the density approximation may be seen in Chapter V. It is noted, however, that generally good agreement between the true density and that predicted can be obtained for an altitude range from 185 km to 370 km and from 370 km to 750 km using

$\rho_0 = 1.60 \times 10^{-10}$ slugs/ft^3 or 0.824×10^{-7} kg/m^3

$\beta = 7.21 \times 10^{-6}$ ft^{-1} or 23.7×10^{-6} m^{-1}

and

$\rho_0 = 1.92 \times 10^{-12}$ slugs/ft^3 or $.988 \times 10^{-9}$ kg/m^3

$\beta = 3.58 \times 10^{-6}$ ft^{-1} or 11.74×10^{-6} m^{-1}

respectively.

Now, denoting successive maneuvers by the subscripts 1, 2, 3, n, it follows that

$$\Delta T_n = \left\{\left(W_0 - W_{p1} - W_{p2} - \cdots - W_{pn-1}\right)\right.$$

(continued)

$$\cdot \left[\frac{e^{\beta h_0}(1 - e^{-\beta \Delta h})}{\beta C_D A g_0 \rho_0 \sqrt{\mu R}}\right]\Bigg\} + \pi\sqrt{\frac{[2(R + h) - \Delta h]^3}{\mu}} \qquad (175)$$

Thus the total time elapsed after n maneuvers is

$$T_s = \sum_{i=1}^{n} \Delta T_i \qquad (176)$$

Now if the corrective term for transfer time is neglected as being small compared to the total time, and the equation for T_s divided by the total amount of propellant used after n maneuvers, the series common to both equations (involving the weights) may be eliminated to arrive at the desired expression

$$T_s / \frac{W_0}{C_D A} = \frac{W_p}{W_0}\left[\frac{e^{\beta h_0}(1 - e^{-\beta \Delta h})}{\beta g_0 \rho_0 \sqrt{\mu R}\left(1 - e^{-\Delta V / I_{sp} g_0}\right)}\right] \qquad (177)$$

This relationship between the propellant mass fraction required to sustain a satellite a specified lifetime is explicitly independent of the number of impulse corrections, and like the continuous thrust method, shows a linear dependence of the propellant mass fraction, W_p/W_0, upon the sustained lifetime, T_s, for a given set of initial conditions. Figures 21 through 24 show the linear relationship as predicted by Eq (177) as a function of the ballistic coefficient for various $\Delta h/h_0$, and initial altitudes for a specific impulse of 300 sec.

One of the values on these curves is for the case where $\Delta h = 0$. This curve was obtained as follows.

$$F = \frac{1}{2} C_D A \rho V^2 = \dot{W} I_{sp}$$

$$W_p = \frac{1}{2} \frac{C_D A \rho V^2}{I_{sp}} T_s$$

$$\frac{T_s}{W_0 / C_D A} = \frac{2W_p I_{sp}}{W_0 \rho V^2} = \frac{2W_p}{W_0} \frac{I_{sp}(R + h)}{\rho \mu}$$

Although it will not be shown here, this is the same limit that would be obtained if Δh and the various maneuver increments (ΔV_i) were allowed to approach zero simultaneously in Eq 177 with the corrective term for time being neglected, (the corrective term must be neglected because the vehicle is never coasting back to the initial orbit; i.e., there is no Hohmann transfer). These figures show that the longest sustained lifetime per unit weight of propellant is obtained from the continuous thrust sustaining method. In the case of satellites utilizing the discrete velocity-addition sustaining method, longer lifetimes are realized (for a given propellant mass fraction) as the increment is decreased in altitude, Δh, the point below the desired altitude at which the first and successive corrective maneuvers are initiated.

Another interesting fact which may be observed by comparing the sustained and unsustained lifetimes is that the advantages of a sustained satellite over an unsustained satellite are greatest at the lower altitudes, where they are needed most.

G. DIFFERENTIAL CORRECTIONS IN ORBIT TRANSFER

The fundamental goal of space vehicle guidance is placing the vehicle at a certain point in space at a certain time, perhaps with a particular velocity. An approximate method of computing guidance commands to accomplish this objective is by differential corrections based on the ideal transfer profile. The sensed data, in the form of deviations from the ideal transfer orbit, are transformed into the desired vehicle velocity component corrections by a matrix of precomputed error sensitivities stored in the vehicle-borne computer.

The primary advantage of the differential correction technique is a simplification of guidance system input calculations performed aboard the vehicle. These calculations involve only matrix multiplication, which can be mechanized in a simple, lightweight vehicle-borne computer.

The technique is feasible wherever deviations from the desired transfer orbit and perturbations to Keplerian motion are reasonably small. Orbit deviations must be small to admit the use of a linear differential approximation. Also, if the deviations are small, the effect of small perturbations on both nominal and incorrect orbits is essentially the same, i.e., the deviation is independent of small perturbations. The orbit correction, being dependent only on the deviation, is thus independent of small perturbations.

The problem may be formulated in several ways (Refs. 4 and 5), depending on choice of coordinates and orbital elements. The formulation considered is that of Lawden (Ref. 4), the solution being obtained by a somewhat different mathematical approach. Let the center of coordinates be located at the center of the force field, the X-axis be the line of intersection of the ideal vehicle transfer orbit and the orbit plane of the target point, the Z-axis be normal to the target point orbit plane, and the Y-axis complete a right-hand system, as shown in the sketch.

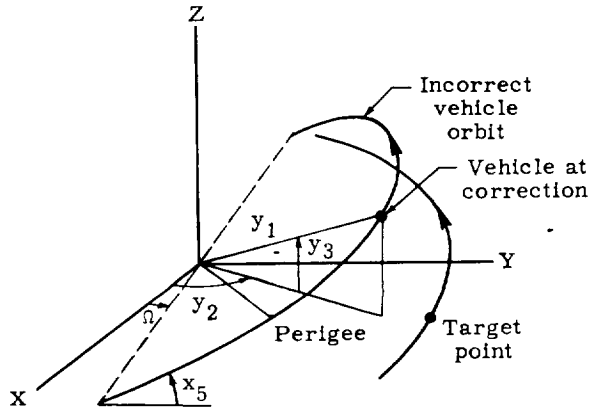

The following nomenclature will be used

x_0 Semimajor axis of the preselected transfer orbit

x_1 Eccentricity of the preselected transfer orbit

x_2 "Curly pi" or sum of the longitude of ascending node and argument of perigee of the transfer orbit

x_3 Eccentric anomaly of the vehicle position at the time of correction

x_4 Eccentric anomaly of the vehicle position in the transfer orbit at the time of rendezvous with the target point

x_5 Inclination of the preselected transfer orbit to the target point orbit plane

x_6 Sum of x_2 and the true anomaly of the vehicle at the time of correction

x_7 180° + longitude of the ascending node of the transfer orbit

x_8 Radius at the rendezvous point

x_9 Eccentric anomaly of the target point in its orbit at the time of rendezvous

y_1 Radius to the vehicle at the time of correction

y_2 Angle in the XY-plane from the X-axis to the projection on the XY-plane of the vehicle radius at the time of correction

y_3 Angle measured in a plane normal to the XY-plane from the XY-plane to the vehicle at the time of correction

y_4 Time between correction and rendezvous

u_1 Radial velocity component of the vehicle at the time of correction

u_2 Vehicle velocity component normal to u_1 and parallel to the XY-plane (at the time of correction)

u_3 Velocity component which completes a right-hand system with u_1 and u_2

v_i Velocity components of the vehicle in the transfer orbit at rendezvous (directions analogous to u_i)

w_i Target point velocity components at rendezvous

a_0 Semimajor axis of the target point orbit

e_0 Eccentricity of the target point orbit

E_0 Eccentric anomaly of the target point at the time of correction

$\tilde{\omega}_0$ Angle in the XY-plane from the X-axis to perigee of the target point orbit.

The problem may be stated as follows. At a certain preselected time, at which errors are to be determined and corrections executed, the vehicle position (y_1, y_2, y_3) is found to be in error relative to the preselected transfer by amounts dy_1, dy_2, dy_3. The velocity components at this point are in error by Δu_1, Δu_2, Δu_3. If the desired velocity at the incorrect point (the velocity to rendezvous $y_4 + dy_u$ later) is $u_i + du_i$, the correction to be applied is $du_i - \Delta u_i$, where the correction relative to the programmed velocity (du_1, du_2, du_3) is to be determined as a function of the dy's. If the velocity, as well as the position, the vehicle is to be matched to that of the target point, a second velocity correction, to be added to the programmed thrust at rendezvous, must be computed.

The required transformation matrix may be obtained by differentiation of the following functions, which describe the Keplerian motion of the vehicle and the target point.

$$
\begin{aligned}
\Phi_0 &= x_4 - x_3 - x_1 (\sin x_4 - \sin x_3) - \frac{y_4}{x_0}\sqrt{\frac{\mu}{x_0}} \\
\Phi_1 &= \tan\frac{x_6 - x_2}{2}\sqrt{\frac{1+x_1}{1-x_1}}\tan\frac{x_3}{2} \\
\Phi_2 &= \tan\frac{x_7 - x_2}{2}\sqrt{\frac{1+x_1}{1-x_1}}\tan\frac{x_4}{2} \\
\Phi_3 &= x_8 - x_0 (1 - x_1 \cos x_4) \\
\Phi_4 &= y_1 - x_0 (1 - x_1 \cos x_3) \\
\Phi_5 &= x_9 - E_0 - e_0 (\sin x_9 - \sin E_0) - \frac{y_4}{a_0}\sqrt{\frac{\mu}{a_0}} \\
\Phi_6 &= \tan\frac{x_7 - \tilde{\omega}_0}{2}\sqrt{\frac{1+e_0}{1-e_0}}\tan\frac{x_9}{2} \\
\Phi_7 &= x_8 - a_0 (1 - e_0 \cos x_9) \\
\Phi_8 &= \tan (x_7 - y_2) - \tan (x_7 - x_6) \cos x_5 \\
\Phi_9 &= \sin y_3 - \sin (x_7 - x_6) \sin x_5
\end{aligned}
\qquad (178)
$$

$$
\begin{aligned}
U_1 &= u_1 - x_1 \sin (x_6 - x_2)\sqrt{\frac{\mu}{x_0 (1 - x_1^2)}} \\
U_2 &= u_2 - \frac{\cos x_5}{\cos y_3}\cdot\frac{\sqrt{\mu x_0 (1 - x_1^2)}}{y_1} \\
U_3 &= u_3 - \frac{\tan y_3}{\tan (x_6 - x_7)}\cdot\frac{\sqrt{\mu x_0 (1 - x_1^2)}}{y_1}
\end{aligned}
$$

The desired velocity components are $u_k + du_k$ where u_k are the programmed velocity components at correction and (in Einsteinian summation notation)

$$du_k = \frac{\partial u_k}{\partial y_m}\, dy_m, \quad k = 1, 2, 3; \; m = 1, 2, 3, 4. \tag{179}$$

The solution of the problem is then complete upon evaluation of the partial derivatives of this expression. These partials are obtained immediately from the Jacobian

$$\Delta = \left| \begin{array}{c|c} a_{ij} & O \\ \hline u_{\ell j} & I \end{array} \right|$$

where

$$a_{ij} = \frac{\partial \Phi_i}{\partial x_j} \qquad i, j = 0, 1, \ldots, 9$$

$$u_{\ell j} = \frac{\partial U_\ell}{\partial x_j} \qquad \ell = 1, 2, 3$$

$$O = [0]_3^{10}$$

$$I = [1]_3^3$$

The partial $\frac{\partial u_k}{\partial y_m}$ of Eq (179) is obtained by dividing the negative of the determinant Δ into the same determinant with the $(10 + k)^{th}$ column replaced by the column vector

$$\left\{ \frac{\partial \Phi_i}{\partial y_m}, \; \frac{\partial U_\ell}{\partial y_m} \right\}$$

For example,

$$\frac{\partial u_1}{\partial y_1} = -\frac{1}{\Delta} \left| \begin{array}{c|c|cc} & \frac{\partial \Phi_0}{\partial y_1} & 0 & 0 \\ & \frac{\partial \Phi_1}{\partial y_1} & 0 & 0 \\ a_{ij} & \cdots & \cdots & \cdots \\ & \frac{\partial \Phi_9}{\partial y_1} & 0 & 0 \\ \hline & \frac{\partial U_1}{\partial y_1} & 0 & 0 \\ u_{\ell j} & \frac{\partial U_2}{\partial y_1} & 1 & 0 \\ & \frac{\partial U_3}{\partial y_1} & 0 & 1 \end{array} \right|$$

This completes the solution for the components of the midcourse differential correction. The thirteenth order determinants (Δ and substituted Δ's) may be evaluated for a particular mission by a computer program and the resulting matrix

$$\left[\frac{\partial u_k}{\partial y_m} \right]$$

stored in the vehicle-borne computer memory.

However, for hand computations, the solution can be expressed in a more convenient form. This is possible because of the large number of zeros in the determinant Δ. Specifically,

$$|a_{ij}| = \begin{vmatrix} a_{00} & a_{01} & 0 & a_{03} & a_{04} & 0 & 0 & 0 & 0 & 0 \\ 0 & a_{11} & a_{12} & a_{13} & 0 & 0 & a_{16} & 0 & 0 & 0 \\ 0 & a_{21} & a_{22} & 0 & a_{24} & 0 & 0 & a_{27} & 0 & 0 \\ a_{30} & a_{31} & 0 & 0 & a_{34} & 0 & 0 & 0 & a_{38} & 0 \\ a_{40} & a_{41} & 0 & a_{43} & 0 & 0 & 0 & 0 & 0 & 0 \\ 0 & 0 & 0 & 0 & 0 & 0 & 0 & 0 & 0 & a_{59} \\ 0 & 0 & 0 & 0 & 0 & 0 & 0 & a_{67} & 0 & a_{69} \\ 0 & 0 & 0 & 0 & 0 & 0 & 0 & 0 & a_{78} & a_{79} \\ 0 & 0 & 0 & 0 & 0 & a_{85} & a_{86} & a_{87} & 0 & 0 \\ 0 & 0 & 0 & 0 & 0 & a_{95} & a_{96} & a_{97} & 0 & 0 \end{vmatrix} \tag{180}$$

which, by Laplace's development of the first five columns, reduces to

$$|a_{ij}| = a_{59}\, a_{67} (a_{85} a_{96} - a_{86} a_{95}) \begin{vmatrix} a_{00} & a_{01} & 0 & a_{03} & a_{04} \\ 0 & a_{11} & a_{12} & a_{13} & 0 \\ 0 & a_{21} & a_{22} & 0 & a_{24} \\ a_{30} & a_{31} & 0 & 0 & a_{34} \\ a_{40} & a_{41} & 0 & a_{43} & 0 \end{vmatrix}$$

where

$$a_{00} = \frac{3}{2}\sqrt{\mu}\, x_0^{-5/2}\, y_4$$

$$a_{01} = \sin x_3 - \sin x_4$$

$$a_{03} = -\frac{y_1}{x_0}$$

$$a_{04} = \frac{x_8}{x_0}$$

$$a_{11} = -\tan\frac{x_3}{2}\sqrt{\frac{1 - x_1}{1 + x_1}}\, \frac{1}{(1 - x_1)^2}$$

$$a_{12} = -\frac{1}{2}\sec^2\frac{x_6 - x_2}{2}$$

$$a_{13} = -\frac{1}{2}\left[\sqrt{\frac{1-x_1}{1+x_1}}\sec^2\frac{x_6 - x_2}{2} + \sqrt{\frac{1+x_1}{1-x_1}}\right]$$

$$a_{21} = -\tan\frac{x_4}{2}\sqrt{\frac{1-x_1}{1+x_1}}\frac{1}{(1-x_1)^2}$$

$$a_{22} = -\frac{1}{2}\csc^2\frac{x_2}{2}$$

$$a_{24} = -\frac{1}{2}\sqrt{\frac{1+x_1}{1-x_1}}\sec^2\frac{x_4}{2}$$

$$a_{30} = -\frac{x_8}{x_0}$$

$$a_{31} = x_0 - x_8$$

$$a_{34} = -x_0 x_1 \sin x_4$$

$$a_{40} = -\frac{y_1}{x_0}$$

$$a_{41} = x_0 - y_1$$

$$a_{43} = -x_0 x_1 \sin x_3$$

$$a_{16} = \frac{1}{2}\sec^2\frac{x_6 - x_2}{2}$$

$$a_{27} = \frac{1}{2}\csc^2\frac{x_2}{2}$$

$$a_{38} = 1$$

$$a_{59} = \frac{x_8}{a_0}$$

$$a_{67} = \frac{1}{2}\csc^2\frac{\tilde{\omega}_0}{2}$$

$$a_{69} = -\frac{1}{2}\sqrt{\frac{1+e_0}{1-e_0}}\sec^2\frac{x_9}{2}$$

$$a_{78} = 1$$

$$a_{79} = -a_0 e_0 \sin x_9$$

$$a_{85} = -\tan x_6 \sin x_5$$

$$a_{86} = \sec^2 x_6 \cos x_5$$

$$a_{87} = \sec^2 y_2 - \sec^2 x_6 \cos x_5$$

$$a_{95} = -\sin x_6 \cos x_5$$

$$a_{96} = -\cos x_6 \sin x_5$$

$$a_{97} = -a_{96}$$

Also

$$\left[u_{\ell j}\right] = \begin{bmatrix} u_{10} & u_{11} & u_{12} & 0 & 0 & 0 & u_{16} & 0 & 0 & 0 \\ u_{20} & u_{21} & 0 & 0 & 0 & u_{25} & 0 & 0 & 0 & 0 \\ u_{30} & u_{31} & 0 & 0 & 0 & 0 & u_{36} & u_{37} & 0 & 0 \end{bmatrix} \tag{181}$$

where

$$u_{10} = \frac{u_1}{2x_0}$$

$$u_{20} = -\frac{u_2}{2x_0}$$

$$u_{30} = -\frac{u_3}{2x_0}$$

$$u_{11} = -\frac{u_1}{x_1(1-x_1^2)}$$

$$u_{21} = \frac{u_2 x_1}{1 - x_1^2}$$

$$u_{31} = \frac{u_3 x_1}{1 - x_1^2}$$

$$u_{12} = -u_1 \cot(x_6 - x_2)$$

$$u_{25} = u_2 \tan x_5$$

$$u_{16} = u_{12}$$

$$u_{36} = u_3 \sec x_6 \csc x_6$$

$$u_{37} = -u_{36}$$

and

$$\left\{\frac{\partial\Phi_i}{\partial y_1}, \frac{\partial U_\ell}{\partial y_1}\right\} = \left\{0,0,0,0,1,0,0,0,0,0,0, \frac{u_2}{y_1}, \frac{u_3}{y_1}\right\}$$

$$\left\{\frac{\partial\Phi_i}{\partial y_2}, \frac{\partial U_\ell}{\partial y_2}\right\} = \{0,0,0,0,0,0,0,0, -\sec^2 y_2, 0,0,0,0\}$$

$$\left\{\frac{\partial\Phi_i}{\partial y_3}, \frac{\partial U_\ell}{\partial y_3}\right\} = \{0,0,0,0,0,0,0,0,0, \cos y_3, 0, -u_2 \tan y_3, -u_3 \sec y_3 \csc y_3\}$$

$$\left\{\frac{\partial\Phi_i}{\partial y_4} \quad \frac{\partial U_i}{\partial y_4}\right\} = \left\{-\frac{1}{x_0}\sqrt{\frac{\mu}{x_0}},\ 0,0,0,0,\right.$$

$$\left. -\frac{1}{a_0}\sqrt{\frac{\mu}{a_0}},\ 0,0,0,0,0,0,0\right\}$$

The determinant $|a_{ij}|$ is interesting in itself since the differentials in the transfer orbit geometry

$$dx_j = \frac{\partial x_j}{\partial y_i}\, dy_i \qquad (182)$$

are given by $|a_{ij}|$ in the same manner that the corrections in vehicle velocity are given directly by Δ. From $|a_{ij}|$, after simplification and factoring, the following error sensitivities are obtained.

$j = 0, \ldots, 4$	$J = 5, \ldots, 9$
$\frac{\partial x_j}{\partial y_1} = (-1)^{j+1}\ \frac{M_{4j}}{D}$	$\frac{\partial x_j}{\partial y_1} = 0\ ,\ j = 5, \ldots, 9$
$\frac{\partial x_j}{\partial y_2} = (-1)^{j+1}\ C_4\ \frac{M_{1j}}{D}$	$\frac{\partial x_5}{\partial y_2} = -k_1,\ \frac{\partial x_6}{\partial y_2} = k_2,\ \frac{\partial x_j}{\partial y_2} = 0,\ j = 7, 8, 9$
$\frac{\partial x_j}{\partial y_3} = (-1)^{j+1}\ C_5\ \frac{M_{1j}}{D}$	$\frac{\partial x_5}{\partial y_3} = \frac{k_2 k_3}{k_4}\ ,\ \frac{\partial x_6}{\partial y_3} = k_1 k_3 k_4,\ \frac{\partial x_j}{\partial x_3} = 0,\ j=7, 8, 9$
$\frac{\partial x_j}{\partial y_4} = (-1)^j \sum_{k=0}^{3} C_k\ \frac{M_{kj}}{D}$	$\frac{\partial x_5}{\partial y_4} = k_1 k_5,\ \frac{\partial x_6}{\partial y_4} = k_5 (1 - k_2),\ \frac{\partial x_7}{\partial y_4} = k_5,\ \frac{\partial x_8}{\partial y_4} = C_3,\ \frac{\partial x_9}{\partial y_4} = \frac{1}{x_8}\sqrt{\frac{\mu}{a_0}}$

(125)

where M_{ij} are the 4 x 4 minors of the determinant

$$D = \begin{vmatrix} d_{00} & d_{01} & 0 & d_{03} & d_{04} \\ 0 & d_{11} & -1 & d_{13} & 0 \\ 0 & d_{21} & -1 & 0 & d_{24} \\ d_{30} & d_{31} & 0 & 0 & d_{34} \\ d_{40} & d_{41} & 0 & d_{43} & 0 \end{vmatrix}$$

and

$$d_{00} = \frac{3y_4}{2x_0^2}\sqrt{\frac{\mu}{x_0}}$$

$$d_{01} = \frac{1}{x_1}\left(\frac{y_4}{x_0}\sqrt{\frac{\mu}{x_0}} + x_3 - x_4\right)$$

$$d_{03} = -\frac{y_1}{x_0}$$

$$d_{04} = \frac{x_8}{x_0}$$

$$d_{11} = \frac{1}{1 - x_1^2}\sin(x_6 - x_2)$$

$$d_{13} = -\left(\sqrt{\frac{1 - x_1}{1 + x_1}} + \frac{2x_1}{\sqrt{1 - x_1^2}}\cos^2\frac{x_6 - x_2}{2}\right)$$

$$d_{21} = \frac{1}{1 - x_1^2}\sin x_2$$

$$d_{24} = -\left(\sqrt{\frac{1 - x_1}{1 + x_1}} + \frac{2x_1}{\sqrt{1 - x_1^2}}\sin^2\frac{x_2}{2}\right)$$

$$d_{30} = -d_{04}$$

$$d_{31} = x_0 - x_8$$

$$d_{34} = -x_0 x_1 \sin x_4$$

$$d_{40} = d_{03}$$

$$d_{41} = x_0 - y_1$$

$$d_{43} = -x_0 x_1 \sin x_3$$

$$C_0 = \frac{1}{x_0}\sqrt{\frac{\mu}{x_0}}$$

$$C_1 = K_5 (1 - \cos x_5)$$

$$C_2 = -K_5$$

$$c_3 = \frac{1}{x_8}\sqrt{\mu\, a_0}\, e_0 \sin x_9$$

$$c_4 = \cos x_5$$

$$c_5 = k_1 k_3 k_4$$

$$k_1 = \frac{\sin x_5}{\tan x_6}$$

$$k_2 = \cos x_5$$

$$k_3 = \frac{\cos^2 y_2 \cos y_3}{\cos^2 x_6}$$

$$k_4 = \sin x_6$$

$$k_5 = \frac{1}{x_8}\sqrt{\frac{\mu}{a_0}}\left[\sqrt{\frac{1-e_0}{1+e_0}} + \frac{2\, e_0}{\sqrt{1-e_0^2}} \sin^2 \frac{\tilde{\omega}_0}{2}\right]$$

The orbit to be achieved by the velocity correction is thus determined in terms of the data.

Special note is made at this point that further development of these determinants is possible resulting in a set of analytic expressions for the corrections. Some of these expressions, however, are very complex in form. For this reason, it is felt that the present form of the solution is most useful.

As an alternative to evaluation of the velocity corrections (du_k) from the 13 x 13 Δ determinants as previously outlined, the corrections may be determined as functions of the orbit element corrections since

$$du_k = \frac{\partial u_k}{\partial x_j}\,\frac{\partial x_j}{\partial y_i}\, dy_i \qquad (184)$$

where $\frac{\partial x_j}{\partial y_i}$ are given by Eq (183) and

$$\frac{\partial u_k}{\partial x_j} = -u_{kj}$$

from Eq (181).

If the velocity, as well as the position, of the vehicle is to be matched with that of the target point, the required correction to the programmed velocity increment at rendezvous may be determined as follows. The velocity components of the vehicle just before rendezvous are

$$v_1 = \sqrt{\frac{\mu}{x_0\,(1-x_1^2)}}\; x_1 \sin(x_7 - x_2)$$

$$v_2 = \frac{\sqrt{\mu\, x_0\,(1-x_1^2)}}{x_8} \cos x_5$$

$$v_3 = \frac{\sqrt{\mu\, x_0\,(1-x_1^2)}}{x_8} \sin x_5 \qquad (185)$$

The deviations of these components from those of the preselected transfer are given by

$$dv_i = \frac{\partial v_i}{\partial x_k}\,\frac{\partial x_k}{\partial y_j}\, dy_j \qquad (186)$$

where the $\frac{\partial x_k}{\partial y_j}$ are given by Eq (183) and the

$\frac{\partial v_i}{\partial x_k}$ are, from Eq (185)

$$\frac{\partial v_1}{\partial x_0} = -\frac{v_1}{2x_0}\;;\quad \frac{\partial v_1}{\partial x_1} = \frac{v_1}{x_1\,(1-x_1^2)}$$

$$\frac{\partial v_1}{\partial x_2} = v_1 \cot x_2\;;\quad \frac{\partial v_1}{\partial x_7} = -v_1 \cot x_2$$

$$\frac{\partial v_2}{\partial x_0} = \frac{v_2}{2x_0}\;;\quad \frac{\partial v_2}{\partial x_1} = -\frac{v_2\, x_1}{1-x_1^2}$$

$$\frac{\partial v_2}{\partial x_5} = -v_2 \tan x_5\;;\quad \frac{\partial v_2}{\partial x_8} = -\frac{v_2}{x_8}$$

$$\frac{\partial v_3}{\partial x_0} = \frac{v_3}{2x_0}\;;\quad \frac{\partial v_3}{\partial x_1} = -\frac{v_3\, x_1}{1-x_1^2}$$

$$\frac{\partial v_3}{\partial x_5} = v_3 \cot x_5\;;\quad \frac{\partial v_3}{\partial x_8} = -\frac{v_3}{x_8}$$

Similarly, from the velocity components of the target point at rendezvous,

$$w_1 = \sqrt{\frac{\mu}{a_0\,(1-e_0^2)}}\; e_0 \sin(x_7 - \tilde{\omega}_0)$$

$$w_2 = \frac{\sqrt{\mu\, a_0\,(1-e_0^2)}}{x_8}$$

$$w_3 = 0\,, \qquad (187)$$

the change in the desired rendezvous velocity from the programmed value is given by

$$dw_1 = w_1 \cot(x_7 - \tilde{\omega}_0)\, dx_7 = -w_1 \cot \tilde{\omega}_0 \frac{\partial x_7}{\partial y_4}\, dy_4$$

$$dw_2 = -\frac{w_2}{x_8}\, dx_8 = -\frac{w_2}{x_8}\,\frac{\partial x_8}{\partial y_4}\, dy_4 \qquad (188)$$

The partials are given by Eq (183). Then the required velocity correction to the stored velocity increment at rendezvous is

$$\Delta v_i = dv_i - dw_i$$

In the previous analyses dy_4 has been considered as an arbitrary increment in the time between correction and rendezvous. If the time of rendezvous is to be maintained at the programmed value, $dy_4 = 0$ and the computations and storage requirements are simplified. On the other hand, if some flexibility is acceptable, then the increment in time may be selected so as to minimize the energy requirement of the correction. Lawden (Ref. 4) gives the value of dy_4 which minimizes the propellant expenditure as

$$dy_4 = -\frac{\delta_3}{\delta_0}\sqrt{\frac{\delta_0\,\delta_2 - \delta_1^2}{\delta_0 - \delta_3^2}} - \frac{\delta_1}{\delta_0} \qquad (189)$$

where

$$\delta_0 = \left(\frac{\partial u_1}{\partial y_4}\right)^2 + \left(\frac{\partial u_2}{\partial y_4}\right)^2 + \left(\frac{\partial u_3}{\partial y_4}\right)^2$$

$$\delta_1 = \sum_{i=1}^{3} \frac{\partial u_i}{\partial y_4}\left(\frac{\partial u_i}{\partial y_1}\, dy_1 + \frac{\partial u_i}{\partial y_2}\, dy_2 + \frac{\partial u_i}{\partial y_3}\, dy_3 - \Delta u_i\right)$$

$$\delta_2 = \sum_{j=1}^{3}\left(\frac{\partial u_i}{\partial y_1}\, dy_1 + \frac{\partial u_i}{\partial y_2}\, dy_2 + \frac{\partial u_i}{\partial y_3}\, dy_3 - \Delta u_i\right)^2$$

$$\delta_3 = \frac{\partial v}{\partial y_4}$$

dy_1, dy_2, dy_3 = position component errors at correction

Δu_i = velocity component errors at correction

v = velocity increment at rendezvous

Many formulations of the differential correction technique are possible. Reference 5 presents rectangular coordinate routine. However, regardless of the form of the data, the approach presented is applicable. By modification of the Φ functions, transformation matrices for any adequate data system may be obtained.

This formulation has been checked for efficacy in several specific examples, one of which is transferred to a 24-hr orbit. The results of these checks indicated a very high degree of approximation in the commanded velocity corrections. In no case were the resultant position and velocity errors greater than 10% of the uncorrected value for errors in position less than 100,000 ft (or 30 km) or more than 3% for errors in initial velocity as large as 20 fps (or 6 mps). In fact the general order of the resultant errors was approximately 3% for errors in initial position in this range and 0.5 to 1% for errors in initial velocity less than 20 fps. The method is thus seen to be ideally suited to midcourse guidance problems and to the problem of small maneuvers.

H. THE STATISTICAL DISTRIBUTION OF THE ELEMENTS OF THE FINAL ORBIT (REF. 6)

Preceding discussions (for example Eqs 134 and 135) related the errors in the resultant orbit elements due to a combination of tracking and control errors. However, these relationships provide no insight as to the probability of occurrence of a given error. This additional information is obtained by relating the probability distributions of the total errors $\Delta a'$ and $\Delta e'$ to the distributions of the individual tracking and control errors. The development of these distributions will be based on the customary assumption that the individual errors (Δr_1, ΔV_1, etc.) are independently and normally distributed.

Since the forms of Eqs 134 and 135 are different, i.e., $\Delta a'$ is the sum of linear differentials and $\Delta e'$ is the square root of the sum of the squares of differential terms. The distribution of both forms will be derived. Consider

$$u = \sum_i a_i x_i, \qquad i = 1, 2, \ldots, k$$

where the a_i are constants and the x_i are independently and normally distributed with means μ_i and variance σ_i^2. Then the moment generating function m (t) for the distribution of the variate u is given as follows:

$$m(t) = \left(\frac{1}{2\pi}\right)^{\frac{k}{2}}\left(\prod_{i=1}^{K}\frac{1}{\sigma_i}\right)\int_{-\infty}^{\infty}\int_{-\infty}^{\infty}\cdots\int_{-\infty}^{\infty}\exp\left[t\sum_i a_i x_i - \frac{1}{2}\sum_i\left(\frac{x_i-\mu_i}{\sigma_i}\right)^2\right]\prod_{i=1}^{K} dx_i$$

where ϵ is the base of natural logarithms (utilized to differentiate from eccentricity).

Transformation to the standard form is convenient.

Now letting ϵ be the base of natural logarithms (to differentiate from eccentricity) and

$$y_i = \frac{x_i - \mu_i}{\sigma_i}$$

then

$$m(t) = \left(\frac{1}{2\pi}\right)^{\frac{k}{2}} \prod_{i=1}^{K} \int_{-\infty}^{\infty} \left(\epsilon^{ta_i\mu_i}\right)\left(\epsilon^{ta_i y_i \sigma_i}\right) \epsilon^{-\frac{1}{2}y_i^2}\, dy_i$$

$$= \left(\frac{1}{2\pi}\right)^{\frac{k}{2}} \prod_{i=1}^{K} \left[\epsilon^{ta_i\mu_i}\, \epsilon^{\frac{1}{2}t^2 a_i^2 \sigma_i^2}\right] \left[\int_{-\infty}^{\infty} \epsilon^{-\frac{1}{2}\left(y_i^2 - 2ta_i y_i \sigma_i + t^2 a_i^2 \sigma_i^2\right)} dy_i\right]$$

$$= \epsilon^{\left[t\sum_i a_i\mu_i + \frac{t^2}{2}\sum_i a_i^2 \sigma_i^2\right]} \qquad (190)$$

However, the moment generating function for the normal distribution is

$$m_n(t) = \epsilon^{t\mu + \frac{1}{2}t^2\sigma^2}$$

Therefore, Eq (190) is the moment generating function for a normal distribution with mean and variance given by

$$\mu = \sum_i a_i\mu_i \qquad (191)$$

$$\sigma^2 = \sum_i a_i^2 \sigma_i^2 \qquad (192)$$

In particular, application of this result to Eq (134) provides the distribution of the error $\Delta a'$. The error in semimajor axis of the corrected orbit is normally distributed with zero mean and variance

$$\sigma^2_{\Delta a'} = 4\sigma^2_{r_1} + 4\frac{r_0^2}{V_0^2}\left(\sigma^2_{\delta V_1} + \sigma^2_{\delta(\Delta V_1)} + \sigma^2_{\delta(\Delta V_2)}\right)$$

That is, the distribution of $\Delta a'$ is

$$f(\Delta a') = \left\{8\pi\left[\sigma^2_{r_1} + \frac{r_0^3}{\mu}\left(\sigma^2_{\delta V_1} + \sigma^2_{\delta(\Delta V_1)} + \sigma^2_{\delta(\Delta V_2)}\right)\right]\right\}^{-1} \epsilon^{-\frac{\Delta a^2 \sigma_{r_1}^2}{8}}$$

$$\epsilon^{-\frac{\Delta a^2 r_0^3}{8\mu}\left(\sigma^2_{\delta V_1} + \sigma^2_{\delta(\Delta V_1)} + \sigma^2_{\delta(\Delta V_2)}\right)}$$

The distribution of the eccentricity error is more difficult to obtain because Eq (135) is not linear. Equation (135) is of the form

$$u = \sqrt{x_1^2 + x_2^2}$$

where x_1 and x_2 are assumed normally and independently distributed, i.e.,

$$n(x_1, x_2) = \frac{1}{2\pi\sigma_{x_1}\sigma_{x_2}}\left[\epsilon^{-\frac{1}{2}\left(\frac{x_1}{\sigma_{x_1}}\right)^2} \epsilon^{-\frac{1}{2}\left(\frac{x_2}{\sigma_{x_2}}\right)^2}\right]$$

The distribution of u may be obtained by eliminating either x_1 or x_2 in terms of u to obtain a density

$$g(u, x_2) = \sum_i n\left[x_1(u, x_2), x_2\right]\left|\frac{\partial x_i}{\partial u}\right|_i$$

where each term in the summation represents one branch of a possibly nonmonotone function $u(x_1)$. The desired distribution, g(u), may then be obtained by integrating over the x_2 in g (u, x_2).

$$g(u) = \int_{-\infty}^{\infty} g(u, x_2)\, dx_2$$

In particular, for

$$u = \sqrt{x_1^2 + x_2^2}$$

$$x_1 = \pm\sqrt{u^2 - x_2^2}$$

$$\left|\frac{\partial x_1}{\partial u}\right| = \frac{u}{\sqrt{u^2 - x_2^2}}$$

Since the function g(u) is not single valued, it must be evaluated on each branch

$$g(u, x_2) = f(x_1^+)\left|\frac{\partial x_1^+}{\partial u}\right| + f(x_1^-)\left|\frac{\partial x_1^-}{\partial u}\right|$$

But

$$f(x_1^+) = f(x_1^-)$$

$$\left|\frac{\partial x_1^{+}}{\partial u}\right| = \left|\frac{\partial x_1^{-}}{\partial u}\right|$$

Thus

$$g(u, x_2) = 2 f(x_1) \left|\frac{\partial x_1}{\partial u}\right|$$

$$g(u, x_2) = 2\left[\frac{1}{2\pi \sigma_{x_1} \sigma_{x_2}} \epsilon^{-\frac{1}{2}\frac{u^2 - x_2^2}{\sigma_{x_1}^2}} \epsilon^{-\frac{1}{2}\frac{x_2^2}{\sigma_{x_2}^2}} \frac{u}{\sqrt{u^2 - x_2^2}}\right]$$

$$g(u) = \frac{u \epsilon^{-\frac{1}{2}\frac{u^2}{\sigma_{x_1}^2}}}{\pi \sigma_{x_1} \sigma_{x_2}} \int_{-\infty}^{\infty} \left\{ \frac{1}{\sqrt{u^2 - x_2^2}} \epsilon^{-\frac{1}{2}\left[x_2^2\left(\frac{1}{\sigma_{x_2}^2} - \frac{1}{\sigma_{x_1}^2}\right)\right]} dx_2 \right\}$$

After the transformation

$$t = x_2^2$$

this expression may be integrated to yield the required distribution

$$g(u) = \left\{ \frac{u}{\sigma_{x_1} \sigma_{x_2}} \epsilon^{-\frac{u^2}{4}\left(\frac{1}{\sigma_{x_1}^2} + \frac{1}{\sigma_{x_2}^2}\right)} I_0\left[\frac{u^2}{4}\left(\frac{1}{\sigma_{x_2}^2} - \frac{1}{\sigma_{x_1}^2}\right)\right] \right\} \qquad (193)$$

$$\left(0 < x_2^2 < u^2\right)$$

$$= 0, \; x_2^2 > u^2$$

This g(u) (and, in particular, the distribution of corrected orbit eccentricity error) is a skewed, single-sided distribution with positive mean and and a shape similar to that of the gamma distribution.

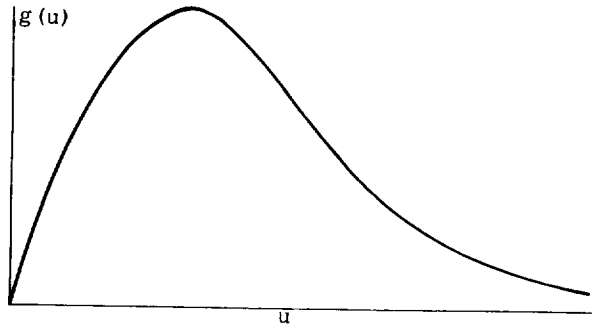

In manipulation of the distribution g(u) the following definitions are convenient.

$$K_1 \equiv \frac{1}{\sigma_{x_1} \sigma_{x_2}}$$

$$K_2 \equiv \frac{1}{4}\left(\frac{1}{\sigma_{x_1}^2} + \frac{1}{\sigma_{x_2}^2}\right)$$

$$K_3 \equiv \frac{1}{4}\left(\frac{1}{\sigma_{x_2}^2} - \frac{1}{\sigma_{x_1}^2}\right)$$

The distribution is then

$$g(u) \equiv K_1 \, u \, \epsilon^{-K_2 u^2} I_0\left(K_3 u^2\right)$$

This final form has been checked both analytically and numerically utilizing randomly selected variates from normal distributions. The results show excellent correlation.

Quantities of some significance in describing the properties of the distribution (e.g., central value, spread, skewness, etc.) are the moments of the distribution. The rth moment of g(u) is

$$\overline{\mu}_r = \int_0^{\infty} u^r \, g(u) \, d u$$

$$= K_1 \int_0^{\infty} u^{r+1} \, \epsilon^{-K_2 u^2} I_0\left(K_3 u^2\right) du \qquad (194)$$

After the transformation $t = u^2$, the integral can be evaluated in various forms.

$$\int_0^{\infty} t^n \, \epsilon^{-K_2 t} I_{\nu}(K_3 t) \, dt =$$

$$\left[\Gamma(n + \nu + 1)\left(K_2^2 - K_3^2\right)^{-\frac{1}{2}(n+1)} P_n^{-\nu}\left(\frac{K_2}{\sqrt{K_2^2 - K_3^2}}\right)\right] \quad K_2 > |K_3|$$

where the generalized Legendre function is given by

$$P_n^m(z) = \frac{1}{\Gamma(1-m)}\left(\frac{z+1}{z-1}\right)^{\frac{m}{2}} {}_2\mathcal{F}_1\left(-n, n+1; 1-m; \frac{1}{2}-\frac{1}{2}z\right)$$

and the hypergeometric series is given by

$${}_m\mathcal{F}_n(a_1, \ldots, a_m; \gamma_1, \ldots, \gamma_n; z) = \sum_{i=0}^{\infty} \frac{(a_1)_i \ldots (a_m)_i}{(\gamma_1)_i \ldots (\gamma_n)_i} \frac{z^i}{i!}$$

Then

$$\bar{\mu}_r = \frac{K_1}{2} \frac{\Gamma\left(\frac{r}{2}+1\right)}{K_2^{\frac{r}{2}+1}} \mathcal{F}\left[\frac{r+2}{4}, \frac{r+4}{4}, 1; \left(\frac{K_3}{K_2}\right)^2\right]$$

$$= \frac{K_1}{2}\left\{\frac{\Gamma\left(\frac{r}{2}+1\right)}{K_2^{\frac{r}{2}+1}} \sum_{i=0}^{\infty} \frac{\left(\frac{r+2}{4}; 1; i\right)\left(\frac{r+4}{4}; 1; i\right)}{i!\,(1; 1; i)} \left(\frac{K_3}{K_2}\right)^{2i}\right\} \quad (195)$$

In particular, the mean of the distribution g(u) is given by

$$\bar{\mu}_1 = \frac{K_1\,\Gamma(3/2)}{2\,K_3^{\frac{3}{2}}} \mathcal{F}\left[\frac{3}{4}, \frac{5}{4}, 1; \left(\frac{K_3}{K_2}\right)^2\right]$$

$$= \frac{K_1\sqrt{\pi}}{4\,K_2^{\frac{3}{2}}}\left[1 + \frac{\frac{3}{4}\cdot\frac{5}{4}}{1\cdot 1}\left(\frac{K_3}{K_2}\right)^2 + \frac{\frac{3}{4}\cdot\frac{7}{4}\cdot\frac{5}{4}\cdot\frac{9}{4}}{(2!)^2}\left(\frac{K_3}{K_2}\right)^4 + \frac{\frac{3}{4}\cdot\frac{7}{4}\cdot\frac{11}{4}\cdot\frac{5}{4}\cdot\frac{9}{4}\cdot\frac{13}{4}}{(3!)^2}\left(\frac{K_3}{K_2}\right)^6 + \ldots\right] \quad (196)$$

The second moment is of interest in determination of the variance of g(u).

$$\bar{\mu}_2 = \frac{K_1}{2}\frac{\Gamma(2)}{K_2^2}\mathcal{F}\left[1, \frac{3}{2}, 1; \left(\frac{K_3}{K_2}\right)^2\right]$$

$$= \frac{K_1}{2\,K_2^2}\left[1 + \frac{3}{2}\left(\frac{K_3}{K_2}\right)^2 + \frac{1}{2!}\,\frac{3}{2}\cdot\frac{5}{2}\left(\frac{K_3}{K_2}\right)^4 + \frac{1}{3!}\cdot\frac{3}{2}\cdot\frac{5}{2}\cdot\frac{7}{2}\left(\frac{K_3}{K_2}\right)^6 + \ldots\right] \quad (197)$$

Then the variance is

$$\sigma_u^2 = \bar{\mu}_2 - (\bar{\mu}_1)^2 \quad (198)$$

Another factor of interest is the probability of occurrence of extreme values of u. Direct computation of areas under the distribution of Eq (193) is rather tedious. However, for large values of the variate u, the modified Bessel function of the first kind of order zero may be approximated by the following series.

$$I_0(x) \approx \frac{\epsilon^x}{\sqrt{2\pi x}}\left(1 + \frac{1^2}{1!\,8x} + \frac{1^2\cdot 3^2}{2!\,(8x)^2} + \frac{1^2\cdot 3^2\cdot 5^2}{3!\,(8x)^3} + \ldots\right)$$

(x large)

If only the fundamental term of this series is retained, the distribution of Eq (193) becomes

$$g(u) \approx \sqrt{\frac{2}{\pi}}\,\frac{1}{\sqrt{\sigma_{x_1}^2 - \sigma_{x_2}^2}}\,\epsilon^{-\frac{u^2}{2}\frac{1}{\sigma_{x_1}^2}}$$

(u large) (199)

Thus, available tabulations of the normal density area

$$n(x) = \frac{1}{\sqrt{2\pi}}\int_x^{\infty} \epsilon^{-\frac{y^2}{2}}\,dy$$

can be used to evaluate probability of occurrence of extreme values of u with good accuracy.

I. TRANSFER TRAJECTORY OPTIMIZATION

1. Variational Approach

The problem of trajectory optimization has received attention in much of the literature referenced. However, the work of D. F. Lawden (Refs. 7, 8, 9) is felt to be particularly meritorious. For this reason, his work has been followed quite closely in this material which is included to provide insight into the general maneuver problem and the basis for the formulation of the differential correction routine discussed later.

The general problem of optimizing a maneuver trajectory with respect to the energy requirement may be expressed as: it is required that two points in space be connected by a curve along which the vehicle can be maneuvered with a minimum energy expenditure. Because aerodynamic, electromagnetic and other forces are extremely complex in nature, only thrust and gravity forces will be considered.

Consider the reference frame in the following sketch:

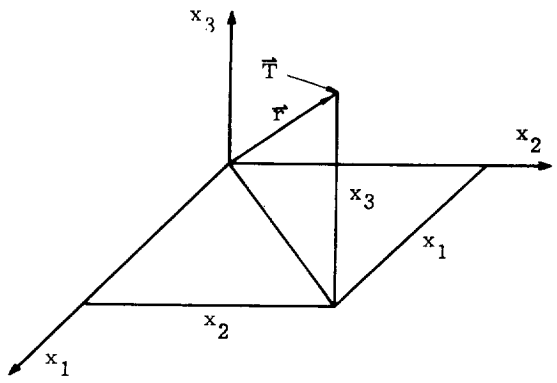

We have

$$m\,\ddot{\vec{r}} = \vec{T} + m\,\vec{g} = \vec{T} - \frac{m\mu}{r^2}\,\hat{r} \qquad (200)$$

where the symbol $\wedge$ denotes a unit vector.

If f_i (i = 1, 2, 3) denote the gravitation components along the three axes at the point (x_1, x_2, x_3) and the time is t we can assume the f_i are known functions of t, t_0, t_1, Λ_k, x_i (where t_0 is the time of departure, t_1 is the time of arrival and the Λ_k are parameters whose values change for different problems). Now we can form the following functions:

$$\phi_i = \dot{V}_i - \frac{T}{m}\,\ell_i - f_i = 0 \qquad (201)$$

$$\phi_{i+3} = \dot{x}_i - V_i = 0 \qquad (202)$$

where again

$$f_i = f_i\,(t, t_0, t_1, \Lambda_k, x_i) \qquad (203)$$

ℓ_i = the direction cosines of the thrust vector

i = 1, 2, 3.

Now noting that $T = c\beta$ (where β is the mass rate of change) and utilizing the cosine identity, we can form the following functions:

$$\phi_i = \dot{V}_i - \frac{c}{m}\,\beta\,\ell_i - f_i = 0 \qquad (204)$$

$$\phi_{i+3} = \dot{x}_i - V_i = 0 \qquad (205)$$

$$\phi_7 = \dot{m} + \beta = 0 \qquad (206)$$

$$\phi_8 = \sum_{i=1}^{3} \ell_i^{\,2} - 1 = 0 \qquad (207)$$

But β is positive and bounded ($\beta_1 \le \beta \le \beta_2$) to overcome problems arising from the fact that the ℓ_i are undefined when $\beta = 0$. However, we shall let $\beta_1 \to 0$ to allow for unpowered flight. β is assumed to be a monotonically increasing function of some parameter of no physical significance $[\alpha = \alpha\,(t)]$ such that as α changes from $-\infty$ to ∞, β changes from β_1 to β_2. Thus, $\frac{d\beta}{d\alpha} = 0$ for some large value of $|\alpha|$. Conversely, the vanishing of $\frac{d\beta}{d\alpha}$ implies either maximum or minimum thrust (Ref. 10).

These eleven functions of t (x_i, V_i, ℓ_i, α and m) must be chosen in such a manner that the energy (or characteristic velocity of the maneuver) is minimized, subject to a particular set of boundary conditions.

Now the boundary conditions for the problem are x_{i0}, x_{if}, $\dot{x}_{i0}$ and $\dot{x}_{if}$. These conditions can be stated as

$$\xi_i = x_{i0} - d_i = 0 \qquad (208)$$

$$\xi_{1+3} = x_{if} - a_i = 0 \qquad (209)$$

$$\xi_{i+6} = V_{i0} - \dot{d}_i = 0 \qquad (210)$$

$$\xi_{i+9} = V_{if} - \dot{a}_i = 0 \qquad (211)$$

where the subscripts 0 and f indicate the initial and final values of x_i and $\dot{x}_i$, respectively, and the d and a denote the points of departure and arrival, respectively. If, in addition, the times of departure and the time of transfer are specified, two additional boundary conditions are

$$\xi_{13} = t_0 - T_0 = 0 \qquad (212)$$

$$\xi_{14} = t_f - T_f = 0 \tag{213}$$

Now we introduce 8 Lagrangian multipliers (λ_j) and form the fundamental function

$$F = \sum_{j=1}^{8} \lambda_j \phi_j \tag{214}$$

Using two sets of running indices (the summation convention) the Euler-Lagrange equations can now be written as:

$$\dot{\lambda}_i + \lambda_{i+3} = 0 \qquad (i, k = 1, 2, 3) \tag{215}$$

$$\dot{\lambda}_{i+3} + \lambda_k \frac{\partial f_k}{\partial x_i} = 0 \tag{216}$$

$$2\lambda_8 \ell_i - \frac{c\beta}{m} \lambda_i = 0 \tag{217}$$

$$\lambda_7 = 2 \frac{c\beta}{m} \lambda_i \ell_i \tag{218}$$

$$\frac{d\beta}{d\alpha} \left(\lambda_7 - \frac{c}{m} \lambda_i \ell_i\right) = 0 \tag{219}$$

It follows from these equations that the λ_i must satisfy

$$\ddot{\lambda}_i = \lambda_k \frac{\partial f_k}{\partial x_i} \tag{220}$$

and

$$\lambda_i = \frac{2m}{c\beta} \lambda_8 \ell_i \tag{221}$$

This latter equation states that the vector composed of the three components λ_i (mutually orthogonal and referred to by Lawden as the primer) is always parallel to the thrust direction except in those cases when $\beta = 0$ (i.e., no thrust).

It further follows from Eq (219) that

$$\frac{d\beta}{d\alpha} = 0 \tag{222}$$

or

$$\lambda_7 = \frac{c}{m} \lambda_i \ell_i \tag{223}$$

The first alternative implies that $\beta \to 0$ or $\beta = \beta_u$ or again that the thrust level is either zero or maximum. If $\beta = 0$ the vehicle coast in an orbit under the influence of gravity alone and λ_7 = constant, $\lambda_8 = 0$ and the ℓ_i are not defined. If $\beta = \beta_u$, the thrust is parallel to the primer as mentioned previously and

$$\lambda_8 = \frac{c\beta_\mu}{2m} \sqrt{\sum_{i=1}^{3} \lambda_i^2} \tag{224}$$

$$\dot{\lambda}_7 = \frac{c\beta_\mu}{m^2} \sqrt{\sum_{i=1}^{3} \lambda_i^2} \tag{225}$$

The second alternative in conjunction with Eq (218) yields

$$\dot{\lambda}_7 = \frac{\beta}{m} \lambda_7 \tag{226}$$

which upon integration gives

$$\lambda_7 = \frac{\text{constant}}{m} \tag{227}$$

However

$$\ell_i = \frac{\lambda_i}{\sqrt{\sum_{i=1}^{3} \lambda_i^2}} \tag{228}$$

therefore

$$\sum_{i=1}^{3} \lambda_i^2 = c \tag{229}$$

This equation states that the primer vector has a constant magnitude which is a contradiction to earlier proofs of Lawden (Ref 8). Therefore, this alternative is not possible, leaving the first alternative (Eq 222) as the only possibility.

Now since the $\dot{V}_i$, ℓ_i and β need only be piecewise continuous in the interval $t_0 \le t \le t_f$, the extremal arc may have corners. If such corners exist, the Weierstrass-Erdman corner conditions must be satisfied for the instants at which thrust is applied or terminated. This implies that the λ_j (j = 1, 2, 3, 4, 5, 6, 7) must be continuous at these times. But since $\dot{\lambda}_i = -\lambda_{i+3}$ (i = 1, 2, 3), the primer and its first derivative must be continuous. Now the corner condition must be satisfied:

$$\left(F - V_i \frac{\partial F}{\partial \dot{V}_i}\right)_+ = \left(F - V_i \frac{\partial F}{\partial \dot{V}_i}\right)_- \tag{230}$$

This equation requires that the following function be continuous

$$-\lambda_i \left(\frac{c\beta}{m} \ell_i + f_i\right) - \lambda_{i+3} V_i + \lambda_7 \beta$$

which in turn requires that

$$\frac{c\beta}{m} \lambda_i \ell_I - \lambda_7 \beta$$

be continuous since f_i and V_i are by definition continuous, and since the λ_i were shown to be continuous for this class of problems (Eq 91). This function is shown to be continuous in Ref 7. Further it is shown that

$$\lambda_i f_i - \dot{\lambda}_i V_i + \beta \left(\frac{c}{m} \lambda_i \ell_i - \lambda_7\right) = \text{constant}$$

where the constant takes on the same value for the entire minimum energy trajectory.

We now form another function, H, from the constraints (Eqs 208 through 213) and the expression for the characteristic velocity of the maneuver.

$$H = c \log \frac{M_0}{M_1} + \eta_i (x_{i0} - d_i) + \eta_{i+3} (x_{i1} - a_i)$$

$$+ \eta_{i+6} (V_{i0} - \dot{d}_i) + \eta_{i+9} (V_{i1} - \dot{a}_i)$$

$$+ \eta_{13} (t_0 - T_0) + \eta_{14} (t_1 - T_1) \qquad (231)$$

At this point it is noted that if the time of transfer and the time of initiation constraints are removed, η_{13} and η_{14} are zero.

Now, from the generalized problem of Mayer, the necessary conditions for the minimization of H can be evaluated

$$\eta_i - \lambda_{i+3,\,0} = 0 \qquad (232)$$

$$\eta_{i+6} - \lambda_{i,\,0} = 0 \qquad (233)$$

$$\eta_{i+3} + \lambda_{i+3,\,f} = 0 \qquad (234)$$

$$\eta_{i+9} + \lambda_{i,\,f} = 0 \qquad (235)$$

$$\frac{c}{M_0} - \lambda_{7,\,0} = 0 \qquad (236)$$

$$- \frac{c}{M_f} + \lambda_{7,\,f} = 0 \qquad (237)$$

$$\int_{t_0}^{t_f} \lambda_i \frac{\partial f_i}{\partial \Lambda_k} \, dt = 0 \qquad (238)$$

$$\eta_{13} + \eta_i \dot{x}_{i0} + \eta_{i+6} \dot{V}_{i0} + \frac{c}{M_0} \dot{M}_0 - \int_{t_0}^{t_f} \lambda_i \frac{\partial f_i}{\partial t_0} \, dt = 0 \qquad (239)$$

$$\eta_{14} + \eta_{i+3} \dot{x}_{if} + \eta_{i+9} \dot{V}_{if} + \frac{c}{M_f} \dot{M}_f - \int_{t_0}^{t_f} \lambda_i \frac{\partial f_i}{\partial t_f} \, dt = 0 \qquad (240)$$

where the subscripts 0 and f refer to the initial and final times for the orbital transfer. If the time restraints are removed (to find the minimum energy trajectory), η_{13} and η_{14} are zero and η_i and η_{i+6} can be eliminated from Eq (239) and η_{i+3} and η_{i+9} can be eliminated from Eq (111) yielding

$$\lambda_i \dot{V}_i - \dot{\lambda}_i V_i - \frac{c}{M_0} \dot{M}_0 = \int_{t_0}^{t_f} \lambda_i \frac{\partial f_i}{\partial t_0} \, dt \qquad (241)$$

$$\lambda_i \dot{V}_i - \dot{\lambda}_i V_i - \frac{c}{M_f} \dot{M}_f = \int_{t_0}^{t_f} \lambda_i \frac{\partial f_i}{\partial t_f} \, dt \qquad (242)$$

The conditions of Eq 232 to Eq 242 must necessarily be satisfied if the external arc is to be optimum with respect to the energy requirement. As is evident from the complexity of these expressions, exact solutions are not easily come by, and general solutions to the optimum transfer problem appear doomed. In fact, numerical evaluation is generally necessary. This conclusion is strengthened when it is noted that the absolute minimum energy maneuver is not the only solution satisfying these conditions. Thus, it is generally necessary to investigate each of the resulting "optimum" solutions. However, several conclusions can be drawn from this work and that reported in Ref. 11.

(1) The optimum trajectory is composed of maximum thrust arcs and coasting arcs.

(2) There are in general only 3 sub arcs in the trajectory, 2 of which are thrust arcs.

(3) The thrust arcs generally occur at the two terminals.

To aid in the visualization of the transfer problem and provide information which is of value in the analysis of trajectory problems, the general problem will be reduced to one of pulse transfer. This assumption is valid for most maneuvers since the magnitude of the correction (ΔV) and the time of burning (t_b) are generally small compared to V_0 or V_1 and the time of transfer, respectively. Under this assumption the optimum trajectory connects the two specified radii with impulses at either end.

Variations in all of the parameters during thrust periods are assumed small. This infers that since the primer vector and its derivatives are continuous during initiation and termination of a thrust phase, they are continuous across any null thrust arc. Thus, Eq 225 reduces to

$$\Delta \lambda_7 = \Delta \frac{c}{M} \sqrt{\sum_{i=1}^{3} \lambda_i^2} \qquad (243)$$

By considering the equations for λ_7 it can be shown that Eq 223 implies that

$$\sqrt{\sum_{i=1}^{3} \lambda_i^2} = 1 \qquad (244)$$

at the beginning of the maneuver.

Now, since the λ_i are the direction ratios for the thrust vector, this equation states that, for the pulse case, they are equal to the direction cosines of the impulse. The other constraints are

$$\lambda_i \dot{V}_i = \frac{c}{M} \beta + \lambda_i f_i \qquad (245)$$

$$\lambda_i f_i - \dot{\lambda}_i V_i = \int_{t_0}^{t_f} \lambda_i \frac{\partial f_i}{\partial t_0} \, dt \qquad (246)$$

$$\lambda_i f_i - \dot{\lambda}_i V_i = -\int_{t_0}^{t_f} \lambda_i \frac{\partial f_i}{\partial f_f}\, dt \qquad (247)$$

$$\lambda_i f_i - \dot{\lambda}_i V_i = \text{constant} \qquad (248)$$

where t_0 and t_f are not specified, and the constant of Eq 248 is zero if the f_i components are time invariant and independent of t_0 and t_1.

Investigations of these equations are reported in Ref. 7 for motion in Keplerian orbits. Therefore, it is not deemed necessary to repeat this material. Rather, conclusions pertaining to these investigations will be presented for the case of transfer between elliptic orbits.

(1) If the orbits intersect, a single impulse can be used to effect the maneuver, and the conditions for optimum transfer are satisfied. However, in some cases this type of transfer is not the absolute minimum energy maneuver (i.e., minimum of the minimum energy maneuvers). For this reason it is necessary to check the energy requirements of each solution satisfying the conditions for minimum energy maneuvers.

(2) If the orbits do not intersect, two impulses are generally required (one at each terminal) to effect the maneuver. This conclusion must be modified in certain classes of transfers as is indicated in the analysis of 3 impulse transfers.

(3) If the eccentricities of the two orbits go to zero, the optimum mode of transfer is via the well known Hohmann ellipse which is tangent at perigee to one circular orbit and tangent at apogee to the other. This conclusion is also modified for certain orbits for 3 impulse-transfers.

(4) If the eccentricities of the two orbits are small, the line of apsides of the minimum energy transfer ellipse aligns itself in the approximate direction of the line of apsides of the terminal ellipse (initial or final) having the greater eccentricity.

(5) If the two terminal ellipses are not coplanar, little in the way of a general conclusion can be made. If, however, the eccentricities of both the initial and final orbits are small, the optimum maneuver occurs when the transfer orbit is tangent to the respective orbits at the points of departure and arrival and when the line of apsides of the transfer orbit is the line of intersection of the two orbital planes.

Utilizing the second of these "general rules" numerical data may be generated relating the parameters of the "optimum" transfer orbit. However, because of the number of variables involved, parametric studies generally prove extremely lengthy in all but the most simple cases. Among these simple cases is the analysis of transfer between circular orbits. For this reason and for the reason that many satellite applications require circular orbits, certain of the parameters will be discussed in the following paragraphs.

Consider the following sketches depicting coplanar and noncoplanar transfer.

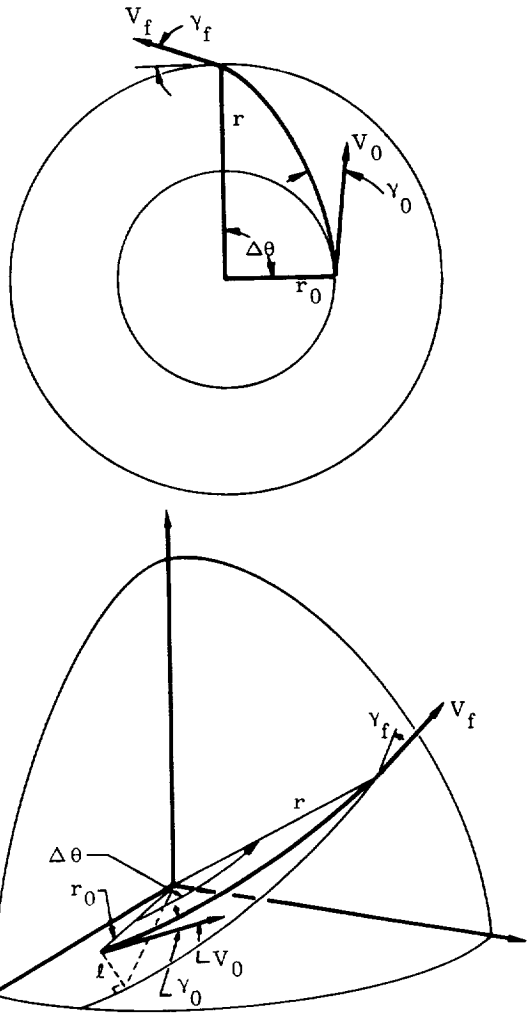

The first of these sketches (showing transfer between circular coplanar orbits) points up the fact that the maneuver required must change both the magnitude and the direction of the velocity in the plane of transfer (both of the effects have been discussed earlier). Thus, it is desired to show what types of orbits will be required to minimize ΔV_{total} for various types of transfer. The equation for this maneuver are:

$$\frac{\Delta V_T}{V_{c1}} = \sqrt{1 + \left(\frac{V_0}{V_{c1}}\right)^2 - 2\,\frac{V_0}{V_{c1}}\cos\gamma} + \sqrt{\frac{r_0}{r_f}}\,\sqrt{1 + \left(\frac{V_f}{V_{c2}}\right)^2 - 2\,\frac{V_f}{V_{c2}}\cos\gamma_2}$$

$$\tan \gamma_0 = \left[\frac{1 - \frac{r_0}{2a}}{\tan \frac{\Delta\theta}{2}} - \frac{\sqrt{\left(1 - \frac{r_0}{2a}\right) \frac{r_0}{r} - \frac{r_0}{2a}\left(1 - \frac{r_0}{2a}\cos^2 \frac{\Delta\theta}{2}\right)}}{\sin \frac{\Delta\theta}{2}} \right]$$

$$\tan \gamma_f = \left[-\frac{1 - \frac{r_f}{2a}}{\tan \frac{\Delta\theta}{2}} + \frac{\sqrt{\left(1 - \frac{r}{2a}\right) \frac{r}{r_0} - \frac{r}{2a}\left(1 - \frac{r}{2a}\cos^2 \frac{\Delta\theta}{2}\right)}}{\sin \frac{\Delta\theta}{2}} \right]$$

$$\frac{V}{V_c} = \frac{\sqrt{\left(\frac{2}{r} - \frac{1}{a}\right)}}{\sqrt{\frac{1}{r}}} = \sqrt{2 - \frac{r}{a}}$$

Thus, if r_f, r_0, r_f and $\Delta\theta$ are specified, the quantity a which will require the smallest value of ΔV_T can be determined. This was done numerically in Ref 12. The results of these computations are presented in Figs. 25, 26 and 27.

The second sketch shows the nonplanar transfer between circular orbits. The equations for this maneuver can be obtained in a simple form if the second impulse alone is responsible for altering the plane of motion. This assumption will not always yield a true minimum energy transfer; however, more rigorous attention to detail leads to a very complex form of solution, thus making such an approach less suited to parametric analyses of this nature.

$$\frac{V_0}{V_{c1}} = \sqrt{\frac{2}{\frac{r}{r_0} - \frac{\cos(\Delta\theta - \gamma_f)}{\cos \gamma_f}}} \cdot \frac{\sin \frac{\Delta\theta}{2}}{\cos \gamma_f}$$

$$\frac{\Delta V_1}{V_{c1}} = \sqrt{2 - \frac{2 - \left(\frac{V_0}{V_{c1}}\right)^2}{\frac{r}{r_0}}}$$

$$\frac{\Delta V_2}{V_{c1}} = \left\{ \left[\sin \Delta\theta - 2\left(\frac{V_0}{V_{c1}}\right) \cos \gamma_f \right. \right.$$

$$(\sin^2 \Delta\theta - \sin^2 \ell\,)^{1/2}$$

$$\left. + \left(\frac{V_0}{V_{c1}}\right)^2 \sin \Delta\theta \right] \left[\left(\frac{r}{r_0}\right) \cdot \sin \Delta\theta \right]^{-1} \Bigg\}^{1/2}$$

$$\frac{\Delta V_T}{V_{c1}} = \frac{\Delta V_1 + \Delta V_2}{V_{c1}}$$

These equations have also been solved numerically to yield the smallest values of ΔV_T. The results of these studies are shown in Figs. 28, 29 and 30.

As was noted in the discussion of the optimum trajectories, and again in the previous paragraph, these solutions may not in general be the minimum energy transfers. However, in all cases, this solution will belong to the set of relative minima.

2. Minimum Energy Transfers

The preceding discussions present the variational formulation of the general maneuver optimization procedure along with several conclusions derivable therefrom. The solution, while rigorous, does not provide data which would be of general interest due to the fact that a lengthy numerical evaluation is necessary to evaluate each optimum solution. This being the case, numerical data for the special case of transfer between circular orbits was also presented. However, two questions arise in regard to the application of the "rules" for approximate maneuver optimization. These questions are:

(1) Under what condition is the two-pulse transfer between circular orbits minimum energy?

(2) What is the minimum energy two-impulse transfer between circular and elliptic orbits?

To answer the first of these questions consider the three-impulse maneuver.

a. Three-pulse transfers between circular orbits

Some of the orbits which have been proposed for various satellite missions require large amounts of energy for the ascent and injection maneuvers because of their extreme altitudes. Thus the three-impulse maneuver philosophy can be divided into three classes:

$$r_2 \geq r_3 > r_1$$

$$r_3 \geq r_2 \geq r_1$$

$$r_3 > r_1 \geq r_2$$

where

r_1 = radius of the initial circular orbit

r_2 = apogee radius of the first transfer orbit (the intermediate radius)

r_3 = radius of the final circular orbit.

The transfers have all been assumed to be of the 180° type since any other transfer would require more energy, and since the primary purpose of this material is to show the existence of three impulse optimum solutions.

Case No. 1 ($r_2 > r_3 > r_1$)

The velocity increment required for this case is defined by the difference in the circular velocity and the perigee velocity for the first transfer orbit, plus the difference in the apogee velocity in the first and second transfer orbits, plus the difference in the perigee velocity in the second transfer orbit and the circular velocity in the desired orbit; i.e.,

$$\Delta V_t = |\Delta V_1| + |\Delta V_2| + |\Delta V_3|$$

$$= (V_{p1} - V_{c1}) + (V_{a2} - V_{a1}) + (V_{p2} - V_{c3})$$

$$\frac{\Delta V_t}{V_{c1}} = \left[\sqrt{\frac{2r_2}{r_2 + r_1}} - 1\right] + \frac{V_{c2}}{V_{c1}}\left[\sqrt{\frac{2r_3}{r_2 + r_3}} - \sqrt{\frac{2r_1}{r_2 + r_1}}\right] + \frac{V_{c3}}{V_{c1}}\left[\sqrt{\frac{2r_2}{r_2 + r_3}} - 1\right]$$

This equation is presented graphically in Fig. 31. The dashed curve denotes the Hohmann transfer. Curves for all r_3/r_1 originate at this single curve since it is, in essence, the limit of the family (i.e., $r_1 = r_3$). The investigation must now be turned to the problem of determining whether or not any of the curves of this family eventually diminish by an amount sufficient to result in a value of $\frac{\Delta V_t}{V_{c1}}$ less than that of the Hohmann transfer; (data for this type of transfer are presented as Fig. 32).

This has been accomplished in Ref. 13, where the equation for $\frac{\Delta V_t}{V_{c1}}$ is differentiated with respect to r_2/r_1 and the resultant equated to zero. The complete solution thus found is:

$$\frac{r_2}{r_1} = \frac{3 + \frac{r_1}{r_3}}{3\left(1 + \frac{r_1}{r_3}\right) - 2\sqrt{3 - \frac{2r_1}{r_3}}}$$

Now by using the constraint $\frac{r_2}{r_1} \geq \frac{r_3}{r_1} > 1$, which is a restatement of the condition assumed in formulating this case, the value of, $\frac{r_3}{r_1}$, i.e., $\frac{r_3^*}{r_1}$ for which the three-pulse approach is more efficient is obtained as 15.582 approximately.

For all $\frac{r_3}{r_1} \geq \frac{r_3^*}{r_1}$, the curves possess no relative maxima or minima and the curves continually decrease. Therefore, the three-pulse method is always more efficient than the Hohmann transfer. If $11.939 < \frac{r_3}{r_1} < \frac{r_3^*}{r_1}$, the solution for those values of $\frac{r_3}{r_1}$ for which $\frac{\Delta V_t}{V_{c1}}$ is less than that for the Hohmann transfer can also be found. However, this value of $\frac{r_3}{r_1}$ is a function of the altitude of the intermediate point which must be placed above a critical altitude greater than the altitude of either of the circular orbits and approaching infinity as $\frac{r_3}{r_1}$ approaches 11.939. If $\frac{r_3}{r_1} < 11.939$, the Hohmann two-pulse transfer is always the more economical approach.

Case No. 2 ($r_3 \geq r_2 \geq r_1$)

The velocity increment required for this case is defined by the difference in circular velocity at the first altitude and the perigee velocity of the first transfer orbit, plus the difference in the apogee velocity of the first transfer orbit and the perigee velocity of the second, plus the difference in the apogee velocity of the second transfer orbit and the circular velocity of the second circular orbit.

$$\frac{\Delta V_t}{V_{c1}} = \left[\sqrt{\frac{2r_2}{r_1 + r_2}} - 1\right] + \frac{V_{c1}}{V_{c2}}\left[\sqrt{\frac{2r_3}{r_2 + r_3}} - \sqrt{\frac{2r_1}{r_1 + r_2}}\right] + \frac{V_{c3}}{V_{c1}}\left[1 - \sqrt{\frac{2r_2}{r_3 + r_2}}\right]$$

When this equation is differentiated with respect to the radius ratio $\frac{r_2}{r_1}$, it can once again be shown that the quantity $\frac{\Delta V_t}{V_{c1}}$ is a single zero derivative which for this case corresponds to a maximum. Further it can be shown that the end points of the curve correspond to the energy requirement for the Hohmann transfer; therefore, this mode of transfer is always less economical than the Hohmann transfer.

Case No. 3 ($r_3 > r_1 \geq r_2$)

The velocity increment required for this case is defined by the difference in the circular velocity of the first orbit and the apogee velocity of the first transfer orbit, plus the difference in the perigee velocity in the second and first transfer orbits, plus the difference in the circular velocity in the final orbit and the apogee velocity of the second transfer orbit; i.e.,

$$\frac{\Delta V_t}{V_{c1}} = \left[1 - \sqrt{\frac{2r_2}{r_1 + r_2}}\right] + \frac{V_{c2}}{V_{c1}} \left[\sqrt{\frac{2r_3}{r_3 + r_2}} - \sqrt{\frac{2r_1}{r_1 + r_2}}\right] + \frac{V_{c3}}{V_{c1}} \left[1 - \sqrt{\frac{2r_2}{r_3 + r_2}}\right]$$

The curves obtained from this equation increase for all $r_2 < r_1$ and have no maximum value. Thus, this approach can never be as efficient as the Hohmann transfer.

b. The two-pulse transfer between coplanar, circular and elliptic orbits

This problem has been formulated in Refs. 14, 15 and 16 and, therefore, will only be summarized in this presentation. Detailed proofs of each step in the formulation are left to the reader.

The problem is that of transferring from one terminal (defined by a scalar distance and a velocity vector) to another. If V_{n1} and V_{r1} are the normal and radial components of velocity at the first position and V_{n2} and V_{r2} the components at the second point, the total velocity pulse required for the transfer (assuming two pulses) is

$$\Delta V = \sqrt{(V_{no} - V_{n1})^2 + (V_{ro} - V_{r1})^2} + \sqrt{(V_{nx} - V_{n2})^2 + (V_{rx} - V_{r2})^2}$$

where

V_{ro}, V_{no} denote velocity components following first pulse (that is, at burnout)

V_{rx}, V_{nx} denote velocity components just prior to second pulse.

Now assuming a conservative field, this equation can be reduced to nondimensional form by using the conservation of angular momentum

$$\frac{\Delta V}{V_{c1}} = \sqrt{\left(\frac{V_{no}}{V_{c1}} - \frac{V_{n1}}{V_{c1}}\right)^2 + \left(\frac{V_{ro}}{V_{c1}} - \frac{V_{r1}}{V_{c1}}\right)^2} + \sqrt{\left(\frac{r_1}{r_2}\frac{V_{no}}{V_{c1}} - \frac{V_{n2}}{V_{c1}}\right)^2 + \left(\frac{V_{rx}}{V_{c1}} - \frac{V_{r2}}{V_{c1}}\right)^2}$$

where

V_{c1} = circular speed at the distance r_1

r_1, r_2 = radial distances for the two terminals.

The problem is now to minimize this quantity under the constraint that the radial velocities are always real, i.e.,

$$\left(1 - \frac{r_1^2}{r_2^2}\right)\left(\frac{V_{no}}{V_{c1}}\right)^2 + \left(\frac{V_{ro}}{V_{c1}}\right)^2 + \left(\frac{r_1}{r_2} - 1\right) \geq 0$$

(This is a restatement of the conservation of total energy)

where

$$0 < \frac{r_1}{r_2} < 1.$$

This minimization is accomplished as follows since in the region of interest the function is differentiable.

$$\frac{\partial\left(\frac{\Delta V}{V_{c1}}\right)}{\partial\left(\frac{V_{ro}}{V_{c1}}\right)} = \frac{\partial\left(\frac{\Delta V}{V_{c1}}\right)}{\partial\left(\frac{V_{no}}{V_{c1}}\right)} = 0$$

Justification for this step is shown in Ref. 15 when the function $\frac{\Delta V}{V_{c1}}$ is shown to have a relative minimum interior to the limits which $\frac{V_{rx}}{V_{c1}}$ can assume, $\left(\text{i.e., } 0 < \frac{V_{rx}}{V_{c1}} < \frac{V_{r2}}{V_{c1}}\right)$. Performing this differentiation and simplifying the resultant equations leads to the conclusion that $\left(\frac{\Delta V}{V_{c1}}\right)_{\min}$ must be compatible with one of the following equations

$$\frac{r_1}{r_2}\frac{V_{no}}{V_{c1}} = \frac{V_{n2}}{V_{c1}}\frac{V_{rx}}{V_{r2}} \pm \left(\frac{V_{rx}}{V_{r2}} - 1\right)\sqrt{\frac{2r_2}{r_2 + r_1}}.$$

After combining terms and using the equations for the partial derivatives obtained previously, four pairs of expressions are obtained

$$\frac{V_{rx} - V_{r2}}{V_{nx} - V_{n2}} = \frac{V_{r2}}{V_{n2} \pm \sqrt{\left(\frac{\mu}{r_1}\right)\frac{2r_2}{r_1 + r_2}}}$$

$$\frac{V_{ro} - V_{r1}}{V_{no} - V_{n1}} = \frac{V_{r1}}{V_{n1} \pm \frac{r_1}{r_2}\sqrt{\left(\frac{\mu}{r_1}\right)\frac{2r_2}{r_1 + r_2}}}$$

When these four equations are divided into two sets both with positive (or negative) radicals and solved for the values of $\frac{V_{no}}{V_{c1}}$ and $\frac{V_{ro}}{V_{c1}}$, four independent solutions are obtained (two for each quadratic equation). The smallest of the four solutions is then the minimum energy (two-pulse) maneuver between the two terminals. This is the basic approach and the solution to the problem first formulated in Ref. 14. In general, it is not possible to select the correct solution analytically; however, in particular cases this selection is possible.

Investigation of these equations is now directed toward the definition of the type of transfer which is most efficient. First, it is obvious that unless the relative radial velocity approaches zero at a given terminal, the condition defined is not one of tangential transfer from the circular orbit or arrival at apogee or perigee in the elliptic orbit. Additional investigations reveal that for nonintersecting circular and elliptic orbits, the optimum path is tangent to the circular orbit but is not, in general, tangent to the elliptic orbit. This fact is illustrated in the following sketch. Numerical studies of the parameters of the optimum path must, of course, be deferred until such time as the orbits in question are completely specified.

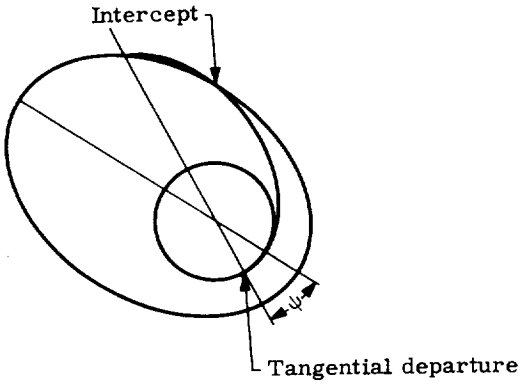

J. THE EFFECTS OF FINITE BURNING TIME

The simplest means of evaluating the effects of burning time on a maneuver in space is to study the numerical simulation of a maneuver, that is, to program a set of equations which describes a maneuver and compare the results to those predicted by an impulsive analysis. This approach, however, is somewhat restrictive because:

(1) The results of the analysis are valid only in the neighborhood of the maneuvers which were simulated.

(2) The results are strongly dependent upon the manner in which the thrust vector is controlled to yield the desired maneuver.

(3) Unless large numbers of simulations are made it is quite possible to overlook the effects of particular variables and trends in the results.

For these reasons, the approach taken here will be to present an analytic approximation to the equations of powered motion which will yield the desired information in a form which exhibits the necessary functional relationships. Consider the following sketch.

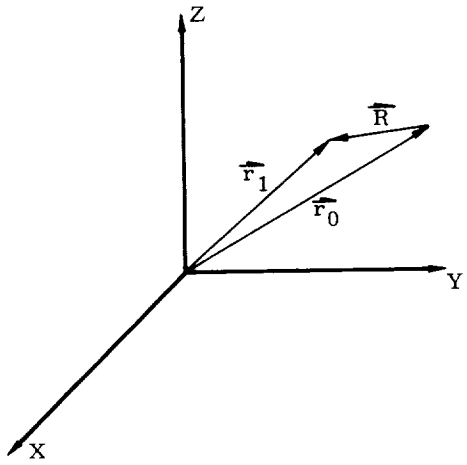

$$\vec{R} = \vec{r}_1 - \vec{r}_0$$

$$\ddot{\vec{R}} = \vec{a}_T + \ddot{\vec{r}}_1 - \ddot{\vec{r}}_0$$

where $\vec{a}_T$ = the thrust acceleration and where the acceleration due to the mutual attraction of the vehicles and the differences in the perturbation accelerations have been neglected. But the radial acceleration vector $\ddot{\vec{r}}_1$ can be developed in terms of r_0 to be

$$\ddot{\vec{r}}_1 = \ddot{\vec{r}}_0 + (\vec{R} \cdot \vec{\nabla})\, \ddot{\vec{r}}_0 + \ldots$$

where

$\ddot{\vec{r}}_0$ = acceleration due to the central force

$$\ddot{\vec{R}} = \vec{a}_T + (\vec{R} \cdot \vec{\nabla})\, \ddot{\vec{r}}_0$$

But

$$\ddot{\vec{r}}_0 = -\frac{\mu}{r_3}\, \vec{r}_0$$

Thus

$$\ddot{\vec{R}} = \vec{a}_T - \frac{\mu}{r_0^2}\left[\frac{\vec{R}}{r_0} - \frac{3\,\vec{r}_0\,(\vec{R} \cdot \vec{r}_0)}{r_0^3}\right]$$

Thus, for motion in a nearly circular orbit the small displacements from the unperturbed position are:

$$\ddot{x} = 3\omega^2 x + 2\omega \dot{y} + a_x \qquad \text{(along radius)}$$

$$\ddot{y} = -2\omega \dot{x} + a_y \qquad \text{(along velocity of origin)}$$

$$\ddot{z} = -\omega^2 z + a_z \qquad \text{(normal to plane)}$$

where ω is the angular rate of the origin about the earth $= \sqrt{\frac{\mu}{r_0^3}}$. Now, following the method of Darby (Ref 17), assume that the thrust is applied as a series of small impulses of magnitude

$$\Delta V = a \Delta T$$

Thus each of the equations listed above can be considered to be unperturbed for a time (i.e., the thrust acceleration is zero) then at a small time later the velocity is changed and the process repeated. Consider the equation for Z.

$$\ddot{z} + \omega^2 z = 0$$

$$z = A \sin \omega (t - T) \qquad t_1 < t < t_2$$

$$\dot{z} = \omega A \cos \omega (t - T)$$

$$= B \cos \omega (t - T)$$

$$\dot{z}_1 = (B + a_z T) \cos \omega (t - T) \qquad t_2 < t < t_3$$

$$d\dot{z} = \lim_{\Delta t_0 \to 0} (\dot{z}_1 - \dot{z}) = a_z \cos \omega (t - T)\, dT$$

Thus

$$\dot{z} = \int_0^t a_z \cos \omega (t - T)\, dT_0$$

$$z = \frac{1}{\omega} \int_0^t a_z \sin \omega (t - T)\, dT$$

and similarly

$$y = \int_0^t a_y \left[\frac{4}{\omega} \sin \omega (t - T) - 3(t - T)\right] dT$$

$$- \frac{2}{\omega} \int_0^t a_x \left[1 - \cos \omega (t - T)\right] dT$$

$$\dot{y} = \int_0^t a_y \left[4 \cos \omega (t - T) - 3\right] dT$$

$$- 2 \int_0^t a_x \left[\sin \omega (t - T)\right] dT$$

$$x = \frac{1}{\omega} \int_0^t a_x \sin \omega (t - T)\, dT$$

$$+ \frac{2}{\omega} \int_0^t a_y \left[1 - \cos \omega (t - T)\right] dT$$

$$\dot{x} = \int_0^t a_x \cos \omega (t - T)\, dT$$

$$+ 2 \int_0^t a_y \sin \omega (t - T)\, dT$$

At this point the solution is no further progressed than would have resulted if the functions x, y, z, $\dot{x}$ and $\dot{z}$ had been expressed as inverse Laplace transforms since the time history of a_x, a_y and a_z has not been specified. However, if it is assumed that once firing is initiated the direction of the thrust vector is unaltered, then, the acceleration will vary with time according to

$$a(t) = \frac{a(0)}{1 - \dot{m} T}$$

where: $\dot{m}$ is the % change in mass, i.e., $\frac{1}{m_0} \frac{dm}{dt}$

At this point the terms $\cos \omega (t - T)$ and $\sin \omega (t - T)$ can be expanded in a power series to yield

$$\cos \omega (t - T) = 1 - \frac{\omega^2 (t - T)^2}{2} + \omega^4 \frac{(t - T)^4}{24} - \cdots$$

$$\sin \omega (t - T) = \omega (t - T) - \omega^3 \frac{(t - T)^3}{6} + \cdots$$

Thus, since ω is a constant, the solution evolves into the evaluation of integrals of the form

$$\int_0^t \frac{(t - T)^n}{1 - \dot{m} T}\, dT \qquad n = 1, 2, 3, 4, \cdots$$

If only two terms of each expansion are retained (i.e., $n < 4$) the results of Darby can be obtained as:

$$\int_0^t \frac{(t - T)}{1 - \dot{m} T}\, dT = \frac{1}{\dot{m}^2} \left[\dot{m}t - (1 - \dot{m}t) \ln \frac{1}{1 - \dot{m}t}\right]$$

$$= \frac{A}{\dot{m}^2}$$

$$\int_0^t \frac{(t - T)^2}{1 - \dot{m} T}\, dT = \frac{1}{\dot{m}^3} \left[(1 - \dot{m}t)^2 \ln \frac{1}{1 - \dot{m}t} - \dot{m}t + \frac{3}{2} (\dot{m}t)^2\right] = \frac{B}{\dot{m}^3}$$

$$\int_0^t \frac{(t - T)^3}{1 - \dot{m}T}\, dT = \frac{1}{\dot{m}^4} \left[(1 - \dot{m}t)^3 \ln \frac{1}{1 - \dot{m}t} - \dot{m}t + \frac{5}{2} (\dot{m}t)^2 - \frac{11}{6} (\dot{m}t)^3\right] = \frac{C}{\dot{m}^4}$$

$$\int_0^t \frac{(t - T)^4}{1 - \dot{m}T}\, dT = \frac{1}{\dot{m}^5} \left[(1 - \dot{m}t)^4 \ln \frac{1}{1 - \dot{m}t} - \dot{m}t + \frac{7}{2} (\dot{m}t)^2 - \frac{13}{3} (\dot{m}t)^3 + \frac{25}{12} (\dot{m}t)^4\right] = \frac{D}{\dot{m}^5}$$

and

$$x = \frac{a_{x0}}{\dot{m}^2} \left(A - \frac{\omega^2}{6 \dot{m}^2} C\right) + \frac{a_{y0}\, \omega}{\dot{m}^3} \left(B - \frac{\omega^2}{12 \dot{m}^2} D\right)$$

$$y = \frac{a_{y0}}{\dot{m}^2}\left(A - \frac{2\omega^2}{3\dot{m}^2}C\right) - \frac{a_{x0}\,\omega}{\dot{m}^3}\left(B - \frac{\omega^2}{12\dot{m}^2}D\right)$$

$$z = \frac{a_{z0}}{\dot{m}^2}\left(A - \frac{\omega^2}{6\dot{m}^2}\right)$$

$$\dot{x} = \frac{a_{x0}}{\dot{m}}\left(\ln\frac{1}{1-\dot{m}t} - \frac{\omega^2}{2\dot{m}^2}B\right) + \frac{2\,a_{y0}\,\omega}{\dot{m}^2}\left(A - \frac{\omega^2}{6\dot{m}^2}C\right)$$

$$\dot{y} = \frac{a_{y0}}{\dot{m}}\left(\ln\frac{1}{1-\dot{m}t} - \frac{2\omega^2}{\dot{m}^2}B\right) - \frac{2\,a_{x0}\,\omega}{\dot{m}^2}\left(A - \frac{\omega^2}{6\dot{m}^2}C\right)$$

$$\dot{z} = \frac{a_{z0}}{\dot{m}}\left(\ln\frac{1}{1-\dot{m}t} - \frac{\omega^2}{2\dot{m}^2}B\right)$$

As is done in Chapter VII (Rendezvous), the set of definitions for A, B, C and D can be simplified for the case where $\dot{m}t_{max}$ (or $\dot{m}t_b$) is small compared to 1, for then

$$\ln\frac{1}{1-\dot{m}t} = -\ln(1-\dot{m}t) = \dot{m}t + \frac{(\dot{m}t)^2}{2} + \frac{(\dot{m}t)^3}{3} + \cdots$$

Thus

$$A = \dot{m}t - (1-\dot{m}t)\left[\dot{m}t + \frac{(\dot{m}t)^2}{2} + \frac{(\dot{m}t)^3}{3} + \cdots\right] = \frac{(\dot{m}t)^2}{2}\left[1 + \frac{\dot{m}t}{3} + \frac{(\dot{m}t)^2}{6} + \frac{(\dot{m}t)^3}{10} + \cdots\right]$$

$$B = \frac{(\dot{m}t)^3}{3}\left[1 + \frac{\dot{m}t}{4} + \frac{(\dot{m}t)^2}{10} + \frac{(\dot{m}t)^3}{20} + \cdots\right]$$

$$C = \frac{(\dot{m}t)^4}{4}\left[1 + \frac{\dot{m}t}{5} + \frac{(\dot{m}t)^2}{15} + \frac{(\dot{m}t)^3}{35} + \cdots\right]$$

$$D = \frac{(\dot{m}t)^5}{5}\left[1 + \frac{\dot{m}t}{6} + \frac{(\dot{m}t)^2}{21} + \frac{(\dot{m}t)^3}{56} + \cdots\right]$$

Now since the motion of the origin of the relative coordinates is known to move in a circle, the position and velocity of the vehicle are known as a function of time. In particular, they are known at the end of burning. Thus, the effects of the burning can be computed by comparing the position and velocity vectors at this time with those that would have resulted at the same time if the maneuver had been impulsive. It is further possible to determine the effect on the six orbital elements since the position and velocity at the end of burning determine these constants uniquely via the equations of Chapter III.

The accuracy of this solution is limited or restricted by four assumptions.

(1) The locus of the origin of coordinates was assumed circular. This assumption can of course be violated if the interval of burning is known by using the average velocity corresponding to that interval and correcting for the radial motion of the origin. The resultant accuracy will of course deteriorate.

(2) The vehicle is assumed to be at the origin with zero velocity at time = 0. Should these conditions not be satisfied, however, suitable constants can be introduced via the medium of the Laplace transform. A similar solution employing nonzero initial boundary conditions is illustrated in Chapter VII (Rendezvous).

(3) Only first-order terms were carried in the expansion of $\vec{r}_1 - \vec{r}_0$. This assumption effectively limits the allowable deviation of the vehicle from the origin of coordinates. Although no analysis of this restriction will be made here, it is noted that for single thrust periods of no more than approximately 2 to 4% of the orbital period and accelerations no larger than 1 g, the total displacements will be no more than 10^6 ft or 0.3×10^6 m. For such displacements the accuracy of the method is still adequate for hand computations of first-order effects.

(4) Higher order terms in $\dot{m}t$ were neglected in the series for A, B, C and D. This assumption is generally not serious due to the rapid convergence of the series for most values of this parameter. However, should this convergence problem be such that additional terms would not resolve the difficulty, the original definition of these constants could be utilized at the expense of simplicity in the form.

Because of the manner in which the variables are related and the large number of ways which can be used to assess the effects of finite burning times, parametric data based on these solutions will not be provided. Rather it is suggested that the computations be made as outlined and that the results be compared to the unperturbed solution utilizing the equations of Chapter III or the differential expression relating elemental errors to position and velocity errors of Chapter VII.

Reference 17 does, however, present a set of figures which relate to the time interval necessary to "anticipate" a maneuver (or lead time) and the difference in the magnitude of the ideal and actual velocity increments as functions of specific impulse, acceleration level, azimuth and flight path angle. Because of the interest in these results they are included.

Figures 33 and 34 show the approximately linear manner in which the lead time varies with both acceleration level and specific impulse. In

both cases the curvature is the result of mass changes and is less noticeable for the small maneuvers.

Figures 35 and 36 show the effects of finite burning time on the magnitude of the velocity increment. These figures show the importance of consideration of these effects in any computations beyond those of a preliminary nature.

Though not shown in figures, several trends can also be noted.

(1) Finite burning times tend to result in a smaller value of eccentricity for a given mass fraction due largely to the fact that work is generally done against gravity forces.

(2) These times tend to produce perigee radii which are greater than their impulse counterparts.

(3) The change in inclination of the plane will tend to be larger for the finite burning time case than for the impulse case.

K. IN-ORBIT PROPULSION SYSTEM

1. Propulsion System Requirements

Each of the maneuvers to be performed in orbit (including injection into the various transfer orbits) requires the application of corrective impulses. The control of these impulses is the determining factor in the evaluation of the utility of the satellite in performing the particular function. In the navigation problem, the control tolerances are specified (based upon some maximum allowable drift rate for the satellites with respect to each other) and the subsystem requirements remain to be evaluated. In order to provide insight into these problems, the following analysis of two different types of propulsion control techniques has been made. These techniques are:

(1) Monitored propulsive inputs.

(2) Monitored velocity increment.

The first of these techniques attempts to control or at least compensate for variations in each of the parameters contributing to the velocity increment. Therefore, errors in each of the parameters will be reflected directly in an error in the velocity pulse. These effects may be evaluated from the following equation (where the loss due to finite burning time is neglected):

$$\Delta V = -g_0 I_{sp} \ln (1 - \zeta) \tag{249}$$

$$\delta(\Delta V) = \frac{\partial(\Delta V)}{\partial t_b} \Delta t_b + \frac{\partial(\Delta V)}{\partial \dot{w}_p} \Delta \dot{w}_p + \frac{\partial(\Delta V)}{\partial I_{sp}} \Delta I_{sp} + \frac{\partial(\Delta V)}{\partial W_0} \Delta W_0$$

$$= \frac{g_0 I_{sp} \zeta}{1 - \zeta} \left[\frac{\Delta t_b}{t_b} + \frac{\Delta \dot{w}_p}{\dot{w}_p} - \zeta (1 - \zeta) \ln (1 - \zeta) - \frac{\Delta W_0}{W_0} \right] \tag{250}$$

$$= \frac{(T/W_0) g_0 \Delta t_b}{1 - \zeta} + \frac{g_0 I_{sp} \zeta}{1 - \zeta} \frac{\Delta \dot{w}_p}{\dot{w}_p} + \zeta^2 \Delta V \frac{\Delta I_{sp}}{I_{sp}} - \frac{g_0 I_{sp} \zeta}{1 - \zeta} \frac{\Delta W_0}{W_0}$$

This equation may be reduced to a more simple form by employing data which is representative of current technology for each of the control parameters. These data are:

$$\Delta t_b \approx 0.030 \text{ sec}$$

$$\Delta \dot{w}_p \approx 0.005 \dot{w}_p$$

$$\frac{\Delta I_{sp}}{I_{sp}} \approx 1/260$$

Thus, for a specific impulse of 300 sec:

$$\delta(\Delta V) = \frac{0.966 \, T/W_0}{1 - \zeta} + \frac{0.161 \, I_{sp} \zeta}{1 - \zeta} + \frac{\zeta^2 \Delta V}{260} - \frac{g_0 I_{sp} \zeta}{1 - \zeta} \left(\sum_{i=1}^{n} \frac{t_{b_i} \Delta \dot{w}_{p_i} + \dot{w}_{p_i} \Delta t_{b_i}}{W_{0_i}} + \frac{\Delta W_0}{W_0} \right) \tag{251}$$

where ΔW_0 is the initial error in the weight of the vehicle. The last group of terms in this equation (the summation) is small compared to the other three for small or even moderately large increments; therefore, it may be neglected. The maximum magnitude of the remaining terms is presented in Fig. 37 as a function of the initial thrust-to-weight ratio. As may be noted from this figure, a system of this type would have difficulty in satisfying extreme accuracy requirements since to limit a maximum error in the velocity increment to less than 0.5 fps appears difficult.

If the velocity increment itself is monitored by integrating the acceleration due to thrust, the maximum error in the increment is a function only of the error in the time of burning and that in the integration itself. Assuming that the integrated accelerometers are accurate to 1 part in 10^5 g (which is the expected accuracy of future integrating accelerometers), the error in the integrated acceleration should be accurate to approximately 1 part in 10^4. Thus, the maximum error is

$$\delta(\Delta V) = \frac{\Delta V}{10^4} + \frac{0.966 \, T/W_0}{1 - \zeta} \tag{252}$$

This equation has also been plotted and appears as Fig. 38a. This figure shows that with control

parameters as quoted the error in the velocity pulse can be controlled to well within 0.5 fps for thrust-weight ratios as high as 0.4 ($\Delta V < 100$ fps). Thus, the precision required for small corrections can be obtained with this system. Since the error plotted in this figure is the maximum expected, this figure implies that the error will generally be negligible. Figure 38b shows the effect of reducing the error in the shutdown time on the resultant velocity error. The parameter in this figure ($\Delta t_b \frac{T}{W_0}$) is immediately recognizable as the error in the total impulse.

2. Selection of Thrust Level and Propellants

While the detailed design of a propulsion system is obviously beyond the scope of an effort of this type, the general sizing and capabilities of such a system can be established.

As shown in Eq (252), if the velocity increment is to be controlled within 0.1 fps for increments of less than 500 fps, the ratio of the error in the impulse to the initial weight must be

$$\frac{T\Delta t_b}{W_0} \leq \left[\delta(\Delta V) - \frac{\Delta V}{10^4}\right] \frac{1-\zeta}{g_0}$$

$$\leq \frac{0.05\,(1-\zeta)}{g} \approx \frac{0.05}{g_0} \cdot \left[1 - \frac{\Delta V}{g_0 I_{sp}}\right]$$

$$\leq 0.0015 \text{ (for } I_{sp} = 300 \text{ sec)}$$

From this it may be seen that (for reasonable errors in the shutdown time, say 0.05 sec) the thrust-to-initial-weight ratio should be ≤ 0.03. It should be noted, however, that the thrust levels should not be extremely low because of the assumption made in the formulation of the corrective maneuvers. For these reasons, an initial thrust-to-weight ratio of say 0.01 should be selected. If this ratio were maintained constant, the thrust for successive corrections would have to decrease according to the following equation.

$$T = 0.01 \left[W_0 - \sum_{i=1}^{m} \dot{w}_p t_{bi}\right]$$

However, since the vehicles in orbit will possess fuel fractions of less than 2/3 in order to assure reasonable payload capabilities, the thrust-to-initial-weight ratio for each correction will always be > 0.03 which is the allowable upper limit. Thus, no provision for thrust variation is necessary.

With thrust level thus established, the remaining propulsion parameters can be evaluated once the propellant characteristics are known. This requires the selection of a propellant or propellant combination capable of performing as required. These considerations are beyond the scope of the present effort and will not be discussed.

The second step in the analysis of the propulsion system is the sizing of the rocket motor and nozzle. This will be accomplished through the utilization of the theoretical relationships developed in gas dynamics and the experimental propulsion systems data available.

The first assumption concerning the motor which must be made pertains to the expansion ratio which is feasible for the nozzle of a motor operating in a vacuum. From this ratio and the average value of the ratio of specific heats for the products of combustion, it is possible to determine the pressure ratio across the nozzle.

$$\frac{p_e}{p_c}\sqrt{1 - \left(\frac{p_e}{p_c}\right)^{\frac{\gamma-1}{\gamma}}} = \frac{A_T}{A_e}\left(\frac{2}{\gamma+1}\right)^{1/\gamma-1}\sqrt{\frac{\gamma-1}{\gamma+1}} \qquad (253)$$

where γ is the average value of the ratio of specific heats of the products of combustion. This equation is of the form

$$\left(\frac{p_e}{p_c}\right)^2 - \left(\frac{p_e}{p_c}\right)^{\frac{3\gamma-1}{\gamma}} - C = 0$$

The simplest solution to this equation is by iteration. Newton's method will be utilized because of convergence

$$X_{n+1} = X_n - \frac{f(X_n)}{f'(X_n)}$$

where, for this solution, X_n is the nth estimate of p_e/p_c. This solution results in the following equation

$$X_{n+1} = X_n - \frac{X_n^2 - X_n^{\frac{3\gamma-1}{\gamma}} - C}{2X_n - \frac{3\gamma-1}{\gamma} X_n^{\frac{2\gamma-1}{\gamma}}}$$

If p_e/p_c is assumed to be $\ll 1$, the first trial of p_e/p_c should be approximately the square root of C.

From this point, it is possible to establish the theoretical thrust coefficient of a gas with the given value of the ratio of specific heats.

$$C_F = \sqrt{\gamma^2 \frac{2}{\gamma-1}\sqrt{\left(\frac{2}{\gamma+1}\right)^{\frac{\gamma+1}{\gamma-1}}\left(1 - \frac{P_e}{P_c}\right)^{\frac{\gamma-1}{\gamma}}}} + \frac{p_e}{p_c}\frac{A_e}{A_i} \qquad (254)$$

Now from the definition of the thrust coefficient

$$C_F = T/A_t P_c$$

it is possible to size the nozzle for any selected chamber pressure. First, however, it should be noted that the theoretical thrust coefficients are approximately 5% higher than indicated from experimental data, thus a better estimate of these areas should account for this discrepancy.

The length of the nozzle may be obtained once the equivalent value of the half angle of divergence has been selected. Care must be exercised in this selection to assure that the flow doesn't separate from the nozzle, and that the nozzle is not excessively long. The length is then obtained as follows:

$$A_e - A_t = \pi \left(r_e^2 - r_t^2 \right) = A_t \left[\left(\frac{r_e}{r_t} \right)^2 - 1 \right]$$

but

$$r_e = r_t + L \tan \alpha$$

thus

$$A_e - A_t = A_t \left[\left(1 + \frac{L}{r_t} \tan \alpha \right)^2 - 1 \right]$$

$$L = \frac{\left(\sqrt{\frac{A_e}{A_t}} - 1 \right) \sqrt{A_t}}{\sqrt{\pi} \tan \alpha} \qquad (255)$$

These data define the general size of the nozzle; however, due to the fact that the optimum nozzle is not conical but rather more nearly a segment of a paraboloid of revolution, they do not define the optimum geometry. This refinement, however, is not deemed necessary due to the fact that the thrust levels are small.

4. Combustion Chamber Sizing

The combustion chamber to be fitted to the nozzle, which has been described in terms of the design parameters utilized, must now be investigated. This may be done through the investigation of an additional parameter, the characteristic chamber length (L*). This parameter, which affects the cycle efficiency, is defined as the ratio of the chamber volume to the nozzle throat area and is a function of the oxidizer-to-fuel weight ratio of the propellants utilized. Experimental data must be utilized for this determination. One such curve is presented in Fig. 39. The curve presented here is an average value curve since the data available were for slightly different propellant combinations operating in different test facilities under different pressures. Nonetheless, these data are sufficient to indicate a characteristic chamber length of approximately 100 in. or greater is recommendable. Similar data for any other propellant combination thus yield the chamber volumes:

$$V_c \approx L^* A_t$$

Before the motor can be sized, however, the geometry of the combustion chamber must be specified as either cylindrical or spherical.

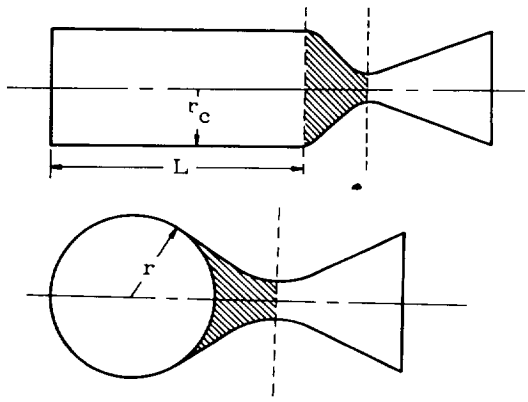

The former is particularly well suited for small motors since production is greatly simplified; the latter is a better design for larger motors due principally to the fact that the surface area exposed for heat transfer within the chamber is minimized for a given volume. Both of these chambers may be defined when a restriction is placed on the ratio of the chamber-to-throat area ratio of the cylindrical motor. This may in turn be accomplished by investigating the pressure drop through the chamber.

$$\frac{P_{inj}}{P_1} = \frac{1 + \gamma M_1^2}{1 + \gamma M_{inj}^2} \qquad (256)$$

where the point 1 is a section passing through the nozzle throat.

$$\frac{P_T}{P_S} = \left[1 + \frac{\gamma - 1}{2} M^2 \right]^{\frac{\gamma}{\gamma - 1}} \qquad (257)$$

Thus

$$\frac{P_{T\,inj}}{P_{T_1}} = \left[\frac{1 + \gamma M_1^2}{1 + \gamma M_{inj}^2} \right] \left[\frac{1 + \frac{\gamma - 1}{2} M_{inj}^2}{1 + \frac{\gamma - 1}{2} M_1^2} \right]^{\frac{\gamma}{\gamma - 1}}$$

If now M_{inj}^2 is small compared to M_1^2.

$$\frac{P_{T\,inj}}{P_{T_1}} = \frac{1 + \gamma M_1^2}{\left(1 + \frac{\gamma - 1}{2} M_1^2 \right)^{\frac{\gamma}{\gamma - 1}}}$$

This is also the ratio of the total pressure at the throat of an ideal motor to that of a tubular motor. This ratio may be related directly to the chamber-to-throat area ratio from the continuity equation as

$$\frac{A_1}{A_T} = \frac{1}{M_1}\left[\frac{2\left(1+\frac{\gamma-1}{2}M_1^2\right)}{\gamma+1}\right]^{\frac{\gamma+1}{2(\gamma-1)}} \qquad (258)$$

The graphical relationship between the total pressures at the throat for tubular and ideal motors and the chamber-to-throat area ratio can thus be plotted in a figure similar to Fig. 40, and the minimum ratio $\frac{A_c}{A_t}$ assessed. Once this is done, the geometry of the chamber is:

$$V_c = L^* A_t = \frac{4}{3}\pi r^3 \text{ (spherical chamber)}$$

$$= \left(\frac{A_c}{A_t}\right) A_t L \text{ (cylindrical chamber)}$$

Thus

$$L = L^* \frac{A_t}{A_c}$$

Note is made that since, as is shown in Fig. 40, $\frac{A_c}{A_t}$ should be equal to or greater than 3.0 and since this ratio corresponds to an awkward length-to-diameter ratio for the chamber (approximately 30), the length may be selected based on other criteria.

5. Propellant Flow Rates

The propellant flow rates for the range of chamber pressures can be obtained once the variation in specific impulse for a given oxidizer-to-fuel weight ratio is established. A review of the abundance of data available will generally reveal no well defined curve for this variation due to differences in assumptions, fuel properties, etc.; therefore, an average curve such as Fig. 41 must be utilized.

Now

$$\dot{w}_p = T/I_{sp}$$

and

$$\dot{w}_f = \frac{1}{1+r}\dot{w}_p = \frac{1}{1+r}T/I_{sp}$$

$$\dot{w}_o = \frac{r}{1+r}\dot{w}_p = \frac{r}{1+r}T/I_{sp}$$

The propellants may be fed to the motor by any of a number of types of pumps. However, two schemes appear particularly attractive for small thrusts. The first utilizes positive displacement pump (which can be electrically driven), a hydraulic accumulator and a pressure regulator to supply the propellants to the nozzle under a constant pressure. This system can have one significant advantage due to the fact that the utilization of the accumulator makes it possible to employ a very small pump which operates between the corrections to keep the system charged. This possibility results in a reduced peak power requirement and a reduced pump-drive unit weight without increasing the size of the accumulator beyond allowable bounds. However, due to the fact that the unit will be constantly pressurized, the seal between the diaphragm and the propellant will require special attention. The second technique utilizes a small vane-type pump of such size as to make an accumulator unnecessary. The accumulator could be used in this application as it was in the other; however, the positive displacement pump is more efficient for this type of operation. Note should be made at this point that a positive propellant feed system is required to assure flow to the pump in either case.

Pumps of both these types exist in the sizes required though it is probable that special materials would be required because of the corrosive nature of the fluids.

The piston pumps are available in a variety of sizes capable of providing exit pressures up to approximately 3000 psia (20.7×10^6 newtons/m^2 at overall efficiencies varying from 85 to 92% (see sketch) for $500 \leq p \leq 3000$ (3.5 to 20.7×10^6 newtons/m^2).

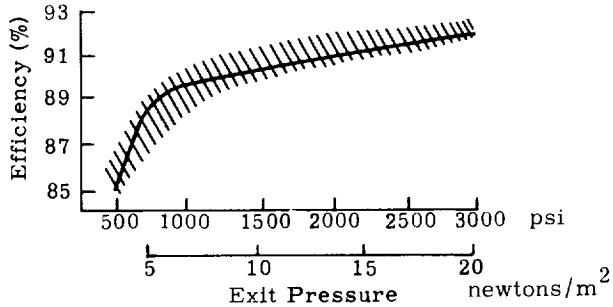

The required power input for these pumps is obtained from the following equations.

$$hp = 0.000583\ (psi)\ (gal/min) =$$

$$\frac{0.00419\ (psi)\ (lb/sec)}{(density)\ (overall\ efficiency)}$$

$$Torque = \frac{(in.^3/rev)\ (psi)}{2}$$

$$rpm = (lb/min) \,/\, (in.^3/rev)\ (lb/in.^3)$$

$$(volumetric\ efficiency)$$

L. MICRO-THRUST STUDY

The purpose of this study is to evaluate the performance and applicability of micro-thrust devices for small corrections in various orbital parameters. For each specific correction maneuver, a definite thrust orientation law (considering thrust magnitude, direction and duration) exists. The analytical expressions derived from the basic laws of celestial mechanics are obtained and their applicability in case of micro-thrust maneuvers investigated. Solutions in closed form are obtained in several cases. Low thrust systems

capable of producing these thrusts are discussed conceptually as well as in detail in the literature. For this reason, such data will not be presented here.

1. Planar Study of Radial Circumferential and Tangential Thrusts

Consider a set of equations of planar motion in polar coordinates. If R is used as the sum of radial accelerations and T as the sum of circumferential accelerations, then

$$\ddot{r} - r\dot{\theta}^2 + \frac{\mu}{r^2} = R$$
$$\frac{1}{r}\frac{d}{dt}\left(r^2\dot{\theta}\right) = T \qquad (259)$$

It is noticed from Eqs (259) that angular momentum is conserved only if there is no component of the tangential thrust applied to the satellite.

Several special cases for thrusting in the two-dimensional micro-thrust problem are discussed in the literature. The most important results of these solutions are summarized below and will serve as an introduction to further discussions.

a. Radial thrust

This problem is treated in Refs. 18 through 20. The outline presented here follows basically Ref. 20.

Equations (259) for the given case become

$$\ddot{r} - r\dot{\theta}^2 + \frac{\mu}{r^2} = R$$
$$r^2\dot{\theta} = \sqrt{\mu p} = \text{constant} \qquad (260)$$

where p is the semiparameter at the instant.

Now introducing nondimensional variables defined in terms of the instantaneous orbital elements.

$R^* = \frac{R}{g_a}$ (acceleration compared to gravity at a)

$r^* = \frac{r}{a}$ (distance in number of semimajor axes)

$t^* = t/\sqrt{a/g_a}$ (time compared to the orbital period)

By these substitutions, the Eqs (260) become (neglecting e^2 terms)

$$\ddot{r}^* - r^*\dot{\theta}^2 + \frac{1}{r^{*2}} = R^*$$
$$r^{*2}\dot{\theta} = 1 \qquad (261)$$

where differentiation is with respect to t*.

Now eliminating $\dot{\theta}$ in Eq (261) yields

$$\ddot{r}^* - \frac{1}{r^{*3}} + \frac{1}{r^{*2}} = R^* \qquad (262)$$

Eq (262) can now be integrated assuming an initially circular orbit at r* = 1 to yield

$$\dot{r}^{*2} = \frac{2}{r^*} - \frac{1}{r^{*2}} + 2R^*(r^* - 1) - 1 \qquad (263)$$

From Eq (263), it is apparent that the radial velocity is zero at the radial distances where

$$2R^* r^{*3} - (2R^* + 1) r^{*2} + 2r^* - 1 = 0 \qquad (264)$$

or

$$r^* = 1$$

and

$$r^* = \frac{1 \pm \sqrt{1 - 8R^*}}{4R^*} \qquad (265)$$

From Eq (265), the fact is seen that the orbit remains bounded for radial accelerations $R^* < \frac{1}{8}$. In the opposite case, $R^* > \frac{1}{8}$, no real roots exist in Eq (265), which indicates that large changes in the planar elements are possible or that escape from the earth's gravitational field may occur if a constant radial acceleration is applied for a sufficiently long time period.

The condition for critical acceleration $R^* = \frac{1}{8}$ implies

$$R = R^* g_a = \frac{1}{8} g_a = \frac{1}{8}\frac{\mu}{a^2} = \frac{1}{8}\left(\frac{r}{a}\right)^2 g$$
$$= \frac{1}{8}\left(\frac{R_0}{a}\right)^2 g_0$$

R_0 = radius of $\oplus$

g_0 = surface gravity.

Since the micro-thrust devices have, in general, a thrust level of 10^{-4} to 10^{-5} g_0, they are obviously not adequate for large orbital changes employing radial thrust applications. Nevertheless, as shown in Ref. 19, such radial micro-thrust can be used effectively to change the eccentricity of an orbit.

If $x_1 > x_2 > x_3$ are the roots of Eq (264), the solutions for a central angle and flight time as functions of the radial distance are:

(1) Radial inward thrust, R* < 0

$$\theta(r^*) = \frac{2\delta}{\gamma\alpha}\left[\frac{\delta}{\beta}\pi\left(\phi, \frac{\alpha}{\beta}, k\right) + cF(\phi, k)\right] + \text{const.} \qquad (266)$$

$$t^*(r^*) = \frac{2\delta}{\gamma}\left[x_3 F(\phi, k) + (x_1 - x_3) E(\phi, k) + \frac{(x_1 - x_2)\sin 2\phi}{2\sqrt{1 - k^2 \sin^2\phi}}\right] + \text{const}$$

where

$$\alpha = -x_3 k^2$$

$$\beta = x_2$$

$$\delta = (x_2 - x_3) k^2$$

$$r^* = \frac{\alpha \sin^2\phi + \beta}{c \sin^2\phi + 1}$$

$$\gamma = (x_2 - x_3) k^2 \sqrt{-2R^* (x_1 - x_3)}$$

$$c = -k^2 = -\frac{x_1 - x_2}{x_1 - x_3}$$

$F(\phi, k)$, $E(\phi, k)$ and $\pi(\phi, \frac{\alpha}{\beta}, k)$ are elliptic integrals of the first, second and third kind.

(2) Radial outward thrust, $0 < R^* < \frac{1}{8}$

$$\theta(r^*) = \frac{2\delta^2}{\gamma\alpha\beta}\pi(\phi, \frac{\alpha}{\beta}, k) + \text{const.}$$

$$t^*(r^*) = \frac{2\delta}{\gamma}\left[x_1 F(\phi, k) - (x_1 - x_3) E(\phi, k)\right] + \text{const.} \quad (267)$$

where

$$\alpha = x_2 - x_3$$

$$\beta = x_3$$

$$r = \alpha \sin^2(\phi + \beta)$$

$$\delta = x_2 - x_3$$

$$\gamma = (x_2 - x_3)\sqrt{2R^*(x_1 - x_3)}$$

$$k^2 = \frac{x_2 - x_3}{x_1 - x_3}$$

$$r^* = \frac{\alpha \sin^2\phi + \beta}{c \sin^2\phi + 1}$$

b. Circumferential thrust

This problem is also solved in Ref. 18, using a series expansion method for large thrust ratios and a simple first order approximation for the very small thrust ratios. For circumferential thrust, the equations of motion corresponding to Eq (261) are

$$\ddot{r}^* - r^* \dot{\theta}^2 + \frac{1}{r^{*2}} = 0$$

$$\frac{d}{dt^*}(r^{*2}\dot{\theta}) = r^* T^* \quad (268)$$

where

$$T^* = T/g_a \quad (269)$$

Eliminating $\dot{\theta}$ from Eqs (268),

$$\frac{d}{dt^*}(r^{*3}\ddot{r}^* + r^*)^{1/2} = r^* T^* \quad (270)$$

for very small accelerations, $r^{*3}\ddot{r}^* << r^*$ and the approximate differential equation is

$$\frac{d}{dt^*} r^{*1/2} = r^* T^* \quad (271)$$

and

$$r^* = \frac{1}{(1 - T^* t^*)^2} \quad (272)$$

which is a good approximation.

c. Tangential thrust

The problem of tangential micro-thrust application is treated in Refs. 21 through 23. It is shown that the mass ratio is slightly smaller for tangential than for circumferential micro-thrust for all but circular orbits. The approximate solution for radius is basically the same as Eq (270), if the first order approximation in T_t^* is considered (T_t = tangential acceleration):

$$r^* \approx \frac{1}{1 - 2 T_t^* \left(\frac{s}{a}\right)} \quad (273)$$

where s = distance traversed by the rocket.

In Ref. 16 the altitude change per revolution is given for the tangential micro-thrust as:

$$\Delta r_{rev} = 4\pi T_t^* r_o \quad (274)$$

and the number of revolutions to reach a certain altitude is

$$n = \frac{1}{8\pi\, T_t^*} \left(\frac{r_o + r_1}{r_1^2} \right) \Delta r \qquad (275)$$

If r_1 tends to infinity, this last equation tends to

$$n_\infty = \frac{1}{8\pi T^*}$$

This equation states that the number of revolutions to escape is inversely proportional to T*. The following sketches obtained from numerical integration exhibit this behavior. Also shown is the fact that the orbit grows in such a manner that most of the revolutions approximate concentric circular orbits. Thus a tangential thrust is a very simple and accurate means of changing the radius of a circular orbit.

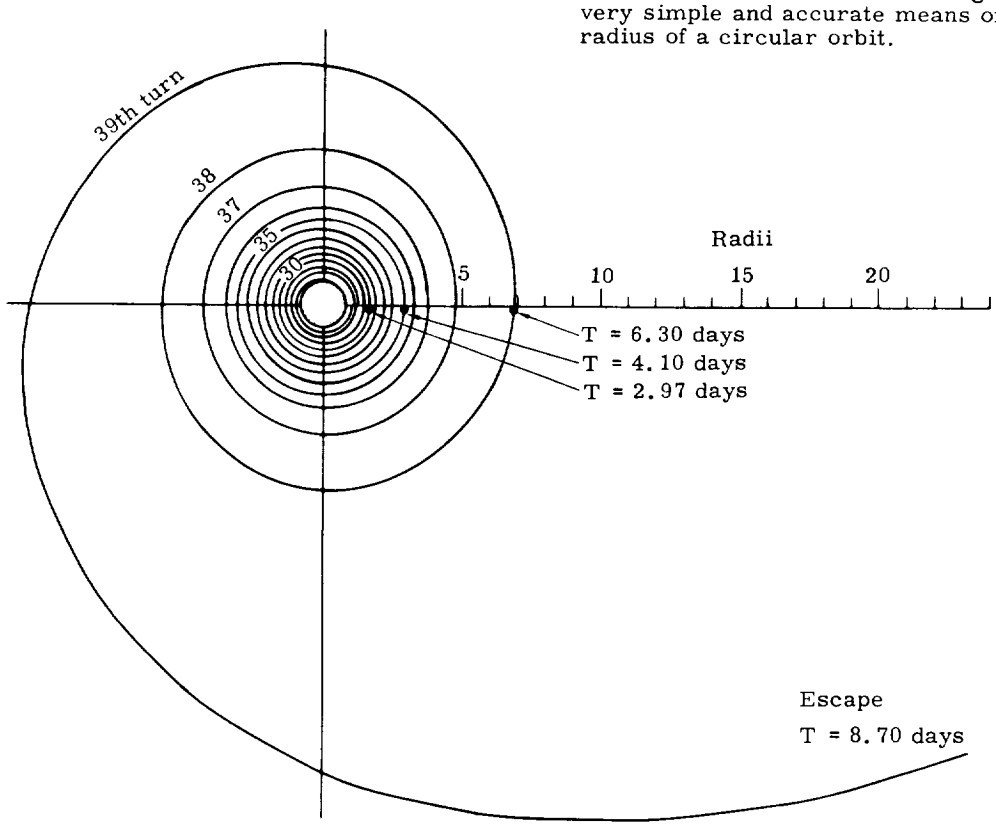

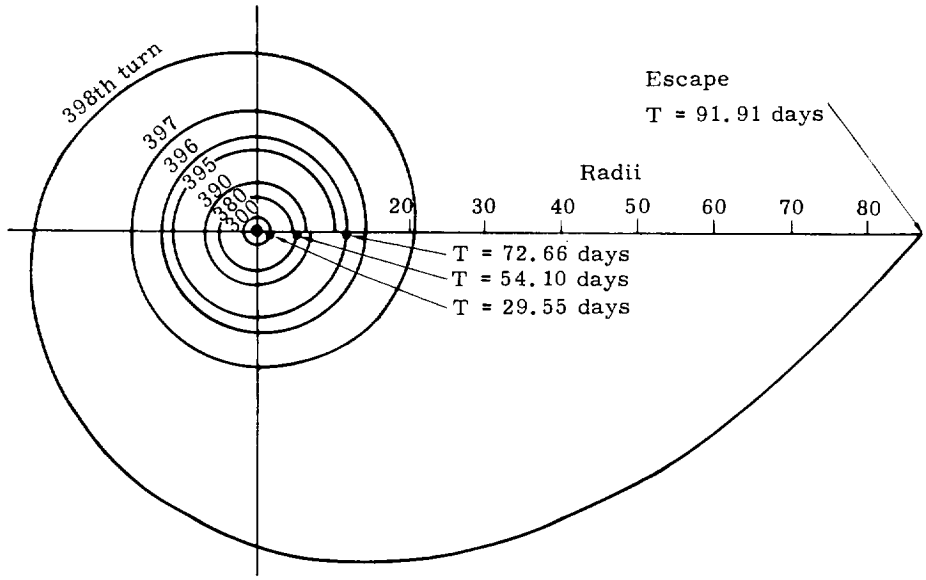

2. The Equations of Motion

The preceding discussion (Eqs (259) through (275)) showed the motion of the vehicle in polar coordinates under the influence of a micro-thrust. Unfortunately, this formulation is not always satisfactory for presenting the most readily comprehended information pertaining to the micro-thrust problem. For this reason, the equations have been written in terms of osculating orbital elements (i.e., the elements of the instantaneous elliptic orbit resulting from thrust termination at that time). This derivation is presented in Chapter IV.

$$
\left[\begin{array}{l}
\dfrac{da}{dt} = \dfrac{2}{n\sqrt{1-e^2}}\left(e\sin\theta \cdot R + \dfrac{p}{r}\,T\right) \\
\dfrac{de}{dt} = \dfrac{\sqrt{1-e^2}}{na}\left[\sin\theta \cdot R + (\cos\theta + \cos E)\,T\right] \\
\dfrac{di}{dt} = \dfrac{r\cos(\omega+\theta)}{na^2\left(1-e^2\right)}\,W \\
\sin i\,\dfrac{d\Omega}{dt} = \dfrac{r\sin(\omega+\theta)}{na^2\sqrt{1-e^2}}\,W \\
\dfrac{d\tilde{\omega}}{dt} = 2\sin^2\dfrac{i}{2}\,\dfrac{d\Omega}{dt} \\
\qquad + \dfrac{\sqrt{1-e^2}}{nae}\left[-\cos\theta \cdot R + \sin\theta\left(1+\dfrac{r}{p}\right)T\right] \\
\dfrac{d\epsilon}{dt} = -\dfrac{2r}{na^2} \cdot R + \dfrac{e^2}{1+\sqrt{1-e^2}}\,\dfrac{d\tilde{\omega}}{dt} \\
\qquad + 2\sqrt{1-e^2}\sin^2\dfrac{i}{2}\,\dfrac{d\Omega}{dt}
\end{array}\right] \qquad (276)
$$

where: $\tilde{\omega} = \omega + \Omega$

and where R, T and ω are the components of acceleration along the radius, the normal to the radius in the plane in the general direction of motion, and normal to the plane in the general direction of north, respectively (see sketch).

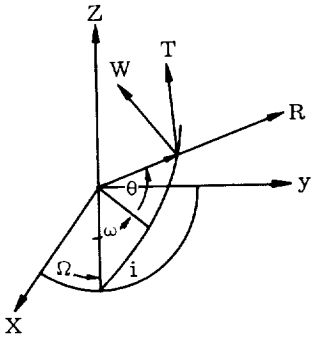

Equations (276) are the basic Lagrange planetary equations, from which special cases for a single component of disturbing acceleration can be derived. The resulting set of differential equations for the orbital parameters can be programmed for a digital computer, and the variations in the orbit computed as a function of time.

The equations can, however, be integrated under several conditions. The resulting equations are presented in following paragraphs. It should be noted, however, that, in certain cases, angular momentum is not conserved for long periods of time (tangential thrust) and that the integration formulas give a good approximation for only a few orbital revolutions.

a. Acceleration perpendicular to orbital plane

In this case both the radial and circumferential components of the acceleration are zero (i.e., R = 0 and T = 0), and the planetary equations for the disturbing acceleration follow from Eqs 276 simply as

$$
\left\{\begin{array}{l}
\dfrac{da}{dt} = \dfrac{de}{dt} = 0 \\
\dfrac{di}{dt} = \dfrac{r\cos(\omega+\theta)}{na^2\sqrt{1-e^2}}\,W \\
\dfrac{d\Omega}{dt} = \dfrac{r\sin(\omega+\theta)}{na^2\sqrt{1-e^2}\sin i}\,W \\
\dfrac{d\tilde{\omega}}{dt} = 2\sin^2\dfrac{i}{2}\,\dfrac{d\Omega}{dt} \\
\dfrac{d\epsilon}{dt} = \dfrac{d\tilde{\omega}}{dt}
\end{array}\right\} \qquad (277)
$$

Define a nondimensional acceleration

$$W^* = \frac{W}{g_a} \qquad (278)$$

where g_a is the gravitational acceleration at a distance corresponding to the semimajor axis.

Since $\mu = n^2 a^3$, this acceleration is equal to

$$g_a = \frac{\mu}{a^2} = n^2 a \qquad (279)$$

and

$$W = n^2 a W^*$$

From the conservation of angular momentum,

$$\frac{d\theta}{dt} = \frac{\sqrt{\mu p}}{r^2}$$

it follows, by using $p = a(1 - e^2)$, that

$$\frac{dt}{d\theta} = \frac{r^2}{na^2\sqrt{1-e^2}} \qquad (280)$$

Substituting Eqs (279) and (280) into Eqs (277):

$$\left\{\begin{aligned}
\frac{di}{d\theta} &= \frac{r^3 \cos(\omega+\theta)}{a^3(1-e^2)}\,W^* = \\
&\quad \frac{(1-e^2)^2 \cos(\omega+\theta)}{(1+e\cos\theta)^3}\,W^* \\
\frac{d\Omega}{d\theta} &= \frac{(1-e^2)^2 \sin(\omega+\theta)}{\sin i\,(1+e\cos\theta)^3}\,W^* \\
\frac{d\tilde{\omega}}{d\theta} &= 2\sin^2\frac{i}{2}\,\frac{d\Omega}{d\theta} \\
\frac{d\epsilon}{d\theta} &= \frac{d\tilde{\omega}}{d\theta}
\end{aligned}\right\} \qquad (281)$$

Assuming the variation in i during a revolution to be extremely small, such that sin i can be considered essentially constant, these expressions can be integrated with respect to the central angle θ.

First, expand the sines and cosines:

$$\left.\begin{aligned}
\sin(\omega+\theta) &= \sin\omega\ \cos\theta + \cos\omega\ \sin\theta \\
\cos(\omega+\theta) &= \cos\omega\ \cos\theta - \sin\omega\ \sin\theta
\end{aligned}\right\} \qquad (282)$$

Substituting this into Eq (281),

$$\Delta i \equiv \int_{\theta_0}^{\theta} di = W^*(1-e^2)^2 \left[\cos\omega \int \frac{\cos\theta\, d\theta}{(1+e\cos\theta)^3} - \sin\omega \int \frac{\sin\theta\, d\theta}{(1+e\cos\theta)^3}\right]\Bigg|_{\theta_0}^{\theta} \qquad (283)$$

$$\Delta\Omega \equiv \int_{\theta_0}^{\theta} d\Omega = W^* \frac{(1-e^2)^2}{\sin i}\left[\sin\omega \int \frac{\cos\theta\, d\theta}{(1+e\cos\theta)^3} + \cos\omega \int \frac{\sin\theta\, d\theta}{(1+e\cos\theta)^3}\right]\Bigg|_{\theta_0}^{\theta} \qquad (284)$$

Both equations can be integrated by the use of the following integration formulas:

$$\int \frac{\sin\theta\, d\theta}{(1+e\cos\theta)^3} = \frac{1}{2e(1+e\cos\theta)^2}\Bigg|_{\theta_0}^{\theta}$$

$$\int \frac{d\theta}{(1+e\cos\theta)^2} = \frac{1}{(1-e^2)^{3/2}}\left[\frac{-e\sqrt{1-e^2}\sin\theta}{1+e\cos\theta} + 2\tan^{-1}\left(\sqrt{\frac{1-e}{1+e}}\tan\frac{\theta}{2}\right)\right]\Bigg|_{\theta_0}^{\theta}$$

$$\int \frac{\cos\theta\, d\theta}{(1+e\cos\theta)^2} = \frac{1}{(1-e^2)^{3/2}}\left[\frac{\sqrt{1-e^2}\sin\theta}{1+e\cos\theta} - 2e\tan^{-1}\left(\sqrt{\frac{1-e}{1+e}}\tan\frac{\theta}{2}\right)\right]\Bigg|_{\theta_0}^{\theta}$$

$$\int \frac{\cos\theta\, d\theta}{(1+e\cos\theta)^3} = \frac{1}{2(1-e^2)}\left[\frac{\sin\theta}{(1+e\cos\theta)^2} + \int \frac{-2e+\cos\theta}{(1+e\cos\theta)^2}\, d\theta\right] = \frac{1}{2(1-e^2)}\,\frac{\sin\theta}{(1+e\cos\theta)^2} + \frac{(1+2e^2)}{2(1-e^2)^2}\,\frac{\sin\theta}{(1+e\cos\theta)} - \frac{3e}{(1-e^2)^{5/2}}\tan^{-1}\left(\sqrt{\frac{1-e}{1+e}}\tan\frac{\theta}{2}\right)\Bigg|_{\theta_0}^{\theta} \qquad (285)$$

After some simplification, the change in orbital inclination caused by a constant micro-thrust perpendicularly oriented to the orbital plane is given by

$$\Delta i = W^* \left\{\frac{(1-e^2)}{2(1+e\cos\theta)^2}\left[\sin\theta\ \cos\omega - \left(\frac{1-e^2}{e}\right)\sin\omega\right] + \frac{(1+2e^2)\sin\theta\ \cos\omega}{2(1+e\cos\theta)} - \frac{3e\cos\omega}{(1-e^2)^{1/2}}\tan^{-1}\left(\sqrt{\frac{1-e}{1+e}}\tan\frac{\theta}{2}\right)\right\}\Bigg|_{\theta_0}^{\theta} \text{ (rad/rev)} \qquad (286)$$

and the change in the longitude of the ascending node is given in the form

$$\Delta\Omega = \frac{W^*}{\sin i}\left\{\frac{(1-e^2)}{2(1+e\cos\theta)^2}\left[\sin\theta\ \sin\omega + \left(\frac{1-e^2}{e}\right)\cos\omega\right] + \frac{(1+2e^2)\sin\theta\ \sin\omega}{2(1+e\cos\theta)} - \frac{3e\sin\omega}{(1-e^2)^{1/2}}\tan^{-1}\left(\sqrt{\frac{1-e}{1+e}}\tan\frac{\theta}{2}\right)\right\}\Bigg|_{\theta_0}^{\theta} \text{ (rad/rev)} \qquad (287)$$

The integrals for the longitude of perigee ($\tilde{\omega}$) and the mean longitude of epoch (ϵ) are both equal and are simply Eq (287) multiplied by $2 \sin^2 \frac{i}{2}$.

Of course, if i should be varying very rapidly, then sin i could not be taken outside the integral sign in Eq (172), and a closed form solution would be extremely difficult, if not impossible, to obtain.

b. Radial acceleration

Setting T = 0 and W = 0 in Lagrange's planetary equations, the following results are obtained:

$$\left\{ \begin{aligned} \frac{da}{dt} &= \frac{2e \sin\theta}{n\sqrt{1-e^2}} R \\ \frac{de}{dt} &= \frac{\sqrt{1-e^2}\sin\theta}{na} R \\ \frac{di}{dt} &= \frac{d\Omega}{dt} = 0 \\ \frac{d\tilde{\omega}}{dt} &= -\frac{\sqrt{1-e^2}\cos\theta}{nae} R \\ \frac{d\epsilon}{dt} &= -\frac{1}{na}\left[2\frac{r}{a} + \frac{e\sqrt{1-e^2}}{1+\sqrt{1-e^2}}\cos\theta\right] R \end{aligned} \right\} \quad (288)$$

At this point it should be noted that for radial acceleration there is no change in the orbital inclination and in the longitude of the ascending node. The orbital plane remains essentially fixed in the inertial space, and only the shape and size of the ellipse are altered.

Now introduce a nondimensional acceleration, $R^* \equiv \frac{R}{g_a}$. Thus as before

$$R = n^2 a R^* \quad (289)$$

For the case of a radial acceleration, the angular momentum is conserved. Thus

$$\frac{dt}{d\theta} = \frac{r^2}{a^2 n \sqrt{1-e^2}}$$

and Eqs (288) become

$$\left\{ \begin{aligned} \frac{da}{d\theta} &= 2ae \frac{(1-e^2)\sin\theta}{(1+e\cos\theta)^2} R^* \\ \frac{de}{d\theta} &= \frac{(1-e^2)\sin\theta}{(1+e\cos\theta)^2} R^* \\ \frac{d\tilde{\omega}}{d\theta} &= -\frac{(1-e^2)^2\cos\theta}{e(1+e\cos\theta)^2} R^* \\ \frac{d\epsilon}{d\theta} &= -\left[\frac{2(1-e^2)^{5/2}}{(1+e\cos\theta)^3} + \frac{e(1-e^2)^2\cos\theta}{(1+\sqrt{1-e^2})(1+e\cos\theta)^2}\right] R^* \end{aligned} \right\} \quad (290)$$

As for micro-thrust applications, the changes in orbital parameters during one revolution are extremely small; thus it is possible to assume $e = e_0$, $a = a_0$, etc., and consider these variables as "almost constants" in integrating Eqs (290). This assumption can be proven analytically for certain cases, and it is a close first approximation for all cases.

The change in semimajor axis during one revolution in the orbit is found as

$$\Delta a = \int da = 2ae R^* (1-e^2) \int \frac{\sin\theta\, d\theta}{(1+e\cos\theta)^2} = \frac{2a R^* (1-e^2)}{(1+e\cos\theta)} \Bigg|_{\theta_0}^{\theta} \quad (291)$$

Similarly, the change in eccentricity for intervals up to 1 rev is

$$\Delta e = \int de = R^* (1-e^2)^2 \int \frac{\sin\theta\, d\theta}{(1+e\cos\theta)^2} = \frac{R^* (1-e^2)^2}{e(1+e\cos\theta)} \Bigg|_{\theta_0}^{\theta} \quad (292)$$

If e = 0, the equation simplifies to

$$\Delta e = \int de = R^* \int \sin\theta\, d\theta = -R^* \cos\theta \Big|_{\theta_0}^{\theta}$$

The variation in the longitude of the perigee again for intervals up to 1 rev is

$$\Delta\tilde{\omega} = \int d\tilde{\omega} = -\frac{(1-e^2)}{e} R^* \int \frac{\cos\theta\, d\theta}{(1+e\cos\theta)^2}$$

or

$$\Delta\tilde{\omega} = -\frac{R^*}{e\sqrt{1-e^2}}\left[\frac{\sqrt{1-e^2}\sin\theta}{1+\cos\theta} - 2e\tan^{-1}\left(\sqrt{\frac{1-e}{1+e}}\tan\frac{\theta}{2}\right)\right]_{\theta_0}^{\theta} \quad (293)$$

Finally, the change in the mean longitude of epoch for this same interval is

$$\Delta\epsilon = \int d\epsilon = -\left[2(1-e^2)^{5/2}\int \frac{d\theta}{(1+e\cos\theta)^3}\right.$$

$$+ \frac{e\,(1 - e^2)^2}{1 + \sqrt{1 - e^2}} \int \frac{\cos\theta \; d\theta}{(1 + e\cos\theta)^2} \Bigg] R^*$$

Integrating and collecting terms,

$$\Delta\epsilon = -R^* \sqrt{1 - e^2} \left\{ \frac{-e\,(1 - e^2)\sin\theta}{(1 + e\cos\theta)^2} \right.$$

$$- 2\tan^{-1}\left(\sqrt{\frac{1-e}{1+e}}\tan\frac{\theta}{2}\right) + \left(\frac{3}{\sqrt{1 - e^2}} + \frac{e}{1 + \sqrt{1 - e}}\right)$$

$$\left. \cdot \left[\frac{-e\sqrt{1 - e^2}\sin\theta}{1 + e\cos\theta} + 2\tan^{-1}\left(\sqrt{\frac{1-e}{1+e}}\tan\frac{\theta}{2}\right)\right]\right\}\Bigg|_{\theta_0}^{\theta}$$

(294)

Equations (291), (292), (293) and (294) define all the changes in orbital parameters for a constant radial micro-thrust applied during a known change in the central angle during 1 orbit.

c. Circumferential acceleration

Last, the case is considered for radial and the normal components of the micro-thrust acceleration equal to zero; i.e., only the component in the orbital plane perpendicular to the radius vector exists. Then, Eqs (276) reduce to

$$\left\{ \begin{array}{l} \dfrac{da}{dt} = \dfrac{2}{n\sqrt{1 - e^2}} \left(\dfrac{p}{r}\right) T \\[2ex] \dfrac{de}{dt} = \dfrac{\sqrt{1 - e^2}}{na} (\cos\theta + \cos E)\, T \\[2ex] \dfrac{di}{dt} = \dfrac{d\Omega}{dt} = 0 \\[2ex] \dfrac{d\tilde{\omega}}{dt} = \dfrac{\sqrt{1 - e^2}}{nae} \sin\theta \left(1 + \dfrac{r}{p}\right) T \\[2ex] \dfrac{d\epsilon}{dt} = \dfrac{e\sqrt{1 - e^2}}{na\left(1 + \sqrt{1 - e^2}\right)} \left(1 + \dfrac{r}{p}\right) T \end{array} \right\} \quad (295)$$

Once more, using a nondimensional acceleration $T^* = \frac{T}{g_a}$, substituting $T = n^2 a\, T^*$ into Eq (295) and remembering from the definition of semiparameter that

$$\frac{p}{r} = (1 - e^2)\frac{a}{r}$$

the following set of differential equations is obtained:

$$\left[\begin{array}{l} \dfrac{da}{d\theta} = 2r\,T^* = \dfrac{2p}{1 + e\cos\theta} T^* \\[2ex] \dfrac{de}{d\theta} = (1 - e^2)^2 \dfrac{(\cos\theta + \cos E)}{(1 + e\cos\theta)^2} T^* \\[2ex] \dfrac{d\tilde{\omega}}{d\theta} = \dfrac{\sin\theta}{e}\left(1 + \dfrac{r}{p}\right)\left(\dfrac{r}{a}\right)^2 T^* \\[2ex] \dfrac{d\epsilon}{d\theta} = \dfrac{e}{1 + \sqrt{1 + e^2}}\left(1 + \dfrac{r}{p}\right)\left(\dfrac{r}{a}\right)^2 T^* \end{array} \right] \quad (296)$$

Here, also, the assumption is made that the changes in orbital parameters during one revolution are extremely small. Thus, Eqs (296) can be integrated as follows, giving the change in semimajor axis

$$\Delta a \equiv \int da = 2\,pT^* \int \frac{d\theta}{1 + e\cos\theta}$$

$$= \frac{2pT^*}{\sqrt{1 - e^2}} \tan^{-1}\left(\frac{\sqrt{1 - e^2}\sin\theta}{1 + e\cos\theta}\right)\Bigg|_{\theta_0}^{\theta} \quad (297)$$

Now

$$\cos E = \frac{e + \cos\theta}{1 + e\cos\theta}$$

Therefore, the change in eccentricity becomes

$$\Delta e \equiv \int de = (1 - e^2)^2\, T^* \left\{ \int \frac{\cos\theta\, d\theta}{(1 + e\cos\theta)^2} \right.$$

$$\left. + e\int \frac{d\theta}{(1 + e\cos\theta)^3} + \int \frac{\cos\theta\, d\theta}{(1 + e\cos\theta)^3} \right\}$$

$$\Delta e = (1 - e^2)^2\, T^* \left\{ \frac{1}{(1 - e^2)^{3/2}} \left[\frac{\sqrt{1 - e^2}\sin\theta}{1 + e\cos\theta} \right.\right.$$

$$\left.\left. - 2e\tan^{-1}\left(\sqrt{\frac{1-e}{1+e}}\tan\frac{\theta}{2}\right)\right] \right.$$

$$\left. + \frac{1}{2(1 - e^2)^{3/2}} \left\{ \frac{-e\sqrt{1 - e^2}\sin\theta}{(1 + e\cos\theta)^2} + \right. \right.$$

(continued)

$$+ \frac{3}{1-e^2}\left[\frac{-e\sqrt{1-e^2}\sin\theta}{1+e\cos\theta} + 2\tan^{-1}\left(\sqrt{\frac{1-e}{1+e}}\tan\frac{\theta}{2}\right)\right]$$

$$- 2\tan^{-1}\left(\sqrt{\frac{1-e}{1+e}}\tan\frac{\theta}{2}\right)\Bigg\} + \frac{1}{2(1-e^2)^{5/2}}\left[\frac{(1-e^2)^{3/2}\sin\theta}{(1+e\cos\theta)^2}\right.$$

$$\left. + \frac{(1+2e^2)\sqrt{1-e^2}\sin\theta}{(1+e\cos\theta)} - 6e\tan^{-1}\left(\sqrt{\frac{1-e}{1+e}}\tan\frac{\theta}{2}\right)\right]\Bigg\}\Bigg|_{\theta_0}^{\theta}$$

(298)

The change in the longitude of perigee is

$$\Delta\tilde{\omega} = \int d\tilde{\omega} = \frac{T^*(1-e^2)^2}{e}\left[\int\frac{\sin\theta\, d\theta}{(1+e\cos\theta)^2} + \int\frac{\sin\theta\, d\theta}{(1+e\cos\theta)^3}\right]$$

and, thus,

$$\Delta\tilde{\omega} = \frac{T^*(1-e^2)^2}{e^2}\left[\frac{1}{(1+e\cos\theta)} + \frac{1}{2(1+e\cos\theta)^2}\right]\Bigg|_{\theta_0}^{\theta}$$

(299)

The change in the mean longitude of epoch is

$$\Delta\epsilon \equiv \int d\epsilon = \frac{T^*e(1-e^2)^2}{1+\sqrt{1-e^2}}\left[\int\frac{d\theta}{(1+e\cos\theta)^2}\right.$$

$$\left. + \int\frac{d\theta}{(1+e\cos\theta)^3}\right]$$

and, finally,

$$\Delta\epsilon = \frac{T^*e\sqrt{1-e^2}}{2\left(1+\sqrt{1-e^2}\right)}\Bigg\{2\left[\frac{-e\sqrt{1-e^2}\sin 0}{1+e\cos\theta}\right.$$

$$\left. + 2\tan^{-1}\left(\sqrt{\frac{1-e}{1+e}}\tan\frac{\theta}{2}\right)\right]$$

$$- \frac{e\sqrt{1-e^2}\sin\theta}{(1+e\cos\theta)^2} + \frac{3}{1-e^2}\left[\frac{-e\sqrt{1-e^2}\sin\theta}{1+e\cos\theta}\right.$$

$$+ \cdot$$

(continued)

$$+ 2\tan^{-1}\left(\sqrt{\frac{1-e}{1+e}}\tan\frac{\theta}{2}\right)$$

$$\left. - 2\tan^{-1}\left(\sqrt{\frac{1-e}{1+e}}\tan\frac{\theta}{2}\right)\right]\Bigg\}\Bigg|_{\theta_0}^{\theta}$$

(300)

d. Conclusions

The equations of the preceding discussions are in the strictest sense only approximate, since the coupling of the equations has been neglected. However, if the interval of time is sufficiently small, the results will be quite accurate. The implication of this is that these expressions could be used to evaluate secular changes and a program written for an electronic computer to sum the various contributions. This is indeed true. The procedure has much to recommend it since the time of computation will be much reduced and the problems of numerical roundoff almost eliminated.

M. REFERENCES

1. Kraft, J. D., "Techniques and Requirements for Orbit Maintenance," ER 12493, Martin Company (Baltimore), 29 June 1962.
2. Levy, Ezra C., "Propulsion Requirement to Counteract One Effect of Earth's Oblateness," Space Technology Laboratories Memo 7720.2-130, 3 January 1961.
3. Bruce, R., "Satellite Orbit Sustaining Techniques," STL Report STL-TM-60-0000-94092, November 1961.
4. Lawden, D. F., and Long, R. S., "The Theory of Correctional Maneuvers in Interplanetary Space," RR-60-1186-11, Radiation Inc., 30 August 1960.
5. "Guidance Requirements for a 24-Hour Satellite," ER 10718-6, Martin Company, 15 October 1959.
6. Kraft, J. D., "Techniques and Requirements for Orbit Maintenance," ER 12493, Martin Company, June 1962.
7. Lawden, D. F., "Optimal Trajectories," Report RR-59-1186-7, Radiation Inc., (Melbourne), May 1959.
8. Lawden, D. F., "Minimal Rocket Trajectories," Journal of the American Rocket Society, Vol. 23, No. 6, 1953.
9. Lawden, D. F., "Fundamentals of Space Navigation," Journal of the British Interplanetary Society, Vol. 13, No. 2, 1954.

10. Miele, A., "General Variational Theory of the Flight Paths of Rocket-Powered Aircraft, Missiles and Satellite Carriers," Report No. A-58-2, Purdue Research Foundation, 1958.

11. Anthony, M., et al., "Variational Approach to Trajectory Optimization," University of Colorado Extension Lectures, Spring Semester 1960.

12. Gedeon, G. S., "Orbital Segment Mechanics," Norair Report ASG-TM-61-43.

13. Hoelker, R. F., and Silber, R., "Bi-Elliptical Transfer Between Circular Coplanar Orbits," ABMA Report DA-TM-2-59, January 1959.

14. Vargo, L. G., "Optimal Transfer Between Two Coplanar Terminals in a Gravitational Field," presented at the Western Regional Meeting, 18 to 19 August 1958 (AAS Preprint No. 58-20).

15. Munick, H., McGill, R., and Taylor, G. E., "Minimization of Characteristic Velocity for Transfer Between Arbitrary Terminals in an Inverse Square Field Using Two Impulses," presented at the ARS 14th Annual Meeting, Washington, D. C., 16 to 20 November 1959 (ARS Preprint No. 959-59). See also abridged version ARS Journal, July 1960.

16. Munick, H., McGill, R., and Taylor, G. E., "Analytic Solutions to Several Optimum Orbit Transfer Problems," Journal of the Astronautical Sciences, Vol. VII, No. 4, Winter 1960.

17. Darby, W. G., "Correction for the Effects of Finite Thrusting Times in Orbit Changing Maneuvers," IAS Preprint 61-154-1848, June 1961.

18. Tsien, H. S., "Takeoff from Satellite Orbit," ARS Journal, Vol. 23, No. 4, July 1953, p 233.

19. "Advances in Astronautical Sciences," Vol. 3 (Proceedings of the Western Regional Meeting of the AAS), Plenum Press, Inc. (New York), August 1958.

20. Copeland, J., "Interplanetary Trajectories Under Low Thrust Radial Acceleration," ARS Journal, Vol. 29, No. 4, April 1959, p 267.

21. Benney, D. J., "Escape from a Circular Orbit Using Tangential Thrust," Jet Propulsion, Vol. 28, No. 3, March 1958, p 167.

22. "Dynamic Analysis and Design Performance Requirements for Satellite Vehicle Guidance Systems," ER 10470-6, Martin Company, January 1959.

23. Bacon, R. H., "Logarithmic Spiral: An Ideal Trajectory for the Interplanetary Vehicle with Engines of Low Sustained Thrust," American Journal of Physics, Vol. 27, No. 3, March 1959, p 164.

N. BIBLIOGRAPHY

Altman, S. P, "Orbital Transfer for Satellites," Los Angeles, 4th Symposium on Ballistic Missiles and Space Technology, August 1959.

Anthony, M., et al., "Variational Approach to Trajectory Optimization," University of Colorado Extension Lectures (Boulder), Spring 1960.

Arthur, P., et al., "Simple Method for Approximating the Characteristics of Low Thrust Trajectories," ARS Journal, Vol. 30, No. 7, July 1960.

Augenstein, B. W., "Dynamic Problems Associated with Satellite Orbit Control," Lockheed Missile Systems Division (Palo Alto, California), 1959. (ASME Paper 59-AV-4).

Bakalyar, G., "Orbital Rendezvous and Point-to-Point Velocity Transfers," Report No. MI-59-61, Martin Company (Denver), November 1959.

Battin, R. H., and Laning, J. H., "A Navigation Theory for Round Trip Reconnaissance Missions to Venus and Mars," Massachusetts Institute of Technology, MIT Instrumentation Laboratory, Cambridge, August 1959.

Brown, H., and Nelson, J. R., "Thrust Orientation Patterns for Orbit Adjustment of Low Thrust Vehicles," ARS Journal, Vol. 30, No. 7, July 1960, pp 635 to 637.

Bruce, R. W., Satellite Orbit Sustaining Techniques (U)," Preprint No. 1448-60, American Rocket Society, 5 to 8 December 1960.

Buchheim, R. W., "Space Flight Trajectories, Navigation and Maneuvers (U)," Report No. P-1387, The Rand Corporation, Santa Monica, California, May 1958.

Burgess, E., "Satellite and Transfer Orbits," Pacific Rocket Society Bulletin, Vol. 4, No. 4, April 1951, pp 5 to 12.

Carstens, J., "Optimum Maneuvers for Launching Satellite into Circular Orbits of Arbitrary Radius and Inclination, Preprint No. 1450-60, American Rocket Society, December 1960.

Cohen, S. R., and Ruggiero, R. R., "Multi-Body Effects on Orbit Transfer (U)," Preprint No. 1478-60, American Rocket Society, 5 to 8 December 1960.

Darby, W. G., "Correction for the Effects of Finite Thrusting Time in Orbit Changing Maneuvers," Preprint No. 61-154-1848, Institute of Aerospace Sciences, June 1961.

De Bra, D., "Orbital Plane-Change Maneuver," Astronautical Sciences Review, Vol. 1, No. 4, October to December 1959.

Demetraides, S., "Orbital Propulsion System for Space Maneuvering," Astronautical Sciences Review, Vol. 1, No. 4, October to December 1959.

Edelbaum, T. N.,
"Propulsion Requirements for Controllable Satellites, Preprint No. 1228-60, American Rocket Society, 1960.

"Some Extensions of the Hohmann Transfer Maneuver," ARS Journal, Vol. 29, No. 11, 1959, pp 864 to 865.

Ehricke, K. A., "Error Analysis of Keplerian Flights Involving a Single Central Force Field and Transfer Between Two Central Force Fields," Navigation, Spring 1958, pp 5 to 23.

Fitzgibbon, M. C., "Satellite Orbit Control System," Preprint No. 59-7, American Astronautical Society, August 1959 (Also, Advances in the Astronautical Sciences, Vol. 5, New York, Plenum Press, 1960).

Fox, R., "Powered Trajectory Studies for Low Thrust Vehicles," ARS Journal, Vol. 31, No. 1, January 1961.

Gundel, B. H., and De Bra, D. B., "Circularization of Elliptic Orbits," Preprint No. 60-36, American Astronautical Society, 1960.

Hord, R. A., "Relative Motion in the Terminal Phase of Interception of a Satellite or Ballistic Missile," NASA TN 4399, September 1958.

Hoelker, R., and Silber, R., "Bi-Elliptic Transfer Between Co-Planar Circular Orbits," 4th Symposium on Ballistic Missile and Space Technology, Los Angeles, California, August 1959.

Johnson, P. G., et al., "Use of Perigee Propulsion for Orbital Launch of Nuclear Rockets," American Astronautical Society, 1960 (Presented at Seattle, Washington, Western National Meeting of the American Astronautical Society, 8 to 11 August 1960).

Kelber, C. C., "Maneuverable Satellite," Western Regional Meeting of the American Astronautical Society, August 1958.

Ketchum, H. B.,
"Navigational Calculations in Space Flight, Part I--Planetary Orbital Distances," Journal of Space Flight, Vol. 5, April 1953.

"Navigational Calculations in Space Flight; Part II--Planetary Orbital Velocities and Gravitational Fields," Journal of Space Flight, Vol. 5, September 1953.

"Navigational Calculations in Space Flight; Part III--Satellite Gravitational Field, Orbital Velocities and Elements of Orbits," Journal of Space Flight, Vol. 5, December 1953.

"Navigational Calculations in Space Flight; Part IV--The Effects of Atmospheric Friction," Journal of Space Flight, Vol. 6, June 1954.

Koskela, P. E., Nicola, L., and Walters, L. G., "The Station Keeping Implications of an Artificial Satellite," Preprint No. 1229-60, American Rocket Society, 1960.

Lass, H., "Low Thrust Takeoff from a Satellite Orbit," ARS Journal, Vol. 31, No. 1, January 1961.

Lawden, D. F.,
"Orbital Transfer Via Tangential Ellipses," Journal of the British Interplanetary Society, Vol. 11, No. 6, November 1952, pp 278 to 279.

"Inter-Orbital Transfer of a Rocket," Journal of the British Interplanetary Society, Vol. 11, No. 6, November 1952, pp 321 to 333.

"Minimal Rocket Trajectories," Jet Propulsion, Vol. 23, November to December 1953.

"Fundamentals of Space Navigation," Journal of the British Interplanetary Society, Vol. 13, No. 2, March 1954, pp 87 to 101.

"Perturbation Maneuvers," Journal of the British Interplanetary Society, Vol. 13, No. 6, November 1954.

"Transfer Between Circular Orbits," Jet Propulsion, Vol. 27, No. 7, July 1956, pp 555 to 558.

"Optimal Trajectories," Report No. RR-59-1186-7, Radiation, Inc. (Orlando), May 1959.

"Necessary Conditions for Optimal Rocket Trajectories," Quarterly Journal of Mechanics and Applied Mathematics, Vol. 12, November 1959.

"The Theory of Correctional Maneuvers in Interplanetary Space," Report No. RR-60-1186-11, Orlando, Florida, Radiation, Inc., August 1960.

"Optimal Program for Correctional Maneuvers," Report No. RR-1186-60-13, Radiation, Inc. (Orlando), 27 September 1960.

Leitmann, G., "On a Class of Variational Problems in Rocket Flight," Journal of the Aerospace Sciences, Vol. 26, September 1959.

Levin, E., "Low Thrust Transfer Between Circular Orbits (U)," Report No. P-1536, The Rand Corporation, Santa Monica, California, October 1958.

Loh, W. H. T., "Minor Circle Flight for Boost Glide on Orbital Re-entry Vehicles," Preprint No. 60-35, American Astronautical Society, 1960.

London, H. S., "Change of Satellite Orbit Plane by Aerodynamic Maneuvering, Report No. 61-5, Institute of Aerospace Sciences, January 1961.

Miele, A.,
"General Variational Theory of the Flight Paths of Rocket-Powered Aircraft, Missiles and Satellite Carriers," Report No. A-58-2, Purdue University, Purdue Research Foundation, Lafayette, 1958.

"Theorem of Image Trajectories," Report No. DI-82-0039, Boeing Airplane Company, Seattle, January 1960.

Morgenthaler, G. W.,
"On Midcourse Guidance in Satellite Interception," Astronautica Acta, Vol. 5, No. 6, 1959.

"On Midcourse Guidance in Satellite Interception, II," Caywood-Schiller Associates, 31 January 1959.

Munick, H., and McGill, R., "Analytical Estimates for Optimum Transfer Paths," ARS Journal, Vol. 30, January 1960.

Munick, H., McGill, R., and Taylor, G. E., "Analytic Solutions to Several Optimum Orbit Transfer Problems," Journal of the Astronautical Sciences, Vol. 7, No. 4, Winter 1960, pp 73 to 77.

Munick, H., et al., "Minimization of Characteristic Velocity for 2 Pulse Orbital Transfers," ARS Journal, Vol. 30, No. 7, July 1960.

Rider, L.,
"Ascent from Inner Circular to Outer Co-Planar Elliptic Orbits," ARS Journal, Vol. 30, No. 3, March 1960.

"Low Thrust Correction of Orbital Orientation," ARS Journal, Vol. 30, No. 7, July 1960, pp 647 to 648.

Schindler, G., "Minimum Time Flight Paths," ARS Journal, Vol. 30, No. 4, April 1960.

Silber, R., "Survey of Characteristic Velocity Requirements for Two-Impulse Transfers Between Circular and Coplanar Exterior Elliptical Orbit with Exposition of Local and Overall Optimum Solutions," NASA TN D-600, March 1961.

Skalafuris, A., et al., "Midcourse Guidance Problem in Satellite Interception," ARS Journal, Vol. 30, No. 1, January 1960.

Smith, F. T., "Optimization of Multistage Orbit Transfer Processes by Dynamic Programming," ARS Journal, Vol. 31, No. 11, November 1961, pp 1553 to 1560.

Szebehely, V. G., "Equations for Thrust Programs," Stockholm, XIth International Astronautical Congress, Trajectories Session, 1960.

Tanguay, A. R., and Hock, D. H., "Space Maneuvers," Space Trajectories, Academic Press (New York), 1960.

Ting, L.,
"Optimum Orbital Transfer by High Thrust Rockets," PIBAL Report No. 633, Polytechnic Institute of Brooklyn, New York, February 1961, 29 pp (Also, AFOSR 163).

"Optimum Orbital Transfer by Impulses," ARS Journal, Vol. 30, No. 11, November 1960.

Townsend, G., Kraft, D., and Kork, J., "Maneuvers," Design Guide to Orbital Flight, McGraw-Hill Book Company (New York), 1962.

Tsien, H. S., "Take-off from a Satellite Orbit (Radial Thrust)," Jet Propulsion, Vol. 23, No. 4, July to August 1953.

Vargo, L., "Generalization of Minimum Impulse Theorem to the Restricted Three Body Problem," Journal of the British Interplanetary Society, Vol. 17, September to October 1959.

Warzecha, L. W., "Performance and Design Considerations for Maneuvering Space Vehicles," Aero/Space Engineering, November 1960, pp 18 to 23.

Wolfe, J. F., and DeBra, D., "Two-Maneuver Ascents to Circular Orbits," J. Astron. Sci., Vol. 7, No. 2, 1960, pp 47 to 48.

Zilczer, P., "Space Navigation by Correlation," Preprint No. 60-18, American Astronautical Society, 1960.

Alderson, J. D., Jr., "Optimum Thrust Programs for High-Altitude Rockets," No GAE/AE-60-1, 88 pages, Wright-Patterson Air Force Base, Ohio, Air Force Institute of Technology, September 1960 (ASTIA No. AD-250795).

Baker, G. A., Jr., Ford, K. W., and Porter, C. E., "Optimal Accuracy Rocket Trajectories," Journal of Applied Physics, Vol. 30, No. 12, December 1959, pp 1925 to 1932.

Bellman, R.,
"An Introduction to the Theory of Dynamic Programming," Report No. R-245, The Rand Corporation (Santa Monica), 1953.

"The Theory of Dynamic Programming," Bulletin of the American Mathematical Society, Vol. 60, No. 6, p 503, November 1954.

Bellman, R., and Dreyfus, S. E.,
"Computational Solutions of Dynamic Programming; VI--on the Optimal Trajectory Problem," Report No. RM-1750, The Rand Corporation (Santa Monica), 16 April 1957 (ASTIA No. AD-123 553).

"An Application of Dynamic Programming to the Determination of Optimal Satellite Trajectories," Journal of the British Interplanetary Society, Vol. 17, Nos. 3-4, May-August 1959, pp 78 to 83.

Bender, D. F., "Optimum Co-Planar Two Impulse Transfers Between Elliptic Orbits," IAS Paper No. 62-4, IAS 30th Annual Meeting, January 1962.

Berman, L. J., "A Digital Computer Study of the Powered Flight Trajectories of Long Range Ballistic Missiles: Part III--Trajectory Optimization by Partial Variation," Report No. ARG-R-1, Massachusetts Institute of Technology (Cambridge), March 1958 (ASTIA No. AD-215 407).

Billik, B. H., "On the Maximum Burnout Velocity of a Vehicle Achieved Through a Throttling Process," Report No. STL 7720, Space Technology Laboratories (Los Angeles), 4 August 1960.

Breakwell, J. V.,
"The Optimization of Trajectories," Report No. AL-2706 NAA, North American Aviation (Los Angeles), August 1957 (Also, Journal of

the Society of Industrial and Applied Mathematics, Vol. 7, No. 2, June 1959, pp 215 to 247) (Also, Flight Dynamics and Space Mechanics, January 1960, LMSD-288139, Vol. III, Chapter 12) (Also, ASTIA No. AD-209 092).

"Optimal Ascent into a Circular Orbit," IAS Vehicle Systems Optimization Symposium (New York), 27-29 November 1961.

Bryson, A. E., and Ross, S. E., "Optimum Rocket Trajectories with Aerodynamic Drag," Jet Propulsion, Vol. 28, No. 7, July 1958, pp 465 to 469 (Also, Preprint 542-57, American Rocket Society, December 1957).

Carstens, J. P., and Edelbaum, T. N., "Optimum Two Impulse Ascents to Circular Orbits," Journal of the Astronautical Sciences, Vol. 7, No. 4, Winter 1960, pp 96 to 97.

"Optimum Maneuvers for Launching Satellites into Circular Orbits of Arbitrary Radius and Inclination," Preprint No. 1450-60, American Rocket Society, December 1960.

Cashmore, D. J., "Minimum Gravitational Losses for Rocket Motion near a Planetary Surface," Journal of the British Interplanetary Society, Vol. 17, No. 2, March-April 1959, pp 52 to 57.

Cicala, C., and Miele, A., "Brachistochronic Maneuvers of a Variable Mass Aircraft in a Vertical Plane," Journal of the Aeronautical Sciences, Vol. 22, No. 8, August 1955, pp 577 to 578.

"Generalized Theory of the Optimum Thrust Programming for the Level Flight of a Rocket-Powered Aircraft," Jet Propulsion, Vol. 26, No. 6, June 1956, pp 443 to 455.

Courant, R., "Calculus of Variations and Supplementary Notes," New York University, Institute of Mathematical Sciences (New York), 1949 to 1950.

Corben, H. C., "A Note on the Optimization of Powered Trajectories in an Arbitrary Gravitational Field," RW Report ERL-IM-150, Thompson Ramo-Wooldridge, 4 December 1957.

Deaton, A. W., and Brandon, P. D., "Saturn Missile SA-7: Optimum Trajectory Shape for Circular Orbit Mission (U)," MTP-AERO-60-8, Marshall Space Flight Center, 14 November 1960.

Desoer, C. A., "Pontriagin's Maximum Principle and the Principle of Optimality," Report 60-326 (U/Rpt.), University of California (Berkeley), 11 November 1960, 9 pages (Also, Journal of the Franklin Institute, Vol. 271, No. 5, May 1961, pp 361 to 367).

Edelbaum, T. N., and Carstens, J. P., "Optimum Maneuvers for Launching Satellites into Circular Orbits of Arbitrary Radius and Inclination," United Aircraft Corporation, Research Laboratories (East Hartford), 1960 (ARS Preprint No. 1450-60).

Eggers, A. J., Allen, H. J. and Neice, S. E., "Comparative Analysis of the Performance of Long-Range Hypervelocity Vehicles," NACA RM A 54 L10, March 1955 (Also, NACA TN-4046, October 1957).

Ehlers, E. E., "On the Trajectories of a Missile in a Constant Gravity Field with the Sine and the Tangent of the Thrust Angle Varying Linearly with Time," Document No. DI-82-0069, Math. Note No. 222, Washington, Boeing Scientific Research Laboratory (Seattle) October 1960 (ASTIA No. AD-245 134).

"Missile Trajectories with Linear Time Variation of the Sine or Tangent of the Thrust Angle," ARS Journal, Vol. 31, No. 5, May 1961, pp 631 to 636.

Egorov, V. A., "On the Solution of a Degenerate Variational Problem and the Optimum Climb of a Space Rocket," Journal of Applied Mathematics and Mechanics, Vol. 22, No. 1, 1959 (Translated).

Ewing, G. M., "A Fundamental Problem of Navigation in Free Space," Quarterly of Applied Mathematics, Vol. XVIII, No. 4, January 1961.

Faulkner, F. D., "The Problem of Goddard and Optimum Thrust Programming," Research Paper No. 11, Naval Postgraduate School (Monterey, California), March 1957 (Also, 3rd Annual Meeting of the American Astronautical Society (New York), 6-7 December 1956) (Also, Proceedings of the American Astronautical Society, 1956, pp 43 to 51).

"Some Results from Direct Methods Applied to Optimum Rocket Trajectories," Proceedings of the 10th International Astronautical Congress, Amsterdam, 1958, Springer-Verlag (Vienna), 1959, Vol. II, pp 694 to 701.

"Complete Elementary Solution to Some Optimum Trajectory Problems," ARS Journal, Vol. 31, No. 1, January 1961, pp 33 to 39.

Foote, J. R., Butler, T., Adney, J. E. and Thatcher, H. C., "Direct Variational Methods and Brachistochrone Problems," AFOSR-101, Holloman Air Force Base, New Mexico, Directorate of Research Analysis, January 1961 (Also, ASTIA No. AD-251 008).

Foulders, C. R., "Minimum-Time Steering Programs for Orbital Transfer with Low-Thrust Rockets," Astronautica Acta, Vol. 7, No. 1, 1961, pp 35 to 49.

Fox, R. H., "Optimum Exhaust Velocity Programming and Propulsion Efficiency," Report UCRL-5135, University of California, Lawrence Radiation Laboratory (Livermore), 26 May 1958 (Also, Journal of the Astronautical Society, Vol. VI, No. 1, Spring 1959, pp 13 to 16.

Fraeijs, De Veubeke, B., "Variational Methods in Optimizing Rocket Performance," Rocket Propulsion, Elsevier Publishing Company (New York), 1960, Chapter 12, pp 772 to 812.

Fried, B. D.,
"On the Powered Flight Trajectory of an Earth Satellite," Jet Propulsion, Vol. 27, No. 6, June 1957, pp 641 to 643.

"The Dynamics of Powered Flight with Application to Trajectory Optimization Problems," Report No. ARL-7-74, Thompson Ramo-Wooldridge Corporation, Physical Research Laboratory, 31 December 1957.

"Trajectory Optimization for Powered Flight in Two or Three Dimensions," Space Technology, John Wiley and Sons, Inc. (New York), 1959, Chapter 4 (Seifert, H. S., ed).

Graham, E. W., "A Class of Optimum Trajectory Problems in Gravitational Fields," Journal of the Aerospace Sciences, Vol. 27, No. 4, April 1960, pp 296 to 303.

Graham, E. W., and Beane, B. J., "Optimum Rocket Trajectories with Atmospheric Resistance," Report No. SM 23745, California, Douglas Aircraft Company (Santa Monica), November 1959 (Also, ASTIA No. AD-235 783).

Granton, J., Jr., et al., "The Trajectory of a Rocket with Thrust," Jet Propulsion, Vol. 28, No. 7, July 1958, pp 472 to 478.

Halkin, H., "Nondegenerate Variational Problems and the Principle of Optimal Evolution," IAS Vehicle Systems Optimization Symposium (New York), 27-29 November 1961.

Hestenes, M. R., "A General Problem in the Calculus of Variations with Applications to Paths of Least Time," Report No. RM-100, California, The Rand Corporation (Santa Monica), March 1950.

Horner, J., and Silber, R., "Impulse Minimization for Hohmann Transfer Between Inclined Circular Orbits of Different Radii," ABMA Report No. DA-TR-70-59, Army Ballistic Missile Agency (Huntsville), 1959.

Jurovics, S. A., and McIntyre, J. E.,
"The Adjoint Method and Its Application to Trajectory Optimization," MD 60-334, North American Aviation (Los Angeles), October 1960.

"Optimum Steering Program for the Entry of a Multistage Vehicle into a Circular Orbit," ARS Journal, Vol. 31, No. 4, April 1961, pp 518 to 523 (Also, MD 60-205, North American Aviation (Los Angeles), May 1960, Revised October 1960).

Kelley, H. J.,
"An Investigation by Variational Methods of Flight Paths for Optimum Performance," SCD Thesis, New York University, Guggenheim School of Aeronautics (New York), May 1958.

"Gradient Theory of Optimal Flight Paths," Preprint No. 1230-60, American Rocket Society, 1960 (Also, ARS Journal, Vol. 30, No. 10, October 1960).

"Successive Approximation Techniques for Trajectory Optimization," IAS Vehicle System Optimization Symposium (New York), 27-29 November 1961.

Krasovskii, N. N., "Sufficient Conditions for Optimization," (Prikl. Mat. Mekh.) Appl. Math. Mech., Vol. 23, No. 3, Pergamon Press (New York), 1959, pp 839 to 843.

Krotov, V, F., "Calculation of the Optimum Trajectory for the Entry of a Rocket into a Particular Circular Trajectory (Orbit) Around the Earth," Mekhanika, MVTU No. 50, Moscow, Oborongiz, 1956, pp 313 to 334.

Kulakowski, L. J., and Stancil, R. T., "Rocket Boost Trajectories for Maximum Burnout Velocity," ARS Journal, Vol. 30, No. 7, July 1960, pp 612 to 618.

Lawden, D. F.,
"Minimal Trajectories," Journal of the British Interplanetary Society, Vol. 9, No. 4, July 1950, pp 179 to 186.

"The Determination of Minimal Orbits," Journal of the British Interplanetary Society, Vol. 11, No. 5, September 1952, pp 216 to 224.

"Minimal Rocket Trajectories," Journal of the American Rocket Society, Vol. 23, No. 6, November 1953.

"Stationary Rocket Trajectories," Quarterly Journal of Mechanics and Applied Mathematics, Vol. 7, Part 4, December 1954, pp 488 to 504.

"Optimum Launching of a Rocket into an Orbit Around the Earth," Astronautica Acta, Vol. 1, Fasc. 4, 1955, pp 185 to 190 (Also, Copenhagen, 6th IAF Congress, 5 August 1955).

"Optimal Programming of Rocket Thrust Direction," Astronautica Acta, Vol. 1, Fasc. 1, January 1955, pp 41 to 46 (Also, Innsbruck, 5th IAF Congress, 6 August 1954).

"Maximum Ranges of Intercontinental Missiles," The Aeronautical Quarterly, Vol. VIII, Part 3, August 1957, pp 269 to 278.

"Mathematical Problems of Astronautics," Mathematical Gazette, October 1957, pp 168 to 179.

"Optimal Rocket Trajectories," Jet Propulsion, Vol. 27, No. 12, December 1957, p 1263.

"The Employment of Aerodynamic Forces to Obtain Maximum Range of a Rocket Missile," The Aeronautical Quarterly, Vol. 9, No. 2, May 1958, pp 97 to 109.

"Optimal Trajectories," Special Report 3, Report RR-59-1186-7, Radiation, Inc. (Melbourne, Fla.), May 1959 (Also, ASTIA No. AD-219 299).

"Necessary Conditions for Optimal Rockets Trajectories," Quarterly Journal of Mechanics and Applied Mathematics, Vol. 12, No. 4, November 1959, pp 476-487.

"Advances in Space Sciences," Interplanetary Rocket Trajectories, Vol. 1, Chapter 1, p 1053, Academic Press (New York), 1959 (Ordway, F. I., III, ed).

"Optimal Powered Arcs in an Inverse Square Law Field," ARS Journal, Vol. 31, No. 4, April 1961, pp 566 to 568.

Leitmann, G.,
"Optimum Thrust Programming for High Altitude Rockets--New Solutions," NOTS TN 5038-9 (China Lake, California), 18 July 1955.

"Integration of the Euler-Legrange Equation and Numerical Example for Optimum Thrust Programming," NOTS TN 5038-10 (China Lake, California), 25 July 1955, 8 pp.

"The Problem of Optimum Thrust Programming," NOTS TN 5038-11 (China Lake, California), 22 September 1955, 11 pp.

"A Calculus of Variations Solution of Goddard's Problem," Astronautica Acta, 1956, Vol. II, Fasc. 2, pp 55 to 62.

"Stationary Trajectory for a High-Altitude Rocket with Drop Away Booster," Astronautica Acta, Vol. II, Fasc. 3, 1956, pp 119 to 124. Correction: Vol. II, Fasc. 4, p 218 (Also, Aeronautical Engineering Review, Vol. 16, 1957, p 63).

"Optimum Thrust Programming for High-Altitude Rockets," Aeronautical Engineering Review, Vol. 16, No. 6, June 1957, pp 63 to 66 (Also, NOTS TN 5038-7, 1955) (Also, University of California, PhD Dissertation).

"A Note on Goddard's Problem," Astronautica Acta, Vol, 3, Fasc. 4, 1957, pp 237 to 240.

"Trajectory Programming for Maximum Range," Journal of the Franklin Institute, Vol. 264, No. 6, December 1957, pp 443 to 452.

"On a Class of Variational Problems in Rocket Flight, Report No. LMSD-5067, Lockheed Missile Systems Division (Sunnyvale), September 1958 (Also, Journal of the Aerospace Sciences, Vol. 26, No. 9, September 1959, pp 586 to 591) (Also, ASTIA No. AD-202-302).

"On a Minimum Fuel Satellite Transfer Trajectory," TM No. 491/2-01-60, The Martin Company (Baltimore), January 1960.

"Optimal Thrust Direction for Maximum Range," Journal of the British Interplanetary Society, Vol. 16, No. 9, September-October 1958, pp 503 to 507.

"Extremal Rocket Trajectories in Position and Time Dependent Force Fields," Preprint 61-30, American Astronautical Society, 7th Annual Meeting, 16 to 18 January 1961.

"The Optimization of Rocket Trajectories--A Survey," Progress in the Astronautical Sciences, North Holland Publishing Company, 1961 (Singer, S. F., ed).

"Minimum Transfer Time for a Power-Limited Rocket, Report No. LMSD-49769, Lockheed Aircraft Corporation (Sunnyvale), 14 August 1959 (Also, Stockholm, XIth International Astronautical Congress, Astrodynamics Colloquium, 1960) (Also, "General Research in Flight Sciences, January 1959-January 1960," Flight Dynamics and Space Mechanics, Report No. LMSD-288139, Vol. III, Chapter 2 Lockheed Aircraft Corporation (Sunnyvale), January 1960). (Also, Journal of Applied Mechanics, Paper No. 61-APM-6, pp 1 to 8) (Also, ASTIA No. AD-225 924).

"Propulsive Efficiency of Rockets," Third International Symposium on Rockets (Tokyo), 1961, Preliminary Preprint.

"Optimization Techniques," Variational Problems with Bounded Control Variables, Academic Press (New York), 1961, Chapter 5.

"On Some Optimum Rocket Trajectories," IAS Vehicle Systems Optimization Symposium (New York), November 27 to 29, 1961.

Leitmann, G. and Cowan, W. D., "A Preliminary Study of the Problem of Obtaining Maximum Range with a Large Surface-to-Surface Rocket (U)," NOTS TN 5038-17, 17 October 1955. Correction: 20 August 1956 (Also, ASTIA No. AD-143 266).

Levinsky, E. S.,
"Variational Procedure for Minimizing Heating Effects During the Re-entry of a Lifting Vehicle," Report No. ZA-309, Convair (San Diego), March 1960.

"Application of Inequality Constraints to Variational Problems of Lifting Re-entry," IAS 29th Annual Meeting, New York, IAS Paper No. 61-21, 23 to 25 January 1961.

Mackay, J. S., "Approximate Solution for Rocket Flight with Linear Tangent Thrust Attitude," ARS Journal, Vol. 30, No. 11, November 1960, pp 1091 to 1093.

McIntyre, J. E.,
"Optimum Trajectory Analysis," Report No. MD 60-309, North American Aviation (Los Angeles), 6 October 1960.

"Application of Optimum Trajectory Analysis to Boost Vehicle Design," IAS Vehicle Systems Optimization Symposium (New York), 27 to 29 November 1961.

Michaels, J. E. and Hartman, M. J.,
"The Determination of Optimum Initial Conditions for Interplanetary Travel from Any Launch Site on Earth," 7th AAS National Annual Meeting (Dallas), January 1961.

Michelson, I.,
"Ultimate Design of High Altitude Sounding Rockets," ARS Journal, Vol. 27, October 1957.

Miele, A.,
"General Variational Theory of the Flight Paths of Rocket-Powered Aircraft, Missiles, and Satellite Carriers," Purdue University, School of Aeronautical Engineering (Lafayette), January 1958, A-58-2 (Also, Astronautica Acta, Vol. 4, 1958, pp 264-288 (Condensed)) (Also, Amsterdam, Proceedings of the IXth International Astronautical Congress, 18 August 1958) (Also, Office of Scientific Research, Technical Note 58-246, Contract AF-18(603)-69) (Also, AFOSR TN 58-246) (Also, ASTIA No. AD-154 148).

"Minimal Maneuvers of High-Performance Aircraft in a Vertical Plane," Purdue University School of Aeronautical Engineering (Lafayette), May 1958, A-58-3 (Also, NASA TN D-155, September 1959) (Also, ASTIA No. AD-255 859).

"Lagrange Multipliers and Quasi-Steady Flight Mechanics," Purdue University, School of Aeronautical Engineering (Lafayette), May 1958, A-58-4. (Also, Journal of Aerospace Sciences, Vol. 26, No. 9, September 1959, pp 592-598).

"Minimality for Arbitrarily Inclined Rocket Trajectories," Jet Propulsion, Vol. 28, July 1958, pp 481-483.

"Stationary Conditions for Problems Involving Time Associated with Vertical Rocket Trajectories," Journal of the Aerospace Sciences, Vol. 25, No. 7, July 1958, pp 467-468.

"Trajectories of Minimum Aerodynamic Heating Including Drag Effects," Report No. SM-27789, Douglas Aircraft Company (Santa Monica), August 1958.

"On the Brachistochronic Thrust Program for a Rocket Powered Missile Traveling in an Isothermal Medium," Report No. SM-27790, Douglas Aircraft Company, Missiles Engineering Department (Santa Monica), August 1958.

"The Application of Green's Theorem to Variational Problems of Linear Type" Report No. SM-27791, Douglas Aircraft Company (Santa Monica), August 1958 (Also, Journal of the Aerospace Sciences, Vol. 25, No. 9, September 1958, pp 581-590).

"Some Recent Advances in the Mechanics of Terrestrial Flight," Jet Propulsion, Vol. 28, No. 9, September 1958, pp 581-587.

"Mathematical Theory of the Optimum Trajectories of a Rocket--Final Report," Purdue University, School of Aeronautical Engineering. (Lafayette), November 1958, A-58-10 (Also, AFOSR TR 58-154) (Also, ASTIA No. AD-206 361).

"Interrelationship of Calculus of Variations and Ordinary Theory of Maxima and Minima for Flight Applications," ARS Journal, Vol. 29, No. 1, January 1959, pp 75-76.

"Variational Apporach to Problems of Hypervelocity Flight, Final Report," Purdue University, School of Aeronautical Engineering (Lafayette), June 1959, A-59-7.

"A General Survey of the Problem of Optimizing Flight Paths of Aircraft and Missiles," Preprint No. 1219-60, American Rocket Society, 9-16 May 1960 (Also, American Rocket Society Semi-Annual Meeting, 9-16 May 1960).

"A Survey of the Problem of Optimizing Flight Paths of Aircraft and Missiles," Document No. D1-82-0050, Boeing (Seattle), July 1960 (Also, ASTIA No. AD-244 056).

"Application of Green's Theorem to the Extremization of Linear Integrals," IAS Vehicle Systems Optimization Symposium (New York), 27-29 November 1961.

Miele, A., and Cappellari, J. O., Jr.,
"Approximate Solutions to Optimum Climbing Trajectory for a Rocket-Powered Aircraft," Purdue University, School of Aeronautical Engineering (Lafayette), July 1957, A-57-4 (Also, NASA TN D-150, September 1959) (Also, ASTIA No. AD-225 566).

"Approximate Solutions to Optimum Flight Trajectories for a Turbojet-Powered Aircraft," Purdue University, School of Aeronautical Engineering (Lafayette), December 1957, A-57-7 (Also, NASA TN D-152, September 1959, 33 pp) (Also, ASTIA No. AD-225 563).

"Topics in Dynamic Programming for Rockets," Purdue University, School of Aeronautical Engineering (Lafayette), July 1958, A-58-5 (Also, Zeitschrift für Flugwissenschaften, Vol. 7, No. 1, 1959) (Also, AFOSR TN 58-685) (Also, ASTIA No. AD-162 218).

"Some Variational Solutions to Rocket Trajectories Over a Spherical Earth," Purdue University, School of Aeronautical Engineering (Lafayette), November 1958, A-58-9 (Also, AFOSR TN 58-1012) (Also, ASTIA No. AD-206 155).

Miele, A., and Cavotti, C. R.,
"Generalized Variational Approach to the Optimum Thrust Programming for the Vertical Flight of a Rocket, Part II: Application of Green's Theorem to the Development of Sufficiency Proofs for Particular Classes of Solutions," Purdue University, School of Aeronautical Engineering (Lafayette), August 1957, A-57-2, v + 30 pp (Also, Zeitschrift für Flugwissenschaften, April 1958, Bd. 6, Heft 4, s. 102-109 (Condensed)) (Also, ASTIA No. AD-136 638).

Miner, W. E.,
"Studies Toward a Minimum Propellant Guidance System," ABMA Report No. DA-TR-15-60 (Huntsville), Army Ballistic Missile Agency, 5 April 1960.

Moskowitz, S., and Ting, Lu
"A Realistic Approach to Problems of Optimum Rocket Trajectories," PIBAL Report No. 625, Polytechnic Institute of Brooklyn (New York), October 1960, 18 pp (Also, ASTIA No. AD-247 226) (Also, ARS Journal, Vol. 31, No. 4, April 1961, pp 551-553).

Mueller, G.,
"Optimum Range of a Wingless Rocket About Rotating Earth," Report No. ATI 169 753, California Institute of Technology (Pasadena), 1952, (PhD Thesis).

Munick, H.,
"An Optimum Transfer Path from an Elliptical Orbit to a Higher Energy Circular Orbit," ARS Journal, Vol. 29, No. 6, June 1959, pp 449-453.

Munick, H., and McGill, R.,
"Minimization of Characteristic Velocity for Two-Impulse Orbital Transfer," ARS Journal, Vol. 30, No. 7, July 1960, pp 638-639.

"Analytical Estimates for Optimum Transfer Paths," ARS Journal, Vol. 30, January 1960, pp 120-121.

Munick, H., McGill, R., and Taylor, G. E.,
"Analytic Solutions to Several Optimum Orbit Transfer Problems," Journal of Astronautical Sciences, Vol. 7, No. 4, Winter 1960, pp 73-77.

Newton, R. R.,
"On the Optimum Trajectory of a Rocket," Journal of the Franklin Institute, No. 3, Vol. 266, September 1958, pp 155-187 (Also, New Orleans, Louisiana, Tulane University, 22 April 1957, Department of Physics Project TU 2-9F, R 5 16-7) (Also, Reprint Series, Report No. 475, Silver Spring, Maryland, The Johns Hopkins University, Applied Physics Laboratory, December 1958).

"On the Optimization of Physical Propulsion Systems," Jet Propulsion, Vol. 28, No. 11, November 1958, pp 752-753.

Olds, R. H.,
"Optimum Variation of Exhaust Velocity During Burning," NAVORD Report 6427, 28 October 1958, p 5 (Also, Jet Propulsion, Vol. 28, No. 6, June 1958, pp 405-406).

Okhotsimskii, D. E., and Eneev, T. M.,
"Some Variation Problems Connected with the Launching of Artificial Satellites of the Earth," Uspekhi Fiz. Nauk, Vol. 63, No. 1, September 1957 (In Russian) (Also, Journal of the British Interplanetary Society, Vol. 16, No. 5, January-February 1958, pp 263-294).

Pfeiffer, C.,
"Theory and Application of the Critical Direction Method of Trajectory Optimization," IAS Vehicle Systems Optimization Symposium (New York), 27-29 November 1961.

Rider, L.,
"A Functional Equation Approach to the Optimization of Plane Change Maneuvers in Space," 22 January 1962 (Report No. TDR-930(2560-30) TN-1, DCAS-TDR-62-6) (Contract No. AF04(647)-930).

Ross, S. E.,
"Variational Solutions to Optimum Rocket Trajectory Problems," Doctorate Thesis, Harvard University (Cambridge), January 1958.

"Minimality for Problems in Vertical and Horizontal Rocket Flight," Jet Propulsion, Vol. 28, No. 1, January 1958, pp 55-56.

"Composite Trajectories Yielding Maximum Coasting Apogee Velocity," ARS Journal, Vol. 29, No. 11, November 1959, pp 843-848.

"Optimum Rocket Trajectories with Aerodynamic Drag," Jet Propulsion, Vol. 28, No. 7, July 1958, pp 465-469.

"Low Acceleration Trajectory Optimization in a Strong Central Force Field," IAS Vehicle Systems Optimization Symposium (New York), 27-29 November 1961.

Rutowski, E. S.,
"Energy Approach to the General Aircraft Performance Problem," Journal of the Aeronautical Sciences, Vol. 21, No. 3, March 1954, pp 187-195 (Also, Annual Summer Meeting of the IAS Aerodynamics Session, 15-17 July 1953--Unrevised form).

Schindler, G. M.,
"Minimum Time Flight Paths," ARS Journal, Vol. 30, No. 4, April 1960, pp 352-355.

Shen, Y. C.,
"General Formulation of the Problem of Optimum Rocket Trajectories," TM-833, Aerojet-General (Azusa, California), November 1959.

"Multiplier Rule in the Calculus of Variations and Its Application to Optimum Performance of Rocket Vehicles," TM-832, Aerojet-General (Azusa, California), November 1959.

"Formulation of the Optimum Rocket Trajectory," ARS Journal, Vol. 31, No. 1, January 1961, pp 89-90.

Simon, W. E.,
"An Extension of the Method of Steepest Descent for Digital Computer Application," Research Report No. R-60-39, The Martin Company (Denver), January 1961.

"Philosophy and Technique for Application of the Modified Method of Steepest Descent

to a Wide Class of Problems," Report No. IOL 214-163-60, North American Aviation (Downey, California), September 1960.

"A Modified Method of Steepest Descent for the General Problem of Finding Extremal Solutions, with Particular Application to Non-linear Least Squares," Report No. IOL 214-139-60, North American Aviation (Downey, California), August 1960.

Smith, E. Q.,
"Optimum Intercept Trajectories for Supersonic Fighters (U)," Naval Air Missile Test Center Technical Memorandum Report 107, 30 August 1957.

Smith, E. Q., and Bok, J. R.,
"Optimum Thrust Programming for Air-to-Air Missiles," Naval Air Missile Test Center Informal Report No. CT-39-56, 20 February 1957 (Part I published in the Bulletin of the 12th Meeting of the Joint Army-Navy-Air Force Solid Propellant Group reporting the Symposium on Design and Performance Optimization, Naval Ordnance Laboratory (White Oak, Maryland), 7-9 May 1956).

Smith, G. C.,
"The Calculation of Minimal Orbits," Astronautica Acta, Vol. 5, No. 5, 1959, pp 253-254.

Stancil, R. T., and Kulakowski, L. J.,
"Rocket Boost Vehicle Mission Optimizations," Preprint No. 1449-60, American Rocket Society (New York), 1960 (Also, Report No. ERR-FW-024, Convair, 27 July 1960, 35 pp) (Also, ASTIA No. AD-255 027).

Stark, H. M.,
"Optimum Trajectories Between Two Terminals in Space," ARS Journal, Vol. 31, No. 2, February 1961, pp 261-262.

Szebehely, V. G.,
"Equations for Thrust Programs," XIth International Astronautical Congress (Stockholm), Trajectories Session, 1960.

Templeman, W. H.,
"Comparison of Minimum Energy Paths and Apogee Designation Paths," ARS Journal, Vol. 29, No. 2, November 1959.

Theodorsen, T.,
"Optimum Path of an Airplane-Minimum Time Climb," Journal of Aerospace Sciences, Vol. 26, No. 10, October 1959, pp 637-642.

Ting, L.
"Approximations in Variational Problems," PIBAL Report No. 610, AFOSR TN 60-789, Polytechnic Inistitute of Brooklyn (New York), July 1960 (Also, Aerospace Engineering, January 1961).

"Approximating Technique for Variational Problems," Aerospace Engineering, January 1961, pp 32-33 and 89-91.

Traenkle, C. A.,
"Design Parameters and Optimization of Missile Trajectories," Zeitschrift fur Flugwissenschaften, Vol. 7, No. 10, October 1959, pp 287-293 (Also, WADC TR 58-580, September 1958) (Also, ASTIA No. AD-204 805).

"Mechanics of the Power and Launching Phase for Missiles and Satellites," Ingenieur Archiv (Festschr), Vol. 28, 1959, pp 335-356) (Also, WADC TR 58-579, September 1958) (Also, ASTIA No. AD-204 804).

"Optimal Programming and Control of Satellite Orbits," ARDC Wright Air Development Center, Ohio, September 1958, WADC TR 58-581 (Also, Zeitschrift fur Flugwissenschaften, 1959) (Also, ASTIA No. AD-204 806).

"Outline of the Mechanics of the Power and Launching Phase for Missiles and Satellites," Technical Paper No. 958-59, 20 pp, American Rocket Society, 16-20 November 1959.

Valentine, F. A.,
"The Problem of Lagrange with Differential Inequalities as Added Side Conditions," Contributions to the Theory of Calculus of Variations, University of Chicago Press, 1933-1937, pp 405-447 (Also, University of Chicago Press, 1937, Dissertation).

Vargo, L. G.,
"A Generalization of the Minimum Impulse Theorem to the Restricted Three-Body Problem," Journal of the British Interplanetary Society, Vol. 17, September-October 1959, pp 124-126.

Wagnet, W. E.,
"Development and Formulation of an Optimum Trajectory Program for Missiles and Satellite Carriers," Report No. 60 H-515, North American Aviation (Los Angeles), September 1960.

Wang, C. J., Lawrence, H. R. and Anthony, G. W.,
"Optimum Thrust Programming of Nuclear Rockets," Preprint No. 691-58, 13 pp, American Rocket Society, 17-21 November 1958.

ILLUSTRATIONS

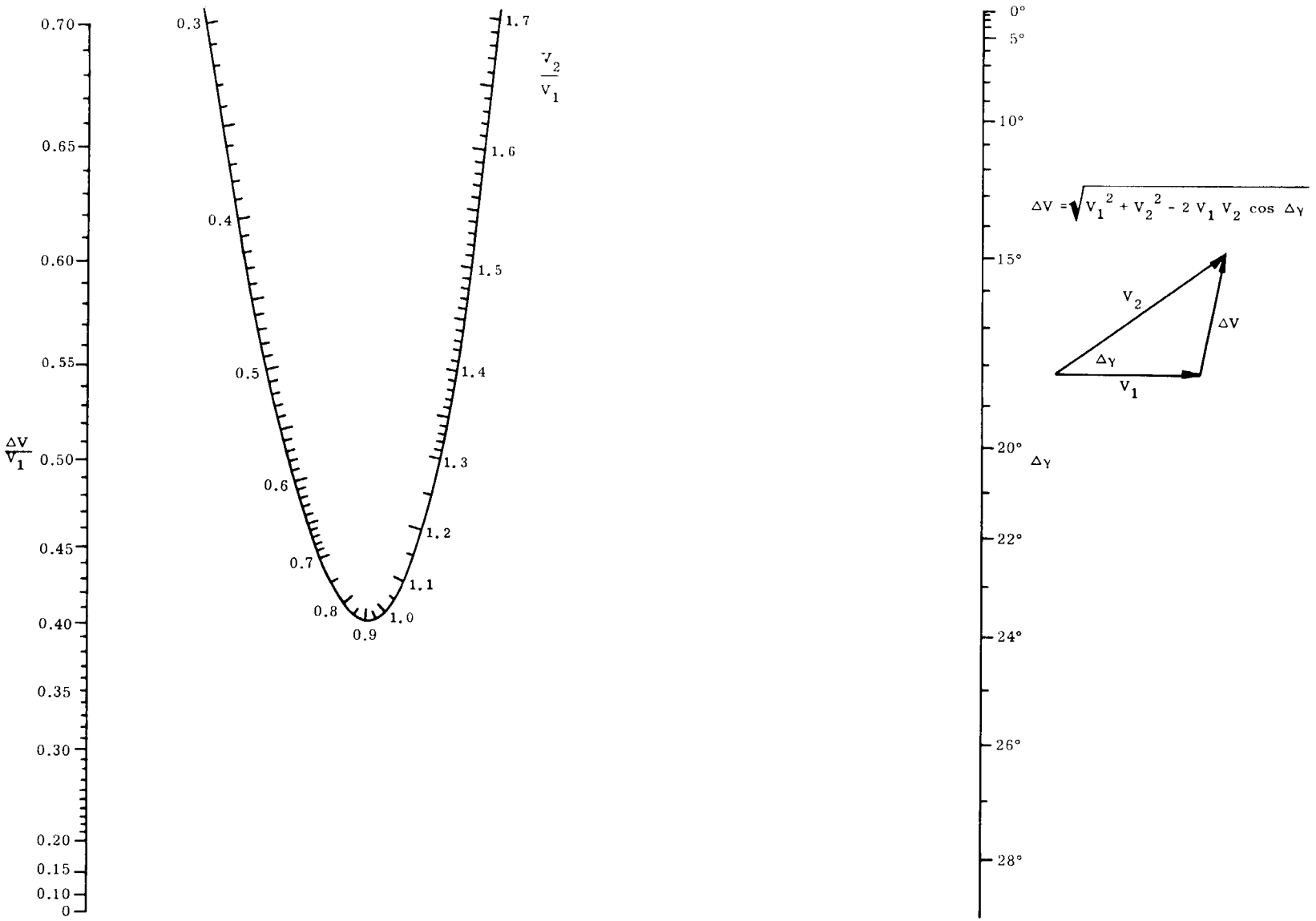

Fig. 1. Solution to the Law of Cosines

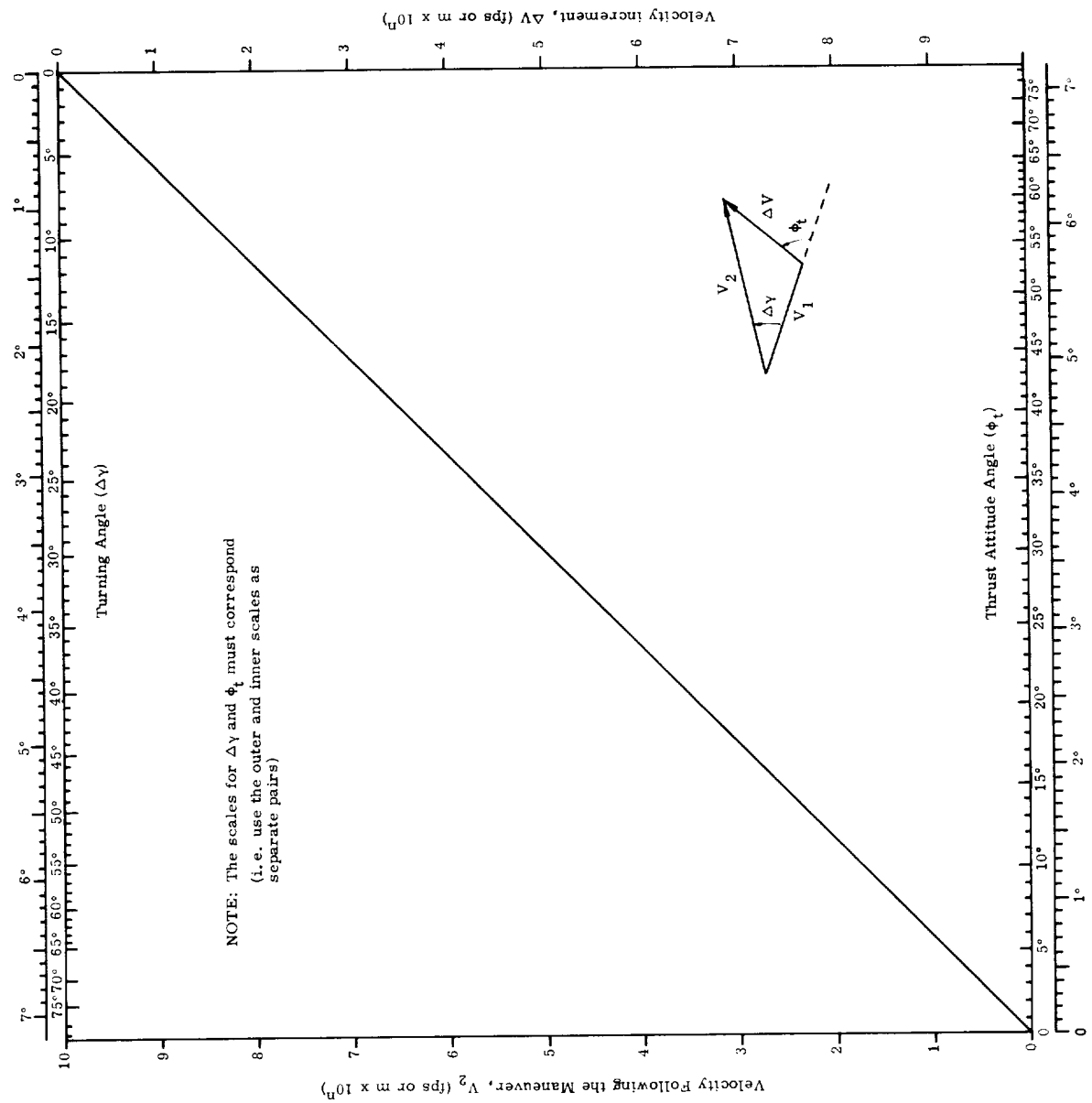

Fig. 2. Solution to the Law of Sines

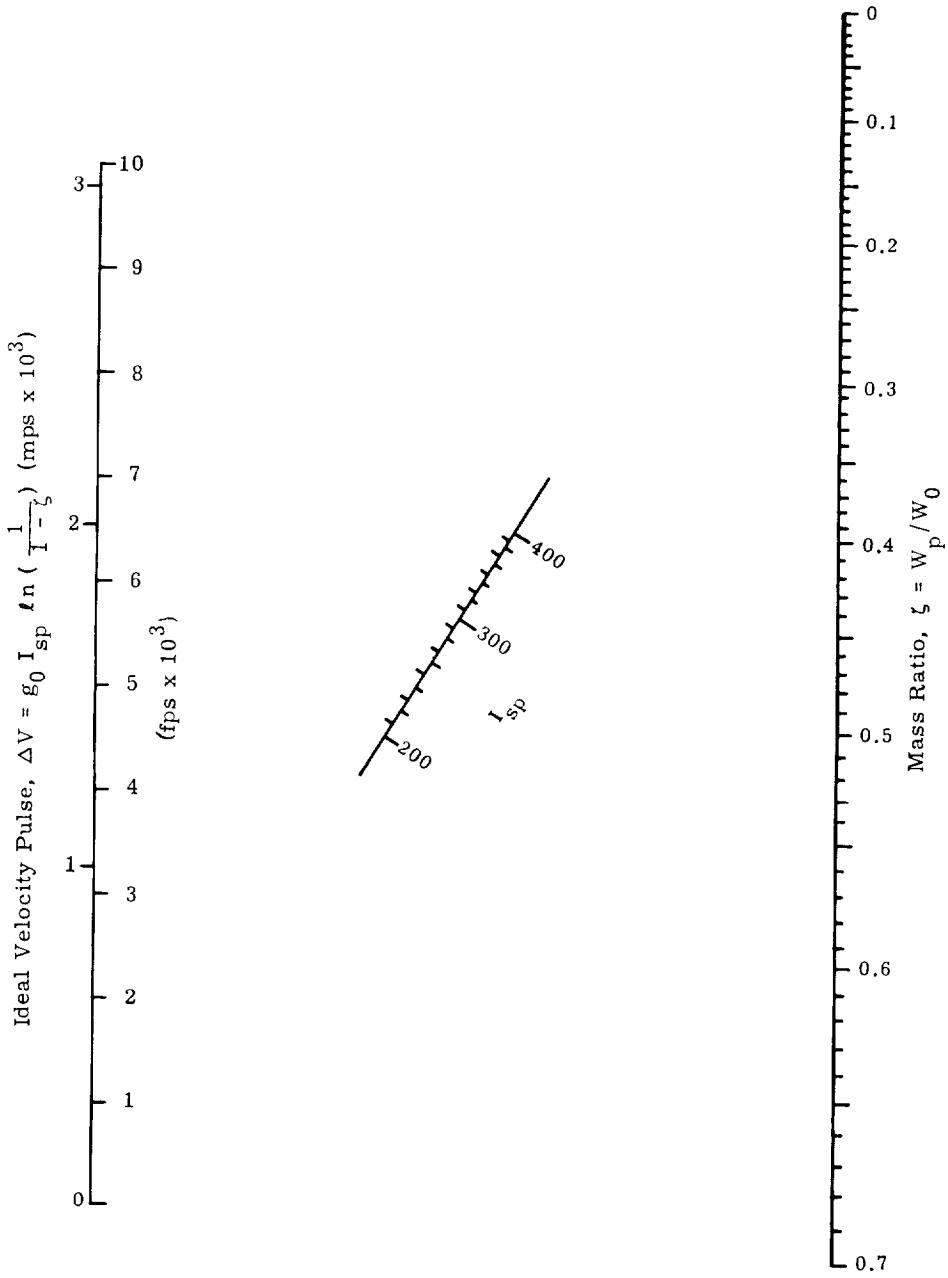

Fig. 3. Total Velocity Increment Required for Two-Pulse Correction to a Circular Orbit

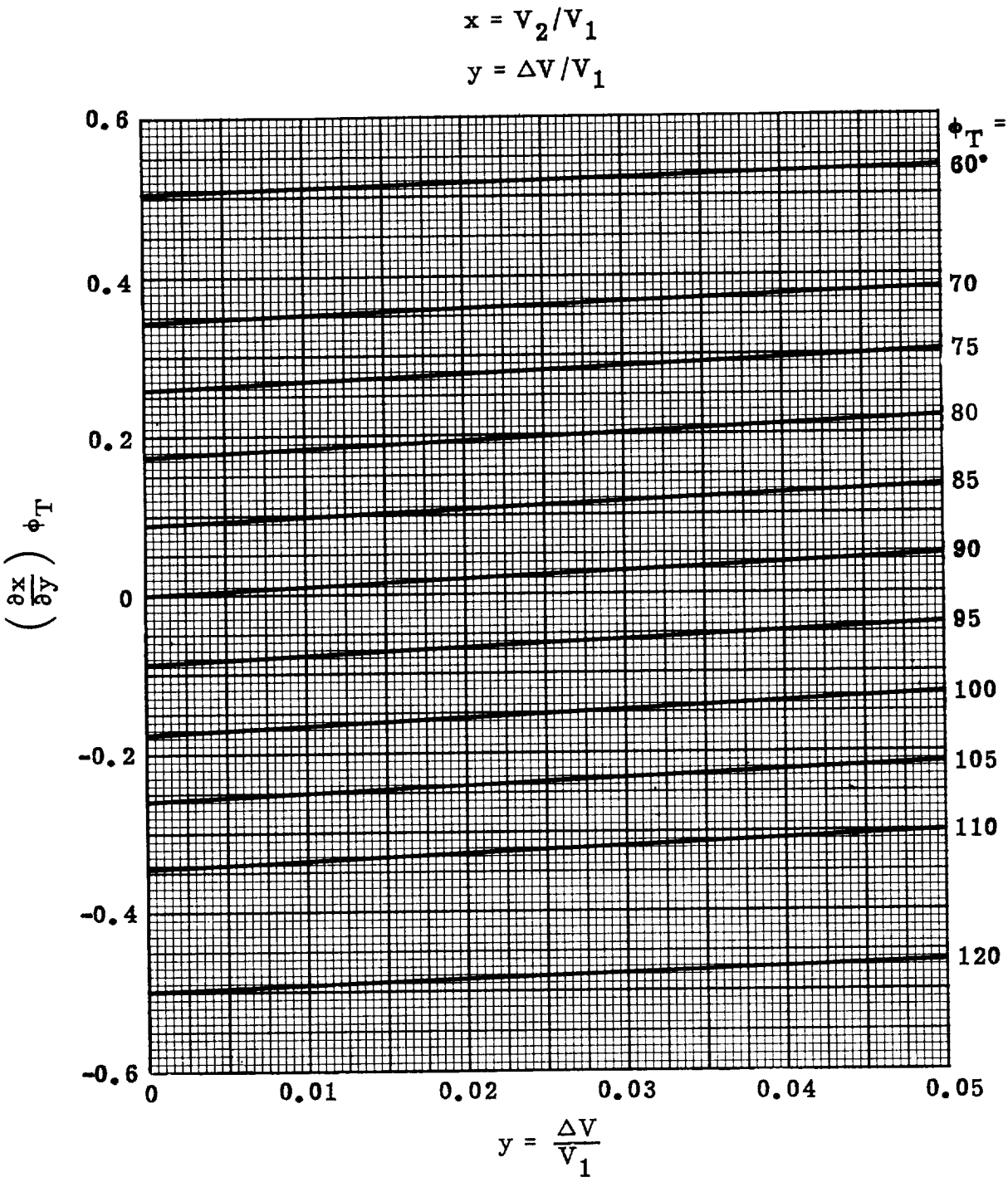

Fig. 4. Effects of Variations in Characteristic Velocity on the Velocity After the Maneuver

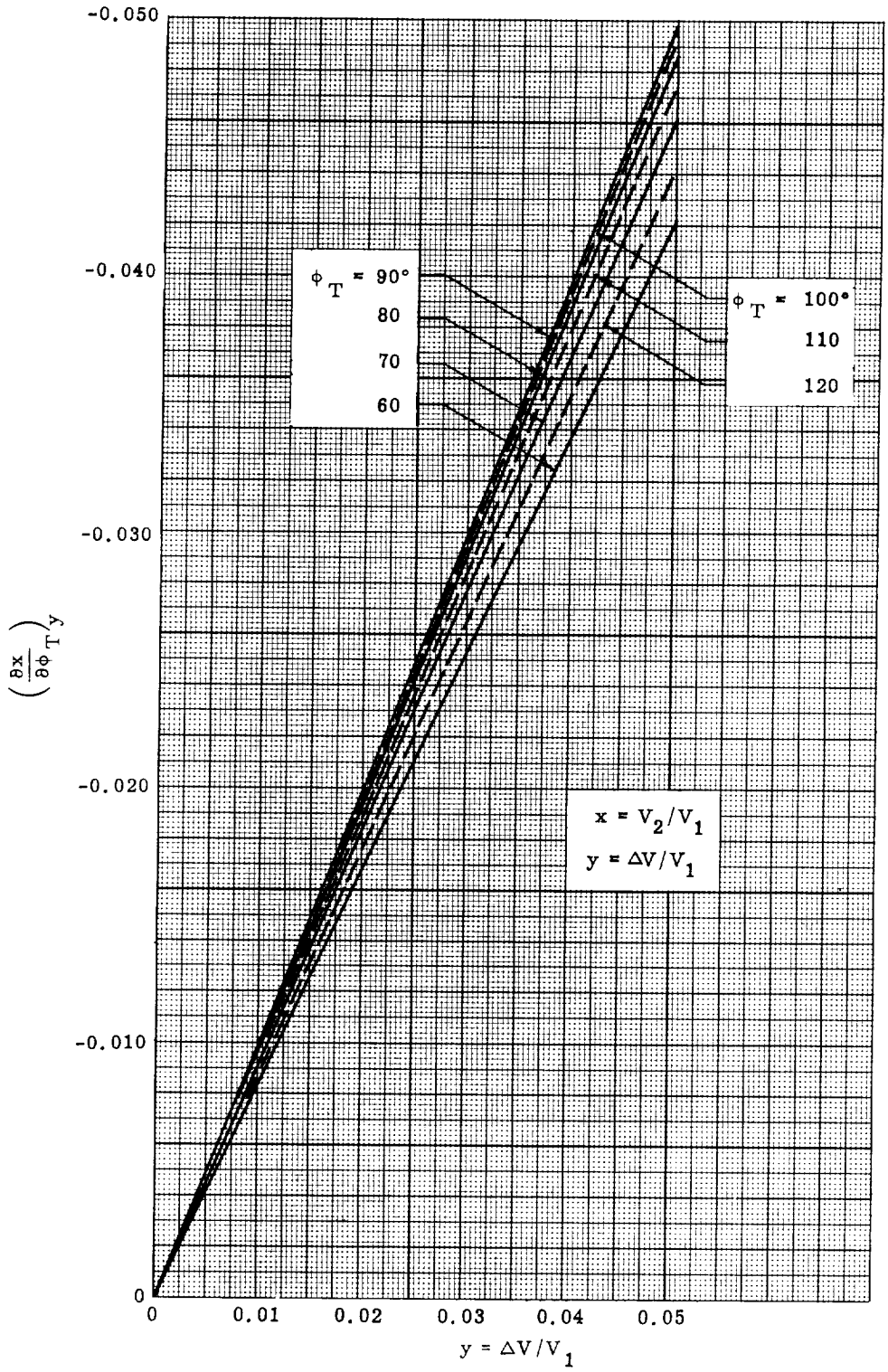

Fig. 5. Effects of Variations in the Pulse Attitude Angle on Vehicle Velocity After the Maneuver

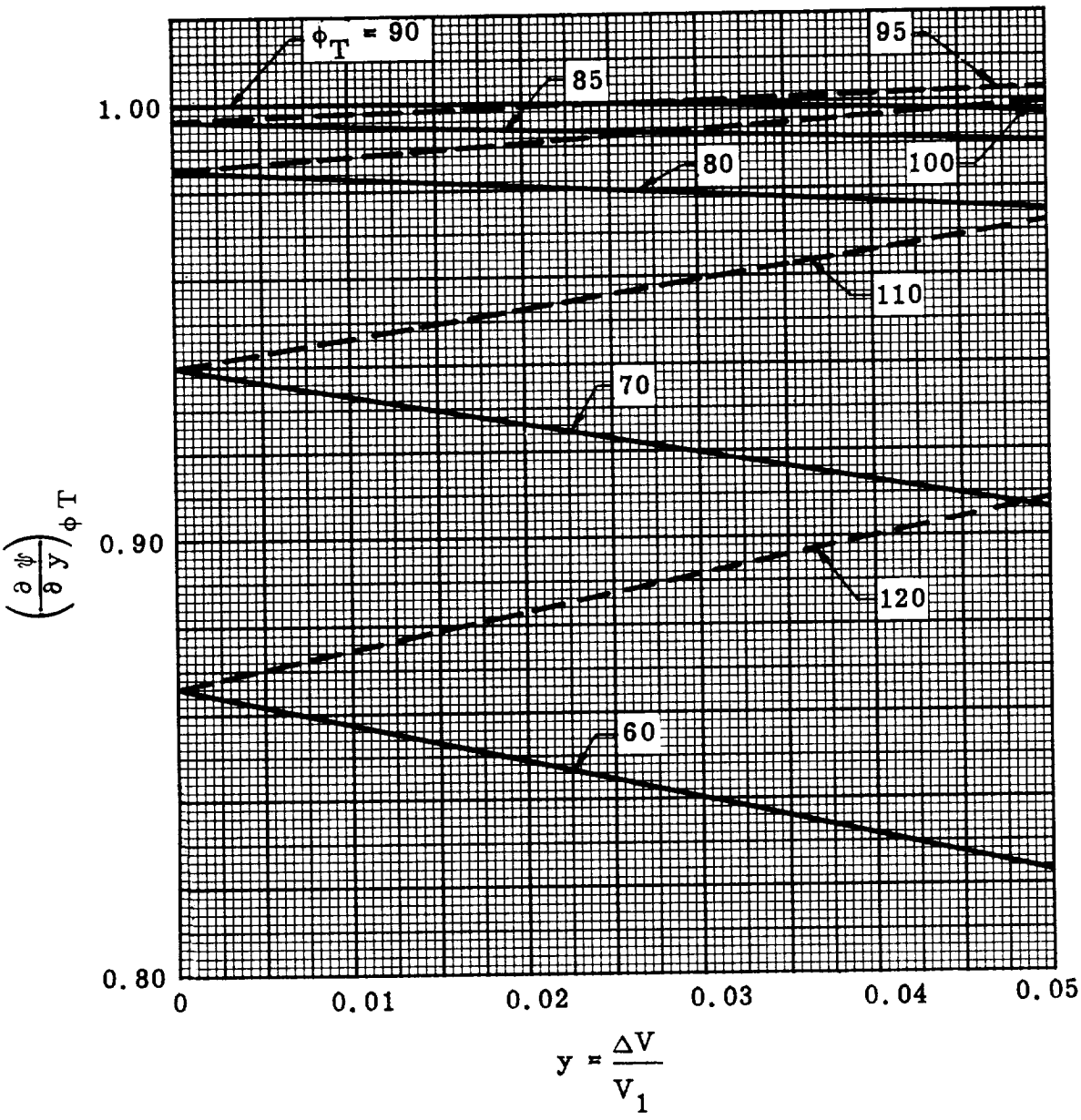

Fig. 6. Effects of Variations in Characteristic Velocity on the Turn Angle

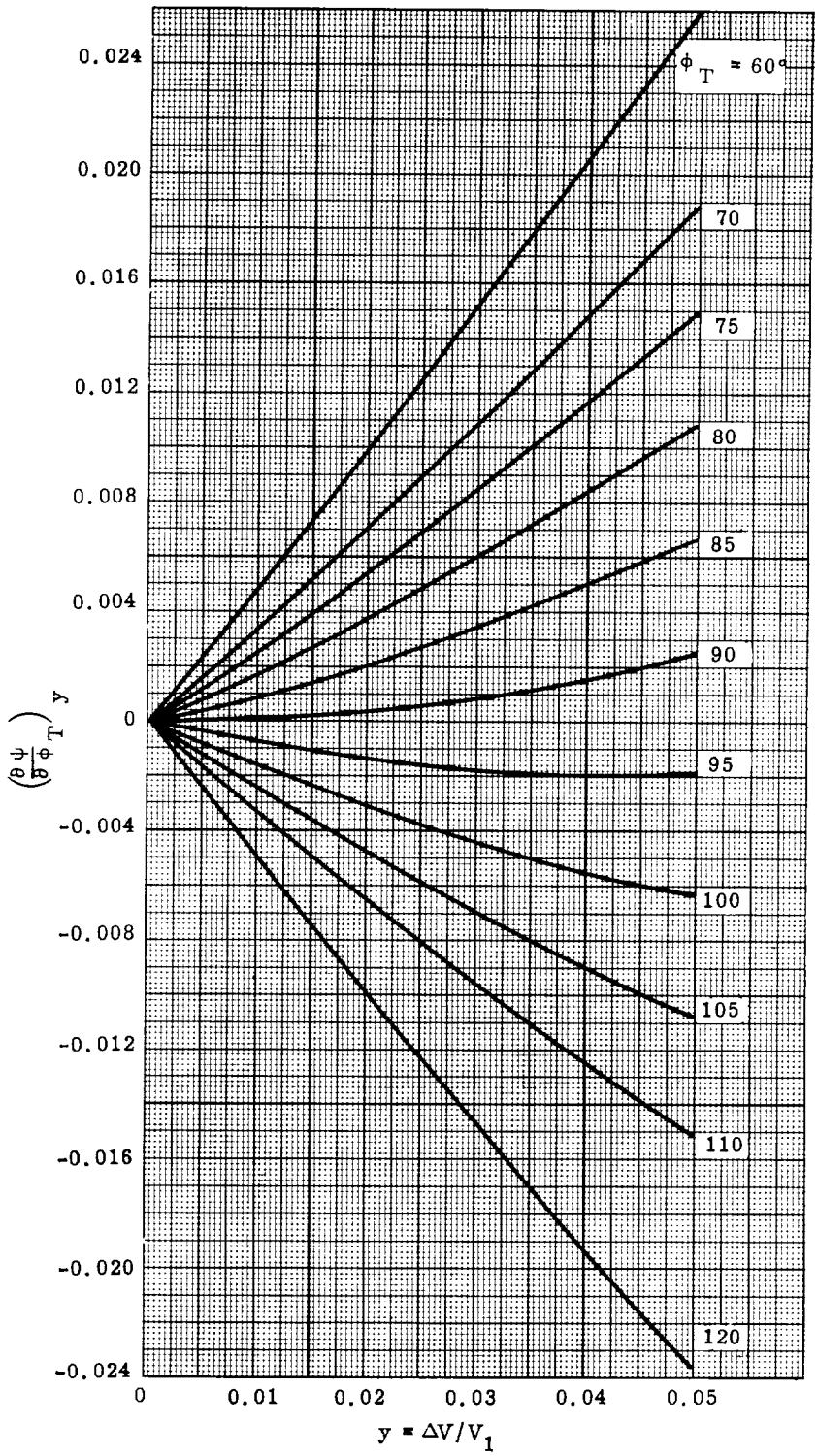

Fig 7. Effects of Variations in Thrust Pulse Angle on the Turn Angle

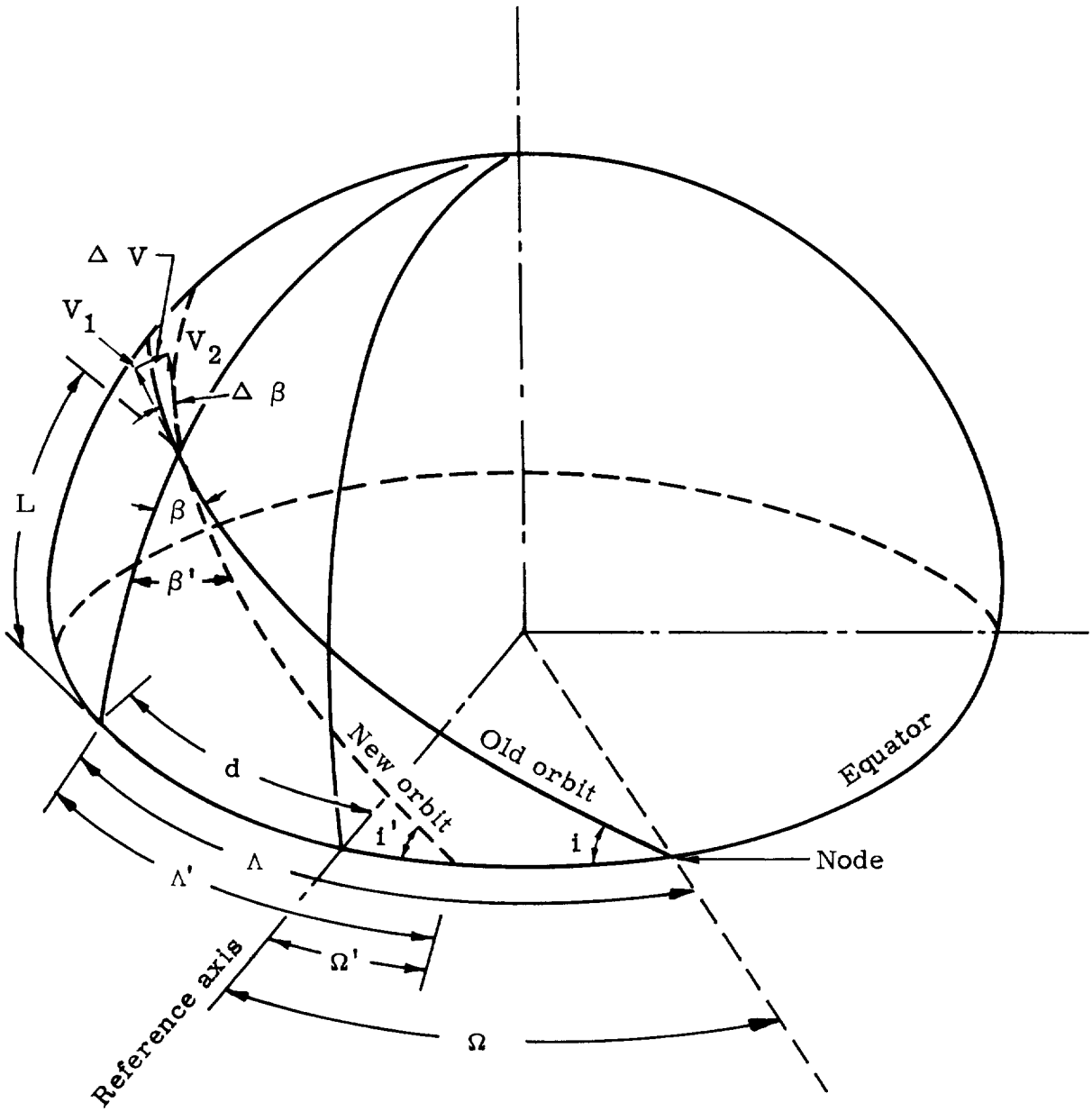

NOTE: No primes denote premaneuver

Primes denote post maneuver

Fig. 8. Maneuvers in Circular Orbits to Change Orbital Inclination and/or the Node

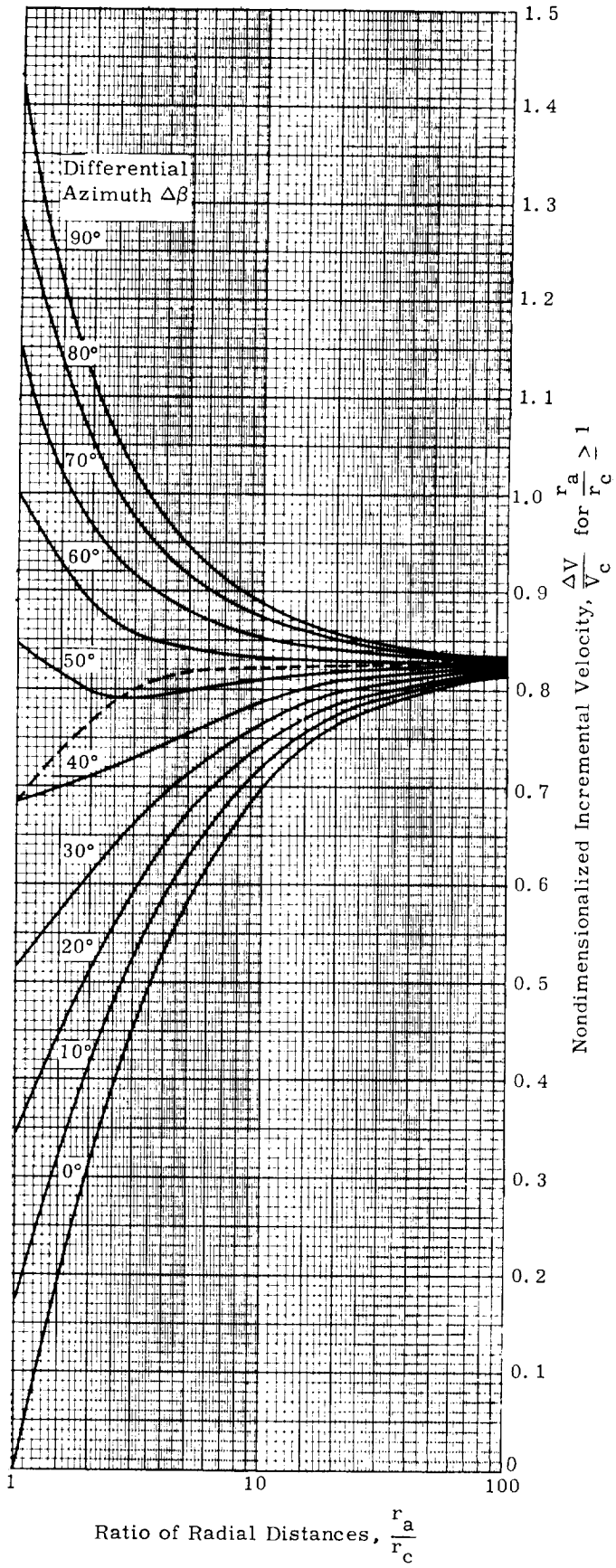

Fig. 9. Nondimensionalized Impulsive Velocity Required to Transfer to a New Altitude, Rotate the Orbital Plane (at that altitude), and Recircularize Upon Arrival at the Initial Orbit

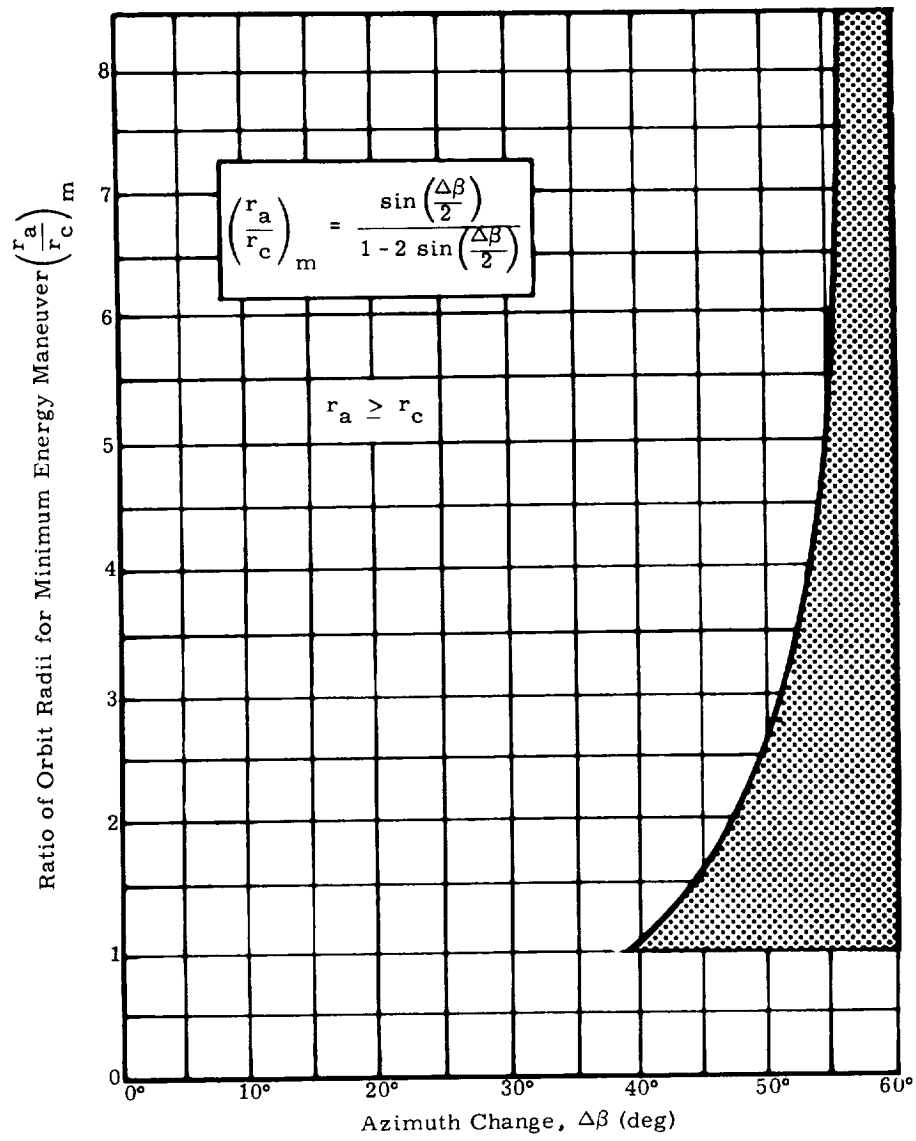

Fig. 10. Ratio of the Interceptor's Apogee Radius to the Radius of the Target's Circular Orbit as a Function of the Azimuth Change for Minimum Energy

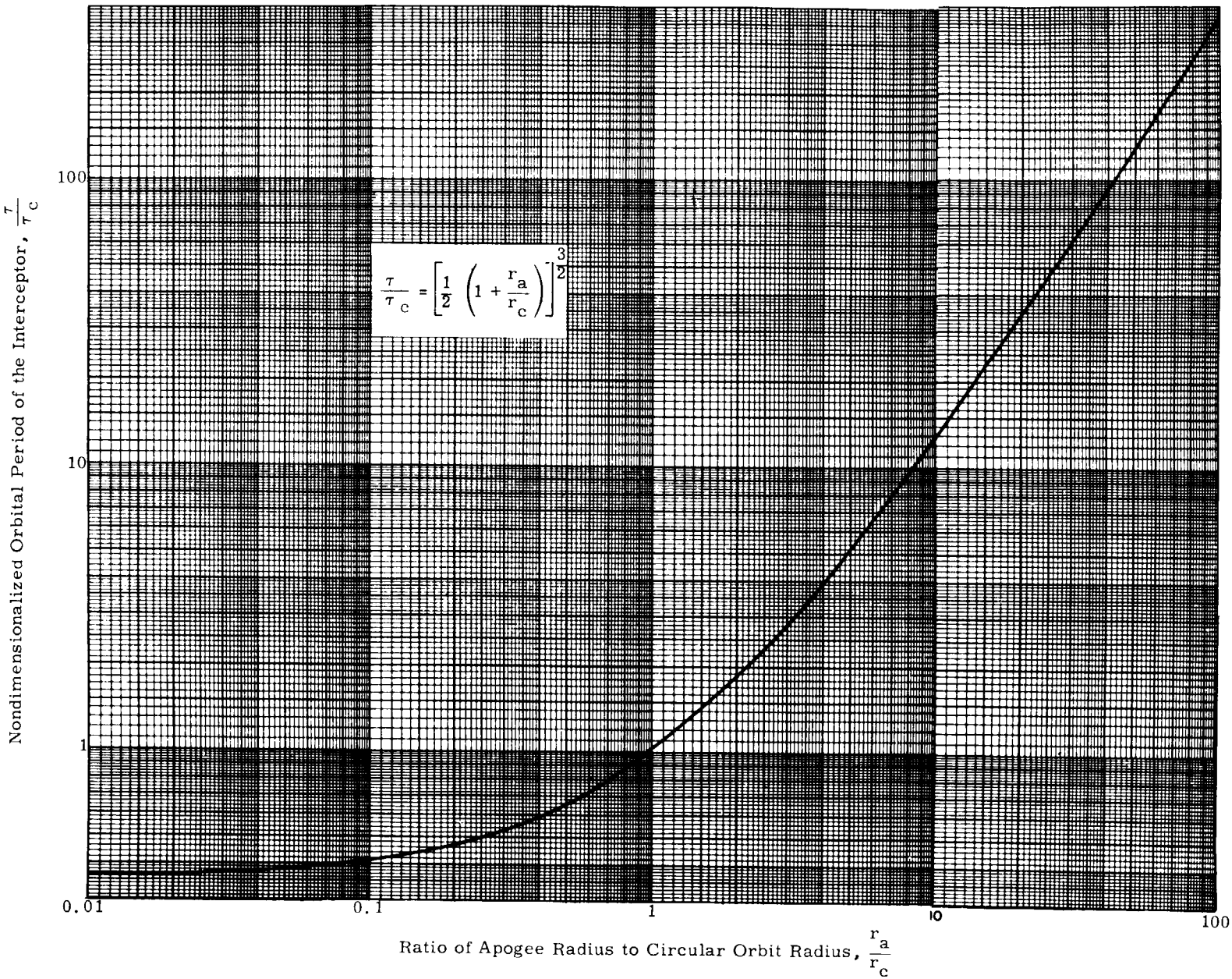

Fig. 11. Nondimensionalized Orbital Period of the Interceptor in Its Maneuvering Orbit (elliptic orbit with apsidal radii equal to r_a and r_c)

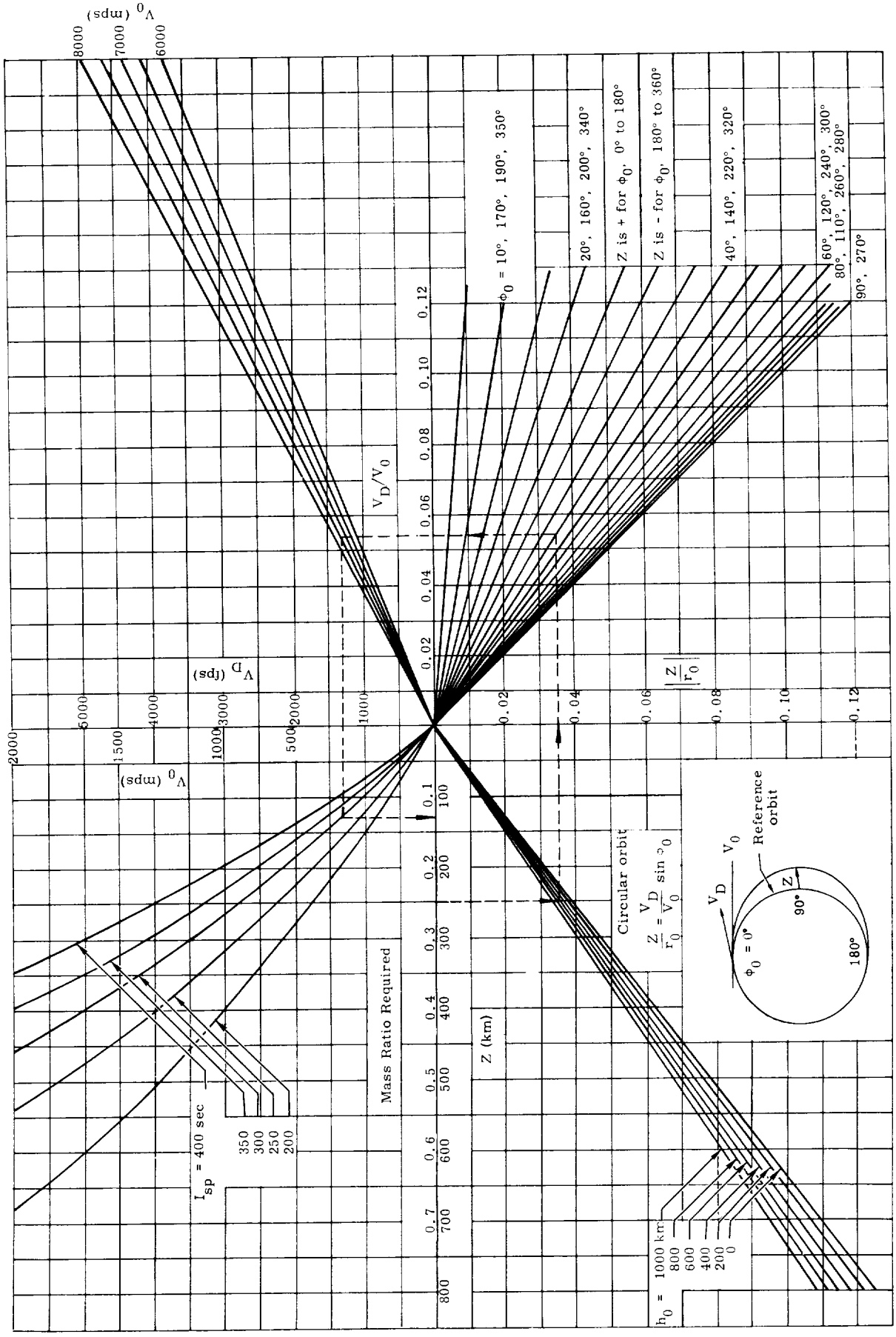

Fig. 12. Fuel Required for Lateral Maneuvers in a Circular Orbit

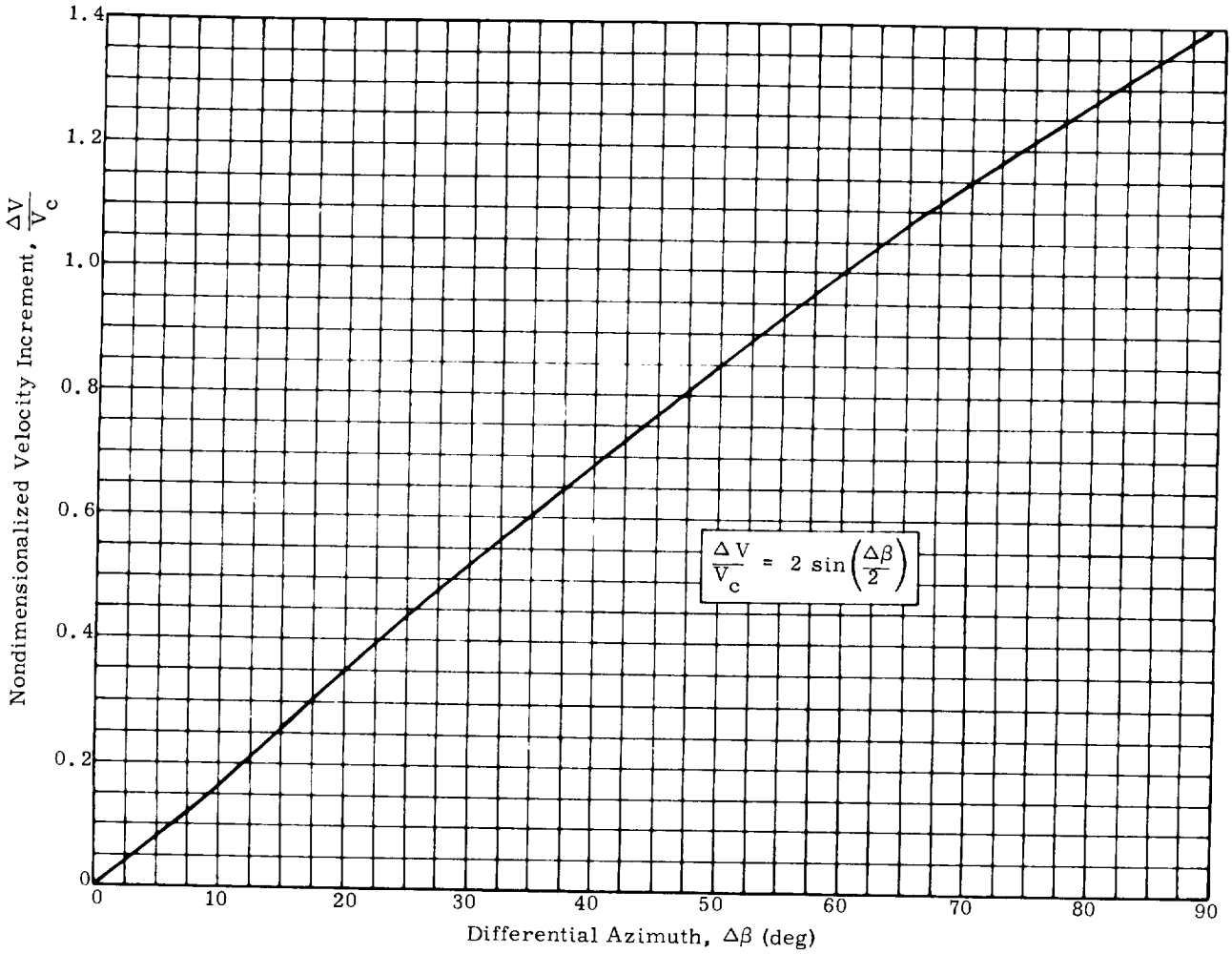

Fig. 13. Nondimensionalized Impulsive Velocity Required to Rotate a Satellite's Orbital Plane

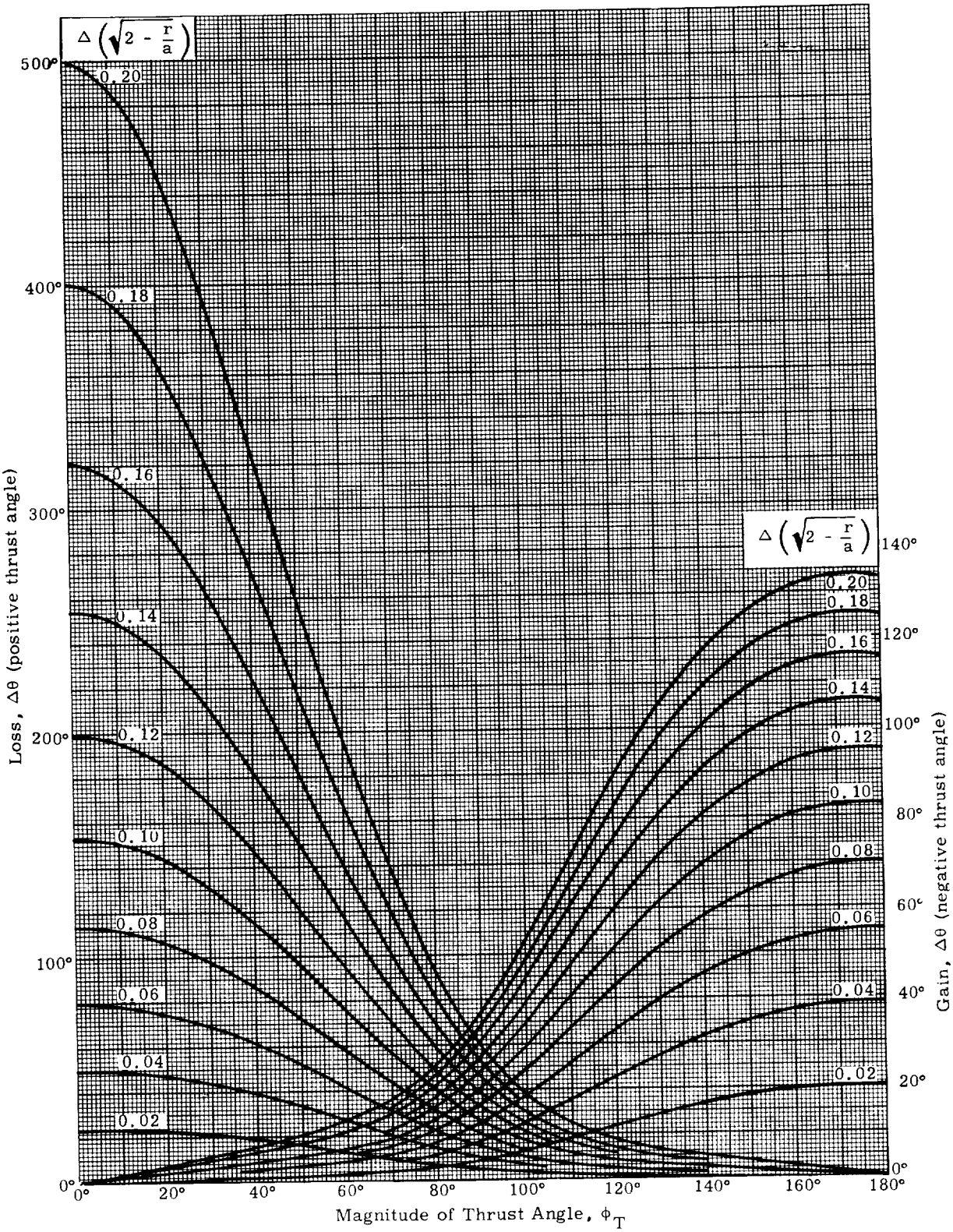

Fig. 14. Maneuver Angle as a Function of Thrust Attitude

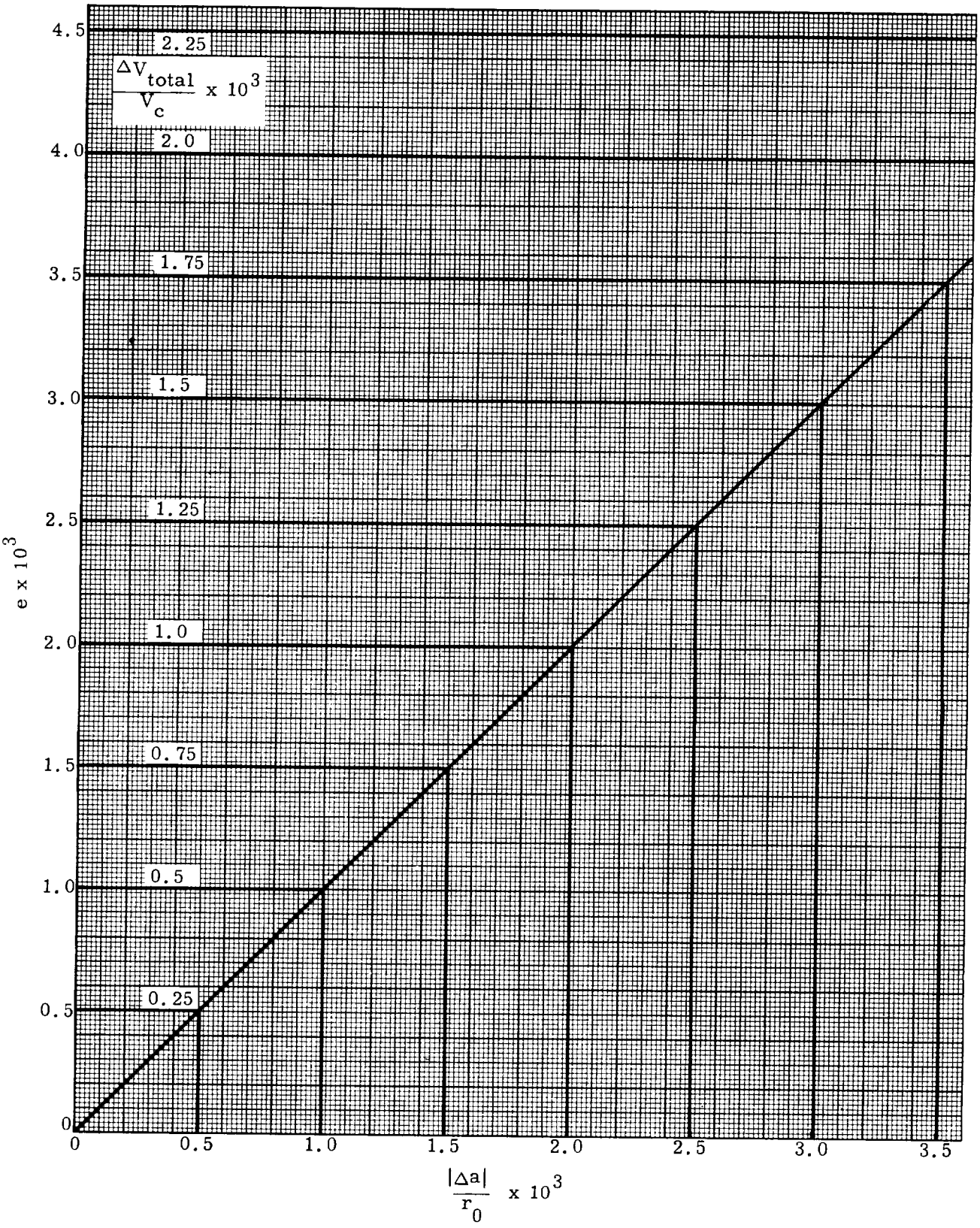

Fig. 15. Total Velocity Increment Required for Two-Pulse Correction to a Circular Orbit

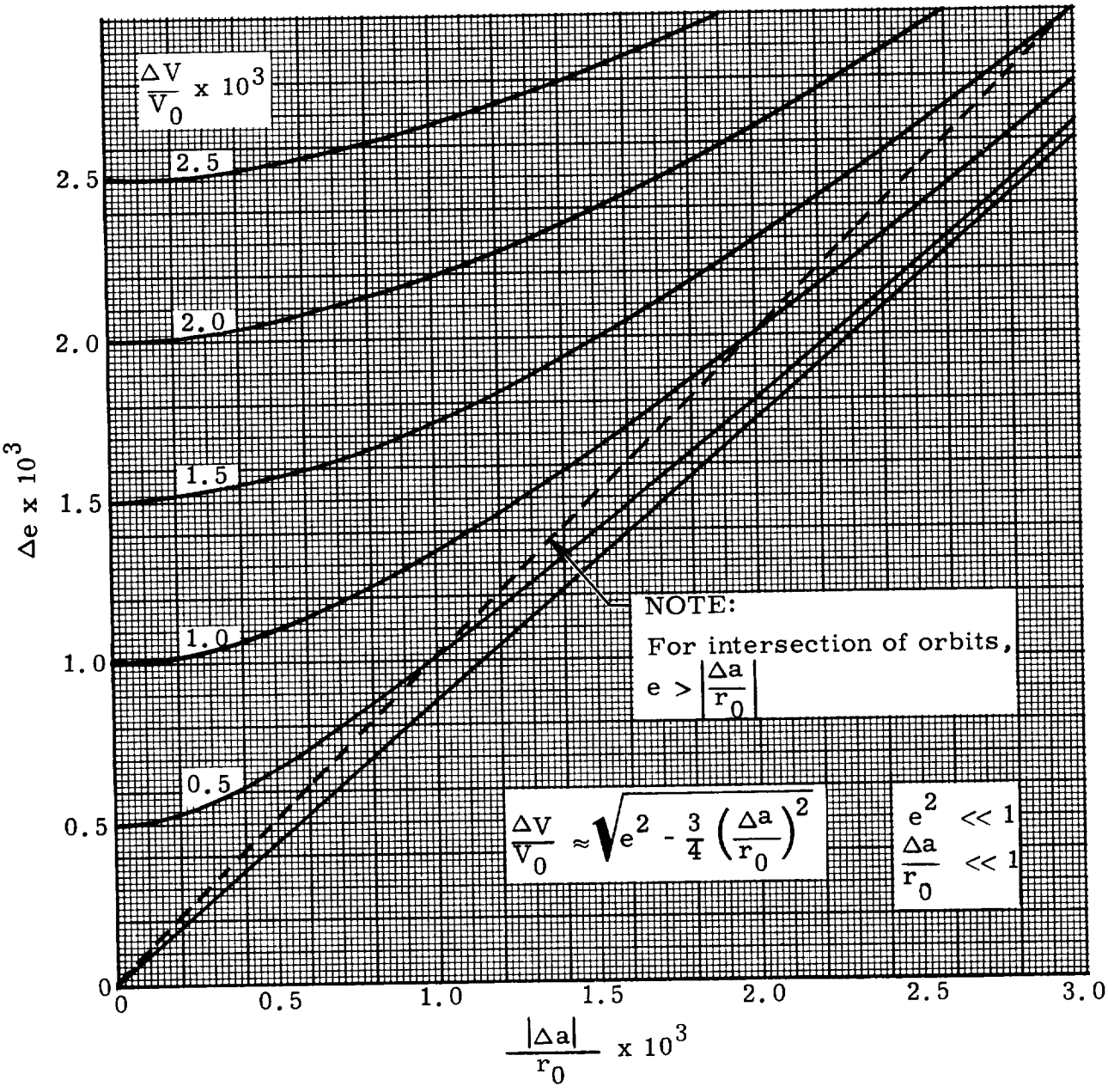

Fig. 16. Velocity Increment for Maintenance of Circular Orbits by an Impulse at Orbit Intersection

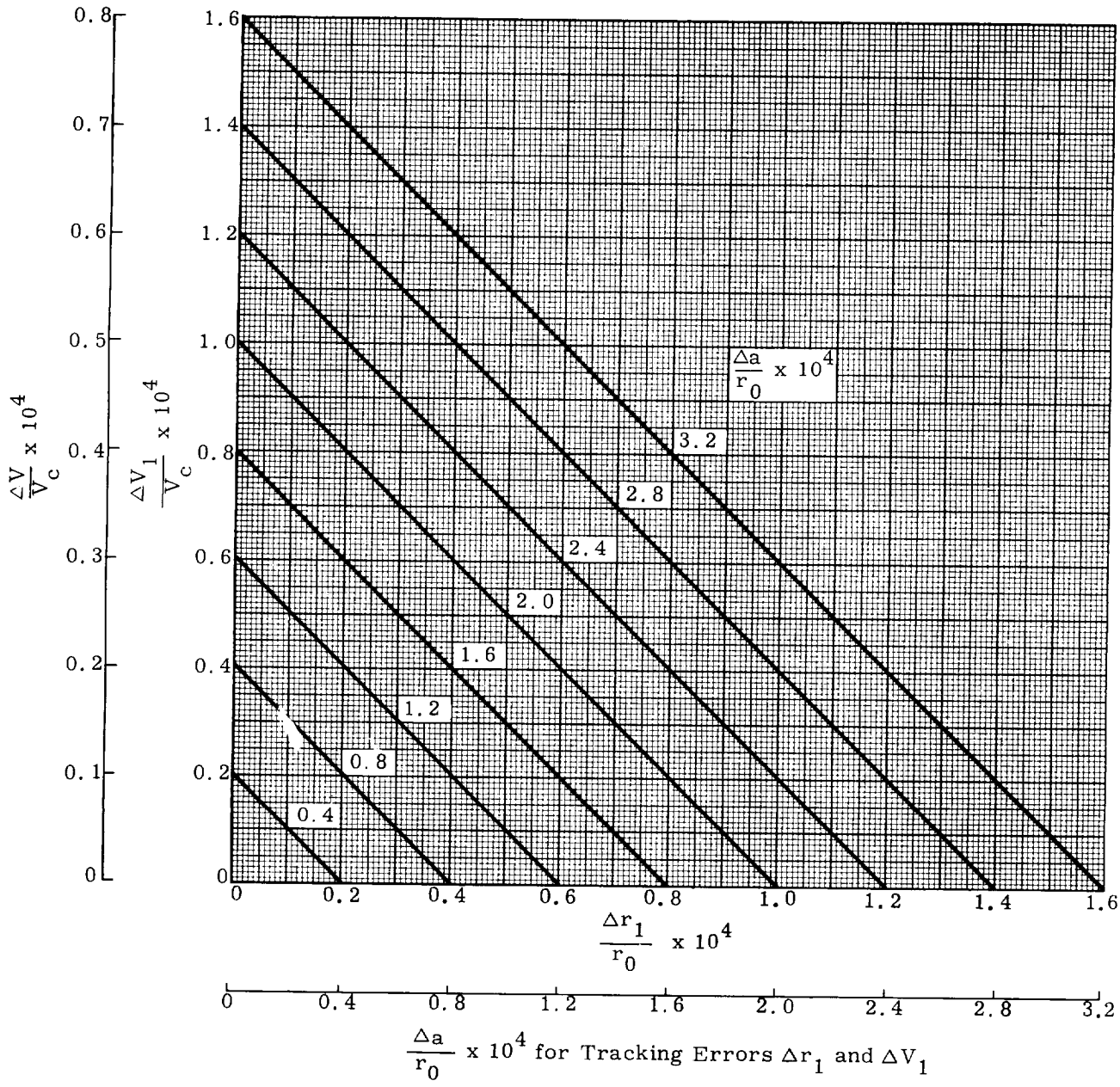

Fig. 17. Error Analysis of Two-Pulse Correction of a Circular Orbit

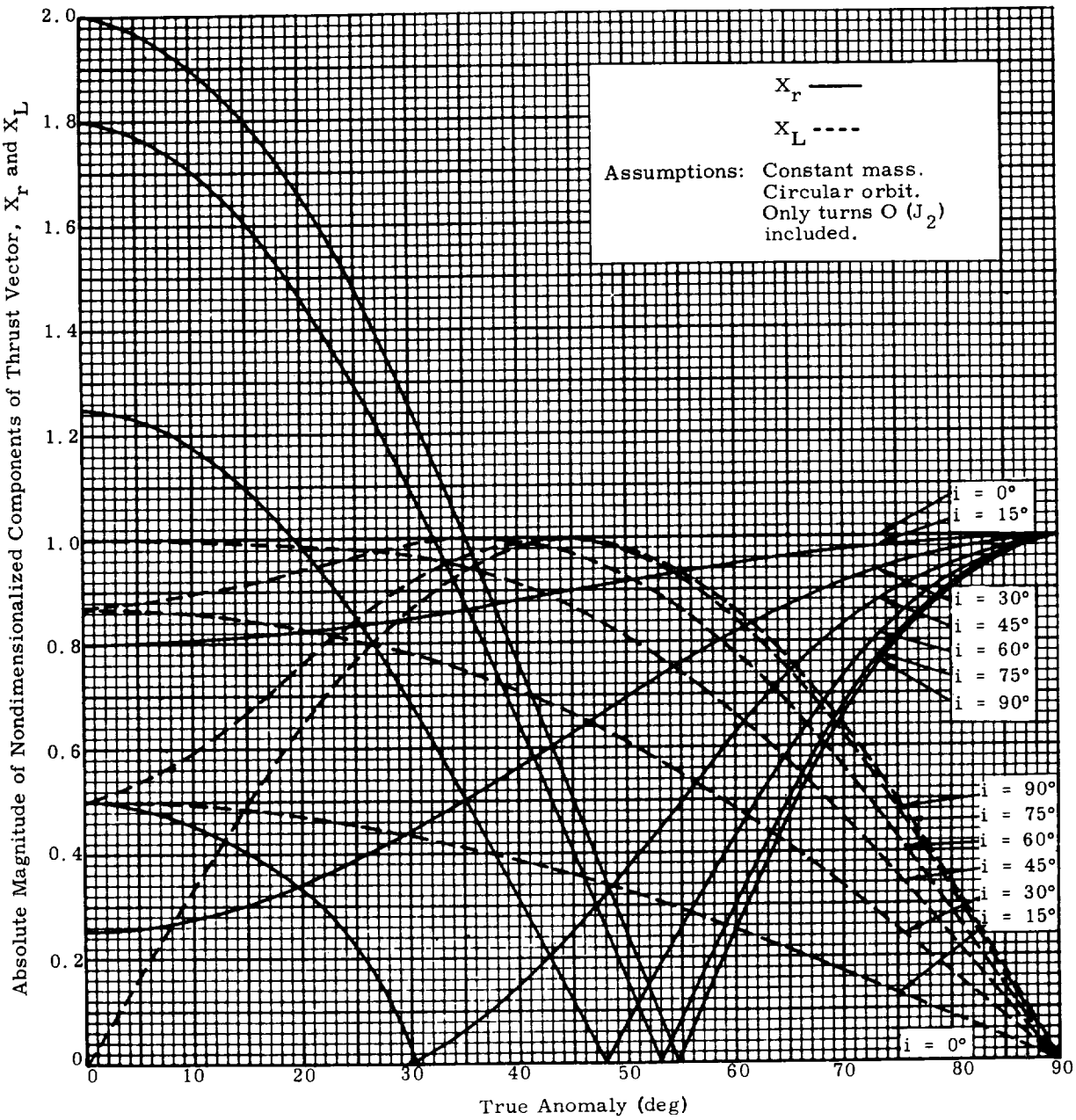

Fig. 18. Absolute Magnitudes of the Nondimensionalized Components of the Thrust Vector as a Function of the True Anomaly for Orbit Inclinations from 0° to 90°

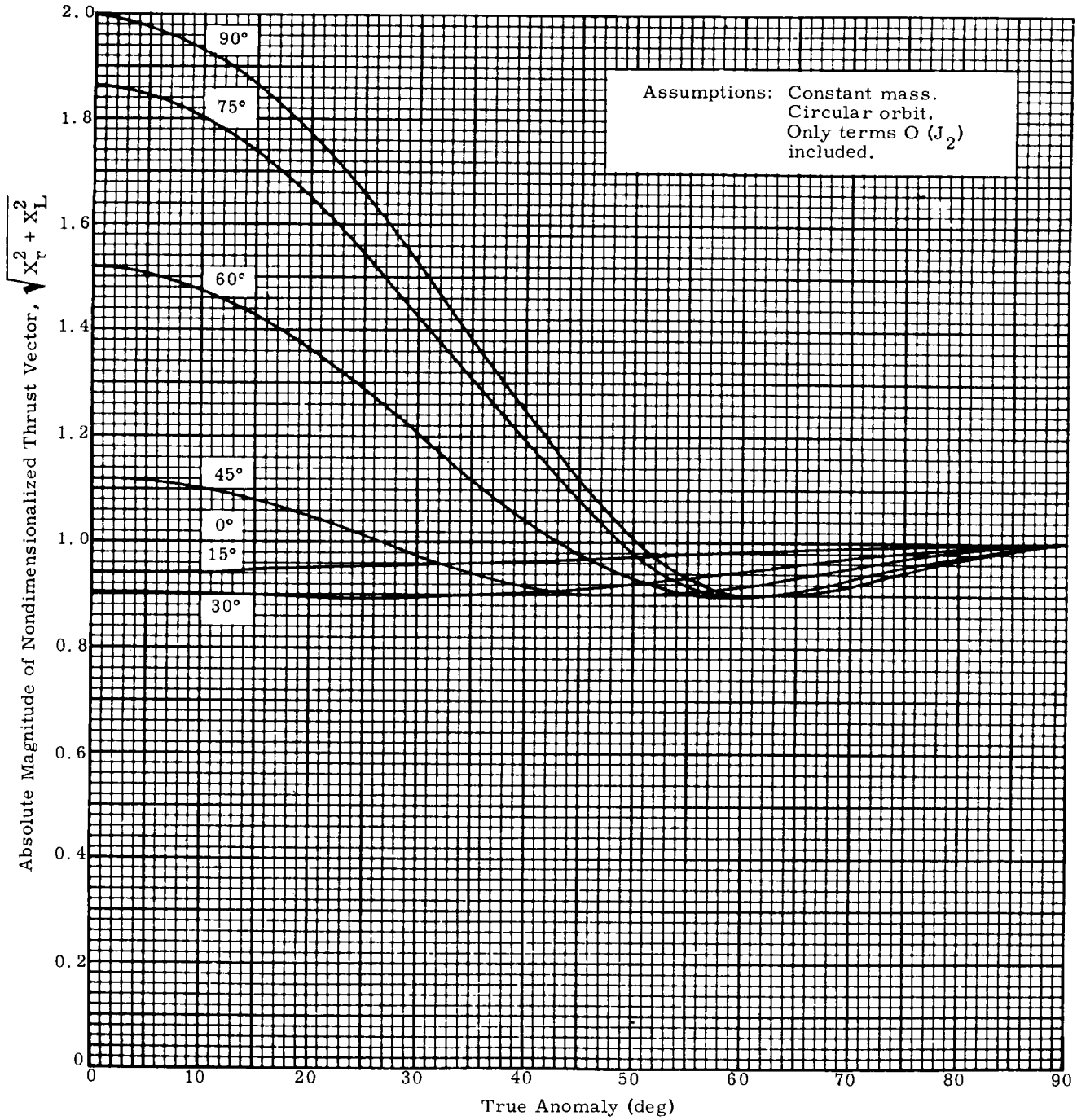

Fig. 19. Absolute Magnitude of the Nondimensionalized Thrust Vector as a Function of True Anomaly

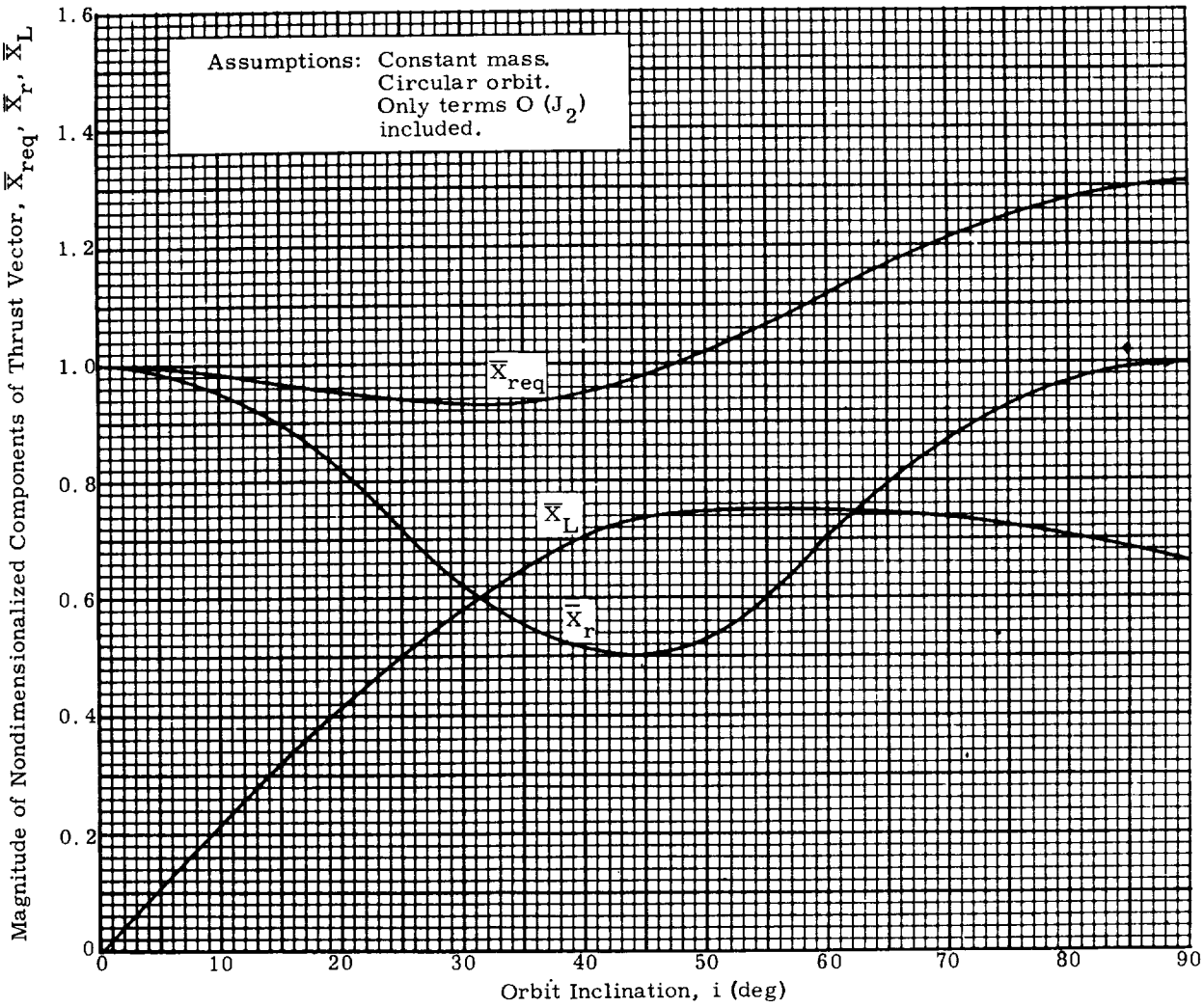

Fig. 20. Magnitudes of the Nondimensionalized Corrective Force and Its Components, Averaged over the Orbit

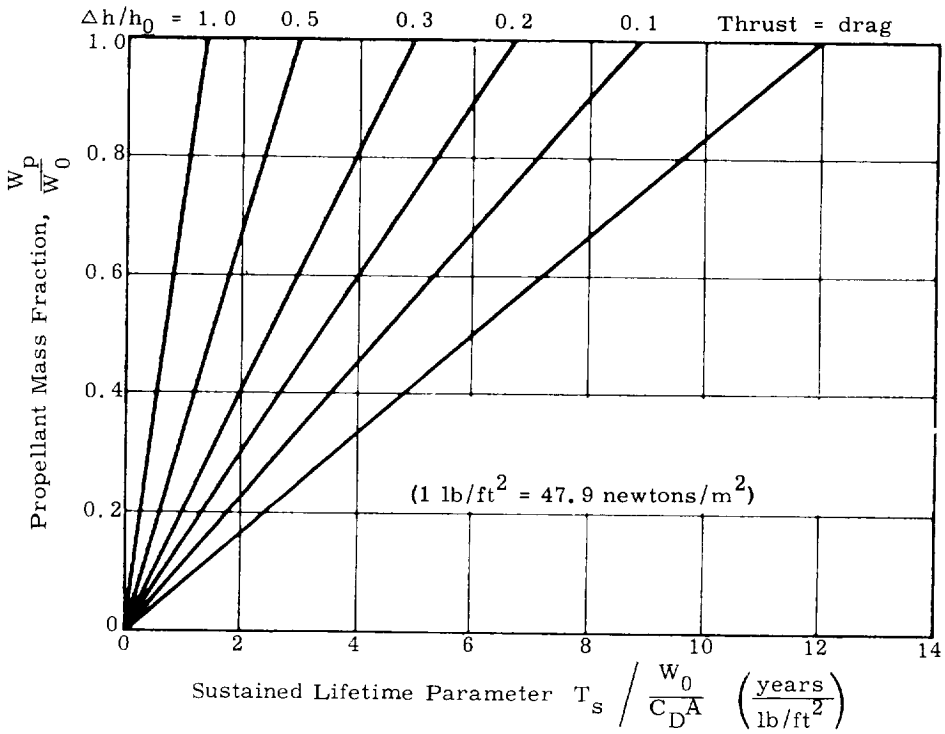

Fig. 21. Discrete Velocity Sustaining System
(h_0 = 300 naut mi = 555 km; I_{sp} = 300 sec)

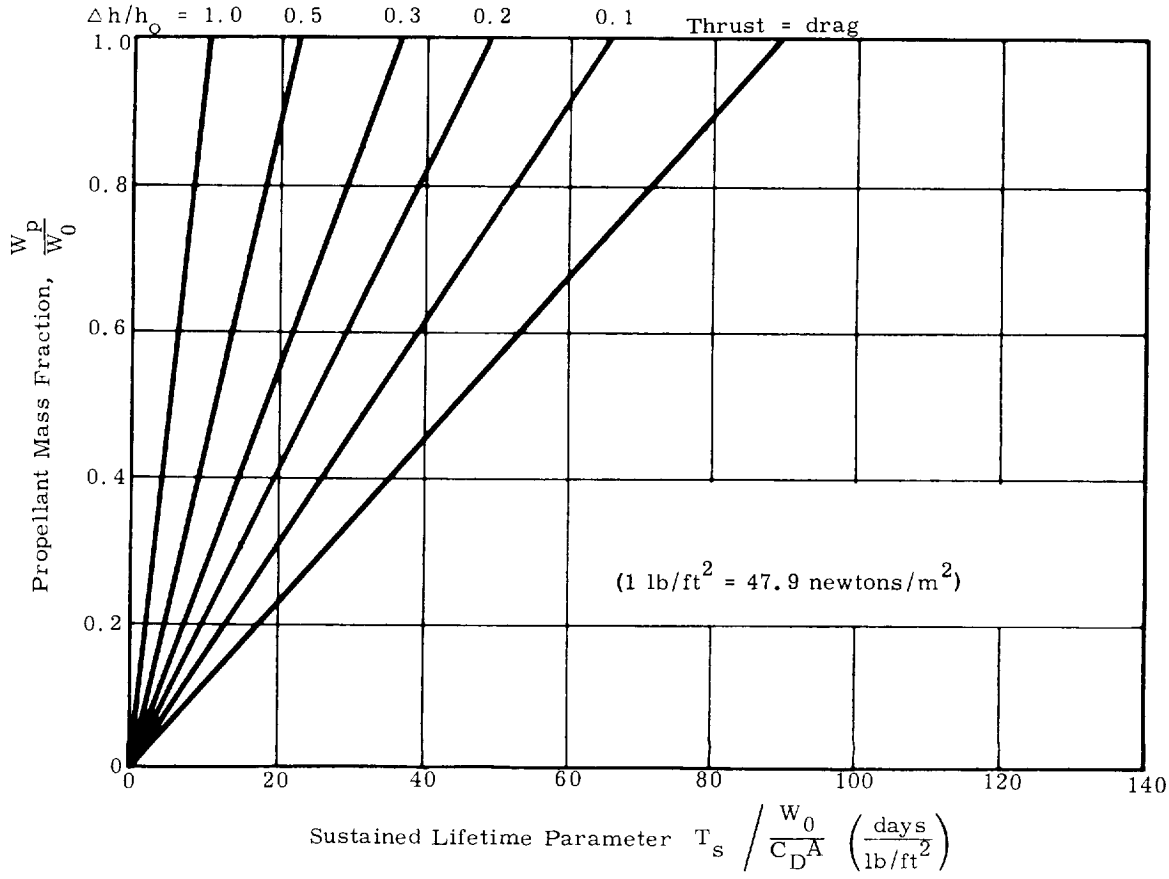

Fig. 22. Discrete Velocity Sustaining System
(h_0 = 200 naut mi = 370 km; I_{sp} = 300 sec)

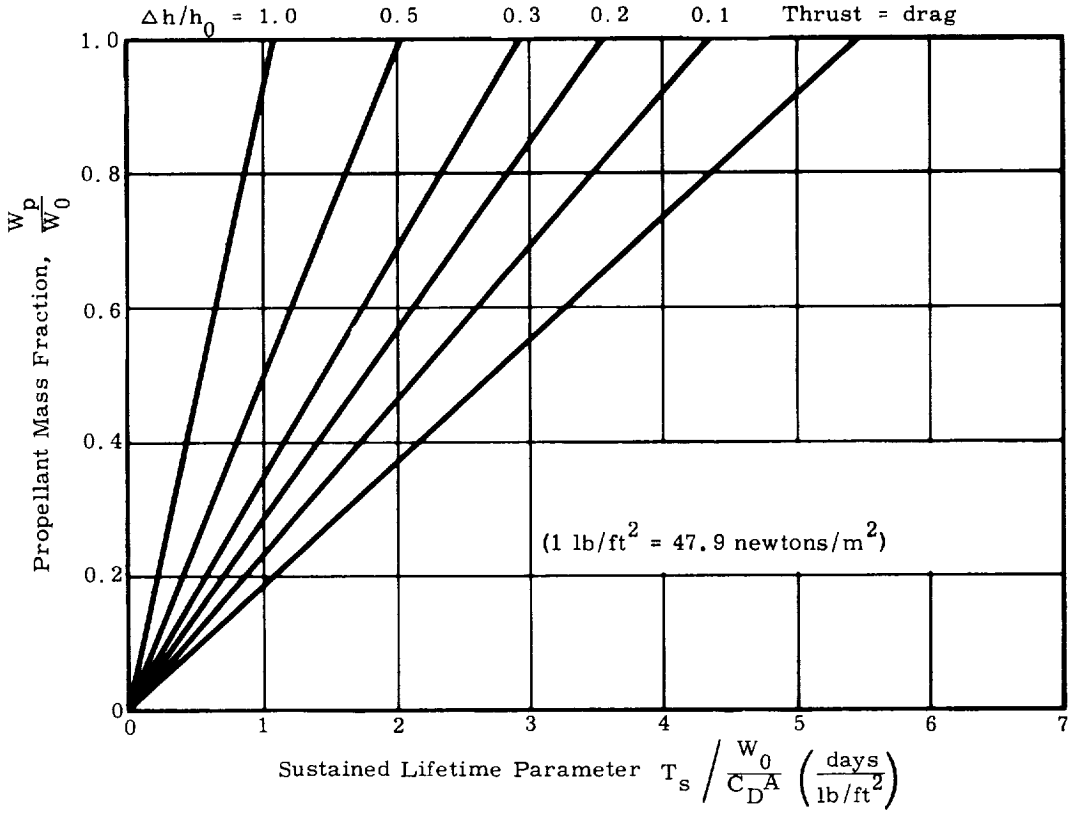

Fig. 23. Discrete Velocity Sustaining System
(h_0 = 100 naut mi = 185 km; I_{sp} = 300 sec)

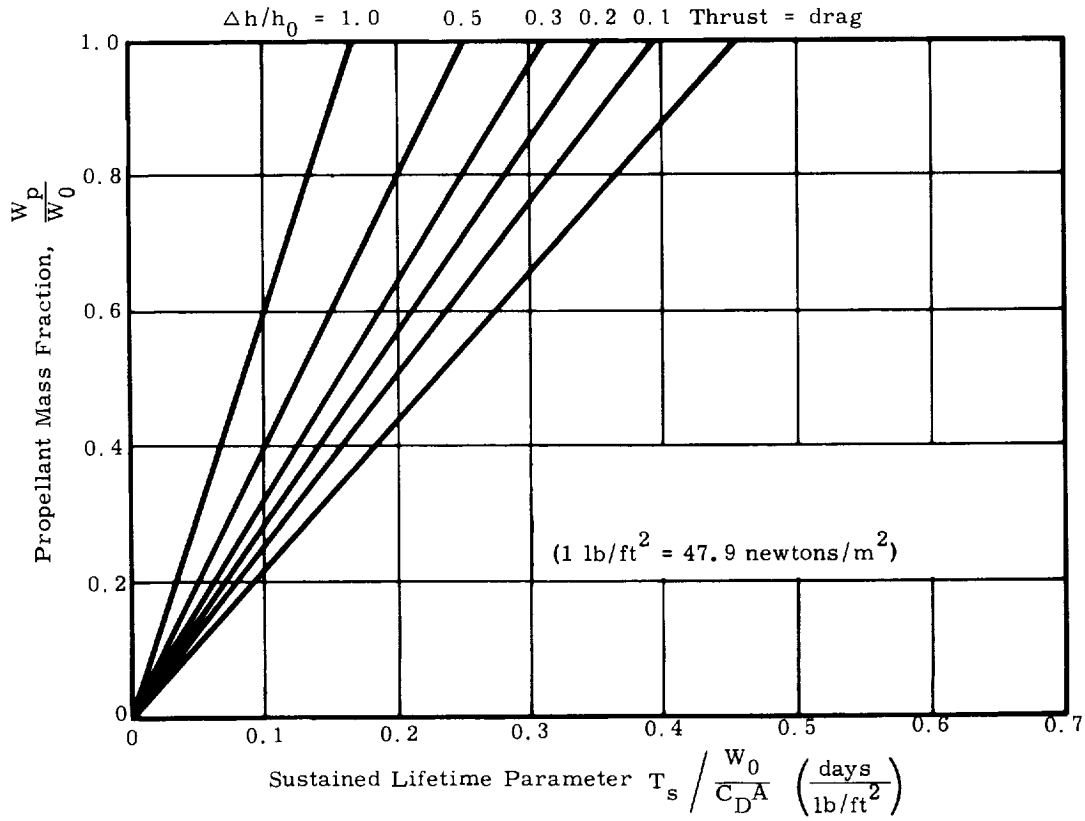

Fig. 24. Discrete Velocity Sustaining System
(h_0 = 50 naut mi = 93 km; I_{sp} = 300 sec)

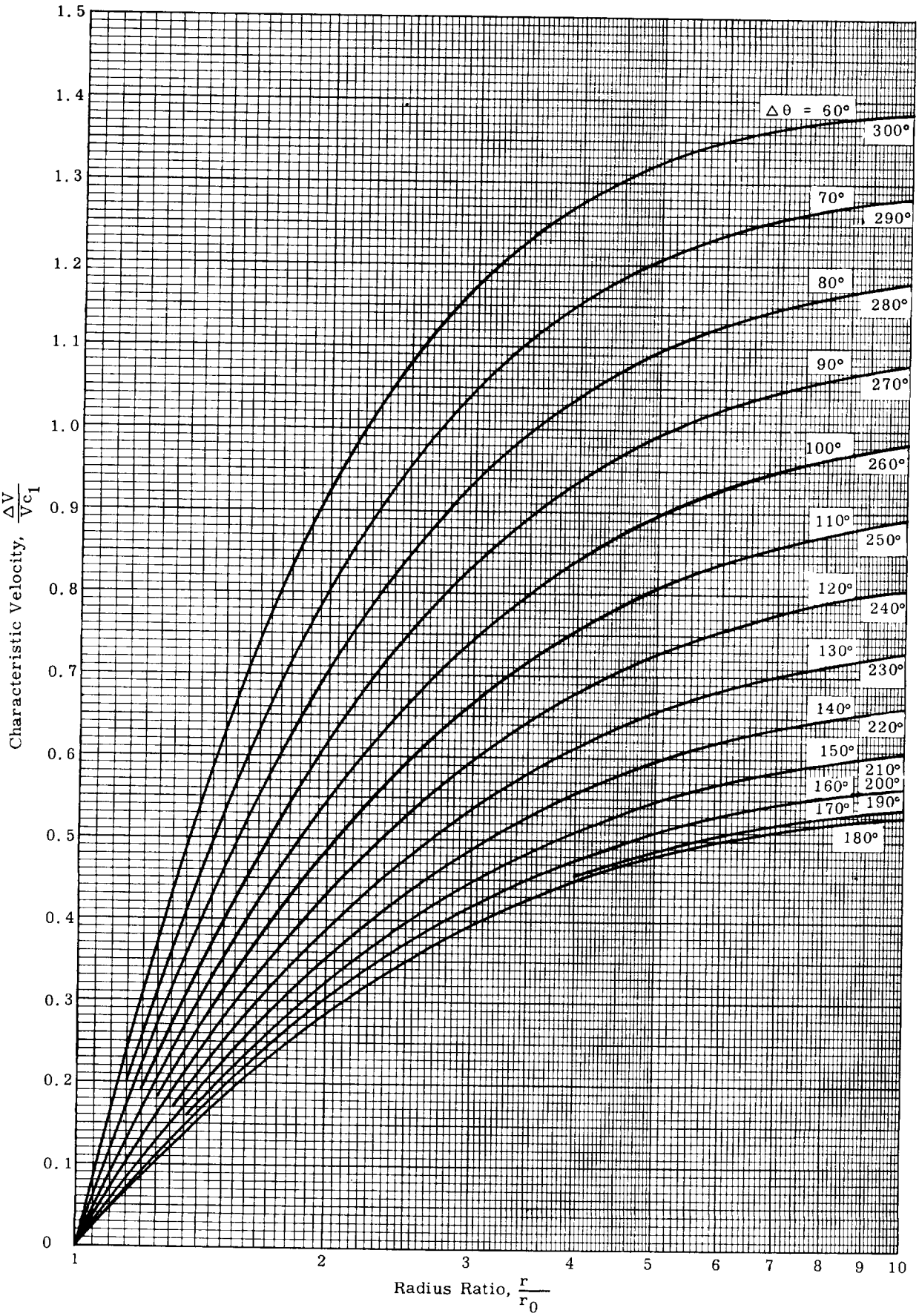

Fig. 25. Velocity Required for Optimum 2-D Transfers Between Circular Orbits

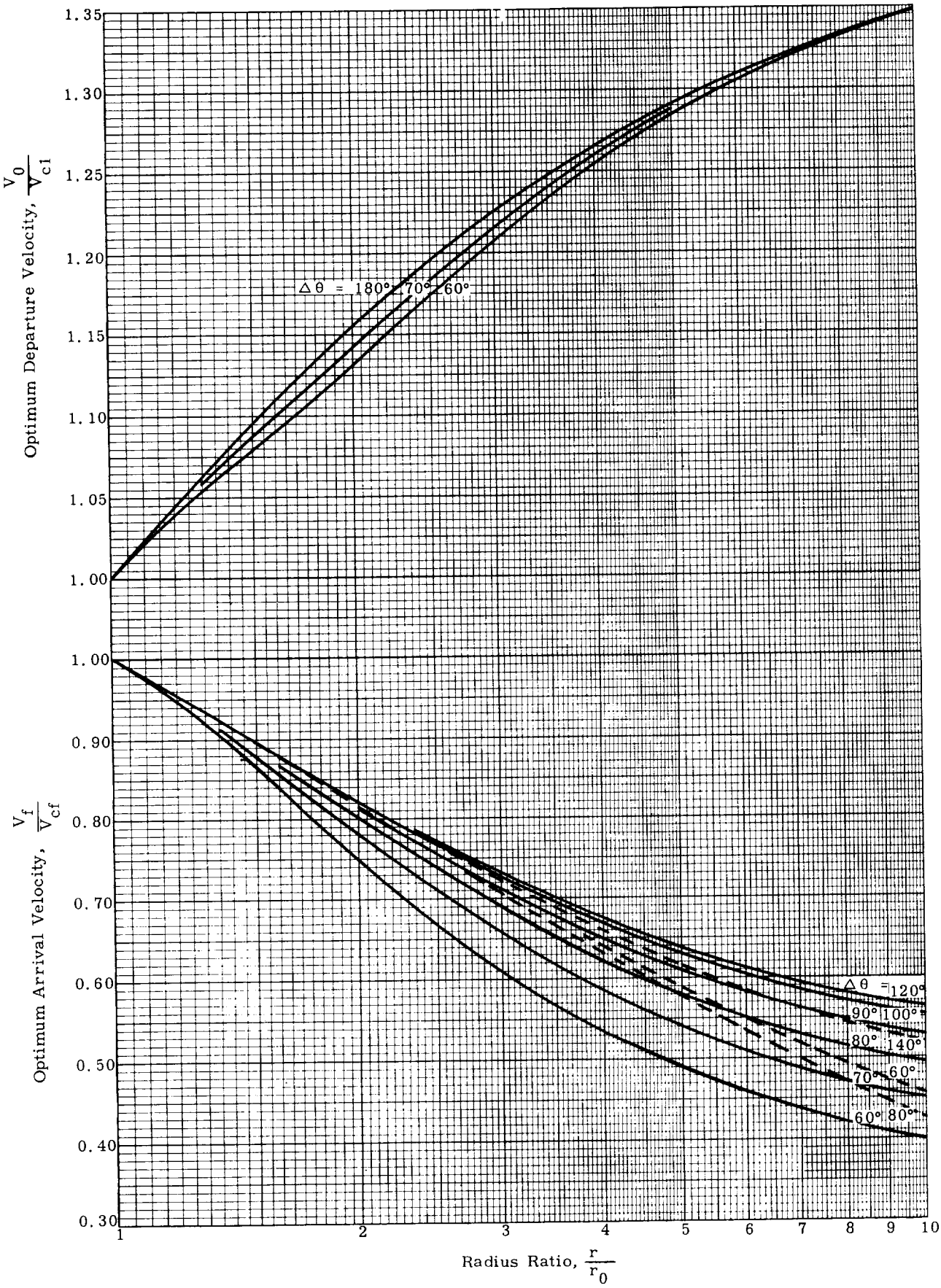

Fig. 26. Independent Impulses for Optimum 2-D Transfers Between Circular Orbits

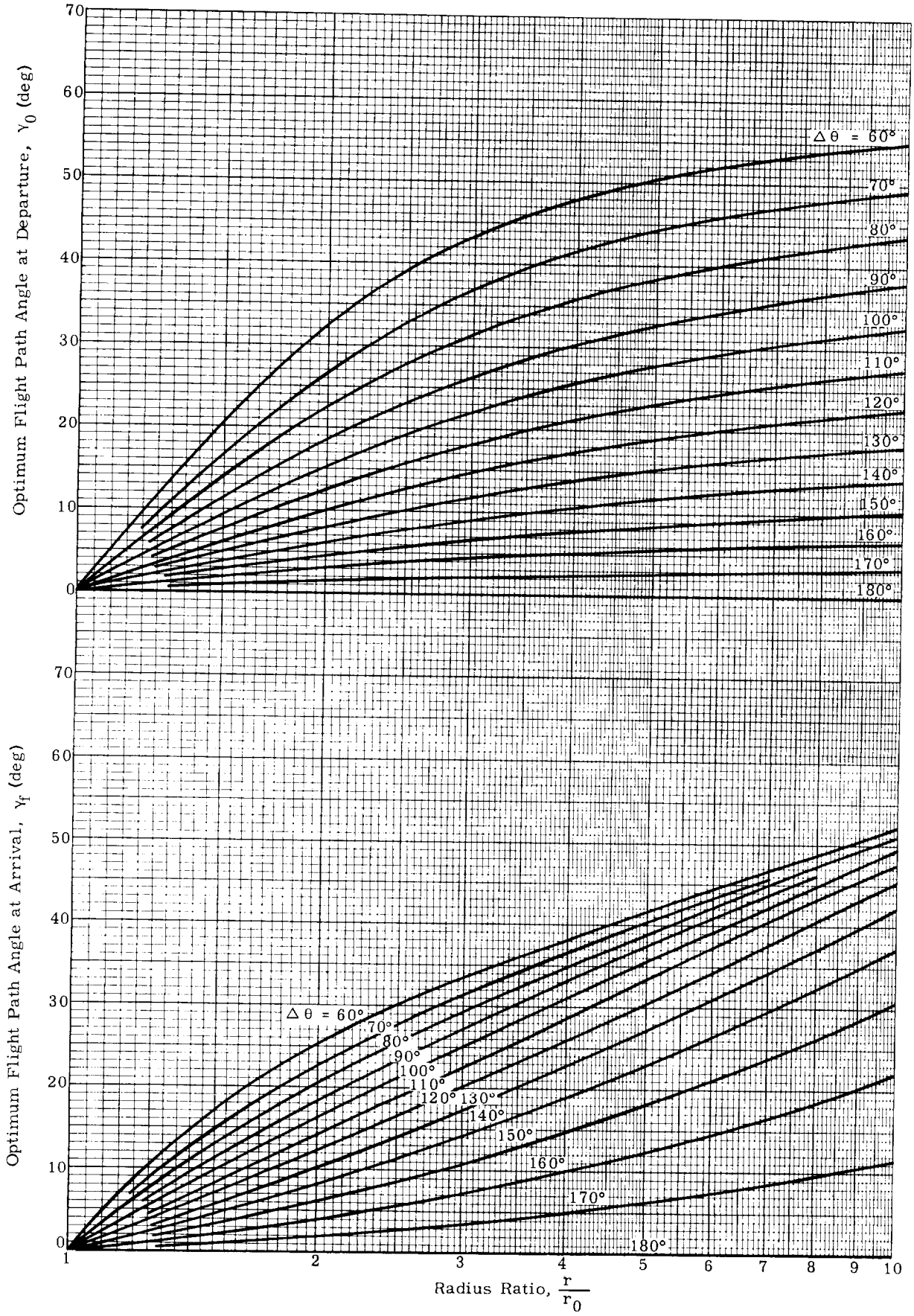

Fig. 27. Flight Path Angles for Optimum 2-D Transfer Between Circular Orbits

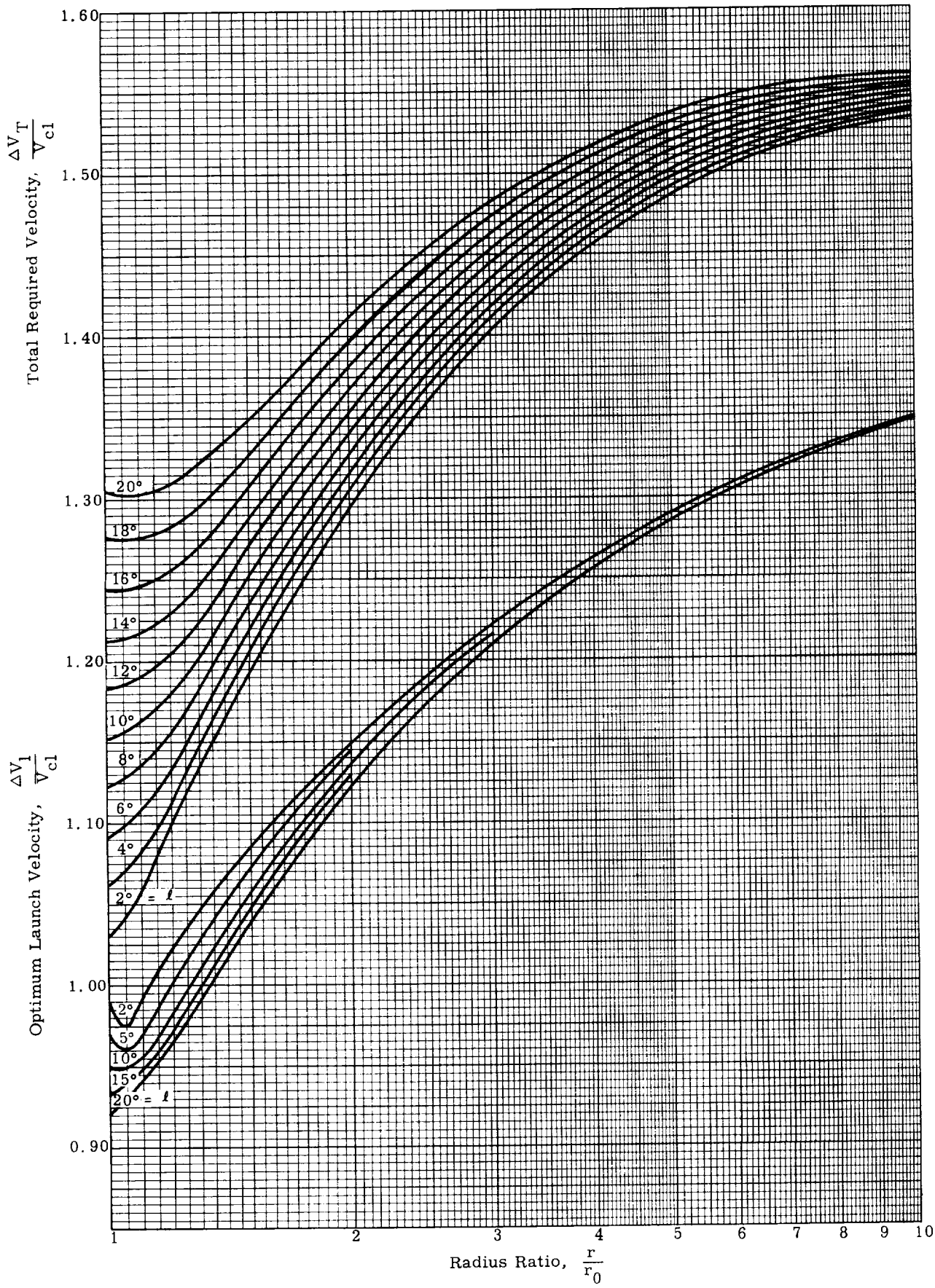

Fig. 28. Velocity Required for Optimum 3-D Transfers Between Circular Orbits

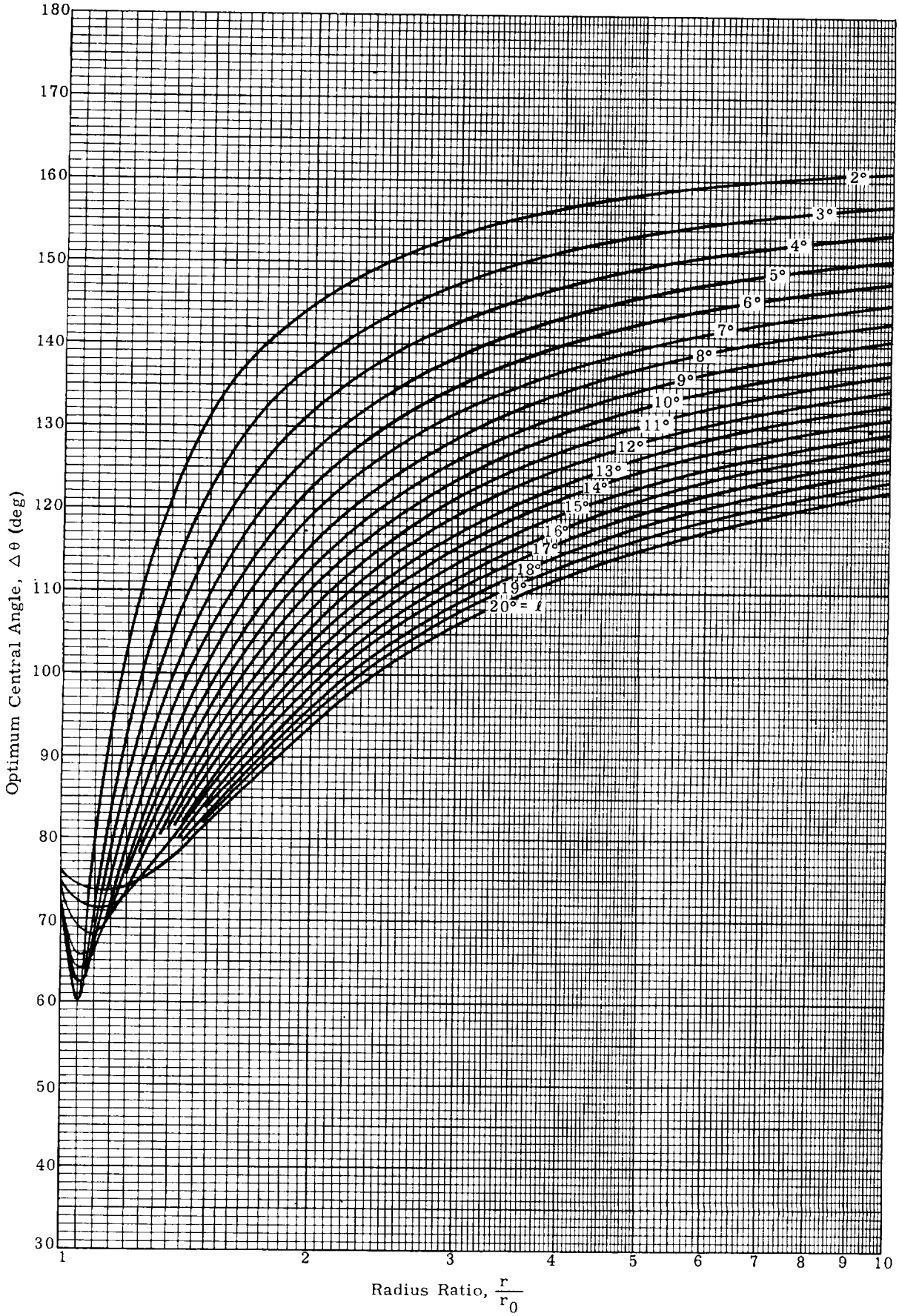

Fig. 29. Central Angles for Optimum 3-D Transfers Between Circular Orbits

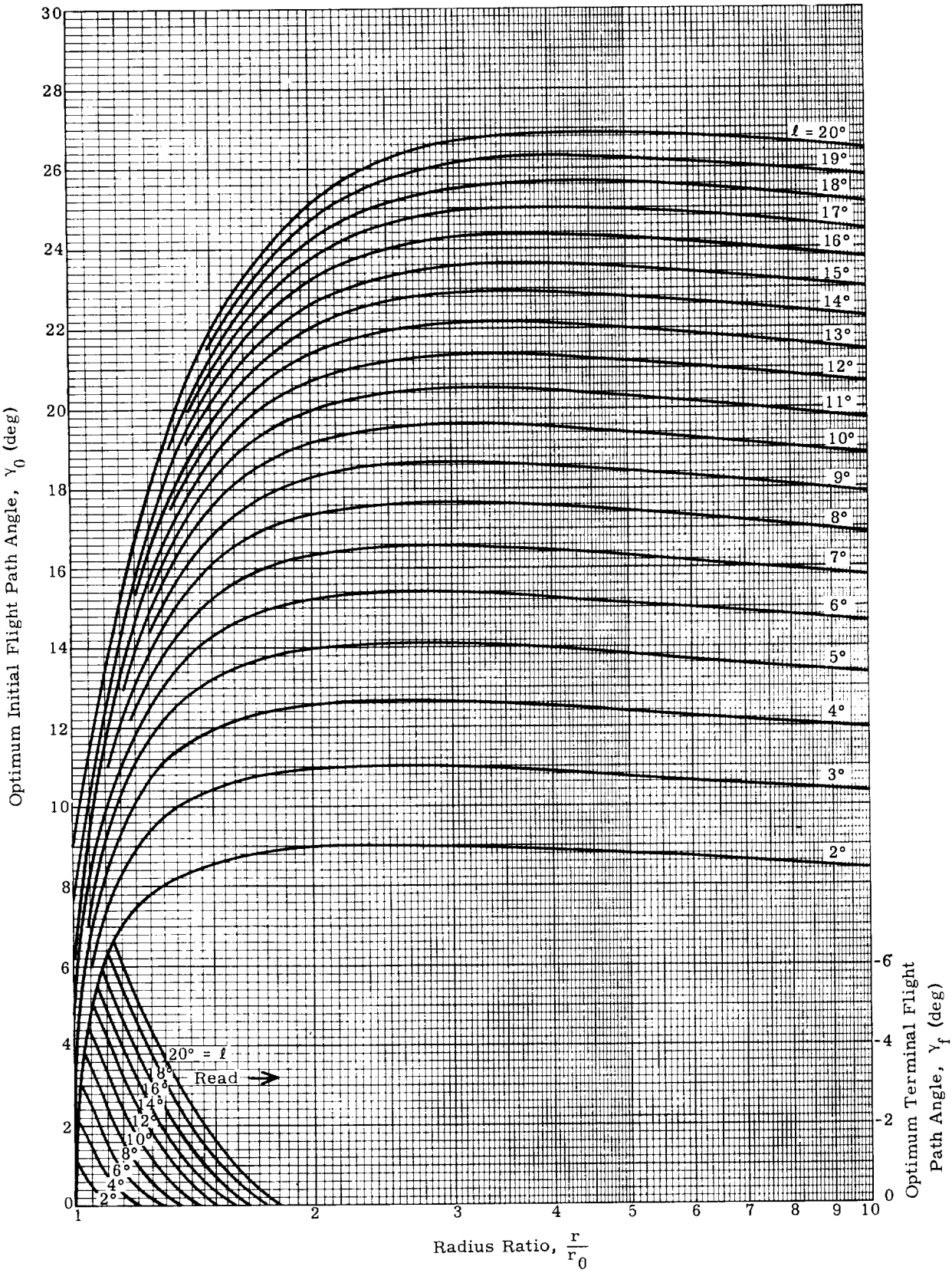

Fig. 30. Flight Path Angles for Optimum 3-D Transfer Between Circular Orbits

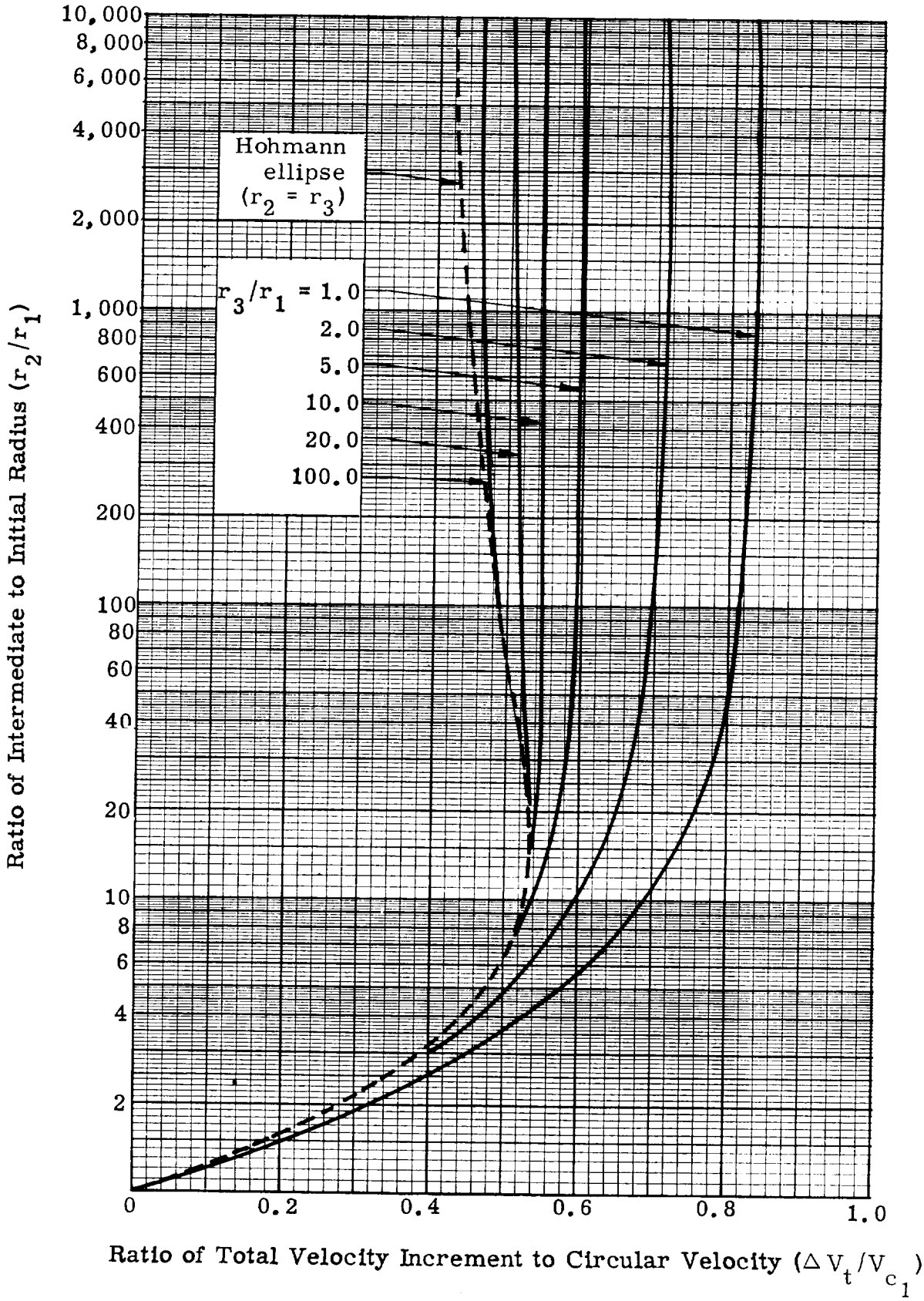

Fig. 31. Total Energy Requirement for the Three-Pulse Transfer Between Circular Orbits as a Function of r_1, r_2 and r_3

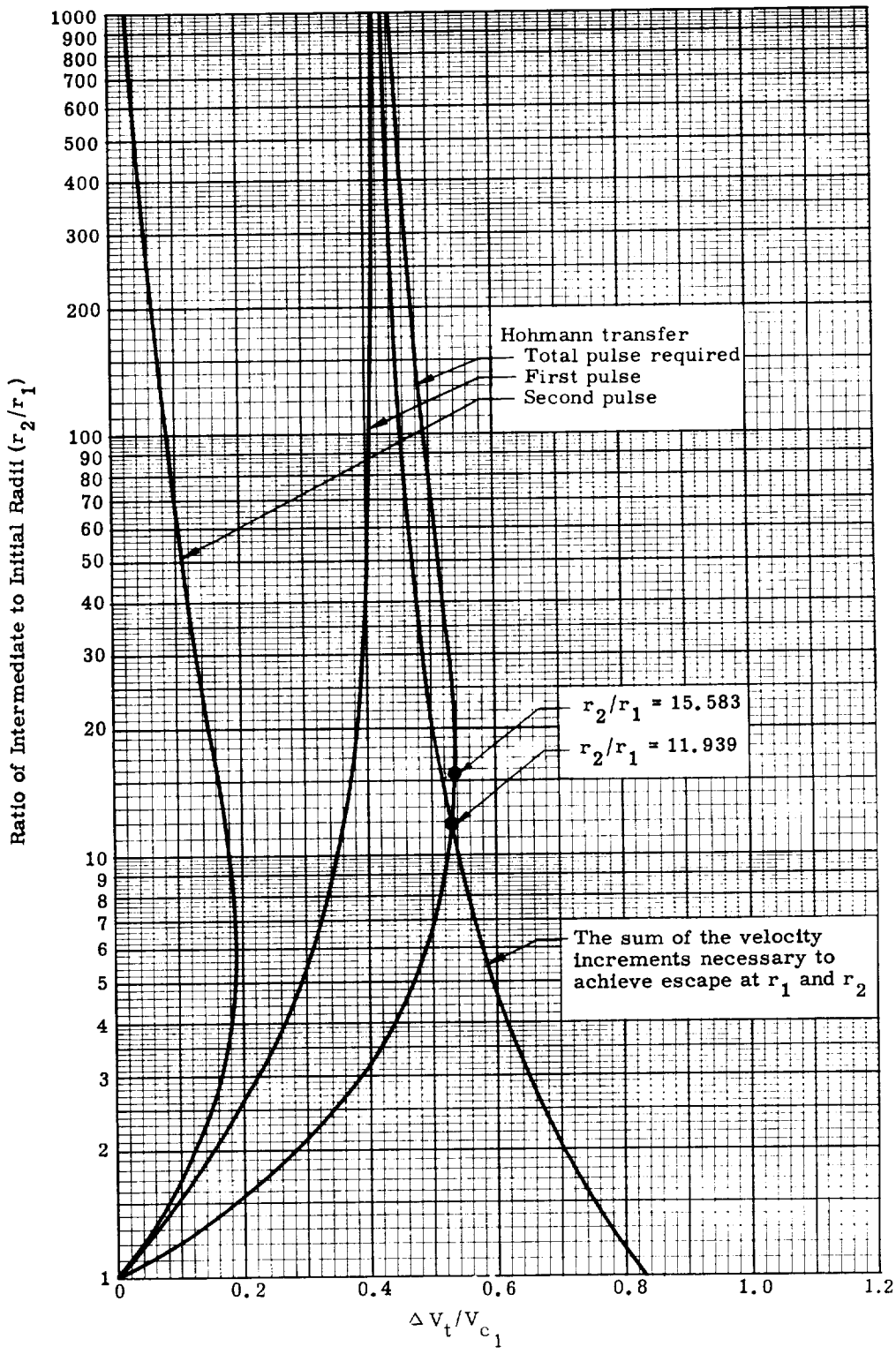

Fig. 32. Energy Requirements for Transfer Between Coplanar Circular Orbits via the Hohmann Ellipse

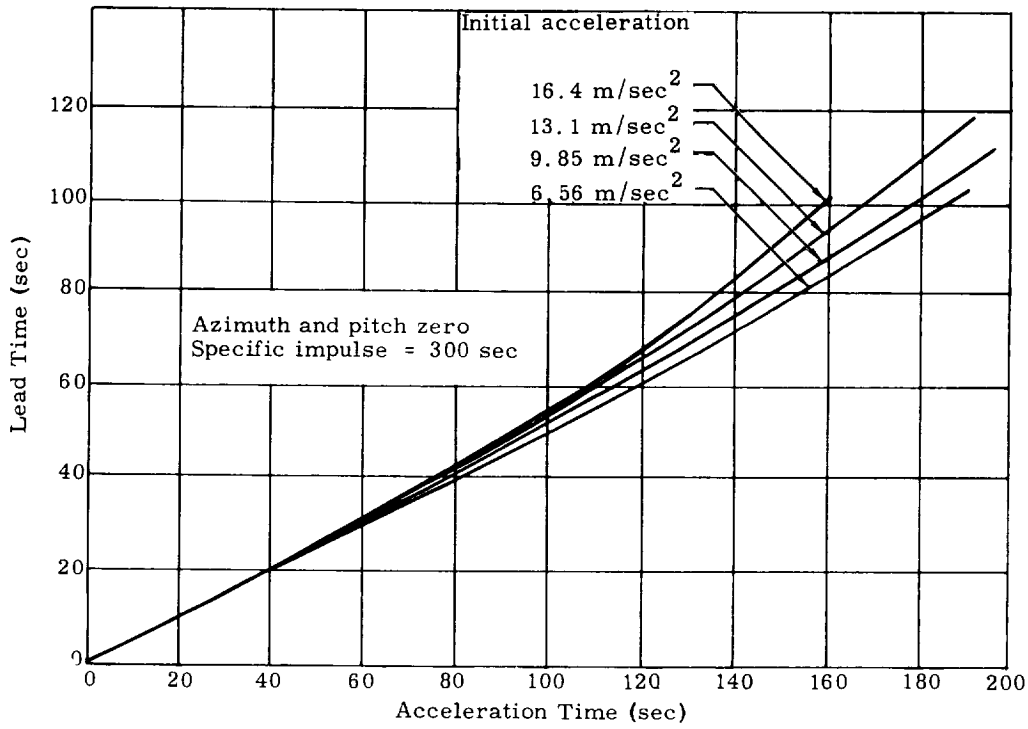

Fig. 33. Lead Time Versus Acceleration Time

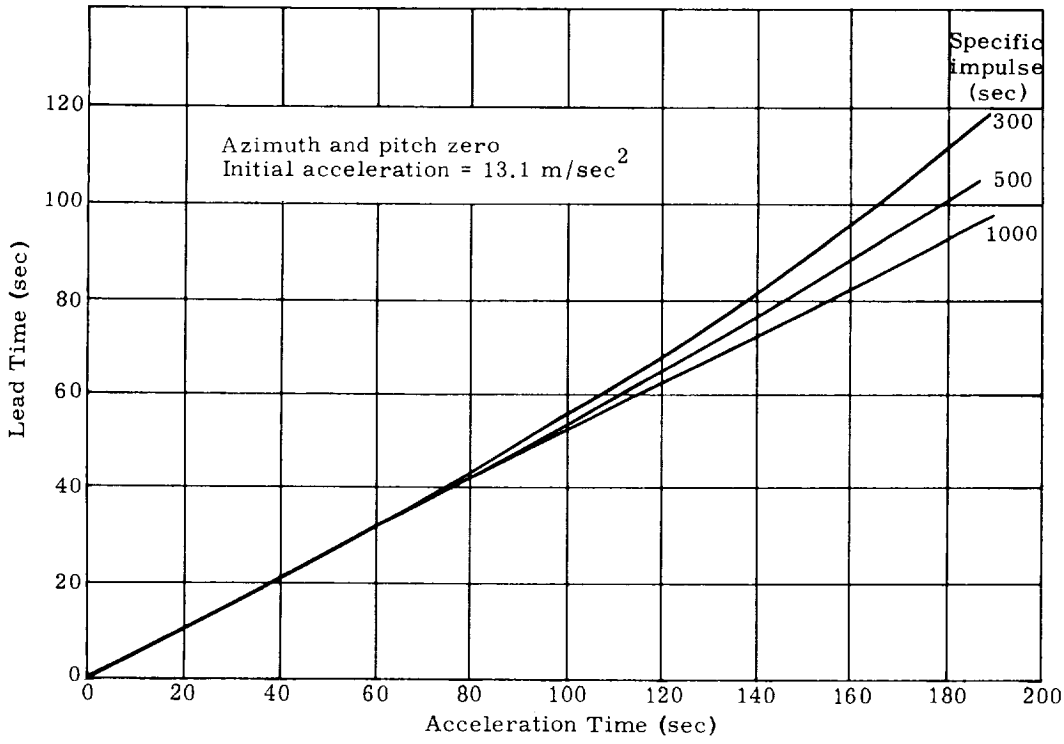

Fig. 34. Lead Time Versus Acceleration Time

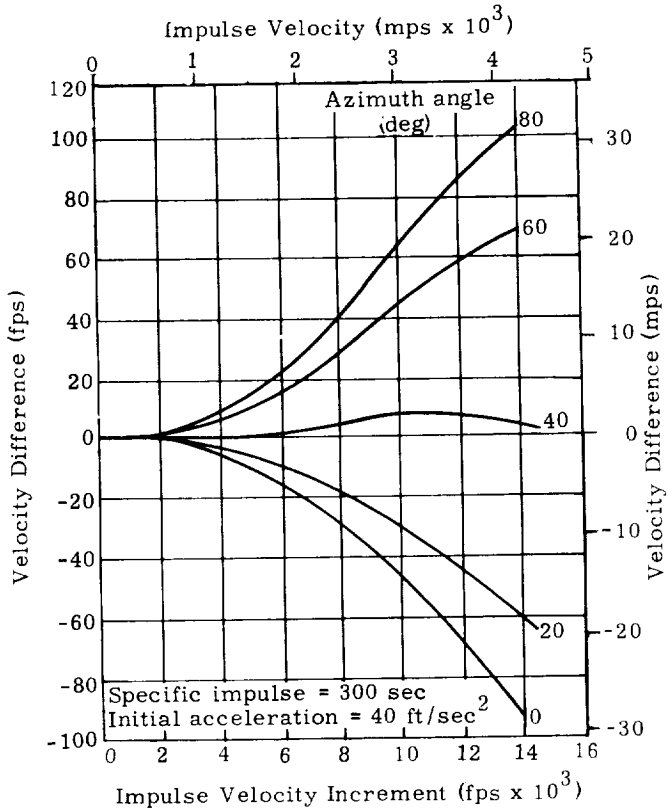

Fig. 35. Velocity Difference Between Finite and Zero Time Acceleration Assumptions

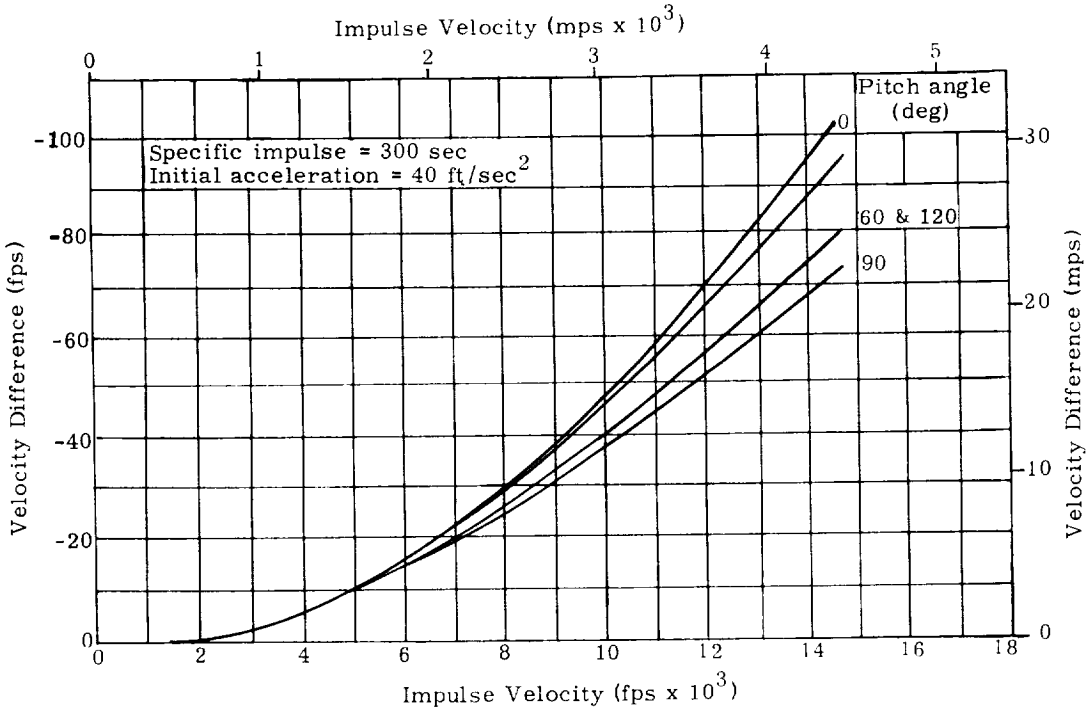

Fig. 36. Difference in Velocity Increments Due to Zero and Finite Thrust Time Assumptions

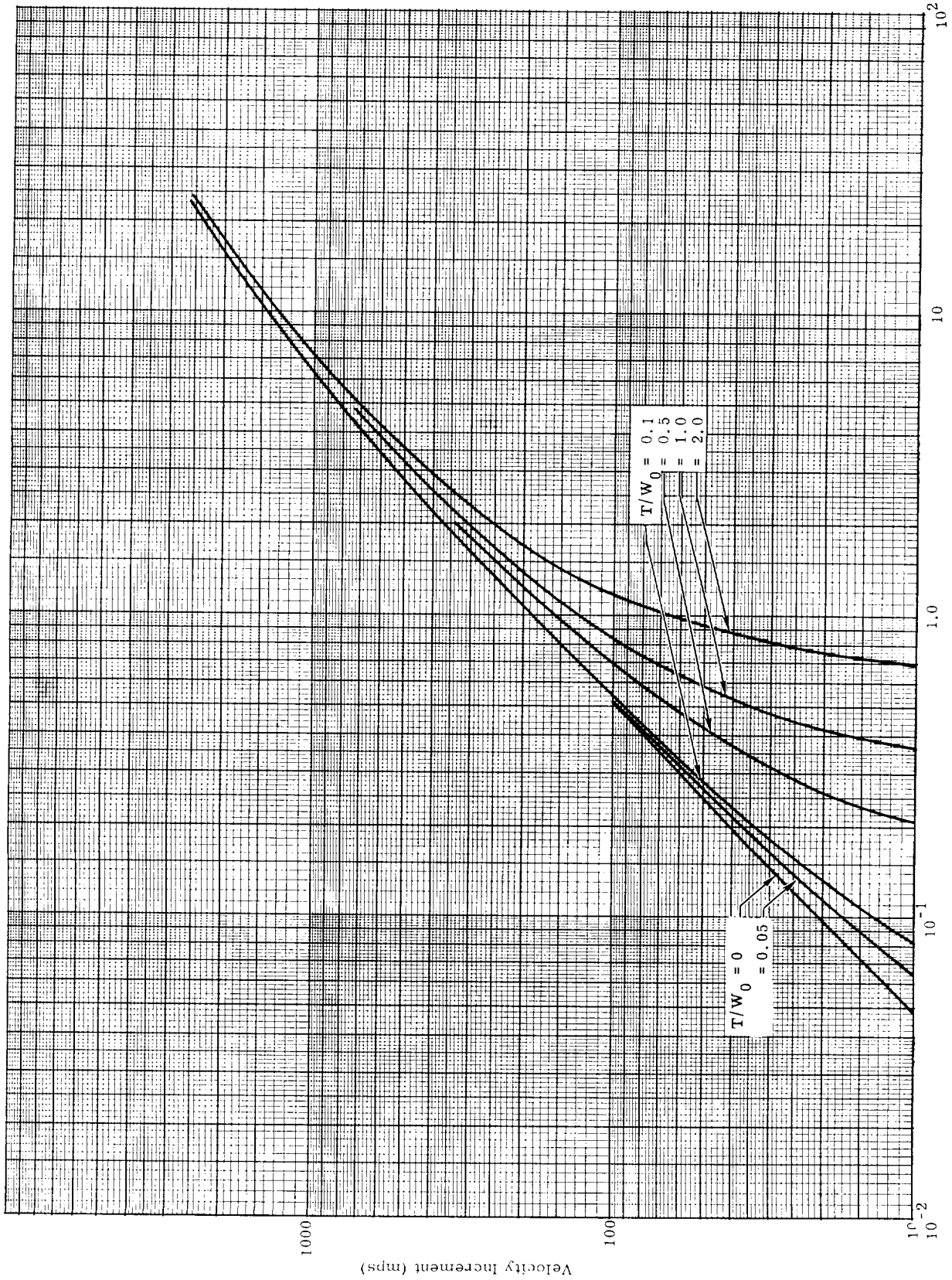

Fig. 37. The Maximum Uncertainty in the Velocity Increment for Present Control Parameters as a Function of the Initial Thrust-to-Weight Ratio (specific impulse = 300 sec)

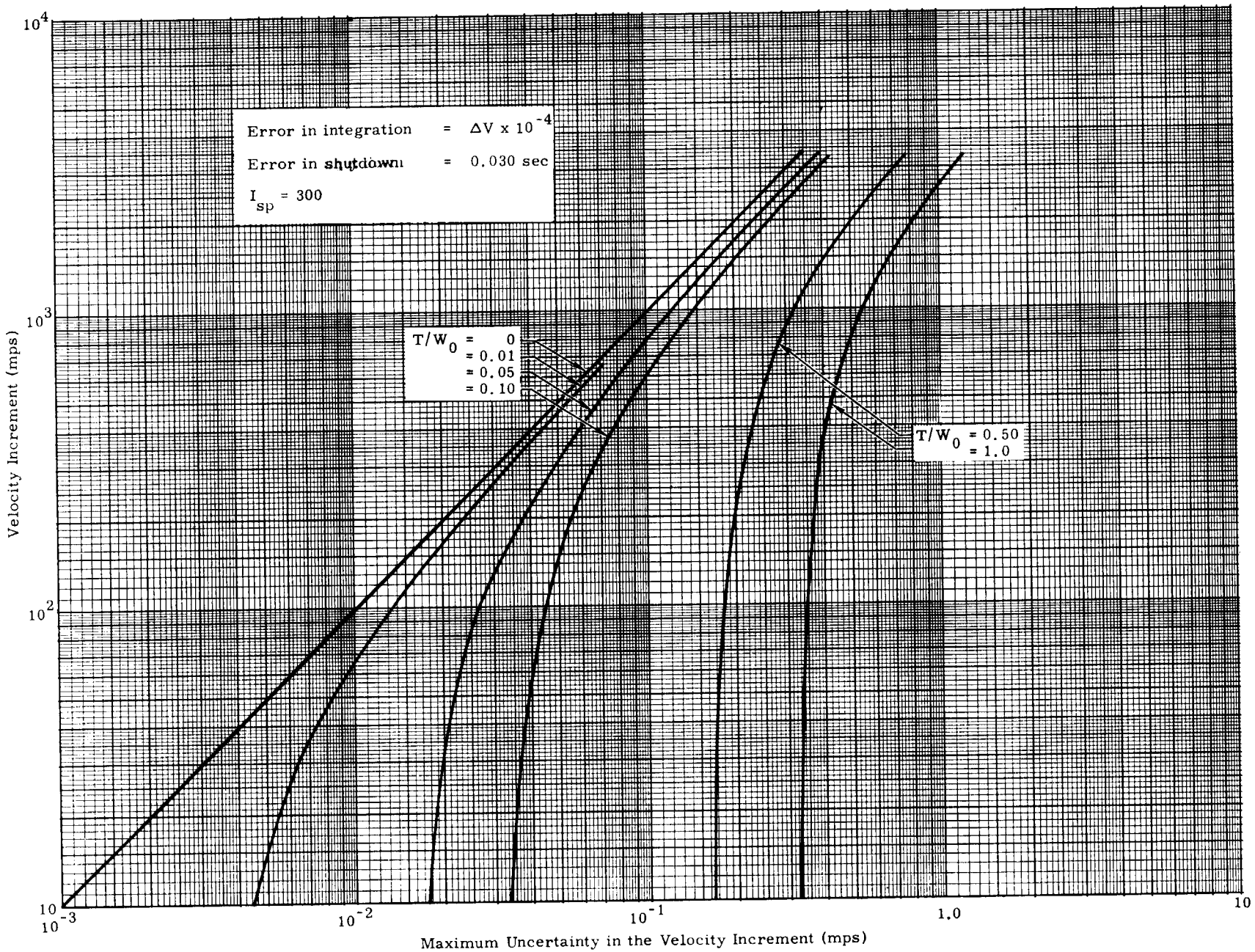

Fig. 38a. The Maximum Error in the Velocity Increment for a Velocity Monitored Propulsion System

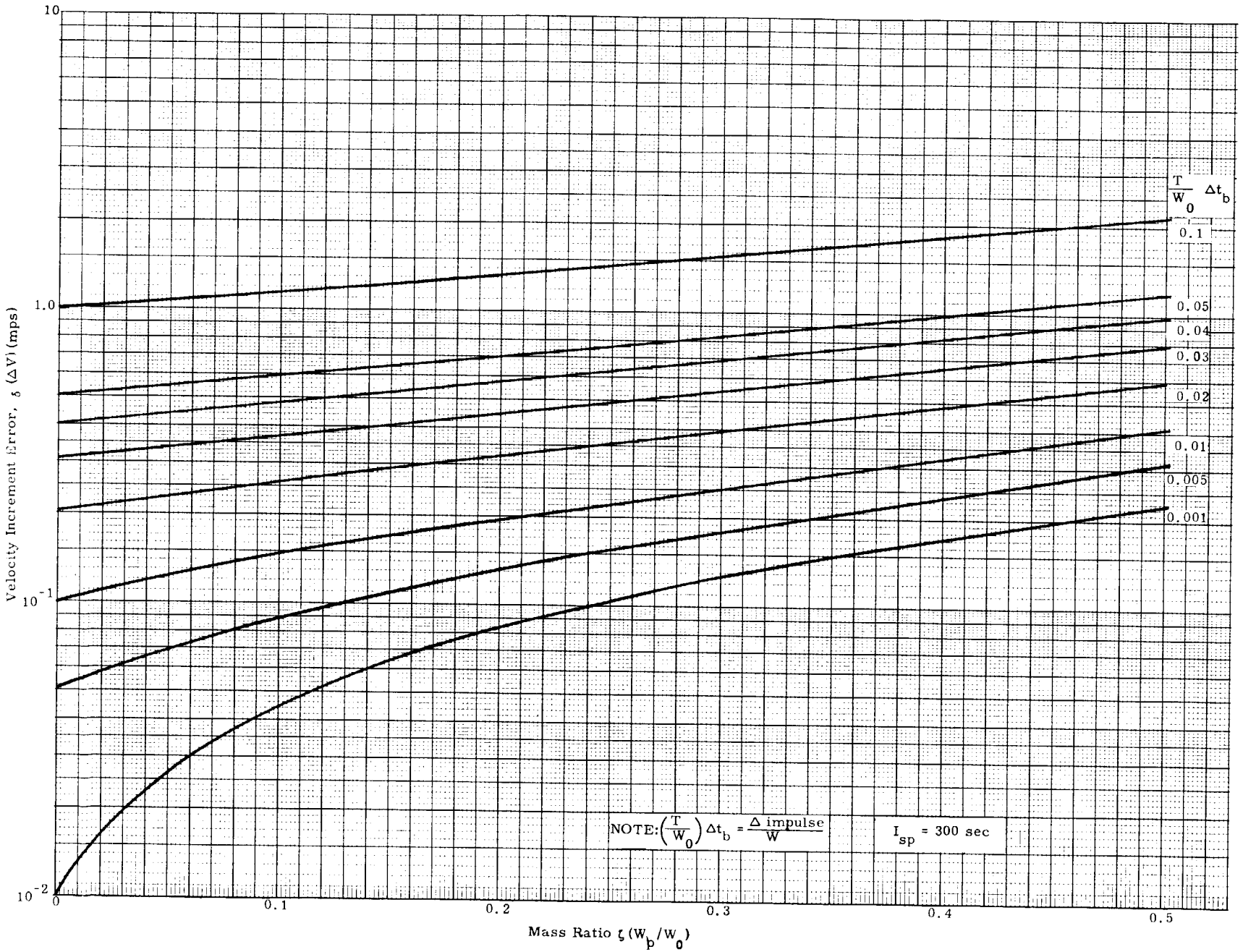

Fig. 38b. The Maximum Error in the Velocity Increment for a Velocity Monitored Propulsion System (error in the integrated velocity increment = 10^{-4} ΔV)

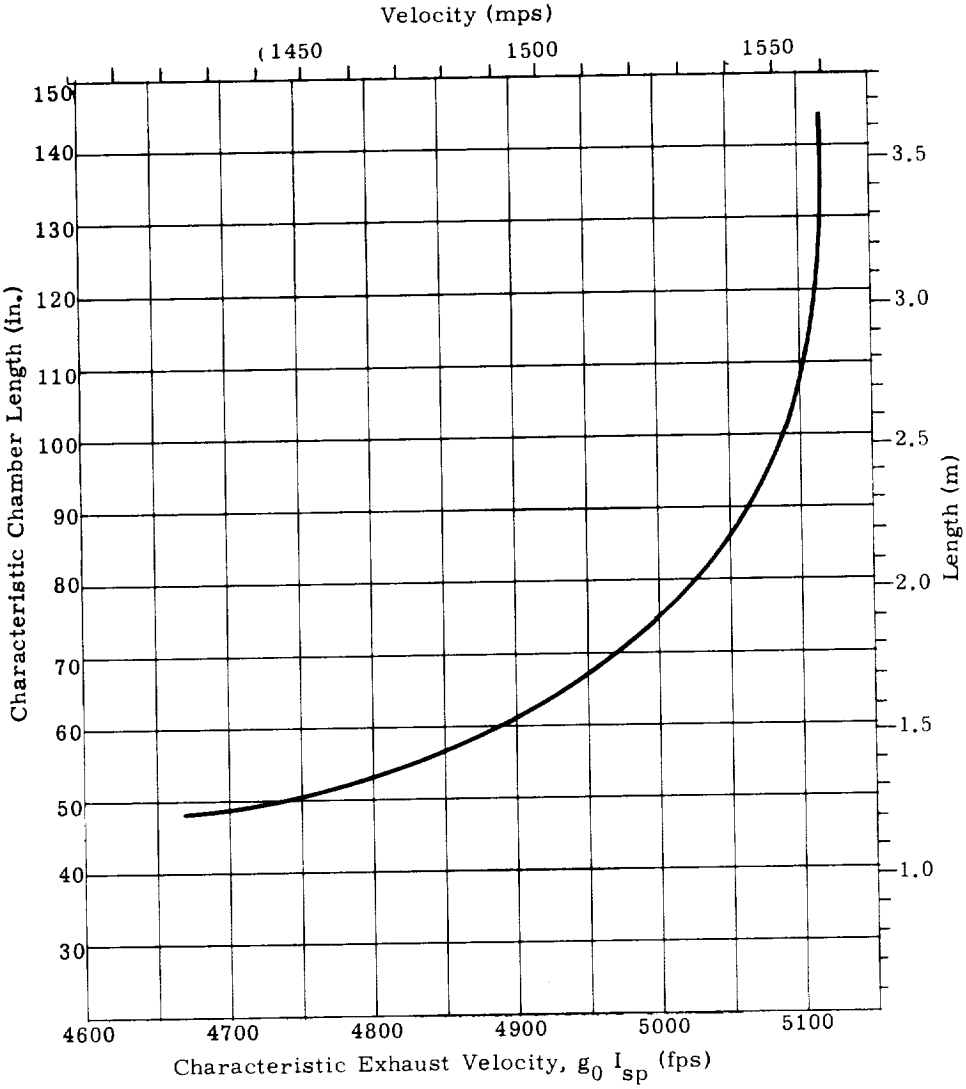

Fig. 39. Characteristic Chamber Length for a UDMH-IRFNA Motor (thrust = 20 to 1000 lb, chamber pressure = 300 to 800 psi, mixture ratio = 2.60:1)(1 psi = 6894 newtons/m^2)

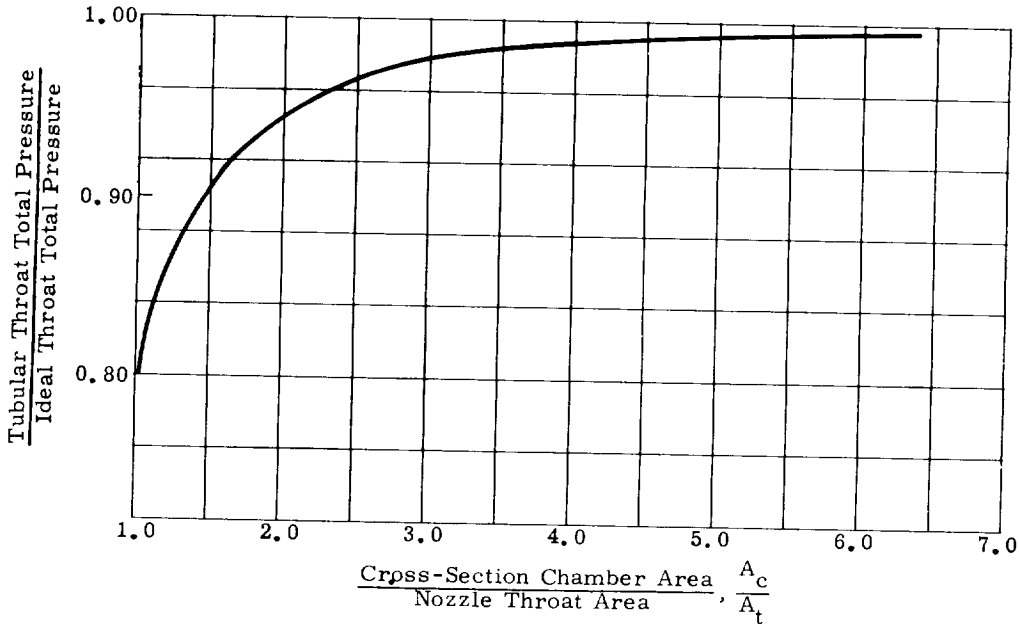

Fig. 40. Relative Total Pressure Loss (measured at the throat) as a Function of Chamber Cross Section for a UDMH-IRFNA Rocket Motor

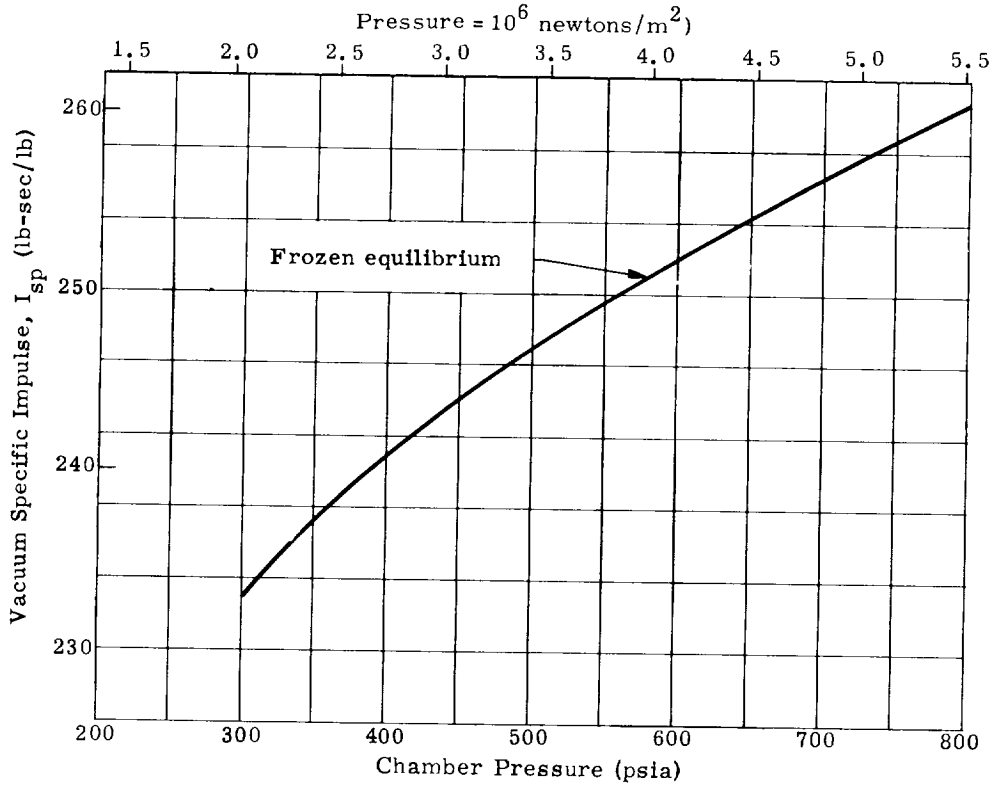

Fig. 41. Sea Level Specific Impulse for a UDMH-IRFNA Motor as a Function of Chamber Pressure (mixture ratio = 2.60:1)
(1 psia = (6894 newtons/m^2)

CHAPTER VII

RENDEZVOUS

Prepared by:

G. E. Townsend, Jr.
Martin Company (Baltimore)
Aerospace Mechanics Department
March 1963

		Page
	Symbols	VII-1
A.	Introduction	VII-3
B.	The Gross Maneuver	VII-3
C.	The Terminal Maneuver	VII-15
D.	References	VII-54
E.	Bibliography	VII-55

LIST OF ILLUSTRATIONS

Figure No.		Page
1	Graphical Solution to Kepler's Equation for E as a Function of M and e	VII-61
2	Launch Azimuth as a Function of Latitude and Inclination	VII-61
3	Launch Site Location for Rendezvous (sample problem)	VII-62
4	Variation of Semimajor Axis with n/m (n/m = 0 to 17)	VII-62
5	Variation of Semilatus Rectum with n/m (n/m = 11 to 17)	VII-62
6	Rendezvous Compatible Orbits (geometric effects)	
	N/m = 16/1	VII-63
	N/m = 31/2	VII-64
	N/m = 15/1	VII-65
	N/m = 29/2	VII-66
	N/m = 14/1	VII-67
7	Finite Burning Time Effects on Rendezvous Compatible Orbits	
	N/m = 15/1, L = 28.5°	VII-68
	N/m = 15/1, L = 34.5°	VII-69
8	Graphical Solution for $\frac{\Delta V}{V}$ in Eq 45a	VII-70
9	Circle Diagram Generatrix of In-Plane Motion	VII-71
10	In-Plane Circle Diagram at Injection	VII-71
11	Parametric Relation for Rendezvous ($\rho = 0$; $\alpha = 0$)	VII-72

LIST OF ILLUSTRATIONS (continued)

Figure No.		Page
12	Ratio of Rendezvous Time to Initial Time-to-Go Versus Initial Downrange Angle	VII-72
13	Rendezvous Geometry at Nodal Crossing	VII-73
14	Rendezvous Using Pure Loft (no period change) . . .	VII-73
15	Rendezvous Using Loft and Period Change	VII-74
16	Output of the Digital Filter (least squares estimate of the input with zero-lag)	VII-75
17	Output of the Digital Filter (least squares, zero-lag estimation of first derivative of the input)	VII-75
18	Output of the Digital Filter (least squares, zero-lag [a = 0] estimation of the second derivative of the input)	VII-75
19	RMS Residual Transverse Error Velocity	VII-76
20	Homing Profile for Extreme Errors	VII-76

VII. RENDEZVOUS

SYMBOLS

Symbols used frequently in this chapter are listed here.

a	semimajor axis (ft or m)
A	right ascension relative to vernal equinox; homing vehicle's yaw relative to target orbit
b	braking distance
e	eccentricity
E	eccentric anomaly (deg or rad)
F	thrust (lb or Newton's)
g	gravitational acceleration = $GM_{\oplus}/r^2$ (fps^2 or mps^2)
G	Newton's Universal Constant of Gravitation
h	angular momentum (ft^2/sec or m^2/sec)
i	inclination to the equatorial plane (deg or rad)
I_{sp}	specific impulse (lb-sec/lb)
J_2	coefficient of the potential function = 1.0823×10^{-3}
L	latitude (deg or rad)
m	mass (slugs or kg)
M	mean anomaly (deg or rad)
$M_{\oplus}$	mass of earth (slugs or kg)
n	number of revolutions; mean motion $\left(\frac{2\pi}{\tau}\right)$
p	semilatus rectum (ft or m)
r, $\dot{r}$, $\ddot{r}$	radial component of position, velocity and acceleration
r_a, r_p	apogee and perigee radii
R_e	equatorial radius of earth
R	radius of equivalent sphere for earth; relative range
$\dot{R}$	relative range rate $(R \cdot V)/R$
s	relative position vector
t	time
t_b	burning time; braking duration
t_G	rectilinear time to go $(R/\dot{R})$
T	normalized position variable for relative motion study = $\omega_0 t$
u_0	deviation in radial velocity for closure = $-V_R$
V	velocity
V_C, V_R, V_N	velocity components in the circumferential direction, radial direction, and normal to the plane, respectively
W_0	initial weight; deviation of velocity from circularity in discussion of relative motion = $-V_C$
x, y, z	Cartesian components of position
α	nondimensional position parameter for relative motion study (y/r)
β	azimuth relative to local north
γ	flight path angle relative to local horizontal
θ	central angle from perigee to instantaneous radius
λ	nondimensional position parameter for relative motion study (z/r)
Λ	longitude relative to prime meridian
μ	earth's gravitation constant = $GM_{\oplus}$
ν	longitude of the satellite relative to the ascending node
ρ	nondimensional position parameter for relative motion study (x/r)
ξ	ratio of propellant mass to initial vehicle mass
σ	standard deviation
τ	orbital period
ω	argument of perigee; angular rate
ω_0	angular rate in a circular orbit
$\dot{\omega}$	change in argument of perigee per revolution due to oblateness
Ω	right ascension of the ascending node
$\dot{\Omega}$	change in Ω per revolution due to oblateness
Ω_e	rotational rate of the earth 1 rev each 86164.091 mean solar sec

Subscripts

a	apogee

b	bias
BO	burnout
f	parameter in final orbit; final
h	homing
L	launch
ℓ	low altitude orbit
n	node; nominal; running integer
p	perigee, proportional
R	along range vector
S	smoothing
t	value in transfer orbit; total; target
T	transverse
y	rotation about local vertical
0	initial, at time = 0
$\oplus$	earth
$\mathbb{C}$	moon

A. INTRODUCTION

With the advent of large instrumented and manned satellites, a requirement has been generated for bringing two or more vehicles together in space. This maneuver is referred to as rendezvous and is differentiated from intercept by the fact that at the time of closure the velocity vectors of the two vehicles must match. The procedure for matching these position and velocity vectors is the subject of this chapter, and the various phases of the maneuver will be studied in detail.

Rendezvous can be broken into a series of problems for the purposes of discussion, these problems being:

(1) The gross maneuver.

(2) The terminal maneuver.

The gross maneuver refers to the powered and coasting periods necessary to place the shuttle or homing vehicle in the vicinity of the target satellite. This maneuver can be performed in a number of ways, among them being:

(1) Rendezvous utilizing an intermediate orbit.

(2) Direct ascent.

(a) Rendezvous compatible orbits.

(b) Direct ascent coupled with plane change maneuvers.

The first of these techniques concerns itself with the reduction of a three-dimensional problem to one of two dimensions by the simple expedient of launching into the plane of motion at the time the launch site is in the plane. Time then passes until the desired relative positions of the two vehicles are obtained; then a planar transfer is initiated.

A second approach (Rendezvous Compatible Orbits) is an attempt to once again reduce the problem to two dimensions but without utilizing the intermediate or parking orbit. This is possible if the orbital elements of the target satellite are judicially selected. Thus, the whole philosophy is predicated on the premise that rendezvous will be required at some future date and the orbit of the target selected accordingly. The third approach treats the problem as one of three dimensions and allows for the expenditure of propellant to turn the velocity vector at the time the vehicle enters the desired plane. Each of these approaches is investigated.

The terminal maneuver refers to the analysis of the procedures necessary to reduce the relative position and velocity of the shuttle vehicle with respect to the target to zero. Because the distances involved are small, this portion of the analysis is conducted utilizing the equations of relative motion which are derived and discussed in the text. The discussions pertain to the various guidance schemes which can be employed utilizing these equations and the behavior of the vehicle under the influence of such a law. Material is also presented which relates the energy and time of closure requirements for such motion, and schemes for data smoothing during closure. The chapter ends with a discussion of long time closure trajectories, and an analysis of homing phase errors.

B. THE GROSS MANEUVER

The analysis of closing with another vehicle requires that the velocity and radius vectors of the target vehicle be matched. In the process, however, it is generally required that as little propellant as possible be expended for maneuvering (i.e., changing the orbital inclination or nodal position). Thus, while not always practical, it is desirable that the analysis be reduced to the problem of nearly coplanar orbital transfer. Two schemes for defining the launch timing for nearly coplanar transfers and the general case of noncoplanar transfers are presented in the following paragraphs. These are:

(1) Launch utilizing parking orbits.

(2) Direct ascent to a rendezvous compatible orbit.

(3) Direct ascent to orbit considering planar adjustment.

The method of approach neglects the perturbative accelerations due to the sun and moon and assumes that the orbits are Keplerian ellipses (making adjustments for the secular perturbations due to the earth's oblateness). Similarly, the orbital decay rates in all orbits are assumed negligible (thus the analysis is restricted to orbits of greater than 200-mi (320-km) altitude or to short times at lower altitudes). And finally, the burning time of the rocket stages is assumed to be short (making it possible to treat the velocity increments obtainable from rocket stages as pulses). Justification for the final assumption is shown in Chapter VI.

1. Development of Equations To Be Utilized

The studies of orbital injection are directed toward the evaluation of the parameters affecting orbital injection and the establishment of the sensor accuracies and computer requirements necessary to produce a desired orbit. For this analysis the transfer orbit is assumed to be an ellipse, and the final orbit either circular or elliptical. To assure the maximum degree of flexibility, injection (i.e., the point at which the final trajectory is obtained) is assumed to occur at a point corresponding to the intersection of the transfer orbit and the desired orbit rather than at apogee of the transfer orbit or at the point of tangency of the two orbits. However, it must be pointed out that both of these methods of injection can also be obtained from the generalized approach as outlined. All of the equations derived are reduced to the fewest variables possible, thus maintaining simplicity both in the analysis and in the application of the equations to a vehicle-borne computer. While not absolutely necessary, the equations are reduced to a nondimensional form, thus assuring that the analysis

is capable of handling transfer between any two elliptical orbits around any central body. The following sketch defines a typical transfer and points out the parameters which must be determined to define the maneuver.

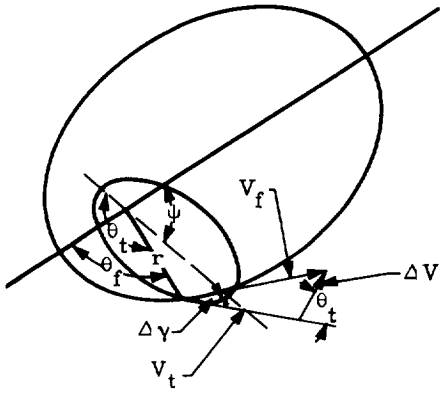

$$\psi = \theta_t - \theta_f \tag{1}$$

$$\Delta\gamma = \gamma_t - \gamma_f \tag{2}$$

$$\Delta V^2 = V_f^2 + V_t^2 - 2 V_f V_t \cos \Delta\gamma \tag{3}$$

$$\Delta V = g_0 I_{sp} \ell n \left(\frac{1}{1-\xi}\right) - \frac{g I_{sp} \xi \sin \gamma}{F/W_0} \tag{4}$$

$$\theta = \cos^{-1}\left[\frac{p - r}{re}\right]$$

$$= \cos^{-1}\left[\frac{\frac{2 r_a}{r} - \left(\frac{r_a}{r_p} + 1\right)}{\frac{r_a}{r_p} - 1}\right] \tag{5}$$

$$\gamma = \cos^{-1}\sqrt{\frac{r_a/r}{\left(\frac{r_a}{r_p} + 1\right) - \frac{r_a/r_p}{r_a/r}}} \tag{6}$$

$$\sqrt{\frac{r}{u}}\, V = \sqrt{\frac{2\left[\left(\frac{r_a}{r_p} + 1\right) - \frac{r_a/r_p}{r_a/r}\right]}{\left(\frac{r_a}{r_p} + 1\right)}} \tag{7}$$

The determination of the radius of intercept is in reality a fairly complex solution since the exact size, shape and orientation of the transfer orbit are not known until the vehicle has been tracked for some interval of time. However, since the actual orbit differs but little from the predicted orbit and since there is an interval of time during coast when tracking data may be processed, it seems reasonable to assume that the actual transfer orbit is defined. Now, since the required information is available, the radius of interception may be evaluated as follows.

$$r = \frac{p_t}{1 + e_t \cos \theta_t}$$

$$= \frac{p_f}{1 + e_f \cos \theta_f} = \frac{p_f}{1 + e_f \cos (\theta_t - \psi)} \tag{8}$$

Therefore:

$$\left(\frac{r_{af}}{r_{pf}} + 1\right) + \left(\frac{r_{af}}{r_{pf}} - 1\right) \cos (\theta_t - \psi) =$$

$$\frac{r_{af}}{r_{at}} \left[\left(\frac{r_{at}}{r_{pt}} + 1\right) + \left(\frac{r_{at}}{r_{pt}} - 1\right) \cos \theta_t\right] \tag{9}$$

and:

$$\frac{2 r_{at}}{r} = \left(\frac{r_{at}}{r_{pt}} + 1\right) + \left(\frac{r_{at}}{r_{pt}} - 1\right) \cos \theta_t \tag{10}$$

The solution for θ_t from Eq (9) is somewhat involved, and the type of solution may well depend upon the material available for the solution and the number of times that the equation must be solved. If a small digital computer in the vehicle is programmed to handle the solution, an iterative solution would probably be the simplest. A direct solution may also be obtained for θ_t after manipulation of the terms in Eq (9); this direct solution is to be preferred for accuracy for manual evaluations of θ_t even though the form of the equation is complex.

$$\cos \theta_t = -A \pm \sqrt{B + A} \tag{11}$$

$$\left.\begin{aligned} A &= \frac{CD}{1 + C^2} \\ B &= \frac{1 - D^2}{1 + C^2} \\ C &= \frac{x - yz \cos \psi}{yz \sin \psi} \\ D &= \frac{(x + 2) - z (y + 2)}{y z \sin \psi} \end{aligned}\right\} \tag{12}$$

$$\left.\begin{aligned} x &= \frac{r_{at}}{r_{pt}} - 1 \\ y &= \frac{r_{af}}{r_{pf}} - 1 \\ z &= \frac{r_{at}}{r_{af}} \end{aligned}\right\} \tag{13}$$

Timing for the injection pulse can be obtained by matching tracking data for the radius to the satellite with the value of the intercept radius as calculated, or the pulse may be initiated at some specified time corresponding to the time of flight from cutoff to the intercept radius. This time of flight may be computed by subtracting the time of flight from perigee to the cutoff radius from that corresponding to travel from perigee to the intercept radius. The time of flight from perigee may be determined as follows.

This approach is entirely general so that the case of tangency of the two orbits can also be evaluated. That case, however, provides another restraint (the flight path angle identity).

$$\cos \gamma = \sqrt{\frac{r_{af}/r}{\left(\frac{r_{af}}{r_{pf}} + 1\right) - \frac{r_{af}/r_{pf}}{r_{af}/r}}}$$

$$= \sqrt{\frac{r_{at}/r}{\left(\frac{r_{at}}{r_{pt}} + 1\right) - \frac{r_{at}/r_{pt}}{r_{at}/r}}}$$

$$r_{tan} = \frac{r_{af}\left(\frac{r_{at}}{r_{pt}} + 1\right) - r_{at}\left(\frac{r_{af}}{r_{pf}} + 1\right)}{\frac{r_{af}}{r_{pt}} - \frac{r_{at}}{r_{pf}}} \qquad (14)$$

The equations of this section have been plotted in nomographic form and are presented in Chapter III. The accuracy afforded by these figures is inadequate for most detailed analyses; however, preliminary calculations are greatly simplified by their use.

2. Launch Utilizing the Intermediate Orbit

a. Formulation

Since the majority of the missions envisioned for satellites suggest orbits inclined at greater than 30° to the equator and since in-orbit maneuvers are not necessary for these orbits, the first approach to be analyzed is that which requires accurate control of the time and azimuth of launch and which utilizes the intermediate orbit.

Kepler's equation defines the time the vehicle coasts in the transfer orbit. This time plus the total time in the intermediate orbit, the time of ascent to the intermediate orbit, and the time from perigee to the point of rendezvous in the target orbit, defines the time (in the target orbit) from perigee to the position of the target vehicle at the time of launch. This time in turn defines the position of the vehicle in its orbit. However, this reverse solution of Kepler's equation is transcendental and requires an independent investigation.

The time from perigee in the final orbit at the time of launch can be computed as

$$t_{1f} = t_{2f} - t_t - n\tau_1 - t_{ascent} \qquad (15)$$

where

$$t_{2f} = \frac{\tau_f}{2\pi}\left[E_{2f} - e_f \sin E_{2f}\right]$$

$$E_{2f} = 2\tan^{-1}\left[\sqrt{\frac{r_{pf}}{r_{af}}}\tan\frac{\theta_{2f}}{2}\right]$$

$$\theta_{2f} = \theta_t - \psi$$

Now

$$E_{1f} - e_f \sin E_1 = \frac{t_{1f}(2\pi)}{\tau_f} = M_{1f} \qquad (16)$$

This equation can be solved using any of a number of iterative processes; however, Newton's method appears to possess best convergence properties.

$$E_{k+1} = E_k - \frac{f(E_k)}{f'(E_k)}$$

$$f(E_k) = E_k - e \sin E_k - M_1$$

$$f'(E_k) = 1 - e \cos E_k$$

and

$$E_{k+1} = \frac{e\left[\sin E_k - E_k \cos E_k\right] + M}{1 - e \cos E_k} \qquad (17)$$

This series has been shown to converge for all E_k and to converge very rapidly if a reasonable estimate of E_k is utilized. Pursuing this thought further, it may be seen that Kepler's equation can be divided into two terms, each of which defines a line.

$$y = \sin E$$

$$y = \frac{1}{e}(E - M)$$

The intersection of these lines is the required solution. This graphical solution, presented in Fig. 1, would be employed as the first estimate of E. (The nomogram of Kepler's equation, Chapter III, may also be utilized.) Once this solution converges for E_1, the initial position of the target vehicle may be evaluated.

$$\theta_{1f} = 2\tan^{-1}\left[\sqrt{\frac{r_{af}}{r_{pf}}}\tan\frac{E_{1f}}{2}\right] \qquad (18)$$

To illustrate the power of this method, consider the following sample problem:

Sample problem

$M = 1.0$

$e = 0.3$

$E_k \approx 1.29$

$$E_{k+1} = \frac{0.3\ [0.960823 - 1.29\ (0.277174)] + 1.0}{1.0 - 0.3\ (0.277174)} = 1.288087$$

$$E_{k+2} = \frac{0.3\ [0.960294 - 1.288087\ (0.278991)] + 1.0}{1.0 - 0.3\ (0.278991)} = 1.288088$$

These equations only partially define the rendezvous problem since only the position of the target vehicle and the corresponding time of launch are evaluated. Consideration must now be given to the position of the launch site. This can be accomplished with spherical trigonometry; however, several quantities, shown in the following sketch must be defined before proceeding.

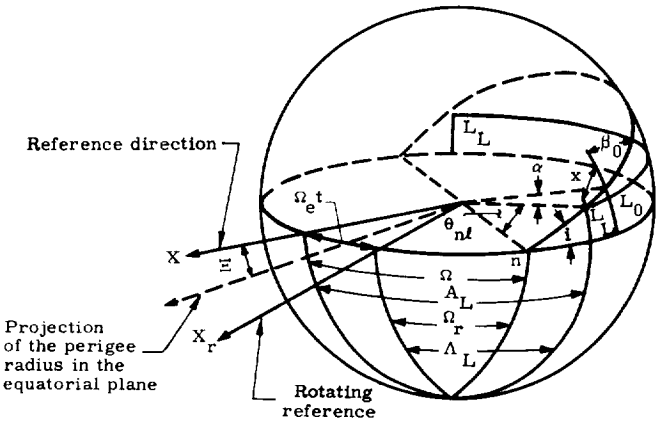

The angle from the ascending node to the radius at which transfer into the final orbit occurs (projected along the equator of a nonrotating earth) is

$$A_s - \Omega = \tan^{-1}\left[\cos i \tan(\omega_t + \theta_t)\right] \qquad (19)$$

where A_s is the right ascension of the satellite at the point of injection into the final orbit, and the latitude of the point of injection is

$$L_s = \sin^{-1}\left[\sin i_t \sin(\omega_t + \theta_t)\right] \qquad (20)$$

Similarly, the angle from the node to the perigee of the transfer orbit and the latitude of perigee may be computed as

$$A_p - \Omega = \tan^{-1}\left[\cos i_t \tan \omega_t\right] \qquad (21)$$

$$L_p = \sin^{-1}\left[\sin i_t \sin \omega_t\right] \qquad (22)$$

Continuing, the position of the required point for injection into the intermediate orbit is

$$A_{BO} - \Omega = \tan^{-1}\left[\cos i_t \tan(\omega_t - \phi)\right] \qquad (23)$$

$$L_{BO} = \sin^{-1}\left[\sin i_t \sin(\omega_t - \phi)\right] \qquad (24)$$

The last remaining step is to define the position of the launch site and the azimuth of burnout. This problem requires the value of the ground range attained in ascent to the low altitude orbit over a nonrotating earth (x).

$$A_L - \Omega = \tan^{-1}\left[\cos i_t \tan\left(\omega_t - \phi - \frac{x}{R_e}\right)\right] \qquad (25)$$

$$L_L = \sin^{-1}\left[\sin i_t \sin\left(\omega_t - \phi - \frac{x}{R_e}\right)\right] \qquad (26)$$

$$\beta_L = \sin^{-1}\left[\frac{\cos i_t}{\cos L_L}\right] \qquad (27)$$

If the assumption is made that the distance and time spent during ascent to the point of burnout are small, the azimuth in which the vehicle must be fired can be computed. This solution follows from the laws of sines and cosines and Eq (27).

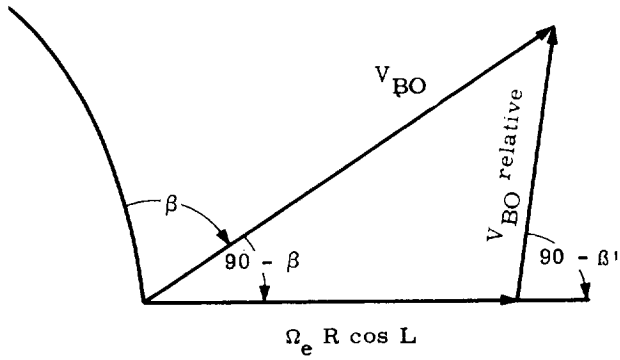

$$V_{BO}^2 = V_{BO}^2 + (\Omega_e R_e \cos L_L)^2 - 2 V_{BO} \Omega_e R \cos L \sin\beta$$

$$= V_{BO}^2 + (\Omega_e R_e \cos L_L)^2 - 2 V_{BO} \Omega_e R \cos i$$

$$\cos\beta' = V_{BO} \cos\beta \left[V_{BO}^2 + (\Omega_e R_e \cos L_L)^2 - 2 V_{BO} \Omega_e R_e \cos i\right]^{-1/2} \qquad (28)$$

The uncorrected launch azimuth (i.e., Eq (27) is presented in Fig. 2. The value of azimuth obtained in this manner is quite close to the corrected value since the velocity component produced by the earth's rotation is only 1524 cos L fps or 465 cos L mps. The magnitude of this vector is, thus, approximately one-tenth of the magnitude of the burnout velocity for most orbital shots with a resultant effect on the cosine of the azimuth between 0.5% and 10% depending on the orbital inclination.

Equations (25) through (28) define the position of the required launch site and the azimuth of launch both in space and relative to the launch site. However, if a particular launch site is to be utilized, consideration must be given to the problem of matching the desired time of launch with the time at which the launch site crosses the desired orbital plane.

$$t_L = t_1$$

where

t_L = the time of launch relative to the reference direction in the plane of the equator.

t_1 = the time from perigee in the final orbit to the vehicle at the launch of the shuttle.

Now

$$t_L = t_{2f} + t^* - t_t - t_{ascent} - n\tau_\ell \left[1 + \frac{\Delta\tau}{\tau}\right] \quad (20)$$

where

t^* = time required by the satellite to travel from the projection of the perigee radius in the equatorial plane to the reference direction (all times are thus related to a common base).

n = number of revolutions in intermediate orbit.

$\Delta\tau$ = oblateness correction to orbital period.

Numerical data can be generated for the time of ascent once it is known what the intermediate orbit will be and to what extent the trajectory from launch to burnout is shaped by the guidance law. It should be noted that since the selection of an intermediate orbit will depend on the duration of t_{ascent}, iteration for this quantity will be necessary.

This time must be matched with the following, if no error in the orbital plane is permissible.

$$t_L = \frac{(\Omega + n\dot{\Omega}_\ell) - \Lambda_L \pm \sin^{-1}\left(\frac{\tan L_L}{\tan i}\right) + \delta\pi}{\Omega_e} \quad (30)$$

where $\delta = 1$ for southerly launches, 0 otherwise.

$\dot{\Omega}_\ell$ = secular regression rate in the intermediate orbit $= \dfrac{-3\pi J_2 \cos i}{\left(\frac{a}{R}\right)^2 (1-e^2)^2}$ $0 < i < 180°$

and where the plus value of $\sin^{-1}\left(\frac{\tan L}{\tan i}\right)$ is used for northerly launches and the minus for southerly launches.

It should be noted at this point that range safety restrictions at both AMR and PMR currently restrict all launches to those in a southerly direction. For this reason only southerly launches are given attention, and therefore, only the negative sign is utilized. For convenience, the term π will also be combined with the angle Ω.

Since the solution of Eqs (29) and (30) may require that the satellite remain in the low altitude orbit for a long period, it may be possible (if small errors in the nodal position are acceptable) to launch at a time when the desired launch site is arbitrarily close to the desired plane. This is done in the following manner.

$$t_L - \frac{(\Omega + n\dot{\Omega}) - \Lambda_L - \sin^{-1}\left(\frac{\tan L_L}{\tan i}\right)}{\Omega_e} \leq \frac{\text{allowable nodal error}}{\Omega_e} \quad (31)$$

Since rendezvous cannot occur until this error has been removed, maneuvering is implied. Equation (31) thus introduces the concept of launch time tolerance (or launch windows as the subject is sometimes called) since

$$\Delta t_L = \frac{\Delta\Omega}{\Omega_e} .$$

It should be noted that the perturbing influence of the earth's oblateness has been included only in those terms involving the low altitude circular orbit. This assumption is reasonable, though not precise, if the final and initial orbits differ markedly in size. However, if more accuracy is desired, or if the various orbits are essentially the same size, the following equations should be employed.

$$t_L = t_{2f} + t^* + \Delta\tau_f\left(\frac{\theta_f}{2\pi}\right) - t_t + \Delta\tau_t\left(\frac{\theta_t}{2\pi}\right) - n\tau_L\left[1 + \frac{\Delta\tau}{\tau}\right] - t_{ascent} \quad (32)$$

$$t_L = \left\{\Omega + n\dot{\Omega}_\ell - \left(\frac{\theta_t}{2\pi}\right)\dot{\Omega}_t - \left(\frac{\theta_f}{2\pi}\right)\dot{\Omega}_f - \Lambda_L - \sin^{-1}\left[\frac{\tan L_L}{\tan i}\right]\right\}\frac{1}{\Omega_e} \quad (33)$$

Because of the large number of variables, it is impossible to obtain an intuitive feel for the manner in which the time in the intermediate orbit varies. However, if certain restrictions are made, a feel can be obtained for certain classes of orbits. If it is assumed that the orbits of interest are both circular and that the transfer is via the Hohmann ellipse, and if it is further assumed that perturbations are neglected because of plotting accuracy, then

$$n = \frac{t_{2f} + t^*}{\tau_L} - \frac{\tau_t}{2\tau_L} - \frac{t_{ascent}}{\tau_L} - \frac{(\Omega - \Lambda_L) - \sin^{-1}\left(\frac{\tan L_L}{\tan i}\right)}{\Omega_e \tau_L}$$

(continued)

$$= \frac{t_{2f} + t^* - t_{ascent}}{\tau_L} - \frac{1}{2}\sqrt{\frac{a_t^3}{a_L^3}} - \frac{(\Omega - \Lambda_L) - \sin^{-1}\left(\frac{\tan L_L}{\tan i}\right)}{\Omega_e \tau_L} \qquad (34)$$

Since the equation generally results in a negative value of t_L, the significance of such values must be discussed. Negative times simply imply that the shuttle vehicle is launched at a time prior to the beginning of the time record; negative times can be avoided by increasing t_{2f} by some integer of the orbital period (1, 2, 3, ---).

b. Sample problem

The rendezvous problem, exclusive of the final closure discussion, has been presented in the preceding sections. A numerical check of the flexibility, accuracy and utilization of the approach is in order. For the purposes of illustration, a target orbit of a 24-hr period is selected. In addition it is assumed that the latitude of the point of injection into the transfer orbit is the latitude of the launch site. The numerical analysis follows.

r_{af} = 42,400 stat mi ≈ 68,300 km

r_{pf} = 10,000 stat mi ≈ 27,900 km

e_f = 0.61832

L_1 = 28.5° N

L_2 = 28.5° N

i_f = i_t = 70°

ω_f = -77.46°

r_{pt} = 4500 stat mi ≈ 7250 km

Elliptical orbits are tangent at point of rendezvous. In addition it is assumed that the type of transfer is specified and the time of ascent is known.

t_{ascent} = 1000 sec

$\sin(\omega + \theta) = \frac{\sin L_2}{\sin i}$

$(\omega + \theta_2)_{24}$ = 30.52°

$(\theta_2)_{24}$ = 107.98°

$$\frac{2 r_a}{r_{tan}} = \left(\frac{r_a}{r_p} + 1\right)_{24} + \left(\frac{r_a}{r_p} - 1\right)\cos(\theta_2)_{24}$$

r_{tan} = 20,000 stat mi ≈ 32,200 km

$$r_{at} = \frac{\frac{r_{tan}}{r_{pt}} - 1}{\frac{r_{tan}}{(r_a)_{24}(r_p)_{24}} - \frac{(r_p)_{24}}{(r_a)_{24}} + 1 + \frac{1}{r_{pt}}}$$

= 23,623 stat mi ≈ 38,000 km

$\frac{r_{at}}{r_{pt}}$ = 5.24956

$$e_t = \frac{\frac{r_{at}}{r_{pt}} - 1}{\frac{r_{at}}{r_{pt}} + 1} = 0.67998$$

$$\cos\theta_t = \frac{\frac{2 r_{at}}{r} - \left(\frac{r_{at}}{r_{pt}} + 1\right)}{\frac{r_{at}}{r_{pt}} - 1} = -0.91474$$

θ_t = 156.17°

$\psi = \theta_t - \theta_{24}$ = 48.19°

$\omega_t = \omega_{24} - \psi$ = - 125.65°

$$a_t = \frac{r_{at} + r_{pt}}{2} = 7.42447 \times 10^7 \text{ ft} \approx 22{,}600 \text{ km}$$

$$\left(\frac{\tau}{2\pi}\right)_t = \sqrt{\frac{a^3}{\mu}} = 5391.75 \text{ sec/rad}$$

$$E_t = 2\tan^{-1}\left[\sqrt{\frac{r_{pt}}{r_{at}}}\tan\frac{\theta_t}{2}\right] = 2.24059 \text{ rad}$$

$$t_t = \frac{\tau}{2\pi}\left[E_t + e_t \sin E_t\right] = 9206.6 \text{ sec}$$

$$E_{24} = 2\tan^{-1}\left[\sqrt{\frac{r_p}{r_a}}\tan\frac{\theta_{24}}{2}\right] = 67.60°$$

= 1.17978 rad

$$(t_2)_{24} = \frac{\tau_{24}}{2\pi}\left[E_{24} - e_{24}\sin E_{24}\right]$$

= 8339.5 sec

$$\tau_\ell = 2\pi\sqrt{\frac{a^3}{\mu}}$$

$$t_L = (t_2)_{24} - t_t - t_{ascent} - n\,\tau_\ell$$

Since $L_L = L_2$, t_L may be written as

$$t_L = -1867.1 - 6133.2\,n'$$

(neglecting perturbations)

This launch time must be made to correspond with that of the launch point as it crosses the orbital plane. This equation, which has all times referenced to the projection of the perigee radius on the equatorial plane, is as follows.

$$t_L = \frac{(\Omega - \Lambda_L) - \sin^{-1}\left[\frac{\tan L_L}{\tan i}\right]}{\Omega_e}$$

$$= \frac{(\Omega - \Lambda_L) - 0.19897}{0.729214 \times 10^{-4}}$$

$$\therefore (\Omega - \Lambda_L) = -n'(0.44724) + 0.06282$$

This equation is immediately recognizable as that of a straight line with a slope of -0.44724 and an ordinate intercept of 0.06282 radian. This equation can be solved for integral values of n' to determine if the desired trajectory can be obtained with the given bits of data. It is obvious that only a few launch sites provide the required timing considerations for this problem. However, if the time in the low altitude orbit is allowed to change by varying the period of this orbit, different results are obtained. This procedure was repeated and the altitude of the circular orbit allowed to vary. The results of these calculations are presented in Fig. 3. This figure shows the limitations on the altitude of the low-altitude orbit. It must be noted that these curves are not, in reality, continuous and that only the points of intersection of vertical lines for integral numbers of revolutions, and the horizontal lines for constant launch site latitude provide the required solution.

$i = 70°$

$L_L = 28.5°$

$L_2 = 28.5°$

$(r_a)_{24}$ = 42,400 stat mi ≈ 68,300 km

$(r_p)_{24}$ = 10,000 stat mi ≈ 27,900 km

t_{ascent} = 1000 sec

No perturbations

The effects of perturbation were not included in this analysis primarily because the magnitude is such that they are rounded off in plotting. However, for comparison purposes these calculations were made for the assumption that all of the influences are encountered in the low-altitude orbit. This assumption is believed to be reasonable because the time in the low-altitude orbit will probably be large compared to that in the transfer orbit, and the effects of the earth's oblateness fall off as the square of the semi-latus rectum. However, by using Chapter IV, it is possible to account for the cyclic perturbations occurring within fractions of revolutions, thus making it possible to account for the perturbing influence of the earth's oblateness for the entire time of flight.

The result of these computations is a slightly different slope for the lines of Fig. 3. The magnitude of this difference is approximately 0.0027 rad/rev and the maximum error produced is 0.046 rad (or 2.6 deg). Although this error is small it should not be neglected since it is capable of producing a linear displacement of approximately 900 stat mi or 1450 km at a radius of 20,000 stat mi or 32,200 km.

3. Compatible Orbits

If rendezvous is seen as a requirement prior to the time the target vehicle is launched, its orbit can be selected in such a manner that the correct relative position between the launch site and the satellite exists at a prescribed time. The selection of such an orbit enables the launch vehicle to utilize a direct ascent trajectory requiring a minimum amount of fuel and guidance. The orbits which satisfy these conditions are referred to as compatible orbits and the periods of such orbits are defined as follows.

$$\Delta t_L = \Delta t_{ascent} + n\tau \left[1 + \frac{\Delta\tau}{\tau}\right] \qquad (35)$$

$$\Delta t_L = \frac{(\Omega_0 + n\Omega) - \Lambda_{L1} \pm \sin^{-1}\left(\frac{\tan L_{L1}}{\tan i}\right) + 2m\pi}{\Omega_e}$$

$$- \frac{\Omega_0 - \Lambda_{L2} \pm \sin^{-1}\left(\frac{\tan L_{L2}}{\tan i}\right)}{\Omega_e} \qquad (36)$$

where

the subscripts 1 and 2 refer to the station from which the first and second satellites were launched in a southerly direction.

The term $\Delta\tau$ is an approximate correction to the orbital period over a spherical earth to account for the earth's equatorial bulge.

Equations (35) and (36) can be solved for the orbital period required to produce rendezvous from a given pair of launch sites after a given interval of time. The result is

$$\tau = \frac{2m\pi + (\Lambda_{L2} - \Lambda_{L1}) \pm \sin^{-1}\left(\frac{\tan L_{L1}}{\tan i}\right)}{n\Omega_e \left[1 + \frac{\Delta\tau}{\tau}\right]}$$

$$+ \frac{\mp \sin^{-1}\left(\frac{\tan L_{L2}}{\tan i}\right) - \Omega_e \Delta t_{asc} + n\dot{\Omega}}{n\Omega_e \left[1 + \frac{\Delta\tau}{\tau}\right]} \qquad (37)$$

To this point no constraints are placed on the values which n can assume. This is accomplished by referring to the spherical triangle shown below.

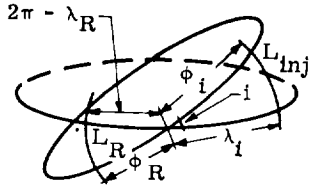

$$\phi = \sin^{-1}\left(\frac{\sin L}{\sin i}\right)$$

For northerly launches from the northern hemisphere, n must be of the form

$$n = p - (\phi_i - \phi_R)$$

and for southerly launches, n must be of the form

$$n = p + (\phi_i - \phi_R)$$

where p is an arbitrary integer and the subscripts i and R refer to the points of injection and rendezvous, respectively. As may be noted, the solution for ϕ is ambiguous unless an additional parameter is specified. The most readily available bit of information is the quadrant (relative to some point in the orbit) of ϕ or of the related angle λ. This information is known for any desired case.

Now, if one simplifying assumption is made, Eq (37) can be reduced to a form which is applicable for the case of a single launch site (i.e., $L_{L1} = L_{L2}$; $\Lambda_{L1} - \Lambda_{L2}$)

$$\tau = \frac{2m\pi - \Omega_e \Delta t_{asc} + n\dot{\Omega}}{n\Omega_e\left[1 + \frac{\Delta\tau}{\tau}\right]} \qquad (38)$$

Because of the interdependence of $\dot{\Omega}$ and τ, an iterative solution to this problem is generally required. However, because $\dot{\Omega}$ is very small, it is generally sufficient to use the value of τ, obtained, neglecting perturbations, to estimate the value of $\dot{\Omega}$ and then to correct the orbital period.

Figures 4 and 5 show the variation in the required semimajor axis for different values of n/m, neglecting perturbations and variations in the ascent trajectories. The auxiliary scale adjacent to the scale for semimajor axis presents the altitude of a circular orbit of the same period.

Table 1 (obtained from Ref. 1) presents the set of orbits obtainable from a launch site at 28.5° (AMR) which makes 15 revolutions per effective earth's rotation as a function of the time interval between easterly launches. The effective rotation of the earth is defined as the time or angular interval between successive passes of a point on earth through a given point in the regressing orbital plane (i.e., $t = \frac{2\pi + n\dot{\Omega}}{\Omega_e}$). Fifteen orbital periods per effective earth's rotation are selected for this presentation because for smaller integers (i.e., 14, 13, etc.), most of the orbits lie in the Van Allen radiation belts, thus making them unsuitable for many satellite missions, and because the only lower orbit suitable (i.e., 16 periods per effective rotation) presents problems due to the extremely short lifetime. Reference 1 also has this to say about the interval between the launches: "The selection of the value of N (the number of revolutions between launches) depends on the specific purpose of the space station. If the orbital inclination of the satellite must be large, a value of N approaching 7 is required. Orbits of this type have the additional advantage that the two possible launch times during each effective earth's revolution are more nearly equispaced; but as N approaches 1, the time spacing between the two possible launches becomes very unequal."

Swanson and Petersen have extended the work published in Ref. 1. This work is presented below as it appeared in Refs. 2 and 3.

For an orbital period corresponding to N revolutions every m earth revolutions to make a south-going pass over the launch base n revolutions after the north-going pass, the following relation must be satisfied.

$$n = \left(\frac{N/m - 1}{2}\right) + \left(\frac{N}{m}\right)M + \frac{1}{\pi}\left[\phi - \frac{N}{m}\nu\right] \qquad (39)$$

where M = integer number of earth revolutions completed between the north-going and south-going pass. For every value of n there is only one value of orbit inclination, i, that will satisfy the equation. No correction for finite burning time is included.

$\nu = \tan^{-1}[\tan\phi \cos i]$

$\phi = \sin^{-1}[\sin L/\sin i]$

L = latitude of launch base

i = inclination of orbit plane

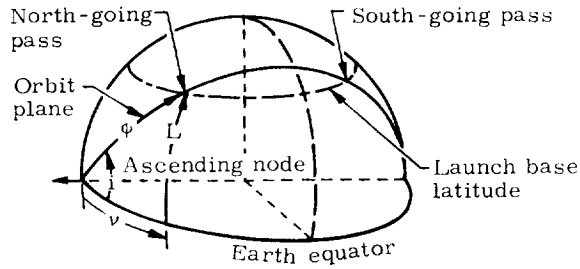

The relationship between n and N/m is presented in Figs. 6a, b, c, d and e.

The preceding figures neglect the effect of finite burning time on the problem. These effects can be observed from the following sketch and Figs. 7a and b.

These figures which present data for Canaveral launches show the effect of both burning time and the number n on the selection of orbital inclination.

TABLE 1

Rendezvous Compatible Orbits Making 15 Revolutions Per Effective Earth's Rotation (Launch from a Latitude of 28.5°)

Central Angle Between Launch and Injection		Revolutions Between Launches (N)												
		1	2	3	4	5	6	7	8	9	10	11	12	13
0	i°	29.13	31.03	34.66	40.72	50.56	65.82	86.60	65.82	50.56	40.72	34.66	31.03	29.13
arc = 0 naut mi	a	3701.7	3702.3	3703.6	3706.3	3711.4	3721.0	3738.0	3721.0	3711.4	3706.3	3703.6	3702.3	3701.7
	h(naut mi)	261.5	262.1	263.4	266.1	271.2	280.8	297.8	280.8	271.2	266.1	263.4	262.1	261.5
5	i°	29.14	31.05	34.71	40.80	50.69	66.05	86.68	66.05	50.69	40.80	34.71	31.05	29.14
arc = 300 naut mi	a	3701.7	3702.3	3703.6	3706.3	3711.5	3721.1	3738.0	3721.1	3711.5	3706.3	3703.6	3702.3	3701.7
	h(naut mi)	261.5	262.1	263.4	266.1	271.3	280.9	297.8	280.9	271.3	266.1	263.4	262.1	261.5
10	i°	29.15	31.11	34.81	41.06	51.04	66.46	86.76	66.46	51.04	41.06	34.81	31.11	29.15
arc = 600 naut mi	a	3701.7	3702.3	3703.7	3706.4	3711.7	3721.4	3738.1	3721.4	3711.7	3706.4	3703.7	3702.3	3701.7
	h(naut mi)	261.5	262.1	263.5	266.2	271.5	281.2	297.9	281.2	271.5	266.2	263.5	262.1	261.5
15	i°	29.17	31.18	35.00	41.46	51.80	67.26	86.90	67.26	51.80	41.46	35.00	31.18	29.17
arc = 900 naut mi	a	3701.7	3702.4	3703.8	3706.6	3712.1	3722.1	3738.2	3722.1	3712.1	3706.6	3703.8	3702.4	3701.7
	h(naut mi)	261.5	262.2	263.6	266.4	271.9	281.9	298.0	281.9	271.9	266.4	263.6	262.2	261.5
20	i°	29.18	31.28	35.28	42.09	53.02	68.52	87.10	68.52	53.02	42.09	35.28	31.28	29.18
arc = 1200 naut mi	a	3701.7	3702.4	3703.9	3707.0	3712.8	3723.0	3738.4	3723.0	3712.8	3707.0	3703.9	3702.4	3701.7
	h(naut mi)	261.5	262.2	263.7	266.8	272.6	282.8	298.2	282.8	272.6	266.8	263.7	262.2	261.5
25	i°	29.19	31.41	35.62	42.86	54.42	69.87	87.32	69.87	54.42	42.86	35.62	31.41	29.19
arc = 1500 naut mi	a	3701.7	3702.4	3704.0	3707.4	3713.6	3724.0	3738.6	3724.0	3713.6	3707.4	3704.0	3702.4	3701.7
	h(naut mi)	261.5	262.2	263.8	267.2	273.4	283.8	298.4	283.8	273.4	267.2	263.8	262.2	261.5
30	i°	29.22	31.55	36.01	43.84	55.86	71.23	87.56	71.23	55.86	43.84	36.01	31.55	29.22
arc = 1800 naut mi	a	3701.7	3702.5	3704.1	3707.8	3714.5	3725.2	3738.8	3725.2	3714.5	3707.8	3704.1	3702.5	3701.7
	h(naut mi)	261.5	262.3	263.9	267.6	274.3	285.0	298.6	285.0	274.3	267.6	263.9	262.3	261.5

(* 1 naut mi = 1.852 km)

L = latitude of launch base i = orbit inclination
ψ^* = burning time measured in degrees of travel of the target satellite. This angle is assumed to be a reasonably small quantity

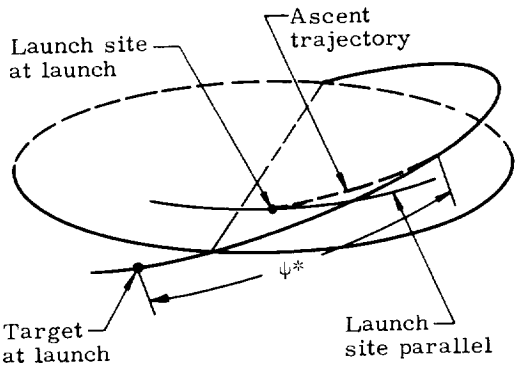

4. Direct Launch

This technique can be analyzed by referring to the development for the intermediate orbit case

$$t_L = t^* + \left(t_{2f}\right) - t_{BO} - t_{ascent} \tag{40}$$

$$t_L = \frac{\Omega - \Lambda_L \pm \sin^{-1}\left(\frac{\tan L}{\tan i}\right)}{\Omega_e} + \frac{\Delta\Omega}{\Omega_e} \tag{41}$$

The significance of all terms in these equations with the exception of the $\Delta\Omega$ term has been discussed in previous paragraphs. The significance of the final term and the energy requirements can be obtained from the following discussion.

$$(A_L - \Omega) = \nu$$

$$\Delta\eta' = \tan^{-1}\left(\frac{\tan L}{\sin \nu}\right) - \tan^{-1}\left(\frac{\tan L}{\sin (\nu + \Delta\Omega)}\right) \tag{42}$$

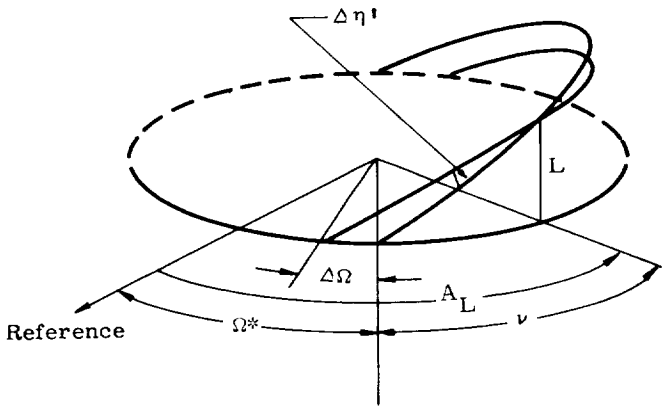

This angle ($\Delta\eta'$) is the projection of the actual change in yaw on the earth. The actual change may be seen from the following sketch to be

$$\Delta\eta = 2 \sin^{-1}\left(\cos \gamma_t \sin \frac{\Delta\eta'}{2}\right) \tag{43}$$

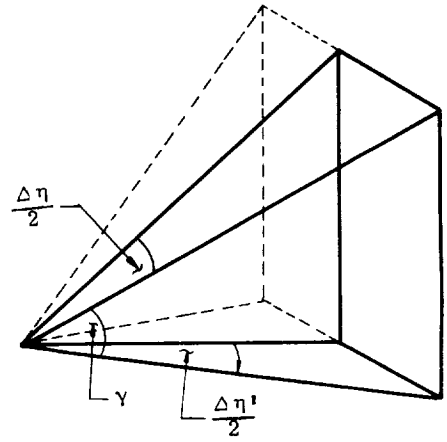

Now the velocity increment to produce this change is

$$\begin{aligned}\Delta V_n &= 2 V_t \sin \frac{\Delta\eta}{2} \\ &= 2 V_t \cos \gamma_t \sin \frac{\Delta\eta'}{2} \\ &= 2 V_t \cos \gamma_t \sin \frac{1}{2}\left[\tan^{-1}\left(\frac{\tan L}{\sin \nu}\right)\right. \\ &\quad \left. - \tan^{-1}\left(\frac{\tan L}{\sin (\nu + \Delta\Omega)}\right)\right]\end{aligned} \tag{44}$$

If the change in yaw is small, and if the correction is made near apogee where the velocity V_t is minimum (just prior to injection into the final orbit), the relationship between the velocity increment and the change in node is

$$\frac{\Delta V_n}{V_a} = \tan^{-1}\left(\frac{\tan L}{\sin \nu}\right) - \tan^{-1}\left(\frac{\tan L}{\sin (\nu + \Delta\Omega)}\right) \tag{45}$$

The significance of negative values of $\frac{\Delta V_n}{V_a}$ is simply that the sign of $\Delta\Omega$ is negative or that the inclination of the transfer orbit is less than that of the desired orbit. A graphical solution to this equation is presented as Fig. 8.

This nodal and inclination correction results in a tolerance in the time of launch assuming that some specified amount of propellant is available for making such a correction.

$$\Delta t_L = \frac{\Delta\Omega}{\Omega_e} \tag{46}$$

$$\sin (\nu + \Delta\Omega) = \frac{\tan L}{\tan\left[\tan^{-1}\left(\frac{\tan L}{\sin \nu}\right) - \frac{\Delta V}{V_a}\right]} \tag{47}$$

$$\sin(\nu + \Delta\Omega) = \sin\nu\cos\Delta\Omega + \sin\Delta\Omega\cos\nu$$

$$\approx \sin\nu + \Delta\Omega\cos\nu$$

$$\therefore \Delta\Omega = \frac{\tan L}{\cos\nu \tan\left[\tan^{-1}\left(\frac{\tan L}{\sin\nu}\right) - \frac{\Delta V}{V_a}\right]} - \tan\nu;$$

$$(\nu \neq \pm\tfrac{\pi}{2}) \qquad (48)$$

and

$$\Delta t_L = \frac{\tan L - \sin\nu \tan\left[\tan^{-1}\left(\frac{\tan L}{\sin\nu}\right) - \frac{\Delta V}{V_a}\right]}{\Omega_e \cos\nu \tan\left[\tan^{-1}\left(\frac{\tan L}{\sin\nu}\right) - \frac{\Delta V}{V_a}\right]} \qquad (49)$$

As an example, consider the case

$L = 30°$

$\nu = (A_L - \Omega^*) = 30°$

$\Delta V_{max} = \pm 1000$ fps $= 305$ mps

$V_a = 10,000$ fps $= 3050$ mps

$\Delta t \approx \pm 1800$ sec

Should L have been negative in this example, ν would have remained unchanged because of the definition of Ω^* which is measured from the reference direction to the last nodal crossing, thus restricting the value of ν to less than 180°. Mathematically this says

$\Omega^* = \Omega \qquad 0 < L \leq 90$

$\Omega^* = \Omega - 180 \qquad 0 > L \geq -90$

With these restrictions, the launch tolerance remains unchanged.

The resultant change in inclination can also be obtained, but it is of lesser significance since its effect on the energy requirements is already included.

From the sketch with Eq (42) and spherical trigonometry

$$\tan L = \tan i \sin\nu \qquad (50)$$

or

$$\tan i_f \sin\nu = \tan(i_f + \Delta i)\sin\left[\nu + \Delta\Omega\right]$$

but

$$\frac{\sin(\nu + \Delta\Omega)}{\sin\nu} = \cos\Delta\Omega + \cot\nu\sin\Delta\Omega$$

$$\frac{\tan(i + \Delta i)}{\tan i} = \frac{1 + \frac{\tan\Delta i}{\tan i}}{1 - \tan i\tan\Delta i} \approx \frac{1}{1 - \Delta i\tan i} \qquad (51)$$

This final approximation is valid under the assumption that the orbital inclination is greater than 30° and that the change in inclination is small.

Thus

$$1 - \Delta i\tan i \approx \cos\Delta\Omega + \cot\nu\sin\Delta\Omega$$

$$\Delta i \approx \frac{1 - \cos\Delta\Omega - \cot\nu\sin\Delta\Omega}{\tan i} \qquad (52)$$

If the nodal change is also small, this equation reduces to

$$\Delta i \approx \frac{-\Delta\Omega\cos\nu}{\tan i\sin\nu} \quad \begin{matrix} i \neq 0 \\ \nu \neq 0 \end{matrix} \qquad (53)$$

C. THE TERMINAL MANEUVER

The preceding discussions have been directed toward the placement of the shuttle or homing vehicle in the vicinity of the target. The following material is intended to provide an insight into the subsequent motion leading to docking or closure. The discussion proceeds as follows.

(1) Relative motion.

(2) Terminal guidance schemes.

(3) Closure times and energy requirements.

(4) Terminal guidance smoothing techniques.

(5) Long time closures.

(6) Homing phase errors

1. Relative Motion (Ref. 5)

In this section, the general relative equations of motion for the rendezvous maneuver are developed and explained. The purpose of this section is to show how the rendezvous dynamics are affected by orbital aspects as well as by vehicle-induced accelerations. The effects of initial conditions on the rendezvous problem will be discussed with respect to velocity and time requirements in sample problems.

a. Motion relative to target

Consider the earth-centered inertial frame shown in the following sketch. The target vehicle

is located by the position vector $\vec{r}_t$, and the homing vehicle by $\vec{r}_h$. The relative range vector $\vec{s}$ is defined from target vehicle to homing vehicle.

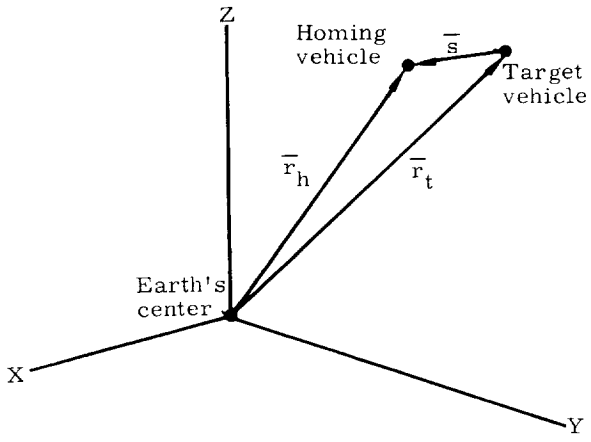

Let:

$\bar{g}(\bar{r})$ = gravitational acceleration for a spherical earth.

$\bar{a}_t$, $\bar{a}_h$ = thrust acceleration of target and homing vehicles.

$\bar{P}(\bar{r}, \dot{\bar{r}})$ = perturbative acceleration due to earth oblateness, moon, sun, atmosphere, and nearby planets combined.

Motion relative to the target, neglecting mutual attraction of the vehicles, is thus governed by

$$\frac{d^2\bar{s}}{dt^2} = \left[\bar{a}_h - \bar{a}_t + \bar{g}(\bar{r}_h) - \bar{g}(\bar{r}_t)\right] + \left[\bar{P}(\bar{r}_h, \dot{\bar{r}}_h) - \bar{P}(\bar{r}_t, \dot{\bar{r}}_t)\right] \quad (54)$$

Simplification of Eq (54) results if the following assumptions apply:

(1) $s << r_t$.

(2) r_t and r_h sufficiently large such that drag effects are small.

(3) Total rendezvous time sufficiently small so that the perturbative accelerations have only first order effects on the motion of each vehicle.

Then, the difference of perturbative accelerations appearing in Eq (54) may be neglected as second order in the perturbation. This follows since the proximity of the two vehicles in space and time yields

$$\bar{P}(\bar{r}_h, \dot{\bar{r}}_h) \sim \bar{P}(\bar{r}_t, \dot{\bar{r}}_t) + d\bar{P}(\bar{r}_t, \dot{\bar{r}}_t)$$

Inasmuch as $\bar{P}$ is itself of first order, $d\bar{P}$ is of second order.

Similarly, if $\bar{g}(\bar{r}_h)$ is developed in a Taylor series about $\bar{r}_t$,

$$\bar{g}(\bar{r}_h) = \bar{g}(\bar{r}_t) + (\bar{s} \cdot \nabla)\,\bar{g}(\bar{r}_t) + \frac{1}{2}(\bar{s} \cdot \nabla)^2\,\bar{g}(\bar{r}_t) + \ldots$$

where

∇ = gradient operator.

Neglecting second and higher order terms

$$\bar{g}(\bar{r}_h) - \bar{g}(\bar{r}_t) = (\bar{s} \cdot \nabla)\,\bar{g}(\bar{r}_t).$$

Substituting

$$\bar{g}(\bar{r}) = -\frac{GM}{r^3}\,\bar{r}$$

where

GM = Universal gravitational constant times mass of the earth.

$= \mu$.

$$\bar{g}(\bar{r}_h) - \bar{g}(\bar{r}_t) = -\frac{GM}{r_t^2}\left[\frac{\bar{s}}{r_t} - 3\bar{r}_t\,\frac{(\bar{s} \cdot \bar{r}_t)}{r_t^3}\right] \quad (55)$$

Thus Eq (54) becomes, valid to first order,

$$\frac{d^2\bar{s}}{dt^2} = \left[\bar{a}_h - \bar{a}_t\right] - \frac{GM}{r_t^2}\left[\frac{\bar{s}}{r_t} - 3\bar{r}_t\,\frac{(\bar{s} \cdot \bar{r}_t)}{r_t^3}\right] \quad (56)$$

This is the equation derived and discussed by Hord in Ref. 4.

The exact solution of Eq (56) for the general case is a difficult analytical task. Aside from the thrust accelerations which are general functionals of $\bar{s}$ and $d\bar{s}/dt$, the orbital nature of the problem, reflected through the gravity terms, complicates the analysis. This complexity, however, underscores the fact that the orbital aspects of the problem should never be overlooked in the general case. To cite an example, consider a coplanar rendezvous in which homing starts when the target is at the apogee of its assumed eccentric orbit. Assume the homing vehicle to be slightly behind the target, at the same altitude, and at sufficient overspeed to be closing on the target. On the

basis of rectilinear considerations one may compute a total closing time by dividing the initial relative range by the closing rate. This time, however, may be completely erroneous and moreover the vehicles may never close to a sufficiently small range for rendezvous purposes. The reason for this is seen by noting the orbital aspects of the situation. The target, initially at apogee, begins to speed up as it travels toward perigee; the homing vehicle, depending on the overspeed, may be at apogee of an elliptic orbit, in a circular orbit, or at perigee of an elliptic orbit. Clearly, the latter two conditions cause an expansion of the homing time, since the homing vehicle either remains at the same speed or slows down as it travels toward apogee. Hence, rendezvous may never occur, or, if it occurs, may undergo extreme time expansion.

Conditions permitting neglect of orbital aspects. If Eq (56) is integrated once with respect to time,

$$\frac{d\bar{s}}{dt} = \left(\frac{d\bar{s}}{dt}\right)_0 + \int_0^t \Delta\bar{a}\, dt - \int_0^t \Delta\bar{g}(\bar{s}, \bar{r}_t)\, dt \qquad (57)$$

where

$$\Delta\bar{a} = \bar{a}_h - \bar{a}_t$$

$$\Delta\bar{g}(\bar{s}, \bar{r}_t) = \frac{GM}{r_t^2}\left[\frac{\bar{s}}{r_t} - 3\,\bar{r}_t\,\frac{(\bar{s}\cdot\bar{r}_t)}{r_t^3}\right]$$

then the condition allowing neglect of the orbital aspects of the problem is obvious, since orbit parameters such as GM and r_t are vested solely in $\Delta\bar{g}(\bar{s}, \bar{r}_t)$. Hence, if

$$\left|\int_0^{T_0} \Delta\bar{g}\, dt\right| << \left|\left(\frac{d\bar{s}}{dt}\right)_0\right| \text{ or } \left|\int_0^{T_0} \Delta\bar{a}\, dt\right| \qquad (58)$$

Eq (57) becomes

$$\frac{d\bar{s}}{dt} \approx \left(\frac{d\bar{s}}{dt}\right)_0 + \int_0^t \Delta\bar{a}\, dt \qquad (59)$$

and permits rectilinear analysis. Note that Eq (58) is a condition on the integrated effect of the gravity differential rather than on the magnitude of $\Delta\bar{g}$ itself.

b. Analysis of relative motion

Certain important special cases of Eq (56) can be analyzed by the method of Gilbert (Ref. 5). One such case is that of thrust-free motion. The method presented below is valid for thrust-free motion, but is easily extended to motion in the presence of impulsive thrusts.

The form of Eq (16) to be analyzed is

$$\frac{d^2\bar{s}}{dt^2} + \frac{GM}{r_t^2}\left[\frac{\bar{s}}{r_t} - 3\,\bar{r}_t\,\frac{(\bar{s}\cdot\bar{r}_t)}{r_t^3}\right] = 0 \qquad (60)$$

The analysis for a target in circular motion is studied first and later extended to targets in orbits of small eccentricities.

(1) Target in circular orbit. Let there be a rotating, relative coordinate frame centered at the target, whose axes as shown in the following sketch are defined by

$\bar{i}_x$ = unit vector along target's radius vector, $\bar{r}_t$

$\bar{i}_y$ completes the right-handed set

$\bar{i}_z$ = unit vector normal to target's orbit plane.

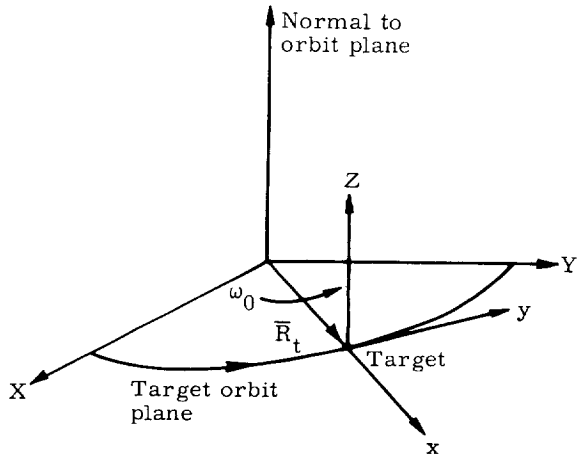

The vector $\bar{s}$ may be resolved into the three orthogonal directions and three coupled second order differential equations obtained.

Since

$$\frac{d^2\bar{s}}{dt^2} = \frac{\delta^2\bar{s}}{\delta t^2} + \left(2\bar{\omega}_0 \times \frac{\delta\bar{s}}{\delta t}\right) + \left(\bar{\omega}_0 \times \bar{\omega}_0 \times \bar{s}\right)$$

where

$\frac{\delta\bar{s}}{\delta t}$ = rate of change of $\bar{s}$ relative to observer in rotating frame

$\frac{\delta^2\bar{s}}{\delta t^2}$ = acceleration of $\bar{s}$ relative to observer in rotating frame

$\bar{\omega}_0$ = angular velocity vector of target in circular motion

Equation (60) becomes

$$\frac{\delta^2\bar{s}}{\delta t^2} + \left(2\bar{\omega}_0 \times \frac{\delta\bar{s}}{\delta t}\right) + \left(\bar{\omega}_0 \times \bar{\omega}_0 \times \bar{s}\right) + \frac{GM}{r_t^2}\left[\frac{\bar{s}}{r_t} - 3\bar{r}_t\,\frac{(\bar{s}\cdot\bar{r}_t)}{r_t^3}\right] = 0. \qquad (61)$$

Whence,

$$\left.\begin{aligned} \frac{d^2x}{dt^2} - 3\omega_0^2 x - 2\omega_0 \frac{dy}{dt} &= 0 \\ \frac{d^2y}{dt^2} + 2\omega_0 \frac{dx}{dt} &= 0 \\ \frac{d^2z}{dt^2} + \omega_0^2 z &= 0. \end{aligned}\right\} \qquad (62a, b, c)$$

These equations have the solution

$$\left.\begin{aligned} x &= \left(2\frac{\dot{x}_0}{\omega_0} - 3y_0\right)\cos\omega_0 t + \frac{\dot{y}_0}{\omega_0}\sin\omega_0 t \\ &\quad + \left(4y_0 - \frac{2\dot{x}_0}{\omega_0}\right) \\ y &= 2\left(\frac{2\dot{x}_0}{\omega_0} - 3y_0\right)\sin\omega_0 t - \frac{2\dot{y}_0}{\omega_0}\cos\omega_0 t \\ &\quad + (6\omega_0 y_0 - 3\dot{x}_0)t + \left(x_0 + \frac{2\dot{y}_0}{\omega_0}\right) \\ z &= z_0\cos\omega_0 t + \frac{\dot{z}_0}{\omega_0}\sin\omega_0 t \end{aligned}\right\} \qquad (62d, e, f)$$

These equations have been presented in numerous references, among them Refs. 6 and 7, and have been utilized in connection with various terminal guidance studies. However, the present goals are best served by altering the form of these equations by introducing a set of normalized variables.

$$\left.\begin{aligned} \rho &\equiv \frac{x}{r_t} \\ \alpha &\equiv \frac{y}{r_t} \\ \lambda &\equiv \frac{z}{r_t} \\ T &\equiv \omega_0 t \end{aligned}\right\} \qquad (63)$$

Note that α is the downrange angle of the homing vehicle relative to the target, while λ is the cross-range angle. The normalized time T is actually the angle of travel of the target from t = 0.

It is also beneficial to define the following normalized rates,

$$\left.\begin{aligned} A &\equiv \frac{\frac{dz}{dt}}{V_0} = \frac{d\lambda}{dT} \equiv \frac{V_N}{V_0} \\ B &\equiv \frac{\frac{dx}{dt} - \omega_0 y}{V_0} = \frac{d\rho}{dT} - \alpha \equiv \frac{V_R}{V_0} \\ C &\equiv \frac{\frac{dy}{dt} + \omega_0 x}{V_0} = \frac{d\alpha}{dT} + \rho \equiv \frac{V_C}{V_0} \end{aligned}\right\} \qquad (64)$$

where

$$\left.\begin{aligned} V_o &= \omega_0 r_t \\ V_C &= \left(\frac{d\bar{r}_h}{dt} - \frac{d\bar{r}_t}{dt}\right)\cdot \bar{i}_y \\ V_R &= \left(\frac{d\bar{r}_h}{dt} - \frac{d\bar{r}_t}{dt}\right)\cdot \bar{i}_x \\ V_N &= \left(\frac{d\bar{r}_h}{dt} - \frac{d\bar{r}_t}{dt}\right)\cdot \bar{i}_z \end{aligned}\right\} \qquad (65)$$

Note that V_C, V_R, V_N are the instantaneous differences of the inertial velocity vectors in the circumferential (y), radial (x), and normal (z) directions, respectively. Hence, C, B, and A are the normalized instantaneous differences of the inertial velocity components.

If the normalized position variables of Eq (63) are substituted in Eq (62), Eqs (66) result.

$$\left.\begin{aligned} \frac{d^2\rho}{dT^2} - 3\rho - 2\frac{d\alpha}{dT} &= 0 \\ \frac{d^2\alpha}{dT^2} + 2\frac{d\rho}{dT} &= 0 \\ \frac{d^2\lambda}{dT^2} + \lambda &= 0 \end{aligned}\right\} \qquad (66)$$

Solutions of Eqs (66), in terms of initial normalized positions and rates, are

$$\left.\begin{aligned} \rho &= 2(\rho_0 + C_0) + (B_0 + \alpha_0)\sin T \\ &\quad - (\rho_0 + 2C_0)\cos T \\ \alpha &= -(\alpha_0 + 2B_0) - 3(\rho_0 + C_0)T \\ &\quad + 2(B_0 + \alpha_0)\cos T \\ &\quad + 2(\rho_0 + 2C_0)\sin T \\ \lambda &= \lambda_0\cos T + A_0\sin T. \end{aligned}\right\} \qquad (67)$$

Also by straightforward differentiation,

$$\left.\begin{aligned} \frac{d\alpha}{dT} &= C - \rho = -3(\rho_0 + C_0) - 2(B_0 + \alpha_0)\sin T \\ &\quad + 2(\rho_0 + 2C_0)\cos T \end{aligned}\right.$$

$$\left.\begin{aligned} \frac{d\rho}{dT} &= B + \alpha = (B_0 + \alpha_0)\cos T \\ &\quad + (\rho_0 + 2C_0)\sin T \\ \frac{d\lambda}{dT} &= A = A_0 \cos T - \lambda_0 \sin T. \end{aligned}\right\} \quad (68)$$

Inasmuch as Eqs (67) and (68) specify three independent position coordinates and their rates, the analytic solution of Eq (60) is complete. The value of the solution, however, is further enhanced if we utilize Gilbert's Method of Circle Diagrams, Ref. 7, to describe the motion.

(2) Gilbert's Method of Circle Diagrams. The information in Eqs (67) and (68) may be portrayed with two phase-plane plots. The out-of-plane variables, λ and A, may be plotted parametrically in a λ-A phase-plane. The remaining variables may be incorporated in a ρ versus $\alpha/2$ plot wherein the complete in-plane behavior is displayed. With such phase-plane plots, the orbital aspects of the problem will be made evident.

In order that we may assign special orbital significance to the normalized variables, the following assumptions are made:

(1) The inclination of the homing vehicle's orbit plane with respect to the target's is small.

(2) The eccentricity of the homing vehicle's orbit is small.

These assumptions are valid for a wide class of rendezvous missions and allow the following interpretation.

- A = homing vehicle's yaw or velocity azimuth angle with respect to the target's orbit
- λ = homing vehicle's cross-range angle with respect to the target's orbit plane
- α = homing vehicle's downrange angle with respect to the target
- ρ = normalized altitude of homing vehicle in excess of r_t.
- C = normalized speed of homing vehicle in excess of $V_0 = \omega_0 r_t$
- γ = $B + \alpha$ = homing vehicle's flight path angle (positive if measured upward from its local horizontal).

Out-of-plane motion. By elimination of T between λ and A, there results

$$A^2 + \lambda^2 = A_0^2 + \lambda_0^2 \quad (69)$$

But for small inclinations i_0,

$$i_0^2 = A_0^2 + \lambda_0^2 \quad (70)$$

Thus,

$$A^2 + \lambda^2 = i_0^2 \quad (71)$$

The locus of Eq (71) is a circle of radius i_0 in the λ-A plane. The argument of the locus point is T. Hence, in one complete orbit revolution on the part of the target, T changes by 2π, returning the locus point to its initial location. The following sketch shows the circle diagram of out-of-plane motion.

The time history of the homing vehicle's cross-range and azimuth angles are portrayed conveniently in the sketch. The angle of travel of the radial segment i_0 is T and is related to time by Eq (63). The value $T = T_N$ corresponds to the crossing of the positive A-axis and defines the ascending (from -z to +z) node.

Important characteristics of the out-of-plane motion are easily obtained from the circle. For example, $z_{max} = R_t \lambda_{max} = R_t i_0$ and $(dz/dt)_{max} = V_0 A_{max} = V_0 i_0$.

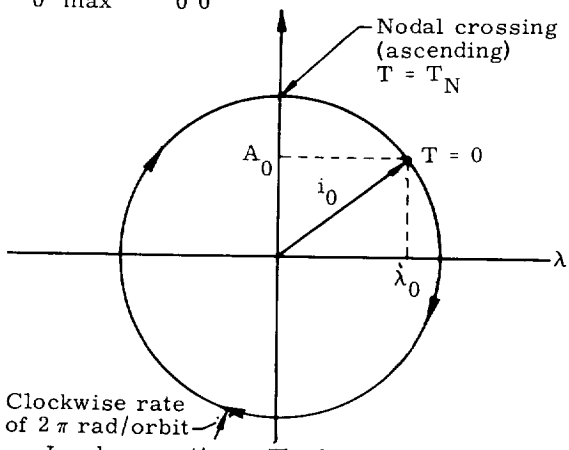

In-plane motion. The homing vehicle's in-plane orbit elements may be written directly in terms of the normalized variables in view of the interpretations allowed by the assumption of $e << 1$.

Hence,

$$\frac{\Delta E}{E_0} \equiv \frac{E - E_0}{E_0} = -2(C_0 + \rho_0) \quad (72)$$

where E = energy of homing vehicle's orbit.

$E_0 = -1/2\, v_0^2$ = energy of target's orbit.

$$e^2 = (\rho_0 + 2C_0)^2 + \gamma_0^2 \quad (73)$$

where e = eccentricity of homing vehicle's orbit.

$$T_p = -\tan^{-1} \frac{\gamma_0}{\rho_0 + 2C_0} \quad (74)$$

where T_p = normalized time to perigee from T = 0

$$\alpha_P = \alpha_0 - 2\gamma_0 - 3(\rho_0 + C_0)\, T_p \qquad (75)$$

where α_P = downrange angle of homing vehicle at perigee passage ($T = T_p$).

Equations (72) through (75) permit the solutions of Eqs (67) and (68) to be written in terms of orbit elements of the homing vehicle.

$$\alpha = \alpha_P - 3(\rho_0 + C_0)(T - T_p) + 2e \sin (T - T_p)$$

$$\rho = 2(\rho_0 + C_0) - e \cos (T - T_p)$$

$$C = -(\rho_0 + C_0) + e \cos (T - T_p)$$

$$\gamma = e \cos (T - T_p). \qquad (76)$$

Portrayal of in-plane motion is obtained by a plot of ρ versus $\alpha/2$. The parametric relation is

$$\left[\rho - 2(\rho_o + C_0)\right]^2 + \left\{\frac{\alpha}{2} - \left[\frac{\alpha_p}{2} - \frac{3}{2}(\rho_0 + C_0)(T - T_p)\right]\right\}^2 = e^2 \qquad (77)$$

or,

$$\left[\rho - 2(\rho_0 + C_0)\right]^2 + \left\{\frac{\alpha}{2} - \left[\frac{\alpha_0}{2} - \gamma_0 - \frac{3}{2}(\rho_0 + C_0)\, T\right]\right\}^2 = e^2. \qquad (78)$$

Equation (77) or its equivalent, Eq (78), represents a circle of radius e in the ρ - $\alpha/2$ plane. The center of the circle is located at $2(\rho_0 + C_0)$ and

$$\left[\frac{\alpha_0}{2} - \gamma_0 - \frac{3}{2}(\rho_0 + C_0)\, T\right]$$

in the ρ and $\alpha/2$ directions, respectively. As the target moves in its orbit an angle T, the point on the circle representing the moving vehicle's relative coordinates travels an angle T counterclockwise. Simultaneously, the center of the circle drifts in the positive $\alpha/2$-direction at the rate of $-3/2(\rho_0 + C_0)$ radians per unit T. The idea of a point traversing a circle of radius e, which drifts at a uniform rate along the $\alpha/2$-direction, is the process by which the ρ - $\alpha/2$ trajectory is most easily visualized. This circle diagram generatrix is shown in Fig. 9.

The locus of relative motion in the ρ - $\alpha/2$ plane is, in general, a trochoid. For $3\left|\rho_0 + C_0\right| < 2e$, the generated curve has loops. For $3\left|\rho_0 + C_0\right| = 2e$, the curve reduces to a cycloid and has cusps. For $3\left|\rho_0 + C_0\right| > 2e$, the curve has neither loops nor cusps and tends toward a straight line for $3\left|\rho_0 + C_0\right| >> 2e$.

The values of the in-plane relative coordinates ρ, C, γ, and α are readily obtained by circle diagram sketches using the generatrix of Fig. 9. The value of α is slightly more difficult to obtain since the simultaneous motions of translation and rotation must be considered. On the other hand, the values of ρ, C, and γ are obtained by simply considering motion along the circle. The value of ρ at any time is equal to the ρ-coordinate of the locus point, and C is equal to $(\rho_0 + C_0) - \rho$. The value of γ is merely equal to horizontal displacement of the locus point from the vertical line joining apogee and perigee (line of apsides). Inasmuch as the argument of the locus point along the circle is T (the angular travel of the target), the values of ρ, C, and γ may be readily calculated.

(3) Sample analysis using circle diagrams. The convenience afforded by Gilbert's circle diagrams in establishing functional relations between various parameters and in generating trajectory requirements overshadows the desirability of graphical plots for the relative motion. In this section the application of Gilbert's method of circle diagrams as an analytical tool is illustrated. For purposes of illustration, the initial conditions will be

(1) Target in circular orbit with radius, r_t

(2) Homing vehicle injected ahead of target with

$$\left.\begin{aligned} x_0 &= 0 \\ y_0 &= s_0 > 0 \\ z_0 &= 0 \\ V_N &= 0 \\ V_C &= -W_0;\ W_0 > 0 \\ V_R &= -u_0;\ u_0 > 0 \end{aligned}\right\} \qquad (79)$$

The situation is shown in the following sketch.

Out-of-plane analysis. Since

$$z_0 = 0$$

$$V_N = \left(\frac{dz}{dt}\right)_0 = 0.$$

Equations (63) and (64) yield

$$\lambda_0 = A_0 = 0. \qquad (80)$$

Accordingly, Eqs (70) and (71) yield

$$i_0 = A(T > 0) = \lambda(T > 0) = 0. \qquad (81)$$

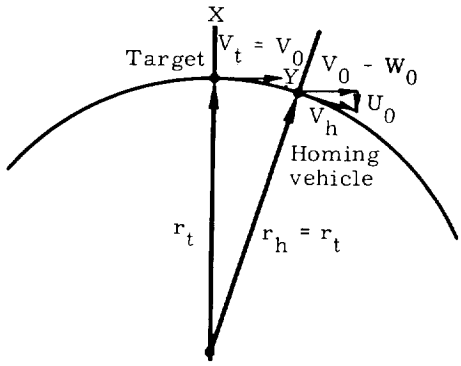

The out-of-plane circle diagram thus degenerates to a point at the origin of the λ-A phase plane, indicating coplanar motion.

In-plane analysis. From Eqs (63) and (64)

$$\left.\begin{aligned} \rho_0 &= 0 \\ \alpha_0 &= \frac{s_0}{r_t} \\ C_0 &= \frac{-W_0}{V_0} \\ \gamma_0 &= B_0 + \alpha_0 = \frac{s_0}{r_t} - \frac{u_0}{V_0} . \end{aligned}\right\} \quad (82)$$

Equations (73), (74) and (75) then yield

$$e^2 = \left(\frac{2W_0}{V_0}\right)^2 + \left(\frac{s_0}{r_t} - \frac{u_0}{V_0}\right)^2 \quad (83)$$

$$T_P = \pi + \tan^{-1}\left(\frac{s_0 V_0}{2W_0 r_t} - \frac{u_0}{2W_0}\right) \quad (84)$$

$$\alpha_p = \left(2\frac{u_0}{V_0} - \frac{s_0}{r_t}\right) - \frac{3W_0}{V_0} T_p . \quad (85)$$

The in-plane circle diagram is shown in Fig. 10 assuming

$$\frac{s_0}{2r_t} < \frac{u_0}{V_0} < \frac{s_0}{r_t} .$$

It is of interest to consider the following special cases

(1) $\gamma_0 = 0$ (homing vehicle's flight path angle is zero)

(2) $W_0 = 0$ (no speed deficit)

(3) Combination of s_0, W_0, γ_0 which causes locus point to pass through origin (coincidence of vehicles).

The circle diagram for $\gamma_0 = 0$ is shown in the following sketch. As can be seen, there exists the possibility of a being always positive, i.e., nonclosure, in spite of the speed deficit, W_0. The limiting condition for downrange angle closure ($\alpha = 0$) is obtained by locating the locus point having minimum $\frac{\alpha}{2}$ and requiring it to be zero. This point occurs when the circle's drift rate cancels out the "speed" of the tip of the radius vector in the negative $\alpha/2$-direction. Since the radius vector rotates at angular rate of 1 rad/unit τ and the radius is $e = 2W_0/V_0$, the speed of the tip of the radius vector is $2W_0/V_0$. Thus, its rate in the negative $\alpha/2$-direction is $2W_0/V_0$ cos T. Equating the rotational and translation rates in the $\alpha/2$-direction,

$$\frac{2W_0}{V_0} \cos T_{min} = \frac{3}{2} \frac{W_0}{V_0}$$

or

$$T_{min} = \cos^{-1} \frac{3}{4} . \quad (86)$$

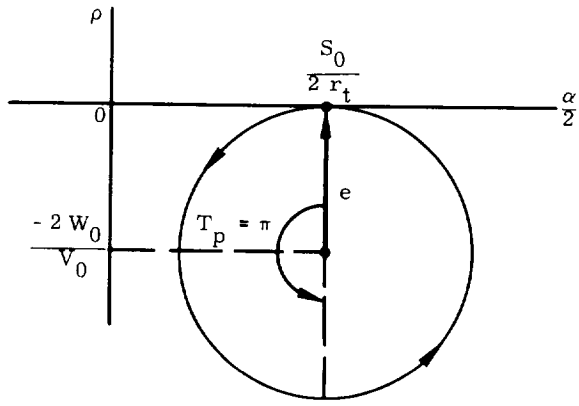

NOTE:
Center drifts to the right $\frac{3}{2}\frac{W_0}{V_0}$ units per unit T

The value of $\left(\frac{\alpha}{2}\right)$ at that point is

$$\left(\frac{\alpha}{2}\right)_{min} = \frac{s_0}{2r_t} - \frac{2W_0}{V_0} \sin T_{min} + \frac{3}{2}\frac{W_0}{V_0} T_{min}$$

$$= \frac{s_0}{2r_t} - 0.24 \frac{W_0}{V_0} . \quad (87)$$

For the limiting case of downrange closure ($\alpha_{min} = 0$).

$$\left(\frac{W_0}{V_0}\right)_{min} = 2.26\ \frac{s_0}{r_t} \quad . \tag{88}$$

That is, if closure is to be obtained, the speed deficit W_0 must be greater than the minimum value specified in Eq (88). The limiting locus is shown in the following sketch along with the locus expected on the basis of rectilinear considerations.

The sketch shows that a rectilinear analysis for the specific injection conditions of $\gamma_0 = 0$ and $W_0 = W_{min}$ is far too optimistic. As indicated, the actual crossover time is given by $T_{min} = \omega_0 t_{min} = 0.724$ compared to $T_G = \omega_0 t_G = 0.442$, where $t_G = s_0/W_0$ is the rectilinear time-to-go. For the limiting case, the time expansion is

$$\frac{t_{min}}{t_G} = \frac{T_{min}}{T_G} = 1.64. \tag{89}$$

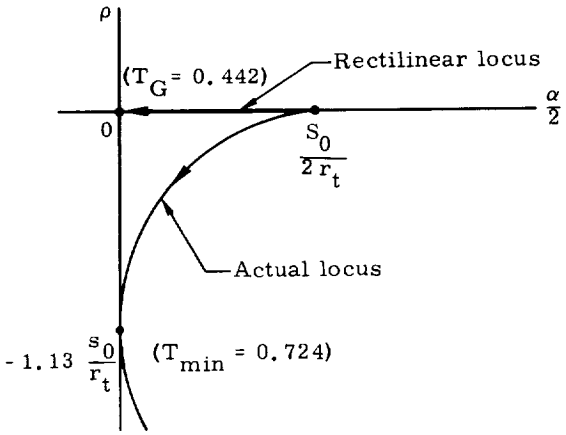

If $W_0 < (W_0)_{min}$ the expansion would be infinite since downrange closure cannot occur. Note also that the orbital nature of the problem causes the homing vehicle to be low in altitude by $1.13\ s_0$ at closure, while rectilinear analysis predicts no altitude deviation. This effect is due to the fact that the speed deficit causes the homing vehicle's injection point to be apogee. The homing vehicle's altitude thus decreases as it progresses toward perigee. This same effect accounts for the expansion in the time of downrange closure, since the homing vehicle's speed increases as it progresses toward perigee.

For the special case of $(W_0 = 0)$ the general circle diagram of Fig. 10 reduces to that of the following sketch.

It is evident that by proper choice of the flight path angle, γ_0, complete coincidence of the vehicles can be obtained. By inspection, the circle will pass through the origin at $T = \pi$ for

$$\gamma_0 = \frac{s_0}{4r_t} \quad . \tag{90}$$

Thus, coincidence occurs after the target moves through $T = \pi$ radians or 180 degrees, if the homing vehicle is lofted an angle

$$\frac{s_0}{4r_t} = \frac{\alpha_0}{4} \quad .$$

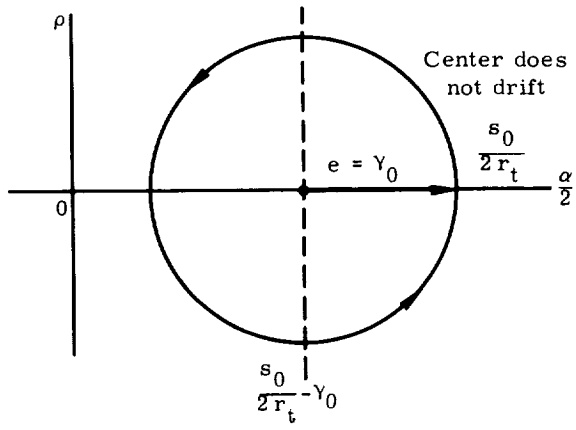

Rendezvous of the vehicles for the more general case of s_0, W_0, $\gamma_0 \neq 0$ may be obtained by considering the general circle diagram of Fig. 10. The first crossing of the $\alpha/2$-axis ($\rho = 0$) for $T > 0$ is at

$$T_1 = 2T_A \tag{91}$$

where

$$T_A = \text{normalized time to apogee} = T_P - \pi$$

$$= \tan^{-1}\ \frac{\gamma_0 V_0}{2W_0} \quad . \tag{92}$$

For complete coincidence we require

$$\alpha\,(T_1) = 0. \tag{93}$$

Hence, the drift of the circle must be such that at $T = T_1$, $\frac{\alpha}{2} = 0$. In Fig. 10, symmetry shows that the $\alpha/2$-component of the radius vector at $T = T_1$ is $-\gamma_0$. Considering the fact that the circle's center was initially at $(s_0/2r_t) - \gamma_0$ and drifted $(3/2)\,(W_0/V_0)\,T_1$ units in the plus $\alpha/2$-direction during the travel from $T = 0$ to $T = T_1$, the value of $\alpha\,(T_1)/2$ is

$$\frac{\alpha(T_1)}{2} = \left(\frac{s_0}{2r_t} - \gamma_0\right) + \frac{3}{2}\,\frac{W_0}{V_0}\,T_1 - \gamma_0 \,. \tag{94}$$

Substituting Eqs (91) and (92) into (94) and invoking the requirement of (93), the following parametric relation is obtained.

$$\frac{s_0}{2r_t} = 2\gamma_0 - 3\,\frac{W_0}{V_0}\tan^{-1}\frac{\gamma_0}{2W_0/V_0} \,. \tag{95}$$

This relation is analogous to the "Hit Equation" of ballistic missile theory (Ref. 8). Figure 11 shows a plot of γ_0 and s_0/r_t for various values of W_0/V_0. The required rendezvous time, t_R, is given by

$$T_R = \omega_0 t_R = T_1 = 2\tan^{-1}\frac{\gamma_0}{2W_0/V_0} \,. \tag{96}$$

Thus, in terms of the target's orbital period, τ_0,

$$\left(\frac{t_R}{\tau_0}\right) = \frac{1}{\pi}\tan^{-1}\frac{\gamma_0}{2W_0/V_0} \,. \tag{97}$$

On the basis of rectilinear analysis, the initial time-to-go is,

$$t_G \equiv \frac{s_0}{W_0} \,. \tag{98}$$

Hence

$$\left(\frac{t_G}{\tau_0}\right) = \frac{1}{2\pi}\,\frac{(s_0/r_t)}{(W_0/V_0)} \,. \tag{99}$$

The ratio of the actual rendezvous time to the initial time-to-go based on rectilinear analysis is thus

$$\frac{t_R}{t_G} = \left(\frac{2W_0/V_0}{s_0/r_t}\right)\tan^{-1}\frac{\gamma_0}{(2W_0/V_0)} \,. \tag{100}$$

The ratio is plotted in Fig. 12 as a function of W_0/V_0 and $\alpha_0 = (s_0/r_t)$. The dependence on α_0 was introduced by utilizing Fig. 11 in a crossplot so that γ_0 could be expressed in terms of α_0 and W_0/V_0.

Note that in this example time compression occurs since $t_R/t_G \leq 1$. This is explained by the fact that for $W_0 > 0$ and $\gamma_0 > 0$, the homing vehicle is on its way toward apogee at the start of the problem. This is obvious in Fig. 10. Thus, the homing vehicle's speed over the lofted flight is less than its initial speed, causing more rapid closure than expected on the basis of rectilinear analysis.

Figure 12 may be used to compute the required rendezvous time. First compute $t_G \equiv s_0/W_0$; then locate the appropriate W_0/V_0 curve, interpolating if need be. The value of t_R/t_G then gives the attenuation factor for a particular $\alpha_0 = s_0/r_t$.

(4) Circle diagram extension to eccentric orbits. In the following paragraphs the basis upon which Gilbert's Method of Circle Diagrams can be extended to targets in eccentric orbits is presented. The eccentricity, however, must be small in order to retain a linear or first-order analysis. Only the in-plane motion is treated since out-of-plane motion is unaffected by target orbit eccentricities.

Circle Diagram of Target Motion. Previously the motion of the homing vehicle relative to a target moving in a circular orbit was analyzed. In this section all motion is referred to the target's mean motion. For small eccentricities the target's mean motion is circular with a radius equal to the semimajor axis. Thus, to obtain a circle diagram of eccentric target motion, it is merely necessary to replace the homing vehicle by the target vehicle and the target vehicle by the mean target in the previous results. The Circle Diagram of Target Motion referred to the mean target is shown in the following sketch. All the features of the in-plane circle diagram which were mentioned in previous sections still hold except that motion is strictly periodic. The center of the circle generatrix does not shift in time.

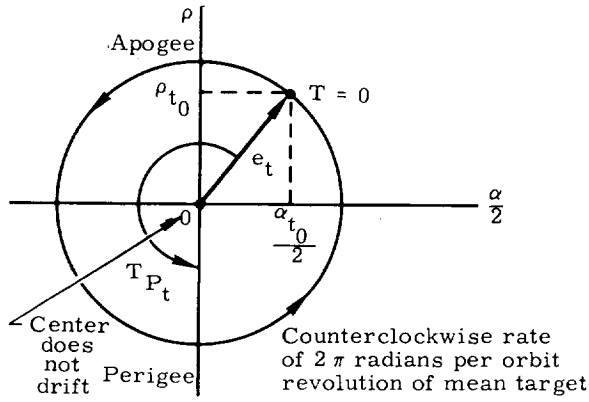

Composite Circle Diagram of Relative Motion. If the homing vehicle's circle diagram, referred to the mean target, is superimposed upon the target's, the composite circle diagram of the following sketch is obtained. Note that the circle diagram differs from that of Fig. 9 merely by the fact that the target locus is a circle of radius e_t (target orbit eccentricity) rather than the origin of the $\rho - \alpha/2$ plane. As e_t approaches zero the locus shrinks to a point at the origin, yielding the circle diagram of Fig. 9.

The relative motion is obtained by plotting both the target and homing vehicle loci and noting the differences in relative coordinates as a function of T (time).

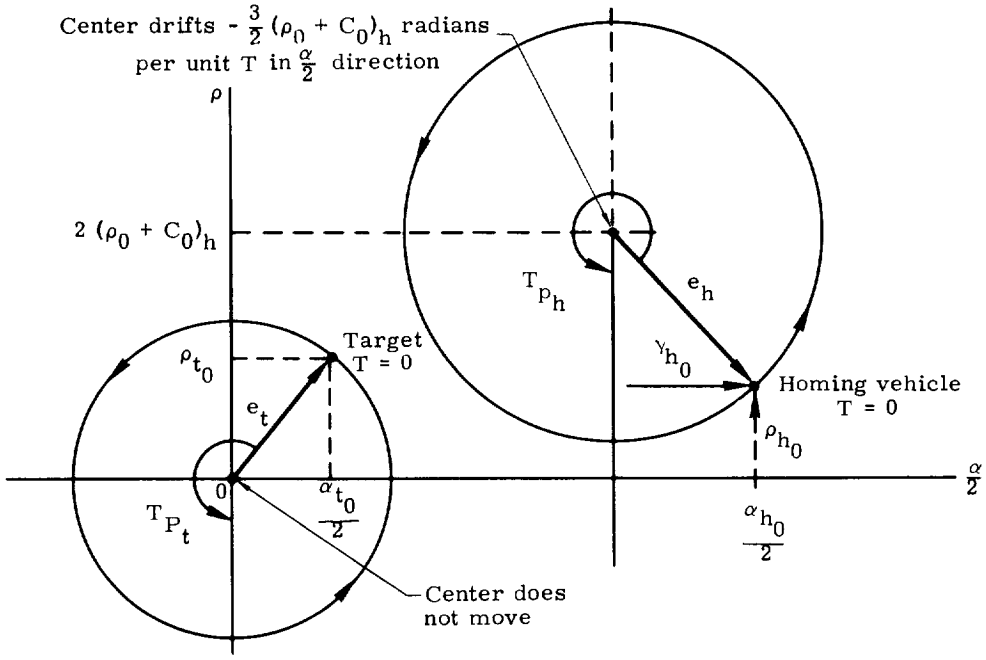

(5) Motion in presence of impulsive thrusts. In the presence of impulsive thrusts, there exists segments of thrust free motion which are separated by discrete changes in velocity. Hence complete motion is obtained by regarding it as a succession of thrust free segments under various initial conditions. Inasmuch as the position coordinates cannot change instantaneously, the final position coordinates before the impulse become the initial position coordinates after the impulse. The complete motion is readily obtained by sketches of circle diagrams. Each impulse changes the size and location of the circle generatrix. The effects of velocity increments in the normal, radial, and circumferential directions are demonstrated below.

Normal velocity increment. For small inclinations between the orbit planes of the target and homing vehicle, a velocity increment, ΔV_N, normal to the target's orbit plane produces an increment ΔA in the homing vehicle's velocity azimuth relative to the target's orbit plane. The relation is linear for small inclinations and velocity increments.

$$\Delta A = \frac{\Delta V_N}{V_0} \qquad (101)$$

The relative out-of-plane motion is illustrated in the following sketch. This sketch shows the situations just prior to the impulse ($T = 0^-$) and just after the impulse ($T = 0^+$). Since position cannot change instantaneously, the crossrange angle, λ, remains unchanged. However, the azimuth angle changes by the amount given in Eq (101). The result is a change in inclination angle. Out-of-plane motion is thus typified by motion along the circle of radius, i_0, until the impulse is applied. After the impulse, the locus point moves along the circle of radius, i_1.

From this sketch it is apparent that inclination may be completely removed by applying a normal impulse at $\Delta A = \mp i_0$ and $\lambda = 0$. The velocity increment required would be

$$\Delta V_N = \mp V_0 i_0 \qquad (102)$$

This corresponds to a velocity increment at the nodal crossings equal and opposite to the existing normal velocity.

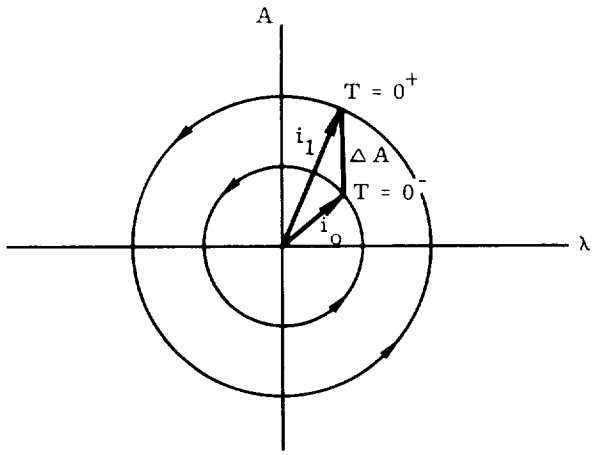

Radial velocity increment. A change in the homing vehicle's velocity vector by an increment, ΔV_R, parallel to the target vehicle's local vertical yields a change in the homing vehicle's flight path angle, B, measured with respect to the target's local horizontal.

$$\Delta B = \frac{\Delta V_R}{V_0} \tag{103}$$

Inasmuch as the homing vehicle's flight path angle measured with respect to its own local horizontal is given by

$$\gamma = B + \alpha$$

then, since α does not change instantaneously,

$$\Delta\gamma = \Delta B = \frac{\Delta V_R}{V_0} \tag{104}$$

The effect of a change in γ is shown in the following sketch. As shown in this sketch, a positive change in the flight path angle causes an increase in the horizontal displacement between the locus point and the center of the generatrix. Inasmuch as the position coordinates cannot change instantaneously, the center must move to the left by the amount, $\Delta\gamma$. This causes the radius to increase, indicating an increase in eccentricity. The center does not shift along the ρ-axis, since the location of the center in such a direction represents the orbit's energy level which is invariant for flight path angle changes.

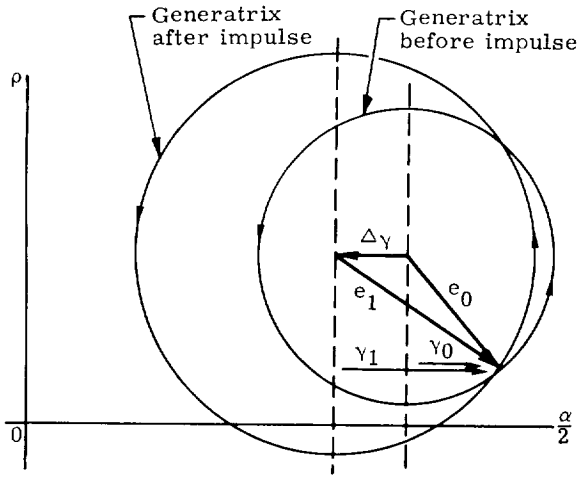

The complete relative motion is thus given by the locus of points generated by the circle of radius e_0 before the impulse and that generated by the circle of radius e_1 after the impulse. Since the energy level is unchanged by the radial impulse, both circles drift in the negative $\alpha/2$-direction at the same rate. It should be noted that if it is desired that the homing vehicle's orbit be circular using a single radial impulse, one should wait until

$$\gamma_0 = \pm e_0$$

and produce

$$\Delta\gamma = \mp e_0$$

by applying

$$\Delta V_R = \mp V_0 e_0 \tag{105}$$

These points correspond to points 90° away from the apsides where the flight path angle possesses extreme values.

Circumferential velocity or speed increments. A change in the homing vehicle's circumferential velocity, ΔV_C, is synonymous with a change in its orbital speed and, hence, a change in orbital energy or period. In terms of the normalized rate, C,

$$\Delta C = \frac{\Delta V_C}{V_0} \tag{106}$$

The effect on the relative motion is indicated in the following sketch. Since the position of the generatrix's center represents the homing vehicle's orbit energy, an increase in the homing vehicle's speed, ΔV_C, causes a vertical shift of the circle's center by the amount $2\Delta C = 2(\Delta V_C/V_0)$. This has two effects. First, the orbit eccentricity changes in general; secondly, the center drifts at a different rate in the $\alpha/2$-direction. As shown in the sketch, the energy level before the impulse is characterized by the ρ-position of the circle's center, $2(\rho_0 + C_0)$. This energy causes the circle to drift in the negative $\alpha/2$-direction at a rate of $3/2\ (\rho_0 + C_0)$. The increase in energy yields a new energy level, $2(\rho_0 + C_0) + 2\Delta C$, and causes the new circle to drift in the negative $\alpha/2$-direction at a rate of $3/2\ (\rho_0 + C_0) + 3/2\ \Delta C$. Thus, for a positive ΔC the new circle moves at a faster rate in the negative $\alpha/2$-direction.

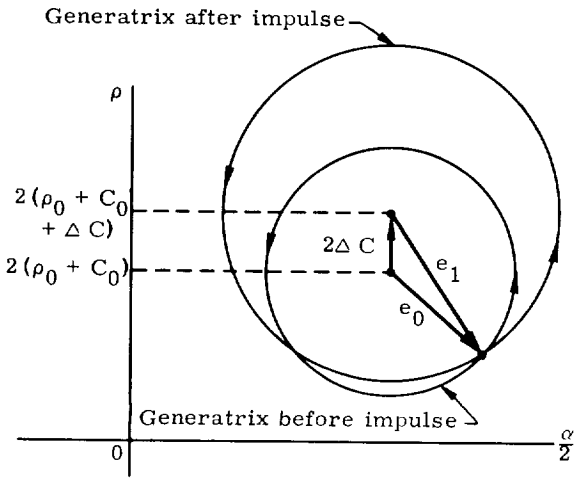

Note that, if desired, orbit eccentricity can be made zero by waiting until the locus point is either at the highest or lowest point of the circle of radius, e_0. If the locus point is at

$$\rho_{max} = 2(\rho_0 + C_0) + e_0$$

the resulting eccentricity, e_1, can be made zero by making $2\Delta C = e_0$ or

$$\Delta V_C = \frac{V_0 e_0}{2} \tag{107}$$

If the locus point is at ρ_{min}, e_1 can be made zero by $2\Delta C = -e_0$ or

$$\Delta V_C = -\frac{V_0 e_0}{2} \tag{108}$$

Comparison of either of these velocity increments with Eq (105) shows that for control of eccentricity circumferential increments can be twice as efficient as radial increments. Note, however, that circumferential increments also produce changes in the orbital energy or period, while radial increments affect only eccentricity.

(6) Sample problem. Assume the vehicles are in circular orbits of equal radii which are inclined at an angle i_0. Assume the phasing to be such that the homing vehicle crosses the target's orbit plane an angle α_0 ahead of the target. This is shown in Fig. 13.

Suppose it is desired that rendezvous be accomplished with only two thrust applications of an impulsive nature. One method by which this may be accomplished is to wait until the situation of Fig. 13 occurs and apply a velocity increment which rotates the homing vehicle's velocity vector into the target's plane while simultaneously changing the flight path angle so that a lofted flight is obtained. The loft should be chosen so that the two vehicles coincide when the homing vehicle returns to its original altitude. The trajectory is shown in Fig. 14. At coincidence, the second impulse is applied to restore the flight path angle to zero and, hence, restore circularity. Since no period changes are involved, the two vehicles will subsequently move in identical orbits and, hence, be in coincidence thereafter.

Another method also converts the situation depicted by this sketch into a coplanar situation but involves changing the flight path angle and period with the first impulse and restoring to the original values with the second impulse upon coincidence. The trajectory is shown in Fig. 15. It is similar to the method of Fig. 14 except that the required rendezvous time is reduced through the use of speed (period) changes as well. Recall that this situation was partially analyzed previously.

Both methods are analyzed below with respect to velocity and time requirements.

Method A: yaw and loft. To convert the situation of Fig. 13 into a coplanar situation a normal velocity component is required. According to Eq (102) we require

$$\Delta V_N = V_0 i_0 \tag{109}$$

Initially, the $\rho - \alpha/2$ phase diagram is as shown in the following sketch. To cause coincidence with a pure radial increment (flight path angle change) requires a flight path angle change of

$$\Delta\gamma_1 = \gamma_0 = \frac{\alpha_0}{4} \tag{110}$$

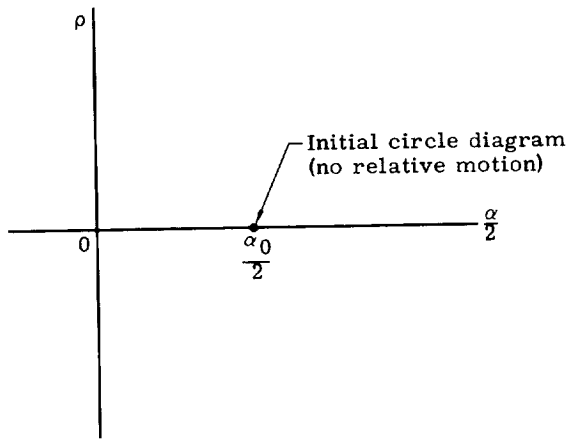

The resulting relative motion is shown in the following sketch. Note that rendezvous occurs at $T = \pi$ or one-half period later. At this time the second impulse must be directed radially outward to remove the existing flight path angle (reduce the ensuing circle diagram to a point at the origin). The second impulse must produce

$$\Delta\gamma_2 = \gamma_0 = \frac{\alpha_0}{4} \tag{111}$$

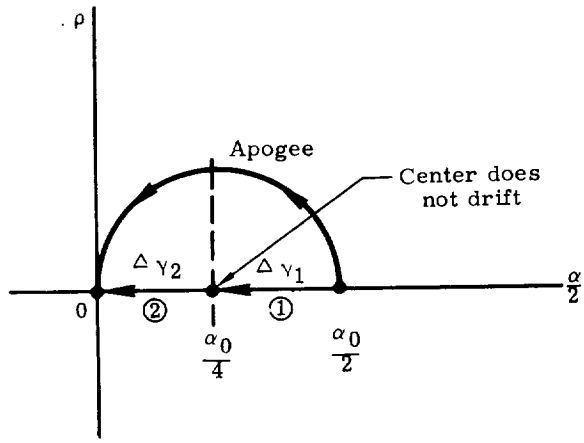

Thus, the actual radial components are

$$(\Delta V_R)_1 = V_0 \Delta\gamma_1 = V_0 \frac{\alpha_0}{4}$$

$$(\Delta V_R)_2 = V_0 \Delta\gamma_2 = V_0 \frac{\alpha_0}{4} \tag{112}$$

Assuming an orientated thrust vector, the radial and normal velocity components of the first impulse require

$$\Delta V_1 = V_0 \sqrt{i^2_0 + \left(\frac{\alpha_0}{4}\right)^2} \tag{113}$$

The second impulse requires

$$\Delta V_2 = (\Delta V_R)_2 = V_0 \frac{\alpha_0}{4} \tag{114}$$

Thus,

$$(\Delta V)_{orien} = \Delta V_1 + \Delta V_2$$

$$= V_0 \left[\frac{\alpha_0}{4} + \sqrt{i^2_0 + \left(\frac{\alpha_0}{4}\right)^2} \right] \tag{115}$$

If separate nozzles are used for increments in the various directions,

$$\Delta V_1 = V_0 \left(i_0 + \frac{\alpha_0}{4} \right) \tag{116}$$

$$\Delta V_2 = V_0 \frac{\alpha_0}{4}$$

Hence,

$$(\Delta V)_{sep} = \Delta V_1 + \Delta V_2 = V_0 \left(i_0 + \frac{\alpha_0}{2} \right) \tag{117}$$

in either case the total rendezvous time, as indicated in Fig. 14 and the preceding sketch ($T = \pi$), is

$$t_R = \frac{\tau_0}{2} \tag{118}$$

where again

τ_0 = target's orbital period.

Method B: yaw, loft and period changes. In either method the yaw velocity required is the same,

$$\Delta V_N = \gamma_0 i_0 \tag{119}$$

The radial and circumferential velocity increments depend on the desired time of rendezvous. Let us suppose that a rendezvous time of $\tau_0/4$ is desired. That is, rendezvous after the target moves through 90° rather than 180° as in Method A. Equation (97) shows that

$$\left(\frac{t_R}{\tau_0}\right) = \frac{1}{\pi} \tan^{-1} \frac{V_p}{2W_0} \tag{120}$$

where $V_p = \gamma_0 V_0$

W_0 = speed (circumferential velocity) reduction.

Thus, for $t_R = \tau_0/4$

$$\frac{V_p}{W_0} = 2 \tan \frac{\pi}{4} = 2 \tag{121}$$

The ratio of the radial velocity increment to the circumferential increment must, hence, be equal to 2 for rendezvous after the target moves through 90°.

Equation (95) shows that for this ratio

$$\frac{\alpha_0}{2} \equiv \frac{W_0}{V_0} \left(4 - \frac{3\pi}{4}\right) \tag{122}$$

is the condition for rendezvous. Thus,

$$W_0 = \frac{V_0 \alpha_0}{8 - \frac{3\pi}{2}} = -\Delta V_{C_1} \tag{123}$$

and

$$V_p = \frac{V_0 \alpha_0}{4 - \frac{3\pi}{4}} = \Delta V_{R_1} \tag{124}$$

Equations (119), (123) and (124) are thus the yaw, speed reduction, and pitch components of the velocity increment applied at point ① in Fig. 15.

The pitch and speed components at point ② (Fig. 15) by symmetry are

$$W_0 = \frac{V_0 \alpha_0}{8 - \frac{3\pi}{2}} = \Delta V_{C_2} \tag{125}$$

$$V_p = \frac{V_0 \alpha_0}{4 - \frac{3\pi}{4}} = \Delta V_{R_2} \tag{126}$$

This may also be obtained from the circle diagram of the following which shows the flight path angle and energy changes required to reduce the circle generatrix to a point when the locus point is at the origin.

As shown in the following sketch, the generatrix is reduced to a point at the origin by shifting the center to the left by $\Delta_{\gamma_2} = \gamma_0$ and upward by $2\Delta C_2 = 2(W_0/V_0)$. These correspond to the velocity components of Eqs (125) and (126).

For an oriented engine nozzle, velocity requirements are as follows.

$$(\Delta V)_1 = \left[(\Delta V_N)^2 + \left(\Delta V_{C_1}\right)^2 + \left(\Delta V_{R_1}\right)^2 \right]^{1/2}$$

$$= V_0 \left[i^2_0 + 5 \left(\frac{\alpha_0}{8 - \frac{3\pi}{2}} \right)^2 \right]^{1/2} \tag{127}$$

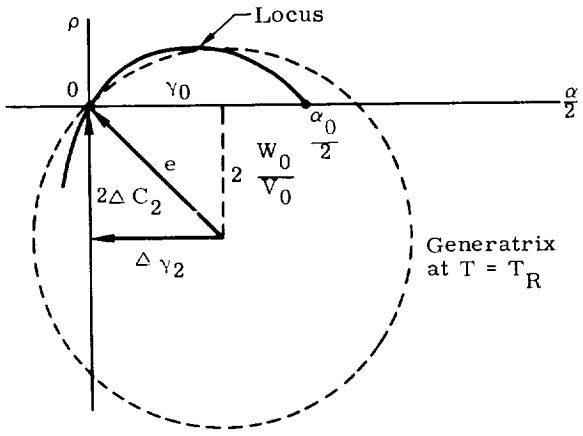

and

$$(\Delta V)_2 = \sqrt{5}\, V_0 \left(\frac{\alpha_0}{8 - \frac{3\pi}{2}} \right) \tag{128}$$

Thus,

$$(\Delta V)_{orien} = (\Delta V)_1 + (\Delta V)_2$$

$$= V_0 \left[i^2_0 + 5 \left(\frac{\alpha_0}{8 - \frac{3\pi}{2}} \right)^2 \right]^{1/2}$$

$$+ \sqrt{5}\, V_0 \left(\frac{\alpha_0}{8 - \frac{3\pi}{2}} \right) \tag{129}$$

For separate nozzles the absolute values of the components are added directly, yielding

$$(\Delta V)_{sep} = V_0 \left[i_0 + 6 \left(\frac{\alpha_0}{8 - \frac{3\pi}{2}} \right) \right] \tag{130}$$

By comparing Eqs (129) and (130) with (115) and (116) the reduction of rendezvous time from $\tau_0/2$ to $\tau_0/4$ can be seen to involve a considerable increase in velocity requirements. Assuming $i_0 = 0$

$$\frac{(\Delta V)_{\tau_0/4}}{(\Delta V)_{\tau_0/2}} = \begin{cases} \dfrac{4\sqrt{5}}{8 - \frac{3\pi}{2}} = 2.72 & \text{for oriented nozzle} \\ \dfrac{12}{8 - \frac{3\pi}{2}} = 3.64 & \text{for separate nozzles.} \end{cases}$$

2. Terminal Guidance Schemes (Ref. 10)

In the previous section the general linear differential equation of relative motion was derived as

$$\frac{d^2\bar{s}}{dt^2} = \bar{a}_h - \bar{a}_t - \frac{GM}{r_t^2} \left[\frac{\bar{s}}{r_t} - 3\bar{r}_t \frac{(\bar{s} \cdot \bar{r}_t)}{r_t^3} \right] \tag{131}$$

where

$\bar{s} \equiv \bar{r}_h - \bar{r}_t$ = relative position of homing vehicle with respect to target.

Equation (131) was derived in terms of motion relative to the target. In this section it is assumed that the homing phase is conducted by the homing vehicle utilizing an onboard guidance system and that the target does not execute thrust maneuvers of either an evasive or cooperative nature.

It is convenient to re-express the differential equation of relative motion so that the target's motion relative to the homing vehicle is obtained. This is readily obtained from Eq (131) by replacing $\bar{s}$ by $-\bar{R}$ where

$\bar{R} \equiv \bar{r}_t - \bar{r}_h$ = range vector of target with respect to homing vehicle (132)

Thus, since the thrust acceleration of the target is zero

$$\bar{a}_t = 0 \tag{133}$$

and the differential equation of motion relative to the homing vehicle is

$$\frac{d^2\bar{R}}{dt^2} = -\bar{a}_h - \frac{GM}{r_t^2} \left[\frac{\bar{R}}{r_t} - 3\bar{r}_t \frac{(\bar{R} \cdot \bar{r}_t)}{r_t^3} \right] \tag{134}$$

The effect of the gravity vector differential is obtained by inspection of Eq (134), that is, the apparent target acceleration is of magnitude

(1) $\dfrac{GM}{r_t^2} \left(\dfrac{R}{r_t} \right)$ directed inward along the line-of-sight.

(2) $\dfrac{GM}{r_t^2} \left(3 \dfrac{\bar{R} \cdot \bar{r}_t}{r_t^3} \right)$, directed upward along the target's local vertical.

Both effects decrease linearly with range. Note that they are not necessarily orthogonal unless the line of sight is normal to the local vertical. For such a situation, however, the vertical acceleration vanishes since it is proportional to $\bar{R} \cdot \bar{r}_t$.

A convenient description of the apparent target acceleration is obtained by resolving it into

components parallel and transverse to the line of sight. This is shown in the following sketch.

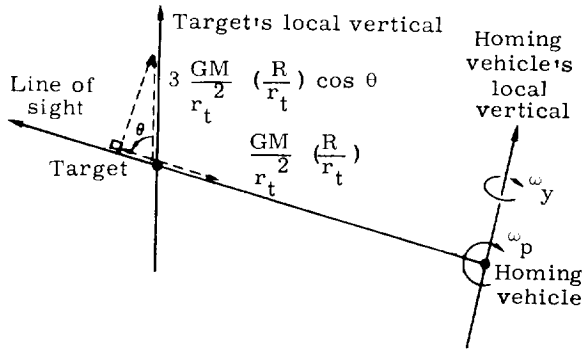

As may be seen in the sketch several new variables have been introduced. These are

θ = angle between target vertical and line-of-sight

ω_p = pitch (angular) rate of the line of sight

ω_y = yaw (angular) rate of the line of sight.

The apparent acceleration outward along the line of sight is

$$\Delta g_R = -\frac{GM}{r_t^2}\left(\frac{R}{r_t}\right)(1 - 3\cos^2\theta) \qquad (135)$$

The apparent acceleration normal to the line of sight tending to increase the pitch rate of the line of sight is

$$\Delta g_p = \frac{GM}{r_t^2}\left(\frac{R}{r_t}\right) \cdot 3\sin\theta\cos\theta \qquad (136)$$

Note that the apparent gravity effects act solely in the plane of the line of sight containing both the target and homing vehicle local verticals. Thus,

$$\Delta g_y = 0 \qquad (137)$$

a. Formulation with respect to line of sight

Since

$$\bar{R} = \bar{i}_R R \qquad (138)$$

where $\bar{i}_R \equiv$ unit vector along line of sight

$$\frac{d\bar{R}}{dt} = \bar{i}_R \frac{dR}{dt} + (\bar{\omega} \times \bar{R}) \qquad (139)$$

where $\bar{\omega} \equiv$ angular rate of line of sight in inertial space

and

$$\frac{d^2\bar{R}}{dt^2} = \bar{i}_R\left[\frac{d^2R}{dt^2} - R\omega^2\right] + \left[2\bar{\omega}\frac{dR}{dt} + \frac{d\bar{\omega}}{dt}R\right] x \bar{i}_R \qquad (140)$$

Equation (134) may be resolved into components along (parallel) and transverse to the line of sight.

The equation of motion along the line of sight is

$$\frac{d^2R}{dt^2} - R\omega^2 = -a_R + \Delta g_R \qquad (141)$$

where the subscript "R" denotes components along the line of sight and the superfluous subscript "h" on the thrust acceleration has been dropped.

The equation of motion transverse (normal) to the line-of-sight is

$$\frac{dh_{\omega_p}}{dt} = R(\Delta g_p - a_p) \qquad (142)$$

$$\frac{dh_{\omega_y}}{dt} = -Ra_y \qquad (143)$$

where

$h_{\omega_p} \equiv R^2\omega_p$ = angular momentum in pitch: (144)

$h_{\omega_y} \equiv R^2\omega_y$ = angular momentum in yaw: (145)

Note that in the absence of transverse thrusts $R^2\omega_y$ is conserved, while $R^2\omega_p$ is not generally conserved due to the torque, $R\Delta g_p$, exerted by the gravity differential.

b. Transverse corrections

The general transverse command logic takes the form

$$\Delta V_T^* = k_1\omega + k_2 V_T + k_3 \qquad (146)$$

where

ΔV_T^* = desired transverse velocity increment

k_1, k_2 = constants of proportionality

V_T = velocity of homing vehicle transverse (normal) to line of sight

k_3 = bias term.

Equation (146) may also be considered a vector statement wherein ΔV_T^*, ω, V_T and k_3 are two-element column vectors whose components are those of yaw and pitch. That is,

$$\Delta V_T^* = \begin{pmatrix} \Delta V_p^* \\ \Delta V_y^* \end{pmatrix} \qquad (147)$$

$$\omega = \begin{pmatrix} \omega_p \\ \omega_y \end{pmatrix} \tag{148}$$

$$V_T = \begin{pmatrix} V_p \\ V_y \end{pmatrix} \tag{149}$$

$$k_3 = \begin{pmatrix} k_{3p} \\ k_{3y} \end{pmatrix} \tag{150}$$

The "constants of proportionality" are then 2 x 2 matrices

$$k_1 = \begin{bmatrix} K^p_{1p} & K^y_{1p} \\ K^p_{1y} & K^y_{1y} \end{bmatrix} \tag{151}$$

$$k_2 = \begin{bmatrix} K^p_{2p} & K^y_{2p} \\ K^p_{2y} & K^y_{2y} \end{bmatrix} \tag{152}$$

where the subscripts indicate those elements belonging to the pitch or yaw velocity command, and the superscripts indicate the elements which scale the pitch and yaw components of ω and V_T. Except in cases where the homing vehicle is called upon to execute roll maneuvers, there will generally be no interchannel crossfeed terms in the command logic. Hence, in most situations the elements outside the principal diagonal are zero.

If k_2 and k_3 are zero while k_1 is equal to the instantaneous range to the target, a collision course results. A lead-collision or biased-collision course may be generated by defining k_3 appropriately so that the homing vehicle in effect steers on a collision course to a point offset from the actual target. If k_2 and k_3 are zero while k_1 is a constant other than the instantaneous range, a proportional navigation results if k_3 is other than zero. For k_1 and k_3 equal to zero while k_2 is -1, a pure pursuit course results since the homing vehicle is directed to fly along the instantaneous line-of-sight. Thus, by proper selection of the constants of proportionality all types of homing schemes are possible including hybrid schemes which do not completely fall into the above classes. It is also possible to fly a slightly different course in pitch than in yaw by choosing the constants of proportionality for the two channels differently. Moreover, the complete homing phase may be a blend of various types by varying the constants of proportionality as a function of range or some other appropriate variable.

Collision course. If range information is available a collision course may be flown. This will tend to minimize the homing time since in nonrotating relative coordinates the motion is completely along the line of sight, which maintains a fixed direction in inertial space. Thus, in nonrotating relative coordinates the motion of the target is radially inward toward the homing vehicle.

Integration of Eqs (144) and (145) with respect to time yields

$$R^2 \omega_p = R_0^2 \omega_{p_0} + \int_0^t R \Delta g_p \, dt - \int_0^t R \, a_p \, dt \tag{153}$$

$$R^2 \omega_y = R_0^2 \omega_{y_0} - \int_0^t R \, a_y \, dt \tag{154}$$

If proportional transverse jets are used (alternately, a gimbaled nozzle) the thrust accelerations are of the form

$$a_p = \frac{\Delta V_p^*}{\tau_p} = \frac{R \omega_p}{\tau_p} \tag{155}$$

$$a_y = \frac{\Delta V_y^*}{\tau_y} = \frac{R \omega_y}{\tau_y} \tag{156}$$

where τ_p and τ_y are the pitch and yaw channel time constants. Substituting Eqs (155) and (156) into (153) and (154) yields

$$\omega_y = \omega_{y_0} \left(\frac{R_0}{R}\right)^2 e^{-\frac{t}{\tau_y}} \tag{157}$$

$$\omega_p = \left(\omega_{p_0} R_0^2 + \int_0^t R \, \Delta g_p \, e^{\frac{\sigma}{\tau_p}} \, d\sigma\right) \frac{e^{-\frac{t}{\tau_p}}}{R^2} \tag{158}$$

Note that if the time constants are small enough that $\frac{R_0}{R}$ does not build up appreciably within, say three time constants, the initial rates ω_{p0} and ω_{y0} are steered out exponentially. In fact, if τ_p, τ_y, and the range rate are small enough such that values of range separated in time by time constants are nearly equal,

$$\omega_y \sim \omega_{y_0} e^{-t/\tau_y} \tag{159}$$

$$\omega_p \sim \omega_{p0} e^{-t/\tau_p} + \frac{\Delta g_p}{R} \tau_p \left(1 - e^{-t/\tau_p}\right) \tag{160}$$

Thus, in the steady state

$$\omega_y = 0 \tag{161}$$

$$\omega_p = \frac{\Delta g_p}{R} \tau_p \tag{162}$$

Note that a pitch rate exists due to the pitch component of the gravity differential. This emphasizes two significant points:

(1) A nonzero steady-state pitch acceleration of

$$a_p = \frac{R}{\tau_p}\,\omega_p = \Delta g_p \qquad (163)$$

will exist.

(2) A precise collision course cannot be realized in pitch if Eq (155) is used, since the gravity differential causes a small steady value of pitch rate to exist. For extensive homing time the pitch displacement of the line-of-sight may be appreciable.

The first point is, of course, clear upon inspection of Eq (142). The obvious remedy for the second point is to make τ_p sufficiently small so that the total displacement is negligible. This, however, is not always possible, since high control loop gains may result in control instability. In the next topic, "Biased-Collision Course," a solution to this problem is indicated.

If impulsive thrusts are used for transverse corrections, the accelerations assume the forms

$$a_p = \Delta V_p^* \delta(t) = r\omega_p \delta(t) \qquad (164)$$

$$a_y = \Delta V_y^* \delta(t) = r\omega_y \delta(t) \qquad (165)$$

where

$\delta(t) \equiv$ Dirac delta or impulse function.

Hence, Eqs (153) and (154) for $t > 0$ become

$$R^2 \omega_p = \int_0^t R\,\Delta g_p\,dt \qquad (166)$$

$$R^2 \omega_y = 0 \qquad (167)$$

Thus, ω_y does not require further corrections in the ideal case, but ω_p soon builds up such that if a set of transverse corrections are scheduled at $t = t_i$, the required velocity increment is

$$\Delta V_p(t_i) = \frac{1}{R_i}\int_0^{t_i} R\,\Delta g_p\,dt \qquad (168)$$

In many cases a control deadzone is used such that corrections are made whenever ω_p exceeds some threshold value. Equation (168) may be used to compute the range at which this occurs. Thus, if the previous correction occurred at $t = t_{i-1}$ when $R = R_{i-1}$, then the threshold value will be exceeded at the range $R = R_i$ given by

$$R^2 = \frac{1}{\Omega_p}\left|\int_{R_{i-1}}^{R_i} \Delta g_p \frac{R\,dR}{\dot{R}}\right| \qquad (169)$$

where

Ω_p = deadzone threshold value for ω_p

$\dot{R}$ = range rate = $\frac{dR}{dt}$ (assumed to be negative).

The magnitude of the correction at such a time is

$$\Delta V_i = R_i\,\Omega_p \qquad (170)$$

Hence, the total pitch velocity increment is

$$(\Delta V_p)_{total} = R_0\,\omega_{p_0} + \sum_{i=1}^{n} \Delta V_i$$

$$= R_0\,\omega_{p_0} + \Omega_p \sum_{i=1}^{n} R_i \qquad (171)$$

The total yaw velocity increment is

$$(\Delta V_y)_{total} = R_0\,\omega_{y_0} \qquad (172)$$

Thus, the total transverse velocity requirement is

$$(\Delta V_T)_{total} = R_0\left(\omega_{p_0} + \omega_{y_0}\right) + \Omega_p \sum_{i=1}^{n} R_i \qquad (173)$$

where it is assumed that ω_{p_0} and ω_{y_0} are positive; if they are not positive, absolute values are to be used in Eqs (171), (172) and (173).

Biased-collision course. In this method the line-of-sight rates are controlled to appropriate bias values. If the biases are zero, a pure collision course results. One particular application of this technique is that which maintains the line of sight at constant angles with respect to the target's local vertical and orbit plane normal. Thus, if the target's body axes are maintained at fixed angles with respect to its local vertical and orbit plane normal, the homing vehicle approaches the target at a fixed aspect in target body coordinates. This is shown in the following sketch for a coplanar situation.

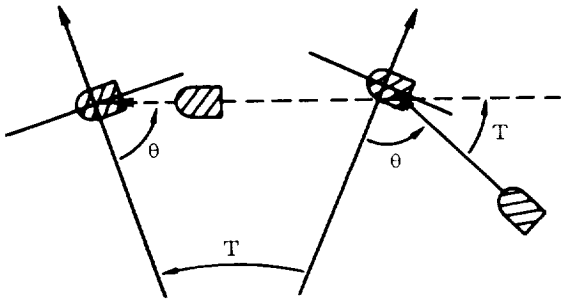

For a target in a circular orbit, the local vertical has an angular rate of

$$\omega_t = \sqrt{\frac{GM}{r_t^3}}$$

Thus, assuming coplanar rendezvous, the line-of-sight rate in pitch must have a magnitude ω_t. If the homing vehicle is behind the target the sign of ω_p must be negative (downward rotation); if ahead, positive. The yaw rotation must be zero in the case of coplanar rendezvous. Thus, there exists biased-collision steering in pitch and pure collision in yaw.

For continuous, proportional steering

$$a_p = \frac{\Delta V_p^*}{\tau_p} = \frac{R(\omega_p - \omega_b)}{\tau_p} \tag{174}$$

$$a_y = \frac{\Delta V_y^*}{\tau_y} = \frac{R\omega_y}{\tau_y} \tag{175}$$

where

$\omega_b \equiv$ desired bias rate

$= \pm\omega_t$.

Substituting the above into the general equations, Eqs (153) and (154) yields upon solution of the differential equations

$$\omega_y = \omega_{y_0}\left(\frac{R_0}{R}\right)^2 e^{-t/\tau_y} \tag{176}$$

$$\omega_p = \omega_{p_0}\left(\frac{R_0}{R}\right)^2 e^{-t/\tau_p} + \frac{1}{r^2}\int_0^t R\left(\Delta g_p + \frac{R\omega_b}{\tau_p}\right) e^{-\frac{(t-\sigma)}{\tau_p}}\, d\sigma \tag{177}$$

As before, if the ratio of range values separated in time by three time constants is approximately unity,

$$\omega_y \sim \omega_{y_0} e^{-t/\tau_y} \tag{178}$$

$$(\omega_p - \omega_b) \sim \left(\omega_{p_0} - \omega_b\right) e^{-t/\tau_p} + \frac{\Delta g_p}{R}\tau_p\left(1 - e^{-t/\tau_p}\right) \tag{179}$$

Thus, in the steady state

$$\omega_y = 0 \tag{180}$$

$$\omega_p = \omega_b + \frac{\Delta g_p}{R}\tau_p \tag{181}$$

This equation shows that the steady pitch rotation obtained using conventional collision steering can be removed by $\omega_b = -\Delta g_p/R\,\tau_p$ and implies use of angular acceleration measurements.

Using Eq (136) in Eq (181) yields

$$\omega_p = \omega_b + 3\frac{GM}{r_t^3}\tau_p \sin\theta_0 \cos\theta_0$$

$$= \omega_b + 3\omega_t^2 \tau_p \sin\theta_0 \cos\theta_0 \tag{182}$$

Then, for $\omega_b = \pm\omega_t$

$$\omega_p = \pm\omega_t\left(1 \mp 3\omega_t \tau_p \sin\theta_0 \cos\theta_0\right) \tag{183}$$

Since the maximum value of $\sin\theta_0 \cos\theta_0$ is $1/2$ and τ_p is usually on the order of seconds, the bracketed term is approximately unity. Thus, in the steady state $\omega_p \cong \omega_b = \pm\omega_t$.

For impulsive thrusts,

$$a_p = \Delta V_p^* \delta(t) = R(\omega_p - \omega_b)\,\delta(t) \tag{184}$$

$$a_y = \Delta V_y^* \delta(t) = R\omega_y\,\delta(t) \tag{185}$$

Hence, after such a correction

$$R^2\omega_p = \int_0^t R\,\Delta g_p\, dt + R^2\omega_b \tag{186}$$

$$R^2\omega_y = 0 \tag{187}$$

As in the case of the collision course, the gravity differential requires subsequent corrections in pitch. Thus, if corrections are made whenever ω_p deviates from ω_b by Ω_p, the range at the time of each correction is given by Eq (169). For the present case since

$$\Delta g_p = 3R\omega_t^2 \sin\theta_0 \cos\theta_0 \tag{188}$$

Equation (169) becomes

$$R_i^2 = \frac{3\omega_t^2 \sin\theta_0 \cos\theta_0}{\Omega_p}\int_{R_{i-1}}^{R_i}\frac{R^2\, dr}{\dot{R}} \tag{189}$$

where the absolute value signs on the right member are implied. If the closing rate, $(-\dot{R})$, is constant between the ith and (i - 1)st corrections

$$R_i^2 = \frac{\omega_t^2 \sin\theta_0 \cos\theta_0}{\Omega_p (-\dot{R})_{i-1}} (R_{i-1}^3 - R_i^3) \quad (190)$$

The total pitch and yaw velocity increments are

$$(\Delta V_p)_{total} = R_0 \Delta\omega_{p_0} + \Omega_p \sum_{i=1}^{n} R_i \quad (191)$$

$$(\Delta V_y)_{total} = R_0 \omega_{y_0} \quad (192)$$

Hence,

$$(\Delta V_T)_{total} = R_0 \left(\Delta\omega_{p_0} + \omega_{y_0}\right) + \Omega_p \sum_{i=1}^{n} R_i \quad (193)$$

By comparison of Eq (193) with Eq (173) it might be inferred that "biased-collision" is most efficient for a coplanar rendezvous since $\Delta\omega_{p_0}$ is involved in biased-collision; whereas the full initial pitch rate, ω_{p_0}, is involved in "pure collision." This is deceiving unless it is realized that faster range closure occurs in pure collision and hence fewer number of pitch corrections are required, since the time-integrated effect of gravity is smaller. Thus, biased-collision does not necessarily require less velocity.

Proportional navigation. Proportional navigation involves transverse accelerations proportional to the line-of-sight rates. That is

$$a_p = K_{a_p} \omega_p \quad (194)$$

$$a_y = K_{a_y} \omega_y \quad (195)$$

If

$$K_{a_p} = \frac{R}{\tau_p} \quad (196)$$

$$K_{a_y} = \frac{R}{\tau_y} \quad (197)$$

then a collision course results. However, in the absence of range information a collision course may be approximated by Eqs (194) and (195) when K_{a_p} and K_{a_y} are constants. This is the prime purpose of proportional navigation.

Substituting Eqs (194) and (195) in Eqs (153) and (154) yields

$$\omega_y = \omega_{y_0} \left(\frac{R_0}{R}\right)^2 Q_y(t) \quad (198)$$

$$\omega_p = \left[R_0^2 \omega_{p_0} + \int_0^t \frac{R \Delta g_p}{Q_p(t)} dt\right] \frac{Q_p(t)}{R^2} \quad (199)$$

where

$$Q(t) \equiv \exp\left(-\int_0^t \frac{K_a}{R} dt\right) \quad (200)$$

Explicit solutions of Eqs (198) and (199) require knowledge of the time variation of range. If we assume that proportional transverse jets are used, then in the absence of accelerations along the line of sight,

$$R \sim R_0 + \dot{R}_0 t \quad (201)$$

It is also assumed that the initial closing rate $(-\dot{R}_0)$ is high enough so that Eq (201) is true in spite of gravity effects and line-of-sight rotations. With Eq (201), Eq (200) becomes

$$Q(t) = \left(\frac{R}{R_0}\right)^m \quad (202)$$

where

$$m \equiv \frac{K_a}{(-\dot{R}_0)} \quad (203)$$

yielding

$$\omega_y = \omega_{y_0} \left(\frac{R}{R_0}\right)^{m-2} \quad (204)$$

$$\omega_p = \left[\omega_{p_0} + \int_0^t \frac{\Delta g_p}{R} \left(\frac{R}{R_0}\right)^{2-m} dt\right] \left(\frac{R}{R_0}\right)^{m-2} \quad (205)$$

If the closing rate is sufficiently high so that $\frac{\Delta g_p}{R}$ can be taken outside of the integral

$$\omega_p \sim \omega_{p_0} \left(\frac{R}{R_0}\right)^{m-2} + \left(\frac{m}{m-3}\right) \frac{\Delta g_p}{K_{a_p}} \left[1 - \left(\frac{R}{R_0}\right)^{m-1}\right] \quad (206)$$

Note that in order to be effective

$$m = \frac{K_a}{(-\dot{R}_0)} > \begin{cases} 2 \text{ for yaw} \\ 3 \text{ for pitch} \end{cases} \qquad (207)$$

Thus, by choosing m sufficiently high (implying high K_{a_p}) in the steady state

$$\omega_y = 0$$

$$\omega_p = \frac{\Delta g_p}{K_{a_p}} \text{ (negligible for } K_{a_p} \text{ high enough).}$$

It is seen then that the proportional navigation course can adequately approximate the collision course for sufficiently high gains and closing rates.

Biased-proportional navigation. This technique is a generalization of proportional navigation, analogous to biased-collision in its generalization of collision steering. If this technique is applied to the coplanar situation analyzed for the case of biased-collision, one obtains

$$\omega_y = \omega_{y_0} \left(\frac{R}{R_0}\right)^{m-2} \qquad (208)$$

$$\omega_p = \left[\omega_{p_0} + \int_0^t \frac{\Delta g_p + K_{a_p} \omega_b}{R} \left(\frac{R}{R_0}\right)^{2-m} dt\right] \left(\frac{R}{R_0}\right)^{m-2} \qquad (209)$$

under the same restrictions imposed on the explicit analysis for proportional navigation. For this case

$$\frac{\Delta g_p}{R} = 3\omega_t^2 \sin\theta_0 \cos\theta_0.$$

Therefore,

$$\omega_p = \omega_{p_0} \left(\frac{R}{R_0}\right)^{m-2} + 3\left(\frac{m}{m-3}\right)\frac{\omega_t^2 \sin\theta_0 \cos\theta_0}{K_{a_p}} \left[1 - \left(\frac{R}{R_0}\right)^{m-1}\right] + \left(\frac{m}{m-2}\right)\omega_b \left[1 - \left(\frac{R}{R_0}\right)^{m-2}\right] \qquad (210)$$

Thus, in the steady state

$$\omega_p \sim 3\left(\frac{m}{m-3}\right)\frac{\omega_t^2 \sin\theta_0 \cos\theta_0}{K_{a_p}} + \left(\frac{m}{m-2}\right)\omega_b \qquad (211)$$

For $\omega_p \sim \pm\omega_t$, it is required that

$$\omega_b = \pm\omega_t \left[\frac{m-2}{m} \mp \left(\frac{m-2}{m-3}\right)\frac{\omega_t^2 \sin\theta_0 \cos\theta_0}{K_{a_p}}\right] \qquad (212)$$

where $m > 3$. For large m (large K_{a_p})

$$\omega_b = \pm\omega_t \qquad (213)$$

As in the case of proportional navigation, this technique can adequately approximate its collision counterpart for sufficiently high gains and closing rates.

c. Homing flight paths

The flight paths produced by the transverse steering techniques presented are simple to derive. For example, in the steady-state, collision and proportional navigation maintain the line of sight in a fixed inertial direction, assuming the flight times are small enough to warrant neglect of the gravity effect. Thus, in a nonrotating frame centered at the target, the homing vehicle closes radially on the target. On the other hand, for the coplanar biased-collision and biased-proportional navigation examples presented, the line of sight is maintained fixed in a rotating frame centered at the target. In this frame the biased-collision and biased-proportional schemes produce an apparent homing vehicle motion radially toward the target. The following two sketches show the flight paths in these frames. The mapping of a flight path from one frame to the other is relatively simple since the two frames differ by a rotational rate.

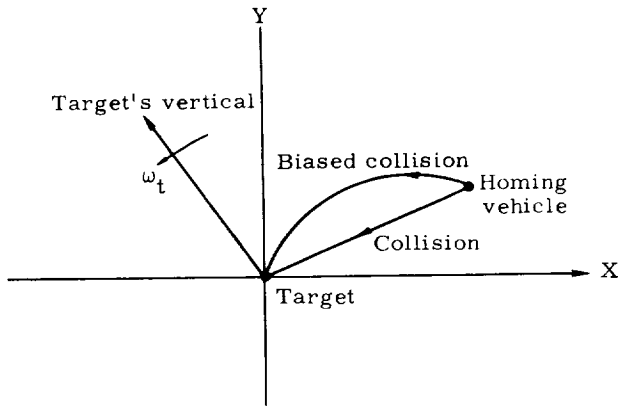

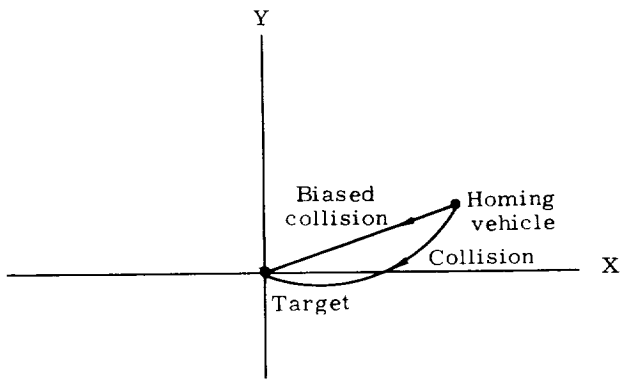

Note that if the target's body axes are continuously aligned with its local vertical, an observer on the target will see the homing vehicle approach along an apparent straight line if biased-collision is used. To this observer the collision course will appear curved. However, assuming no thrust accelerations along the line of sight and identical initial conditions, the homing vehicle reaches the target sooner along the collision course.

d. Motion along the line of sight (longitudinal)

The governing differential equation for this maneuver is Eq (141) which is repeated at this point.

$$\frac{d^2 R}{dt^2} - R\omega^2 = -a_R + \Delta g_R \tag{214}$$

where

$$\Delta g_R = -\frac{GM}{r_t^2}\left(\frac{R}{r_t}\right)(1 - 3\cos^2\theta) \tag{215}$$

For a target in circular orbit, the differential equation can be written as

$$\frac{d^2 R}{dt^2} + R\,\omega_t^2\left[(1 - 3\cos^2\theta) - \frac{\omega^2}{\omega_t^2}\right] = -a_R \tag{216}$$

where

ω_t = target's angular rate.

For the cases treated it was seen that biased-collision and biased-proportional navigation yield

$$\frac{d^2 R}{dt^2} - R\,\omega_t^2\,(3\cos^2\theta_0) = -a_R \tag{217}$$

whereas collision and proportional navigation yield

$$\frac{d^2 R}{dt^2} + R\,\omega_t^2\,(1 - 3\cos^2\theta) = -a_R \tag{218}$$

The above equations show that the gravity effects reduce the closing rate in the case of biased-collision and biased-proportional navigation. However, the gravity effects may actually increase the closing rate or at worse reduce it to a lesser extent in collision and proportional navigation. Hence, all else being equal, the latter produce shorter homing times. The differences are small when rapid rendezvous is involved. However, for extended or long-time rendezvous the differences may be significant.

Neglect of orbital aspects. The homogeneous solution of Eq (217) admits hyperbolic functions whose arguments are proportional to ω_t. For Eq (218) since $\theta = \theta_0 \pm \omega_t t$, Mathieu functions, whose arguments are likewise proportional to ω_t, are admitted. These homogeneous solutions represent the perturbative effect of the orbital aspects of the problem. If the homing phase is restricted to small homing times such that the arguments of the homogeneous functions differ negligibly from zero, the range variation will be approximately that which is obtained by letting $\omega_t = 0$ in Eqs (217) and (218). In such instances all techniques analyzed in subsection d have range variations governed by

$$\frac{d^2 R}{dt^2} \simeq -a_R \tag{219}$$

In all ensuing work in this chapter it is assumed that Eq (219) is valid. The condition which must be satisfied for this to hold is

$$\omega_t\, t_R << 1 \tag{220}$$

or

$$t_R << \frac{\tau_0}{2\pi} \tag{221}$$

where

$t_R \equiv$ rendezvous (homing) time.

This implies, of course, that the initial closing rate must be sufficiently high so that the integrated effects of the gravity differential are negligible. If this is not the case, the problem becomes one of extended or long-time rendezvous, requiring the use of Eq (217) or (218).

e. Single longitudinal correction

Satellite rendezvous requires closing rate control and differs from interception because of this requirement. It is assumed that the homing vehicle possesses an initial closing rate $(-\dot{R}_0)$ such that longitudinal corrections may be devoted solely to closing rate reductions or braking. The initial closing rate is established either by the booster or homing vehicle upon injection.

The most obvious technique is one involving a single thrust application at the last possible moment, such that range and closing rate go to zero upon completion of the correction. This technique produces minimum flight times since the initial closing rate is not reduced until just prior to rendezvous.

Impulsive thrust. In the ideal case of an impulsive thrust, the initial closing rate is removed at R = 0. Thus, the rendezvous and interception problems are virtually identical in this ideal case. The rendezvous time is the same as that of interception. That is,

$$t_R = t_{G_0} = \frac{R_0}{(-\dot{R}_0)} \tag{222}$$

where

t_{G_0} ≡ initial time-to-go.

The longitudinal velocity requirement is just

$$\Delta V_L = (-\dot{R}_0) \tag{223}$$

Constant acceleration. Physically all thrusts are finite and, hence, regard must be given to the resultant nonzero braking distance. For constant thrust and negligible mass change, the braking acceleration is constant. The distance traveled over the time it takes to remove the closing rate is defined as the braking distance b and is given by

$$b = \frac{(-\dot{R}_0)^2}{2a_0} \tag{224}$$

where

$$a_0 = \frac{F_0}{m_0} = \text{initial thrust-to-mass ratio.}$$

Thus, the homing vehicle is allowed to close at the rate $(-\dot{R}_0)$ until R = b, whereupon the braking acceleration a_0 is applied so that R = 0 when $\dot{R} = 0$. This results in a rendezvous time of

$$t_R = t_{G_0} + \frac{\Delta t_b}{2} \tag{225}$$

where

$$\Delta t_b \equiv \text{braking duration} = \frac{(-\dot{R}_0)}{a_0} \tag{226}$$

Constant thrust. For the general case of constant thrust wherein mass variation is non-negligible

$$a_R(t) = -\frac{F_0}{m_0 - \dot{m}_0 t} \tag{227}$$

where

$\dot{m}_0$ ≡ mass flow rate > 0.

$$= \frac{F(t)}{g_0 I_{sp}}$$

For this case, the required braking distance is Refs. 10 and 11.

$$b = \left(e^{\dot{R}_0/c} - (1 + \dot{R}_0/c)\right)\left(-\frac{cm}{\dot{m}}\right) \tag{228}$$

where

c ≡ effective mass exit velocity.

$$= g_0 I_{SP}$$

The rendezvous time is

$$t_R = t_{G_0} + \frac{c}{a_0}\left(\frac{c}{(-\dot{R}_0)} - \left(1 + \frac{c}{\dot{R}_0}\right)e^{\dot{R}_0/c}\right) \tag{229}$$

The following sketch shows a typical R versus $\dot{R}$ phase plane for this closure. Impulsive, constant acceleration and constant thrust braking are illustrated. It is noted, however, that the difference between the latter two is exaggerated.

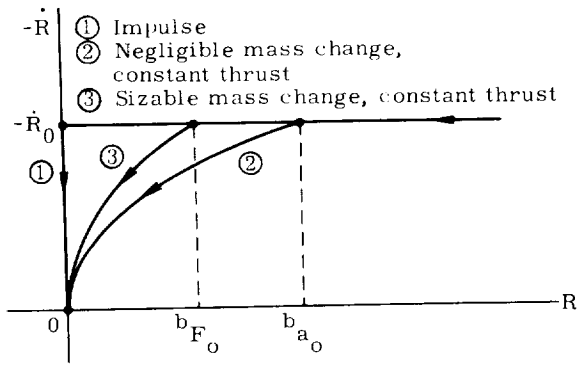

Multiple longitudinal corrections. There are many reasons for reducing the closing rate in multiple steps rather than in a single step. The most obvious reason is the presence of system errors which can cause significant range and range rate dispersions if large closing rates are removed in a single step. Therefore, there exists the possibility of biasing the nominal point of closing rate reduction so that the closing rate is nominally zero at some range R_b. Small vernier jets can then be used to adjust for position and residual range rate errors. However, for large initial closing rates, the residual errors may be quite high and may require considerable expenditure of gas since the thrust level and specific impulses of pneumatic jets are low. Compounding this is the weight penalty incurred by the tankage to contain such large pneumatic volumes. Thus, even if such fine jets are used, there still exists the desirability of multiple step reductions so that the single step braking thrust will not leave large residual errors for the vernier system.

The underlying idea of multiple step reduction of the closing rate is this: divide up the total closing rate to be reduced in smaller increments and allocate these increments at various ranges so that percent-type errors in the velocity increments are also allocated rather than occurring all at once near the target. Errors in each correction are than removed by each subsequent correction, assuming that sufficient time exists between corrections for closed-loop control.

If done properly, the closing rate control can be effected without need of a bilateral thrust capability during the multiple step reductions.

This is done by constraining each correction to yield a certain minimum closing rate even in the presence of system errors. Thus, each successive correction need only decrease the closing rate. This permits the use of a unilateral thrust, resulting in a weight saving since a comparable rear-mounted longitudinal engine is not required. In addition, since the closing rate decreases monotonically, the longitudinal velocity requirement is no more than the initial closing velocity $(-\dot{R}_0)$. There is the matter of the differential gravity effect and injection dispersions. However, these are also required of the single step technique.

It should be made clear that these refinements occur at the expense of a longer flight time. That is, under the constraint of minimum velocity requirement and unilateral thrust, final dispersions are traded off against time. However, except for emergency rendezvous, the longer homing time is usually more acceptable than the weight penalty which otherwise occurs.

A method for selecting the nominal closing rate profile which utilizes the minimum number of reductions is now described. To simplify the presentation, impulsive corrections are assumed. This is not a restriction, however, since, for nonimpulsive thrust, it is only necessary to start each correction at a range which is greater by the amount of distance traveled during each thrust period. Thus, if it is required that the closing rate be reduced from $(-\dot{R}_0)$ to $(-\dot{R}_1)$ at some range, the difference between the braking distances b_0 and b_1 yields the amount of lead distance. The corresponding difference between the stretch-out times yields the amount by which the total homing time is increased over the impulsive case.

Suppose the final braking correction is scheduled at a range R_B which provides a suitable bias such that errors in range measurement do not cause an overshoot in position and, possibly, premature impact. In addition, suppose the nominal closing rate at this point is made sufficiently high to ensure against negative closing rates in the presence of system dispersions. The following sketch shows this in the $(-\dot{R})$ versus R phase plane. The 3σ contour of dispersions is shown, assuming a bivariate gaussian distribution in closing rate and range.

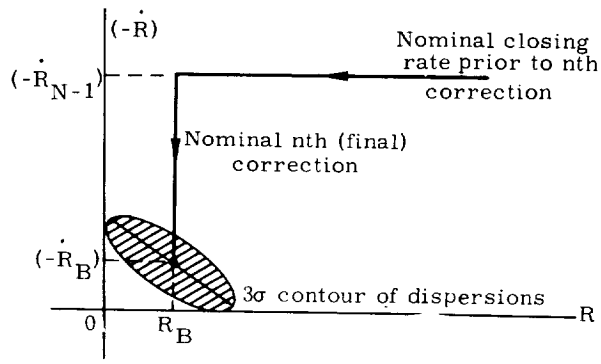

It is implicitly assumed that the range dispersion is acceptable with regard to specifications or that use of small bilateral verniers for clocking maneuvers can comfortably accommodate the range errors. The primary concern then is to ensure that the closing rate dispersion is also within allowable limits. From this sketch it is apparent that the closing rate bias $(-\dot{R}_B)$ must be at least equal to the expected 3σ closing rate error if range is to decrease monotonically. Hence, for large dispersions in the final closing rate $(-\dot{R}_N)$ the bias becomes large and may be unacceptable in terms of vernier fuel and tank weight requirements. To avoid this the following process may be used to obtain the desired closing rate profile. Let

- N = total number of required corrections (to be determined)
- V_i = closing rate following ith correction
- ΔV_i = velocity increment of ith correction
- ΔV_i^* = commanded velocity increment of ith correction
- k_i, β_i = proportional (percent-type) and additive errors in execution of ΔV_i^*
- D_i = desired or nominal closing rate following ith correction
- ϵ_i = error in measurement of V_i.

The proportional error k_i is the per-unit error in execution of ΔV_i^* and may result from either accelerometer bias, scale factor errors, or from thrust and I_{sp} variations if corrections are metered on a time basis. The additive error β_i is the effect of residual impulse uncertainties.

Since

$$V_i = V_{i-1} - \Delta V_i \tag{230}$$

$$\Delta V_i^* = (V_{i-1} + \epsilon_{i-1}) - D_i \tag{231}$$

and

$$\Delta V_i = (1 + k_i)\,\Delta V_i^* + \beta_i \tag{232}$$

It is possible to write for the general correction

$$V_i = D_i - k_i (D_{i-1} - D_i) - (\epsilon_{i-1} + \beta_i) \quad (233)$$

if all cross-products of errors are assumed to be negligible. In particular for the Nth (final) correction,

$$D_N = (-\dot{R}_B)$$

yielding

$$\left[V_N - (-\dot{R}_B)\right] = -k_N \left[D_{N-1} - (-\dot{R}_B)\right] - \alpha_N \quad (234)$$

where

$\left[V_N - (-\dot{R}_B)\right]$ = closing rate error after Nth correction

$\alpha_N \equiv$ total additive error of Nth correction

$$\equiv \epsilon_N + \beta_N \quad (235)$$

Hence, if the 3σ dispersion in the final closing rate is allowed to be no greater than C [and by the preceding sketch $(-\dot{R}_B) \equiv C$], then it is required that

$$D_{N-1} \leq C + \left(\frac{C^2 - 9\sigma^2_{\alpha_N}}{9\sigma^2_{k_N}} \right)^{1/2} \quad (236)$$

Thus, if a single step correction (N = 1) is to be used, the following relation must hold.

$$D_0 = (-\dot{R}_0) \leq C + \left(\frac{C^2 - 9\sigma^2_{\alpha_1}}{9\sigma^2_{k_1}} \right)^{1/2} \quad (237)$$

If this is not the case, then a single step correction cannot be used and hence N must be greater than 1. This implies a prior correction at a range

$$R = R_{N-1} > R_N = R_B.$$

For this prior correction, the unilateral thrust constraint is invoked, requiring that $V_{N-1} > 0$. Using Eq (233) with i = N - 1, this is established with 3σ probability if

$$D^2_{N-1} > 9\sigma^2_{k_{N-1}} (D_{N-2} - D_{N-1})^2 + 9\sigma^2_{\alpha_{N-1}} \quad (238)$$

If D_{N-1} is assumed to be at the maximum value allowed by Eq (236) (to minimize the nominal closing time),

$$D_{N-2} < \underset{D_{N-1}}{\text{Max}} \left[D_{N-1} + \left(\frac{D^2_{N-1} - 9\sigma^2_{\alpha_{N-1}}}{9\sigma^2_{k_{N-1}}} \right)^{1/2} \right] \quad (239)$$

where the notation implies the maximum value with respect to D_{N-1}. Thus, in order for a two step reduction to be possible,

$$D_0 = (-\dot{R}_0) < \underset{D_1}{\text{Max}} \left[D_1 + \left(\frac{D^2_1 - 9\sigma^2_{\alpha_1}}{9\sigma^2_{k_1}} \right)^{1/2} \right] \quad (240)$$

where $(D_1)_{\text{max}}$ is given by Eq (236) for N = 2.

Usually, it is not necessary to proceed beyond the case of N = 2 since the presence of a small number $\sigma^2_{k_1}$ in the denominator of the square root expression in Eq (240) yields a very large number. In addition, the fact that the maximum value of D_1 is involved in Eq (240) further enhances the situation. However, should the initial closing rate be extremely high, so that Eq (240) does not hold, N must be made greater than 2. This implies a prior correction at

$$R = R_{N-2} > R_{N-1} > R_N = R_B$$

Again for this prior correction the unilateral thrust constraint is invoked, and an expression similar to Eq (238) results. If the maximum value of D_{N-2} is used, a constraint on D_{N-3}, similar to that of Eq (239), results.

$$D_{N-3} < \underset{D_{N-2}}{\text{Max}} \left[D_{N-2} + \left(\frac{D^2_{N-2} - 9\sigma^2_{\alpha_{N-2}}}{9\sigma^2_{k_{N-2}}} \right)^{1/2} \right] \quad (241)$$

where $(D_{N-2})_{\text{max}}$ is given by Eq (239). If three reductions are to suffice, then Eq (241) requires that

$$D_0 = (-\dot{R}_0) < \underset{D_1}{\text{Max}} \left[D_1 + \left(\frac{D^2_1 - 9\sigma^2_{\alpha_1}}{9\sigma^2_{k_1}} \right)^{1/2} \right]$$

which is identical to Eq (240), except that the unity subscripts apply to the first of three scheduled reductions, and, if written out cumulatively instead of recursively, implies

$$D_0 = (-\dot{R}_0) < \left\{ \begin{matrix} \text{Max} & \text{Max} \\ D_1 & D_2 \end{matrix} \cdot \left[D_2 + \sum_{i=1}^{2} \left(\frac{D_{N-1}^2 - 9\sigma^2_{\alpha_{N-i}}}{9\sigma^2_{k_{N-i}}} \right)^{1/2} \right] \right\} \quad (242)$$

where $(D_1)_{\max}$ and $(D_2)_{\max}$ are given by Eqs (236) and (239) for N = 3.

What has taken place so far is an exercise in dynamic programming (Ref. 12) to determine the minimum number of reductions N necessary to satisfy the criterion C under the constraint of unilateral thrust. By inference, the general allocation policy for N reductions may be written as

$$D_{N-i} < \underset{D_{N-i+1}}{\text{Max}} \left[D_{N-i+1} + \left(\frac{D_{N-i+1}^2 - 9\sigma^2_{\alpha_{N-i+1}}}{9\sigma^2_{k_{N-i+1}}} \right)^{1/2} \right] \quad (243)$$

for

$$i = 2, 3, \ldots, N$$

where

$$D_0 = (-\dot{R}_0) \quad (244)$$

$$\text{Max } D_{N-1} = C + \left(\frac{C^2 - 9\sigma^2_{\alpha_N}}{9\sigma^2_{k_N}} \right)^{1/2} \quad (245)$$

The process is continued until it is found that

$$D_0 = (-\dot{R}_0) < \text{Max } D_{N-i} \quad (246)$$

whereupon N is determined. The process also yields the desired closing rates at each step. Hence, upon satisfaction of Eq (246) all D_i's are determined.

There now remains the problem of allocating the desired set of closing rates at appropriate times or ranges. Generally, the choice should be made so that a sufficient amount of tracking and smoothing time exists between consecutive step reductions. Also, the reductions should be spaced so that the transverse channels have sufficient time to steer out errors. The non-impulsive nature of each thrust application must also be taken into account. Thus, generally, the time between reductions is

$$\Delta t_i = \Delta t_{s_i} + \Delta t_{\ell_i} + \Delta t_{B_i} \quad (247)$$

where

Δt_i = time between ith and i - first reduction

Δt_{s_i} = ith smoothing time

Δt_{ℓ_i} = ith lag time (computing time, valve lag, etc.)

Δt_{B_i} = burning time of ith correction

The range difference between the ith and (i - 1)st correction is thus

$$\Delta R_i = \left(\Delta t_{s_i} + \Delta t_{\ell_i} \right) D_{i-1} + \Delta b_i \quad (248)$$

where

$\Delta b_i \equiv$ distance traveled in braking from D_{i-1} to D_i. (249)

Equations (248) and (249) then allow for the computation of the spacing of step reductions and, hence, the generation of the nominal closing rate profile. For any given set of spacings between corrections, the closing rate profile is the minimum time profile under unilateral constraints. This follows, since at each step the closing rate is assigned the highest possible value under unilateral thrust constraints.

g. Other rendezvous schemes

So far the work presented in this section has been based on the differential equations of relative motion. This approach is, however, not necessary as will be illustrated in the two remaining schemes to be discussed.

Combined injection and terminal guidance. By timing the initiation of thrust and providing thrust of a variable magnitude and direction, it is possible to perform the injection and any maneuvers necessary for closure simultaneously. The most notable studies conducted for this scheme have been conducted at the MIT Instrumentation Laboratory (see Refs. 13, 14, 15 and 16). These studies are concerned with a guidance equation of the form

$$\bar{f}_c = S_1 \bar{\ell}_r \left[\dot{R} + f(R) \right] + S_2 \left[R \bar{\omega}_{LS} \right] \quad (250)$$

where

$\bar{f}_c$ = commanded acceleration vector

S_1, S_2 = sensitivity coefficients

$\dot{R}$ = range rate

R = range

$\bar{\omega}_{LS}$ = angular velocity of the line of sight

$f(R)$ = desired range rate as a function of range

$\bar{\ell}_R$ = unit vector along the line of sight

For the studies conducted to this date, the $f(R)$ utilized has been $K\sqrt{R}$. This selection was made based on trials of several functions satisfying the boundary conditions for $f(R)$ (namely that $f(R)$ be defined for all R and go to zero at $R = 0$). A variety of values have been investigated for S_i and for K. With regard to K, the implications are that some linear function of the required velocity increment (i.e., $a + b\Delta v$) may be advantageous from the standpoint of propulsion system performance.

Because of the extreme initial closure velocities (as great as 4500 mps) and the limited range of the radar unit, it is, in general, necessary to begin the injection maneuver with a programmed thrust. Then at some time during the maneuver after the target is acquired, the guidance equation must be utilized. This sequencing is desirable in other respects as well, since it allows the planar change to be made while the velocity is near minimum, thus conserving the energy available.

A single variable thrust gimbaled motor (along with an adequate control system) comprises the propulsion system. The utilization of a single motor is made possible by restricting the initial conditions for closure to lie within a region ahead of and slightly below the target. Under these conditions the target overtakes the shuttle during the injection maneuver. The energy requirements for these maneuvers closely approximate the minimum (for small changes in the plane of motion).

The purpose of the variable thrust motor is to provide additional tolerance in the relative position of the two vehicles at the time the injection maneuver is initiated. In this manner it is possible to simultaneously compensate for errors in the ascent trajectory and launch timing.

The data obtained for the necessary computations are taken from a single radar unit mounted to the vehicle on a set of gimbals. The range and range rate are measured directly, whereas the angular velocity of the line of sight is computed from signals taken from the dish gimbals and the inertial platform.

An elementary functional block diagram of this system is shown in the following sketch.

Positive closure. Utilizing the analytic solutions for positive and velocity presented in the discussion of relative motion for nearly circular orbits, a purely numerical study of rendezvous has been conducted. The guidance scheme for this technique requires that the vehicle be accelerated toward the target with some given velocity. Then at a specified distance and range rate, thrust is again initiated to drive both the range and range rate to zero. This scheme has been investigated in studies conducted within the Martin Company.

In order to maintain the vehicle antennas in known orientations with respect to the earth, and to simplify the attitude control function to one of stabilization, the vehicle considered is assumed to be aligned with its fore and aft axis parallel to the orbital plane of the target satellite. Furthermore it is assumed that the fore-aft axis and the lateral axis lie in the plane normal to radius vector to the satellite. Thrust units are located so as to provide fore-aft, left-right and up-down accelerations. The attitude reference for this orientation is provided by an inertial platform.

Analog studies have been conducted to investigate vehicle to target closure employing on-off thrusts applied through the cg of the shuttle vehicle. The basic scheme utilized in these runs

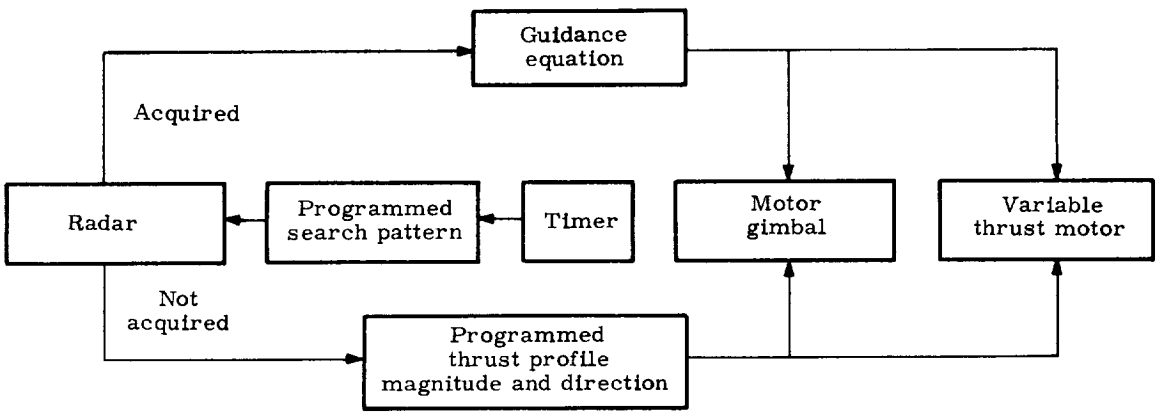

is illustrated in the following sketch. This sketch shows the relative range and range-rate phase plane (where Points A and B are two representative conditions existing at the time of radar lock-on).

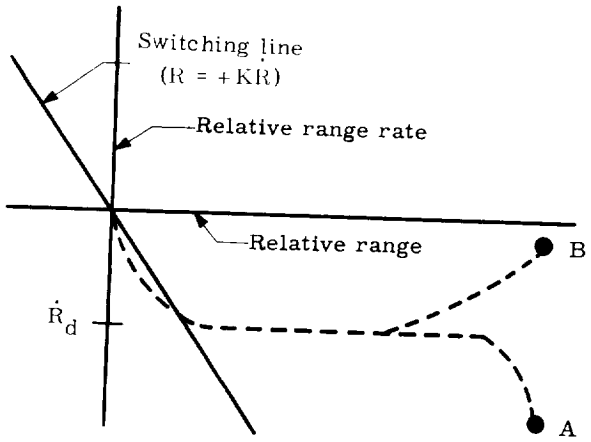

Thrust is applied in all cases to produce a given specified closure rate, $\dot{r}_d$. The vehicle is then allowed to coast until the switching line conditions are reached. At this point thrust is again initiated and the range and range rates are nulled to zero. The choice of K in the switching line equation is determined by knowledge of the acceleration available from the motors. Thrust must be initiated sufficiently early to avoid overrunning the target. Because of the on-off nature of the propulsion system, a dead spot must be provided to prevent chattering. In addition, it is necessary to bias the preselected closure velocity since the relative velocity components will change even in the absence of thrust due to slight differences in the orbits of the two vehicles and the differences in the perturbations effecting them.

The guidance law for each thrust component (neglecting the velocity bias previously discussed) is of the form

$$\left.\begin{aligned} T = +T_0 &\left\{ \begin{aligned} &\left[(R-\epsilon)+K\dot{R}\right] > D\,;\ \dot{R} > -\dot{R}_d \\ &\text{or} \\ &\left[(R-\epsilon)+K\dot{R}\right] < -D\,;\ \dot{R} > \dot{R}_d \end{aligned} \right\} \\ T = -T_0 &\left\{ \begin{aligned} &\left[(R-\epsilon)+K\dot{R}\right] > D\,;\ \dot{R} < -\dot{R}_d \\ &\left[(R-\epsilon)+K\dot{R}\right] < -D\,;\ \dot{R} < \dot{R}_d \end{aligned} \right\} \\ T = 0 \qquad -D < &\left[(R-\epsilon)+K\dot{R}\right] < D \end{aligned}\right\} \quad (251)$$

where

ϵ = stand off distance

D = dead spot (±) about ϵ

$\dot{R}_d$ = preselected closure rate.

It can be shown that closure from any point in a region about the target vehicle is possible. However, the most economic utilization of the propellant occurs when the shuttle is initially ahead of the target with a slightly lower velocity. If the vehicle is initially behind the target, two possibilities exist. First, thrust can be applied to produce closure without regard to propellant consumption. Or secondly, the orbital period of the shuttle vehicle can be adjusted so as to produce a gradual closure with respect to the target, and then at such time as the vehicles are appropriately located, the previous routine can be employed.

Studies conducted with initial separations of approximately 32 km and velocities of approximately 90 mps indicate that thrust-to-weight ratios of 0.1 to 0.2 g are quite adequate for control. Closure times for these runs were generally in the order of 400 to 800 sec with a fuel requirement of approximately $\frac{W_0}{8}$ which checks very closely to the estimate obtained from

$$\Delta V = g_0 I_{sp} \ell n \frac{1}{1-\xi}.$$

The motion of the shuttle vehicle under the influence of this set of control laws is illustrated in the following sketch which shows the projected motion in the vertical-longitudinal plane and the lateral longitudinal plane.

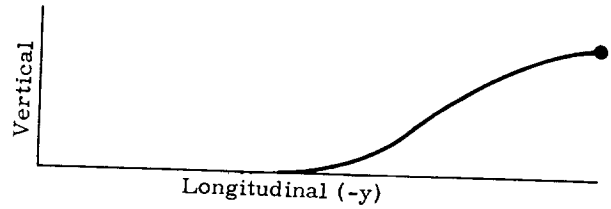

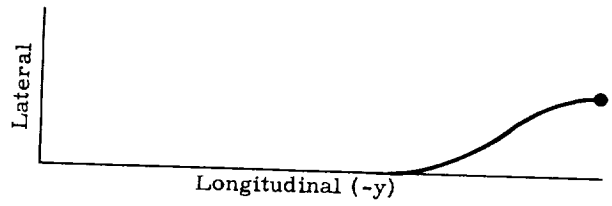

Signals for implementing this guidance law are derived from the radar data. Range (r) and range rate ($\dot{r}$) along the line of sight are measured by the tracking radar; the Euler angles defining relative position are provided by pickoffs on the radar dish gimbals, and the angular rate of the line of sight as computed from the signals from the rate gyros on the radar dish gimbals and the angular rate of the vehicle which is slaved to some reference (for example, local vertical).

h. Use of explicit control

The preselection of a nominal closing rate profile implies a fixed number of corrections at fixed ranges. In the early stages of mission planning, this is perhaps necessary for determination of sensor, propulsion, and time requirements in relation

to final accuracies and desired payload. However, whenever the question of optimization arises, the selection of a nominal profile can become an involved process, particularly when many corrections are necessary. Moreover, when the statistical interactions are considered, there may be some disadvantages in the idea of a fixed profile. Under such involved circumstances, it may be desirable to allow the vehicle to adjust the closing rate as a function of the conditions which exist at the time, rather than purely on the basis of range or time. Such a scheme would involve estimating the final range and closing rate dispersions which would result upon application of the final braking thrust, and an eventual adjustment of the closing rate if the estimated dispersions were unsatisfactory. Thus, the times and number of thrust applications would depend upon the particular circumstances encountered during homing, with due regard for system constraints.

3. Closure Times and Energy Requirements

The requirements for time and mass fraction to produce terminal closure under any one of the guidance laws discussed in the previous section can be obtained by programming the equations of motion for numerical solution and by substitution of given sets of initial conditions into the program. Although this technique has been employed frequently in the literature, it has the disadvantage that the solution is accurate only in the neighborhood of the initial set of conditions. Thus, for the present purposes a better approach is to present an analytic approximation which is reasonably valid than to discuss numerical solutions. This technique should have the advantage of pointing up the significant parameters.

Consider the two space curves representing the motion of the two vehicles in the following sketch.

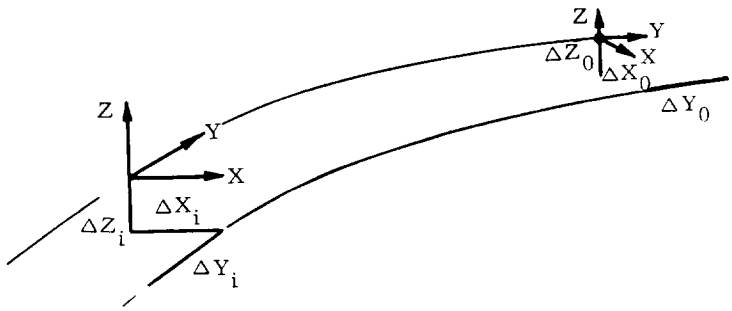

Given the position and velocity errors at a time corresponding to injection it is possible to compute the required change in position and velocity at a time in the future at which rendezvous is desired. This information is sufficient for a first order estimate of energy requirement if guidance schemes are not considered. (The energy requirement will be no more valid than this due to the fact that coupling of the differential equations will be neglected.)

The differential equations governing this maneuver are

$$\vec{F} = \dot{m}\vec{C} = (m_0 - \dot{m}t)\ddot{\vec{R}} \qquad (252)$$

or in terms of the various components of position

$$F_x = \dot{m}_x C = \left[m_0 - (\dot{m}_x + \dot{m}_y + \dot{m}_z)t\right] \ddot{x}(t)$$

$$= (m_0 - \dot{m}t)\ddot{x}$$

(where $\dot{m}$ represents the total mass flow rate assumed constant)

and the boundary conditions are $\vec{R} = \vec{R}_0$ and $\vec{V} = \vec{V}_0$ at $t = 0$ and $\vec{R} = \vec{V} = 0$ at $t = t_b$. The ground rule is that thrust be maintained constant. This, in turn, means that the induced velocity will be canceled at some point in the maneuver by reversing the thrust for the remaining burning time. It is noted that this is the general requirement. If the initial conditions are proper for a given thrust level and burning time, it will be possible to eliminate the necessity for thrust reversal. This will be seen in the discussions which follow.

Each of the components of position can be obtained as a function of burning time (prior to thrust reversal) by integrating

$$\ddot{x}(t) = \frac{\frac{F_x}{m_0}}{\left(1 - \frac{\dot{m}}{m_0}t\right)}$$

$$\dot{x}(t) = \frac{F_x}{m_0}\left[-\frac{m_0}{\dot{m}}\,\ell n\left(1 - \frac{\dot{m}}{m_0}t\right)\right] + C_1.$$

Now evaluating $\dot{x}$ at $t = 0$, yields $C_1 = \dot{x}_0$, thus

$$\dot{x}(t) = -\frac{F_x}{\dot{m}}\,\ell n\left(1 - \frac{\dot{m}}{m_0}t\right) + \dot{x}_0$$

$$x(t) = -\frac{F_x}{\dot{m}}\left(-\frac{m_0}{\dot{m}}\right)\left[\left(1 - \frac{\dot{m}}{m_0}t\right)\left\{\ell n\left(1 - \frac{\dot{m}}{m_0}t\right) - 1\right\}\right] + \dot{x}_0 t + C_2.$$

Again evaluating at $t = 0$ yields

$$x(t) = \frac{F_x m_0}{\dot{m}^2}\left[\left(1 - \frac{\dot{m}t}{m_0}\right)\left\{\ell n\left(1 - \frac{\dot{m}t}{m_0}\right) - 1\right\}\right]$$

(continued)

$$+ \dot{x}_0 t + x_0 + \frac{F_x m_0}{\dot{m}^2}$$

$$= \frac{F_x m_0}{\dot{m}^2}\left[\left(1 - \frac{\dot{m}t}{m_0}\right)\ell n\left(1 - \frac{\dot{m}t}{m_0}\right) + \frac{\dot{m}t}{m_0}\right] \quad (253)$$

$$+ \dot{x}_0 t + x_0$$

and similarly for y and z. But this solution is valid only for $t < t_1$ where t_1 is the time at which this component of thrust is reversed. At times greater than t_1 the same procedure must be utilized but T_x must be of the opposite sense.

$$\dot{x}(t) = \frac{F_x}{\dot{m}}\left[\ell n\left(1 - \frac{\dot{m}t}{M_0}\right)\right] + C_3$$

where

$$M_0 = m_0 - \dot{m}t_1$$

But $\dot{x}$ must be $\dot{x}_1$ at $t = t_1$. Thus

$$C_3 = \dot{x}_1 - \frac{F_x}{\dot{m}}\left[\ell n\left(1 - \frac{\dot{m}t_1}{M_0}\right)\right]$$

and

$$\dot{x}(t) = \frac{F_x}{\dot{m}}\left[\ell n\left(1 - \frac{\dot{m}t}{M_0}\right) - \ell n\left(1 - \frac{\dot{m}t_1}{M_0}\right) - \ell n\left(1 - \frac{\dot{m}t_1}{M_0}\right)\right] + \dot{x}_0$$

$$= \frac{F_x}{\dot{m}}\left[\ell n\left(1 - \frac{\dot{m}t}{M_0}\right) - \ell n\left\{\left(1 - \frac{\dot{m}t_1}{M_0}\right)\cdot\left(1 - \frac{\dot{m}t_1}{m_0}\right)\right\}\right] + \dot{x}_0.$$

At this point the relationship between t_1 for this coordinate and t_b can be determined by requiring that $\dot{x} = 0$ at $t = t_b$. Thus

$$1 - \frac{\dot{m}t_b}{M_0} = \left(1 - \frac{\dot{m}t_1}{M_0}\right)\left(1 - \frac{\dot{m}t_1}{m_0}\right) e^{-\dot{x}_0 \frac{\dot{m}}{F_x}}$$

or

$$t_b = \frac{M_0}{\dot{m}}\left[1 - \left(1 - \frac{\dot{m}t_1}{M_0}\right)\left(1 - \frac{\dot{m}t_1}{m_0}\right) e^{-\dot{x}_0 \frac{\dot{m}}{F_x}}\right] \quad (254)$$

$$\approx 2t_1 - 2\frac{\dot{m}t_1^2}{m_0} \text{ for } \dot{x}_0 = 0$$

Now continuing to the definition of x(t) yields

$$x(t) = \frac{F_x}{\dot{m}}\left[-\frac{M_0}{\dot{m}}\left(1 - \frac{\dot{m}t}{M_0}\right)\left\{\ell n\left(1 - \frac{\dot{m}t}{M_0}\right) - 1\right\}\right.$$

(continued)

$$\left. - t\,\ell n\left\{\left(1 - \frac{\dot{m}t_1}{M_0}\right)\left(1 - \frac{\dot{m}t_1}{m_0}\right)\right\}\right]$$

$$+ \dot{x}_0 t + C_4$$

where

$$x(t) = x_1 \text{ at } t = t_1.$$

Thus

$$C_4 = x_1 + \frac{F_x}{\dot{m}}\left[\frac{M_0}{\dot{m}}\left(1 - \frac{\dot{m}t_1}{M_0}\right)\left\{\ell n\left(1 - \frac{\dot{m}t_1}{M_0}\right) - 1\right\}\right.$$

$$\left. + t_1\,\ell n\left\{\left(1 - \frac{\dot{m}t_1}{M_0}\right)\left(1 - \frac{\dot{m}t_1}{m_0}\right)\right\}\right] - \dot{x}_0 t_1$$

$$= \frac{F_x}{\dot{m}^2}\left[m_0\left(1 - \frac{\dot{m}t_1}{m_0}\right)\ell n\left(1 - \frac{\dot{m}t_1}{m_0}\right) + \frac{\dot{m}t_1}{m_0}\right.$$

$$+ M_0\left(1 - \frac{\dot{m}t_1}{M_0}\right)\left\{\ell n\left(1 - \frac{\dot{m}t_1}{M_0}\right) - 1\right\}$$

$$\left. + t_1\,\ell n\left\{\left(1 - \frac{\dot{m}t_1}{M_0}\right)\left(1 - \frac{\dot{m}t_1}{m_0}\right)\right\}\right] + x_0$$

Now at $t = t_b$, $x = 0$, therefore

$$-x_0 = \frac{F_x}{\dot{m}^2}\left[-M_0\left(1 - \frac{\dot{m}t_b}{M_0}\right)\left\{\ell n\left(1 - \frac{\dot{m}t_b}{M_0}\right) - 1\right\}\right.$$

$$- \dot{m}(t_b - t_1)\,\ell n\left\{\left(1 - \frac{\dot{m}t_1}{M_0}\right)\left(1 - \frac{\dot{m}t_1}{m_0}\right)\right\}$$

$$+ m_0\left(1 - \frac{\dot{m}t_1}{m_0}\right)\ell n\left(1 - \frac{\dot{m}t_1}{m_0}\right) + \dot{m}t_1$$

$$\left. + M_0\left(1 - \frac{\dot{m}t_1}{M_0}\right)\left\{\ell n\left(1 - \frac{\dot{m}t_1}{M_0}\right) - 1\right\}\right] \quad (255)$$

This expression can be simplified by eliminating t_b from the equation using

$$t_b = \frac{M_0}{\dot{m}}\left[1 - A\left(1 - \frac{\dot{m}t_1}{M_0}\right)\left(1 - \frac{\dot{m}t_1}{m_0}\right)\right]$$

$$A = e^{-\dot{x}_0 \dot{m}/F_x} \quad (256)$$

or

$$t_b = \frac{M_0}{\dot{m}}(1 - A) + A\,2t_1\left(1 - \frac{\dot{m}}{m_0}t_1\right)$$

$$= \frac{M_0}{\dot{m}}(1 - A) + 2At_1\frac{M_0}{m_0} \quad (257)$$

Now letting $\frac{\dot{m}t_1}{m_0} = \xi_1$.

$$t_b = \frac{m_0}{\dot{m}} (1 - \xi_1)(1 - A) + 2A(1 - \xi_1) t_1$$

$$1 - \frac{\dot{m} t_b}{M_0} = 1 - \left[(1 - A) + 2A\xi_1\right]$$

$$= A - 2A\xi_1 = A(1 - 2\xi_1).$$

Thus

$$- x_0 = \frac{F_x}{\dot{m}^2} \Bigg[- A m_0 (1 - \xi_1)(1 - 2\xi_1) \left\{ \ell n\, A (1 - 2\xi_1) - 1 \right\} - \left\{ m_0 (1 - \xi_1)(1 - A) + m_0 \xi_1 \cdot (2A(1 - \xi_1) - 1) \right\} \ell n (1 - 2\xi_1) + \dot{m}_0 (1 - \xi_1) \ell n (1 - \xi_1) + m_0 \xi_1 + m_0 (1 - \xi_1) \left(1 - \frac{\xi_1}{1 - \xi_1}\right) \cdot \left\{ \ell n \left(1 - \frac{\xi_1}{1 - \xi_1}\right) - 1 \right\} \Bigg]$$

$$- x_0 = \frac{F_x m_0}{\dot{m}^2} \Bigg[- A (1 - 3\xi_1 + 2\xi_1^2) \ell n (1 - 2\xi_1) + (1 - 3\xi_1 + 2\xi_1^2)(1 - \ell n A) - \left\{ (1 - \xi_1)(1 - A) + \xi_1 \left[2A(1 - \xi_1) - 1 \right] \right\} \ell n (1 - 2\xi_1) + (1 - \xi_1) \ell n (1 - \xi_1) + \xi_1 + (1 - 2\xi_1) \left\{ \ell n (1 - 2\xi_1) - \ell n (1 - \xi_1) - 1 \right\} \Bigg].$$

Now adding and subtracting $(1 - 3\xi_1 + 2\xi_1^2) \ell n (1 - 2\xi_1)$ within the bracket yields

$$- x_0 = m_0 \frac{F_x}{\dot{m}^2} \left\{ \left[\xi_1 \ell n (1 - \xi_1) + 2\xi_1^2 \right] + (1 - 3\xi_1 + 2\xi_1^2) \left[(1 - A) \ell n (1 - 2\xi_1) - \ell n A \right] \right\} \quad (258)$$

This equation is solved for t_1; then the equation for t_b completes the solution. However, if ξ is of the order of 0.1 or less as it is for most maneuvers a further simplification can be achieved by expansion of $\ell n (1 - \xi)$

$$\ell n (1 - \xi) = - \xi - \xi_2^2.$$

Thus

$$- x = m_0 \frac{F_x}{\dot{m}^2} \left\{ \left[\xi_1^2 - \frac{\xi_1^3}{2} \right] + (1 - 3\xi_1 + 2\xi_1^2) \left[(1 - A)(- 2\xi_1 - 2\xi_1^2) - \ell n A \right] \right\}$$

$$\frac{\dot{m}^2 x_0}{m_0 F_x} = \ell n A + 2\xi_1 (1 - A) + \xi_1^2 (- 1 + 8(1 - A)) + \xi^3 \left(- \frac{1}{2} - 2(1 - A)\right) + \cdots \quad (259)$$

This is a cubic equation which can be solved by successive approximations. Since there exist three such equations (one for each of the coordinates) parametric data seems extremely impractical. However, the form of the solution is sufficiently simple to facilitate hand computions for any given set of initial conditions.

Once t_1 and t_b are known, the total mass fraction is simply

$$\xi = \frac{\dot{m} t_b}{m_0} = \frac{T t_b}{C m_0} \quad (260)$$

and the corresponding impulsive velocity is

$$\Delta V = g_0 I_{sp} \ell n \frac{1}{(1 - \xi)} \approx g_0 I_{sp} \xi = g_0 I_{sp} \frac{\dot{m} t_b}{m_0} = g_0 I_{sp} \frac{T}{C} \frac{t_b}{m_0} \quad (261)$$

Thus, in this fashion it is possible to evaluate the energy requirements for a rendezvous maneuver which approximates the guided maneuver.

Example. Consider a maneuver in the x-direction for which the initial conditions are $x = R_0 = x_0$, $\dot{x} = 0$, $t = t_b$, and $\frac{F}{W_0} = B$ or $\frac{F}{m_0} = B g_0$, where B is an unspecified constant. Since $\dot{x} = 0$, $A = 1$.

Thus

$$\frac{\dot{m}^2 x_0}{m_0 F_x} \approx - \xi_1^2 + O(\xi^3)$$

but

$$F_x = - \frac{F x_0}{R_0} = - F.$$

Thus

$$\frac{\dot{m}^2 x_0}{m_0 F} = \left(\frac{\dot{m} t_1}{m_0} \right)^2$$

$$t_1^2 = \frac{m_0 x_0}{F} = \frac{x_0}{B g_0}$$

and

$$t_b = 2t_1\left(1 - \frac{\dot{m}t_1}{m_0}\right)$$

$$\frac{\dot{m}}{m_0} = \frac{\dot{W}}{W_0} = \frac{F}{W_0 I_{sp}} = \frac{B W_0}{W_0 I_{sp}} = \frac{B}{I_{sp}}$$

$$t_b = 2\left[\left(\frac{x_0}{B g_0}\right)^{1/2} - \frac{1}{I_{sp}}\left(\frac{x_0}{g_0}\right)\right]$$

or

$$B = \frac{x_0/g_0}{\left(\frac{t_b}{2} + \frac{x_0}{I_{sp}\, g_0}\right)^2}.$$

Also

$$\xi_b = \frac{\dot{m}}{m_0}\, t_b$$

$$= \frac{2B}{I_{sp}}\left[\left(\frac{x_0}{B g_0}\right)^{1/2} - \frac{1}{I_{sp}}\left(\frac{x_0}{g_0}\right)\right] \qquad (262)$$

This expression shows the importance of several parameters. First, ξ_b will be larger for the higher acceleration levels (large B). This behavior results from the excessive propellant burned to cancel the velocity induced from t = 0 to t = t_1. The higher consumption, however, resulted in a lower value of closure time (t_b). The second parameter is the specific impulse (I_{sp}). This parameter enters into two stages: first, higher values of specific impulse reduce t_b, and second, the higher values of I_{sp} reduce $\dot{m}$. The contribution of both efforts is observed in the functional form of ξ_b, Eq (262).

To provide an idea of the magnitude of the required propellant fraction, consider

$x_0 = 10^5$ ft = 0.3048×10^5 m

B = 0.1

$g_0 = 32.2$ ft/sec$^2 \approx 980$ cm/sec^2

$I_{sp} = 300$ sec

$$\xi_b = \frac{0.2}{0.300}\left[\frac{10^3}{5.68} - \frac{1}{300}\,\frac{10^5}{32.2}\right]$$

$$= 0.666\left[0.176 - 0.013\right] = 0.108$$

$$t_b = \xi_b \frac{m_0}{\dot{m}} = \xi_b\left(\frac{I_{sp}}{B}\right)$$

$$= 0.108\,\frac{(300)}{0.1} = 322 \text{ sec}$$

$t_1 = 170$ sec

$$\Delta V \approx g_0 I_{sp} \xi_b = 32.2\,(300)\,(0.108)$$

= 1030 fps or 315 mps

Now consider the some problem but with acceleration levels of 0.075, 0.05, 0.03 and 0.01.

	B = 0.1	B = 0.075	B = 0.05	B = 0.03	B = 0.01
ξ_b	0.108	0.0955	0.0783	0.0616	0.0364
t_b (sec)	322	382	469	616	1103
t_1 (sec)	170	203	244	318	562
ΔV fps	1030	922	756	594	352
ΔV mps	315	281	231	181	107

The first observation is that the energy requirements are large. This fact is due to the assumption that the closure velocity was zero initially (as may be seen in Eq (259), and the fact that the assumed range at t = 0 was large. To provide an appreciation of the validity of the solution, however, a numerical check was made of this set of initial conditions utilizing a line of sight guidance law. The results of this investigation proved the validity of this approximation since the agreement of the results for the same closure times was essentially the same as those predicted.

A more realistic approach utilizing the fact that the vehicle should be placed ahead of the target at a slightly lower velocity in order to produce an inverse tail chase would of necessity reduce these energy requirements to the numbers more conventionally quoted. In fact by selecting the proper value of F and t_b for a given $\dot{x}_0\, \dot{y}_0\, \dot{z}_0$ it would be possible to eliminate the first type of thrust (i.e., toward the target) and accelerate continuously to the desired rendezvous. To provide more specific information for a particular guidance system, it is necessary to produce a numerical simulation of the maneuver. This has been accomplished for two of the rendezvous schemes, the first being a constant line of sight in inertial space and the second being a combination of a differential correction procedure and Method I. Table 2 presents typical numerical results for these techniques for a circular target orbit of approximately 180 km. Burnout occurs at 37 km for all runs, and two ascent range angles (cut off to apocynthian 180° and 90°) are presented. The differences in the numerical results are due to the fact that more energy is required for injection for the 90° ascents and the fact that the relative velocities near apocynthian for the 180° ascents are sufficiently lower to require longer closure times. As may be seen from Eq (259), the maneuver requirements for a lunar rendezvous and for an earth rendezvous would be the same. The same cannot, however, be said for that portion of the velocity required to inject into the orbit. Thus, the total maneuver requirements should be increased by the amount of the difference in the injection velocities to provide a better estimate of the total requirements for earth rendezvous

$$\Delta V_{\text{correction}} = (V_c - V_a)_{\oplus} - (V_c - V_a)_{\text{(}}$$

TABLE 2

Numerical Rendezvous Results

	Position			Velocity			Uncorrected Miss Distance	Method I		Method II	
ϕ Ascent	x_0(m)	y_0(m)	z_0(m)	$\dot{x}_0$(mps)	$\dot{y}_0$(mps)	$\dot{z}_0$(mps)	(km)	t	ΔV (mps)	t	ΔV (mps)
90	0	-33,109	-16,620	0	43.6	61.0	0	560	81.1	587	71.6
90	0	-35,693	-9,897	0	43.6	61.0	8.83	608	84.4	627	78.9
90	3,426	-35,528	-9,897	0	43.6	61.0	--	609	89.9	628	79.2
90	3,426	-28,554	-23,343	0	43.6	61.0	9.06	540	100.3	563	88.7
90	0	-28,760	-23,343	0	43.6	61.0	--	538	93.0	561	87.4
90	37,040	0	0	-64.6	0	0	0	557	71.9	580	71.9
90	33,617	0	6,723	-64.6	0	0	--	538	91.4	559	82.6
90	33,617	0	-6,723	-64.6	0	0	--	535	91.7	556	82.6
90	40,466	0	-6,723	-64.6	0	0	--	622	92.7	644	83.8
90	40,466	0	6,723	-64.6	0	0	8.98	616	92.7	644	83.8
180	0	-19,886	-31,299	0	-15.1	56.1	0	1081	66.1	1093	36.9
180	0	-27,729	-24,256	0	-15.1	56.1	14.48	1261	69.8	1269	45.1
180	23,706	-14,388	-24,256	0	-15.1	56.1	--	1162	101.5	470	57.0
180	23,706	-5,667	-27,891	0	-15.1	56.1	--	968	112.2	977	72.5
180	0	-5,667	-36,604	0	-15.1	56.1	--	843	66.8	853	64.6
180	37,040	0	0	-26.1	0	0	0	1061	40.8	1071	40.5
180	37,040	0	6,743	-26.1	0	0	--	1102	59.1	1112	51.8
180	45,003	0	6,743	-26.1	0	0	15.41	1207	64.6	1220	59.1
180	60,747	0	6,743	-26.1	0	0	--	1366	91.4	1383	68.3

Method 1 The inertial line of sight is maintained fixed.

Method 2 A computation is made using the equations of relative motion to yield a correction of position. Then as a final phase, the inertial line of sight is held constant as thrust nulls velocity and position errors.

NOTES:

x normal to track
y along track (i.e., along V)
z along radius

4. Terminal Guidance Smoothing Techniques

Tracking noise, in particular that which arises in radar skin tracking, has a profound effect on the probability of success in the rendezvous mission. Frequently, the basic accuracy of a homing tracker is not sufficient to allow guidance command computations without some smoothing. In this section two techniques for the smoothing of transverse angular rates of the line of sight are discussed. Emphasis is placed on the angular rates inasmuch as the effects of noise in these measurements are more severe than those in range. The two techniques are:

(1) Angular momentum smoothing.

(2) Sample data (digital) filtering.

The first technique takes advantage of the fact that the product of the square of range and the inertial angular rate of the line of sight is very nearly preserved during thrust-free flight. Thus, the average of this product over many points in time yields a near-optimal estimate of the "angular momentum" of the target-homing vehicle system. Division of this estimate by the square of the most recent value of range (suitably smoothed and updated) yields a near-optimal, updated estimate of the line-of-sight rate. Alternatively, division of the estimate of angular momentum by the most recent value of range yields a near-optimal, updated estimate of the transverse velocity.

The second technique is that of digital filtering of the line-of-sight rate, assumed to be of the form of a signal polynomial plus uncorrelated noise. This technique is the conventional sample data minimum mean square error scheme discussed by Blum (Ref. 17). While the angular momentum smoothing scheme is simple and effective, range measurements must be available. Sample data filtering on the angular rates does not depend on range information and is, hence, applicable to both collision and proportional navigation.

A third technique not discussed here is that of analog filtering of continuous data outputs from the tracker. The smoothing may involve either a straightforward low-pass filtering of the tracking outputs or the use of Wiener filters. The interested reader is directed to Refs. 18 through 26 on the topic of optimum mean square error filters for continuous processes.

The forms of the true rates ω_y and ω_p are suggested in the discussion of homing techniques formulated with respect to the line of sight. For thrust-free motion

$$\left.\begin{aligned} h_{\omega_p} &= R_0^2 \omega_{p_0} + \int_0^t R \Delta g_p \, dt \\ h_{\omega_y} &= R_0^2 \omega_{y_0} \end{aligned}\right\} \qquad (263)$$

where

$$\left.\begin{aligned} h_{\omega_p} &= R^2\omega_p \\ h_{\omega_y} &= R^2\omega_y \end{aligned}\right\} \quad (264)$$

Thus, for angular momentum smoothing, the yaw signal, h_{ω_y}, is a constant, while that of pitch is very nearly so if the gravity torque is small. For sample data filtering of the rates, ω_p and ω_y, substitution of Eq (264) into Eq (263) shows that

$$\left.\begin{aligned} \omega_p &= \frac{R_0^2\omega_{p_0}}{R^2} + \frac{1}{R^2}\int_0^t R\Delta g_p\, dt \\ \omega_y &= \frac{R_0^2\omega_{p_0}}{R^2} \end{aligned}\right\} \quad (265)$$

Over smoothing times much less than the total homing time, ω_p and ω_y, may be closely approximated by general polynomials in time. For example, if the closing rate is reasonably constant over the smoothing time,

$$\begin{aligned} R &\cong R_0 - (-\dot{R}_0)\, t \\ &\cong R_0\left(1 - \frac{t}{t_{G_0}}\right) \end{aligned} \quad (266)$$

where

$$t_{G_0} = \text{initial time-to-go} = \frac{-\dot{R}_0}{R_0} \quad (267)$$

Thus,

$$\begin{aligned} \omega_y &= \frac{\omega_{y_0}}{\left(1 - \frac{t}{t_{G_0}}\right)^2} \\ &= \omega_{y_0}\left(1 + 2\,\frac{t}{t_{G_0}} - 5\frac{t^2}{t_{G_0}^2} + \ldots\right) \end{aligned} \quad (268)$$

and similarly for ω_p except that an additional expansion is required due to the presence of the gravity torque.

Thus, in both schemes it can be said that the true signal is a polynomial in time. In the case of angular momentum smoothing the behavior is nearly a constant in pitch and truly a constant in yaw. The angular rates are polynomials of higher order depending on the smoothing time. For very short smoothing times a linear variation is valid. For moderate to reasonably long smoothing times a second or third order polynomial is valid.

a. Angular momentum smoothing

Let

$$h_{p,y} = \text{estimate of } h_{\omega_p},\ h_{\omega_y}$$

then assuming a large number of samples, N, over the smoothing interval,

$$h_{p,y} = \frac{1}{N}\sum_{i=1}^{N}\left(h_{\omega_{p,y}}\right)_i \quad (269)$$

may be used to smooth the angular momentum over thrust-free periods. In the following, the range measurements are considered to be noiseless since current trackers have range accuracies giving rise to negligible transverse guidance errors. The input to the smoothing process may be written as

$$\left.\begin{aligned} \left(h_{\omega_p}\right)_i &= R_0^2\omega_{p_0} + R_i^2\delta\omega_{p_i} \\ &\quad + \int_{t_0}^{t_0+t_i} R\Delta g_p\, dt \\ \left(h_{\omega_y}\right)_i &= R_0^2\omega_{y_0} + R_i^2\delta\omega_{y_i} \end{aligned}\right\} \quad (270)$$

where

$\delta\omega_p$ = pitch rate noise of line of sight

$\delta\omega_y$ = yaw rate noise of line of sight.

Thus,

$$\left.\begin{aligned} h_p &= R_0^2\omega_{p_0} + \frac{1}{N}\sum_{i=1}^{N} R_i^2\delta\omega_{p_i} \\ &\quad + \frac{1}{N}\sum_{i=1}^{N}\int_{t_0}^{t_0+t_i} R\Delta g_p\, dt \\ h_y &= R_0^2\omega_{y_0} + \frac{1}{N}\sum_{i=1}^{N} R_i^2\delta\omega_{y_i} \end{aligned}\right\} \quad (271)$$

At the end of the smoothing interval at which the estimates are to apply, the true values of the angular momenta are

$$h_p = R_0^2 \omega_{p_0} + \int_{t_0}^{t_0 + t_N} R\Delta g_p \, dt$$

$$h_y = R_0^2 \omega_{y_0} \qquad (272)$$

Hence, the errors in the estimates are

$$\delta h_p = \frac{1}{N} \sum_{i=1}^{N} R_i^2 \delta\omega_{p_i} - \frac{1}{N} \sum_{i=1}^{N} \int_{t_0+t_i}^{t_0+t_N} R\Delta g_p \, dt$$

$$\delta h_y = \frac{1}{N} \sum_{i=1}^{N} R_i^2 \delta\omega_{y_i} \qquad (273)$$

Utilizing the apparent gravity effects (discussed earlier) and the fact that range decreases monotonically, Eq (273) are seen to be bounded by

$$(\delta h_p)_{max} = \frac{R_0}{N} \sum_{i=1}^{N} \delta V_{p_i} + \frac{3}{4} \frac{GM}{r_t^3} R_0^2 t_N$$

$$(\delta h_y)_{max} = \frac{R_0}{N} \sum_{i=1}^{N} \delta V_{y_i} \qquad (274)$$

where

$$\delta V_{p_i} = R_i \delta\omega_{p_i}$$

$$\delta V_{y_i} = R_i \delta\omega_{y_i} \qquad (275)$$

Hence,

$$(\delta V_p)_{max} = \frac{(\delta h_p)_{max}}{R} = \left(\frac{R_0}{R}\right) \frac{1}{N} \sum_{i=1}^{N} \delta V_{p_i} + \frac{3}{4} \frac{GM}{r_t^3} \frac{R_0^2}{R} t_N$$

$$(\delta V_y)_{max} = \frac{(\delta h_y)_{max}}{r} = \left(\frac{R_0}{R}\right) \frac{1}{N} \sum_{i=1}^{N} \delta V_{y_i} \qquad (276)$$

Using Eq (266) with $t = t_N << t_{G_0}$

$$(\delta V_p)_{max} \cong \frac{1}{N} \sum_{i=1}^{N} \delta V_{p_i} + \frac{3}{4} \frac{GM}{r_t^3} Rt_N$$

$$(\delta V_y)_{max} \cong \frac{1}{N} \sum_{i=1}^{N} \delta V_{y_i} \qquad (277)$$

Thus, since the samples are uncorrelated, the maximum values for the standard deviations are

$$\max \sigma_{V_p} = \frac{1}{\sqrt{N}} \left(\sigma_{V_{p_i}}\right)_{max}$$

$$\max \sigma_{V_y} = \frac{1}{\sqrt{N}} \left(\sigma_{V_{y_i}}\right)_{max} \qquad (278)$$

and the maximum mean pitch velocity error is

$$\max \mu_{V_p} = \frac{3}{4} \frac{GM}{r_t^3} Rt_N \qquad (279)$$

The fact that the velocity error due to the gravity torque is negligible is apparent upon substitution of some numbers. For a target in a circular orbit of 500 naut mi or 926 km altitude and a relative range of 25 naut mi or 46.3 km, a smoothing time of 10 sec yields

$$\max \mu_{V_p} \cong 1 \text{ fps or } 0.3 \text{ mps}$$

At a relative range of 5 mi or 8.7 km this maximum error becomes 0.2 fps or 0.036 mps; at 1 mi or 1.73 km; 0.04 fps or 0.012 mps. Thus, while the bias error is initially large, it quickly drops to a negligible level at small ranges where fine accuracy is required. This is to be expected since the differential gravity acceleration diminishes as range goes to zero. Thus, Eqs (278) and (279) remain as the principal errors, showing that the angular momentum smoothing scheme yields residual transverse velocity errors which decrease with the square root of the number of samples used in the process.

b. Sample data filtering

Blum (Ref. 17) presents an exact formula for the output noise power of an optimum digital filter designed to make a zero-lag estimate of the input or its derivatives. The input model consists of a polynomial signal plus stationary uncorrelated noise. Graphs and tables of the rms error for the zero-lag estimation of the 0th, 1st and 2nd derivatives are given as a function of the input polynomial up to degree 5 and memory spans up to 10 sample points.

The work of Blum in sampled data filters is discussed in this section, to the extent of introducing the variables and notation used in his graphs and tables, and the results that he derives.

Consider a set of equally spaced data points (u, y_u) $u = 1, 2, \ldots, M$. The problem is to fit a least squares polynomial of degree n to these points and to estimate the Kth derivative of the observed data from the curve fit at any point on the u scale.

For the purpose of the analysis it is convenient to utilize orthogonal polynomials in the curve fitting procedure. Thus let the true polynomial be given by

$$P(u) = \sum_{L=0}^{n} \alpha_L \xi_L(u), \quad u = 1, 2, \ldots, M \tag{280}$$

where the polynomials $\xi_L(u)$ are orthogonal, (Ref. 28) e.g., satisfy the following relationships

$$\sum_{u=1}^{M} \xi_h(u)\xi_L(u) = 0, \quad h \neq L, \tag{281}$$

$$\sum_{u=1}^{M} \xi_L{}^2(u) = S(L, M). \tag{282}$$

It is assumed that the observations y_u are given by

$$y_u = P(u) + N(u).$$

The N(u) are assumed to be random, stationary, and uncorrelated errors.

Then the least squares estimates $\hat{\alpha}_L$ of the coefficients α_L are obtained by minimizing

$$I = \sum_{u=1}^{M} \left[\sum_{L=0}^{n} \hat{\alpha}_L \xi_L(u) - y_u \right]^2 \tag{283}$$

with respect to each of the parameters $\hat{\alpha}_L$.

Thus one obtains

$$\frac{\partial I}{\partial \hat{\alpha}_L} = \sum_{u=1}^{M} 2\left[\sum_{v=0}^{n} \hat{\alpha}_v \xi_v(u) - y_u \right] \xi_L(u) = 0, \quad L = 0, 1, \ldots, n. \tag{284}$$

Solving Eq (284) for α_L one obtains

$$\hat{\alpha}_L = \sum_{u=1}^{M} \frac{y_u \xi_L(u)}{S(L, M)}, \quad L = 0, 1, \ldots, n. \tag{285}$$

By substituting Eq (285) one obtains the curve fit relationship

$$Y(u) = \sum_{L=0}^{n} \hat{\alpha}_L \xi_L(u). \tag{286}$$

To evaluate the estimate of the Kth derivative at $u = M + \alpha$ one need only take the Kth derivative of both sides of Eq (286) (considering u as a continuous variable), and obtain

$$\left.\frac{d^K Y(u)}{du^K}\right|_{u=M+\alpha} \equiv Y^{(K)}_{(M+\alpha)} = \sum_{L=K}^{n} \hat{\alpha}_L \left.\frac{d^K}{du^K} \xi_L(u)\right|_{u=M+\alpha} \tag{287}$$

Let

$$\left.\frac{d^K}{du^K} \xi_L(u)\right|_{u=M+\alpha} \equiv \xi_L{}^{(K)}(M + \alpha) \tag{288}$$

Now, substituting Eqs (285) and (287) yields

$$Y^{(K)}(M + \alpha) = \sum_{L=K}^{n} \sum_{u=1}^{M} \frac{y_u \xi_L(u) \xi_L{}^{(K)}(M + \alpha)}{S(L, M)} \tag{289}$$

Let

$$W^*_{M-u} = \sum_{L=K}^{n} \frac{\xi_L(u)\xi_L{}^{(K)}(M + \alpha)}{S(L, M)}, \quad u = 1, 2, \ldots, M \tag{290}$$

then

$$Y^{(K)}_{M+j}(M + \alpha + j) = \sum_{u=1}^{M} W^*_{M-u} y_{u+j}, \quad j = 0 \pm 1 \pm 2 \ldots. \tag{291}$$

Equation (291) is directly interpreted as the input-output relationship of a digital filter with weighting sequence $W^*_0, W^*_1, \ldots, W^*_{M-1}$. The input is the sequence y_{u+j} and the output is $Y_{M+j}(M + j + \alpha)$. The output is available in real time after the last data point is sampled and estimates the Kth derivative of the input at $u = M + \alpha + j$. The filter has a finite memory over the interval $(M - 1)T$.

Since the estimators $\hat{\alpha}_L$ are unbiased, the error in estimate is given by (j = 0),

$$\Delta = \left[Y_M^{(K)}(M+\alpha) - \sum_{L=K}^{n} \alpha_L \xi_L^{(K)}(M+\alpha) \right]$$

$$\Delta = \sum_{u=1}^{M} W^*_{M-u} N(u). \tag{292}$$

The mean square error of estimate is given by

$$\sigma_\Delta^2 = \alpha_N^2 \sum_{u=1}^{M} \left[W^*_{M-u} \right]^2 \tag{293}$$

(σ_N^2 = noise mean square error).

Substituting Eqs (281) and (282) into Eq (293) yields,

$$\frac{\sigma_\Delta^2}{\sigma_N^2} \equiv \delta^2(M, \alpha, K, n) = \sum_{L=K}^{n} \frac{\left[\xi_L^{(K)}(M+\alpha) \right]^2}{S(L, M)} \tag{294}$$

which is the main result of this section.

Equation (294) has been derived for unit time between samples. If the interval between samples is given by T, then Eq (290) is modified as follows:

$$W^*_{M-u,\,T} = \frac{1}{(T)^K} W_{M-u}, \tag{295}$$

and Eq (294) becomes

$$\frac{\sigma_\Delta^2 (T)^{2K}}{\sigma_N^2} = \delta^2(M, \alpha, K, n). \tag{296}$$

Note that

$$\delta^2(M, \alpha, K, n) = \delta^2(M, \alpha, K, n-1) + \frac{\left[\xi_n^{(K)}(M+\alpha) \right]^2}{S(n, -M)}, \tag{297}$$

so that increasing the degree of curve fit is never associated with a decrease in α_Δ^2 since the second term of Eq (297) is positive definite for fixed M, α, and K.

Special case. Special formulas for δ^2 are as follows. Let K = 0, α = 0, -1, -2, . . . , (M - 1) then

$$\delta^2(M, \alpha, 0, n) = W^*_{-\alpha}.$$

As an example, when α = 0, K = 0, one obtains a zero-lag estimate of the input. The mean square error output is then proportional to W_0, the coefficient which multiplies the latest data point, e. g. ,

$$\sigma_\Delta^2 = \sigma_N^2 \cdot W_0^*.$$

Other relationships on the δ which may be useful are as follows. Let the order of the derivative equal the order of degree of curve fit, e. g. , K = n, then

$$\delta^2(M, \alpha, n, n) = \frac{(n!)^2}{S(n, M)} \tag{298}$$

and is independent of α.

Let the order of the derivative equal one less than the degree of the curve fitting polynomial, e. g. , K = n - 1, then

$$\delta^2(M, \alpha, n-1, n) = \delta^2(M, \alpha, n-1, n-1) + \left[\frac{M + 2\alpha - 1}{2} \right]^2 \delta^2(M, \alpha, n, n) \tag{299}$$

$$= \frac{[(n-1)!]^2}{S(n-1, M)} + \left[\frac{M + 2\alpha - 1}{2} \right]^2 \frac{[n!]^2}{S(n, M)} \tag{300}$$

When α = - (M - 1)/2; e. g. , the midpoint of the curve fitting interval,

$$\delta(M, \alpha = -\left[\frac{M-1}{2} \right], n-1, n) = \delta^2(M, \alpha, n-1, n-1). \tag{301}$$

This represents the minimum δ^2 obtainable with respect to α.

Tables 3, 4 and 5 present the exact values of δ using Eq (296). Figures 11, 12 and 13 present a plot of δ using Eq (294) for M = 10 to 100 for purposes of interpolation.

Equation (296) is identical with the results one would obtain from Blum (Ref. 30) as are the values of the weighting sequence.

The interpretation of the parameter α is as follows: when α = 0, one obtains a zero-lag estimate with respect to the latest data point, when - (M - u $\rightarrow$ 1) < α > 0, one obtains an extrapolation, and when (M - 1) < α < 0, one obtains interpolation of the input polynomial. A more

detailed discussion of σ_Δ^2 as a function of α is available (Ref. 28).

Table 6 contains a summary of a few useful properties of the orthogonal polynomials. A listing of the orthogonal polynomials in consistent notation is shown in Table 5 of Ref. 29.

The functions satisfy the following recursion relationship

$$\xi_{v+1}(u) \equiv \xi_1(u)\,\xi_v(u) - \frac{v^2(M^2 - v^2)}{4(4v^2 - 1)}\,\xi_{v-1}(u) \quad (302)$$

As indicated, the recursion is an identity so that by repeated differentiation one obtains

$$\xi_{v+1}^{(L)}(u) \equiv \xi_1(u)\,\xi_v^{(L)}(u) + L\,\xi_v^{(L-1)}(u) - \frac{v^2(M^2 - v^2)}{4(4v^2 - 1)}\,\xi_{v-1}^{(L)}(u), \quad (303)$$

where

$$\xi_x^{(L)}(u) = 0,\ L < 0,\ x < 0,\ L > x, \text{ and}$$

where $\xi_L^{(L)} = L!$

so that

$$\xi_{v+1}^{(L)}(M+\alpha) \equiv \left[\frac{2\alpha + M - 1}{2}\right]\xi_v^{(L)}(M+\alpha) + L\,\xi_v^{(L-1)}(M+\alpha) - v^2\,\frac{\left[M - v^2\right]}{4(4v^2 - 1)}\,\xi_{v-1}^{(L)}(M+\alpha). \quad (304)$$

Finally, the sum of squares S(L, M) is given by Ref. 30.

$$S(L, M) = \frac{(L!)^4 \prod_{j=-L}^{+L}(M - j)}{(2L)!\,(2L+1)!} \quad (305)$$

Higher order polynomials to degree 10 are listed by Allen (Ref. 31). A very complete table of the values of $\xi_v(u)$ for v = 0, to 5, u from v + 2 to 104 is made available by Anderson and Houseman (Ref. 30).

c. Conclusion

An exact equation for the mean square error of the output of an optimum digital filter has been presented. The formula was derived using curve fitting concepts to demonstrate the relationship between the concepts of parameter estimation in curve fitting and weighting function optimization in linear filtering.

Equation (290) represents a convenient formula for computing the weighting sequence of the digital filter.

From Tables 3, 4 and 5, one may determine the exact value of δ for small M.

In Figures 16, 17 and 18, the values of δ can be determined for those values of M not tabulated. For M > 100, one can extrapolate linearly on log-log paper.

TABLE 3

Table of $\delta(M, \alpha, K, n)$, $\alpha = 0$, K = 0 for Evaluating the RMS Error for Zero-Lag ($\alpha = 0$) Estimation of the Input (K = 0) as a Function of the Degree of the Curve Fitting Polynomial (n) and the Number of Data Points (M)

M/n →		0	1	2	3	4	5
2	δ	0.70711					
3	δ	0.57735	0.91287				
4	δ	0.50000	0.83666	0.97468			
5	δ	0.44721	0.77460	0.94112	0.99283		
6	δ	0.40825	0.72375	0.90633	0.97996	0.99801	
7	δ	0.37796	0.68139	0.87287	0.96362	0.99348	0.99946
8	δ	0.35355	0.64550	0.84162	0.94548	0.98665	0.99796
9	δ	0.33333	0.61464	0.81278	0.92660	0.97800	0.99533
10	δ	0.31623	0.58775	0.78625	0.90762	0.96802	0.99157
20	δ	0.22361	0.43095	0.60892	0.74985	0.85231	0.92022
50	δ	0.14142	0.27865	0.40784	0.52578	0.63011	0.71946
95	δ	0.10260	0.20359	0.30142	0.39471	0.48223	0.56299
1001	δ	0.031607	0.063167	0.094632	0.12596	0.15709	0.18800

TABLE 4

Table of $\delta(M, \alpha, K, n)$, $\alpha = 0$, K = 1 for Evaluating the RMS Error for Zero-Lag ($\alpha = 0$) Estimation of the First Derivative of the Input (K = 1) as a Function of the Degree of the Curve Fitting Polynomial (n) and the Number of Data Points (M)

M/n →		1	2	3	4	5
2	δ	1.414				
3	δ	0.70711	2.5495			
4	δ	0.44721	1.5652	3.83695		
5	δ	0.31623	1.1148	2.52566	5.5839	
6	δ	0.23905	0.85252	1.90348	3.6802	8.2418
7	δ	0.18898	0.68138	1.52189	2.8226	5.2190
8	δ	0.15430	0.56167	1.26041	2.3028	3.9614
9	δ	0.12910	0.47377	1.06943	1.9445	3.2351
10	δ	0.11010	0.40685	0.92389	1.6794	2.7476
20	δ	0.038778	0.14855	0.35079	0.65608	1.0684
50	δ	0.0097999	0.038494	0.093871	0.18201	0.30714
95	δ	0.0037414	0.014821	0.036558	0.071883	0.12326
1001	δ	0.000109380	0.00043711	0.0010913	0.0021790	0.0038054

TABLE 5

Table of $\delta(M, a, K, n)$, a = 0, K = 2 for evaluating the RMS error for zero-lag (a = 0) estimation of the second derivative of the input (K = 2) as a function of the degree of the curve fitting polynomial (n) and the number of data points (M)

M/n →		2	3	4	5
3	δ	2.4495			
4	δ	1.0	6.7823		
5	δ	0.53452	3.2071	14.017	
6	δ	0.32733	1.8919	7.0312	26.312
7	δ	0.21822	1.2440	4.3582	13.334
8	δ	0.15430	0.87535	2.9852	8.4113
9	δ	0.11396	0.64578	2.1729	5.8714
10	δ	0.087039	0.49355	1.6494	4.3527
20	δ	0.015094	0.087123	0.29179	0.74414
50	δ	0.0015194	0.0089549	0.030657	0.079685
95	δ	0.00030512	0.0018129	0.0062672	0.016468
1001	δ	0.84641×10^{-6}	0.50735×10^{-5}	0.17741×10^{-4}	0.47264×10^{-4}

TABLE 6

Orthogonal Polynomials

$$\xi_0(u) = 1$$

$$\xi_1(u) = (u - \bar{u}),\ \bar{u} = \frac{M+1}{2}$$

$$\xi_2(u) = (u - \bar{u})^2 - \frac{M^2 - 1}{12}$$

$$\xi_3(u) = (u - \bar{u})^3 - (u - \bar{u})\left[\frac{3M^2 - 7}{20}\right]$$

$$\xi_4(u) = (u - \bar{u})^4 - (u - \bar{u})^2\left[\frac{3M^2 - 13}{14}\right] + \frac{3(M^2 - 1)(M^2 - 9)}{560}$$

$$\xi_5(u) = (u - \bar{u})^5 - (u - \bar{u})^3\left[\frac{5(M^2 - 7)}{18}\right] + (u - \bar{u})\left[\frac{15M^4 - 230M^2 + 407}{1008}\right]$$

5. Long Time Closure

If relatively long times are acceptable for closure, several computational schemes may be employed. One such method has been developed by D. F. Lawden and is reported in Ref. 31. The solution outlined is directed primarily toward the correction of interplanetary orbits but is sufficiently general that it may be utilized for this problem as well. The major disadvantage of this solution for manual computation is the iteration procedure required to define the modified or closure orbit.

A general solution may be obtained by considering the requirements for closure (i.e., the radius identity at the point of rendezvous and specified time of closures). This analysis yields two equations with 3 unknowns (Δa, Δe and $\Delta\omega$); however, these new variables are in turn functions of Δr which is a known error and ΔV_1 and $\Delta\gamma_1$ which are the differences in velocity and flight path angle immediately after the corrective pulse relative to those of the target vehicle at the same time. This analysis yields the following equations when second order terms in Δa, Δe and $\Delta\omega$ are neglected.

$$\left[1 - \frac{2e_f \Delta e}{1 - e_f^2}\right]\left[1 + \frac{\Delta a}{a}\right] = \frac{1 + (e_f + \Delta e)\cos(\theta_{f2} + \Delta\omega)}{1 + e_f \cos\theta_{f2}}$$

$$\frac{\Delta t\, 2\pi}{\tau} = E_{t2} - E_{t1} - (e_f + \Delta e)(\sin E_{t2} - \sin E_{t1})$$

$$E_{t1} = 2\tan^{-1}\left[\sqrt{\frac{1-(e_f+\Delta e)}{1+(e_f+\Delta e)}}\ \tan\ \frac{(\theta_{f2} - \Delta\theta - \Delta\phi + \Delta\omega)}{2}\right]$$

$$E_{t2} = 2\tan^{-1}\left[\sqrt{\frac{1-(e_f+\Delta e)}{1+(e_f+\Delta e)}}\ \tan\ \frac{(\theta_{f2} + \Delta\omega)}{2}\right]$$

where

Δa, Δe and $\Delta\omega$ are the required changes in the orbital parameters as defined in the following discussion of the variation of parameters technique.

θ_{f2} is the angle from perigee to the point of rendezvous in the target orbit.

$\Delta\theta$ is the angle subtended by the target vehicle in moving from t_1 to t_2.

$\Delta\phi$ is the central angle between the two vehicles at t_1

The resultant equations for this solution are so complex in nature that the solution appears unattractive.

A third method may be obtained by adapting the "Variational Method for General Orbital Errors Analysis" reported in Chapter 12. The equations for this solution are summarized below.

$$\theta_{f2} = \theta_{f2}(\theta_{f1}, t_{closure}, e_f)$$

$$\Delta\phi_2 = \Delta\omega - \frac{(1+e\cos\theta_{f2})^2}{(1-e^2)^{3/2}}\left[\sqrt{\frac{\mu}{a^3}}\,\Delta t_p + \frac{3M\Delta a}{2a}\right] + \frac{\sin\theta_{f2}\,(2 + e\cos\theta_{f2})}{1 - e^2}\Delta e \qquad (306)$$

$$\Delta r_2 = \left[\frac{1 - e^2}{1 + e\cos\theta_{f2}} - \frac{3eM\sin\theta_{f2}}{2(1-e^2)^{1/2}}\right]\Delta a - a\cos\theta_{f2}\,\Delta e - \sqrt{\frac{\mu}{a}}\,\frac{e\sin\theta_{f2}\,\Delta t_p}{(1-e^2)^{1/2}} \qquad (307)$$

$$\Delta a = \frac{2(1 + e\cos\theta_{f1})^2\,\Delta r_1}{(1 - e^2)^2} + \qquad \text{(continued)}$$

$$+ 2\sqrt{\frac{a^3}{\mu}}\ \frac{(1+2e\cos\theta_{f1}+e^2)\Delta V_1}{1-e^2} \qquad (308)$$

$$\Delta e = \frac{(e+\cos\theta_{f1})(1+e\cos\theta_{f1})\Delta r_1}{a(1-e^2)^2}$$

$$+ 2(e+\cos\theta_{f1})\sqrt{\frac{a(1-e^2)}{\mu(1+2e\cos\theta_{f1}+e^2)}}\ \Delta V_1$$

$$+ \frac{(1-e^2)\sin\theta_{f1}}{1+e\cos\theta_{f1}}\ \Delta\gamma_1 \qquad (309)$$

$$\Delta\omega = \frac{\sin\theta_{f1}(1+e\cos\theta_{f1})\Delta r_1}{ae(1-e^2)}$$

$$+ 2\sin\theta_{f1}\sqrt{\frac{a(1-e^2)}{\mu(1+2e\cos\theta_{f1}+e^2)}}\ \Delta V_1$$

$$- \left[2 + \frac{(1-e^2)\cos\theta_{f1}}{e(1+e\cos\theta_{f1})}\right]\Delta\gamma_1 \qquad (310)$$

$$\Delta t_p = \sqrt{\frac{a^3}{\mu}}\left\{\frac{(1-e^2)^{3/2}}{(1+e\cos\theta_{f1})^2}\left[(\Delta\omega - \Delta\phi_1)\right.\right.$$

$$\left.\left. + \frac{\sin\theta_{f1}(2+e\cos\theta_{f1})}{1-e^2}\Delta e\right] - \frac{3M\Delta a}{2a}\right\} \qquad (311)$$

This analysis assumes that the orbits of the target and shuttle vehicle during closure are very similar and treats the displacement at the initially selected point of rendezvous, or any other point where the vehicles are sufficiently close, as an error in the position at that time of the target vehicle. The solution is made in the following sequence:

(1) The required changes in a, e, ω and t_p are computed in terms of known errors Δr_1 and $\Delta\phi_1$, and the desired parameters ΔV_1 and $\Delta\gamma_1$.

(2) These equations in terms of two unknowns are then substituted into the equations for Δr_2 and $\Delta\phi_2$.

(3) The equations for errors in position at point 2 are equated to 0 and the resultant equations solved simultaneously for ΔV_1 and $\Delta\gamma_1$.

(4) With knowledge of the velocity and flight path angle both before and after the application of the corrective pulse, the magnitude and direction of the pulse required may be computed from the law of cosines.

This analysis is general and could be employed for the case of short time closure as well (this implies large changes in a, e, ω, t_p) were it not for the fact that second order terms in ΔV_1, $\Delta\gamma_1$ and Δr_1 have been neglected in the derivation. This does not preclude the possibility of including these terms in the definition of Δa, Δe, $\Delta\omega$ and Δt_p; however, this incorporation is felt to be excessively laborious.

Sample problem. The utilization of this closure analysis is illustrated in the following sample problem.

$a_{24} = 1.38337 \times 10^8$ ft = 42165.1 km

$e_{24} = 0.61832$

$\theta_{f1} = 107.90°$

$t_{f1} = 8339.5$ sec

$V_{f1} = 12840$ fps = 3913.63 m/sec

$r_{f1} = 20{,}000$ stat mi = 32186.9 km

$\Delta r_1 = 16.6426$ stat mi = 26.7837 km

$\Delta\phi_1 = 0.019222$ rad

$V_{t1} = 8776$ fps = 2675 m/sec

$t_{closure} = 20{,}000$ sec

$\gamma'_{t1} = 36.008°$

Note:

X'_{t1} parameter in transfer orbit before initiating closure

X_{t1} parameter in closure orbit at time of pulse

X_{f1} parameter in target orbit at time of pulse

X_{f2} parameter in target orbit at rendezvous

X_{24} target 24-hr orbit

$t_{f2} = 28340$ sec

$$M_{f2} = \frac{2\pi t_{f2}}{\tau} = 2.066592$$

From Fig. 1

$E_K \approx 2.46$ rad

$$E_{K+1} = \frac{e(\sin E_K - E_K\cos E_K) + M}{1 - e\cos E_K}$$

$= 2.457386$ rad $= 140.7984°$

$$\theta_{f2} = 2\tan^{-1}\left[\sqrt{\frac{1+e}{1-e}}\ \tan\frac{E_{f2}}{2}\right] = 160.3768°$$

$$\Delta a = \frac{2(1+e\cos\theta_{f1})\Delta r_1}{(1-e^2)^2} + 2\sqrt{\frac{a^3(1+2e\cos\theta_{f1}+e^2)}{\mu(1-e^2)}}\Delta V_1$$

$$= (30.1577 + 3.49074\,\Delta V_1) \times 10^4 \text{ (ft)}$$

where ΔV_1 is expressed in feet per second.

$$\Delta e = \frac{(e + \cos\theta_{f1})(1 + e\cos\theta_{f1})\,\Delta r_1}{a(1-e^2)} + 2(e + \cos\theta_{f1})\sqrt{\frac{a(1-e^2)}{\mu(1 + 2e\cos\theta + e^2)}}\,\Delta V_1 + \frac{(1-e^2)\sin\theta_{f1}\,\Delta\gamma}{1 + e\cos\theta_{f1}}$$

$$= \left[2.08560 + 0.482328\,\Delta V_1 + 7261.03\,\Delta\gamma\right] \times 10^{-4}$$

$$\Delta\omega = \frac{\sin\theta_{f1}(1 + e\cos\theta_{f1})\,\Delta r_1}{ae(1-e^2)} + \frac{2\sin\theta}{e}\sqrt{\frac{a(1-e^2)}{\mu(1 + 2e\cos\theta_{f1} + e^2)}}\,\Delta V_1 - \left[2 + \frac{(1-e^2)\cos\theta_{f1}}{e(1 + e\cos\theta_{f1})}\right]\Delta\gamma$$

$$= (12.80025 + 2.396265\,\Delta V_1 - 16188.96\,\Delta\gamma_1) \times 10^{-4}$$

$$\Delta t_p = \sqrt{\frac{a^3}{\mu}}\left\{\frac{(1-e^2)^{3/2}}{(1+e\cos\theta_{f1})^2}\left[\Delta\omega - \Delta\phi_1 + \frac{\sin\theta_{f1}(2+e\cos\theta_{f1})\,\Delta e}{1-e^2}\right] - \frac{3M\Delta a}{2a}\right\}$$

$$\Delta t_p = \left[1.016824(\Delta\omega - \Delta\phi_1) + 2.832749\,\Delta e\right] - 0.452128 \times 10^{-8}\,\Delta a \times 10^4$$

$$= -190.165412 + 2.224632\,\Delta V_1 + 4107.37\,\Delta\gamma_1$$

Now since it is desired to rendezvous at θ_{f2}, it is known that $\Delta\phi_2 = \Delta r_2 = 0$. Re-evaluating the equations for $\Delta\phi$ and Δr at θ_{f2} and equating them to zero yields

$$\Delta\phi_2 = \Delta\omega - \frac{(1+e\cos\theta_{f2})^2}{(1-e^2)^{3/2}}\left[\sqrt{\frac{\mu}{a^3}}\,\Delta t_p + \frac{3M\Delta a}{2a}\right] + \frac{\sin\theta_{f2}(2 + e\cos\theta_{f2})\,\Delta e}{1-e^2}$$

$$0 = \Delta\omega - 0.262335 \times 10^{-4}\,\Delta t_p - 0.806135 \times 10^{-8}\,\Delta a + 0.770742\,\Delta e$$

$$\Delta r_2 = \left[\frac{1-e^2}{1 + e\cos\theta_{f2}} - \frac{3Me\sin\theta_{f2}}{2(1-e^2)^{1/2}}\right]\Delta a - a\cos\theta_{f2}\,\Delta e - \sqrt{\frac{\mu}{a}}\,\frac{e\sin\theta_{f2}\,\Delta t_p}{(1-e^2)^{1/2}}$$

$$0 = 0.660121\,\Delta a + 1.303016 \times 10^8\,\Delta e - 0.266530 \times 10^4\,\Delta t_p$$

Substituting for Δa, Δe, $\Delta\omega$ and Δt_p their equivalents in terms of ΔV_1 and $\Delta\gamma_1$ yields

$$0.629591\,\Delta V + 11670.08\,\Delta\gamma = 39.983576$$

$$2.33986\,\Delta V + 8366.51\,\Delta\gamma = -73.310088$$

Solving these equations simultaneously produces

$$\Delta V_1 = -53.998 \text{ fps} = -16.459 \text{ m/sec}$$

$$\Delta\gamma_1 = 0.00634 \text{ rad} = 0.3632°$$

These values of ΔV_1 and $\Delta\gamma_1$ are relative to those of the target vehicle at point one. The solution for the required maneuver follows:

$$V_{t1} = V_{f1} + \Delta V = 12786 \text{ fps} = 3897.2 \text{ m/sec}$$

$$V'_{t1} = 8775.5 \text{ fps} = 2674.8 \text{ m/sec}$$

$$\Delta\gamma = (\gamma_{f1} + \Delta\gamma_1) - \gamma'_{t1}$$

$$\gamma_{f1} = \tan^{-1}\left[\frac{e_f\sin\theta_{f1}}{1 + e_f\cos\theta_{f1}}\right] = 36.012°$$

$$\Delta\gamma = 0.3712°$$

The law of cosines yields the required pulse

$$\Delta V_1^2 = (V'_{t1})^2 + (V_{t1})^2 - 2V'_{t1}\,V_{t1}\cos\Delta\gamma$$

$$= 4011 \text{ fps} = 1223 \text{ m/sec}$$

This pulse represents half of the total maneuver. A second pulse is required at the point at which the two vehicles finally close. This second pulse must be sufficient to turn the shuttle vehicle and supplement its velocity vector. The laws of sines and cosines and the energy equation must be employed to define this second pulse.

$$r_{f2} = \frac{p}{1 + e\cos\theta_{f2}} = \frac{(r_{f1}V_{f1}\cos\gamma_{f1})^2}{\mu(1 + e_f\cos\theta_{f1})}$$

$$= 2.046322 \times 10^8 \text{ ft} = 62371.9 \text{ km}$$

$$V_{f2} = \sqrt{\mu\left(\frac{2}{r_2} - \frac{1}{a_f}\right)} = 5985.4 \text{ fps} = 1824.3 \text{ m/sec}$$

$$V_{t2} = \sqrt{\mu\left(\frac{2}{r_2} - \frac{1}{a_f + \Delta a}\right)} = 5886.3 \text{ fps} = 1794.1 \text{ m/sec}$$

$$\gamma_{f2} = \frac{e_f \sin \theta_{f2}}{1 + e_f \cos \theta_{f2}} = 26.4495°$$

$$\gamma_{t2} = \frac{(e_f + \Delta e) \sin (\theta_{f2} + \Delta\omega)}{1 + (e_f + \Delta e) \cos (\theta_{f2} + \Delta\omega)} = 27.7571°$$

$$\Delta\gamma_2 = 1.3076°$$

$$\Delta V_2^2 = (V_{f2})^2 + (V_{t2})^2 - 2\, V_{f2}\, V_{t2} \cos \Delta\gamma_2$$

$$= 168 \text{ fps} = 51.2 \text{ m/sec}$$

$$\Delta V_T = 4011 + 168 = 4279 \text{ fps.} = 1304 \text{ m/sec}$$

This value of ΔV_T represents the total impulse required for injection and correction of the orbits. It must not be compared to the impulse requirements for closure alone.

As was noted earlier in the discussion of this approach, the accuracy deteriorates as the deviation from the reference trajectory (in this case the target orbit from θ_{f1} to θ_{f2}) increases. The accuracy afforded by this technique as a function of the distances involved has not been determined.

In an analogous manner the differential corrections formulation presented in Chapter VI (Maneuvers) may be adapted for producing closure. The restrictions for usage are, however, roughly the same. Because this approach is discussed in detail in Chapter VI, no further discussion will be presented at this point.

6. Homing Phase Errors

Due to several error sources, errors will result in an inability to control both the transverse and the longitudinal motion of the shuttle vehicle. These sources and their effects are the subject of the following paragraphs. Particular sensors will not be discussed because of the rapid changes being made in the design and utilization of such equipments.

a. Transverse errors

Due to the effect of radar tracking noise, accelerometer error and engine shutoff uncertainty, a transverse velocity error remains at the end of the transverse correction pulses, including the final one.

Radar tracking noise arises from:

(1) Receiver thermal noise.

(2) Amplitude scintillation of the target.

(3) Angular scintillation of the target.

(4) Radar antenna servo jitter.

(5) Radar range measurement noise.

The first four sources result in a random error in the measured line-of-sight angle. This error has a nearly flat spectrum at frequencies below about 1 cps and is heavily attenuated at higher frequencies by action of the radar angle tracking loop. The standard deviations of the angular noise due to these sources are related to range as follows:

(1) Receiver noise varies with the square of range.

(2) Amplitude scintillation is invariant with range.

(3) Angular scintillation varies inversely with range.

(4) Servo jitter is invariant with range.

Since the computer accepts angular rate data, the angular noise is effectively differentiated before use. The computer then performs an arithmetic averaging of the angle rate noise over a smoothing period T. (Actually, the computer operates on H rather than ω but this is unimportant in the present discussion.) Since T is large compared to the reciprocal of angle noise bandwidth, the resulting angle rate noise after smoothing is given by

$$\omega_{RMS} = \frac{\psi_{RMS}}{T}$$

where ψ_{RMS} is the standard deviation of the total angle noise at the radar output due to all four noise sources. The error in measured transverse velocity due to radar tracking noise varies as the product of range and angle rate noise. Thus the velocity error due to radar tracking noise has the following relationship to range:

(1) Receiver noise varies with the cube of range.

(2) Amplitude scintillation varies directly with range.

(3) Angular scintillation is invariant with range.

(4) Servo jitter varies directly with range.

Figure 19 shows the transverse velocity error resulting from typical radar errors, plotted against range, with T = 10 sec.

The transverse velocity error due to radar range noise is a second order effect since the error is a product of range error and the small angular rate of the line of sight. The accelerometer error in terminating thrust has a negligible effect for a similar reason. The error due to transverse engine shutoff uncertainty is small and constant for any correction period, and is only important at the end of the last correction. Its value may be held less than 0.6 fps or 0.2 mps (3 σ) for a reasonable choice of engine thrust level.

Figure 19 shows a worst possible profile of transverse velocity during the homing phase. The correction threshold function shown has been chosen empirically and is not necessarily optimum. The 3σ noise envelope shown is just three times the value of the curve of Fig. 19. The pessimistic assumption has been made in Fig. 20 that the magnitude of the residual error at the end of each correction period is 3σ. This has been done for the purpose of sizing the propellant tanks of the homing vehicle for the worst case. The initial transverse error of 250 fps or 76 mps corresponds to a worst case for the launch guidance system.

In determining an acceptable correction threshold function it must be remembered that too high a threshold will generally result in a propellant penalty since corrections are unnecessarily delayed. Too low a threshold will result in frequent small corrections which are undesirable for several reasons, among them the fact that insufficient smoothing time is available between corrections.

Using typical numbers for a final transverse correction occurring at a range of 200 ft or 61 m a 3σ value of transverse velocity of less than 1.5 fps or 0.46 mps may be achieved, considering all sources of error.

b. Longitudinal errors

The longitudinal error analysis is quite straightforward for the system proposed. The errors in R and $\dot{R} = (-V_c)$ at the termination of any but the final longitudinal thrust period are quite unimportant, provided that the nominal closing profile (Fig. 10) has been chosen intelligently. Intelligent choice of this profile, that is, proper choice of the parameters of Eq (263) permits sufficiently long coast times, so that R and $\dot{R}$ may be adequately smoothed before the next correction begins. If this is done, errors in the radar measurement of r and $\dot{r}$ occurring at the beginning of a prior correction pulse, as well as accelerometer error, thrust acceleration uncertainty and thrust shutoff uncertainty occurring during the prior correction pulse, only serve to alter the range at which the subsequent correction begins (that is, lengthen or shorten the coast period before the next correction). No accumulation of error results.

The profile is also chosen so that the final correction in close velocity is small and begins at very close range. The terminal error in r and $\dot{r}$ results from the following sources:

(1) Radar measurement error of r at initiation of final longitudinal correction.

(2) Radar measurement error of $\dot{r}$ at initiation of final longitudinal correction.

(3) Accelerometer error.

(4) Thrust acceleration uncertainty (uncertainty in predicted a_i).

(5) Thrust shutoff uncertainty.

Items (1) and (4) produce only a terminal range error. Items (2), (3) and (5) are primarily responsible for a terminal closing velocity error. For a small final correction, the terminal range error is primarily due to item (1), and for a good radar is surely less than 50 ft or 15 m (3σ). The 3σ terminal closing velocity error due to item (2) is about 1 to 2 fps or 0.3 to 0.6 mps for a good radar. The 3σ error due to item (3) may be held to less than 0.4 fps or 0.12 mps with almost any decent accelerometer. The 3σ error due to item (5) may be held to less than 1 fps or 0.3 mps by proper choice of longitudinal engine size. Thus, the total 3σ error in terminal closing velocity is no more than 2.25 fps or 0.686 mps.

The total terminal velocity, including transverse velocity, is therefore no more than 2.7 fps or 0.82 mps (3σ). This velocity defines the quality of rendezvous obtainable with the vehicle described. If desired, a vernier system could be incorporated on the vehicle to effect either a soft contact with the target, or else a standoff position with respect to the target (Ref. 32).

D. REFERENCES

1. Petersen, N. V., Swanson, R. S., "Rendezvous in Space," Aerospace Engineering, Vol. 19, No. 5, May 1960.

2. Swanson, R. S. and Petersen, N. V., "Summary Report of Rendezvous Compatible Orbits," (ASG-TM-61-10), Northrop Corp., Norair Division, 1961.

3. Gedeon, G. S., et al., "Flight Performance Manual for Orbital Operations," Norair Division of Northrop Corp., Report NOR 61-208, September 1961.

4. Hord, R. A., "Relative Motion in the Terminal Phase of Interception of a Satellite or a Ballistic Missile," NACA TN 4399, September 1958.

5. Gilbert, E. O., "Orbit Control and Analysis Techniques for Equatorial 24-Hour Satellites," STL/TN-60-0000-27149, Space Technology Laboratories, August 1960.

6. Seifert, H. S., "Space Technology," John Wiley and Sons, 1959.

7. Clohessy, W. H., and Wiltshire, R. S., "Terminal Guidance System for Satellite Rendezvous," Journal of the Aerospace Sciences, Vol. 27, No. 9, September 1960.

8. Wheelon, A. D., "Free Flight of a Ballistic Missile," Space Technology Laboratories, Inc.

9. Anonymous, "The Rendezvous Maneuver," Chapter 4 of Flight Performance Handbook for Orbital Operations, STL (Redondo Beach), September 1961.

10. Passera, A. L., "Conditional-Switching Terminal Guidance (A Terminal Guidance Technique for Satellite Rendezvous)," IRE Transactions on Aeronautical and Navigational Electronics, Vol. ANE-7, No. 4, December 1960.

11. Nason, M. L., "Terminal Guidance Technique for Satellite Interception Utilizing a Constant Thrust Rocket Motor," ARS Journal, Vol. 30, No. 9, September 1960.

12. Bellman, Richard, "Dynamic Programming," Princeton University Press, Princeton, New Jersey, p 18, 1957.

13. Felleman, P., and Sears, N., "A Guidance Technique for Achieving Satellite Rendezvous," Aerospace Engineering, Vol. 19, May 1960.

14. Sears, N., and Felleman, P., "Continuously Powered Terminal Maneuver for Satellite Rendezvous," ARS Journal, Vol. 30, No. 8, August 1960.

15. Sears, N., and Felleman, P., "Terminal Guidance for a Satellite Rendezvous," ARS Preprint 778-59, 1959.

16. MIT Instrumentation Laboratory Reports, not reviewed here because of classification.

    (a) "Satellite Rendezvous Guidance System," Report R-257, October 1959. SECRET

    (b) "Satellite Rendezvous Guidance System," Study Report R-260, June 1960. SECRET

    (c) "Satellite Rendezvous Guidance System," Study Report R-289, September 1960. SECRET

    (d) "Space Mission Navigation and Guidance Techniques," Report R-234, March 1959. SECRET

17. Blum, M., "On the Mean Square Noise Power of a Linear Discrete Filter Operating on Polynomial Plus White Noise Input," IRE Transaction on Information Theory, December 1957.

18. Ling, Donald P., "Radio-Inertial Guidance," part of Space Technology edited by H. Seifert, John Wiley and Sons, New York, 1959, pp 25 to 108, 25-18.

19. Wiener, N., "The Extrapolation, Interpolation and Smoothing of Stationary Time Series," John Wiley and Sons, New York, 1949.

20. Bode, H. W., and Shannon, C. E., "A Simplified Derivation of Linear Least Square Smoothing and Prediction Theory," Proc IRE, 38, pp 417 to 425, 1950.

21. Darlington, S., "Linear Least Squares Smoothing and Prediction," BSTJ, 37, pp 1221 to 1294, 1958.

22. Bendat, J. S., "Optimum Filters for Independent Measurements of Two Related Perturbed Messages," IRE Trans Prof Group Circuit Theory, CT-4, pp 14 to 19, 1957.

23. Laning, J. H., and Battin, R. H., "Random Processes in Automatic Control," McGraw-Hill, New York, 1956.

24. Tukey, J. W., and Blackman, R. B., "The Measurement of Power Spectra from the Point of View of the Communications Engineer," Part I, BSTJ, 37, pp 185 to 282 (1958); Part 2, BSTJ, 37, pp 485 to 569 (1958).

25. Aseltine, J. A., "Transform Method in Linear System Analysis," McGraw-Hill Book Co., Inc., New York, 1958.

26. Van Valkenburg, M. E., "Introduction to Modern Network Synthesis," Wiley, New York, 1960.

27. Fischer, R. A., and Yates, F., "Statistical Tables for Biological, Agricultural and Medical Research," Oliver and Boyd, Edinburgh, Scotland, 1938.

28. Blum, M., "An Extension of the Minimum Mean Square Prediction Theory for Sampled Input Signals," IRE Transactions, Vol. IT-2, pp 176 to 184, September 1956.

29. Anderson, R. L., and Houseman, E. E., "Tables of Orthogonal Polynomial Values Extended to N = 104," Iowa State College of Agriculture and Mechanical Arts, Ames, Iowa, Res Bulletin 297; April 1942.

30. Allen, F. E., "The General Form of the Orthogonal Polynomials for Simple Series with Proofs of Their Simple Properties," Proc Roy Soc, Edinburgh, Vol. 50, pp 310 to 320, 1935.

31. Lawden, D. F., "Correction of Interplanetary Trajectories," Journal of the British Interplanetary Society, July 1954.

32. Schroeder, W., "A Terminal Guidance Scheme for Docking Satellites," Space Technology Laboratores, Inc., Summer 1961.

E. BIBLIOGRAPHY

Bakalyar, G.,
"Orbital Rendezvous and Point to Point Velocity Transfers," The Martin Company, Denver, Colorado, Report No. MI-59-61, November 1959.
"Continuous Thrust Rendezvous Transfers Approximately Mass Extremized (U)," The Martin Company, Denver, Colorado, Report No. R-61-22, August 1961.

Blizard, R. B., "Terminal Rendezvous Between a Ferry and a Satellite (U)," The Martin Company, Denver, Colorado, Report No. R-61-21, August 1961.

Brissenden, Roy F., and Lineberry, Edgar C., Jr., "Visual Control of Rendezvous," Aerospace Technologists, Guidance and Control Br., Aerospace Mechanics Div., Langley Research Center, NASA, IAS 30th Annual Meeting, IAS Paper No. 62-42.

Brissenden, R. F., Burton, B. B., Foudriat, E. D., and Whitten, J. B., "Analog Simulation of a Pilot-Controlled Rendezvous," NASA TN D-747, April 1961.

Brunk, W. E., and Flaherty, R. J., "Methods and Velocity Requirements for the Rendezvous of Satellites in Circumplanetary Orbits," NASA TN 81, October 1959.

Carney, T. M., "An Automatic Terminal Guidance System for Rendezvous with a Satellite," NASA TN D-923, August 1961.

Cicolani, L. S., "Trajectory Control in Rendezvous Problems Using Proportional Navigation," NASA TN D-772, April 1961.

Clohessy, W., and Wiltshire, R.,
"Problems Associated with Assembly of Multiunit Satellites in Orbit," The Martin Company, Denver, Colorado, ASME Paper No. 59-AV-25.

"Terminal Guidance System for Satellite Rendezvous," Los Angeles, California, IAS National Summer Meeting, June 1959, Paper No. 59-93. (Also, Journal of the Aerospace Sciences, Vol. 27, No. 9, September 1960.)

Duke, W. M., et al., "Error Analysis Considerations for Satellite Rendezvous," American Rocket Society, Preprint No. 1198-60, May 1960.

Eggleston, John M., "A Study of the Optimum Velocity Change to Intercept and Rendezvous," NASA TN D-1029, February 1962.

Eggleston, J. M., and Beck, H. D., "A Study of the Positions and Velocities of a Space Station and a Ferry Vehicle During Rendezvous and Return," NASA TR R-87, 1961.

Eggleston, J. M., and Dunning, R. S., "Analytical Evaluation of a Method of Midcourse Guidance for Rendezvous with Earth Satellites," NASA TN D-883, June 1961.

Faulkner, F. D.,
"Complete Solution to a Simple Rendezvous Problem," Monterey, California, Naval Postgraduate School, July 1960.
"Optimum Interception of a Ballistic Missile at Intermediate Range," Naval Postgraduate School, Res Paper 29, October 1961.

Felleman, P. G., and Sears, N. E., Jr., "A Guidance Technique for Achieving Rendezvous," Aerospace Engineering, Vol. 19, May 1960, pp 76 to 77.

Garber, T. B., "Ascent Guidance for Satellite Rendezvous," Aerospace Engineering, Vol. 19, No. 5, May 1960.

Grubin, C., "Docking Dynamics for Rigid-Body Spacecraft," Inst Aerospace Sci Paper 62-43, January 1962.

Heiss, W. H., Macek, W. M., Price, R. C., and Stark, E. W., "Space Rendezvous Terminal Sensors," National Aerospace Electronics Conference, Dayton, Ohio, Proceedings, 8 to 10 May 1961 (NAECON, Dayton, Ohio, 1961), pp 64 to 75.

Hord, R. A., "Relative Motion in the Terminal Phase of Interception of a Satellite or Ballistic Missile," NASA TN 4399, September 1958.

Hord, R. A., and Dürling, B. J., "Analysis of a Linear System for Variable-Thrust Control in the Terminal Phase of Rendezvous," NASA TN D-953, September 1961.

Hornby, H., "An Analytical Study of Orbital Rendezvous for Least Fuel and Least Energy," NASA TN D-1207, March 1962.

Jacobs, E., Morgenthaler, G., and Sevastian, R.,
"A Simplified Model for Computing Probability of Satellite Interception by a Preguided Missile," Chicago, Caywood-Schiller Associates, May 1959.
"Probability of Satellite Interception by an Air Launched Preguided Missile," ARS Journal, Vol. 31, No. 3, March 1961, pp 352 to 355.

Kamm, L. J., "SATRAC: Satellite Automatic Terminal Rendezvous and Coupling (U)," American Rocket Society, Preprint No. 1497-60, 5 to 8 December 1960.

Kaste, O., and Novak, D., "Study of Rendezvous Mission," Baltimore, Maryland, The Martin Company, Engineering Report No. ER 11522, October 1960. (Also, MLV Technical Note No. 13.)

Kidd, A. T., "Terminal Maneuvers for Satellite Ascent Rendezvous," Institute of Aerospace Sciences, Preprint No. 61-206-1900, June 1961.

Leitmann, G., "An Optimum Pursuit Problem," Journal of the Franklin Institute, Vol. 263, No. 6, June 1957, pp 499 to 503.

Levin, E., and Ward, J., "An Orbital Rendezvous Simulator," Astronautical Science Review, Vol. 1, No. 4, October to December 1959, pp 15 to 16, 21.

Levin, E., et al., "Manned Control of Orbital Rendezvous," Aerospace Engineering, Vol. 19, No. 5, May 1960.

Lindorfer, W., "Optimization of Missile Intercept Range," IAS Vehicle Systems Optimization Symposium, New York, 27 to 29 November 1961.

Lorell, J., "Velocity Increments Required to Reduce Target Miss on Coasting Trajectories," Institute of Aerospace Sciences, Preprint No. 60-30, January 1960.

Miller, D. M., "A Statistical-Mechanical Estimate of Orbital Collision Probabilities," Calif Inst Tech Jet Propulsion Lab. TR 32-211, March 1962.

Morgenthaler, G. W., "On Midcourse Guidance in Satellite Interception, II," Chicago, Caywood-Schiller Associates, January 1959. (Also Astronautica Acta, Vol. 5, No. 6, 1959, pp 328 to 346.

Munick, H., and McGill, R., "Analytical Estimates for Optimum Transfer Paths," ARS Journal, Vol. 30, No. 1, January 1960.

Nason, M. C.,
"Terminal Guidance Technique for Satellite Interception Utilizing a Constant Thrust Rocket Motor," ARS Journal, Vol. 30, No. 9, September 1960.
"Terminal Guidance and Rocket Fuel Requirements for Satellite Interception," American Rocket Society, Preprint No. 777-59, April 1959.

Niemi, N. J., "An Investigation of a Terminal Guidance System for a Satellite Rendezvous," American Rocket Society, Paper No. 1176-60, 1960.

Parker, G. H., and Daly, W. A., "Preliminary Design of a Satellite Rendezvous Vehicle," American Rocket Society, Preprint No. 1481-60, December 1960.

Petersen, N. V., "Rendezvous in Space--Effects of Launch Conditions," Aerospace Engineering, Vol. 19, May 1960.

Petersen, N. V., and Swanson, R. S., "Rendezvous Compatible Orbits," Astronautical Science Review, Vol. 1, October to December 1959, pp 13 to 14, 20.

Petersen, N. V., Swanson, R. S., and Hoover, L. R., "An Astrovehicle Rendezvous-Guidance Concept," Institute of Aerospace Sciences, Preprint No. 60-12, 1960.

Potter, N. S., "Controlled Rendezvous of Orbiting Space Stations," American Rocket Society, Preprint No. 1483-60, December 1960, also, ARS Journal, Vol. 31, No. 8, August 1961, pp 1096 to 1102.

Roberson, R. E., "Path Control for Satellite Rendezvous," American Astronautical Society, Preprint No. 60-15, January 1960. (Also, "Advances in Astronautical Sciences," Vol. 6, New York, The Macmillan Company, 1960.)

Schroeder, W., "A Terminal Guidance Scheme for Docking Satellites," ARS Preprint 1952-61, August 1961.

Sears, N. E., "Satellite-Rendezvous Guidance System (U)," Massachusetts Institute of Technology, Instrumentation Laboratory, Cambridge, Massachusetts, Report No. R-331, May 1961.

Sears, N. E., and Felleman, P. G.,
"Terminal Guidance for Satellite Rendezvous," American Rocket Society, Paper No. 778-59, April 1959.
"Continuously Powered Terminal Maneuver for Satellite Rendezvous," ARS Journal, Vol. 30, No. 8, August 1960, pp 734 to 739.

Shapiro, M.,
"Attenuated Intercept Satellite Rendezvous System," ARS Journal, Vol. 31, No. 12, December 1961, pp 1733 to 1744.
"An Attenuated Intercept Satellite Rendezvous System," Institute of Aerospace Sciences, Preprint No. 61-155-1849, June 1961.

Simon, E., Jr., "A Proposed Control System to Facilitate the Terminal Phase of Manned Rendezvous," American Rocket Society, Preprint No. 1480-60, 1960.

Skalafuris, A. J., and Schiller, D. H., "On Midcourse Guidance Problems in Satellite Interception," Chicago, Caywood-Schiller Associates, September 1958. (Also, ARS Journal, Vol. 30, pp 41 to 45, January 1960.)

Smith, R. A., "Establishing Contact Between Orbiting Vehicles," Journal of the British Interplanetary Society, Vol. 10, No. 6, November 1951, pp 295 to 299. (Also, London, 2nd International Congress on Astronautics, Symposium on Satellite Vehicles, 1951.)

Spradlin, L. W., "The Long-Time Satellite Rendezvous Trajectory," Aerospace Engineering, Vol. 19, June 1960.

Steffan, K. F., "A Satellite Rendezvous Terminal Guidance System," American Rocket Society, Preprint No. 1494-60, December 1960. (Also, ARS Journal, Vol. 31, No. 11, November 1961.)

Steinhoff, E., "Orbital Rendezvous and Guidance," Aerospace Engineering, Vol. 19, May 1960.

Straly, W. H.,
"Utilizing the Chasing Technique in Rendezvous," American Rocket Society, Preprint No. 2295-61, October 1961.
"The Phasing Technique in Rendezvous," ARS Journal, Vol. 32, No. 4, April 1962, p 620.

Swanson, R. S., and Petersen, N. V., "The Influence of Launch Conditions on the Friendly Rendezvous of Astrovehicles, American Astronautical Society, Preprint No. 59-16, August 1959. (Also, "Advances in Astronautical Sciences," New York, Plenum Press, 1960, Vol. 5.)

Swanson, R. S., Petersen, N. V., and Soule, P. W., "Station Keeping of Satellites in Rendezvous Compatible Orbits," ARS Preprint 1954-61, August 1961.

Swanson, R. S., et al., "An Astrovehicle Rendezvous Guidance Concept," Advances in Astronautical Sciences, The Macmillan Company, New York, Vol. 6, 1960.

Tempelman, W. H., "3-D Analysis of Minimum Energy Intercepts, Transfers and Rendezvous Using n Impulses," American Rocket Society, Preprint No. 1474-60, December 1960.

Townsend, G. E.,
"Satellite Rendezvous," Design Guide to Orbital Flight, McGraw-Hill Book Company, New York, 1962, Chapter 8.
"A Generalized Analytic Method of Satellite Rendezvous," The Martin Company, Baltimore, Maryland, Engineering Report No. ER 10882, October 1959.

Tsien, H. S., "Takeoff from a Satellite Orbit (radial thrust)," Jet Propulsion, Vol. 23, No. 4, July to August 1953.

Ward, J. W., and Williams, H. M., "Orbital Docking Dynamics," ARS Preprint 1953-61, August 1961.

Weber, R. J., and Pouson, N. M., "Achieving Satellite Rendezvous," ARS Journal, Vol. 29, No. 8, August 1959.

Wiltshire, R. S., and Clohessy, W. H., "Terminal Guidance for Rendezvous in Space," Astronautical Science Review, Vol. 1, No. 4, pp 9 to 10, October to December 1959.

ILLUSTRATIONS

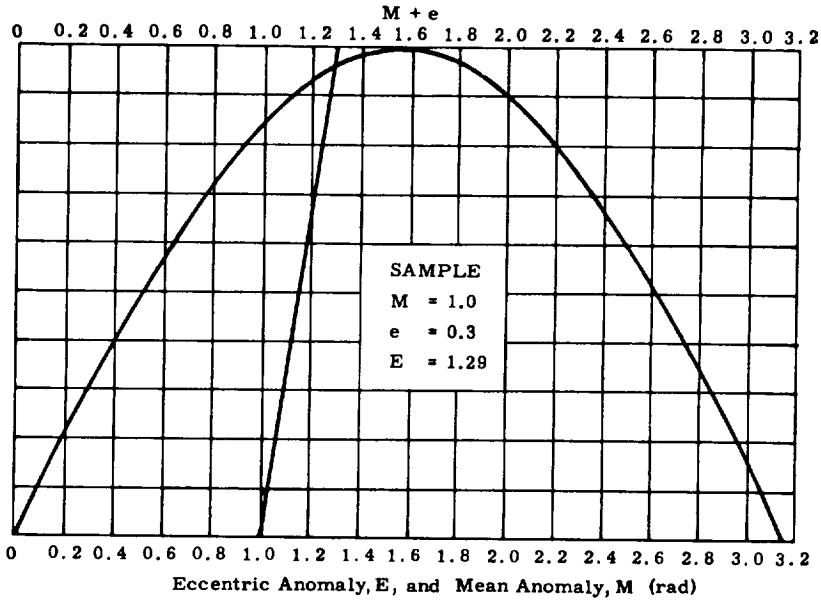

Fig. 1. Graphical Solution to Kepler's Equation for E as a Function of M and e

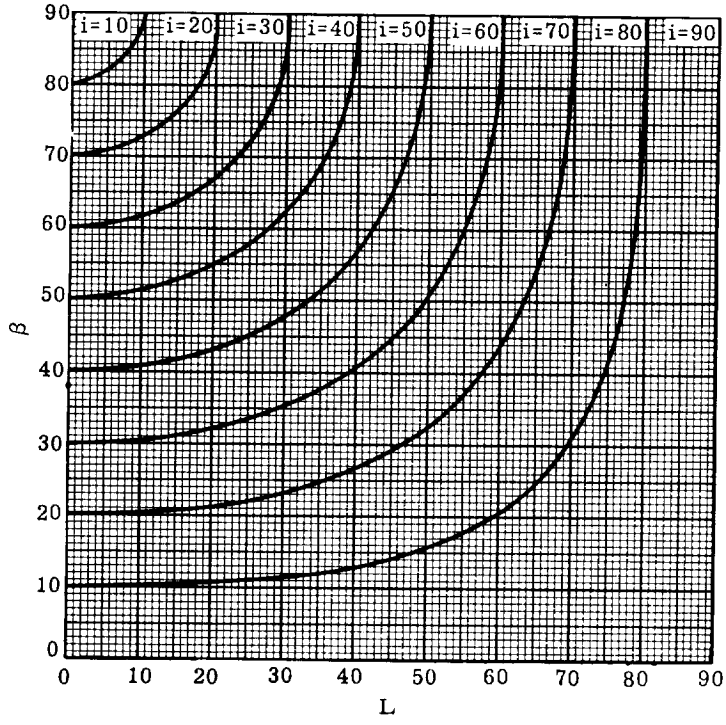

Fig. 2. Launch Azimuth as a Function of Latitude and Inclination

$i = 70°$
$L_L = 28.5°$
$L_2 = 28.5°$
$(r_a)_{24} = 42,400$ stat mi
$= 68,300$ km
$(r_p)_{24} = 10,000$ stat mi
$= 16,090$ km
$t_{ascent} = 1000$ sec

Fig. 3. Launch Site Location for Rendezvous (sample problem)

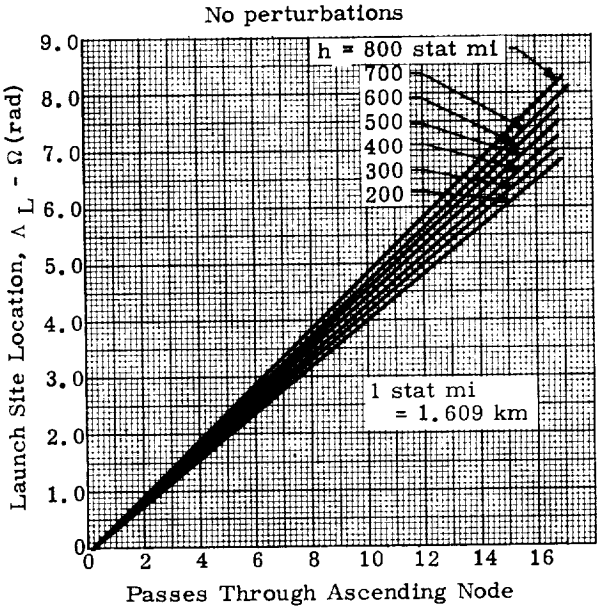

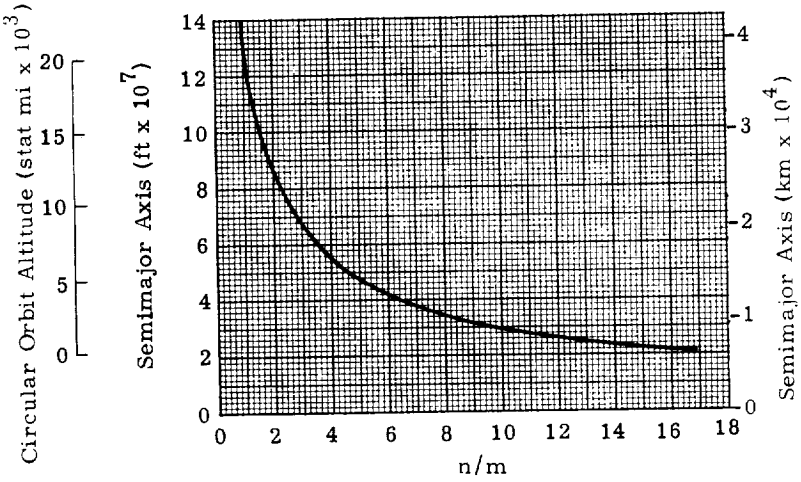

Fig. 4. Variation of Semimajor Axis with n/m (n/m = 0 to 17)

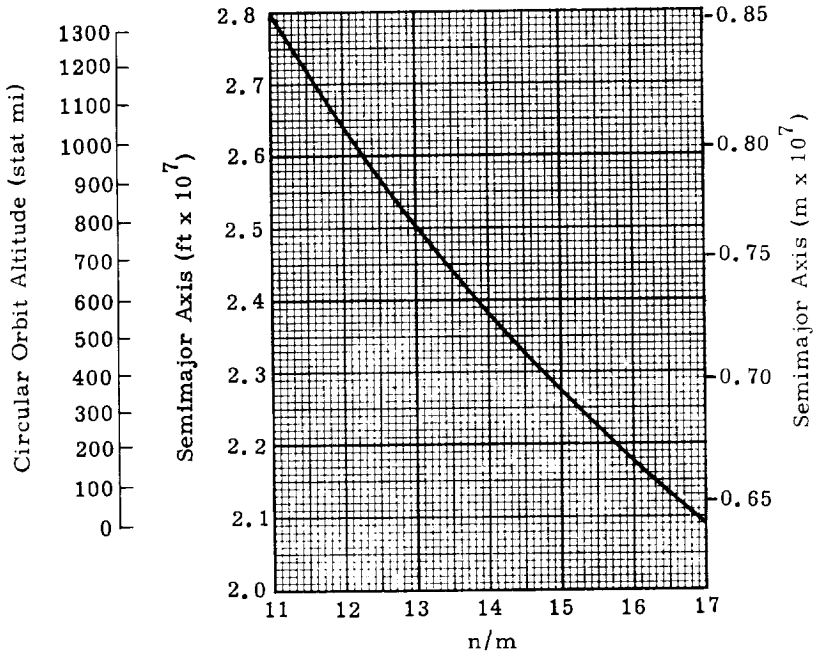

Fig. 5. Variation of Semilatus Rectum with n/m (n/m = 11 to 17)

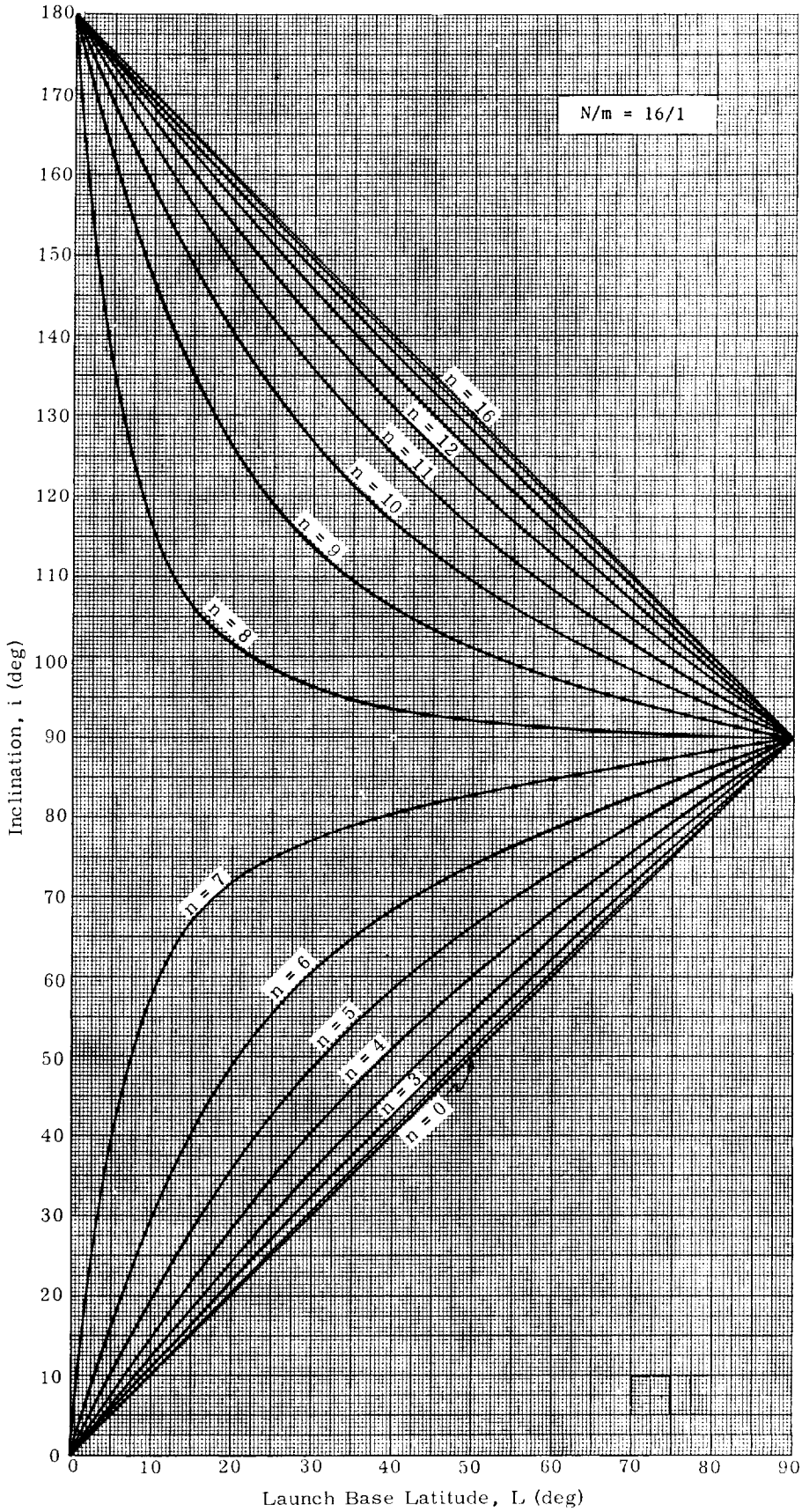

Fig. 6. Rendezvous Compatible Orbits (geometric effects)

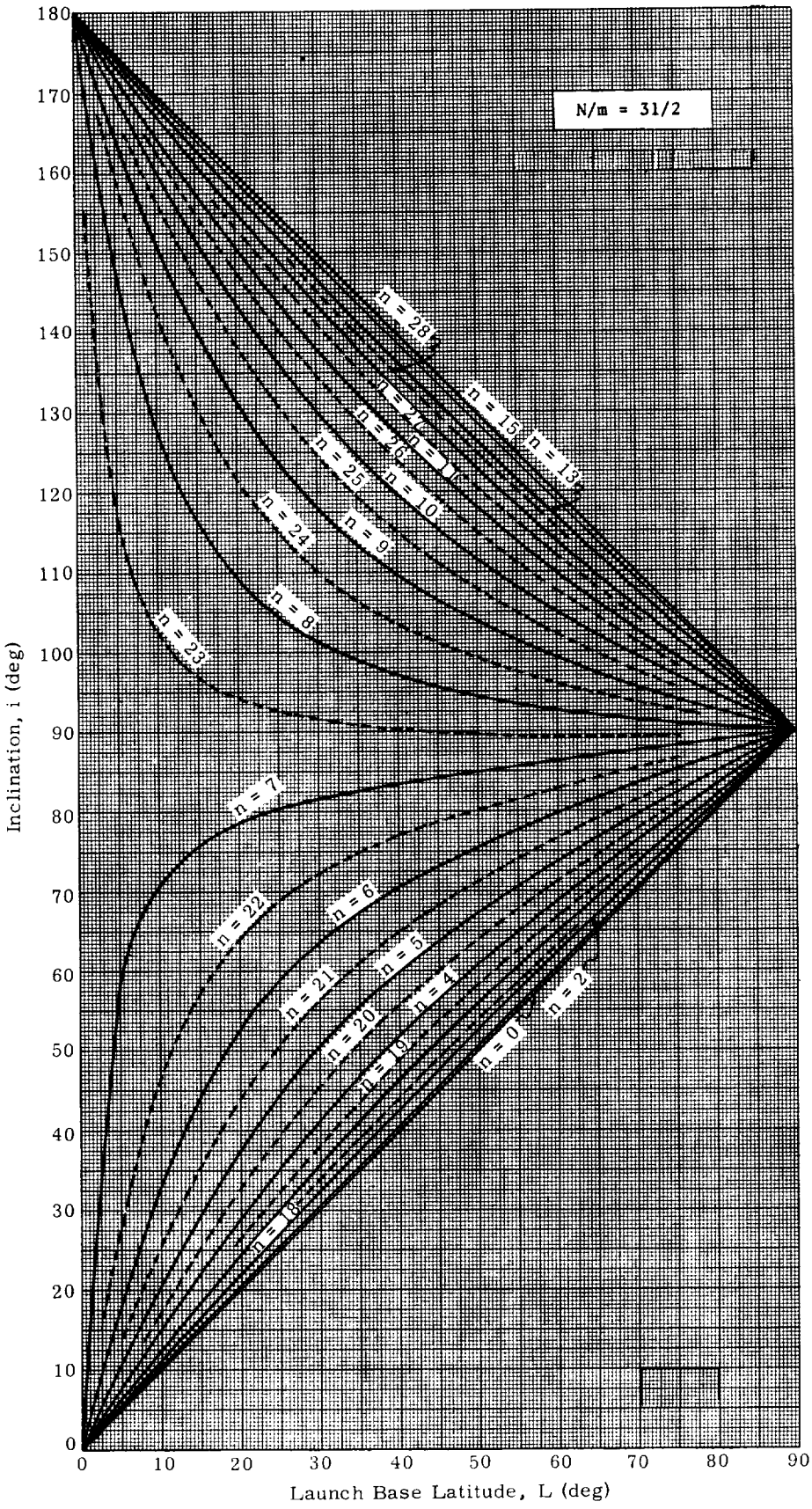

Fig. 6. Continued

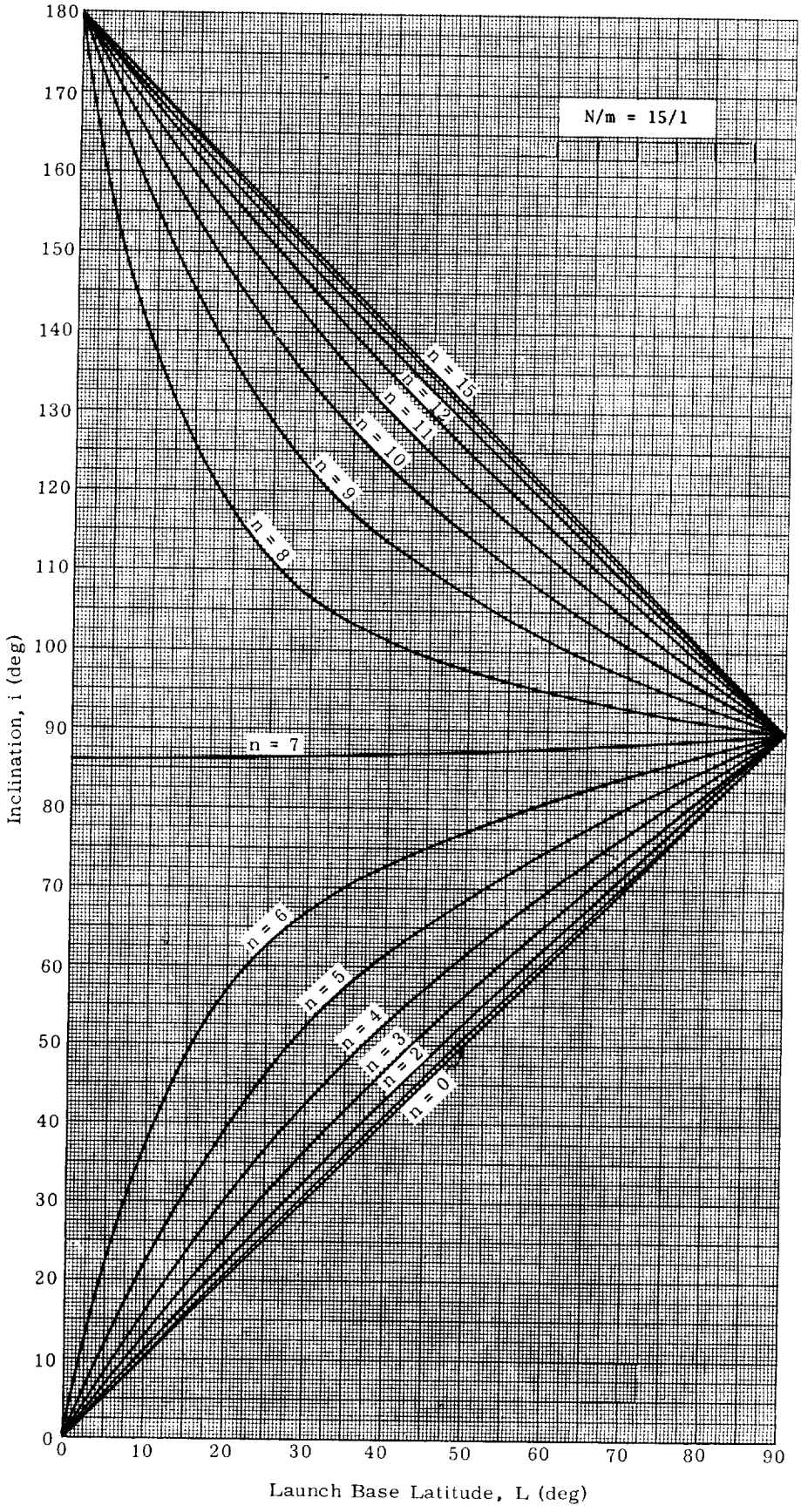

Fig. 6. Continued

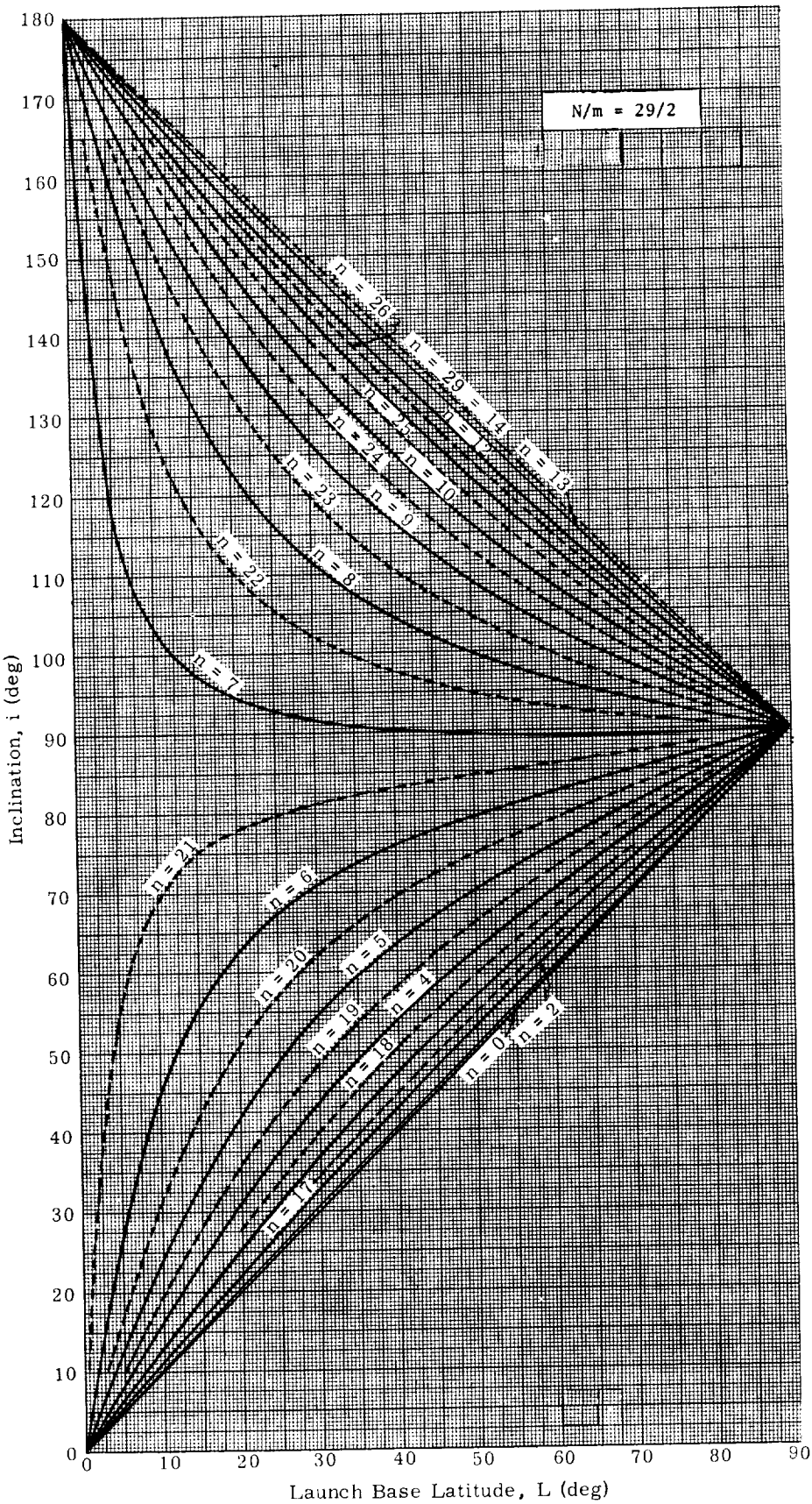

Fig. 6. Continued

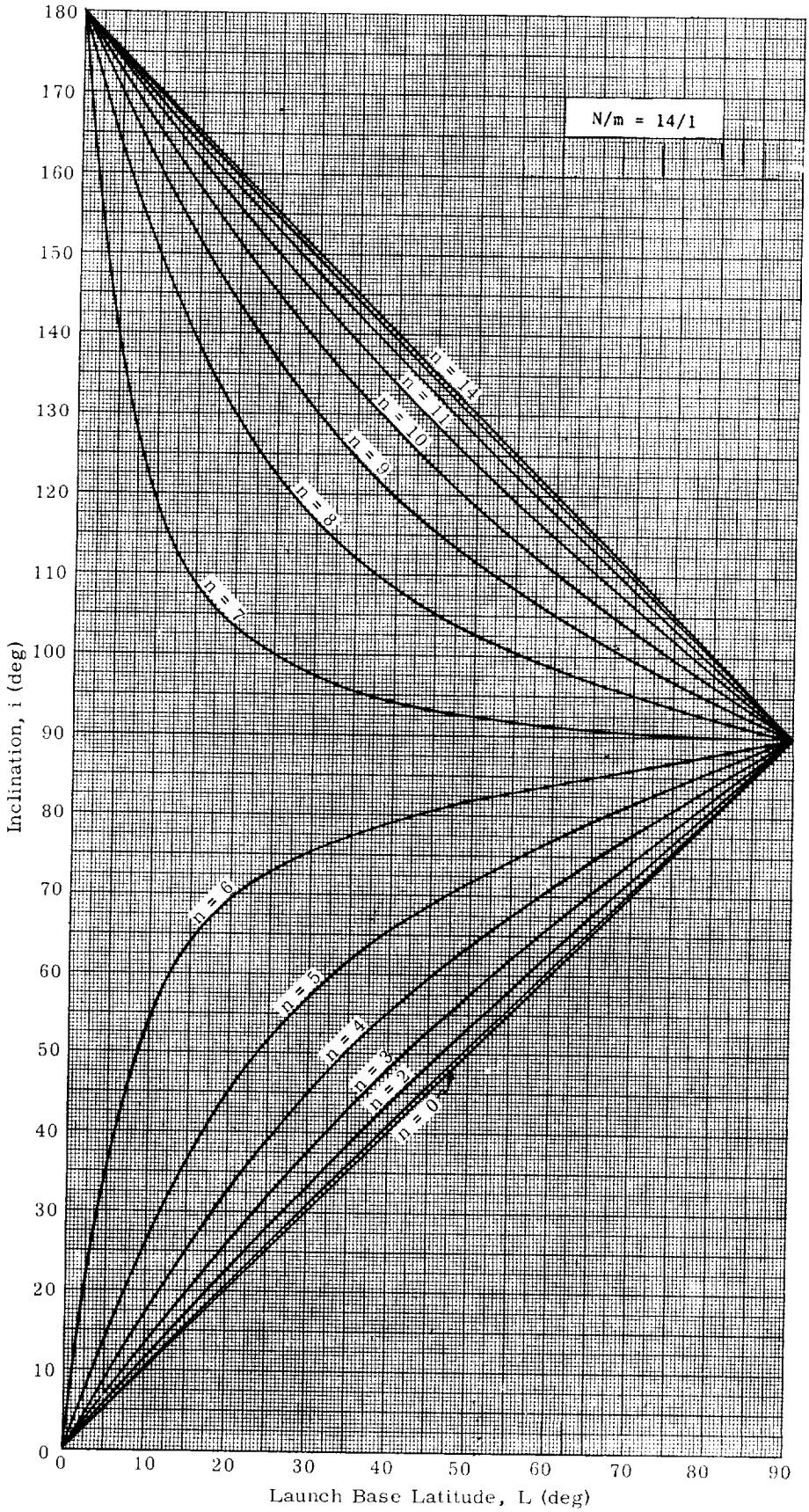

Fig. 6. Continued

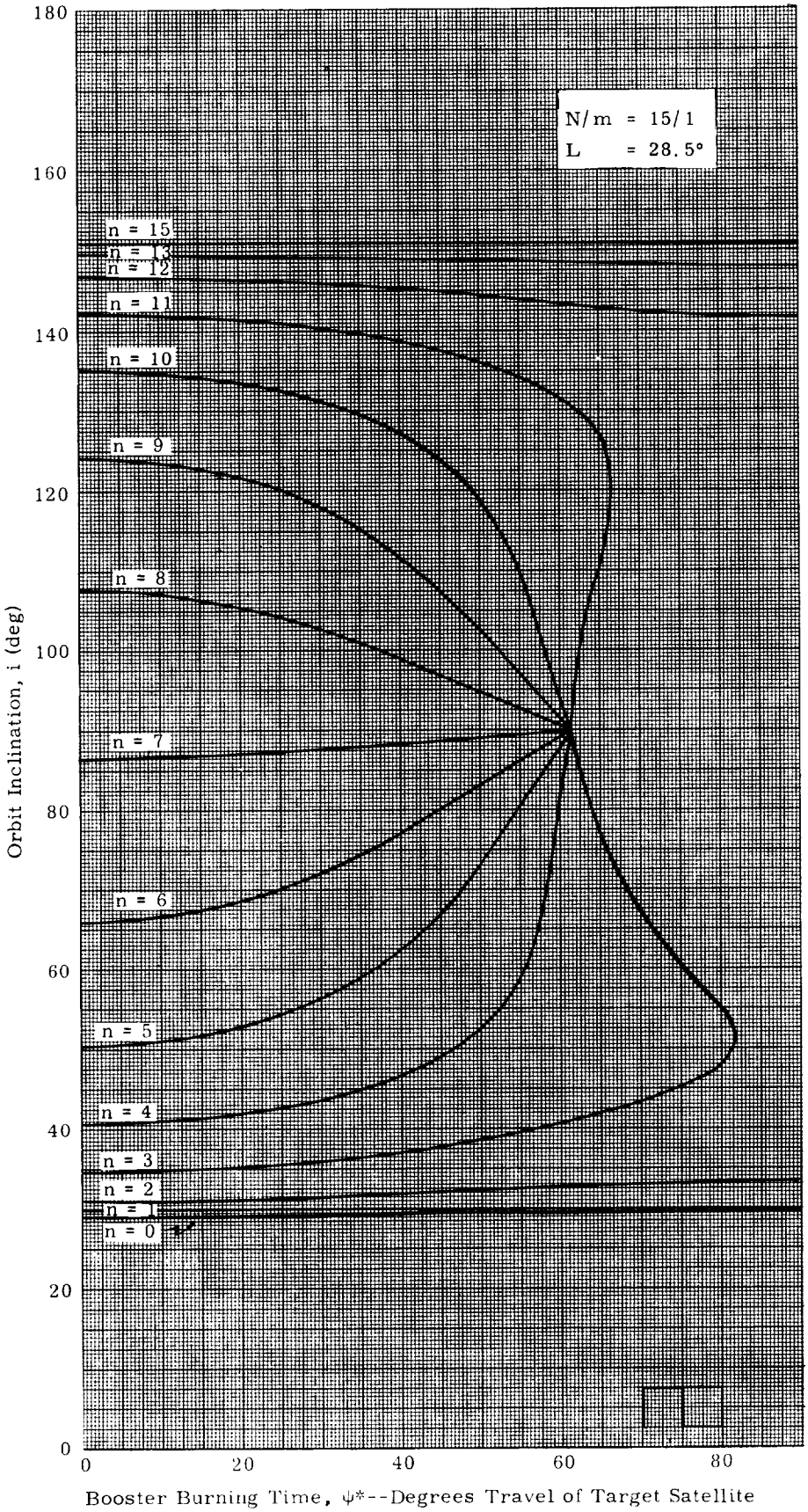

Fig. 7. Finite Burning Time Effects on Rendezvous Compatible Orbits

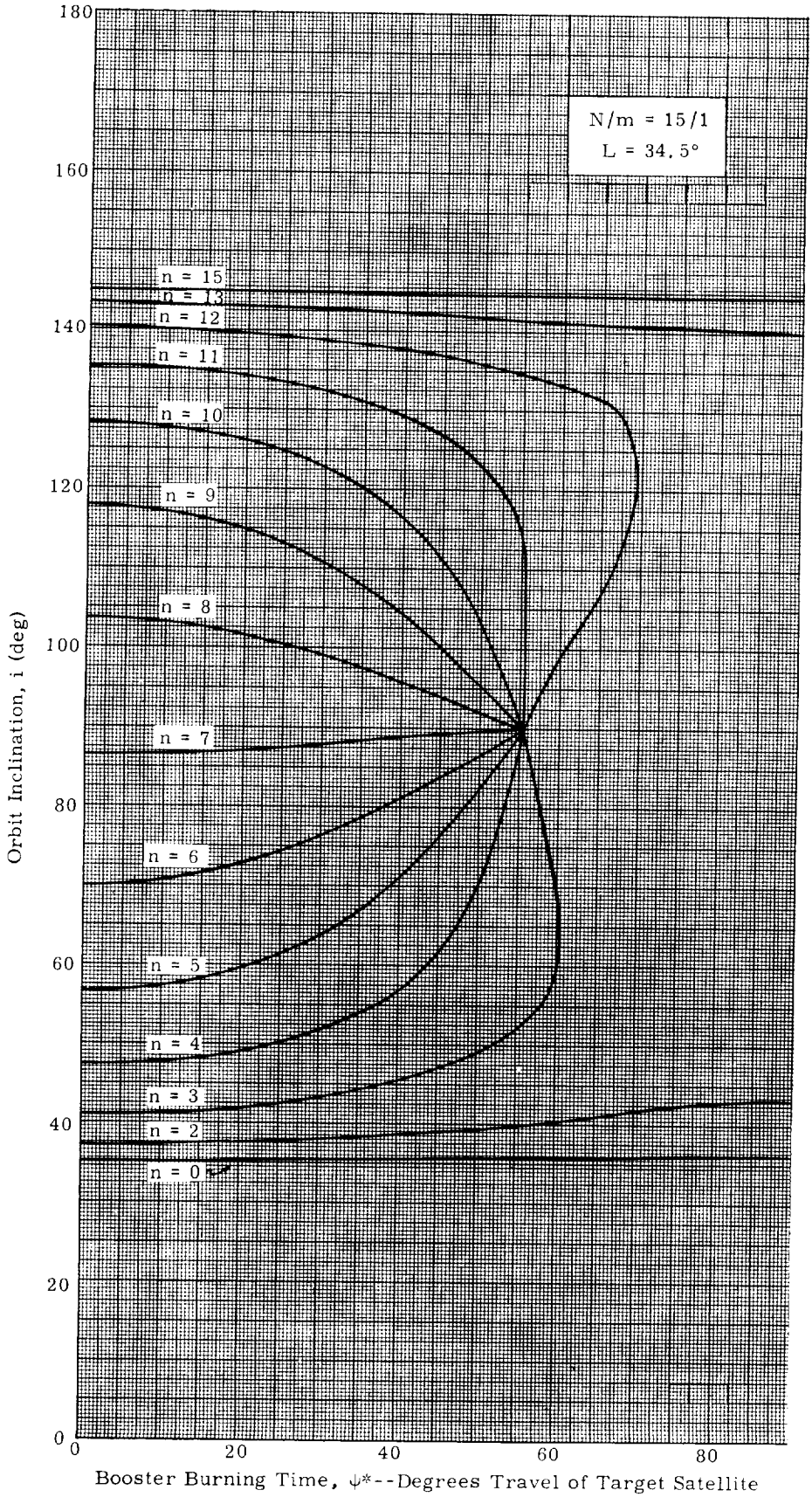

Fig. 7. Continued

The solution for the energy requirement utilized in adjusting the plane of the transfer orbit near its apogee for direct launches

$$\frac{\Delta V}{V} = \left|\beta_2 - \beta_1\right|$$

Example

$L = 40°$
$\nu = 70°$
$\nu + \Delta\Omega = 80°$

$$\frac{\Delta V}{V} = 0.73 - 0.71 = 0.02$$

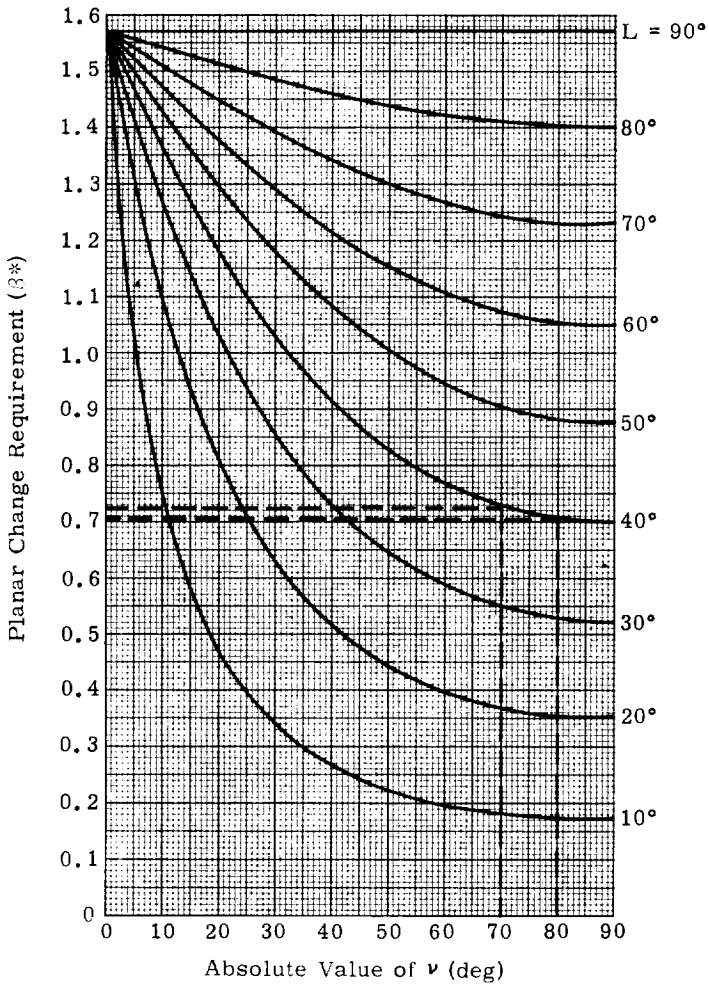

Fig. 8. Graphical Solution for $\frac{\Delta V}{V}$

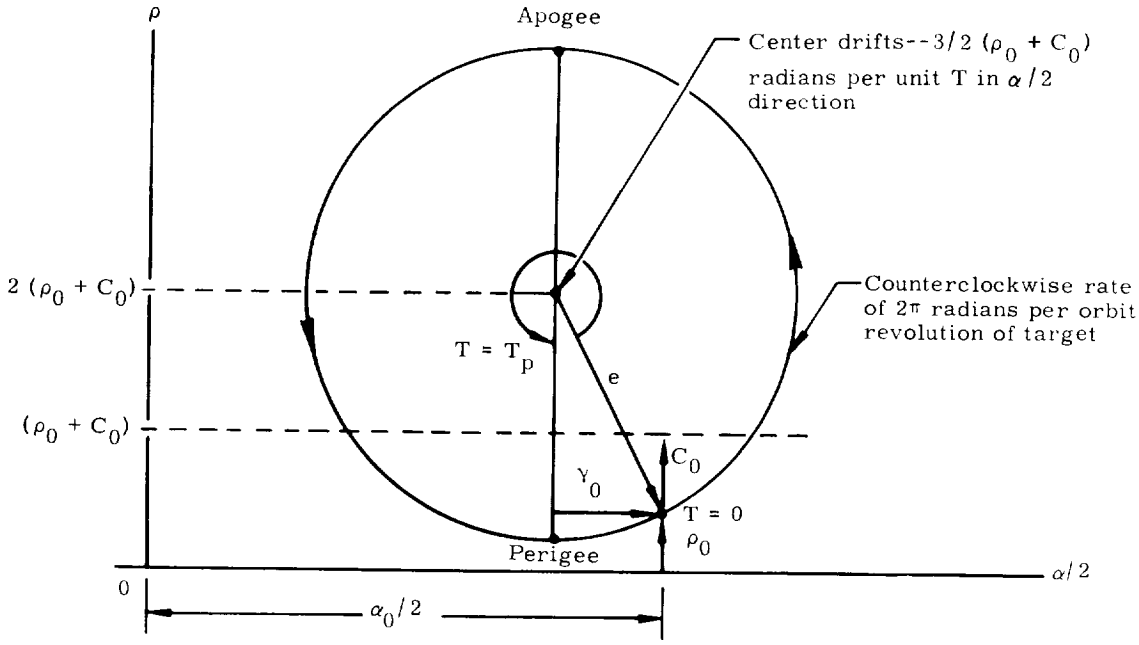

Fig. 9. Circle Diagram Generatrix of In-Plane Motion

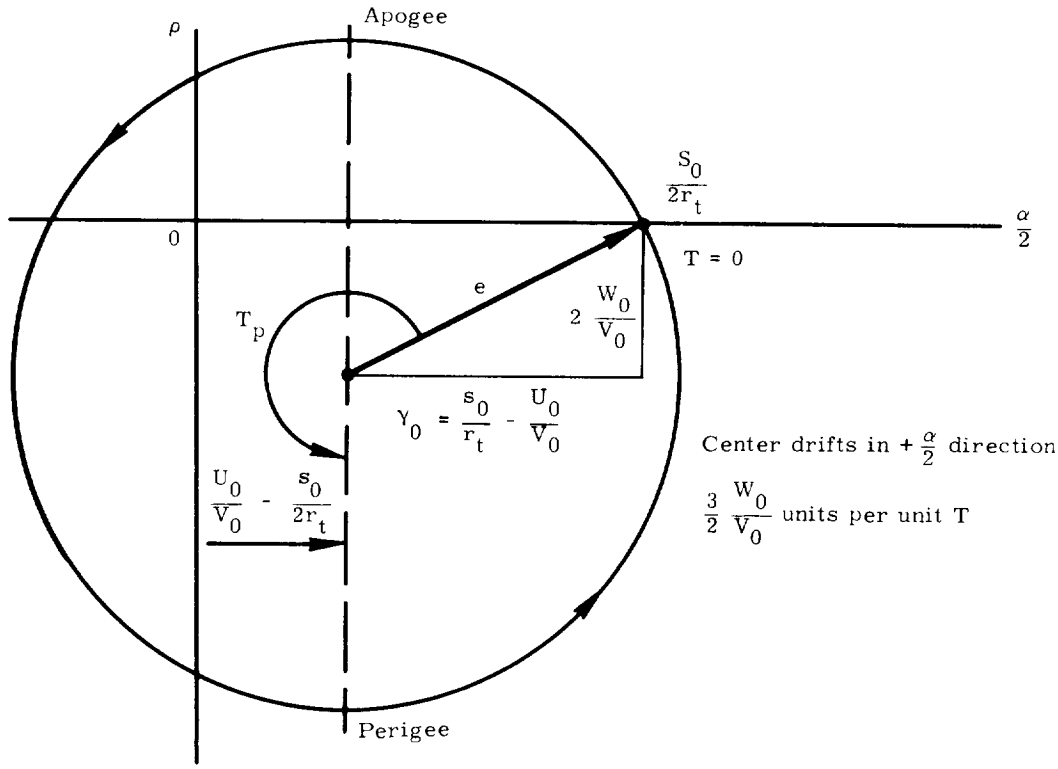

Fig. 10. In-Plane Circle Diagram at Injection

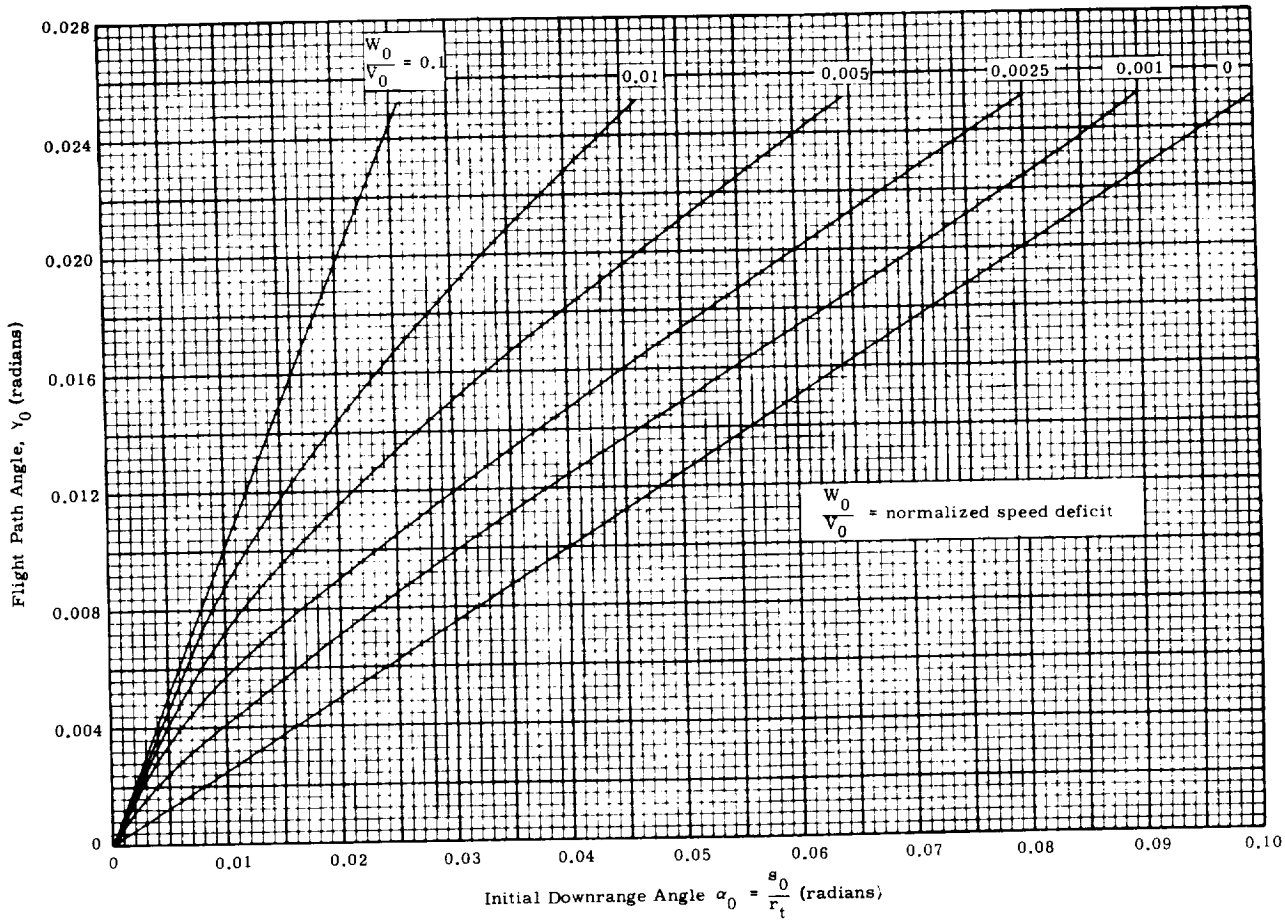

Fig. 11. Parametric Relation for Rendezvous ($\rho = 0$, $\alpha = 0$)

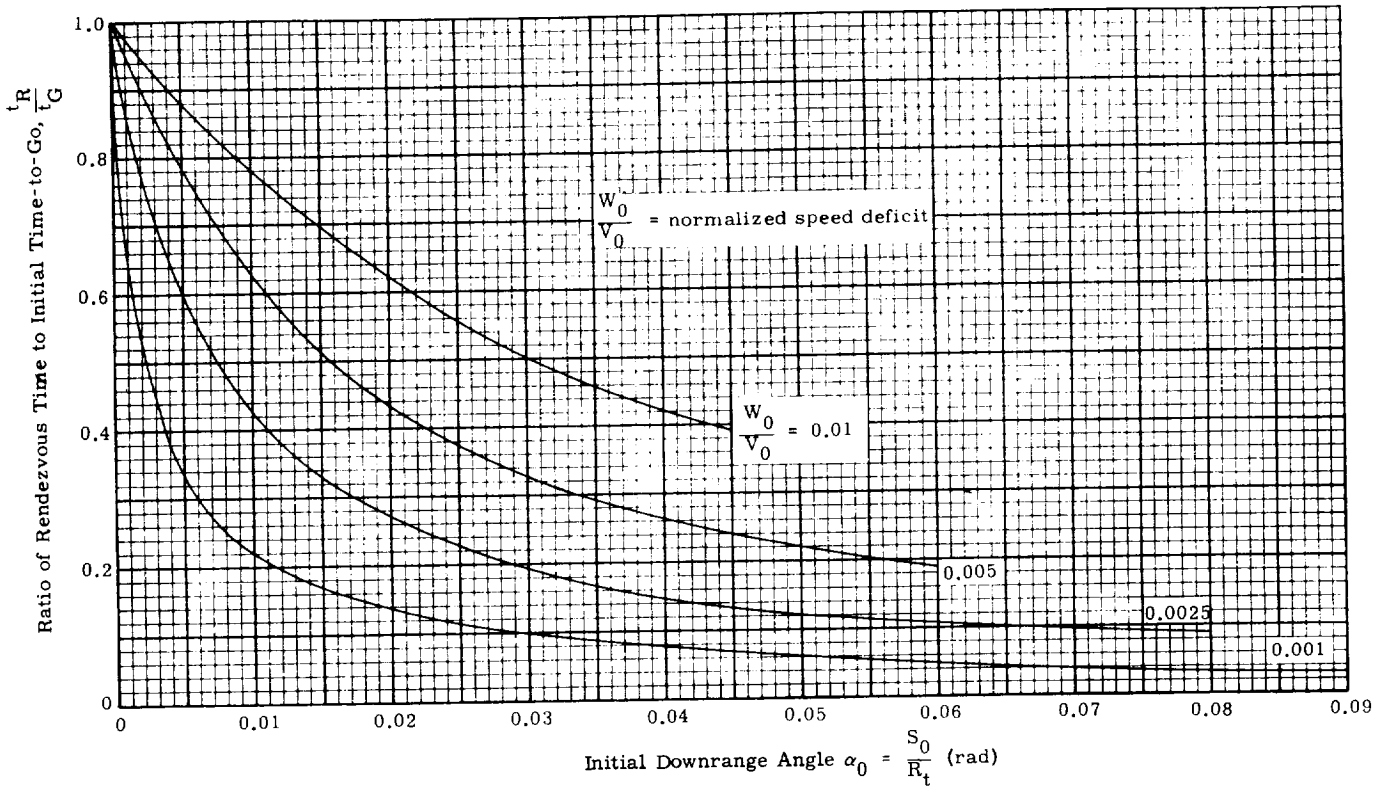

Fig. 12. Ratio of Rendezvous Time to Initial Time-to-Go Versus Initial Downrange Angle

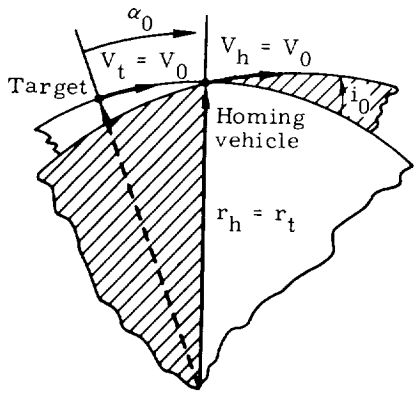

Fig. 13. Rendezvous Geometry at Nodal Crossing

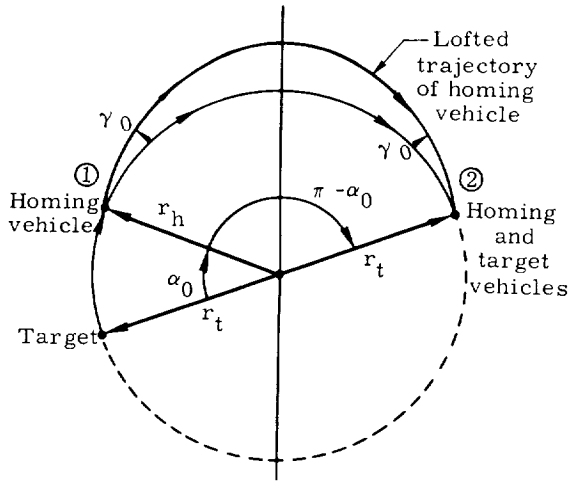

Fig. 14. Rendezvous Using Pure Loft (no period change)

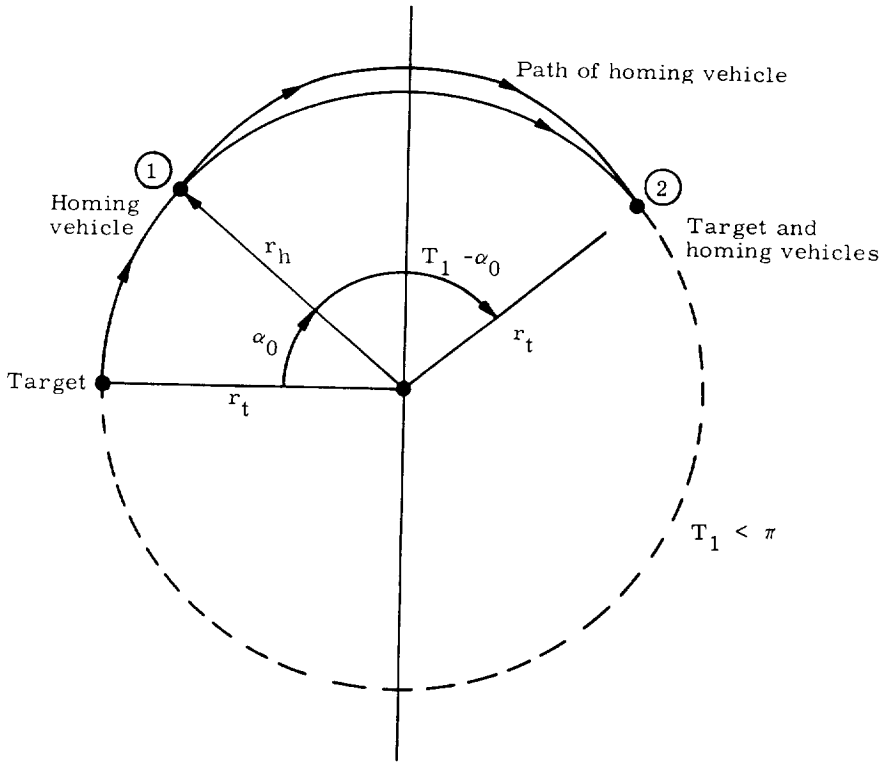

Fig. 15. Rendezvous Using Loft and Period Change

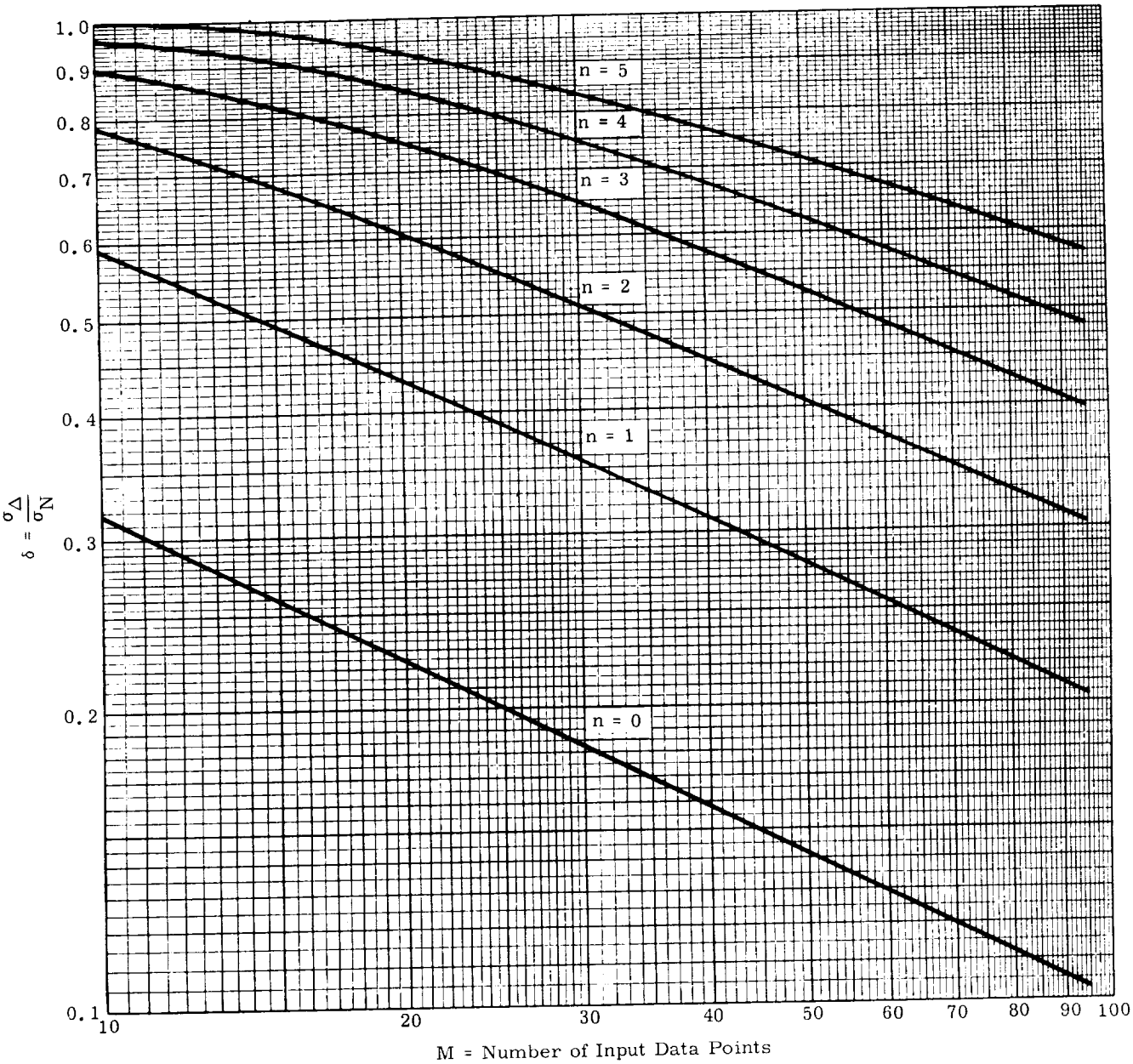

$\delta = \frac{\sigma_\Delta}{\sigma_N}$

σ_Δ = rms error output (zero-lag estimation)

σ_N = rms error of noise

n = degree of polynomial passed without error

(M - 1) T = memory span of filter

Fig. 16. Output of the Digital Filter (least squares estimate of the input with zero-lag)

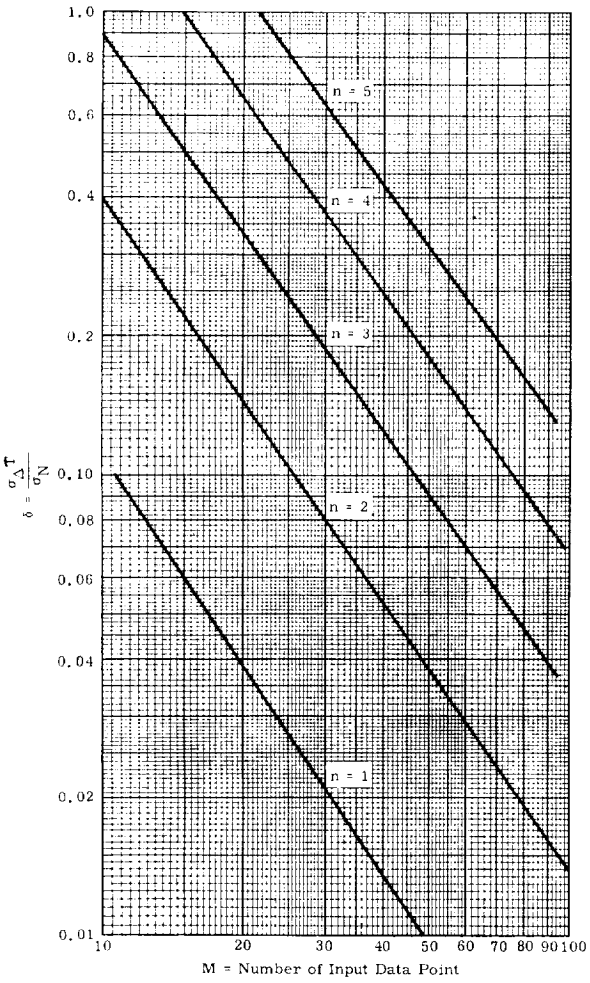

σ_Δ = rms of output

σ_N = rms of input

$\delta = \frac{\sigma_\Delta T}{\sigma_N}$

n = degree of polynomial passed by filter without error

T = interval between samples

(M - 1)T = finite memory of filter

Fig. 17. Output of the Digital Filter (least squares, zero-lag estimation of first derivative of the input)

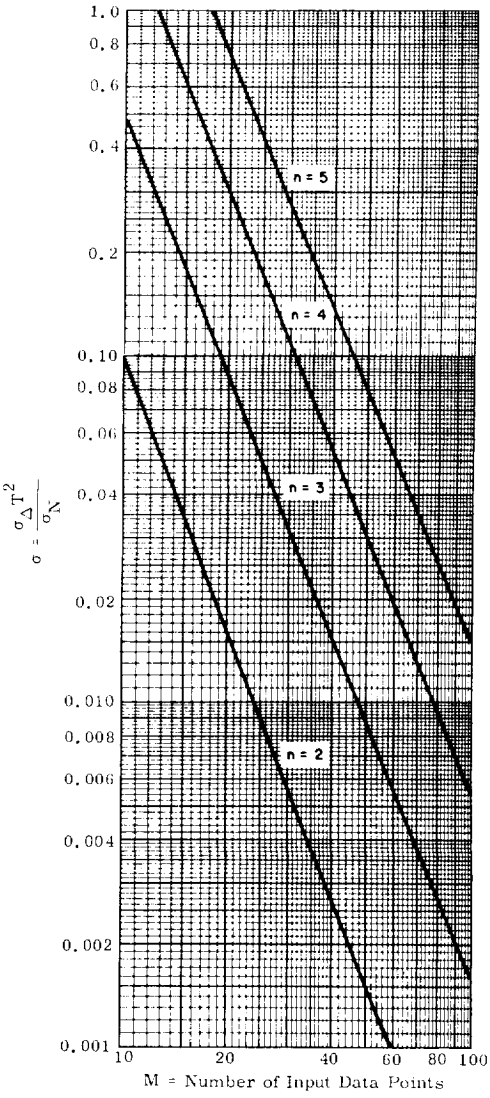

σ_Δ = rms of the output

σ_N = rms of the noise

$\delta = \frac{\sigma_\Delta T^2}{\sigma_N}$

n = degree of polynomial passed without error

T = interval between samples

(M - 1)T = finite memory of filter

Fig. 18. Output of the Digital Filter (least squares, zero-lag [a = 0] estimation of the second derivative of the input)

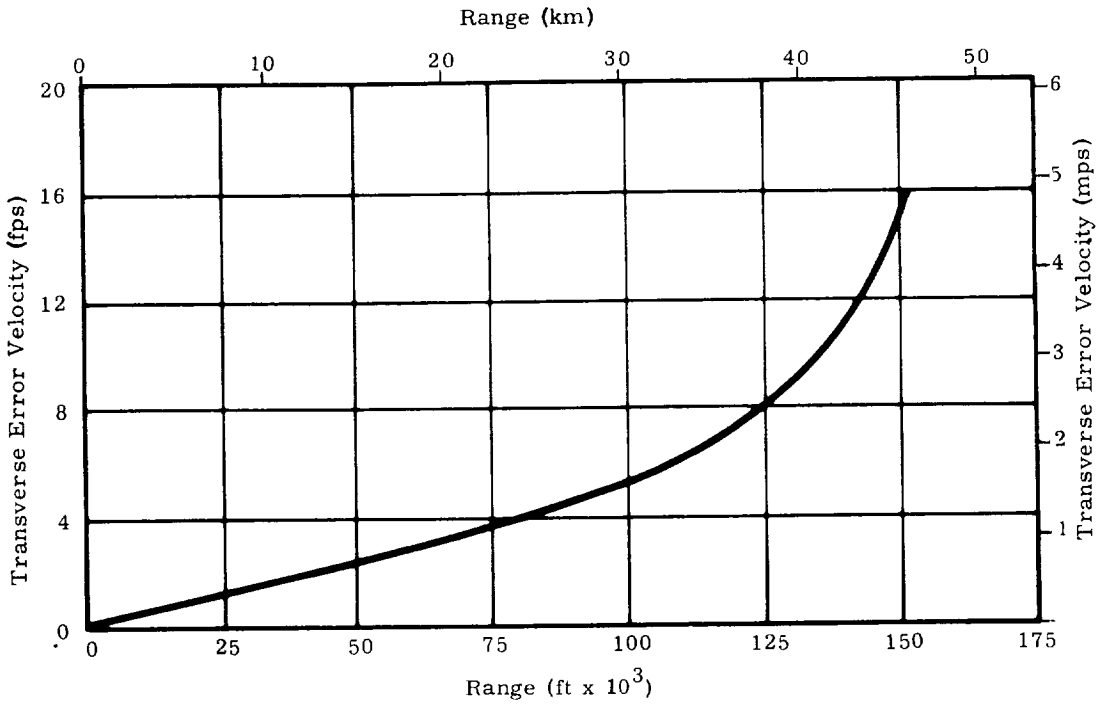

Fig. 19. RMS Residual Transverse Error Velocity

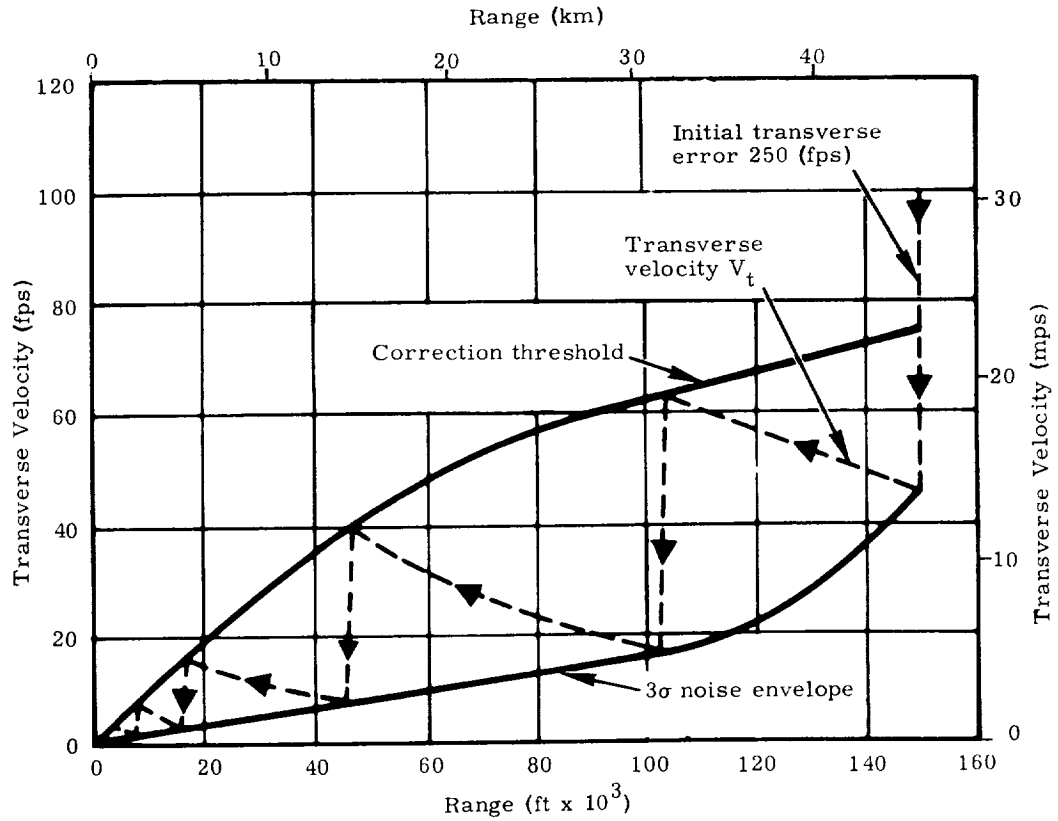

Fig. 20. Homing Profile for Extreme Errors
(1 ft = 0.3048 m)

CHAPTER VIII

ORBITAL DEPARTURE

Prepared by:

G. E. Townsend, Jr.
Martin Company (Baltimore)
Aerospace Mechanics Department
March 1963

		Page
	Symbols	VIII-1
A.	Introduction	VIII-3
B.	The Generalized Return Problem	VIII-3
C.	Planar Analysis of Departure from Low Altitude Orbits.	VIII-17
D.	Three-Dimensional Impulse Analysis for the Case of Circular Orbits	VIII-23
E.	Analysis of Orbital Departure Frequency	VIII-24
F.	Conclusions	VIII-30
G.	References	VIII-30
H.	Bibliography.	VIII-30
	Illustrations	VIII-31

LIST OF ILLUSTRATIONS

Figure	Title	Page
1	Geometry of the Return Problem.	VIII-33
2	Geometry of the Return Problem (expanded view). .	VIII-33
3a	3-D Geometry of the Return Shuttle Problem ($i \geq L_x$)	VIII-34
3b	Characteristic Angles of the Return Shuttle Trajectory	VIII-34
4a	Solution of Flight Time Equation	VIII-35
4b	Flight Time Versus Departure Angle	VIII-36
5	Critical Angle for the Return Flight-Time Solution.	VIII-37
6a	Location of the Return Shuttle in the Orbit Plane . .	VIII-37
6b	Altitude from Sea Level for the Return Shuttle . . .	VIII-38
7	Ground Track of the Return Shuttle	VIII-39
8	Flight Time Error Analysis	VIII-40
9	Error in Re-entry Parameters as Functions of Altitude and Retrorocket Mass Ratios	VIII-41
10	The Ratio of the Velocity Pulse Obtainable from a Rocket Stage to the Ideal Pulse Neglecting Finite Burning Times	VIII-42
11	Re-Entry Parameters as Functions of δ and T/W_0 .	VIII-43
12a	Re-Entry Parameters as Functions of Initial Thrust-to-Weight Ratio and Retrorocket Mass Ratio	VIII-44
12b	Re-Entry Parameters as Functions of Initial Thrust-to-Weight Ratio and Retrorocket Mass Ratio	VIII-45

LIST OF ILLUSTRATIONS (continued)

Figure	Title	Page
12c	Re-Entry Parameters as Functions of Initial Thrust-to-Weight Ratio and Retrorocket Mass Ratio	VIII-46
13	Range Attained in Descending from Re-Entry to Sea Level	VIII-47
14a	Mass Ratio Required to Exit from a 100-Stat Mi (161 km) Circular Orbit	VIII-48
14b	Mass Ratio Required to Exit from a 100-Stat Mi (161 km) Circular Orbit	VIII-48
14c	Mass Ratio Required to Exit from a 100-Stat Mi (161 km) Circular Orbit	VIII-49
15	Variations in the Re-Entry Conditions Due to Small Variations in Orbital Altitude and Velocity	VIII-50
16	Re-Entry Parameters as Functions of Initial Altitude and Retrorocket Mass Ratio	VIII-51
17	Re-Entry Parameters as Functions of Initial Orbital Altitude and Mass Ratio of the Retrorocket	VIII-52
18a	Re-Entry Parameters as Functions of Initial Orbital Velocity and Retrorocket Mass Ratio	VIII-53
18b	Re-Entry Parameters as Functions of Initial Velocity and Mass Ratio of the Retrorocket	VIII-54
18c	Re-Entry Parameters as Functions of Initial Velocity and Retrorocket Mass Ratio	VIII-55
18d	Re-Entry Parameters as Functions of Initial Velocity and Retrorocket Mass Ratio	VIII-56

LIST OF ILLUSTRATIONS (continued)

Figure	Title	Page
18e	Re-Entry Parameters as Functions of Initial Orbital Velocity and Retrorocket Mass Ratio.	VIII-57
19a	Re-Entry Parameters as Functions of ζ and γ_1 . .	VIII-58
19b	Re-Entry Parameters as Functions of ζ and γ_1 . .	VIII-59
19c	Re-Entry Parameters as Functions of ζ and γ_1 . .	VIII-60
19d	Re-Entry Parameters as Functions of ζ and γ_1 . .	VIII-61
19e	Re-Entry Parameters as Functions of ζ and γ_1 . .	VIII-62
20a	Variations in Re-Entry Position, Time and Flight Path Angle (per Second Error in t_B) with Initial Velocity and Retrorocket Mass Ratio	VIII-63
20b	Variations in Re-Entry Position, Time and Flight Path Angle (per Second Error in t_B) with Variations in Initial Velocity and Retrorocket Mass Ratio	VIII-64
20c	Variations in Re-Entry Position, Time and Flight Path Angle (per Second Error in t_B) with Variations in Initial Velocity and Retrorocket Mass Ratio	VIII-65
20d	Variations in Re-Entry Position, Time and Flight Path Angle (per Second Error in t_B) with Initial Velocity and Retrorocket Mass Ratio	VIII-66
20e	Variations in Re-Entry Position, Time and Flight Path Angle (per Second Error in t_B) with Initial Velocity and Retrorocket Mass Ratio	VIII-67

LIST OF ILLUSTRATIONS (continued)

Figure	Title	Page
21	Variations in Re-Entry Location, Time, Flight Path Angle, and Velocity with Initial Velocity as Functions of Retrorocket Mass Ratio and h_1	VIII-68
22a	Variations in Re-Entry Location, Time, Flight Path Angle and Velocity with Altitude as Functions of h_1 and Retrorocket Mass Ratio.	VIII-69
22b	Variations in Re-Entry Position, Time, Flight Path Angle and Velocity with Altitude as Functions of h_1 and Retrorocket Mass Ratio.	VIII-70
22c	Variations in Re-Entry Position, Time, Flight Path Angle and Velocity with Altitude as Functions of h_1 and Retrorocket Mass Ratio.	VIII-71
23a	Errors in the Re-Entry Parameters Due to a 1° Error in γ_1.	VIII-72
23b	Errors in the Re-Entry Parameters Due to a 1° Error in γ_1	VIII-73
23c	Errors in the Re-Entry Parameters Due to a 1° Error in γ_1	VIII-74
23d	Errors in the Re-Entry Parameters Due to a 1° Error in γ_1	VIII-75
23e	Errors in the Re-Entry Parameters Due to a 1° Error in γ_1	VIII-76
24	Optimum ΔK and γ for 3-D Departure	VIII-77
25	Optimum Central Angle and Arrival Path Angle for 3-D Departure	VIII-78
26	Optimum Central Angle and ΔK as a Function of d .	VIII-79
27	Plane Change Angle and Flight Path Angle as Functions of Mass Range Angle	VIII-80

Symbols

A	Reference area for C_D; right ascension (rad)
A_e	Exit area of rocket nozzle
a	Semimajor axis of the ellipse
B	Ballistic coefficient, $C_D A/2m$
D	Aerodynamic drag
D_m	Lateral maneuver distance
E	Eccentric anomaly
e	Eccentricity of the ellipse
g	Gravity at altitude
g_0	Gravity at sea level
h	Altitude above a spherical earth
I_{sp}	Specific impulse of the retrorocket
i	Orbital inclination
J_2	Coefficient of second harmonic of earths potential function 1.0823×10^{-3}
K	$\sqrt{2 - \frac{r}{a}}$
L	Aerodynamic lift; latitude
M	Mean anomaly
m	Mass of the vehicle
n	Number of revolutions; mean motion
P	Pressure
p	Semilatus rectum of ellipse
R	Radius of spherical earth
R_e	Equatorial radius of earth
r	Radius from the center of force
r_m	Mixture ratio (oxidizer/fuel)
T	Thrust
t	Time
t_B	Burning time
V_c	Circular orbital speed = $\sqrt{\mu/r}$
V	Velocity
W	Weight
W_p	Weight propellant
$\dot{W}_p$	Propellant flow rate
X	Range
$\bar{X}$ and $\bar{Y}$	Inertial components of the radius (2 dimensional)
$\dot{\bar{X}}$ and $\dot{\bar{Y}}$	Inertial components of velocity (2 dimensional)
$\ddot{\bar{X}}$ and $\ddot{\bar{Y}}$	Inertial components of acceleration (2 dimensional)
Z	Displacement perpendicular to the orbital plane
α	Angle of attack, cross range angle,
α	range angle
β	Azimuth from north
γ	Flight path angle referenced to local horizontal
$\bar{\gamma}$	Angle formed by $\dot{\bar{X}}$ and $\dot{\bar{Y}}$
Δ_i^j	Finite difference operator
δ	Thrust altitude with respect to the velocity vector
δ'	Supplement of the eccentric anomaly
ζ	Mass ratio (W_p/W_0)
θ	Central angle from perigee to the instantaneous radius
Λ	Longitude
μ	Gravitational constant $(1.407645) 10^{16}$ ft^3/sec^2 or 3.986005×10^{14} m^3/sec^2)
υ	Nondimensional velocity V/V_c
ρ	Density
ρ_B	bulk density $= \frac{r_m + 1}{\frac{r_m}{\rho_{ox}} + \frac{1}{\rho_{fuel}}}$
τ	Orbital period over a spherical earth (sec)
ϕ	Central angle between points in an orbit (deg); central angle $(\theta + \omega)$
ψ	Angle between major axes of 2 orbits
Ω	Longitude of the ascending node

Ω_e	Rotational rate of earth (7.292115 x 10^{-5} rad/sec)
$\dot{\Omega}$	Secular change in the right ascension of the ascending node due to the earth's oblateness (rad/rev)
ω	Argument of perigee

Subscripts

AD	Ascent and descent
a	Apogee or ambient
BO	Burnout
$c\ell$	Low altitude circular orbit
f	First or original orbit
i	Impact, intersection
L	Launch
o	Initial
p	Perigee
r	Rotating
SL	Sea level
t	Terminal
X	Impact

Superscript

*	Denotes point of injection from initial to transfer orbit

A. INTRODUCTION

Most satellite missions eventually require that the satellite or a portion thereof be recovered from orbit. This recovery process has been broken into two phases for presentation in the manual: departure and re-entry. The latter is discussed in Chapter IX and the former is presented here. The purpose of the departure discussions is to provide insight into: the timing limitations for return to a point on earth, the energy requirements, the error sensitivities for that portion of the trajectory occurring above the re-entry altitude (≈400,000 ft or 122 km).

In the analysis of the departure of a satellite from orbit, two general approaches present themselves for consideration:

(1) Departure at those times necessary to arrive at a position in the plane of motion at the same time that the impact site lies in the plane.

(2) Departure any time that the fuel required to maneuver onto a collision trajectory is equal to or less than some prescribed limit.

However, there are orbits which do not meet the requirements imposed by either of these approaches (e.g. some of the 24-hr orbits). Thus, it is necessary before investigating these approaches to first analyze the general problem of return from orbit utilizing an intermediate orbit (i.e. the reverse rendezvous technique of Chapter VII). Once this is done departure from the parking orbit (assumed to be nearly circular) can be discussed.

It should be noted at this point that the parking orbit approach is not a firm requirement since by properly restricting the times of departure and the descent trajectories, the position of the re-entry point can be matched to almost any specified point ($L \leq i$) without the use of the parking orbit. However, the only means for producing re-entry from an arbitrary orbit at a prescribed position and at a preselected time (assuming very limited or no maneuvering during descent) is the parking orbit. Other significant advantages will be discussed in turn during the presentation of the material.

B. THE GENERALIZED RETURN PROBLEM

1. Return Trajectories

Transfer from the elliptical orbit into a low altitude circular orbit is now considered. The time limitations (i.e., arrival at a given time over a fixed point) are not considered initially because time-imposed conditions can be obtained later by variations of the general return trajectory.

The transfer orbit is assumed to be an ellipse whose major axis is inclined at some unknown angle (ψ) to the major axis of the original orbit. Injection into the transfer orbit is accomplished tangentially at a departure point r^*, θ^* as shown in Fig. 1. A nonzero flight path angle at departure is specified because:

(1) Limitations may exist on the velocity pulses given by the rocket booster.

(2) Arrival time and location of the intersection with the low altitude orbit can be adjusted by changes in the departure angle.

(3) This approach results in a more generalized solution, where perigee departure is included as a particular case.

In order to ensure the certainty of intersection with the final low altitude circular orbit, a requirement exists that the perigee radius of the transfer orbit must be equal to or less than the radius of the final orbit. This can be given mathematically as

$$r_{pt} \leq r_{cl} \text{ or } r_{cl} = r_{pt} + \Delta r \qquad (1)$$

where Δr is determined by the probable errors caused by the guidance limitations at the departure point. In order to avoid the atmospheric effects distorting the transfer trajectory, the low altitude orbit should be at least 200 stat mi 322 km above sea level. In any case, the perigee radius of the transfer orbit has to be fixed before the maneuver. This considerably simplifies the solution for the remaining properties of the transfer orbit.

Knowing the parameters of the original orbit and having specified the departure time or the departure angle (θ^*), the departure radius is determined as

$$r^* = \frac{p_f}{1 + e_f \cos \theta^*} \cdot \qquad (2)$$

For greater generality, this can also be given in a nondimensional parameter form, using the perigee distance of the original orbit as a reference distance as

$$\frac{r^*}{r_{pf}} = \frac{1 + e_f}{1 + e_f \cos \theta^*} \cdot \qquad (2b)$$

At the departure point, the two ellipses are further assumed to be tangent, as shown in Fig. 1 for efficiency of propellant consumption. This means that the flight path angles are identical, i.e.,

$$\gamma_t = \gamma_f \equiv \gamma^* .$$

where: flight path angle is defined from the conservation of angular momentum by

$$V r \cos \gamma = \sqrt{p\mu},$$

Thus

$$\cos^2 \gamma = \frac{1}{\frac{r}{r_p}\left(1 + \frac{r_p}{r_a} - \frac{r}{r_a}\right)} \cdot \qquad (3)$$

where the sign of the flight angle is determined by the quadrant of the original ellipse.

Using $\gamma_t^* = \gamma^*$ and writing Eq (3) for the radii of the transfer ellipse and the initial orbit, it follows that the apogee radius of the transfer orbit is given by

$$\frac{r_{at}}{r^*} = \frac{\left(1 - \frac{r_{pt}}{r^*}\right)\cos^2\gamma^*}{\cos^2\gamma^* - \frac{r_{pt}}{r^*}} . \qquad (4)$$

From Eq (4), the semimajor axis of the transfer ellipse is obtained as

$$\frac{a_t}{r^*} = \frac{1}{2}\left[\frac{\cos^2\gamma^* - \left(\frac{r_{pt}}{r^*}\right)^2}{\cos^2\gamma^* - \frac{r_{pt}}{r^*}}\right] . \qquad (5)$$

Next, in order to determine the properties of the transfer orbit completely, the central angle from perigee (θ_t^*) is obtained. At the departure point, the following expression holds:

$$r^* = \frac{p_f}{1 + e_f \cos\theta^*} = \frac{p_t}{1 + e_t \cos\theta_t^*} .$$

Solving this for θ_t^*,

$$\cos\theta_t^* = \frac{\frac{r_{pt}}{r_{pf}}}{1 - \frac{r_{pt}}{r_{at}}}\left[\left(1 + \frac{r_{pf}}{r_{af}}\right) + \left(1 - \frac{r_{pf}}{r_{af}}\right)\cos\theta^* - \frac{r_{pf}}{r_{pt}}\left(1 + \frac{r_{pt}}{r_{at}}\right)\right] . \qquad (6a)$$

Using Eq (2b), this can be rewritten in a shorter form as

$$\cos\theta_t^* = \frac{2\frac{r_{pt}}{r^*} - \left(1 + \frac{r_{pt}}{r_{at}}\right)}{1 - \frac{r_{pt}}{r_{at}}} . \qquad (6b)$$

Assuming that transfer will be initiated near apogee of the transfer orbit, the quadrant of the initial central angle in the transfer orbit is determined by the rule:

if $0 \leq \theta^* \leq 180°$ then $90° < \theta_t^* \leq 180°$

if $180° \leq \theta^* \leq 360°$ then $180° \leq \theta_t^* < 270°$

Now from the geometry of the problem, the angle between the major axes of the transfer and target orbits is

$$\psi = 180° + \theta^* - \theta_t^* . \qquad (7)$$

Next, the magnitude of the velocity impulse applied at θ^* is determined (direction ΔV^* is opposite to the direction of motion for the assumed tangential transfer). Since the departure radius and semimajor axes for both ellipses are already computed, this velocity impulse is found by the numerical difference of the velocity required in the original orbit and the velocity corresponding to the transfer orbit at this particular point.

$$\Delta V^* = V_f^* - V_t^* . \qquad (8)$$

These velocities may be found from the energy equation.

$$V = \sqrt{\mu\left(\frac{2}{r} - \frac{1}{a}\right)} \qquad (9)$$

Equations (8) and (9) determine the required velocity impulse as

$$\Delta V^* = \sqrt{\frac{\mu}{r^*}}\left[\sqrt{2 - \frac{r^*}{a_f}} - \sqrt{2 - \frac{r^*}{a_t}}\right] \qquad (10)$$

Injection into the low altitude circular orbit is now accomplished at either the intersection point r_{1t} or point r_{2t}, as shown in Fig. 2.

In a manner similar to that of Eq (6b), the intersection central angle is given by

$$\cos\theta_{it} = \frac{2\frac{r_{pt}}{r_{it}} - \left(1 + \frac{r_{pt}}{r_{at}}\right)}{1 - \frac{r_{pt}}{r_{at}}} , \qquad (11)$$

where

$i = 1, 2$

$r_{it} = r_{cl}$

θ_{1t} is in the fourth quadrant and θ_{2t} is in the first quadrant for all reasonable return trajectories.

Now the maneuver angle at the circular orbit is defined by:

$$\cos^2\Delta\gamma_i = \frac{1}{\frac{r_{cl}}{r_{pt}}\left(1 + \frac{r_{pt}}{r_{at}} - \frac{r_{cl}}{r_{at}}\right)} \qquad (12)$$

where the following rules apply:

$$\Delta\gamma_1 \leq 0 \quad \text{(negative)}$$

$$\Delta\gamma_2 \geq 0 \quad \text{(positive)}$$

and the pulse required is

$$\Delta V_1^2 = V_{1t}^2 - 2V_{1t}\, V_{1\ell} \cos \Delta\gamma_1 + V_{1\ell}^2 \qquad (13)$$

or

$$\left(\frac{\Delta V_1}{V_{1\ell}}\right)^2 = \left(\frac{V_{1t}}{V_{1\ell}}\right)^2 - 2\left(\frac{V_{1t}}{V_{1\ell}}\right)\cos \Delta\gamma_1 + 1. \qquad (14)$$

where

$$V_{1t} = \sqrt{2 - \frac{r_{c\ell}}{a_t}}\ \sqrt{\frac{\mu}{r_{c\ell}}}$$

$$V_{1\ell} = \sqrt{\frac{\mu}{r_{c\ell}}}\,.$$

Thus, the following equation results:

$$\left(\frac{\Delta V_1}{V_{c\ell}}\right)^2 = \left(3 - \frac{r_{c\ell}}{a_t}\right) - 2\left(2 - \frac{r_{c\ell}}{a_t}\right)^{1/2} \cos \Delta\gamma_1 \qquad (15)$$

Now the angle at which the thrust must be applied with respect to the velocity vector (δ) is found by the law of sines.

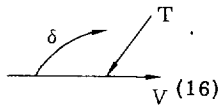

$$\sin \delta_1 = \left(\frac{V_{c\ell}}{\Delta V_1}\right) \sin \Delta\gamma_1 \qquad (16)$$

To avoid the ambiguities in the sign of Eq (16), the law of cosines can also be applied to the angle δ, resulting in

$$\cos \delta_1 = \frac{+\sqrt{2 - \frac{r_{c\ell}}{a_t}} - \cos \Delta\gamma_1}{\left(\frac{\Delta V_1}{V_{c\ell}}\right)}\,. \qquad (17)$$

At r_{2t}, a similar analysis can be applied since the drag loss is negligible for half a revolution and a symmetry about the major axis exists.

This analysis determines the trajectories and velocity pulses for a return into a circular orbit. The flight times and the positioning problems are considered in Subsection 3.

2. Departure Error Analysis

The problem arises concerning the effect of small errors of altitude, velocity or flight path angle on the perigee conditions. Partial derivatives of the perigee radius and velocity, with respect to initial conditions, are obtained in terms of eccentricity and central angle. In the conversion from the usual r, V and γ relationships, the following equations are found to be most useful:

$$\frac{r}{r_p} = \frac{1 + e}{1 + e \cos \theta} \qquad (18)$$

$$\left(\frac{V}{V_c}\right)^2 = \frac{1 + 2\, e \cos \theta + e^2}{1 + e \cos \theta} \qquad (19)$$

$$\left(\frac{V_c}{V_{ca}}\right)^2 = \frac{1 + e \cos \theta}{1 - e} \qquad (20)$$

$$\cos^2 \gamma = \frac{(1 + e \cos \theta)^2}{1 + 2\, e \cos \theta + e^2} \qquad (21)$$

The partials of r_p can be nondimensionalized as follows:

$$\frac{V}{r}\,\frac{\partial r_p}{\partial V} = \frac{2\,(1 + e \cos \theta)\,(1 - \cos \theta)}{(1 + e)^2} \qquad (22)$$

$$\frac{\partial r_p}{\partial r} = \frac{(1 - e)\,(1 + \cos \theta)}{(1 - e^2)^2}\,(2 - e - e^2 - \cos \theta + e \cos \theta) \qquad (23)$$

$$\frac{1}{r}\,\frac{\partial r_p}{\partial \gamma} = -\sin \theta. \qquad (24)$$

The partials of V_p are derived from the conservation of angular momentum

$$V_p\, r_p = V\, r \cos \gamma.$$

Differentiating,

$$\frac{\partial (V_p\, r_p)}{\partial V} = V_p \frac{\partial r_p}{\partial V} + r_p \frac{\partial V_p}{\partial V} = r \cos \gamma. \qquad (25)$$

Using Eqs (18) to (22), the final form of the partial is obtained.

$$\frac{\partial V_p}{\partial V} = \frac{e - 1 + 2 \cos \theta}{(1 + 2\, e \cos \theta + e^2)^{1/2}}\,. \qquad (26)$$

Using the method of Eq (25), the following equations are obtained:

$$\frac{r}{V}\frac{\partial V_p}{\partial r} = \frac{\cos\theta - 1}{(1 + 2e\cos + e^2)^{1/2}} \qquad (27)$$

$$\frac{1}{V}\frac{\partial V_p}{\partial \gamma} = \frac{(1+e)\sin\theta}{(1 + e\cos\theta)(1 + 2e\cos\theta + e^2)^{1/2}} \qquad (28)$$

As seen in Fig. 1, the departure usually occurs close to the apogee of the transfer ellipse, i.e., $\theta_t^* \approx 180°$. For this case

$$\cos\theta_t^* \approx -1$$

$$\cos\theta_t^* \approx 0.$$

Therefore, the partial derivatives for the case of departure point being near to the apogee of the transfer ellipse reduce to the following:

(1) Errors in perigee radius.

$$\frac{V_a}{r_a}\frac{\partial r_p}{\partial V_a} = \frac{4(1-e)}{(1+e)^2} = \left(2\frac{r_p}{r_a}\right)\left(1 + \frac{r_p}{r_a}\right) \qquad (29)$$

$$\frac{\partial r_p}{\partial r_a} = \frac{(1-e)(3+e)}{(1+e)^2} = \frac{r_p}{r_a}\left(2 + \frac{r_p}{r_a}\right) \qquad (30)$$

$$\frac{1}{r_a}\frac{\partial r_p}{\partial \gamma} = 0. \qquad (31)$$

(2) Errors in perigee velocity.

$$\frac{\partial V_p}{\partial V_a} = \frac{e-3}{1-e} = -\left(2 + \frac{r_a}{r_p}\right) \qquad (32)$$

$$\frac{r_a}{V_a}\frac{\partial V_p}{\partial r_a} = -\frac{2}{1-e} = -\left(1 + \frac{r_a}{r_p}\right) \qquad (33)$$

$$\frac{1}{V_a}\frac{\partial V_p}{\partial \gamma} = 0. \qquad (34)$$

In Eqs (22) to (34), it is implied that all the quantities pertain to the transfer ellipse.

The important point to notice is the insensitivity of the perigee radius and velocity to errors in flight path angle for near-apogee departures, as shown by Eqs (31) and (34).

For small deviations from the required departure conditions, the perigee errors can be approximated from the given partials by

$$\Delta r_p \approx \frac{\partial r_p}{\partial r_a}\Delta r_a + \frac{\partial r_p}{\partial V_a}\Delta V_a + \frac{\partial r_p}{\partial \gamma}\Delta\gamma \qquad (35)$$

and

$$\Delta V_p \approx \frac{\partial V_p}{\partial r_a}\Delta r_a + \frac{\partial V_p}{\partial V_a}\Delta V_a + \frac{\partial V_p}{\partial \gamma}\Delta\gamma \qquad (36)$$

By substituting Eqs (29) to (31) into (35), the radial errors for a near-apogee departure are obtained:

$$\frac{\Delta r_p}{r_a} \approx \frac{1-e}{(1+e)^2}\left[(3+e)\frac{\Delta r_a}{r_a} + 4\frac{\Delta V_a}{V_a}\right] \qquad (37)$$

or in terms of apogee and perigee radii:

$$\frac{\Delta r_p}{r_a} \approx \frac{r_p}{r_a}\left[\left(2 + \frac{r_p}{r_a}\right)\frac{\Delta r_a}{r_a} + 2\left(1 + \frac{r_p}{r_a}\right)\frac{\Delta V_a}{V_a}\right]. \qquad (38)$$

Similarly, the velocity error is found by substituting Eqs (32) to (34) into (36).

$$\frac{\Delta V_p}{V_a} \approx -\left(\frac{1}{1-e}\right)\left[2\frac{\Delta r_a}{r_a} + (3-e)\frac{\Delta V_a}{V_a}\right] \qquad (39)$$

or

$$\frac{\Delta V_p}{V_a} \approx -\left[\left(1 + \frac{r_a}{r_p}\right)\frac{\Delta r_a}{r_a} + \left(2 + \frac{r_a}{r_p}\right)\frac{\Delta V_a}{V_a}\right]. \qquad (40)$$

3. Timing Considerations

Assume that the trajectory problem of the return vehicle is defined as follows:

(1) The vehicle must arrive in a low altitude orbit over a specified impact area at some predetermined time.

(2) There are possible limitations on the velocity pulses to be employed during the maneuver.

Immediately, it becomes clear that unless the orbital plane for the return phase is different from that of the original orbit, only two times of

arrival in the low altitude orbit are acceptable during each day. These times correspond to the times at which the impact point crosses the orbital plane.

The following analysis of the return problem is quite general. However, because the number of variables involved is large, only those cases for which the orbital plane is unaltered are treated.

The initial location (at time t_0) of the final intersection point is determined by using spherical trigonometry and the symbols defined in Fig. 3a.

$$\sin L_0 = \sin i \sin \phi_0 . \tag{41}$$

Equation (41) applies only if $L_0 \leq i$. In case the inclination angle is less than the latitude of the impact area (note that $L_0 \equiv L_x$), a change in orbital inclination must be accomplished before or during the departure maneuver. The equations for such a maneuver are presented in Chapter VI.

From spherical trigonometry, the first intersection of the two planes is

$$\cos (\Lambda_0 - \Omega_0) = \frac{\cos \phi_0}{\cos L_x} . \tag{42}$$

The second intersection is

$$\Lambda_0' - \Omega_0 = \pi - \cos^{-1}\left(\frac{\cos \phi_0}{\cos L_x}\right). \tag{42a}$$

Next, the initial angular distance from the intersection point (P_i) to the impact point (P_x) is

$$\Delta\Lambda_0 = \Lambda_0 - \Lambda_x$$

$$= (\Omega_0 - \Lambda_x) + \cos^{-1}\left(\frac{\cos \phi_0}{\cos L_x}\right). \tag{43}$$

During each revolution of the earth there are two intersection points, P_i and P_i'

Time to intersection for the first day is

$$t_{j1} = \frac{\Delta\Lambda_0}{\dot{\Omega}_e} = \frac{\Omega_0 - \Lambda_x}{\dot{\Omega}_e} + \frac{1}{\dot{\Omega}_e}\cos^{-1}\left(\frac{\cos \phi_0}{\cos L_0}\right). \tag{44}$$

Time to intersection for n days is

$$t_j = t_{j1} + (n - 1)\, d + \frac{n\dot{\Omega} d}{\dot{\Omega}_e \tau} \quad (j = n = 1, 2, 3 \ldots) \tag{45}$$

where d = sidereal day (86,164 sec)

Or using Eq (44),

$$t_j = \frac{\Omega_0 + n\dot{\Omega} d/\tau - \Lambda_x}{\dot{\Omega}_e} + \frac{1}{\dot{\Omega}_e}\cos^{-1}\left(\frac{\cos \phi_0}{\cos L_0}\right) + (n - 1)\, d \tag{46}$$

where $j = n = 1, 2, 3, \ldots$

Equation (46) gives the only possible flight times for target interception.

By changing the inclination at the original orbit in inertial space (i.e., changing i and/or Ω_0), a small range of possible intersection times can be achieved. Large changes in inclination become prohibitive due to exceedingly high mass ratios and should not be considered for most vehicles.

From the geometry of Fig. 3b,

$$\psi = 180° - (\theta_t^* - \theta^*) \tag{47}$$

and

$$\theta_\ell = 360° - \omega + \phi_0 + \theta_t^* - \theta^*. \tag{48}$$

Now, after the equation for the necessary intercept flight time has been derived and the angles for the transfer trajectory have been defined, a solution of the departure angle is required in mathematical form.

$$\theta^* = f(\theta_0, \Omega_0, i, \omega, p_f, e_f, r_\ell, \Lambda_x, L_x, t_t) . \tag{49}$$

To get the exact relationship indicated by Eq (49), an expression for the total flight time must be derived in terms of all other pertinent variables. In such an equation there is only one unknown (i.e., θ^*) and the proper value of the total flight time, corresponding to some fixed value determined by Eq (46), can be obtained by variations of θ^*.

In general, the total flight time is the sum of three separate components.

(1) Time in original orbit before departure (t_1).

(2) Time in transfer orbit (t_2).

(3) Time in the final low altitude orbit until the impact area is reached (t_3).

Consider the case where the departure angle from perigee (θ^*) is less than the initial central angle (θ_0), or $\theta^* < \theta_0$. Then, the components of flight time will be as follows.

(1) Original orbit

$$t_1 = \frac{\tau_f}{2\pi}\left[2\pi + (E^* - E_0) + e(\sin E_0 - \sin E^*)\right]$$

where

$$E = 2 \tan^{-1}\left[\sqrt{\frac{1-e}{1+e}}\ \tan\frac{\theta}{2}\right]$$

$$\sin E = \frac{\sqrt{1-e^2}\sin\theta}{1+e\cos\theta} \qquad (50)$$

(2) Transfer orbit

$$t_2 = \frac{\tau_t}{2\pi}\left\{2\pi - E_t^* + e_t \sin E_t^*\right\} \qquad (51)$$

(3) Low altitude circular orbit

$$t_3 = \frac{\tau_\ell}{2\pi}\theta_\ell = \sqrt{\frac{r_\ell^3}{\mu}}\,(2\pi - \omega + \phi_0 + \theta_t^* - \theta^*) \qquad (52)$$

The total flight time is given as

$$t_t = t_1(\theta^*) + t_2(\theta^*) + t_3(\theta^*) \qquad (53)$$

where it is desired that t_t be one of the characteristic time values given by Eq (46).

If the departure angle from perigee is greater than the initial central angle ($\theta^* > \theta_0$), then the transfer orbit is initiated before the next perigee passage and Eq (50) becomes

$$t_t = \frac{\tau_f}{2\pi}\left\{(E^* - E_0) + e(\sin E_0 - \sin E^*)\right. \qquad (54)$$

Equations (51), (52) and (53) remain identical even for the case of $\theta^* > \theta_0$.

The transformation of Eq (53) into (49) is obviously extremely complicated, if not impossible. Thus, it is necessary to revert to a trial-and-error method. One such method is described below.

4. Iteration Procedure for the Departure Angle

The approach presupposes that either the computer possesses plotting and curve-reading abilities, or that the first approximation of the departure angle is known.

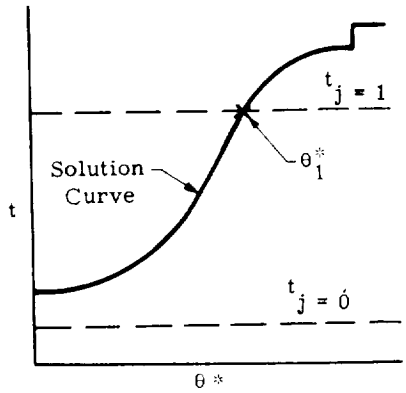

For a particular return mission, the most obvious method of solution is as follows.

(1) Determine the target point intercept times with the orbit plane (t_j).

(2) Establish the total flight time solution curve for a whole revolution in original orbit by the procedure shown in Table 1. Relatively large increments of central angle (e.g., $\Delta\theta^* = 30°$) can be used.

(3) Find the first intersection point (θ_1^*) of the solution curve and target intercept times.

(4) Determine the accurate departure angle by a linear iteration process.

(a) Use Eq (53) to compute t_{t1} for the first approximation of θ_1^*.

$$\text{If}\left\{\begin{array}{l} t_j > t_{t1}, \text{ assume } \theta_2^* = \theta_1^* + 1 \\ t_j < t_{t1}, \text{ assume } \theta_2^* = \theta_1^* - 1 \end{array}\right\}.$$

(b) Compute t_{t2} for θ_2^*.

NOTE: t_{t1} and t_{t2} should be on the opposite sides of t_j. If both are on the same side, i.e.,

$$\left\{\begin{array}{l} t_{t1} > t_j \\ t_{t2} > t_j \end{array}\right\} \text{ or } \left\{\begin{array}{l} t_{t1} < t_j \\ t_{t2} < t_j \end{array}\right\},$$

use θ_2^* as θ_1^* and repeat step (4a).

(c) From θ_1^* and θ_2^*, compute the second approximation by the linear relationship

$$\theta_3^* = \frac{t_j - B}{A} \qquad (55)$$

where

$$A = \frac{t_{t1} - t_{t2}}{\theta_1^* - \theta_2^*} \qquad (56a)$$

$$B = \frac{t_{t2}\,\theta_1^* - t_{t1}\,\theta_2^*}{\theta_1^* - \theta_2^*}. \qquad (56b)$$

(d) Compute t_{t3} for θ_3^*. As for each linear approximation, the two points used must be on opposite sides of t_j line, the following rules apply.

$$\text{If}\begin{cases} t_{t3} > t_j, \text{ use min } \theta_k^* \\ t_{t3} < t_j, \text{ use max } \theta_k^* \end{cases} \text{where } \left\{ \theta_k : \theta_1^*,\ \theta_2^* \right\} .$$

(e) Compute the third approximation by using θ_3^* in connection with the correct θ_k^*.

Thus,

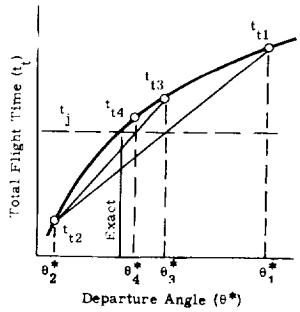

$$\theta_4^* = \frac{t_j - B'}{A'} \qquad (57)$$

$$A' = \frac{t_{tk} - t_{t3}}{\theta_k^* - \theta_3^*} \qquad (58a)$$

$$B' = \frac{t_{t3}\theta_k^* - t_{tk}\theta_3^*}{\theta_k^* - \theta_3^*} \qquad (58b)$$

The iteration usually converges very rapidly because θ_1^* and θ_2^* are already within ± 1° of the exact answer desired. The geometrical interpretation of the convergence is shown in the preceding sketch. The reason for taking θ_k^* as one of the initial points is to avoid $(\theta_k^* - \theta_3^*) \to 0$ as the exact answer is approached. With this method, the values of $(\theta_k^* - \theta_3^*)$ remain finite for all approximations.

Table 1 presents the necessary variables arranged in the order of computation, and the equations used to aid in the visualization of the solution procedure.

TABLE 1
Return Shuttle Computations

	Variable	How Determined	Remarks
Desired Intercept Times	ϕ_o	Eq(41b)	
	t_j	Eq(46)	
Total Flight Curve	r^*	Eq(2a)	First assume θ^*
	$\cos^2 \gamma^*$	Eq(3)	
	r_{at}/r^*	Eq(4)	
	$\cos \theta_t^*$	Eq(6b)	
	a_t	$a_t = 1/2\,(r_{at} + r_{pt})$	
	e_t	$e_t = \frac{r_{at}}{a_t} - 1$	
	$\tau_t/2\pi$	$\frac{\tau_t}{2\pi} = \frac{a_t^3}{\mu}$	
	$\tau_\ell/2\pi$	$\frac{\tau_\ell}{2\pi} = \frac{r_\ell^3}{\mu}$	
	t_1	Eq(50) or (54)	
	t_2	Eq(51)	
	t_3	Eq(52)	
	t_t	$t_t = t_1 + t_2 + t_3$	Plot t_t vs θ^* (Fig. 4a)
Ground Track	M_i	$M_i = \frac{2\pi}{\tau} t_i$	For simplicity assume t_i in full hours
	θ_i	by iteration	
	L	Eq(59)	
	Λ	Eq(60)	

It should be noted that for a first approximation t_1, t_2, t_3 and θ_i can be found from Keplerian flight time curves (Chapter III). These curves are accurate to four significant figures and satisfactory for slide rule computations. After the flight time curve is plotted and the first estimate of departure angle is obtained, the exact equations should be used.

The desired intercept times and the ground track are computed only once (intercept times are independent of departure angle, and ground track is determined for only one final value of θ^*).

For the total flight time curve, values of θ^* are assumed at sufficient intervals (e.g., $\Delta\theta^* = 30°$) and t_t is found for each θ^*. From a plot of t_t versus θ^*, the intersections with the desired intercept times are determined.

5. Sample Problem

Assume that the following orbital and target parameters are specified (target refers to the specified low altitude orbit).

$\theta_0 = 0°$

$i = 70°$

$\omega = 270°$

$\Omega_0 = 135°\ E = +135°$

$\Lambda_x = 80°\ W = -80°$

$L_x = 28°\ N = +28°$

$\tau_f = 86,164.09$ sec (24-hour orbit)

$p_f = 1.037528 \times 10^8$ ft = 31623.9 km

$e_f = 0.500000$

$r_{af} = 2.075055 \times 10^8$ ft = 63247.7 km

$r_{pf} = 0.691685 \times 10^8$ ft = 21082.6 km

$r_\ell = r_{pt} = 0.224869 \times 10^8$ ft = 6854.0 km

The angle (ϕ_0) from the ascending node of the orbital plane to the intercept point of the target path and orbital plane is from Eq (41).

$$\phi_0 = \sin^{-1}\left(\frac{\sin 28°}{\sin 70°}\right) \approx \sin^{-1}(0.500)$$

$$\begin{cases} \phi_0 \approx 30° \\ \phi_0' \approx 150° \end{cases}$$

From Eq (43),

$$\Delta\Lambda_0 \approx 135° - (-80°) + \cos^{-1}\left(\frac{\cos 30°}{\cos 28°}\right)$$

$$\begin{cases} \Delta\Lambda_0 \approx 226.5° \\ \Delta\Lambda_0' \approx 383.5° \end{cases}$$

There is also the possibility of considering the angle $\Delta\Lambda_0' \approx 383.5° - 360° \approx 23.5°$, because $\Delta\Lambda_0'$ is actually ahead at the target point. Time to reach the first intersection points is as follows.

$$t_{j=1} \approx \frac{226.5}{4.18 \times 10^{-3}} = 54,200 \text{ sec} = 15.06 \text{ hr}$$

$$t_{j=1}' \approx \frac{383.5}{4.18 \times 10^{-3}} = 91,800 \text{ sec} = 25.5 \text{ hr}$$

$$t_{j=1}'' \approx \frac{23.5}{4.18 \times 10^{-3}} = 5620 \text{ sec} = 1.56 \text{ hr}$$

The second set of possible flight times is derived from Eq (45).

$$t_{j=2} = 54,200 + (2 - 1)\ 86,200 = 140,400 \text{ sec} = 39.0 \text{ hr}$$

$$t_{j=2}' = 91,800 + (2 - 1)\ 86,200 = 178,000 \text{ sec} = 49.5 \text{ hr}$$

This means that during each day there are two possible arrival times over the target area.

Next, the total flight time is computed for $\theta^* = 0°, 30°, 60° \ldots 360°$, using Table 1 in connection with Chapter III. The sample calculations are given later for $\theta^* = 137°$.

The results for the departure angle within the first revolution of the 24-hr orbit are shown in Fig. 4a. The solid line gives the total flight times for the ascent crossing at the target latitude during the first revolution in the low altitude orbit. For the descent crossing during the first revolution, and for all crossings during succeeding revolutions in the low altitude orbit, the solid line retains its shape but will be displaced along the time axis by some constant flight time.

The first time the target crosses the orbital plane (1.56 hr) it falls short of the necessary transfer time. Therefore, this solution is imaginary.

For the given sample problem, the first possible departure angle is approximately $\theta^* \approx 137°$, corresponding to a flight time of 15 hr.

The important feature of Fig. 4a is the discontinuity in the total flight time solution. This irregularity is caused by the fact that overshooting the target interception by even a small angle results in the requirement for another revolution in the 24-hr orbit. For the given case, the third theoretically possible target intercept time is seen to fall into the region of discontinuity, indicating that this arrival time also represents an imaginary solution.

Of course, a possibility exists that the target intercept could be made during a succeeding revolution in the low altitude orbit. The optimum number of such revolutions will depend primarily upon the purpose of the return shuttle.

For example, the target intercept could be made at 25.5 hr by leaving at $\theta^* \approx 236°$ and staying for more than one full revolution in the low altitude orbit.

To explain the discontinuity at $\theta^*_{critical}$, flight times in the 24-hr orbit, the transfer orbit and the low altitude orbit are given separately in Fig. 4b. At $\theta^*_{critical} \approx 312°$, the overshooting of the target will require another revolution in the low orbit.

The determination of the critical departure angle is best accomplished by plotting θ_ℓ versus θ^*, as shown in Fig. 5. The flight time discontinuity exists at $\theta_\ell = 0°$.

Figure 4a indicates that $t_1 \approx 15$ hr is the most promising total maneuver time. Therefore, this solution is recomputed with more accuracy than that afforded by the preliminary slide rule results. From Eq (41),

$$\phi_0 = 29.9736°.$$

Time to reach the first intercept point is

$$t_{j=1} = \frac{\Omega_0 - \Lambda_x}{\Omega_e} + \frac{1}{\Omega_e} \cos^{-1}\left(\frac{\cos \phi_0}{\cos L_x}\right)$$

$$= 54,129.917 \text{ sec} = 15.036088 \text{ hr}.$$

The departure angle ($\theta^* = 137°$) is used to find t_{t1} by the procedure given in Table 1. All the steps are indicated for the sample problem in the following paragraphs.

(1) Departure radius

$$r^* = \frac{p_{24}}{1 + e_{24} \cos \theta^*} = 1.635645 \times 10^8 \text{ ft}$$
$$= 49,854.4 \text{ km}$$

(2) Cosine flight path angle

$$\cos^2 \gamma^* = \frac{1}{\frac{r^*}{r_{p24}}\left(1 + \frac{r_{p24}}{r_{a24}} - \frac{r^*}{r_{a24}}\right)} = 0.775799$$

(3) Apogee radius

$$\frac{r_{at}}{r^*} = \frac{\left(1 - \frac{r_{pt}}{r^*}\right)\cos^2 \gamma^*}{\cos^2 \gamma^* - \frac{r_{pt}}{r^*}} = 1.048287$$

(4) Central angle

$$\cos \theta_t^* = \frac{2\frac{r_{pt}}{r^*} - \left(1 + \frac{r_{pt}}{r_{at}}\right)}{1 - \frac{r_{pt}}{r_{at}}}; \quad \theta_t^* = 170.2047°$$

(5) Semimajor axis

$$a_t = \frac{1}{2}(r_{at} + r_{pt}) = 0.969747 \times 10^8 \text{ ft}$$
$$= 29557.8 \text{ km}$$

(6) Eccentricity

$$e_t = \frac{r_{at}}{a_t} - 1 = 0.768115$$

(7) Period of transfer orbit

$$\frac{\tau_t}{2\pi} = \sqrt{\frac{a_t^3}{\mu}} = 8048.71 \text{ sec}$$

(8) Period of low altitude orbit

$$\frac{\tau_\ell}{2\pi} = \sqrt{\frac{r_\ell^3}{\mu}} = 898.74 \text{ sec}$$

As $\theta^* > \theta_0$, from Eq (54),

$$t_1 = 20,276.50 \text{ sec} = 5.632361 \text{ hr}.$$

From Eq (51), the following is obtained.

$$t_2 = 31,796.37 \text{ sec} = 8.832325 \text{ hr}$$

(9) Angle in low orbit

$$\theta_\ell = 360° - \omega + \phi_0 + \theta_t^* - \theta^* = 153.1783°$$
$$= 2.673465 \text{ rad}$$

$$t_3 = \frac{\tau_\ell}{2\pi}\theta_\ell = 2402.75 \text{ sec} = 0.667430 \text{ hr}$$

(10) Total flight time

$$t_{t1} = t_1 + t_2 + t_3 = 15.132112 \text{ hr}$$

(11) Error in flight time

$$\Delta t_1 = t_t - t_j = 345.7 \text{ sec} = 5.76 \text{ min}$$

As $t_{t1} > t_j$, $\theta_2^* = \theta_1^* - 1 = 136°$ and, by the previous method, $t_{t2} = 14.960314$ hr.

Using the iteration process given in Eqs (55), (56a) and (56b), the next approximation is obtained.

$$A = \frac{t_{t1} - t_{t2}}{\theta_1^* - \theta_2^*} = 0.171802 \text{ hr/deg}$$

$$B = \frac{t_{t2}\theta_1^* - t_{t1}\theta_2^*}{\theta_1^* - \theta_2^*} = -8.404758 \text{ hr}$$

Finally,

$$\theta_3^* = \frac{t_j - B}{A} = 136.4411^\circ .$$

Using $\theta_3^* = 136.44^\circ$, $t_{t3} = 15.036515$ hr is obtained for the second approximation.

Since $t_{t3} > t_j$, by the rules given in subsection 5, min θ_k^* (i.e., θ_2) has to be used. Thus, Eqs (57), (58a) and (58b) become

$$A' = \frac{t_{t2} - t_{t3}}{\theta_2^* - \theta_3^*} = 0.173187 \text{ hr/deg}$$

$$B' = \frac{t_{t3}\,\theta_2^* - t_{t2}\,\theta_3^*}{\theta_2^* - \theta_3^*} = -8.592722 \text{ hr}$$

giving the third approximation as

$$\theta_4^* = \frac{t_j - B}{A} = 136.4376^\circ.$$

Thus, for the present example, the second and third approximations are almost identical and, for practical purposes, the convergence to the exact value is obtained. The following table presents the convergence of the solutions.

Approximation	θ^* (deg)	Error in Total Flight Time † (sec)
First	137	345.7
Second	136.44	1.535
† $t_t = 54,129.917$ sec	136.4376	0.050

Since the shape and inclination of the transfer ellipse (θ_t^*, a_t, e_t, etc.,) were determined during the last iteration, it is relatively simple to obtain the location of the return shuttle in the orbit plane. The locations of the return shuttle treated here are given in Fig. 6a.

Altitude from sea level is given in Fig. 6b, as computed from the basic relationships.

$$r = \frac{p}{1 + e \cos\theta} \quad \text{and} \quad r = R + h$$

where R is the radius of earth at the given latitude. By neglecting the oblateness perturbation effects of the earth the ground track can be computed from the following equations.

(1) Latitude

$$L = \sin^{-1}\left[\sin i \sin(\omega + \theta)\right] \tag{59}$$

(2) Longitude

$$\Lambda = \tan^{-1}\left[\cos i \tan(\omega + \theta)\right] + \Omega_0 - \Omega_e t \tag{60}$$

where

$$\Omega_e = 0.004178074 \text{ deg/sec.}$$

The computed ground track for the sample problem is given in Fig. 7. Assuming the initial time to be zero hour, it gives the successive positions and a service time scale up to the desired landing point (Florida in the present case).

It should be noted that up to 12 hr, the transfer ground track deviates only slightly from the basic 24-hr ground track (given in dotted lines). The reason for this can be seen by comparing Figs. 6a and 7.

6. Flight Time Error Analysis

The total flight time error per unit departure angle can be approximated by taking the slopes of the total flight time curve (Fig. 4b). The solid line of Fig. 8 presents the slopes of the return flight time curve. Another approach utilizes the total flight time equation

$$t_t(\theta^*) = t_1(\theta^*) + t_2(\theta^*) + t_3(\theta^*), \tag{61}$$

Thus

$$\frac{dt_t}{d\theta^*} = \frac{dt_1}{d\theta^*} + \frac{dt_2}{d\theta^*} + \frac{dt_3}{d\theta^*} \tag{62}$$

Since the period and eccentricity of the 24-hr orbit are dependent of θ^*, the first derivative in Eq 62 is found by using Kepler's equation

$$M = E - e \sin E \tag{63}$$

where

$$M = nt = \frac{2\pi t}{\tau}.$$

Differentiating with respect to central angle

$$\frac{dM}{d\theta} = (1 - e \cos E)\frac{dE}{d\theta}, \tag{64}$$

but

$$E = \sin^{-1}\left(\frac{\sqrt{1 - e^2}\sin\theta}{1 + e\cos\theta}\right), \tag{65}$$

therefore

$$\frac{dE}{d\theta} = \frac{\sqrt{1 - e^2}}{1 + e\cos\theta}. \tag{66}$$

From Eqs (64) and (66),

$$\frac{dM}{d\theta} = \frac{(1 - e^2)^{3/2}}{(1 + e\cos\theta)^2}. \tag{67}$$

Using the definition of M, the error due to time spent in the 24-hr section of the return path is found from Eq (67).

$$\frac{dt_1}{d\theta^*} = \frac{\tau_f}{2\pi} \frac{(1 - e^2)^{3/2}}{(1 + e \cos \theta^*)^2} \tag{68}$$

Equation (68) is presented as the dotted line on Fig. 8. It is obviously symmetrical about 180°, as expected.

a. Approximate analysis

The low altitude orbit contribution to Eq (61) is approximately constant for the whole revolution of θ^* (Fig. 4b). Thus,

$$t_3 \approx \frac{\tau}{2\pi} (300° - \theta^*)$$

and

$$\frac{dt_3}{d\theta^*} \approx - \frac{\tau_\ell}{2\pi} = - 898.74 \text{ sec/rad} =$$

$$- 15.686 \text{ sec/deg.} \tag{69}$$

To obtain the contribution of the transfer orbit, the following approximation may be used first. Assuming that the transfer orbit is always entered at apogee (i.e., $r^* \approx r_{at}$), the time spent in transfer orbit is one-half of a period.

$$t_2 \approx \frac{\tau_t}{2} = \pi \sqrt{\frac{a_t^3}{\mu}} \tag{70}$$

Due to the previous assumptions,

$$a_t \approx \frac{1}{2} (r^* + r_{pt}) \tag{71}$$

and

$$a_t^3 \approx \frac{1}{8} \left(\frac{p_f}{1 + e_f \cos \theta^*} + r_{pt} \right)^3 . \tag{72}$$

Substituting Eq (72) into Eq (70) and differentiating with respect to θ^*,

$$\frac{dt_2}{d\theta^*} \approx \frac{3\pi e_f}{4\sqrt{\mu}} \left(\frac{r^{*2}}{p_f} \right) \left(\frac{r^* + r_{pt}}{2} \right)^2 \sin \theta^* . \tag{73}$$

The slope of the total flight time curve is the sum of these three components (i.e., the sum of Eqs (68), (69) and (73)).

b. Exact analysis

Actually, the transfer orbit is not usually entered at apogee, but rather at some small displacement from apogee. Since the vehicle moves very slowly in this region, the flight times may change considerably.

Thus, Eq (73) can be justified only for a preliminary estimate, and an exact analysis is needed. The exact derivative is obtained by differentiating the expression for t_2 assuming that γ^* is negative

$$t_2 = \frac{\tau_t}{2\pi} \left\{ 2\pi - M_t \right\} . \tag{74}$$

Differentiating Eq (74) with respect to θ^*,

$$\frac{dt_2}{d\theta^*} = \frac{1}{2\pi} \frac{d\tau_t}{d\theta^*} \left\{ 2\pi - M_t \right\} - \frac{\tau_t}{2\pi} \frac{dM_t}{d\theta^*} . \tag{75}$$

To evaluate these derivatives it is now necessary to define

$$A \equiv \frac{r_{pt}^2}{r_{af} r_{pf}} \tag{76a}$$

$$B \equiv \frac{r_{pt}}{r_{af}} + \frac{r_{pt}}{r_{pf}} , \tag{76b}$$

Thus

$$\cos \theta_t^* = \frac{B + 2 - \frac{r^*}{r_{pt}} (1 + A) - 2 \frac{r_{pt}}{r^*}}{\frac{r^*}{r_{pt}} (1 - A) + B - 2} \tag{77}$$

$$e_t = \frac{\frac{r^*}{r_{pt}} (1 - A) + B - 2}{\frac{r^*}{r_{pt}} (1 + A) - B} \tag{78}$$

$$a_t = \frac{1}{2} r^* \left[\frac{1 - \frac{r_{pt}}{r^*} B + A}{1 - B + \frac{r^*}{r_{pt}} A} \right] \tag{79}$$

Also, from Eqs (77) and (78), it follows that

$$1 + e_t \cos \theta_t^* = \frac{2 \left(1 - \frac{r_{pt}}{r^*} \right)}{\frac{r^*}{r_{pt}} (1 + A) - B} \tag{80}$$

Using the relationship

$$\frac{\tau_t}{2\pi} = \sqrt{\frac{a_t^3}{\mu}}$$

the first derivative is

$$\frac{d\tau_t}{d\theta^*} = \frac{3\pi}{\mu}\, a_t^{1/2}\left(\frac{da_t}{d\theta^*}\right)$$

$$= \frac{3\pi}{\mu}\, a_t^{1/2}\left(\frac{da_t}{dr^*}\right)\frac{dr^*}{d\theta^*} \quad . \tag{81}$$

From Eq (79) and also from

$$\frac{dr^*}{d\theta^*} = \frac{r^{*2}}{p_f}\, e_f \sin\theta^*, \tag{82}$$

it follows that

$$\frac{da_t}{d\theta^*} = \frac{1}{2}\,\frac{1 - B + A}{\left(1 - B + \frac{r^*}{r_{pt}} A\right)^2}\,\frac{r^{*2}}{p_f}\, e_f \sin\theta^*. \tag{83}$$

From Eqs (79), (81) and (83),

$$\frac{d\tau_t}{d\theta^*} = \left[\frac{3\sqrt{2}\pi}{4\sqrt{\mu}}\,\frac{r^{*5/2}}{p_f}\, e_f \left(\frac{1 - \frac{r_{pt}}{r^*} B + A}{1 - B + \frac{r^*}{r_{pt}} A}\right)\right]^{1/2} \cdot \left[\frac{1 - B + A}{\left(1 - B + \frac{r^*}{r_{pt}} A\right)^2}\right] \sin\theta^*. \tag{84}$$

To obtain the second term in Eq (75), it should be noted that in this case τ_t = constant is implied, and

$$\frac{\tau_t}{2\pi}\,\frac{dM_t}{d\theta^*} = \frac{1}{n}\,\frac{dnt}{d\theta^*} = \frac{dt}{d\theta^*} = \frac{dt}{d\theta_t^*}\,\frac{d\theta_t^*}{d\theta^*} \tag{85}$$

The first quantity in Eq (85) follows from Kepler's Law

$$\frac{dt}{d\theta_t^*} = \frac{r^{*2}}{\sqrt{\mu p_t}} \quad . \tag{86}$$

Substituting Eq (80) into Eq (86), (since $p = r(1 + e\cos\theta)$.

$$\frac{dt}{d\theta_t^*} = \frac{r^{*3/2}}{\sqrt{\mu}}\sqrt{\frac{\frac{r^*}{r_{pt}}(1 + A) - B}{2\left(1 - \frac{r_{pt}}{r^*}\right)}} \tag{87}$$

To obtain the second quantity in Eq (85), the following shorthand notation of Eq (77) is used.

$$\cos\theta_t^* = f(r^*) \tag{88}$$

Differentiating Eq (88) with respect to θ^*

$$-\sin\theta_t^*\,\frac{d\theta_t^*}{d\theta^*} = \frac{df}{d\theta^*}\,\frac{dr^*}{d\theta^*} \quad . \tag{89}$$

From Eq (77), it follows that

$$\frac{df}{dr^*} = -\frac{2}{r_{pt}}\left[\left(\frac{r_{pt}}{r^*}\right)^2 (2 - B) - 2\,\frac{r_{pt}}{r^*}(1 - A) + B - 2A\right]\left[\frac{r^*}{r_{pt}}(1 - A) + B - 2\right]^{-2} \tag{90}$$

From Eqs (89), (90) and (82),

$$\frac{d\theta_t^*}{d\theta^*} = \frac{2r^{*2}}{r_{pt}\, p_f}\, e_f\left[\left(\frac{r_{pt}}{r^*}\right)^2 (2 - B) - 2\,\frac{r_{pt}}{r^*}(1 - A) + B - 2A\right]\left\{\left[\frac{r^*}{r_{pt}}(1 - A) + B - 2\right]^{-2} \cdot \frac{\sin\theta^*}{\sin\theta_t^*}\right\}. \tag{91}$$

Substituting Eqs (87) and (91) into (85),

$$\frac{\tau_t}{2\pi}\,\frac{dM_t}{d\theta^*} = \frac{r^{*3/2}}{\mu}\sqrt{\frac{\frac{r^*}{r_{pt}}(1+A) - B}{2\left(1 - \frac{r_{pt}}{r^*}\right)}}\,\frac{d\theta_t^*}{d\theta^*}. \tag{92}$$

It should be noted that Eqs (91) and (92) are zero at the points where

$$\frac{r_{pt}}{r^*} = \frac{B - 2A}{2 - B}. \tag{93}$$

The third error in time, i.e., the total flight time error contributed by the low altitude orbit is simply.

$$\frac{dt_3}{d\theta^*} = \frac{\tau_\ell}{2\pi}\,\frac{d\theta_\ell}{d\theta^*} \tag{94}$$

since the period τ_ℓ is a constant.

As shown previously

$$\theta_\ell = 360° - \omega + \varphi_0 + \theta_t^* - \theta^*$$

therefore, Eq (94) becomes

$$\frac{dt_3}{d\theta^*} = \frac{\tau_\ell}{2\pi}\left(\frac{d\theta_t^*}{d\theta^*} - 1\right). \tag{95}$$

Finally, the equations for the flight time error are given as follows.

(1) Approximate equation

$$\frac{dt_t}{d\theta^*} \approx \frac{\tau_f}{2\pi} \frac{\left(1 - e_f^2\right)^{3/2}}{\left(1 + e_f \cos\theta^*\right)^2} + \frac{3\pi e_f}{4\sqrt{\mu}} \left(\frac{r^{*2}}{p_f}\right)\left(\frac{r^* + r_{pt}}{2}\right)^2 \sin\theta^* \quad (96)$$

-899

(2) Exact equation

$$\frac{dt_t}{d\theta^*} = \frac{\tau_f}{2\pi} \frac{\left(1 - e_f^2\right)^{3/2}}{\left(1 + e_f \cos\theta^*\right)^2} + \frac{1}{2\pi} \frac{d\tau_t}{d\theta^*} \left\{2\pi - M_t\right\} - \frac{\tau_t}{2\pi} \frac{dM_t}{d\theta^*} + \frac{\tau_\ell}{2\pi} \left(\frac{d\theta_t^*}{d\theta^*} - 1\right) \quad (97)$$

where

$\frac{d\tau_t}{d\theta^*}$ is given by Eq (84)

$\frac{\tau_t}{2\pi} \frac{dM_t}{d\theta^*}$ is given by Eq (92b)

$\frac{d\theta_t^*}{d\theta^*}$ is given by Eq (91).

In Fig. 8, the results of Eqs (96) and (97) are compared to the solid curve obtained from measuring the slopes of curves in Fig. 4b. It is seen that the approximate equation gives only the general trends and should not be used where exact numerical values are needed.

c. Limiting cases for the exact flight-time error analysis

In the previous material, the error analysis for the return shuttle flight times was derived. Due to the geometry of the problem, Eqs (91) and (92) become indeterminate for $\theta^* = 0°$ and 180°. This is caused by the fact that for the apogee and perigee departures from orbit, the corresponding transfer orbits are entered at apogee. Mathematically, as $\theta^* \to 0°$ and 180°, $\theta_t^* \to 180°$ and

$$\left(\frac{\sin\theta^*}{\sin\theta_t^*}\right) \longrightarrow \frac{0}{0} . \quad (98)$$

Equation (98) calls for a limiting procedure, since it is intuitively clear that the ratios must be finite.

Since

$$\cos\theta^* = \frac{1}{e_f}\left(\frac{p_f}{r^*} - 1\right) , \quad (99)$$

$$\sin^2\theta^* = 1 - \cos^2\theta^* = \frac{1}{e_f^2}\left[\left(\frac{p_f}{r^*}\right)\left(2 - \frac{p_f}{r^*}\right) - \left(1 - e_f^2\right)\right] . \quad (100)$$

Next, defining two new constants

$$u \equiv \frac{r_{pt}}{r_{af}} \quad (101a)$$

$$v \equiv \frac{r_{pt}}{r_{pf}} \quad (101b)$$

which correspond to the previous constants as follows.

$$A = u\,v \quad (102a)$$

$$B = u + v \quad (102b)$$

From the definition of eccentricity, it follows that

$$e_f = \frac{v - u}{v + u} \quad (103)$$

and

$$p_f = r_{pf}\,(1 + e_f) = \frac{2\,v\,r_{pf}}{u + v} . \quad (104)$$

Therefore, Eq (100) is shown to become, after substituting Eqs (101), (103) and (104),

$$\sin^2\theta^* = \frac{4(u + v)}{(v - u)^2}\left\{\frac{r_{pt}}{r^*}\left[1 - \left(\frac{r_{pt}}{r^*}\right)\cdot\left(\frac{1}{u + v}\right) - \frac{uv}{u + v}\right]\right\} . \quad (105)$$

From Eqs (77) and (102), it follows that

$$\sin^2\theta_t^* = 4\left[-\left(\frac{r_{pt}}{r^*}\right)^2 + \frac{r_{pt}}{r^*}(u + v + 2) - uv\left(\frac{r^*}{r_{pt}}\right)^2 + \frac{r^*}{r_{pt}}(u + v + 2uv) - 2(u + v) - (1 + uv)\right] \cdot \left[\frac{r^*}{r_{pt}}(1 - uv) + u + v - 2\right]^{-2} \quad (106)$$

Now, defining

$$x \equiv \frac{r_{pt}}{r^*} , \tag{107}$$

the following relationships exist.

$$\theta^* \to 0° \quad \text{means } x \to v \tag{108}$$

$$\theta^* \to 180° \text{ means } x \to u . \tag{109}$$

The problem of deriving the actual limits is somewhat simplified by the theorem that the square of the limit is equal to the limit of the square.

From Eqs (105), (106) and (107),

$$\frac{\sin^2 \theta^*}{\sin^2 \theta_t^*} = \frac{(u+v)\left[\frac{1}{x^2}(1-uv)+u+v-2\right]^2}{(v-u)^2} \frac{1}{I_x} \tag{110}$$

where

$$I_x = \frac{-x^2 + x(u+v+2) - \frac{uv}{x^2} + \frac{1}{x}(u+v+2uv)}{x - \frac{x^2}{u+v} - \frac{uv}{u+v}} + \frac{-2(u+v)-(1+uv)}{x - \frac{x^2}{u+v} - \frac{uv}{u+v}} . \tag{111}$$

Since the cases of interest in this investigation are elliptic orbits, $u \neq v$, the behavior of $\frac{1}{I_x}$ alone must be investigated.

Because Eq (111) still gives an indeterminate form $\frac{0}{0}$, L'Hospital's rule has to be used and

$$\lim_{x \to u \text{ or } v} (I_x) = \lim_{x \to u,\, v} \left\{ \left[-2x + u + v + 2 + \frac{2uv}{x^3} - \frac{1}{x^2}(u+v+2uv) \right] \cdot \left[1 - \frac{2x}{u+v} \right]^{-1} \right\} \tag{112}$$

Finally, from Eqs (109), (110) and (112),

$$\lim_{\theta^* \to 0°} \left(\frac{\sin \theta^*}{\sin \theta_t^*} \right) = \frac{1-v}{v-u} . \tag{113}$$

Similarly,

$$\lim_{\theta^* \to 180°} \left(\frac{\sin \theta^*}{\sin \theta_t^*} \right) = \frac{1-u}{v-u} , \tag{114}$$

or simply

$$\lim_{\theta^* \to 180°} \left(\frac{\sin \theta^*}{\sin \theta_t^*} \right) = \lim_{\theta^* \to 0°} \left(\frac{\sin \theta^*}{\sin \theta_t^*} \right) + 1. \tag{115}$$

For the sample problem (24-hour orbit)

$$\left.\begin{aligned} r_{pt} &= 0.224869 \times 10^8 \text{ ft} \\ &= 6854.0 \text{ km} \\ r_{a24} &= 2.075055 \times 10^8 \text{ ft} \\ &= 63,247.7 \text{ km} \\ r_{p24} &= 0.691685 \times 10^8 \text{ ft} \\ &= 21,082.6 \text{ km} \end{aligned}\right\} \quad \begin{aligned} u &= \frac{r_{pt}}{r_{a24}} = 0.108368 \\ v &= \frac{r_{pt}}{r_{p24}} = 0.325103 \end{aligned}$$

and from Eqs (113) and (114),

$$\lim_{\theta^* \to 0°} \left(\frac{\sin \theta^*}{\sin \theta_t^*} \right) = 3.113927$$

$$\lim_{\theta^* \to 180°} \left(\frac{\sin \theta^*}{\sin \theta_t^*} \right) = 4.113927.$$

d. Error analysis by numerical differentiation

Since the total flight time curve (Fig. 4b) was computed in the sample problem, a numerical differentiation method can also be used.

First, assemble a central difference table in the following form.

θ_{-2}	$(t_t)_{-2}$				
		Δ^1_{-2}			
θ_{-1}	$(t_t)_{-1}$		Δ^2_{-2}		
		Δ^1_{-1}		Δ^3_{-2}	.....
θ_0	$(t_t)_0$		Δ^2_{-1}		
		Δ^1_0		Δ^3_{-1}	.....
θ_1	$(t_t)_1$		Δ^2_0	.....	
		Δ^1_1	.....		
θ_2	$(t_t)_2$	.....			
.....	.....				

where Δ^n is the n th difference of the value of t_t, when θ is increased to $\theta + \Delta\theta$.

It can be shown that for this central difference table, Stirling's interpolation formula is

$$t_t = (t_t)_0 + \frac{\delta\theta}{\Delta\theta}\left(\frac{\Delta^1_0 + \Delta^1_{-1}}{2}\right) + \frac{\delta\theta^2}{2!\,\Delta\theta^2}\Delta^2_{-1} + \frac{\delta\theta(\delta\theta^2 - \Delta\theta^2)}{3!\,\Delta\theta^3}\left(\frac{\Delta^3_{-1} + \Delta^3_{-2}}{2}\right) + \ldots \tag{116}$$

where

$\delta\theta$ is a small variation between θ_0 and θ_1

$\Delta\theta$ is the equal increment $\theta_1 - \theta_0$, $\theta_0 - \theta_{-1}$, ...

The slope of the total flight time curve is obtained by differentiating Eq (116) and setting $\delta\theta = 0$ in the result. Thus,

$$\frac{dt_t}{d\theta^*} = \frac{1}{\Delta\theta}\left(\frac{\Delta^1_0 + \Delta^1_{-1}}{2} - \frac{\Delta^3_{-1} + \Delta^3_{-2}}{12} + \frac{\Delta^5_{-2} + \Delta^5_{-3}}{60} - \ldots\right) . \qquad (117)$$

(Fig. 4b), the rough values for t_t were obtained from which the following table is constructed.

θ (deg)	t_t (sec)	Δ^1	Δ^2	Δ^3
0	12,910			
		3020		
30	15,930		2490	
		5510		+1470
$(60)_0$	$(21,440)_0$		3960	
		$(9470)_0$		-330
90	30,910		$(3630)_0$	
		13,100		
120	44,010			

From Eq (117),

$$\left(\frac{dt_t}{d\theta^*}\right)_{\theta^* = 60^\circ} = \frac{1}{30^\circ}\left(\frac{9470 + 5510}{2} - \frac{-330 + 1470}{12}\right)$$

$$= 246.5 \text{ sec/deg.}$$

The results of numerical differentiation are also given in Fig. 8, and they fit rather closely the slopes measured from Fig. 4b. Since numerical differentiation is extremely simple, as compared to the exact analysis, it should be used for all preliminary calculations.

NOTE: In the numerical differentiation method presented here, the difference columns should not be carried further than is consistent with the accuracy of the data. Otherwise, the higher order approximations could be less accurate than the lower ones. Thus, the differences should be carried only to the point where marked irregularities start to appear.

C. PLANAR ANALYSIS OF DEPARTURE FROM LOW ALTITUDE ORBITS

For high altitude orbits, where all estimates of atmospheric drag are negligible, orbital lifetime may be measured in terms of years. Thus, should impact with the earth be desired at a specific time and location, some device must be employed to alter the vehicle's velocity and/or flight path angle an amount sufficient to cause the vehicle to re-enter. Re-entry as used here is actually a misnomer due to the fact that there are finite values of atmospheric pressure for the entire range of altitudes to be investigated. The term, however, will be used throughout this section to refer to an altitude below which atmospheric drag is of such magnitude as to cause the vehicle's trajectory to degenerate and impact with the earth in one half of one revolution or less. Previous machine runs and calculations have revealed that for vehicles of ballistic or low lift design this re-entry altitude may be considered to be 300,000 ft (91.5 km). Therefore, for the purposes of this analysis, since drag is of negligible magnitude above the re-entry altitude, the atmosphere will be assumed to terminate at an altitude of 300,000 ft (91.5 km). The earth will be assumed to be both spherical and non-rotating. Thus the vehicle trajectories involved will be portions of Keplerian ellipses. Special note should be made at this point that even though the approaches made here are valid for vehicles of high lift design, the altitude at which drag must be considered may increase to 400,000 ft (122 km) or more. Motion within the earth's atmosphere will not be treated here; it is reported in Chapter IX. Since Section B resulted in a plane which continues the impact point at a given time the analysis of departure can be treated as 2 dimensional. The following paragraphs present this information both for the impulse and finite burning cases.

1. Analytic Approach to Orbital Departure

A method of analysis which neglects the effects of finite burning times will now be developed to provide a means of obtaining relatively accurate approximations of the re-entry parameters and retrorocket size requirements.

The velocity increment obtainable from a given rocket is:

$$\Delta V = g_0 I_{sp} \ln\left(\frac{1}{1-\zeta}\right) - g t_B \sin\gamma . \qquad (118)$$

$$= g_0 I_{sp} \ln\left(\frac{1}{1-\zeta}\right) - g \frac{I_{sp}\zeta}{T/W_0} \sin\gamma .$$

If the assumption is made that the burning time is extremely short or that the flight path angle remains very close to 0° during burning, Eq (118) reduces to

$$\Delta V = g_0 I_{sp} \ln\left(\frac{1}{1-\zeta}\right) . \qquad (119)$$

This equation is plotted in Chapter VI.

For most cases in which departure is desired from low altitude orbits, the mass ratio required is quite small and one further simplification in this expression may be made by noting that:

$$\ln\left(\frac{1}{1-\zeta}\right) = \zeta + \frac{\zeta^2}{2} + \frac{\zeta^3}{3} + \ldots$$

$$\approx \zeta \text{ for small values of } \zeta .$$

Therefore:

$$\Delta V = g_0 I_{sp} \zeta. \tag{120}$$

This equation may be rewritten to include propellant characteristics by substituting for ζ its equivalent

$$\zeta = \rho_0 g_0 V_P/W_0 .$$

Thus:

$$\Delta V = g_0^2 I_{sp} \rho_0 V_P/W_0 .$$

Where

V_P = total propellant volume

ρ_0 = bulk density of propellant combination

$$= \frac{r_m + 1}{\frac{r_m}{\rho_{oxidizer}} + \frac{1}{\rho_{fuel}}}$$

r_m = mixture ratio $\sim \frac{\text{weight of oxidizer}}{\text{weight of fuel}}$

$I_{sp} = \frac{\text{unit force thrust}}{\text{weight of propellant flow/sec}}$

Since the assumption has been made that the burning time is infinitesimal, the velocity increment obtained from a given retrorocket may be treated as a pulse and the laws of sines and cosines can be used to relate the velocity and the direction before and after the pulse. For the purposes of this analysis, the thrust vector will be in the plane of the orbit; therefore, both the change in flight path angle and the required thrust attitude angle may be computed.

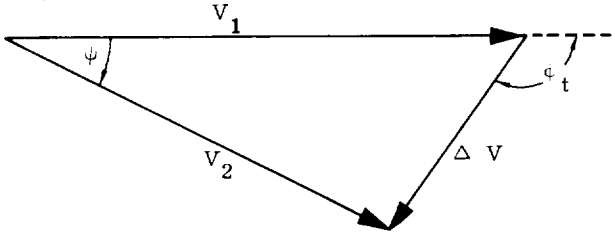

NOTE:
If the thrust vector lies in the orbital plane, $\psi = \Delta\gamma$ and $\phi_t = \delta$. (δ = the thrust attitude angle discussed in Section B.)

$$\Delta V^2 = V_1^2 + V_2^2 - 2V_1 V_2 \cos \Delta\gamma \tag{121}$$

$$\left(\frac{\Delta V}{V_1}\right)^2 = \left(\frac{V_2}{V_1}\right)^2 - 2\frac{V_2}{V_1}\cos\Delta\gamma + 1$$

$$\frac{\sin\delta}{V_2} = \frac{\sin\Delta\gamma}{\Delta V}$$

$$\sin\delta = \frac{V_2/V_1}{\Delta V/V_1}\sin\Delta\gamma. \tag{122}$$

Equation (121) is also presented in Chapter VI.

Now since the equation of any conic may be written as

$$\frac{V^2}{\mu} = \frac{2}{r} + \text{constant} \tag{123}$$

$$\frac{V_1^2}{2} - \frac{\mu}{r_1} = \frac{V_2^2}{2} - \frac{\mu}{r_2} . \tag{124}$$

a means of determining the vehicle velocity at any radius, if velocity and radius are known at some other point in the conic, is available. Point 2 is assumed to be that of re-entry at a radius of 2.12029×10^7 ft (6462.64 km). Thus, the velocity at re-entry may be determined once the velocity at burnout has been obtained. The energy equation is plotted in Chapter III.

The re-entry flight path angle can be obtained from the conservation of angular momentum and the radius, velocity and flight path angle at burnout of the retrorocket.

$$\cos\gamma_2 = \cos\gamma_1 \frac{r_1 V_1}{r_2 V_2} . \tag{125}$$

Equation (125) can be used in conjunction with the energy equation to yield the relationship between the flight path angle at burnout of the retrorocket and that at re-entry.

If a tolerance is placed on the entry angle (e.g. 0 - 2°), the retropulse cannot be selected independently of other considerations. This fact may appear obvious, but is rigorously shown by combining the equations for the conservation of energy and angular momentum.

$$r_1 v_1 \cos\gamma_1 = r_2 v_2 \cos\gamma_2$$

$$r_1 \left| \vec{V}_0 + \vec{\Delta V} \right| \cos(\gamma_0 - \Delta\gamma)$$

$$= r_{entry} \sqrt{\left| \vec{V}_0 + \vec{\Delta V} \right|^2 - \frac{2\mu}{r} + \frac{2\mu}{r_{entry}}} \cos\gamma_{entry}$$

In order to determine the values of range and time of flight required for descent to re-entry, it is necessary to first consider the ellipse in question.

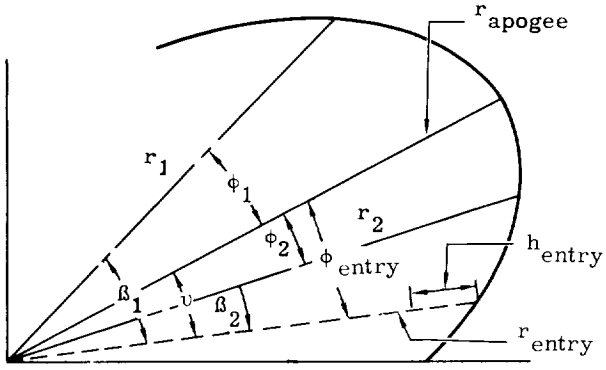

The range attained may be seen to be

$$X = R\beta \tag{126}$$

R = The radius of the earth

The problem then is to define the angle β in terms of the known quantities of the ellipse. This problem may be simplified by observing that

$$\beta = \upsilon - \phi. \tag{127}$$

Where

ϕ_1 is negative and ϕ_2 is positive and where the central angle from a given radius to apogee is

$$\phi = \cos^{-1}\left[\frac{r - p}{re}\right]. \tag{128}$$

Therefore:

$$\beta = \cos^{-1}\left[\frac{r_e - p}{r_e e}\right] \pm \cos^{-1}\left[\frac{r - p}{re}\right], \tag{129}$$

where:

$r_e = r_{entry}$

To define the time of flight a procedure similar to that employed to define the angle β is used. That is, the time of flight from one point to another is equal to the difference between the times from these points to apogee. The time of flight from a given point to apogee is defined by Eq (130)

$$t_a = \frac{\tau}{2\pi}\left[\delta' - e \sin \delta'\right]. \tag{130}$$

Where

δ' is measured in radians

$$\delta' = \cos^{-1}\left[\frac{\cos\phi - e}{1 - e\cos\phi}\right]. \tag{131}$$

The time of flight is thus

$$t_f = t_{entry} - t_a$$

where

δ'_{entry} is evaluated at $\phi = \phi_{entry}$

δ'_a is evaluated at $\phi = \phi_1$ or ϕ_2

t'_a is negative if vehicle passes through apogee before re-entry

Thus the complete maneuver can be described analytically under the assumption of impulsive burning.

This section has shown the results of flight path corrections and departures for the case in which instantaneous pulses were considered. Figure 9 shows the percentage deviation in the re-entry parameters obtained using this method as compared to that which includes the effects of finite burning time. The horizontal lines drawn at ± 4% error were arbitrarily selected to show the minimum mass ratios which could be considered as pulses in order to maintain this desired accuracy in all re-entry parameters as a function of initial altitude. A continuation of this analysis would be necessary to limit the maximum mass ratios which could be considered as pulses for the same accuracy limitation.

Figure 10 presents the error in the ideal velocity pulse due to finite burning times.

2. Orbital Departure from 100-stat mi (161-km) Orbits with Finite Burning Time

Finite burning time will now be included in the analysis as an additional variable: however, since no closed solution exists for this problem, the digital computer and a stepwise trajectory program were employed. This program considers the vehicle to be a point mass and the earth to be spherical. The trajectory during burning of a rocket or during travel within the sensible atmosphere is obtained by stepwise integration. The time interval for each integration is determined by the accuracy limitation placed on the extrapolated values of certain critical quantities. The equations for this program are presented in the simplified form required for this effort.

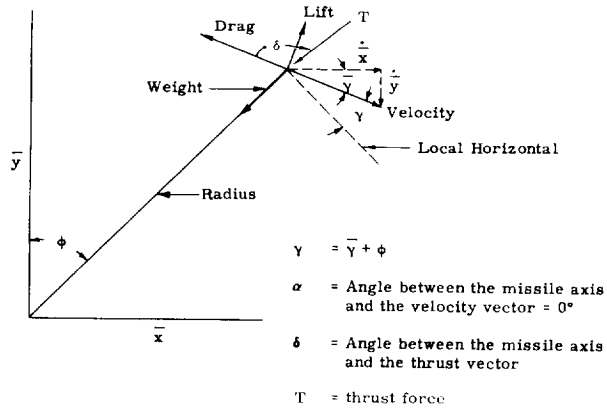

$$\dot{V} = \frac{T}{m}\cos(\alpha + \delta) - \frac{D}{m} - \frac{\mu}{r^2}\sin\gamma \tag{132}$$

$$= -\frac{T}{m} - \frac{\mu}{r^2}\sin\gamma = A$$

$$\dot{\bar{\gamma}} V = \frac{T}{m} \sin(\alpha + \delta) + \frac{L}{m} - \frac{\mu}{r^2} \cos \gamma \tag{133}$$

$$= -\frac{\mu}{r^2} \cos \gamma = B$$

$$\ddot{\bar{y}} = A \sin \bar{\gamma} + B \cos \bar{\gamma} \tag{134}$$

$$\ddot{\bar{x}} = A \cos \bar{\gamma} - B \sin \bar{\gamma} \tag{135}$$

$$\sin \gamma = \sin \bar{\gamma} \cos \phi + \cos \bar{\gamma} \sin \phi \tag{136}$$

$$\cos \gamma = \cos \bar{\gamma} \cos \phi - \sin \bar{\gamma} \sin \phi \tag{137}$$

where

$$\sin \bar{\gamma} = \frac{\dot{\bar{y}}}{V}$$

$$\cos \bar{\gamma} = \frac{\dot{\bar{x}}}{V}$$

$$\sin \phi = \frac{\bar{x}}{r}$$

$$\cos \phi = \frac{\bar{y}}{r}$$

$$T = T_{SL} + A_e (P_{SL} - P_a)$$

$$T_{SL} = T_{Vac} - A_e P_{SL} \tag{138}$$

$$m = \frac{W_0}{g_0} \left[1 - \frac{\dot{W}_p t}{W_0} \right] \tag{139}$$

$$\dot{W}_p = \text{constant}.$$

Once the retrorocket burns out, the trajectory is assumed to be unperturbed down to the altitude at which drag becomes appreciable. The equations for this portion of the trajectory are those of motion in a Keplerian ellipse.

For the purposes of this analysis two rocket parameters $\frac{W_p}{W_0}$ and $\frac{T}{W_0}$ (mass ratio and initial thrust-to-weight ratio) are investigated. In addition the thrust attitude angle (δ) was varied to show the effects of these quantities on the conditions at re-entry.

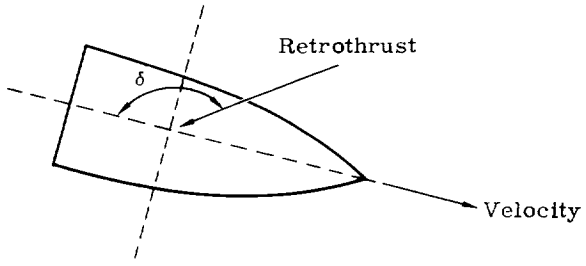

NOTE:
δ is measured in the plane of the trajectory.

The magnitude of the radial component of velocity is small, thus work done by the radial component of thrust will be small. It may, therefore, appear that a value of δ of 180° is optimum for all cases in which departure is desired; such is not the case. In the case of low altitude orbits small changes in the burnout altitude and flight path angle can affect the mass ratio required for orbital departure and on the re-entry parameters. This analysis, therefore, treats departure from a 100-stat mi (161 km) orbit separately from similar analysis for orbits of increased altitude.

There are many possible criteria which might be considered in the determination of an optimum retrorocket configuration. The selected configuration might be one for which the re-entry velocity is minimum, the re-entry flight path angle is minimum, the mass ratio required for departure is minimum or one which ensures a given value of range from the time of initiation to impact with the earth. The vehicle itself must also be considered in this process due to the sensitivity of some vehicles to small changes in the re-entry parameters.

Minimization of the re-entry flight path angle is not a realistic constraint for the vehicle configurations discussed due to the fact that the maximum values of both deceleration and aerodynamic heating can be held with allowable tolerances for manned re-entry for angles up to approximately -2°. Thus, this constraint need not be considered.

Since maneuver, either before initiating re-entry or sometime thereafter, is anticipated to assure impact in a given area, the criteria selected for the evaluation of retrorocket configurations should provide the maximum degree of flexibility in this respect. The analysis of maneuvering showed that the maximum displacement of the impact point in a plane normal to that of the unaltered trajectory, for a given amount of propellant, is obtained if the central angle measured from the radius at which the correction is made to that at which the trajectory impacts with the earth is 90° (10,000-km range). Thus, the selection of the retrorocket configuration which is near optimum for an orbit of this altitude is, determined by this value of total range and the minimum amount of propellant required for successful departure. This criteria must be modified, however, if the re-entry angle exceeds the allowable tolerances placed upon it.

Specific impulse will not be included in this analysis as a variable; however, because the mass ratios are small, the data presented here can be converted to obtain approximate answers corresponding to values of I_{sp} other than the assumed 300 sec. This can be accomplished by employing Eq (120).

$$\triangle V = g_0 I_{sp} \zeta = C$$

$$\zeta_1 I_{sp_1} = \zeta_2 I_{sp_2}$$

Figure 11 shows the variations in range, re-entry velocity and re-entry flight path angle as

functions of δ and $\frac{T}{W_0}$ for one value of mass ratio (0.1). This figure clearly shows that the range obtained in descent to 300,000 ft (91.5 km) can be minimized for a value of δ less than 180°. Also shown is the convergence of the curves of the higher values of $\frac{T}{W_0}$ implying that little is to be gained by increasing its magnitude above some value as yet undetermined (0.5, see Section 3. It is interesting to note that re-entry velocity which is a function of initial velocity, altitude, and velocity increment of the retrorocket is least sensitive to changes in thrust-to-weight ratio. This fact substantiates the assumption made in the impulse analyses that the velocity increment loss (a function of $\frac{T}{W_0}$) due to gravity is negligible for small values of mass ratio.

Figures 12a, b and c present time of flight required for descent from 100 stat mi (161 km) to 300,000 ft (91.5 km) and the re-entry parameters at 300,000 ft (91.5 km) as functions of thrust-to-weight ratio, mass ratio, and values of δ of 180, -135, and -90°, respectively. It is interesting to note that the hand computed instantaneous pulse points fared into the digital results for the δ = 180° case. The sensitivity of both range and time of flight to small changes in mass ratio may be observed to decrease as mass ratio increases; this portion of the analysis, however, will be discussed later.

If now a curve such as the one shown in Fig. 13 is employed to determine values of total range attained in descending to sea level Figs. 14a, b, and c may be obtained. These curves point up most effectively the proper combination of δ, $\frac{T}{W_0}$ and mass ratio required to accomplish a minimum energy orbital departure for a given range. Examination of these figures reveals that the minimum propellant requirement for a given value of total range is obtained for this special case for a value of δ of approximately -135°. Further examination indicates that both re-entry flight path angle and the required mass ratio are minimum for the higher thrust-to-weight ratio (0.5), again for a given value of total range.

Since the results obtained thus far pertain to only one set of initial conditions and since it is desired to show the effects of small variations in the conditions prior to initiation of the retrorocket on the re-entry parameters, another series of runs has been made. However, due to the scope of the program involved only one retrorocket configuration has been investigated. This particular configuration was selected to provide a minimum energy orbital departure for a total range of 5000 naut mi or 9270 km (δ = -135°, T/W = 0.5, ζ = 0.042, L/D = 0.5). The results of this series of runs are presented in Fig. 15.

3. Orbital Departure from Nearly Circular Orbits (100 ≤ h ≤ 500 stat mi i.e. 161 to 805 km) with Finite Burning Times

This section treats departure from orbits whose altitudes vary from 100 to 500 stat mi (161 to 805 km), whose velocities at the firing of the retrorocket vary between 100 ft/sec more than and 100 ft/sec less than the velocity of circularity (v_c ± 30.5 m/sec) at the orbital altitude, and whose flight path angles will be between ±4°.

As was discussed in the previous paragraphs, the work done by the radial component of thrust is small; therefore, as the orbital altitude increases, the value of δ which provides for a minimum energy orbital departure rapidly changes from -90 to 180°. The value of δ to be used for the remainder of this study dealing with orbits of 100-stat mi (161-km) altitude and more will be 180°. The initial thrust-to-weight ratio will also be assigned a value to restrict the scope of the program which must be undertaken to provide the data for this report. Figure 16, a plot of the re-entry parameters as functions of orbital altitude and thrust-to-weight ratio, shows the reduced sensitivity of all of the re-entry quantities to thrust-to-weight ratio as $\frac{T}{W_0}$ increases. This figure indicates that no improvement in the re-entry parameters or reductions in the required mass ratio are to be realized by increasing $\frac{T}{W_0}$ to more than 1.5 and little above 0.5; therefore, a value of $\frac{T}{W_0}$ of 0.5 is used for the remainder of this analysis.

Figure 17 presents re-entry velocity, flight path angle, time of flight required for descent and the range attained in descent to 300,000 ft (91.5 km) as functions of the initial altitude and retrorocket mass ratio for several initially circular orbits. This figure clearly defines the minimum mass ratio required for departure from several initially circular orbits. Any mass ratio less than that which produces 0° as a re-entry angle would produce an elliptical orbit, the initial perigee of which would be above the nominally selected re-entry altitude, and the initial apogee of which would be approximately the altitude at burnout. This orbit would decay, possibly quite rapidly due to the existence of an atmosphere above the re-entry altitude, and the vehicle would eventually re-enter; these figures, however, are for those applications in which the vehicle would re-enter the sensible atmosphere, as defined, in one-half of one revolution or less. The time of flight for a vehicle traveling in a trajectory which did not initially pass within the atmosphere would be determined approximately by its closest approach to the earth and the quantity $\frac{C_D A}{2m}$.

Figures 18a, b, c, d, and e present the re-entry parameters as functions of orbital altitude, orbital velocity and retrorocket mass ratio (γ_1 = 0°). Conclusions pertaining to the minimum mass ratios acceptable for orbital departure for velocities other than that of circularity can be obtained from these figures in the manner discussed for Fig. 17.

Figures 19a, b, c, d, and e present the re-entry parameters as functions of retrorocket mass ratio, orbital altitude and flight path angle prior to firing the retrorocket. Several of these figures show discontinuities and bulges which at first glance may appear to be in error; however,

it must be noted that these irregularities occur for mass ratios which are marginal from the standpoint of energy required for successful orbital exit and only in the range of flight path angles from approximately -2° to +2°. This situation can best be explained by stating that a variation in the value of γ_1 (either positive or negative) produces an elliptical orbit one portion of which lies below the altitude at which the retrorocket is fired. The net result of this displacement of the perigee is to reduce the amount of propellant required for a successful departure from orbit or to make exit less marginal for a given amount of propellant.

Small thrust-to-initial-weight ratios $\left(\frac{T}{W_0} = 0.01\right)$ for orbital departure have also been considered. This device burned for the major portion of the time required for descent, thus, providing a force which could also be employed for minor maneuver or flight path corrections during descent. It was thought that significant reduction in the re-entry flight path angle could be realized with this approach; however, the results indicated little margin of superiority in this respect and showed an increase in the amount of propellant required.

4. Error Sensitivities for Departure from Nearly Circular Orbits Assuming Finite Burning Times

Generally, since the orbital velocity, altitude and flight path angle at any given time are not known exactly, it is desired to show the effects of errors in each of these orbital parameters prior to initiation of a retrorocket and in the retrorocket burning time on the re-entry parameters being evaluated. Due to the fact that no purely analytical expressions can be obtained which include the effects of retrorocket burning time on these errors, each error was evaluated manually by determining the slopes of the curves presented in the previous sections. An extension of this analysis to include such things as variations in the peak values of deceleration and vehicle skin temperatures due to the atmosphere, in the impact angle and velocity, and in impact dispersion, will not be made here due to the fact that each of these quantities is a complex function of the configuration of the re-entry vehicle.

The error in a given re-entry parameter resulting from any of the errors being investigated can be evaluated from the data presented here in the following manner.

$$\Delta X_1 = \Delta t_B \left(\frac{\Delta X}{\Delta t_B}\right) \quad (140)$$

$$\Delta X_2 = \Delta V_1 \left(\frac{\Delta X}{\Delta V_1}\right) \quad (141)$$

$$\Delta X_3 = \Delta h_1 \left(\frac{\Delta X}{\Delta h_1}\right) \quad (142)$$

$$\Delta X_4 = \Delta \gamma_1 \left(\frac{\Delta X}{\Delta \gamma_1}\right) \quad (143)$$

where

X can be any of the four re-entry quantities considered (range, flight time, velocity, and flight path angle).

The resultant error in any of the re-entry parameters due to an error in more than one of the quantities t_B, V_1, h_1 and γ_1 can now be evaluated through the utilization of the chain rule, i.e.,

$$\Delta X_{total} = \Delta X_1 + \Delta X_2 + \Delta X_3 + \Delta X_4. \quad (144)$$

This assumption is permissible only because the independent error terms are small for most cases; if a higher degree of accuracy is desired or if these independent errors are large, the method of successive approximations must be employed to improve the accuracy of the estimate. Once the resultant error has been determined, the actual value of the re-entry parameter may be obtained by adding the resultant error to the nominal value of quantity as defined in previous sections.

It is noted at this point that this procedure will not yield the most probable value of the error if the maximum errors in each parameter are substituted into the chain. To obtain this probable error, it is necessary to refer to statistical discussions similar to that presented in Chapter VI.

Due to the fact that it is at present impossible to place a vehicle in an exact predetermined orbit, it is necessary to provide the vehicle with a retrorocket large enough to remove the vehicle from the major portion of orbits into which injection is likely. This fact makes it necessary to physically control the burning time (and consequently the mass ratio) of the retrorocket in order to prevent the vehicle from assuming a trajectory which would produce maximum values of skin temperature and/or deceleration which exceed the limits placed on the trajectory by structural and personnel considerations.

Figures 20a, b, c, d and e present the errors in the re-entry parameters due to an error in t_B (assumed to be 1 sec) as functions of the orbital conditions prior to firing the retro-rocket and of the retrorocket mass ratio. The selection of this value of Δt_B is not intended to reflect the accuracy anticipated in controlling this quantity but rather is intended to make the data more readily applicable for all values of Δt_B. Actually, this error can be limited to approximately 0.05 sec barring malfunction for most motors of the size necessary for this maneuver.

Figure 21 presents the changes in the re-entry quantities due to an error of 1 ft/sec (0.3 mps) in V_1 as a function of the retrorocket mass ratio and the orbital conditions prior to firing the retrorocket. Very little data is available pertaining to the accuracies obtainable from the various velocity sensing schemes and mechanisms, but it is felt that vehicle velocity should be known within a

range of 1 to 10 parts in 100,000. These inaccuracies correspond to errors in V_1 from approximately 0.2 to 1.0 fps (±0.06 to ± 0.3 mps).

Figures 22a, b and c present the variations in the re-entry parameters due to a 1-stat mi (1.61 km) error in h_1. The accuracies obtainable even with present radar indicate that it would be unreasonable to assume an error in h_1 greater than approximately 300 ft $\left(\frac{1}{17.6}\right.$ stat mi or 91.5 m$\left.\right)$ will exist. Since all of the errors being evaluated are small even for an error in h_1 of 1.6 km, the effects of an error in h_1 of only 91 m are negligible. As may be observed from the energy equation, variations in altitude h_1 will have a definite effect on the re-entry velocity, an effect which is not reflected here. This apparent discrepancy is due to the fact that the assumed error in h_1 is so small that actual variations in the value of the re-entry velocity could not be obtained in this manner from the data.

Figures 23a, b, c, d and e present the errors in the re-entry parameters due to a 1° error in the flight path angle. This error can be the result of the fact that the flight path angle prior to the maneuver was not known correctly or to the fact that the impulse from the retrorocket was not applied in the proper direction. In either case very little data is available pertaining to the accuracy to which this quantity can be obtained; however, it is felt that if sufficiently accurate data is available this angle should be known to the order of 0.01 to 0.1 degree.

The data presented in this section indicates that the resultant errors in all of the re-entry parameters with the exception of range attained in descent will be quite small for the estimated errors in t_B, V_1, h_1 and γ_1. Range, however, is quite sensitive to errors in each of these quantities thus pointing up the probability of a marked impact dispersion pattern. The determination of this pattern, however, will not be attempted due to the necessity of including the vehicle ballistic coefficient and aerodynamic lift in such analysis. In any event, the presence of an atmosphere below the re-entry altitude will magnify the dispersion pattern existing at re-entry due to the aerodynamic uncertainties and the fact that γ and V were also affected by the previous errors.

D. THREE-DIMENSIONAL IMPULSE ANALYSIS FOR THE CASE OF CIRCULAR ORBITS

The approach in the previous sections has been to reduce the recovery problem to one of two dimensions by utilizing an intermediate orbit. The philosophy for this approach is governed by the consideration of the energy required for maneuvering. However, because timing errors can result, and because under some circumstances it may be desirable to recover promptly, it is also necessary to consider the three-dimensional nature of the problem (see following sketches).

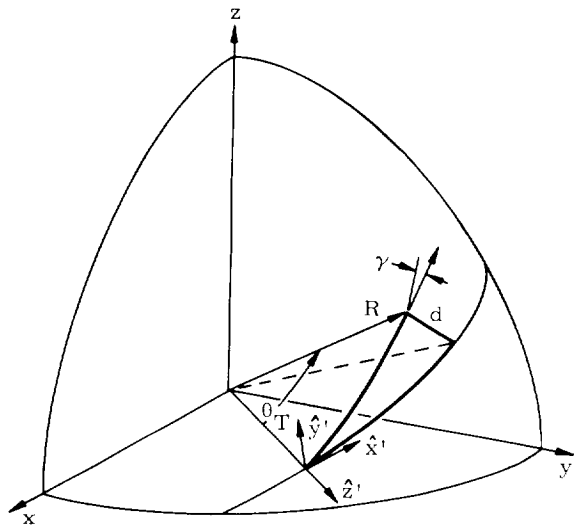

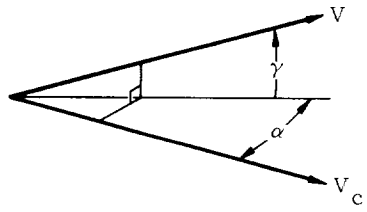

This particular problem has been analyzed by Fosdick and Anthony (Ref. 1). For this reason the complete solution will not be repeated here. However, it is noted that the problem is not unlike those discussed in Chapter VI (Maneuvers). The referenced paper gives the following:

(1) The direction cosines of the impulse in vehicle centered coordinates

$$\ell = \frac{\Delta\vec{V} \cdot \hat{X}'}{\Delta V} = (\nu \cos \alpha \cos \gamma - 1)/D^*$$

$$m = \frac{\Delta\vec{V} \cdot \hat{Y}'}{\Delta V} = (\alpha \cos \gamma \sin \alpha)/D^*$$

$$n = \frac{\Delta\vec{V} \cdot \hat{Z}'}{\Delta V} = (\nu \sin \gamma)/D^*$$

where

$D^* = (1 - 2\nu \cos \alpha \cos \gamma + \nu^2)^{1/2}$

α = The angle in the horizontal plane at the initial radius through which the velocity vector is rotated

γ = The flight path angle of the velocity vector following the impulse

$\nu = \frac{V}{V_c}$

$$\nu = \left\{ \left[1 - \cos\theta_T\right] \left[\cos^2\alpha \quad (1 - \cos\theta_T + \frac{r - R}{R} \cdot + \tan\alpha \sin\theta_T\right]^{-1} \right\}^{1/2}$$

(2) Turn angle and impulse magnitude

$$\sin\alpha = \frac{\sin d}{\sin\theta_T}$$

$$\frac{\Delta V}{V_c} = \nu^2 + 1 - 2\nu\cos\gamma\cos\alpha$$

(3) Flight path angle.

To this point only the initial and final radii and the angle between have been fixed. Thus, the transfer ellipse is not unique and γ cannot be fixed. This condition is altered if the time of flight (or flight path angle or velocity at a point in the ellipse) is specified since then the ellipse is unique. The reason that this was not done was to leave an area for possible optimization of the impulsive correction.

Ref. 1 also reports some results obtained for the analytic optimization of the position of deorbit. The solution is, however, fairly lengthy. Gedeon (Ref. 2) took this work and developed some interesting results by numerical optimization of the following equation obtainable from Ref. 1.

$$\Delta K = \sqrt{1 - 2K\cos\gamma\sqrt{\sin^2\theta_T - \frac{\sin^2 d}{\sin\theta_T}} + K^2}$$

where: $K = \frac{\sin\theta_T/2}{\cos\gamma} \cdot \sqrt{\frac{2}{\frac{r_0}{r_1} - \frac{\cos(\theta_T - \gamma)}{\cos\gamma}}}$

r_0 = initial radius

r_1 = radius at which the displacement occurs

ΔK = The change in the quantity $\sqrt{2 - \frac{r}{a}}$

= a measure of ΔV since $a = \frac{r\mu}{2u - r\left|\vec{V} + \Delta\vec{V}\right|^2}$

$$= -2\frac{r}{K}\frac{\vec{V}\cdot\Delta\vec{V}}{\mu} \quad \frac{|\Delta V|^2}{|V|^2} \ll |$$

The results of these procedures are presented in Figures 24 through 27. One important factor should be noted. These figures have the parameter r_0/r_1; thus, they can be utilized for generating data down the re-entry altitude (or to impact if the effects of the atmosphere on the trajectory can be assumed negligible in the case of interest).

This being the case, the angle γ, takes on special value since it is the re-entry angle discussed previously and in Chapter IX.

This material completes this portion of the 3-D recovery discussion. As was noted previously, however, additional material on this problem and on maneuvers can be found in Chapter VI.

E. ANALYSIS OF ORBITAL DEPARTURE FREQUENCY

1. Defining Equations

For the purpose of defining the acceptable times of orbital departure from the low altitude orbit, a model of the earth and of the satellite orbit have been selected. The earth is assumed to be spherical and rotating at a uniform rate (see the following sketch). In order to partially compensate for errors involved in assuming a spherical earth, the orbital plane is assumed to be regressing about the equator at a uniform rate. The orbit of the satellite will be considered to be affected by drag forces; however, all other accelerations (such as second order oblateness effects, sun, moon, etc.) are neglected.

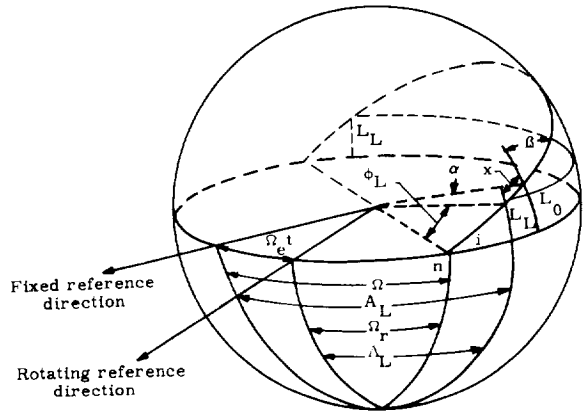

$$\alpha = \frac{X}{R_s} = \frac{\text{arc}}{\text{radius}}$$

Utilizing this sketch and the assumptions listed above, it is now possible to solve for the sidereal time at which the impact point lies in a prescribed plane.

$$t_{exit} = \frac{\Omega_0 + n\dot{\Omega} - (\Lambda + \Delta\Lambda \text{ maneuver})}{\Omega_e} + \frac{f_{impact}(L, i) + 2m\pi}{\Omega_e}$$

where: $\Delta\Lambda$ maneuver = angular displacement corresponding to thrust or aerodynamic maneuverability.

$$\dot{\Omega} = -3\pi J_2 \left(\frac{R}{p}\right)^2 \cos i \qquad 0° \leq i \leq 180°$$

m = positive integer for number of days; selected sufficiently large that $t \geq 0$

$$f(L, i) = \sin^{-1} \frac{\tan L_L}{\tan i}$$ northerly launches or southerly approach

$$= \pi - \sin^{-1} \frac{\tan L_L}{\tan i}$$ northerly approach southerly launches $0° < i < 90°$

$$= \pi + \sin^{-1} \frac{\tan L_L}{\tan i}$$ northerly approach southerly launch $90° < i < 180°$

n = number of revolutions in orbit (non-integer)

Similarly there is an expression for the time at which the launch point crosses the plane

$$t_{launch} = \left(\Omega_0 - \Lambda_{launch} - \Delta\Lambda_{launch\ maneuver} + f_{launch}(L, i) \right) \Omega_e^{-1}$$

Thus, the time duration for the satellite in orbit is $t_{exit} - t_{launch}$ or

$$t_{in\ orbit} = \left[(\Lambda + \Delta\Lambda)_{impact} - (\Lambda + \Delta\Lambda)_{launch} + n\dot{\Omega} + 2m\pi + f_{impact}(L, i) - f_{launch}(L, i) \right] \Omega_e^{-1}$$

It is noted at this point that though f_{impact} and f_{launch} have the same functional form, the numerical values of L_L, L_i, i and i_i need not be the same. Thus, this equation can reflect the effects of maneuvering in orbit in the interim between launch and recovery.

A second equation for the time in orbit may be written as

$$t_{in\ orbit} = n\tau_0 + \sum_{i=1}^{n} \Delta\tau_i + t_{AD}$$

where

n = the number of revolutions in the orbit (noninteger)

τ_0 = the period of the initial orbit over an oblate earth

$\Delta\tau_i$ = change in the i^{th} period due to drag shown in the next sketch

t_{AD} = the time required for ascent and descent.

Now, the two equations for $t_{in\ orbit}$ can be equated and solved for the unknown "n" which will be required to place the satellite and the impact point in the desired positions for recovery.

$$n = \left[(\Lambda + \Delta\Lambda)_{impact} - (\Lambda + \Delta\Lambda)_{launch} + 2m\pi + f_{impact}(L, i) - f_{launch}(L, i) - \left(\sum_{i=1}^{n} \Delta\tau_i + t_{AD} \right) \Omega_e \right] \left[\tau_s \Omega_e \left(1 + \frac{\Delta\tau}{\tau_s} - \frac{\dot{\Omega}}{\Omega_e} \right) \right]^{-1}$$

where

$\frac{\Delta\tau}{\tau_s}$ = oblateness correction for orbital period, see Chapter IV

τ_s = the orbital period over a spherical earth.

2. Drag Correction

Since the corrective term (i.e., the series) is a function of n (shown in the following sketch), the solution requires iteration.

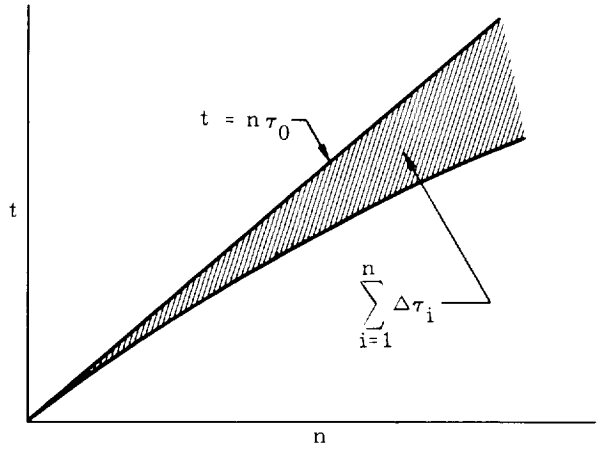

This process, however, is greatly simplified due to the fact that the size of the correction is small. Thus n can be estimated neglecting the correction and then refined. This refinement can be obtained in the following fashion.

$$a = \frac{r_a + r_p}{2}$$

$$\Delta a_{secular} = \frac{(\dot{h}_a + \dot{h}_p)}{2} \tau$$

$$\Delta\tau_{secular} = \frac{3}{2} \frac{\tau}{a} (\Delta a_D + \Delta a_0)$$

$$= -\frac{3}{4}\frac{\tau^2}{a}\left[G_1(z) + G_2(z)\right]\left[1 - e\right]^{1/2} 2B\rho_p\sqrt{\mu r_p}$$

where

Δa_D = the drag correction for secular changes in the semimajor axis

Δa_0 = the oblateness correction for secular changes in the semimajor axis = 0

$G_1(z)$, $G_2(z)$ = drag parameters for elliptic orbits, discussed in Chapter V

ρ_p = atmosphere density at perigee

$B = \frac{C_D A}{2m}$

Thus, as the elements are defined as a function of the revolution number, the correction corresponding to that revolution can be computed.

The approach above is vigorous but is somewhat more involved than desirable because it is necessary to compute a correction on each revolution. In view of the fact that the corrections are in general small and that the atmospheric uncertainties preclude high accuracies, an alternative solution is available for the case of circular and near circular orbits. This approach makes use of the fact that in a restricted range of altitudes the following approximations are valid.

$$\Delta\tau = (4\pi\rho B\sqrt{\mu r_p})\left(\frac{3}{2}\sqrt{\frac{a}{\mu}}\right)\Delta t = -6\pi B a\,\Delta t$$

But

$$t \approx n\tau_0$$

$$\Delta t \approx \tau_0\,\Delta n$$

Now replacing a by $(a_0 - 4\pi\rho a_0^2 Bn)$ yields:

$$\Delta\tau \approx -6\pi B\tau_0(a_0 - 4\pi\rho a_0^2 Bn)\rho\,\Delta n$$

and for nearly circular orbits

$$\rho \approx \rho_0 \exp K(a_0 - a) \approx \rho_0 \exp K(4\pi\rho_0 a_0^2 Bn)$$

$$\Delta\tau = \left\{-6\pi B\tau_0\left[(a_0 - 4\pi\rho_0 a_0^2 Bn \exp K(4\pi\rho_0 a_0^2 Bn)\right]\right.$$

$$\left.\cdot\,\rho_0 \exp K(4\pi\rho_0 a_0^2 Bn)\,\Delta n\right\}$$

Now adopting a shorthand notation to prevent bookkeeping problems with the constants, the equation for $\Delta\tau$ becomes

$$\Delta\tau = (A_1 + A_2 ne^{A_3 n})e^{A_3 n}\,\Delta n$$

$$A_1 = -6\pi B\tau_0 a_0\rho_0$$

$$A_2 = +24\pi^2 B^2\tau_0 a_0^2\rho_0$$

$$A_3 = 4\pi\rho_0 a_0^2 BK$$

If, at this point it is further assumed that the series $\sum_{i=1}^{n}\Delta i$ can be approximated by the integral, a simple expression can be obtained.

$$\sum_{i=1}^{n}\Delta\tau_i = \int_0^n (A_1 + A_2 ne^{A_3 n})e^{A_3 n}\,dn$$

$$= \frac{A_1}{A_3}e^{A_3 n} + \frac{A_2(2A_3 n - 1)}{(2A_3)^2}e^{2A_3 n}$$

This expression should be utilized for the evaluation of the series for most of the cases of interest. However, for special cases where $|2A_3 n| < 1$, it is of interest to look at the series expansion of the right-hand side of the previous equation.

$$\sum_{i=1}^{n}\Delta\tau_i = \frac{A_1}{A_3}\left(1 + A_3 n + \frac{(A_3 n)^2}{2} + \frac{(A_3 n)^2}{6} + \ldots\right)$$

$$+ \frac{A_2(2A_3 n - 1)}{(2A_3)^2}\left(1 + 2A_3 n\right.$$

$$\left. + \frac{(2A_3 n)^2}{2} + \frac{(2A_3 n)^3}{6} + \ldots\right)$$

$$= \left(\frac{A_1}{A_3} - \frac{A_2}{4A_3^2}\right) + n\left(A_1 + \frac{A_2}{2A_3}\right)$$

$$+ n^2\left(\frac{A_1 A_3}{2} + \frac{A_2}{2}\right) + n^3\left(\frac{A_1 A_3^2}{6}\right.$$

$$\left. + \frac{2A_2 A_3}{3}\right) + \text{other terms.}$$

This form of the series is preferable for the previously noted special cases because of the simple form.

It is noted at this point that either form for the correction will be more accurate if the altitude range is small. Thus, a logical extension could be obtained by breaking the decay range into regions which the assumptions were valid. This approach would entail the computation of several sets of constants A_i (i = 1, 2, 3).

3. Launch Maneuver Correction

To this point each factor in the definition of the quantity n has been discussed except the quantities $\Delta\Lambda_{launch}$ and $\Delta\Lambda_{impact}$. The first maneuver ($\Delta\Lambda_L$) is the direct result of launching into a plane other than the orbital plane and utilizing a portion of the propellant for the purpose of turning the vehicle into the desired plane. The magnitude of this maneuver thus depends on the amount of surplus propulsion available, the type of trajectory to be flown and the type of guidance law which is utilized. Although no detailed discussions of powered flight are presented in this volume, the related discussions for the case where the plane is altered impulsively can be presented. Consider the following sketch and the spherical relationships derivable therefrom:

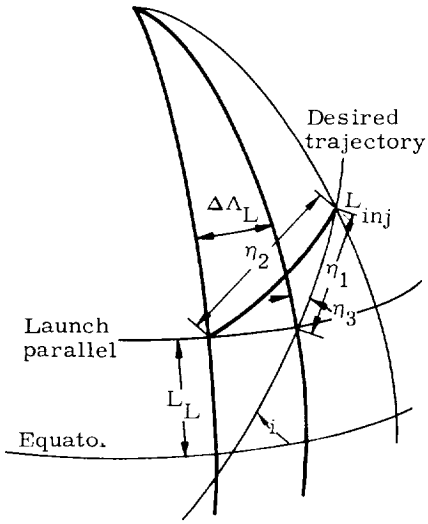

$$\sin\phi = \frac{\sin L}{\sin i}$$

$$\eta_1 = \phi_{inj} - \phi_L$$

$$= \sin^{-1}\left(\frac{\sin L_{inj}}{\sin i}\right) - \sin^{-1}\left(\frac{\sin L_L}{\sin i}\right)$$

$$\eta_2 = \frac{\text{ascent range}}{\text{Earth's radius}}$$ (i.e., the plane change is assumed to occur at point of injection into orbit but prior to injection for fuel economy)

$$\eta_3 = \beta_L$$

$$= \sin^{-1}\left(\frac{\cos i}{\cos L_L}\right)$$

Now the determination of $\Delta\Lambda$ can proceed based on Eqs (65) and (68) of Chapter XIII.

$$\sin(\Lambda - \Lambda_0) = \frac{\sin\alpha \sin\beta}{\cos L}$$

$$\sin L = \sin L_0 \cos\alpha + \cos L_0 \sin\alpha \cos\beta$$

or

$$\cos\beta = \frac{\sin L - \sin L_0 \cos\alpha}{\cos L_0 \sin\alpha}$$

These equations are the parametric equations for a polar cap with center at L_0, Λ_0 and of radius of α. The azimuth angle β is then the independent variable for generating the locus of points L, Λ. These two equations can be utilized as follows:

Let

$$\alpha = \eta_1$$

$$\beta = \eta_3$$

$$\Lambda_0 = 0$$

then

$$\sin\Lambda_1 = \frac{\sin\eta_1 \sin\eta_3}{\cos L_{inj}}$$

Now let

$$\alpha = \eta_2$$

$$L_0 = L_{inj} \text{ and } L = L_L$$

$$\cos\beta = \frac{\sin L_L - \sin L_{inj}\cos\eta_2}{\cos L_{inj}\sin\eta_2}$$

and

$$\sin(\Lambda_2 - \Lambda_1) = \frac{\sin\eta_2 \sin\beta}{\cos L_L}$$

At this point it is noted that the quantity of interest $\Delta\Lambda_L$ may be obtained to be:

$$\Delta\Lambda_L = \Lambda_2 - \Lambda_0 = \Lambda_2$$

This derivation tacitly assumed that the launch site would cross the orbital plane, thus as a consequence this value of $\Delta\Lambda_L$ is valid only for the cases for which

$$i > |L_L|$$

By varying the formulation above other cases can, however, be included.

4. Landing Maneuver Correction

The second maneuver to be discussed ($\Delta\Lambda_{impact}$) is, as was noted, the result of either

aerodynamic maneuverability or thrust. In either case, however, $\Delta\Lambda_{impact}$ is highly dependent on the guidance philosophy. This being the case, only the simplest of the possible maneuvers can be considered. The following sketch illustrates this problem for a lateral maneuver distance D_m and a descent range R.

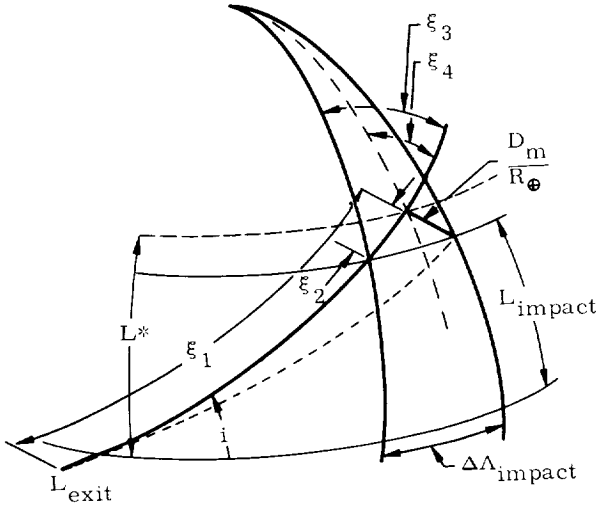

$$\xi_1 = \cos^{-1}\left[\frac{\cos\ \frac{R}{R_\oplus}}{\cos\ \frac{D_m}{R_\oplus}}\right]$$

$$\xi_2 = \xi_1 - \phi_2 + \phi_1$$

where

$$\phi_1 = \sin^{-1}\left(\frac{\sin L_{exit}}{\sin i}\right)$$

$$\phi_2 = \sin^{-1}\left(\frac{\sin L_{impact}}{\sin i}\right)$$

$$\xi_3 = \sin^{-1}\left(\frac{\cos i}{\cos L_{impact}}\right)$$

$$L^* = \sin^{-1}\left(\sin i \sin(\xi_2 + \phi_2)\right)$$

$$\xi_4 = \sin^{-1}\left(\frac{\cos i}{\cos L^*}\right)$$

Now, as before, the spherical segment equations can be utilized to yield $\Delta\Lambda_{impact}$.

let

$$\alpha = \xi_1$$

$$\beta = \xi_3$$

$$\Lambda_0 = 0$$

$$L_0 = L_{impact}$$

$$\sin\Lambda_1 = \frac{\sin\xi_1 \sin\xi_3}{\cos L^*}$$

Now let

$$\alpha = \frac{D_m}{R}$$

$$\beta = \xi_3$$

$$\Lambda_0 = \Lambda_1$$

$$L_0 = L^*$$

$$\sin(\Lambda_2 - \Lambda_1) = \frac{\sin\left(\frac{D_m}{R}\right)\sin\xi_4}{\cos L_{impact}}$$

and finally

$$\Delta\Lambda_{impact} = \Lambda_2 - \Lambda_0 = \Lambda_2$$

No stipulation has been made as to the restriction on the validity of this value of Λ_2; however, in the derivation an assumption has been made nonetheless. This assumption is that

$$i > |L_{impact}| + \frac{D_m}{R}$$

While this assumption is somewhat restrictive, it provides information for most of the orbits of practical value. Those orbits which are excluded will be discussed later.

Attention may now be turned to the description of the parameters assumed in this final discussion, R and D_m. The first quantity must be estimated from the combination of the free flight trajectory down to a re-entry altitude, the aerodynamic characteristics of the body and the re-entry conditions. This material is found in Chapters III and IX. The second quantity (D_m), however, must be handled in a slightly different fashion. If the maneuver is the result of a small impulsive correction, the lateral maneuverability is approximately

$$D_m = r_0 \frac{\Delta V}{V_0} \sin(\theta - \theta_0) \text{ (see Chapter VI)}$$

where

r_0 = initial radius

V_0 = initial velocity

$\theta - \theta_0$ = central angle from point of maneuver to impact

Whereas, if the maneuver results from aerodynamic forces

$$\left.\begin{aligned} D_m &\approx 623\left(\frac{L}{D^*}\right)^{1.875} \text{ naut mi} \\ &\approx 1155\left(\frac{L}{D^*}\right)^{1.875} \text{ km} \end{aligned}\right\} \frac{L}{D^*} < 1.0$$

$$\left.\begin{aligned} D_m &\approx 910\left(\frac{L}{D^*}\right) \text{ naut mi} \\ &\approx 1688\left(\frac{L}{D^*}\right) \text{ km} \end{aligned}\right\} 0.75 < \frac{L}{D^*} < 2.0$$

where

D_m = maximum distance normal to the orbital plane that is obtainable in descent from 300,000 ft (91.4 km).

L/D^* = component of the L/D ratio normal to the plane of motion.

These latter relations were suggested by numerical integration of actual motions, although it is noted that the former relation $\left(\frac{L}{D^*} < 1\right)$ has some theoretical basis. (The theoretical constants are different.)

5. The Form of n

Now since each term in the definition of n is a known quantity, the number of revolutions having occurred at any time that the impact point is in or near the plane of motion can be evaluated. The attention must, therefore, be turned to those values of n which are acceptable for a particular problem. Consider the following sketch:

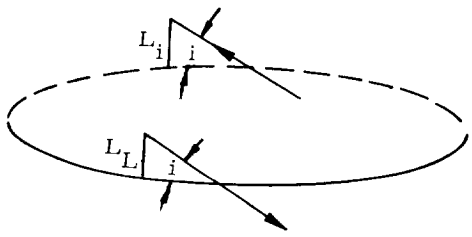

From this sketch, it is apparent that the number of revolutions must be of this form:

$$n' = p + \frac{1}{2\pi}\left[\pi + \sin^{-1}\left(\frac{\sin L_L}{\sin i}\right) + \sin^{-1}\left(\frac{\sin L_i}{\sin i}\right)\right]$$

southerly launches approach from the south

$$= p + \sin^{-1}\left(\frac{\sin L_L}{\sin i}\right) - \sin^{-1}\left(\frac{\sin L_i}{\sin i}\right)$$

southerly launches approach from north

$$n' = p - \sin^{-1}\left(\frac{\sin L_L}{\sin i}\right) + \sin^{-1}\left(\frac{\sin L_i}{\sin i}\right)$$

northerly launch approach from north

$$= p + \sin^{-1}\left(\frac{\sin L_L}{\sin i}\right) - \sin^{-1}\left(\frac{\sin L_i}{\sin i}\right)$$

northerly launch approach from south

where

p is a positive integer

n' is related to n in following paragraph

But portions of these distances will be required for ascent and descent. Since those distances are not explicitly in the equations for time in orbit (the times required are included), a correction to the value of n' must be made and the resultant form for n must be

$$n = n' - \frac{R_{ascent}}{R_\oplus} - \frac{R_{descent}}{R_\oplus}$$

The procedure is now to generate values of n for the various passes of the impact point through the plane of motion and compare these numbers to those required for successful return. In this comparison if $\pm D_m$ allows the computation of the required n, then a suitable maneuver can result in sucessful return. This process is sufficiently simple in that it can be performed manually if necessary; however, digital computers prove to be a definite asset. Once n is known, it can be determined whether the approach was from the north or south, what maneuverability is required, and even the time at which deorbit should occur.

6. Alternative Methods

As was noted in previous paragraphs, there have been assumptions made which restrict the applicability of the approach to orbits for which $i > |L_{impact}| + \frac{D_m}{R_\oplus}$. Though this assumption may not be too restrictive for some orbits, it proves troublesome for others. One approach around this impasse is to compute the ground swath defined by the maneuverability of the vehicle. (Ground swaths are discussed in Chapter XIII.) When the ground swath contains the impact site then recovery is possible. If several of these ground swaths are then computed in the vicinity of the positions which yielded satisfactory call-downs, the amount of maneuverability and the direction and the time for deorbit can be found. The approach is very simple and is not restricted as to applicability; however, the number of computations required even for relatively short durations in orbit is large and automatic computation is almost essential.

A third purely graphical approach involves the plotting of the ground track (see Chapter XVIII) for the orbit on vellum for a suitable map. (This track will be approximately constant for the entire duration in orbit under the assumption that large maneuvers or large changes resulting from drag do not occur.) Then the positions of the ascending nodes can be plotted on the map including the effects of drag, oblateness, etc. After this step, the maneuver envelope is superimposed on the ground track as the track is laid alternately on each of the ascending nodes and the possible call-downs are recorded. This final approach thus combines the advantages of both of the previous approaches in that it is not restricted to latitudes, can be performed manually and readily exhibits the information desired. Much work is still required, however, in order to develop the data.

Each of these three methods has its merits, and each has been utilized for analyses of this type. The selection of a method should be based on the method of computation, the information required in the analysis, and the availability of data in various forms.

F. CONCLUSIONS

In this chapter the geometry and the landing site intercept timing considerations for a generalized return trajectory from an elliptical orbit into a low altitude circular orbit are presented mathematically. An error analysis of the final low altitude orbit characteristics is derived for small errors in the departure velocity, altitude and flight path angle. The following conclusions are reached.

(1) The return trajectory is extremely sensitive to errors in departure velocity. A vernier correction of the velocity vector seems mandatory immediately after the initial departure injection for certain classes of orbits.

(2) Errors in departure radius cause an error of roughly the same order of magnitude at the perigee arrival.

(3) In case of departure close to the apogee of the transfer ellipse, the errors caused by deviations in flight path angle are extremely small and can be neglected for engineering purposes.

In the timing analysis of the return shuttle, it is shown that two possible target arrival times exist for each day. The solution for the exact departure angle required for a target intercept is best accomplished by an iterative method. For the sample problem the convergence of the iteration method is very rapid. The second approximation gives an answer within two decimal places and within 1.5 sec of total flight time (t_t = 54, 129.92 sec).

Three flight time error analyses are investigated. First, the approximate analytical method is seen to give only an order of magnitude result. Second, the exact analytical method is seen to be somewhat cumbersome algebraically, so far as manual computations are concerned (on the other hand, a digital computer can handle the exact equations easily). Third, the numerical differentiation method is found to be simple, fast and sufficiently accurate.

Call-down from an intermediate altitude circular orbit or from low altitude circular orbits in general is shown to be extremely sensitive to all error sources. Indeed, if a given landing point is selected with a very small allowable error, the only means of achieving a satisfactory landing at a prescribed time is with a maneuverable reentry vehicle. Lateral maneuverability seems to afford the most rewarding avenue of investigation from this point of view.

The anlaysis of orbital departure with finite burning times shows the effect of thrust attitude and magnitude on the re-entry parameters. The analysis also shows that the optimum thrust vector is not always opposite in direction from that of the velocity vector and that thrust levels above approximately 1/2 mg alter the descent trajectory very little.

G. REFERENCES

1. Fosdick, G. and Anthony, M., "Three-Dimensional Pulse Optimization for Vehicles Disorbiting from Circular Orbits," ARS paper 61-156-1850, 13 June 1961.

2. Gedeon, G. S., "Flight Performance Manual for Orbital Operations," Norair Div Northrop Corp. (Hawthorne) Report NOR 61-208, September 1961.

H. BIBLIOGRAPHY

See Chapters III, V, VI, VII and IX for references pertinent to the problem of recovery. In addition, the following are offered.

Bull, G., Enkenhus, K. and Tiddy, G., "Exit and Re-entry Problems," Aerospace Engineering, Vol. 17, No. 6, June 1958.

Detra, R., Ryddell, F. and Rose, P., "Controlled Recovery of Nonlifting Satellites," ARS Journal, Vol. 30, No. 9, September 1960, p 892.

Fosdick, G. and Anthony, M., "3-D Pulse Optimization for Vehicles Disorbiting from Circular Orbits," ARS paper 61-156-1850, June 1961.

Hakes, R. C., "Some Fundamental Problems Associated with Injecting, Orbiting and Recovering Man from Orbit," presented at 27th Annual Meeting of IAS, New York, 26 to 29 January 1959.

Hoglund, R. and Thale, J., "Recovery from a Satellite Orbit," ARS Preprint 650-58, 1958.

Low, G. M., "Nearly Circular Transfer Trajectories for Descending Satellites," NASA report No. 3, Lewis Research Center.

Rosamond, D. L., "Satellite Recovery Techniques for Optimization of Touchdown Accuracy," Journal of Aerospace Sciences, Vol. 28, No. 3, March 1961.

Townsend, G. and Kork, J., "Satellite Recovery," Chapter 9 in Design Guide to Orbital Flight, McGraw-Hill Book Co., New York, 1962.

ILLUSTRATIONS

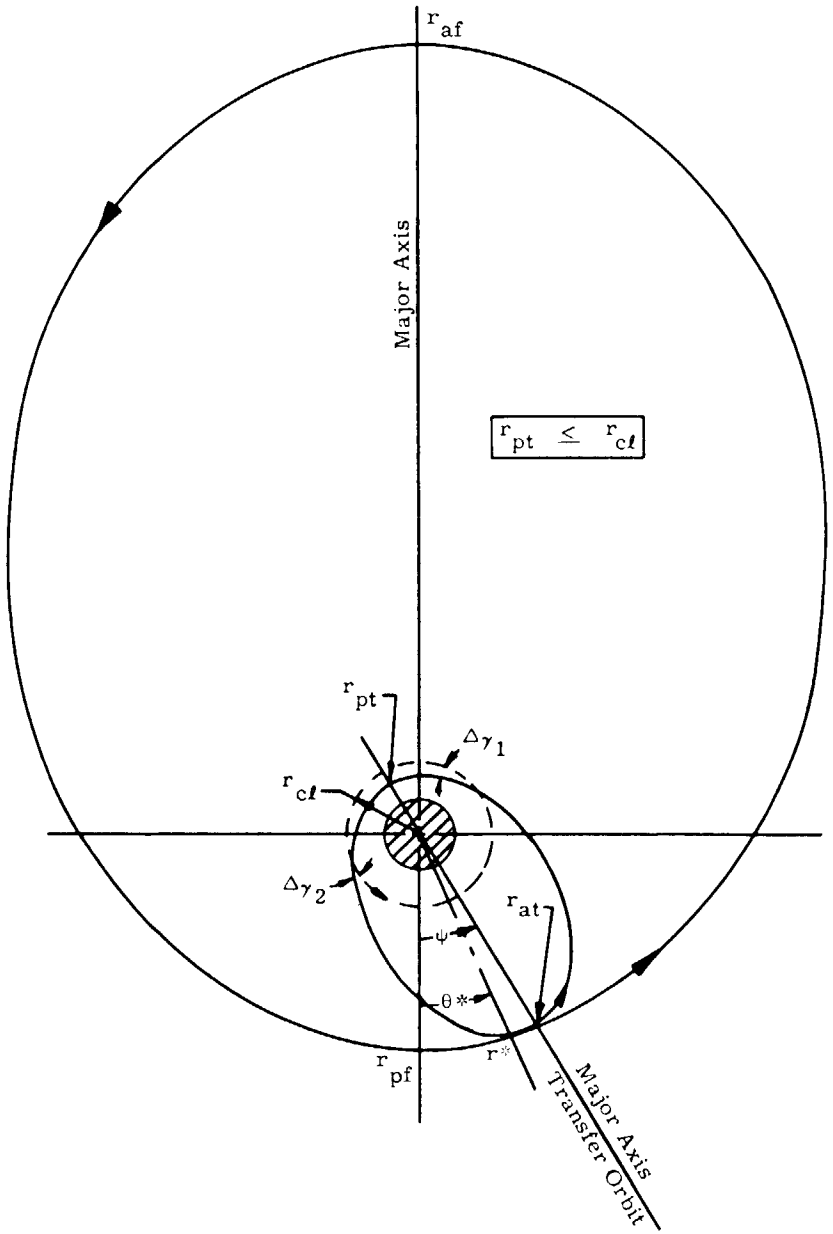

Fig. 1. Geometry of the Return Problem

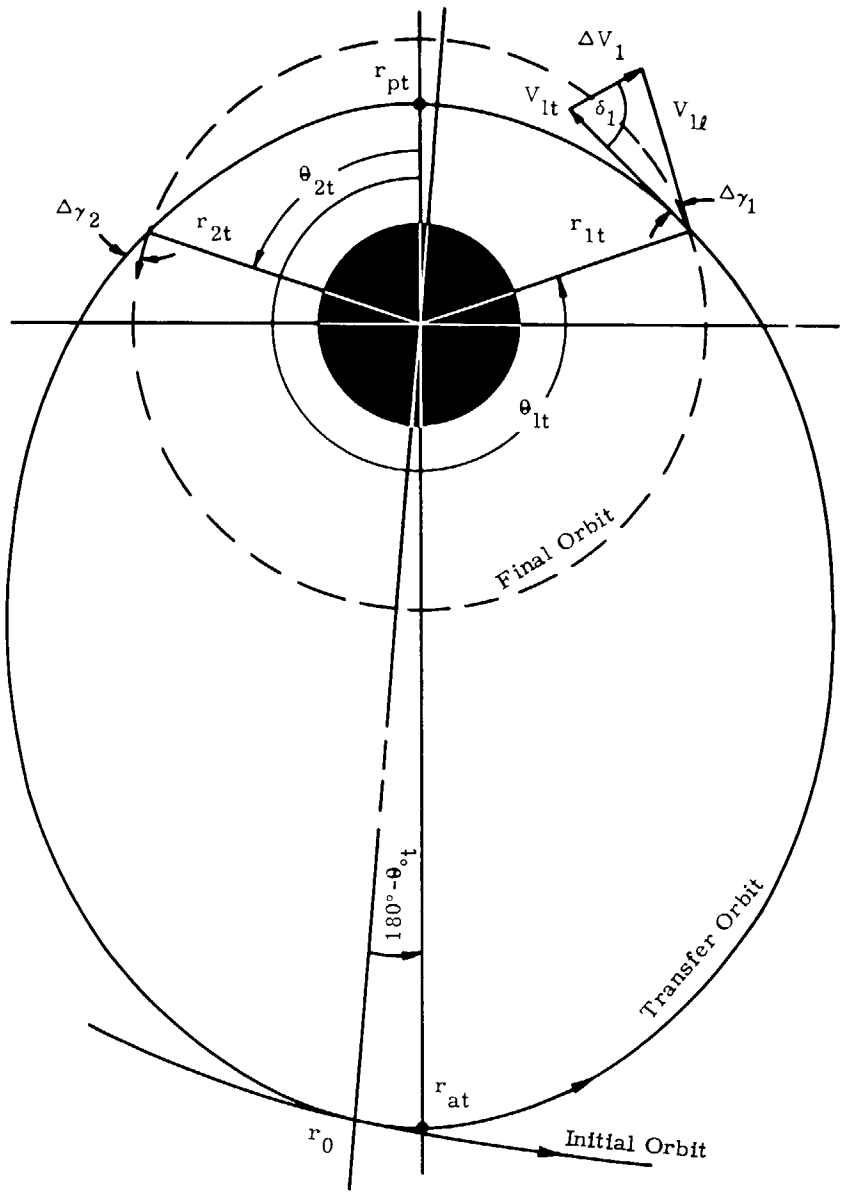

Fig. 2. Geometry of the Return Problem (expanded view)

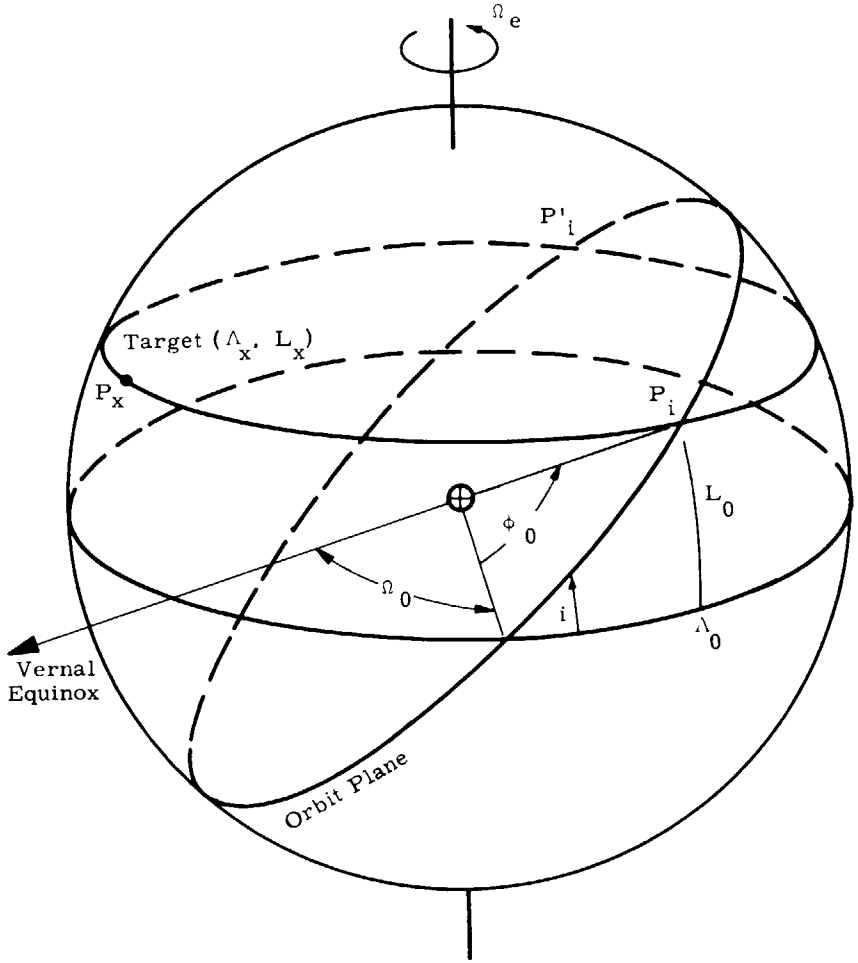

Fig. 3a. 3-D Geometry of the Return Shuttle Problem ($i \geq L_x$)

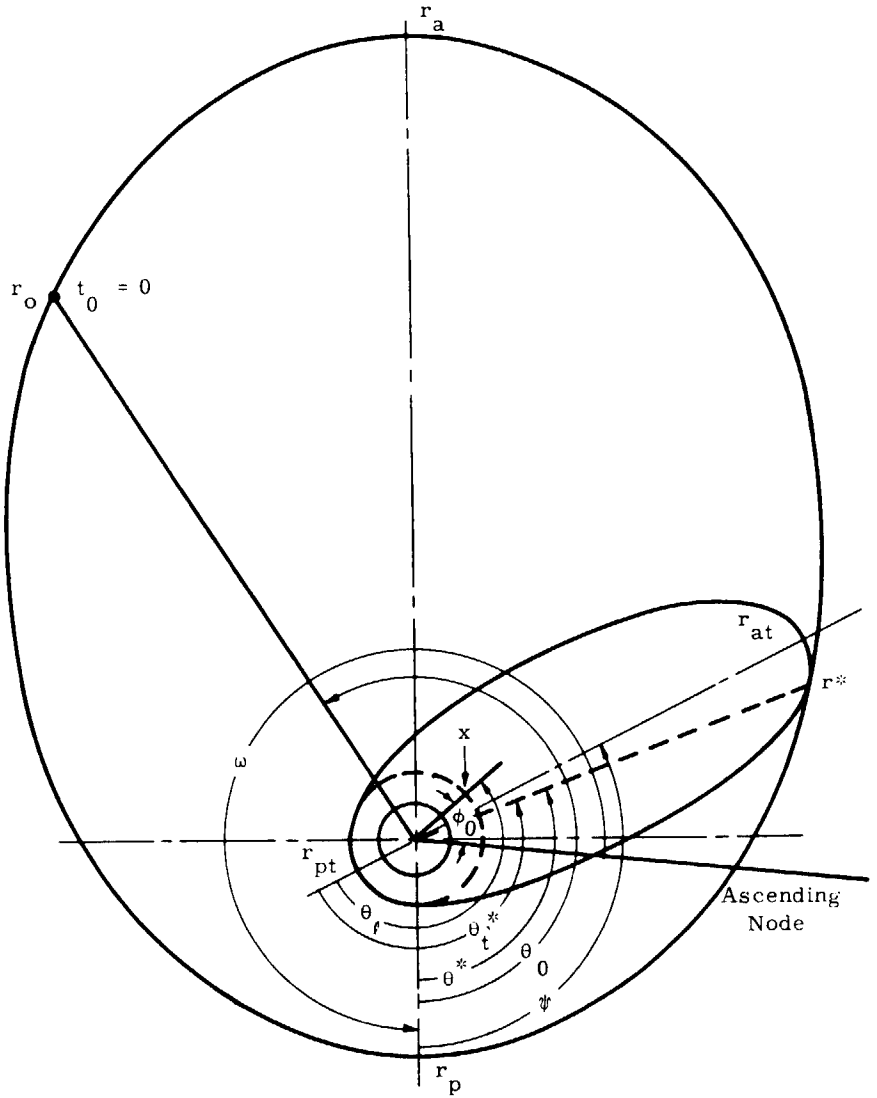

Fig. 3b. Characteristic Angles of the Return Shuttle Trajectory

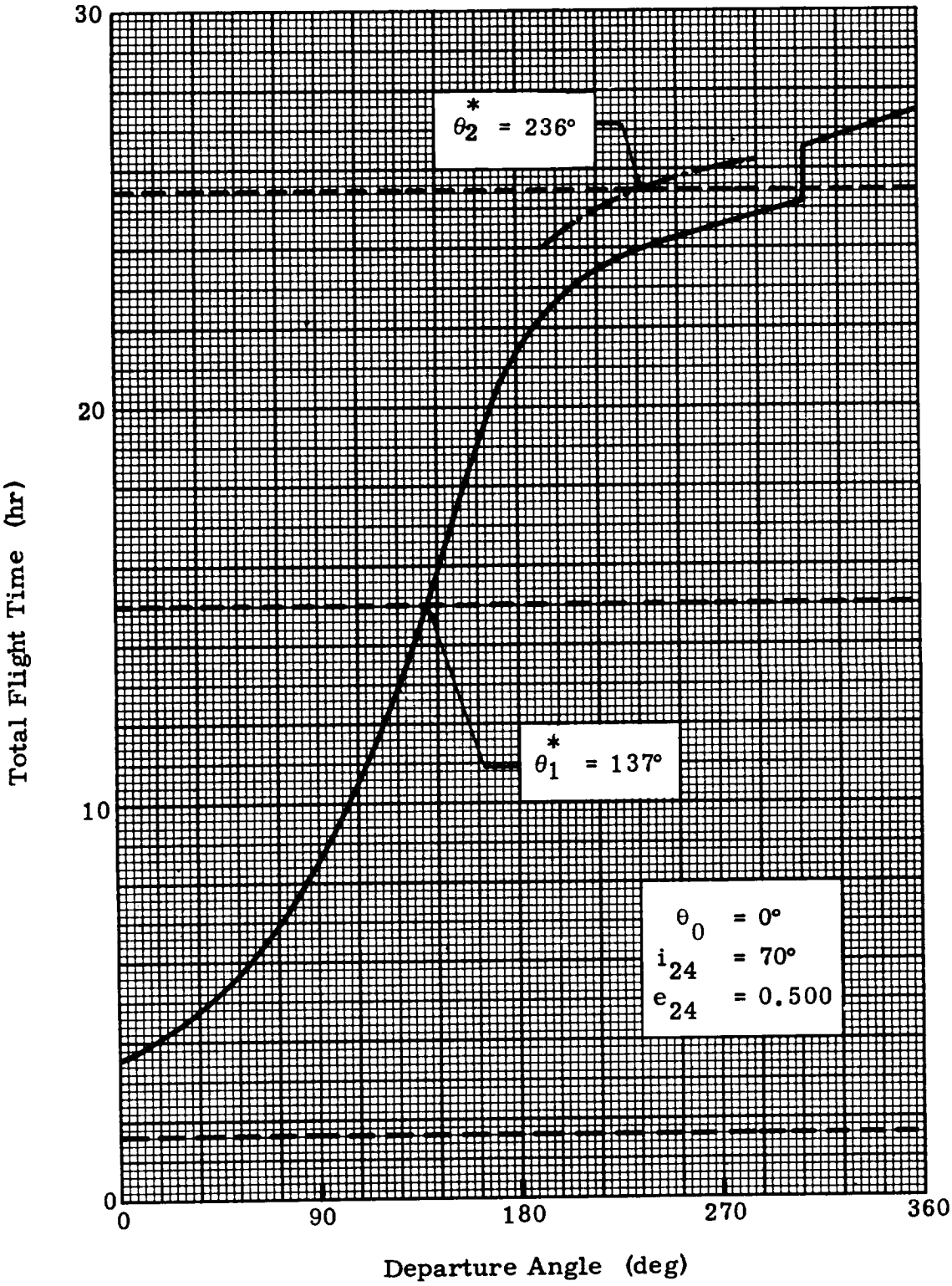

Fig. 4a. Solution of Flight Time Equation

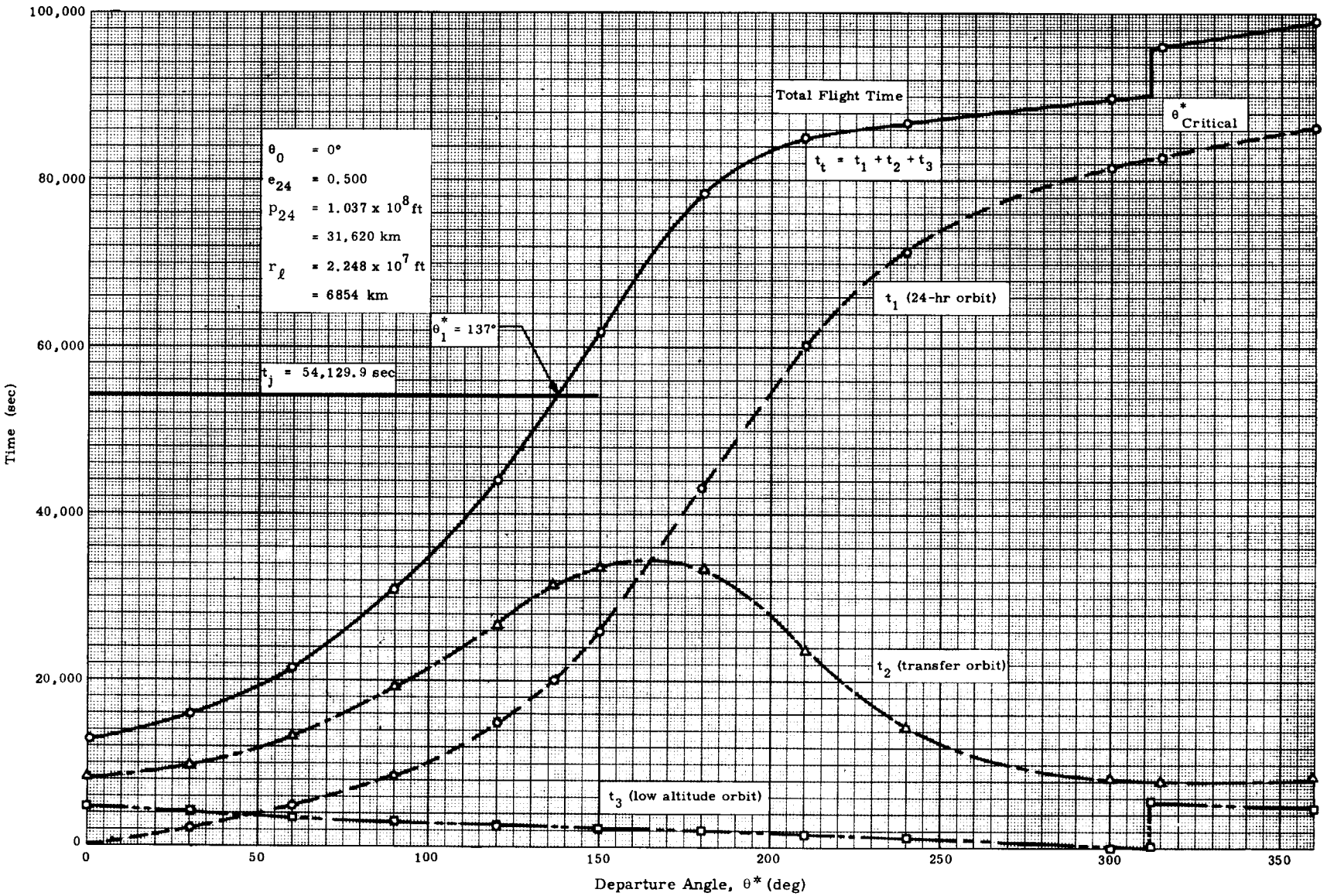

Fig. 4b. Flight Time Versus Departure Angle

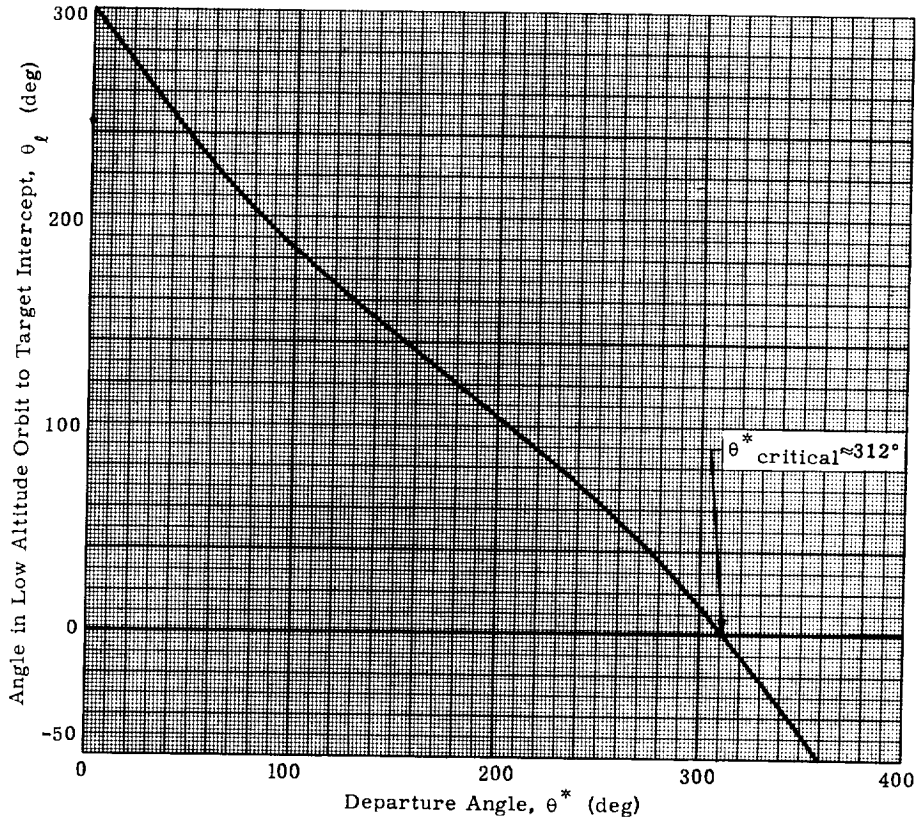

Fig. 5. Critical Angle for the Return Flight-Time Solution

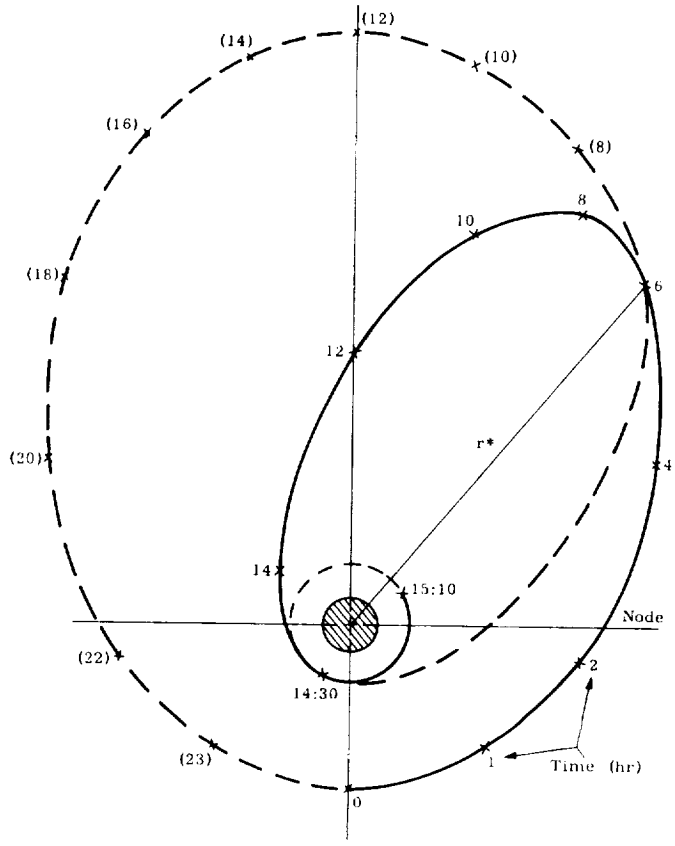

Fig. 6a. Location of the Return Shuttle in the Orbit Plane

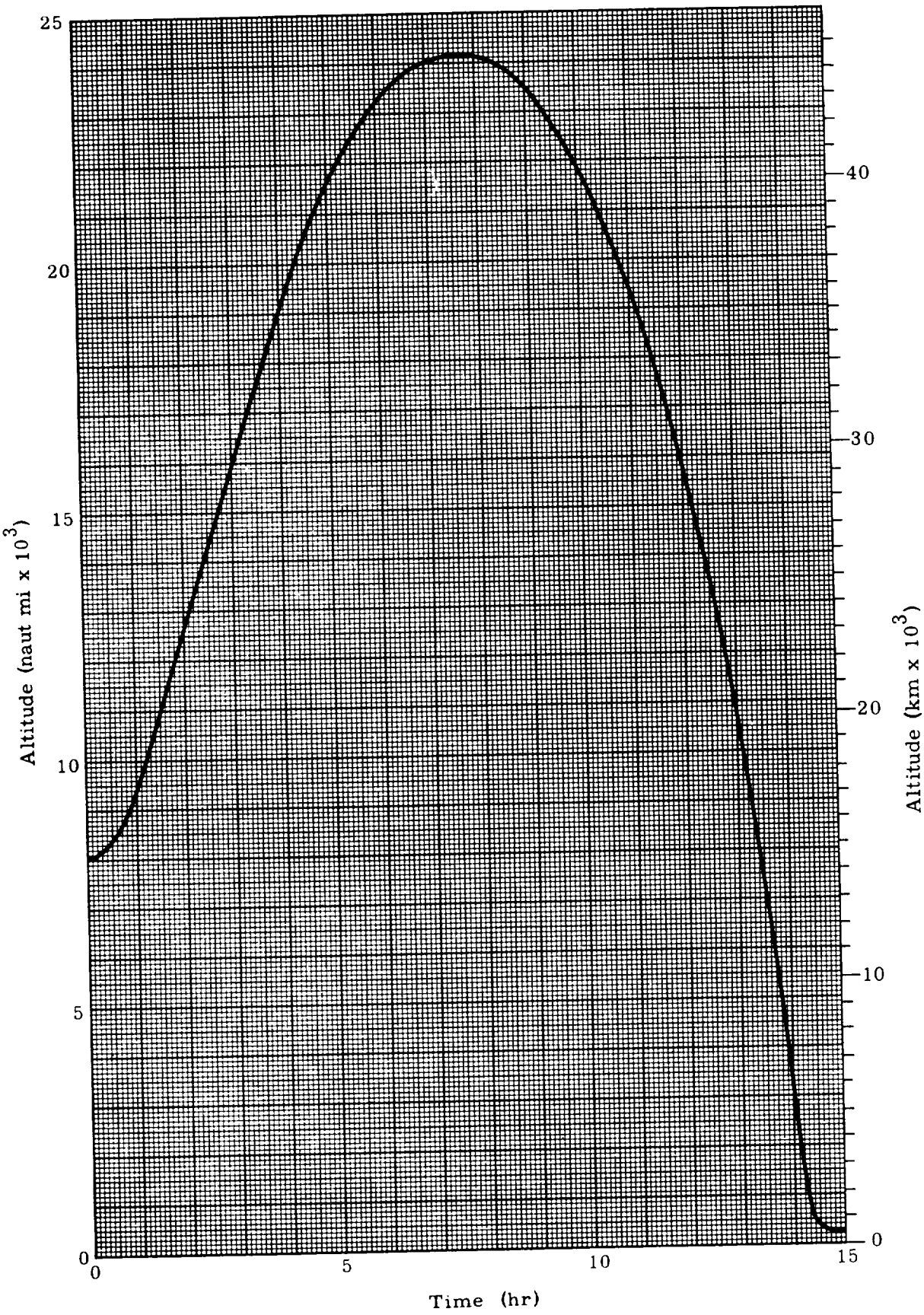

Fig. 6b. Altitude from Sea Level for the Return Shuttle

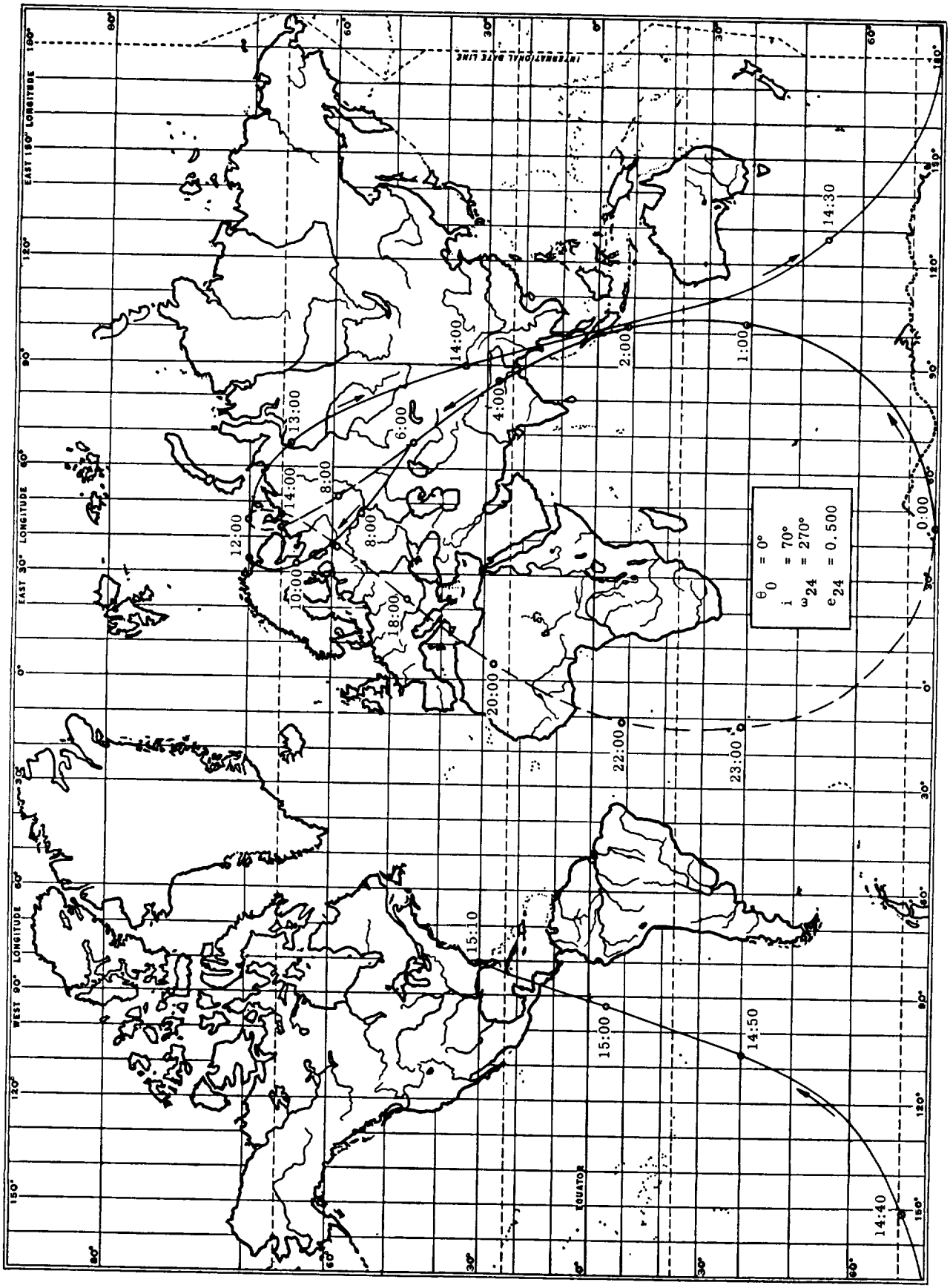

Fig. 7. Ground Track of the Return Shuttle

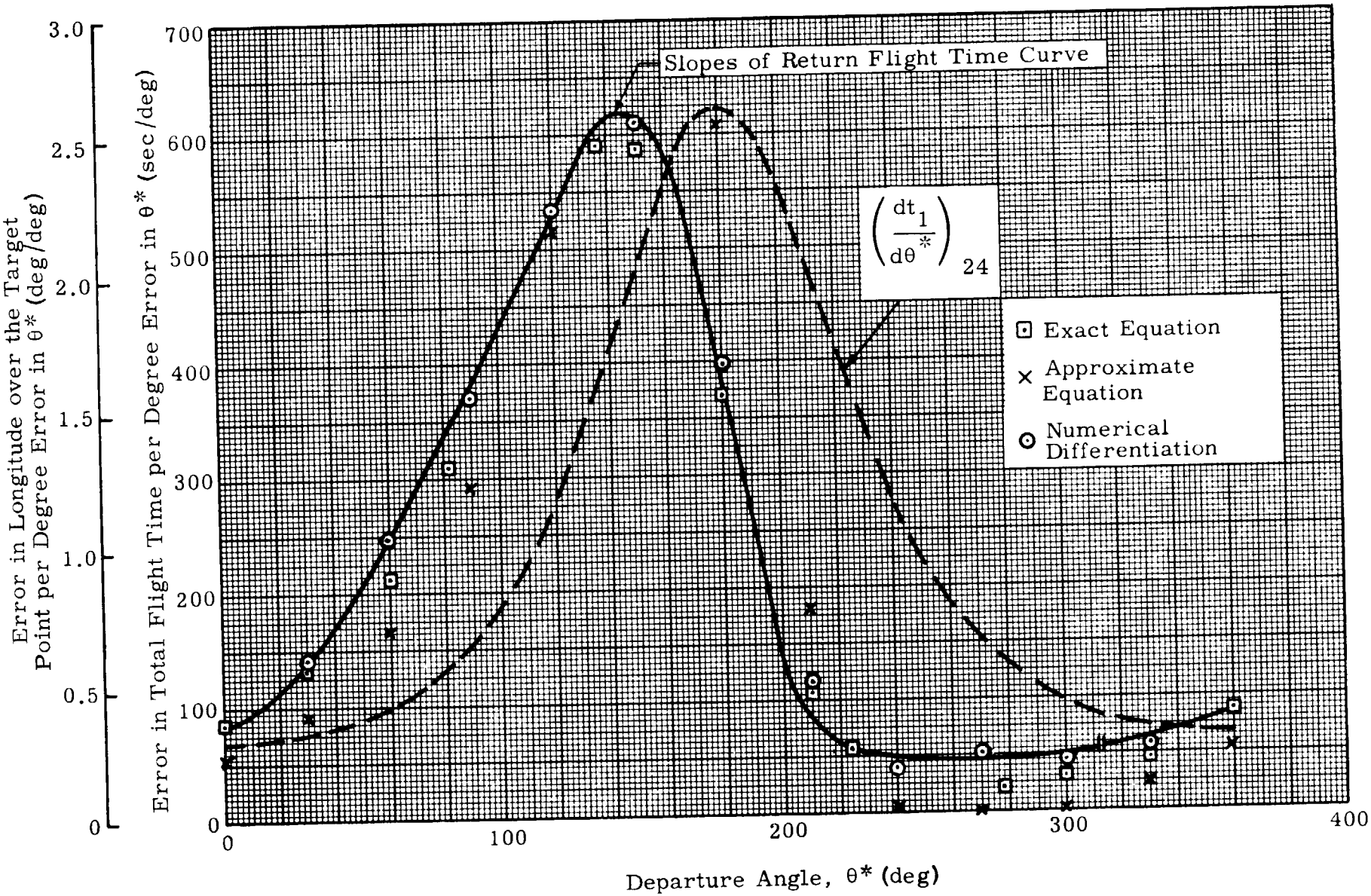

Fig. 8. Flight Time Error Analysis

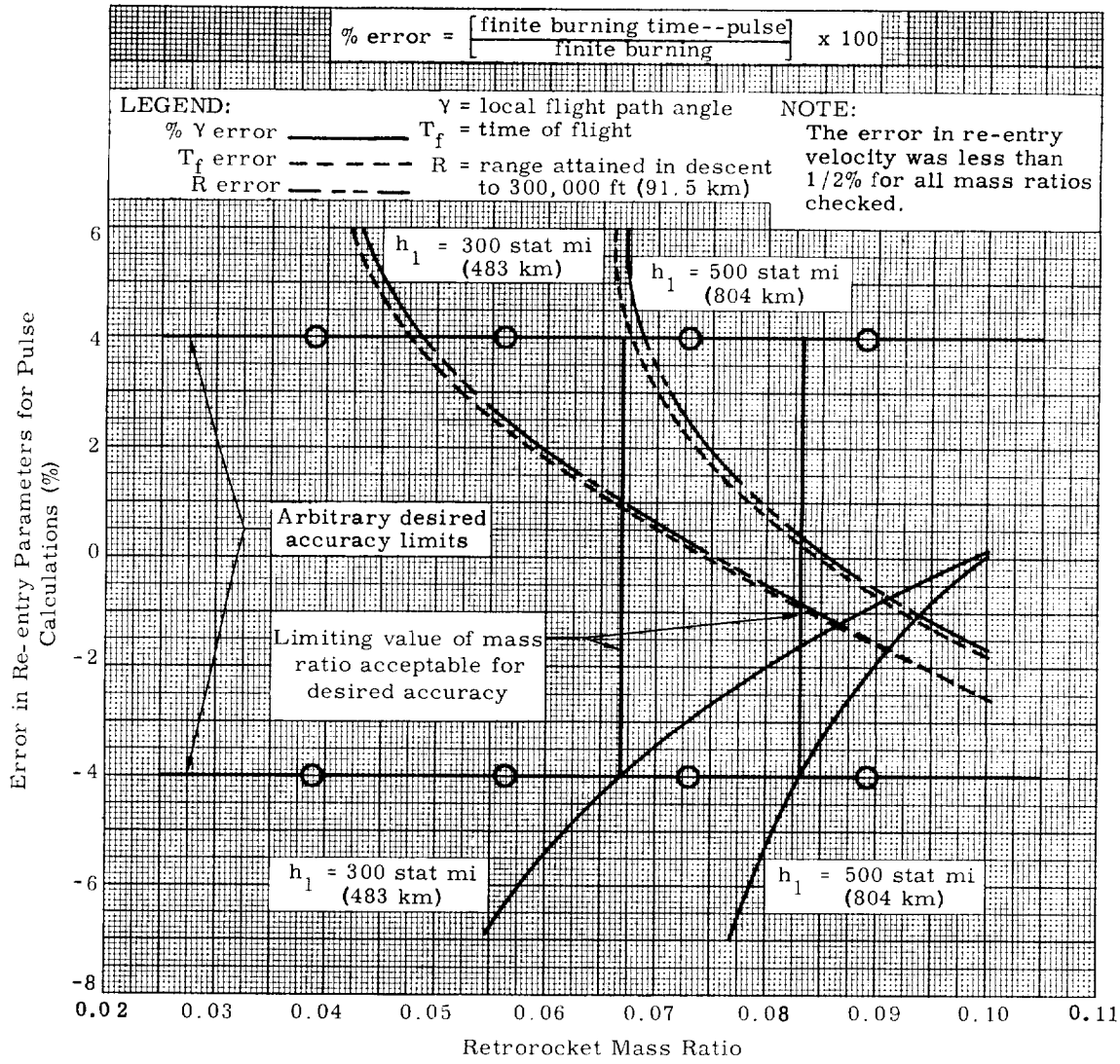

Fig. 9. Error in Re-entry Parameters as Functions of Altitude and Retrorocket Mass Ratios (1 stat mi ≈ 1.609 km)

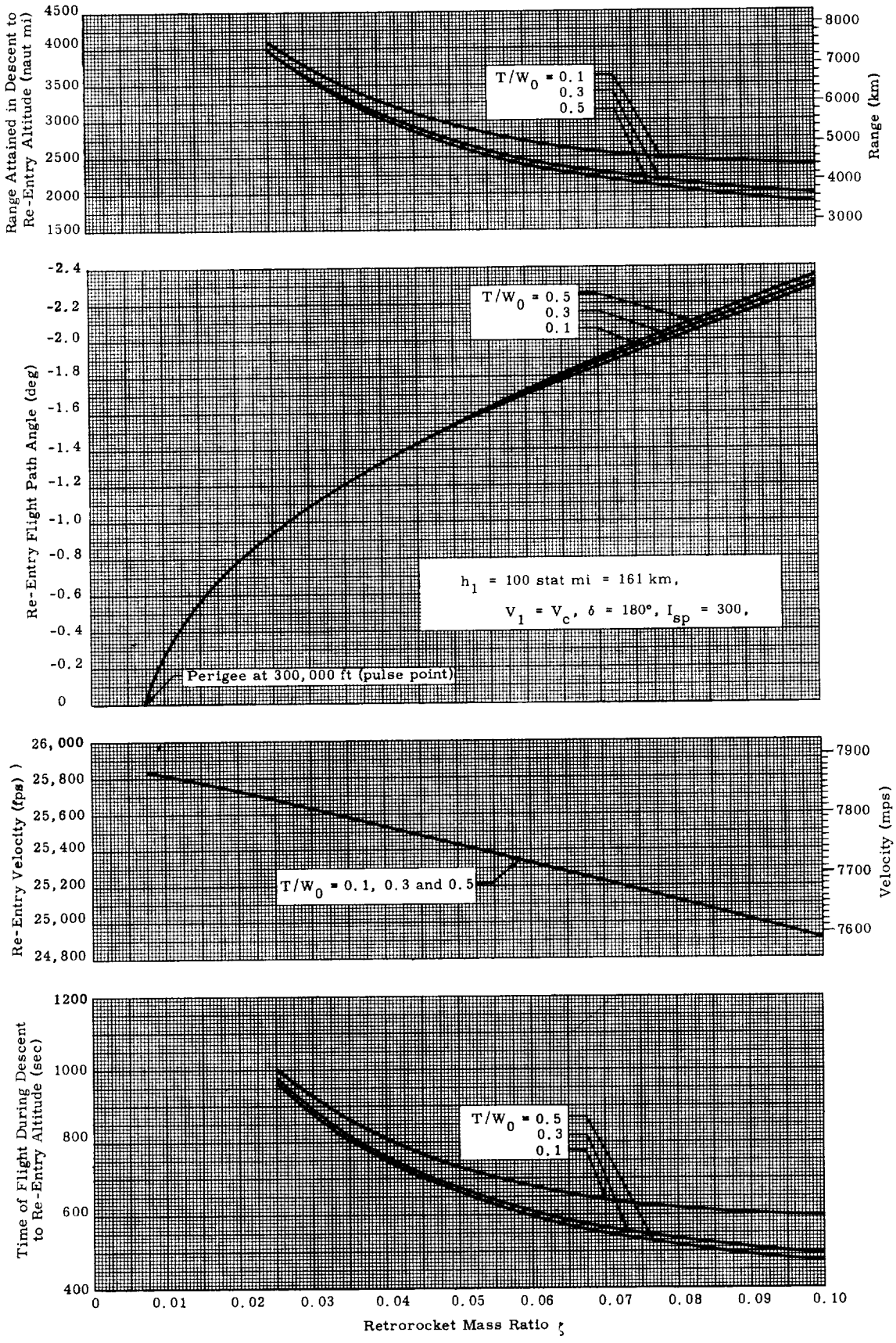

Fig. 10. The Ratio of the Velocity Pulse Obtainable from a Rocket Stage to the Ideal Pulse Neglecting Finite Burning Times

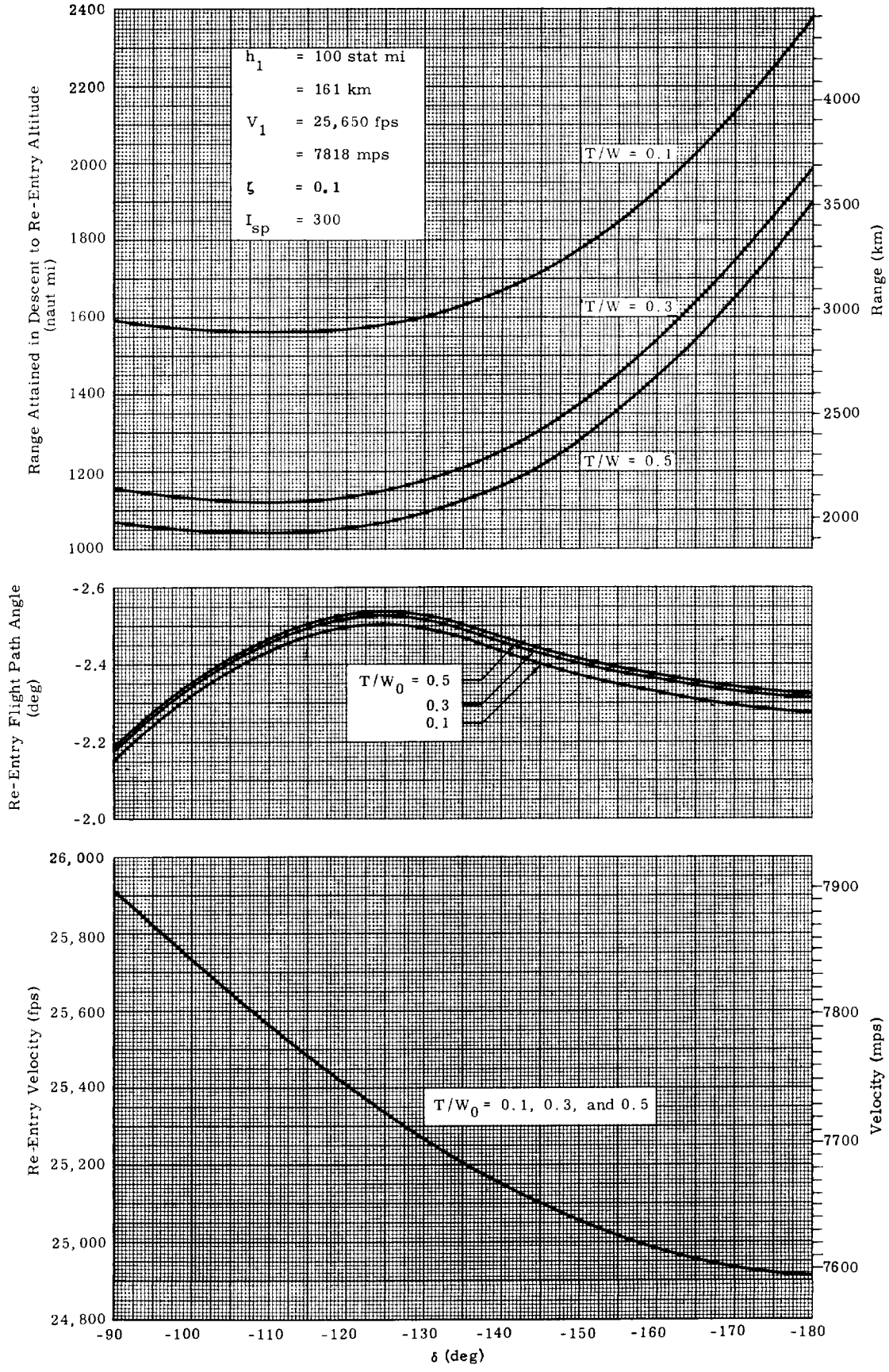

Fig. 11. Re-Entry Parameters as Functions of δ and T/W_0

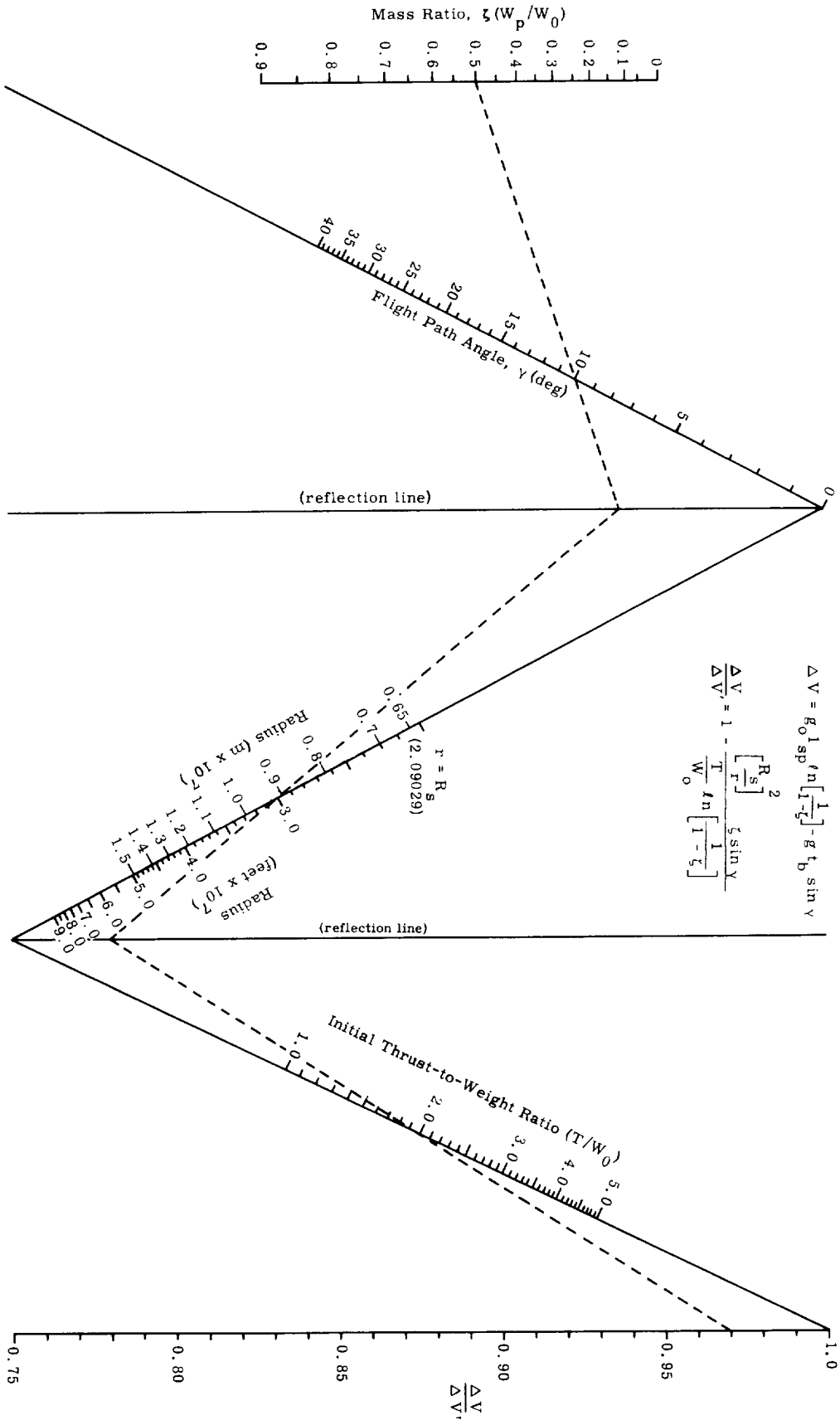

Fig. 12a. Re-Entry Parameters as Functions of Initial Thrust-to-Weight Ratio and Retrorocket Mass Ratio

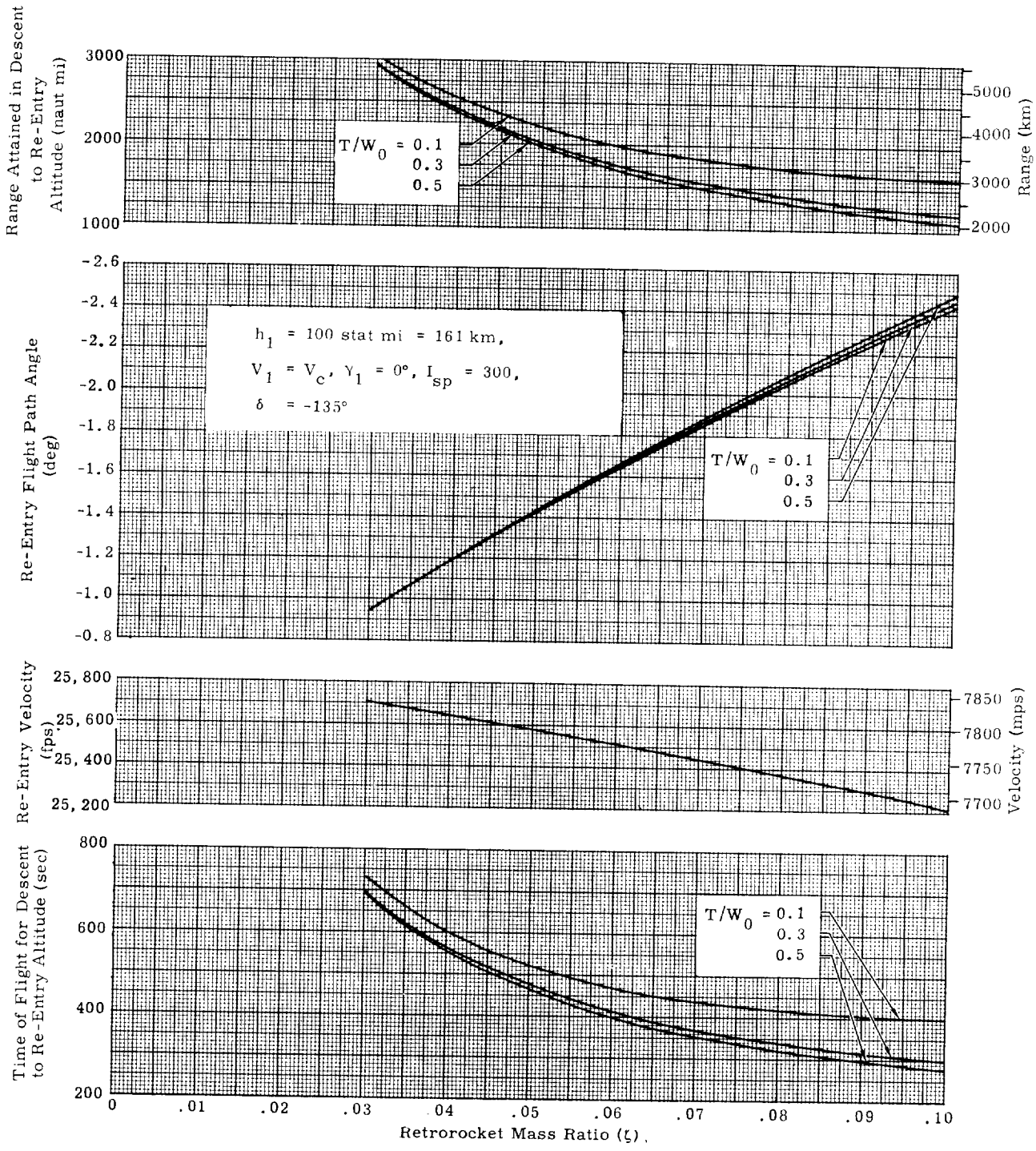

Fig. 12b. Re-Entry Parameters as Functions of Initial Thrust-to-Weight Ratio and Retrorocket Mass Ratio

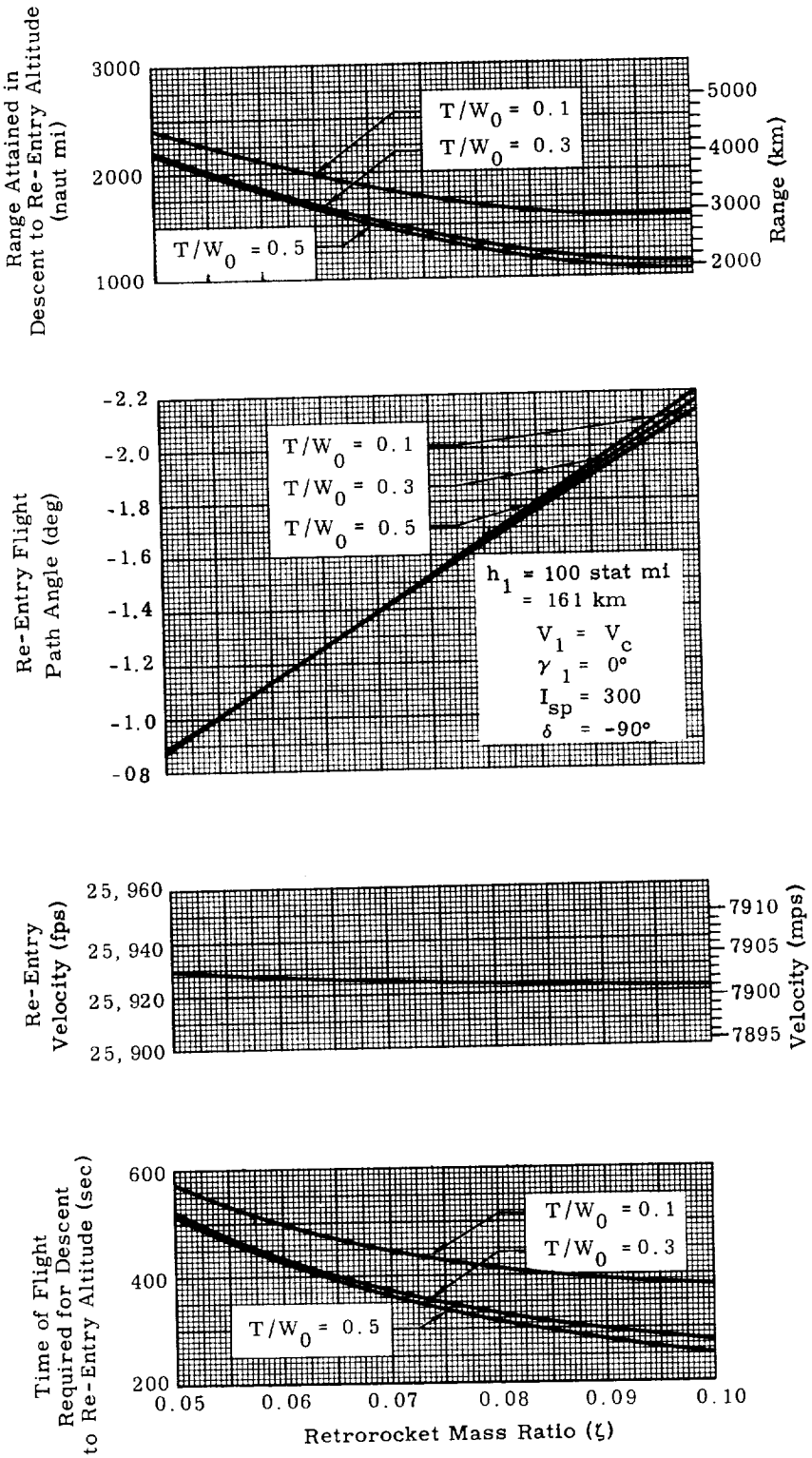

Fig. 12c. Re-Entry Parameters as Functions of Initial Thrust-to-Weight Ratio and Retrorocket Mass Ratio

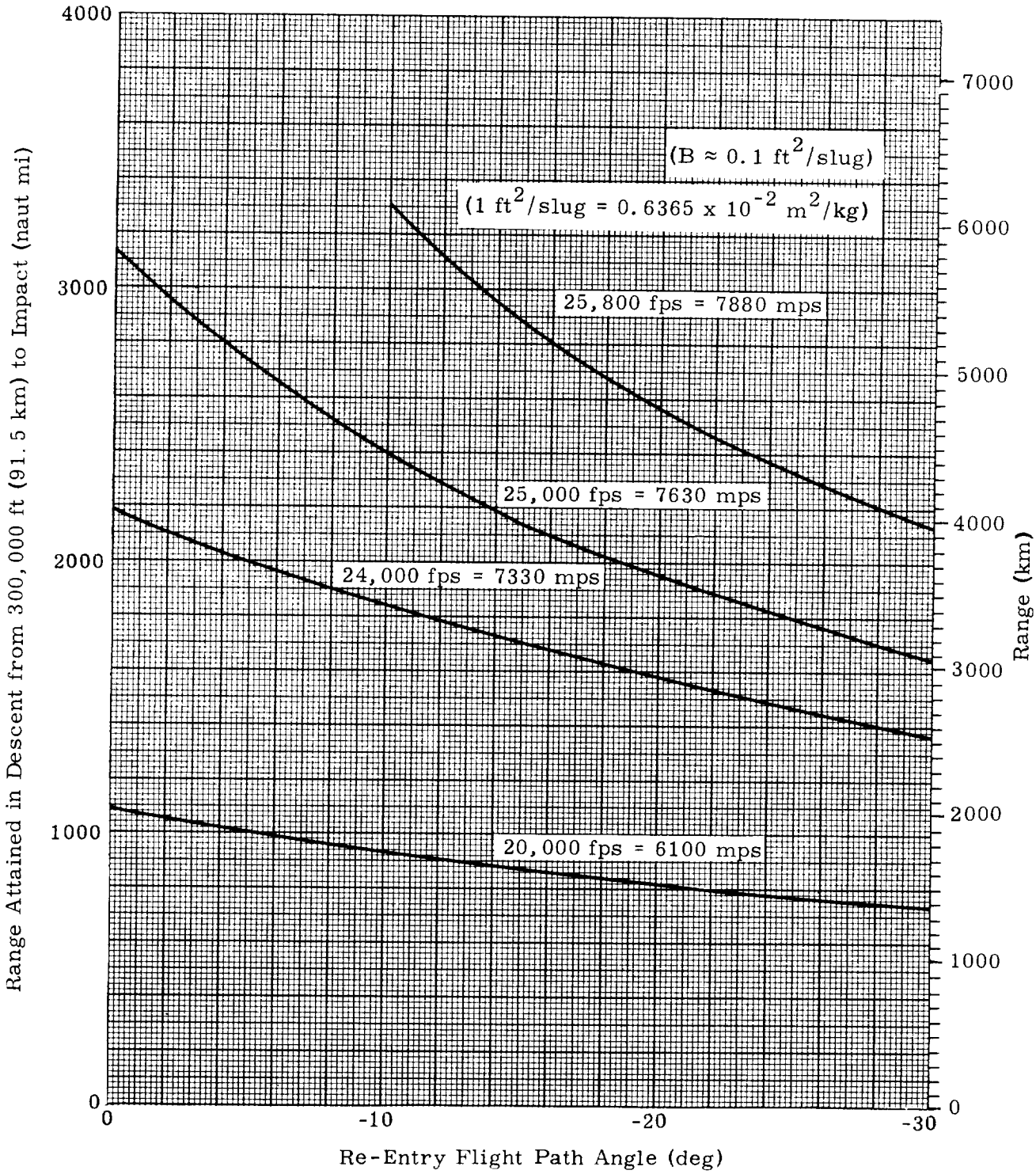

Fig. 13. Range Attained in Descending from 300,000 ft (91.5 km) to Sea Level

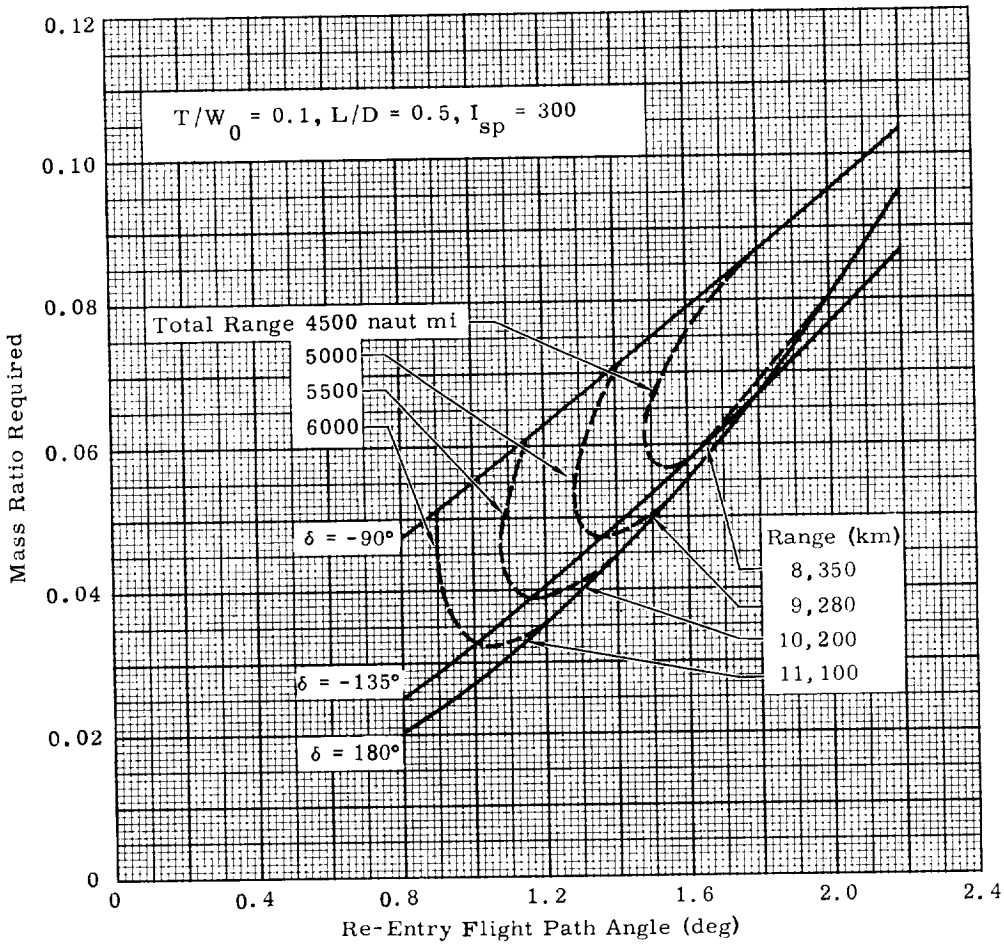

Fig. 14a. Mass Ratio Required to Exit from a 100-Stat Mi (161 km) Circular Orbit

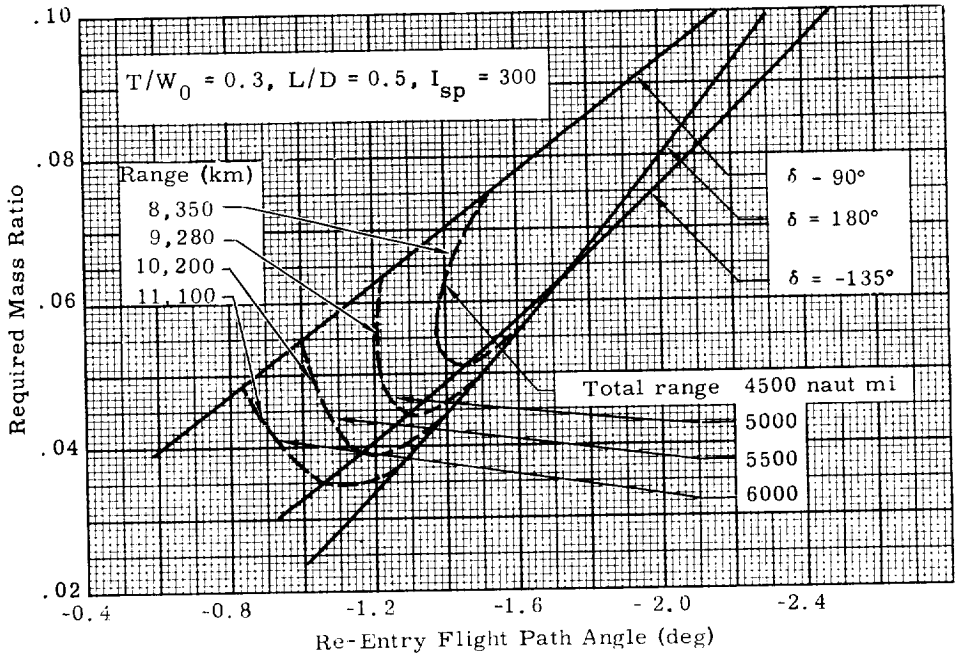

Fig. 14b. Mass Ratio Required to Exit from a 100-Stat Mi (161 km) Circular Orbit

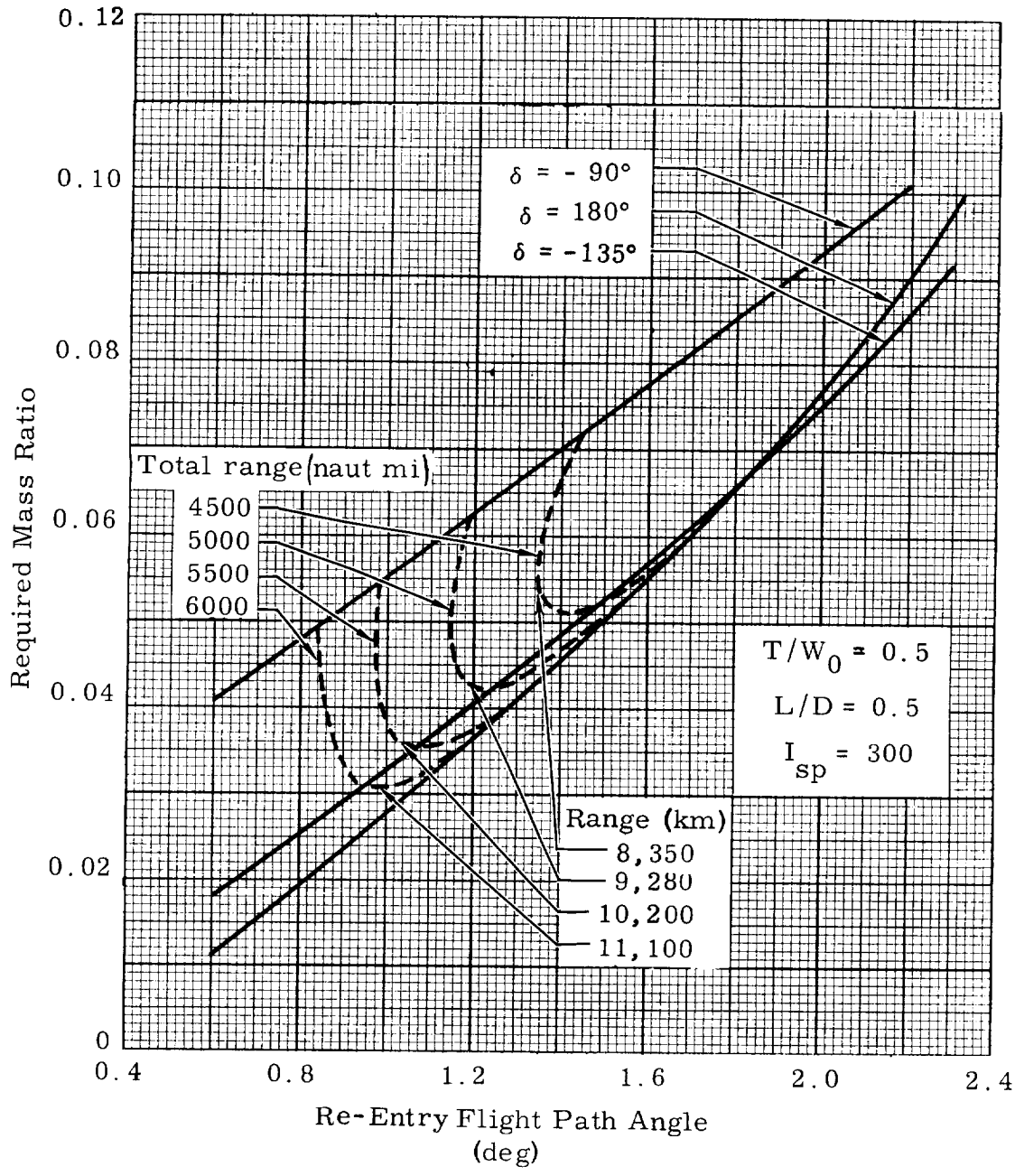

Fig. 14c. Mass Ratio Required to Exit from a 100-Stat Mi (161 km) Circular Orbit

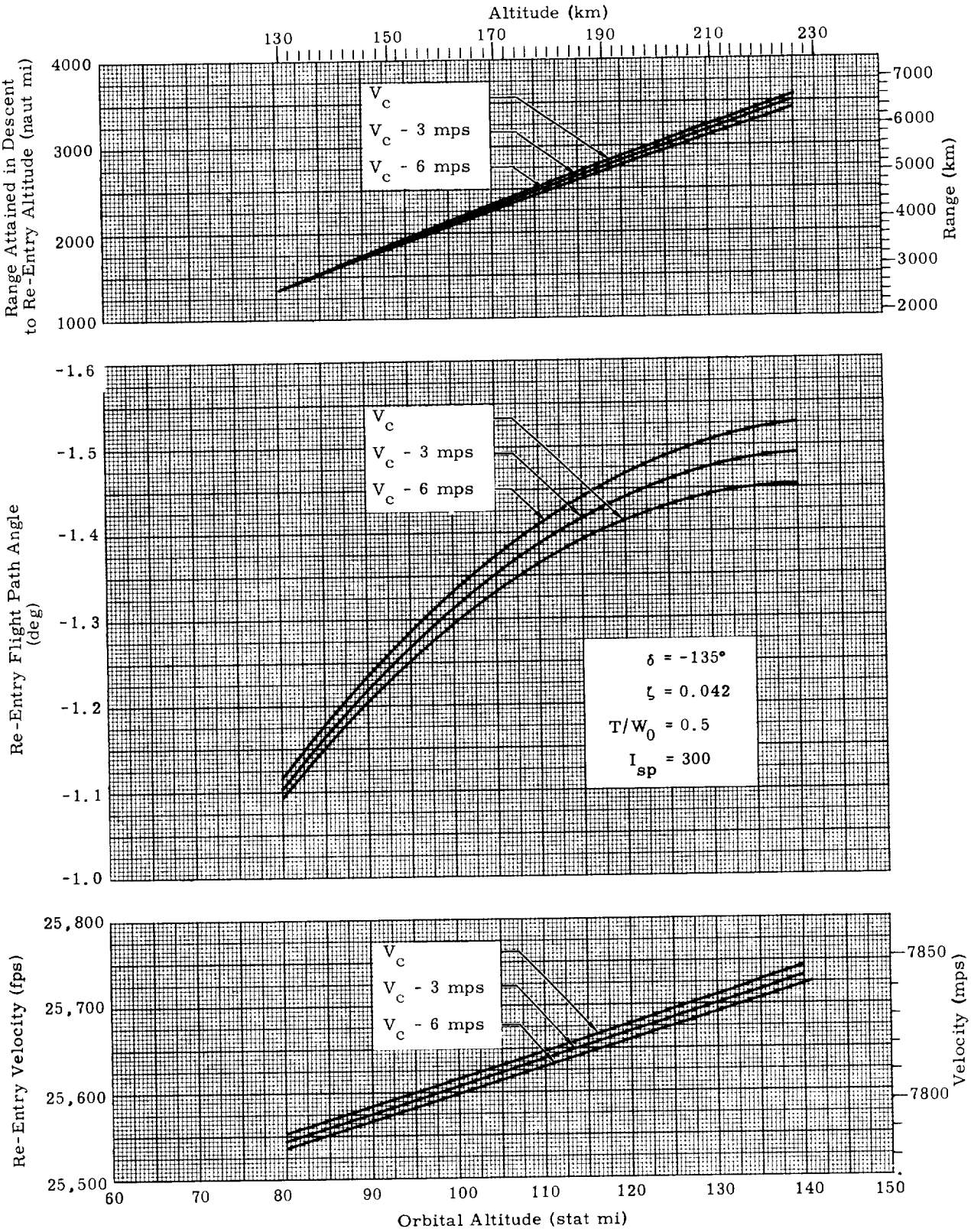

Fig. 15. Variations in the Re-Entry Conditions Due to Small Variations in Orbital Altitude and Velocity

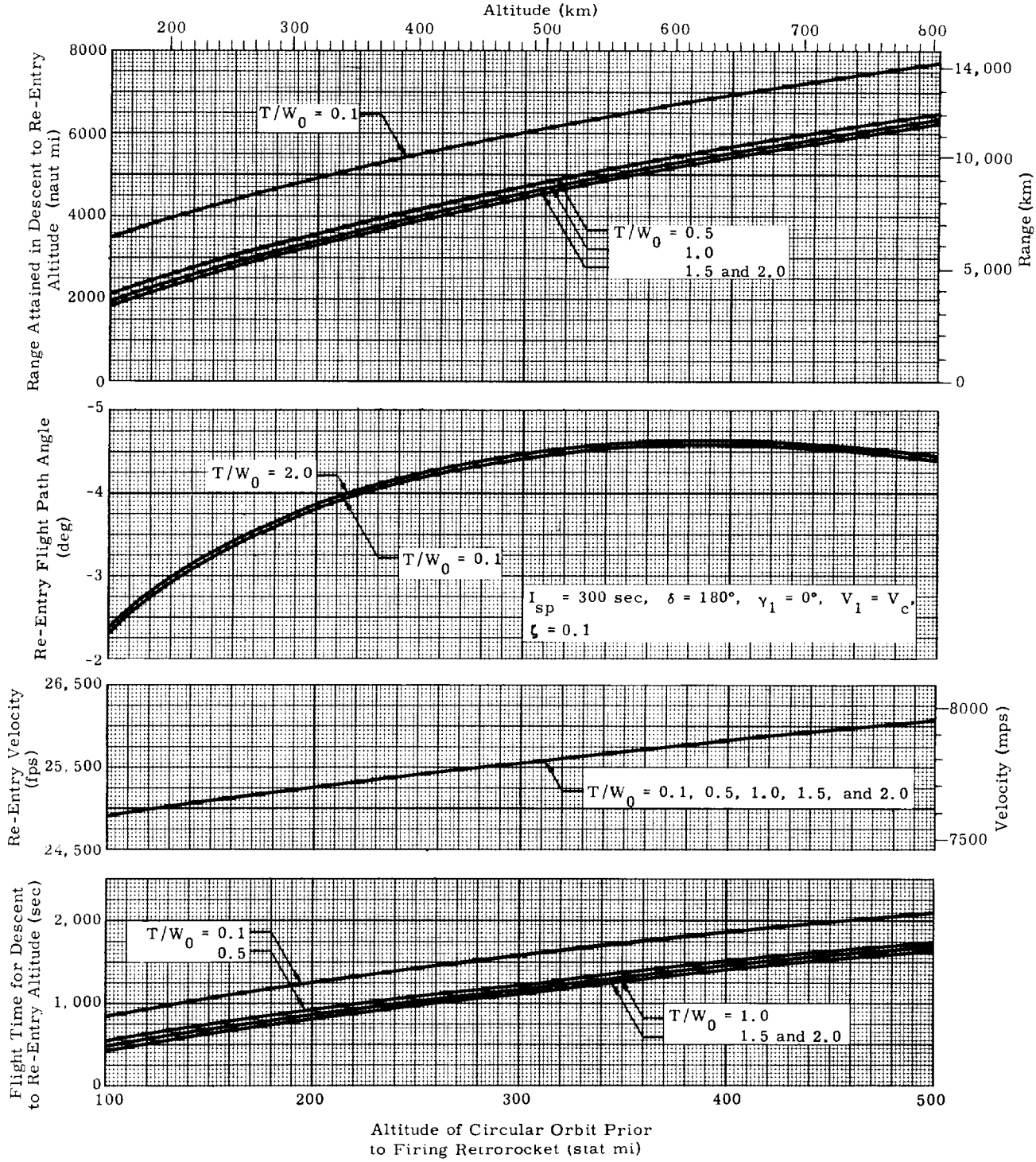

Fig. 16. Re-Entry Parameters as Functions of Initial Altitude and Retrorocket Mass Ratio

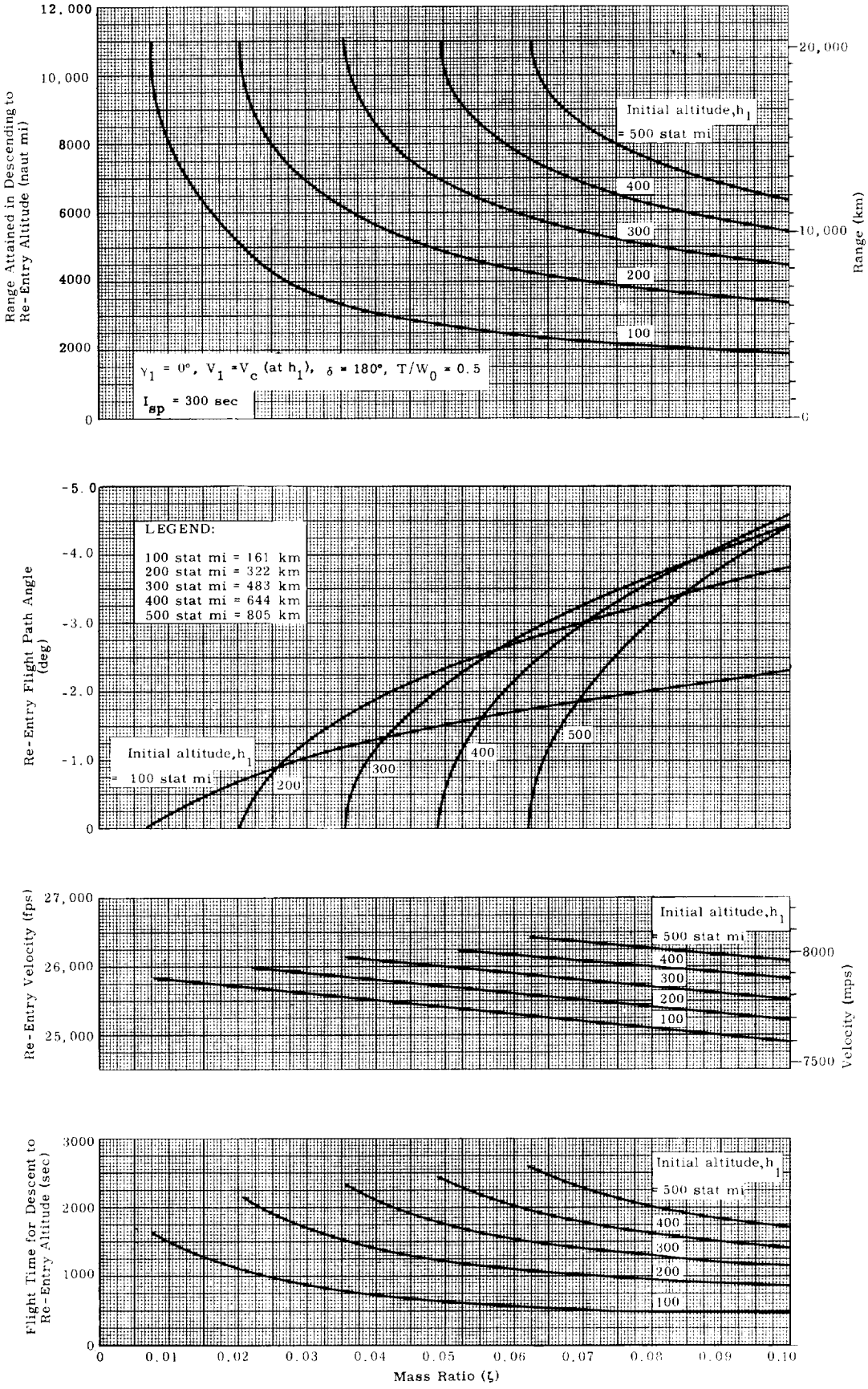

Fig. 17. Re-Entry Parameters as Functions of Initial Orbital Altitude and Mass Ratio of the Retrorocket

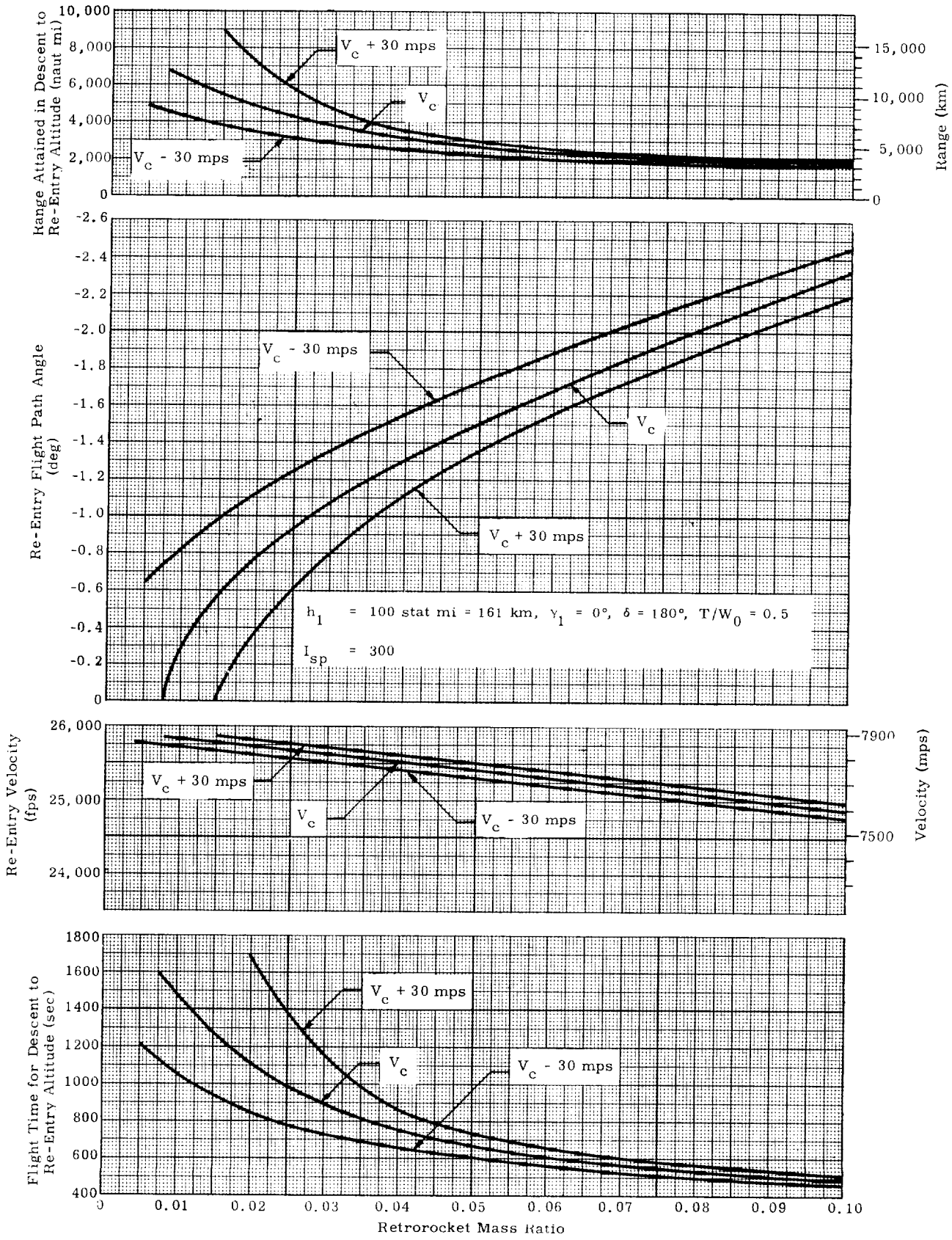

Fig. 18a. Re-Entry Parameters as Functions of Initial Orbital Velocity and Retrorocket Mass Ratio (30 mps = 100 fps)

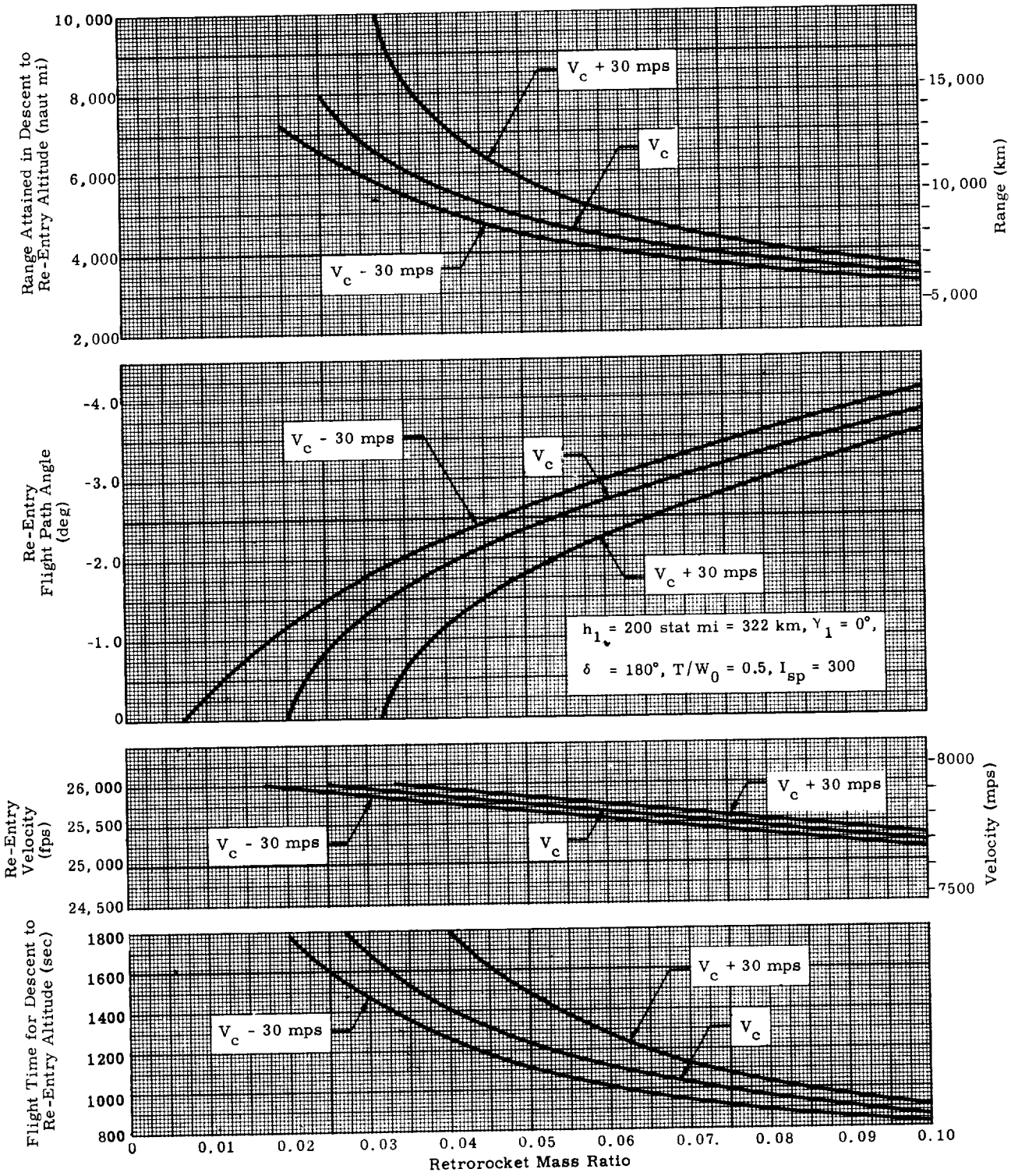

Fig. 18b. Re-Entry Parameters as Functions of Initial Velocity and Mass Ratio of the Retrorocket (100 fps $\approx$ 30 mps)

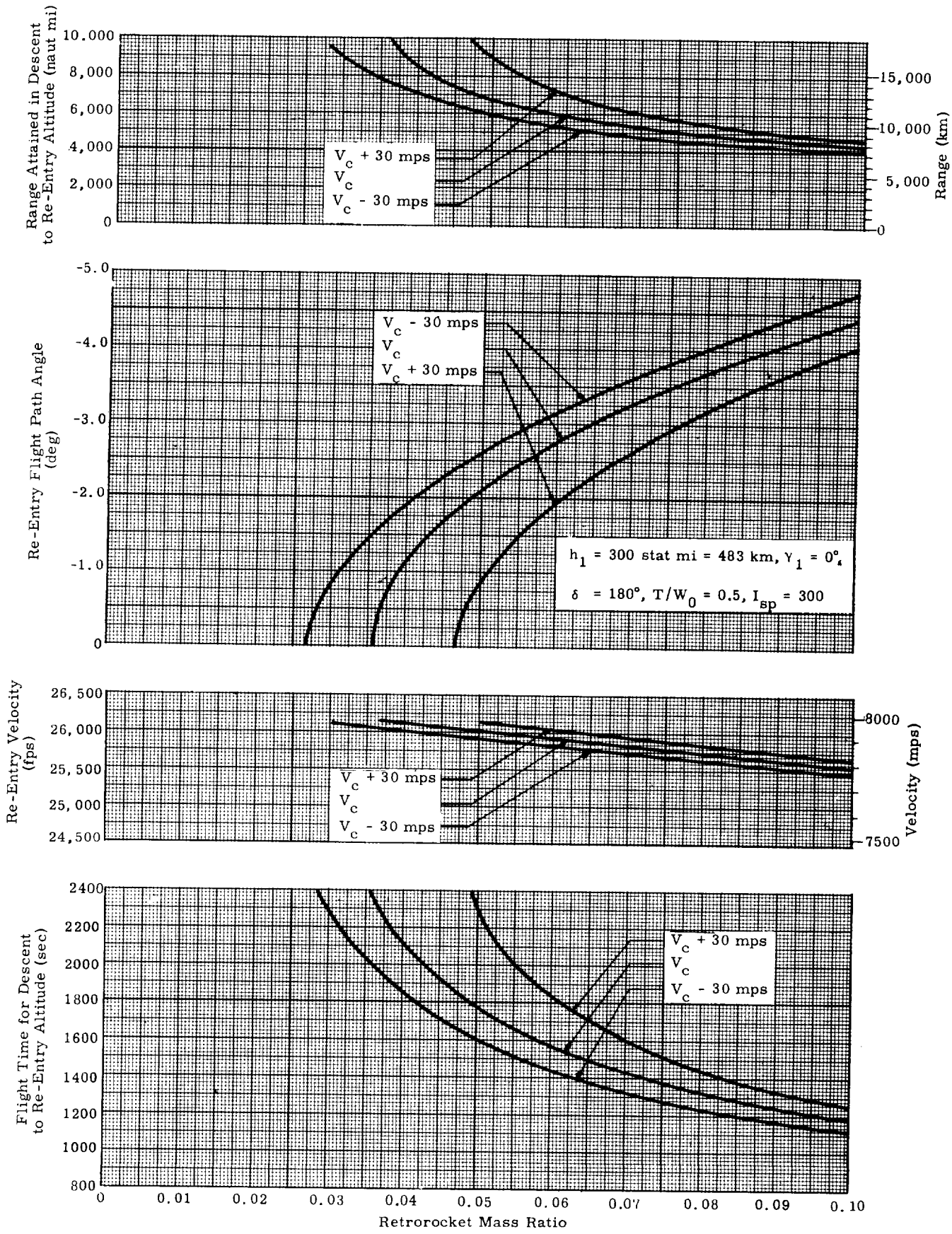

Fig. 18c. Re-Entry Parameters as Functions of Initial Velocity and Retrorocket Mass Ratio (100 fps $\approx$ 30 mps)

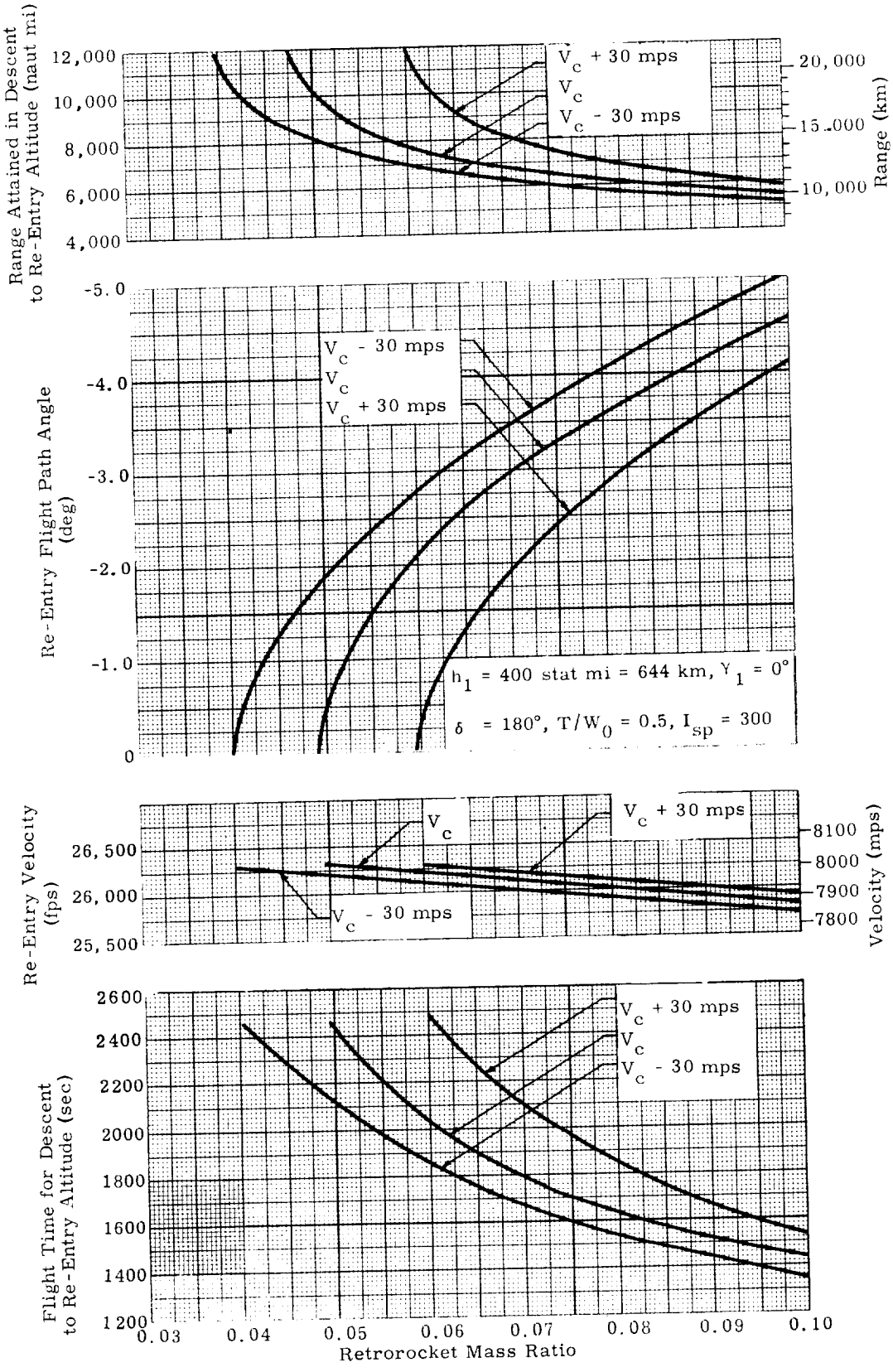

Fig. 18d. Re-Entry Parameters as Functions of Initial Velocity and Retrorocket Mass Ratio (100 fps ≈ 30 mps)

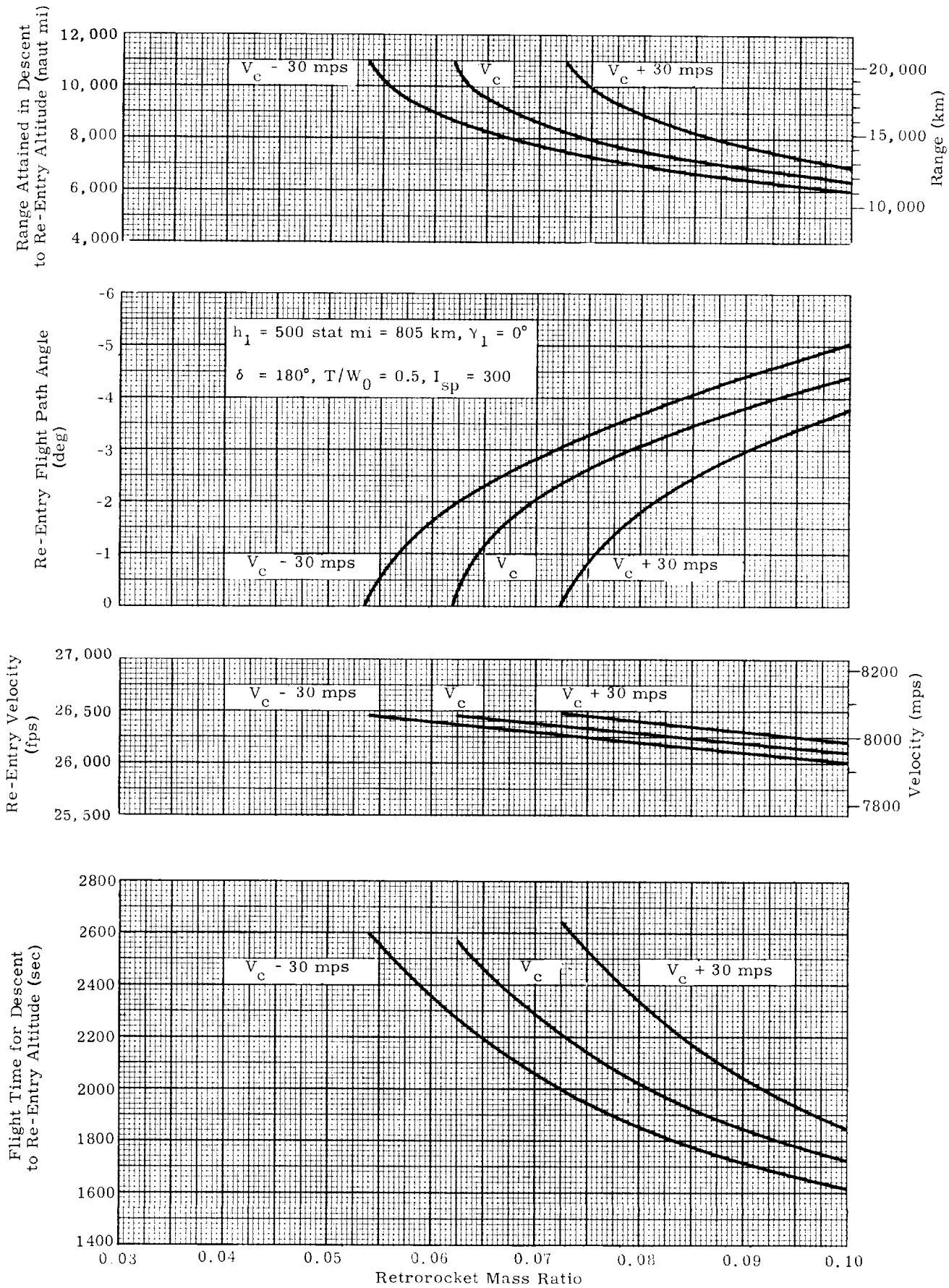

Fig. 18e. Re-Entry Parameters as Functions of Initial Orbital Velocity and Retrorocket Mass Ratio (100 fps ≈ 30 mps)

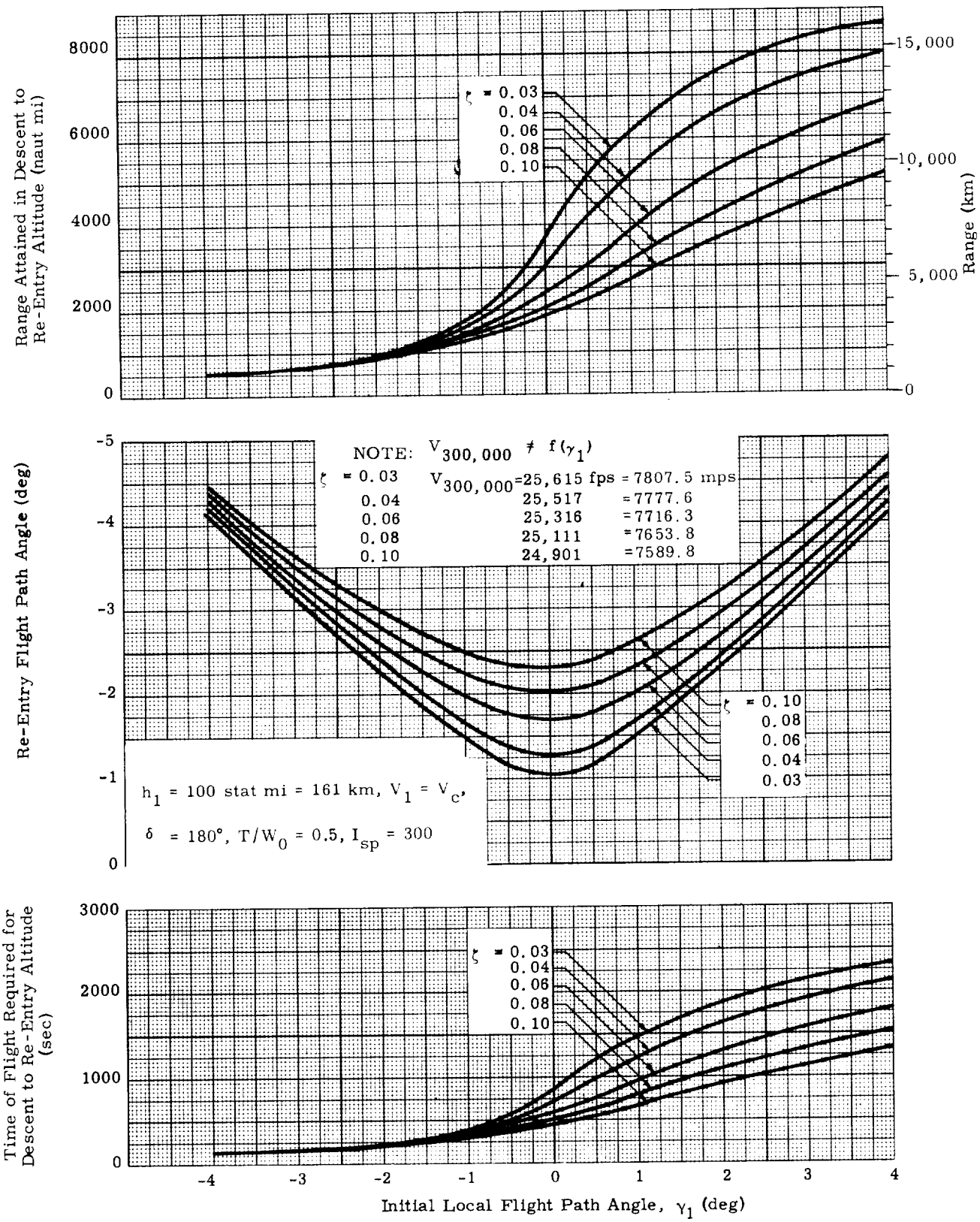

Fig. 19a. Re-Entry Parameters as Functions of ζ and γ_1

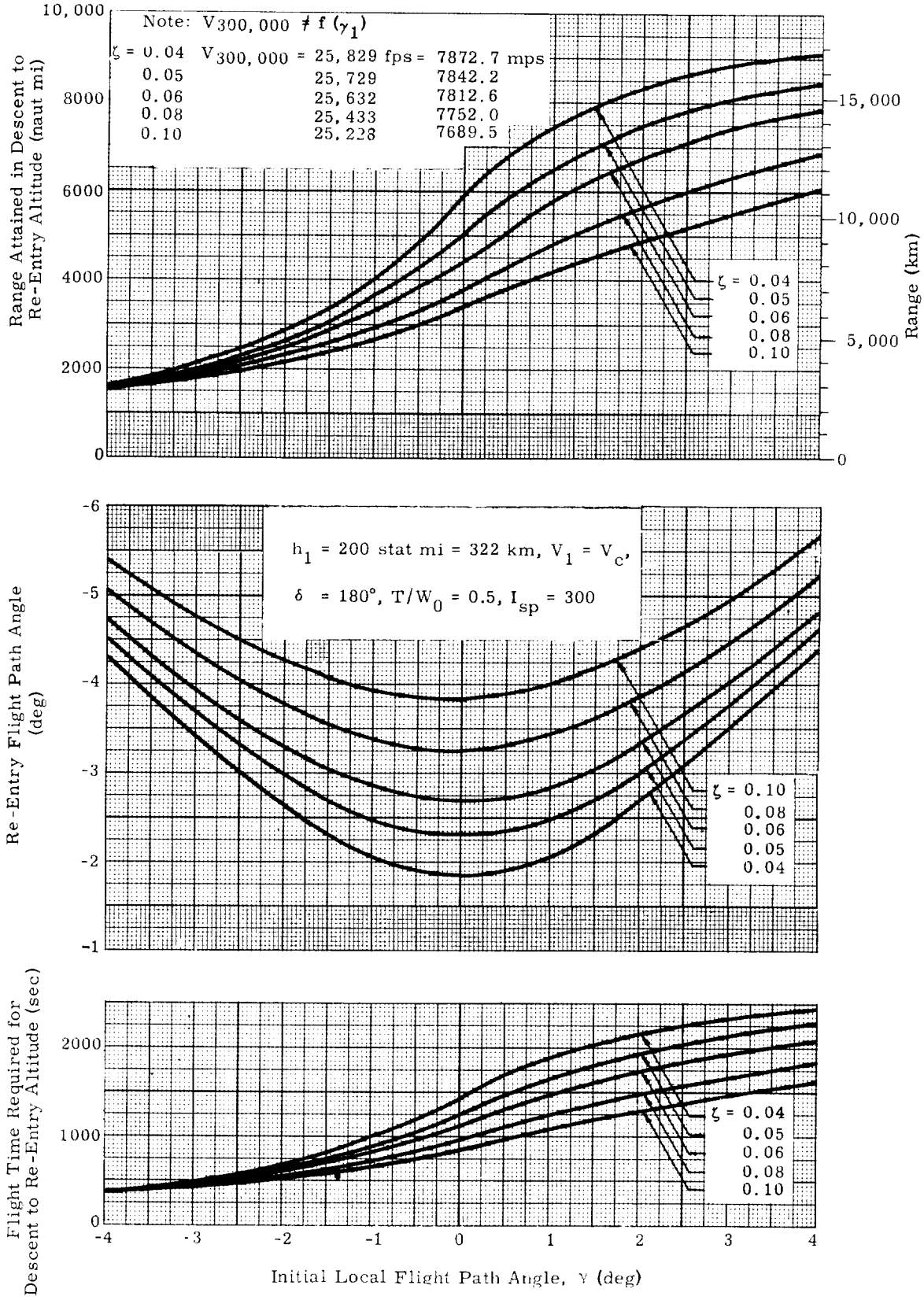

Fig. 19b. Re-Entry Parameters as Functions of ζ and γ_1

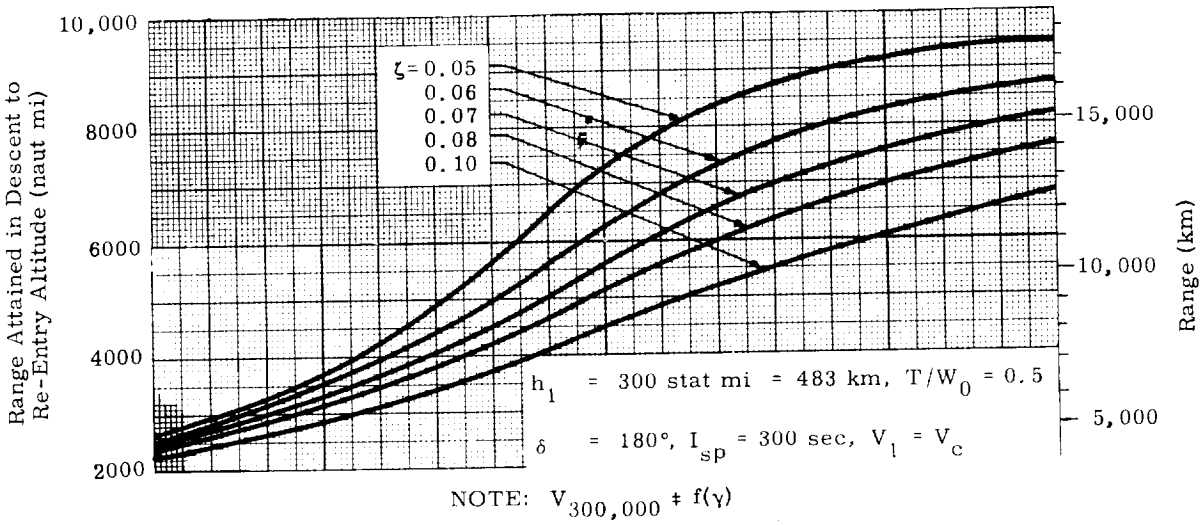

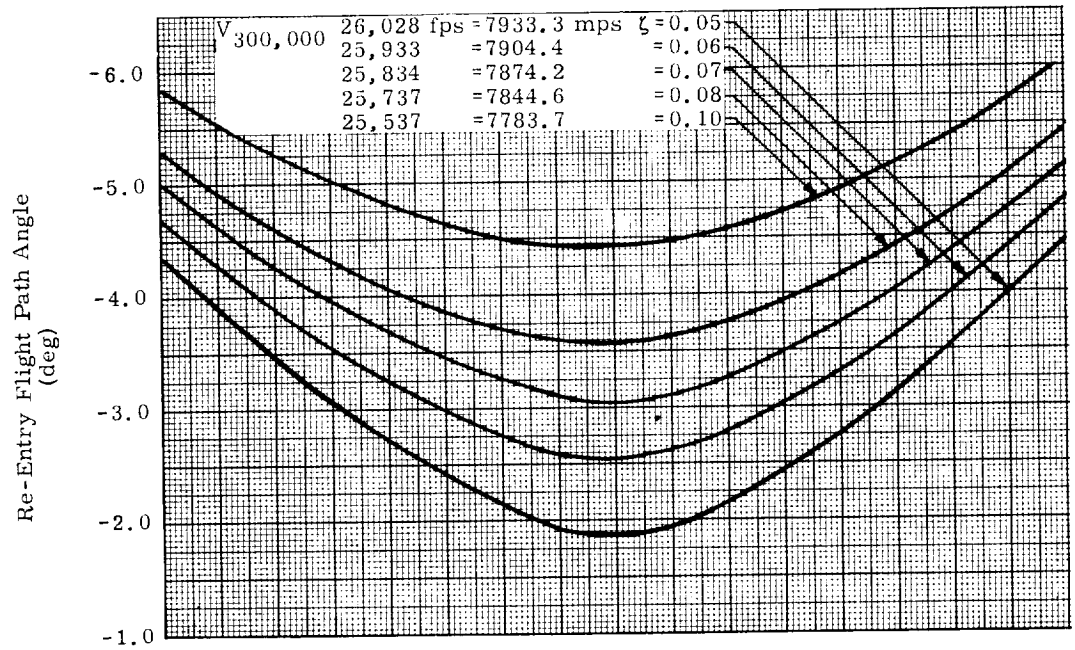

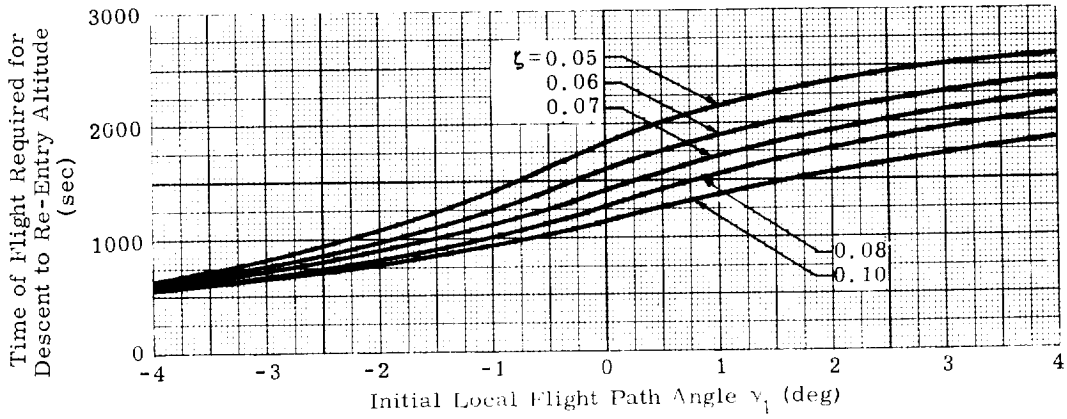

Fig. 19c. Re-Entry Parameters as Functions of ζ and γ_1

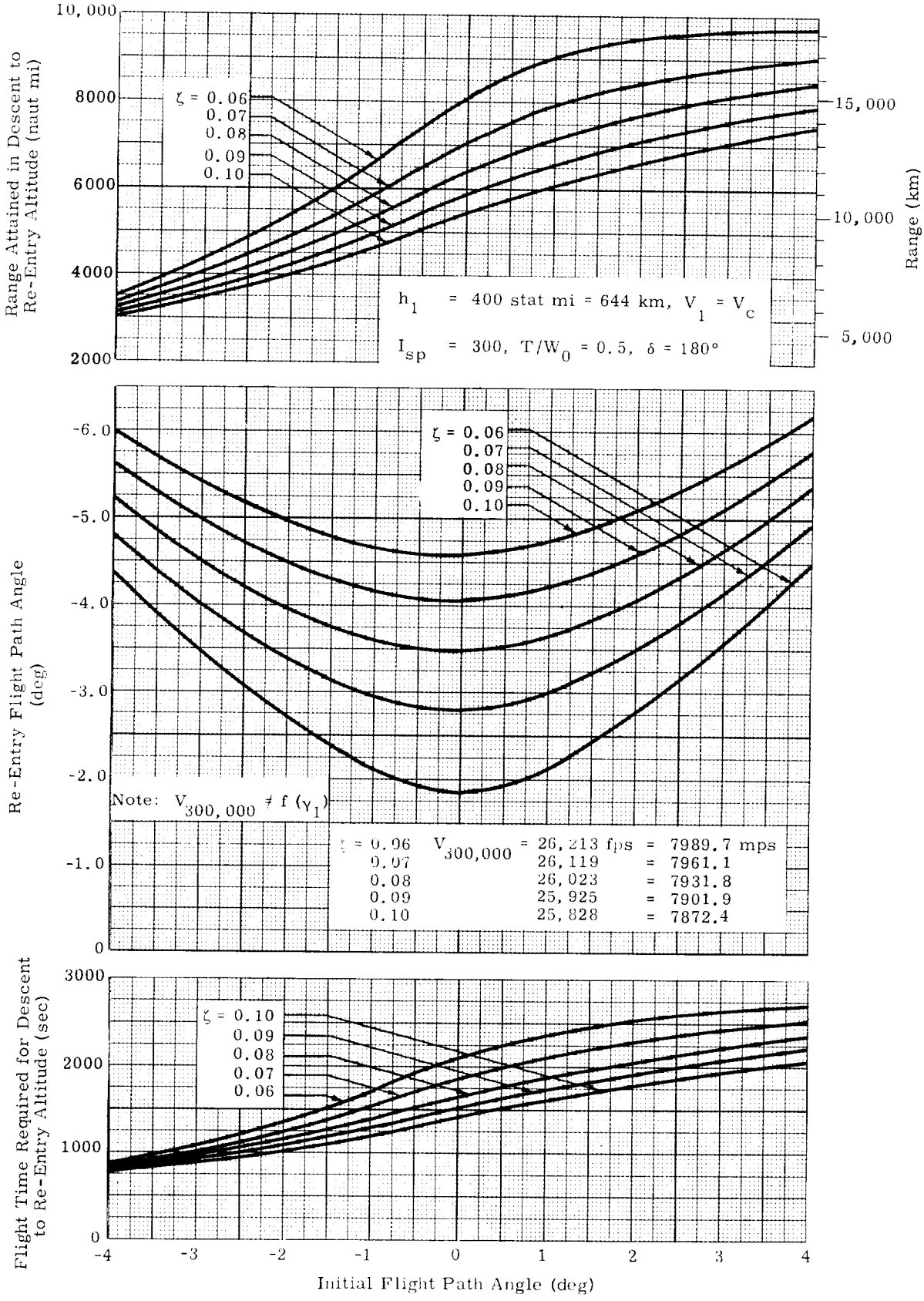

Fig. 19d. Re-Entry Parameters as Functions of ζ and γ_1

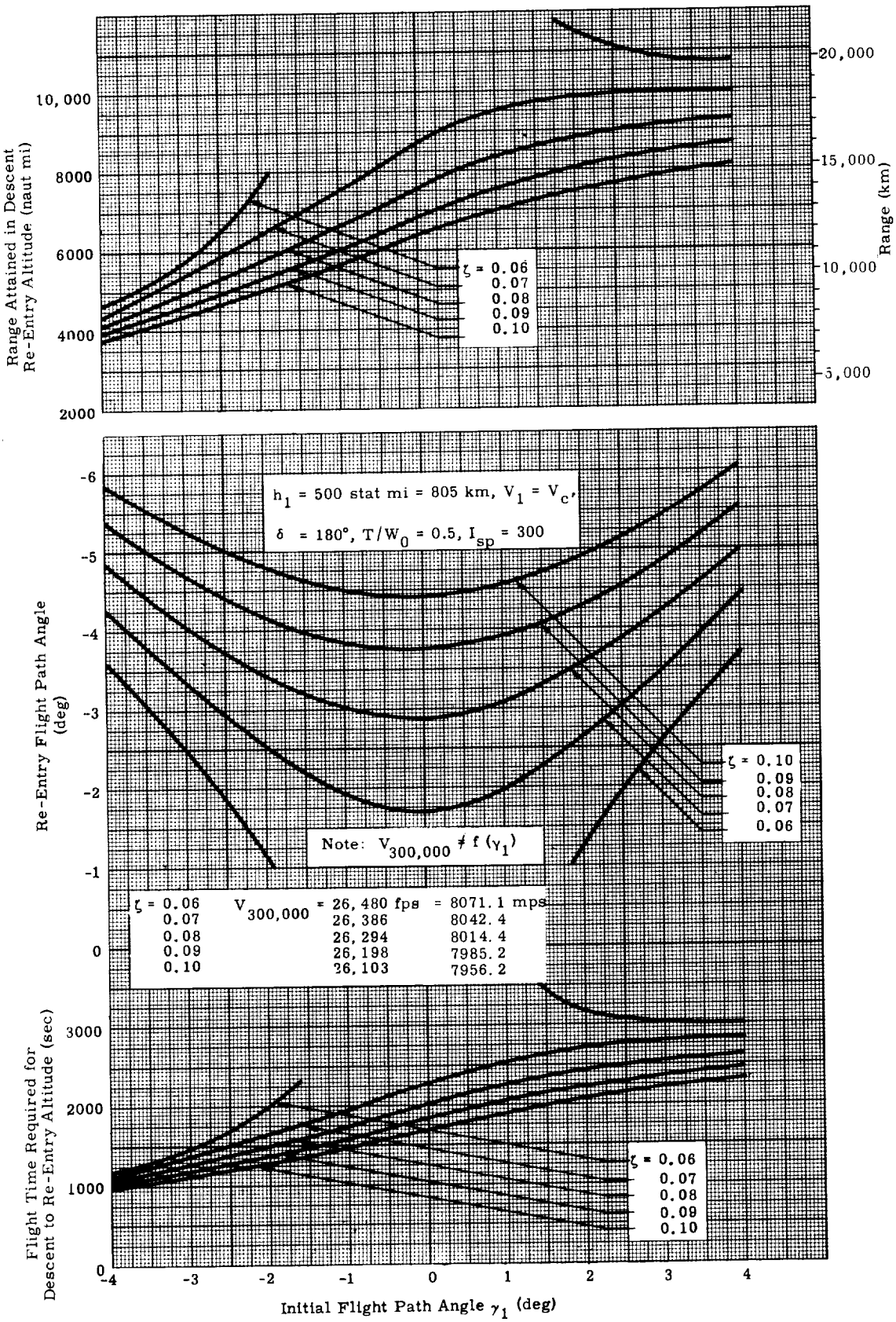

Fig. 19e. Re-Entry Parameters as Functions of ζ and γ_1

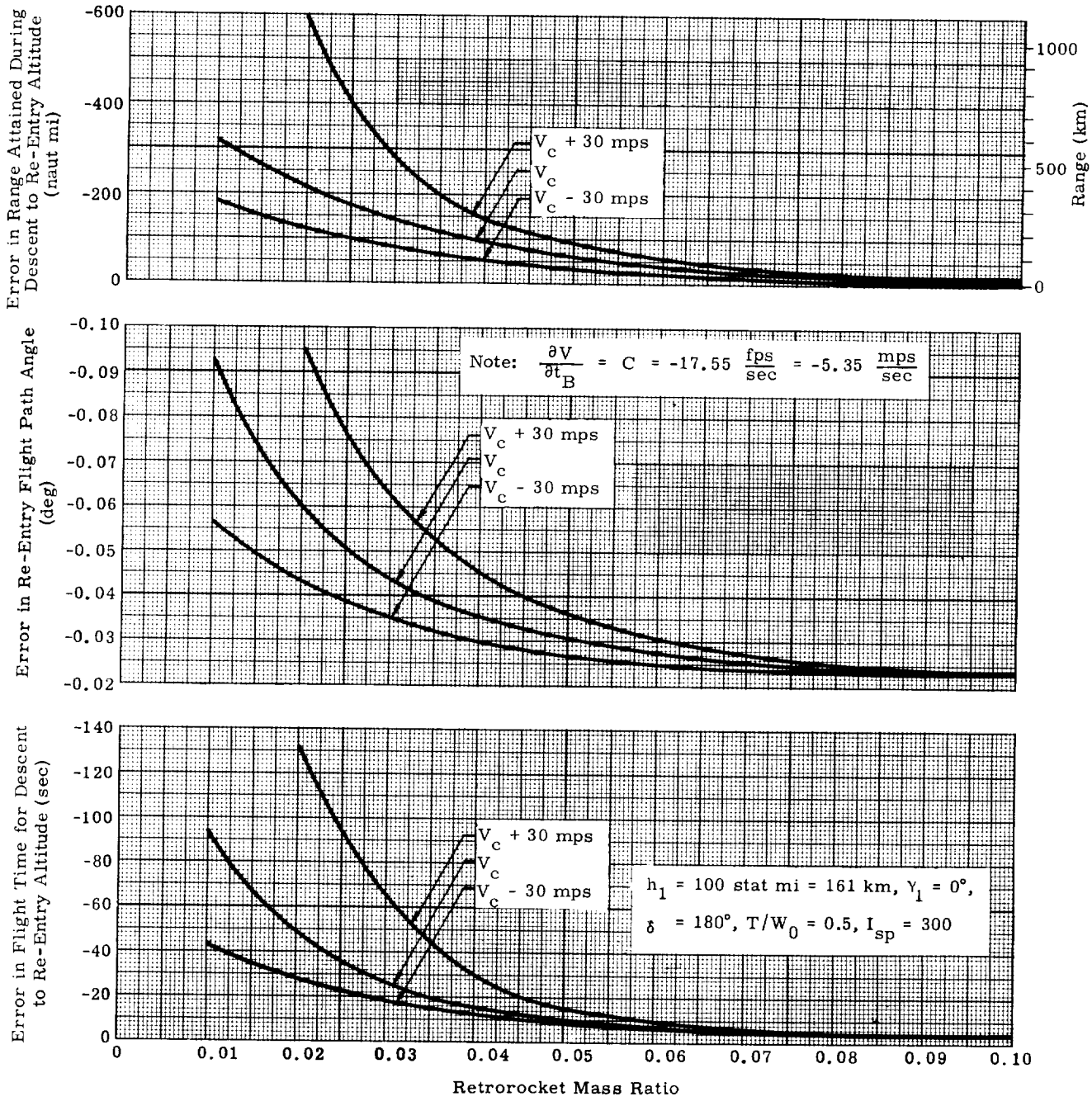

Fig. 20a. Variations in Re-Entry Position, Time and Flight Path Angle (per Second Error in t_B) with Initial Velocity and Retrorocket Mass Ratio (100 fps ≈ 30 mps)

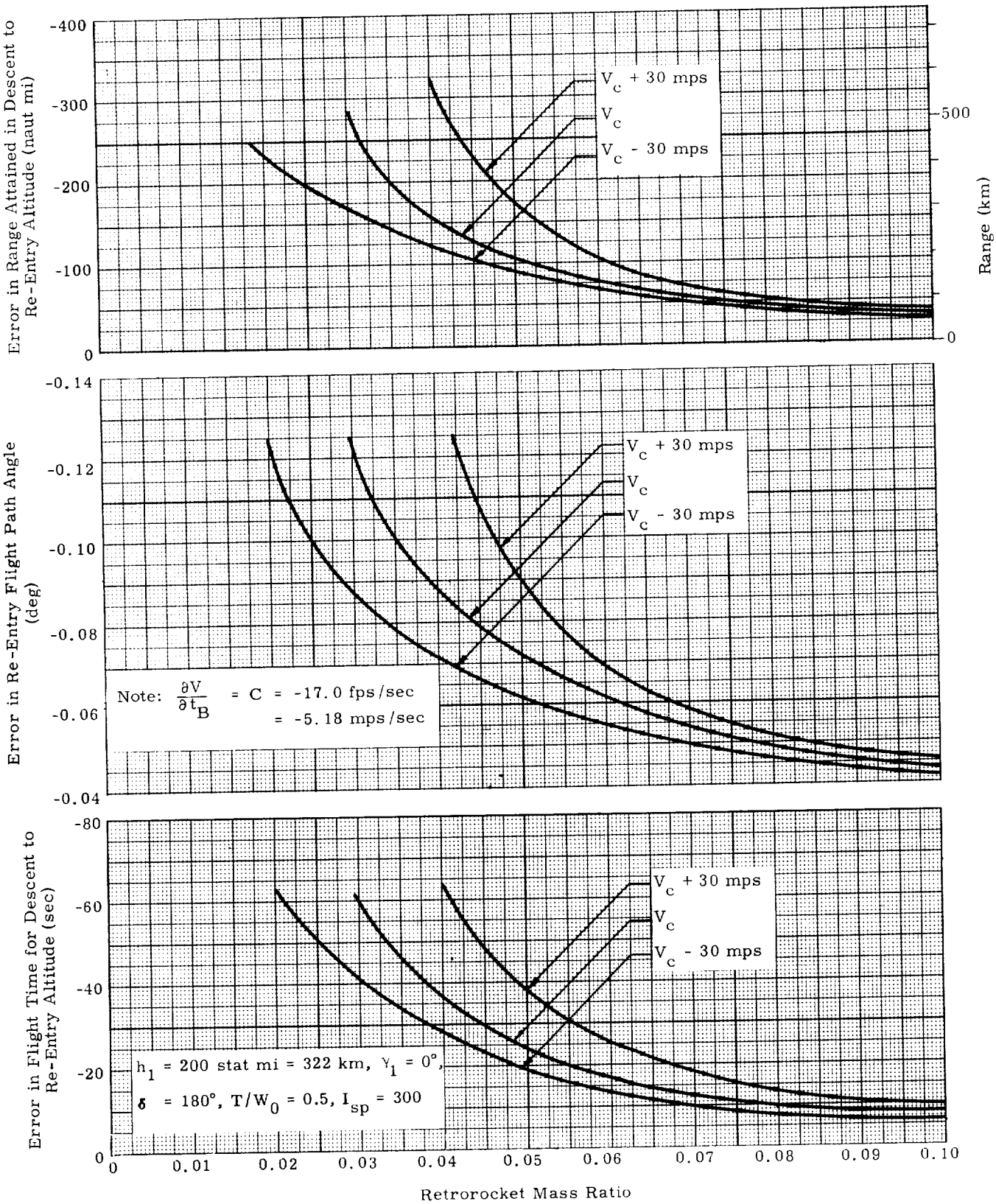

Fig. 20b. Variations in Re-Entry Position, Time, and Flight Path Angle (per Second Error in t_B) with Variations in Initial Velocity and Retrorocket Mass Ratio (100 fps ≈ 30 mps)

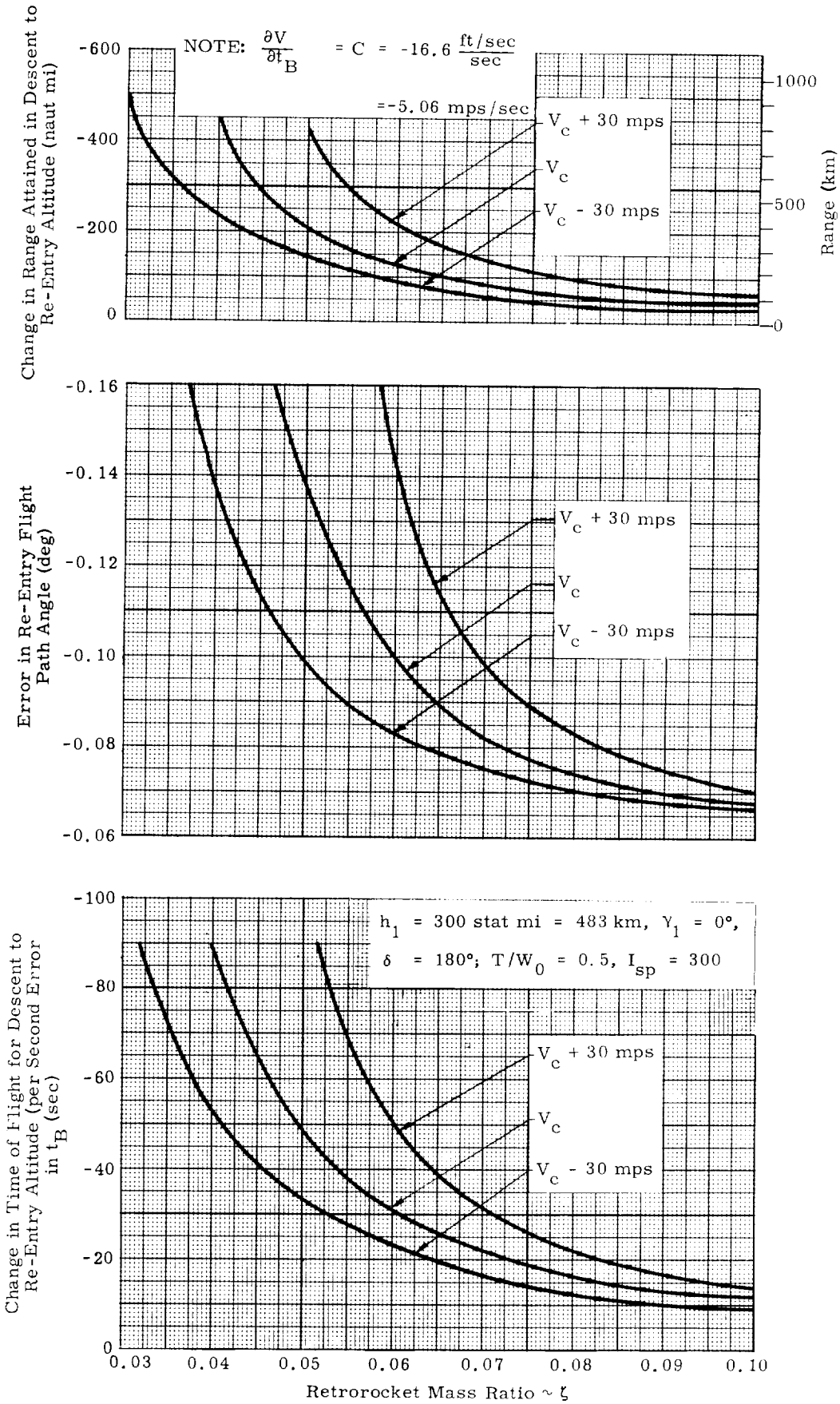

Fig. 20c. Variations in Re-entry Position, Time and Flight Path Angle (per Second Error in t_B) with Variations in Initial Velocity and Retrorocket Mass Ratio (100 fps = 30 mps)

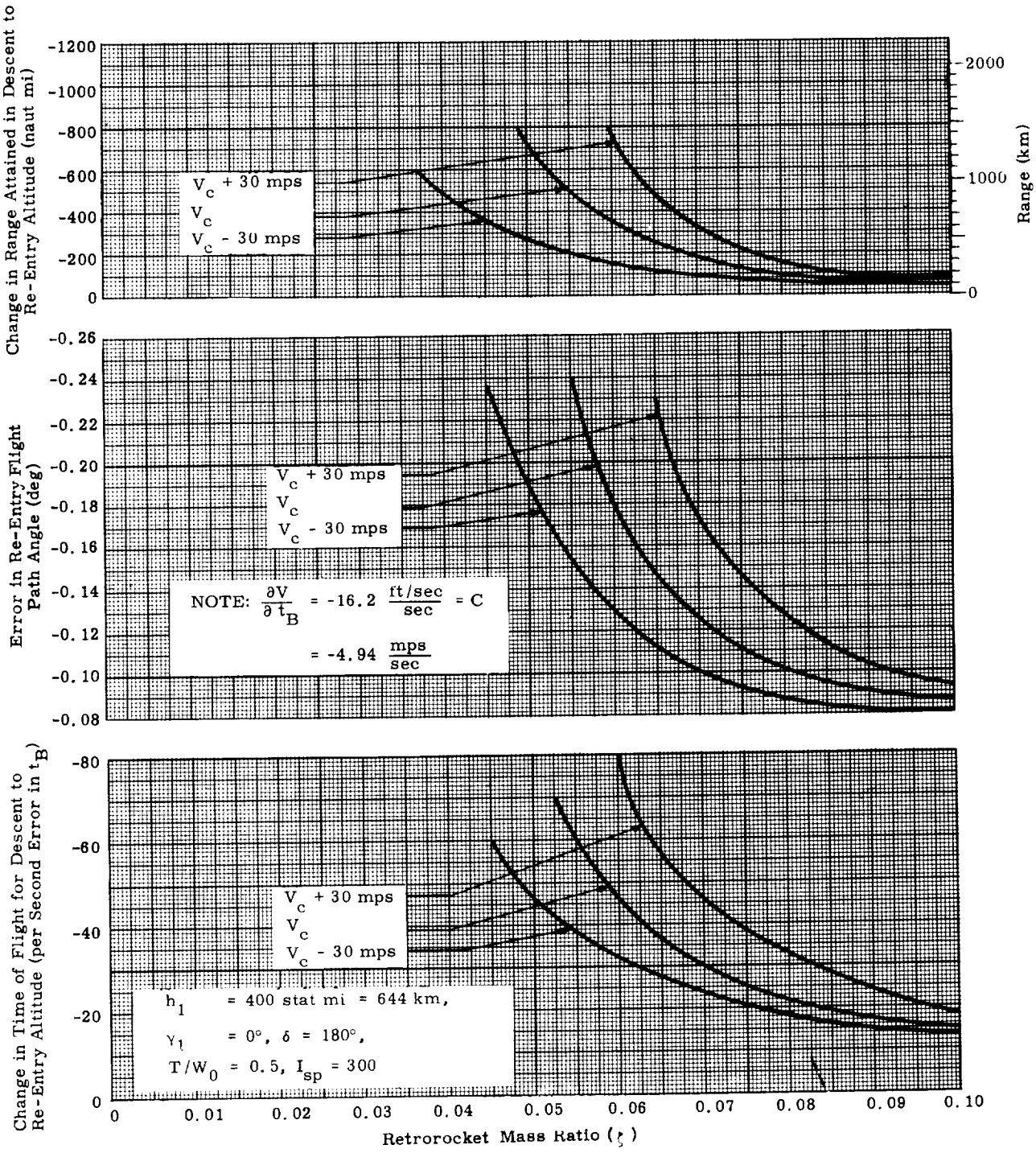

Fig. 20d. Variations in Re-Entry Position, Time and Flight Path Angle (per Second Error in t_B) with Initial Velocity and Retrorocket Mass Ratio (100 fps ≈ 30 mps)

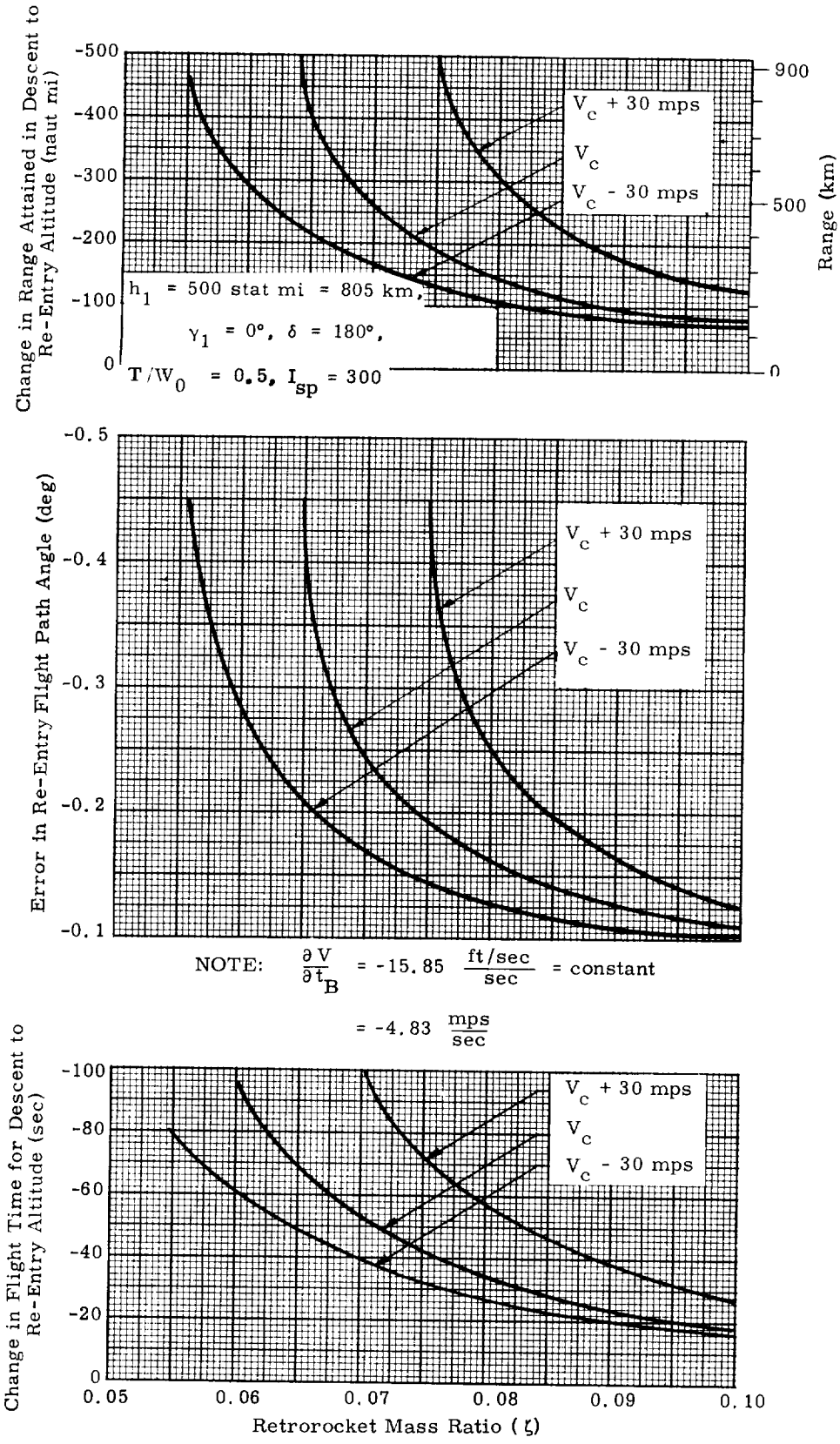

Fig. 20e. Variations in Re-Entry Position, Time and Flight Path Angle (per Second Error in t_B) with Initial Velocity and Retrorocket Mass Ratio (100 fps ≈ 30 mps)

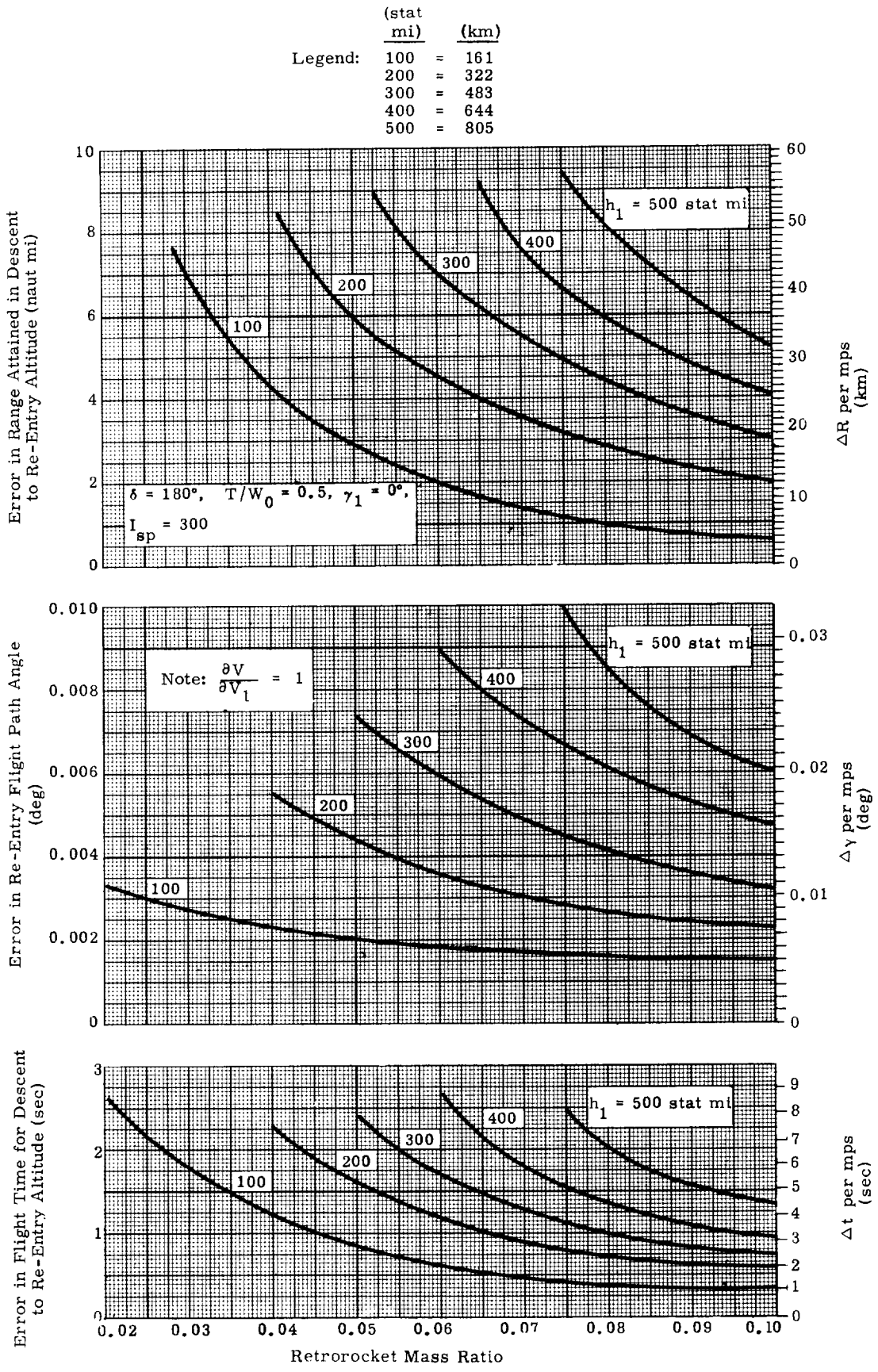

Fig. 21. Variations in Re-Entry Location, Time, Flight Path Angle, and Velocity with Initial Velocity as Functions of Retrorocket Mass Ratio and h_1

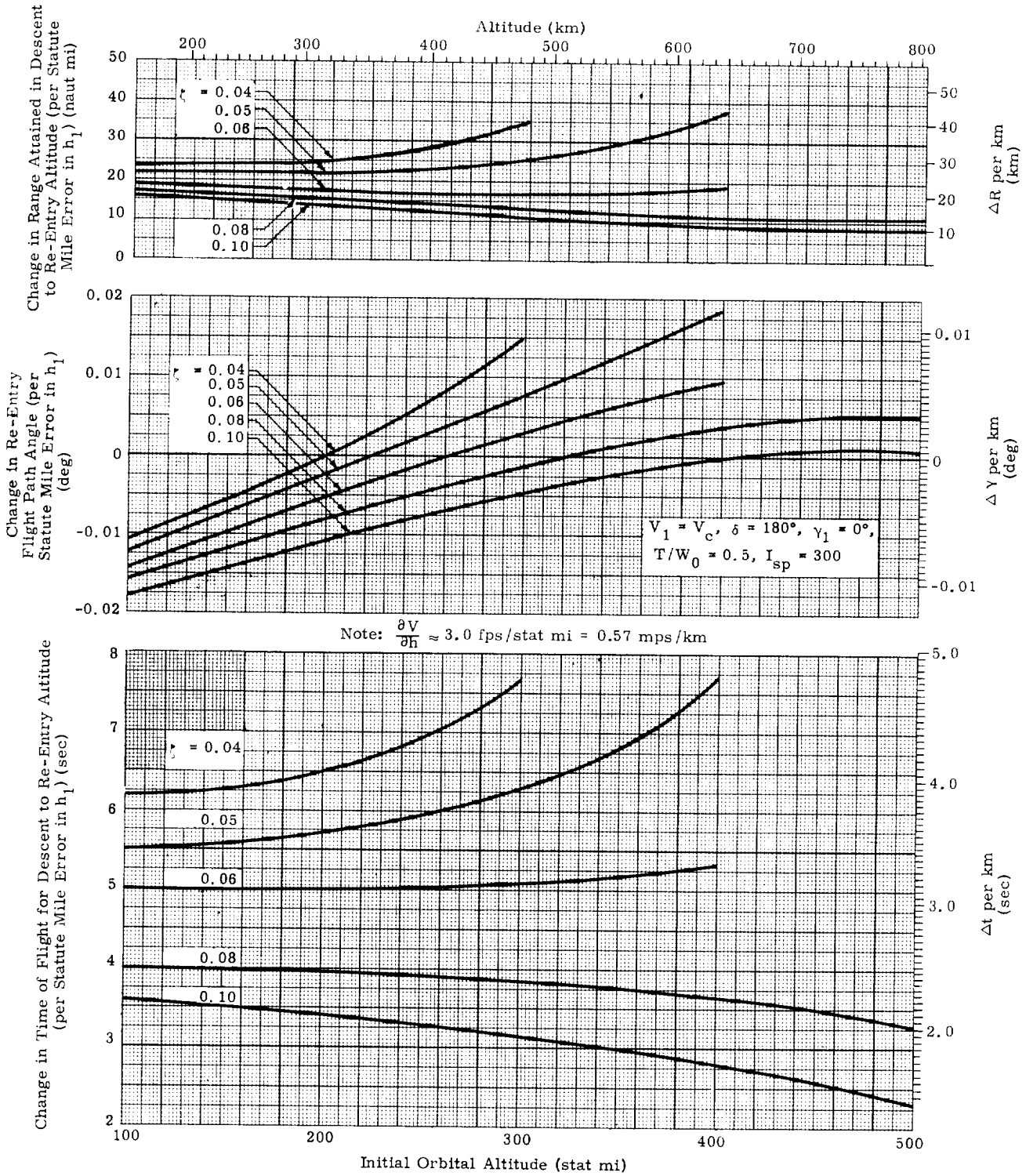

Fig. 22a. Variations in Re-Entry Location, Time, Flight Path Angle and Velocity with Altitude as Functions of h_1 and Retro-rocket Mass Ratio

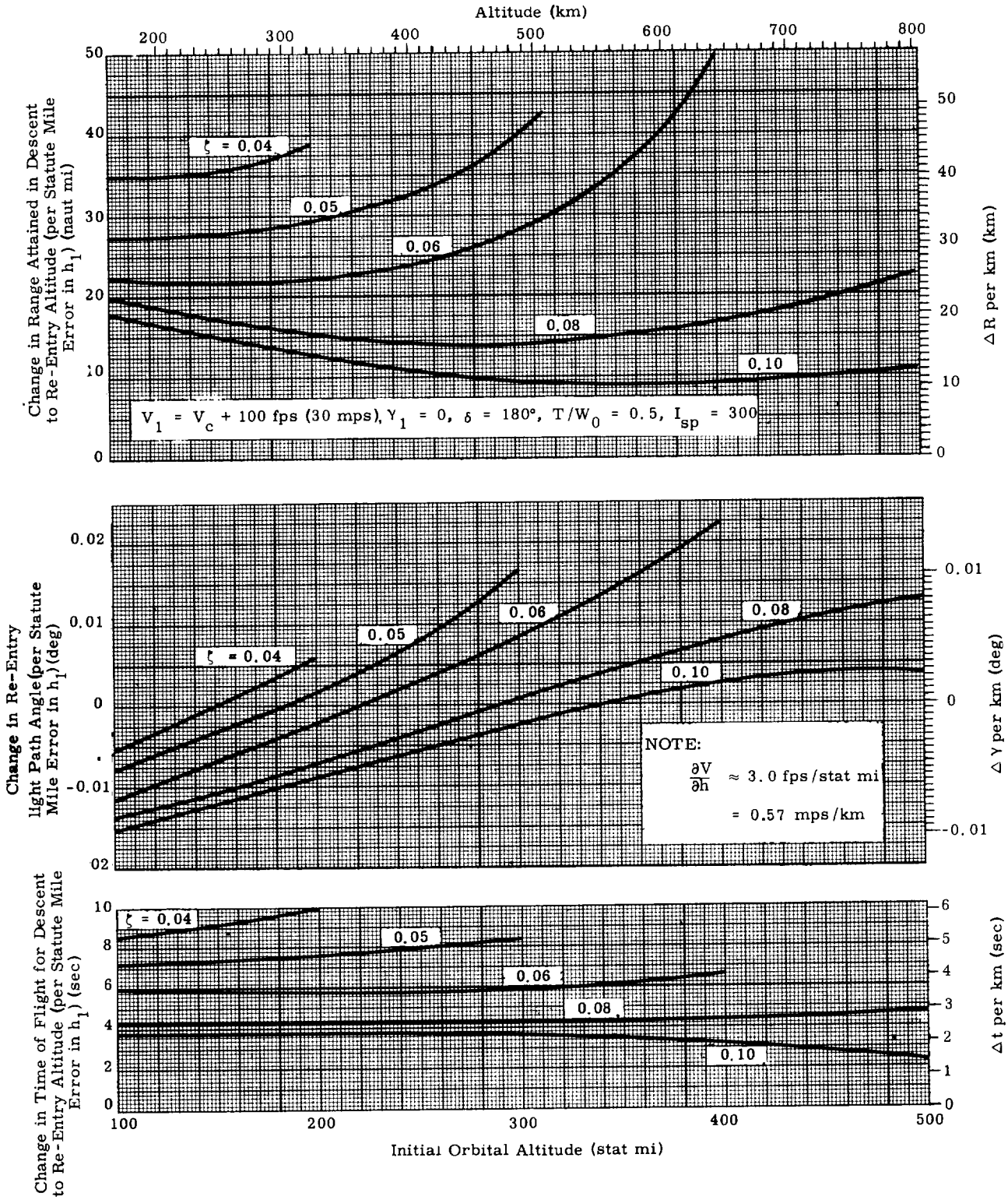

Fig. 22b. Variations in Re-Entry Position, Time, Flight Path Angle and Velocity with Altitude as Functions of h_1 and Retrorocket Mass Ratio

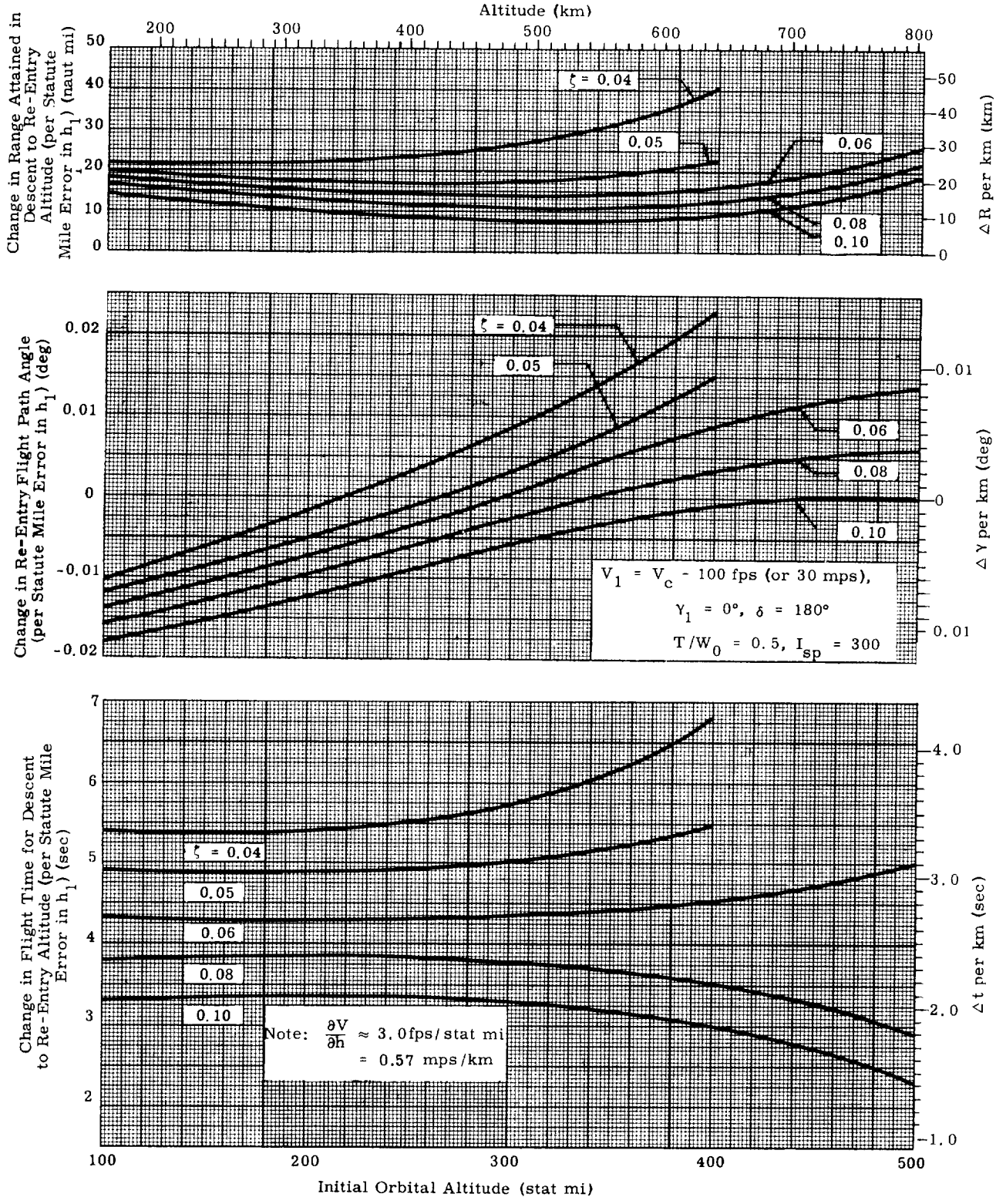

Fig. 22c. Variations in Re-Entry Position, Time, Flight Path Angle and Velocity with Altitude as Functions of h_1 and Retro-rocket Mass Ratio

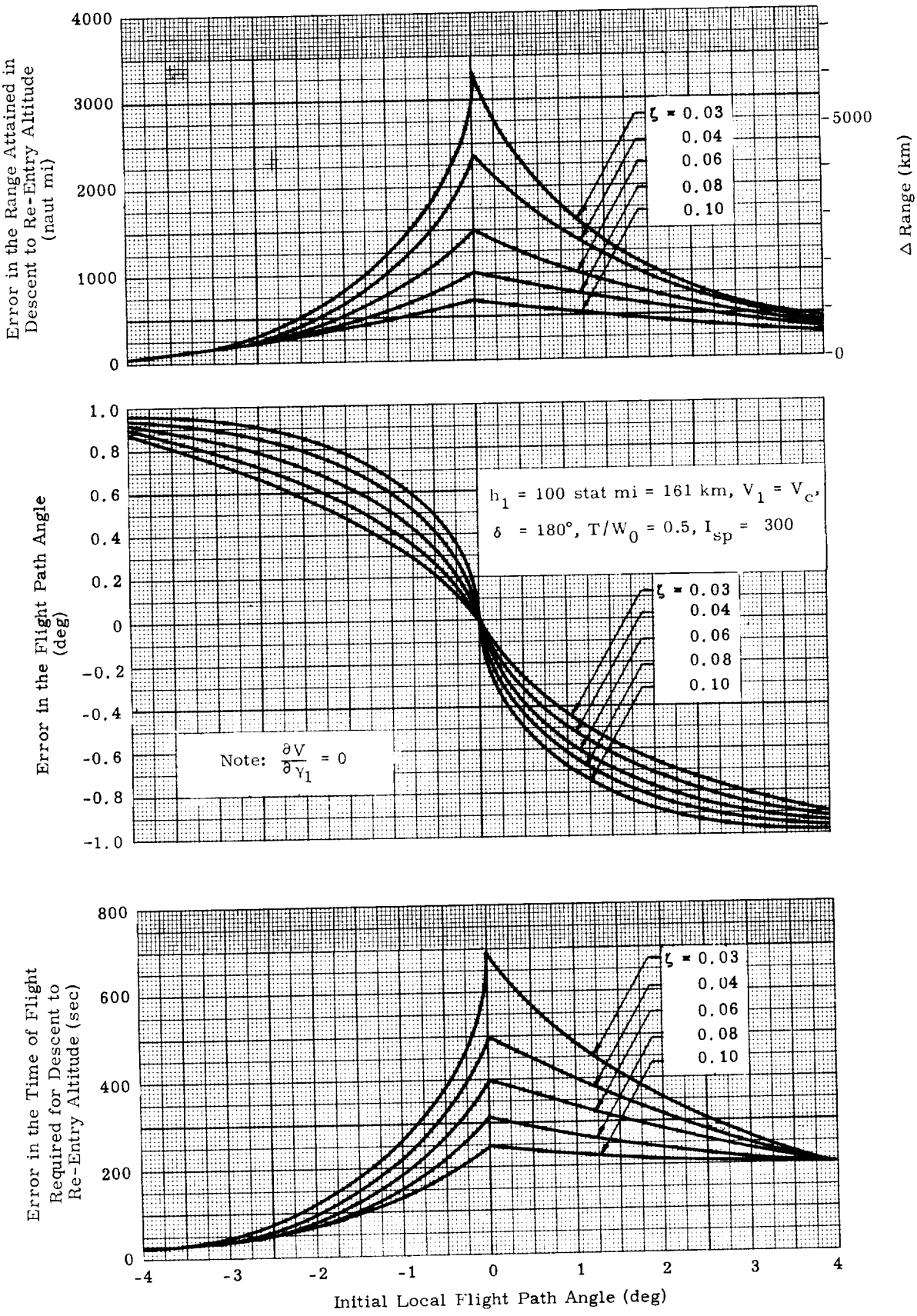

Fig. 23a. Errors in Re-Entry Parameters Due to a 1° Error in γ_1

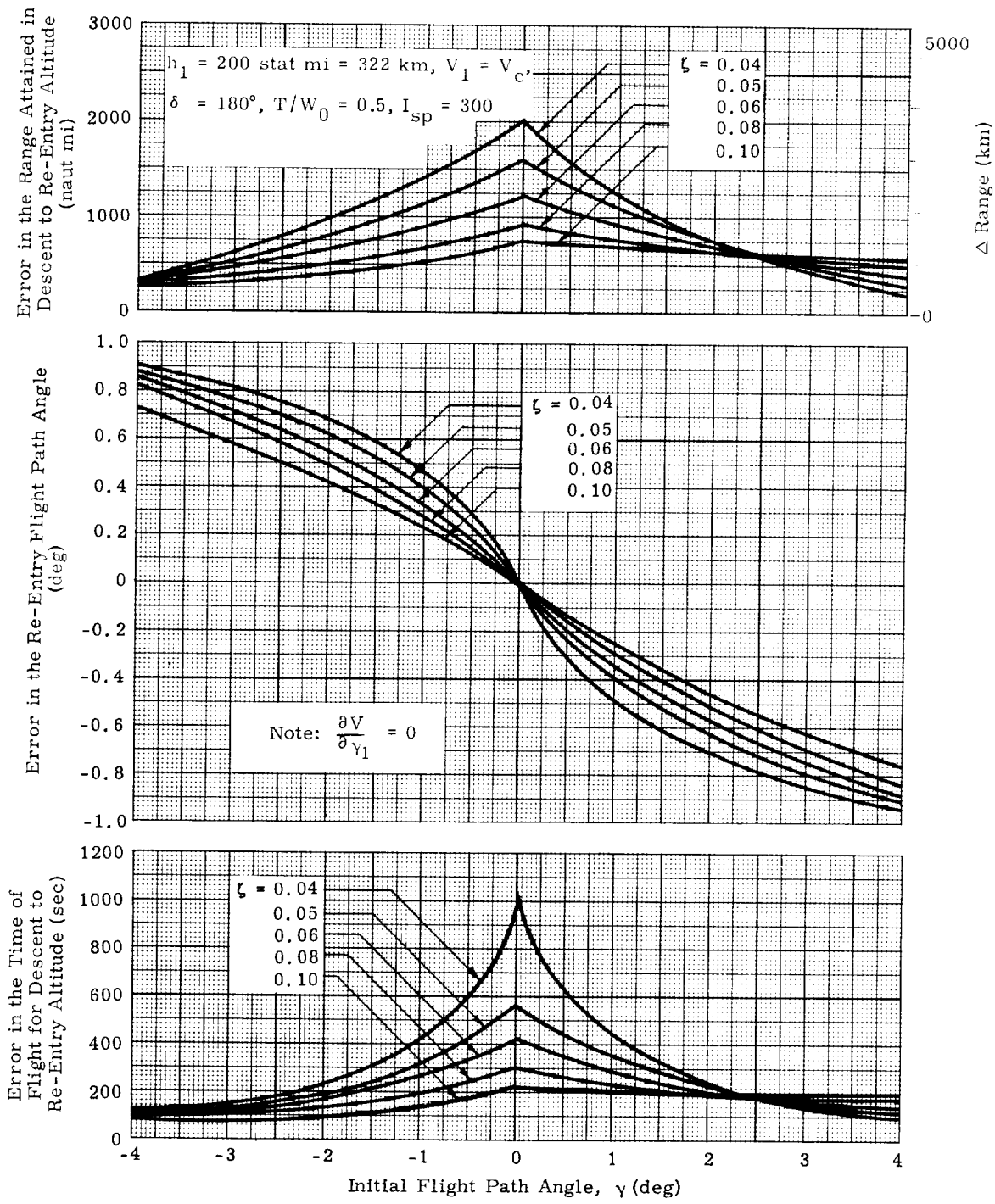

Fig. 23b. Errors in the Re-Entry Parameters Due to a 1° Error in γ_1

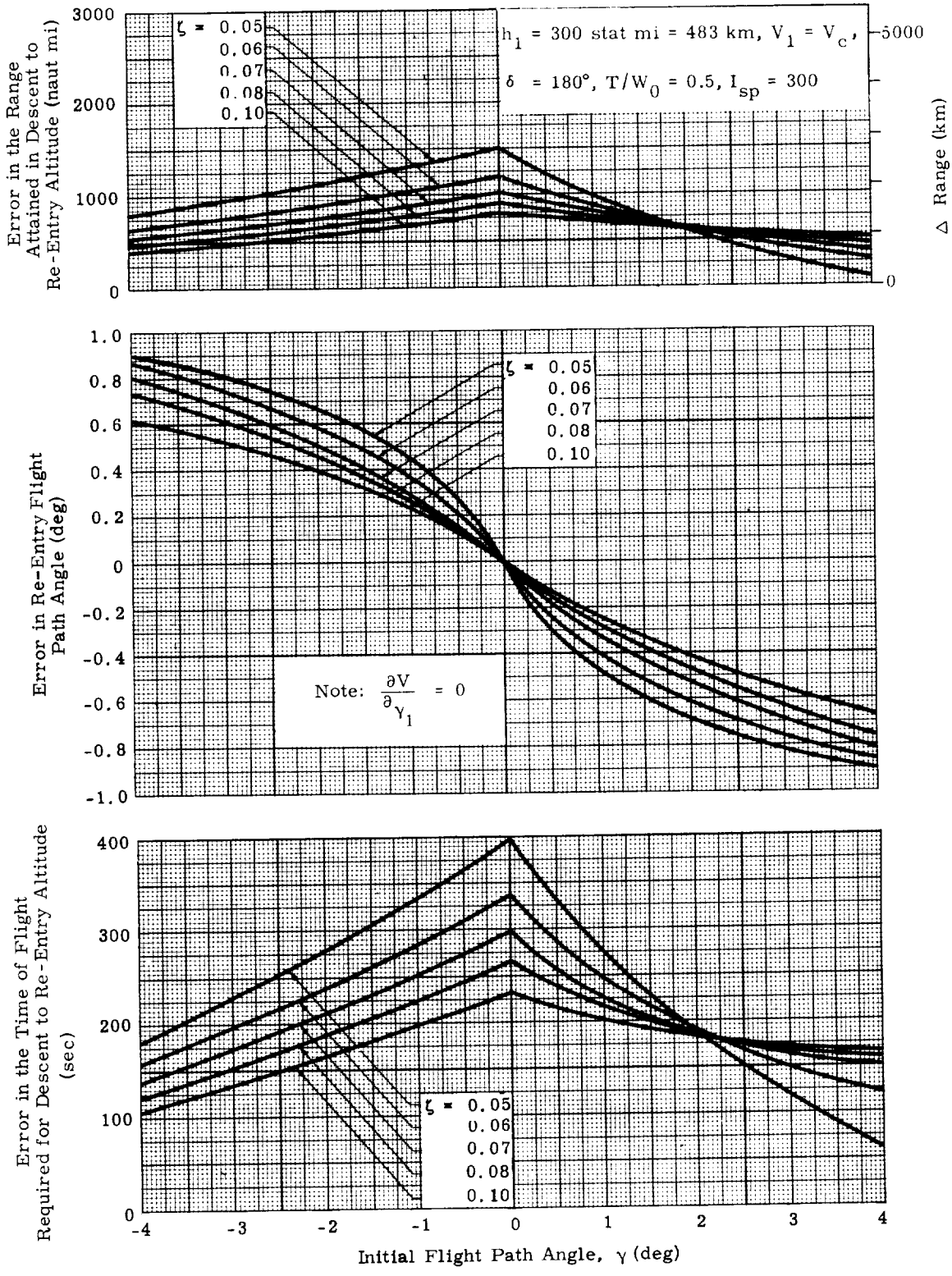

Fig. 23c. Errors in the Re-Entry Parameters Due to a 1° Error in γ_1

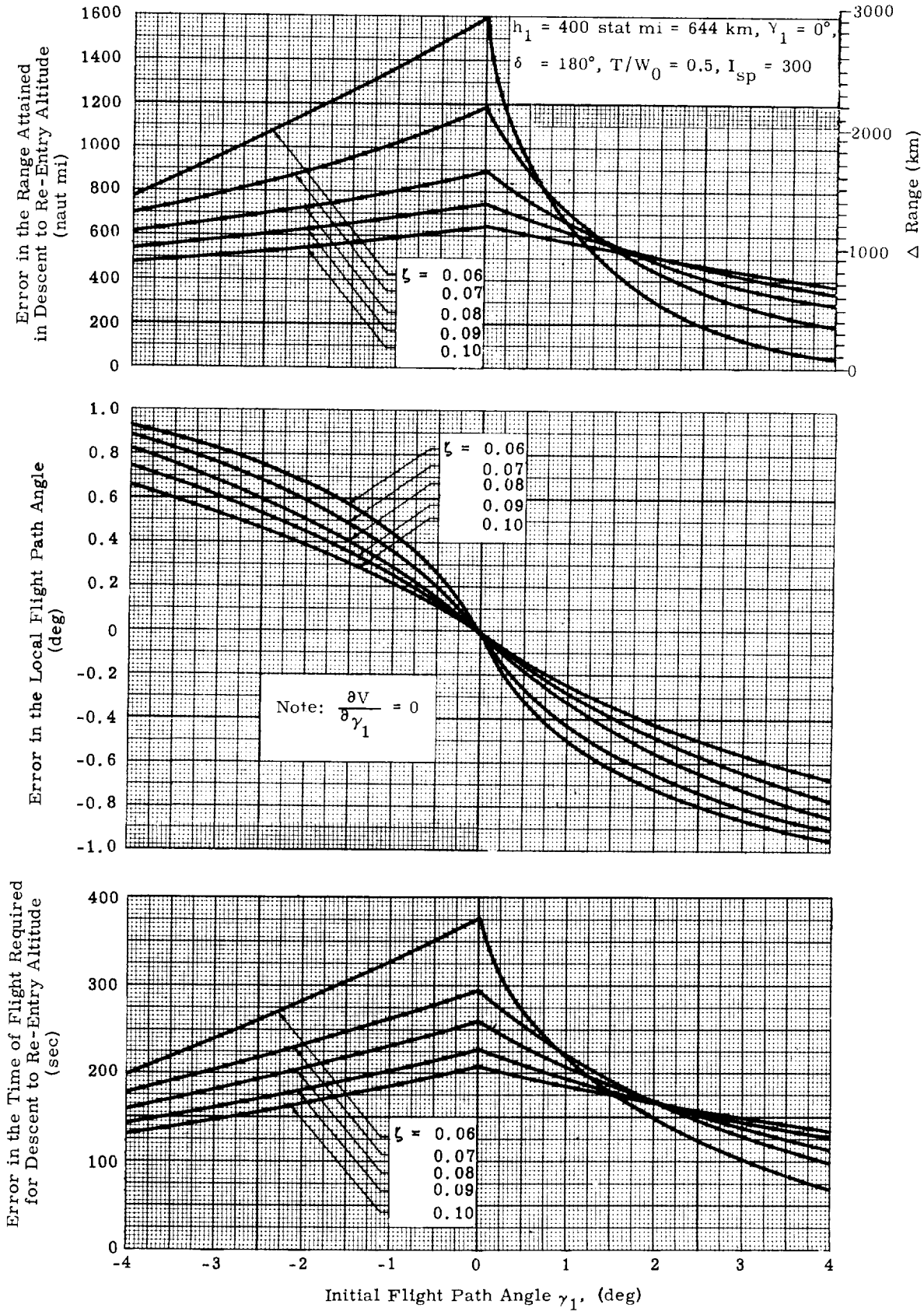

Fig. 23d. Errors in the Re-Entry Parameters Due to a 1° Error in γ_1

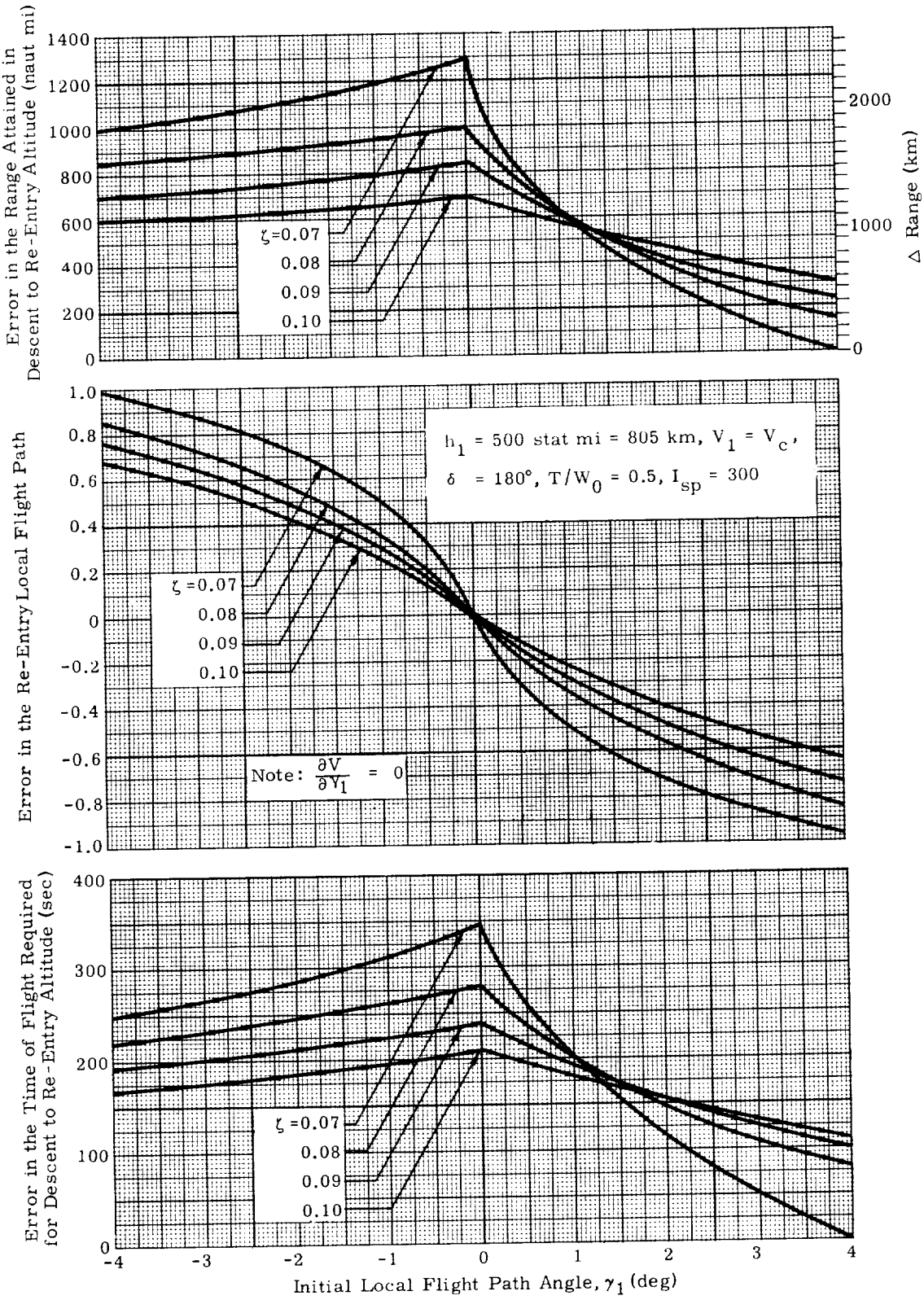

Fig. 23e. Errors in the Re-Entry Parameters Due to a 1° Error in γ_1

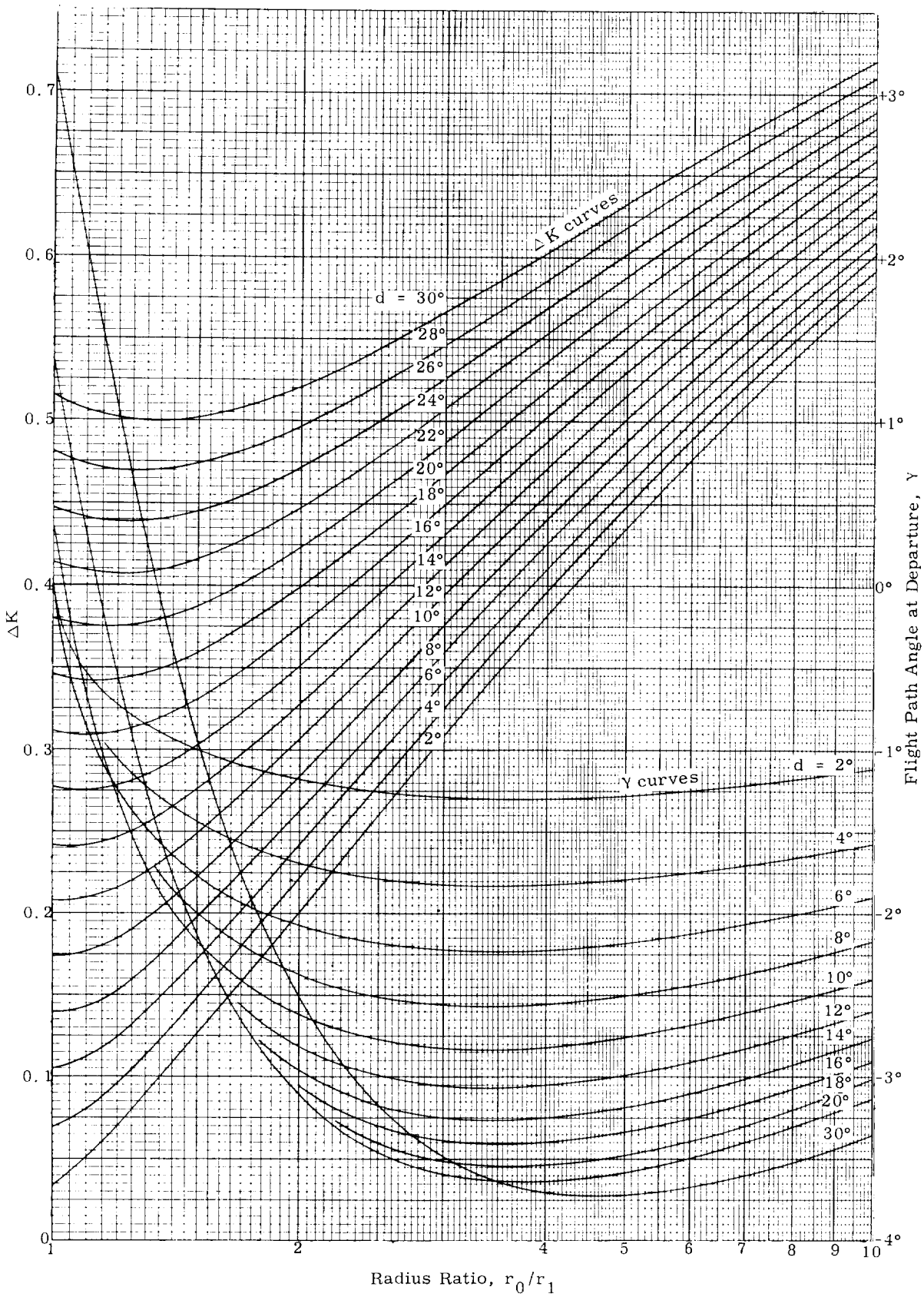

Fig. 24. Optimum ΔK and γ for 3-D-Departure

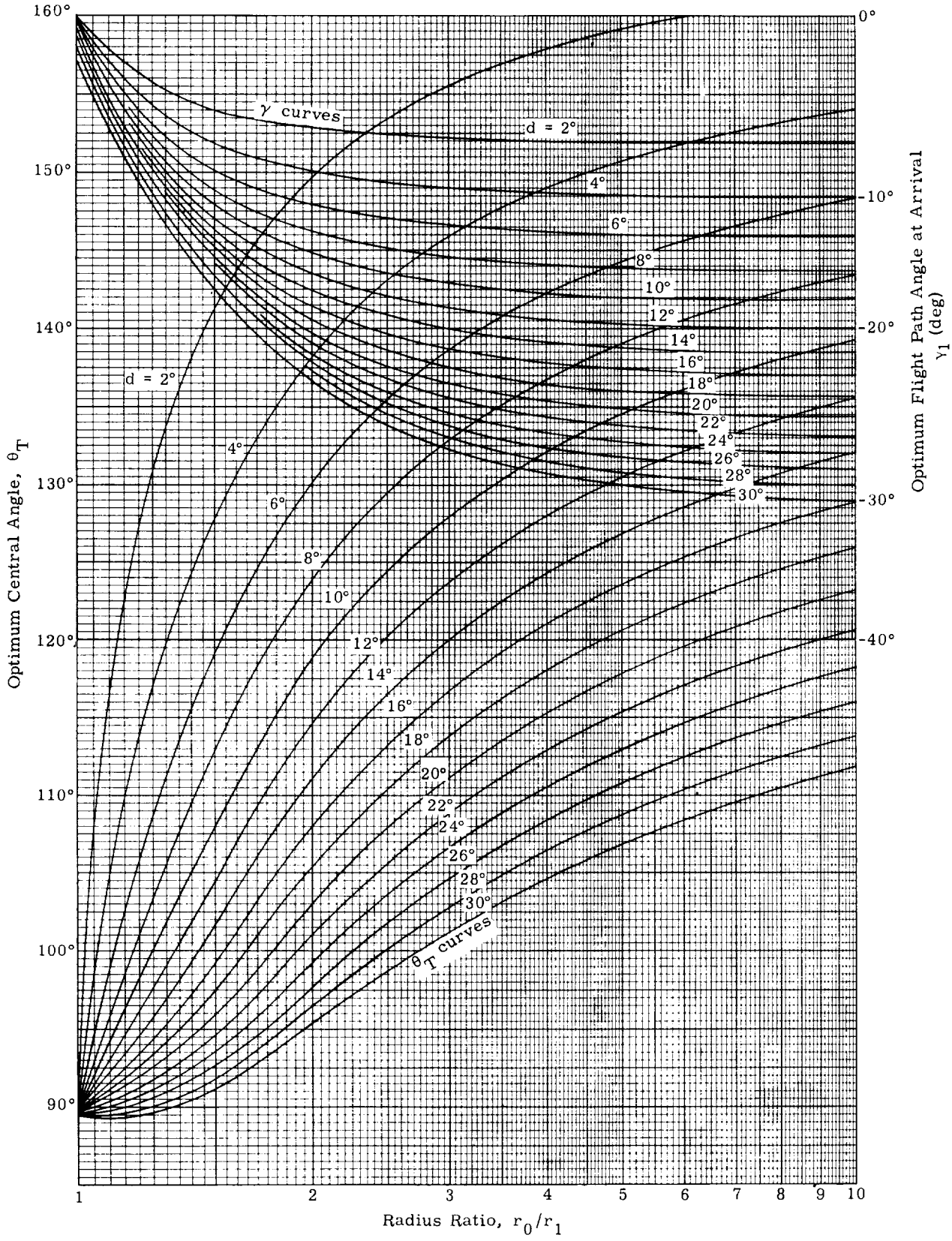

Fig. 25. Optimum Central Angle and Arrival Path Angle for 3-D Departure

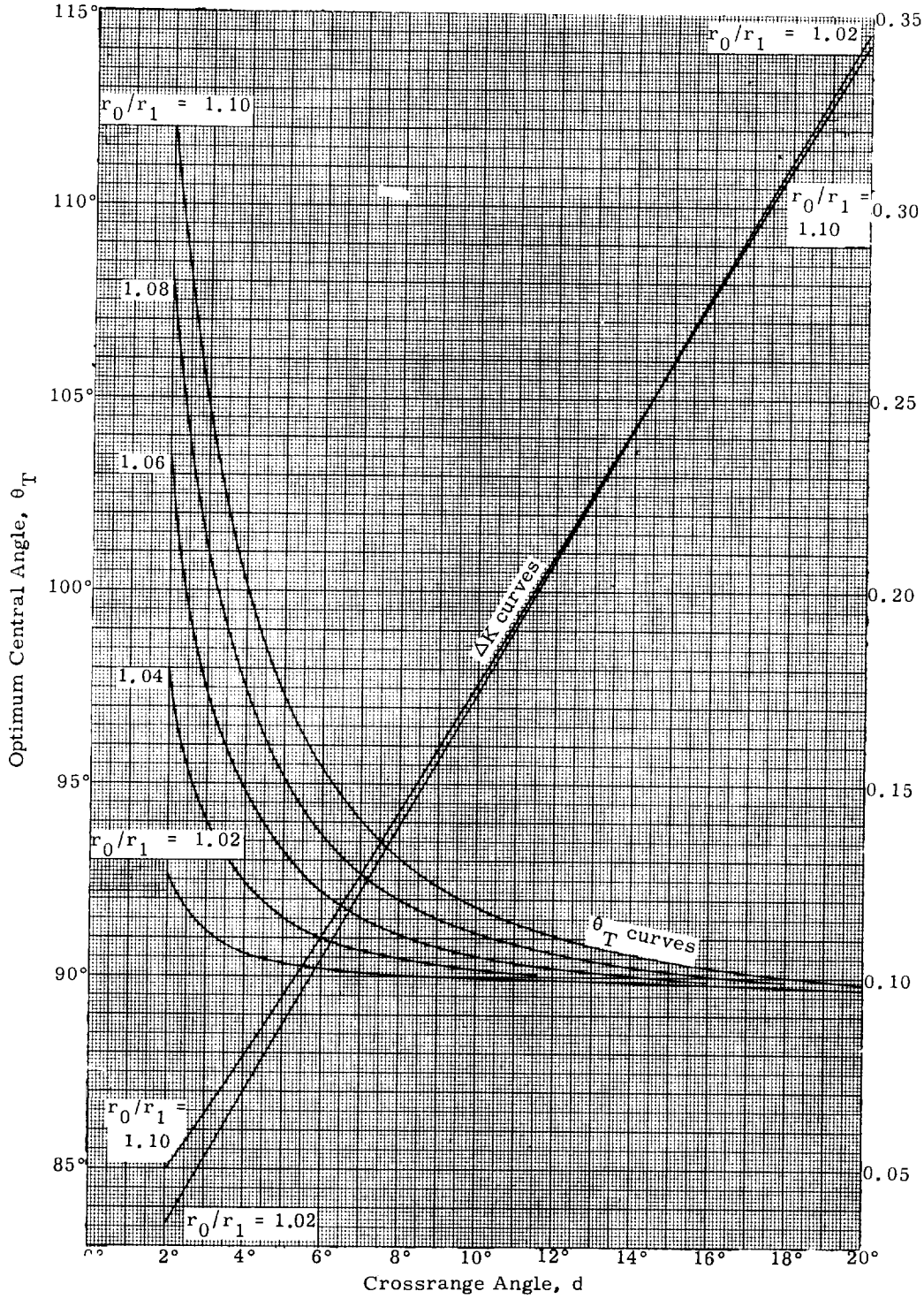

Fig. 26. Optimum Central Angle and ΔK as a Function of d

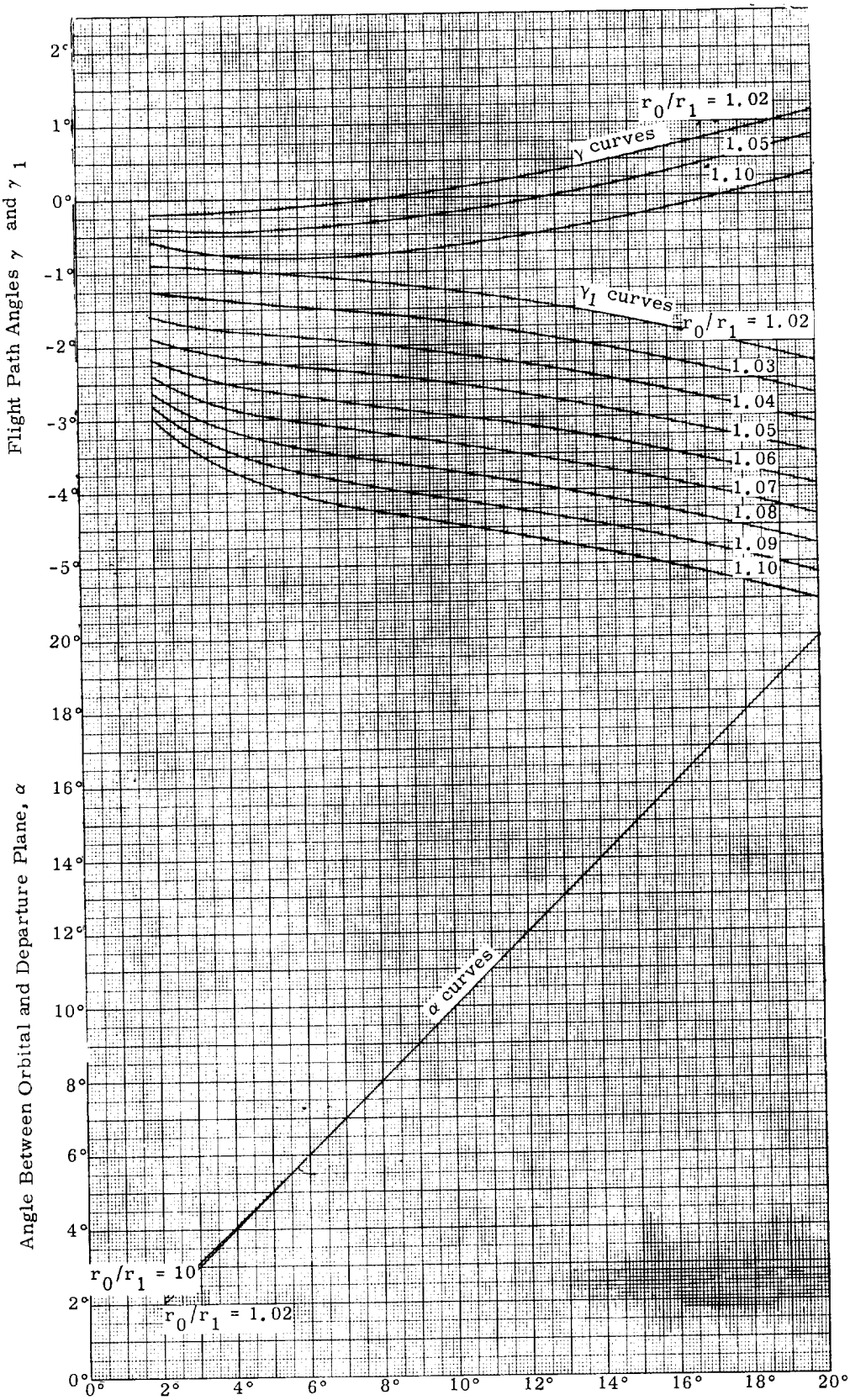

Fig. 27. Plane Change Angle and Flight Path Angle as Functions of Mass Range Angle

CHAPTER IX

SATELLITE RE-ENTRY

Prepared by

J. D. Kraft
Martin Company (Baltimore)
Aerospace Mechanics Department
March 1963

		Page
	Symbols	IX-1
A.	Introduction	IX-2
B.	Re-Entry Trajectories	IX-2
C.	Deceleration	IX-12
D.	Re-Entry Heating	IX-14
E.	Range and Time to Impact	IX-17
F.	Maneuverability	IX-18
G.	References	IX-21
H.	Bibliography	IX-22
	Illustrations	IX-29

LIST OF ILLUSTRATIONS

Figure	Title	Page
1	Values of z Functions for Entry from Decaying Orbits into Planetary Atmosphere	IX-31
2	Values of z Functions for Entry from Orbital Velocity at Initial Angles of Descent; $\overline{u}_0 = 1$	IX-32
3	Values of z Functions for Atmosphere Braking of Nonlifting Vehicles ($\overline{u}_0 = 1.4$, L/D = 0)	IX-34
4	Velocity Profile and Flight Path Angle Variation for Satellite Re-Entry	IX-35
5	Velocity Variation with Altitude (h_0 = 300,000 ft = 91,440 m, v_0 = 25,000 fps = 7,620 mps, L/D = 0) . .	IX-36
6	Flight Path Angle Variation with Altitude (h_0 = 300,000 ft = 91,440 m; v_0 = 25,000 fps = 7620 mps)	IX-41
7	Characteristic Re-Entry Altitude-Velocity Profiles for Lifting Vehicles	IX-44
8	Altitude Peak of First Skip (v_0 = 25,000 fps = 7,620 mps, h_0 = 400,000 ft = 122,000 m)	IX-45
9a	Entry Vehicle Comparison, Velocity-Altitude Profile	IX-47
9b	Effect of Entry Velocity on Altitude-Velocity Profile	IX-48
9c	Effect of Entry Angle on Velocity-Altitude Profiles .	IX-49
9d	Effect of Programmed C_L on Velocity-Altitude Profile	IX-50
9e	Program of C_L with Mach Number	IX-50
10a	Terminal Velocity	IX-51
10b	Terminal Flight Path Angle	IX-52

LIST OF ILLUSTRATIONS (continued)

Figure	Title	Page
11a	Entry Vehicle Comparison, Altitude-Time History . . .	IX-53
11b	Re-entry Vehicle Comparison--Time History	IX-54
11c	Re-Entry History with and Without Rotating Air Mass	IX-55
12a	Effect of Lift-Drag Ratio on Deceleration for Entry into Earth Atmosphere From Decaying Orbits	IX-56
12b	Deceleration Profile and Load Factor for Satellite Re-Entry	IX-56
12c	Deceleration Variation with Altitude for Satellite Re-Entry	IX-57
13a	Maximum Decelerations for Ballistic Re-Entry	IX-58
13b	Optimum Ballistic Coefficients (to minimize re-entry decelerations)	IX-58
14a	Controlled Descent, General Ballistic Coefficient Variation	IX-59
14b	Controlled Descent, General Acceleration Profile . . .	IX-59
15	Length of Time Spent at Decelerations Equal to and Larger than the Shown Value	IX-60
16	Effect of Re-Entry Conditions on Maximum Total Decelerations (L/D = 0.5)	IX-62
17a	Maximum Load Factor Versus L/D (W/C_DA = 438 psf or B = 0.234 x 10^{-3} m^2/kg)	IX-62
17b	Maximum Load Factor Versus L/D (W/C_DA = 50 psf or B = 2.04 x 10^{-3} m^2/kg)	IX-63
17c	Maximum Total Acceleration Versus L/D Ratio (W/C_DA = 50 psf or B = 2.04 x 10^{-3} m^2/kg)	IX-63

LIST OF ILLUSTRATIONS (continued)

Figure	Title	Page
18	Maximum Re-Entry Load Factor Versus Ballistic Coefficient (h_0 = 400,000 ft = 121,920 m, v_0 = 25,000 fps = 7620 mps)	IX-64
19	Maximum Re-Entry Load Factor Versus Flight Path Angle (v_0 = 25,000 ft/sec = 7620 mps, h_0 = 400,000 ft = 121,920 m)	IX-65
20	Maximum Re-entry Load Factor Versus Velocity (h_0 = 400,000 ft, γ_0 = - 1°)	IX-66
21	Maximum Re-Entry Load Factor Versus L/D	IX-68
22	Effect of Re-Entry Angle on Peak Deceleration, v_0 = v_c, $W/C_L A$ = 20 psf = 957 newton/m^2, L/D = 2 (Ref. 14)	IX-68
23	Maximum Re-Entry Dynamic Pressure (v_0 = 25,000 fps = 7620 mps; h_0 = 400,000 ft = 121,920 m)	IX-69
24	Maximum Re-Entry Dynamic Pressure Versus γ_0 (v_0 = 25,000 fps = 7620 mps, h_0 = 400,000 ft = 121,920 m)	IX-72
25	Maximum Re-entry Dynamic Pressure Versus Velocity (γ_0 = - 1°; h_0 = 400,000 ft = 121,920 m)	IX-73
26	Maximum Re-Entry Dynamic Pressure Versus L/D (v_0 = 25,000 fps = 7620 mps)	IX-75
27	Maximum Re-Entry Dynamic Pressure Versus L/D (γ_0 = -1°; h_0 = 400,000 ft = 121,920 m)	IX-76
28	Effects of Lift, Drag and Wing Loading on Maximum Dynamic Pressure	IX-78

LIST OF ILLUSTRATIONS (continued)

	Title	Page
29	Radius-Emissivity Parameter ($R^{1/8} \times \epsilon^{1/4}$) Versus Stagnation Nose Radius.	IX-78
30a	Heat Transfer Rate q_s at the Stagnation Point of a Blunt Body of 1-ft Nose Radius as a Function of Air Density Ratio, ρ/ρ_0	IX-79
30b	Ratio of the Heat Input Rate q_s to the Rate at Which Energy Is Dissipated by Drag $\frac{1}{2}\rho v^3$ as a Function of Air Density Ratio ρ/ρ_0	IX-79
31a	Effect of Re-Entry Angle on Maximum Heat Flux ($v_0 = v_c$, $W/C_L A$ = 20 psf, L/D = 2)	IX-80
31b	Equilibrium Radiation Temperature Versus Heat Transfer Rate	IX-80
32	Comparison of Radiation Equilibrium Method with an Exact Skin Temperature Computation (free fall from 1,000,000 ft = 304,800 m)	IX-81
33a	Nose Temperature Histories for Different Flight Conditions	IX-82
33b	Stagnation Point Temperature Profiles for Equilibrium Glides	IX-83
33c	Temperature Data for Inertial Velocity and Altitude . .	IX-84
34a	Maximum Equilibrium Nose Temperature Versus $W/C_L A$ for Equilibrium Glides	IX-85
34b	Altitude for Maximum Equilibrium Nose Temperature Versus $W/C_L A$ (equilibrium glides)	IX-85
34c	Altitude for Maximum Stagnation Nose Temperature (h_0 = 400,000 ft, v_0 = 25,000 fps)	IX-86
35	Maximum Re-Entry Stagnation Point Nose Temperature (h_0 = 400,000 (121,920 m), v_0 = 25,000 fps (7620 mps)	IX-87

LIST OF ILLUSTRATIONS (continued)

Figure	Title	Page
36	Maximum Re-Entry Stagnation Point Nose Temperature Versus γ_0 (h_0 = 400,000 ft = 121,920 m, v_0 = 25,000 fps = 7620 mps)	IX-88
37	Effect of Re-Entry Conditions on Maximum Stagnation Point Temperature (L/D = 0.5)	IX-90
38	Maximum Re-Entry Stagnation Point Temperature Parameter Versus Velocity (h_0 = 400,000 ft = 121,920 m; γ_0 = - 1°)	IX-91
39	Maximum $T_W R^{1/8} \epsilon^{1/4}$ Versus Re-Entry Velocity (h_0 = 400,000 ft = 121,920 m, $\frac{W}{C_D A}$ = 50 psf = 2390 Newtons/m^2	IX-93
40	Maximum Re-Entry Stagnation Point Nose Temperature Versus Velocity (h_0 = 400,000 ft = 121,920 m; $W/C_D A$ = 438 psf = 21,000 newtons/m^2	IX-95
41	$T_W R^{1/8} \epsilon^{1/4}$ Versus Lift-Drag Ratio (h_0 = 400,000 ft = 121,920 m)	IX-97
42	Equilibrium Temperature History, with and Without Rotating Air Mass	IX-98
43a	Maximum Stagnation Point Temperature Parameter Versus Ballistic Coefficient (ballistic re-entry--L/D = 0)	IX-98
43b	Maximum Radiation-Equilibrium Temperature at Laminar Stagnation Point for Entry from Decaying Orbits into Earth Atmosphere	IX-99
44	Effect of Lift-Drag Ratio on Maximum Laminar Heating Rate at Stagnation Point for Entry from Decaying Orbits	IX-99
45a	Surface Temperature Parameter $\epsilon^{1/4} R^{1/8} T_w$ as a Function of Air Density Ratio ρ/ρ_0. Simple drag bodies	IX-100

LIST OF ILLUSTRATIONS

Figure	Title	Page
45b	Lift Parameter $C_L A/W$ as a Function of Air Density Ratio ρ/ρ_0 for Several Values of the Drag Parameter $W/C_D A$. Constant Heat Transfer Trajectories.	IX-100
45c	Lift Parameter $C_L A/W$ as a Function of Air Density Ratio ρ/ρ_0 for Several Values of the Surface Temperature Parameter $\epsilon^{1/4} R^{1/8} T_w$ Constant Heat Transfer Trajectories	IX-101
46	Rate of Change of Stagnation Point Temperature Parameter as a Function of Re-Entry Angle (h_0 = 400,000 ft = 121,920 m, (v_0 = 25,000 fps = 7620 mps) .	IX-102
47	Maximum Surface Temperature for Entry into Various Planets from Decaying Orbits $v_0/v_c = 1$, $\gamma_0 = 0°$	IX 103
48	Range to Impact Versus Re-entry Angle	IX-104
49	Range Attained in Descent from 300,000 ft (91,440 m) ft to Sea Level (L/D = 0).	IX-105
50	Range to Impact from 400,000 ft = 121,920 m (v_0 = 25,000 fps = 7620 mps).	IX-107
51	Range to Impact from 400,000 ft = 121,920 m(γ_0 = -1°)	IX-109
52	Impact Range Versus Re-Entry Velocity ($\frac{W}{C_D A}$ = 50 psf = 2390 newtons/m^2, h_0 = 400,000 ft = 121,920 m) .	IX-111
53	Range to Impact from 400,000 ft (121,920 m) Versus L/D (v_0 = 25,000 fps = 7620 mps).	IX-115
54	Range Versus Lift-Drag, $\frac{W}{C_D A}$ = 50 psf (Applies for $5 < \frac{W}{C_D A} < 500$ psf; h_0 = 400,000 ft)	IX-116

LIST OF ILLUSTRATIONS (continued)

Figure	Title	Page
55	Equilibrium Glide Range (not dependent on $W/C_L A$) . .	IX-118
56a	Variation in Range as a Function of Angle of Attack and Entry Angle. (Nonrotating Earth; h_0 = 350,000 ft = 106,700 m; v_0 = 25,863 fps = 7870 mps; W/A = 20 lb/ft^2 = 956 newton/m^2)	IX-118
56b	Variation in Range as a Function of Initial Velocity and Entry Angle for Ballistic Vehicles (α = 90), (Nonrotating Earth; h_0 = 350,000 ft = 106,800 m; W/A = 20 lb/ft^2 = 955 newtons/m^2)	IX-119
56c	Variation in Range as a Function of Angle of Attack and Initial Velocity. (Nonrotating Earth; h_0 = 350,000 ft = 160,800 m; γ_0 = 1°)	IX-119
57	Time to Impact Versus Ballistic Coefficient (v_0 = 25,000 fps = 7620 mps)	IX-120
58	Time Versus Range to Impact from 400,000 ft = 121,920 m (v_0 = 25,000 fps = 7620 mps)	IX-120
59	Time to Impact Versus Re-Entry Velocity (h_0 = 400,000 ft = 121,920 m, $W/C_D A$ = 50 psf = 2390 newton/m^2)	IX-122
60	Re-Entry Time Versus L/D for Various Velocities ($\frac{W}{C_D A}$ = 50 psf = 2390 newtons/m^2; h_0 = 400,000 ft = 121,920 m)	IX-123
61	Velocity at Apogee Versus Range	IX-124
62	Range and Time to Impact for Ballistic Entry.	IX-125
63a	Conditions for Impact--Ballistic Case	IX-125
63b	Conditions for Impact, Lifting Case	IX-126
63c	Minimum Entry Angle for Capture (at escape velocity)	IX-126

LIST OF ILLUSTRATIONS (continued)

Figure	Title	Page
64	Range Corrections with Ballistic Coefficient Increments	IX-127
65a	Variation in Range as a Function of Angle of Attack and Entry Angle for Headings of 90° and 150° (Rotating Earth; h_0 = 350,000 ft = 106,680 m; v_0 = 25,743 fps = 7846 mps; W/A = 20 lb/ft^2 = 957 newtons/m^2)	IX-128
65b	Variation in Range and Maximum Deceleration as a Function of Heading and Initial Latitude (Rotating Earth; h_0 = 350,000 ft = 106,650 m; v_0 = 25,743 fps = 7846 mps; W/A = 20 lb/ft^2 = 957 newtons/m^2)	IX-128
66a	Effect of Roll Angle on Lateral Range	IX-129
66b	Lateral Range Capability ($v_0 = v_c$)	IX-129
66c	Effect of Entry Angle on Lateral Range	IX-130
66d	Effect of Velocity at Initiation of Maneuver on Lateral Range	IX-130
67a	Effect of Re-Entry Angle on the Azimuth Angle and Range to Maximum Lateral Deflection Point	IX-131
67b	Effect of Wing Loading on Azimuth Potential (γ_0 = 2°; constant altitude and equilibrium glide)	IX-132
67c	Effect of Wing Loading on Range to Maximum Azimuth Potential (γ_0 = -2°; constant altitude and equilibrium glide)	IX-132

LIST OF ILLUSTRATIONS (continued)

Figure	Title	Page
68	Total Maneuverability Envelope	IX-133
69	Range and Lateral Displacement for Lifting Body Re-Entry	IX-134

IX. SATELLITE RE-ENTRY

SYMBOLS

a	acceleration
A	reference area
B	ballistic coefficient, $\frac{C_D A}{2m}$
C_D	drag coefficient
C_L	lift coefficient
D	drag force $= \frac{1}{2} \rho v^2 C_D A$
g	gravitational acceleration
G	resultant acceleration magnitude experienced in addition to that due to gravity
h	altitude; also, enthalpy
k	conductivity
°K	degrees Kelvin
L	lift force $= \frac{1}{2} \rho v^2 C_L A$
Le	Lewis number
ℓ	characteristic length
m	vehicle mass
N	load factor, $\frac{G}{g}$
Nu	Nusselt number $= \frac{h\ell}{k}$
Pr	Prandtl number
q_s	Heating rate at the stagnation region
r	geocentric radius vector
R	earth radius
°R	degrees Rankine
Re	Reynolds number $= \frac{\rho v \ell}{\mu}$
R_s	body radius of curvature at the stagnation point
t	time
T_w	temperature at the vehicle wall
u	component of velocity normal to the radius vector in the trajectory plane
$\bar{u}$	normalized velocity component, $\frac{u}{v_c}$
v	velocity magnitude
v_c	circular orbit velocity magnitude
$\bar{v}$	normalized velocity, $\frac{v}{v_c}$
w	radial component of velocity
W	vehicle weight
x	longitudinal range
y	altitude
Y	side force
z	drag parameter $= \rho_0 B \sqrt{\frac{r}{\beta}} \bar{u} e^{-\beta y}$
β	logarithmic slope of the exponential atmospheric density function
γ	flight path angle with respect to the local horizontal
ϵ	emissivity
θ	flow inclination angle with respect to the free stream
λ	lateral range
μ	viscosity
ν	kinematic viscosity
ρ	density of the atmosphere
ρ_0	sea-level or reference density of the atmosphere
$\bar{\rho}$	normalized density $= \frac{\rho_\infty}{\rho_0}$
σ	radiation constant
ϕ	bank angle

Subscripts

e	entry condition
s	value at the stagnation point
0	initial value
∞	ambient value

A. INTRODUCTION

For missions involving manned satellites and recovery of scientific instrument payloads, re-entry of the vehicle into the atmosphere is an important problem area. The principal considerations involved are (1) protection of the vehicle structure and payload against the deceleration and loading encountered in entry, (2) protection of the vehicle structure and payload against the thermal environment, (3) assurance of dynamic stability of the entering vehicle, and (4) achieving sufficiently accurate trajectory control and landing point prediction. An investigation of any of these factors must rely on an analysis of the vehicle trajectory. This chapter, therefore, presents an entry trajectory analysis and subsequently considers the four previously noted mission considerations. Design information given is in the form of both analytic solutions and data generated by numerical methods.

B. RE-ENTRY TRAJECTORIES

During the re-entry phase of the satellite mission, aerodynamic forces become necessarily more important, and the relatively simple perturbed Keplerian orbit relationships can no longer be used. The equations of motion involve nonlinear drag terms, since air drag is a function of V^2 and atmospheric density, ρ, and ρ is a complicated function of altitude.

These nonlinear differential equations cannot be reduced to an exact closed form solution with present mathematical methods. Thus, two possible solution procedures must be investigated.

(1) Closed form solutions of approximate differential equations.

(2) Numerical parametric solutions of the exact differential equations using a high speed digital computer.

1. Approximate Analytic Solutions

A multitude of approximate analytic solutions to the equations of motion has appeared in the literature during the past few years. Many of these solutions differ somewhat in their simplifying assumptions as well as in mathematical approach. Therefore, in an attempt to consider the problem with both depth and scope, two somewhat different approximate analyses are presented in detail in Subsections a and b, following; and a rather comprehensive itemization of other solutions existing in the literature, together with pertinent assumptions and limitations, is given in Subsection c.

a. First approximate method (Ref. 1)

Chapman (Ref. 1) presents an interesting approximate solution as well as a convenient approach to numerical solution of the equations of motion. Assumptions include (1) spherically symmetric planet and atmosphere, (2) exponentially varying atmospheric density, (3) negligible peripheral velocity of the planet compared to the velocity of the entering vehicle, (4) small fractional change in radial distance compared to the fractional change in velocity in a given increment of time (i.e., $|\frac{dr}{r}| \ll |\frac{du}{u}|$), (5) small component of lift in the horizontal direction compared to the drag (i.e., $|\frac{L}{D}\tan\gamma| \ll 1$) and (6) a point mass vehicle. The derivation proceeds as follows: in the absence of forces normal to the trajectory plane, the motion may be described in two dimensions by the vector acceleration.

$$\vec{a} = \left(\frac{dw}{dt} - \frac{u^2}{r}\right)\vec{e}_r + \left(\frac{du}{dt} + \frac{uw}{r}\right)\vec{e}_\phi \qquad (1)$$

where $\vec{e}_r$ and $\vec{e}_\phi$ are unit vectors in the r and ϕ directions, r is the radius vector from the planet center to the entering body, and w and u are velocity components along and normal to the instantaneous radius vector, respectively. The

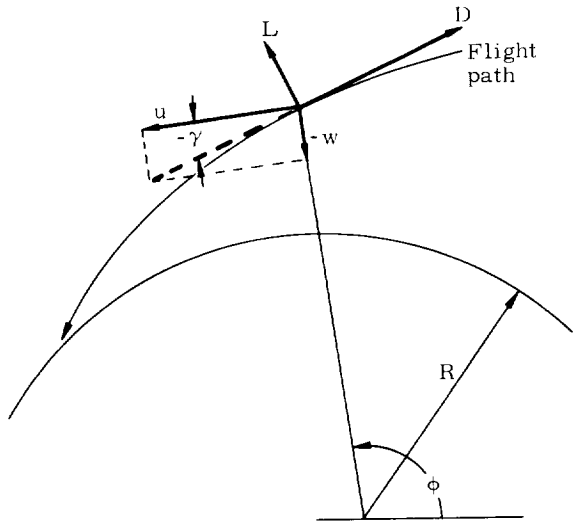

flight path angle with respect to local horizontal, γ (negative for descent) is

$$\gamma = \tan^{-1}\frac{w}{u} \qquad (2)$$

The vector force is

$$\vec{f} = (-mg + L\cos\gamma - D\sin\gamma)\,\vec{e}_r - (D\cos\gamma + L\sin\gamma)\,\vec{e}_\phi, \qquad (3)$$

so that two component equations of motion may be written from Eqs (1), (2) and (3):

$$-\frac{d^2y}{dt^2} = -\frac{dw}{dt} = g - \frac{u^2}{r} - \frac{L}{m}\cos\gamma + \frac{D}{m}\sin\gamma \qquad (4)$$

$$\frac{du}{dt} = -\frac{uw}{r} - \frac{D}{m}\left(\cos\gamma + \frac{L}{D}\sin\gamma\right) \qquad (5)$$

Ref. (1) neglects the term $\frac{uw}{r}$ in Eq (5), which is equivalent to assumption (4),

$$\frac{|\frac{uw}{r}|}{|\frac{du}{dt}|} = \frac{u}{r}\frac{|\frac{dr}{dt}|}{|\frac{du}{dt}|} = \frac{|\frac{dr}{r}|}{|\frac{du}{u}|} \ll 1.$$

This situation is realistic only when drag is large, so that the solutions will not apply to orbit motion above the sensible atmosphere. Then, using the exponential approximation to atmospheric density,

$$\rho = \rho_0 \, e^{-\beta y}, \tag{6}$$

and assumption (5),

$$\left| \frac{L}{D} \tan \gamma \right| \ll 1,$$

Eq (5) yields

$$\frac{du}{dt} = -\frac{\rho_0 \, e^{-\beta y}}{2 \dfrac{m}{C_D A}} \frac{u^2}{\cos \gamma} \tag{7}$$

since

$$D = \frac{1}{2} \rho \, V^2 \, C_D \, A \tag{8}$$

where

V = velocity magnitude = $\sqrt{u^2 + w^2}$

C_D = drag coefficient

A = reference cross-section area of entry vehicle

The variable u may be normalized by setting

$$\bar{u} = \frac{u}{v_c} = \frac{u}{\sqrt{gr}} . \tag{9}$$

Then

$$\frac{du}{dt} = \frac{d\left(\sqrt{gr}\,\bar{u}\right)}{dt} = \sqrt{gr} \, \frac{d\bar{u}}{dt} \tag{10}$$

since, from approximation (4) and the differential of Newton's law of gravitation, $g = \dfrac{\mu}{r^2}$,

$$\frac{dg}{g} = -2 \frac{dr}{r} ,$$

derivatives of g and r may be neglected relative to derivatives of u or $\bar{u}$. From Eq (10), Eq (7) for the normalized variable becomes

$$\frac{d\bar{u}}{dt} = -B \, \rho_0 \, e^{-\beta y} \frac{\bar{u}^2}{\cos \gamma} \sqrt{gr} \tag{11}$$

where B is the ballistic coefficient, $B = \dfrac{C_D A}{2m}$. Similarly, rewriting Eq (4) using Eqs (8) and (9) gives

$$-\frac{1}{g}\frac{dw}{dt} = -\frac{1}{g}\frac{d^2y}{dt^2} = 1 - \bar{u}^2 + \rho_0 \, B \, \frac{r\bar{u}^2}{\cos^2 \gamma} e^{-\beta y} (\sin \gamma - \frac{L}{D} \cos \gamma) \tag{12}$$

Reference (1) reduces the transformed pair of motion equations, Eqs (11) and (12), to a single equation by transforming to a dimensionless dependent variable z defined by

$$z \equiv \rho_0 \, B \sqrt{\frac{r}{\beta}} \, u \, e^{-\beta y} \tag{13}$$

Then, with assumption (4),

$$\frac{1}{\bar{u}} \frac{dz}{d\bar{u}} - \frac{z}{\bar{u}^2} = -\rho_0 \, B \sqrt{r\beta} \, e^{-\beta y} \frac{dy}{du}$$

$$= -\beta \frac{z}{\bar{u}} \frac{dy}{dt} \frac{dt}{d\bar{u}} . \tag{14}$$

But, from Eq (11),

$$\frac{d\bar{u}}{dt} = -\sqrt{g\beta} \, \frac{\bar{u} z}{\cos \gamma} \tag{15}$$

and

$$\frac{dy}{dt} = w = \bar{u} \sqrt{gr} \tan \gamma$$

so that Eq (14) becomes

$$\frac{dz}{d\bar{u}} - \frac{z}{\bar{u}} = \sqrt{\frac{\beta}{g}} \frac{\cos \gamma}{\bar{u}} \frac{dy}{dt} = \sqrt{\beta r} \sin \gamma. \tag{16}$$

Then

$$\frac{1}{g}\frac{dw}{dt} = \sqrt{\frac{r}{g}} \frac{d}{dt}\left(\frac{\bar{u} \sin \gamma}{\cos \gamma}\right) = \frac{1}{\sqrt{\beta g}} \frac{d\bar{u}}{dt}\left(\frac{u}{\cos \gamma} \frac{d^2 z}{du^2} + \frac{\bar{u}\sqrt{\beta r} \, \sin^2 \gamma}{\cos^2 \gamma} \frac{d\gamma}{d\bar{u}}\right) \tag{17}$$

and

$$\bar{u} \frac{d}{d\bar{u}}\left(\frac{dz}{d\bar{u}} - \frac{z}{\bar{u}}\right) = \bar{u}\sqrt{\beta r} \, \frac{d}{d\bar{u}} (\sin \gamma)$$

$$= \bar{u} \frac{d^2 z}{d\bar{u}^2} - \frac{dz}{d\bar{u}} + \frac{z}{\bar{u}} \tag{18}$$

$$= \bar{u} \frac{d^2 z}{d\bar{u}^2} - \sqrt{\beta r} \sin \gamma.$$

From the first form of Eq (18), Eq (15) and Eq (17),

$$-\frac{1}{g}\frac{dw}{dt} = -\frac{1}{g}\frac{d^2 y}{dt^2} = \frac{\bar{u} z}{\cos^2 \gamma} \left[\left[\bar{u} \frac{d^2 z}{d\bar{u}^2} + \tan^2 \gamma \left[u \frac{d}{d\bar{u}} \left(\frac{dz}{d\bar{u}} - \frac{z}{\bar{u}} \right) \right] \right] \right] \tag{19}$$

and from Eqs (12), (13) and (16),

$$-\frac{1}{g}\frac{dw}{dt} = -\frac{1}{g}\frac{d^2 y}{dt^2} = 1 - \bar{u}^2 + \frac{\bar{u} z}{\cos^2 \gamma} \left(\frac{dz}{dt} - \frac{z}{\bar{u}} - \sqrt{\beta r} \, \frac{L}{D} \cos \gamma \right) \tag{20}$$

A comparison of Eqs (19) and (20) gives the final equation to be solved.

$$u \frac{d}{d\bar{u}}\left(\frac{dz}{d\bar{u}} - \frac{z}{\bar{u}} \right) - \frac{1 - \bar{u}^2}{uz} \cos^4 \gamma$$

$$\sqrt{\beta r}\, \frac{L}{D} \cos^3 \gamma = 0 \qquad (21)$$

where

$$\sqrt{\beta r} \sin \gamma = \frac{dz}{d\bar{u}} - \frac{z}{\bar{u}}$$

Consequently, the pair of component motion equations, Eqs (4) and (5), has been reduced to a single second order differential equation by transforming to the dependent variable z and the independent variable $\bar{u}$, subject to the assumptions noted.

The nonlinear differential Eq (21) may be solved by numerical integration; since Eq (21) depends only on the ratio of lift and drag coefficients, numerical solution of this equation has certain advantages over straightforward integration of the two component equations of motion, which depend on both coefficients. Alternatively, Eq (21) may be used to generate various approximate solutions.

(1) Approximation for straight line trajectories and ballistic vehicles

For the case of entry of a ballistic vehicle along a spiral path characterized by a constant flight path angle with respect to local horizontal $\bar{\gamma}$, Eq (18) gives

$$\frac{d}{d\bar{u}} (\sin \gamma) = 0 = \bar{u} z_1'' - \sqrt{\beta r} \sin \bar{\gamma} \qquad (22)$$

where z_1 is the z function defined by Eq (13) for this special case. Successive integration of Eq (22) yields, for initial conditions $\bar{u} = \bar{u}_0$, $z = 0$ (entry from high altitudes),

$$z_1' = \sqrt{\beta r} \sin \bar{\gamma} \ln \bar{u} + \text{costant}$$

and

$$\frac{z_1}{\bar{u} \sqrt{\beta r} \sin \bar{\gamma}} = \ln \frac{\bar{u}}{\bar{u}_0} = B \frac{\rho_0 e^{-\beta y}}{\beta \sin \bar{\gamma}} \qquad (23)$$

This solution is applicable in either of two circumstances: (1) the rather impractical case in which lift is programmed to maintain a constant flight path angle, or (2) the case of ballistic vehicles entering at such steep flight path angles that the difference of gravitational and centrifugal forces is small compared to the vertical component of drag force, so that the trajectory is essentially a straight line. This latter situation is that considered in Ref. 2, and Eq (23) is the solution obtained in that reference.

(2) Approximation for gliding vehicles

For the case of small entry angles ($|\sin \gamma| \approx |\gamma| << \frac{L}{D}$ and $\cos \gamma \approx 1$) with large $\frac{L}{D}$ and gliding hypersonic flight ($\bar{u} \approx 1$), the basic differential equation, Eq (21), gives the approximate solution

$$z_2 = \frac{1 - \bar{u}^2}{\bar{u} \sqrt{\beta r}\, \frac{L}{D}} \qquad (24)$$

which is the same as the gliding flight solution given by Ref. 3 and considered in Ref. 4.

(3) Approximation for a skipping vehicle

For the case in which the difference in gravitational and centrifugal forces, i.e., the term

$$\frac{1 - \bar{u}^2}{\bar{u} z} \cos^4 \gamma$$

of the basic equation, Eq (21), is relatively small, as for a skipping vehicle, Ref. 1 provides an approximate solution.

$$\frac{z_3}{\bar{u}} = \frac{z_0}{\bar{u}_0} + \sqrt{\beta r} \left[\sin \gamma_0 \ln \frac{\bar{u}}{\bar{u}_0} - \frac{\cos^3 \gamma_{av}}{2} \frac{L}{D} \ln^2 \frac{\bar{u}}{\bar{u}_0} \right] \qquad (25)$$

with

$$\sin \gamma = \sin \gamma_0 - \left(\cos^3 \gamma_{av} \right) \frac{L}{D} \ln \frac{\bar{u}}{\bar{u}_0} \qquad (26)$$

For $\frac{L}{D} = 0$ these equations reduce to Eq (23).

b. Second approximate method (Ref. 5)

Wang and Ting (Ref. 5) derive approximate solutions from the equations of motion expressed in the form of tangential and normal components.

$$\frac{dv}{dt} = - \frac{D}{m} - g \sin \gamma \qquad (27)$$

$$\frac{v d\gamma}{dt} = \frac{L}{m} - \left(g - \frac{v^2}{r} \right) \cos \gamma \qquad (28)$$

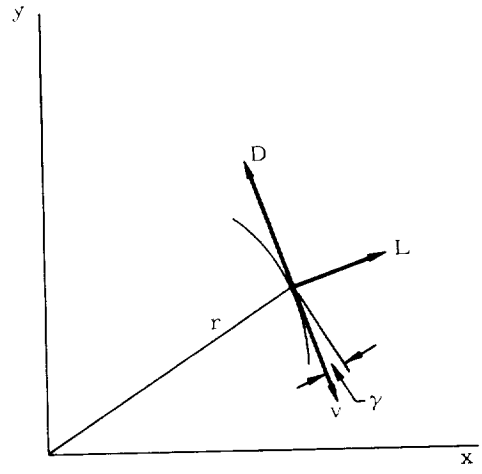

where

v = vehicle velocity magnitude

$D = \frac{1}{2}\rho v^2 C_D A$

= drag force

$L = \frac{1}{2}\rho v^2 C_L A$ (29)

= lift force

g = acceleration due to gravity

r = radial distance of vehicle from the center of the earth

m = mass of vehicle

γ = local flight path angle, positive for ascent

Since this formulation differs from that of Ref. 1 and provides somewhat more accurate approximate solutions, the derivation will be presented in some detail for reference. Assumptions, although noted in the derivation, are collected for convenience in the following list.

(1) The earth and its atmosphere are spherically symmetric.

(2) The atmospheric density varies exponentially.

(3) The atmosphere does not rotate.

(4) $\cos\gamma \approx \gamma_e$. For grazing entry, the local flight path angle is always small so that $\cos\gamma \approx 1$ and can be approximated by $\cos\gamma_e$. For steep entry, the flight path angle does not change greatly from the entry value, and the approximation is again valid.

(5) The aerodynamic coefficients C_L and C_D are assumed constant in the given solutions. (An extension does not require this assumption.)

(6) Although γ is not assumed to be very small, accuracy deteriorates because of series truncation assuming $1 - \cos\gamma \approx \gamma^3$. For reasonable accuracies, $\gamma < 60°$.

(7) The vehicle is considered as a point mass.

With the assumption of exponential atmospheric density, Eq (6) takes the form

$$\rho = \rho_0 e^{-\beta h}$$

$$\frac{d\rho}{dt} = -\beta\rho\frac{dh}{dt} = -\beta\rho v\sin\gamma$$

and from Eqs (8) and (29), Eqs (27) and (28) become

$$\frac{dv}{v} = -\frac{C_D A}{2m\beta\sin\gamma}d\rho + \frac{g}{\beta\rho v^2}d\rho \qquad (30)$$

$$\sin\gamma\, d\gamma = -\frac{C_L A}{2m\beta}d\rho - \left(\frac{1}{r} - \frac{g}{v^2}\right)\frac{\cos\gamma_e}{\beta\rho}d\rho \qquad (31)$$

where the approximation $\cos\gamma \approx \cos\gamma_e$ has been made in Eq (31). The limitations imposed by this approximation are noted in the previous list of assumptions, Assumption (4). The quantities in parenthesis in Eq (31) represent the centrifugal and gravitational forces and are sometimes neglected in approximate solutions if entry velocities may be assumed close to circular orbit velocity. Reference 5 obtains a higher order solution by approximating the velocity in the centrifugal force term by the velocity-density relation given in Ref. 6,

$$\ln\frac{v}{v_e} = \frac{B}{\beta\sin\gamma_e}(\rho - \rho_e) \qquad (32)$$

where

$$B = \frac{C_D A}{2m}$$

Then, expanding the centrifugal force term in series,

$$\frac{g}{v^2} = \frac{g}{v_e^2}\left[1 + C_1\ln\frac{v}{v_e} + C_2\ln^2\frac{v}{v_e} + \dots\right]$$

$$\approx \frac{g}{v_e^2}\left[1 + \frac{C_1 B}{\beta\sin\gamma_e}(\rho - \rho_e) + C_2\left(\frac{B}{\beta\sin\gamma_e}\right)^2(\rho - \rho_e)^2\right] \qquad (33)$$

where C_1 and C_2 are constant coefficients which can be determined by collocation. Substitution of Eq (33) in Eq (31) and integration gives, for constant C_L,

$$\cos\gamma = \cos\gamma_e + B_1(\rho - \rho_e) + B_2\ln\frac{\rho}{\rho_e} + B_3 f_1(\rho) \qquad (34)$$

where

$$B_1 = \frac{C_L A}{2m\beta},\quad B_2 = \frac{\cos\gamma_e}{\beta r},\quad B_3 = -\frac{g\cos\gamma_e}{\beta v_e^2}$$

$$f_1(\rho) = \left[(1 + B_4C_1 + B_4^2C_2)\ln\frac{\rho}{\rho_e} - (B_4C_1 + 2B_4^2C_2)\frac{\rho - \rho_e}{\rho_e} + \frac{1}{2}B_4^2C_2\left(\frac{\rho^2 - \rho_e^2}{\rho_e^2}\right)\right]$$

$$B_4 = -\frac{B\rho_e}{\beta\sin\gamma_e}$$

For constant C_D integration of Eq (30) proceeds as

$$\ln \frac{v_e}{v} = -\frac{B}{\beta}\int_{\rho_e}^{\rho} \frac{d\rho}{\sin\gamma} - \frac{g}{\beta}\int_{\rho_e}^{\rho} \frac{d\rho}{\rho v^2} \qquad (35)$$

Evaluation of the integrals is facilitated by the following expansions.

$$\frac{1}{\sin\gamma} \approx \frac{1}{\gamma - \frac{1}{6}\gamma^3} \approx \frac{1}{\gamma} + \frac{\gamma}{6}, \qquad 1 >> \gamma^4 \qquad (36)$$

or

$$\frac{1}{\sin\gamma} = \frac{1}{\sin\left[\gamma_e - (\gamma_e - \gamma)\right]} \approx \frac{1}{\sin\gamma_e - (\gamma_e - \gamma)\cos\gamma_e}$$

$$\approx \frac{1}{\sin\gamma_e} + \frac{\cos\gamma_e}{\sin^2\gamma_e}(\gamma_e - \gamma), \qquad (37)$$

$$\gamma > \frac{\pi}{4}, \quad 1 >> (\gamma - \gamma_c)$$

Also, $\cos\gamma \approx 1 - \frac{\gamma^2}{2}$ in Eq 34. Then integration of Eq (35) gives the following solutions:

Case I. K_2 positive, $\gamma_e < 45°$

$$\ln \frac{v_e}{v} = \frac{B_3}{\cos\gamma_e} f_1(\rho) + \frac{B_5}{\sqrt{K_2}} f_2(\rho) + f_3(\rho) \qquad (38)$$

where

$$B_5 = \frac{B}{\beta}\left[1 + \frac{4K_2\bar{\gamma}^2 - K_1^2}{48K_2}\right]$$

$$f_2(\rho) = \rho\ell n\left\{\left[K_1 + 2(1-\sigma)K_2 + 2\left[K_2\bar{\gamma}^2 + (K_1 + K_2 - \sigma K_2)(1-\sigma)K_2\right]^{1/2}\right]\cdot\left[-2\sqrt{K_2}\,\bar{\gamma} + K_1\right]^{-1}\right\}$$

$$f_3(\rho) = \frac{B\rho}{24\beta K_2}\left\{\left[2K_2(1-\sigma) + K_1\right]\left[\bar{\gamma}^2 + K_1(1-\sigma) + K_2(1-\sigma)^2\right]^{1/2} + K_1\bar{\gamma}\right\}$$

$$\bar{\gamma}^2 = \gamma_e^2 - \left[2B_1 - \frac{2C_1B_3B_4}{\rho_e} + C_2B_3B_4^2\frac{(\rho - 3\rho_e)}{\rho_e^2}\right](\rho - \rho_e) - 2\left[B_3 + B_2 + C_1B_3B_4 + C_2B_3B_4^2\right]\ln\frac{\rho}{\rho_e}$$

$$K_1 = 2\left[B_1\rho + B_3 + B_2 - C_1B_3B_4\frac{(\rho - \rho_e)}{\rho_e} + C_2B_3B_4^2\frac{(\rho - \rho_e)^2}{\rho_e^2}\right]$$

$$\sigma = \frac{\rho_e}{\rho}$$

$$K_2 = B_3 + B_2 + C_1B_3B_4 - C_2B_3B_4^2\frac{(\rho^2 - \rho_e^2)}{\rho_e^2}$$

Case II. K_2 negative, $\gamma_e < 45°$

$$\ln \frac{v_e}{v} = \frac{B_3}{\cos\gamma_e} f_1(\rho) + \frac{B_5}{\sqrt{-K_2}} f_4(\rho) + f_3(\rho) \qquad (39)$$

where

$$f_4(\rho) = \rho\left[\sin^{-1}\frac{K_1}{\sqrt{K_1^2 - 4K_2\bar{\gamma}^2}} - \sin^{-1}\frac{K_1 + 2(1-\sigma)K_2}{\sqrt{K_1^2 - 4K_2\bar{\gamma}^2}}\right]$$

Case III. K_2 positive, $\gamma_e > 45°$

$$\ln \frac{v_e}{v} = \left(\frac{-1}{\sin\gamma_e} + \frac{\gamma_e\cos\gamma_e}{\sin^2\gamma_e}\right)\frac{B}{\beta}(\rho - \rho_e) - \frac{B_6}{\sqrt{K_2}} f_2(\rho) - 6f_3(\rho) \qquad (40)$$

where

$$B_6 = \frac{B\cos\gamma_e(4K_2\bar{\gamma}^2 - K_1^2)}{8\beta\sin^2\gamma_e K_2}$$

Case IV. K_2 negative, $\gamma_e > 45°$

$$\ln \frac{v_e}{v} = \left(\frac{-1}{\sin\gamma_e} + \frac{\gamma_e\cos\gamma_e}{\sin^2\gamma_e}\right)\frac{B}{\beta}(\rho - \rho_e) - \frac{B_6}{\sqrt{-K_2}} f_4(\rho) - 6f_3(\rho) \qquad (41)$$

These solutions can be used to determine the velocity at any point between entry and minimum γ.

c. Other approximate analytic solutions

The following list of approximate analytic solutions has been collected, along with pertinent assumptions and limitations for reference convenience.

(1) Reference (7)

Assumptions. (1) spherically symmetric earth and atmosphere, (2) exponential atmospheric density, (3) nonrotating atmosphere, (4) constant gravitational attraction, (5) ballistic entry

(6) the quantity $\frac{1}{\beta R}\ \frac{\cos\gamma}{\rho}\left(\frac{gR}{v^2}-1\right)$ is considered constant in integration over ρ or γ, and (7) point mass

Solution.

$$\cos\gamma = \frac{\cos\gamma_e}{1+\frac{1}{\beta R}\left(\frac{gR}{v^2}-1\right)\left(1-\frac{\rho_e}{\rho}\right)} \tag{42}$$

$$\left(\frac{v}{v_e}\right)^2 = \left(\frac{4}{\beta R}\right)\left(\frac{gR}{v_e^2}\right) F(\gamma) + \left[\left[\left(1-\frac{4}{\beta R}\right)\left(\frac{gR}{v_e^2}\right) F(\gamma_e) \exp\left[\frac{-R C_D A (\gamma_e-\gamma)\rho}{m\cos\gamma\left(\frac{gR}{v^2}-1\right)}\right]\right]\right] \tag{43}$$

where

$$F(\gamma) \equiv \left[\ln\left(\frac{-\gamma}{2}\right) - C_1\gamma + \frac{1}{4}(C_1\gamma)^2 - \frac{1}{18}(C_1\gamma)^3\right] e^{C_1\gamma} + \left[\frac{(C_1\gamma)^3}{720 C_1^4} + \frac{(C_1\gamma)^2}{240 C_1^4} + \left(\frac{1}{120 C_1^4}+\frac{1}{12 C_1^2}\right)C_1\gamma + \left(\frac{1}{120 C_1^4}+\frac{1}{12 C_1^2}\right)\right] \text{(for } \gamma \text{ small)}$$

or

$$F(\gamma) \equiv -C_2\left[C_1\sin\gamma+\cos\gamma\right] - C_3\left[\frac{1}{2}C_1\sin 2\gamma + \cos 2\gamma\right] + C_4\sin^2\gamma\,(C_1\sin\gamma + 3\cos\gamma)$$

(for γ large)

$$C_1 = \left[\frac{\cos\gamma_m}{\rho_m R}\ \frac{m}{C_D A}\left(\frac{gR}{v_m^2}-1\right)\right]^{-1}$$

where m designates a reference point

$$C_2 = \frac{1}{2}\left[\frac{1}{\cos\gamma_e} + \frac{1}{\cos^2\gamma_e}(C_1^2+9) - 6\left(\frac{1}{\cos^3\gamma_e}\right)\right]\left[(C_1^2+1)(C_1^2+9)\right]^{-1}$$

$$C_3 = \frac{1}{2}\left[\cos^2\gamma_e\,(C_1^2+4)\right]^{-1}$$

$$C_4 = \frac{1}{2}\left[\cos^3\gamma_e\,(C_1^2+9)\right]^{-1}$$

Special Cases.

(i) For $\beta R > 200$ and $\gamma < 45°$ ($\beta R \approx 900$ for earth)

$$\left(\frac{v}{v_e}\right)^2 = \exp\left[\frac{C_D A}{m} R \left(\frac{\gamma-\gamma_e}{\cos\gamma}\right)\left(\frac{gR}{v^2}-1\right)\right]^{-1} \tag{44}$$

(ii) For constant γ (from Eq (42), this occurs for ρ small or close to ρ_e or for v large or close to gR). Then,

$$\cos\gamma = \cos\gamma_e \tag{45}$$

$$\left(\frac{v}{v_e}\right)^2 = \exp\left[\frac{C_D A}{m\beta}\ \frac{(\rho-\rho_e)}{\sin\gamma_e}\right] \tag{46}$$

(Compare with Eq (23).)

(2) Reference (8)

Assumptions. (1) spherically symmetric earth and atmosphere, (2) exponential atmospheric density, (3) nonrotating atmosphere, (4) small γ ($\sin\gamma \approx \gamma$ and $\cos\gamma \approx 1$) and the component of g along the flight path angle is small, (5) constant C_L and C_D, (6) constant gravity and constant $\frac{1}{r}$ over range of re-entry, (7) point mass.

Solution.

$$v^2 = \bar{v}^2 - 2\sqrt{\frac{g}{r}}(h-h_e) \tag{47}$$

where

$$\bar{v} = \frac{\bar{v}}{\bar{v}_1}\ \frac{\bar{v}_1}{v_e}\ v_e$$

$$\frac{v_1}{v_e} = \exp\left(-\frac{\gamma-\gamma_e}{\frac{L}{D}}\right)$$

$$\frac{\bar{v}}{\bar{v}_1} = \exp\left[\left[\frac{-4g\,e^{\phi_e}}{v_e^2\left(\frac{L}{D}\right)^2\beta}\left\{\left[\frac{v_e^2}{gr}\,e^{-\phi_e} - \left(1+\frac{k^2}{2}\right)\right]\frac{1}{2k}\left[\ell n\frac{k+\phi}{k+\phi_e} - \ell n\frac{k-\phi}{k-\phi_e}\right] - \frac{1}{2}\left(1+\frac{k^2}{6}\right)\left[\ell n\frac{k+\phi}{k+\phi_e} + \ell n\frac{k-\phi}{k-\phi_e}\right] - \frac{1}{2}(\phi_e-\phi) + \frac{1}{12}\left(\phi_e^2-\phi^2\right)\right\}\right]\right]$$

$$k^2 = \frac{8 K_D}{\beta r \frac{L}{D}} \left[e^{-\beta h_e} + \frac{\beta r \gamma_e^2}{2 \frac{L}{D} K_0} \right]$$

$$\phi = - \frac{2\gamma}{\frac{L}{D}}$$

$$K_D = \frac{C_D A \rho_0 r}{2m}$$

(3) Reference (9)

Assumptions. (1) spherically symmetric earth and atmosphere, (2) exponential atmospheric density, (3) nonrotating atmosphere, (4) γ is small, (5) constant aerodynamic coefficients C_L and C_D (6) $v \approx v_e$ in the gravitation term of the force equation $\frac{v^2}{r} \cos \gamma$, (7) constant r over the range of integration, (8) constant g, (9) point mass.

Solution.

$$\gamma^2 = \gamma_e^2 - \frac{C_L A}{m\beta} (\rho - \rho_e) - \left[\frac{2}{r\beta} - \frac{2}{\beta v_e^2} \right] \ln \frac{\rho}{\rho_e} \tag{48}$$

$$\ln \frac{v_e}{v_m} = \frac{C_D A}{2m\beta\sqrt{C}} \ln \left[\frac{\sqrt{a + b\rho_m + C\rho_m^2} + \sqrt{C}\rho_m + \frac{\beta}{2\sqrt{C}}}{\sqrt{a + b\rho_e + C\rho_e^2} + \sqrt{C}\rho_e + \frac{\beta}{2\sqrt{C}}} \right] \tag{49}$$

where

$$a = \gamma_e^2 - \left[\frac{1}{r\beta} - \frac{g}{\beta v_e^2} \right] \left[2 \ln \frac{\rho_m}{\rho_e} - 3 \right] + \frac{C_L A}{m\beta} \rho_e$$

$$b = - \left[\frac{C_L A}{m\beta} + \frac{4}{\rho_m} \left(\frac{1}{r\beta} - \frac{g}{\beta v_e^2} \right) \right]$$

$$C = \frac{1}{\rho_m^2} \left(\frac{1}{r\beta} - \frac{g}{\beta v_e^2} \right)$$

and the subscripts e and m signify values at entry and at peak acceleration or minimum flight path angle, respectively.

(4) Reference (2)

See Eq (23).

(5) Reference (10)

See Eq (46) or (23).

(6) Reference (11)

Assumptions. (1) spherically symmetric earth and atmosphere, (2) exponential atmospheric density, (3) point mass, (4) $1 - \frac{v^2}{gr} \approx 0$ in the equations of motion, (5) $\sin \gamma << \frac{\rho v^2 C_D A}{2 mg}$ (i.e., the component of gravity along the flight path is negligible compared to the aerodynamic drag load, (6) constant $\frac{C_L}{C_D}$.

Solution.

$$\frac{v}{v_e} = \exp \left[- \frac{C_D}{C_L} (\gamma - \gamma_e) \right] \tag{50}$$

$$(\rho - \rho_e) = 2\beta \frac{m}{C_D A} \frac{C_D}{C_L} (\cos \gamma - \cos \gamma_e) \left(\text{for constant } \frac{C_L A}{m} \right) \tag{51}$$

or

$$\rho = \rho_e + \beta \frac{m}{C_D A} \frac{C_D}{C_L} (\gamma_e^2 - \gamma^2) \quad 1 >> \gamma^3$$

2. Numerical Solutions and Graphical Presentations

Since the equations of motion for entry (Eqs (4) and (5), or Eq (21), or Eqs (27) and (28)) cannot be solved analytically without use of simplifying assumptions, numerical integration offers the only means of highly accurate computation of general trajectories. Many techniques are possible in numerical solution, depending on the chosen formulation of the equations of motion and on the method of numerical integration used. Three formulations of the equations of motion are given in Eqs (4) and (5), Eq (21), and Eqs (27) and (28), and various numerical integration techniques are discussed in Chapter IV. In general, selection of a formulation and integration technique must be based upon the nature of the particular entry mission. However, it should be noted that Eq (21), although not completely exact, has an advantage in that only ratios of lift and drag coefficients are involved.

Consideration of numerical entry analyses will be limited to presentation of the solutions and will not consider the methods. The solutions are of interest for two reasons:

(1) Comparison of the numerical solutions with the results of approximate analytic analyses provides a check on the validity of these analytic solutions.

(2) The numerical solutions, presented in the form of parametric graphs, are useful in making preliminary design estimates.

Reference 1 provides various solutions determined numerically from the entry problem formulation of Section B.1.a. For entry of ballistic vehicle from a decaying orbit ($\gamma_e = 0°$, $\bar{u}_0 = 1$), Eq (2) reduces to

$$\bar{u}\frac{d}{d\bar{u}}\left[\frac{dz}{d\bar{u}} - \frac{z}{\bar{u}}\right] - \frac{1-\bar{u}^2}{\bar{u}z} + \sqrt{\beta r}\,\frac{L}{D} = 0 \qquad (52)$$

$$z_0 = 0,\ z_0' = 0$$

The solution of this equation, which has to be evaluated only once for each value of $\sqrt{\beta r}\,\frac{L}{D}$ is plotted in Fig. 1a for nonlifting vehicles and in Fig. 1b for lifting vehicles. It should be noted that in the case of circular decay, the lifting vehicle does not "skip," but follows a smooth equilibrium glide trajectory. For nonlifting vehicles entering from circular velocities and nonzero entry angles ($\bar{u}_0 = 1$, $\gamma_0 < 0$), Eq (21) reduces to

$$\bar{u}\frac{d}{d\bar{u}}\left[\frac{dz}{d\bar{u}} - \frac{z}{\bar{u}}\right] - \frac{1-\bar{u}^2}{\bar{u}z}\cos^4\gamma = 0 \qquad (53)$$

The z functions for this case are plotted in Fig. 2a. With lift and $\bar{u}_0 = 1$, $\gamma_0 < 0$, Eq (52) applies with $z_0 = 0$ and $Z_0' = \sqrt{\beta r}\gamma_0$. Solutions for this case are plotted in Figs. 2b through 2e. All exhibit severe skips except when $\gamma_0 = 0$.

In Fig. 3 the theoretical solutions for the atmospheric braking of ballistic vehicles entering at escape speeds are shown for different values of maximum deceleration during the first pass. The parameters used are $(30\bar{u}\,\mathbf{z})_{\text{first max.}}$ which correspond to the altitudes of deepest penetration during the first pass. Figure 3 shows, for example, that if $(30\bar{u}\,\mathbf{z})_{\text{first max.}} = 0.46$, then entry is completed on the seventh pass.

Figure 4 represents a numerical integration run on the IBM 704 digital computer, considering natural decay from a near-circular orbit. Velocity and flight path angle variations are given as functions of geometrical altitude above the sea level. Superimposed are the results obtained from the analytical solution given in Fig. 1a and the corresponding flight path angles given in Table 1. Correlation is seen to be good, justifying the approximations made in Ref. 1. [Table 1 also gives the ranges in terms of earth radii and the flight times from the initial re-entry altitude.]

Figures 5a to 5e show the velocity-altitude profiles for ballistic re-entry, as obtained by numerical integrations of the exact equations of motion. Using the ballistic coefficient (B) as a constant parameter, parametric trajectory curves are given for initial flight path angles of -1°, -2°, -3°, -5° and -10° for an initial velocity of 25,000 fps (7620 mps) and an initial altitude of 300,000 ft (91.4 km). It should be noted that these results also apply to any altitudes higher than 300,000 ft (91.4 km), since the drag effects above this altitude are extremely small for conventional ballistic coefficients. Interpolations between the curves can be accomplished.

In Fig. 5a the comparison with the analytical methods of Ref. 3 is presented, showing that for B = 0.5 to 5.0 ft^2/slug (0.00318 to 0.0318 m^2/kg) relatively good agreement exists.

The corresponding local flight path angle versus altitude histories is shown in Figs. 6a to 6e. In Fig. 6a the comparison of analytical and numerical results is seen once more to be satisfactory for a first approximation.

Characteristic re-entry altitude-velocity profiles for lifting vehicles with L/D = 1 and L/D = 3 are indicated in Fig. 7 for an initial re-entry flight path angle of -10°.

Figures 8a, 8b and 8c present the peak altitudes of first skip for lifting re-entry vehicles in parametric form for L/D = 0.5 to 3.0.

Figure 9a compares the velocity-altitude profiles for various re-entry vehicles, both ballistic and lifting type. The severity of skips increases with increasing lift-to-drag ratios and atmospheric effects become significant at much higher altitudes in the case of lifting bodies, as compared to simple ballistic vehicles.

Figure 9b investigates the effects of variable entry velocities on the velocity-altitude profiles of a lifting body with L/D = 0.5. It should be noticed that a definite "skip envelope" exists for all entries regardless of the initial velocity and basically the same trajectories are reached at 100,000 ft (30.48 km) altitude.

The initial flight path angle produces somewhat larger deviations between the members of the same trajectory family as indicated in Fig. 9c.

The effects of programmed C_L on velocity-altitude profile are shown in Fig. 9d. The corresponding programs of C_L as functions of Mach number are given in Fig. 9e.

It should be noted that considerable variations in the lift coefficient are required for a relatively smooth trajectory and even small deviations from the desired lift coefficent program result in a pronounced phugoid motion of the vehicle.

Figure 10a presents the terminal velocities as a function of L/D for various parametric values $\frac{W}{C_D A}$, While Fig. 10b gives terminal flight path angles for lifting vehicles.

A comparison between the trajectories of ballistic, lifting and winged bodies is given in Fig. 11a. Further comparisons of velocities, flight path angles, dynamic pressures, accelerations and nose temperatures for the above three

TABLE I

Values of z Functions and Related Quantities for $\frac{L_1}{D} = 0$ and $\bar{U}_0 = 1$ (Ref. 1)

$\bar{V}_1 = 1.0$ $\sqrt{(Br)_e}L/D = 0$

.00 DEG.

$\bar{U}$	Z	G	Y DEG.	$\bar{Q}$	S	T
.999	.00005	.00	-.15	.000	.000	.0
.995	.00058	.02	-.33	.275	.716	581.4
.990	.00163	.05	-.47	.431	.886	720.1
.985	.00299	.09	-.58	.535	.961	781.7
.980	.00461	.14	-.67	.614	1.006	818.6
.970	.00846	.25	-.82	.736	1.059	862.7
.960	.01301	.37	-.96	.828	1.091	889.3
.950	.01817	.52	-1.07	.903	1.112	907.6
.900	.05116	1.38	-1.56	1.154	1.166	954.5
.850	.09348	2.39	-1.98	1.309	1.190	976.6
.800	.14306	3.44	-2.36	1.419	1.205	990.7
.750	.19860	4.48	-2.73	1.503	1.214	1001.0
.700	.25915	5.46	-3.11	1.568	1.222	1009.2
.650	.32387	6.34	-3.50	1.619	1.228	1016.1
.600	.39203	7.09	-3.91	1.661	1.232	1022.1
.550	.46290	7.68	-4.36	1.694	1.236	1027.6
.500	.53570	8.09	-4.86	1.722	1.239	1032.7
.450	.60958	8.30	-5.43	1.743	1.242	1037.7
.400	.68355	8.30	-6.09	1.761	1.245	1042.6
.350	.75637	8.06	-6.89	1.775	1.247	1047.5
.300	.82646	7.58	-7.89	1.785	1.249	1052.8
.250	.89161	6.86	-9.21	1.793	1.251	1058.4
.200	.94852	5.91	-11.08	1.799	1.253	1064.9
.150	.99158	4.74	-14.03	1.803	1.255	1072.6
.100	1.00892	3.41	-19.50	1.805	1.256	1083.1
.050	.95725	2.05	-33.16	1.806	1.258	1100.0

-.50 DEG.

$\bar{U}$	Z	G	Y DEG.	$\bar{Q}$	S	T
.999	.00026	.01	-.50	.000	.000	.0
.995	.00137	.04	-.56	.151	.202	164.3
.990	.00291	.09	-.63	.260	.285	231.4
.985	.00462	.14	-.69	.341	.330	268.5
.980	.00648	.19	-.75	.406	.360	293.5
.970	.01065	.31	-.87	.512	.400	326.7
.960	.01536	.44	-.98	.595	.426	348.5
.950	.02058	.59	-1.08	.665	.445	364.4
.900	.05309	1.43	-1.54	.907	.495	407.8
.850	.09449	2.41	-1.94	1.060	.518	429.4
.800	.14308	3.44	-2.32	1.170	.532	443.4
.750	.19769	4.46	-2.69	1.254	.542	453.7
.700	.25741	5.42	-3.07	1.319	.550	461.9
.650	.32144	6.29	-3.47	1.371	.555	468.9
.600	.38905	7.04	-3.88	1.412	.560	475.0
.550	.45951	7.63	-4.34	1.446	.564	480.5
.500	.53205	8.04	-4.84	1.473	.567	485.7
.450	.60583	8.25	-5.41	1.495	.570	490.7
.400	.67984	8.25	-6.07	1.513	.573	495.6
.350	.75286	8.02	-6.88	1.526	.575	500.6
.300	.82328	7.55	-7.88	1.537	.577	505.8
.250	.88890	6.84	-9.21	1.545	.579	511.5
.200	.94640	5.90	-11.09	1.551	.581	517.9
.150	.99016	4.73	-14.04	1.555	.583	525.7
.100	1.00822	3.40	-19.52	1.557	.584	536.2
.050	.95713	2.05	-33.18	1.558	.586	553.2

-1.00 DEG.

$\bar{U}$	Z	G	Y DEG.	$\bar{Q}$	S	T
.999	.00052	.02	-1.00	.000	.000	.0
.995	.00264	.08	-1.03	.107	.102	83.1
.990	.00536	.16	-1.07	.187	.146	118.5
.985	.00817	.24	-1.10	.247	.171	139.1
.980	.01105	.32	-1.14	.297	.188	153.5
.970	.01704	.50	-1.21	.379	.212	173.5
.960	.02334	.67	-1.28	.446	.229	187.5
.950	.02993	.85	-1.35	.503	.242	198.2
.900	.06704	1.81	-1.69	.711	.278	230.2
.850	.11045	2.82	-2.02	.850	.298	248.0
.800	.15943	3.83	-2.35	.953	.310	260.2
.750	.21336	4.81	-2.69	1.033	.319	269.6
.700	.27166	5.72	-3.05	1.096	.326	277.4
.650	.33380	6.53	-3.42	1.146	.332	284.0
.600	.39921	7.22	-3.83	1.188	.336	289.9
.550	.46731	7.75	-4.27	1.221	.340	295.3
.500	.53744	8.12	-4.77	1.248	.343	300.4
.450	.60886	8.29	-5.33	1.270	.346	305.3
.400	.68066	8.26	-6.00	1.287	.349	310.3
.350	.75170	8.01	-6.80	1.301	.351	315.3
.300	.82048	7.52	-7.81	1.312	.353	320.5
.250	.88491	6.81	-9.14	1.320	.355	326.2
.200	.94177	5.87	-11.03	1.325	.357	332.7
.150	.98559	4.71	-14.00	1.329	.359	340.5
.100	1.00458	3.39	-19.50	1.332	.360	351.0
.050	.95536	2.05	-33.19	1.333	.362	368.0

-1.50 DEG.

$\bar{U}$	Z	G	Y DEG.	$\bar{Q}$	S	T
.999	.00078	.02	-1.50	.000	.000	.0
.995	.00394	.12	-1.52	.088	.068	55.5
.990	.00792	.24	-1.54	.153	.098	79.4
.985	.01195	.35	-1.57	.203	.115	93.3
.980	.01602	.47	-1.59	.244	.127	103.2
.970	.02428	.71	-1.64	.312	.143	117.2
.960	.03272	.94	-1.69	.369	.155	127.1
.950	.04132	1.18	-1.74	.417	.164	134.7
.900	.08677	2.35	-2.00	.597	.192	158.6
.850	.13605	3.47	-2.26	.721	.207	172.7
.800	.18889	4.54	-2.53	.815	.217	182.8
.750	.24501	5.53	-2.83	.888	.225	190.9
.700	.30408	6.40	-3.14	.948	.231	197.7
.650	.36579	7.16	-3.48	.996	.236	203.7
.600	.42976	7.77	-3.85	1.035	.240	209.1
.550	.49558	8.22	-4.27	1.068	.244	214.2
.500	.56274	8.50	-4.74	1.094	.247	219.0
.450	.63065	8.59	-5.28	1.115	.250	223.8
.400	.69854	8.47	-5.93	1.132	.252	228.5
.350	.76543	8.15	-6.71	1.146	.254	233.4
.300	.82999	7.61	-7.71	1.157	.257	238.6
.250	.89031	6.85	-9.03	1.165	.258	244.3
.200	.94346	5.87	-10.91	1.170	.260	250.7
.150	.98432	4.70	-13.89	1.174	.262	258.6
.100	1.00164	3.38	-19.41	1.177	.264	269.1
.050	.95288	2.04	-33.16	1.178	.265	286.2

TABLE 1 (continued)

$\bar{V}_1 = 1.0$ $\sqrt{(\beta r)_\oplus} L/D = 0$

			Y			
			-2.00 DEG.			
$\bar{U}$	Z	G	DEG.	$\bar{Q}$	S	T
.998	.00109	.03	-2.00	.000	.000	.0
.995	.00419	.13	-2.02	.062	.044	35.9
.990	.00946	.28	-2.04	.123	.070	56.9
.985	.01476	.44	-2.06	.168	.084	68.4
.980	.02009	.59	-2.08	.205	.094	76.3
.970	.03080	.90	-2.12	.266	.107	87.4
.960	.04161	1.20	-2.16	.316	.116	95.1
.950	.05250	1.50	-2.19	.359	.123	101.2
.900	.10818	2.93	-2.40	.519	.145	120.1
.850	.16579	4.24	-2.61	.631	.157	131.5
.800	.22515	5.42	-2.84	.716	.166	139.9
.750	.28608	6.46	-3.08	.784	.172	146.8
.700	.34838	7.34	-3.36	.839	.178	152.6
.650	.41183	8.06	-3.65	.884	.182	157.9
.600	.47615	8.61	-3.99	.921	.186	162.8
.550	.54101	8.98	-4.37	.952	.189	167.4
.500	.60602	9.15	-4.80	.978	.192	171.8
.450	.67066	9.13	-5.31	.998	.195	176.3
.400	.73430	8.91	-5.92	1.015	.197	180.8
.350	.79607	8.47	-6.67	1.028	.199	185.5
.300	.85481	7.83	-7.63	1.039	.201	190.5
.250	.90882	6.98	-8.92	1.046	.203	196.0
.200	.95545	5.94	-10.78	1.052	.205	202.3
.150	.99006	4.72	-13.73	1.056	.206	210.1
.100	1.00221	3.37	-19.25	1.058	.208	220.6
.050	.95100	2.03	-33.07	1.060	.210	237.7

			Y			
			-2.50 DEG.			
$\bar{U}$	Z	G	DEG.	$\bar{Q}$	S	T
.998	.00131	.04	-2.50	.000	.000	.0
.995	.00523	.16	-2.51	.055	.035	28.7
.990	.01179	.35	-2.53	.110	.056	45.6
.985	.01835	.54	-2.55	.150	.067	54.8
.980	.02493	.73	-2.56	.183	.075	61.2
.970	.03809	1.11	-2.59	.238	.086	70.1
.960	.05128	1.48	-2.62	.283	.093	76.4
.950	.06450	1.84	-2.66	.322	.099	81.3
.900	.13084	3.54	-2.82	.467	.117	96.8
.850	.19754	5.05	-3.00	.569	.127	106.3
.800	.26446	6.37	-3.19	.648	.134	113.4
.750	.33144	7.48	-3.40	.711	.140	119.2
.700	.39831	8.40	-3.64	.762	.144	124.3
.650	.46486	9.11	-3.90	.805	.148	129.0
.600	.53083	9.61	-4.20	.840	.152	133.3
.550	.59593	9.89	-4.54	.869	.155	137.5
.500	.65978	9.97	-4.94	.893	.157	141.6
.450	.72192	9.83	-5.41	.913	.160	145.7
.400	.78173	9.48	-5.97	.929	.162	149.9
.350	.83843	8.92	-6.68	.942	.164	154.3
.300	.89094	8.16	-7.60	.952	.166	159.1
.250	.93770	7.20	-8.85	.960	.168	164.4
.200	.97630	6.07	-10.66	.966	.169	170.6
.150	1.00252	4.77	-13.57	.969	.171	178.2
.100	1.00683	3.38	-19.06	.972	.173	188.7
.050	.95040	2.02	-32.92	.973	.174	205.8

			Y			
			-3.00 DEG.			
$\bar{U}$	Z	G	DEG.	$\bar{Q}$	S	T
.998	.00157	.05	-3.00	.000	.000	.0
.995	.00628	.19	-3.01	.050	.029	23.9
.990	.01413	.42	-3.03	.100	.047	38.0
.985	.02197	.65	-3.04	.137	.056	45.7
.980	.02981	.88	-3.05	.168	.063	51.0
.970	.04547	1.33	-3.08	.218	.071	58.4
.960	.06110	1.76	-3.11	.259	.078	63.7
.950	.07670	2.19	-3.13	.295	.083	67.8
.900	.15417	4.18	-3.27	.428	.098	80.9
.850	.23067	5.90	-3.42	.523	.106	89.0
.800	.30604	7.37	-3.59	.595	.113	95.1
.750	.38010	8.59	-3.77	.654	.117	100.2
.700	.45264	9.55	-3.98	.702	.121	104.7
.650	.52345	10.26	-4.21	.742	.125	108.8
.600	.59224	10.73	-4.47	.775	.128	112.6
.550	.65868	10.94	-4.78	.803	.131	116.4
.500	.72238	10.92	-5.14	.826	.133	120.1
.450	.78284	10.67	-5.57	.845	.135	123.9
.400	.83945	10.19	-6.10	.861	.137	127.8
.350	.89140	9.49	-6.76	.873	.139	131.9
.300	.93762	8.59	-7.63	.883	.141	136.4
.250	.97661	7.50	-8.82	.891	.143	141.5
.200	1.00608	6.25	-10.57	.896	.144	147.5
.150	1.02214	4.86	-13.41	.900	.146	155.0
.100	1.01610	3.40	-18.85	.902	.147	165.3
.050	.95150	2.02	-32.73	.904	.149	182.3

			Y			
			-4.00 DEG.			
$\bar{U}$	Z	G	DEG.	$\bar{Q}$	S	T
.997	.00209	.06	-4.00	.000	.000	.0
.995	.00628	.19	-4.01	.032	.017	14.2
.990	.01672	.50	-4.02	.080	.033	27.0
.985	.02714	.81	-4.03	.113	.041	33.3
.980	.03754	1.11	-4.04	.141	.046	37.6
.970	.05825	1.70	-4.06	.185	.053	43.4
.960	.07885	2.28	-4.08	.221	.058	47.5
.950	.09934	2.85	-4.10	.253	.062	50.7
.900	.19994	5.43	-4.21	.370	.073	60.8
.850	.29733	7.63	-4.33	.453	.080	67.0
.800	.39125	9.45	-4.46	.518	.085	71.8
.750	.48144	10.90	-4.60	.570	.089	75.8
.700	.56758	12.00	-4.76	.613	.092	79.3
.650	.64935	12.76	-4.95	.649	.095	82.6
.600	.72634	13.18	-5.16	.679	.097	85.7
.550	.79810	13.29	-5.41	.704	.099	88.8
.500	.86408	13.09	-5.71	.725	.101	91.9
.450	.92362	12.61	-6.07	.743	.102	95.0
.400	.97594	11.86	-6.52	.757	.105	98.4
.350	1.02004	10.88	-7.10	.769	.106	101.9
.300	1.05466	9.67	-7.86	.778	.108	105.9
.250	1.07811	8.29	-8.93	.785	.110	110.5
.200	1.08804	6.75	-10.53	.790	.111	116.0
.150	1.08071	5.13	-13.19	.794	.113	123.0
.100	1.04853	3.50	-18.43	.796	.114	132.8
.050	.95978	2.01	-32.24	.798	.116	149.7

types of re-entry bodies are given in Fig. 11b as functions of time. Finally, Fig.11c represents the effects of the rotating atmosphere on the entry of a lifting body with L/D = 0.5 and $\frac{W}{C_L A}$ = 155 lb/ft^2 $\left(7420 \frac{\text{newtons}}{\text{m}^2}\right)$. It can also be seen from the note that for entry from 300,000 ft (91.4 km) the range for a rotating air mass is 72.5 naut mi (135 km) longer than the value for a stationary air mass.

C. DECELERATION

Deceleration magnitude is one of the several factors to be considered in safeguarding the payload of an entering vehicle. External loading on the vehicle, due to air pressure created by motion of the vehicle through the atmosphere, varies directly with deceleration and ballistic coefficient. Another consideration involving deceleration is that of human tolerance to stress, which is a function not only of peak deceleration and rate of onset of deceleration, but of orientation of the body and duration of the stress.

1. Analytic Solutions

From the force equation for an entering body (for example Eq (3)) the total acceleration magnitude is

$$a = \left[\left(-g + \frac{L}{m} \cos \gamma - \frac{D}{m} \sin \gamma \right)^2 + \left(\frac{D}{m} \cos \gamma + \frac{L}{m} \sin \gamma \right)^2 \right]^{1/2} \quad (54)$$

and the resultant acceleration magnitude experienced in addition to that due to gravity can be written as

$$G = \left[\left(\frac{L}{m} \cos \gamma - \frac{D}{m} \sin \gamma \right)^2 + \left(\frac{D}{m} \right)^2 \left(\cos \gamma + \frac{L}{D} \sin \gamma \right)^2 \right]^{1/2} \quad (55)$$

or

$$G = \frac{C_D A}{2m} \rho V^2 \cos \gamma \left[\left(-\frac{L}{D} + \tan \gamma \right)^2 + \left(1 + \frac{L}{D} \tan \gamma \right)^2 \right]^{1/2} \quad (56)$$

This acceleration G is that actually experienced by a pilot or instrument package, i.e., the acceleration due to external forces (lift and drag) alone. Expressed in units of g, this quantity is sometimes referred to as the load factor, $N = \frac{G}{g}$. Two simple cases are of interest.

(1) Ballistic entry

For L = 0, Eq (55) reduces to

$$G = \frac{C_D A}{2m} \rho V^2 \quad (57)$$

L = 0

(2) lifting entry at small entry angles

From Eq (56)

$$G \approx \frac{C_D A}{2m} \rho V^2 \cos \gamma \left[1 + \left(\tan \gamma - \frac{C_L}{C_D} \right)^2 \right]^{1/2} \quad (58)$$

$$\left[1 >> \left| \frac{L}{D} \tan \gamma \right| \right]$$

For small entry angles

$$G \approx \frac{C_D A}{2m} \rho V^2 \left[1 + \left(\frac{C_L}{C_D} \right)^2 \right]^{1/2} \quad (59)$$

$$\left[\cos \gamma \approx 1, \frac{C_L}{C_D} >> \left| \tan \gamma \right| \right]$$

The maximum deceleration experienced can be determined from the previous equations by setting

$$\frac{dG}{dt} = 0$$

For the case of Eq (59), small entry angles, or Eq (57), ballistic entry, this condition gives

$$v^2 \frac{d\rho}{dt} + 2\rho v \frac{dv}{dt} = 0$$

From Eqs (29) and (27),

$$\left[1 + \frac{2g}{\beta v_m^2} \right] \sin \gamma_m = - \frac{C_D A}{m} \frac{\rho_m}{\beta} \quad (60)$$

or

$$\sin \gamma_m \approx - \frac{C_D A}{m} \frac{\rho_m}{\beta} \quad \left[1 >> \frac{2g}{\beta v_m^2} \right] \quad (61)$$

In the notation of Ref. 1, or Section B.1.a.,

$$N_{max} \approx \sqrt{\beta r} \, (\bar{u}z)_{max} \sqrt{1 + \left(\frac{L}{D} \right)^2} \quad \left[|\gamma| << \frac{L}{D}, \cos \gamma \approx 1 \right] \quad (62)$$

2. Numerical Solutions and Graphical Presentations

Fig. 12a from (Ref. 1) gives horizontal deceleration, $\frac{du}{dt}$, for entry into the earth's atmosphere from decaying orbits. From Eqs (10) and (15),

$$\frac{du}{dt} \approx - g \sqrt{\beta r} \frac{\bar{u}z}{\cos \gamma} \quad (63)$$

$$\approx 30 \, \bar{u}z \, , \, (g), \, 1 >> \gamma$$

Consequently, Fig. 2 is useful in generating Fig. 12a.

In Fig. 12b are shown the results of numerical integrations of the exact equations of motion by an IBM 704 digital computer for a zero lift decay trajectory from a near-circular orbit. From Fig. 12b it can be seen that below approximately 50,000 ft, the deceleration approaches zero because in this range terminal velocity is reached (drag = weight). On the same figure, the re-entry load factors

$$N = \frac{G}{g}$$

are also indicated. At least for small re-entry angles, both curves coincide (for practical purposes) in the region where really significant g loads are encountered. It should also be noted that the analytical values are considerably higher than the actual decelerations (theoretical max = 8.35 g and actual max = 6.9 g).

Furthermore, maximum deceleration is also a function of the ballistic coefficient, as indicated by Fig. 12c. For different entry angles the shapes of the curves presented in Fig. 12c are essentially maintained; only the region of maximum deceleration shifts out with decreasing γ_0.

The variations in maximum decelerations are given in Fig. 13a, which also gives the corresponding altitudes where they occur. Given a certain re-entry angle (e.g., γ_0 = 0 deg) and the ballistic coefficient of the satellite (e.g., B = 2 ft^2/slug), 0.0127 m^2/kg), the magnitude of the maximum acceleration and its point of occurrence (for the given example; $(\dot{v}/g_{max})$ = 6.65 and $h_{max\ acc}$ = 185, 000 ft) (56.4 km) can be determined. From Fig. 13a it can also be seen that for a fixed ballistic coefficient, optimum re-entry decelerations are always connected with a zero initial angle. However, for a fixed re-entry angle, there exists a variable optimum ballistic coefficient which minimizes the decelerations. These optimum ballistic coefficients are given as functions of γ_0 in Fig. 13b. The corresponding values of maximum deceleration are also given. It can be seen that the design values for ballistic coefficients in the range $1.0 < B < 1.5$ ft^2/slug (0.00637 to 0.00956 m^2/kg) are desirable.

Drag decelerations may be controlled by varying the configuration parameters. Figure 14a shows the effects of variations in the configuration parameters for normalized altitude variations (Ref. 12). The normalized altitude represents distances on either side of the original altitude for maximum deceleration. Figure 14b indicates the acceleration profiles for these programmed configuration changes. Taking the most drastic deceleration reduction (namely 60% of the maximum uncontrolled deceleration) only 4 g's are encountered if the configuration parameter is changed roughly by a factor of 8.

For manned satellite re-entry, the critical parameter is not the magnitude of maximum acceleration, but time spent at a given acceleration. Figure 15a compares the effects of re-entry angles on cumulative deceleration times (for B = 1.0 ft^2/slug 0.00637 m^2/kg) with human tolerance as given in Ref. 13. It should be noted that the tolerance curves seem to be the maximum permissible values and blackouts can possibly occur, even if the dotted lines are not reached. Although the interpretation of the curves for human tolerance is not clear, it appears that for a pilot in a sitting position (with a g suit), the re-entry angles must be less than 2°, preferably less than 1°. For a pilot in a prone position, re-entry must be less than 4°.

Figure 15b compares the effects of ballistic coefficients on deceleration times for $\gamma_0 = -1°$. It indicates that, for small re-entry angles, a relatively large range of ballistic coefficients permissible for manned re-entry exists. With the given data, the permissible range would be $0.5 < B < 5.0$ ft^2/slug (0.00318 to 0.0318 m^2/kg) for a pilot with a g suit in a sitting position. For a pilot in the prone position, $0.1 < B < 25.0$ ft^2/slug (0.000637 to 0.16 m^2/kg) seems to be safe.

The material presented for the ballistic entry was extended to show the effects of aerodynamic lift during re-entry. The data presented were obtained from an iterative solution by the 704 digital computer of a point mass moving in an inverse-square force field. Because the aerodynamic forces at 300,000 ft (91.4 km) are sufficiently high to cause an immediate skipping of the vehicle at the higher lift-to-drag ratio, the re-entry altitude was increased to 400,000 ft (122 km).

Figure 16 presents the effects of re-entry conditions on the maximum total deceleration for a lifting body. This is a specific example for a vehicle with $W/C_L A$ = 146.9 psf (7040 newton/m^2 and L/D = 0.5. It also indicates a trend that for small re-entry angles decelerations decrease as orbital velocity is approached.

Figure 17a shows the effects of increasing L/D ratios on the decrease of total deceleration for a fixed re-entry angle and velocity. For example, in case of $\gamma_0 = -1°$, maximum deceleration is decreased roughly by a factor of 1/5 as L/D increases from 0 to 0.5. Similar curves are presented in Figs. 17b and c.

Maximum load factors for a variation of ballistic coefficients with lift-to-drag ratios from zero to three are shown in Figs. 18a, b and c for initial re-entry flight path angles of -1°, -5° and -10°.

For the initial flight path angles considered, a re-entry vehicle with an L/D = 1 reduces intolerable or excessive accelerations experienced in a ballistic re-entry to within comfortable limits. It should be pointed out that the modest reductions achieved by increasing lift-to-drag ratios greater than 1 can lead to an excessive increase in the amplitude and number of cycles of a moderate skipping trajectory.

To facilitate interpolations between the curves, load factors are given as functions of the initial flight path angle γ_0, in Figs. 19a, b and c. Figures 20a, b and c show that for a ballistic re-entry the magnitude of the acceleration peaks between initial velocities of 10,000 and 25,000 fps (3048 and 7620 mps), but decreases throughout the complete velocity range for a lifting re-entry.

Figure 21 gives the maximum entry load factors as a function of L/D ratio for $\gamma_0 = -1°$ and $W/C_D A = 5$ psf considering initial velocities between 10,000 and 25,000 fps (3048 and 7620 mps).

Figure 22 indicates the peak decelerations for the constant altitude--equilibrium glide entry program (Ref. 14) as a function of initial entry flight path angle. For a suggested operational limit it is seen that $\gamma_0 \geq -7°$ is advisable for L/D = 2.

A parametric set of curves, similar to the deceleration presentation, is given for maximum re-entry dynamic pressures (dynamic pressure = $\frac{1}{2}\rho V^2$) in Figs. 23a to 27c. A comprehensive curve, expressing the effects of lift, drag and wing loading on the maximum re-entry dynamic pressure is presented in Fig. 28 for $\gamma_0 = -1°$, $v_0 = 25{,}000$ fps and $h_0 = 300{,}000$ ft (7620 mps and 91.4 km).

Figures 23a to c show that maximum entry dynamic pressures are essentially linear functions of ballistic coefficients throughout the initial flight path angles investigated.

In Figs. 25a to c the decrease of dynamic pressure with increase of initial entry velocity is an effect of the centrifugal force acting on the vehicle in earth's gravitational field during the hypersonic portion of the trajectory where the maximum values of the dynamic pressure are occurring.

D. RE-ENTRY HEATING

Two modes of heat transfer to an entry vehicle exist during the entry phase of flight. These are the laminar and turbulent aerodynamic boundary layer heat transfer and the radiant transfer of energy to the vehicle surface from the hot gas between the shock wave and the vehicle. The relative magnitude of these two modes of heat transfer are functions of vehicle shape and entry velocity. In general, the blunter the vehicle and the higher the entry velocity, the greater the radiation heat transfer rate relative to the aerodynamic rate. The radiation heat transfer rate is the earliest to reach its maximum during the entry trajectory; next is the laminar rate and finally the turbulent rate. As the entry angle is decreased, both the rate and total radiant heat transfer decrease; whereas, for aerodynamic heat transfer, only the rate decreases while the total increases.

Protection against this thermal environment may be accomplished in a number of ways, and the methods chosen are dependent primarily upon the magnitudes of both the total and the rate of heat transfer. If both rate and total are sufficiently low, a simple heat sink made of copper or beryllium may be adequate. The simple heat sink is heat rate limited only to prevent the outer surface from melting. If the total heat that must be absorbed is large, the weight of the heat sink becomes excessive. For rates that are relatively low, it is possible to absorb the heat in a thin skin and reradiate it to the external environment. For example, if a thin skin can withstand a temperature of 5000° R it can reradiate up to 300 Btu/ft^2-sec so that the heat protection system now becomes a matter of insulating the remainder of the vehicle from this high temperature skin. On the other hand, at low heat rates it is also possible to use low temperature ablating materials for heat absorption. This alleviates the insulation problem, but weight is now required as ablating material rather than insulation. At high heat transfer rates and for high total heating, the use of high surface temperature ablating materials is required.

Analysis of aerodynamic heating of re-entry vehicles becomes much more complicated than the trajectory analysis since heat transfer terms introduce new nonlinearities into the differential equations. The main difficulty with an exact skin temperature history calculation is the necessity of knowing all the characteristics of a particular re-entry body shape, its heat shield thickness, heat conductivities and related heat transfer parameters, surface interactions with the air-flow (ionization, melting, ablation, etc.) and certain further important heat transfer characteristics. The number of variables involved makes a parametric representation necessarily rather involved.

1. Analytic Solutions

During entry, intense heating occurs at the stagnation region of the entering body. It is customary to relate the heating rate at any point on the body, q, to the heating rate at the stagnation point, q_s. In hypersonic flow the heating rate at a stagnation point can be written (Ref. 1) as

$$q_s = \frac{C}{\sqrt{R_s}} \left[\frac{\rho_\infty}{\rho_0}\right]^n \left[\frac{v}{v_c}\right]^m \qquad (64)$$

where the constants C, n and m depend on the type of boundary layer flow, and

R_s = body radius of curvature at the stagnation point

ρ_∞ = density of the ambient atmosphere

ρ_0 = sea-level atmospheric density

v = vehicle velocity

$v_c = \sqrt{gr}$ = circular orbit velocity at altitude.

For laminar flow n = 0.5 and m ≈ 3.1. As in the case of analytic trajectory solutions (Section B.1.c), more than a few methods have been developed for computing the laminar heating rates at a stagnation region. A collection of these methods appears

in Ref. 15 and is presented in the following list.

Laminar Heating Rate at Stagnation Region

(1) Ref. 16

$$q_s = \frac{Nu}{D} k \left[T_w - T_\infty \right] \qquad (65)$$

where

Nu = Nusselt number

$$k_1 \left[\frac{v_\infty D}{2} \right]^{0.5} Pr^{0.4}$$

for a sphere ($k_1 = 1.696 \times 10^{-3}$ in English units, ft-lb-sec; $= 5.169 \times 10^{-4}$ in mks)

D = drag

k = conductivity

T_w = temperature at the wall

T_∞ = temperature of the free stream

v_∞ = free stream velocity

Pr = Prandtl number = 0.71

(2) Ref. 17

$$q_s = \frac{k_w (T_s - T_w)}{\sqrt{\nu_w}} \quad \frac{Nu}{\sqrt{Re_w}} \left[\frac{d v_\delta}{dx} \right]_s^{0.5} \qquad (66)$$

where

$\frac{Nu}{Re_w}$ = ratio of Nusselt number to the square root of the Reynolds number (= 0.62 for Pr = 0.71, small $\frac{T_w}{T_s}$ and axially symmetric heating)

$\frac{d v_\delta}{dx}$ = stagnation point, velocity gradient

0 = flow inclination angle with respect to the free stream

s = subscript denoting value at stagnation point

w = subscript denoting value at the wall

ν = kinematic viscosity, $\frac{\mu}{\rho}$

(3) Ref. 18

(extreme cooling, small $\frac{T_w}{T_s}$)

$$q_s = \left\{ \frac{(0.5) 2^{0.5n}}{Pr^{2/3}} \left[\rho_s \mu_s v_\infty \right]^{1/2} \right.$$

(continued)

$$\left. \cdot h_s \left[\frac{d v_\delta}{v_\infty d 0} \right]_s^{0.5} \sqrt{\frac{R_{sh}}{R_s^2}} \right\} \qquad (67)$$

when

n = 0 for a planar body (two-dimensional flow)

n = 1 for a body of revolution (axially symmetric flow)

R_{sh} = shock radius $\sim R_s + 0.1 R_s$

h = enthalpy

μ = viscosity

$\frac{d v_\delta}{v_\infty d 0}$ = dimensionless stagnation point velocity gradiant (= 0.408 for spherical body, Newtonian flow and a 1.2 ratio of specific heats)

(4) Ref. 19

$$q_s = \left\{ \frac{26,300}{\sqrt{R_s}} \left[\frac{\rho_\infty}{\rho_0} \right]^{0.5} \left[\frac{v_\infty}{v_c} \right]^{3.15} \right.$$

$$\left. \cdot \left| \frac{h_s - h_w\ 6}{h_s - 3.2 \times 10^0} \right| \right\} \frac{kcal}{m^2 - sec} \qquad (68)$$

(5) Ref. 20

$$q_s = \left\{ \frac{0.54 \times 2^{n/2}}{Pr^{0.6} \sqrt{R_s}} \left[\frac{\rho_w \mu_w}{\rho_s \mu_s} \right]^{0.1} \right.$$

$$\cdot\ \cdot\ (\rho_s \mu_s v_\infty)^{0.5} (h_s - h_w) \left[\frac{d v_\delta}{v_\infty d 0} \right]_s^{0.5}$$

$$\left. \cdot \left[1 + (Le^m - 1) \frac{h_D}{h_s} \right] \right\} \qquad (69)$$

where

Le = Lewis number $\neq 1$ (Le $\sim$ 1.4)

m = 0.52 for equilibrium boundary layer flow

= 0.63 for frozen boundary layer flow

n = 0 or 1 as in case (3)

(6) Ref. 21

$$q_s = K' \frac{1 - \frac{h_w}{h_s}}{\sqrt{R_s}} \quad 2^{0.5n} (\rho_\infty)^{0.5} (u_\infty)^3 \qquad (70)$$

where u_∞ is the component of ambient flow velocity parallel to the surface

and $K' = 15.5 \times 10^{-9}$ Btu/sec-(slug)$^{1/2}$-(ft)^3 = 36.1×10^{-9} kcal/sec-(kg)$^{1/2}$-(m)^3.

The previous solutions apply for the case of laminar stagnation point heating, which generally applies for the nose and leading edge of gliding vehicles. However, Ref. 15 provides the following solution for turbulent flow.

$$q = \left\{ 7.5 \left[\frac{\theta^{0.6} \cos^{1.6} \theta}{0.542 \left(1 - \beta^2 \theta^2\right)^{0.7}} \right] \left[\frac{0.408}{\beta} \right]^{0.6} \frac{\bar{\rho}^{0.8}}{R_s^{0.2}} \cdot \left[\frac{v_\infty}{1000} \right]^3 \left[1 - \frac{h_w}{h_s} \right] \right\} \quad \text{kcal/m}^2\text{-sec} \quad (71)$$

where

$$\beta = \left[\frac{dv_\delta}{v_\infty d\theta} \right]_s$$

ρ = altitude density ratio, $\frac{\rho_\infty}{\rho_0}$

During entry the gas behind the shock wave in the stagnation region becomes very hot, and radiation from this hot gas is a source of heat transmission in addition to the convective heat input. Reference 21 provides the following empirical equation for the radiative heating rate:

$$q = 11.2 R_s \bar{\rho}^{1.5} \left[\frac{v_\infty}{10{,}000} \right] \quad \text{kcal/m}^2\text{-sec} \quad (72)$$

2. Numerical Solutions and Graphical Presentations

The equations for heat transfer rates presented in the previous section obviously vary somewhat in complexity and in degree of approximation. For generation of graphical data to be used in preliminary design work, a very simple solution has the advantages of involving fewer parameters to be varied and necessitating fewer calculations. For this reason, the solution chosen for generation of graphical data is that of Eq (64)

$$q_s = \frac{17{,}000}{R_s^{1/2}} \left[\frac{\rho_\infty}{\rho_s} \right]^{1/2} \left[\frac{v}{v_c} \right]^3 \text{Btu/ft}^2\text{-sec}$$

$$= \frac{25{,}400}{R_s^{1/2}} \left[\frac{\rho_\infty}{\rho_0} \right]^{1/2} \left[\frac{v}{v_c} \right]^3 \text{kcal/m}^2\text{-sec} \quad \text{(hypersonic flight)}$$

Furthermore, maximum stagnation point wall temperatures are presented in the parametric form

$$T_{ws} \cdot R_s^{1/8} \cdot \epsilon^{1/4}$$

to make the results independent of the nose radius at the stagnation point, R_s, and skin emissivity, ϵ. The values of the "radius-emissivity parameter" $R_s^{1/8} \cdot \epsilon^{1/4}$ are plotted in Fig. 29. The radiation heat loss is given by

$$q_{rad} = \epsilon \sigma T_{ws}^4 \quad (73)$$

where σ = radiation constant = 0.482×10^{-12} Btu/ft^2-sec-(°R)^4 = 1.372×10^{-11} kcal/m^2-sec-(°K)^4. At equilibrium, all of the heat flow from the boundary layer is radiated back into the atmosphere (i.e., the heat flux to the interior of the structure is negligible), and the maximum temperature attained by the stagnation region of the body is determined by equating the two heat flows:

$$T_{ws} R_s^{1/8} \epsilon^{1/4} = \left[\frac{17{,}000}{\sigma} \right]^{1/4} \left[\frac{\rho_\infty}{\rho_0} \right]^{1/8} \left[\frac{v}{v_c} \right]^{3/4}$$

(°R-ft$^{1/8}$ or 2.092° K-km$^{1/8}$) (74)

The maximum aerodynamic heating at the stagnation region of the nose can then be computed as:

$$q_s = \left[T_{w_s} R_s^{1/8} \epsilon^{1/4} \right]^4 \frac{\sigma}{\sqrt{R_s}} \quad (75)$$

The graphical information on re-entry heating presented in Figs. 30 through 47 is based primarily on Eqs (74) and (75), together with the related trajectory equations (Section B).

Figure 30a (Ref. 22) presents the approximate heat transfer rates for a blunt body of 1-ft (0.3 m) nose radius traveling at satellite velocities both for free molecule and for continuous flow. The definitions and ranges of flow regimes are given in Chapter 5. Figure 30b shows the ratios of heat input rates with respect to rate of energy dissipation by drag ($1/2\ \rho v^3$).

The effects of entry angles on maximum heat flux are given in Fig. 31a (Ref. 14). For example, as the re-entry angle is increased from -1° to -4°, the maximum heat flux is increased roughly by a factor of 4. Assuming radiation equilibrium temperatures of the satellite skin, Fig. 31b gives skin temperatures as a function of heat transfer rates for different values of the constant of emissivity, ϵ.

The assumption of radiation equilibrium becomes inadequate for steep ballistic entries or large heat shields. Figure 32 (Ref. 23) shows a sample history of aerodynamic heating, comparing the radiation equilibrium method with an exact skin temperature computation for a vertical entry. Temperature histories of the outer and inner surface of a 0.25-in. pyrex skin are shown for free fall from 1,000,000 ft (304.8 km).

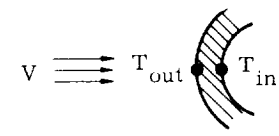

The estimated maximum temperatures are seen to be as follows:

T_{rad} = 2480° R = 1380° K

T_{out} = 1660° R = 920° K

T_{in} = 1080° R = 600° K

Thus, for the case considered, radiation equilibrium gives unrealistically high estimates, as the most important parameter for recovery programs is usually the temperature at the inner surface of the heat shield. In connection with Fig. 32, it should be further noted that below 100,000 ft (30.5 km) it would be advantageous to jettison the hot heat shield for the case investigated.

Figure 33a shows the trajectories for a family of re-entry vehicles, indicating the stagnation point radiation temperatures in dotted lines. Following a solid line of velocity-altitude variation, the corresponding skin temperature parameters can be read from the intersections with the dotted lines. Figure 33b presents the corresponding temperature profiles as a function of altitude. From theoretical considerations it can be shown that the maximum temperature occurs at $\frac{V}{V_c} = 0.81$, which agrees with the numerical results of the machine computations.

A family of curves similar to Fig. 33a is plotted for the initial altitude at 400,000 ft (122 km) in Fig. 33c.

Fig. 34a shows the maximum equilibrium nose temperatures as a function of the lift characteristics for equilibrium glides. It can be seen that the maximum equilibrium temperatures can be reduced by increasing the L/D ratios. The corresponding altitudes for maximum temperatures are expressed in Fig. 34b. The effects of the initial flight path angle on the altitude for maximum stagnation nose temperature are given in Fig. 34c.

In Figs. 35 through 41 the results of all the important Martin Company numerical integration results are collected. Maximum re-entry stagnation point nose temperatures are presented successively versus the ballistic coefficient, B, the initial entry angle, γ_0, the initial velocity, v_0, and lift-to-drag ratios, L/D.

Figures 35a through 36c show the maximum radiation-equilibrium temperature at the laminar stagnation point as a function of ballistic coefficient, lift-to-drag ratio and initial re-entry angles.

It can be seen that though aerodynamic lift reduces the higher temperatures experienced during a ballistic re-entry, the magnitude of the reduction is reduced as the initial flight path angle decreases. The effects of initial re-entry velocity are shown in Fig. 37 for L/D = 0.5 and in Figs. 38a through 40d for three ballistic coefficients and various values of L/D and entry angle.

The effect of considering a rotating air mass is presented in Fig. 42 for the equilibrium temperature history.

A comparison of the maximum temperature parameters for ballistic entry is shown in Fig. 43a for various initial flight path angles. Also shown is a comparison between the stagnation point and spherical nose solutions.

Figure 43b presents the maximum temperature parameters for various L/D ratios (Ref. 1). It can be used for various planetary atmosphere, if the proper logarithmic atmospheric densitys slope, b, is inserted in connection with the radial distance, r.

Obviously the preliminary design estimates based on the stagnation point solution may be considerably altered, if the particular shape of the vehicle nose is known. An indication of the dependency on body shape is given by Fig. 44 from Ref. 1.

Parametric temperature histories versus density ratios are given in Fig. 45a (Ref. 22) for simple drag bodies. Figures 45b and c present lift parameter requirements for constant heat transfer trajectories (Ref. 22).

The slopes of the stagnation point temperature parameter are given in Figs. 46a through 46c for three ballistic coefficients.

Finally the effects of lift-drag ratios on the maximum surface temperature parameter for entry into various planetary atmospheres is given in Fig. 47 (Ref. 1). It should be noted that optimum conditions are encountered at L/D from roughly 0.8 to 1.0 for most planets.

E. RANGE AND TIME TO IMPACT

Range to impact for ballistic vehicles is given as a function of the initial flight path angle in Fig. 48 for h_0 = 300,000 ft (91.4 km) and v_0 = 25,000 fps (7620 mps).

Figures 49a through e present the data obtained from a series of computer runs, giving the values of range attained in descent from 300,000 ft to sea level. Data are plotted as functions of re-entry velocity, re-entry flight path angle and ballistic coefficient for a zero-lift re-entry.

Figures 50a through c show range from 400,000 ft (122 km) for different ballistic coefficients, lift-to-drag ratios and re-entry angles. It is interesting to note that for a constant re-entry angle, range is rather insensitive to ballistic coefficient for the higher lift-to-drag ratios.

Figures 51a through 52g show the range to impact versus initial velocity for various parametric values of lift-drag ratios, L/D, and initial flight path angles, γ_0.

Further parametric studies of impact ranges are compiled in Figs. 53 through 54c, as functions of initial flight path angles and lift-drag ratios.

Equilibrium glide range variations as a function of initial velocities are indicated in Fig. 55.

The range characteristics of a high-drag, low variable lift vehicle (flat plate at almost 90° angles of attack) are treated in Figs. 56a to 56c (Ref. 25). Figure 56a expresses the variation in range as a

function of angle of attack and entry flight path angles. Figure 56b analyzes the range variations for ballistic vehicles as functions of initial velocities and entry angles, while Fig. 56c gives the range as a function of angle of attack and initial entry velocity.

Figure 57 shows times to impact for various ballistic coefficients, lift-drag ratios and re-entry angles. It should be observed that for high lift-drag ratios the flight time is rather sensitive to entry angles and ballistic coefficients.

Parametric curves of range versus flight time for lifting bodies are shown for three values of B in Figs. 58a to 58c, using γ_0 = -1, -5° and -10°. The effects of initial entry velocity are expressed for L/D = 0.5, 1.25 and 2.0 in Figs. 59a to 59c. In Fig. 60 time to impact is expressed as a function of L/D, using as parameters the initial flight path angles and initial velocities.

Range is shown as a function of velocity at apogee for lifting vehicles traveling at sub-satellite speeds in Fig. 61, cross-plotting flight times as additional parameters.

For fast estimates of ballistic vehicle range and time to impact, a comprehensive parametric family of curves is presented in Fig. 62 for a large number of ballistic coefficients and initial flight path angles.

F. MANEUVERABILITY

Even if deceleration and heating are adequately controlled during entry, recovery of the vehicle is not assured unless it is capable of landing in a predesignated area. The size of the landing area could range from a very large region for parachute recovery by a large search group to an area comparable to that of an airport for glide-landing vehicles. It is apparent, in the latter case, that the vehicle must be capable of fairly extensive maneuvers during the entry phase if recovery is to be possible without long periods of waiting in orbit for a favorable landing site approach. Consequently, vehicle maneuverability is another problem in the area of entry requiring investigation.

As a first consideration in the problem of maneuvering a vehicle from certain initial conditions to a successful landing, the possibility that a landing, or even an impact, on the earth might not be possible for the given initial conditions, should be noted. Trajectories which are too high overshoot because they encounter too little atmospheric drag to slow the vehicle for entry; on the other hand, trajectories which are too low result in the vehicle experiencing too much deceleration for safe recovery.

Figures 63a and 63b show the range of values for both re-entry velocity and flight path angle necessary to ensure ballistic vehicle and lifting body impact with the earth in one revolution or less. Results apply for two initial altitudes, 300,000 and 400,000 ft (91.4 and 122 km). Several values of the ballistic coefficient from 0 to 1.07 are included.

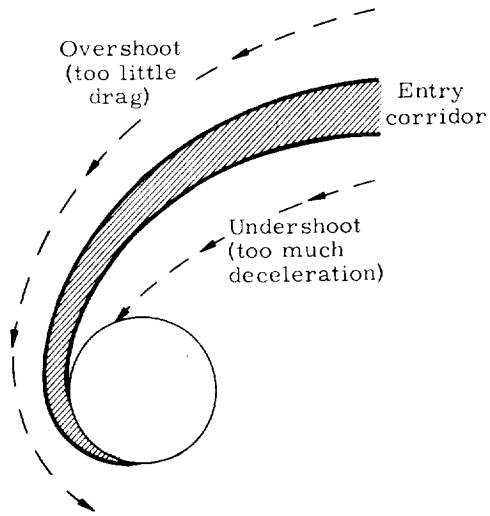

Figure 63c (Ref. 14) indicates the limitations on the minimum entry angles for capture of vehicles traveling at escape velocities.

Example:

$$W/C_L A = 50 \text{ lb/ft}^2 \ (2390 \text{ newtons/m}^2),$$

$$v_0 = v_e = \sqrt{2}\, v_c$$

For positive lift, vehicle is captured, if

$$\gamma_0 < -5.05°$$

For negative lift, vehicle is captured, if

$$\gamma_0 < -4.50°$$

Entry corridor conditions are considered in greater detail in Ref. 26.

Within certain bounds, the longitudinal and lateral range to the landing site may be varied by modifying the vehicle area or orientation (i.e., modifying the effective drag or lift). Figure 64 illustrates the correction of longitudinal range by varying the ballistic coefficient. This figure presents two graphs showing the ballistic coefficient increments needed to compensate for errors in entry angle if a fixed longitudinal range is to be attained.

Example:

$B_0 = 1.0 \text{ ft}^2/\text{slug} \ (0.00637 \text{ m}^2/\text{kg})$ } Range = 530 stat mi (Fig. 62) (853 km)

Programmed re-entry angle $\gamma_0 = -2$ deg }

Actual re-entry angle $\gamma_0' = -3$ deg

Thus, error = -1 deg (new range = 416 stat mi (670 km), Fig. 62).

From Fig. 64 $\dfrac{\Delta B_1}{B_0} = -0.8$

Therefore, approximately 80% of B (∝ drag area) should be discarded in order to reach the predetermined range of 530 stat mi (853 km).

For the high-drag, low-lift vehicle already treated in Figs. 56a to 56c ($\alpha \approx 90°$, see Ref. 25). the variation of range as a function of angle of attack and initial flight path angle is shown for two azimuth angles in Fig. 65a. These changes in design range, created by the rotation of the earth, must be counteracted for a particular heading by proper changes in the angle of attack (i.e., changing the L/D ratio).

Figure 65b gives for the same type of entry vehicles the whole spectrum of variation of range as a function of heading for initial latitudes of 0° and 45°. Maneuver capabilities compensating these effects may be mandatory where exact impact at the point of destination is desired.

Reference 27 provides approximate analytic solutions for the lateral maneuverability available from banking the vehicle. These solutions, together with pertinent assumptions, are presented here for convenience in reference. They are based on equations of motion expressed in the following form (see Eqs (27) and (28)

$$m v \frac{dv}{ds} = - D - m g \sin \gamma \tag{76}$$

$$m v \frac{2 d\gamma}{ds} = L - m \cos \gamma \left(g - \frac{v^2}{r}\right) \tag{77}$$

$$m v^2 \frac{d\psi}{ds} = Y \tag{78}$$

where

Y = side force normal to L and D.

If the side force Y is produced by banking the vehicle, and if the vehicle exhibits a constant aerodynamic lift-drag ratio of $\left(\frac{L}{D}\right)_0$, then a bank angle ϕ results in

$$\frac{L}{D} = \left(\frac{L}{D}\right)_0 \cos \phi \tag{79}$$

$$\frac{Y}{D} = \left(\frac{L}{D}\right)_0 \sin \phi \tag{80}$$

1. Equilibrium-Glide Solution

Assumptions: vehicle weight is balanced by lift plus centrifugal force in the vertical direction (small γ).

$$\frac{\lambda}{R} \approx \frac{\pi^2}{24} \left(\frac{L}{D}\right)_0^2 \sin \phi \cos \phi \qquad \left[\psi << 1,\ v_0 = v_c,\ v_f = 0\right] \tag{81}$$

or, more generally

$$\frac{\lambda}{R} = \frac{L}{D}\left[\left(-\xi_0 + \frac{\xi_0^3}{3!} - \frac{\xi_0^5}{5!}\right)\Phi_0 + \left(1 - \frac{3}{3!}\xi_0^2 + \frac{5}{5!}\xi_0^4\right)\frac{Y}{D}\Phi_1 + \left(\frac{3}{3!}\xi_0 - \frac{10}{5!}\xi_0^3\right)\left(\frac{Y}{D}\right)^2 \Phi_2 + \left(-\frac{1}{3!} + \frac{10}{5!}\xi_0^2\right)\left(\frac{Y}{D}\right)^3 \Phi_3 + \frac{5}{5!}\xi_0\left(\frac{Y}{D}\right)^4 \Phi_4 + \frac{1}{5!}\left(\frac{Y}{D}\right)^5 \Phi_5\right] \tag{82}$$

$$\frac{x}{R} \approx \frac{L}{D}\left[\left(-1 + \frac{\xi_0^2}{2!} - \frac{\xi_0^4}{4!}\right)\Phi_0 + \left(-\frac{2}{2!}\xi_0 + \frac{4}{4!}\xi_0^3\right)\frac{Y}{D}\Phi_1 + \left(\frac{1}{2!} - \frac{6}{4!}\xi_0^2\right)\left(\frac{Y}{D}\right)^2 \Phi_2 + \frac{4}{4!}\xi_0\left(\frac{Y}{D}\right)^3 \Phi_3 - \frac{1}{4!}\left(\frac{Y}{D}\right)^4 \Phi_4\right] \tag{83}$$

$$\approx \frac{1}{2}\frac{L}{D} \ln \frac{1 - \bar{v}^2}{1 - \bar{v}_0^2} \quad \text{for} \quad \frac{Y}{D} = \xi_0 = 0 \tag{84}$$

where

λ = lateral range

x = longitudinal range

R = radius of earth

$\Phi_n = \int_{\bar{v}}^{\bar{v}} \frac{\bar{v} (\ln \bar{v})^n}{\bar{v}_0 \, 1 - \bar{v}^2} \, d\bar{v}$ in the difference between initial and final values tabulated as function of $\bar{v}$ in Table 2.

$\bar{v} = \frac{v}{v_c} = \bar{v}_0 \exp\left[-\frac{\psi}{(Y/D)}\right]$

$\bar{v}_0$ = normalized velocity at initiation of maneuver

$\xi = \frac{Y}{D} \ln \bar{v}$

2. Orbit Decay at Large Bank Angles ($\phi \approx 90°$)

Assumptions: zero lift in vertical plane $\frac{Y}{D} = \left(\frac{L}{D}\right)_0$, entry in decay from a satellite orbit.

$$\frac{\lambda}{R} = \sqrt{\frac{3}{2\beta R}\left[\frac{Y}{D}\right]}\,\psi \tag{85}$$

Figure 66a expresses the effects of roll angles on the lateral range for the study conducted in Ref. 27. It is seen roll angles equal to approximately 45° result in a maximum lateral range. Figure 66b represents the lateral range capabilities for increasing L/D ratios. The following empirical approximate equations can be fitted to these curves as follows, assuming the initial altitudes of 300,000 ft: (91.4 km)

TABLE 2

Values of the Function ϕ_n

∇	Φ_0	Φ_1	Φ_2	Φ_3	Φ_4	Φ_5	∇	Φ_0	Φ_1	Φ_2	Φ_3	Φ_4	Φ_5
1.00	∞	0	0	0	0	0	0.49	0.1373	0.2492	-0.0773	0.0341	-0.0175	0.0097
.99	1.9585	.0050	.0000	.0000	.0000	.0000	.48	.1309	.2538	-.0806	.0366	-.0192	.0109
.98	1.6145	.0100	-.0001	.0000	.0000	.0000	.47	.1248	.2584	-.0840	.0391	-.0211	.0123
.97	1.4143	.0150	-.0002	.0000	.0000	.0000	.46	.1189	.2629	-.0875	.0417	-.0231	.0139
.96	1.2730	.0200	-.0004	.0000	.0000	.0000	.45	.1131	.2674	-.0910	.0445	-.0253	.0156
.95	1.1640	.0250	-.0006	.0000	.0000	.0000	.44	.1076	.2719	-.0947	.0475	-.0277	.0176
.94	1.0754	.0300	-.0009	.0000	.0000	.0000	.43	.1022	.2764	-.0984	.0506	-.0303	.0197
.93	1.0009	.0350	-.0012	.0001	.0000	.0000	.42	.0970	.2808	-.1022	.0538	-.0331	.0221
.92	.9367	.0400	-.0016	.0001	.0000	.0000	.41	.0920	.2852	-.1061	.0572	-.0361	.0247
.91	.8804	.0450	-.0021	.0001	.0000	.0000	.40	.0872	.2896	-.1100	.0608	-.0393	.0276
.90	.8304	.0500	-.0026	.0002	.0000	.0000	.39	.0825	.2940	-.1140	.0646	-.0428	.0309
.89	.7853	.0550	-.0031	.0002	.0000	.0000	.38	.0780	.2983	-.1182	.0685	-.0466	.0345
.88	.7445	.0600	-.0038	.0003	.0000	.0000	.37	.0736	.3026	-.1224	.0726	-.0506	.0384
.87	.7071	.0649	-.0044	.0004	.0000	.0000	.36	.0694	.3068	-.1266	.0769	-.0549	.0428
.86	.6728	.0699	-.0051	.0005	-.0001	.0000	.35	.0653	.3110	-.1310	.0814	-.0596	.0477
.85	.6410	.0749	-.0059	.0006	-.0001	.0000	.34	.0614	.3152	-.1354	.0862	-.0646	.0530
.84	.6114	.0799	-.0068	.0008	-.0001	.0000	.33	.0576	.3193	-.1400	.0911	-.0700	.0589
.83	.5838	.0848	-.0076	.0009	-.0001	.0000	.32	.0540	.3234	-.1445	.0963	-.0758	.0654
.82	.5580	.0898	-.0086	.0011	-.0002	.0000	.31	.0505	.3274	-.1492	.1016	-.0821	.0726
.81	.5337	.0948	-.0096	.0013	-.0002	.0000	.30	.0472	.3314	-.1540	.1073	-.0888	.0806
.80	.5108	.0997	-.0107	.0016	-.0003	.0000	.29	.0439	.3354	-.1588	.1132	-.0959	.0893
.79	.4892	.1047	-.0118	.0018	-.0003	.0001	.28	.0408	.3393	-.1636	.1193	-.1036	.0990
.78	.4688	.1096	-.0130	.0021	-.0004	.0001	.27	.0378	.3431	-.1686	.1257	-.1119	.1097
.77	.4493	.1146	-.0143	.0024	-.0005	.0001	.26	.0350	.3469	-.1736	.1324	-.1207	.1214
.76	.4309	.1195	-.0156	.0028	-.0006	.0001	.25	.0323	.3506	-.1787	.1393	-.1303	.1344
.75	.4133	.1245	-.0170	.0032	-.0007	.0002	.24	.0297	.3543	-.1839	.1466	-.1405	.1488
.74	.3966	.1294	-.0185	.0036	-.0008	.0002	.23	.0272	.3579	-.1891	.1541	-.1514	.1647
.73	.3806	.1343	-.0200	.0041	-.0009	.0002	.22	.0248	.3614	-.1944	.1620	-.1632	.1822
.72	.3653	.1392	-.0216	.0046	-.0011	.0003	.21	.0226	.3649	-.1997	.1702	-.1757	.2015
.71	.3507	.1441	-.0232	.0051	-.0013	.0004	.20	.0204	.3683	-.2051	.1787	-.1892	.2229
.70	.3367	.1490	-.0249	.0057	-.0015	.0004	.19	.0184	.3716	-.2105	.1876	-.2037	.2466
.69	.3232	.1539	-.0267	.0064	-.0017	.0005	.18	.0165	.3748	-.2160	.1968	-.2192	.2728
.68	.3103	.1588	-.0285	.0071	-.0020	.0006	.17	.0147	.3780	-.2214	.2063	-.2359	.3019
.67	.2979	.1637	-.0304	.0078	-.0023	.0007	.16	.0130	.3810	-.2269	.2162	-.2538	.3341
.66	.2860	.1686	-.0324	.0086	-.0026	.0009	.15	.0114	.3840	-.2325	.2265	-.2730	.3699
.65	.2745	.1734	-.0345	.0095	-.0030	.0010	.14	.0099	.3868	-.2380	.2372	-.2936	.4097
.64	.2635	.1782	-.0366	.0104	-.0034	.0012	.13	.0085	.3896	-.2435	.2482	-.3157	.4540
.63	.2528	.1831	-.0388	.0114	-.0039	.0014	.12	.0073	.3922	-.2490	.2597	-.3394	.5034
.62	.2426	.1879	-.0411	.0125	-.0044	.0016	.11	.0061	.3948	-.2544	.2715	-.3650	.5585
.61	.2327	.1927	-.0434	.0136	-.0049	.0019	.10	.0050	.3972	-.2598	.2836	-.3924	.6023
.60	.2231	.1975	-.0458	.0148	-.0055	.0022	.09	.0041	.3994	-.2651	.2961	-.4218	.6896
.59	.2139	.2023	-.0483	.0161	-.0062	.0026	.08	.0032	.4015	-.2703	.3089	-.4534	.7676
.58	.2050	.2071	-.0509	.0175	-.0069	.0030	.07	.0025	.4035	-.2754	.3220	-.4874	.8556
.57	.1964	.2118	-.0535	.0190	-.0077	.0034	.06	.0018	.4053	-.2803	.3354	-.5238	.9553
.56	.1881	.2166	-.0562	.0205	-.0086	.0039	.05	.0013	.4069	-.2849	.3488	-.5628	1.0686
.55	.1801	.2213	-.0590	.0222	-.0096	.0045	.04	.0008	.4083	-.2892	.3623	-.6046	1.1981
.54	.1724	.2260	-.0618	.0239	-.0106	.0051	.03	.0005	.4094	-.2932	.3754	-.6488	1.3466
.53	.1649	.2307	-.0648	.0257	-.0118	.0058	.02	.0002	.4104	-.2966	.3880	-.6950	1.5176
.52	.1576	.2353	-.0678	.0276	-.0130	.0066	.01	.0001	.4110	-.2992	.3990	-.7415	1.7134
.51	.1506	.2400	-.0709	.0297	-.0144	.0075	.00	.0000	.4112	-.3005	.4059	-.7777	1.9075
.50	.1438	.2446	-.0740	.0319	-.0159	.0085							

for $L/D \leq 1.0$ (due east): $\lambda \approx 623 \left(\frac{L}{D}\right)^{1.875}$ (naut mi) $= 1155 \left(\frac{L}{D}\right)^{1.875}$ (km)

for $0.75 \leq \frac{L}{D} \leq 2.0$ (due east): $\lambda \approx 910 \quad \frac{L}{D}$ - 300 (naut mi) $= 1688 \left(\frac{L}{D}\right)$ - 556 (km)

The effects of the entry angle on the maximum lateral range are shown in Fig. 66c for roll angle of 45° and (L/D) = 1.0, while the effects of initial velocity are indicated in Fig. 66d.

In Ref. 14, the maneuvering performance of a re-entry vehicle is considered for a trajectory consisting of three parts:

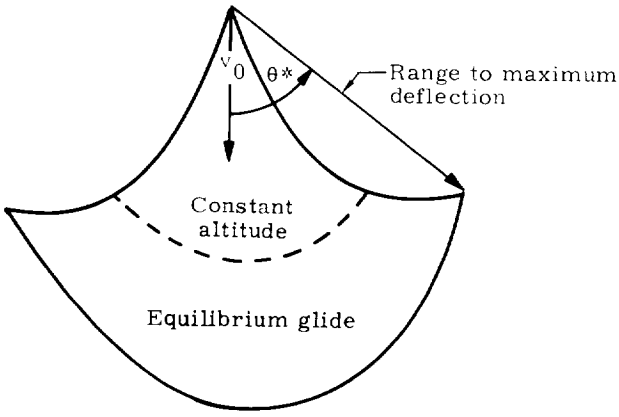

(1) Initial pull-out at $\left(\frac{L}{D}\right)_{max}$.

(2) Constant altitude glide at $\frac{L}{D} \leq \left(\frac{L}{D}\right)_{max}$.

(3) Equilibrium glide at $\left(\frac{L}{D}\right)_{max}$.

Range to maximum deflection point and the corresponding azimuth angle, θ*, are defined as shown in the above sketch.

The effects of re-entry angle on θ* and range are presented in Fig. 67a for $\frac{W}{C_L A}$ = 20 psf (958 newtons/m^2 and $\frac{L}{D}$ ratios of 0.5, 1 and 2. It can be seen that the range capabilities are greatly reduced by large re-entry angles, the resulting ranges for $-10 \leq \gamma_0$ being almost independent of $\frac{L}{D}$. The reverse is true for azimuth angles.

Figures 67b and c give the effects of wing loading on the range to maximum deflection point and the maximum azimuth angle for $\gamma_0 = -2°$ and $\frac{L}{D}$ ratios 0.5, 1 and 2.

Figure 68a shows a typical maneuverability envelope for $\frac{W}{C_L A}$ = 20 psf (958 newtons/m^2) and $v_0 = v_c$ (entry at circular orbit speeds). North pole is considered as the initial point of the trajectory calculations. For an initial flight path angle of -2°, the maneuver envelopes for the lift-drag ratios of 0.5, 1 and 2 are plotted. A comparison for γ_0 = -4° and $\frac{L}{D}$ = 2 is shown in dotted lines.

Similar maneuver envelopes are also shown in Fig. 68b for $\frac{W}{C_L A}$ = 100 psf (4787 newtons/m^2) and γ_0 = -6° for an entry at escape speeds.

Finally, Fig. 69 shows the maneuverability (that is the locus of impact points) of a lifting body as computed on the Martin Marietta powered trajectory program, using a maximum L/D = 0.5; the minimum which could be trimmed is 0.3. Bank angles varied from 0° for the fore and aft case to 60° for the maximum lateral deviation. Initial conditions were h_0 = 300,000 ft (91.4 km) v_0 = 25,500 fps (7770 mps) and γ_0 = -1°. An additional variable on the plot is the altitude at which initial deviation from the basic approach is effected (300,000, < 250,000, 225,000, 200,000 or 150,000 ft; (91.4 < 76.2, 68.6, 61.0, 45.7 km). Essentially, no maneuverability is afforded for initial altitude below 150,000 ft (45.7 km).

G. REFERENCES

1. Chapman, D. R., "An Approximate Analytical Method for Studying Entry into Planetary Atmospheres," NACA TN 4276, May 1958.

2. Allen, H. J., and Eggers, A. J., Jr., "A Study of the Motion and Aerodynamic Heating of Missiles Entering the Earth's Atmosphere at High Supersonic Speeds," NACA TN 4047, October 1957.

3. Sänger, E., "Raketen-Flugtechnik," R. Oldenbourg, Berlin, 1933.

4. Eggers, A. J., Jr., Allen, H. J., and Neice, S. E., "A Comparative Analysis of the Performance of Long-Range Hypervelocity Vehicles," NACA TN 4046, 1957.

5. Wang, K., and Ting, Lu, "Approximate Solutions for Reentry Trajectories with Aerodynamic Forces," Astronautics Acta, Fasc 8, pp 28 to 41, 1962.

6. Allen, H. J., and Eggers, A. J., Jr., "A Study of the Motion and Aerodynamic Heating of Ballistic Missiles Entering the Earth's Atmosphere at High Supersonic Speed," NACA Report 1381 1958.

7. Loh, W. H. T., "Ballistic Re-entry at Small Angles of Inclination," ARS Journal, Vol. 32, No. 5, May 1962, pp 718 to 721.

8. Bendor, E., Krenkel, A. R., and Kottler, C., "Trajectories of Lifting Bodies Entering Planetary Atmospheres at Shallow Angles," Fifth Symposium on Ballistic Missile and Space Technology, Academic Press, New York, 1960, pp 89 to 112.

9. Wang, K., and Ting, L., "An Approximate Analytic Solution of Re-entry Trajectory with

Aerodynamic Forces," ARS Journal, Vol. 30, No. 6, June 1960, pp 565 to 566.

10. Phillips, R. L., and Cohen, C. B., "Use of Drag Modulation to Reduce Deceleration Loads During Atmospheric Entry," ARS Journal, Vol. 29, No. 6, June 1959, pp 414 to 422.

11. Lees, L., Hartwig, F. W., and Cohen, C. B., "Use of Aerodynamic Lift During Entry into the Earth's Atmosphere," ARS Journal, Vol. 29, No. 9, September 1959, pp 633 to 641.

12. Robinson, A. C., Wolarer, L. E , and Besonis, A. J., "A Study of Nonlifting Satellites Re-entering the Earth's Atmosphere," WADC Aero Research Lab Working Paper, March 1958.

13 White, C., and Benson, O., "Physics and Medicine of the Upper Atmosphere," The University of New Mexico Press, Albuquerque, 1952.

14. Mandell, D. S., "Maneuvering Performance of Lifting Re-entry Vehicles," ARS Journal, Vol. 32, No. 3, March 1962, pp 346 to 354.

15. Hankey, W. L., Jr., Neumann, R. D., and Flinn, E. H., "Design Procedures for Computing Aerodynamic Heating at Hypersonic Speeds," WADC Technical Report 59-610, June 1960.

16. Sibulkin, M. J., "Heat Transfer Near the Forward Stagnation Point of a Body of Revolution," Journal of Aeronautical Sciences Vol. 19, No. 8, August 1952, pp 580 to 581.

17. Cohen, C. B., and Reshotko, E., "Heat Transfer at the Forward Stagnation of Blunt Bodies," NACA TN 3513, July 1955.

18. Lees, L., "Laminar Heat Transfer over Blunt Bodies at Hypersonic Flight Speeds," Jet Propulsion, Vol. 26, No. 4, April 1956, pp 259 to 269, 274.

19. Detra, R. W., Kemp, N. H., and Riddell, F. R., "Addendum to 'Heat Transfer to Satellite Vehicles Re-entering the Atmosphere,'" Jet Propulsion, Vol. 27, No. 4, December 1957, pp 1256 to 1257.

20. Fay, J. A., and Riddell, F. R., "Theory of Stagnation Point Heat Transfer in Dissociated Air," Journal of Aeronautical Sciences, Vol. 25, No. 2, February 1958, pp 73 to 86.

21. Lees, L., "Recovery Dynamics--Heat Transfer at Hypersonic Speed in a Planetary Atmosphere," Space Technology, John Wiley and Sons, Inc., 1958.

22. Kemp, N. H., and Riddell, F. R. "Heat Transfer to Satellite Vehicles Re-entering the Atmosphere," Jet Propulsion, Vol. 27, No. 2, February 1957, pp 132 to 137.

23. Kork, J., "A Practical Calculation Method of Aerodynamic Heating at the Stagnation Point," Master's Thesis, University of Maryland, May 1958.

24. Gazley, C., Jr., and Masson, D. J., "A Recoverable Scientific Satellite," Rand Report RM-1844, 1956.

25. Cheatham, D. C., Young, J. W., and Eggleston, John, "The Variation and Control of Range Traveled in the Atmosphere by a High-Drag Variable-Lift Entry Vehicle," NASA TN D-230, March 1960.

26. Chapman, D. R., "An Analysis of the Corridor and Guidance Requirements for Supercircular Entry into Planetary Atmospheres," NASA Technical Report R-55, 1960.

27. Slye, R. E., "An Analytical Method for Studying the Lateral Motion of Atmosphere Entry Vehicles," NASA TN D-325, September 1960.

H. BIBLIOGRAPHY

Adler, A. A., "Calculation of Re-entry Velocity Profile," Jet Propulsion, Vol. 28, No. 12, December 1958, pp 827 to 828.

Allen, H. J., "Motion of a Ballistic Missile Angularly Misaligned with the Flight Path upon Entering the Atmosphere and Its Effect upon Aerodynamic Heating, Aerodynamic Loads and Miss Distance," NACA TN 4048, October 1957

Allen, H. J., and Eggers, A. J., Jr., "A Study of the Motion and Aerodynamic Heating of Missiles Entering the Earth's Atmosphere at Supersonic Speeds," NACA TN 4047, October 1957.

Ambrosio, A., "A General Atmospheric Entry Function and Its Characteristics," ARS Journal, Vol. 32, No. 6, June 1962, p 906.

Austin, R. W., "Trajectory Control of Lifting Re-entry Vehicles," IAS National Aerospace Support and Operations Meeting, Orlando, Florida, 4 December 1961.

Baker, R. M. L., Jr.,
"Encke's Method and Variation of Parameters as Applied to Re-entry Trajectories," Advances in Astronautical Sciences, New York, Plenum Press, Vol. 3, August 1958.
"Variation of Parameters as Applied to Re-entry Trajectories," American Astronautical Society Western Regional Meeting, 18 to 19 August 1958.
"Application of Astronomical Perturbation Techniques to the Return of Space Vehicles," ARS Journal, Vol. 29, No. 3, March 1959, pp 207 to 211.
"3-Dimensional Drag Perturbation Technique," ARS Journal, Vol. 30, No. 8, August 1960, pp 748 to 753.

Becker, J., "Re-entry from Space," Scientific American, Vol. 204, No. 1, January 1961, pp 49 to 57.

Berman, L. J., "Optimum Soft Landing Trajectories: Part I--Analysis" (U), Massachusetts Institute of Technology, Department of Aeronautics and Astronautics, Cambridge, Massachusetts, Report No. AFOSR 519, March 1961.

Bidwell, J. M., and Skulsky, R. S., "Maneuvering Re-entry for Maximum Lateral Range," The Martin Company, Denver, Colorado, Report No. MI 60-36.

Blum, R., "Re-entry Trajectories--Flat Earth Approximation," ARS Journal, Vol. 32, No. 4, April 1962, p 616.

Boissevain, A. G., "The Effect of Lateral- and Longitudinal-Range Control on Allowable Entry Conditions for a Point Return from Space," NASA TN D-1067, July 1961.

Bowersox, R. B., et al., "Trajectory of a Vehicle Departing from a Circular Orbit, Lockheed Aircraft Corporation, Sunnyvale, California, Report No. LMSD-703049, July 1960.

Bressler, D. C., "Effects of Initial Re-entry Flight Conditions on a Recoverable Space Vehicle," The Martin Company, Baltimore, Maryland, Engineering Report No. ER 10625M, 1959.

Bull, G. V., Enkenhus, K. R., and Tiddy, G. H., "Exit and Re-entry Problems," Aero/Space Engineering, Vol. 17, No. 6, June 1958.

Bush, L. R., "A Study of the Accurate Re-entry and Precision Landing of an Orbital Earth Satellite, Part I," Cornell Aeronautical Laboratory, CAL Report No. VF-1351-H-1, 30 June 1959. (Also, ASTIA No. AD 245, 153.)

Brunner, M. J., "The Aerodynamic and Radiant Heat Input to Space Vehicles Which Re-enter at Satellite and Escape Velocity," American Rocket Society, Preprint No. 1558-60, December 1960.

Bryson, A. E., Denham, W. F., Carroll, F. J., and Mikand, K., "Determination of the Lift or Drag Program that Minimizes Re-entry Heating with Acceleration or Range Constraints Using a Steepest Descent Computation Procedure," Institute of the Aeronautical Sciences, Paper No. 61-6, 1961.

Cappellari, J. O., "The Effect of Drag Modulation on the Maximum Deceleration Encountered by a Re-entering Ballistic Missile," Purdue University, School of Aeronautical Engineering, Lafayette, Indiana, Report No. A-59-6, June 1959.

Chapman, D. R.,
"An Approximate Analytical Method for Studying Entry into Planetary Atmospheres," NASA TR R-11, 1959. (Also, NACA TN 4276, May 1958.)
"An Analysis of the Corridor and Guidance Requirements for Supercircular Entry into Planetary Atmospheres," NASA TR R-55.

Chapman, D. R., and Kapphahn, A. K., "Tables of Z Functions for Atmosphere Entry Analyses," NASA TR R-106, 1961.

Cheatham, D. C., Young, J. W., and Eggleston, J., "The Variation and Control of Range Traveled in the Atmosphere by a High-Drag Variable-Lift Entry Vehicle," NASA TN D-230, March 1960.

Cross, D. B.,
"A Study of Entry into the Earth's Atmosphere," American Astronautical Society, Preprint No. 58-48, December 1958.
"Re-entry Trajectory Analysis," The Martin Company, Denver, Colorado, Martin-Denver Course in Space Flight Dynamics, Lecture No. 13, 1960.
"Flight Dynamics and Heating Problems for Atmospheric Entry," The Martin Company, Denver, Colorado, Report No. R-60-12, May 1960.

Czarnecki, E. G., "Lifting Re-entry Vehicles," Astronautics, Vol. 6, No. 6, June 1961, pp 27 to 31, 50, 52.

Daskin, W., et al., "The Use of Lift for Re-entry from Satellite Trajectories," Jet Propulsion, Vol. 27, No. 11, November 1957, pp 1184 to 1189.

Detra, R. W., "Controlled Recovery of Nonlifting Satellites," ARS Journal, Vol. 30, No. 9, September 1960.

Detra, R. W., and Hidalgo, H., "Generalized Heat Transfer Formulas and Graphs for Nose Cone Re-entry into the Atmosphere," ARS Journal, Vol. 31, No. 3, March 1961, p 318.

Detra, R. W., Kemp, N. H., and Riddell, F. R., "Addendum to Heat Transfer to Satellite Vehicles Re-entering the Atmosphere," Jet Propulsion, Vol. 27, No. 12, December 1957.

Detra, R. W., and Riddell, F. R., "Controlled Recovery of Nonlifting Satellites," AVCO Research Laboratory and Advanced Development Division, Report No. RR 54, May 1959.

DiChristina, V., "Re-entry Performance of a High-Altitude Probe," Inst. Aerospace Sci., Paper 62-31, January 1962.

Dryer, M., "Propulsive Control of Atmospheric Entry Lifting Trajectories" (U), The Martin Company, Denver, Colorado, Report No. R-60-9, May 1960, 27 pp.

Edwards, R. H., and Campbell, G. S., "Prediction of Peak Temperature for Satellite Entries with Lift," ARS Journal, Vol. 30, No. 5, May 1960, p 496.

Eggers, A. J., Jr., Allen, H. J., and Neice, S. E., "A Comparative Analysis of the Performance of Long-Range Hypervelocity Vehicles," NASA TN 4046, October 1957.

Eggers, A. J., Jr., Hansen, C. F., and Cunningham, B. E., "Stagnation-Point Heat Transfer to Blunt Shapes in Hypersonic Flight, Including Effects of Yaw," NACA TN 4229, April 1958.

Eggleston, J. M., and Cheatham, D. C., "Piloted Entries into the Earth's Atmosphere," Institute of Aeronautical Sciences, Preprint No. 59-98, June 1959.

Ehricke, K. A.,
"On the Descent of Winged Orbital Vehicles," Astronautica Acta, Vol. 1, Fasc 3, 1955, pp 137 to 155.
"On Mechanics of Descent to Celestial Body," Journal of Astronautics, Vol. 2, No. 4, 1955, pp 137 to 144.
"Re-entry of Spherical Bodies into the Atmosphere at Very High Speeds," American Rocket Society, Spring Meeting, Washington, D. C., Reprint No. 428-57, April 1957.
"The Satelloid," Astronautica Acta, Vol. II, Fasc 2, 1956, pp 64 to 100.

Etkin, B., "The Entry of Manned Maneuverable Space Craft into Planetary Atmospheres," Toronto University, Inst. Aerophys., UTIA Rev. 20, October 1961.

Fay, J. A., and Riddell, F. R., "Theory of Stagnation-Point Heat Transfer in Dissociated Air," J. Aeronautical Science, Vol. 25, February 1958, pp 73 to 85.

Fay, J. A., "Hypersonic Heat Transfer in the Air Laminar Boundary Layer," AVCO Report AMP 71, March 1962.

Ferri, A., and Ting, L., "Practical Aspects of Re-entry Problems" (U), Polytechnic Institute of Brooklyn, Department of Aerospace Engineering, New York, Report No. PIBAL 705, July 1961.

Ferri, A., Feldman, L., and Daskin, W., "The Use of Lift for Re-entry from Satellite Trajectories," Jet Propulsion, Vol. 27, No. 11, November 1957.

Fine, J. H., "Stability of Flight Paths of Lifting Vehicles During Entry into Planetary Atmospheres," Toronto University, Inst. Aerophys., July 1961.

Fisher, L., "Landing Energy Dissipation for Manned Re-entry Vehicles," NASA TN D-453, 1960.

Gaines, L. M., and Surber, T. E., "Prediction of Optimum Approach and Landing Techniques for Manned Re-entry Gliders," North American Aviation, Inc., presented at the National IAS - ARS Joint Meeting, 13 to 16 June 1961, Ambassador Hotel, Los Angeles, California, IAS Paper 61-115-1809.

Galman, B. A.,
"Direct Re-entry at Escape Velocity," American Astronautical Society, Preprint No. 60-86, April 1960.
"Some Fundamental Considerations for Lifting Vehicles in Return from Satellite Orbit," General Electric Company, Philadelphia, Pennsylvania, Report No. GE-MSVD TIS R595D355, May 1959.

Garber, T. B.,
"Effects of Aerodynamic Forces upon the ICBM Re-entry Trajectory," The Rand Corporation, Santa Monica, California, Report No. RM 1782, August 1956.
"On the Rotational Motion of a Body Re-entering the Atmosphere," Journal of Aerospace Science, Vol. 26, No. 7, July 1959, p 443.

Gazley, C., Jr.,
"Recovery of a Circum-Lunar Instrument Carrier," The Rand Corporation, Santa Monica, California, Report No. P-119, 19 August 1957.
"The Penetration of Planetary Atmosphere," The Rand Corporation, Report No. P-1322, Santa Monica, California, February 1958.
"Deceleration and Heating of a Body Entering a Planetary Atmosphere from Space," Report No. P-955, The Rand Corporation, Santa Monica, California, 18 February 1957. (Also, Vistas in Astronautics, New York, Pergamon Press, Inc., 1958, Vol. 1, pp 8 to 32.)
"Atmospheric Entry of Manned Vehicles," The Rand Corporation, Research Memorandum RM-2579, Santa Monica, California, January 1960, p 42. (Also, Institute of Aerospace Sciences Space Stations Symposium, April 1960.)
"Atmospheric Entry," Handbook of Astronautical Engineering, McGraw-Hill Book Company, New York, 1961 (Koelle, ed.)

Gazley, C., Jr., and Masson, D. J., A Recoverable Scientific Satellite," Report No. RM-1844, The Rand Corporation, Santa Monica, California, 1956.

Grant, F. C.,
"Analysis of Low-Acceleration Lifting Entry from Escape Speed," NASA TN D-249, June 1960.
"Dynamic Analysis of a Simple Re-entry Maneuver for a Lifting Satellite," NASA TN D-47, September 1959.
"Importance of the Variation of Drag with Lift in Minimization of Satellite Entry Acceleration," NASA TN D-120, October 1959.
"Modulated Re-entry," Joint Conference on Lifting Manned Hypervelocity and Re-entry Vehicles, Langley Field, Virginia, April 1960.

Groves, G. V., "Velocity of a Body Falling Through the Atmosphere and the Propagation of Its Shock Wave to Earth," Journal of Atmospheric and Terrestrial Physics, Vol. 10, No. 2, February 1957, pp 73 to 83.

Guess, A. L., and Peline, V. P., "The Sensisitivity of Ballistic Satellite Re-entry Trajectory Prediction to Differences in the Geophysical Properties," The Martin Company, Baltimore, Maryland, Report No. AP TN 60-3. (Also, Lockheed Aircraft Corporation, Sunnyvale, California, Report No. LMSD-447470.)

Hendrix, C. E., "Proposal for a Simple System for Achieving Soft Landing of a Rocket Vehicle," Naval Ordnance Test Station, China Lake, California, NOTS TP 2495, NavWEPS Report 7084.

Jackson, C. M., Jr., "Estimates of Minimum Energy Requirements for Range-Controlled Return of a Non-Lifting Satellite from a Circular Orbit," NASA Technical Note D-980, November 1961.

Hermann, R., "Ascent and Re-entry," Space Trajectories, Academic Press, New York, 1960.

Hilderbrand, R. B., "Aerodynamic Fundamentals," Handbook of Astronautical Engineering, McGraw-Hill Book Company, New York, 1961 (Koelle, ed.).

Hill, F. A. F., "Satellite Re-entry with Lightly Loaded Lifting Vehicles," Massachusetts Institute of Technology, Naval Supersonic Laboratory, Cambridge, Massachusetts, Technical Report No. 429, December 1959.

Hoglund, R., and Thale, J., "Recovery from a Satellitic Orbit," American Rocket Society, Preprint 650-58, 1958.

Hoshizaki, H., "Heat Transfer in Planetary Atmospheres at Super-Satellite Speeds, ARS Journal, Vol. 32, No. 10, p 1544.

Hunziker, R. R., "Re-entry Trajectories for Impact Prediction and Radar Acquisition," ARS Journal, Vol. 32, No. 8, August 1962, p 1261.

Kaeppeler, H. J., and Kubler, M. E., "Die Rückkehr von Geflugelten Geräten von Aussenstationsbahnen," Bericht uber den V. Internationalen Astronautischen Kongress. Vienna, Springer Publication, 1955 (F Hecht, ed.).

Katzen, E. D., "Terminal Phase of Satellite Entry into the Earth's Atmosphere," ARS Journal, Vol. 29, No. 2, February 1959, pp 147 to 148.

Katzen, E. D., and Levy, L. L., Jr., "Atmosphere Entries with Vehicle Lift-Drag Ratio Modulated to Limit Deceleration and Rate of Deceleration - Vehicles with Maximum Lift-Drag Ratio of 0.5," NASA Technical Note D-1145, December 1961.

Kemp, N. H., and Riddell, F. R., "Heat Transfer to Satellite Vehicles Re-entering the Atmosphere," Jet Propulsion, Vol. 27, No. 2, February 1957, pp 132 to 137.

Kemp, N. H., Rose, P. H., and Detra, R. W., "Laminar Heat Transfer Around Blunt Bodies in Dissociated Air," Journal of the Aerospace Sciences, Vol. 26, 1959, pp 424 to 450.

Kennet, H., and Strack, S. L., "Stagnation Point Radiative Transfer," ARS Journal, Vol. 31, No. 3, March 1961, p 370.

Kepler, D. I., "Concepts Influencing the Selection of a Configuration for Atmospheric Re-entry," American Rocket Society, Paper No. 786-59, April 1959.

King-Hele, D. G., "The Descent of an Earth-Satellite Through the Upper Atmosphere," Journal of the British Interplanetary Society, Vol. 15, December 1956, pp 314 to 323.

Kork, J., "Satellite Re-entry," Design Guide to Orbital Flight, McGraw-Hill Book Company, New York, Chapter X, 1962.

Lees, L.,
Ablation in Hypersonic Flow, New York, Seventh Anglo-American Aeronautical Conference, October 5 to 7, 1959.
"Laminar Heat Transfer Over Blunt-Nosed Bodies at Hypersonic Flight Speeds," Jet Propulsion, Vol. 26, No. 4, 1956, pp 259 to 269, 274.
"Recent Developments in Hypersonic Flow," Jet Propulsion, Vol. 27, No. 11, November 1957, pp 1162 to 1178.
"Recovery Dynamics--Heat Transfer at Hypersonic Speeds in a Planetary Atmosphere," Space Technology, New York, John Wiley and Sons, 1959.

Lees, L., Hartwig, F. W., and Cohen, C. B., "The Use of Lift During Entry into the Earth's Atmosphere," American Rocket Society, Preprint No. 785-59, April 1959. (Also, ARS Journal, Vol. 29, No. 9, September 1959).

Legalley, D. P., ed., "Re-entry and Vehicle Design," Ballistic Missile and Space Technology, Academic Press, New York, Vol. 4, 1960, p 422.

Levin, A. D., and Hopkins, E. J., "Re-entry Glide Maneuvers for Recovery of a Winged First-Stage Rocket Booster."

Levinsky, E. S., "Application of Inequality Constraints to Variational Problems of Lifting Re-entry," Institute of Aerospace Sciences, Report No. 61-21, January 1961.

Levy, L. L., Jr., "Atmosphere Entries with Spacecraft Lift-Drag Ratios Modulated to Limit Decelerations," NASA Technical Note D-1427, October 1962.

Lew, H. G., "Re-entry Physics," General Electric Company, Missile and Space Vehicle Department, Philadelphia, Pennsylvania, Contract No. DA 36-034-ORD-3187 (RD), December 1960. (Martin Library No. 6173-S-19.)

Linnell, R. D., "Vertical Re-entry into the Earth's Atmosphere for Both Light and Heavy Bodies," Jet Propulsion, Vol. 28, No. 5, pp 329-331, May 1958.

Loh, W. H. T.,
"Mechanics of Re-entry," 4th Symposium on Ballistic Missiles and Space Technology, Los Angeles, California, August 1959.
"Dynamics and Thermodynamics of Re-entry," Journal of the Aerospace Sciences, October 1960, pp 748 to 762.
"A Second Order Theory of Entry Mechanics into a Planetary Atmosphere," Institute of Aerospace Sciences, June 1961, Preprint No. 61-116-1810.
"Supercircular Gliding Entry," ARS Journal, Vol. 32, No. 9, September 1962, p 1398.
"Ballistic Re-entry at Small Angles of Inclination," ARS Journal, Vol. 32, No. 5, May 1962, p 718.

Luidens, R. W., "Approximate Analysis of G-Loads and Heating During Atmospheric Entries and Passes with Constant Aerodynamic Coefficients," NASA TN D1280, July 1962.

Mandell, D. S.
"A Study of the Maneuvering Performance of Lifting Re-entry Vehicles, Part I, Initial Atmospheric Re-entry," General Electric Company, Missile and Space Vehicle Department, Philadelphia, Pennsylvania, Flight Mechanics Data Memo No. 2:23, October 1960. (Also, American Rocket Society, Preprint No. 1555-60, December 1960.)
"Maneuvering Trajectory Program," General Electric Company, Missile and Space Vehicle Department, Philadelphia, Pennsylvania, Report No. TIS R50SD398, November 1960.
"Maneuvering Performance of Lifting Re-entry Vehicles," Vol. 32, No. 3, ARS Journal, March 1962, p 346.

Marshall, F. J., "Optimum Re-entry via a Variable Control Force," American Rocket Society, Preprint No. 956-59, 1959.

Miele, A., and Cavoti, C. R., "Variational Approach to the Re-entry of a Ballistic Missile, Parts I and II," Purdue University, School of Aeronautical Engineering, Lafayette, Indiana, Reports Nos. A-59-1 and A-59-3.

Miercort, F. A., "Re-entry into an Exponential Atmosphere, Ignoring Gravity," Martin-Denver, SR 1420-5, 30 November 1961, p 6.

Miller, B. P., "Approximate Velocity, Position and Time Relationship for Ballistic Re-entry," Vol. 31, No. 3, ARS Journal, March 1961, p 437.

Moe, M. M., "An Approximation to the Re-entry Trajectory," ARS Journal, Vol. 30, No. 1, ARS Journal, 1960, pp 50 to 53.

Morth, R. and Speyer, J. L., "Divergence from Equilibrium Glide Path at Supersatellite Velocities," ARS Journal, Vol. 31, No. 3, p 448.

Nielson, J. N., "Three-Dimensional Satellite Orbits with Emphasis on Re-entry Dynamics and Oblateness Effects," Aero/Space Engineering, Vol. 18, No. 4, April 1959, pp 60 to 66.

Nonweiler, T. R. F.,
"Problems of Interplanetary Navigation and Atmospheric Re-entry," Journal of the Royal Aeronautical Society, Vol. 64, 1960, pp 155 to 160.
"The Motion of an Earth Satellite on Re-entry to the Atmosphere," IXth International Astronautical Congress, Amsterdam, Vol. II, 1958, p 842. (Also, Astronautica Acta, Vol. 5, 1959.)

Norling, R. A., "Normal Dispersion of a Re-entry Body," ARS Journal, Vol. 30, No. 7, July 1960, p 652.

Offenhartz, E., Weisblatt, H., and Flagg, R. F., "Stagnation Point Heat Transfer Measurement at Super-Satellite Speeds," J. Royal Aeronautical Soc. Vol. 66, January 1962, p 53.

Olstad, W. B., "A Study of the Feasibility of Inflatable Re-entry Gliders," NASA TN D-538, 1960.

Phillips, R. L., and Cohen, C. B., "Use of Drag Modulation to Reduce Deceleration Loads During Atmospheric Entry," ARS Journal, Vol. 29, No. 6, June 1959.

Plascott, R. H., "The Re-entry of Manned Earth Satellites," Royal Aeroplane Establishment, Farnborough, England, Technical Note No. 2640, August 1959.

Probstein, R. F., "Methods of Calculating the Equilibrium Laminar Heat Transfer Rate at Hypersonic Flight Speeds," Jet Propulsion, Vol. 26, 1956, pp 497 to 499.

Quillinan, J. H., London, J. and Aston, B. A., "Configuration Selection of Re-entry Vehicles," Institute of Aeronautical Sciences, Preprint No. 59-97, June 1959.

Remmler, K. L., "Tumbling Bodies Entering the Atmosphere," ARS J. 32, 92-94, 1962.

Reshotko, E., "Simplified Method for Estimating Compressible Laminar Heat Transfer with Pressure Gradient," NACA TN 3888, December 1956.

Reshotko, E. and Cohen, C. B., "Heat Transfer at the Forward Stagnation Point of Blunt Bodies," NACA TN 3513, July 1955.

Rasamond, D. L., "Satellite Recovery Techniques for Optimization of Touchdown Accuracy," Institute of Aeronautical Sciences, Preprint No. 59-92, June 1959.

Riddell, F. R. and Detra, R. W., "Returning Alive from Space," American Astronautical Society, January 1958.

Riddell, F. R., and Winkler, H. B., "Meteorites and Re-entry of Space Vehicles at Meteor Velocities, ARS Journal, Vol. 32, No. 10, October 1962, p 1523.

Robinson, A. C., and Besonis, A. J., "On the Problems of Re-entry into the Earth's Atmosphere," USAF WADC TR 58-408, August 1958. (Also ASTIA No. AD 203790.) (Also, Journal of the Astronautical Sciences, No. 7, 1960, pp 7 to 21.)

Robinson, A. C., and Poli, C. R., "Development of Normalized Six-Degree-of-Freedom Equations for Analog Simulation of Atmospheric Re-entry," Synthesis and Analysis Division, Directorate of Systems Dynamic Analysis, Aeronautical Systems Division, Wright-Patterson Air Force Base, Ohio. (Task No. 70958) (ASD TR 61-448), November 1961.

Robinson, A. C., Wolaver, L. E. and Besonis, A. J., "A Study of Nonlifting Satellites Re-entering the Earth's Atmosphere," WADC Aero Research Laboratory Working Paper, March 1958.

Rogallo, F. M., and Lowry, J. G., "Flexible Re-entry Gliders," Society of Automotive Engineers, Inc., New York, Preprint No. 175C, 1960.

Rose, P. H., "Re-entry from Lunar Missions," AVCO Rpt AMP 69, December 1961.

Rute, L., "A Study of Aerodynamic Effects of Isothermal and Temperature Gradient Atmospheres on Re-entry Trajectories," Polytechnic Institute of Brooklyn, Department of Aerospace Eng and Applied Mechanics, AFOSR 2411, March 1962.

Scala, S., "Heating Problems of Entry into Planetary Atmospheres from Super Circular Orbiting Velocities," Proceedings of Symposium on Aerothermoelasticity, Aeronautical Systems Division, Wright-Patterson AFB, Ohio TR 61-645, October 1961.

Scherberg, M. G. and Rubin, T., "Decelerations of Ballistic Type Missile on Re-entry into Atmosphere," WADC TN WCRR53-2, February 1953.

Skulsky, R. S. and Summers, L. J., "Parametric Studies on Ballistic Re-entry Trajectories," The Martin Company, Denver, Colorado, Report MI-60-36, May 1960.

Slye, R. E., "An Analytical Method for Studying the Lateral Motion of Atmosphere Entry Vehicles," NASA TN D-325, September 1960.

Smith, R. H., "Supercircular Entry and Recovery with Maneuverable Manned Vehicles," Institute of Aerospace Sciences, Preprint No. 61-114-1808, June 1961.

Strack, S. L., "Radiant Heat Transfer Around Re-entry Bodies," ARS Journal, Vol. 32, No. 5, May 1962, p 744.

Surber, T. E. and Gaines, L. M., "Prediction of Optimum Approach and Landing Techniques for Manned Lifting Re-entry Gliders," Institute of Aerospace Sciences, Preprint No. 61-115-1809, June 1961.

Swanson, B. L.,
"A Study of Methods for Simulating the Atmosphere Entry of Vehicles with Small-Scale Models"
"Appendix A, B--Turbulent Heating Rates"
"Appendix C--Simulation of Highly Elliptic, Parabolic, and Hyperbolic Entries," NASA TN D-90, 1960, 51 pp.

Townsend, G. and Kork, J., "Satellite Recovery," Design Guide to Orbital Flight, McGraw-Hill Book Company, New York, Chapter 9, 1962.

Turnacliff, R. D. and Hartnett, J. P., "Generalized Trajectories for Free-Falling Bodies of High Drag," American Rocket Society, Preprint No. 543-57, December 1957.

Vargo, L. G., "Criteria for Orbital Re-entry," Jet Propulsion, Vol. 28, No. 1 January 1958, p 54.

Wang, K. and Ting, L., "An Approximate Analytic Solution of Re-entry Trajectory with Aerodynamic Forces," ARS Journal Vol. 30, No. 6, June 1960, p 565.
"Approximate Solutions for Re-entry Trajectories with Aerodynamic Forces," Astronaut Acta, 8, 28-41, 1962.

Warden, R. V., "Ballistic Re-entries with a Varying W/C_DA," ARS Journal, Vol. 31, No. 2, pp 208 to 213, February 1961.

Wick, B. H., "Radiative Heating of Vehicles Entering the Earth's Atmosphere," presented to the Fluid Mechanics Panel of Advisory Group for Aeronautical Research and Development, Brussels, Belgium, 3 to 6 April 1962.

Wong, T. J., et al., "Motion and Heating During Atmosphere Re-entry of Space Vehicles," NASA TN D-334, 1960.

"The Use of Aerodynamic Lift During Entry into The Earth's Atmosphere," Space Technology, Inc., Los Angeles, Cal., 20 November 1958.

"Trajectory Control for Vehicles Entering the Earth's Atmosphere at Small Flight-Path Angles," Langley Research Center, Langley Field, Va., February 1959.

"Variational Procedure for Minimizing Heating Effects During the Re-entry of a Lifting Vehicle: Heat Transfer to Slender Hypersonic Delta Wings Near 90° Incidence," Aeronautical Systems Division, Dir/Aeromechanics, Flight Dynamics Lab, Wright-Patterson AFB, Ohio, WADD TR 60-369, Vol. II, Final Report, April 1962.

"On the Mechanics of Descent to a Celestial Body," American Rocket Society, Report No. 146 A-54.

"Proceedings of the Recovery of Space Vehicles Symposium," Los Angeles, Cal., 31 August to 1 September 1960.

New York, Institute of the Aeronautical Sciences, 1960

"Recovery Technology and Space Operations," Evans, H. L.
"A Guided Parachute System," Kane, M. T.
"A Minimum Weight Landing System for Interplanetary Spacecraft," Ewing, E. G.
"Introduction to Dyna-Soar Recovery Session," Moore, W. L.
"The Effect of Search and Retrieval on Escape System Performance and Space Crew Safety," Edwards, H. H. and Garnett, R. J.

"Re-entry of Spherical Bodies into the Atmosphere at Very High Speed," American Rocket Society, Report No. 22128-57.

ILLUSTRATIONS

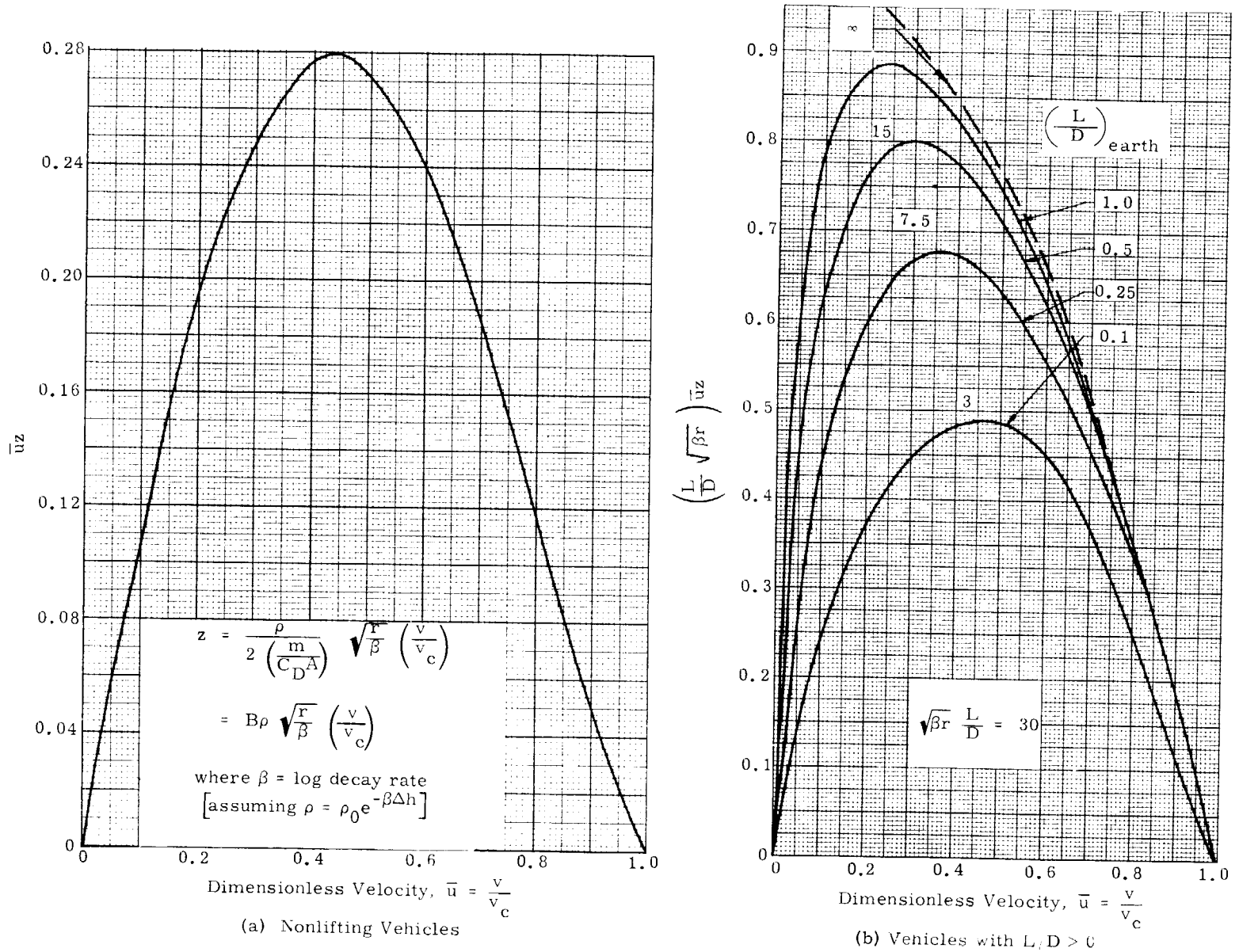

Fig. 1. Values of z Functions for Entry from Decaying Orbits into Planetary Atmosphere (Ref. 1)

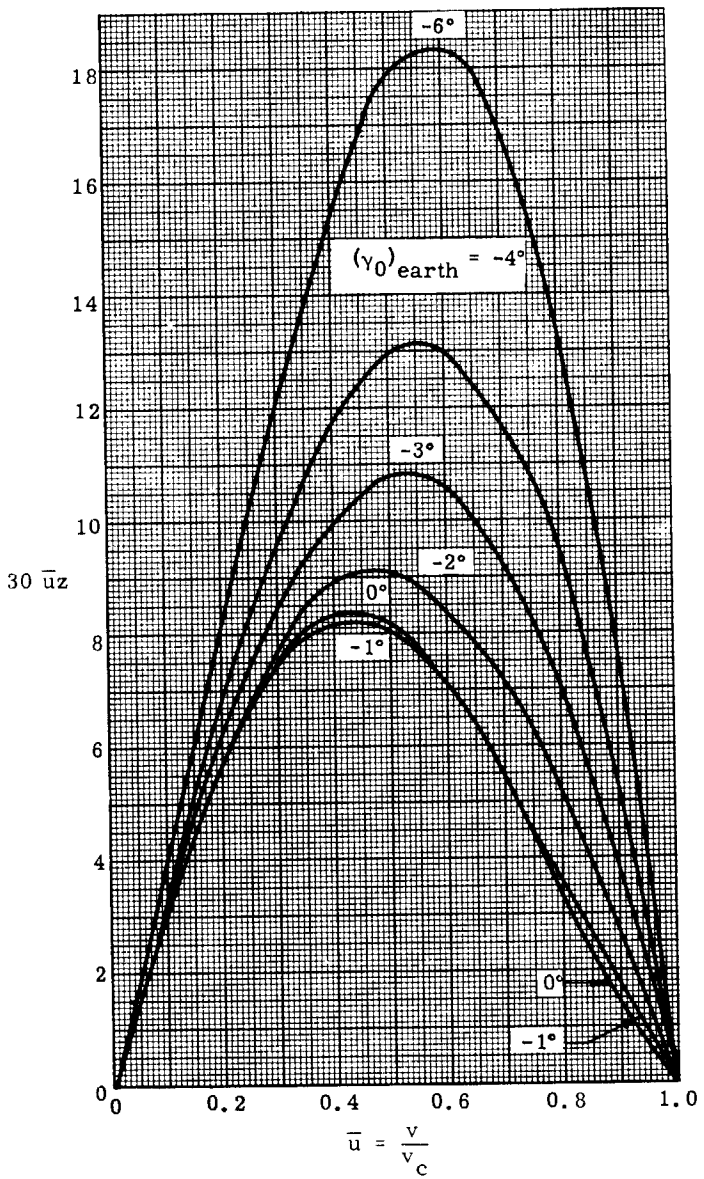

(a) Nonlifting Vehicles, L/D = 0

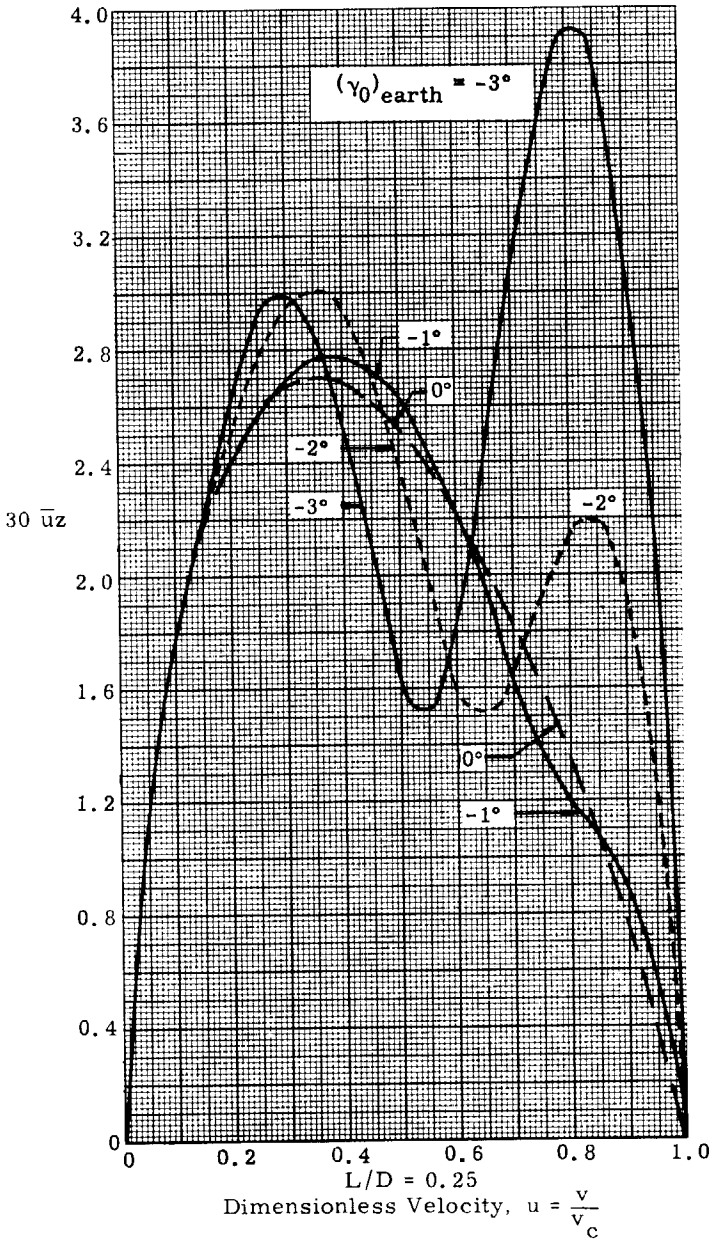

(b) Vehicles with L/D > 0 = 0.25

Fig. 2. Values of z Functions for Entry from Orbital Velocity at Initial Angles of Descent; $\bar{u}_0$ = 1 (Ref. 1)

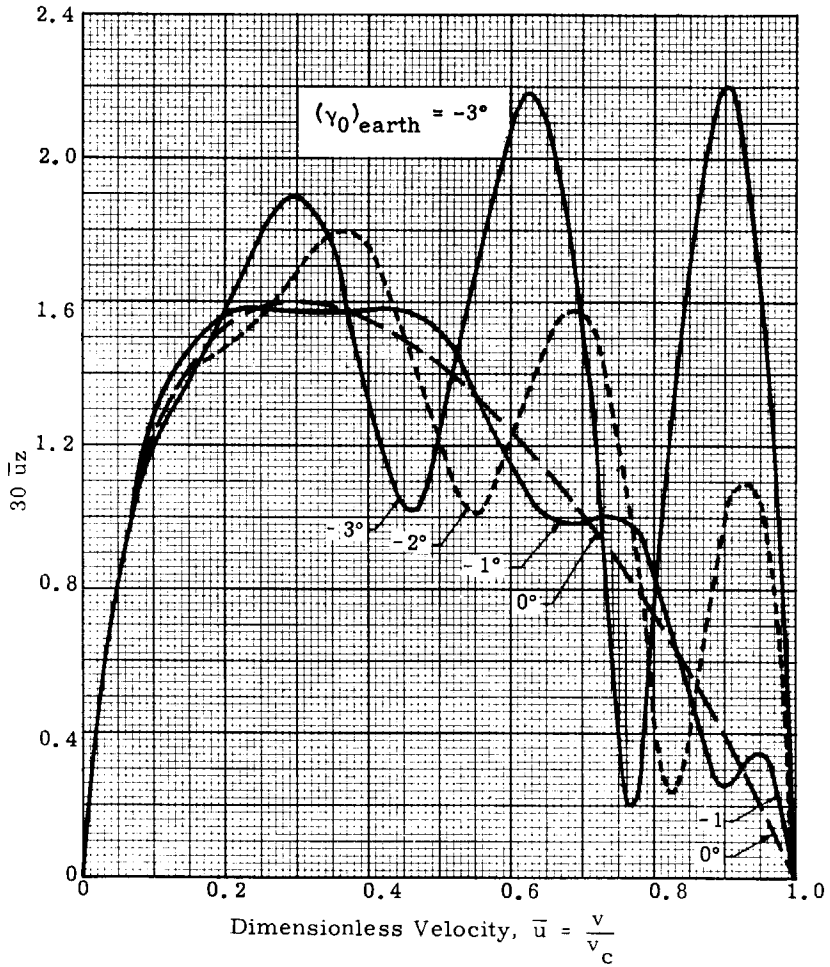

(c) Vehicles with L/D = 0.5

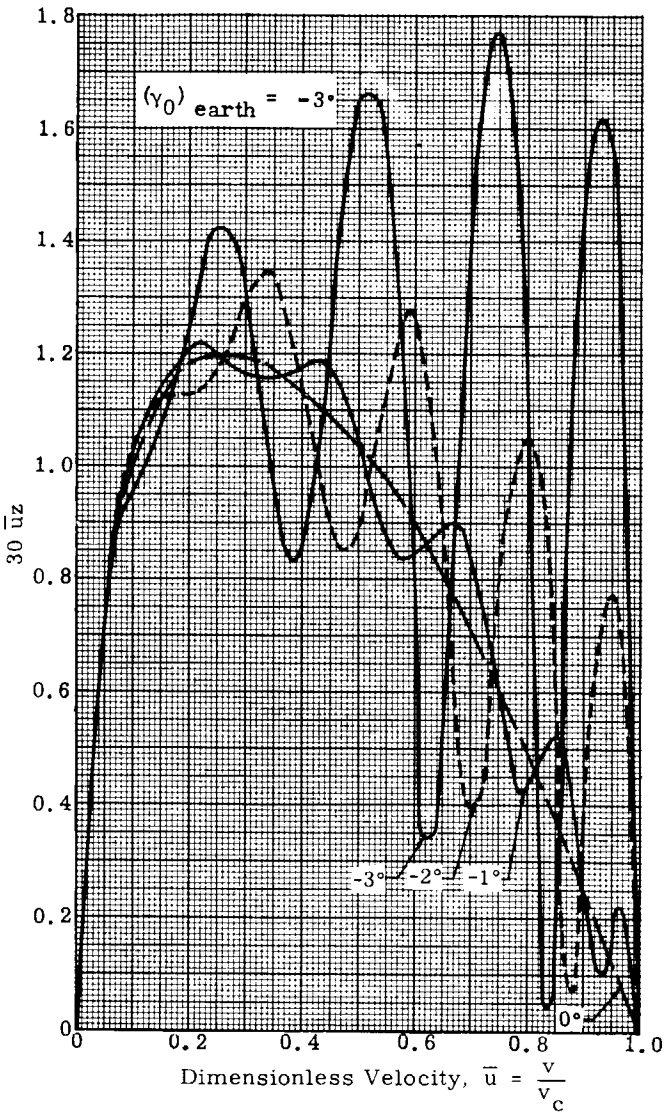

(d) Vehicles with L/D = 0.7

Fig. 2. (continued)

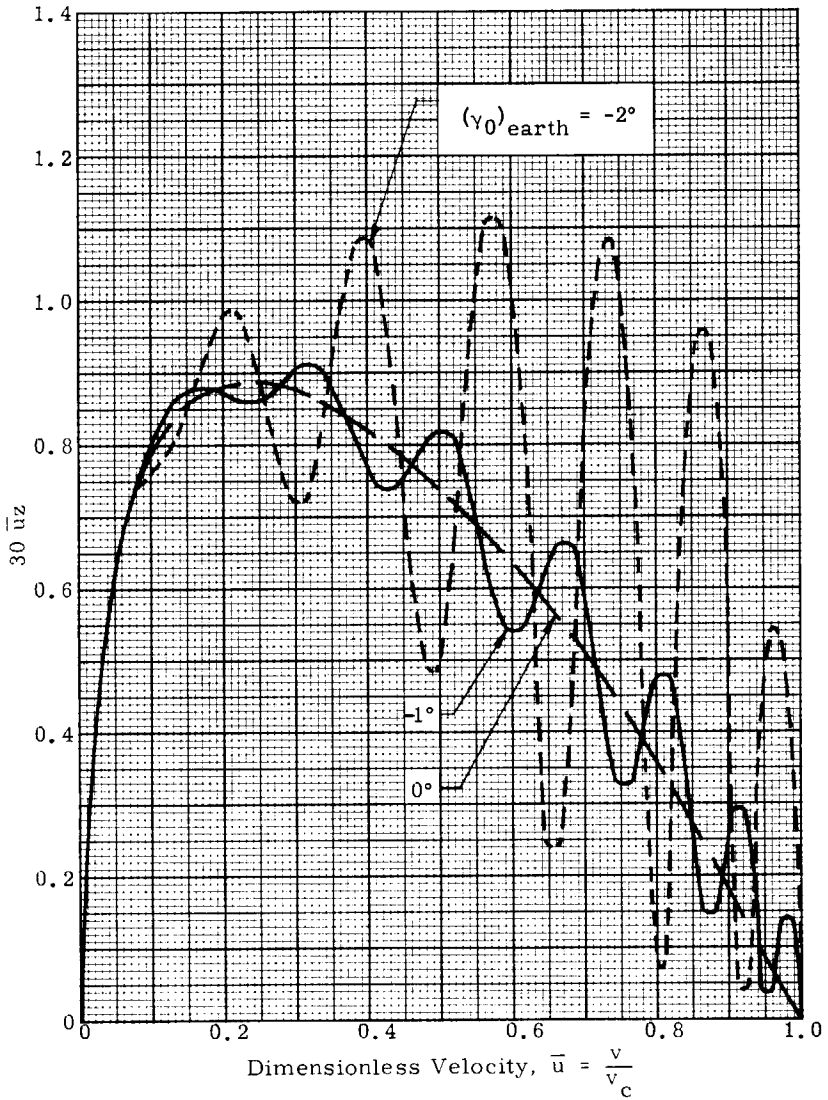

(e) Vehicles with L/D = 1

Fig. 2. (continued)

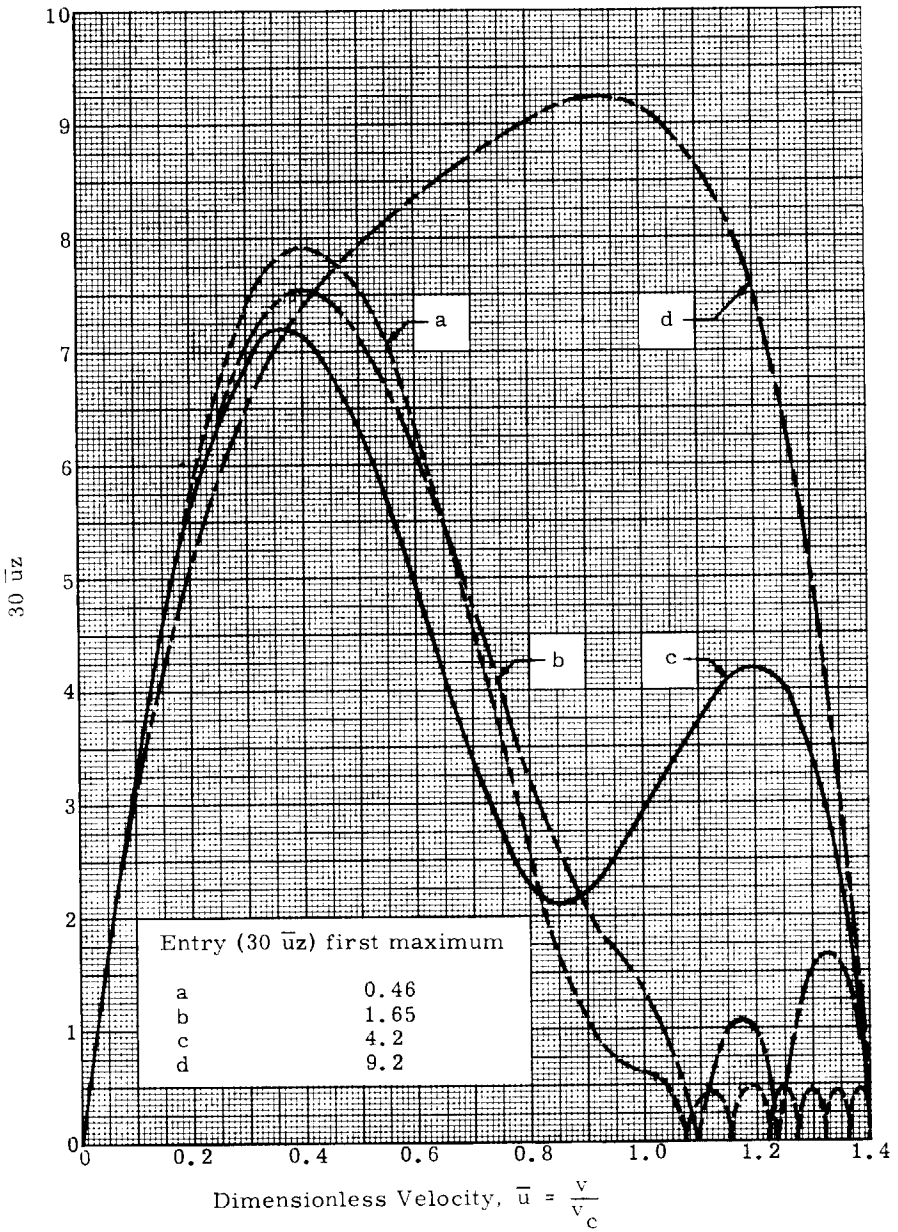

Fig. 3. Values of z Functions for Atmosphere Braking of Nonlifting Vehicles ($\bar{u}_0$ = 1.4, L/D = 0) (Ref. 1)

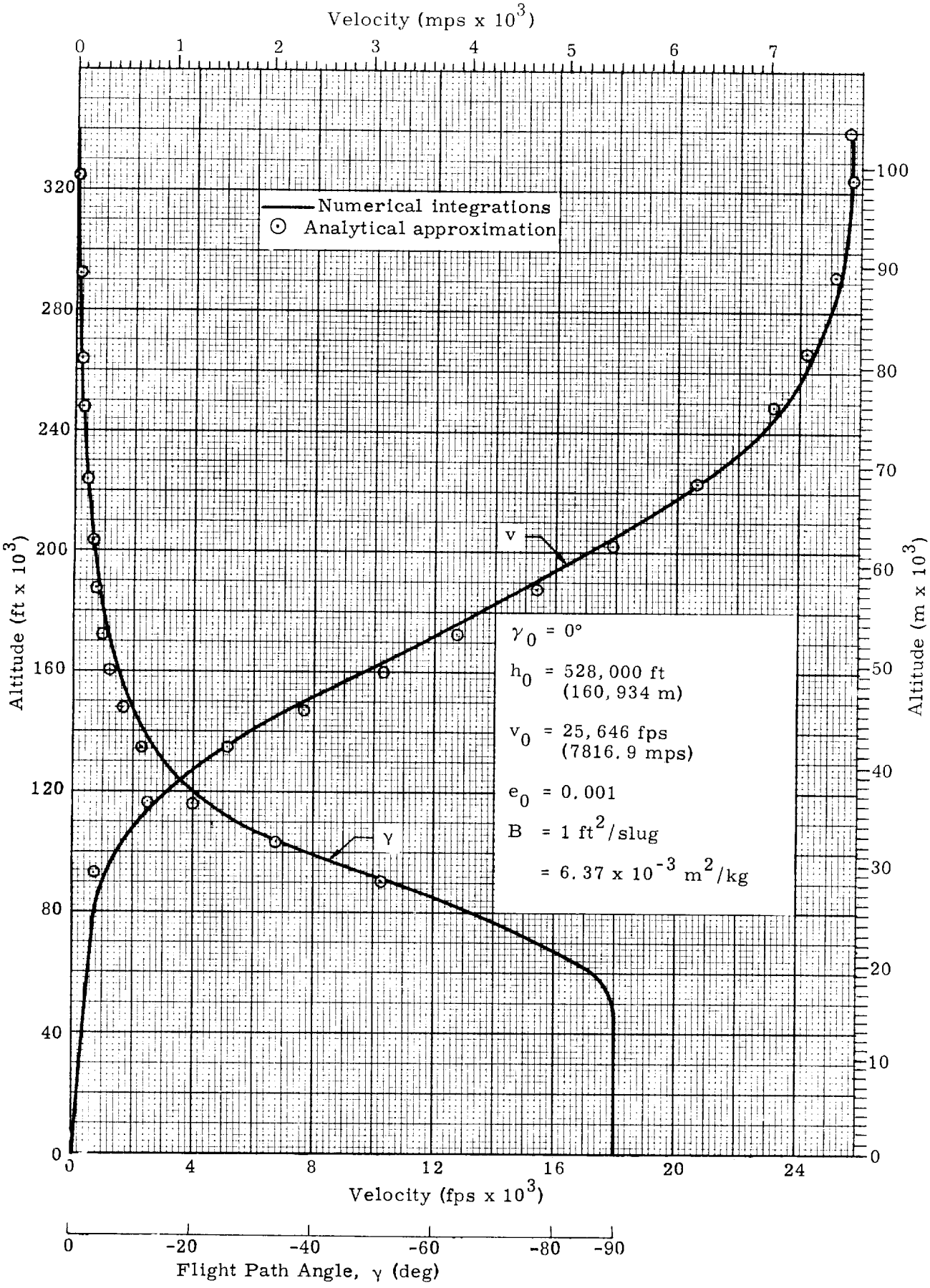

Fig. 4. Velocity Profile and Flight Path Angle Variation for Satellite Re-Entry

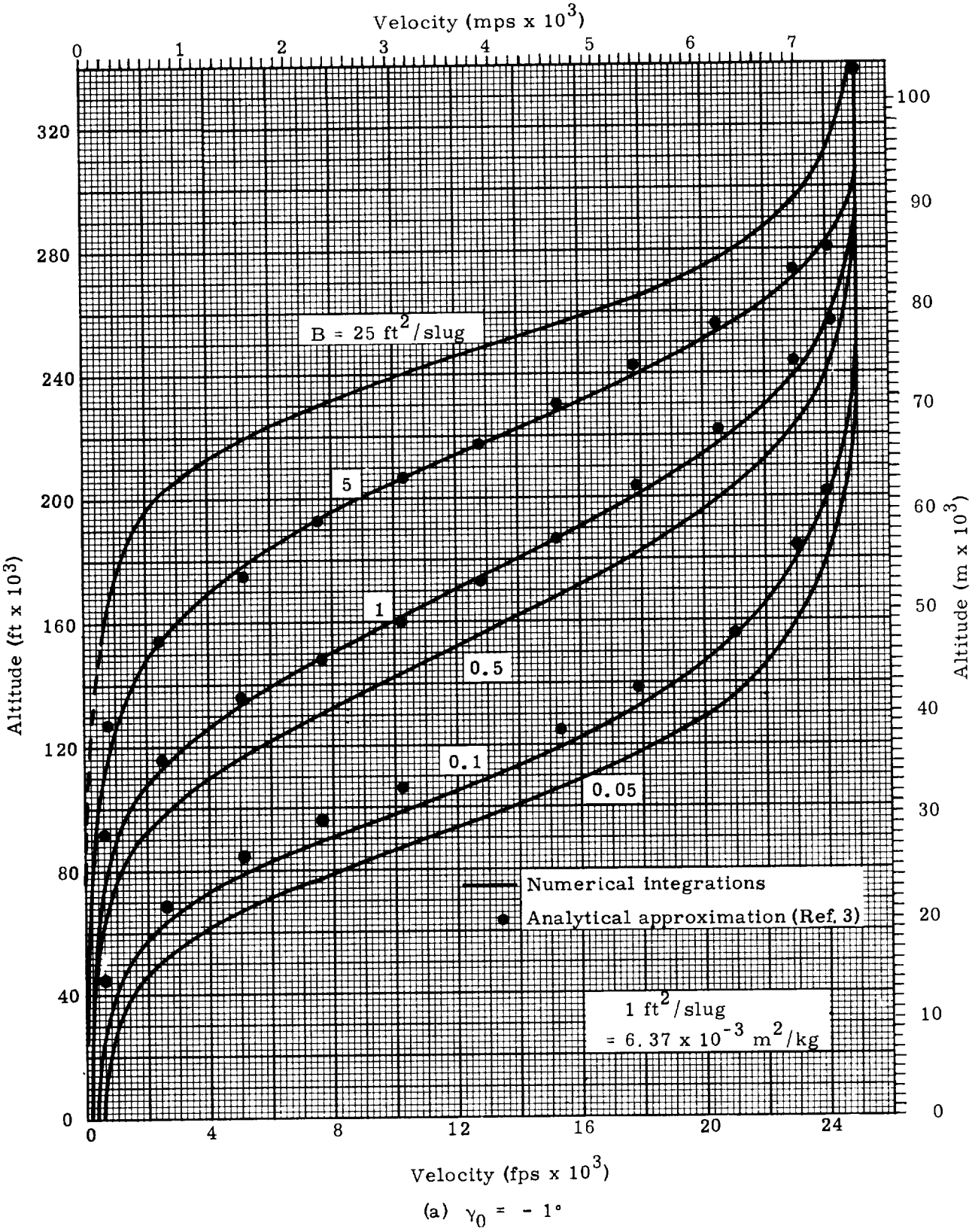

(a) $\gamma_0 = -1°$

Fig. 5. Velocity Variation with Altitude (h_0 = 300,000 ft = 91,440 m, v_0 = 25,000 fps = 7,620 mps, L/D = 0)

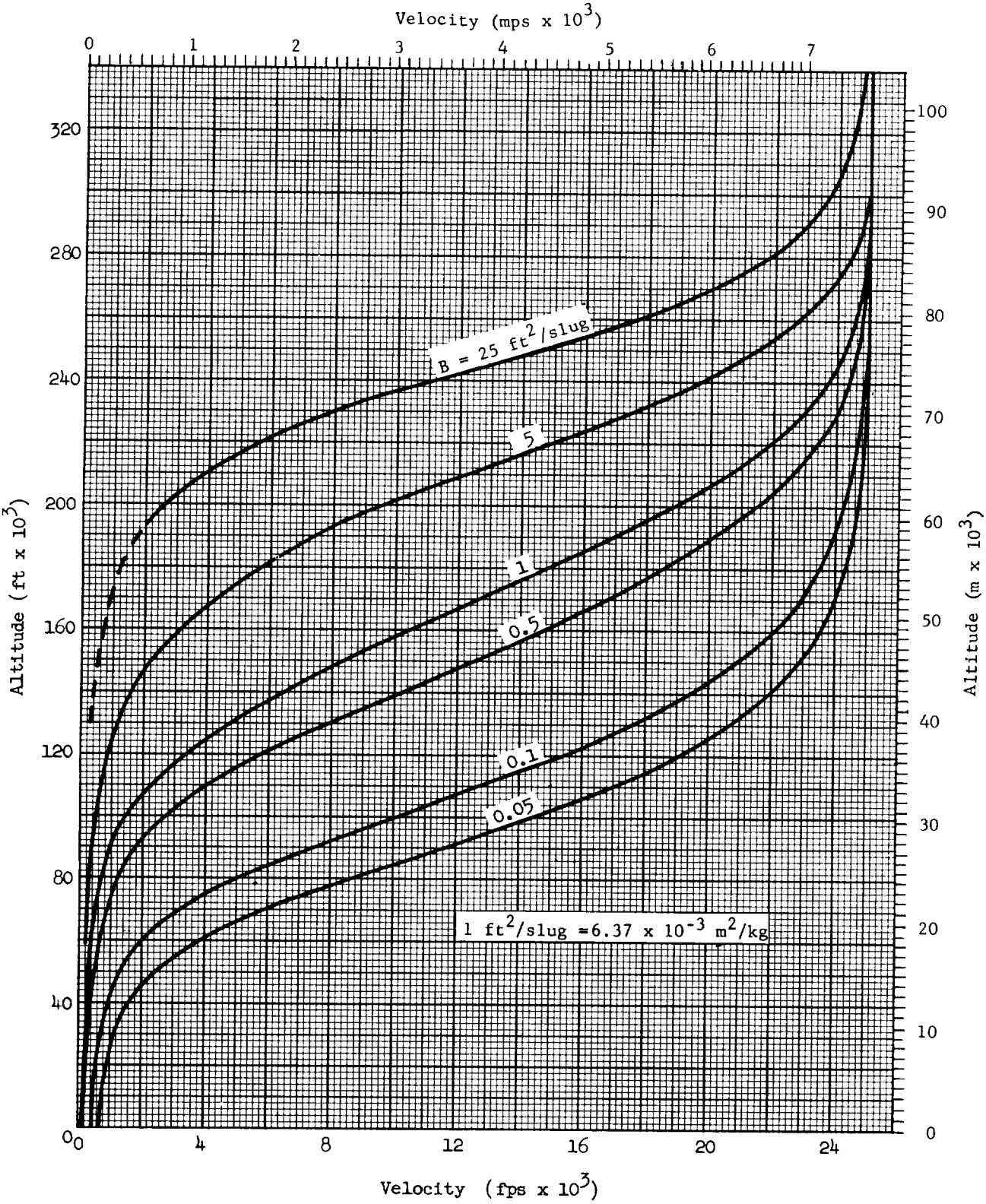

(b) $\gamma_0 = -2°$

Fig. 5. (continued)

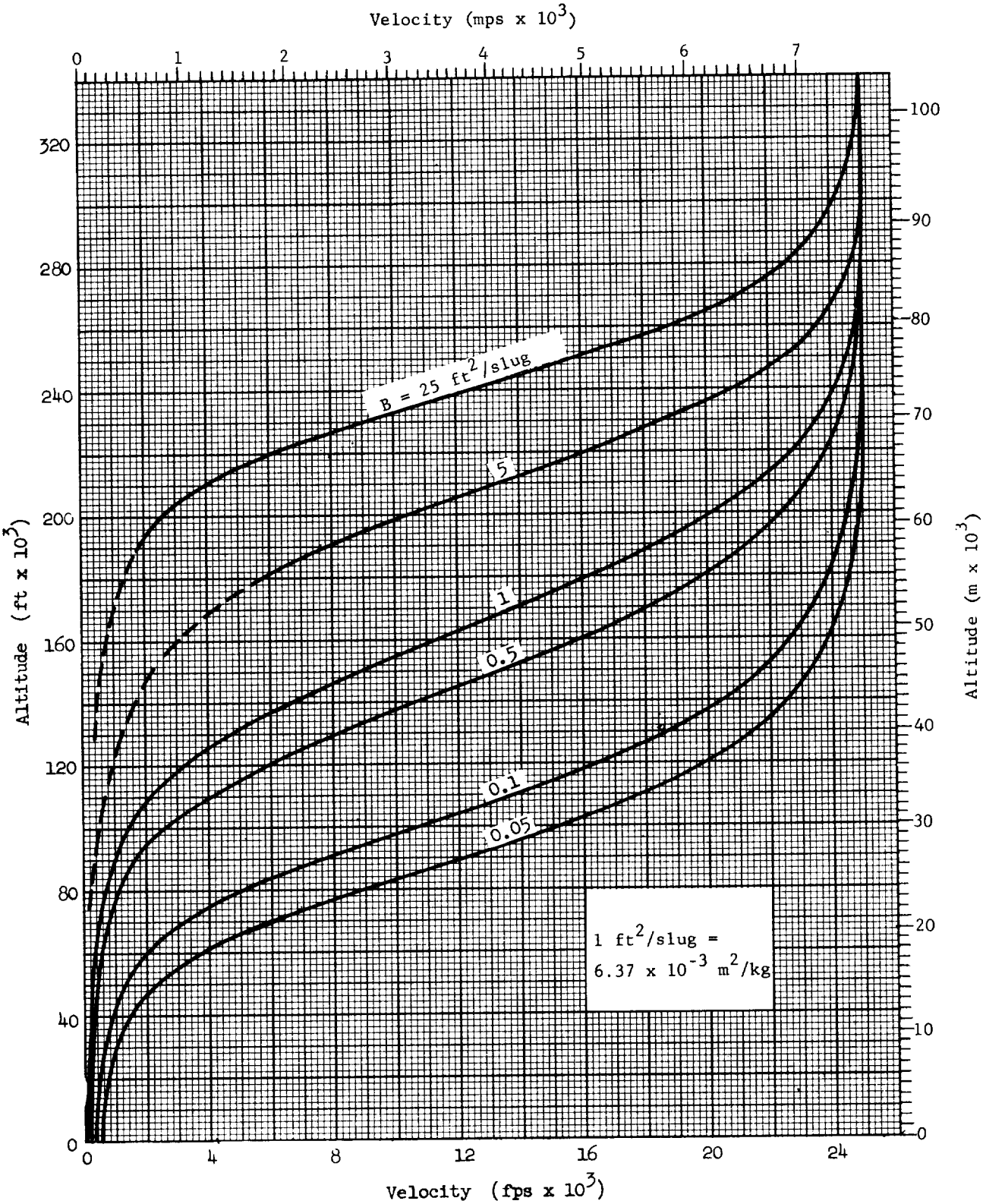

(c) $\gamma_0 = -3°$

Fig. 5. (continued)

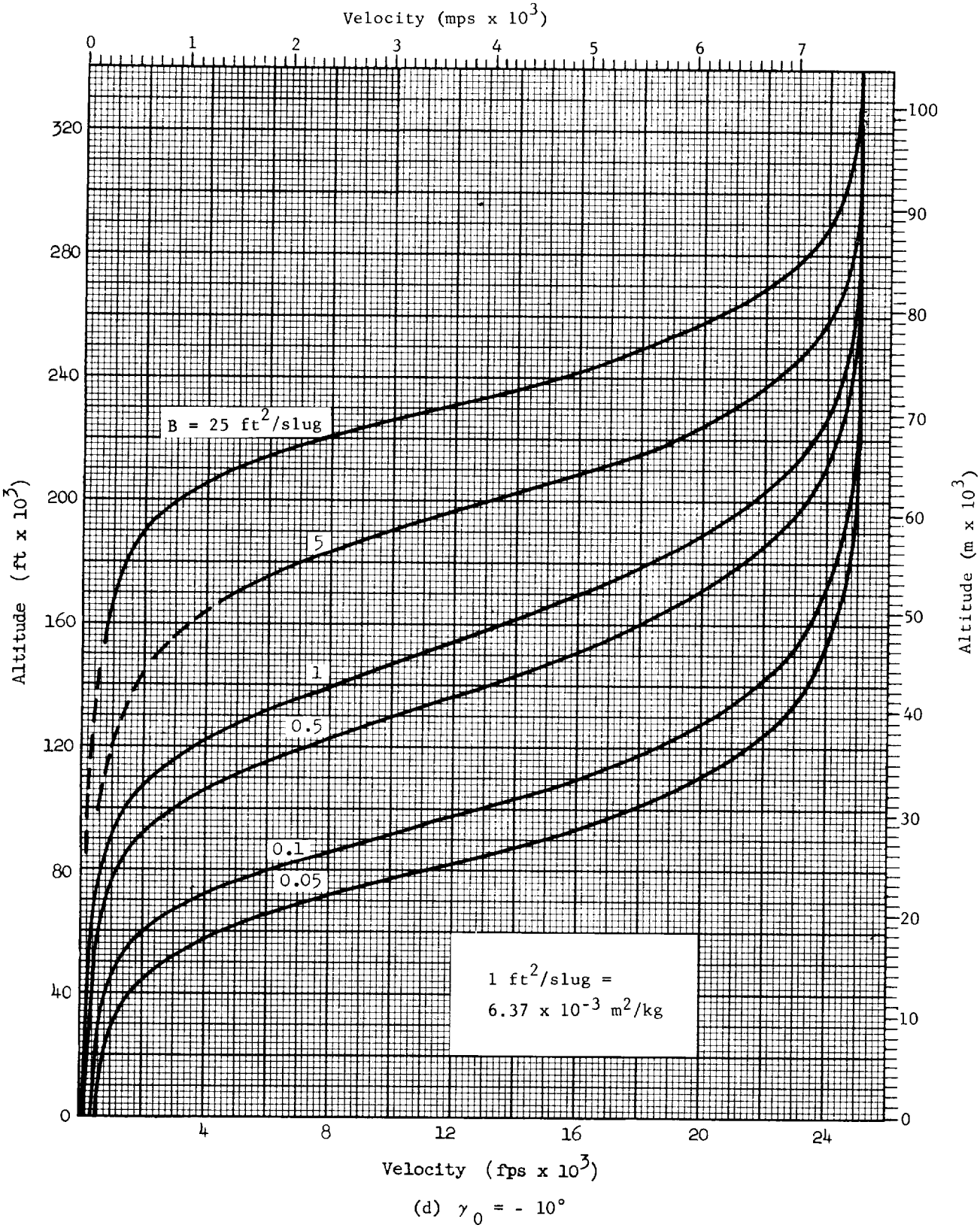

(d) $\gamma_0 = -10°$

Fig. 5. (continued)

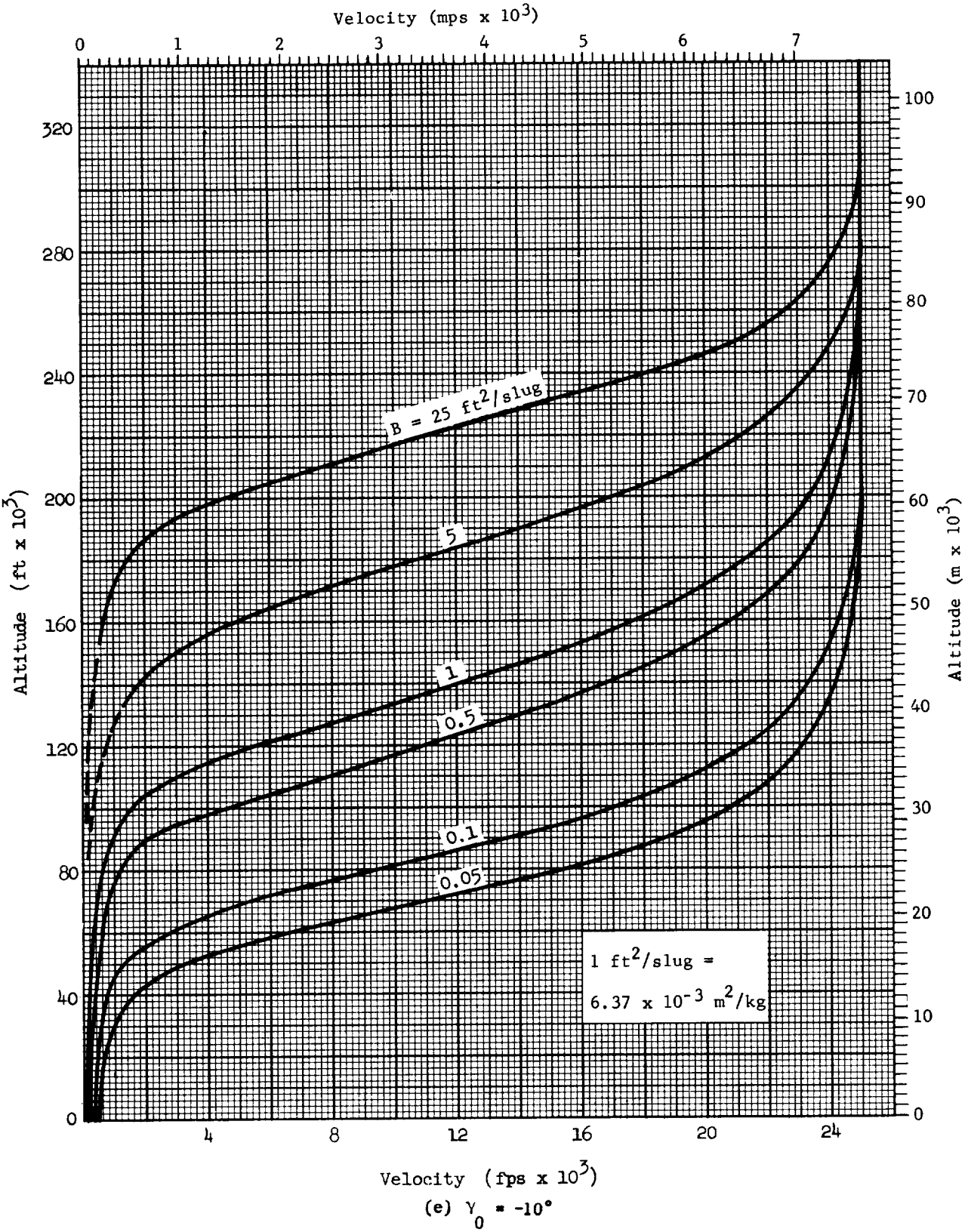

(e) $\gamma_0 = -10°$

Fig. 5. (continued)

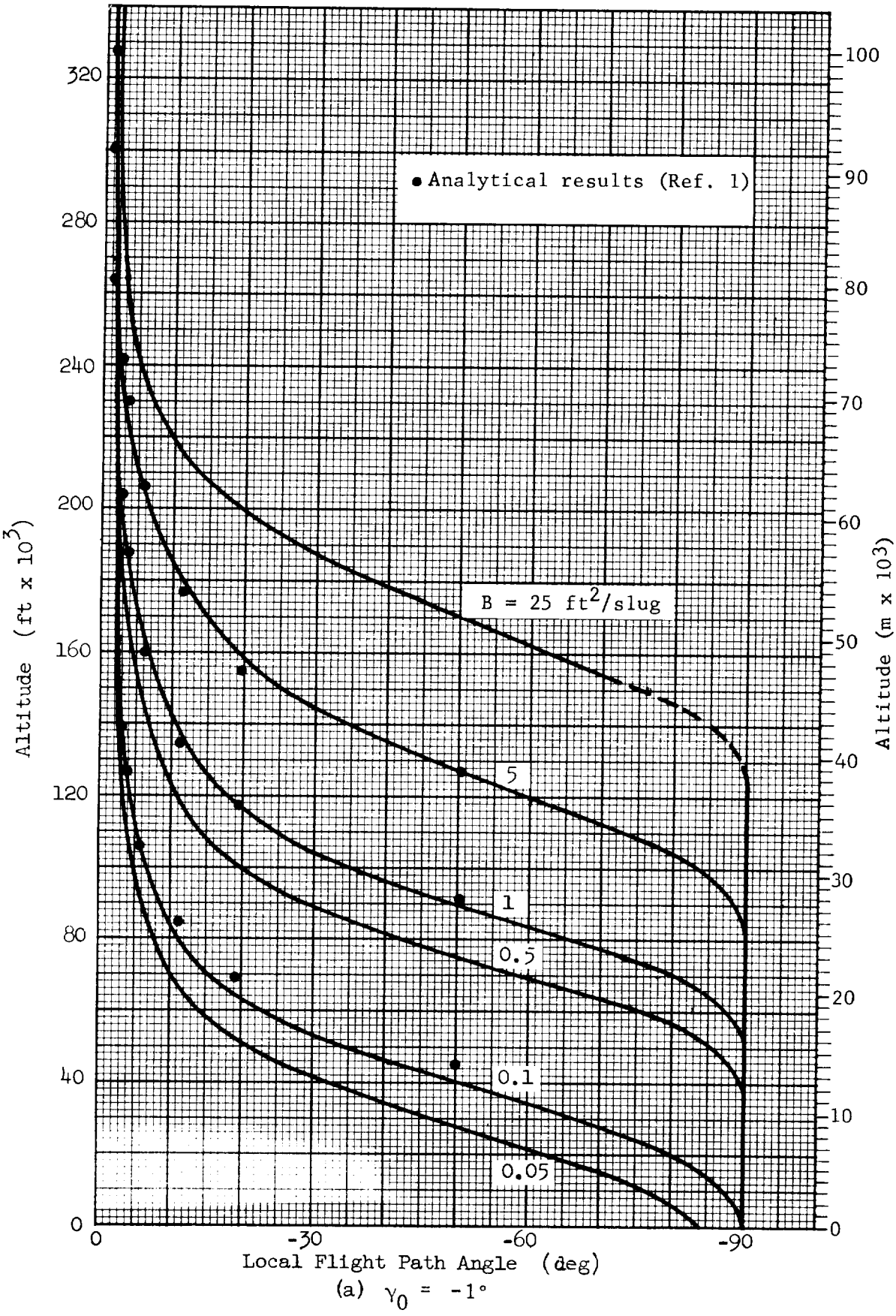

Fig. 6. Flight Path Angle Variation with Altitude (h_0 = 300,000 ft = 91,440 m; v_0 = 25,000 fps = 7620 mps)

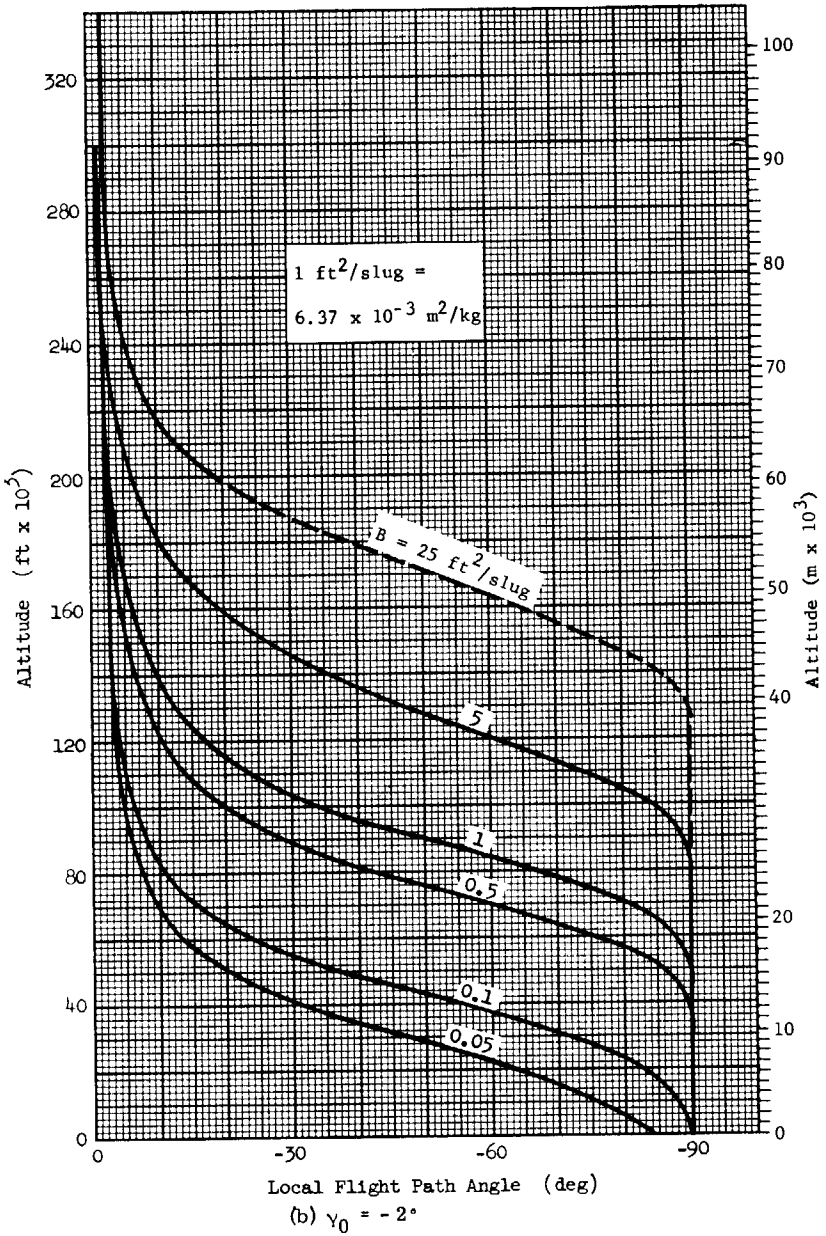

(b) $\gamma_0 = -2°$

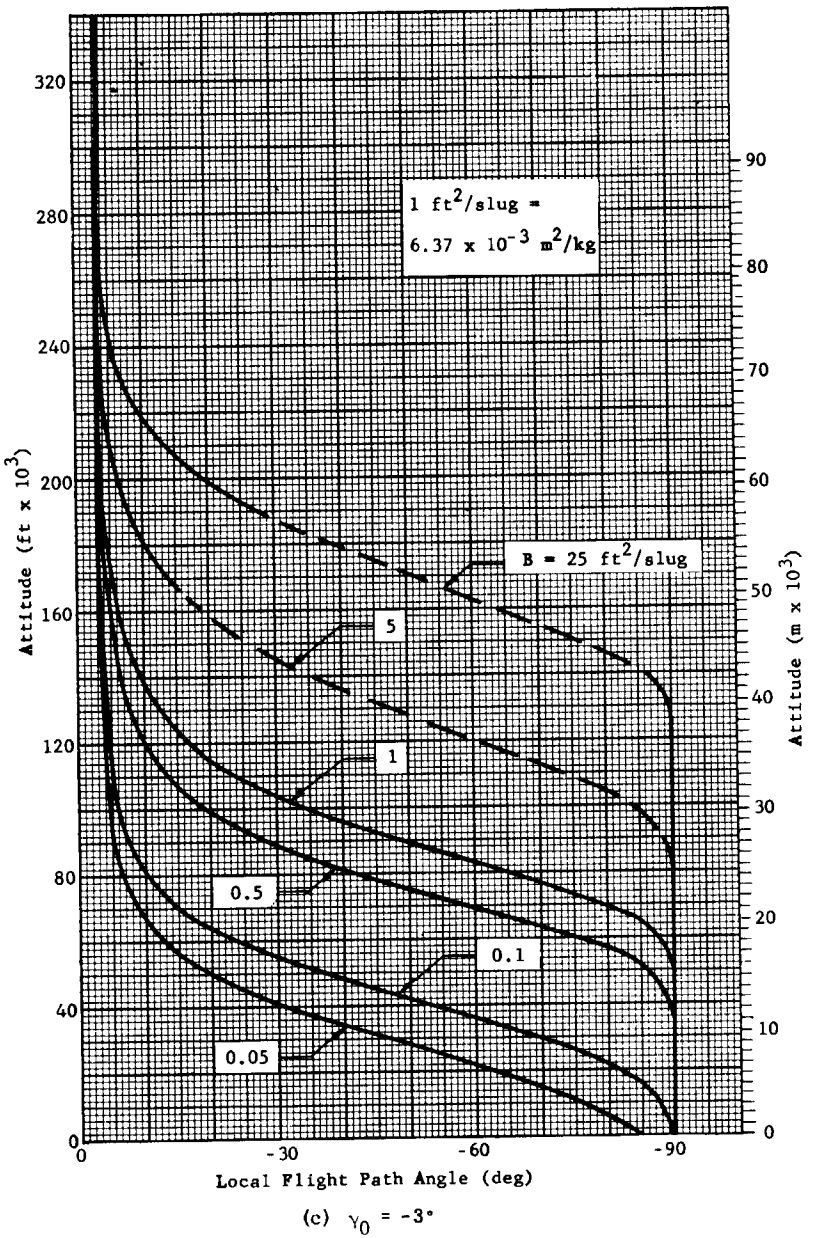

(c) $\gamma_0 = -3°$

Fig. 6. (continued)

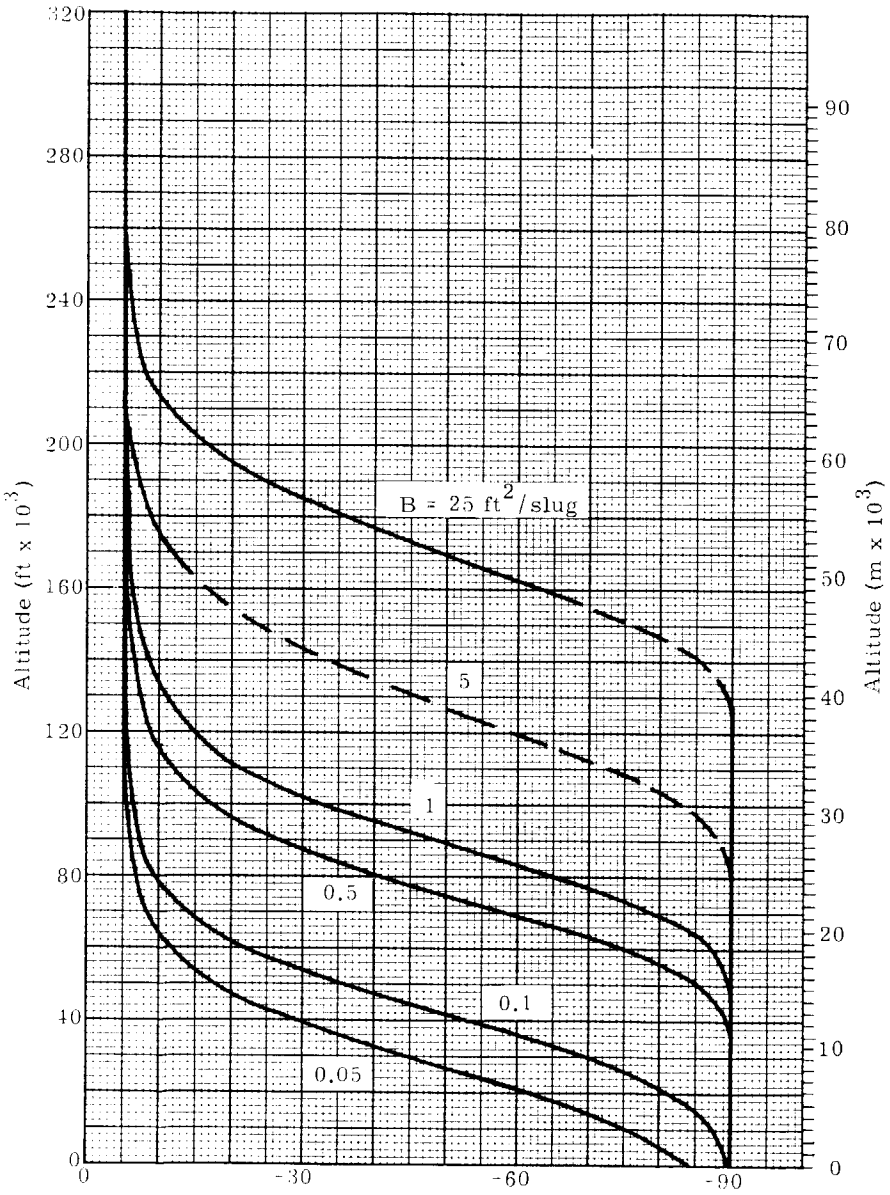

(d) $\gamma_0 = -5°$

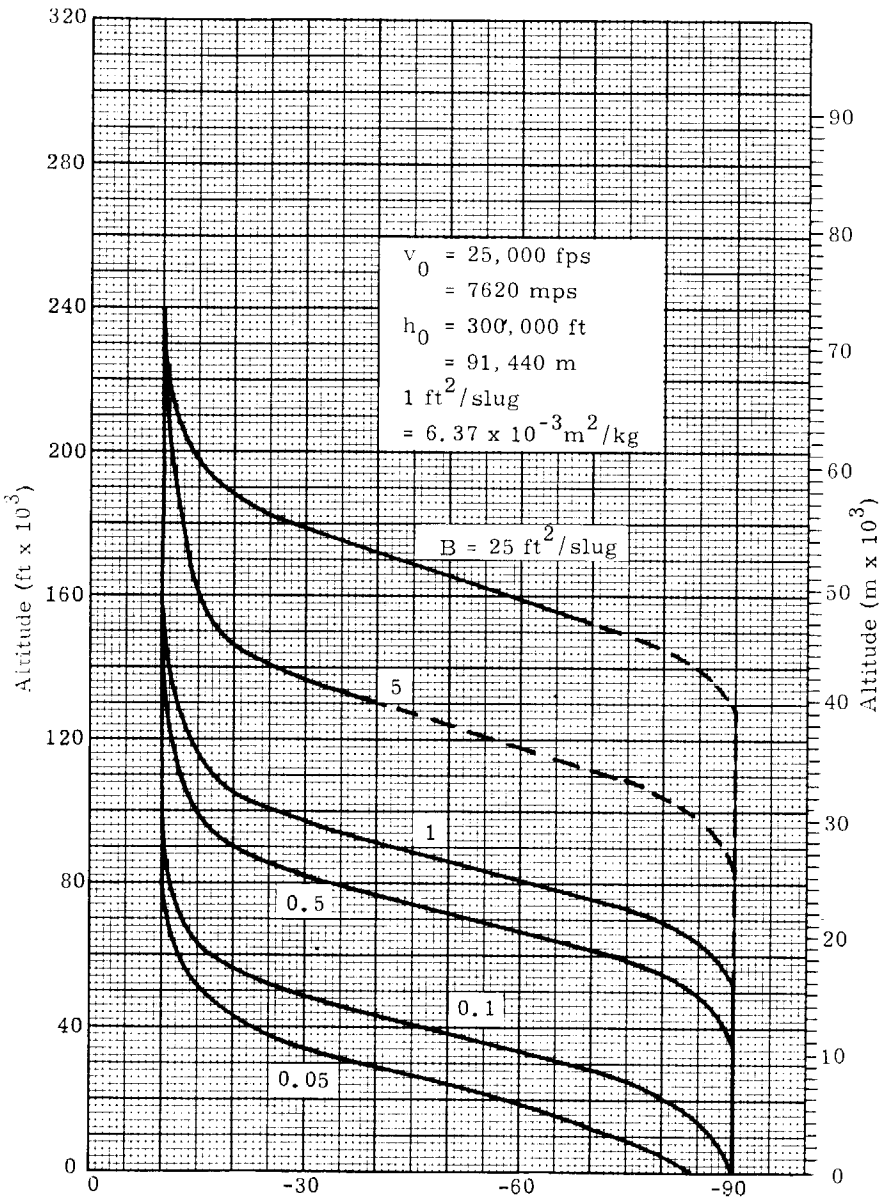

(e) $\gamma_0 = -10°$

Fig. 6. (continued)

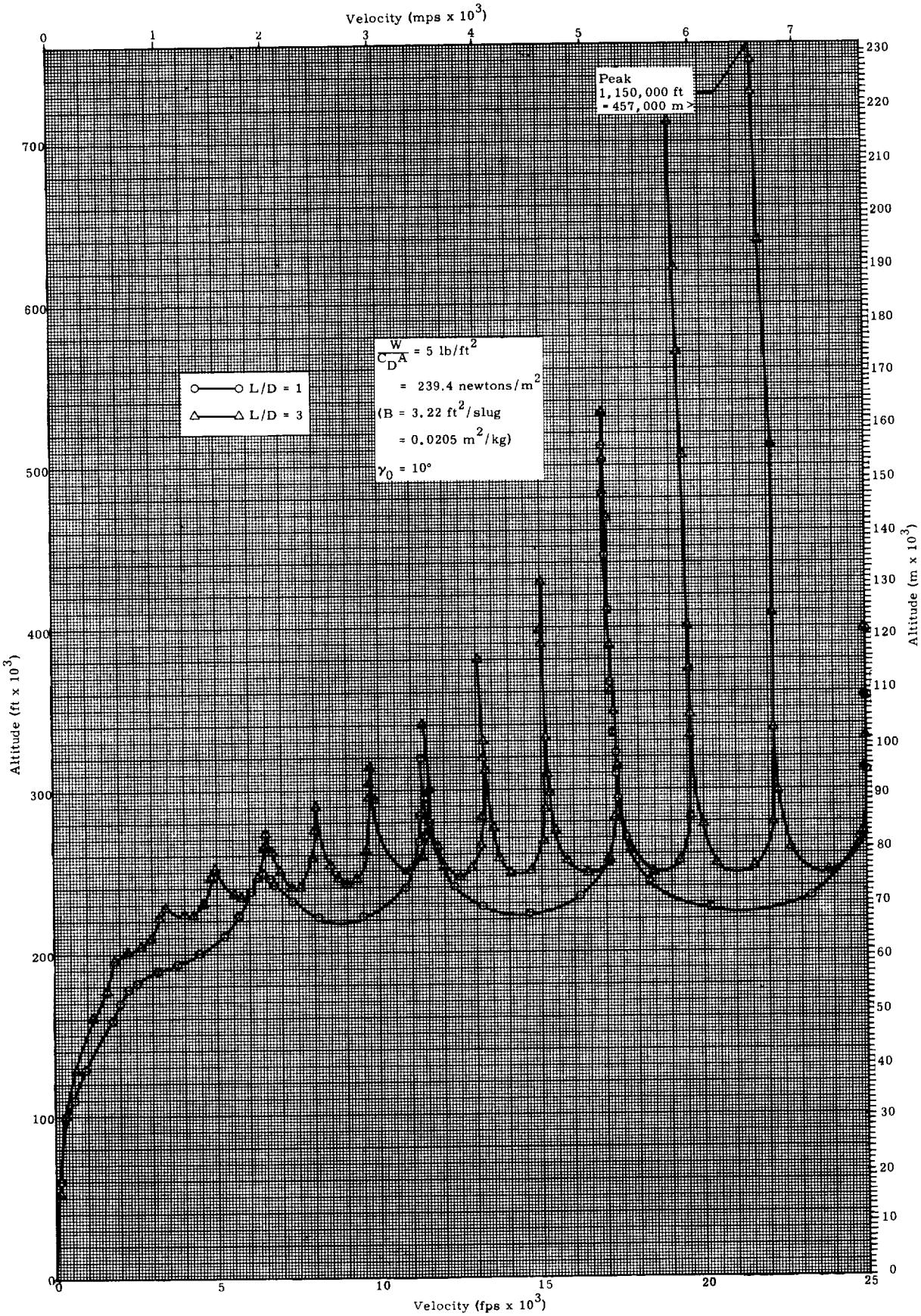

Fig. 7. Characteristic Re-Entry Altitude-Velocity Profiles for Lifting Vehicles

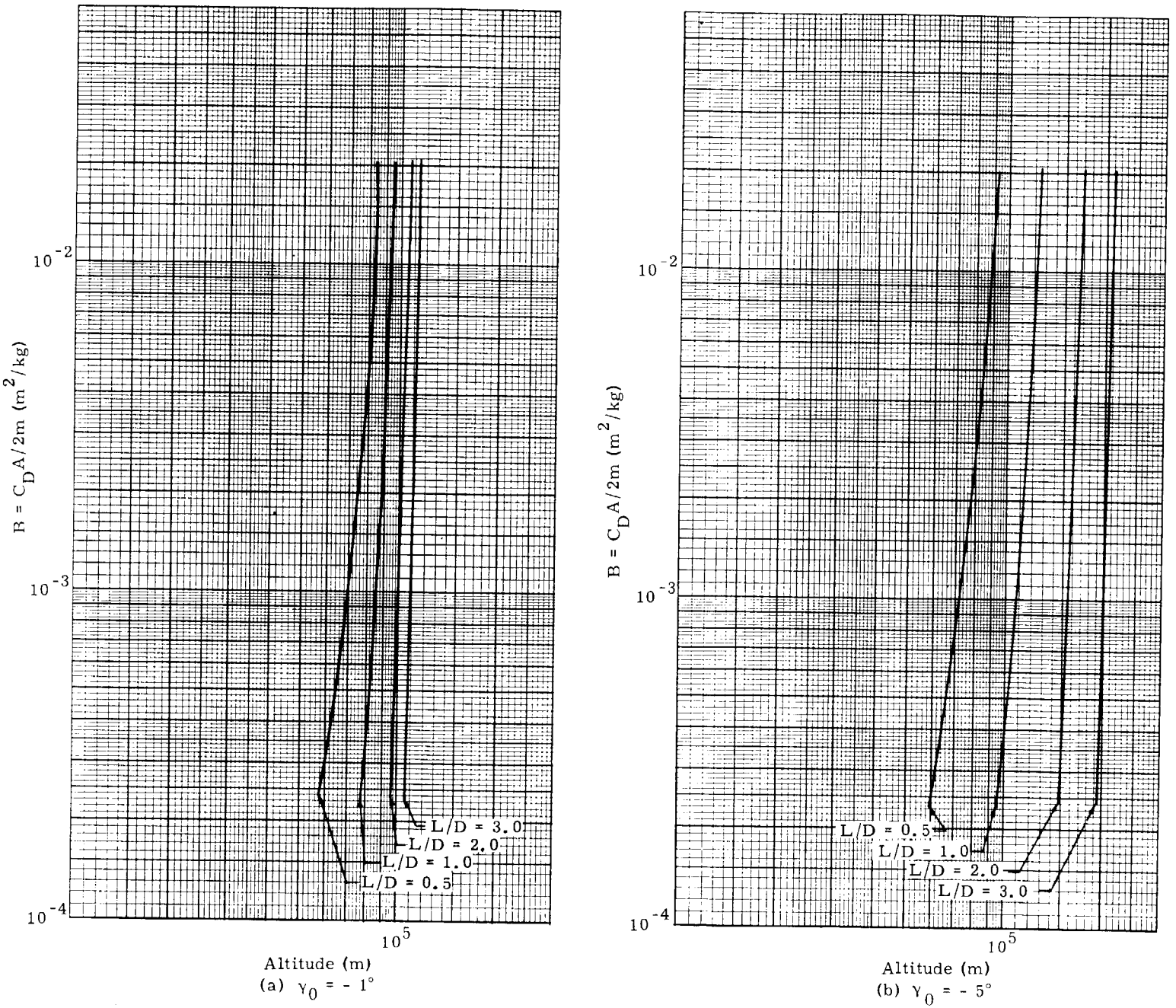

Fig. 8. Altitude Peak of First Skip (v_0 = 25000 fps = 7,620 mps, h_0 = 400,000 ft = 122,000 m)

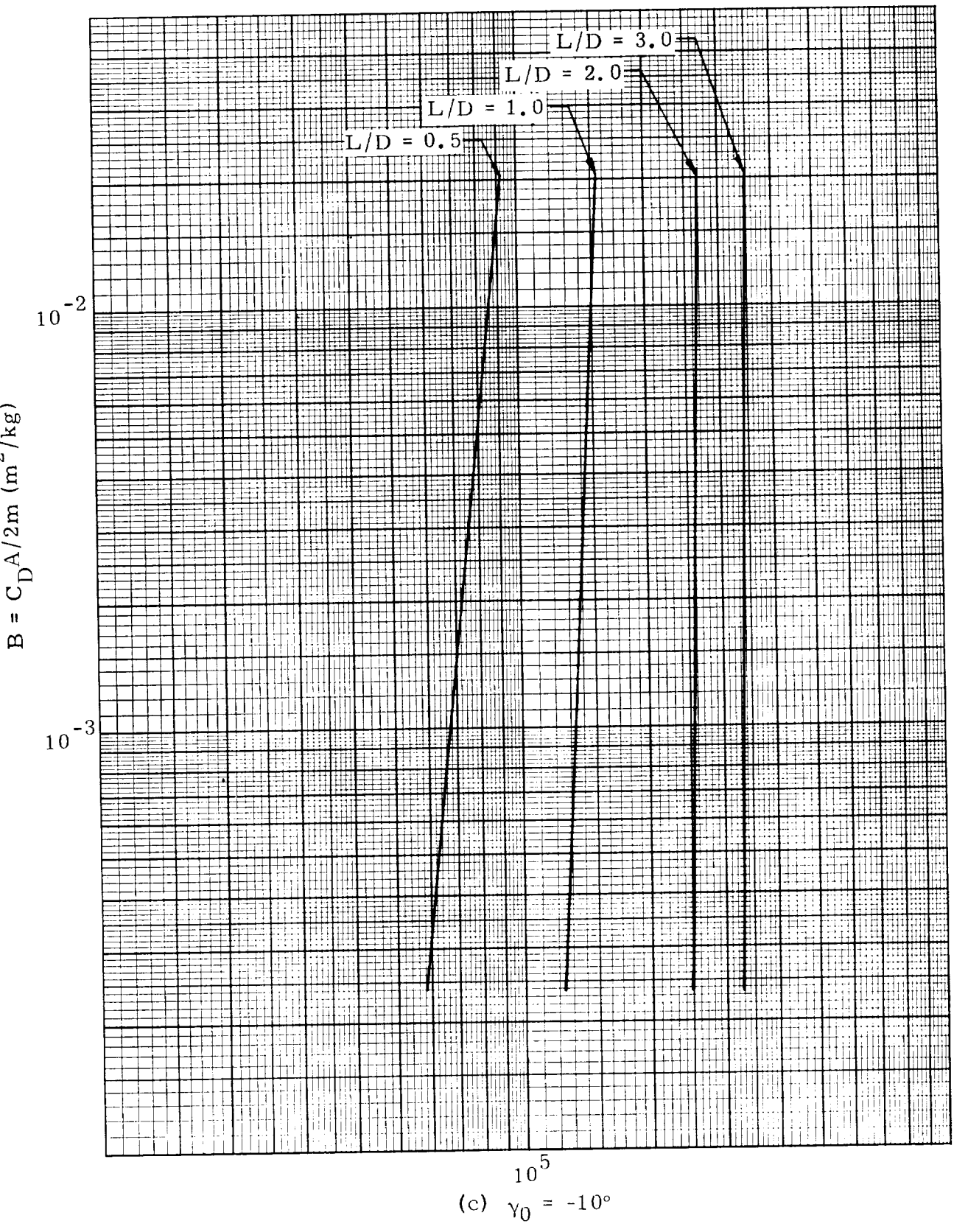

Fig. 8. (continued)

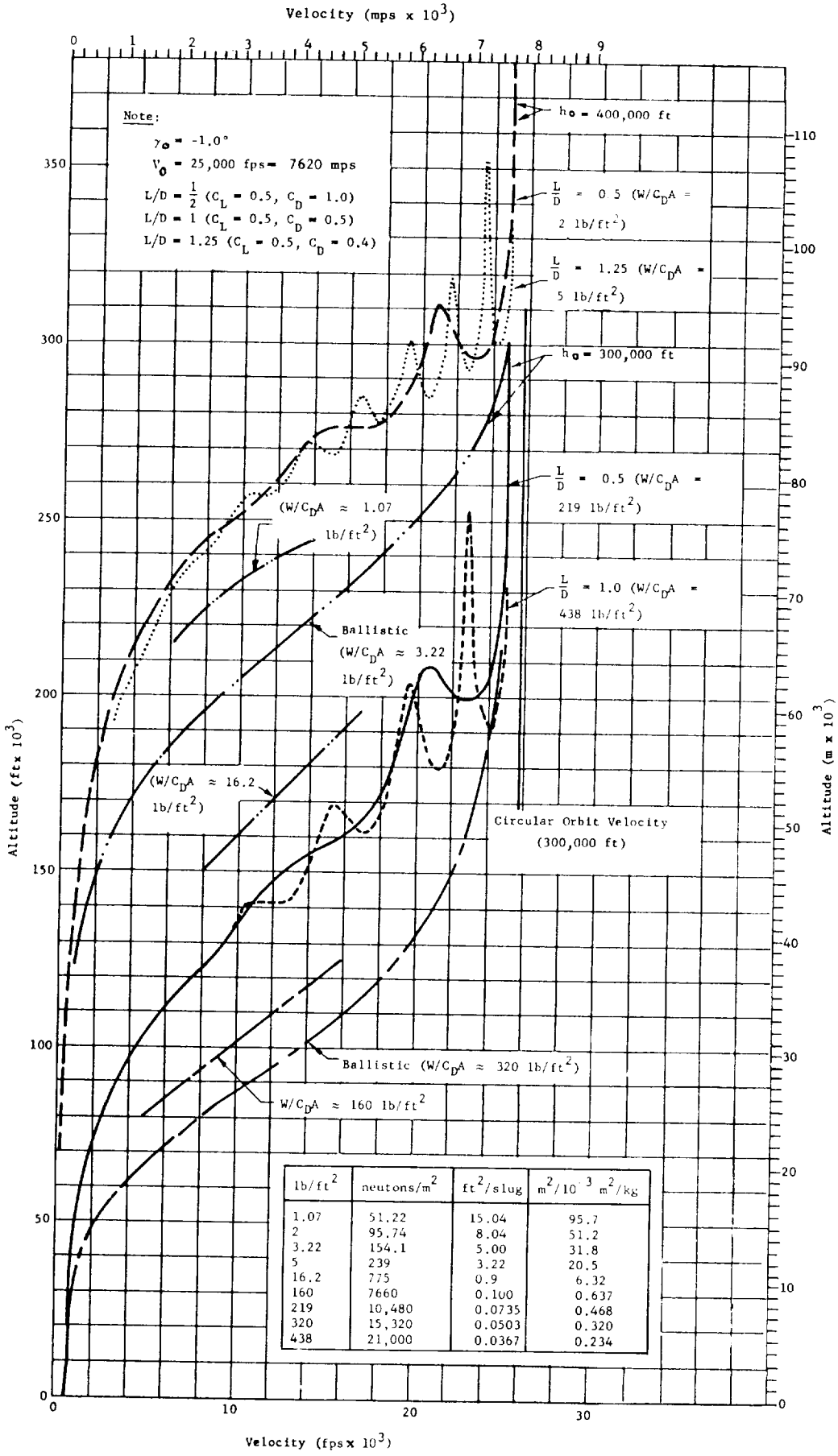

lb/ft^2	neutons/m^2	ft^2/slug	m^2/10^{-3} m^2/kg
1.07	51.22	15.04	95.7
2	95.74	8.04	51.2
3.22	154.1	5.00	31.8
5	239	3.22	20.5
16.2	775	0.9	6.32
160	7660	0.100	0.637
219	10,480	0.0735	0.468
320	15,320	0.0503	0.320
438	21,000	0.0367	0.234

Fig. 9a. Entry Vehicle Comparison, Velocity-Altitude Profile

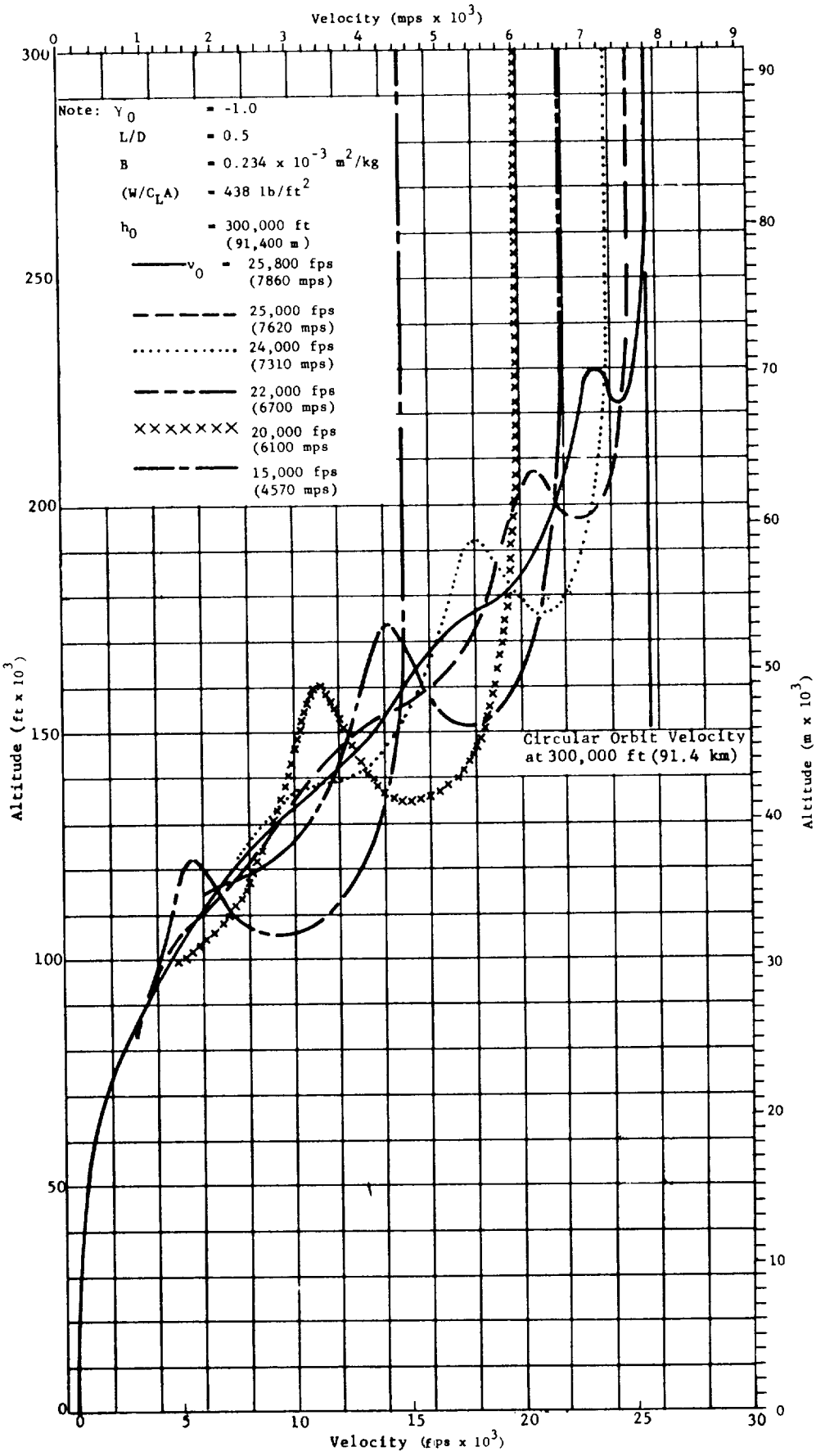

Fig. 9b. Effect of Entry Velocity on Altitude-Velocity Profile

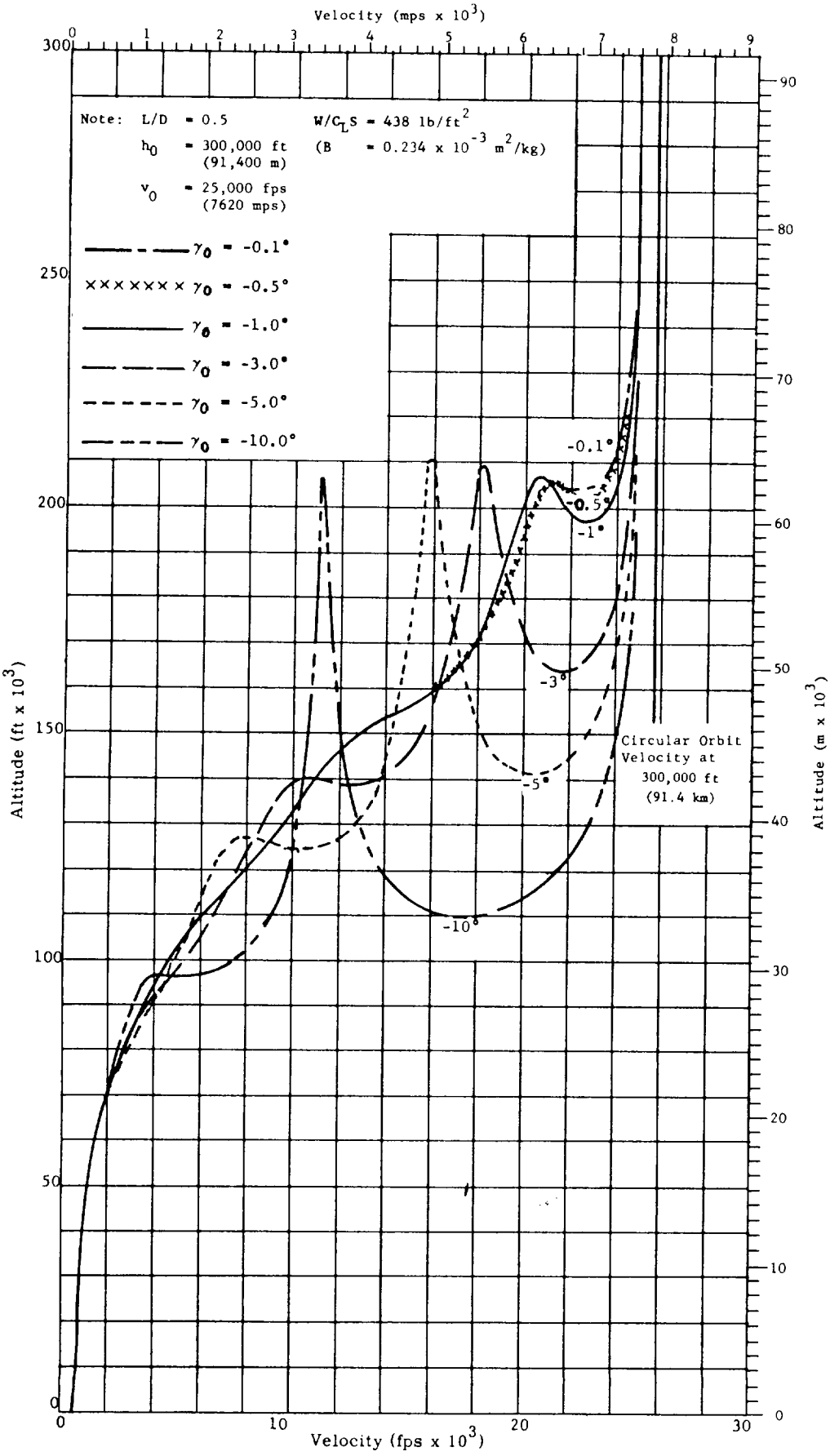

Fig. 9c. Effect of Entry Angle on Velocity-Altitude Profiles

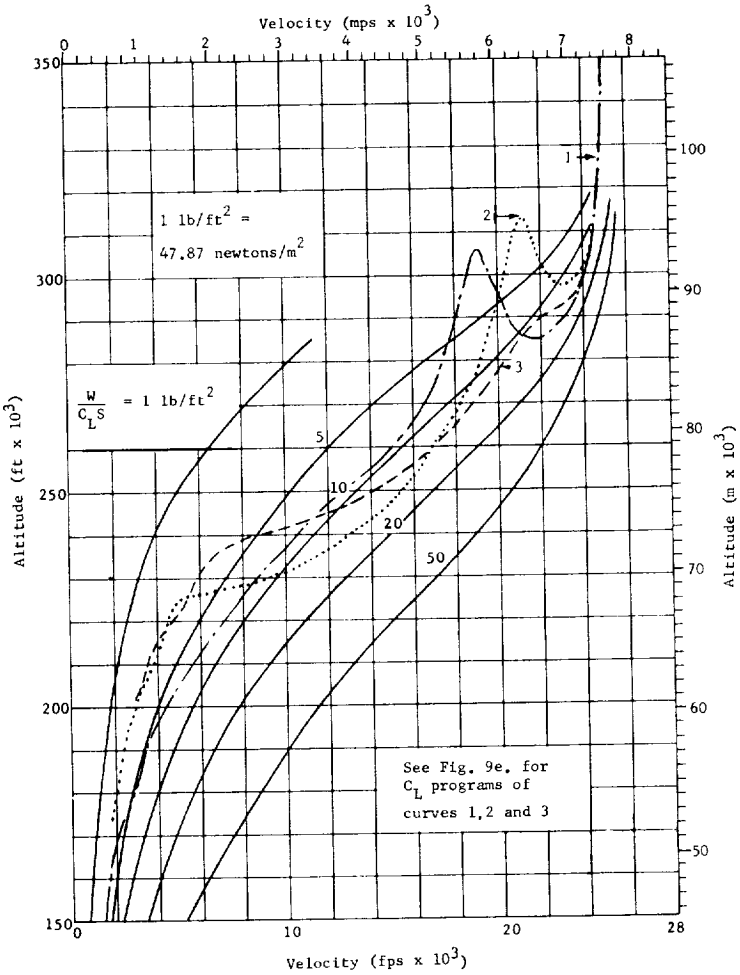

Fig. 9d. Effect of Programmed C_L on Velocity-Altitude Profile

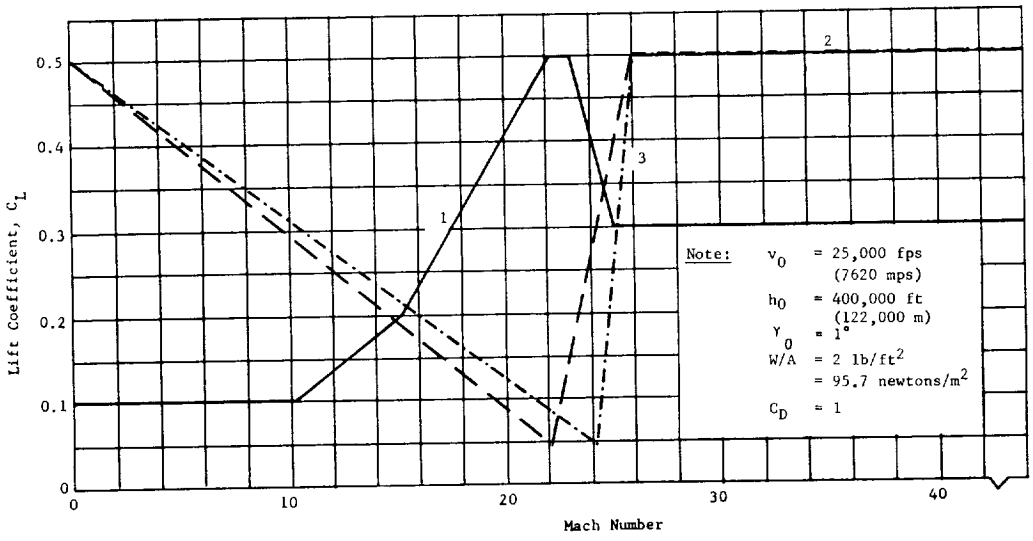

Fig. 9e. Program of C_L with Mach Number

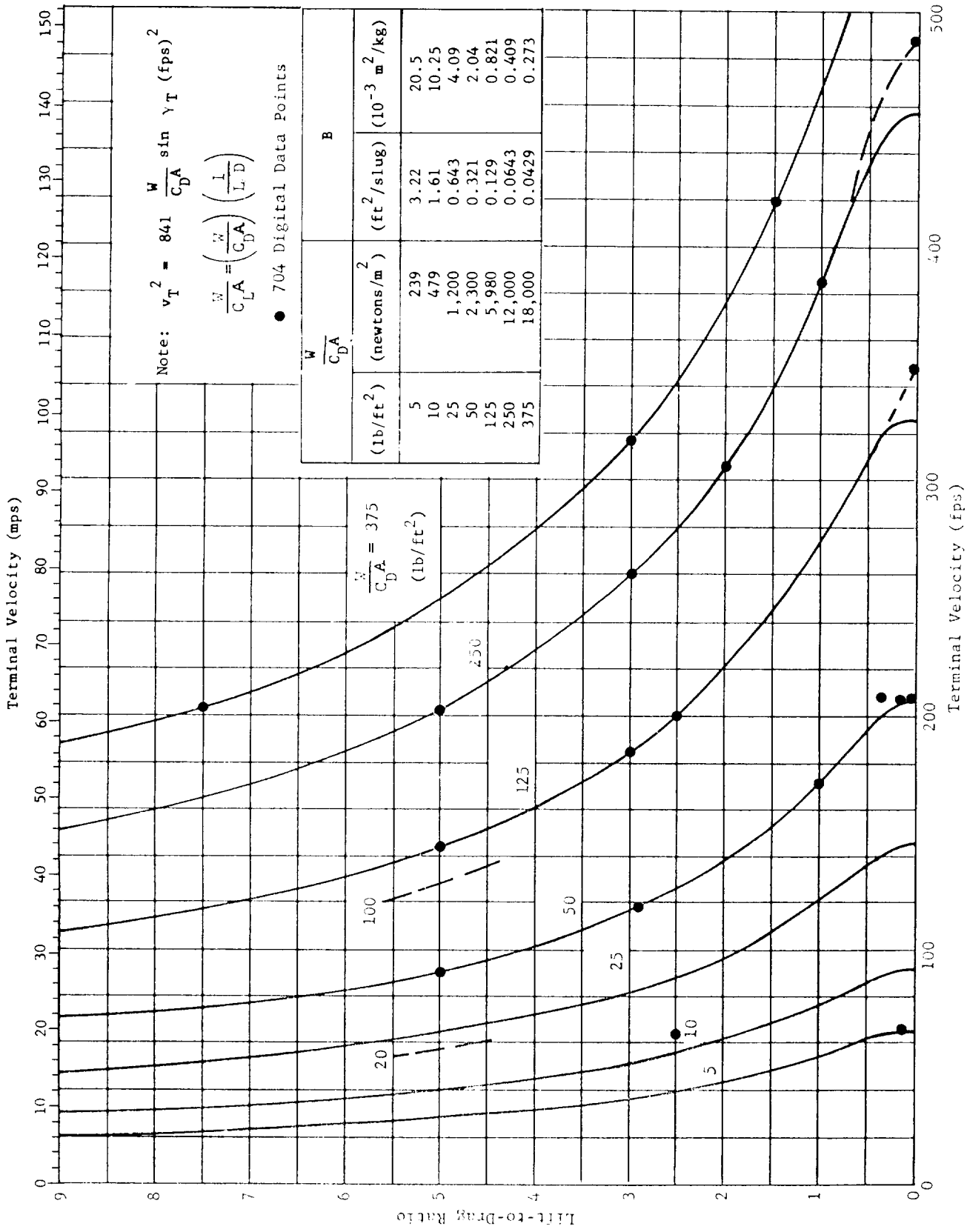

Fig. 10a. Terminal Velocity

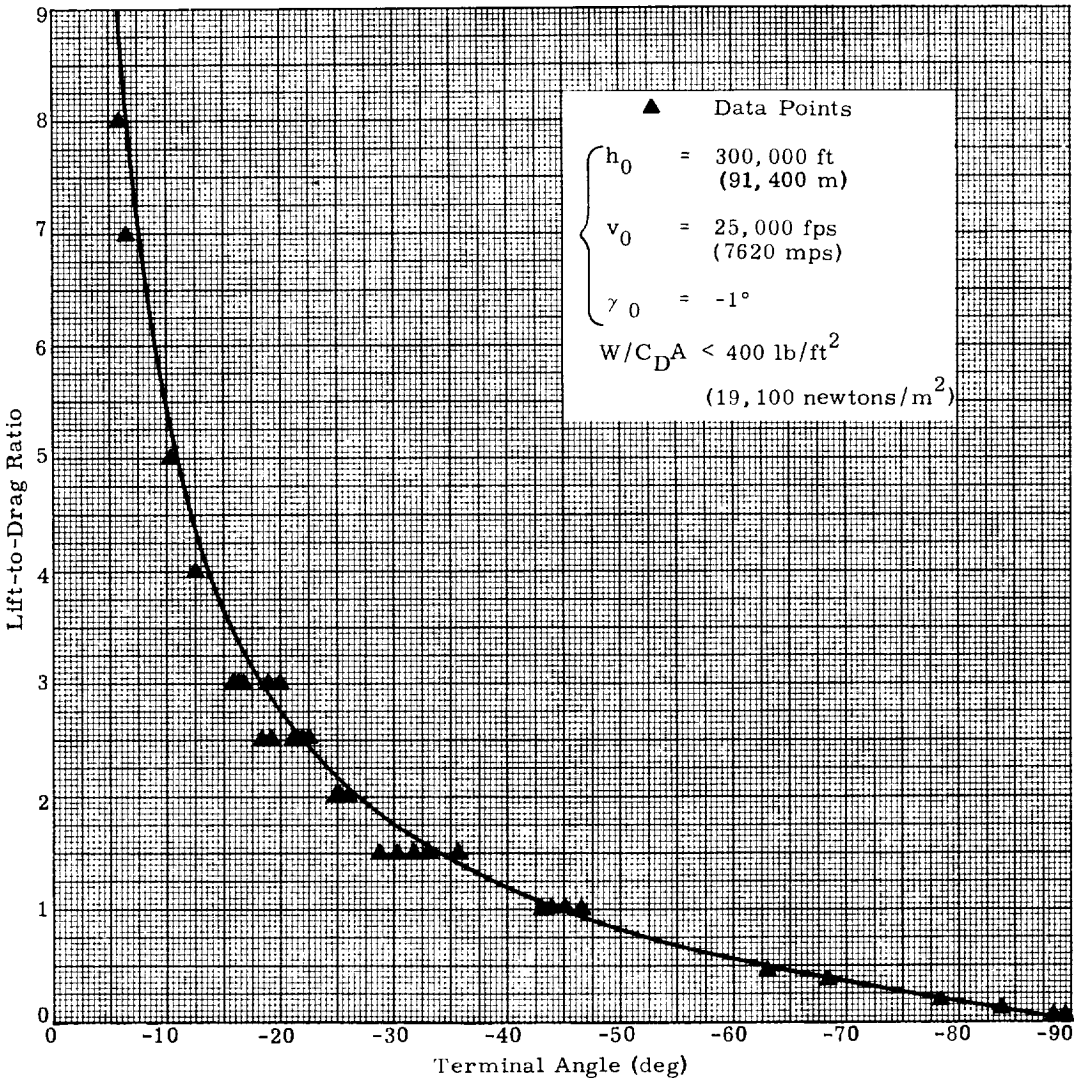

Fig. 10b. Terminal Flight Path Angle

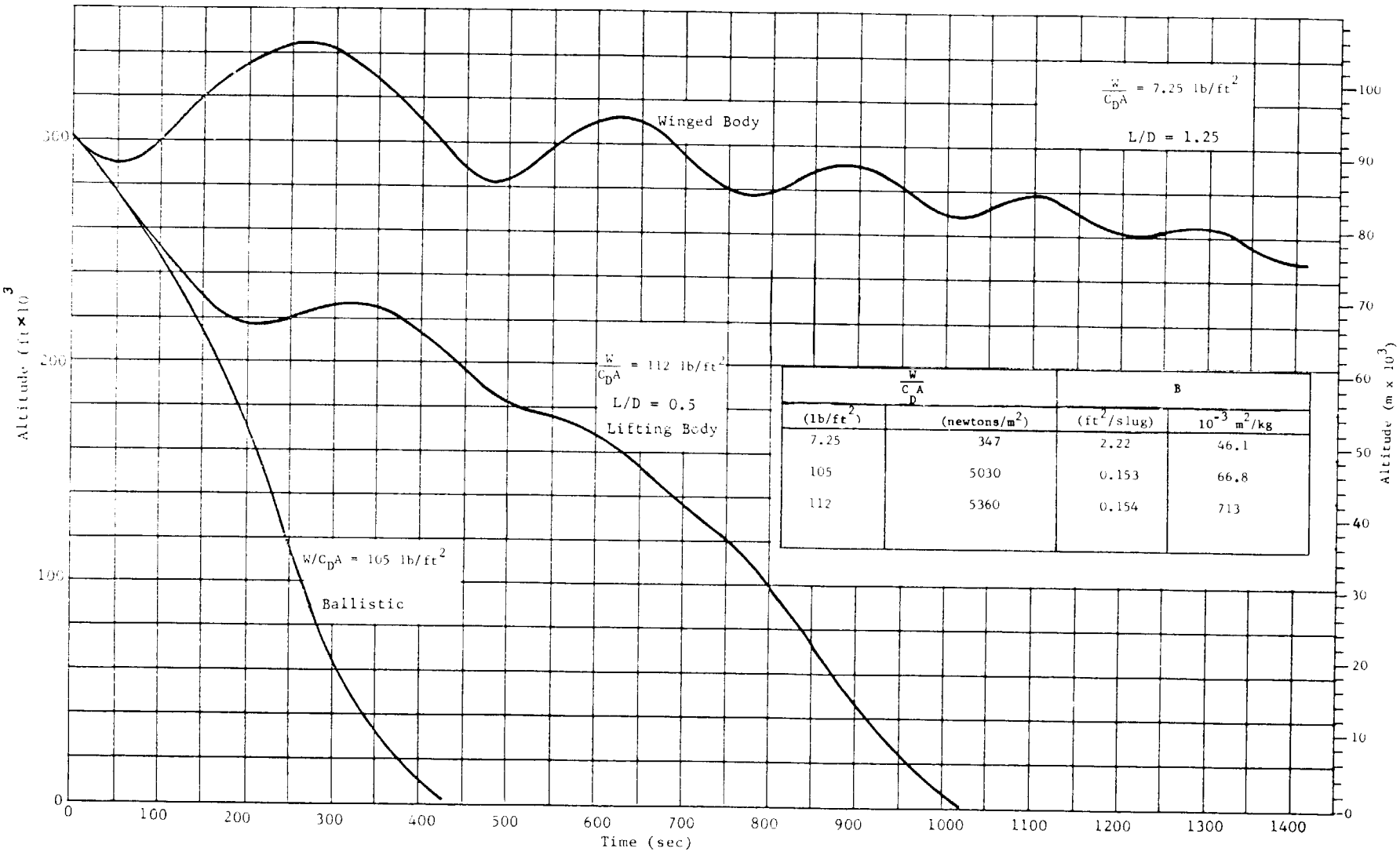

$\frac{W}{C_D A}$		B	
(lb/ft^2)	(newtons/m^2)	(ft^2/slug)	10^{-3} m^2/kg
7.25	347	2.22	46.1
105	5030	0.153	66.8
112	5360	0.154	713

Fig. 11a. Entry Vehicle Comparison, Altitude-Time History

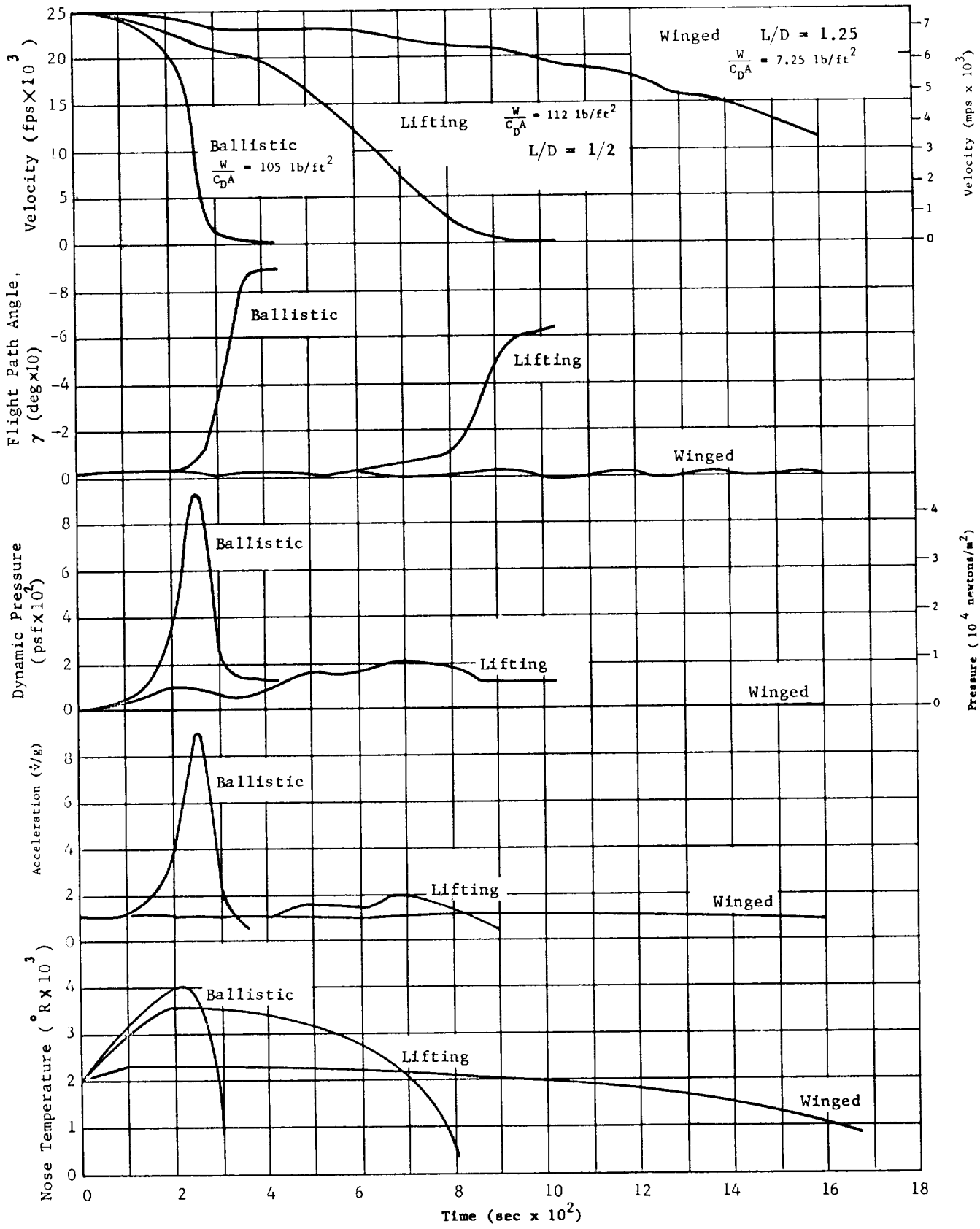

Fig. 11b. Re-entry Vehicle Comparison--Time History

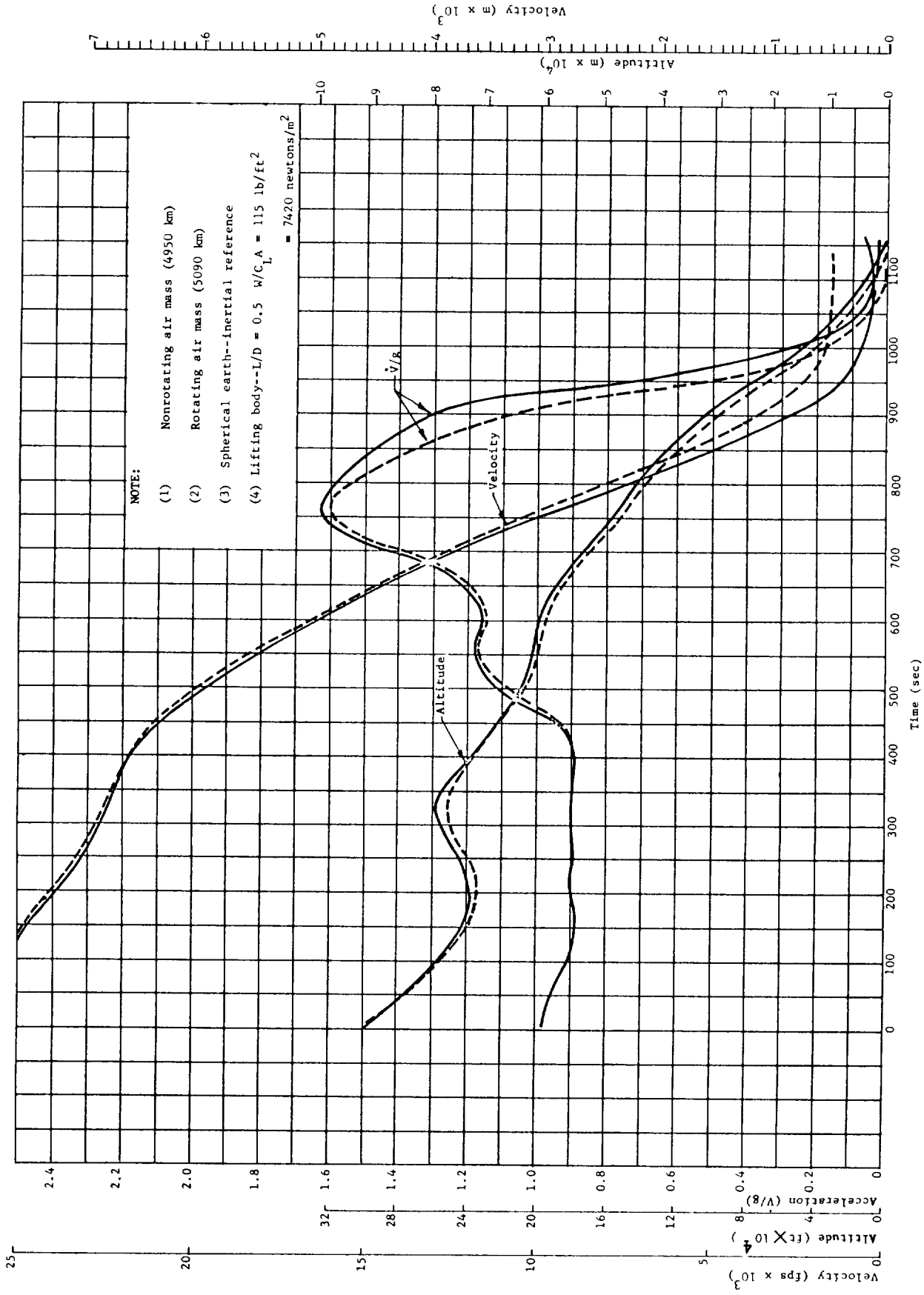

Fig. 11c. Re-Entry History with and Without Rotating Air Mass

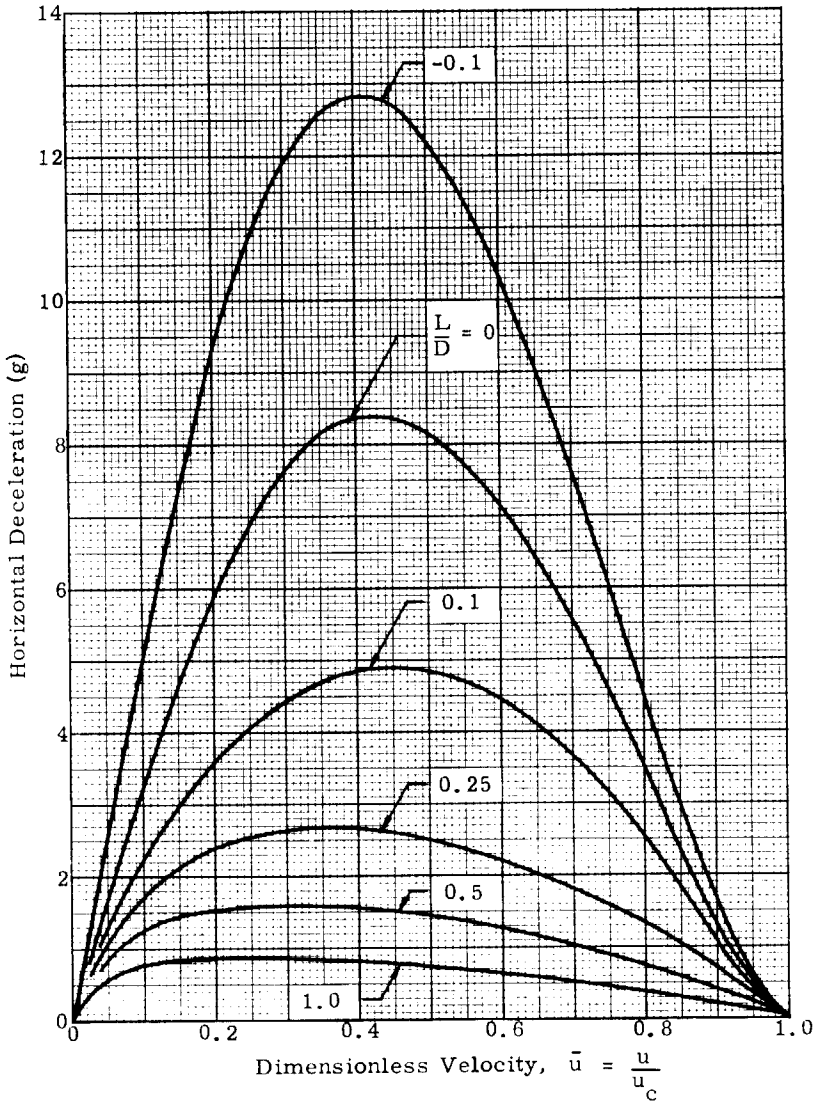

Fig. 12a. Effect of Lift-Drag Ratio on Deceleration for Entry into Earth Atmosphere From Decaying Orbits (Ref. 1)

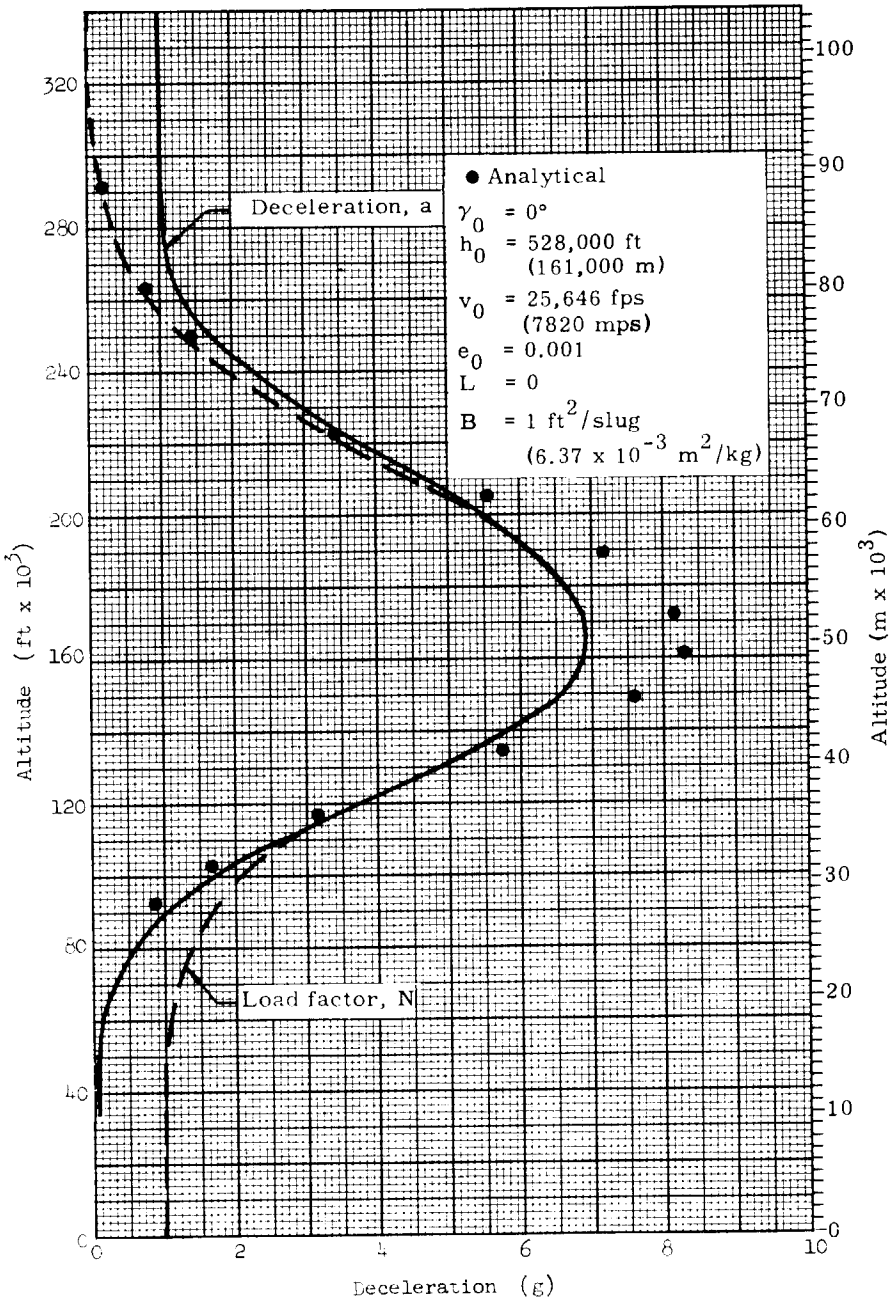

Fig. 12b. Decelleration Profile and Load Factor for Satellite Re-Entry

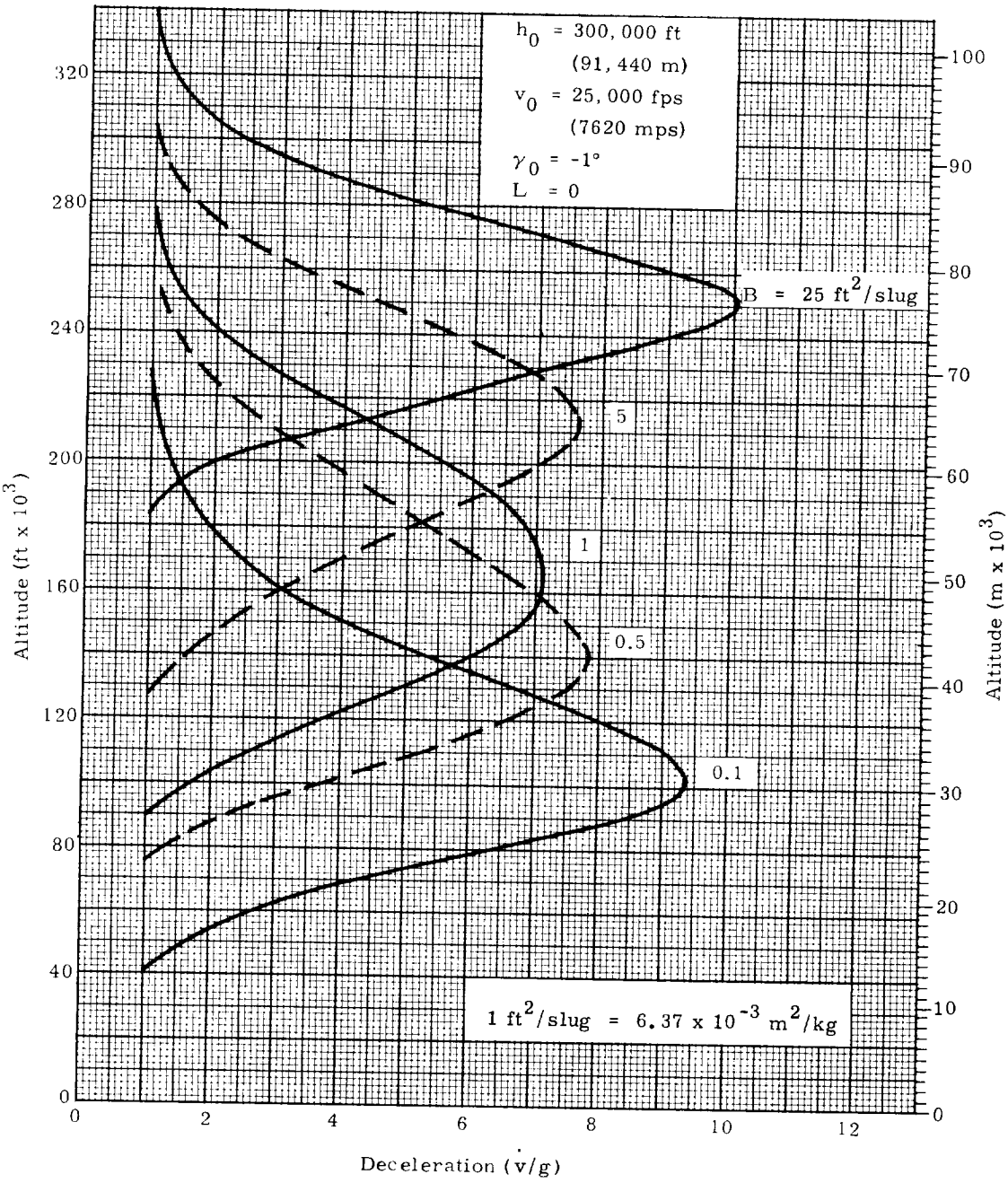

Fig. 12c. Deceleration Variation with Altitude for Satellite Re-Entry

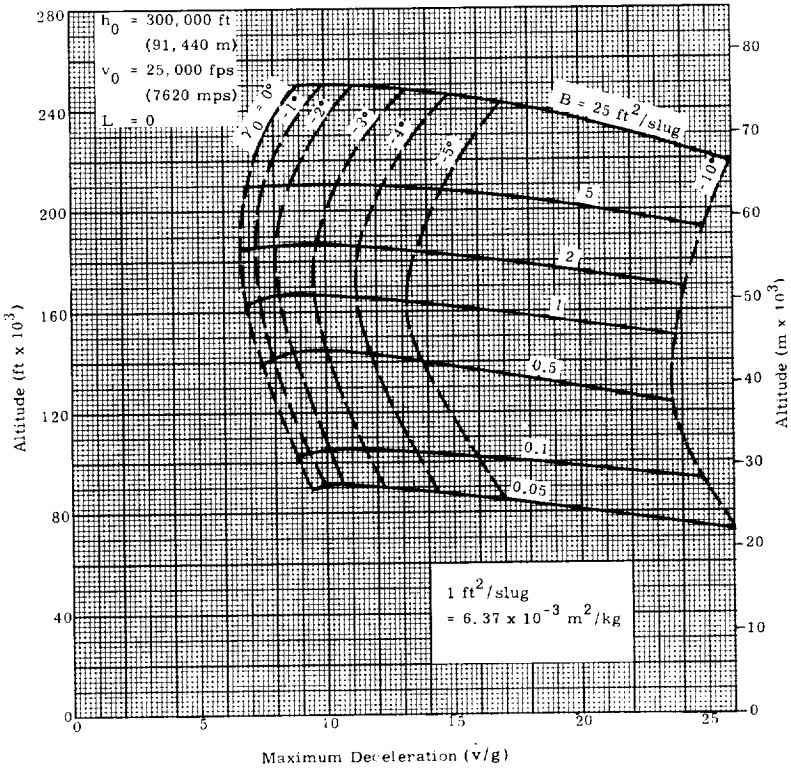

Fig. 13a. Maximum Decelerations for Ballistic Re-Entry

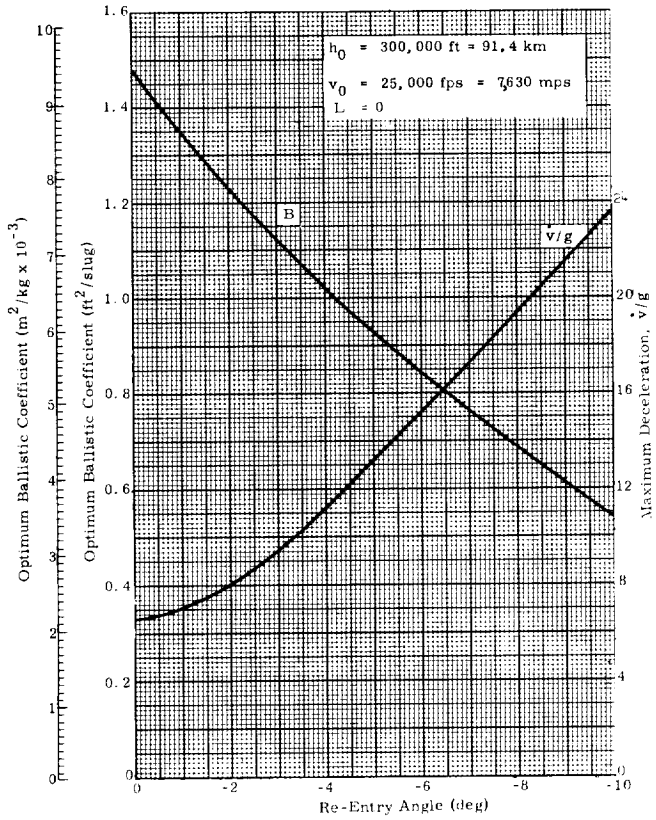

Fig. 13b. Optimum Ballistic Coefficients (to minimize re-entry decelerations)

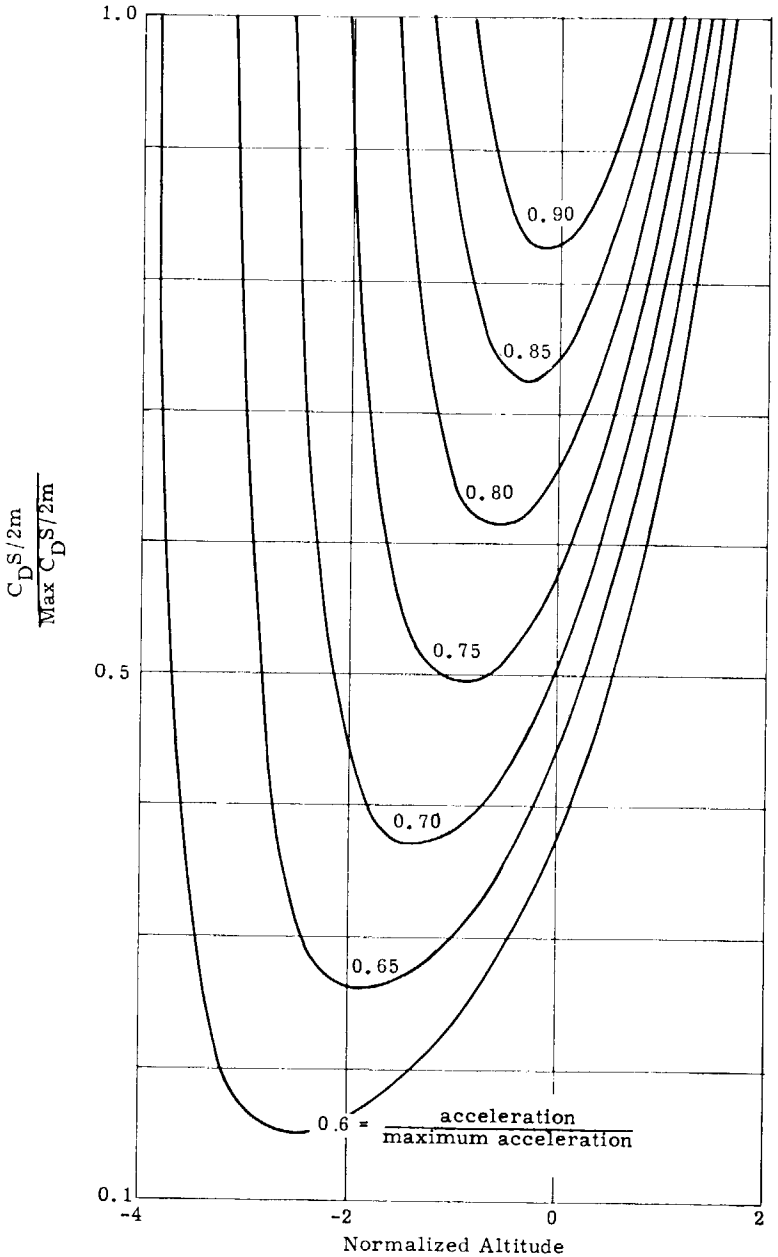

Fig. 14a. Controlled Descent, General Ballistic Coefficient Variation (Ref. 12)

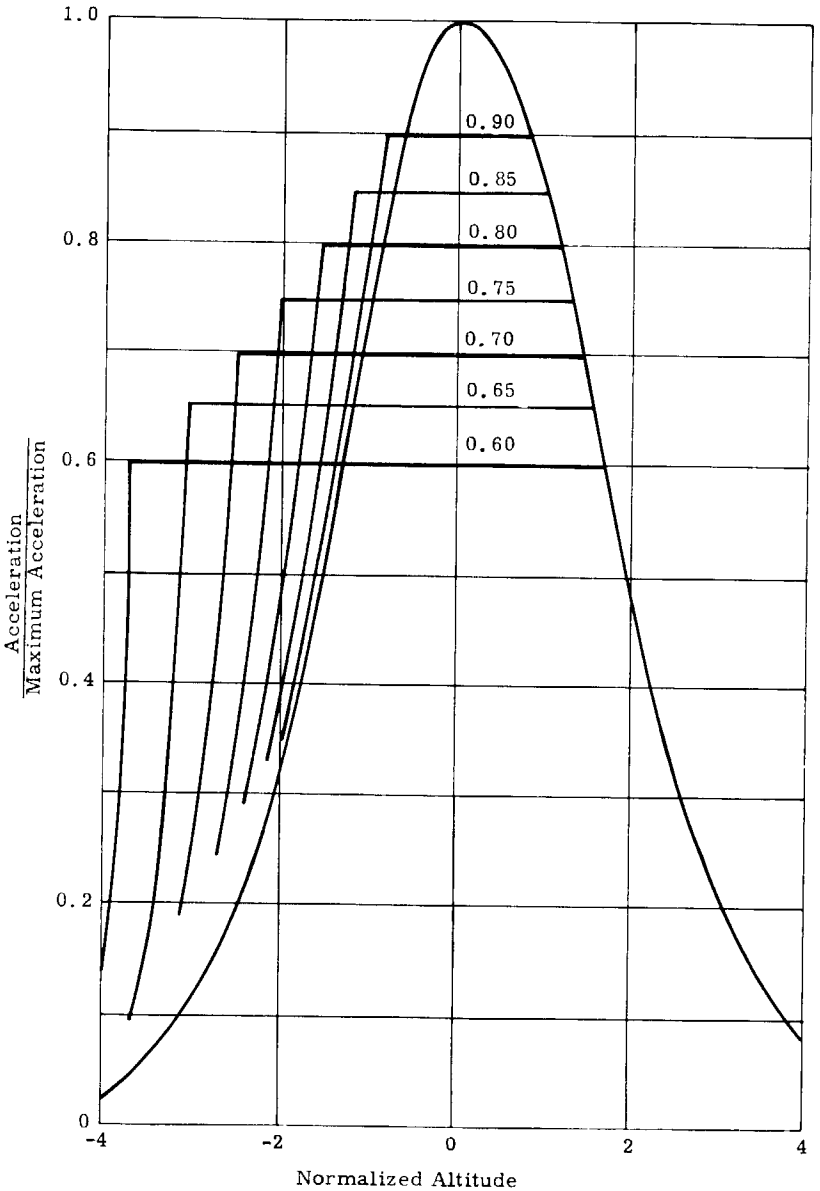

Fig. 14b. Controlled Descent, General Acceleration Profile

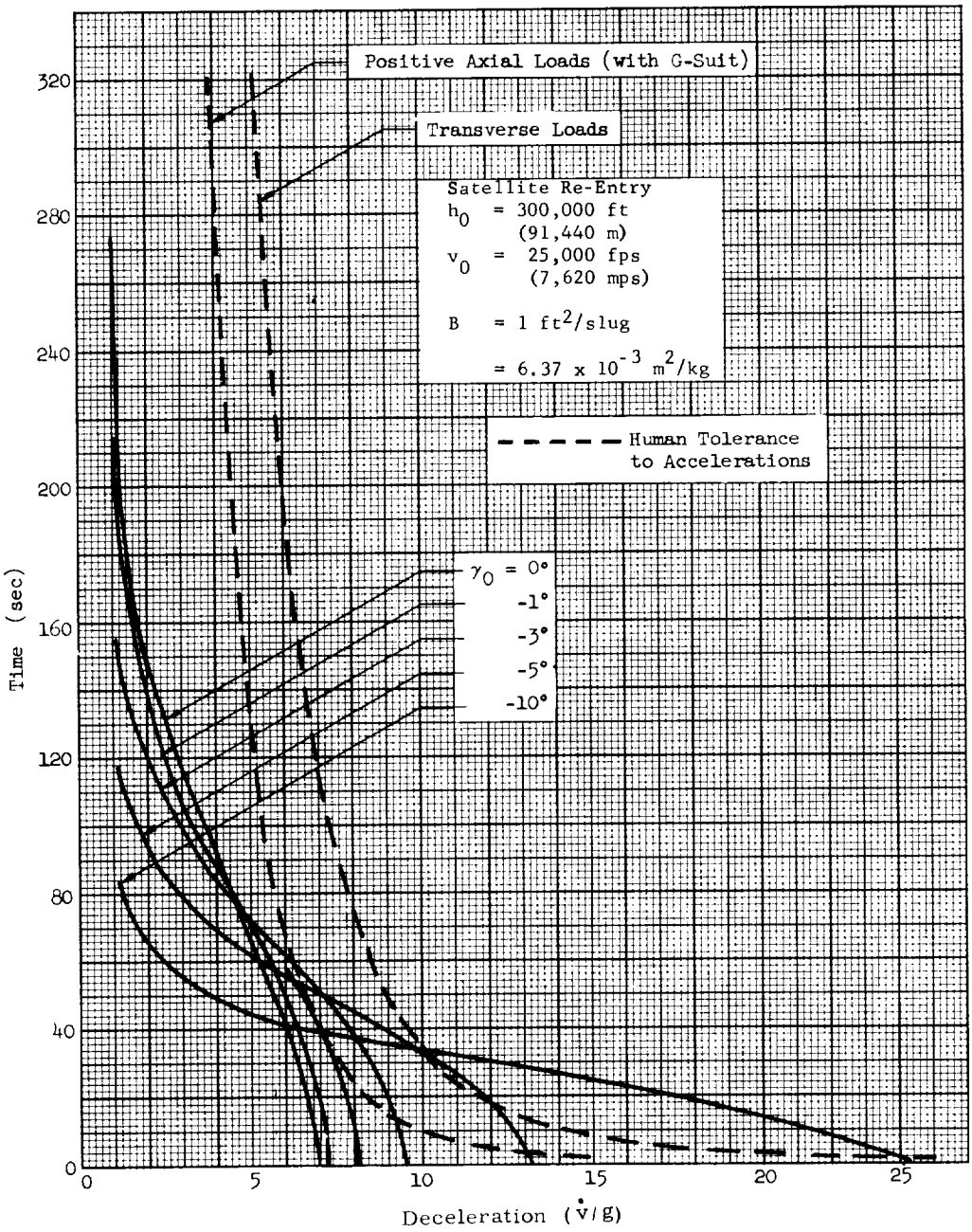

(a) Constant ballistic coefficient

Fig. 15. Length of Time Spent at Decelerations Equal to and Larger than the Shown Value

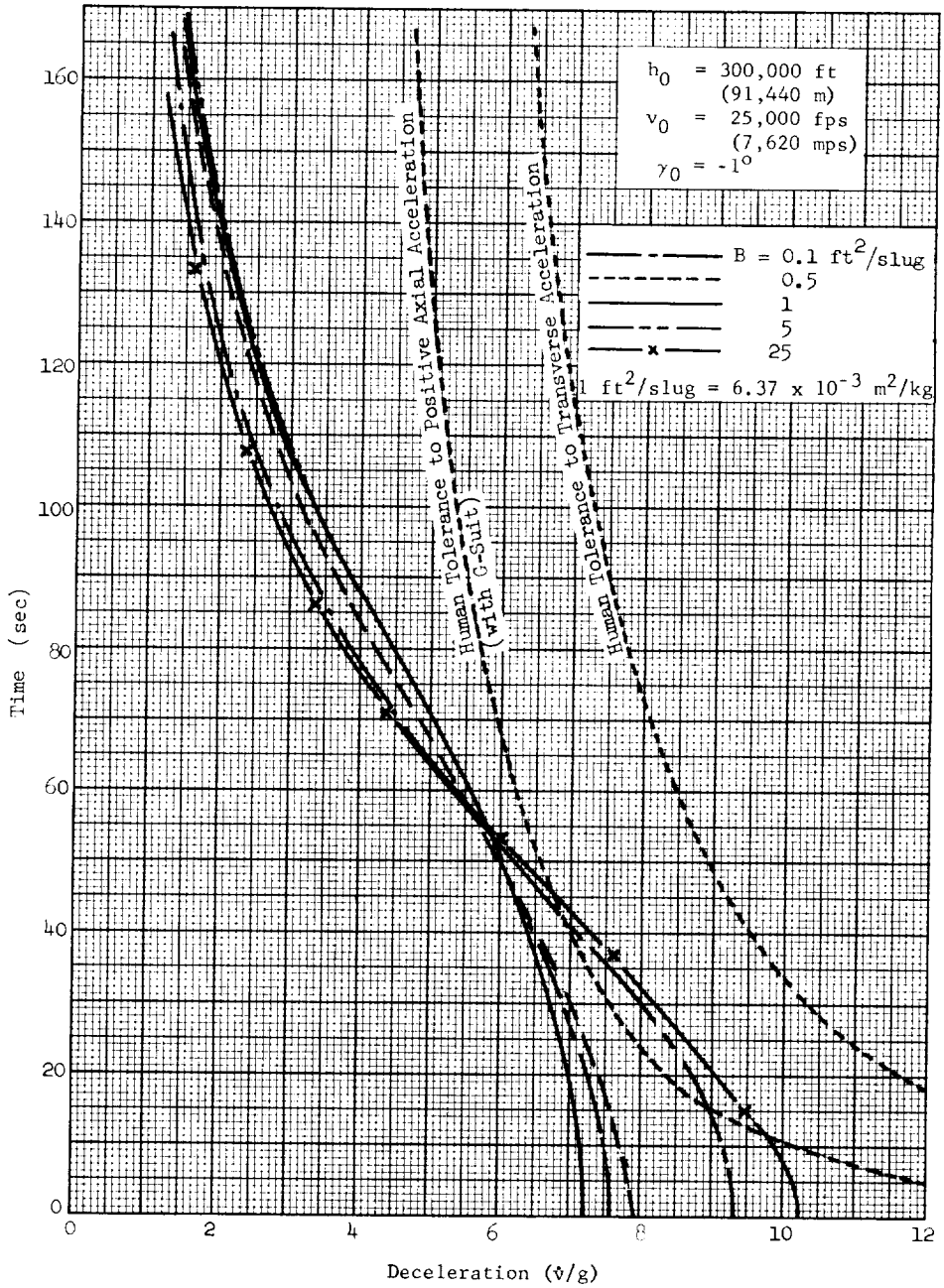

(b) Constant re-entry angle

Fig. 15. (continued)

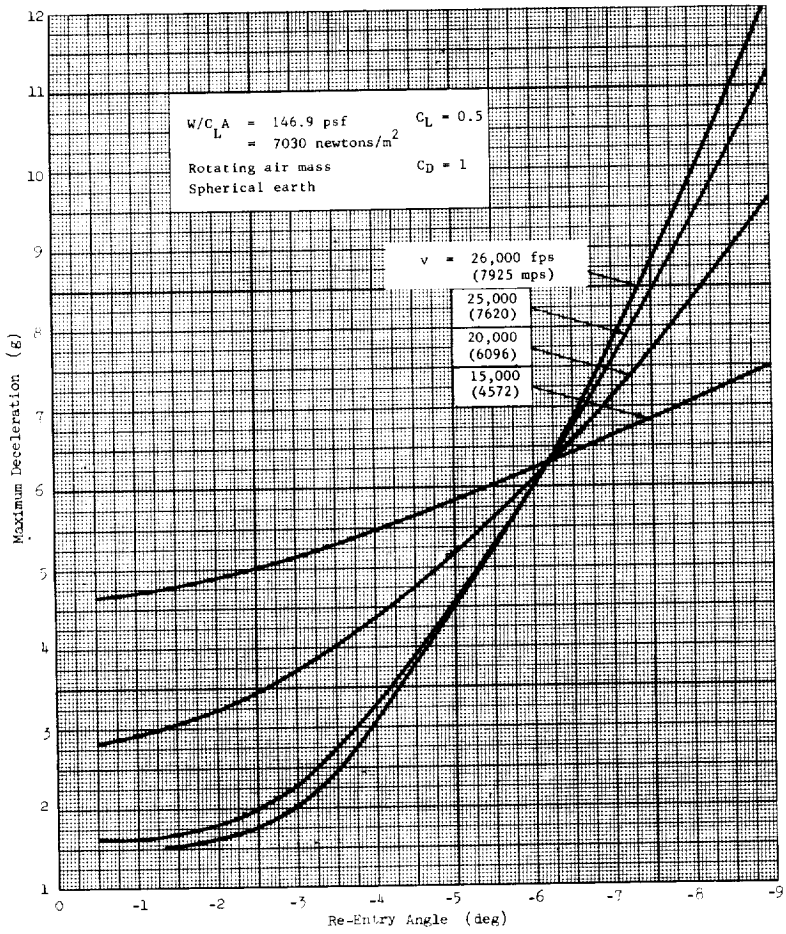

Fig. 16. Effect of Re-Entry Conditions on Maximum Total Decelerations (L/D = 0.5)

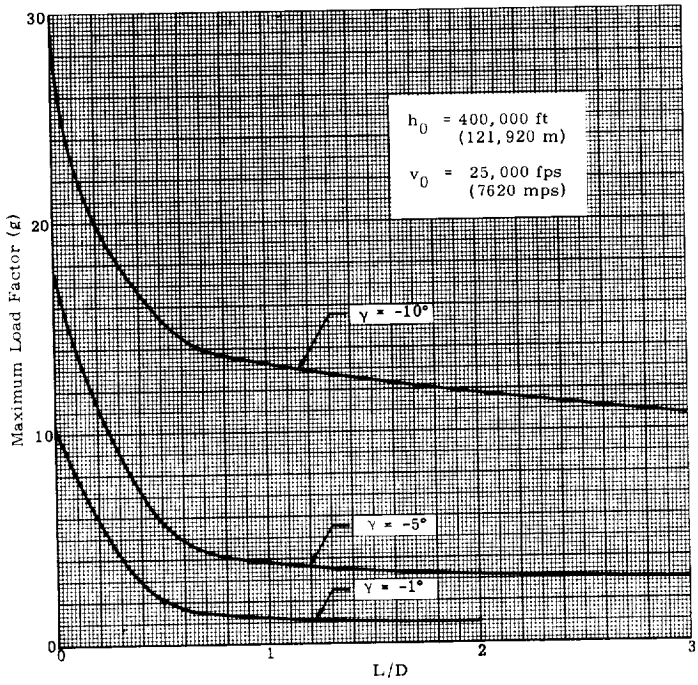

Fig. 17a. Maximum Load Factor Versus L/D (W/C_DA = 438 psf or B = 0.234 x 10^{-3} m^2/kg)

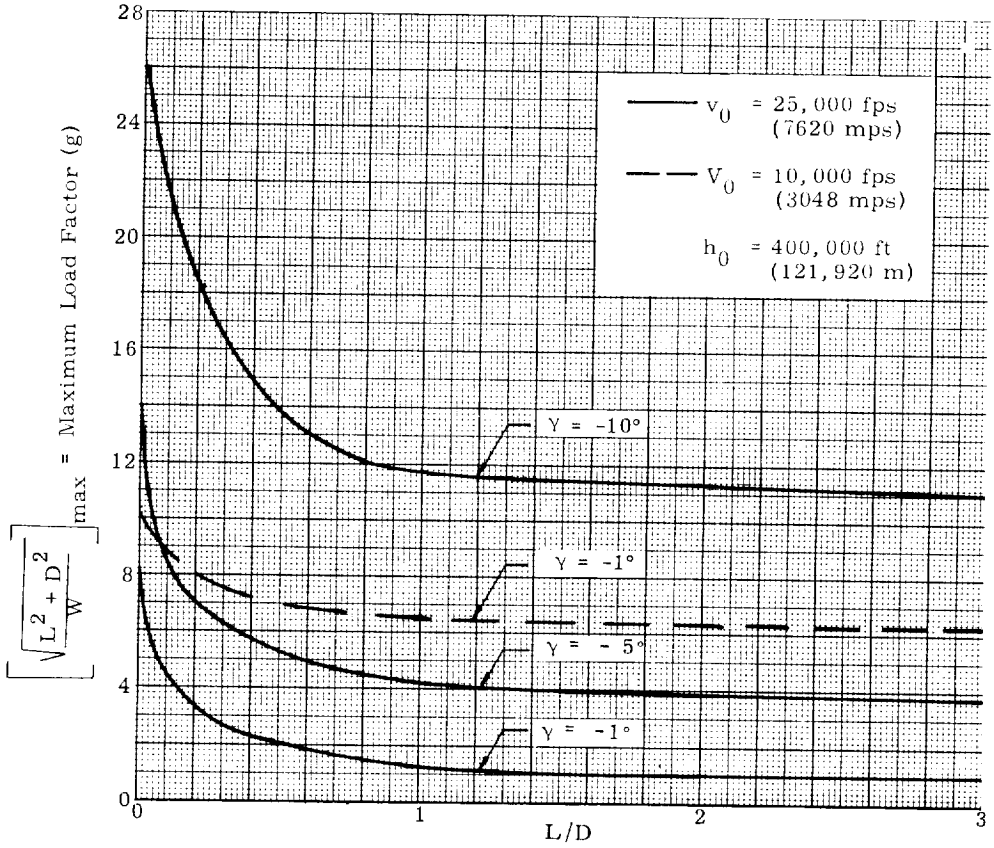

Fig. 17b. Maximum Load Factor Versus L/D (W/C_DA = 50 psf or B = 2.04 x 10^{-3} m^2/kg)

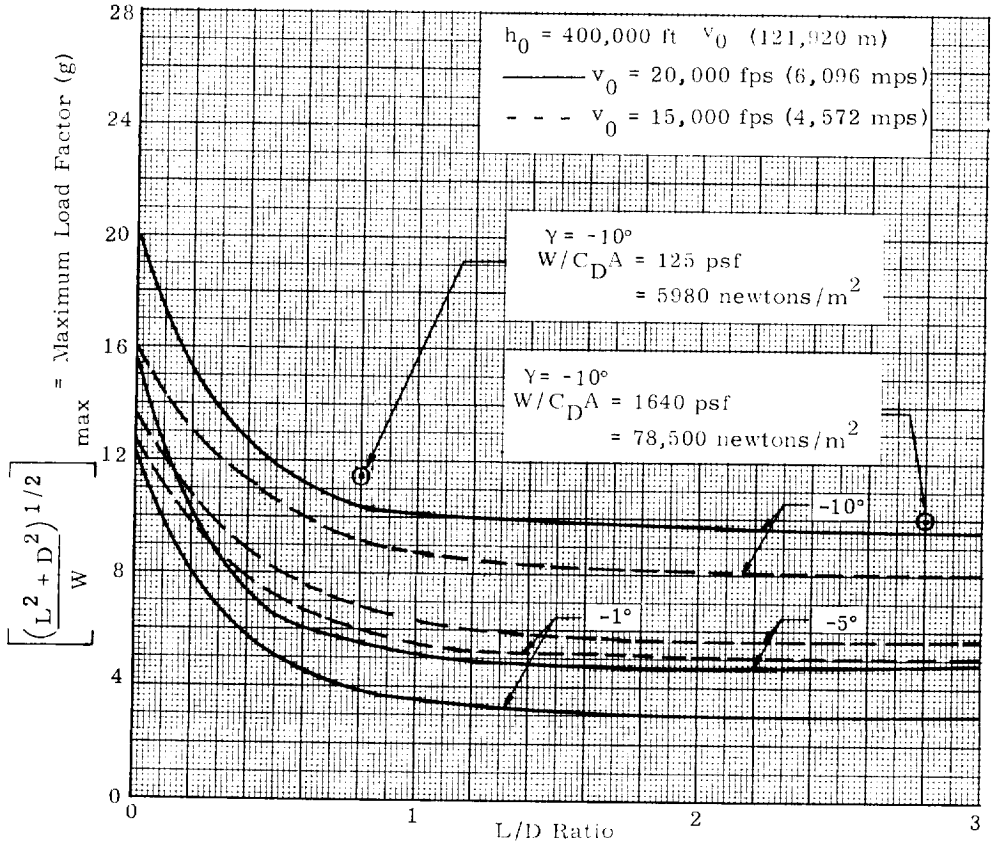

Fig. 17c. Maximum Total Acceleration Versus L/D Ratio (W/C_DA = 50 psf or B = 2.04 x 10^{-3} m^2/kg)

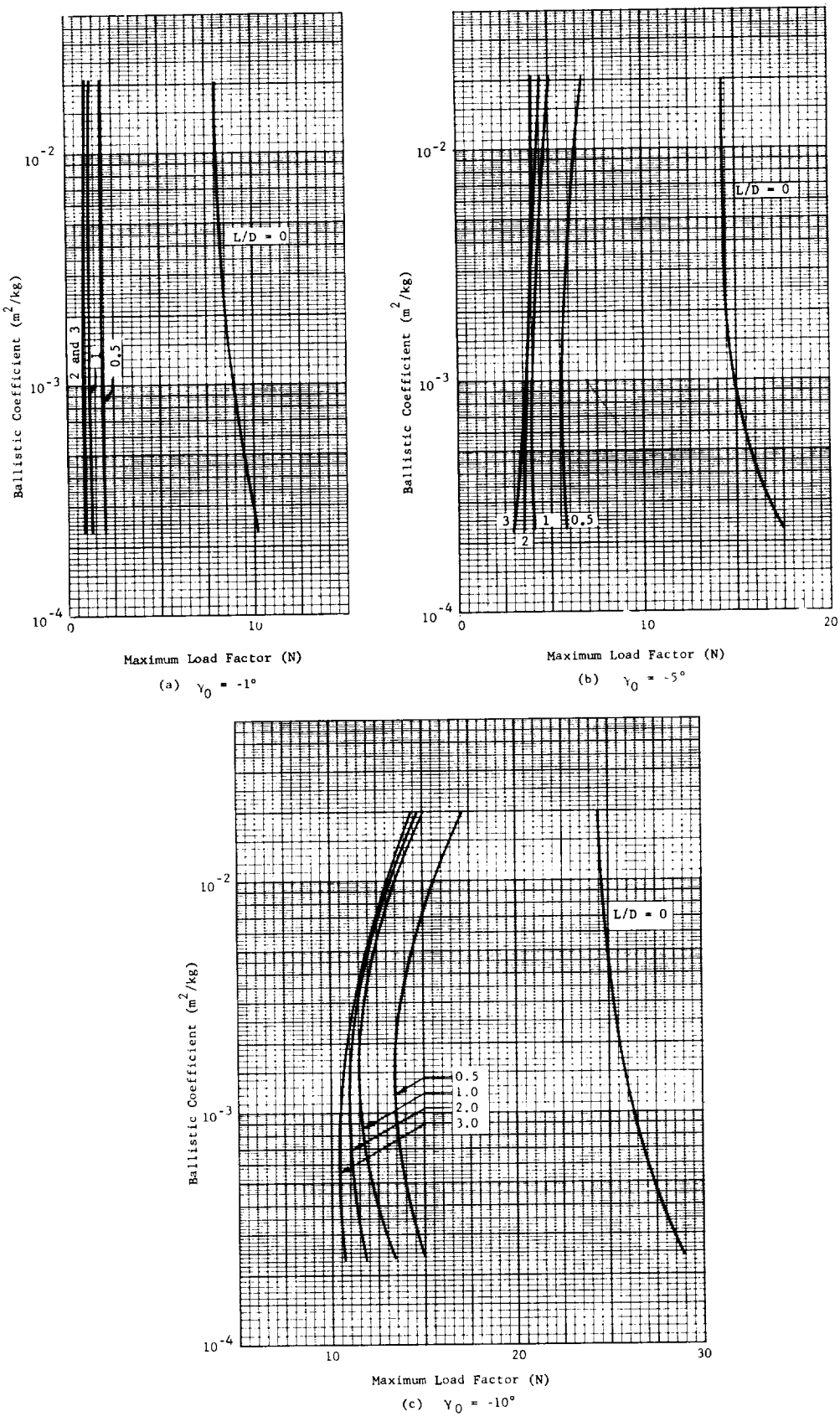

Fig. 18. Maximum Re-Entry Load Factor Versus Ballistic Coefficient (h_0 = 400,000 ft = 121,920 m; v_0 = 25,000 fps = 7620 mps)

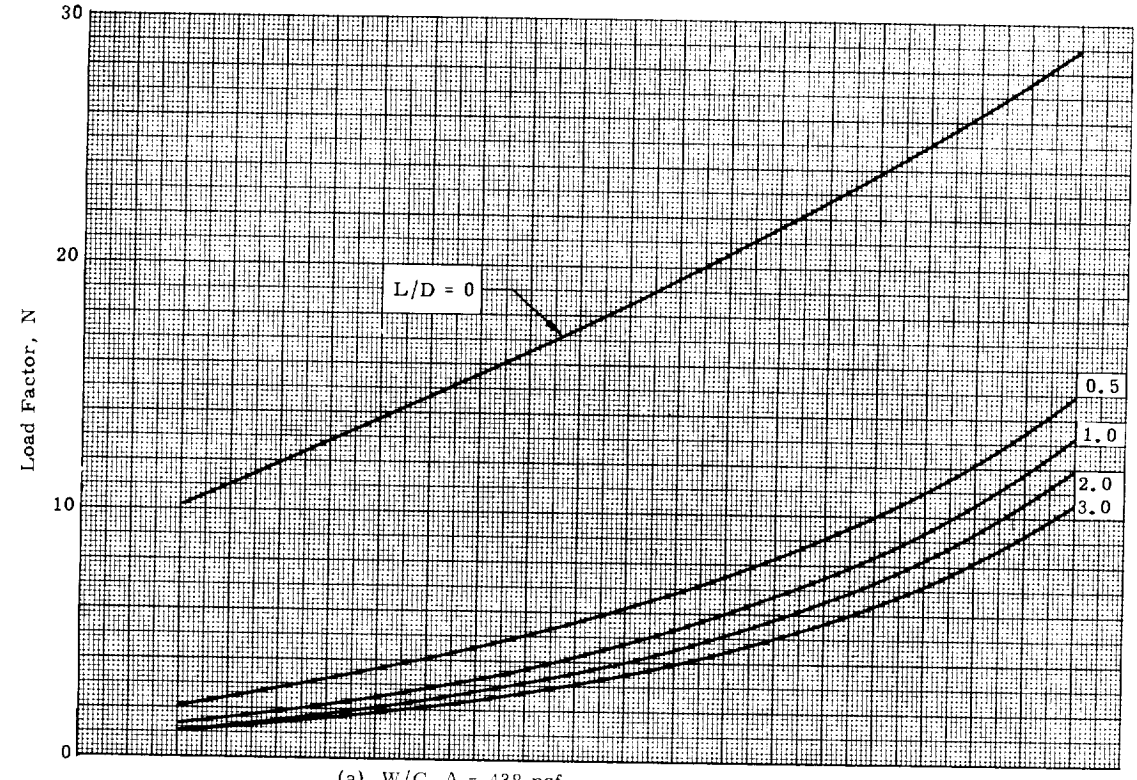

(a) W/C_DA = 438 psf

B = 0.037 ft^2/slug = 0.234 x 10^{-3} m^2/kg

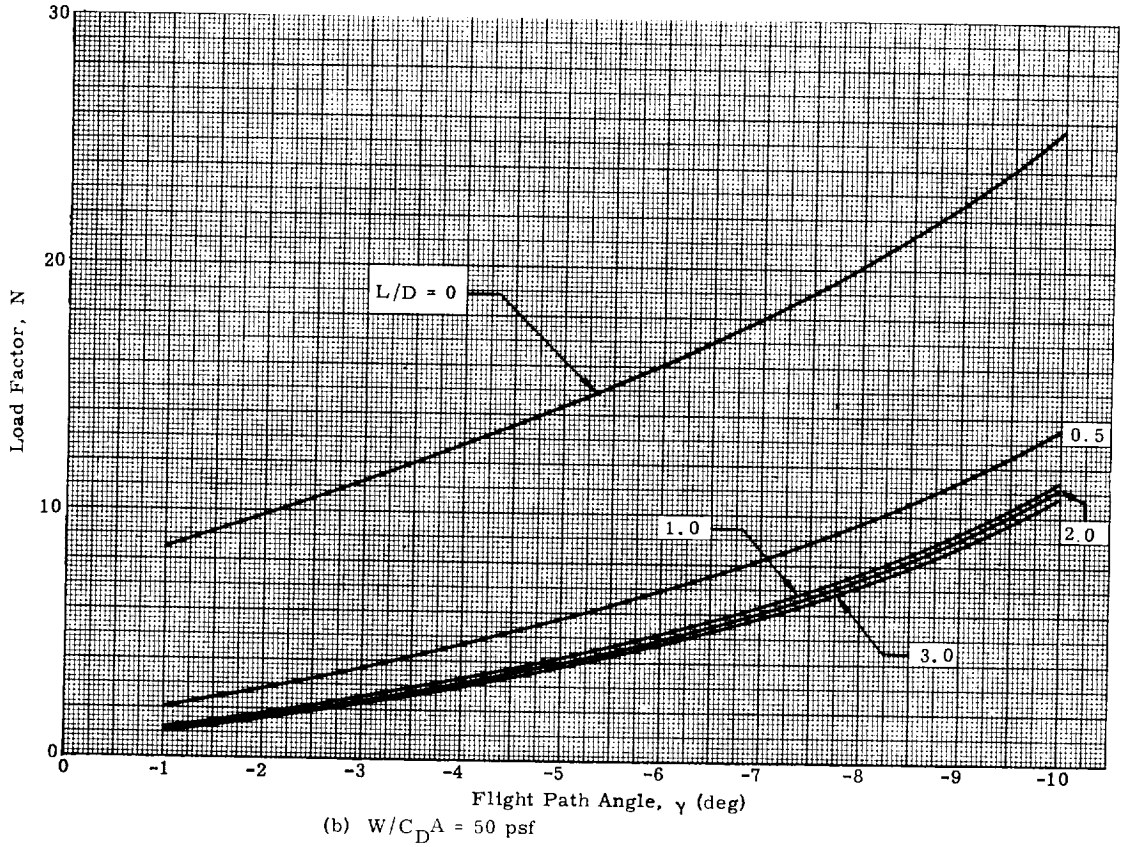

(b) W/C_DA = 50 psf

B = 0.322 ft^2/slug = 2.04 x 10^{-3} m^2/kg

Fig. 19. Maximum Re-Entry Load Factor Versus Flight Path Angle (v_0 = 25,000 fps = 7620 mps; h_0 = 400,000 ft = 121,920m)

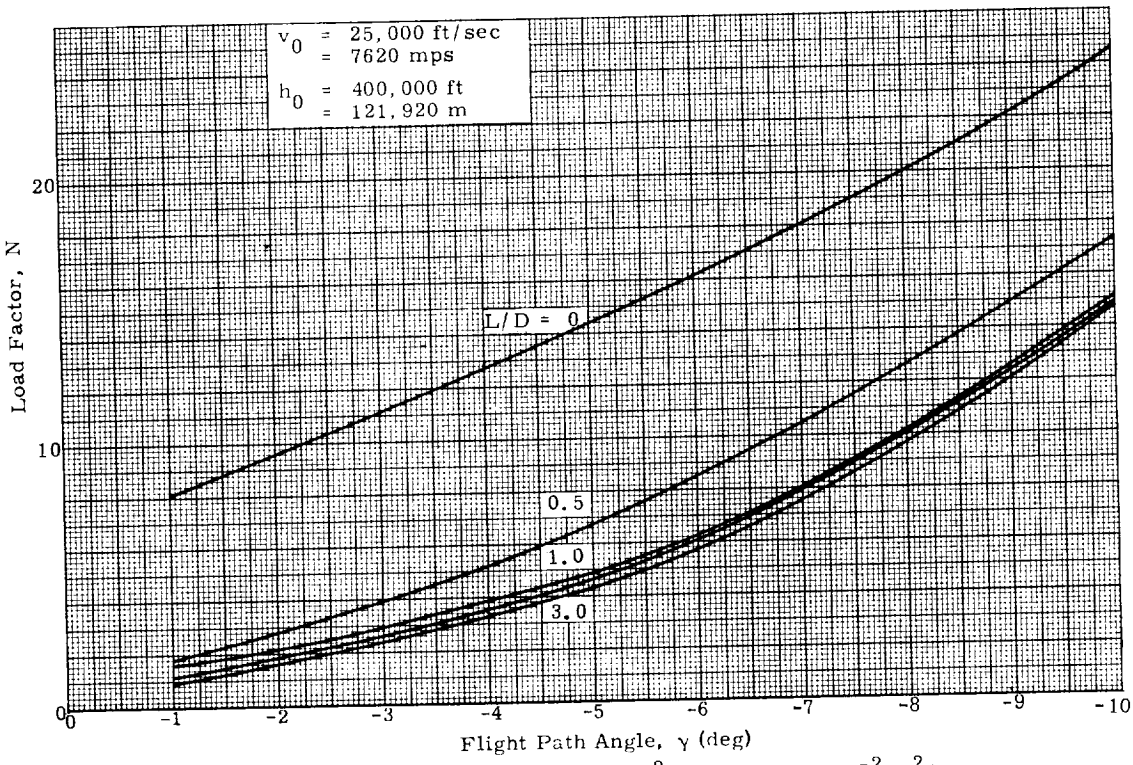

(c) W/C_DA = 5 psf, B = 3.22 ft^2/slug = 2.05 x 10^{-2} m^2/kg

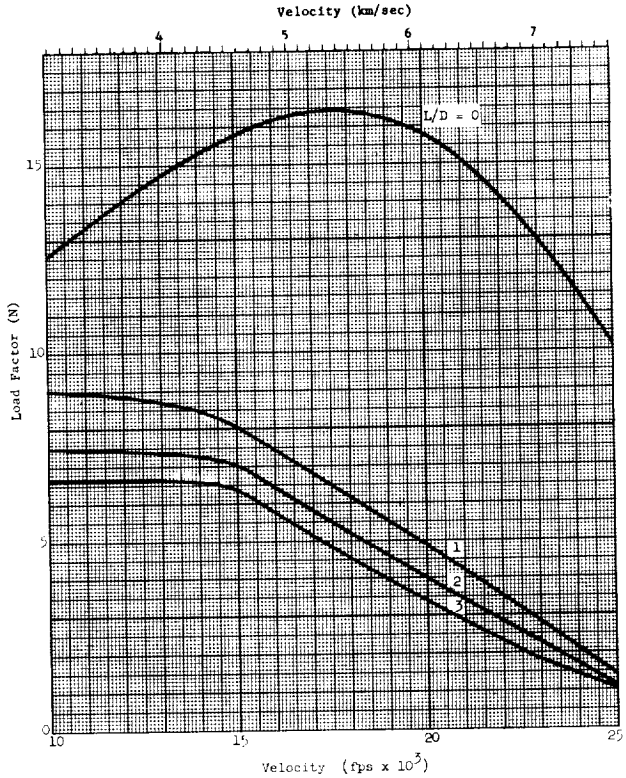

(a) B = 0.0367 ft^2/slug; W/C_DA = 438 psf
= 0.234 x 10^{-3} m^2/kg = 21,000 newton/m^2

Fig. 20. Maximum Re-entry Load Factor Versus Velocity (h_0 = 400,000 ft, γ_0 = -1°)

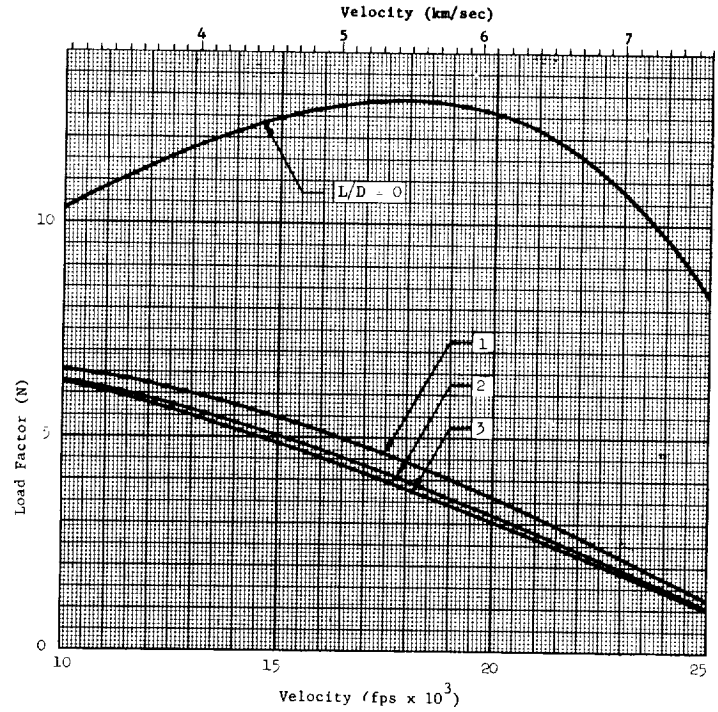

(b) B = 0.322 ft^2/slug; W/C_DA = 50 psf

= 2.04 x 10^{-3} m^2/kg = 2390 newtons/m^2

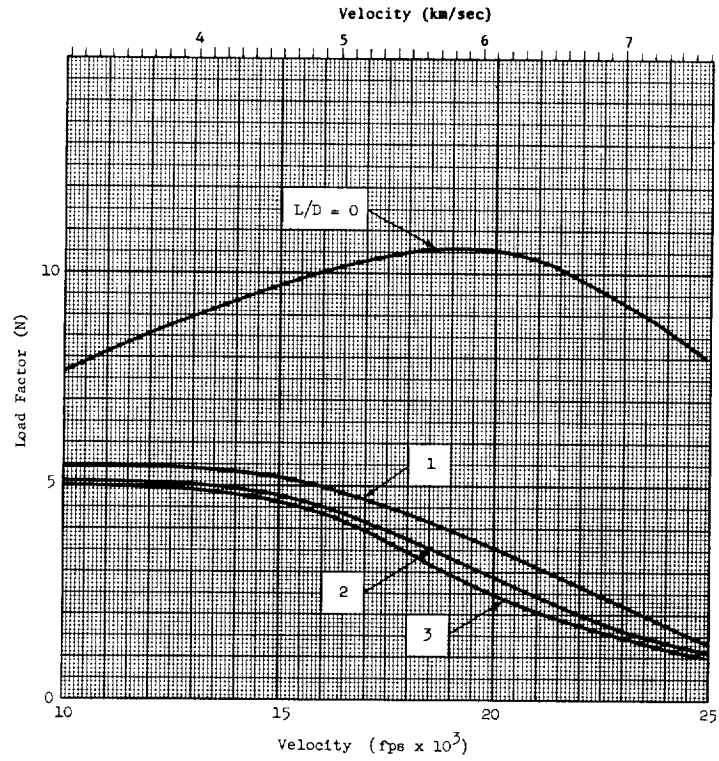

(c) W/C_DA = 5 psf = 239 newtons/m^2, B = 3.22 ft^2/slug = 2.05 x 10^{-2} m^2/kg

Fig. 20. Continued

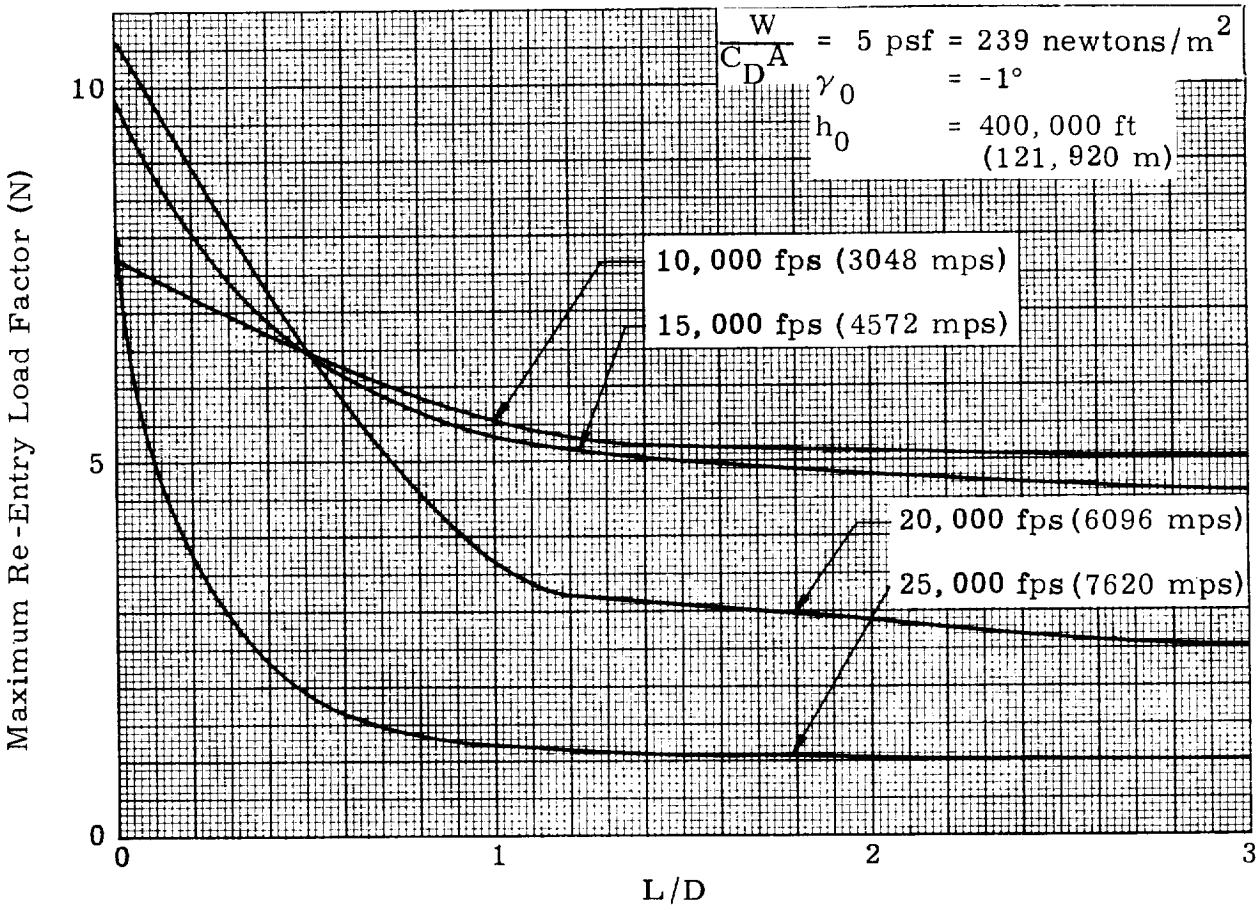

Fig. 21. Maximum Re-Entry Load Factor Versus L/D

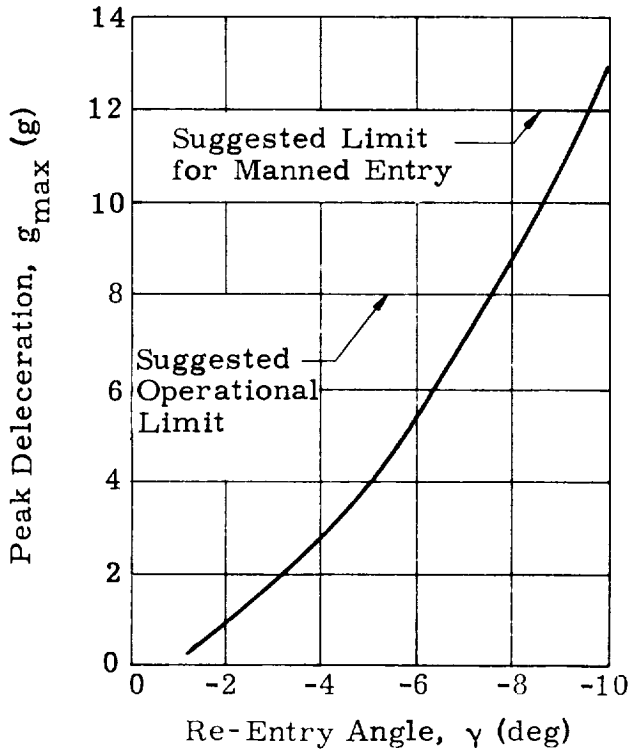

Fig. 22. Effect of Re-Entry Angle on Peak Deceleration, $v_0 = v_c$, $W/C_L A$ = 20 psf = 957 newton/m^2, L/D = 2 (Ref. 14)

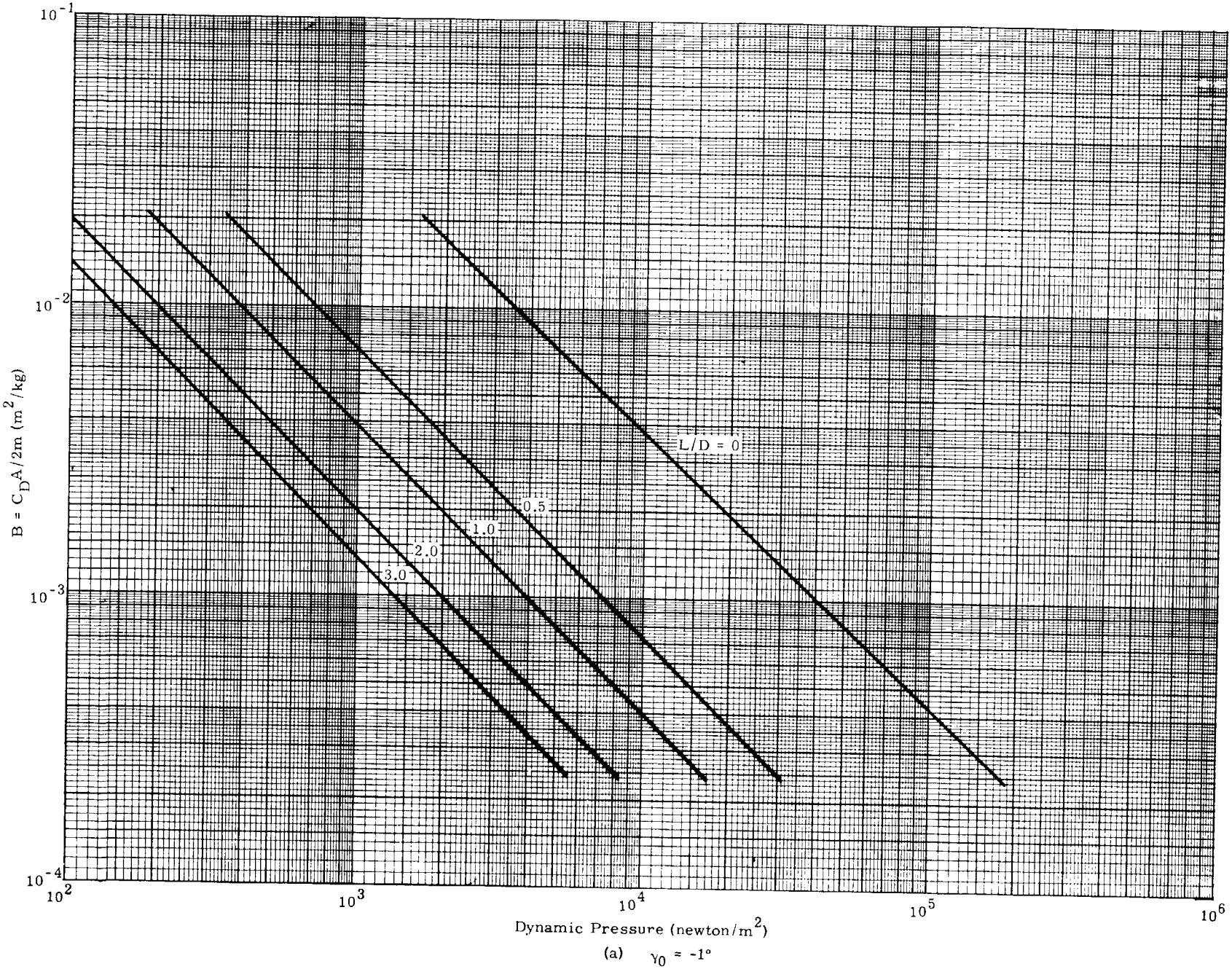

(a) $\gamma_0 = -1°$

Fig. 23. Maximum Re-Entry Dynamic Pressure (v_0 = 25,000 fps = 7620 mps; h_0 = 400,000 ft = 121,920 m)

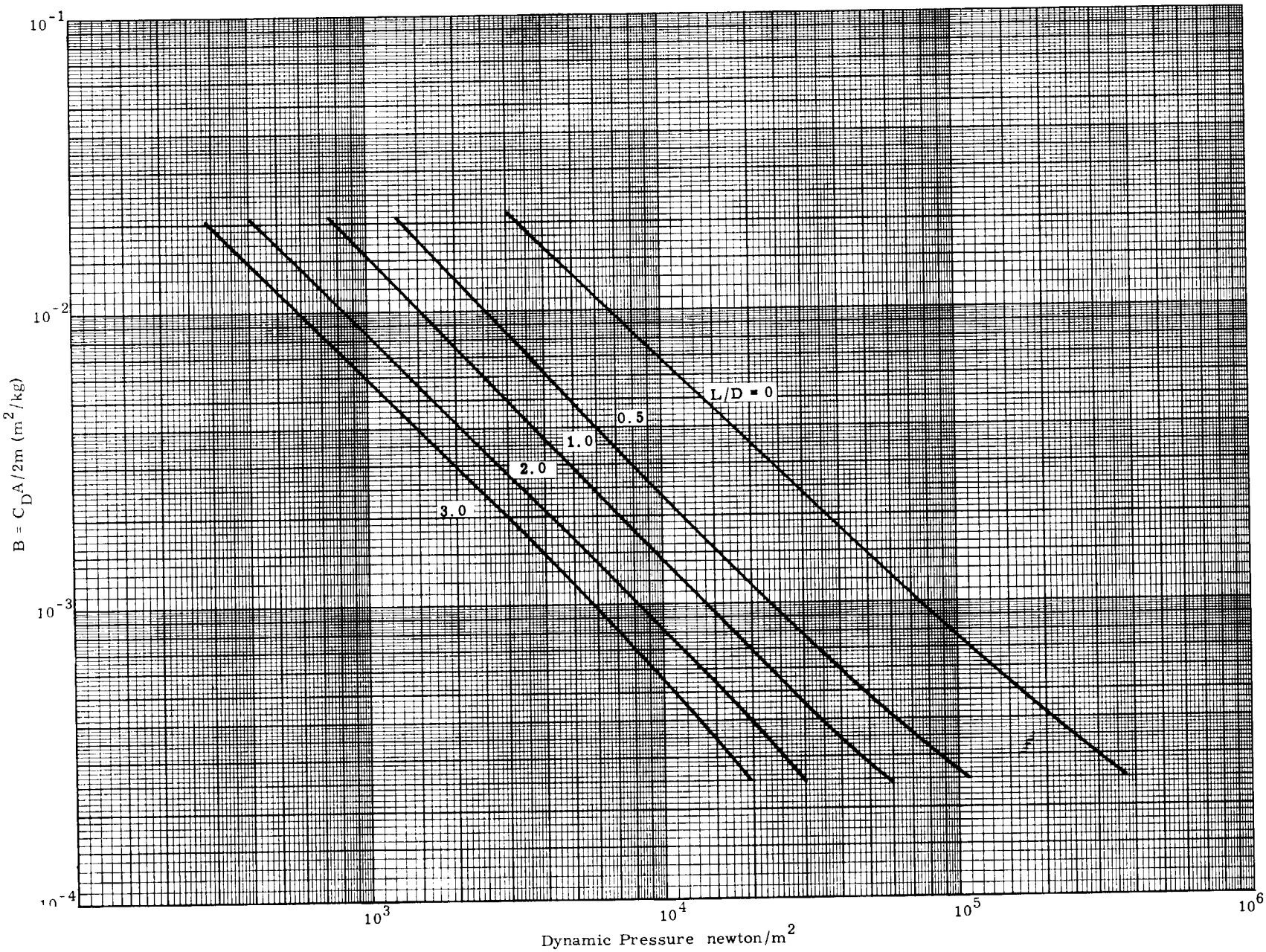
10^{-1}
10^{-2}
10^{-3}
10^{-4}
$B = C_D A/2m$ (m^2/kg)
L/D = 0
0.5
1.0
2.0
3.0
10^3
10^4
10^5
10^6
Dynamic Pressure newton/m^2

(b) $\gamma_0 = -5°$

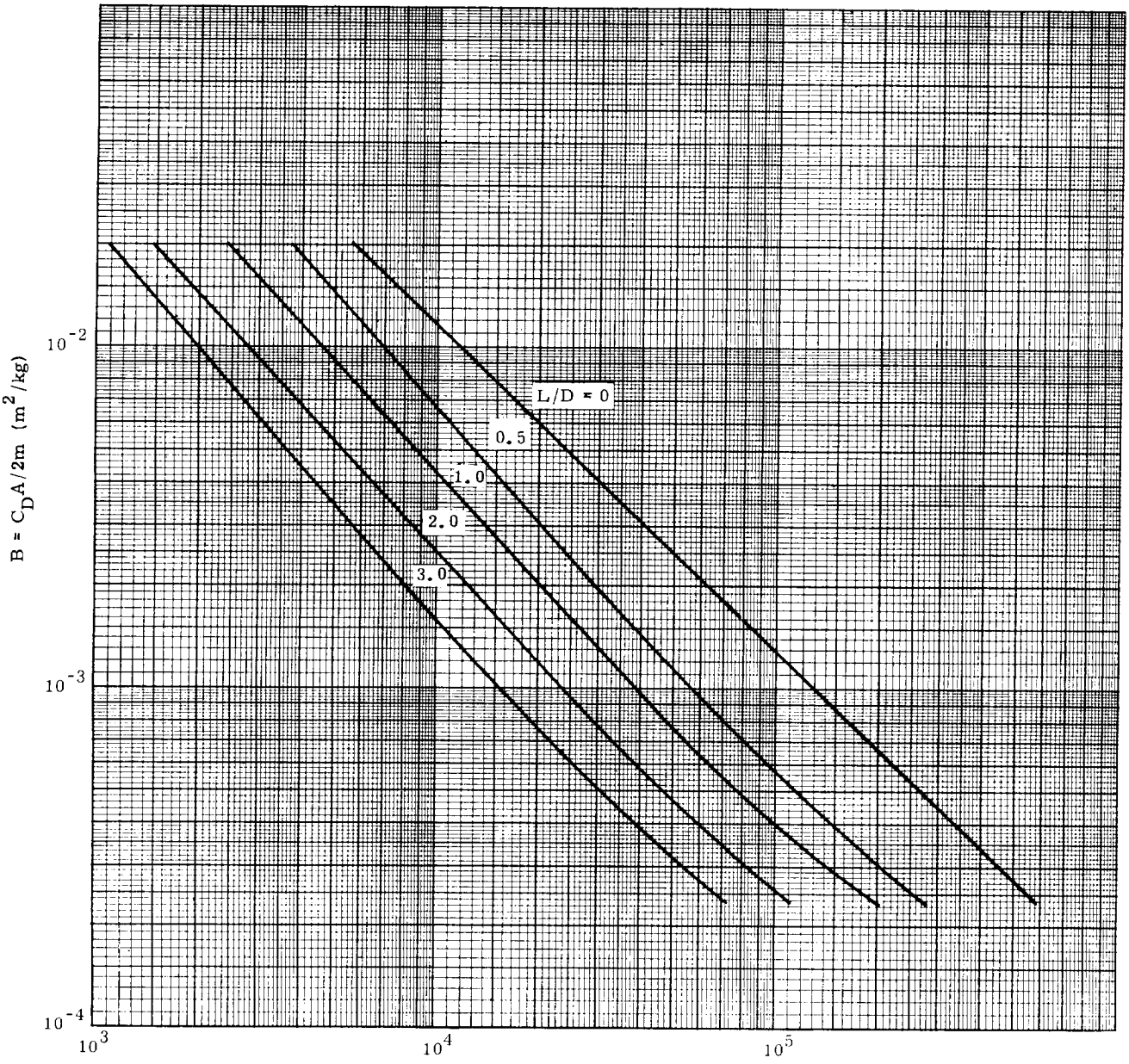

(c) $\gamma_0 = -10°$

Fig. 23. (continued)

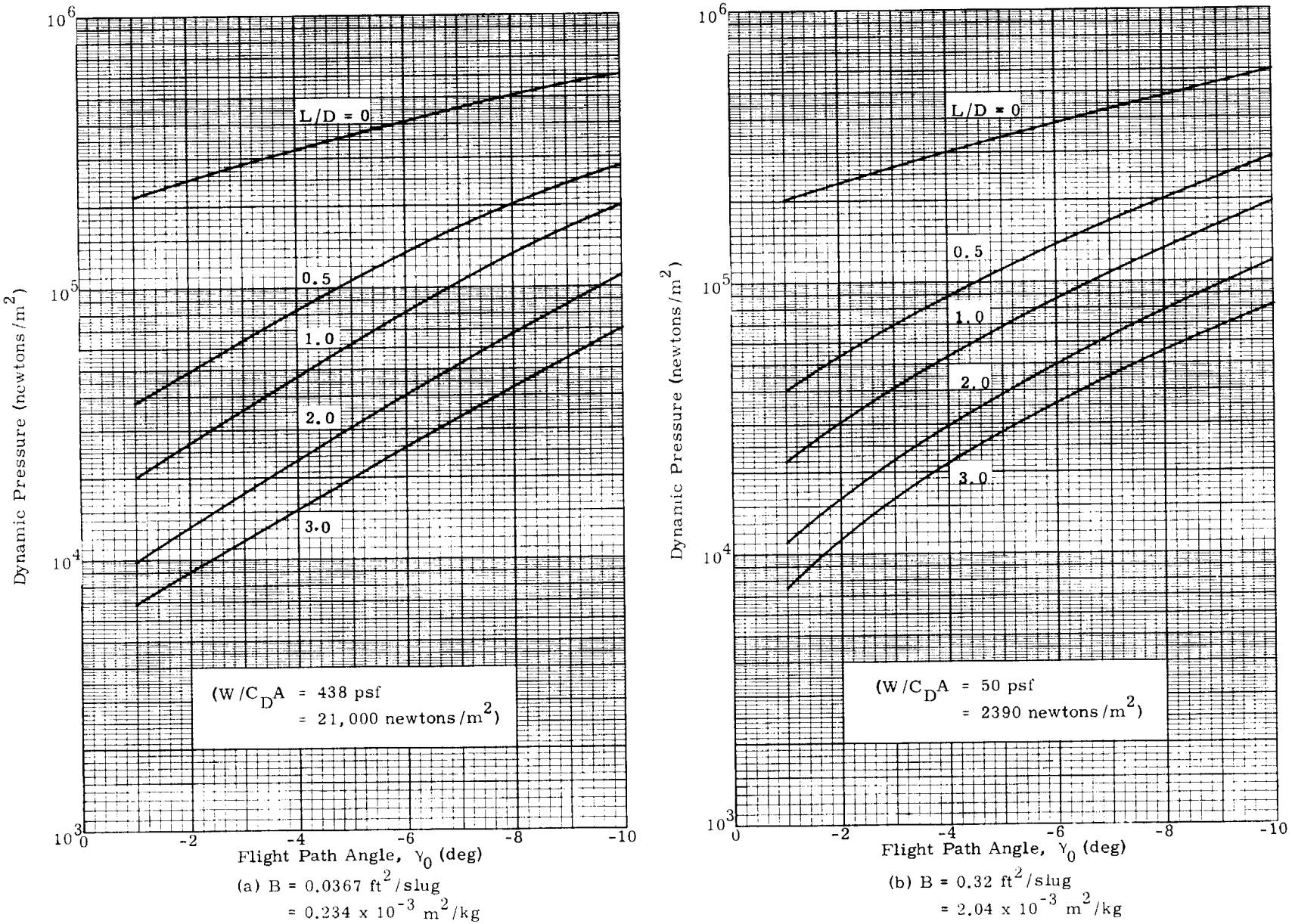

Fig. 24. Maximum Re-Entry Dynamic Pressure Versus γ_0 (v_0 = 25,000 fps = 7620 mps, h_0 = 400,000 ft = 121,920 m)

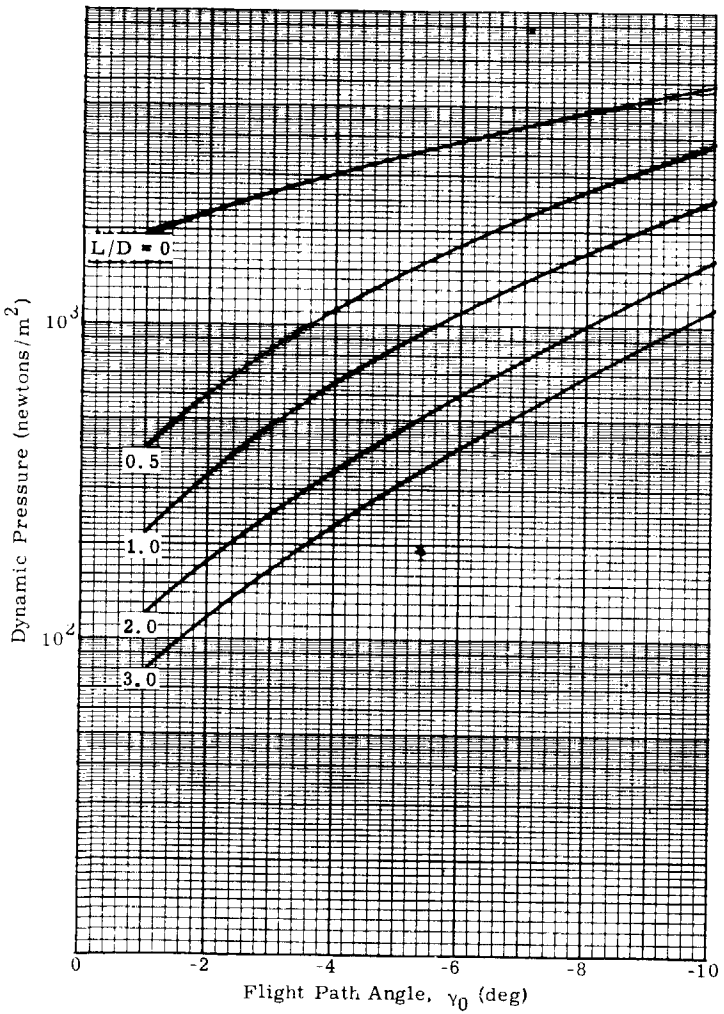

(c) W/C_DA = 5 psf = 239 newtons/m^2,
B = 3.2 ft^2/slug = 20.5 x 10^{-3} m^2/kg

Fig. 24. (continued)

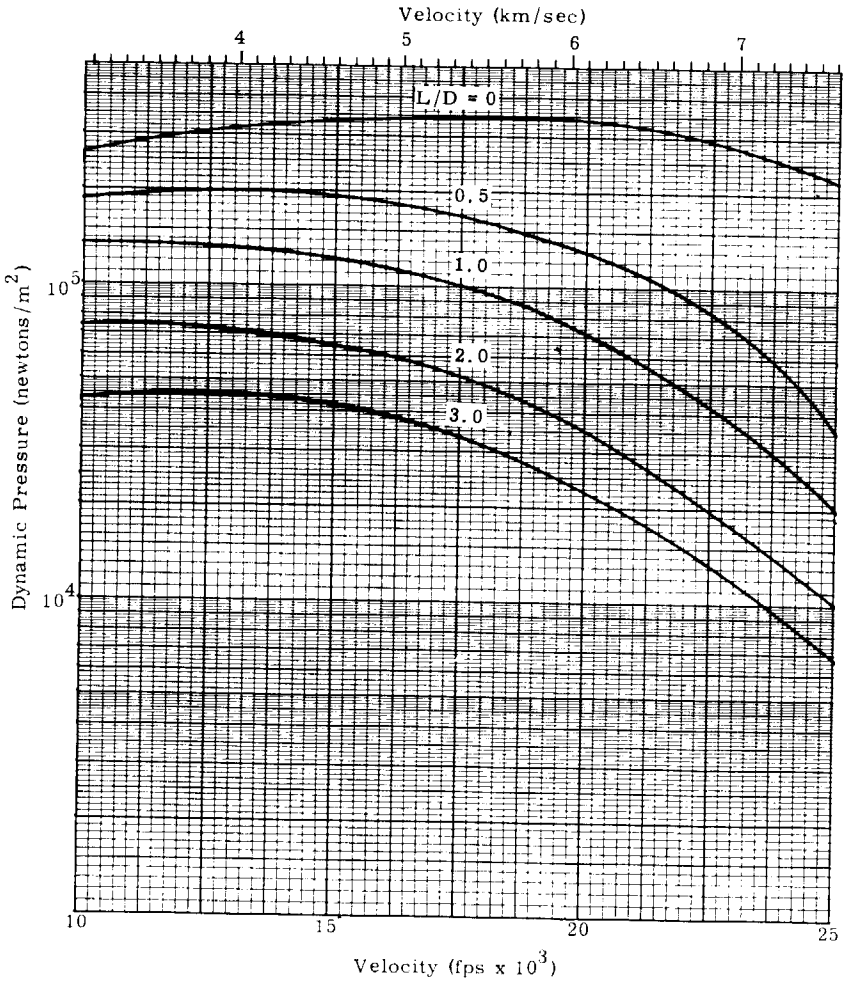

(a) W/C_DA = 438 psf
= 21,000 newtons/m^2

Fig. 25. Maximum Re-entry Dynamic Pressure Versus Velocity
(γ_0 = -1°; h_0 = 400,000 ft = 121,920 m)

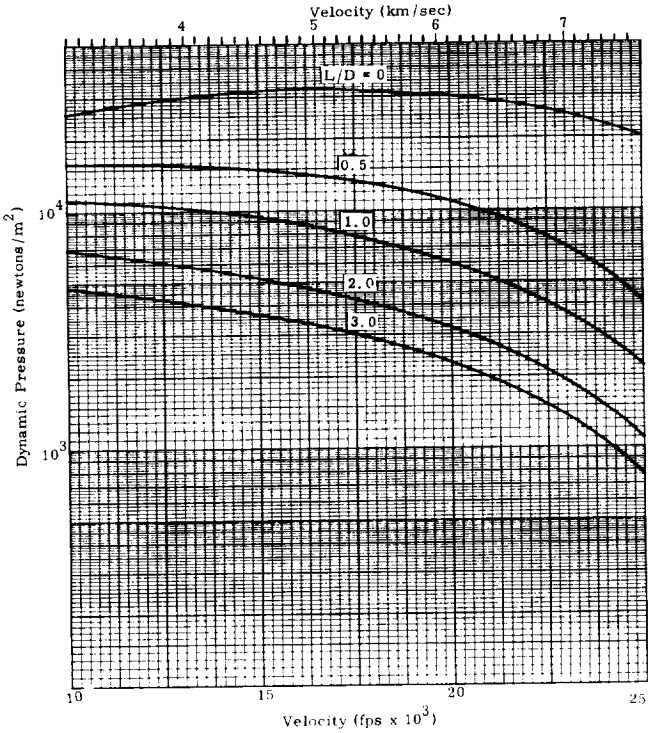

(b) W/C_DA = 50 psf
= 2390 newtons/m^2

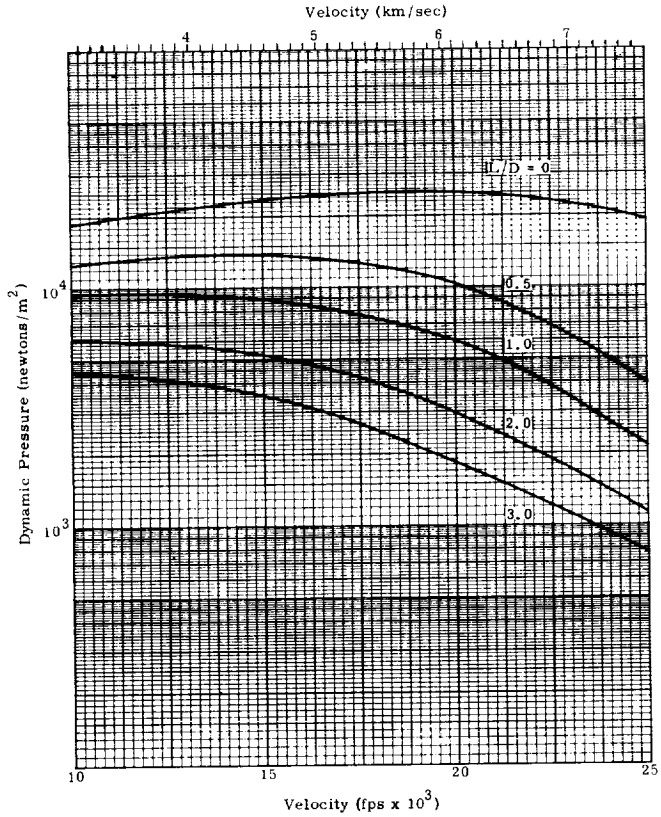

(c) W/C_DA = 5 psf
= 239 newtons/m^2

Fig. 25. (continued)

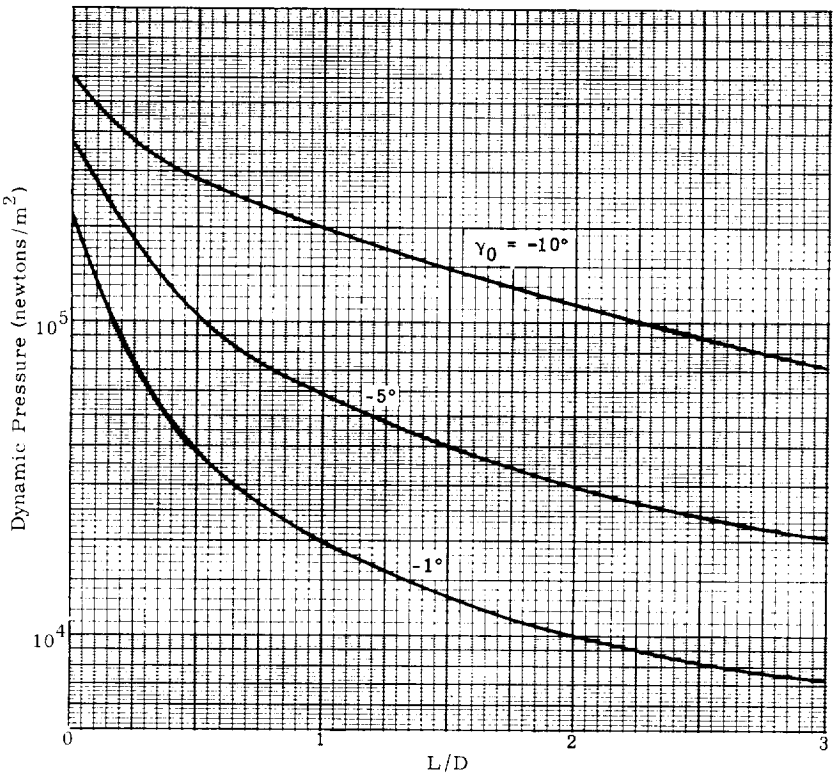

(a) W/C_DA = 438 psf = 21,000 newtons/m^2

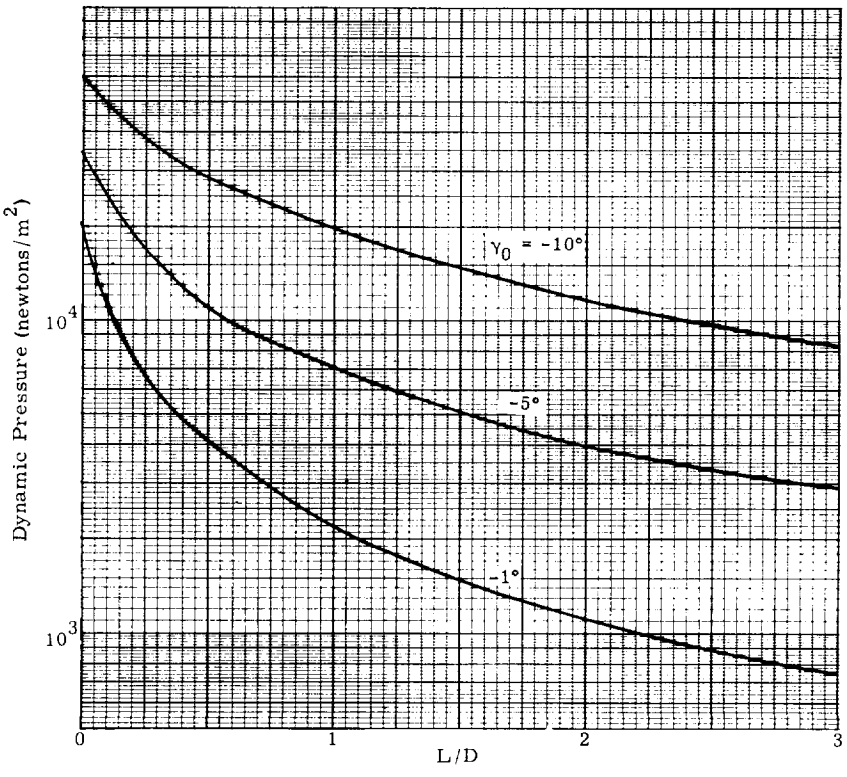

(b) W/C_DA = -50 psf = 2390 newtons/m^2

Fig. 26. Maximum Re-Entry Dynamic Pressure Versus L/D
(v_0 = 25,000 fps = 7620 mps)

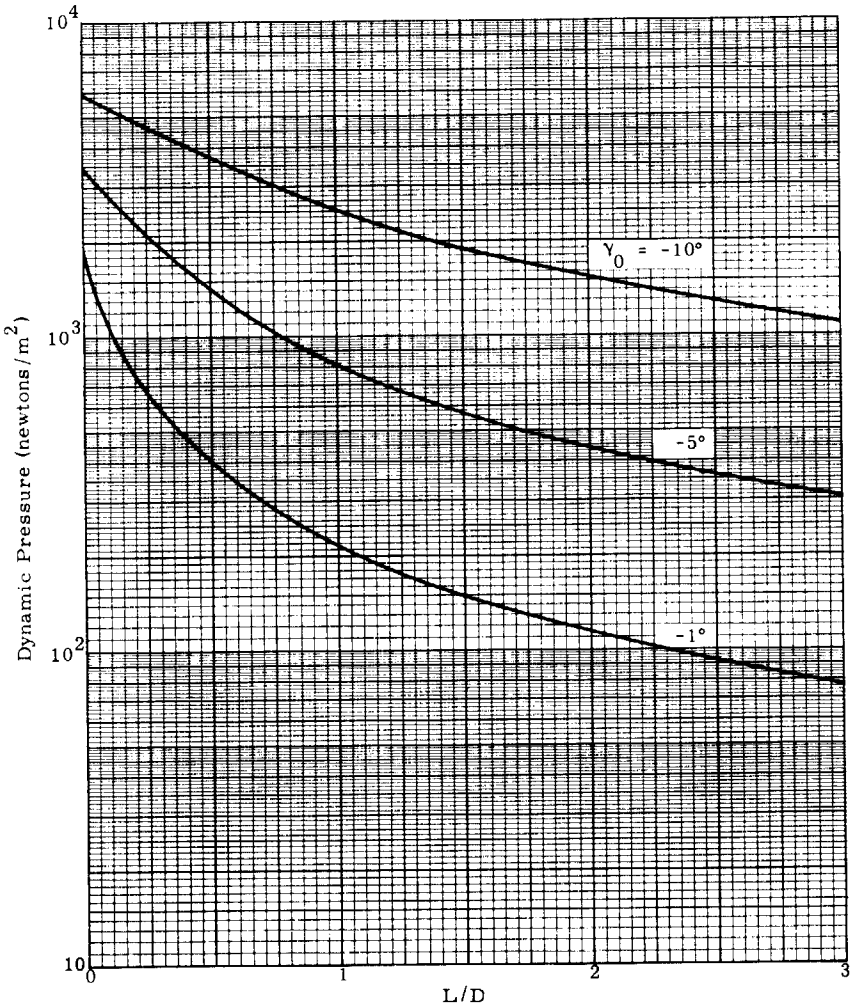

(c) W/C_DA = 5 psf = 239 newtons/m^2

Fig. 26. (continued)

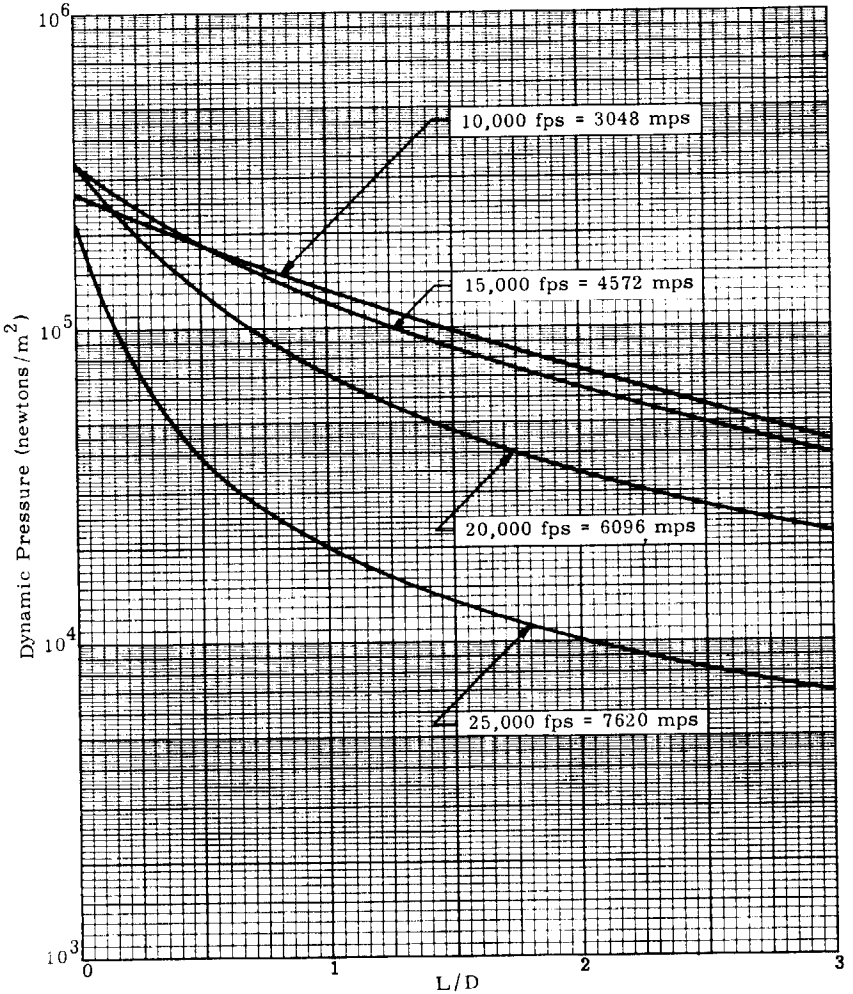

(a) W/C_DA = 438 psf = 21,000 newtons/m^2

Fig. 27. Maximum Re-Entry Dynamic Pressure Versus L/D (γ_0 = -1°; h_0 = 400,000 ft = 121,920 m)

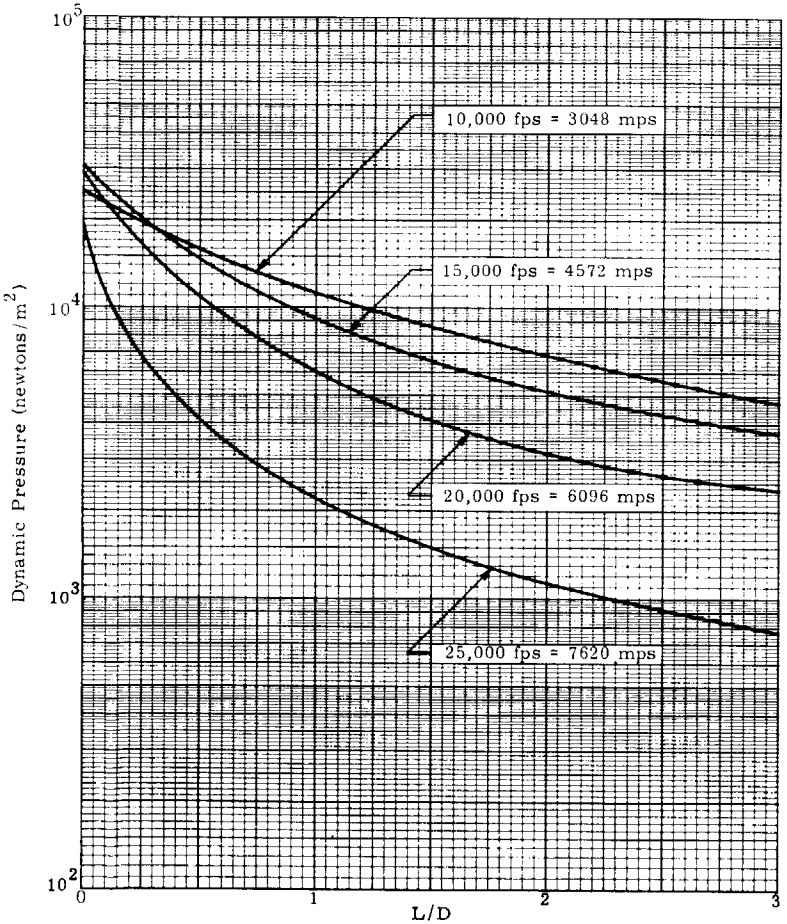

(b) W/C_DA = 50 psf = 2390 newtons/m^2

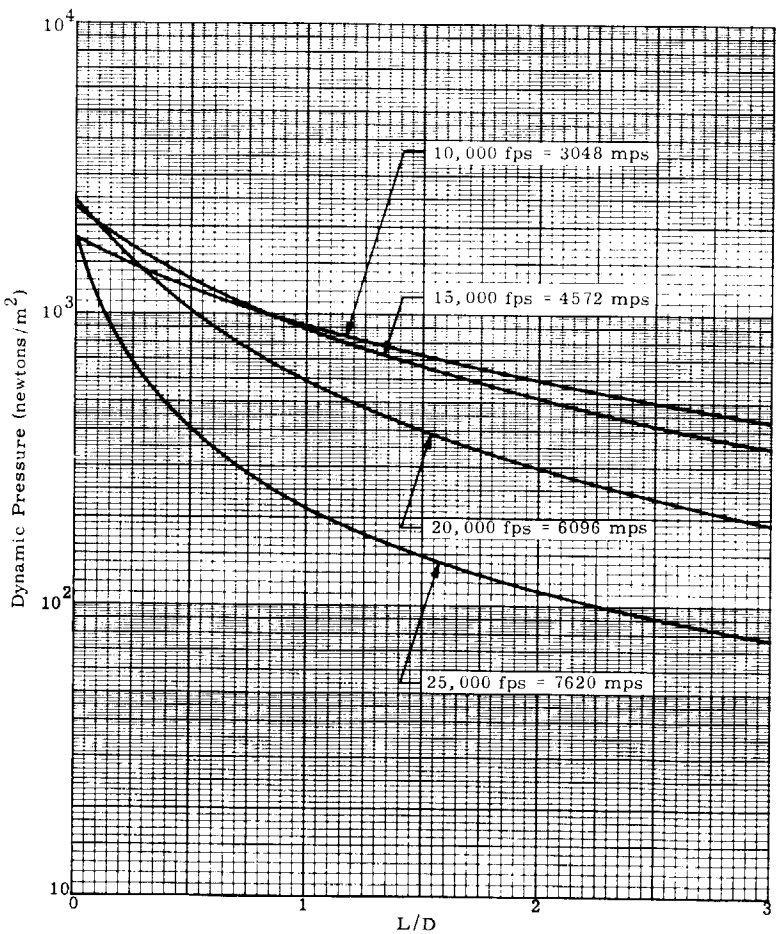

(c) W/C_DA = 5 psf = 239 newtons/m^2

Fig. 27. (continued)

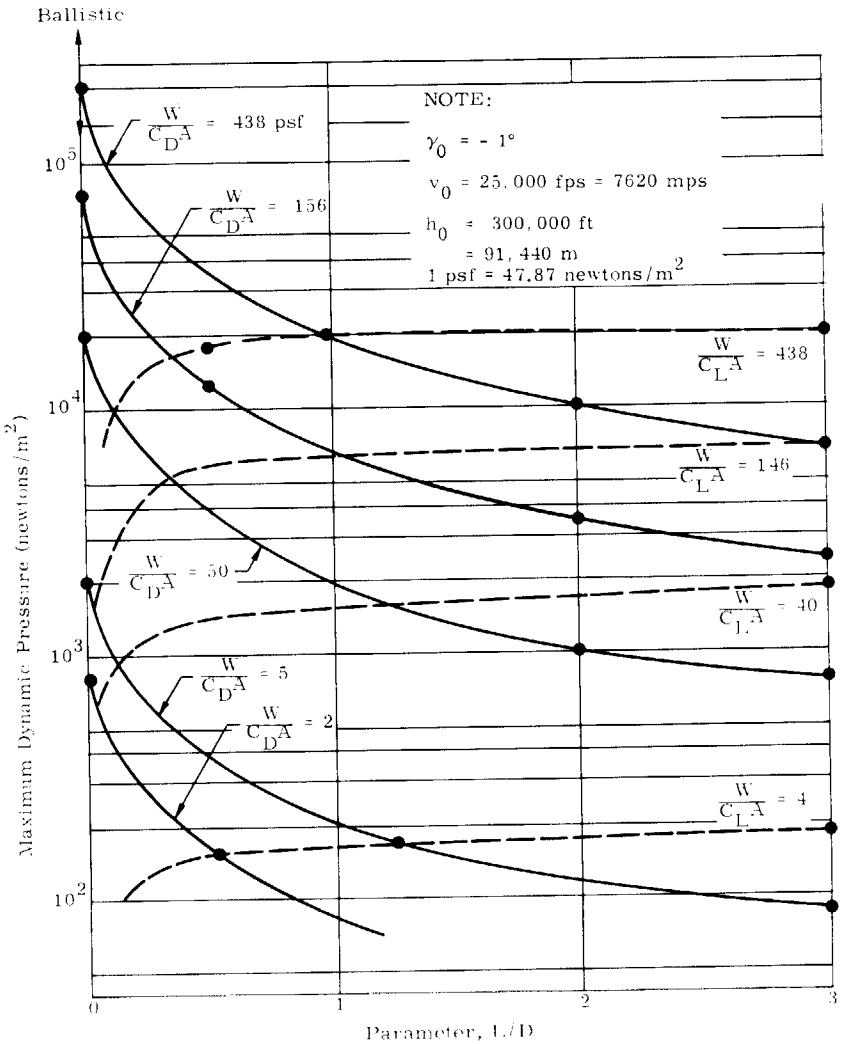

Fig. 28. Effects of Lift, Drag and Wing Loading on Maximum Dynamic Pressure

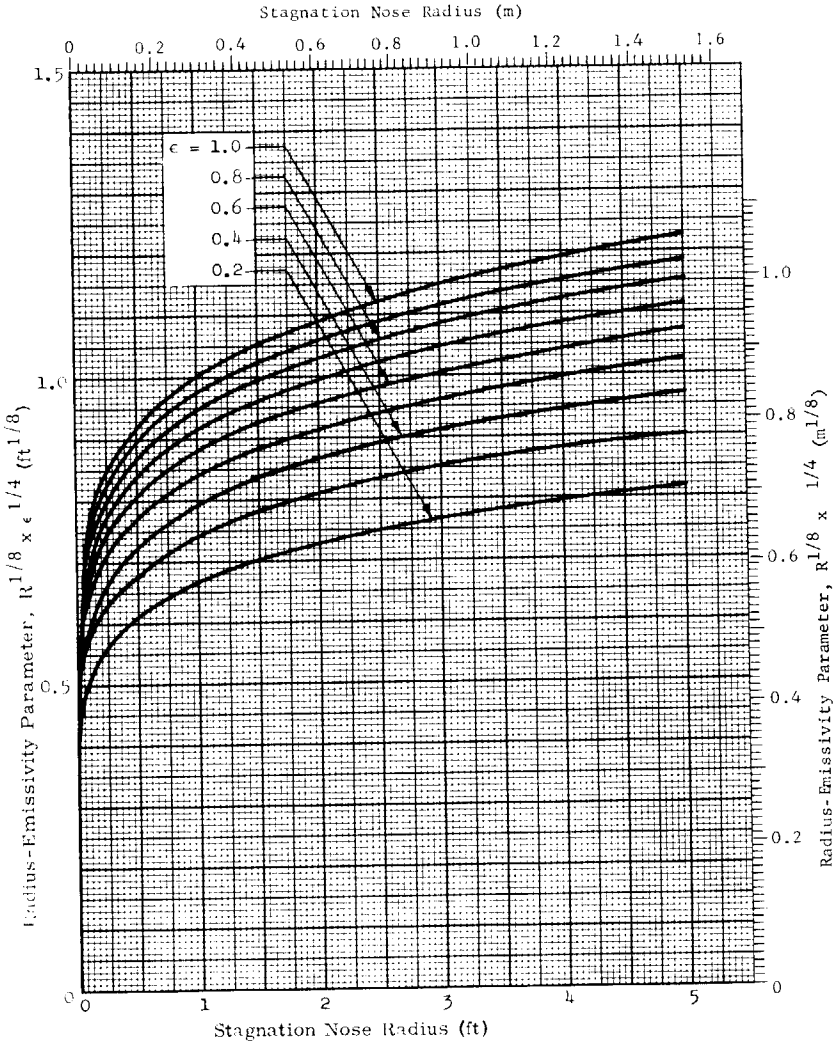

Fig. 29. Radius-Emissivity Parameter ($R^{1/8} \times \epsilon^{1/4}$) Versus Stagnation Nose Radius

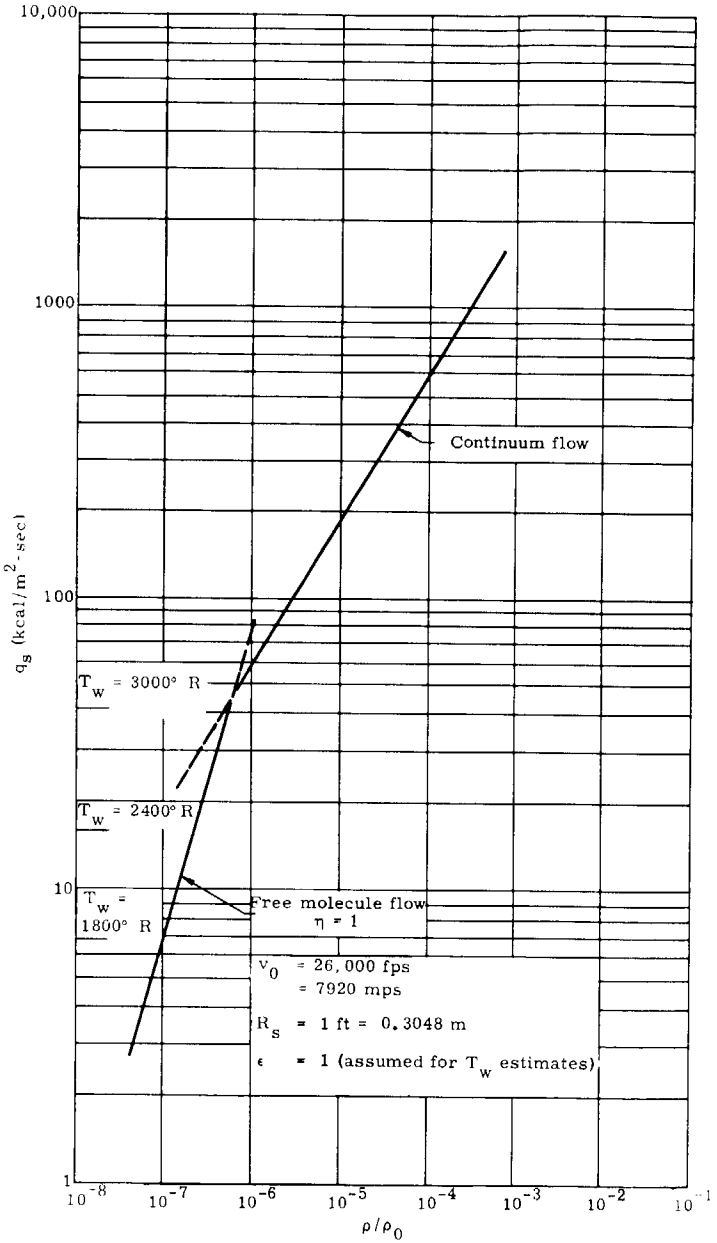

Fig. 30a. Heat Transfer Rate q_s at the Stagnation Point of a Blunt Body of 1-ft Nose Radius as a Function of Air Density Ratio, ρ/ρ_0 (Ref. 22)

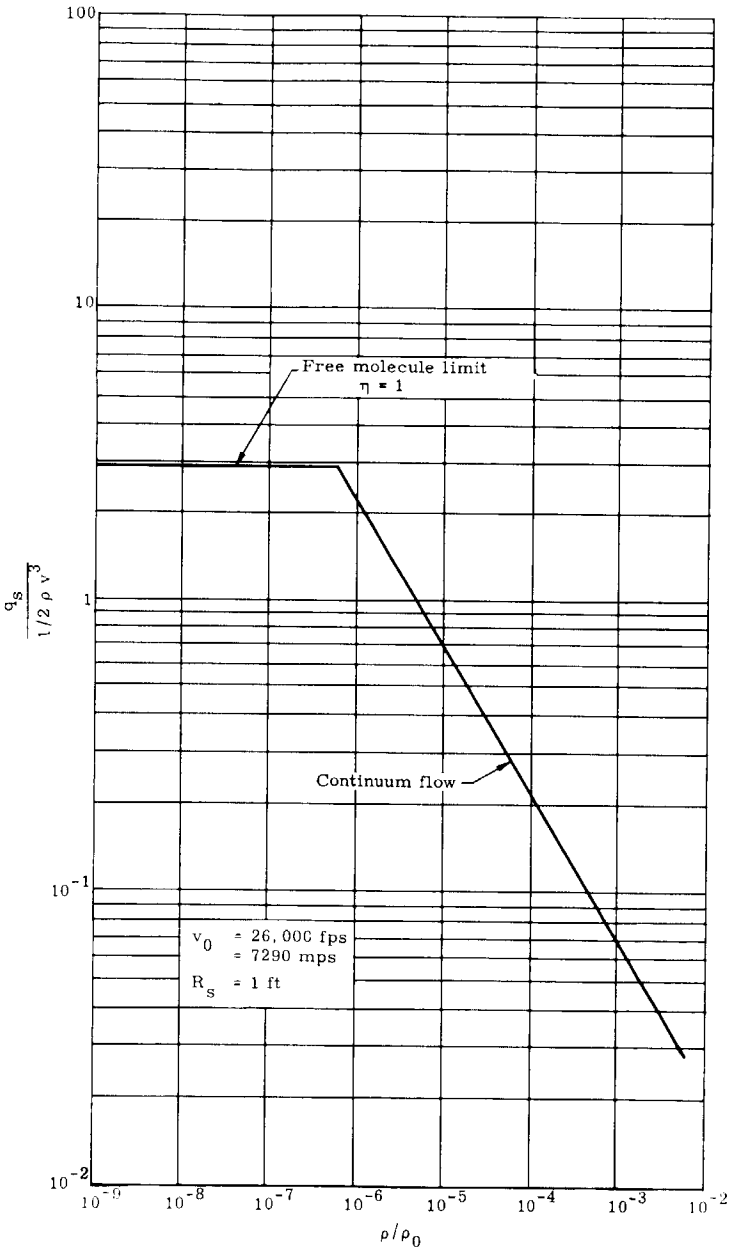

Fig. 30b. Ratio of the Heat Input Rate q_s to the Rate at Which Energy Is Dissipated by Drag $\frac{1}{2}\rho v^3$ as a Function of Air Density Ratio ρ/ρ_0 (Ref. 22)

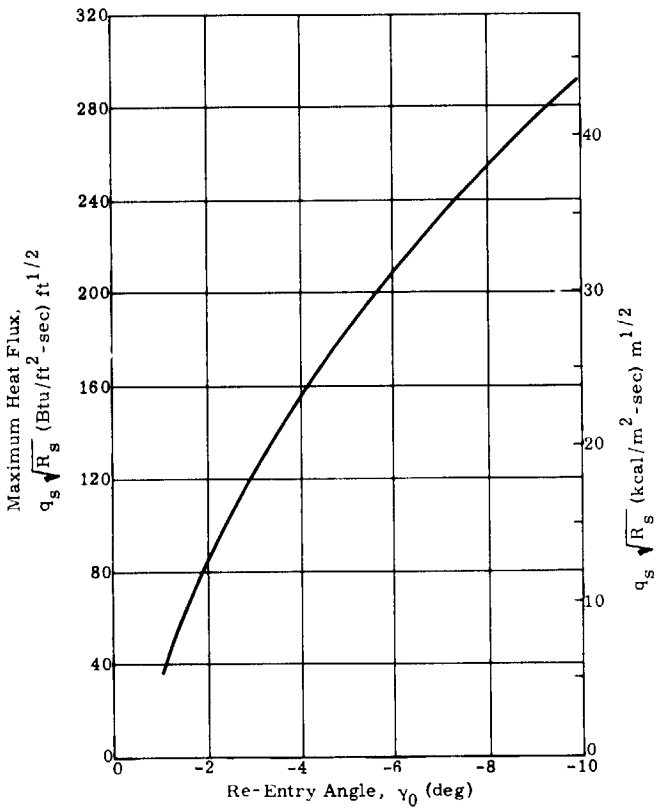

Fig. 31a. Effect of Re-Entry Angle on Maximum Heat Flux ($v_0 = v_c$, W/C_LA = 20 psf, L/D = 2) (Ref. 14)

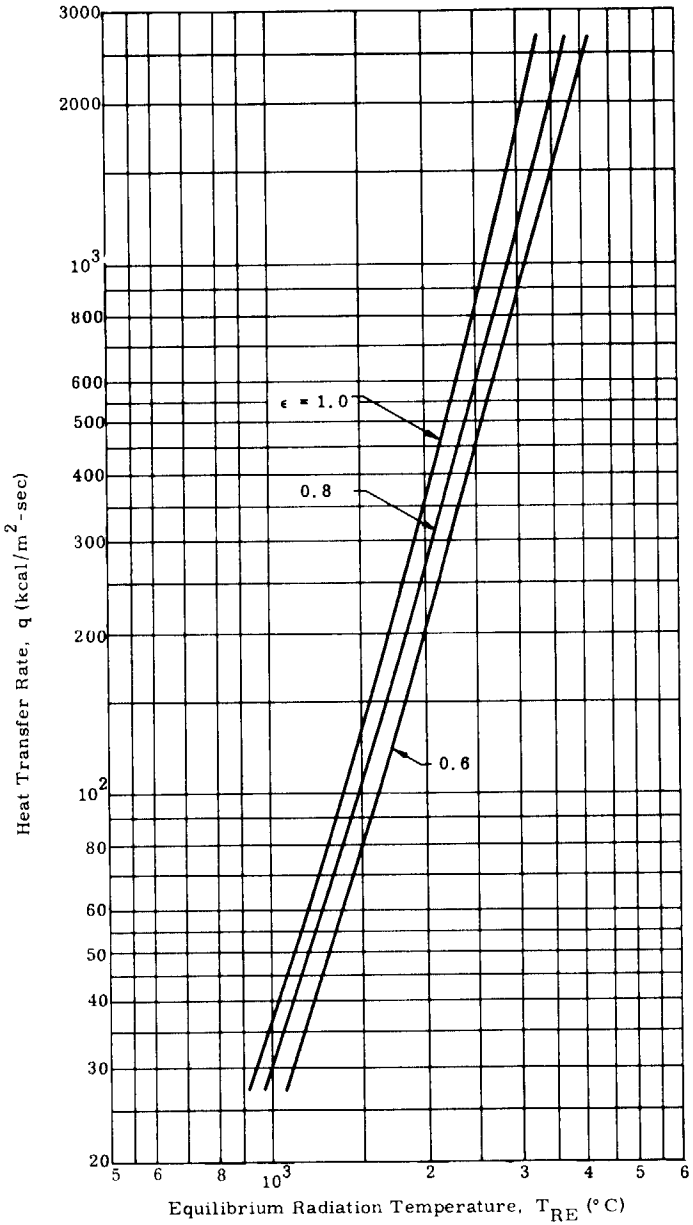

Fig. 31b. Equilibrium Radiation Temperature Versus Heat Transfer Rate (Ref. 14)

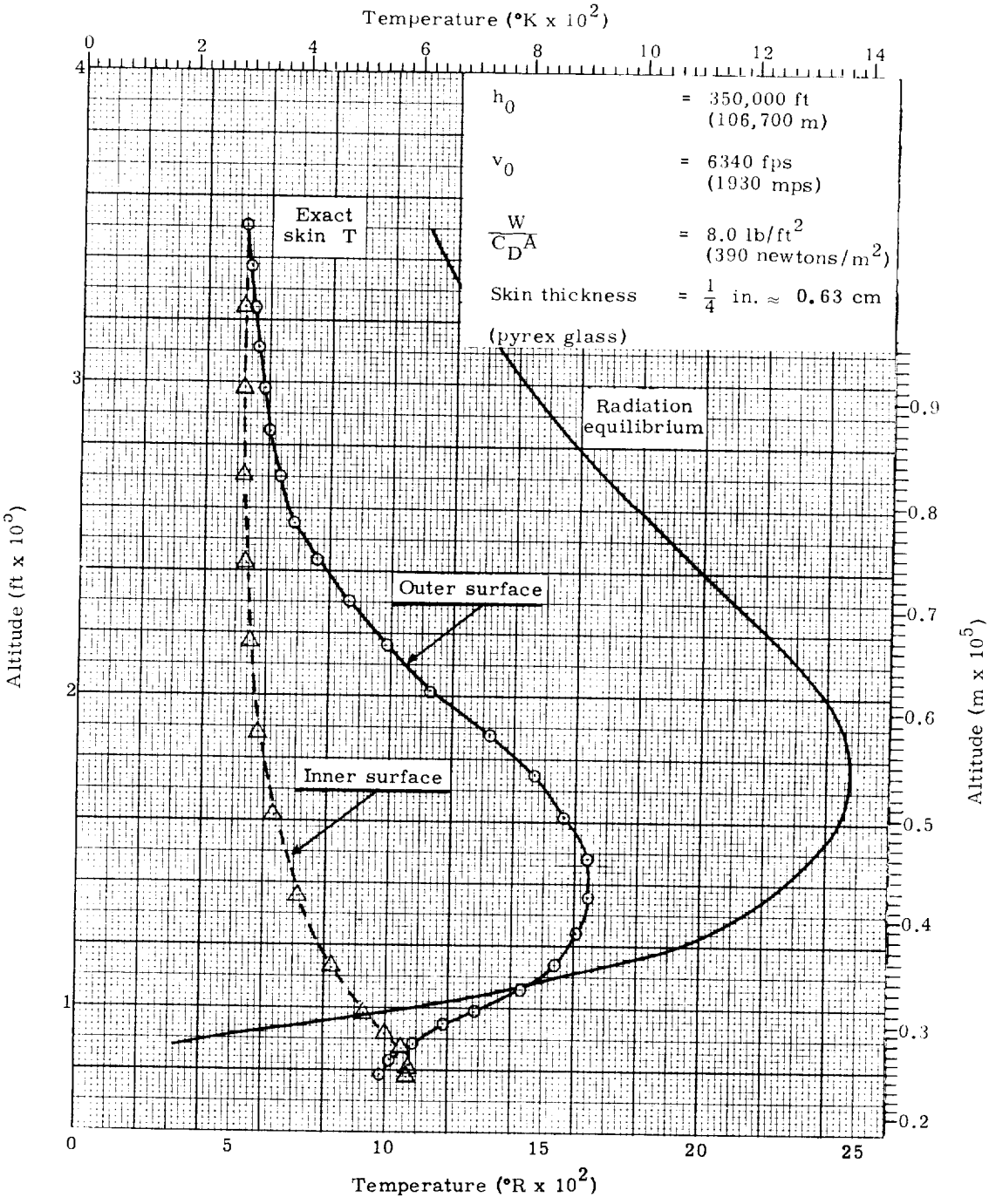

Fig. 32. Comparison of Radiation Equilibrium Method with an Exact Skin Temperature Computation (free fall from 1,000,000 ft = 304,800 m) (Ref 23)

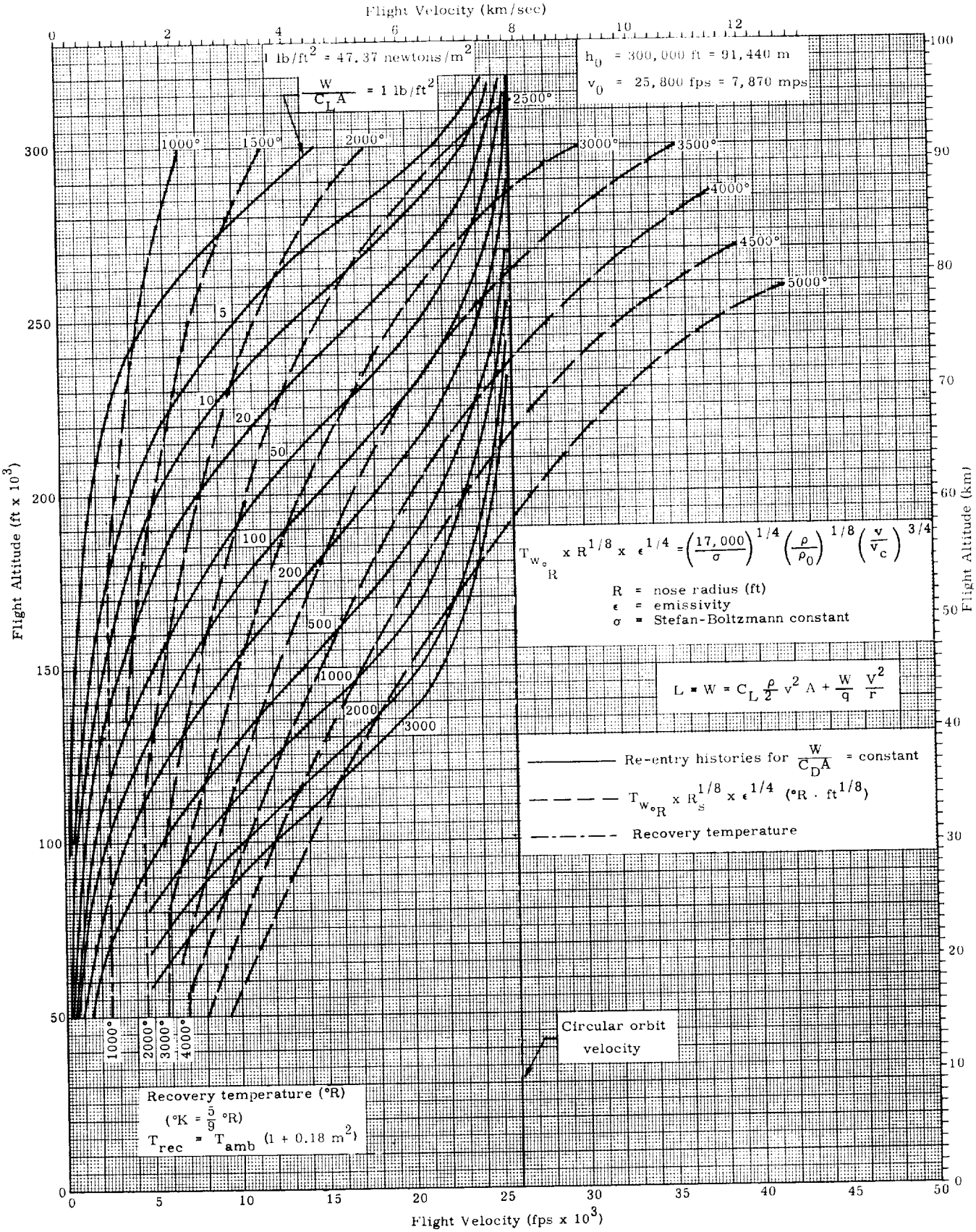

Fig. 33a. Nose Temperature Histories for Different Flight Conditions

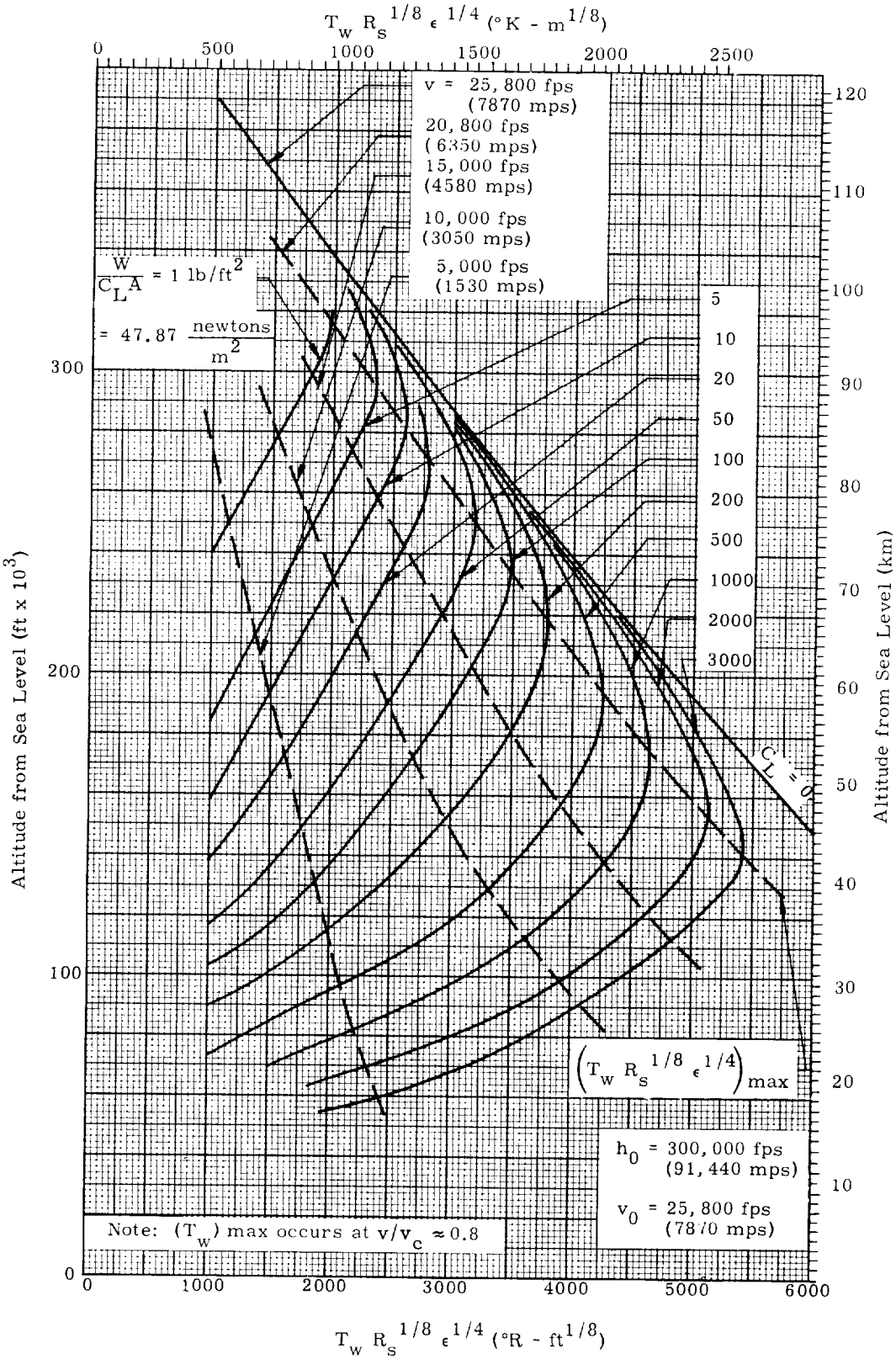

Fig. 33b. Stagnation Point Temperature Profiles for Equilibrium Glides

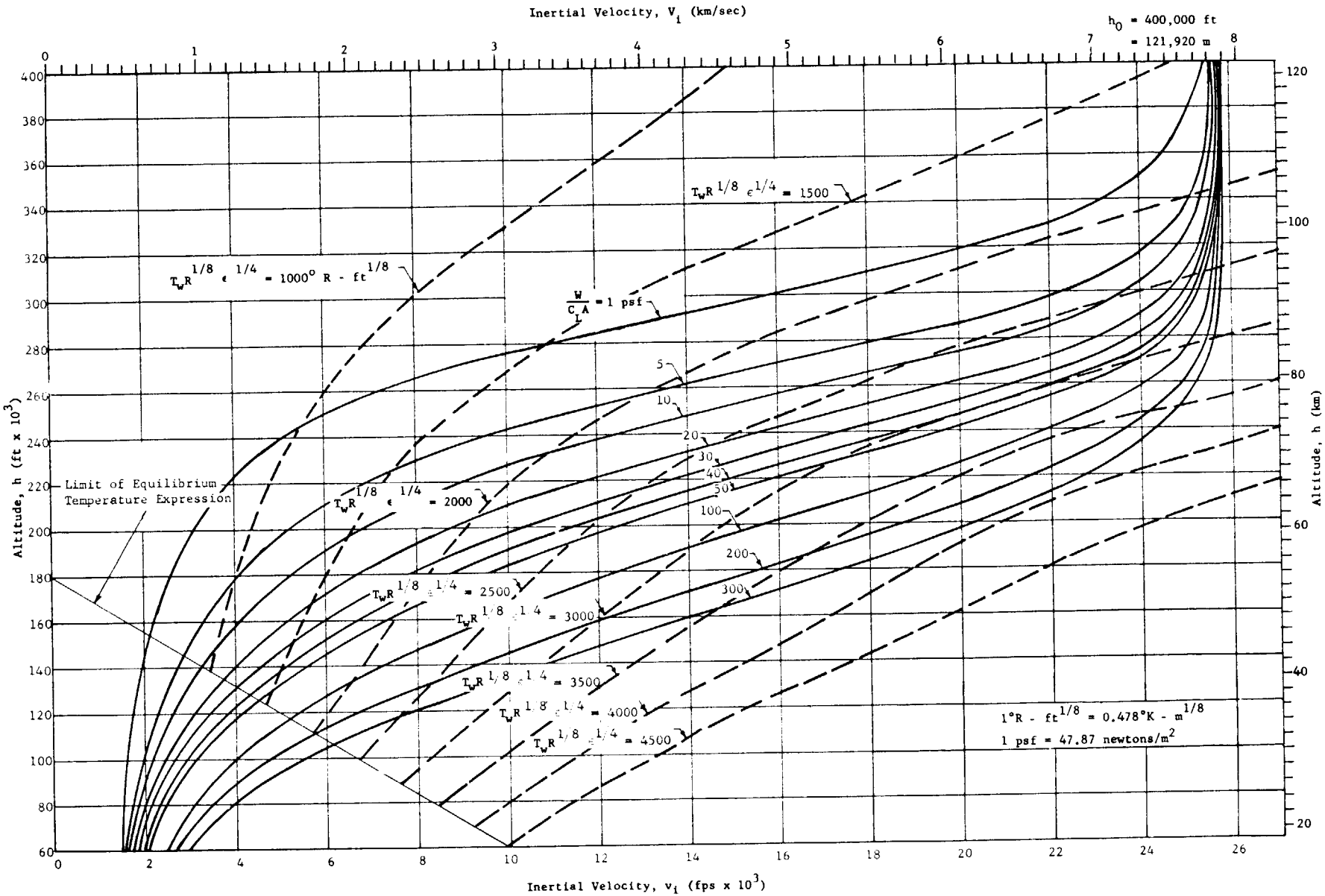

Fig. 33c. Temperature Data for Inertial Velocity and Altitude

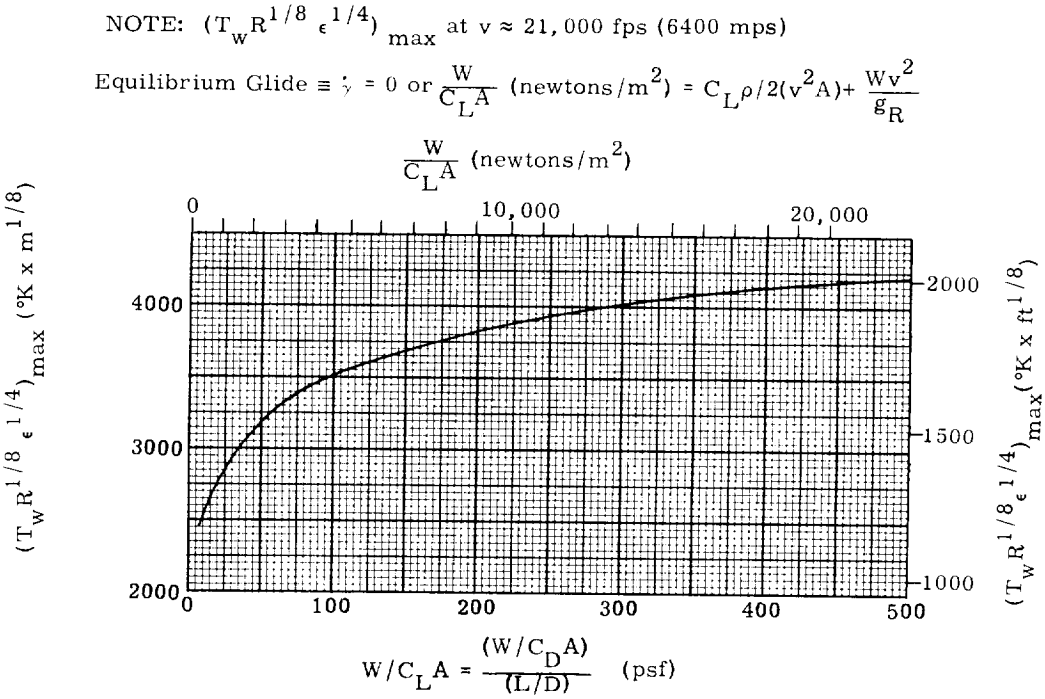

Fig. 34a. Maximum Equilibrium Nose Temperature Versus $W/C_L A$ for Equilibrium Glides

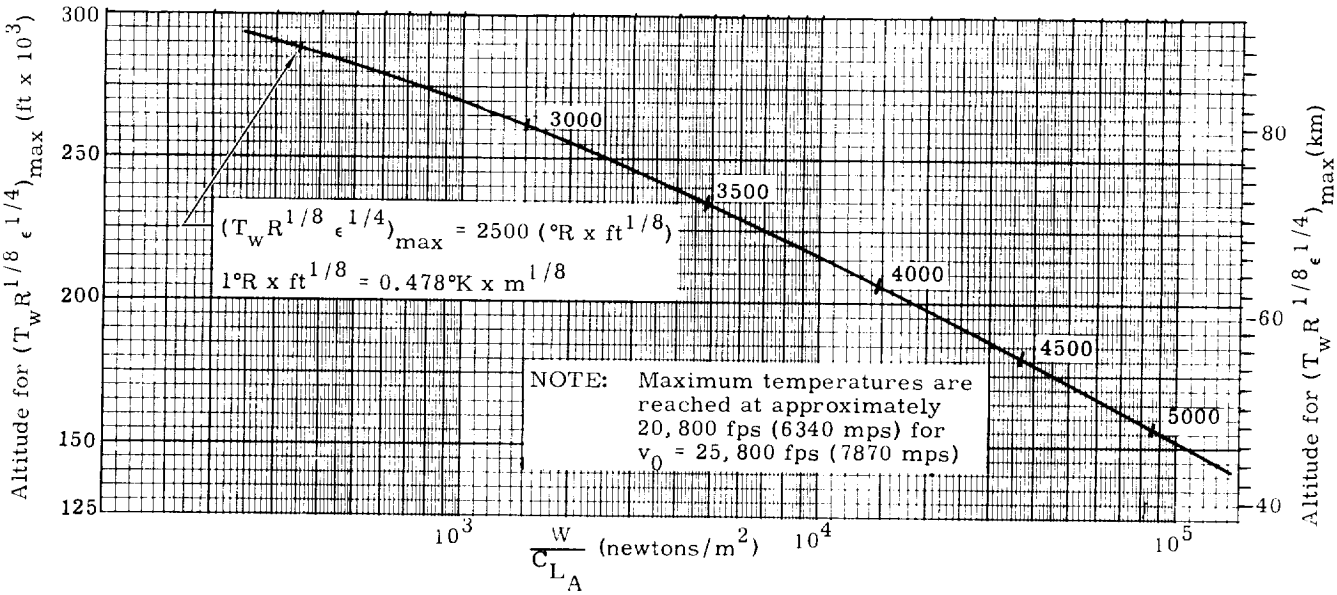

Fig. 34b. Altitude for Maximum Equilibrium Nose Temperature Versus $W/C_L A$ (equilibrium glides)

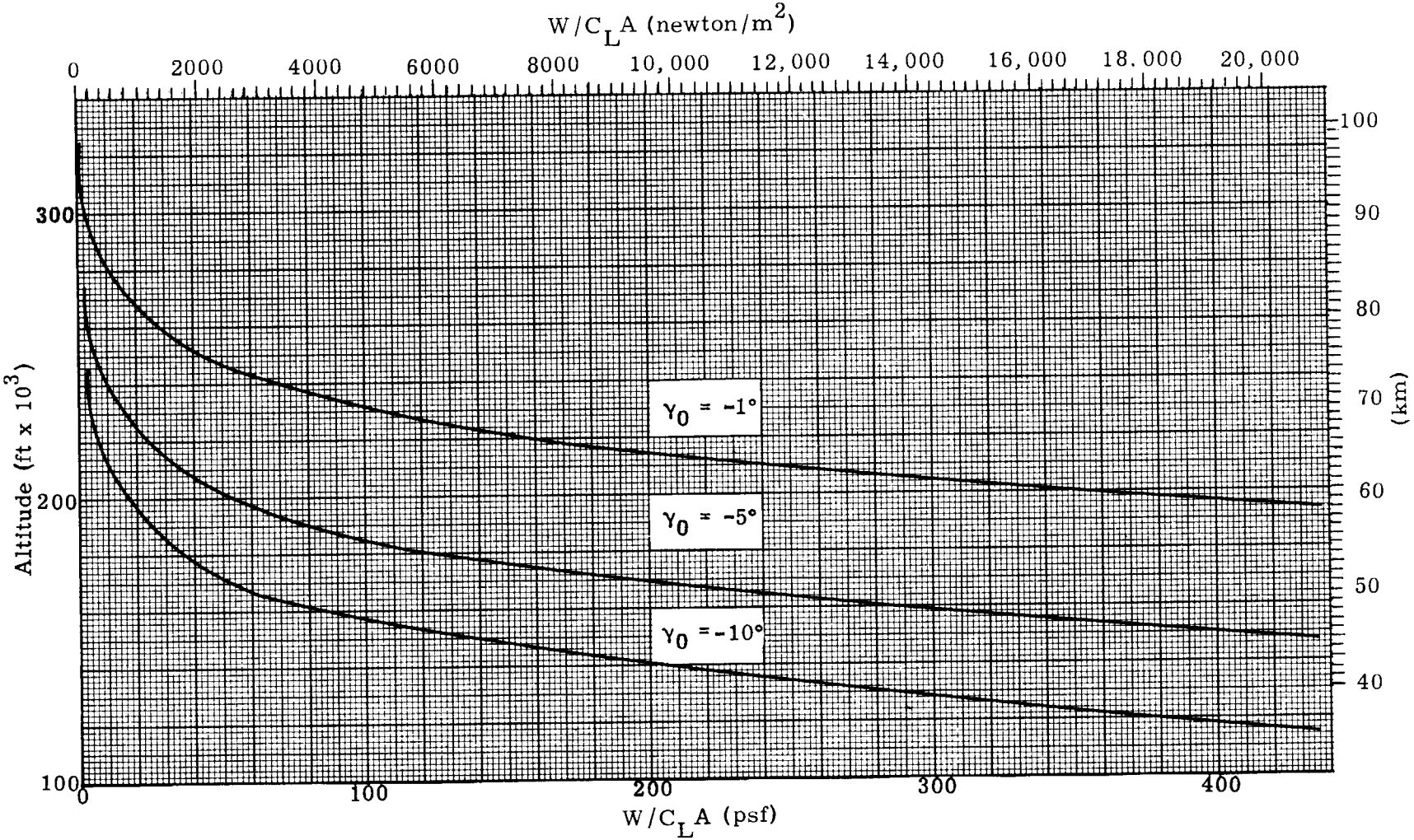

Fig. 34c. Altitude for Maximum Stagnation Nose Temperature (h_0 = 400,000 ft, v_0 = 25,000 fps)

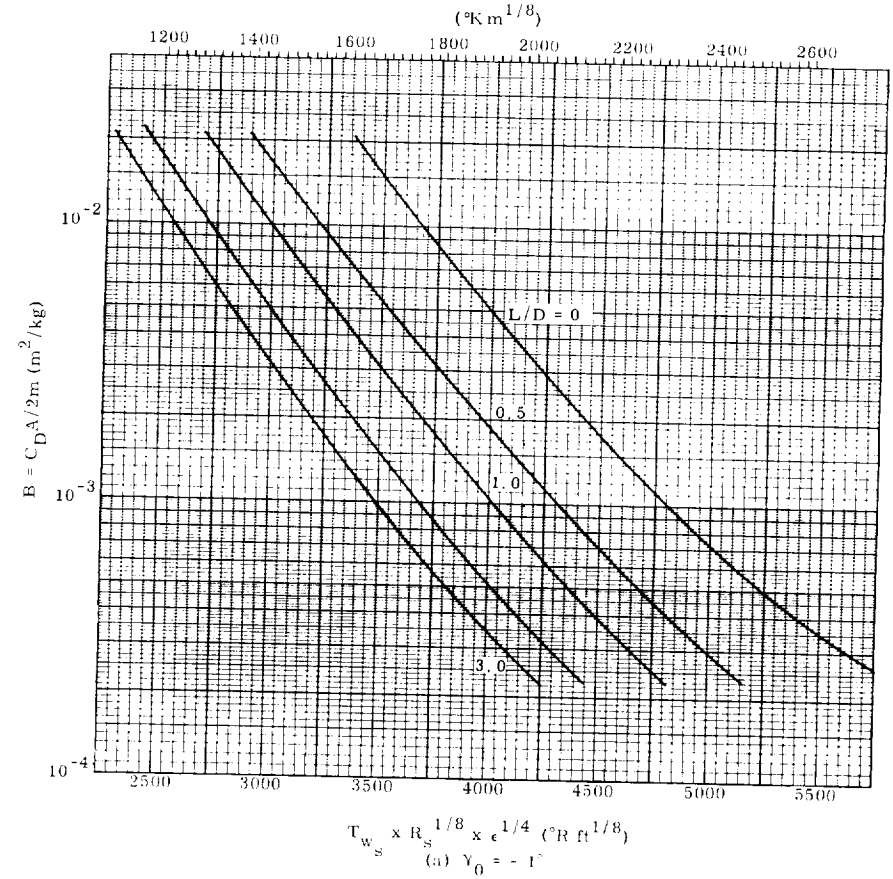

(a) $\gamma_0 = -1°$

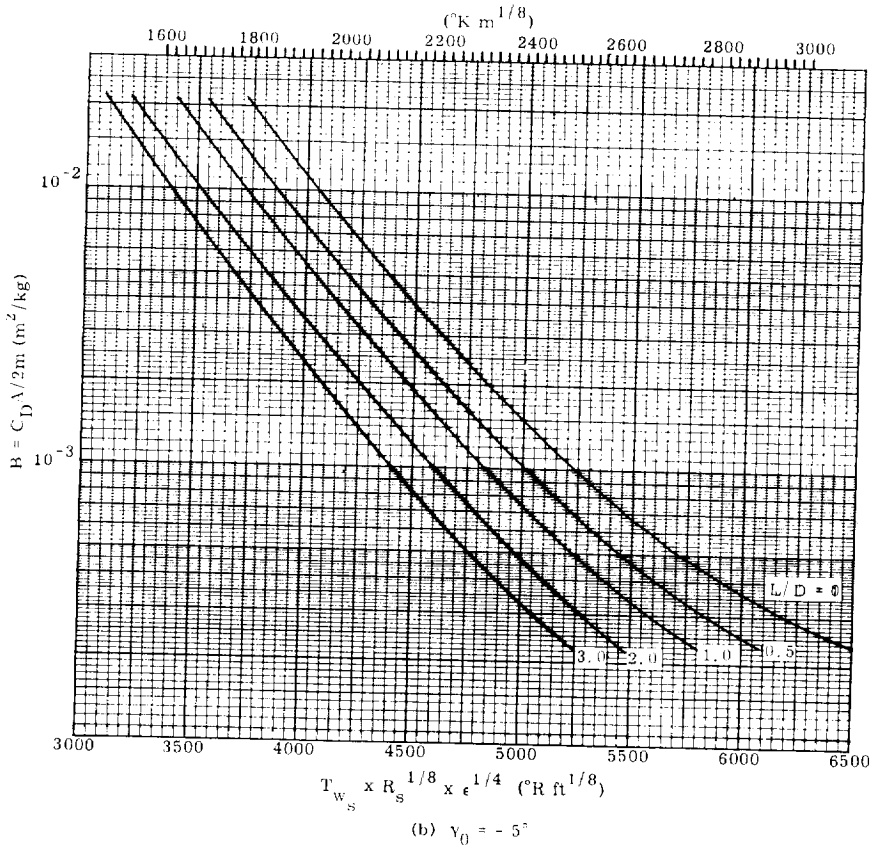

(b) $\gamma_0 = -5°$

Fig. 35. Maximum Re-Entry Stagnation Point Nose Temperature (h_0 = 400,000 (121,920 m), v_0 = 25,000 fps (7620 mps)

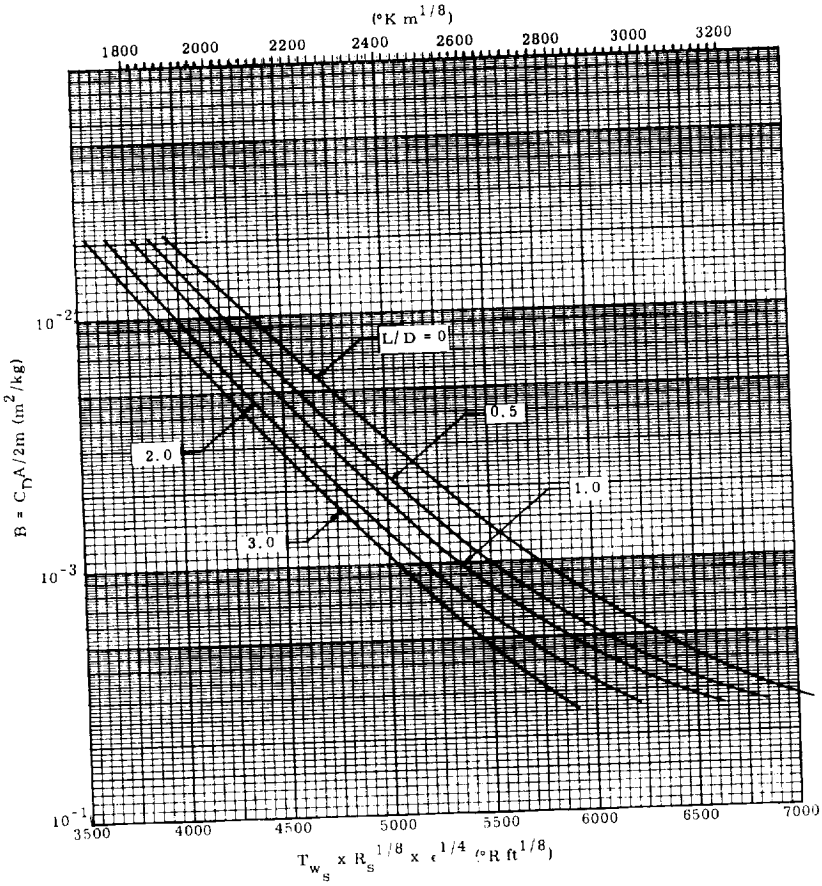

(c) $\gamma_0 = -10°$

Fig. 35. (continued)

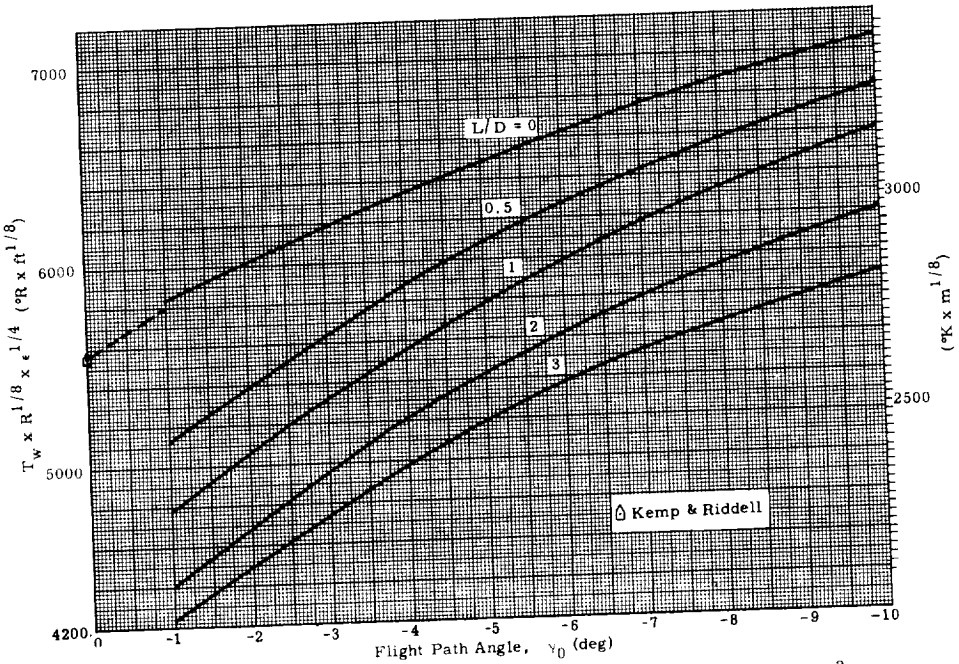

(a) $B = 0.037\ ft^2/slug = 0.234 \times 10^{-3}\ m^2/kg$, $W/C_D A = 438\ psf = 21000\ newton/m^2$

Fig. 36. Maximum Re-Entry Stagnation Point Nose Temperature Versus γ_0
(h_0 = 400,000 ft = 121,920 m, v_0 = 25,000 fps = 7620 mps)

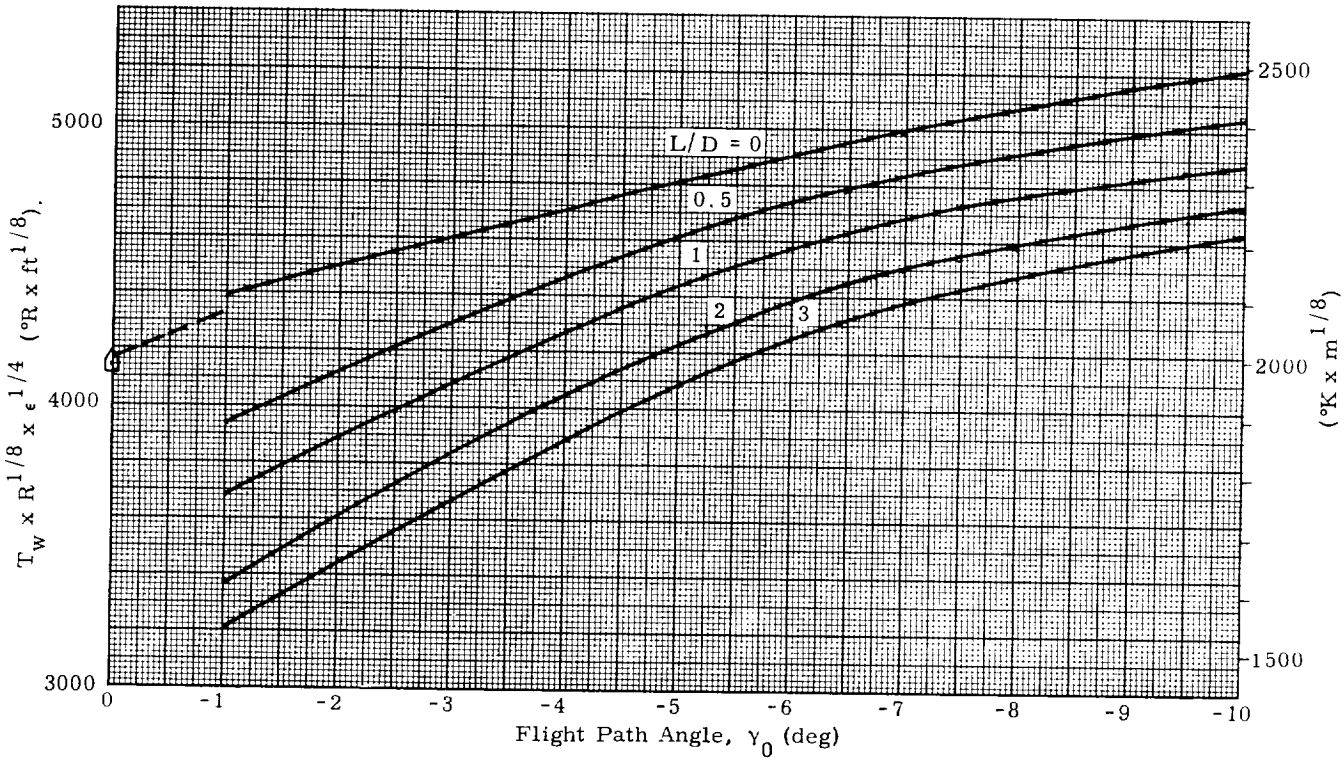

(b) B = 0.322 ft^2/slug = 2.05 x 10^{-3} m^2/kg, W/C_DA = 50 psf = 2390 newton/m^2

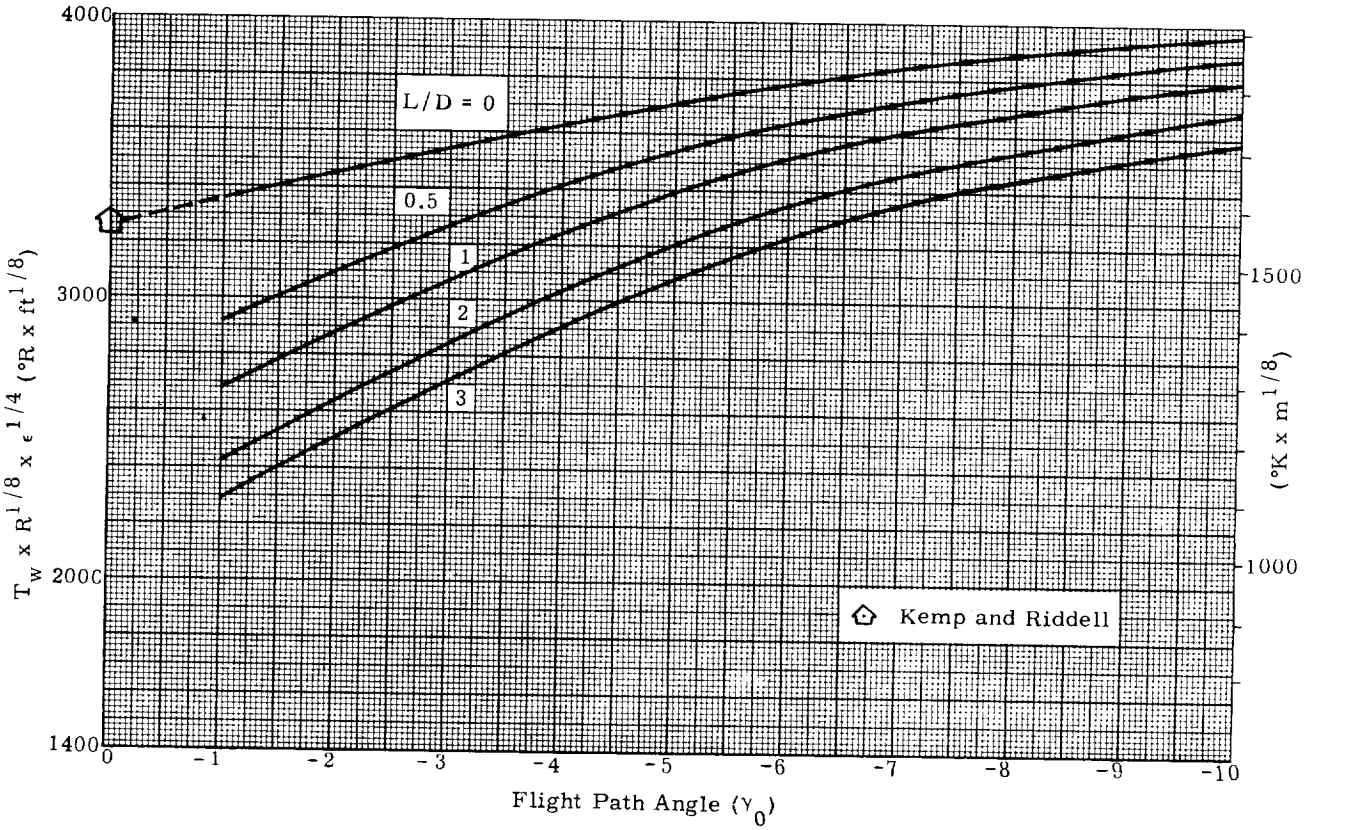

(c) B = 22 ft^2/slug = 0.0205 m^2/kg, W/C_DA = 5 psf = 239 newton/m^2

Fig. 36. (continued)

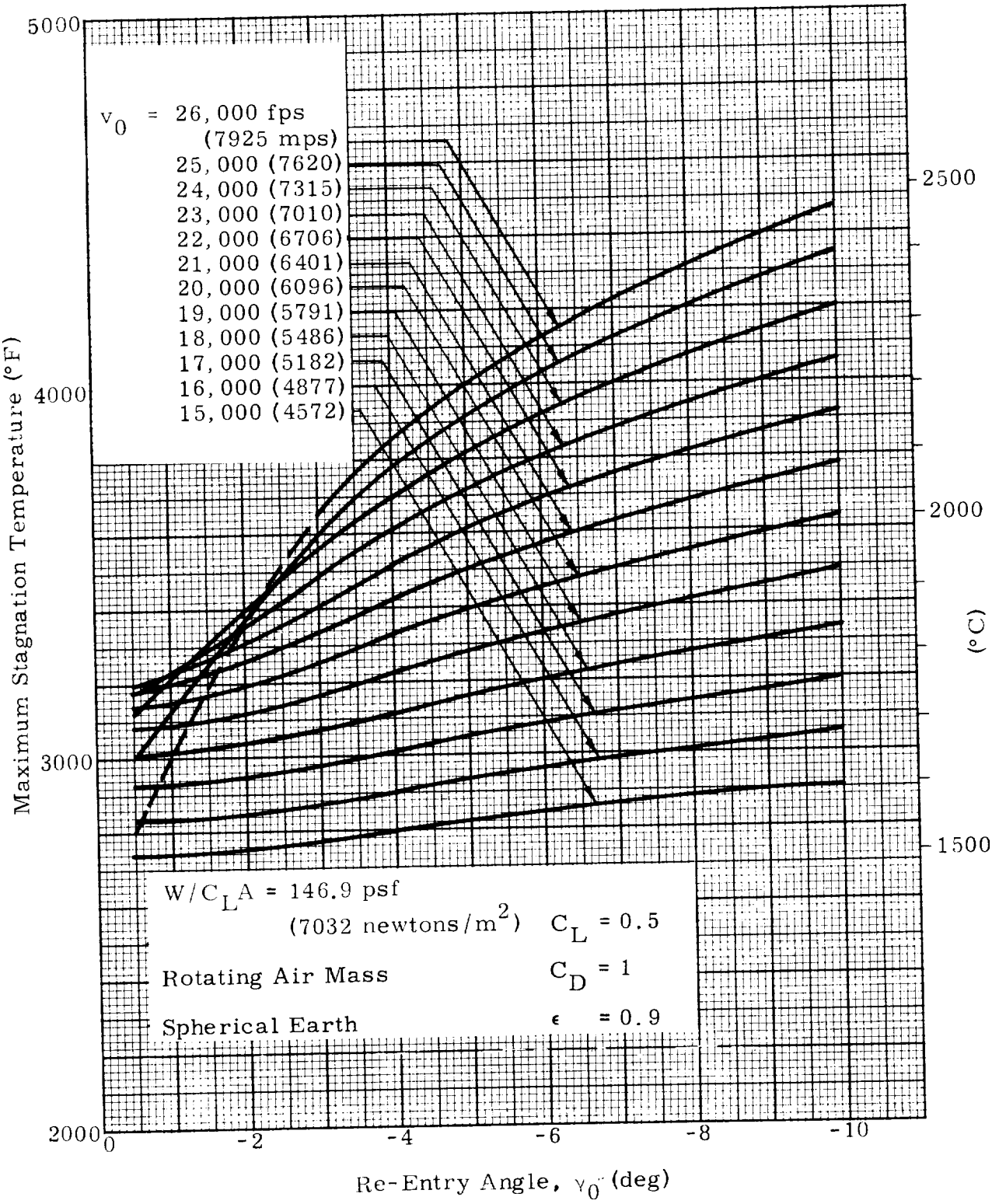

Fig. 37. Effect of Re-Entry Conditions on Maximum Stagnation Point Temperature (L/D = 0.5)

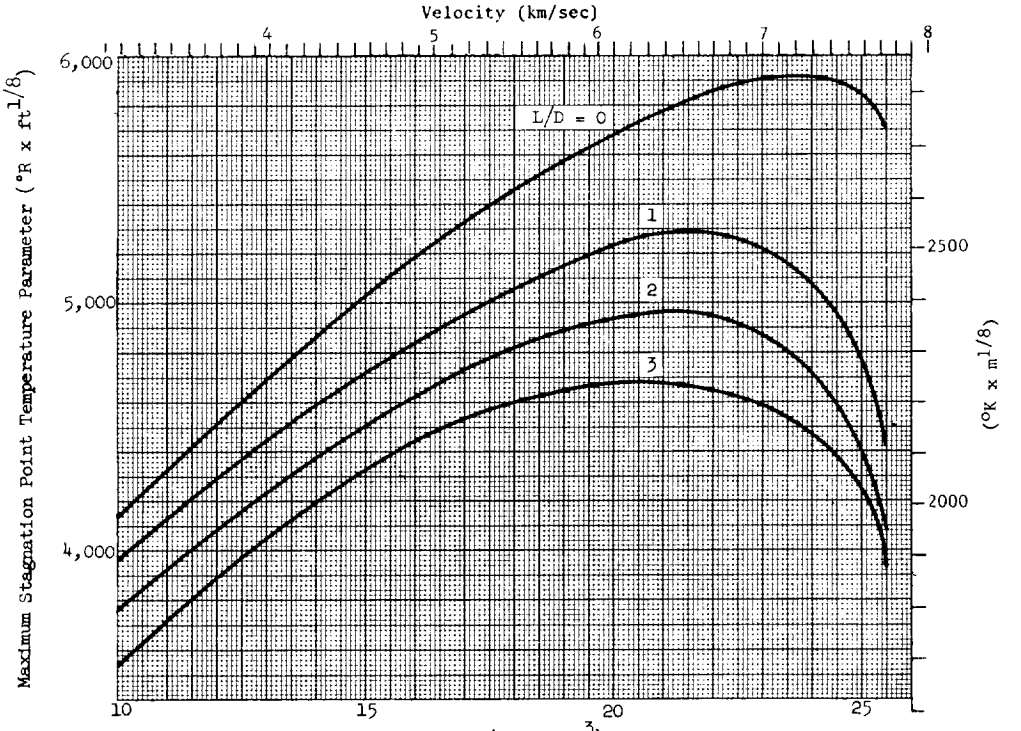

(a) B = 0.0367 $ft^2/slug$ = 0.234 x 10^{-3} m^2/kg

$\frac{W}{C_D A}$ = 438 lb/ft^2 = 21,000 $newtons/m^2$

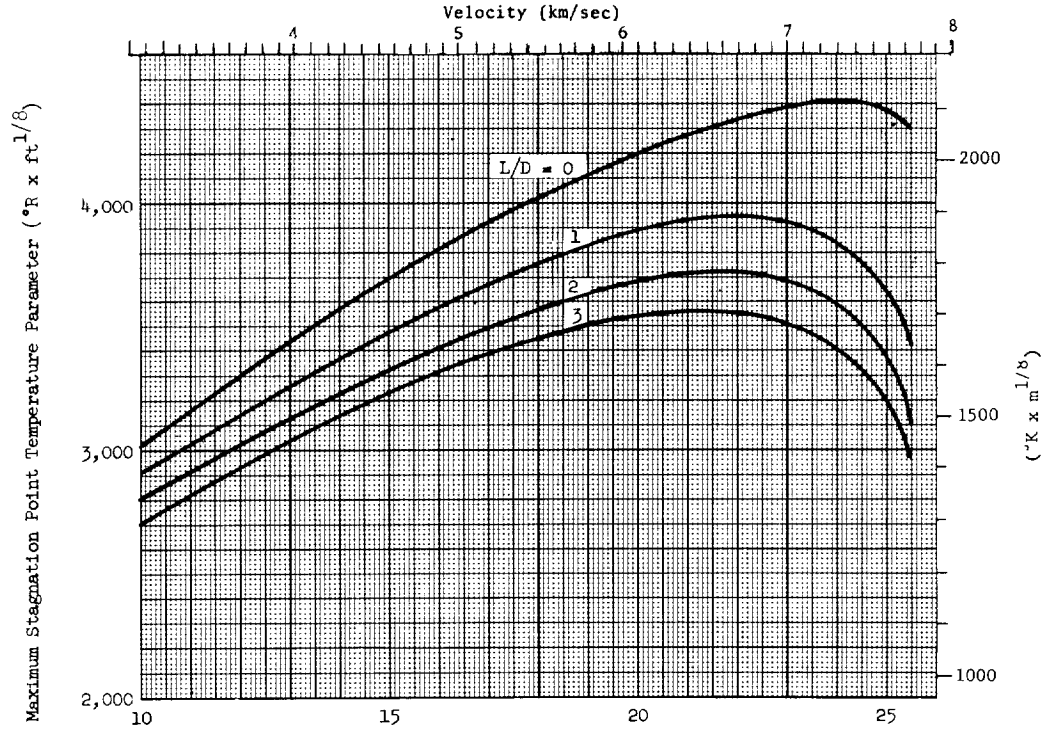

(b) B = 0.322 $ft^2/slug$ = 2.05 x 10^{-3} m^2/kg

$\frac{W}{C_D A}$ = 50 lb/ft^2 = 2390 $newtons/m^2$

Fig. 38. Maximum Re-Entry Stagnation Point Temperature Parameter Versus Velocity (h_0 = 400,000 ft = 121,920 m; γ_0 = -1°)

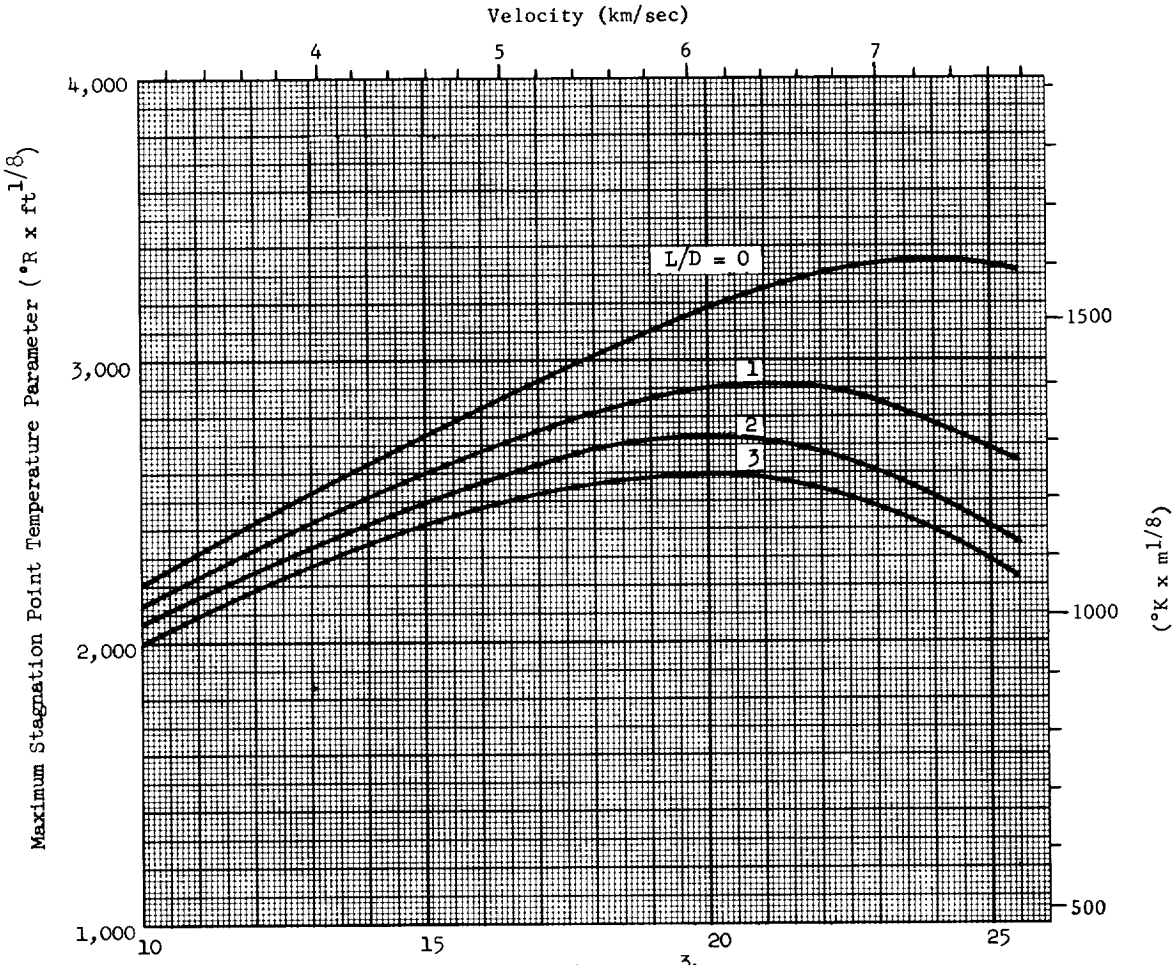

(c) B = 3.22 $ft^2/slug$ = 20.5 x 10^{-3} m^2/kg

$\frac{W}{C_D A}$ = 5 lb/ft^2 = 239 $newtons/m^2$

Fig. 38. (continued)

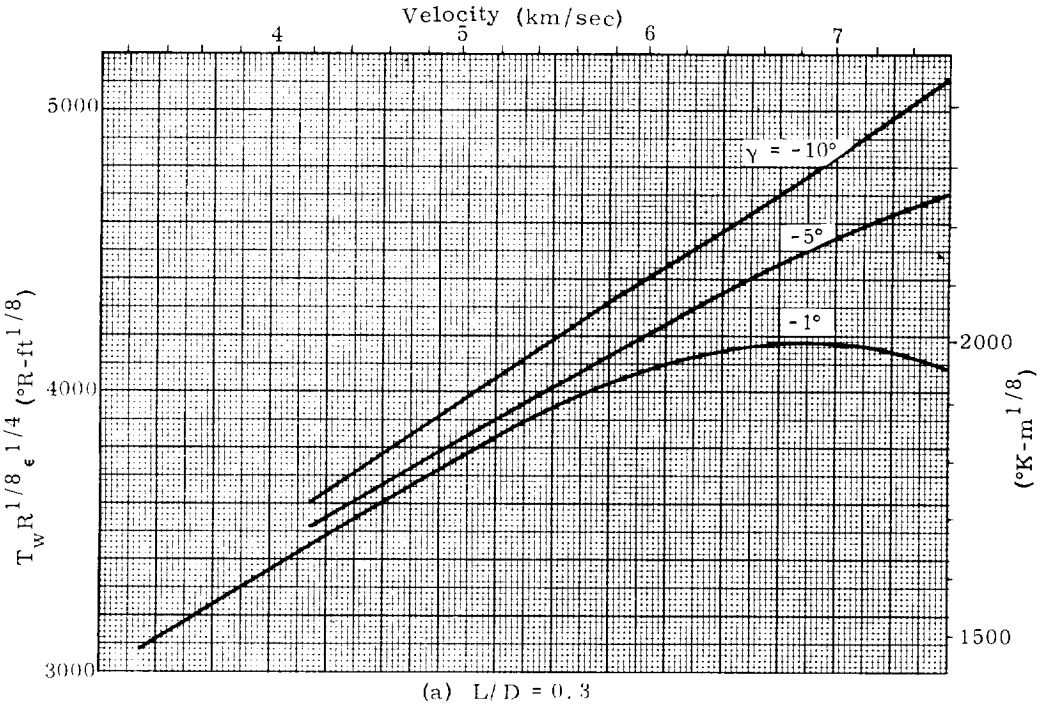

(a) L/D = 0.3

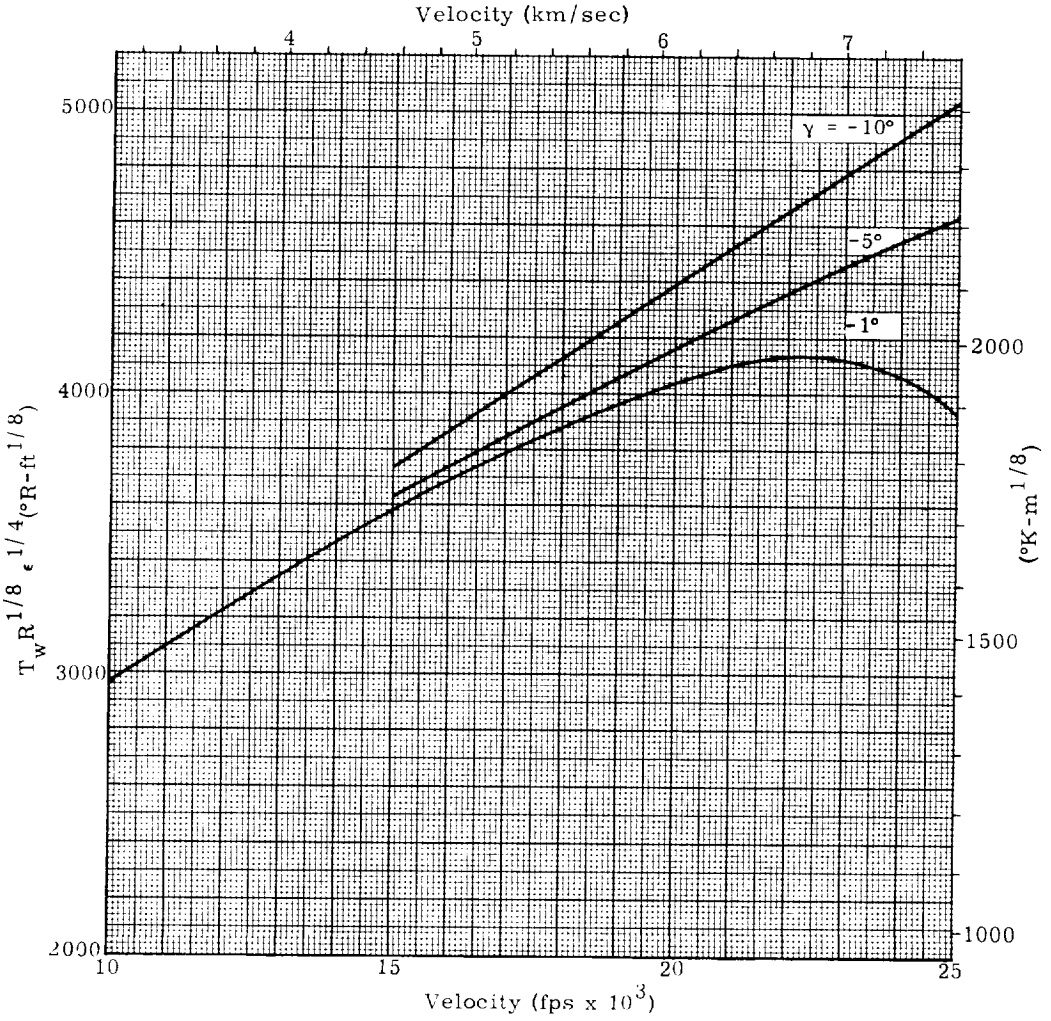

(b) L/D = 0.5

Fig. 39. Maximum $T_w R^{1/8} \epsilon^{1/4}$ Versus Re-Entry Velocity (h_0 = 400,000 ft = 121,920 m, $\frac{W}{C_D A}$ = 50 psf = 2390 newtons/m^2

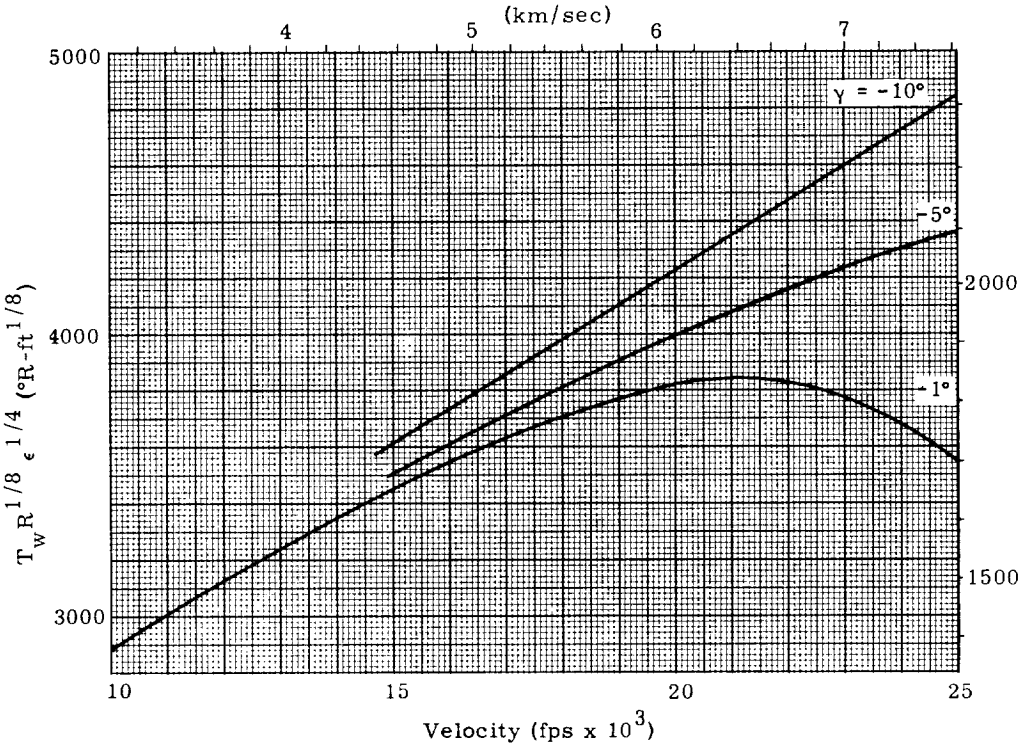

(c) L/D = 1.25

$$\left[\left(TR^{1/8}\,\epsilon^{1/4}\right)_{\frac{W}{C_D A}} = X\right] \cong \left[\left(TR^{1/8}\,\epsilon^{1/4}\right)_{\frac{W}{C_D A}} = 50\right]\left(\frac{X}{50}\right)^{1/8} \cong \left[1200\,(q)^{1/4}_{\frac{W}{C_D A}} = X\right] \text{ Btu/ft}^2\text{-sec}$$

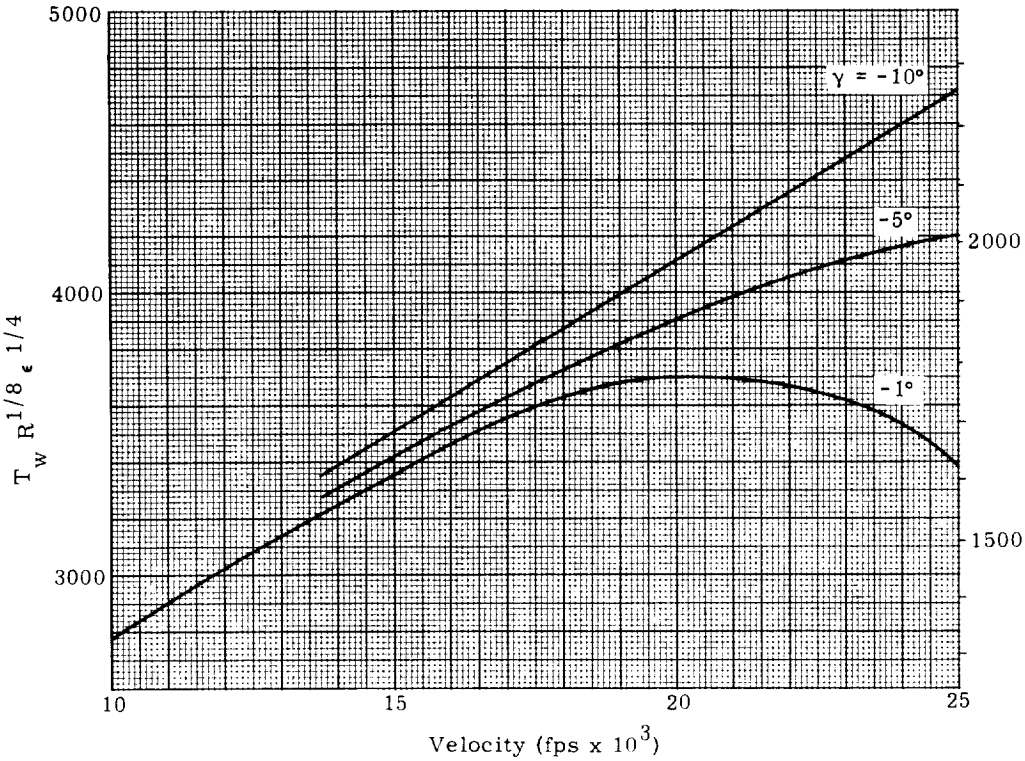

(d) L/D = 2

Fig. 39. (continued)

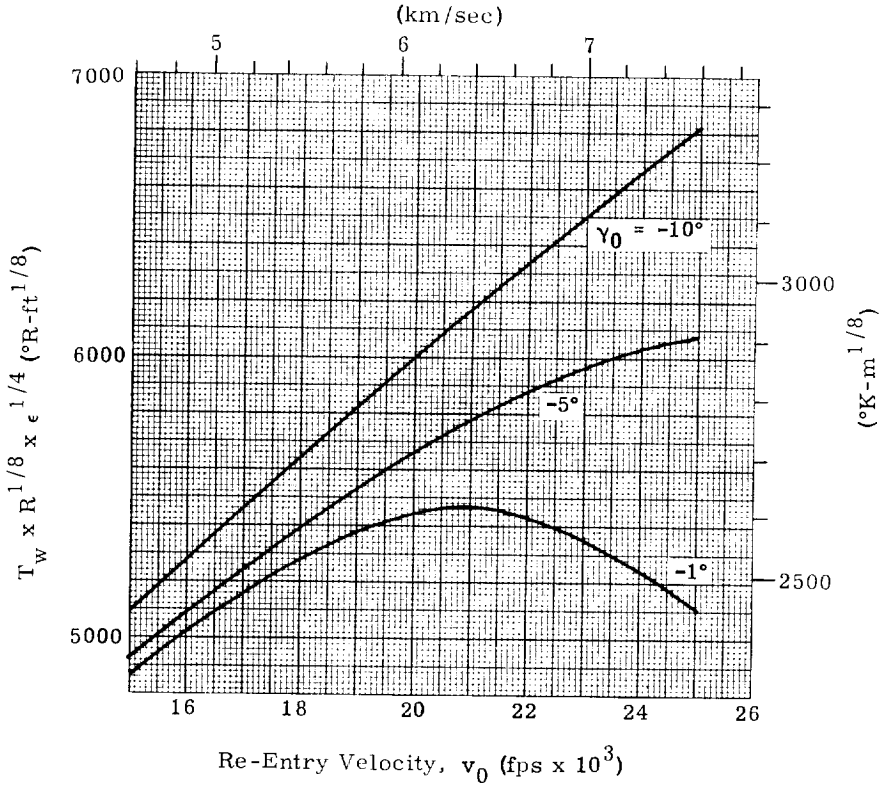

(a) L/D = 0.5

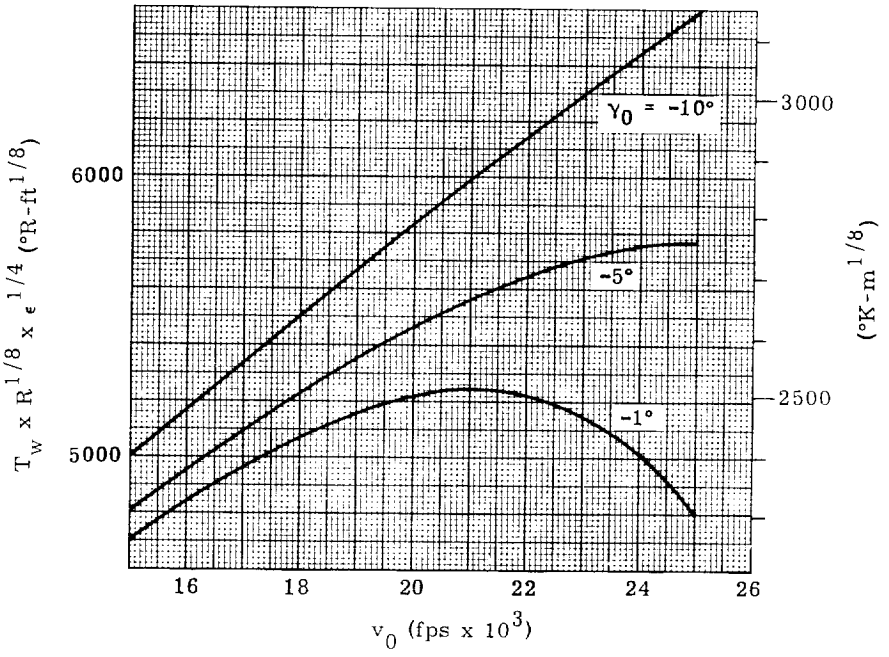

(b) L/D = 1.0

Fig. 40. Maximum Re-Entry Stagnation Point Nose Temperature Versus Velocity (h_0 = 400,000 ft = 121,920 m; W/C_DA = 438 psf = 21,000 newtons/m^2

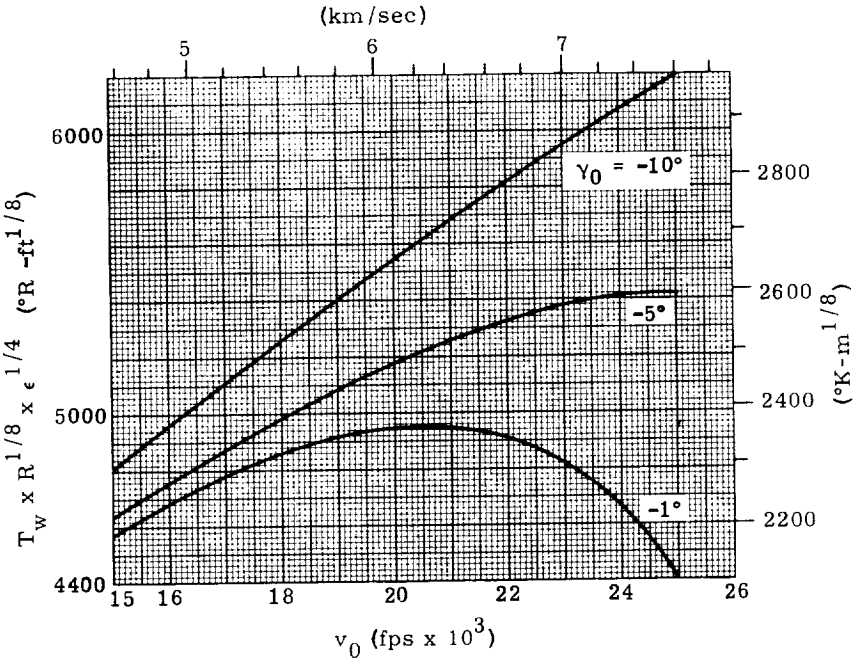

(c) L/D = 2

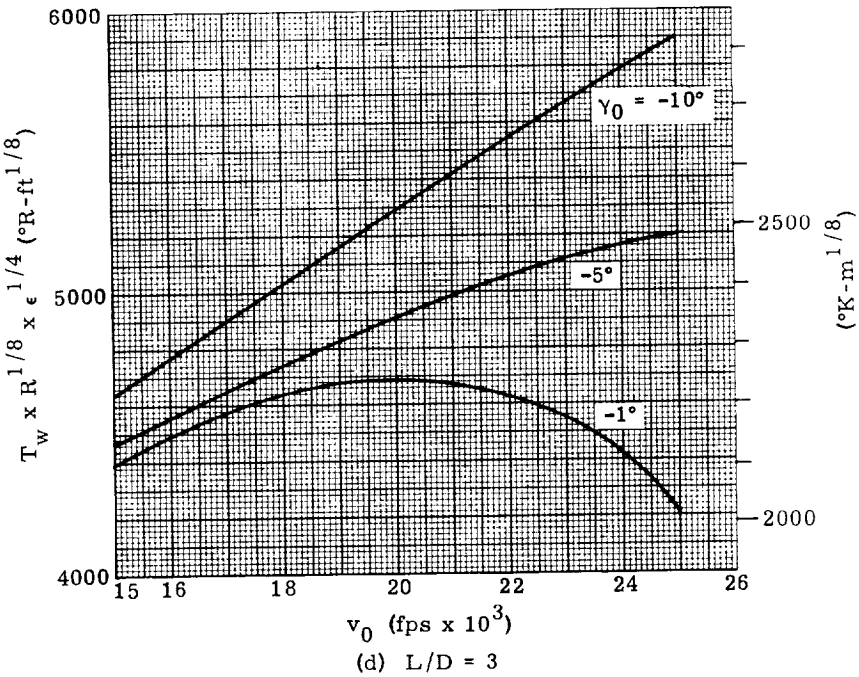

(d) L/D = 3

Fig. 40. (continued)

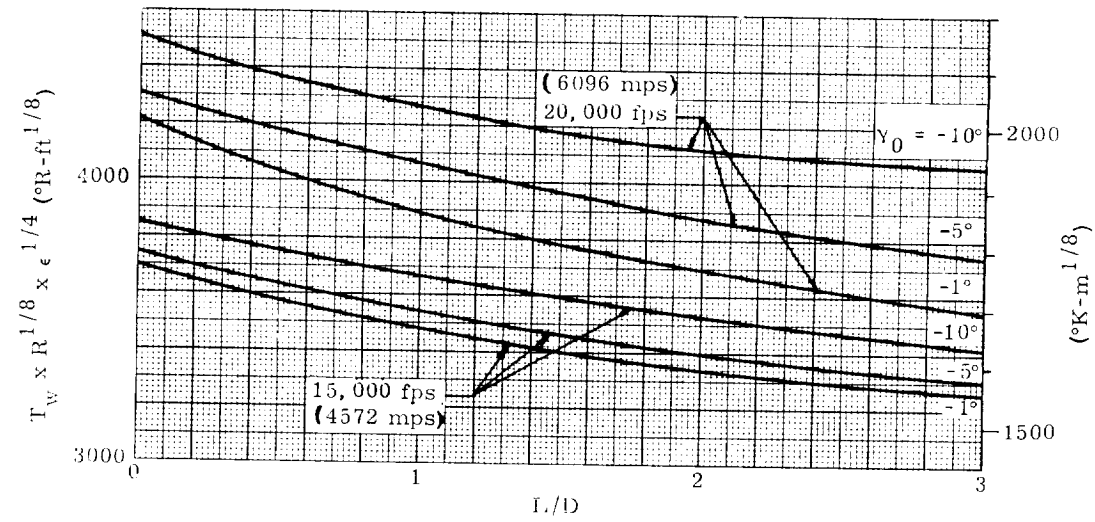

$$\left(T_w R^{1/8} \epsilon^{1/4}\right) W/C_D A = X \simeq \left(T_w R^{1/8} \epsilon^{1/4}\right) W/C_D A = 50 \left(\frac{X}{50}\right)^{1/8} \simeq 1200\,(q)^{1/4} \quad W/C_D A = X \text{ Btu/ft}^2\text{-sec}$$

(a) $W/C_D A$ = 50 psf = 2390 newtons/m^2

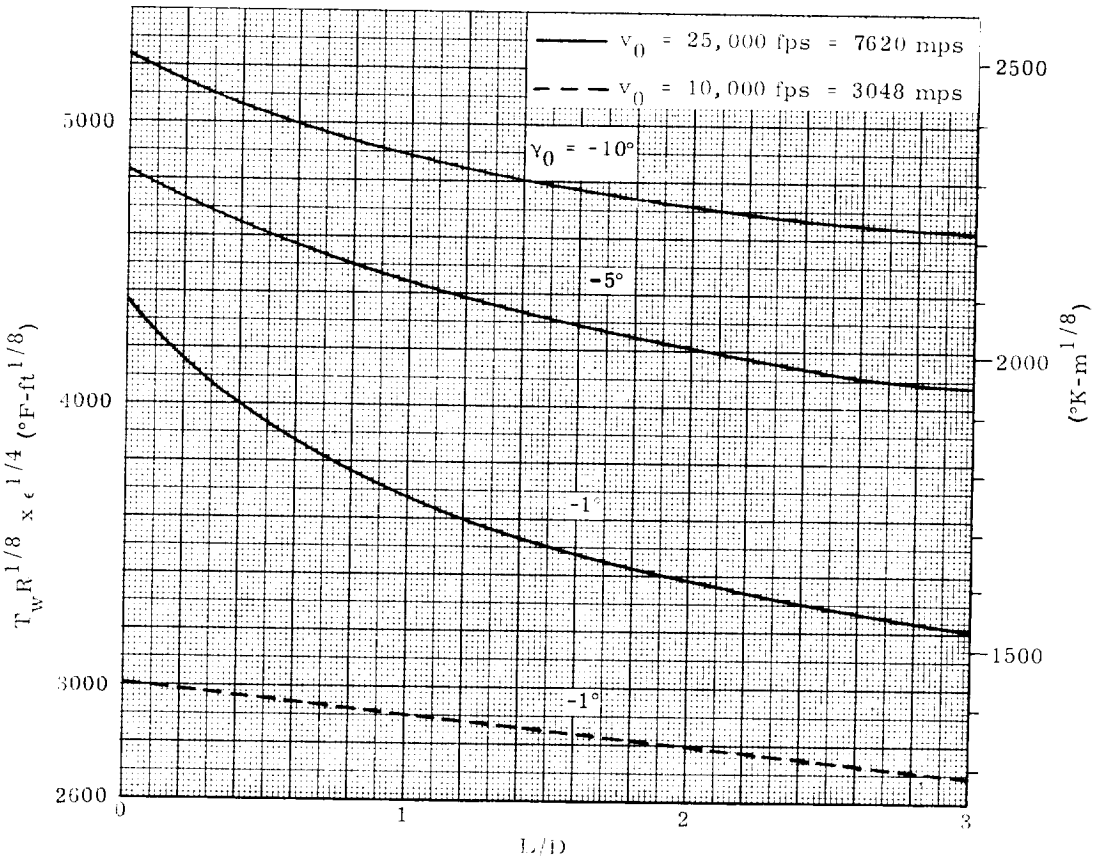

(b) $W/C_D A$ = 50 psf = 2390 newtons/m^2

Fig. 41. $T_w R^{1/8} \epsilon^{1/4}$ Versus Lift-Drag Ratio (h_0 = 400,000 ft = 121,920 m)

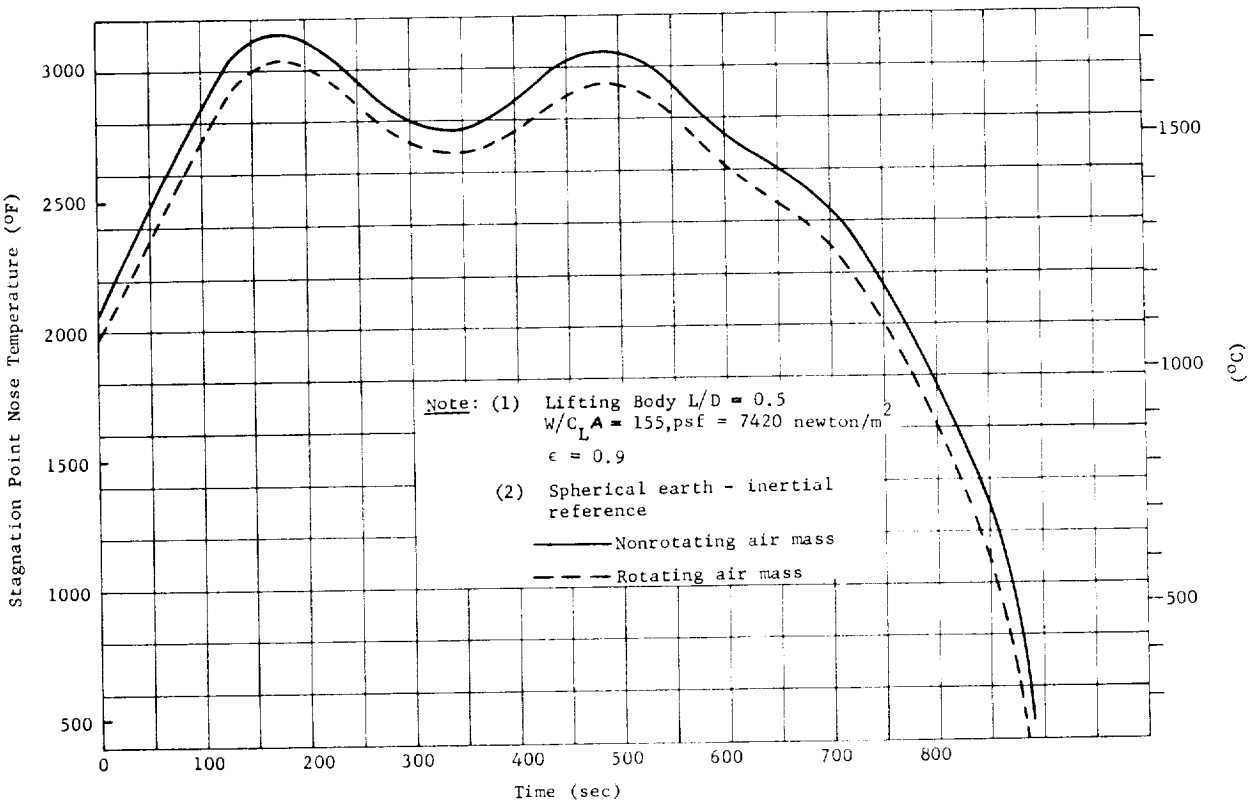

Fig. 42. Equilibrium Temperature History, with and Without Rotating Air Mass

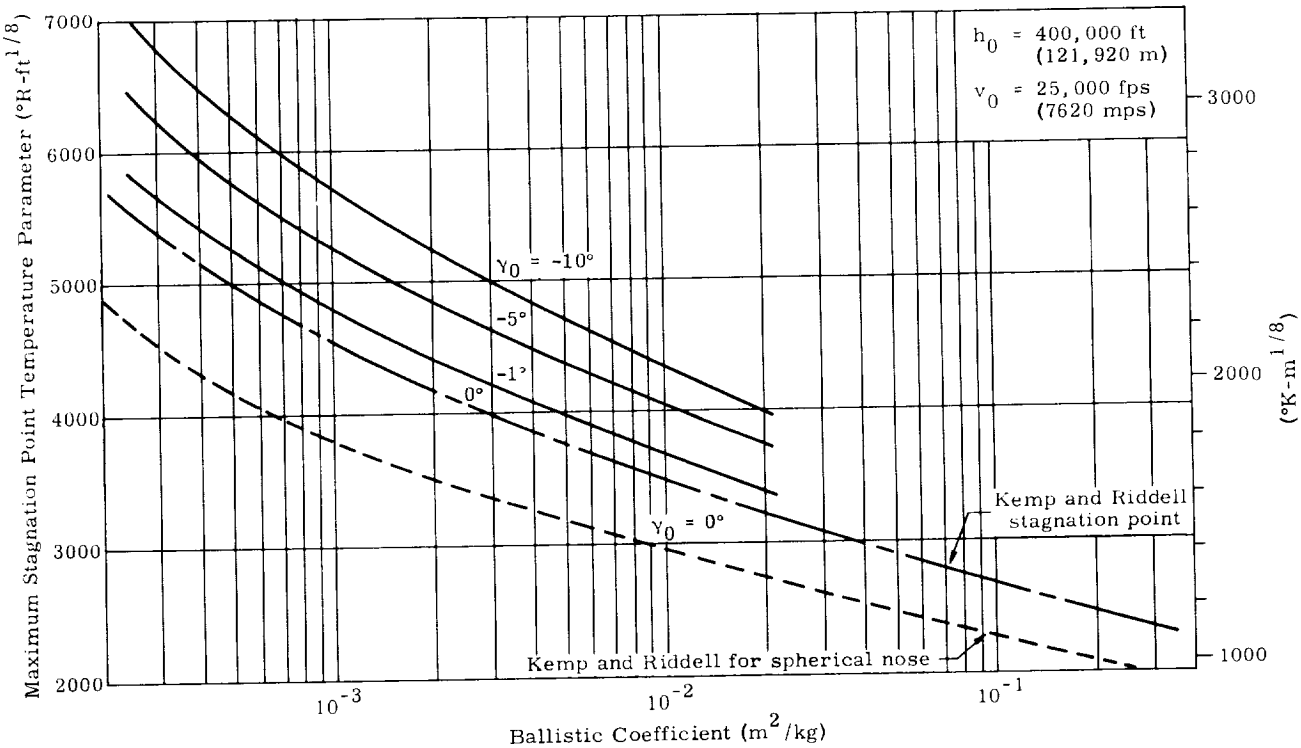

Fig. 43a. Maximum Stagnation Point Temperature Parameter Versus Ballistic Coefficient (ballistic re-entry--L/D = 0)

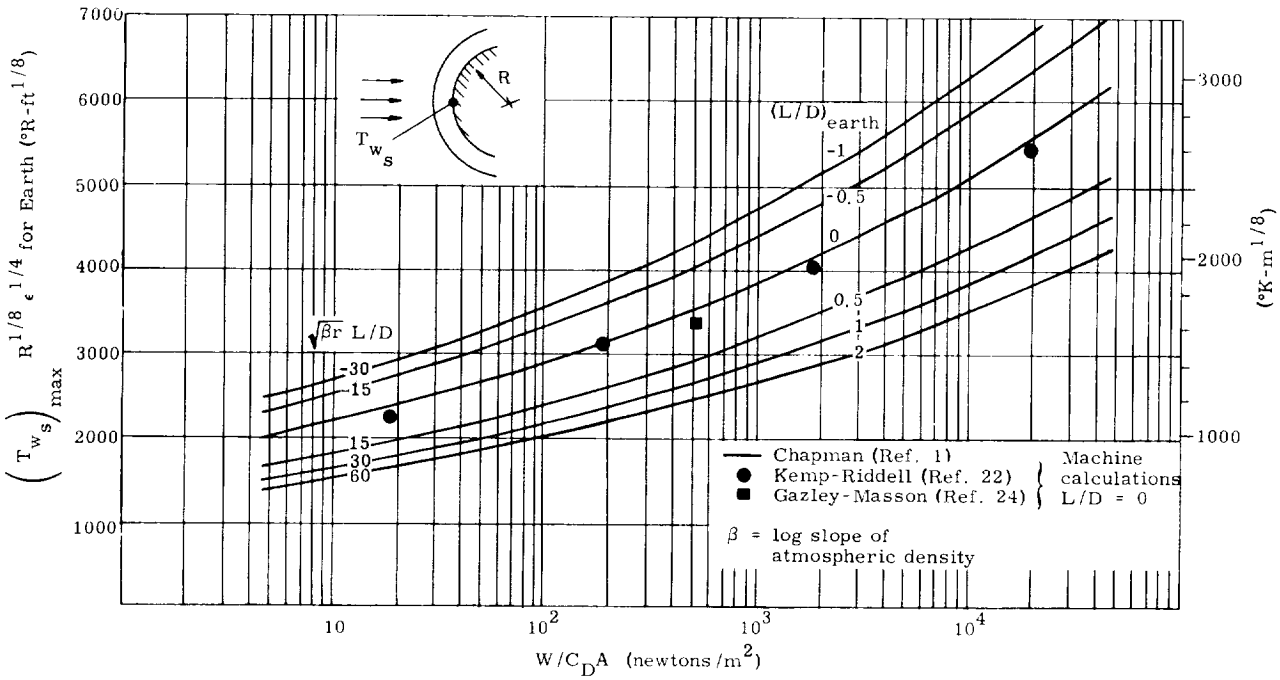

Fig. 43b. Maximum Radiation-Equilibrium Temperature at Laminar Stagnation Point for Entry from Decaying Orbits into Earth Atmosphere (Ref. 1)

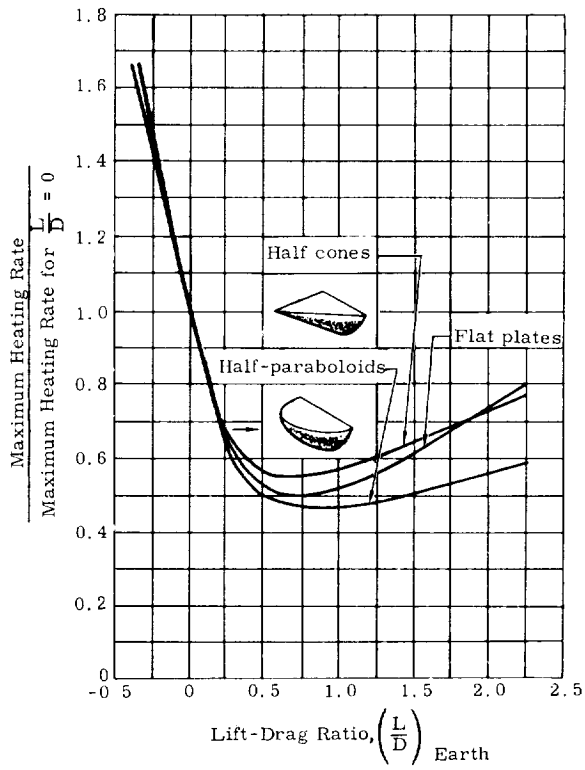

Fig. 44. Effect of Lift-Drag Ratio on Maximum Laminar Heating Rate at Stagnation Point for Entry from Decaying Orbits

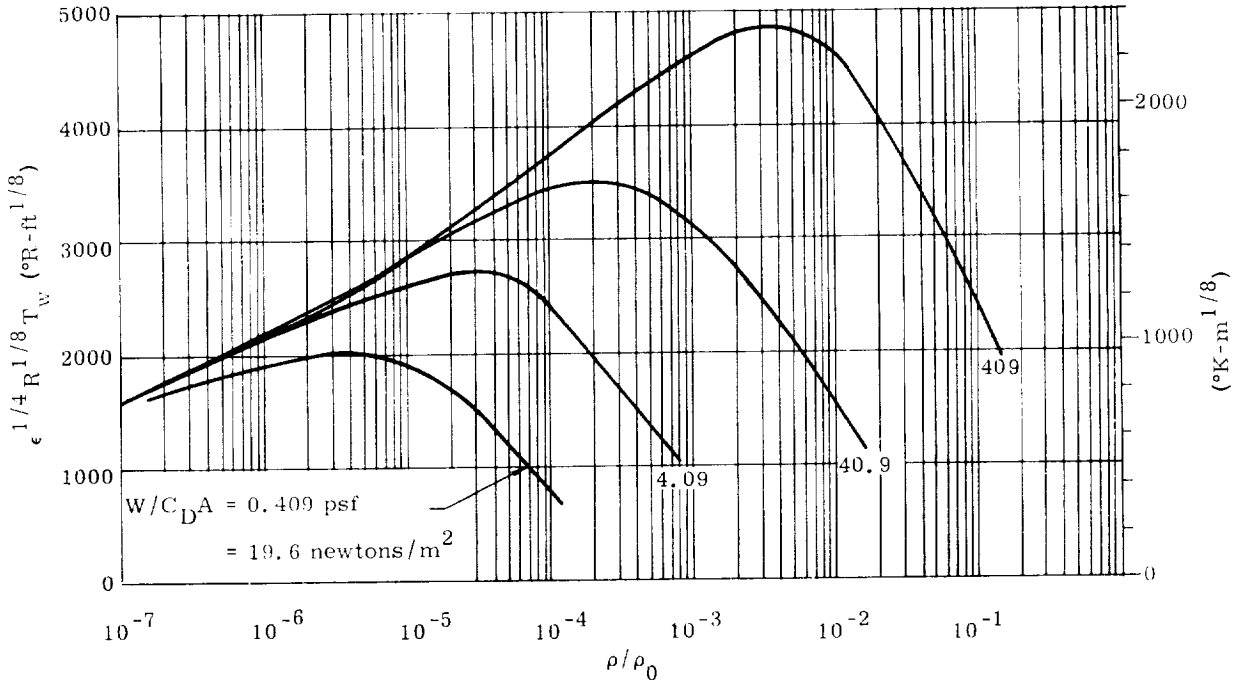

Fig. 45a. Surface Temperature Parameter $\epsilon^{1/4} R^{1/8} T_w$ as a Function of Air Density Ratio ρ/ρ_0. Simple drag bodies (Ref. 22)

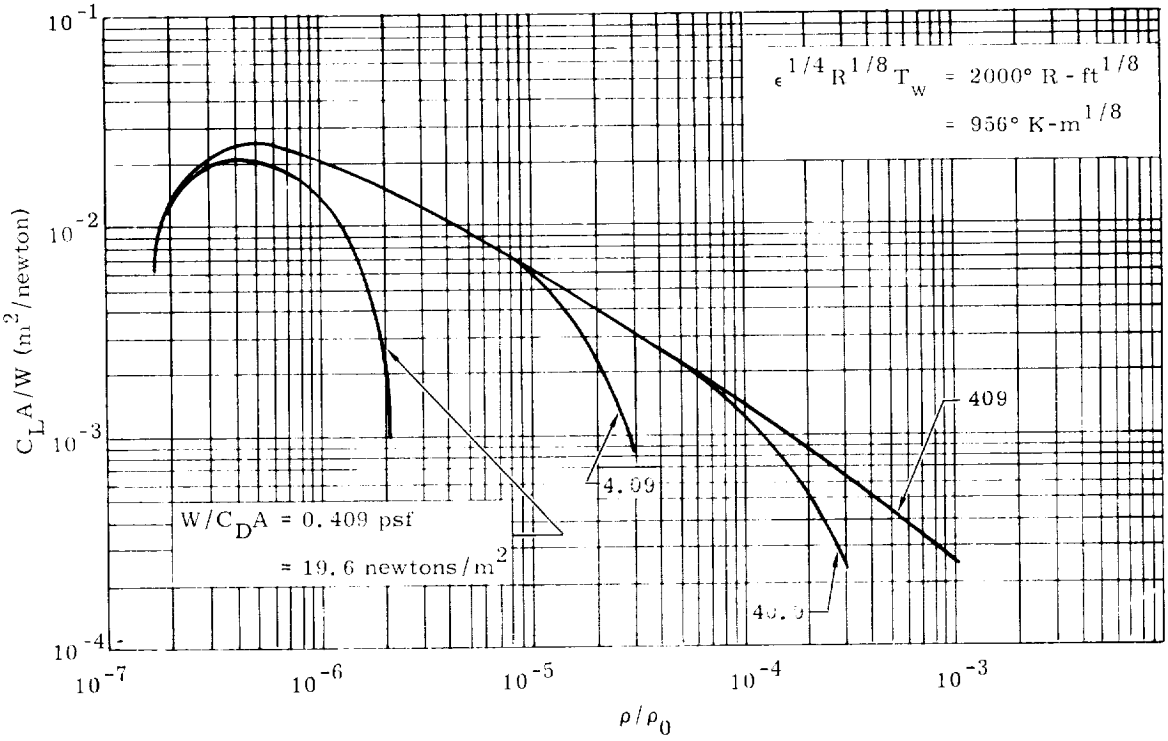

Fig. 45b. Lift Parameter $C_L A/W$ as a Function of Air Density Ratio ρ/ρ_0 for Several Values of the Drag Parameter $W/C_D A$. Constant Heat Transfer Trajectories (Ref. 22)

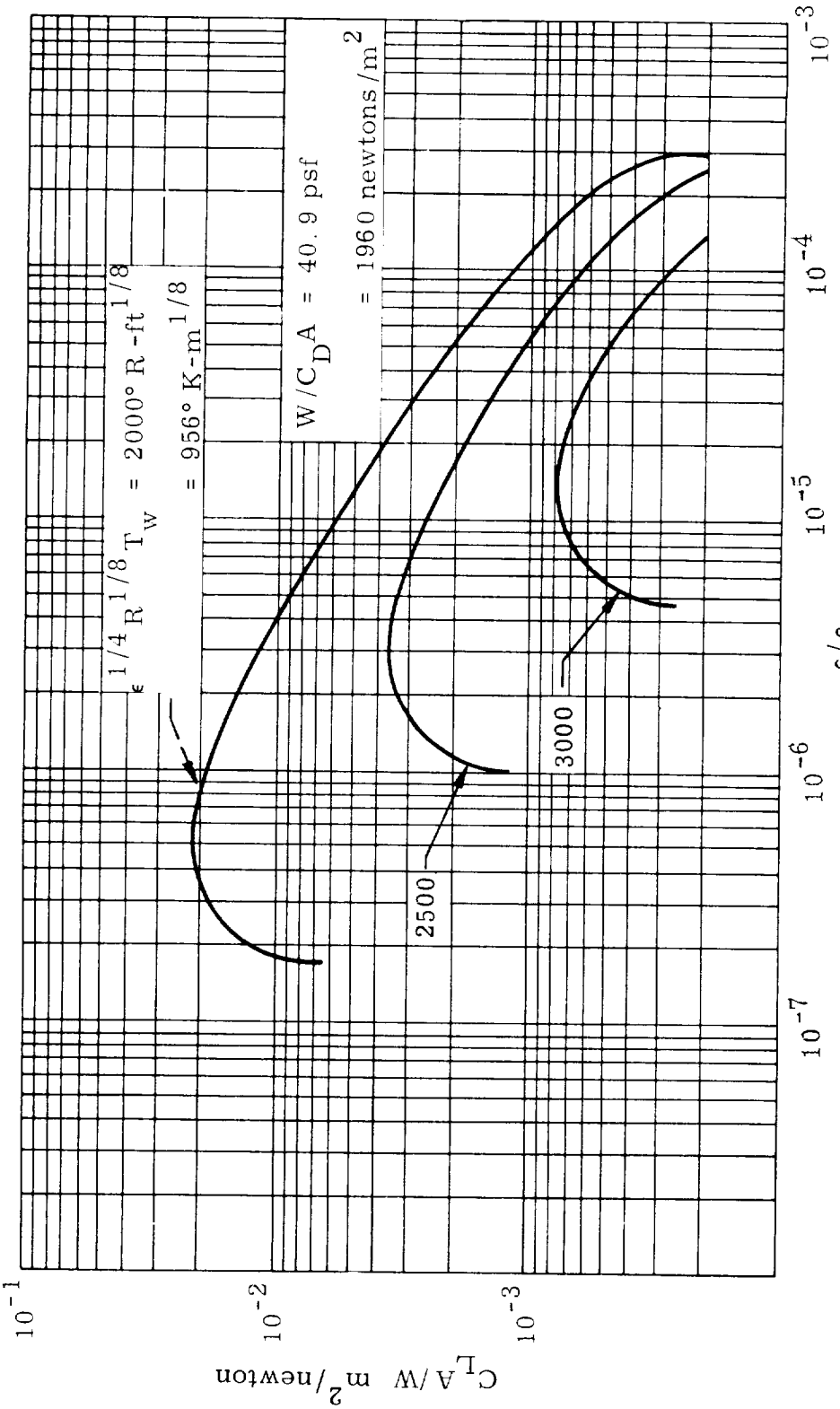

Fig. 45c. Lift Parameter $C_L A/W$ as a Function of Air Density Ratio ρ/ρ_0 for Several Values of the Surface Temperature Parameter $\epsilon^{1/4} R^{1/8} T_w$. (Constant Heat Transfer Trajectories) (Ref. 22)

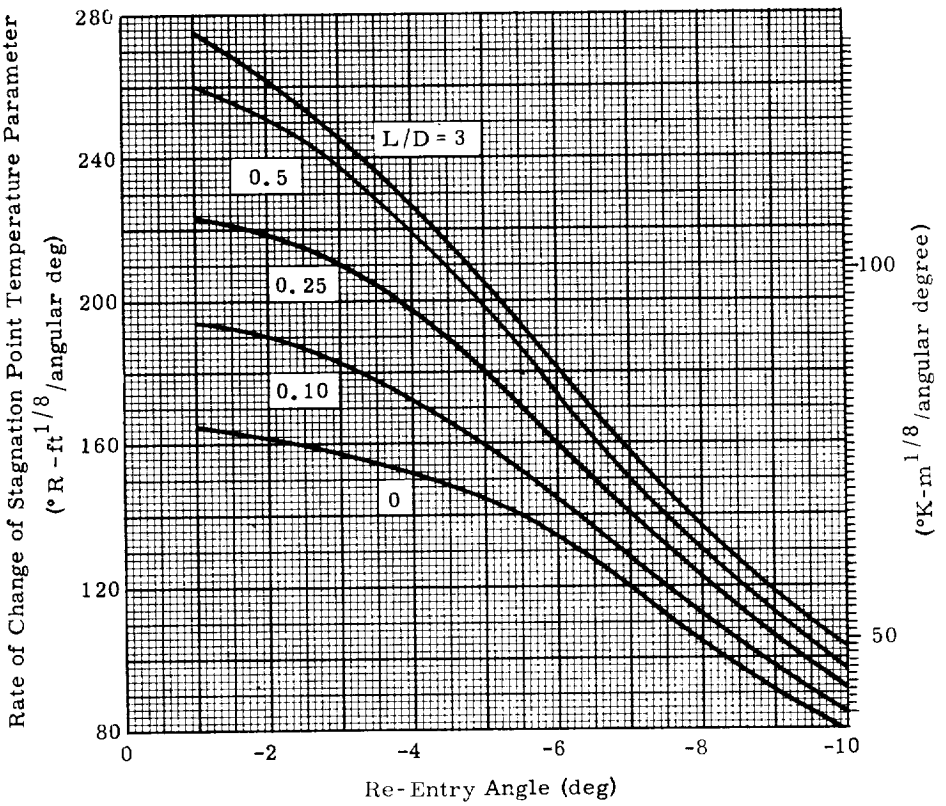

(a) B = 0.0367 ft^2/slug = 0.234 x 10^{-3} m^2/kg

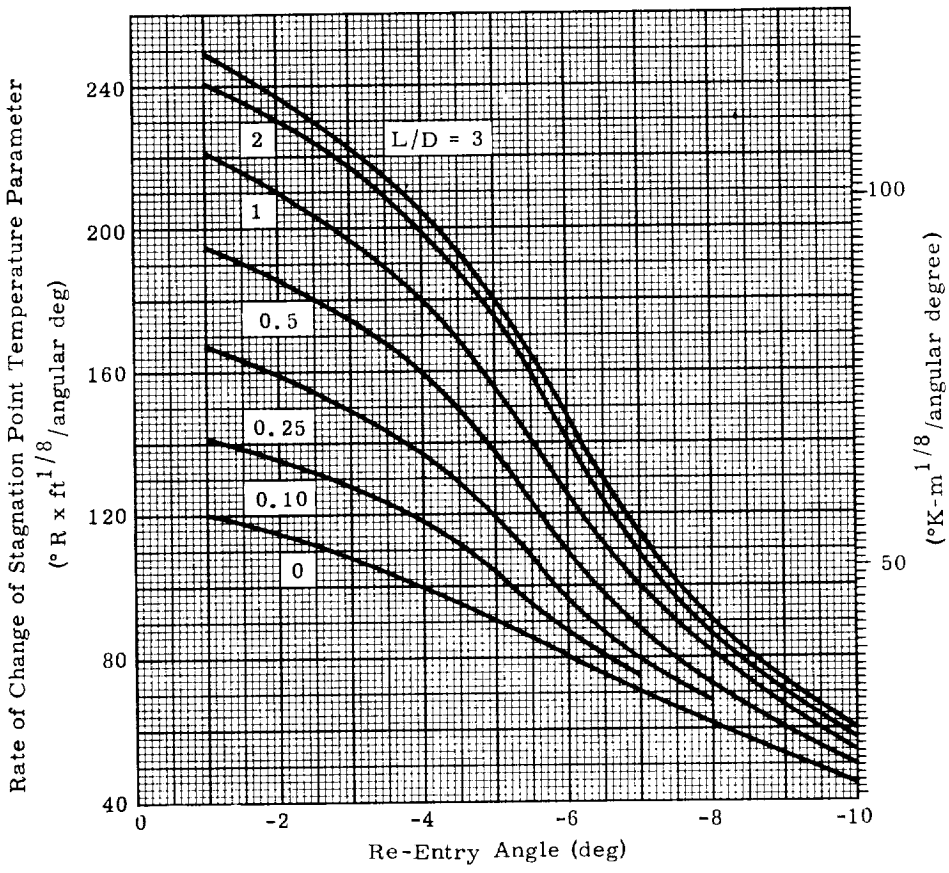

(b) B = 0.322 ft^2/slug = 2.05 x 10^{-3} m^2/kg

Fig. 46. Rate of Change of Stagnation Point Temperature Parameter as a Function of Re-Entry Angle (h_0 = 400,000 ft = 121,920 m, v_0 = 25,000 fps = 7620 mps)

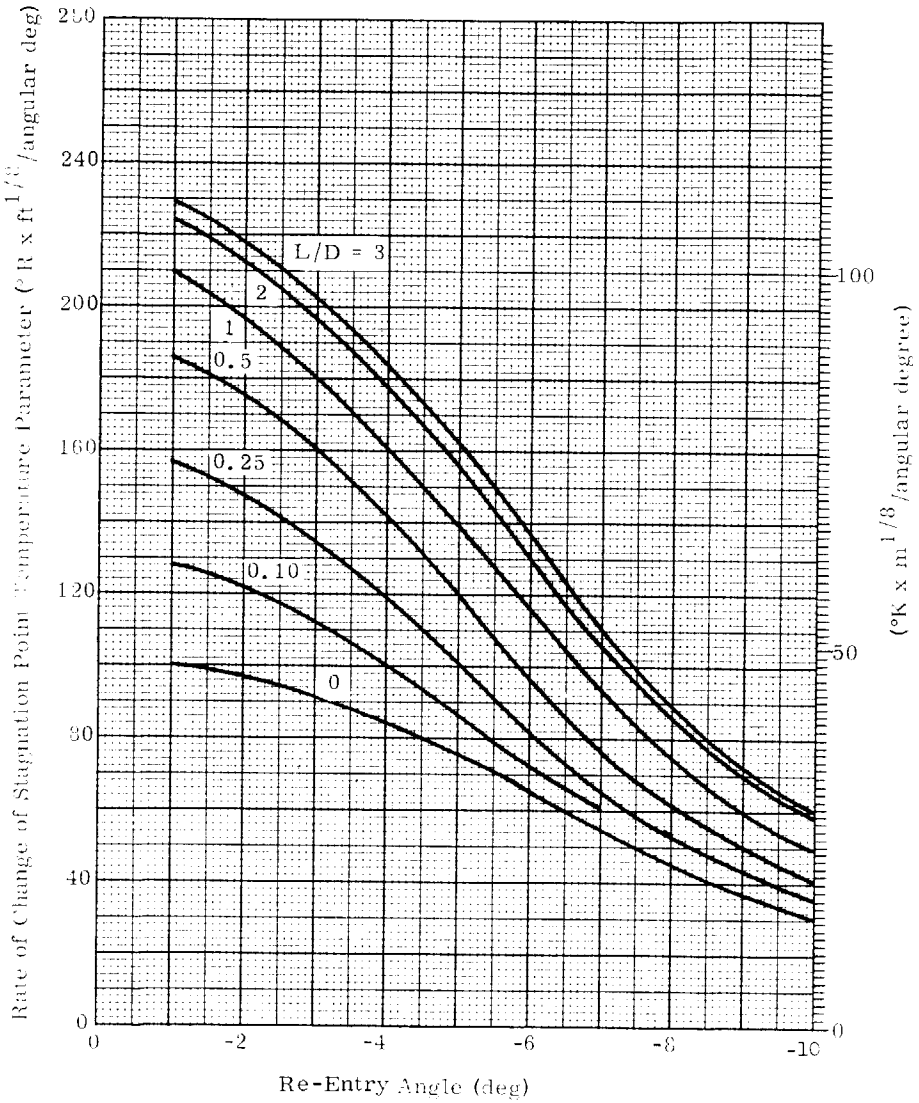

(c) B = 3.22 ft^2/slug = 20.5 x 10^{-3} m^2/kg

Fig. 46. (continued)

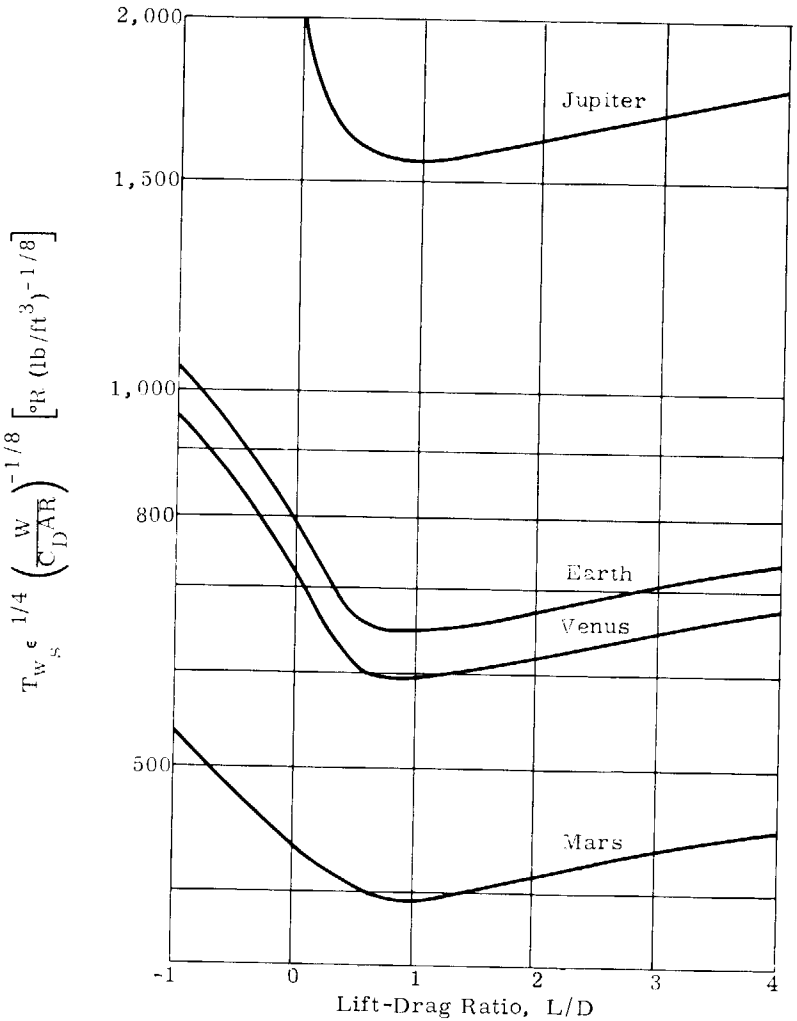

$T_{w_s} \epsilon^{1/4} \left(\frac{W}{C_D A R}\right)^{-1/8}$ [°R (lb/ft^3)$^{-1/8}$]

Fig. 47. Maximum Surface Temperature for Entry into Various Planets from Decaying Orbits

(V_0/V_c = 1, γ_0 = 0°) (Ref 1)

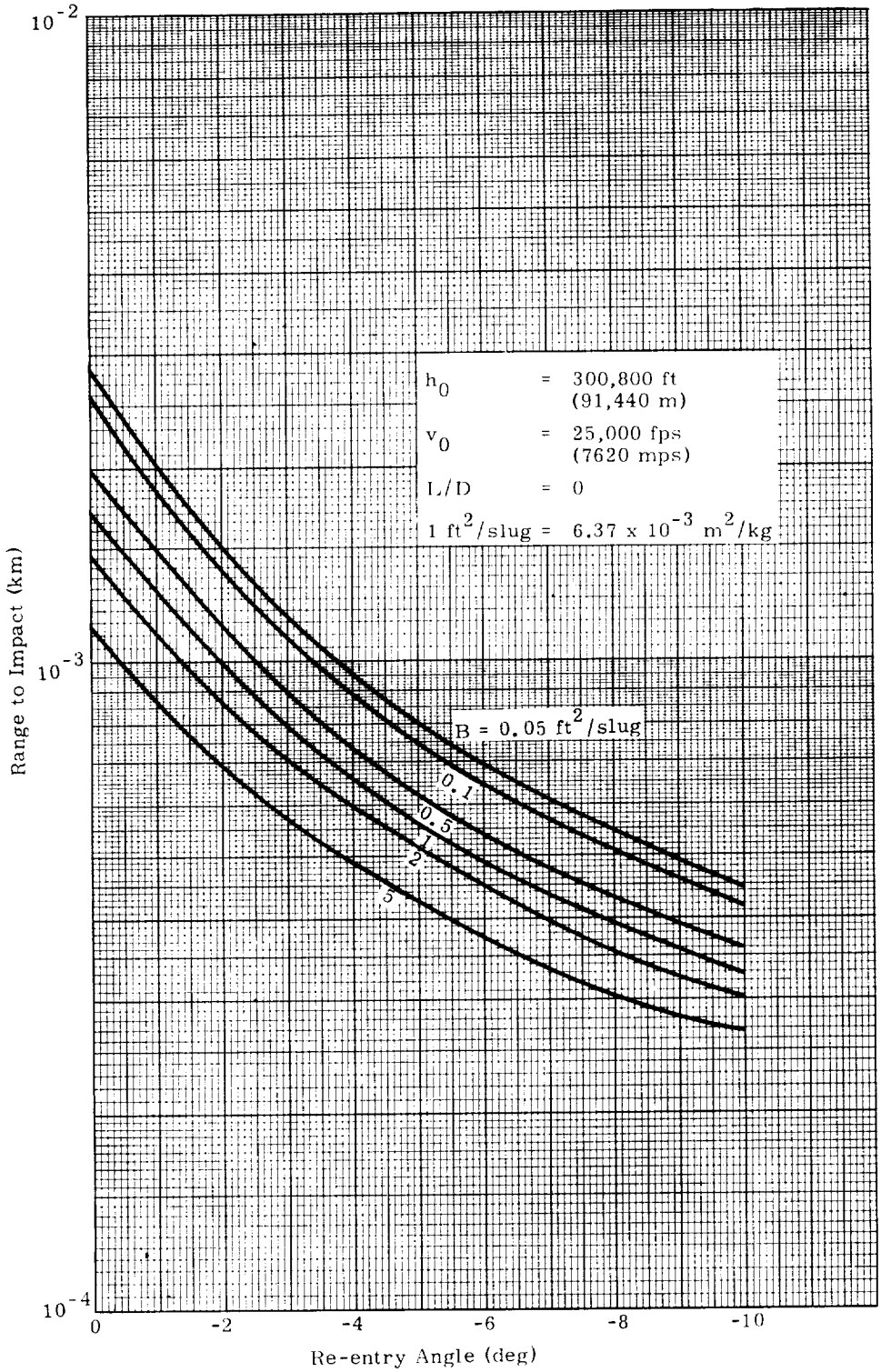

Fig. 48. Range to Impact Versus Re-entry Angle

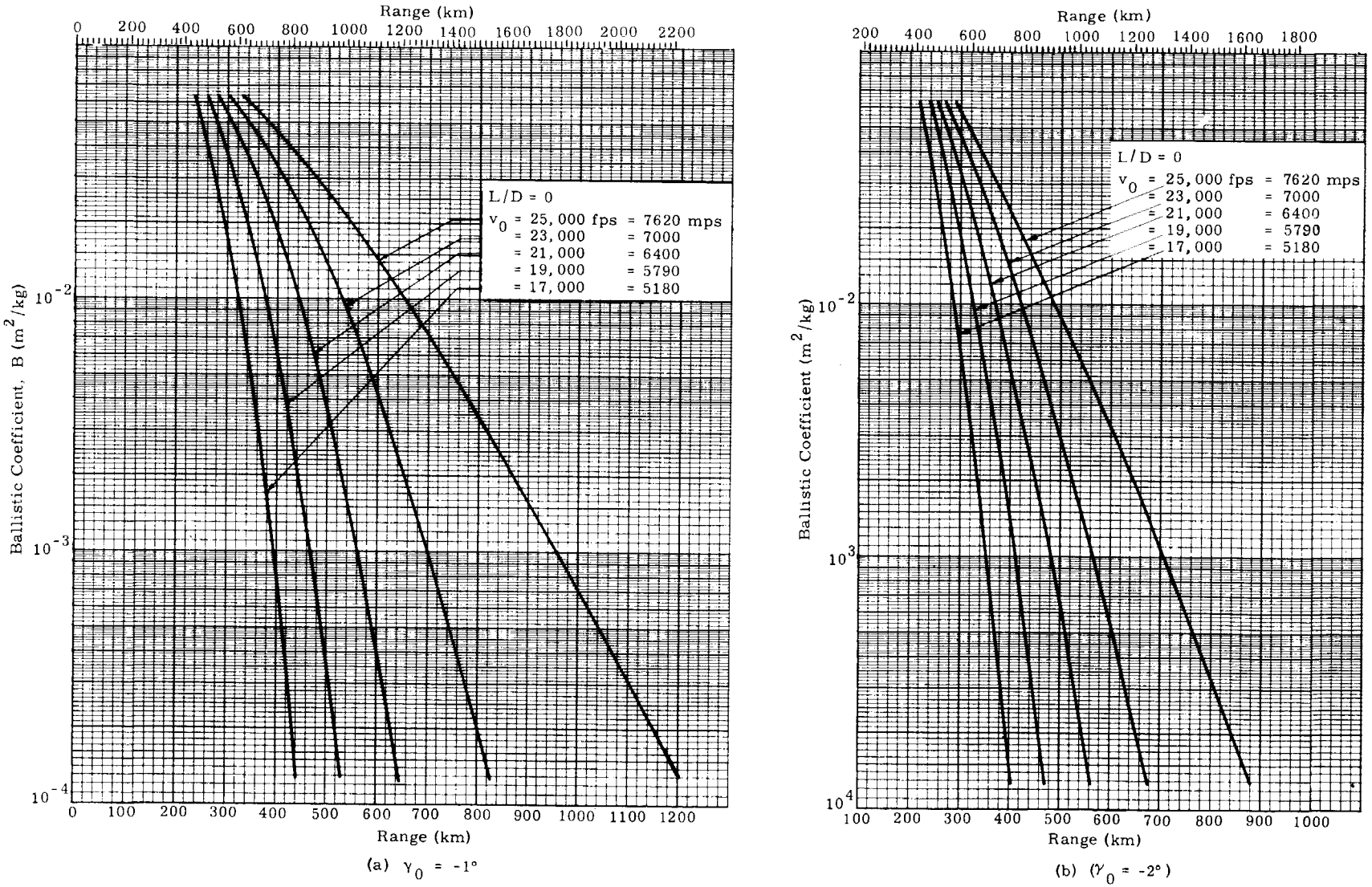

Fig. 49. Range Attained in Descent from 300,000 ft (91,440 m) to Sea Level (L/D = 0)

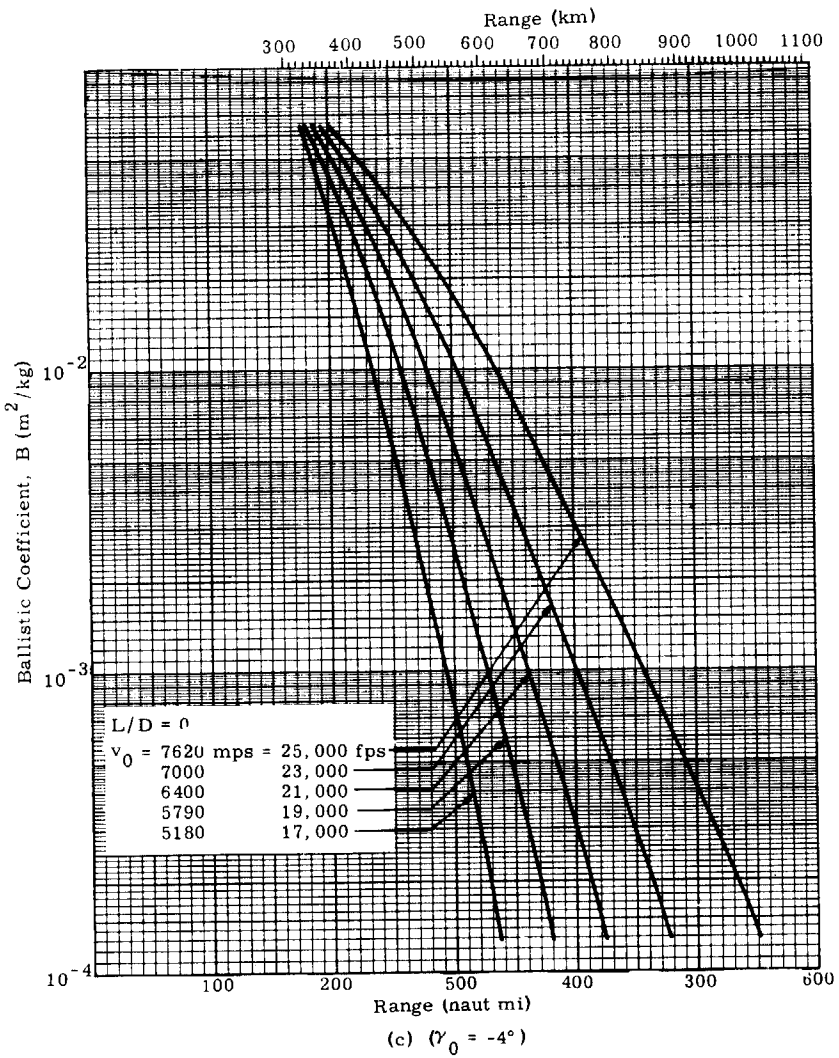

(c) (γ_0 = -4°)

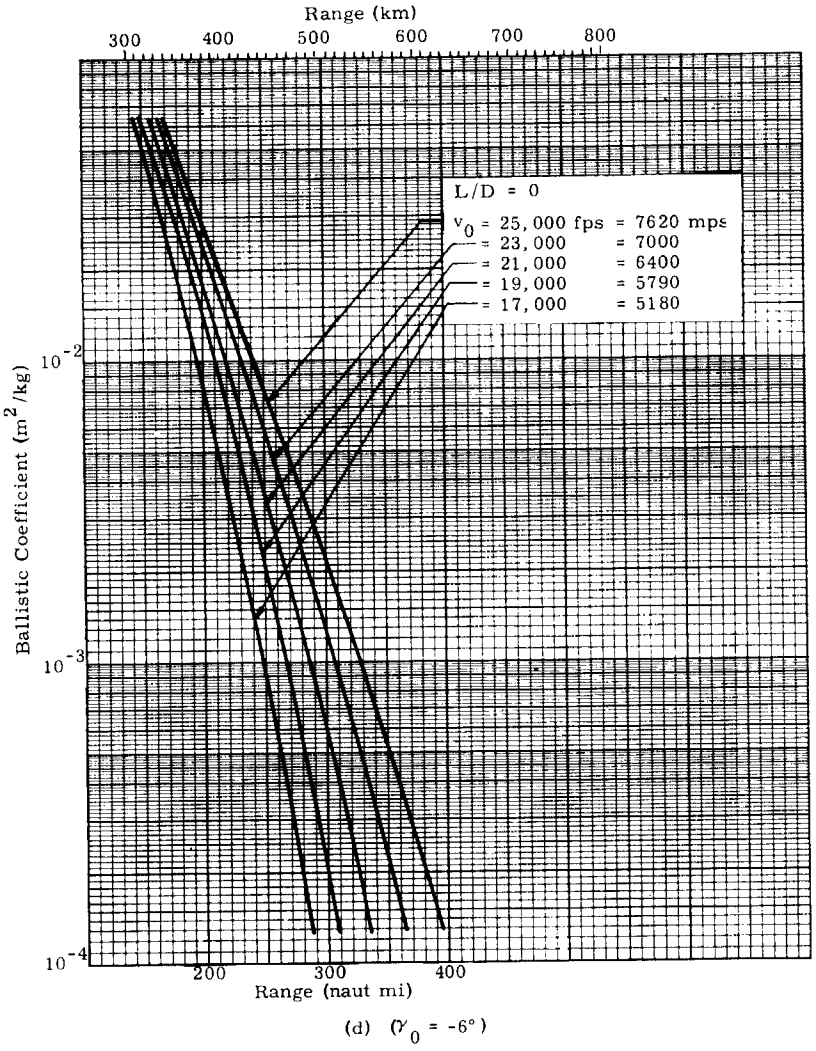

(d) (γ_0 = -6°)

Fig. 49. (continued)

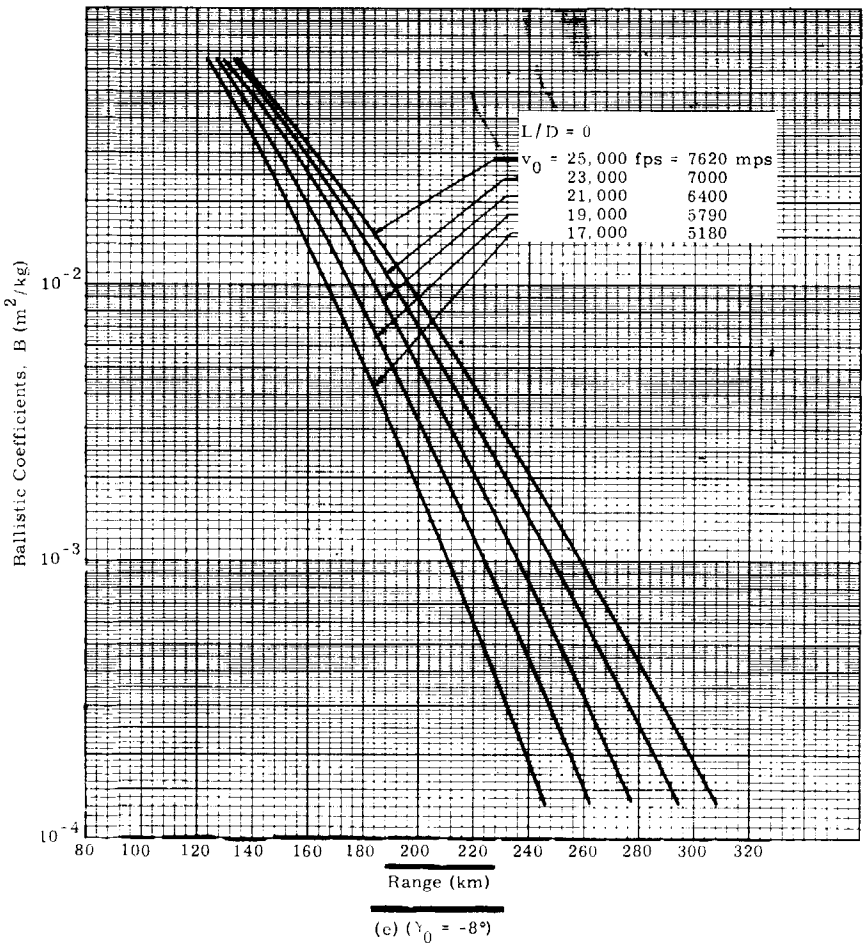

(c) (γ_0 = -8°)

Fig. 49. (continued)

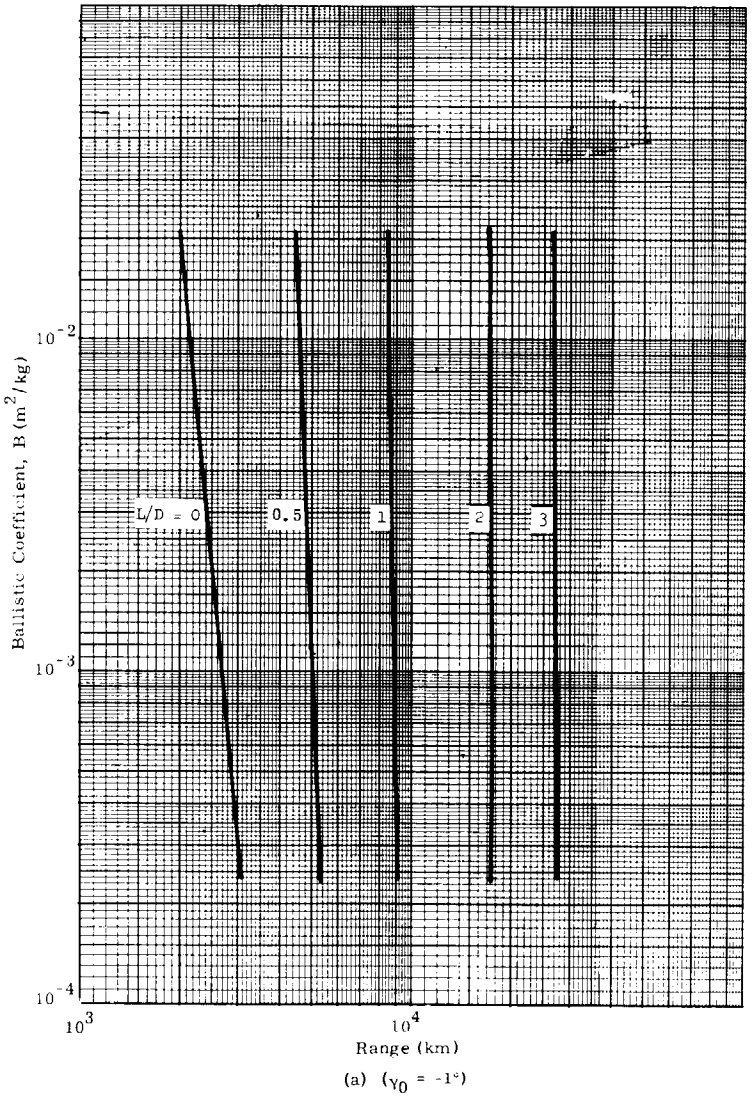

(a) (γ_0 = -1°)

Fig. 50. Range to Impact from 400,000 ft = 121,920 m (v_0 = 25,000 fps = 7620 mps)

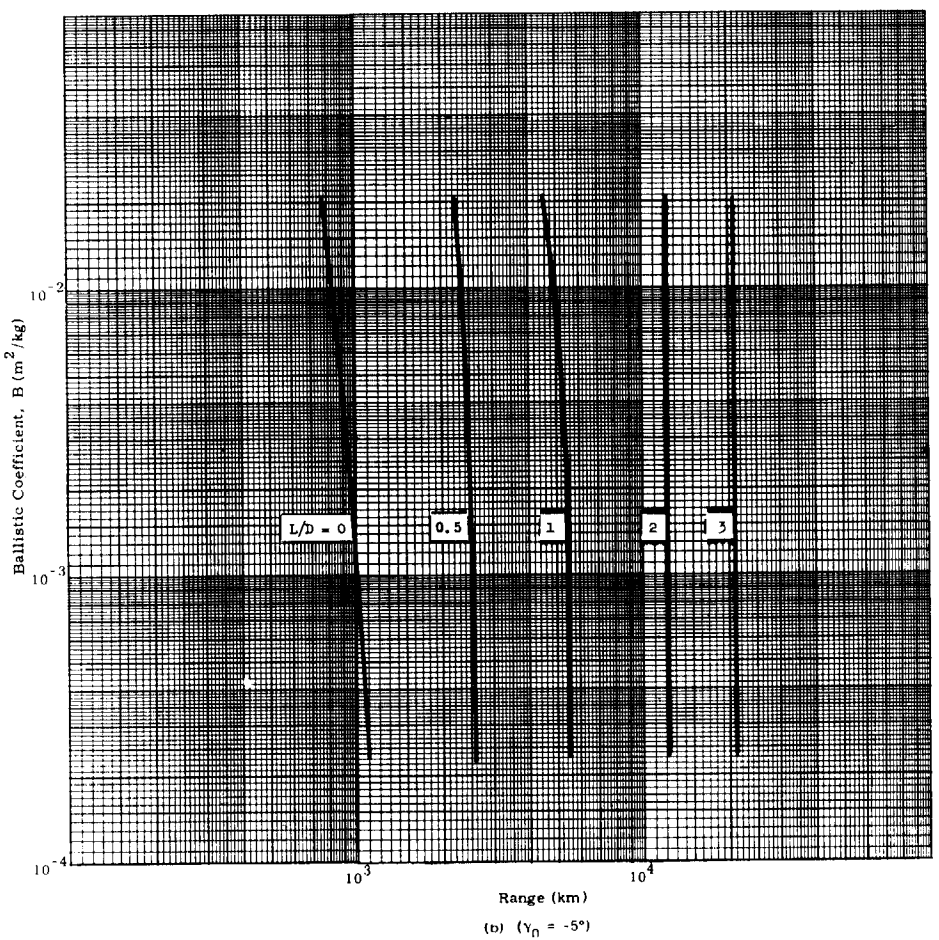

(b) (γ_0 = -5°)

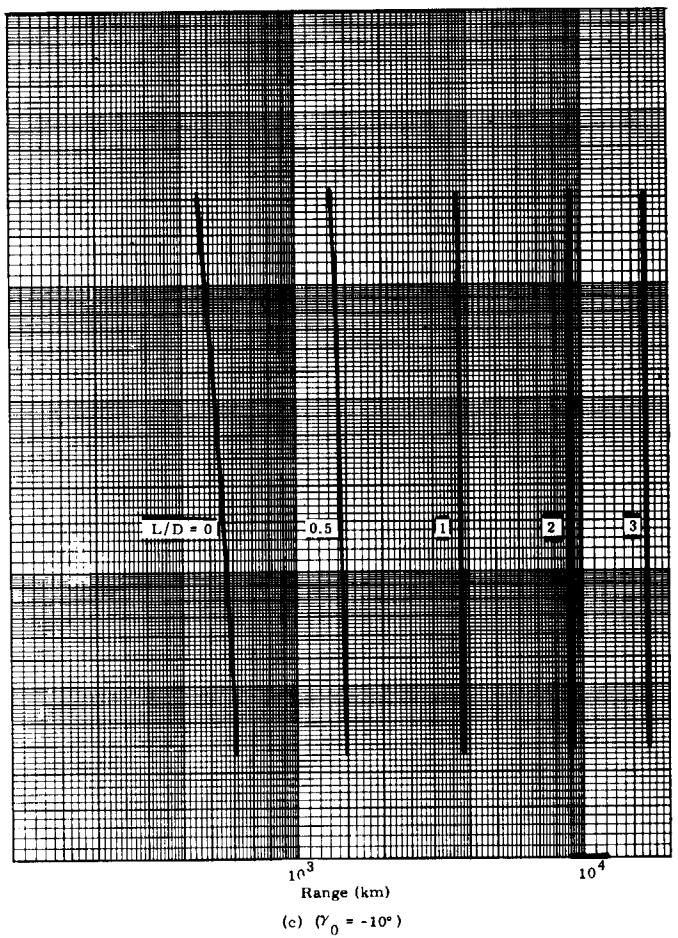

(c) (γ_0 = -10°)

Fig. 50. (continued)

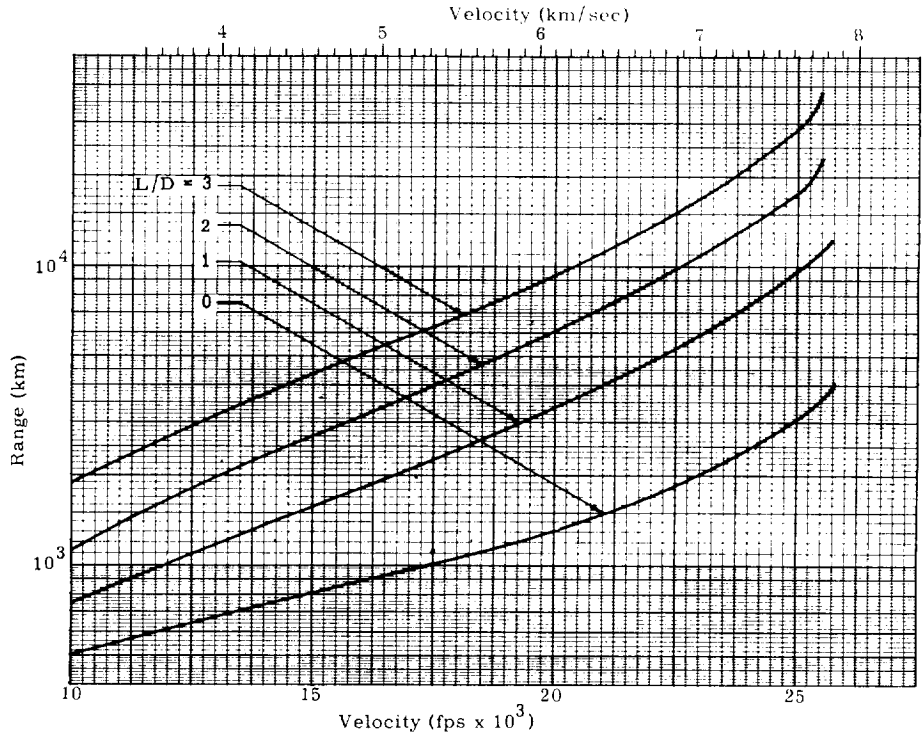

(a) W/C_DA = 438 psf = 21,000 newton/m^2,
B = 0.0367 ft^2/slug = 0.234 x 10^{-3} m^2/kg

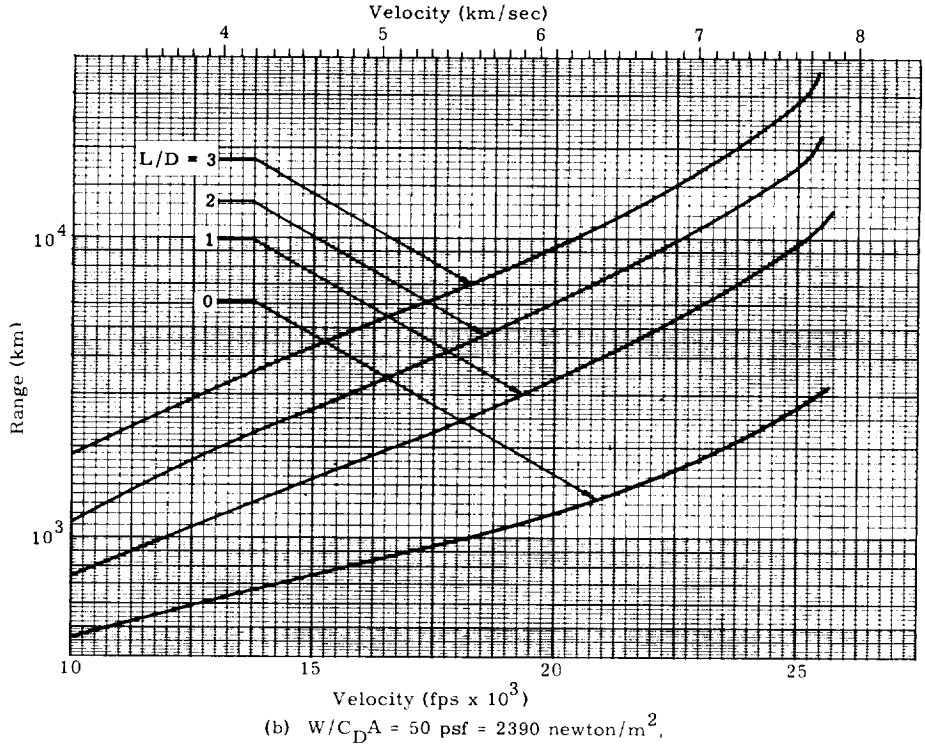

(b) W/C_DA = 50 psf = 2390 newton/m^2,
B = 0.322 ft^2/slug = 2.04 x 10^{-3} m^2/kg

Fig. 51. Range to Impact from 400,000 ft = 121,920 m (γ_0 = -1°)

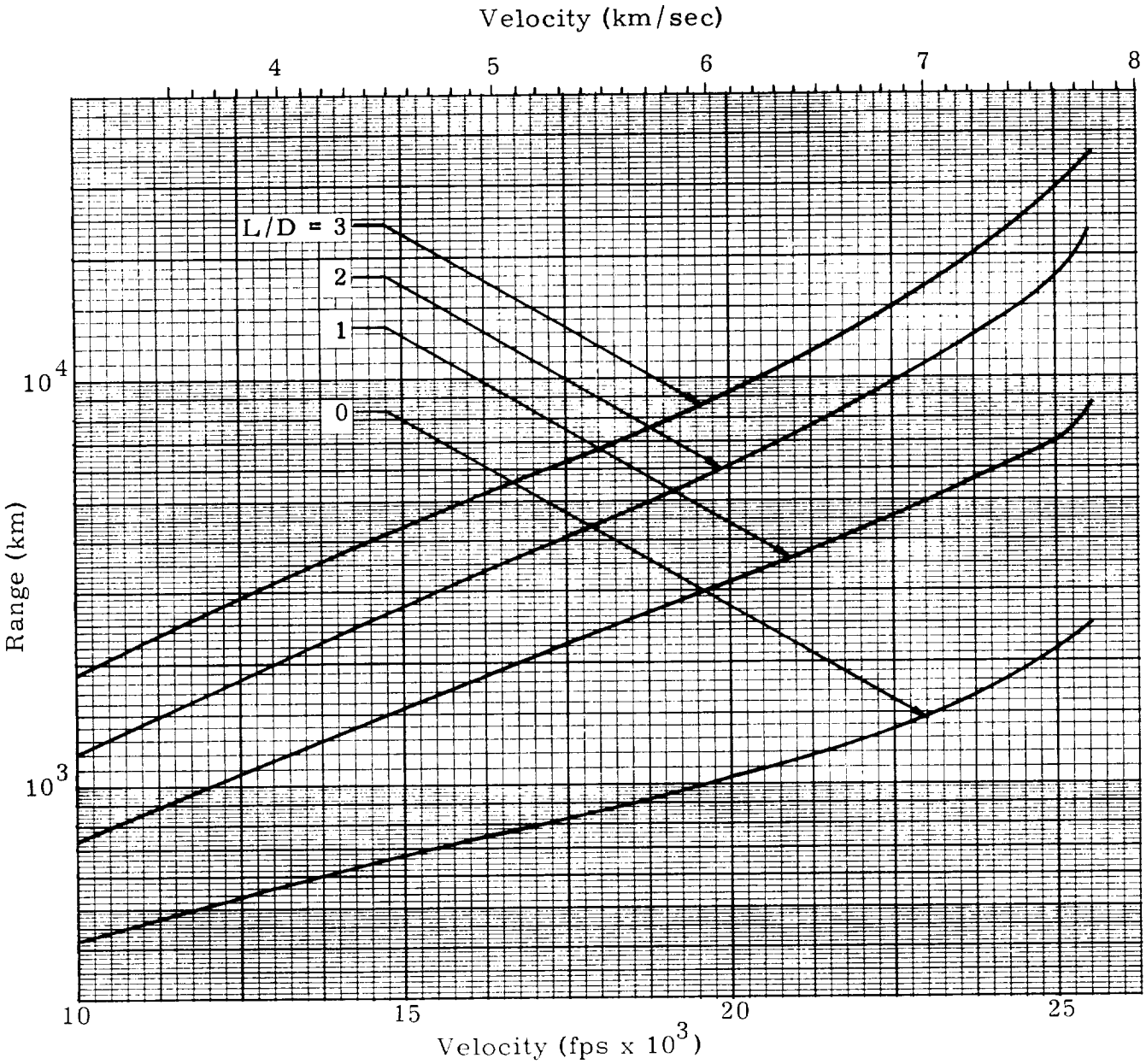

(c) W/C_DA = 5 psf = 239 newton/m^2,

B = 3.22 ft^2/slug = 2.05 x 10^{-2} m^2/kg, γ = -1°

Fig. 51. (continued)

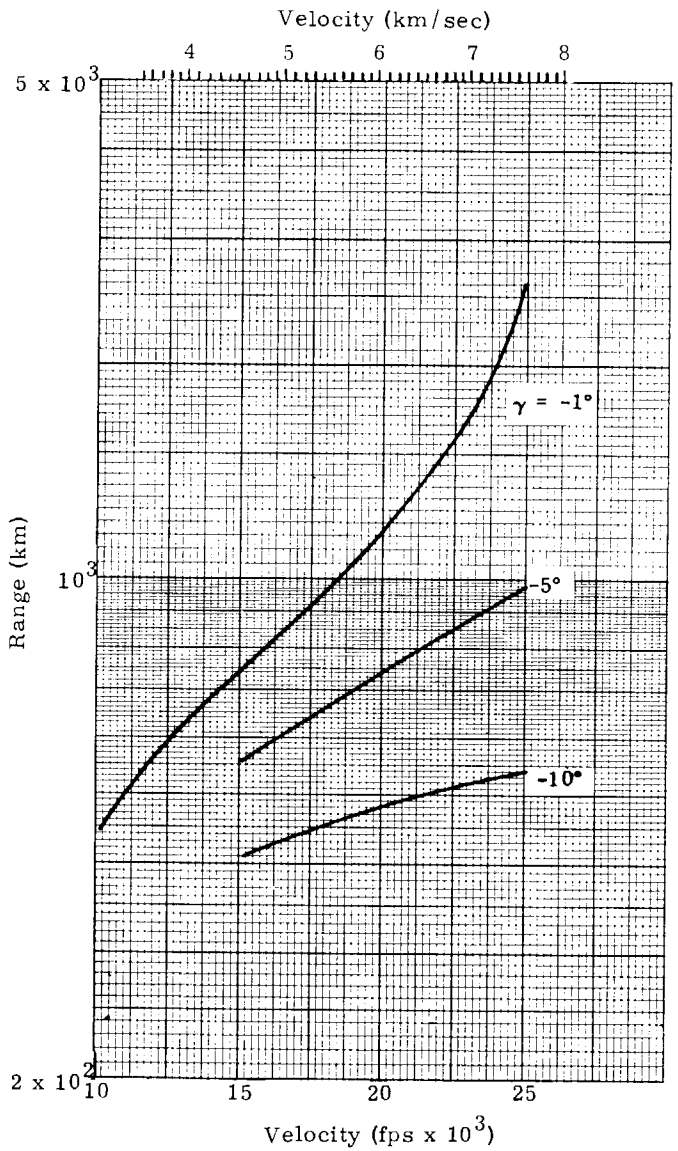

(a) L/D = 0

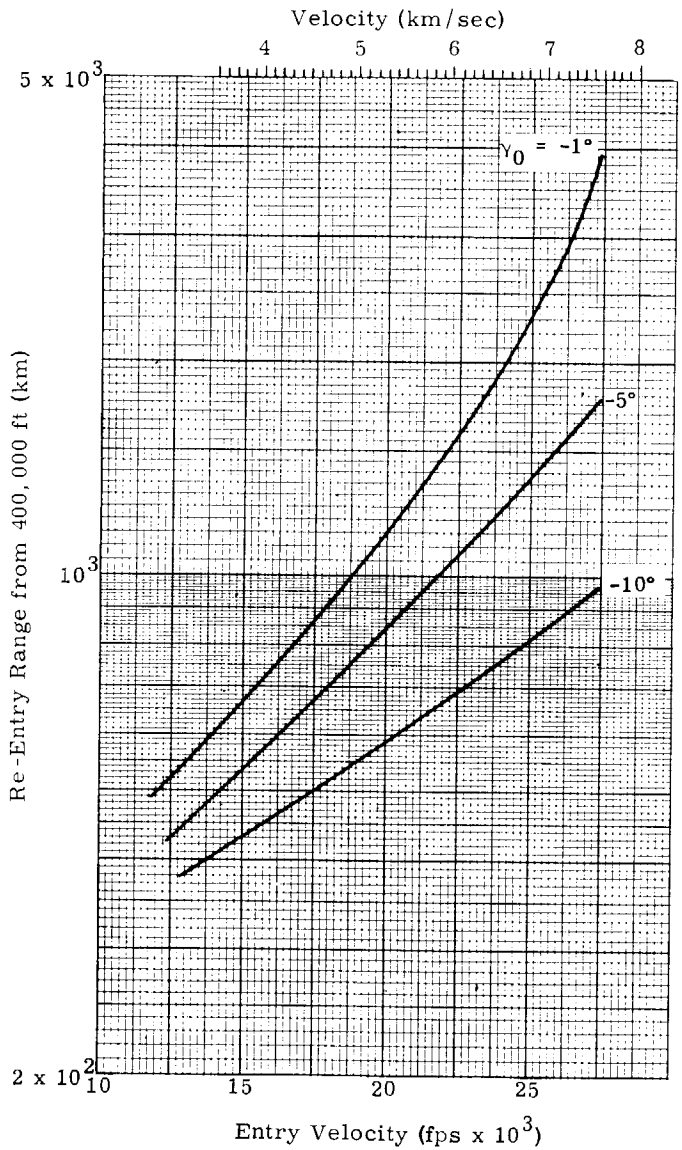

(b) L/D = 0.3

Fig. 52. Impact Range Versus Re-Entry Velocity($\frac{W}{C_D A}$ = 50 psf = 2390 newton/m^2, h_0 = 400,000 ft = 121,920 m)

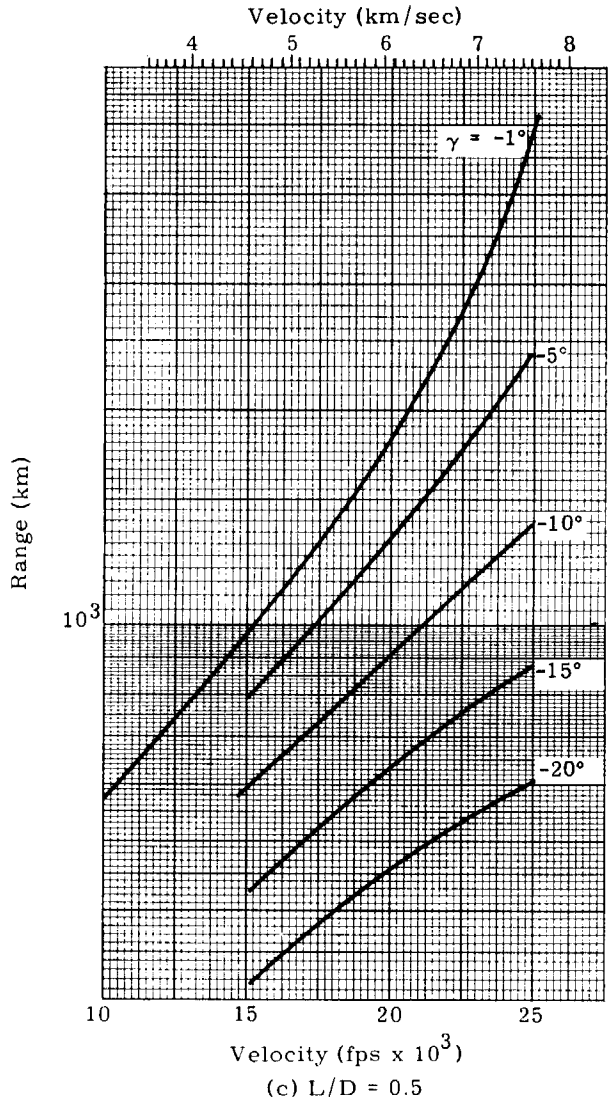

(c) L/D = 0.5

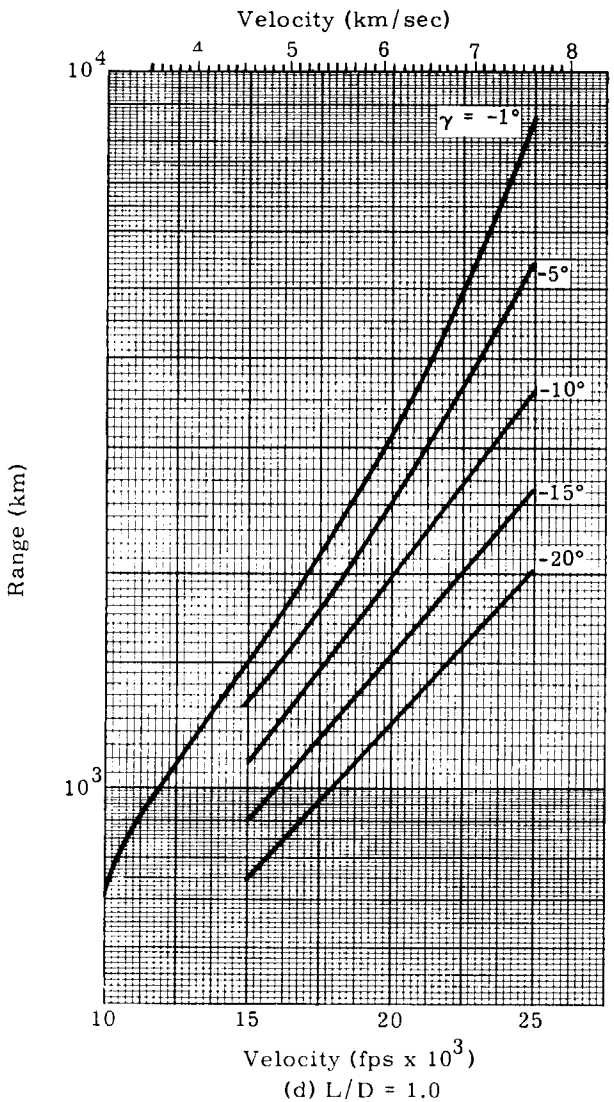

(d) L/D = 1.0

Fig. 52. (continued)

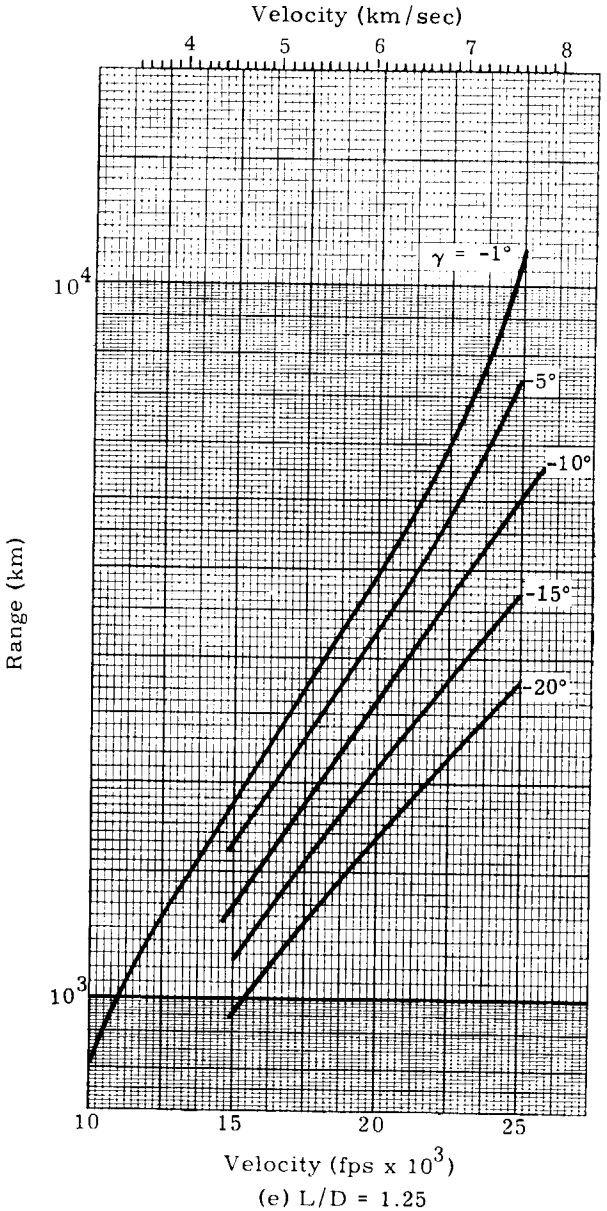

(e) L/D = 1.25

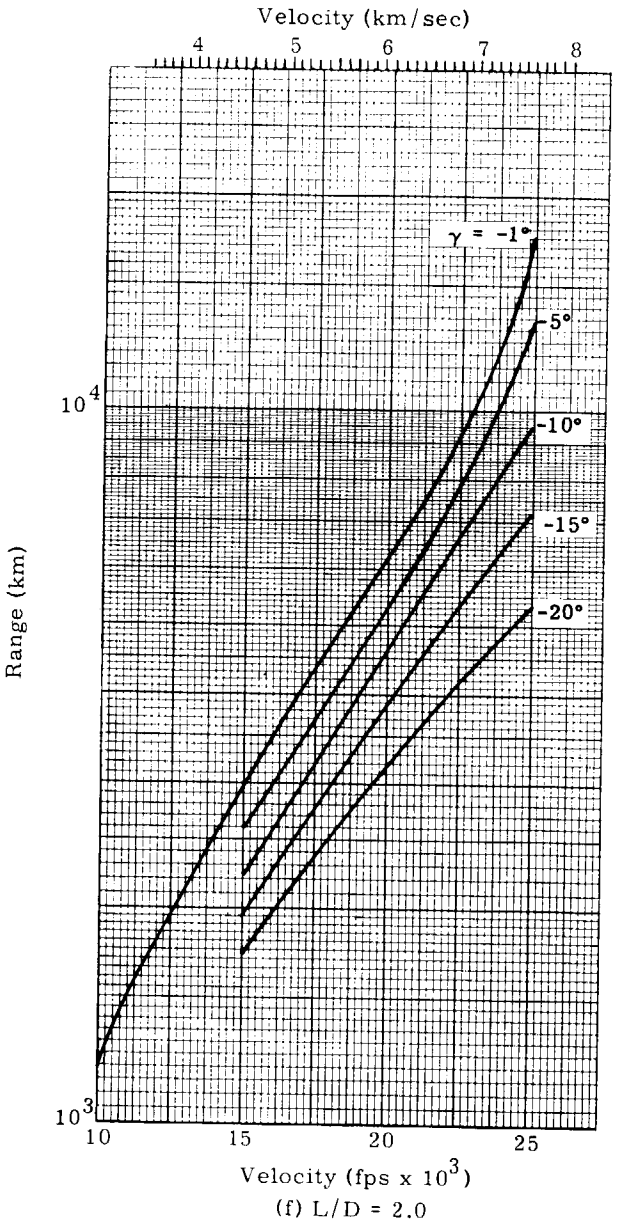

(f) L/D = 2.0

Fig. 52. (continued)

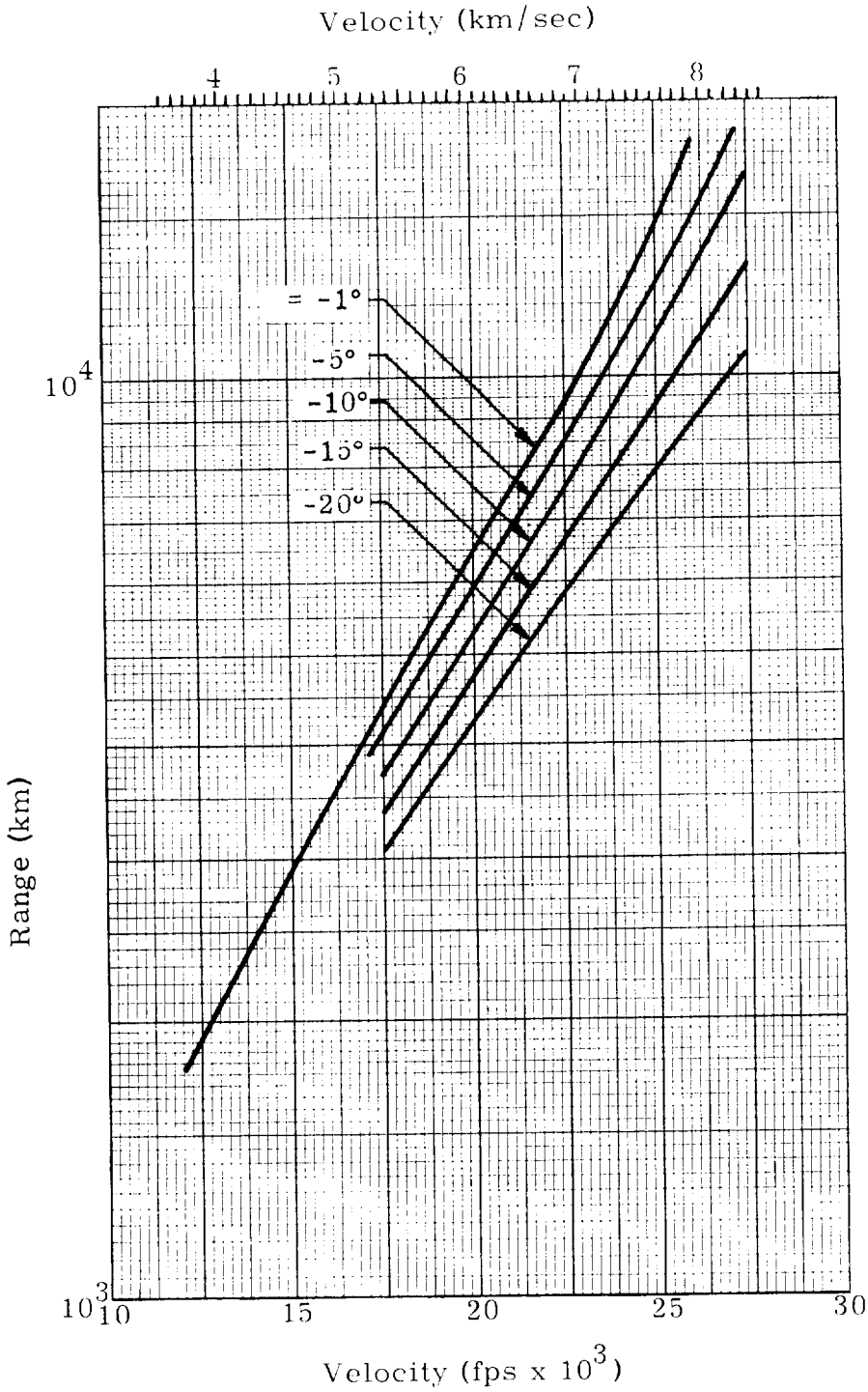

(g) L/D = 3.0

Fig. 52. (continued)

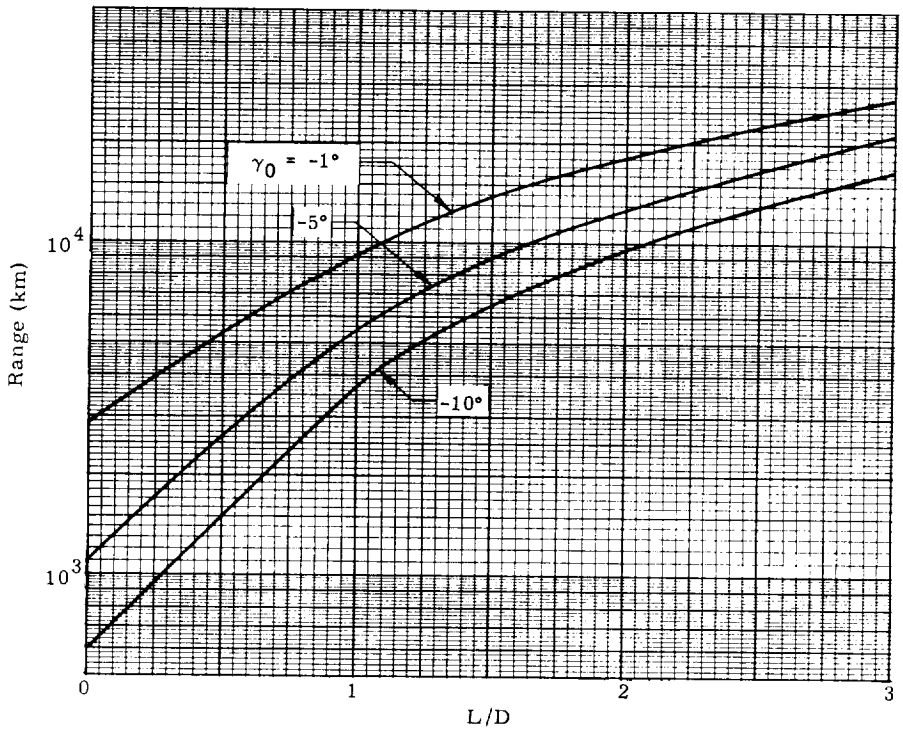

(a) W/C_DA = 438 psf = 21,000 newton/m^2

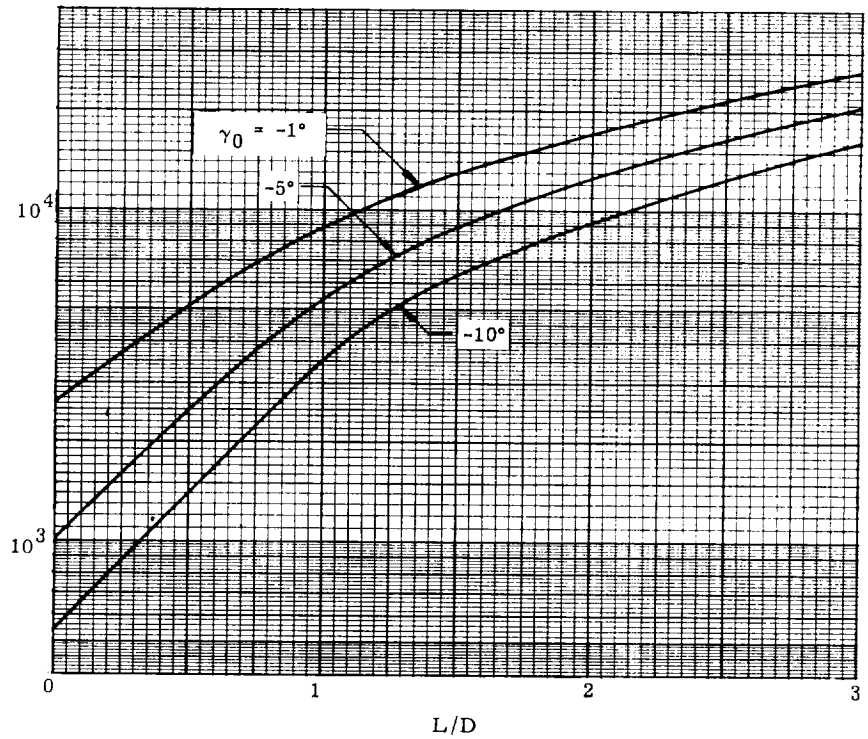

(b) W/C_DA - 50 psf = 2390 newton/m^2

Fig. 53. Range to Impact from 400,000 ft (121,920 m) Versus L/D (v_0 = 25,000 fps = 7620 mps)

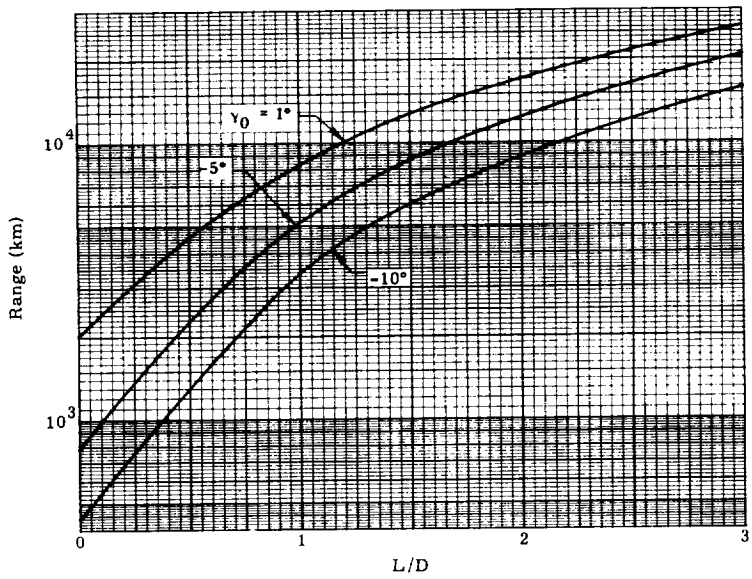

(c) W/C_DA = 5 psf = 239 newton/m^2

Fig. 53. Continued

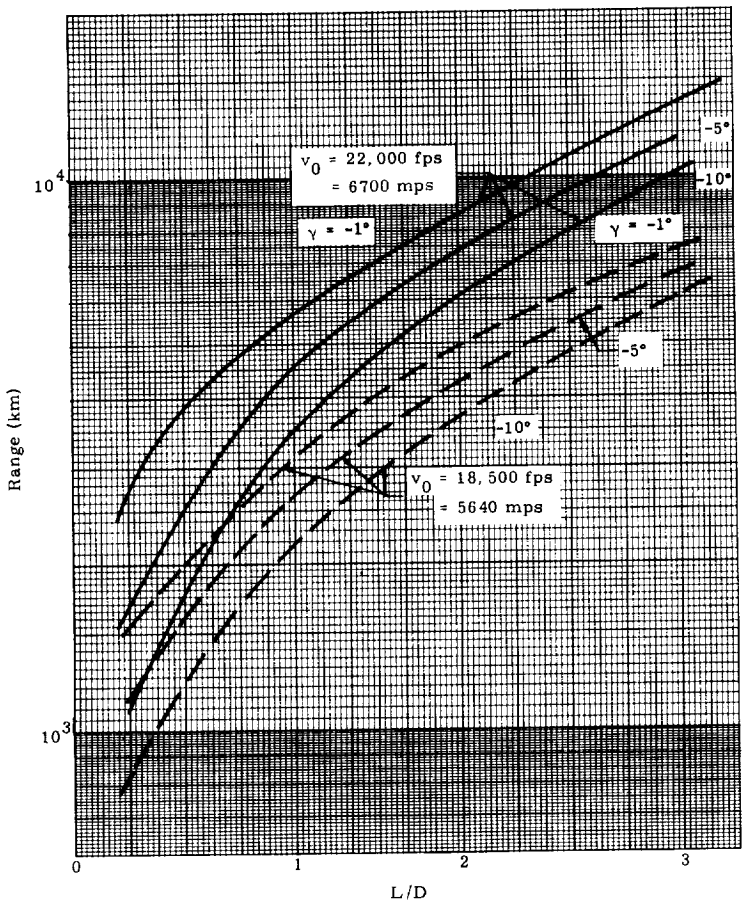

(a) v_0 = 18,500 fps and v_0 = 22,000 fps

Fig. 54. Range Versus Lift-Drag Ratio, $\frac{W}{C_DA}$ = 50 psf (Applies for 5< $\frac{W}{C_DA}$ < 500 psf; h_0 = 400,000 ft)

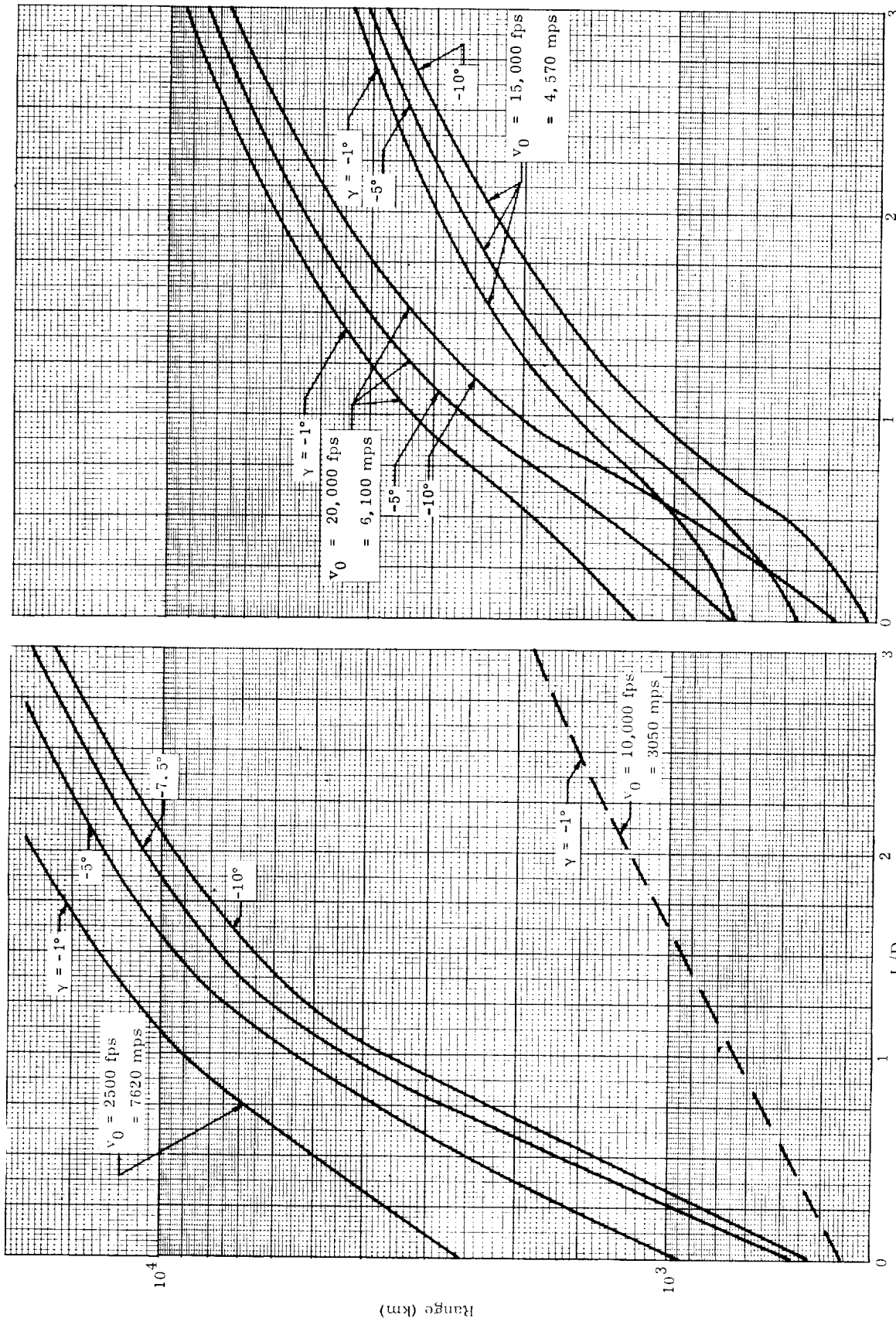

(b) v_0 = 25,000 and 10,000 fps (7620 and 3050 mps)

(c) v_0 = 20,000 and 15,000 fps (6100 and 4570 mps)

Fig. 54. (continued)

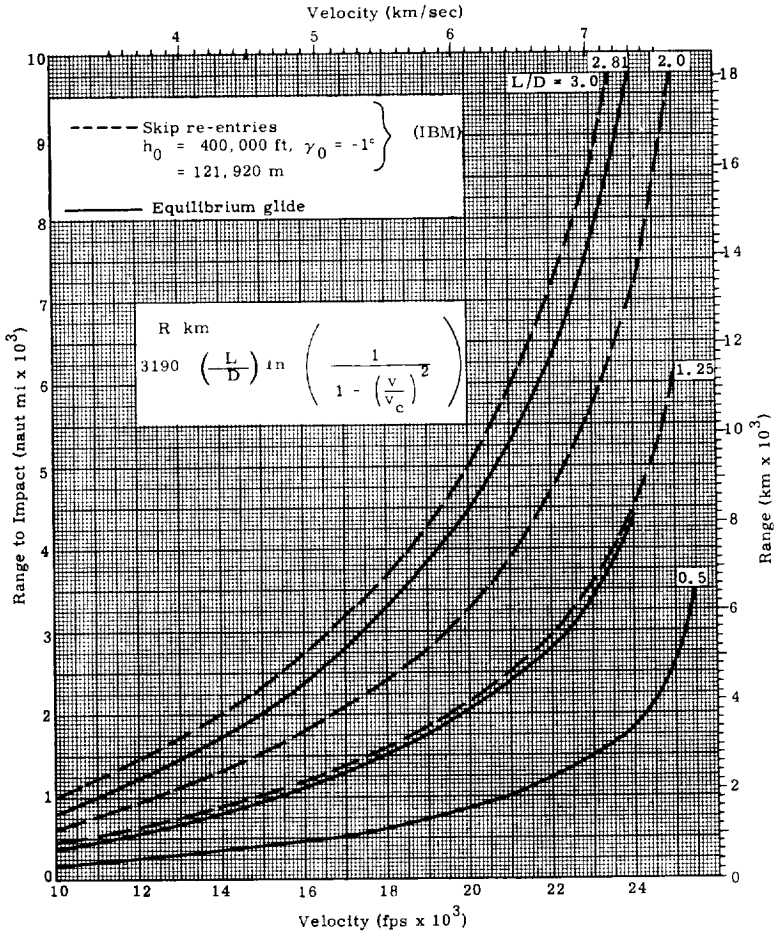

Fig. 55. Equilibrium Glide Range (not dependent on $W/C_L A$)

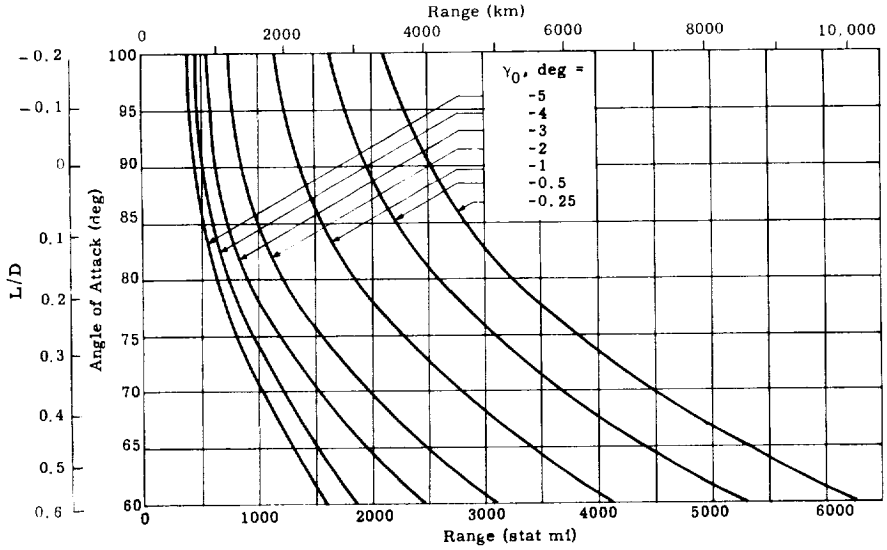

Fig. 56a. Variation in Range as a Function of Angle of Attack and Entry Angle. (Nonrotating Earth; h_0 = 350,000 ft = 106,700 m; v_0 = 25,863 fps = 7870 mps; W/A = 20 lb/ft^2 = 956 newton/m^2) (Ref. 25)

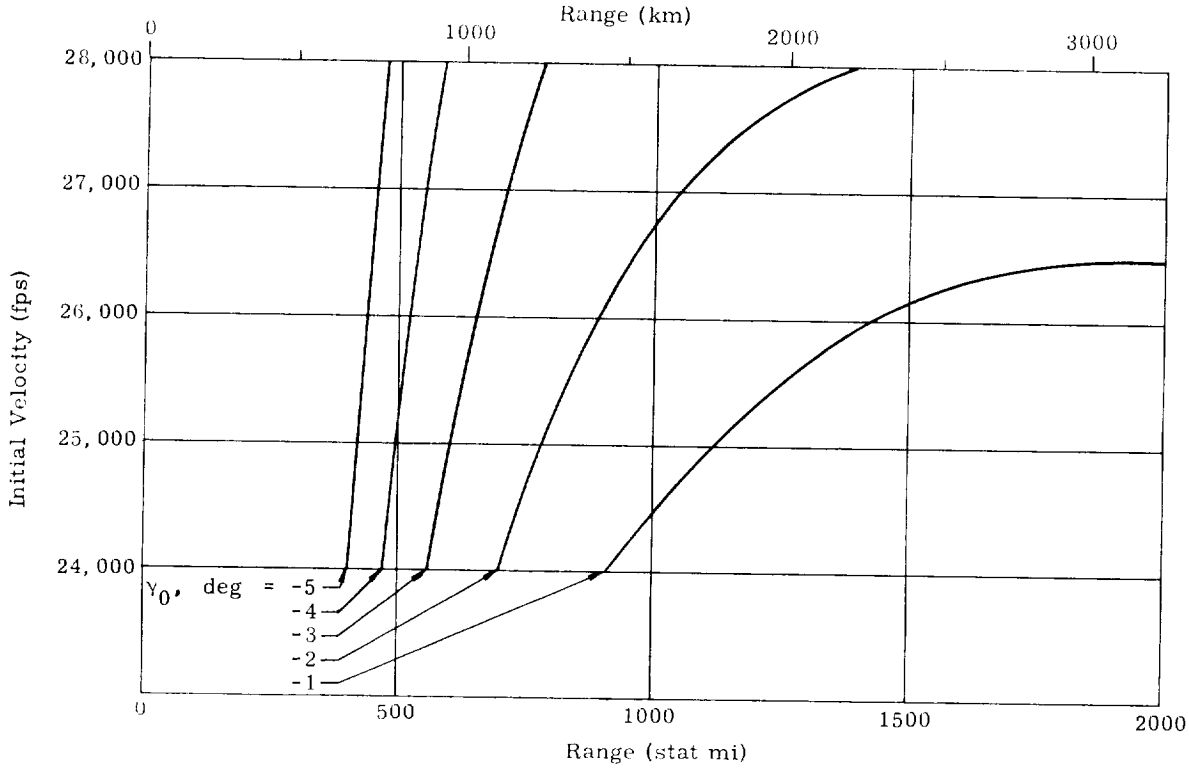

Fig. 56b. Variation in Range as a Function of Initial Velocity and Entry Angle for Ballistic Vehicles (α = 90), (Nonrotating Earth; h_0 = 350,000 ft = 106,800 m; W/A = 20 lb/ft^2 = 955 newtons/m^2] [Ref. 25]

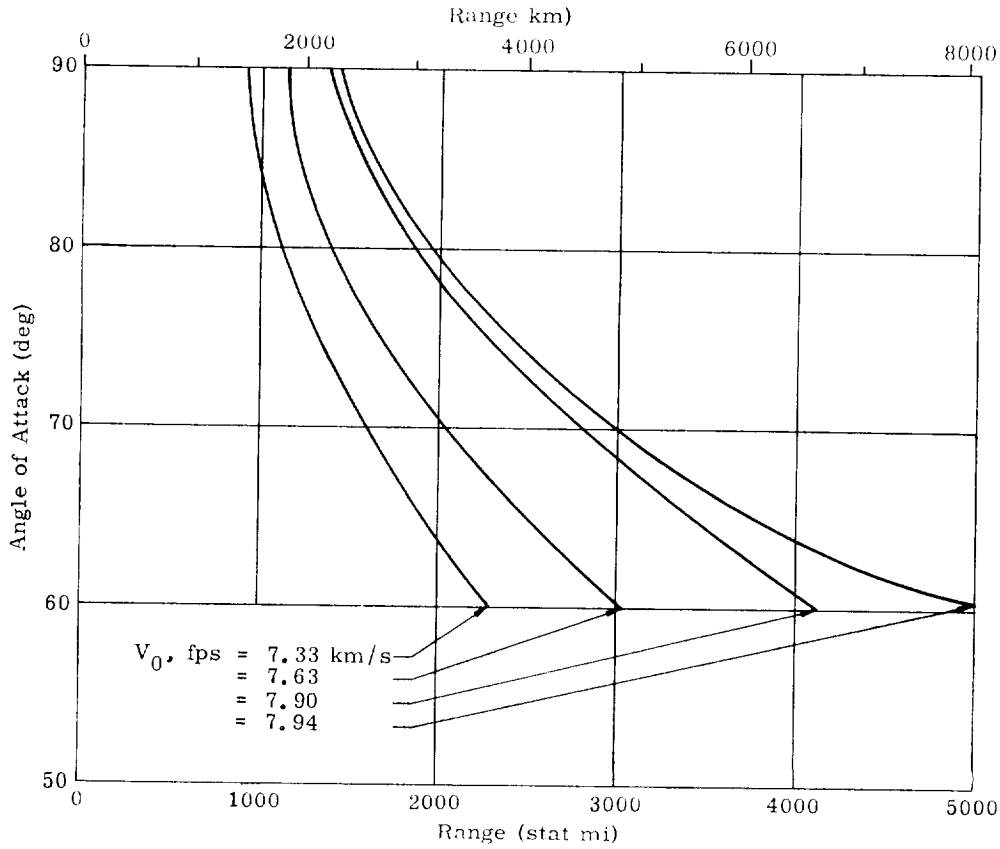

Fig. 56c. Variation in Range as a Function of Angle of Attack and Initial Velocity. (Nonrotating Earth; h_0 = 350,000 ft = 160,800 m; γ_0 = -1°) (Ref 25)

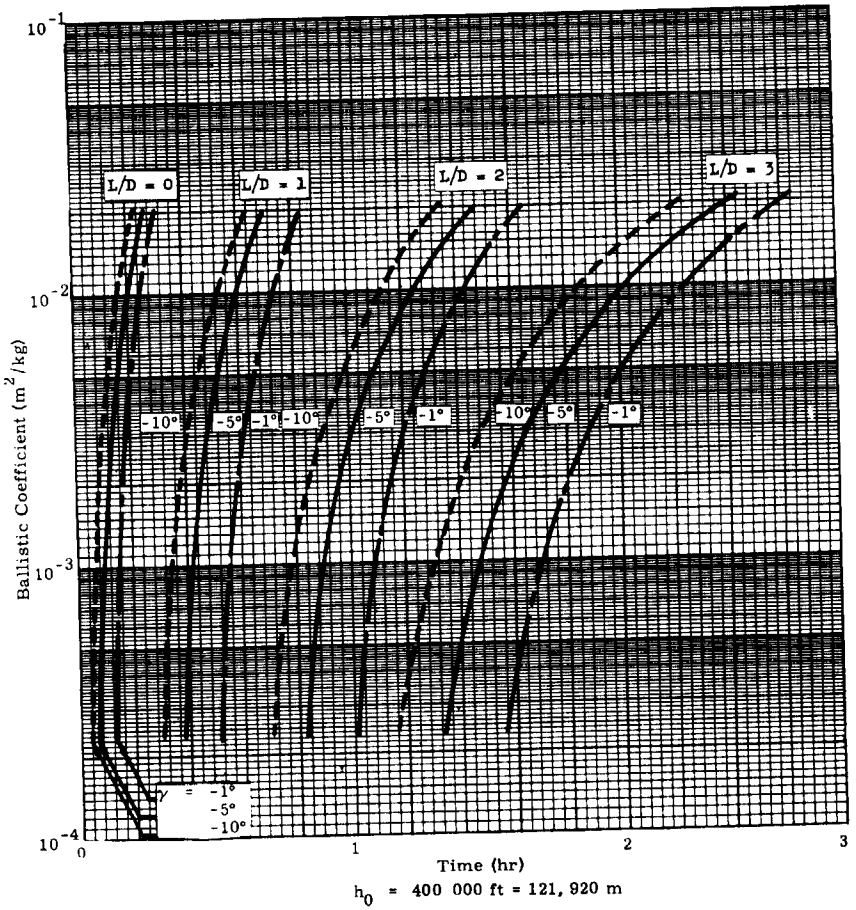

Fig. 57. Time to Impact Versus Ballistic Coefficient (v_0 = 25,000 fps = 7620 mps)

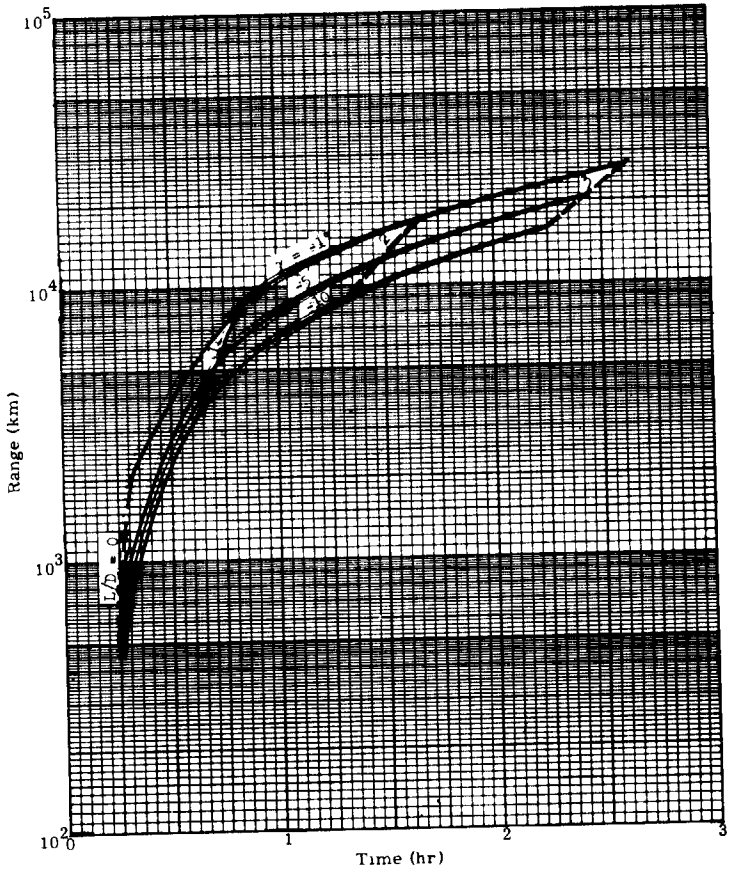

(a) B = 322 ft²/slug = 2.05 x 10^{-2} m²/kg

Fig. 58. Time Versus Range to Impact from 400,000 ft = 121,920 m (v_0 = 25,000 fps = 7620 mps)

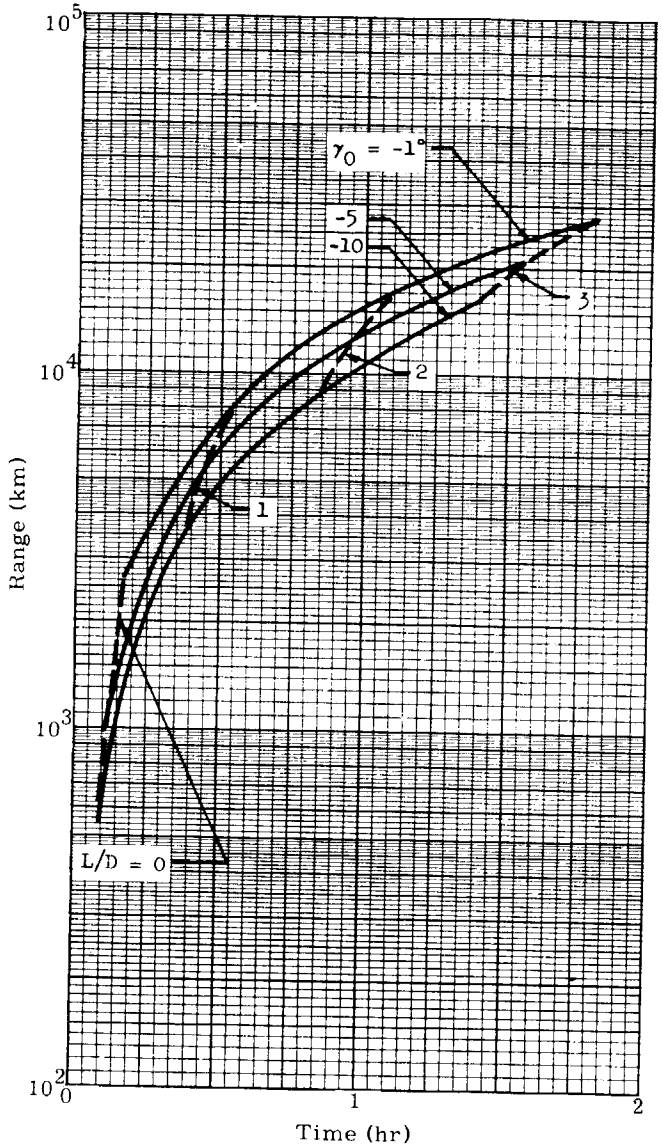

(b) B = 0.322 ft^2/slug = 2.05 x 10^{-3} m^2/kg

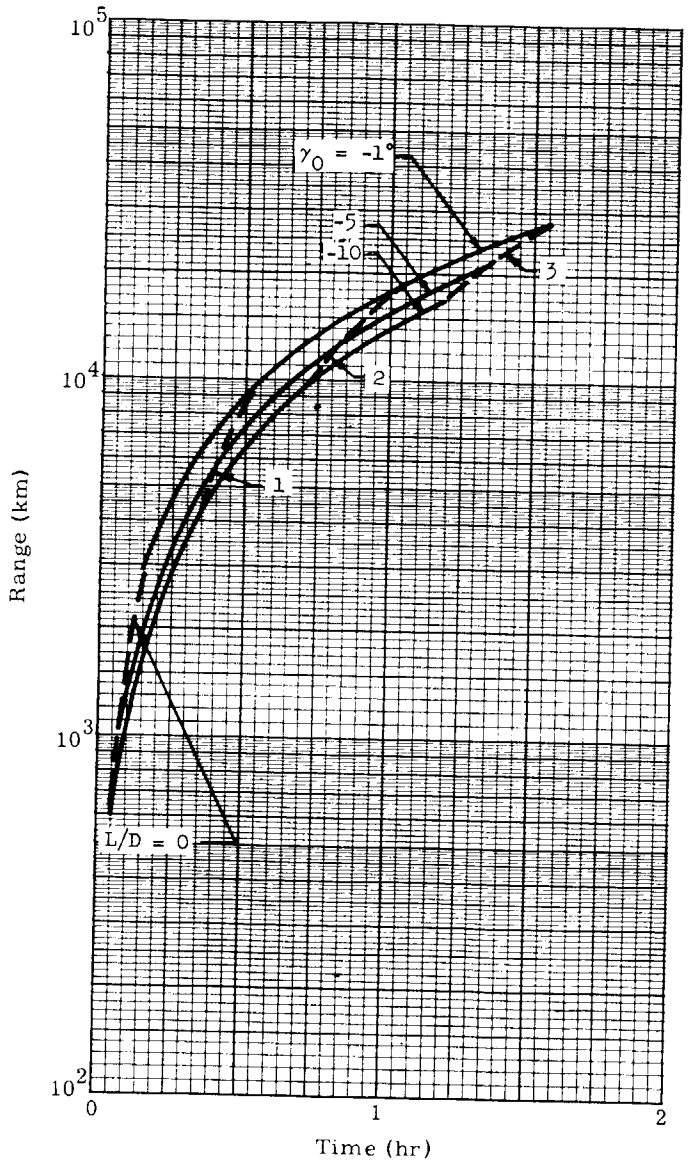

(c) B = 0.0367 ft^2/slug = 0.234 x 10^{-3} m^2/kg

Fig. 58. Continued

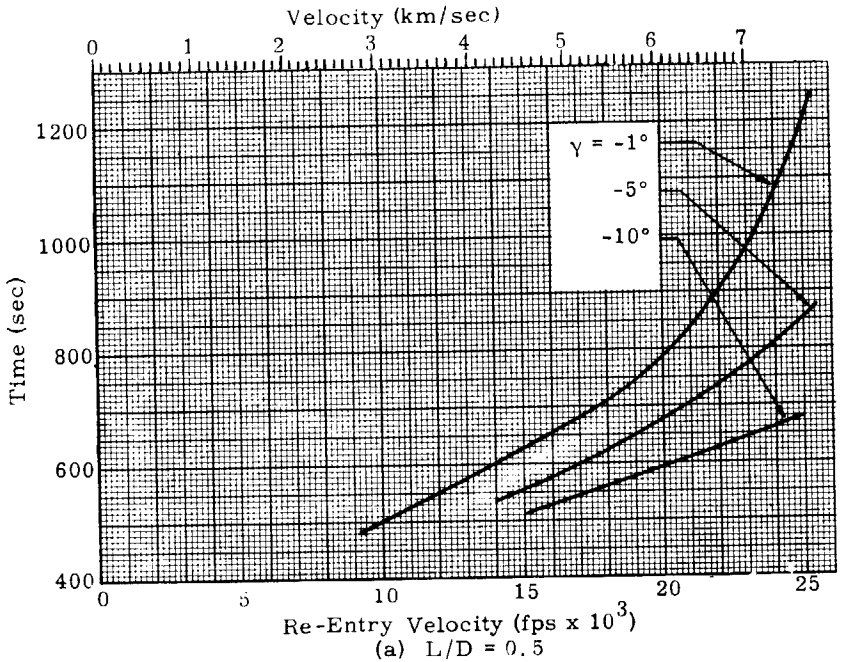

(a) L/D = 0.5

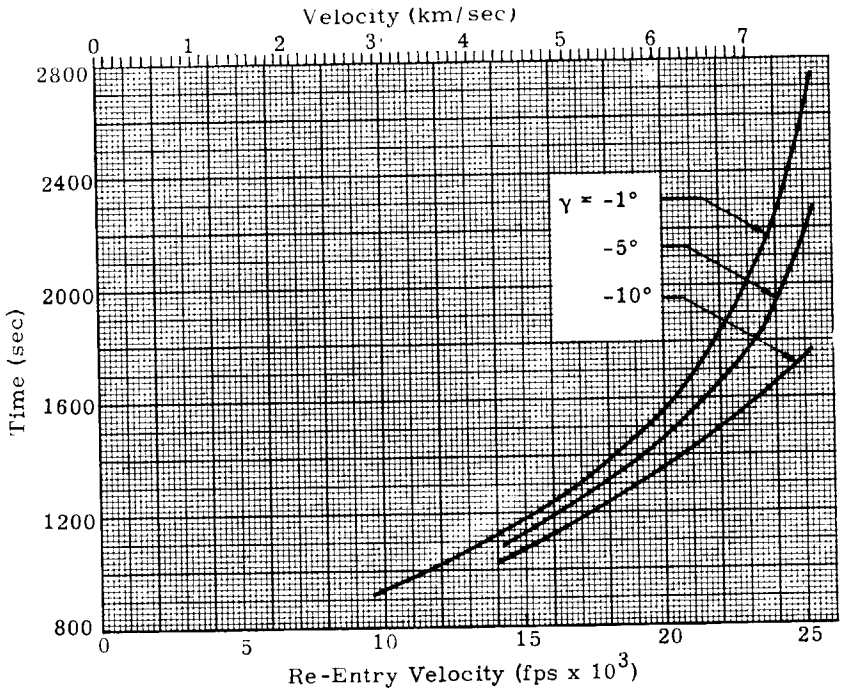

(b) L/D = 1.25

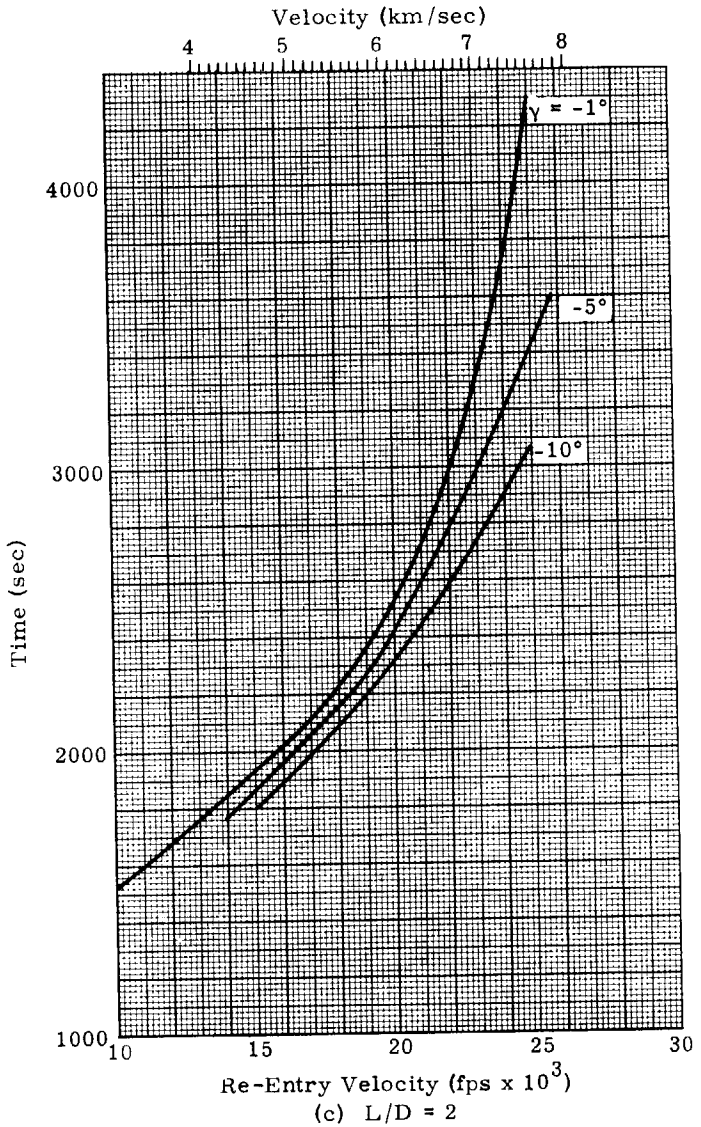

(c) L/D = 2

Fig. 59. Time to Impact Versus Re-Entry Velocity (h_0 = 400,000 ft = 121,920 m, W/C_DA = 50 psf = 2390 newtons/m^2)

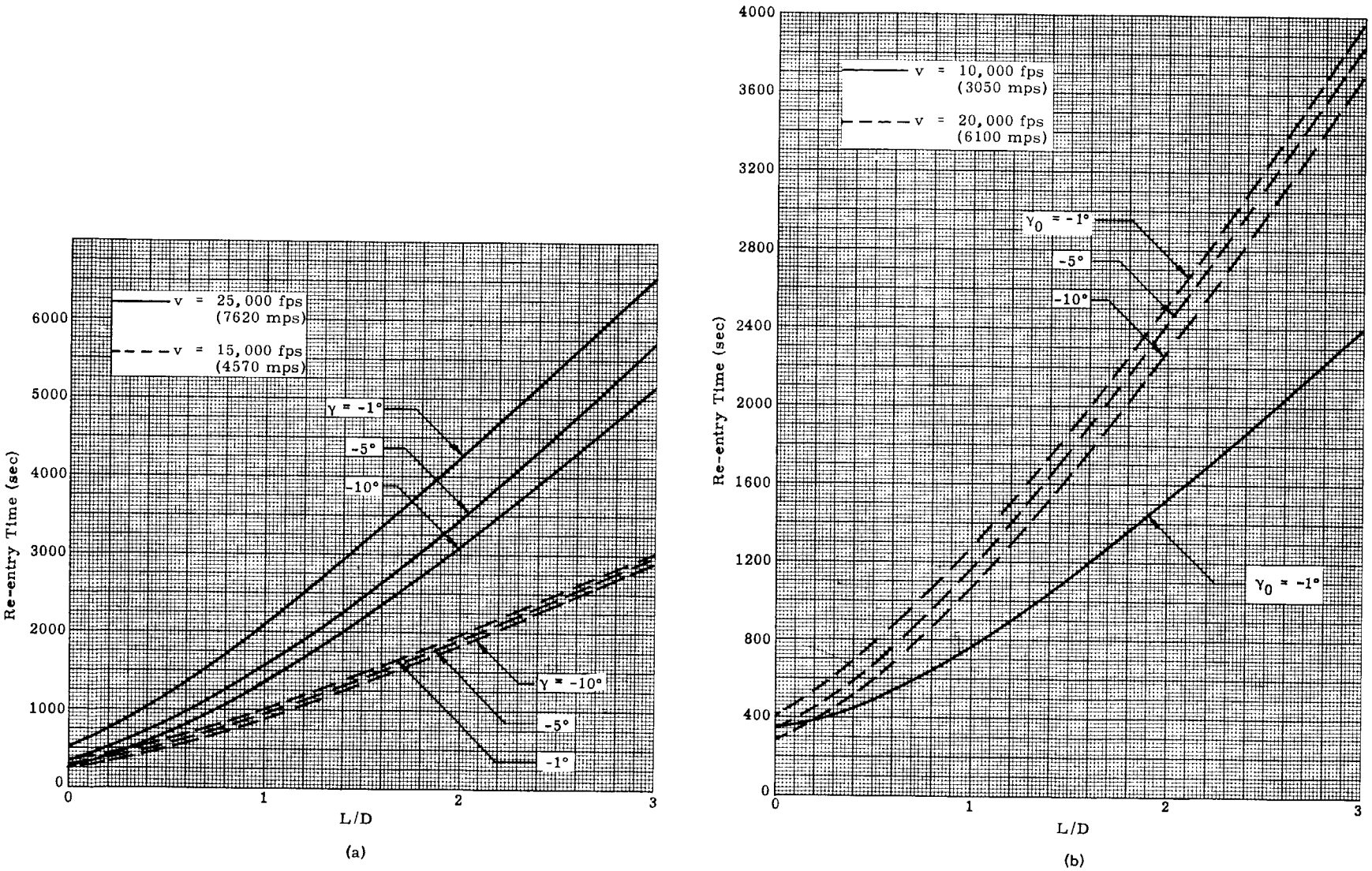

Fig. 60. Re-Entry Time Versus L/D for Various Velocities($\frac{W}{C_D A}$ = 50 psf = 2390 newtons/m^2; h_0 = 400,000 ft = 121,920 m)

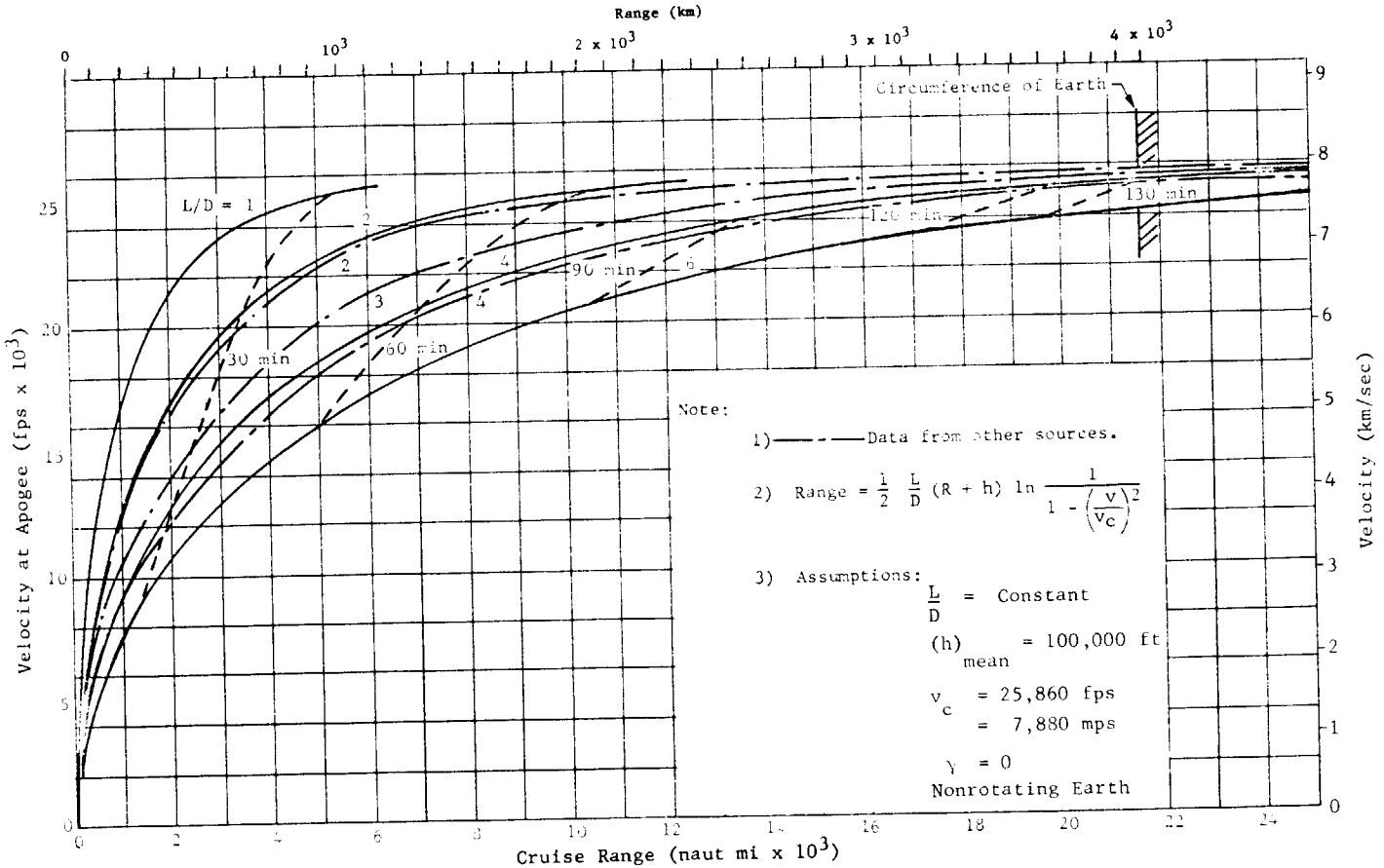

Fig. 61. Velocity at Apogee Versus Range

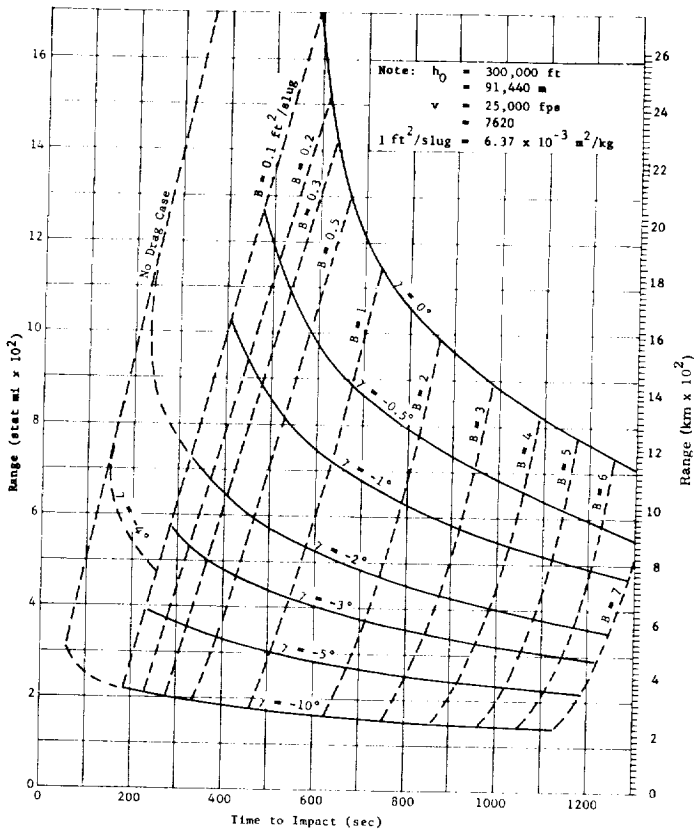

Fig. 62. Range and Time to Impact for Ballistic Entry

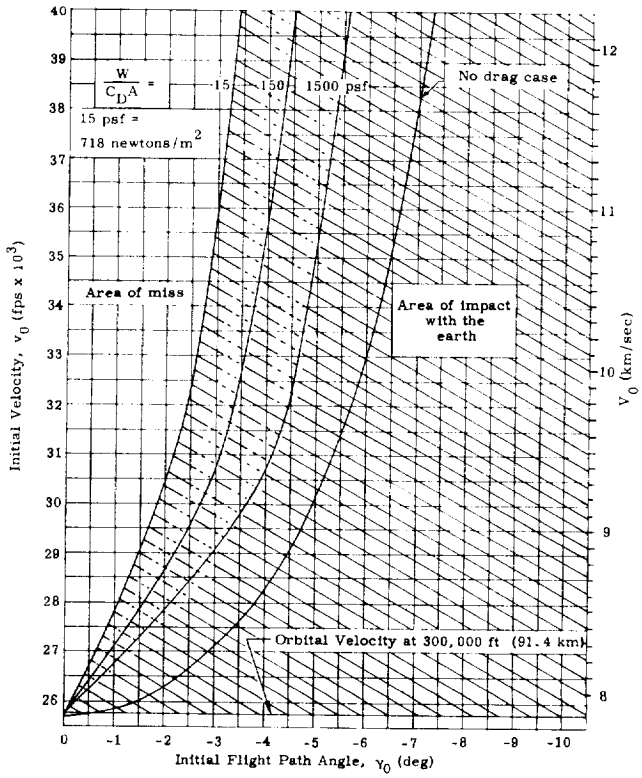

Fig. 63a. Conditions for Impact--Ballistic Case

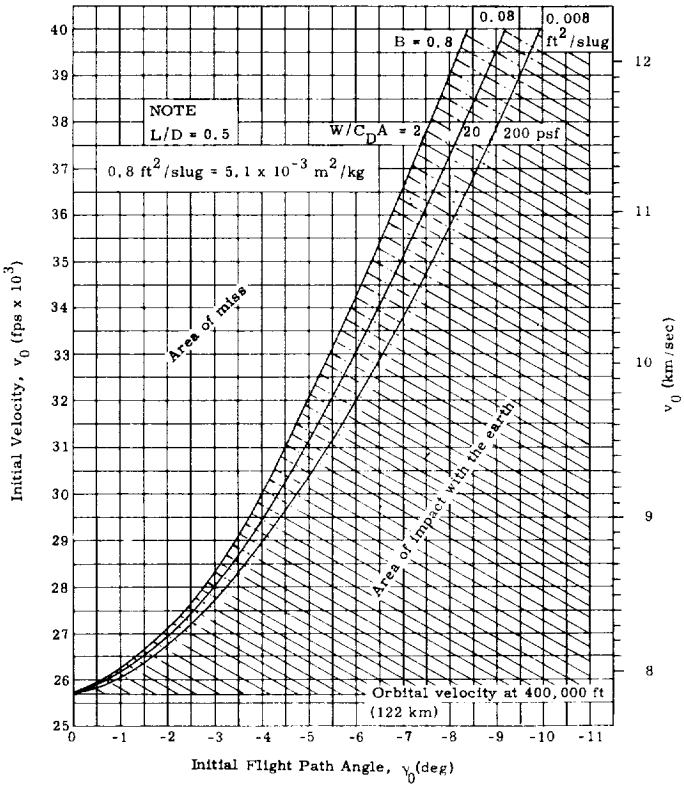

Fig. 63b. Conditions for Impact, Lifting Case

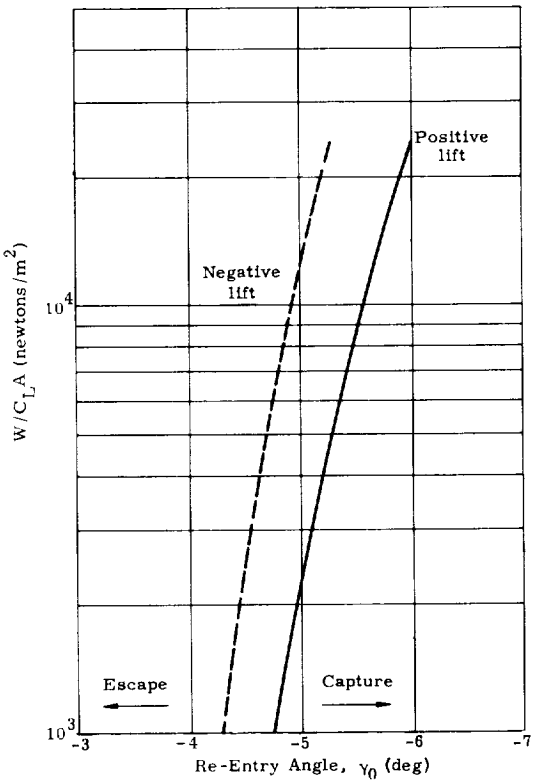

Fig. 63c. Minimum Entry Angle for Capture (at escape velocity) (Ref. 14)

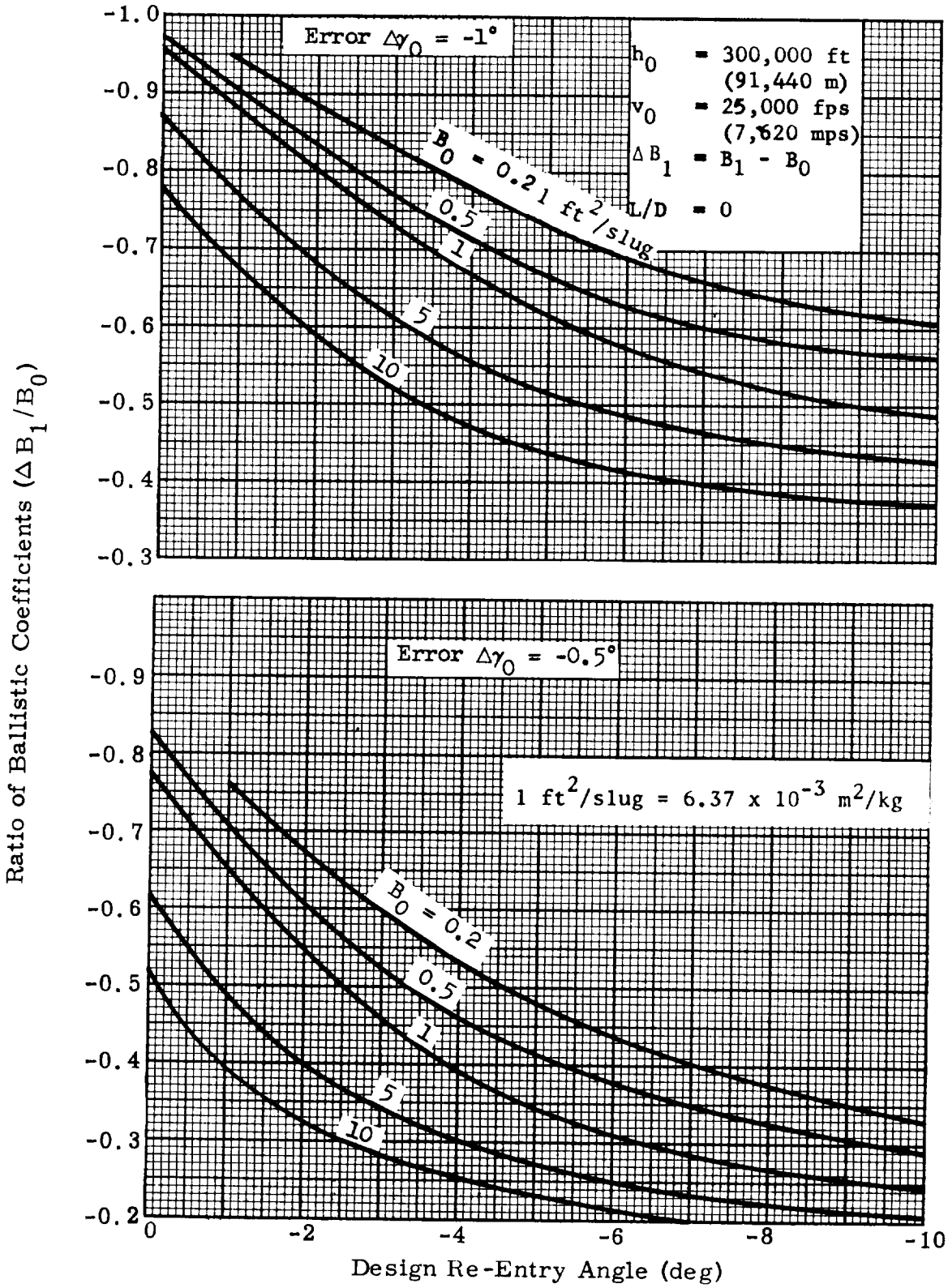

Fig. 64. Range Corrections with Ballistic Coefficient Increments

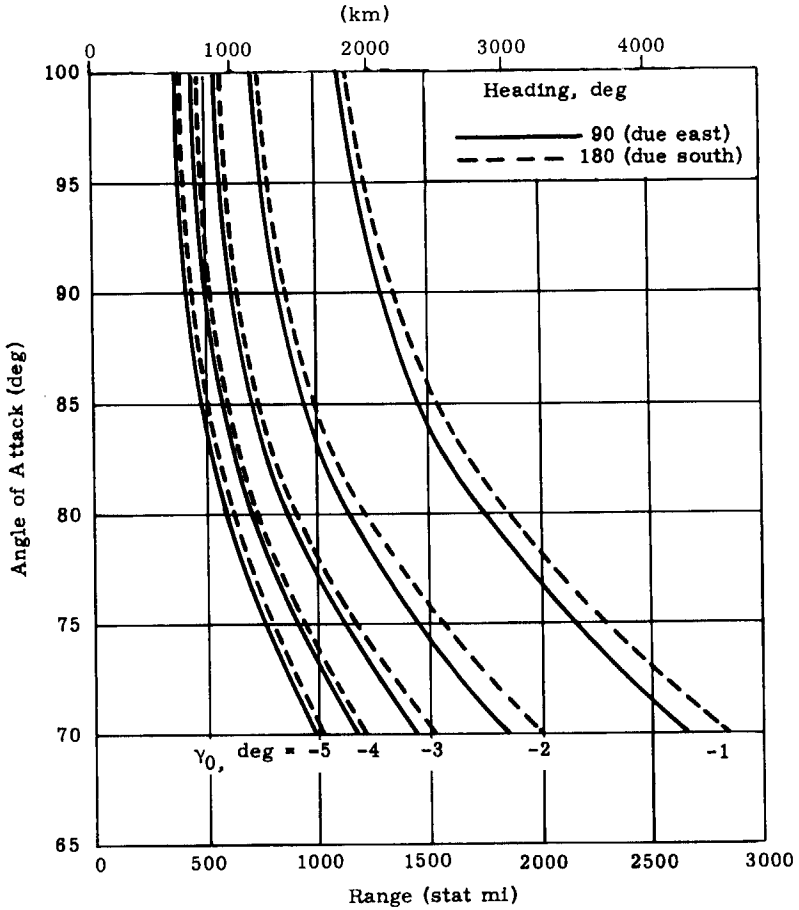

Fig. 65a. Variation in Range as a Function of Angle of Attack and Entry Angle for Headings of 90° and 150° (Rotating Earth; h_0 = 350,000 ft = 106,680 m; v_0 = 25,743 fps = 7846 mps; W/A = 20 lb/ft^2 = 957 newtons/m^2) (Ref. 25)

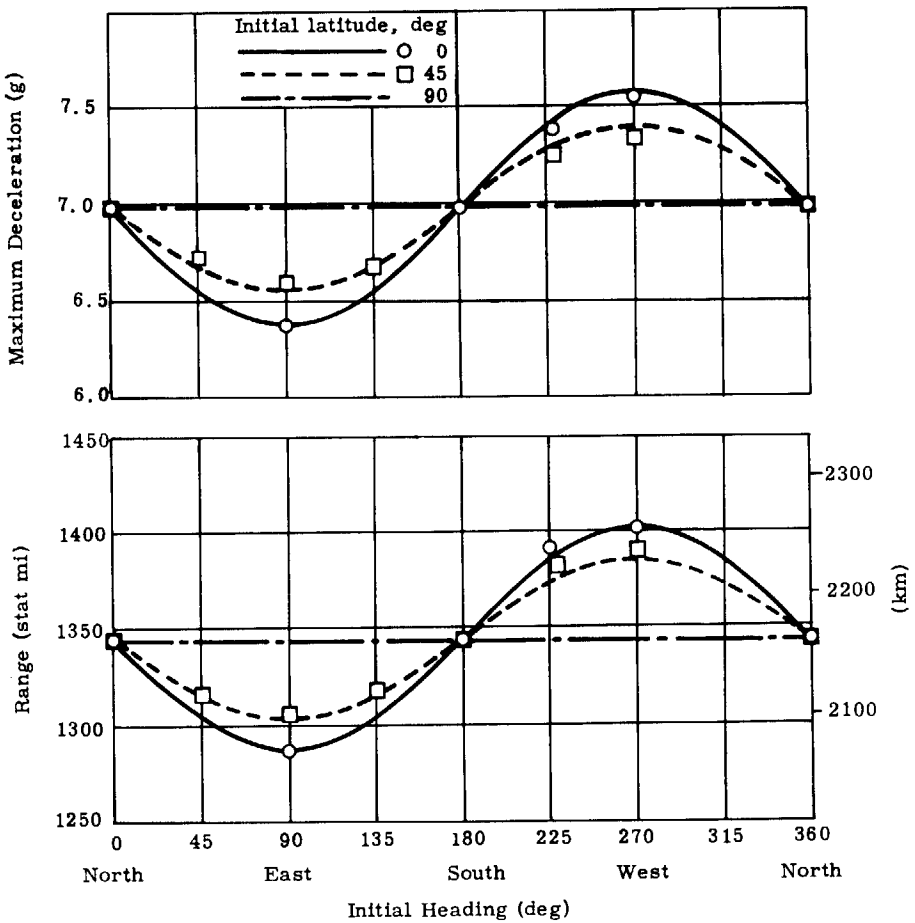

Fig. 65b. Variation in Range and Maximum Deceleration as a Function of Heading and Initial Latitude (Rotating Earth; h_0 = 350,000 ft = 106,650 m; v_0 = 25,743 fps = 7846 mps; W/A = 20 lb/ft^2 = 957 newtons/m^2) (Ref. 25)

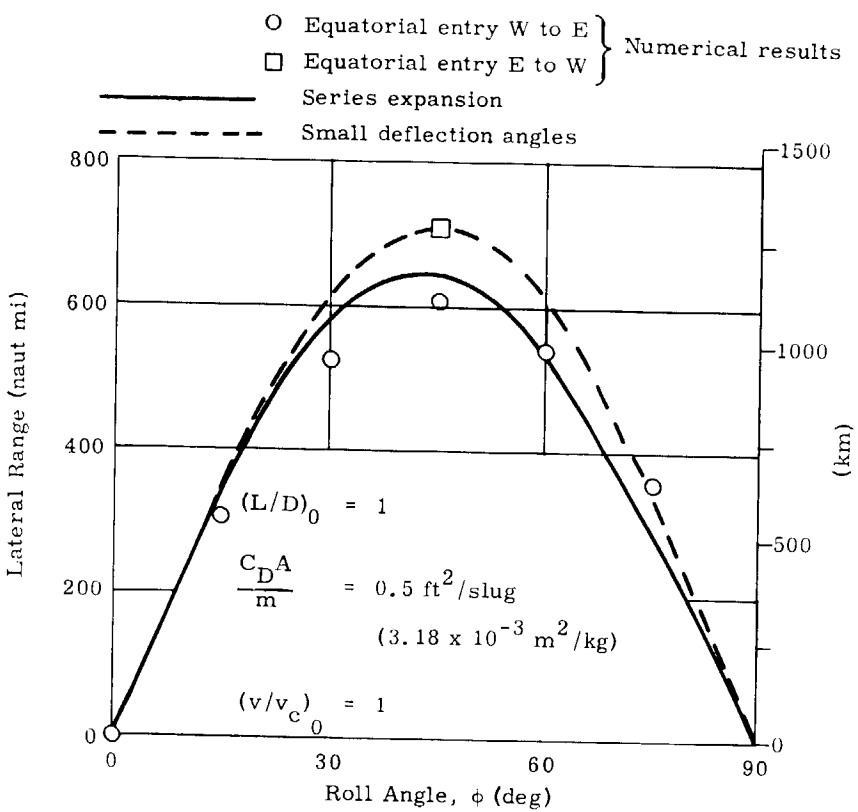

Fig. 66a. Effect of Roll Angle on Lateral Range (Ref. 27)

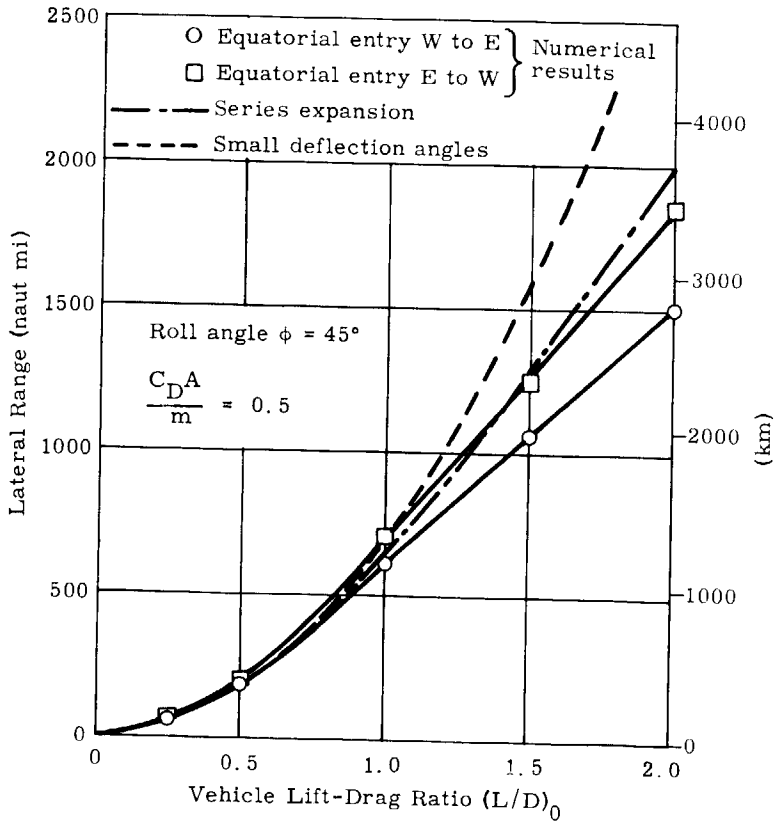

Fig. 66b. Lateral Range Capability ($v_0 = v_c$) (Ref. 27)

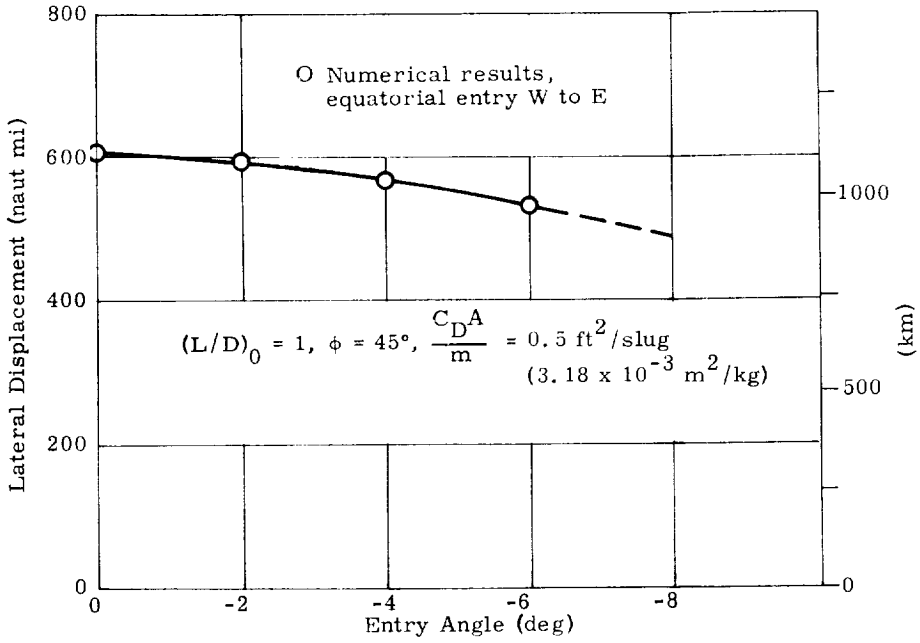

Fig. 66c. Effect of Entry Angle on Lateral Range (Ref 27)

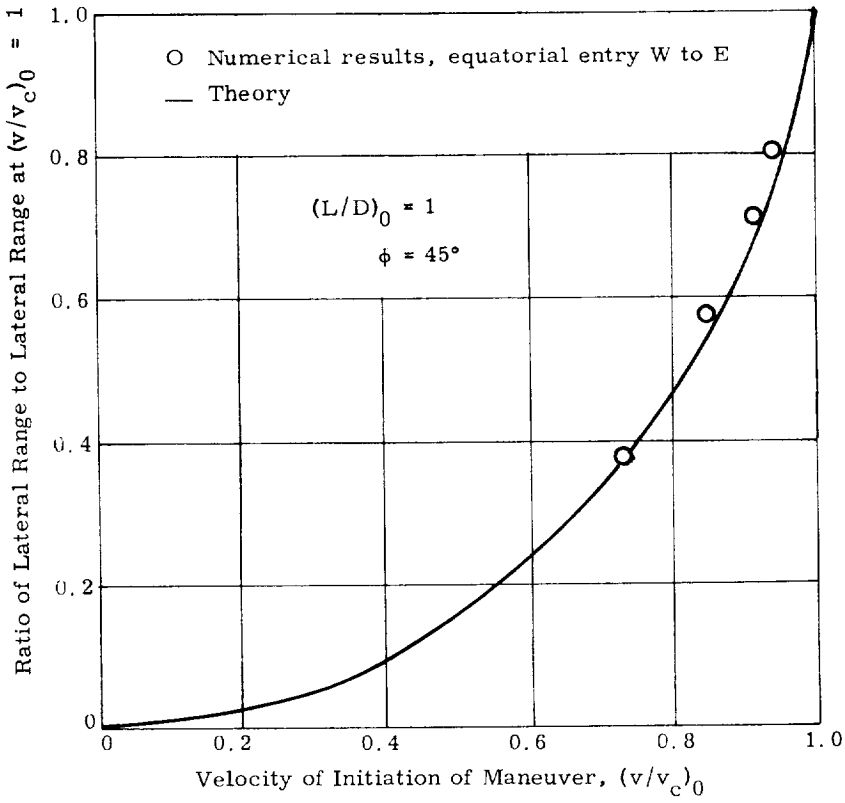

Fig. 66d. Effect of Velocity at Initiation of Maneuver on Lateral Range (Ref 27)

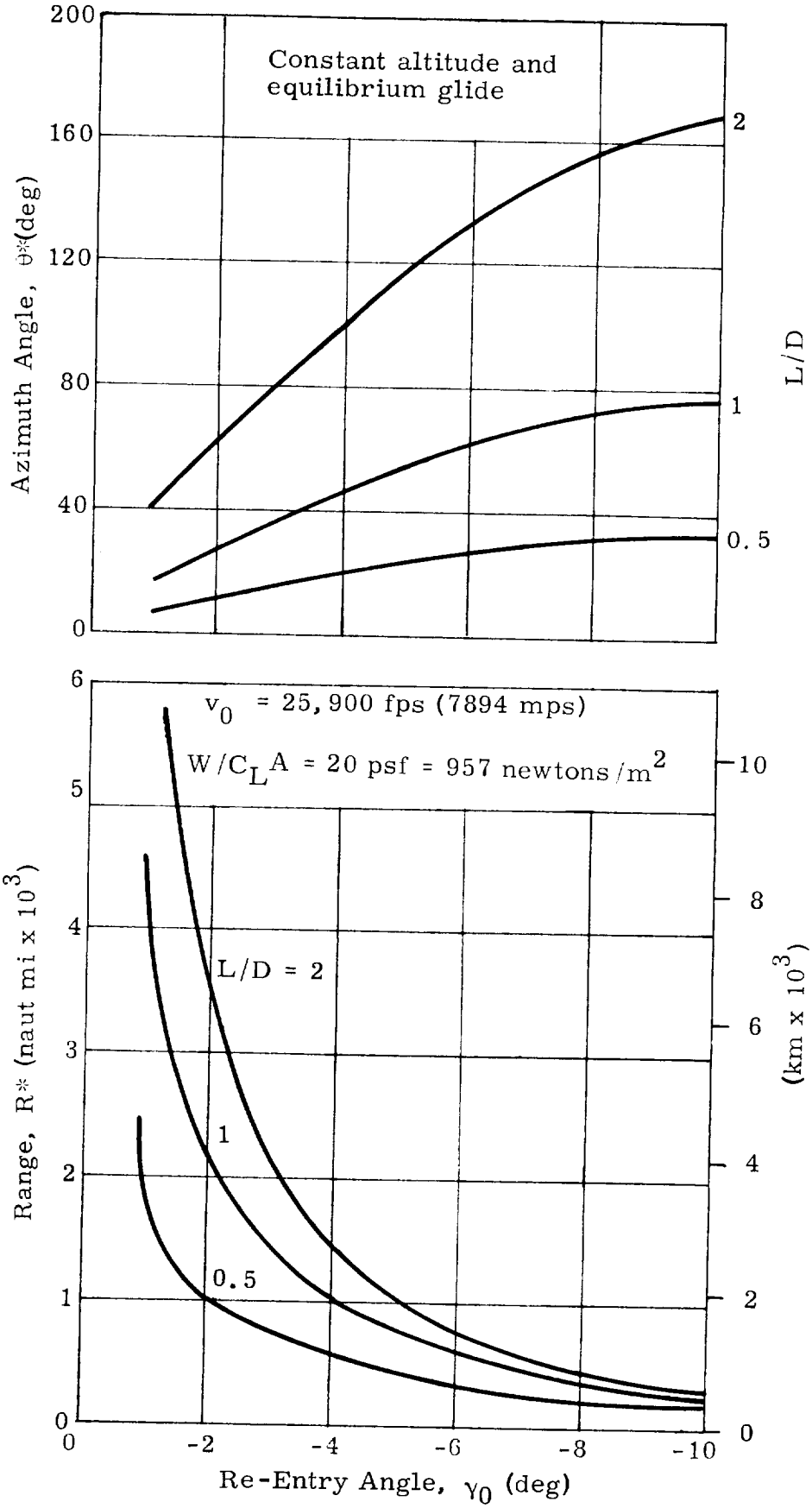

Fig. 67a. Effect of Re-Entry Angle on the Azimuth Angle and Range to Maximum Lateral Deflection Point (Ref 14)

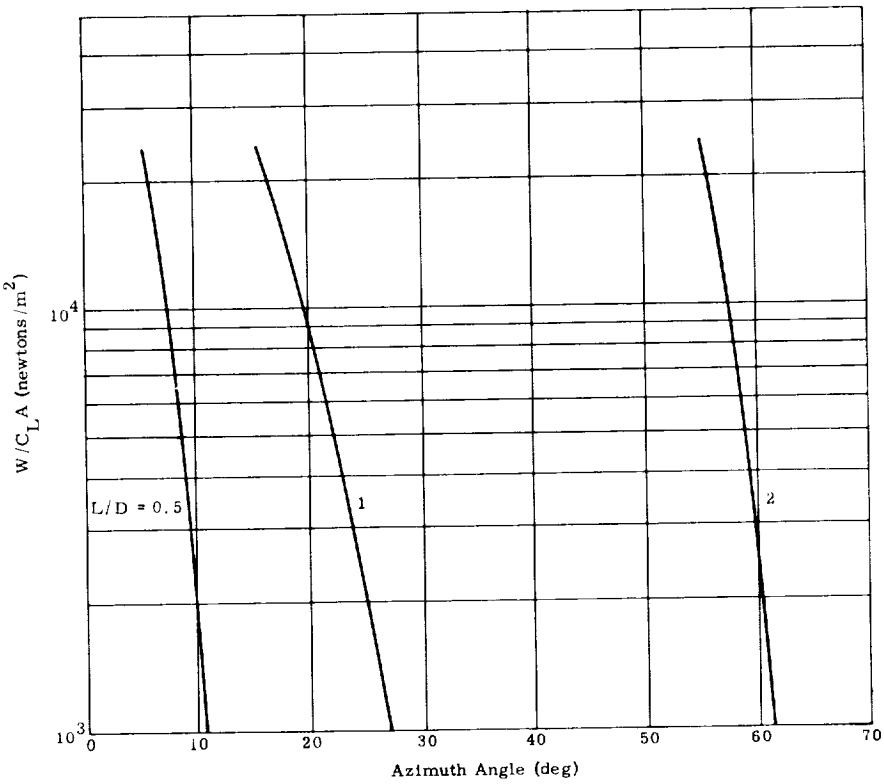

Fig. 67b. Effect of Wing Loading on Azimuth Potential (γ_0 = 2°; constant altitude and equilibrium glide) (Ref. 14)

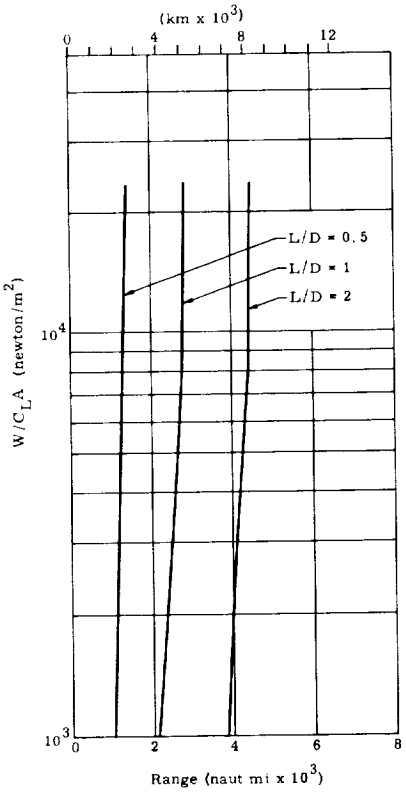

Fig. 67c. Effect of Wing Loading on Range to Maximum Azimuth Potential (γ_0 = -2°; constant altitude and equilibrium glide) (Ref. 14)

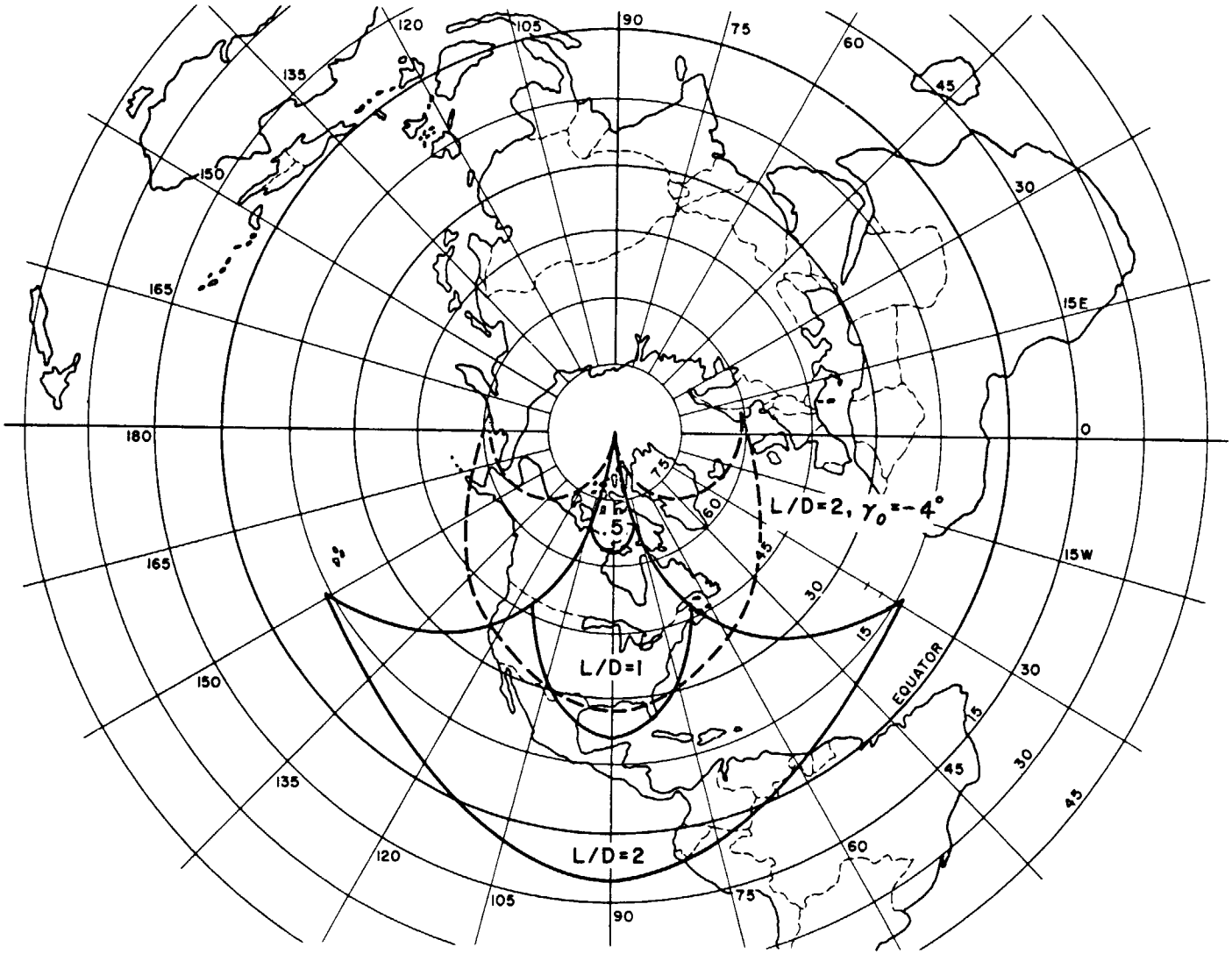

(a) $v_0 = v_c$, $\gamma_0 = -2°$, $W/C_L A$ = 20 psf = 957 newtons/m^2 (Ref. 14)

Fig. 68. Total Maneuverability Envelope

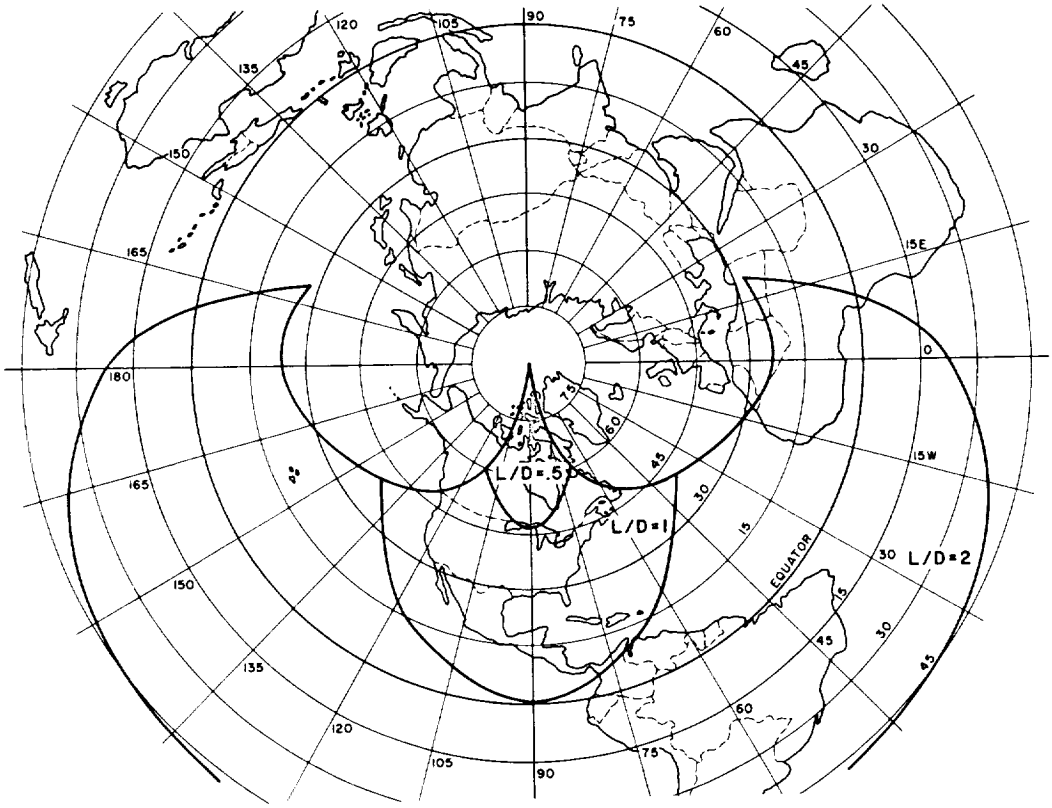

(b) $v_0 = \sqrt{2}\, v_c$, $\gamma_0 = -6°$, $W/C_L A = 100$ psf = 4787 newtons/m^2 (Ref. 14)

Fig. 68. (continued)

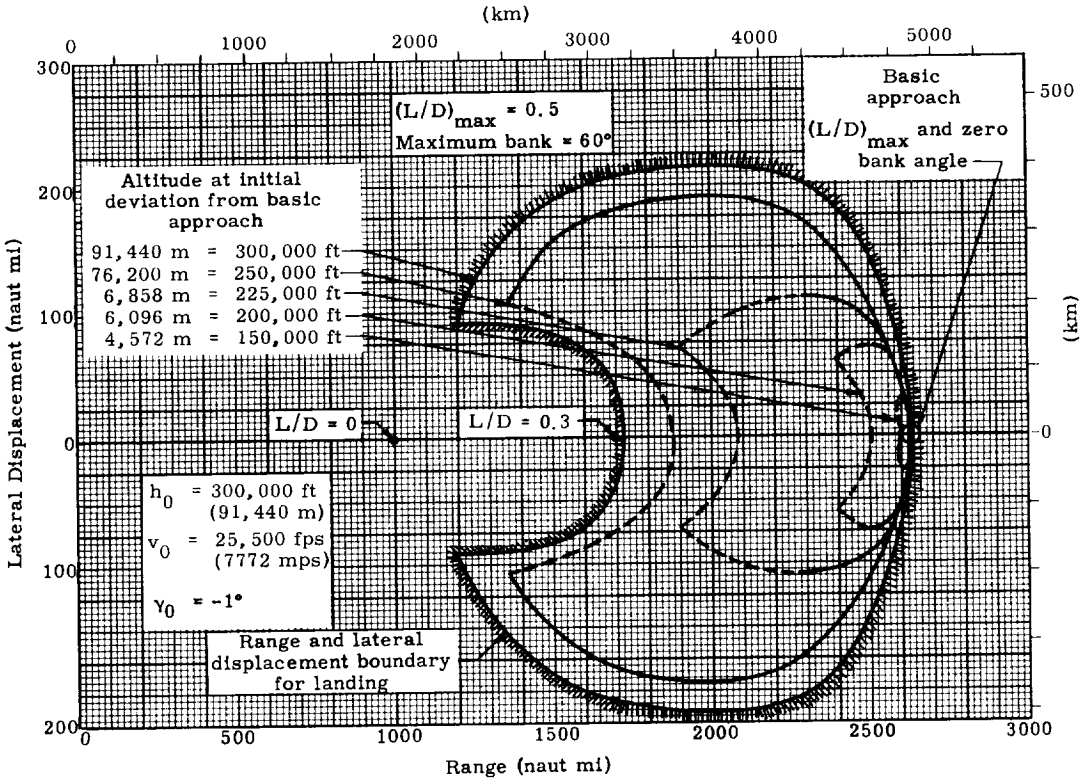

Fig. 69. Range and Lateral Displacement for Lifting Body Re-Entry